#200 #200

FAO Fisheries Report No. 200 Supplement
FAO, Informes de Pesca, N° 200 Suplemento

FIR/R200 Suppl. (En/Es)

CICAR – II

SYMPOSIUM ON PROGRESS IN MARINE RESEARCH IN THE CARIBBEAN AND ADJACENT REGIONS

Held in Caracas, 12-16 July 1976

Papers on oceanography, metereology, geology and geophysics

LIBRARY
JUL 2 1979
FISH & WILDLIFE SERVICE

ICCRA – II

SIMPOSIO SOBRE ADELANTOS EN LAS INVESTIGACIONES MARINAS EN EL CARIBE Y REGIONES ADYACENTES

celebrado en Caracas, 12-16 de julio de 1976

Contribuciones sobre oceanografía, meteorología, geología y geofísica

FOOD AND AGRICULTURE ORGANIZATION OF THE UNITED NATIONS
ORGANIZACION DE LAS NACIONES UNIDAS PARA LA AGRICULTURA Y LA ALIMENTACION

Digitized by the Internet Archive
in 2025

https://archive.org/details/fao-fisheries-and-aquaculture-report_1976-07_supplement

Cooperative Investigations of the Caribbean and Adjacent Regions - II

Investigaciones Cooperativas del Caribe y Regiones Adyacentes - II

SYMPOSIUM ON PROGRESS IN MARINE RESEARCH IN THE CARIBBEAN AND ADJACENT REGIONS

Caracas, Venezuela, 12-16 July 1976

SIMPOSIO SOBRE ADELANTOS EN LAS INVESTIGACIONES MARINAS EN EL CARIBE Y REGIONES ADYACENTES

Caracas, Venezuela, 12-16 julio 1976

Papers on oceanography,
meteorology, geology
and geophysics

Contribuciones sobre oceanografía,
meteorología, geología y
geofísica

Edited by

Redactado por

Harris B. Stewart Jr.

FOOD AND AGRICULTURE ORGANIZATION OF THE UNITED NATIONS
ORGANIZACION DE LAS NACIONES UNIDAS PARA LA AGRICULTURA Y LA ALIMENTACION

Rome, December 1978

Roma, Diciembre 1978

PREPARATION OF THIS REPORT

This publication forms part of the Proceedings of the Symposium on Advances in Marine Research in the Caribbean and Adjacent Regions (CICAR-II Symposium) held in Caracas, Venezuela, 6-12 July 1976. The Symposium was the conclusion of the international programme Cooperative Investigations of the Caribbean and Adjacent Regions. The present volume, issued by FAO in its Fisheries Reports series, contains the full texts in their original language of papers on physical and chemical oceanography, marine geology and geophysics.

PREPARACION DE ESTE DOCUMENTO

Esta publicación forma parte de las Actas del Simposio sobre Adelantos en Investigaciones Marinas en el Mar Caribe y Regiones Adyacentes (Simposio CICAR-II) que tuvo lugar en Caracas, Venezuela del 12 al 16 de julio de 1976. El Simposio fue la conclusión del programa internacional Investigaciones Cooperativas del Mar Caribe y Regiones Adyacentes. El presente volumen, editado por la FAO en su serie de Informes de Pesca, contiene el texto íntegro en su lengua original de las comunicaciones sobre oceanografía física y química, geología marina y geofísica, y meteorología.

Las contribuciones sobre pesquerías, biología marina y acuicultura se encuentran en el Informe de Pesca No. 200.

Distribution/Distribución

FAO Department of Fisheries
FAO Regional Fishery Officers
Member countries
Unesco
IOC
Participants and organizers
Selector SM
ACMRR

Departamento de Pesca de la FAO
Funcionarios de Pesca Regionales de la FAO
Países miembros
Unesco
COI
Selector SM
CAIRM

Bibliographic Entry/Cita bibliográfica

Stewart, H.B. Jr. (Ed.)(1978)
FAO Fish.Rep., (200)Suppl.:638 p.
Cooperative Investigations of the
Caribbean and Adjacent Regions - II.
Symposium on Progress in Marine Research
in the Caribbean and Adjacent Regions,
Caracas, Venezuela, 12-16 July 1976.
Papers on oceanography, meteorology,
geology and geophysics
Investigaciones Cooperativas del Caribe
y Regiones Adyacentes - II. Simposio
sobre Adelantos en las Investigaciones
Marinas en el Caribe y Regiones Adyacentes,
Caracas, Venezuela, 12-16 julio 1976.
Contribuciones sobre oceanografía,
meteorología, geología y geofísica

Conferences - Caracas (Venezuela). Reports.
Physical oceanography. Chemical oceanography.
Meteorology. Atmospheric conditions.
Oceanographic data. Ocean-atmospheric
system. Marine geology. Sedimentology.
ASW, Caribbean

FOREWORD

The CICAR-II Symposium held in Caracas, Venezuela in July 1976 was called to present the advances in marine research achieved during the period of the Cooperative Investigations of the Caribbean and Adjacent Regions (CICAR), 1968-1975. The Symposium was sponsored by the Intergovernmental Oceanographic Commission (IOC), a part of the United Nations Educational, Scientific and Cultural Organization (Unesco) with the assistance of the Food and Agriculture Organization (FAO) and the World Meteorological Organization (WMO). The Government of Venezuela generously provided facilities and made local arrangements for the proceedings.

The success of the Symposium was the result of the efforts of many people in countries throughout the region, of whom only a few can be mentioned here. The programme was organized by an International Steering Committee of which H.B. Stewart Jr. (U.S.A.) was Chairman and the members were A. Ayala Castañares (Mexico), I. Emilsson (Unesco/Mexico), I. Goodbody (Jamaica), A. Mena M. (Cuba), R. Molinari (U.S.A.), H. Pérez Nieto (Venezuela), H. Postma (SCOR/Netherlands), T. Rass (U.S.S.R.) and T. van't Hof (Netherlands). The Local Arrangements Committee in Venezuela was headed by J.A. Galavis S. and included H. Pérez Nieto, J.d'Angelo B. and A. Ahmad. The International Coordinator of CICAR, J.S. Kenny (Trinidad and Tobago) served as Chairman of the Symposium.

This volume contains the papers on oceanography, meteorology, geology and geophysics. A previous publication (FAO Fisheries Report No. 200) contains the papers on fisheries, aquaculture and marine biology.

Enquiries concerning the content of the papers should be directed to the authors.

Harris B. Stewart Jr.
Editor-in-Chief
NOAA Atlantic Oceanographic and
Meteorological Laboratories
Virginia Key
Miami, Florida 33149
U.S.A.

PREAMBULO

El Simposio CICAR-II, celebrado en Caracas, Venezuela, en julio de 1976, se convocó para presentar los adelantos conseguidos en materia de investigaciones marinas durante el período de las Investigaciones cooperativas en el mar Caribe y regiones adyacentes (ICCRA) 1968-1975. El simposio fue patrocinado por la Comisión Oceanográfica Intergubernamental (COI), y una parte de la Organización de las Naciones Unidas para la Educación, la Ciencia y la Cultura (Unesco), y tuvo colaboración de la Organización de las Naciones Unidas para la Agricultura y la Alimentación (FAO) y la Organización Meteorológica Mundial (OMM). El Gobierno de Venezuela proporcionó generosamente las instalaciones y servicios, y se hizo cargo de los preparativos locales.

El buen éxito del simposio se debió a los esfuerzos de muchas personas de diversos países de la región, de las cuales tan sólo algunas pueden mencionarse en el presente documento. El programa fue organizado por el Comité Organizador Internacional, cuyo Director era H.B. Stewart Jr. (EE.UU.), y cuyos miembros eran A. Ayala Castañares (México), I. Emilsson (Unesco/México), I. Goodbody (Jamaica), A. Mena M. (Cuba), R. Molinari (EE.UU.) H. Pérez Nieto (Venezuela), H. Postma (CCIO/Países Bajos), T. Rass (U.R.S.S.) y T. van't Hof (Países Bajos). El Comité organizador Venezolano estuvo presidido por J.A. Galavís S., y de él formaban parte H. Pérez Nieto, J. d'Angelo B. y A. Ahmad. El Coordinador Internacional del ICCRA, J.S. Kenny (Trinidad y Tabago), actuó como Presidente del simposio.

Este documento contiene las comunicaciones relativas a oceanografía, meteorología, geología y geofísica. Una publicación anterior (FAO, Informes de la Pesca, No. 200) contiene las contribuciones sobre pesquerías, acuicultura y biología marina.

Las solicitudes de información sobre el contenido de los documentos deberán dirigirse a los autores de los mismos.

Harris B. Stewart Jr.
Editor-in-Chief
NOAA Atlantic Oceanographic and
Meteorological Laboratories
Virginia Key
Miami, Florida 33149
U.S.A.

CONTENTS
INDICE

Pages/Paginas

VAN'T HOF, T. and W. LANGERAAR, A short history of CICAR 1 - 8

Physical Oceanography Session
Sesión de Oceanografía Física

ADEM, J., Predicción de la temperatura media mensual en la superficie de los océanos utilizando un modelo termodinámico 19 - 20

FEBRES ORTEGA, G. y L.E. HERRERA, Circulación y transporte de masa de agua en el caribe suroriental 21 - 33

HERRERA L.E. and G. FEBRES ORTEGA, Divergencia anemogénica horizontal de las aguas superiores de Venezuela oriental, Mar Caribe 35 - 50

MERRELL, W.J. et al., A description of the circulation observed in the eastern Gulf of Mexico during CICAR Survey Month II, May 1972 51 - 61

METCALF, W.G., Water exchange between the Atlantic Ocean and the Caribbean Sea 63 - 77

MOFJELD, H.O. and M. WIMBUSH, Tides in the Gulf of Mexico and the Caribbean Sea 79 - 102

MOLINARI, R.L., An overview of the Cayman Sea-Gulf of Mexico circulation based on CICAR Survey Month and other data 103 - 118

NELEPO, B.A. et al., Soviet investigations of the dynamics and properties of the waters of the Caribbean Sea and Gulf of Mexico 119 - 131

PASKAUSKY, D.F. and W.D. NOWLIN, A comparison of summer and winter drifter movements with the American Mediterranean 133 - 137

RUIZ RENTERIA, F., La velocidad del sonido en la región suroccidental del Golfo de Mexico 139 - 154

VASQUES DE LA CERDA, A.M., Circulación del agua en el suroeste del golfo de México 155 - 171

VISSER, M.P., Physical Oceanography in the waters off Surinam and French Guyana during 1970-71 173 - 184

VOLTOLINA, D., Hydrological conditions in the central zone of the Venezuelan Caribbean Sea, February 1975 185 - 210

Chemical Oceanography Session
Sesión de Oceanografía Quimica

ATWOOD, D.K., Review of the Chemical Oceanography Session 211 - 219

BARCELONA, M.J. and D.K. ATWOOD, Gypsum-organic interactions in tropical seawater 221 - 231

VAN BENNEKOM, A.J. and S.B. TIJSSEN, Nutrients on and off the Guyana shelf related to upwelling and Amazon outflow 233 - 253

Pages/Paginas

BERBERIAN, G.A. and R.B. STARR, The circulation between the Cayman Sea and the Gulf of Mexico as deduced from nutrient distributions 255 - 266

BOTELLO, A.V., E. HICKS and E.F. MANDELLI, Estudios preliminares sobre los niveles de algunos contaminantes en la laguna de Términos, Campeche, México 267 - 280

CEDEÑO FERMIN, G., Carbohidratos disueltos en aguas de la región nororiental de Venezuela 281 - 295

FANNING, K.A., Dissolved silica and the American Mediterranean 297 - 298

FROELICH, P.N. and D.K. ATWOOD, Dissolved silicate and salinity structure of the upper waters of the Venezuela basin, Caribbean Sea 299 - 314

FORSTER, W.O. et al., Radionuclide and trace element associations with plankton and possible vertical transport mechanisms in the Caribbean 315 - 328

JEFFREY, L.M. and R.M. GERSHEY, Organic matter in the Cariaco Trench 329 - 347

OKUDA, T., Condiciones hidroquímicas de las aguas superiores de la Fosa de Cariaco y áreas adyacentes 349 - 362

VELEZ, B.J. et al., Adhesion enhancing organics in the Eastern Caribbean Sea 363 - 374

Marine Geology/Geophysics Session
Sesión de Geología y Geofísica Marinas

CARDER, K.L. et al., A nepheloid layer associated with the Guiana Current 375 - 385

KEIGWIN, L.D., Jr., Late cenozoic paleoceanography of the Panama, Colombia and Venezuela basins 387 - 392

KLINGEBIEL, A. and G. VERNETTE, Marine geology research on the Colombian Caribbean shelf 393 - 398

PETER, G., Summary of NOAA geological-geophysical studies during CICAR expeditions 399 - 417

SCHUBERT, C., Quaternary marine terraces of La Blanquilla Island, northeastern Venezuelan offshore 419 - 428

THUNELL, R.C., Late quaternary calcium carbonate dissolution history, Western Gulf of Mexico 429 - 444

Meteorology and Air/Sea Interaction Session
Sesión en Meteorología y Interacción Aire-Mar

AUGSTEIN, E., The role of the atmospheric boundary layer in air-sea interaction processes in the tropics 445 - 461

ETTER, P.C., A climatic heat budget study of the Gulf of Mexico 463 - 478

OSTAPOFF, F. and S. WORTHEM, Air-sea interactions during conditions of squalls and deep convection 479 - 486

Pages/Paginas

PERDOMO DE MATA, M. y K. HUBSCHMANN, Temporada de lluvias en las costas venezolanas durante el año 1975 487 - 503

WORTHEM, S. and F. OSTAPOFF, The response of the tropical North Atlantic to meteorological forcing functions 505 - 530

Interdisciplinary Topics Session
Sesión en Temas Interdisciplinarios

DUNCAN, C.P. *et al.*, Energy from the sea: ocean thermal energy conversion possibilities in the Caribbean 531 - 546

LEGECKIS, R., Present and planned satellite observations of the Gulf of Mexico and the Caribbean Sea 547 - 560

MANDELLI, E.F., Guidelines for regional baseline studies of contaminants in coastal areas 561 - 568

WINTERFELD, T., Distribution of physical and chemical oceanographic data in the CICAR region 569 - 580

Multidisciplinary Topics Session
Sesión en Temos Multidisciplinarios

DARBYSHIRE, J. *et al.*, Investigation of mixing processes of North Sound Lagoon, Grand Cayman 581 - 595

MAUL, G.A., The 1972-73 cycle of the Gulf Loop Current Part II: mass and salt balances of the basin 597 - 619

NELEPO, B.A., Basic results of research carried out by the Marine Hydrophysical Institute of the Ukrainian SSR Academy of Sciences in the International Oceanographic Programme "CICAR" 621 - 636

ZERNETSKY, B.F., Estructura geológica y principales fases de desarrollo de la parte oriental de la región del Caribe 637 - 638

A SHORT HISTORY OF CICAR

by

T. VAN 'T HOF[1]
Operations Coordinator of CICAR
Carmabi, Curaçao, Netherlands Antilles

CONTENTS

1. INTRODUCTION
2. PREPARATORY PHASE
3. OPERATIONAL PHASE
4. EVALUATION PHASE
5. CONCLUSION
6. REFERENCES

Abstract

A cooperative study of the Caribbean area was proposed in 1967 by the Netherlands delegation to the Intergovernmental Oceanographic Commission (IOC) of Unesco. The fifth IOC Assembly in October 1967 declared the "Cooperative Investigation of the Caribbean and Adjacent Regions" (CICAR) an official IOC programme. The field phase of CICAR was initiated in 1970, after a preparatory symposium and the formation of an International Coordination Group (ICG) in Curaçao in 1968.

A comprehensive scientific programme was drawn up during the second and third sessions of the ICG and critically reviewed at the fourth session in 1971. Organizational arrangements included a regional data centre (the National Oceanographic Data Center in Washington), an operations centre and a biological sorting centre.

The field work of CICAR extended over a period of six years, during which over 40 research vessels belonging to ten different nations participated in the investigations. The overall scientific programme of CICAR was essentially a combination of various national programmes. The CICAR Survey Month programme, however, was a truly cooperative exercise, while CICAR also generated several bilateral cooperative research activities.

During the period of its field operations, CICAR developed from a cooperative investigation into a framework for international cooperation in marine sciences in general. It is this development that most likely made the ICG wish to extend the duration of CICAR to six years and that illustrated the necessity to establish a new body for international cooperation in the Caribbean area.

Resumen

En 1967, la delegación holandesa propuso a la Comisión Oceanográfica Internacional (COI) de la Unesco un estudio cooperativo de la zona del Caribe. La quinta Asamblea de la COI declaró, en octubre de 1967, que las "Investigaciones cooperativas del Caribe y regiones adyacentes" (ICCRA) eran un programa oficial de la COI. Después de un simposio preparatorio. celebrado en 1968, y de la creación, en Curaçao, de un Grupo Internacional de Coordinación (GIC), se inició, en 1960, la fase de trabajos prácticos.

---

[1] Present address: Ministry of Education and Sciences
Department of Space Technology and Oceanography
The Hague, Netherlands

En la segunda y tercera reuniones del GIC se preparó un amplio programa científico, que fue sometido a un examen crítico durante la cuarta reunión, en 1971. Entre las medidas administrativas figuraba la creación de un centro regional de datos (el Centro Nacional de Datos Oceanográficos, en Washington), un centro de operaciones, y un centro de clasificación biológica.

Los trabajos prácticos de las ICCRA duraron seis años y en ellos participaron cuarenta buques de investigación científica pertenecientes a diez naciones. El programa científico global de las ICCRA era, en esencia, una combinación de varios programas nacionales, mientras que las expediciones mensuales de las ICCRA eran actividades realmente cooperativas, que coincidieron con otras varias actividades bilaterales de investigacion también de las ICCRA, de carácter cooperativo.

Durante el período de duración de los trabajos prácticos, las ICCRA se transformaron de investigaciones cooperativas, en el marco general para le cooperación internacional en ciencias marinas, y es muy probable que, precisamente a causa de este desarrollo, las ICCRA desearan ampliar a seis anos la duración de sus actividades, poniendo de manifiesto la necesidad de crear un nuevo organismo de cooperación internacional en la zona del Caribe.

1. INTRODUCTION

Mr. Chairman, ladies and gentlemen: I am very honoured by the invitation to present an introductory paper on the history of CICAR at this first session of the Symposium. This Symposium is regarded as the conclusion of CICAR and it is fitting to look back at such moments. History always teaches us a lesson and we need this particular lesson to be able to conduct future cooperative studies with even more success.

2. PREPARATORY PHASE

Let us go back to 1965, four years after the establishment of the Intergovernmental Oceanographic Commission (IOC) when the former Chief Hydrographer of the Royal Netherlands Navy and the Director of the Netherlands Institute for Sea Research met at a summer residence on a little island off the Britanny coast of France. As usual they could not resist talking oceanography. Both were familiar with the Caribbean Sea and interested in its scientific problems. They agreed that insufficient knowledge existed concerning its circulation, resources, bathymetry and geological history, and that a cooperative approach was needed to solve problems and give answers to a multitude of questions. It was not to be "just a plan" that would disappear like so many others because of lack of follow-up. In 1967 the Netherlands delegation to the IOC proposed a cooperative study of the Caribbean area; the fifth session of the IOC, October 1967, declared the Cooperative Investigation of the Caribbean and Adjacent Regions (CICAR) an official IOC programme.

Preparations for the field phase of CICAR included a Symposium on Investigations and Resources of the Caribbean and Adjacent Regions held in 1968 at Curaçao, Netherlands Antilles. The purpose of this Symposium was to review existing knowledge and to prepare recommendations to CICAR. Immediately following the Symposium the International Coordination Group (ICG) for CICAR met for the first time. The eleven IOC Member States expressed an interest in participating in CICAR. These were Cuba, Federal Republic of Germany, France, Guatemala, Jamaica, Mexico, Netherlands, United Kingdom, U.S.A., U.S.S.R. and Venezuela. Later, Brazil, Colombia, Panama and Trinidad and Tobago were to bring the membership of the ICG for CICAR to fifteen. Each CICAR Member State appointed a National Coordinator and at its first session the ICG elected Rear Admiral W. Langeraar as International Coordinator for CICAR. Most of the elements that would later become part of the organizational structure of CICAR, were discussed during this meeting. Consideration was given to the desirability of establishing an "operations centre" or "coordinating nerve centre", a biological sorting centre and a data centre. It was proposed that an editorial committee be set up, and that a "liaison bulletin" be used for the dissemination of up-to-date information on CICAR operations. The concept of "disciplinary coordinators" was brought up in the discussions and, also at this first meeting, an "assistant international coordinator" was elected. The United Kingdom strongly recommended that a full-time salaried International Coordinator be appointed to work out of the operational centre when it was established within the Caribbean region.

Most of these ideas and suggestions did become reality sooner or later. A CICAR Operations Centre was established at Curaçao in 1970 and it functioned throughout the duration of CICAR (until the end of 1975) with funds provided by the Government of the Netherlands. The Operations Coordinator became the full-time salaried coordinator who was to work from the operational centre. The U.S. National Oceanographic Data Center (NODC) served the cooperative investigation outstandingly and performed all the duties it could expect from a regional data centre. In 1972, the Mexican Government with the support of Unesco set up a biological sorting centre for CICAR known as Centro de Preclasificación Oceánica de México (CPOM) or Mexican Oceanic Sorting Center.

The Subject Leader system; specialists with specific responsibilities in the conception and implementation of scientific programmes in their own disciplines, filled the role of "disciplinary coordinators". Two Assistant International Coordinators have served CICAR, one for fisheries and one for meteorology. Their tasks were similar to those of the Subject Leaders. However, a separate status distinguished these disciplines which are areas of special concern for FAO and WMO respectively.

The establishment of coordinating machinery for CICAR was not as laborious as the establishment of a comprehensive scientific programme. At the Curaçao meeting the CICAR National Coordinators presented the mainly provisional national programmes for CICAR and a first attempt was made to identify the overall scientific programme for CICAR. The scientific programme was to be the main subject of the discussions during the two following sessions of the ICG in Washington, 1969 and Mexico City in 1970.

Although the programme evolved continuously, its main features were clearly recognizable by 1969. The main objectives of the physical oceanography programme studies were on the movement of water masses into, out of and within the Caribbean Sea and Gulf of Mexico, including tidal movements and upwelling phenomena. The main objectives of the meteorological programme were to study the exchange of energy between ocean and atmosphere and to provide meteorological information to the various sub-programmes of CICAR.

The chemical oceanographic programme was to study background levels of pesticides and petroleum products and to elucidate the budgets of nutrients, salt and dissolved gases. These studies would include both a systematic coverage of the whole area and detailed investigations of trenches, deep basins and areas of upwelling. The need for close coordination between chemical and physical oceanographic observations was obvious. In the field of marine geology and geophysics the main objectives were to investigate: the age and origin of the Caribbean; the nature of the submarine ridges; the deep structure of the island arcs and the sediment discharge into the region. A geotraverse was proposed from the Atlantic to the Pacific as a cooperative project. The following commentary on the geology and geophysics programme recorded at the Mexico session of the ICG illustrates that project proposals were not always implemented: "It is apparent that the optimistic recommendations of the second meeting of the ICG for CICAR at Washington D.C., 1969 are unlikely to be achieved."

A separate bathymetry programme was proposed, primarily to assist the preparation and updating of the General Bathymetric Chart of the Oceans (GEBCO) and to eliminate so-called "doubtful hydrographic data".

The main objectives of the marine biology programme were the study of primary production, plankton and secondary production, comprehensive taxonomic studies and marine pollution. The fisheries programme included: the study of eggs, larvae and juveniles of pelagic fish; the study of coastal lagoons and mariculture; the appraisal of shrimp resources and the appraisal and management of turtle stocks.

3. OPERATIONAL PHASE

Most programmes entered the operational stage in 1970, which was designated as the year of reconnaissance. The Operations Coordinator began his duties in 1970 and put the Coordination and Communication Manual for CICAR to work. This manual instructed masters of participating research vessels to submit to the Operations Coordinator daily reports including the ship's position and the status of the observations. These position reports were sent in the form of coded telegrams. The Operations Coordinator, in turn, sent out daily ships' availability reports, thus informing all participating ships of the others' positions. The system functioned well during the first year of the CICAR operations but was later abandoned in favour of a less strict reporting scheme (1972).

In 1971 the first evaluation of CICAR was carried out by Dr. Mamayev (IOC) with the assistance of Dr. Kesteven. The evaluation was followed by a critical review of the comprehensive scientific programme for CICAR which was drawn up in Mexico City by the third session of the ICG for CICAR. It was only at this session that the objectives of CICAR were clearly defined. They were worded in recommendation 4.1 as follows:

(1) to contribute to the development of scientific research in the CICAR region;
(2) to secure the maximum participation of coastal countries in this region;
(3) to achieve a better scientific understanding of the region;
(4) to carry out, rapidly and effectively, certain particular projects of research with well-defined scientific and economic objectives, and

(5) to establish the basis for further international coordination in the CICAR area.

Meanwhile the concept of standard sections, already put forward in 1968, proved to be the basis of a true international programme. The standard sections, a number of strategic lines located east and west of the Lesser Antilles Arc, in the Central Caribbean, across the Antillean passages and in the Gulf of Mexico were meant to be occupied by research vessels two or three times a year in connexion with the circulation studies. The basic sampling programme to be carried out at the standard sections consisted of a BT observation and a cast of watersamplers to determine salinity, temperature and oxygen.

In 1971 the ICG for CICAR designated certain months as CICAR Survey Months. The Survey Months were periods during which as many research vessels as possible would carry out synoptic or near-synoptic observations with special emphasis on standard sections. A set of meteorological observations and a "standard biological station" were added to the physicochemical measurements that were to be carried out at standard sections, thus making the programme one of broad interest. In a later stage Dr. Donald K. Atwood, Subject Leader for Chemical Oceanography was charged with the responsibility of preparing a Standard Chemical Station for CICAR. His recommendations concerning the parameters to be measured and the methodology to be followed were included along with a description of the other standard stations and of the standard sections in a publication compiled and edited by the Operations Coordinator, Guide to CICAR Standard Observations.

During CICAR a total of eleven months were designated CICAR Survey Months. The actual dates were determined first on an ad hoc basis, but from 1974 onwards the months of February, June and October became Survey Months.

Reviewing the operational activities, we see that the majority took place in 1970-72. This is understandable if we consider the original idea of a three-year field phase. At the fifth session of the ICG (1972) it was generally agreed to extend the field programme until the end of 1973; however, some Member States were not prepared for an extension. Most ship schedules are planned some two years ahead and an extension of CICAR had not been planned. It is quite questionable whether the arguments that would justify an extension of CICAR in its then existing form were sufficiently investigated. However, in my opinion it is important that the CICAR Member States realized that if CICAR was not extended something valuable might be lost and that no measures had been taken to ensure a follow-up, replacement or ways to retain the acquired cooperation. Numerous discussions have been held on this subject since and several recommendations of the ICG state that cooperative marine science activities should be continued and that CICAR should be succeeded by an organizational structure that can coordinate such activities. I will return to this point later.

3.1 Training (TEMA)

We cannot relate the history of CICAR without touching on the aspects of training, education and mutual assistance (TEMA). The need for increasing the number of qualified marine scientists in most countries of the CICAR area was recognized as a prerequisite for their participation in the cooperative investigations at an adequate level. The contribution of CICAR to TEMA has probably not been as effective as required. However, in general, CICAR has facilitated the accommodation of marine scientists on foreign research cruises and generated numerous bilateral TEMA provisions. Two training cruises deserve special attention: the NOAA Carib cruise, by the NOAA ship DISCOVERER in the fall of 1972, and the cruise of the AKADEMIK KURCHATOV, in early 1973. Both cruises offered research opportunities under the guidance of experienced marine scientists to nationals of some five or six Caribbean and Latin American countries. During NOAA Carib, mechanical BTs were left with each of the participating groups. Similarly the U.S. National Marine Fisheries Service provided training in the use of bongo and neuston nets and provided the trainees with this equipment. In this case the effect was twofold; not only was training provided, but also the provision of standard sampling equipment aided the comparability of results. The workshop on ichthyoplankton at the Mexican Oceanic Sorting Centre fulfilled an important training need for identification of fish larvae. Finally the CICAR oceanographic methods Intercalibration

Experiment (CINTEX) provided a two-week practical training course in chemical oceanographic methods at the University of Puerto Rico, Mayaguez and on board the R/V CRAWFORD. CINTEX is unique in the history of CICAR because it was the only experiment of its kind, and because the participation was disappointing in spite of a thorough preparation and the complete absence of financial problems.

Although it is not directly relevant to TEMA I would like to mention at this time the shrimp consultations which were convened by FAO. These consultations, in which the major shrimp fishing countries participated, formed an important aid in the collection of statistical data and in shrimp stock evaluation.

4. EVALUATION PHASE

Even though there was a decrease in the operational activities of CICAR after 1972 this certainly did not affect the implementation of the overall objectives of CICAR. In 1973, at Cartagena, the sixth session of ICG for CICAR recommended that CICAR be continued until at least the end of 1975 and that the CICAR officers and the servicing arrangements such as the regional data centre, the operations centre and the sorting centre, continue their duties until or beyond that date. The sorting centre which became operational in mid-1972, initially experienced some practical problems. Some countries seem to have been reluctant to provide material to the centre. Consequently the sorting centre did not receive many requests from scientists for collections. It was understood that the centre needed to establish useful reference collections in order to generate interest on the part of scientists, but that it also needed to establish a good reputation in order to convince scientists to send the samples necessary for such collections.

The NODC, as the regional data centre for CICAR, not only reported all data submitted as part of CICAR and the format in which they were available, but also compiled and edited a CICAR bibliography and provided for CICAR news in the NODC newsletter. The work of NODC, in combination with that of the operations centre, was of great importance for checking the submittal of CICAR Data Inventories (CICARDI) and subsequent submittal of the actual data. Apart from its tasks in the communication with research vessels, the most useful function of the operations centre probably has been to act as a clearing-house for information. This function could be fulfilled adequately because the Operations Coordinator was able to travel throughout the area and to establish and maintain contacts with all CICAR officers and scientists involved in CICAR investigations. The Operations Coordinator kept track of all the ships' activities. It is interesting to compare his records with the assessment of ship-time available for CICAR made by the ICG at the Curaçao session in 1968. At that time it was estimated that a total of 310-330 ship-months would be committed to CICAR to be effected by about 23 ships. Although the number of participating vessels actually amounted to about 40, the total ship-time committed to CICAR for the period 1970-75 was considerably less than the estimate - about 150 ship-months.

The wish to secure ways and means for continued cooperation in the CICAR area was present early in the history of CICAR. In 1971 recommendation 4.1 on the objectives of CICAR states that one of the goals of CICAR shall be "to establish the basis for further international coordination in the CICAR area" and recommendation 4.6 draws attention to the desirability of continuation of the collaboration developed through CICAR after its termination. In recommendation 5.11 made in 1972, the ICG was much more specific about future actions and recommends that a small group of experts be established to develop proposals for future cooperative marine activities. This recommendation resulted in the formation of an *ad hoc* working group for the continuation of cooperative work in the CICAR area. The working group carried out a preliminary analysis of CICAR and proposed a set of objectives for future cooperative activities. Among the recommendations of this working group was the proposal that an analysis of the CICAR operations be carried out by outside experts. Such an analysis was carried by a consultant to the IOC, Dr. Albert Koers, who submitted his evaluation: "CICAR: past, present and future" in the autumn of 1974. The evaluation and analysis of CICAR have contributed significantly to discussions on future means for marine science cooperation in the Caribbean area. In 1975 recommendation 7.10 redefines the objectives of future cooperative studies. In recommendation 7.11 the ICG - for the first time - set forth its proposal for the structure of a future coordinating body.

We should realize that extensions of CICAR have been of great value in that they provided the opportunity to carry out analyses for the IOC Secretariat to put forward proposals on future arrangements, and to promote a dialogue between CICAR Member States and the IOC on a future structure, without losing the existing mechanism for coordination and all the benefits of the acquired cooperation.

5. CONCLUSION

I have now come to the point where the past touches the present and history ends. At this time I should also say that I do not believe in objective history. The facts of history may be true but the narrator makes history subjective. I know that I have given you not only a pure historical account but have also included a personal opinion. But now it is time to summarize, conclude and stress once more the merits of CICAR.

Curaçao, 1968 - Caracas, 1976: It has been almost eight years since the first Symposium was held to identify major research problems of the area and prepare recommendations on the scientific programmes for CICAR. Dr. Albert Koers, in his excellent evaluation study, has noted that it would be extremely difficult to evaluate CICAR's scientific achievements because the comprehensive programme included so many small sub-programmes and individual projects. However, we can say without hesitation that CICAR has made very significant contributions to the development of marine science capabilities and the establishment of a national marine science structure in several countries of the CICAR area. These two developments made it possible for some nations to actively participate in CICAR and were an important tool in identifying research priorities, establishing national programmes and defining the needs for training and education.

I would like to categorize four phases of CICAR: a preparatory phase, including the First Symposium and the first two sessions of the ICG for CICAR; an operational phase during which most field activities took place; an evaluation phase including the work of the ad hoc working group on the continuation of cooperative work in the CICAR area in 1973, the evaluation study "CICAR: past, present and future", and of course the present CICAR Symposium. There is no clear separation between the second and the third phase nor between the third and fourth, which I will call the consolidating phase. We find ourselves at the basis of this phase, which started with the meeting of oceanographic experts on the future cooperation and future programmes in Puerto Rico, 1976 and the decision to establish the IOC Association for the Caribbean and Adjacent Regions (IOCARIB). It must be considered the great merit of CICAR that we are now consolidating regional marine science cooperation in this new structure.

6. REFERENCES

Hof, T. van't (Operations Coordinator of CICAR) (Comp.), Guide to CICAR standard observations
1974 with special reference to CICAR survey months and standard sections. pag.var. (mimeo)

IOC, Summary report. Fifth session of the Intergovernmental Oceanographic Commission.
1968 Paris, 19-27 October 1967. Paris, Unesco/IOC, SC/CS/150 + Corr.:pag.var.

__________, Draft summary report. Second meeting of the International Coordination Group
1969 for CICAR. Washington, D.C., 2-5 June 1969. Paris, Unesco/IOC, SC/IOC-VI/INF 147:pag.var.

__________, Revised draft summary report. Fourth session of the International Coordination
1971 Group for CICAR. Port of Spain, Trinidad and Tobago, 29 March 1971. Paris, Unesco/IOC, SC/IOC/CG-8(IV)/12:pag.var.

IOC, Summary report. First meeting of the International Coordination Group for CICAR.
1969 Curaçao, Netherlands Antilles, 25-26 November 1968. Paris, Unesco/IOC, SC/
IOC-VI/INF-143; SCE/9/895:pag.var.

————————, Summary report. Third meeting of the International Coordination Group for
1970 CICAR. Mexico, D.F., 23-26 February 1970. Paris, Unesco/IOC, SC/IOC/CG-8(III)/
5(Rev.):pag.var.

————————, Summary report. Fifth session of the International Coordination Group for
1972 CICAR. La Habana, Cuba, 20-24 June 1972. Paris, Unesco/IOC, SC.72/CONF.72/
10a10c/CICAR.V/2:pag.var.

————————, Summary report. Sixth session of the International Coordination Group for
1973 CICAR. Cartegena, Colombia, 16-20 July 1973. Paris, Unesco/IOC, VI/30a.SC.73/
CONF.212/1:pag.var.

————————, CICAR: past, present and future. An evaluation study of a regional IOC
1974 programme. Prepared by A.W. Koers, Consultant to IOC. Paris, Unesco/IOC,
IOC/INF.2380aSC.75/CONF.202/COL. 5:52 p.

————————, Summary report of the ninth session of the Assembly. Paris, 22 October -
1975 4 November 1975. Paris, Unesco

————————, Summary report. Seventh session of the International Coordination Group for
1975 CICAR. Mexico, D.F., 14-17 April 1975. Paris, Unesco/IOC, IOC/CICAR.VII/
30aSC.75/CONF.212/COL. 1:pag.var.

PREDICCION DE LA TEMPERATURA MEDIA MENSUAL EN LA SUPERFICIE DE LOS OCEANOS UTILIZANDO UN MODELO TERMODINAMICO

por

J. ADEM
Instituto de Geofísica
Universidad Nacional Autónoma de México
México 20, D.F.

Resumen

Un modelo termodinámico del sistema atmósfera-océano-continente se aplica para predecir las temperaturas medias mensuales en el hemisferio norte.

La evaluación de la predicción del signo de los cambios, de un mes al siguiente, en las anomalías de la temperatura en la superficie oceánica, para los océanos Pacífico y Atlántico, muestra una habilidad substancialmente superior que la predicción de un retorno a los valores normales.

Se presenta un análisis sobre la posibilidad de mejorar las predicciones para el área de CICAR.

Abstract

A thermodynamic model of the atmosphere-ocean-continent system is applied to predict mean monthly temperatures in the Northern Hemisphere.

A statistical evaluation of the predictions of the sign of the month-to-month changes in the anomalies of ocean surface temperature for the Pacific and the Atlantic Oceans shows substantially higher rates of success than consistent predictions of a return toward normal.

An analysis of the possibility of improving the predictions for the CICAR area is presented.

El modelo usado en las predicciones numéricas de temperatura de océanos que se presentan aquí está descrito en detalle en varios artículos (Adem, 1962, 1963, 1964, 1964a, 1965, 1965a, 1970, 1970a, 1975). Por lo tanto, solamente se da una descripción breve sobre dicho modelo.

La conservación de energía térmica se aplica a la capa superior de los océanos (hasta una profundidad de 100 a 50 m), la capa superior de los continentes (de profundidad despreciable) y la capa atmosférica (de unos 10 kilómetros de altura). Las ecuaciones son las siguientes:

para la atmósfera: $$c_v a_o \frac{\partial T'_m}{\partial t} + AD_1 - c_v a_o K \nabla^2 T'_m = E_T + G_5 + G_2 \quad (1)$$

para los océanos: $$h\left(\frac{\partial T'_s}{\partial t} + v_s \cdot \nabla T'_s - K_s \nabla^2 T'_s\right) + W = \frac{1}{\rho_s c_s}(E_s - G_2 - G_3) \quad (2)$$

para los continentes: $$0 = E_s - G_2 - G_3 \quad (2')$$

donde ∇ es el operador gradiente bi-dimensional horizontal; t es el tiempo, $T'_m = T_m - T_{m_o}$ donde T_m es la temperatura media troposférica, T_{m_o} es una temperatura constante y $T'_m \ll T_{m_o}$; a_o es una constante, c_v es el calor específico del aire a volumen constante, AD_1 es la advección por el viento medio, K es el coeficiente de intercambio horizontal para la atmósfera, E_T el exceso de radiación en la atmósfera, G_5 es el calor ganado por condensación de vapor de agua en las nubes, G_2 el calor sensible dado de la superficie a la atmósfera por transporte vertical turbulento; $T'_s = T_s - T_{s_o}$ donde T_s es la temperatura en la superficie, T_{s_o} es una constante y $T'_s \ll T_{s_o}$; $\vec{v}_s$ es la corriente oceánica horizontal, K_s es el coeficiente de intercambio horizontal para el océano, E_s es el exceso de radiación en la superficie, G_3 es el calor perdido por evaporación en la superficie, W es el calor ganado por las surgencias, h es la profundidad de la capa oceánica ρ_s la densidad de las aguas y c_s el calor específico.

Para los continentes, los términos de almacenamiento y transporte son relativamente pequeños y, por lo tanto, se han tomado como cero.

Desde 1962 se han llevado a cabo experimentos numéricos con estas ecuaciones. En la mayoría de los experimentos se ha usado un modelo en que los transportes horizontales de calor por corrientes oceánicas por la mezcla horizontal turbulenta de las aguas se desprecian; en este caso, usando diferencias finitas hacia atrás para las derivadas en el tiempo y parametrizaciones adecuadas para las funciones de calentamiento, la solución se reduce a resolver una ecuación diferencial elíptica del siguiente tipo:

$$K\nabla^2 T'_m + F_1 \frac{\partial T'_m}{\partial x} + F_2 \frac{\partial T'_m}{\partial y} + F_3 T'_m = F_4 \quad (3)$$

donde F_1, F_2 F_3 y F_4 son funciones conocidas que dependen de la posición geográfica.

Para introducir el transporte por las corrientes oceánicas medias y por mezcla turbulenta, así como por surgencias, un método diferente de integración se usa que consiste en integrar la ecuación para la capa del océano con diferencias finitas hacia adelante y la ecuación para la atmósfera con diferencias hacia atrás.

Las parametrizaciones usadas para las funciones de transporte y calentamiento se han descrito en varios artículos por el autor (Adem, 1962, 1964, 1965a, 1970, 1970a) y no se van a discutir aquí.

El modelo se ha aplicado para hacer predicciones mensuales de las anomalías medias de temperatura y precipitación en el hemisferio norte.

Utilizando como datos iniciales las anomalías mensuales de las temperaturas en la superficie de los océanos, y en el nivel de los 700 milibarios, así como anomalías en la cubierta de nieve y hielo, se predicen, para el mes siguiente, las anomalías de la temperatura superficial del océano y continentes, de la temperatura de la atmósfera a los 700 milibarios, de la precipitación, de las funciones de calentamiento y circulaciones asociadas con ellas (Adem 1964, 1965a, 1970, 1970a).

También se ha integrado el modelo para períodos largos de tiempo, en estudios de paleoclimatología y de fluctuaciones y cambios climáticos por Shaw y Donn (1968, 1971) y Donn y Shaw (1975).

La variable más importante en el modelo es la temperatura media mensual en la superficie de los continentes y océanos. Las predicciones tienen una fuerte dependencia de la temperatura de los océanos en el mes anterior, lo cual se debe a la gran capacidad calorífica de los océanos, que almacenan energía que es liberada lentamente e influye por lo tanto en el estado del tiempo y el clima, sirviendo como memoria del sistema océano-continente-atmósfera y permitiendo, a través de las interacciones y mecanismos de retroalimentación que existen en la superficie, hacer predicciones termodinámicas para períodos de un mes or una estación, y quizá para más largos períodos.

Las aplicaciones del modelo a la predicción del tiempo y a la predicción climática se han presentado en varios artículos ya mencionados anteriormente. En este trabajo nos concentraremos únicamente en la predicción mensual de la temperatura de los océanos.

El modelo actualmente en operación incluye la región mostrada en la Fig. 1 con 512 puntos, equidistantes en el plano de la proyección estereográfica utilizada. La distancia entre los puntos es de 817 km; por lo tanto, se aplica a anomalías alisadas de gran escala, capaces de representarse con esta rejilla.

Se han llevado a cabo experimentos numéricos y predicciones para evaluar la importancia de los diferentes términos que aparecen en la ecuación (2).

Así, la Fig. 2 muestra una predicción en la que se ha despreciado el transporte horizontal de calor por corrientes oceánicas medias y por intercambio turbulento. También se ha despreciado el transporte vertical de calor en el fondo de la capa superficial oceánica. La predicción (parte A) corresponde al cambio de las anomalías de temperatura de marzo a abril de 1966; la comparación con el cambio observado (parte B) muestra que en una gran porción del hemisferio norte, el signo y el orden de magnitud del cambio están correctamente predichos.

El modelo utilizado en esta predicción incluye un acoplamiento termodinámico en la superficie de los océanos y continentes, y aunque en los océanos no incluye transporte horizontal de calor, sí lo incluye en la atmósfera. Los cambios de la temperatura del océano en este modelo se deben principalmente a la evaporación y al transporte vertical turbulento de calor sensible de la superficie del océano a la atmósfera.

Este modelo ha sido aplicado por el autor a 73 casos (Adem, 1975) cuya comparación con los correspondientes valores observados corrobora la habilidad de predicción del modelo.

Para determinar el valor del método de predicción se utiliza una verificación objetiva, que consiste en evaluar la habilidad del modelo en predecir correctamente el signo de los cambios de las anomalías de un mes al siguiente, calculando el porcentaje de signos correctamente predicho. Como predicción de control se usa el retorno a los valores normales que consiste en tomar el signo del cambio de las anomalías igual al signo opuesto al que tienen las anomalías del mes anterior.

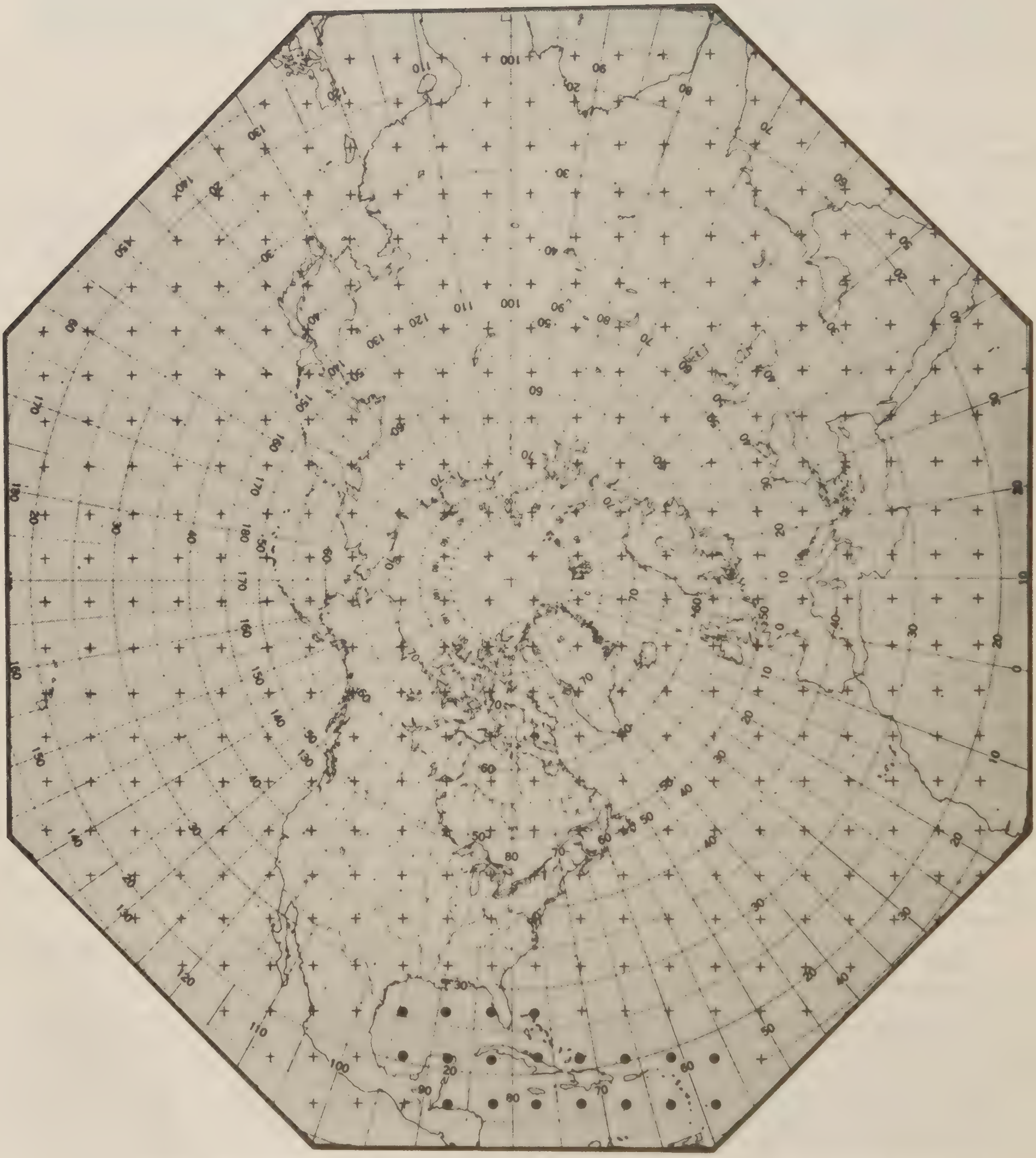

Fig. 1 Región de integración del modelo termodinámico y puntos de la rejilla utilizada

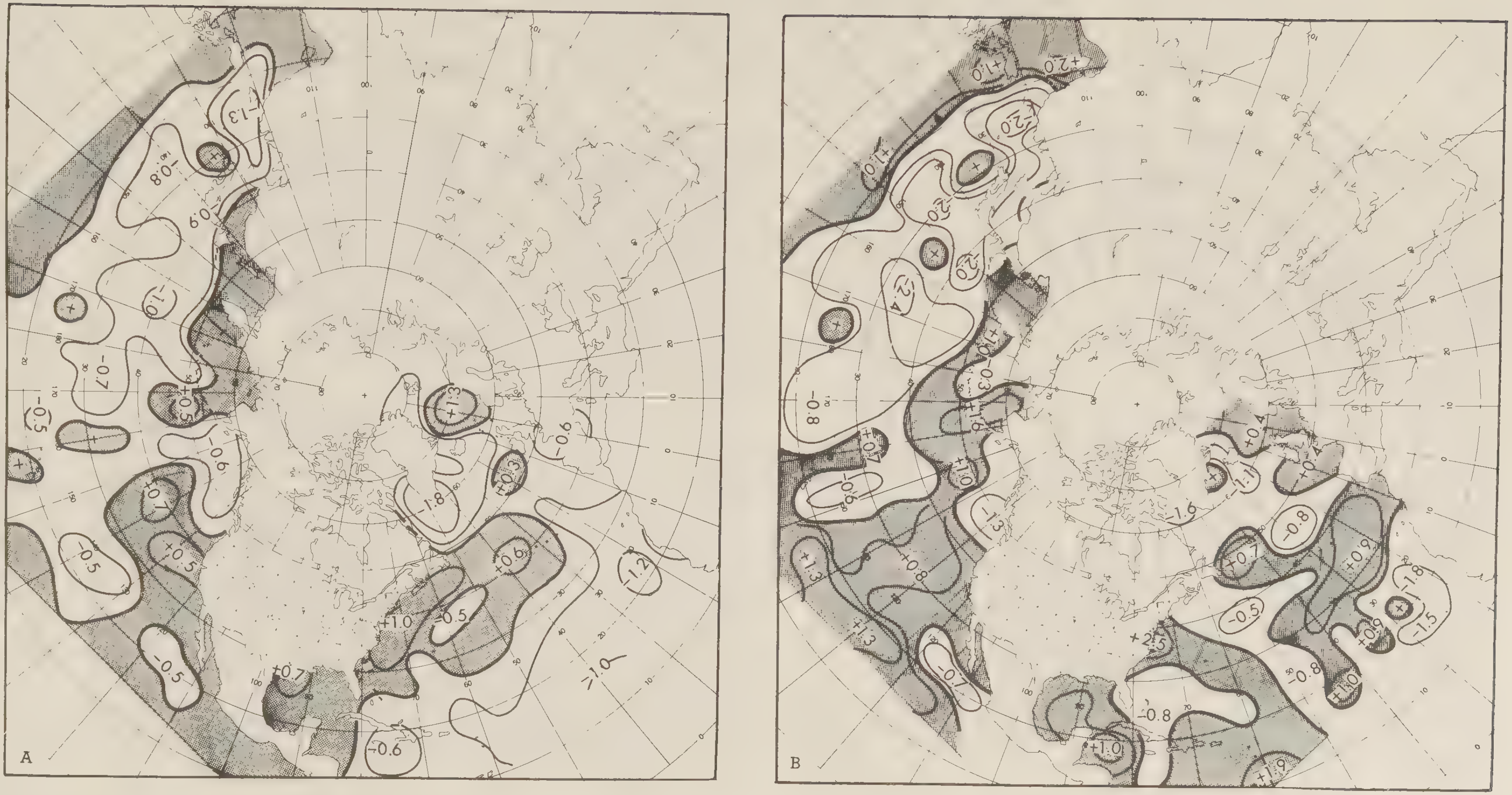
A
-1.3
-0.8
-0.9
-1.0
-0.7
-0.5
+0.5
-0.6
+0.7
+0.5
-0.5
-0.5
+0.7
-0.6
+1.0
-0.5
+0.6
-1.2
-1.0
-1.8
+0.3
-0.6
+1.3
B
+2.0
+1.0
-2.0
-2.0
+1.0
-2.0
-2.4
-0.8
+0.7
-0.6
+1.3
+1.3
-0.7
-0.8
+1.0
-0.3
+1.6
+1.0
-1.3
-1.6
-1.1
+0.4
+0.4
-0.8
+0.7
-0.5
+0.9
-1.8
-1.5
+0.9
-0.8
+1.0
+2.5
-0.8
+1.0
+1.9

Fig. 2 Cambio de las anomalías de la temperatura de la superficie de los océanos de marzo a abril de 1966, en décimas de grados centígrados
(A) predicho por el modelo;
(B) observado

Las predicciones de control tienen por sí mismas cierta habilidad, la cual debe ser superada por las correspondientes predicciones hechas con el modelo, de tal modo que el exceso sobre el control del porcentaje de signos correctamente predicho por el modelo indica la habilidad de predicción del modelo.

La evaluación de las 73 predicciones mencionadas anteriormente ya ha sido discutida ampliamente en un artículo previo (Adem, 1975). El resumen de dicha evaluación se presenta en el Cuadro I que muestra los porcentajes de signos de los cambios de las anomalías de temperatura correctamente predichos para las cuatro estaciones para todo el período considerado de 73 meses, utilizando el modelo así como el método de retorno a normal (R a N), para el área del Océano Pacífico, así como para el área que incluye tanto el Océano Pacífico como el Atlántico. De este cuadro es evidente que las predicciones del modelo son superiores que las del control para todas las estaciones del año, y que los mejores resultados se obtienen en invierno en el Océano Pacífico, para el que el modelo predice correctamente 64,1 por ciento de los signos de los cambios en las anomalías de un mes al siguiente, con un exceso de 6 por ciento sobre el control.

El porcentaje mayor se obtiene en verano y es de 65,1 sobre el área que incluye el Atlántico y el Pacífico, pero en este caso, el exceso sobre el control es únicamente de 3 por ciento. Sobre todo el período y en ambos océanos, el porcentaje total correctamente predicho es de 63,2 por ciento con un exceso sobre el control de 3,7, mientras que sobre el Pacífico es de 63,4 con un exceso sobre el control de 4,7.

En las 73 predicciones mencionadas, en las ecuaciones (1) y (2) se utilizaron diferencias hacia atrás como una aproximación de las derivadas respecto al tiempo, reduciéndose la integración de las ecuaciones a resolver la ecuación (3). Además de estas predicciones, se han llevado a cabo otras utilizando diferencias de tiempo hacia adelante en la ecuación (2), con intervalos de tiempo de un mes o menores. Algunas de dichas predicciones ya se han analizado en otros artículos (Adem, 1970, 1975).

De los experimentos numéricos llevados a cabo por Namias (1959) y por el autor (Adem, 1970) es evidente que las anomalías en las corrientes horizontales debidas a las anomalías en el viento geostrófico producen importantes cambios en las anomalías de las temperaturas de la superficie de los océanos. Sin embargo, en el número limitado de casos evaluados por el autor no se ha evidenciado una mejoría en las predicciones cuando se incluye este término en las ecuaciones. Esto puede deberse, sin embargo, al hecho de que la parametrización usada es muy cruda o a que en las predicciones se ha usado un paso de tiempo de un mes, lo cual, según estudios del autor, introduce errores de truncación grandes cuando se incluye este término (Adem, 1971). Deben, por lo tanto, llevarse a cabo experimentos numéricos con pasos de tiempo menores, además de tratar de mejorar la parametrización de este término de transporte horizontal de energía.

El efecto de las surgencias es importante únicamente en ciertas localidades, como ocurre enfrente de California, donde según Roden (1972) existen velocidades del orden de $4 \times (10^{-3}$cm seg$^{-1})$, las cuales, de acuerdo con los cálculos llevados a cabo por el autor (Adem, 1970) pueden ser de significación para producir anomalías de temperatura en la superficie de los océanos de magnitud no despreciable. Sin embargo, es evidente de la escala de la distribución horizontal de las corrientes verticales que la distancia entre los puntos de la rejilla en este caso debe ser menor que la usada en el modelo actual.

El término que, desde que se iniciaron los experimentos ha mostrado gran habilidad de predicción, es el de difusión o mezcla turbulenta, en el que se ha usado un coeficiente de intercambio del orden 10^8cm^{2}seg^{-1}.

Cuando se incluye únicamente dicho término, la ecuación (2) se reduce a

$$\frac{T_s}{t} = K_s \nabla^2 T_s \qquad (4)$$

La solución de esta ecuación depende de la temperatura superficial oceánica inicial y del coeficiente de intercambio (K_s). El carácter de dicha solución, que se ha discutido por el autor previamente (Adem, 1971) muestra una tendencia de las anomalías a disminuir, pero la razón de cambio a la que las anomalías disminuyen depende de su tamaño, de modo que las menores desaparecen antes que las mayores.

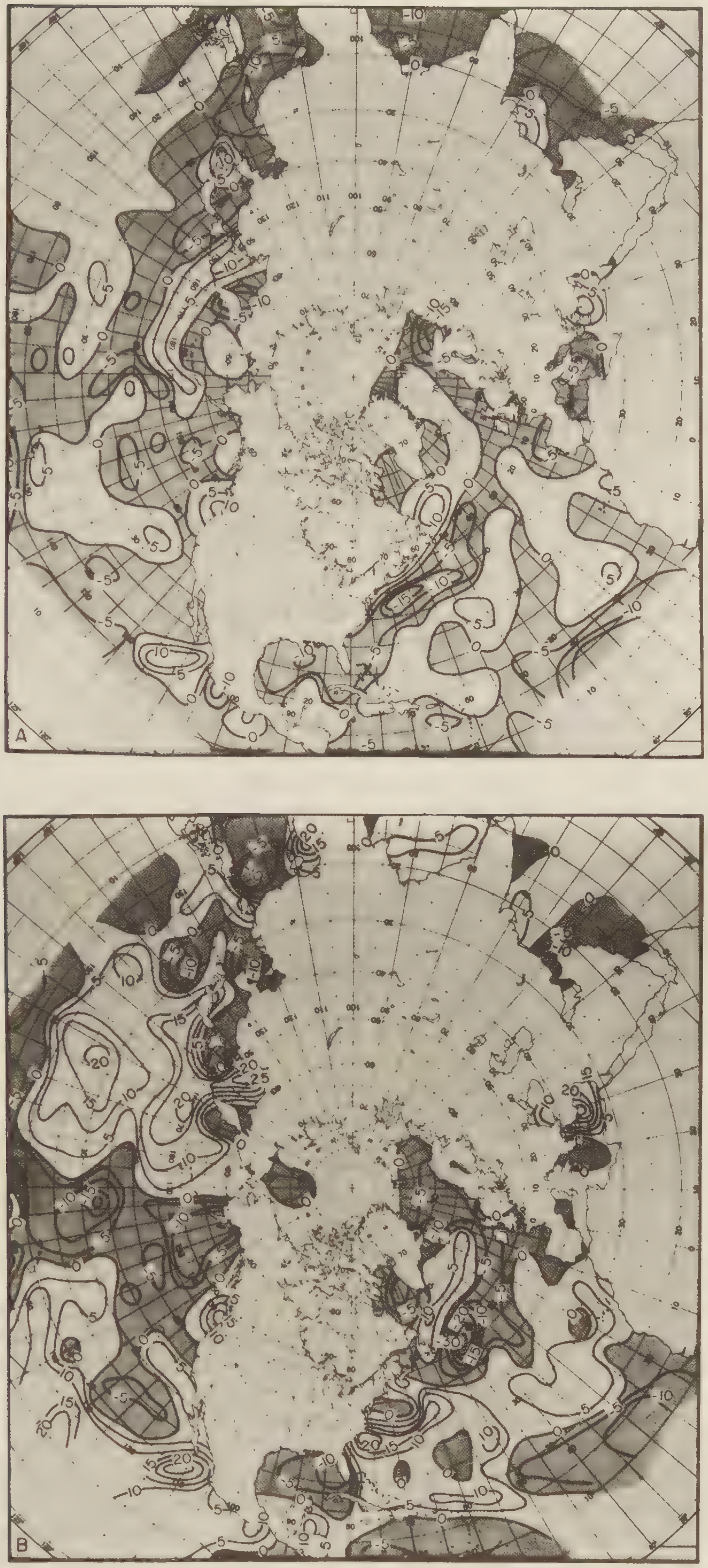

Fig. 3 Cambio de las anomalías de la temperatura de la superficie de los océanos de noviembre a diciembre de 1972, en décimas de grados centígrados
(A) predicho por el modelo;
(B) observado

Un ejemplo de una predicción utilizando la ecuación (4) con diferencias adelantadas en el tiempo se muestra en la Fig. 3. En 3(A) aparece la predicción del cambio de las anomalías de noviembre a diciembre 1972 y en 3B los correspondientes cambios observados.

Las predicciones de 24 casos (de enero 1970 a diciembre 1970 y de junio 1972 a mayo 1973) utilizando la ecuación (4), publicadas recientemente (Adem, 1975) son aún superiores a las correspondientes al modelo que incluye únicamente evaporación, transporte vertical turbulento de calor sensible y radiación (HE). Los resultados se muestran en el Cuadro II. En la primera línea están los valores del control (retorno a normal): en el Pacífico 58,7 por ciento, en el Atlántico 57,9 por ciento y en ambos océanos 58,3 por ciento del signo del cambio de las anomalías de un mes al siguiente correctamente predicho para el período de dos años considerado. En la segunda línea, se muestran los excesos sobre el control, usando el modelo HE: en el Pacífico 4, en el Atlántico 5,7 y en ambos océanos 4,8. En la tercera línea los excesos sobre el control cuando se usa el modelo en que existe solamente difusión turbulente con pasos de tiempo adelantados de 5 días (TU(5)): en el Pacífico 6,9, en el Atlántico 9,1 y en ambos océanos 8,1. Finalmente, en la última línea se muestran los excesos sobre el control cuando se usa también el modelo con difusión turbulenta, pero con un solo paso de tiempo de 30 días (TU(30)). Este cuadro demuestra que los mejores resultados se obtienen con el modelo que incluye sólo difusión turbulenta y en el que se usan pasos de tiempo de 5 días.

Es interesante determinar la habilidad del modelo actual para predecir el cambio de anomalías de temperatura en el Golfo de México y en el Mar Caribe. Con tal finalidad, hemos evaluado las predicciones de los 12 casos de junio 1972 a mayo 1973, aplicando el modelo de difusión turbulenta con pasos de tiempo de 5 días. Los círculos negros en la Fig. 1 son los puntos donde se hizo la verificación para la región del Golfo de México y el Mar Caribe. El Cuadro III muestra los valores de la predicción del modelo y del método de retorno a los valores normales, así como la diferencia entre estos dos métodos. Se incluye la evaluación para el área total del Pacífico y Atlántico, así como para el área que comprende el Golfo de México y el Mar Caribe.

El Cuadro IV muestra los correspondientes valores para las cuatro estaciones y para el promedio anual, tanto para el área total (Pacífico y Atlántico) como para el área que incluye el Golfo de México y el Mar Caribe. El promedio anual de signos del cambio de las anomalías correctamente predicho por el modelo es de 65,3 por ciento para el caso del Pacífico y el Atlántico, con un exceso sobre retorno a normal de 7,6 por ciento; en cambio, el porcentaje en la región del Golfo de México y Mar Caribe es de 69,7 con un exceso sobre retorno a normal de 11,3 por ciento.

En ambos casos, el exceso sobre el control del porcentaje de signos correctamente predicho por el modelo es máximo en invierno y mínimo en verano; sin embargo, el porcentaje de puntos correctamente predicho por el modelo es en ambos casos mínimo en invierno y máximo en verano. En los dos casos, el modelo muestra cierta habilidad de predicción, y las predicciones para todas las estaciones son mejores en el área del Golfo de México y el Mar Caribe, que en el área total (Pacífico y Atlántico).

Estos resultados son muy alentadores y sirven de punto de partida para los experimentos numéricos que se están llevando a cabo en el Instituto de Geofísica de la Universidad Nacional Autónoma de México para mejorar la predicción mensual y estacional de las temperaturas de océanos, tanto a escala hemisférica como a menor escala, para aplicarse en el Golfo de México, el Mar Caribe y en otras áreas oceánicas de especial interés.

La mejoría de las predicciones depende de la disponibilidad de mejores datos, tanto oceanográficos como meteorológicos. A este respecto, para el caso del Golfo de México y del Mar Caribe, se cuenta con un acervo de datos, enriquecido recientemente con los de CICAR. Sin embargo, para llevar a cabo predicciones operacionalmente, es indispensable contar con datos en tiempo real, igual que en el caso de las predicciones meteorológicas.

Además, se requiere la realización de numerosos experimentos, incluyendo funciones de transporte y de calentamiento cada vez más realistas; y para obtener mayor resolución y poder incluir con mayor precisión corrientes y surgencias, es indispensable reducir la distancia entre los puntos de la rejilla. Finalmente, para evitar los efectos de la frontera del modelo actual en la región del CICAR, es indispensable mover hacia el sur dicha frontera.

CUADRO I

Porcentaje correctamente predicho del signo de los cambios de las anomalías de la temperatura superficial de los océanos de un mes al siguiente para los 73 meses de diciembre 1965 a diciembre 1970 y de junio 1972 a mayo 1973

	Pacífico			Pacífico y Atlántico		
Estación	Modelo	R a N	Exceso	Modelo	R a N	Exceso
Invierno	64,1	58,1	6,0	62,4	58,3	4,1
Primavera	63,3	58,0	5,3	63,3	59,5	3,8
Verano	63,4	59,7	3,7	65,1	62,1	3,0
Otoño	62,8	58,9	3,8	61,9	58,0	3,9
Promedio para todo el período	63,4	58,7	4,7	63,2	59,5	3,7

CUADRO II

Promedios para el período completo de 24 meses (de enero 1970 a diciembre 1970 y de junio 1972 a mayo 1973) del porcentaje correctamente predicho de los signos de los cambios de un mes al siguiente de las anomalías de la temperatura superficial de los océanos, utilizando diversos modelos simplificados

Caso	Pacífico	Atlántico	Ambas océanos
R a N (porcentaje)	58,7	57,9	58,3
HE (exceso)	4,0	5,6	4,8
TU(5) (exceso)	6,9	9,1	8,1
TU(30) (exceso)	5,9	7,8	6,8

CUADRO III

Porcentaje correctamente predicho del signo de los cambios de un mes al siguiente de las anomalías de la temperatura superficial de los océanos, utilizando un modelo que incluye únicamente mezcla horizontal turbulenta, para los 12 meses de junio 1972 a mayo 1973

	Pacífico y Atlántico			Golfo de México y Mar Caribe		
Mes	Modelo	Regreso al normal	Exceso	Modelo	Regreso al normal	Exceso
1972						
Junio	65,4	62,9	2,5	78,9	84,2	-5,3
Julio	63,9	60,9	3,0	73,7	52,6	21,1
Agosto	69,8	65,4	4,5	73,7	73,7	0
Septiembre	69,8	57,9	11,9	84,2	63,2	21,0
Octubre	62,4	57,4	5,0	47,4	47,4	0
Noviembre	60,9	50,0	10,9	47,4	26,3	21,0
Diciembre	68,8	54,4	14,4	78,9	47,4	31,5
1973						
Enero	60,9	38,6	22,3	68,4	47,4	21,0
Febrero	63,3	66,3	-3,0	63,2	63,2	0
Marzo	69,3	67,8	1,5	84,2	73,7	10,5
Abril	61,9	52,0	9,9	68,4	47,4	21,0
Mayo	66,8	58,9	7,9	68,4	73,7	-5,3

CUADRO IV

Valores estacionales del porcentaje correctamente predicho del signo de los cambios de un mes al siguiente de las anomalías de la temperatura superficial de los océanos, utilizando un modelo que incluye únicamente mezcla horizontal turbulenta, para los 12 meses de junio 1972 a mayo 1973

	Pacífico y Atlántico			Golfo de México y Mar Caribe		
Estación	Modelo	Regreso al normal	Exceso	Modelo	Regreso al normal	Exceso
Invierno	64,3	53,1	11,2	70,2	52,7	17,5
Primavera	66,0	59,6	6,4	73,6	64,9	8,7
Verano	66,4	63,1	3,3	75,4	70,2	5,2
Otoño	64,4	55,1	9,3	59,6	45,6	14,0
Promedio para todo el período	65,3	57,7	7,6	69,7	58,4	11,3

REFERENCIAS

Adem, J., 1962 On the theory of the general circulation of the atmosphere. Tellus, 14:102-15

__________, 1963 Preliminary computation of the maintenance and prediction of seasonal temperatures in the troposphere. Mon.Weather Rev., 91:375-86

__________, 1964 On the physical basis for the numerical prediction of monthly and seasonal temperatures in the troposphere-ocean-continent system. Mon.Weather Rev., 92:91-104

__________, 1964a On the normal thermal state of the troposphere-ocean-continent system in the Northern Hemisphere. Geofís.Int., Mex., 4:3-32

__________, 1965 Preliminary model for computing mid-tropospheric and surface temperatures from satellite data. J.Geophys.Res., 70:376-86

__________, 1965a Experiments aiming at monthly and seasonal numerical weather prediction. Mon.Weather Rev., 93:495-503

__________, 1970 On the prediction of mean monthly ocean temperature. Tellus, 22:410-30

__________, 1970a Incorporation of advection of heat by mean winds and by ocean currents in a thermodynamic model for long-range weather prediction. Mon.Weather Rev., 98:776-86

__________, 1971 Further studies on the thermodynamic prediction of ocean temperatures. Geofís.Int., Mex., 11:7-45

__________, 1975 Numerical-thermodynamical prediction of mean monthly ocean temperatures. Tellus, 27:542-51

Donn, W.L. 1975 y D.M. Shaw, The evolution of climate. In Proceedings of the WMO/IAMAP Symposium on long-term climatic fluctuations, Norwich, August 1975. Paper no. (WMO-421XII)

Namias, J., 1959 Recent seasonal interactions between north Pacific waters and the overlying atmospheric circulations. J.Geophys.Res., 64:631-46

Roden, G.I., 1972 Large-scale upwelling off northwestern Mexico. J.Phys.Oceanog., 2:184-9

Shaw, D.M. 1968 y W.L. Donn, Milankovitch radiation variations: a quantitative evaluation. Science, Wash., 162:1270-2

__________, 1971 A thermodynamic study of arctic paleoclimatology. Quaternary Res., 1:175-87

CIRCULACION Y TRANSPORTE DE MASA DE AGUA EN EL CARIBE SURORIENTAL

por

G. FEBRES ORTEGA[1/] y L.E. HERRERA
Instituto Oceanográfico, Universidad de Oriente, Cumaná, Venezuela

CONTENIDO

1. INTRODUCCION
2. CALCULOS GEOSTROFICOS
3. CIRCULACION
4. TRANSPORTE
5. REFERENCIAS

Resumen

La circulación geostrófica de las aguas cercanas a las Antillas Menores, sector sureste del Mar Caribe, ha sido calculada a base de una red relativamente densa de estaciones oceanográficas ocupadas por el Instituto Oceanográfico, Cumaná, Venezuela, a bordo de la M/N LA SALLE, durante el mes de agosto de 1972. El flujo geostrófico, relativo a 1 000 db, es descrito mediante secciones verticales meridionalmente orientadas (60°00', 62°00', 63°00', 63°45' y 64°30' long. W). También se presenta la distribución de la altura dinámica de la superficie del mar. El transporte de masa de agua fue calculado para segmentos significativos de las secciones meridionales, así como en líneas aproximadamente zonales, a fin de establecer un balance del agua transportada hacia o fuera de la región. En el Océano Atlántico (60°00' long. W), la circulación de agua se caracteriza por una alternación en la dirección de las corrientes, asociada a la presencia de meandros. El flujo principal hacia el Mar Caribe se observa entre las Islas San Vicente y Dominica (21,5 Sverdrups) por donde entran dos corrientes: una que avanza desde el SE, entre Barbados y Tabago, y otra que penetra desde el NW, al sur de Dominica. El flujo neto al sur de San Vicente es muy pequeño. Un giro ciclónico al este de Tabago devuelve un elevado volumen de las aguas transportadas por la Corriente de Guayana. En el interior del Mar Caribe, la circulación hacia el oeste muestra dos ejes principales, con una contracorriente intercalada y otra contracorriente cerca de la costa (Contracorriente Costera de Venezuela).

Abstract

The geostrophic circulation of the waters near the Lesser Antilles, SE sector of the Caribbean Sea, has been calculated on the basis of a relatively dense network of oceanographic stations occupied by the Instituto Oceanográfico, Cumaná, Venezuela, onboard the R/V LA SALLE, during the month of August 1972. The geostrophic flow is described by means of longitudinal vertical sections (60°00', 62°00', 63°00', 63°45' and 64°30' long. W). The dynamic height distribution at the sea surface is also presented. The water mass transport was calculated for significant segments of the longitudinal sections, as well as for nearly zonal lines, in order to establish the balance of water transport in and out

---

[1/] Actualmente en Intecmar, Universidad Simón Bolívar, Caracas, Venezuela

of the region. In the Atlantic Ocean ($60^\circ00'$ long. W), the water circulation is characterized by an alternation in current direction associated with the presence of meanders. The main inflow to the Caribbean Sea is observed between the Islands St. Vincent and Dominica (21.5 Sverdrups) where two current branches enter: one moving from the SE, between Barbados and Tobago, and another penetrating from the NW, south of Dominica. The net inflow south of St. Vincent is very small. A cyclonic gyre east of Tobago returns a large volume of the waters transported by the Guiana Current. Within the Caribbean Sea, the westward circulation shows two main axes, with an intercalated countercurrent and another countercurrent near the coast (Venezuelan Coastal Countercurrent).

1. INTRODUCCION

Varios investigadores han señalado que existe una estrecha dependencia entre la estructura horizontal y vertical del Mar Caribe y del Océano Atlántico adyacente. La barrera física que impone el arco antillano a la libre comunicación entre estos cuerpos de agua, da lugar a que su intercambio se efectúe de manera compleja, con entradas y salidas de agua confinadas a los pasos interinsulares y con una consecuente deformación de las líneas de flujo. Por otra parte, se sabe que la circulación atlántica cerca de la Guayana se caracteriza por presentar grandes cambios temporales, así como por la ocurrencia de meandros. Este patrón de circulación ha sido atribuido a influencias batimétricas, al apilamiento de agua contra las Antillas y a las variaciones del régimen de vientos y descarga de los ríos suraméricanos (Fukuoka, 1971, 1971a; Mazeika, 1973; Febres Ortega, 1974). La advección asociada a las corrientes de Guayana, norecuatorial y del Caribe, presenta fluctuaciones semianuales provocadas por las variaciones estacionales de velocidad y dirección de los Vientos Alisios. Estas variaciones han sido analizadas por Fuglister (1951), fundamentalmente en base a información sobre deriva de barcos. Con referencia a este trabajo, Wüst (1964) señala que la corriente de Guayana, la más intensa de ellas, tiene una celeridad media de 41,6 cm/s y una amplitud anual de variación de 28,2 cm/s. El máximo de la velocidad ocurre entre abril y mayo y el mínimo en septiembre, en concordancia con la migración norte-sur de la Convergencia Intertropical. La celeridad de la corriente en la parte centro-oriental del Mar Caribe alcanza a 31,3 cm/s, con una amplitud anual de 13,4 cm/s. La corriente norecuatorial presenta una celeridad media de apenas 14,3 cm/s y una amplitud de 2,7 cm/s. Según Wüst (1964), estos valores demuestran que la corriente del Caribe resulta de la combinación de las de Guayana y norecuatorial. Con respecto a la penetración de aguas atlánticas al Caribe, deduce que el eje principal de la corriente cerca del arco antillano, se localiza superficialmente entre 10° y 13° lat. N. No obstante, para la primera mitad del año sus mapas de corrientes superficiales no destacan mayores diferencias en las velocidades del agua entre Trinidad y 15°N. Hacia finales de año las corrientes son menos intensas; la mayor parte del flujo hacia el Caribe se produce en el sur, principalmente por el paso de Granada.

Observaciones directas de las corrientes, tales como las de Pillsbury (1890), confirman la ocurrencia de importantes variaciones en la dirección de las corrientes de los pasos interinsulares. Las mediciones efectuadas en el Paso de Granada en 1888, mostraron exclusivamente movimiento hacia el este, mientras que en 1889 sólo se registraron corrientes hacia el oeste. Durante marzo y abril de 1970, Stalcup y Metcalf (1972) recopilaron una valiosa información sobre las corrientes en las Antillas Menores. Según ellos, el mayor influjo hacia el Caribe ocurrió por los pasos de Granada y San Vicente, y las corrientes más débiles por los de Dominica y Santa Lucía. Sus datos muestran, no obstante, que las velocidades y direcciones de las corrientes y, consecuentemente, los volúmenes de agua transportados entre las islas, sufren variaciones temporales muy significativas. En este sentido, Stalcup y Metcalf (1972) sugieren que este patrón de circulación puede estar relacionado con la posible ramificación de la corriente principal al este de las Antillas.

Por las evidencias citadas, puede sugerirse que la mayor penetración de las aguas atlánticas al Mar Caribe, especialmente de las que integran la corriente de Guayana, podría efectuarse indistintamente por uno o varios de los pasos interinsulares, dependiendo de la zona sobre la cual se concentra transitoriamente el efecto de los meandros de Guayana. En este trabajo se examinan con cierto énfasis los detalles de la circulación y del transporte de aguas en el sureste del Caribe, pretendiendo definir más claramente el flujo entre las islas antillanas.

2. CALCULOS GEOSTROFICOS

Para la descripción de la circulación geostrófica se han utilizado los datos obtenidos por el Instituto Oceanográfico de la Universidad de Oriente durante el crucero LS 7203, realizado en agosto de 1972 a bordo de la M/N LA SALLE (Fig. 1). Para el análisis primario de los datos se trazaron curvas características de todas las estaciones y se compararon con curvas compuestas trazadas para grupos de estaciones cercanas. El flujo geostrófico se determinó por medio de las distribuciones de altura dinámica relativa a 1 000 db. Esta superficie de referencia es aparentemente la más adecuada para el sector suroriental del Caribe, de acuerdo a los valores calculados por Gordon (1967) por el método de Defant y debido a que no se aleja excesivamente de las profundidades de umbral de los pasos Antillanos. Según Stalcup et al. (1971) estas últimas son: Granada, 740 m; San Vicente, 890 m; Santa Lucía, 980 m y Dominica, 950 m. Las velocidades geostróficas fueron calculadas para secciones verticales meridionalmente orientadas (60°00', 62°00', 63°00', 63°45' y 64°30' long. W). Se determinaron, además, la distribución de la altura dinámica de la superficie del mar y los transportes de masa de agua para segmentos significativos de las secciones meridionales, así como para líneas aproximadamente zonales.

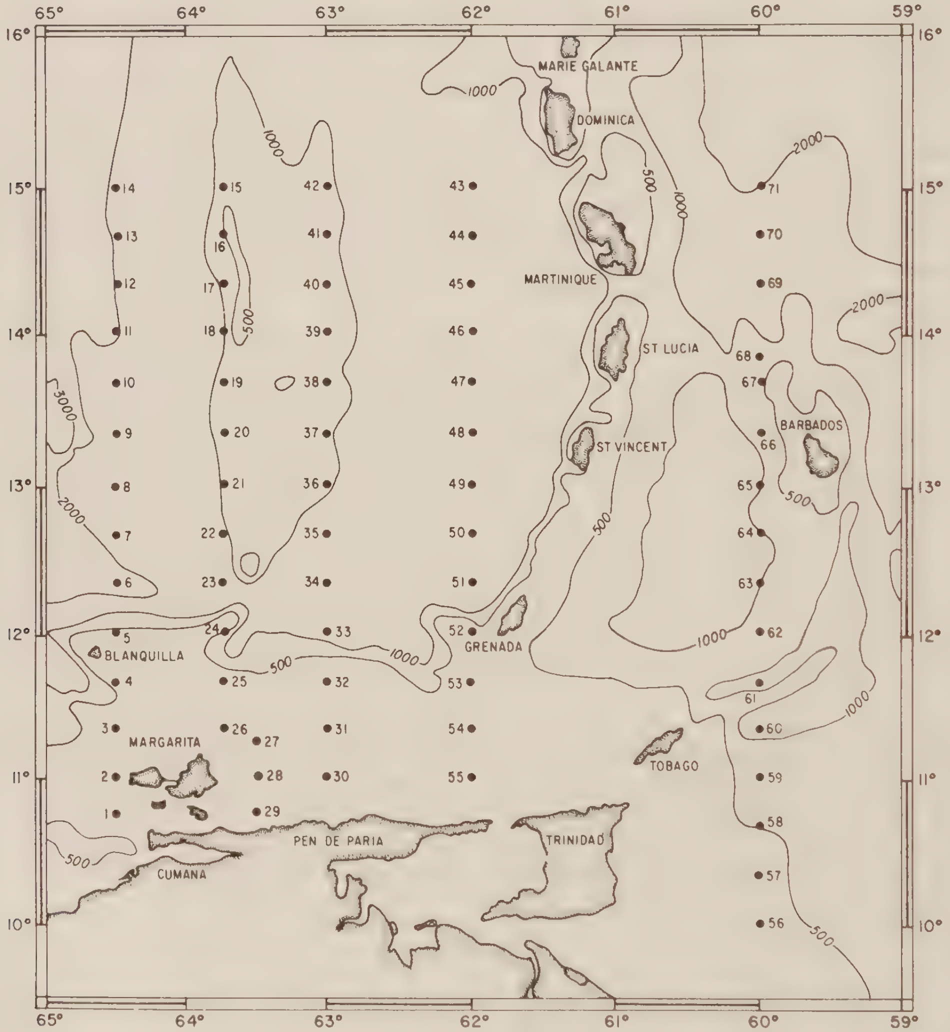
65°
64°
63°
62°
61°
60°
59°
16°
15°
14°
13°
12°
11°
10°
MARIE GALANTE
DOMINICA
MARTINIQUE
ST LUCIA
ST VINCENT
BARBADOS
GRENADA
TOBAGO
TRINIDAD
BLANQUILLA
MARGARITA
PEN DE PARIA
CUMANA
1000
2000
3000
500
1
2
3
4
5
6
7
8
9
10
11
12
13
14
15
16
17
18
19
20
21
22
23
24
25
26
27
28
29
30
31
32
33
34
35
36
37
38
39
40
41
42
43
44
45
46
47
48
49
50
51
52
53
54
55
56
57
58
59
60
61
62
63
64
65
66
67
68
69
70
71

Fig. 1 Localización de las estaciones oceanográficas del crucero LS 7203 Agosto de 1972

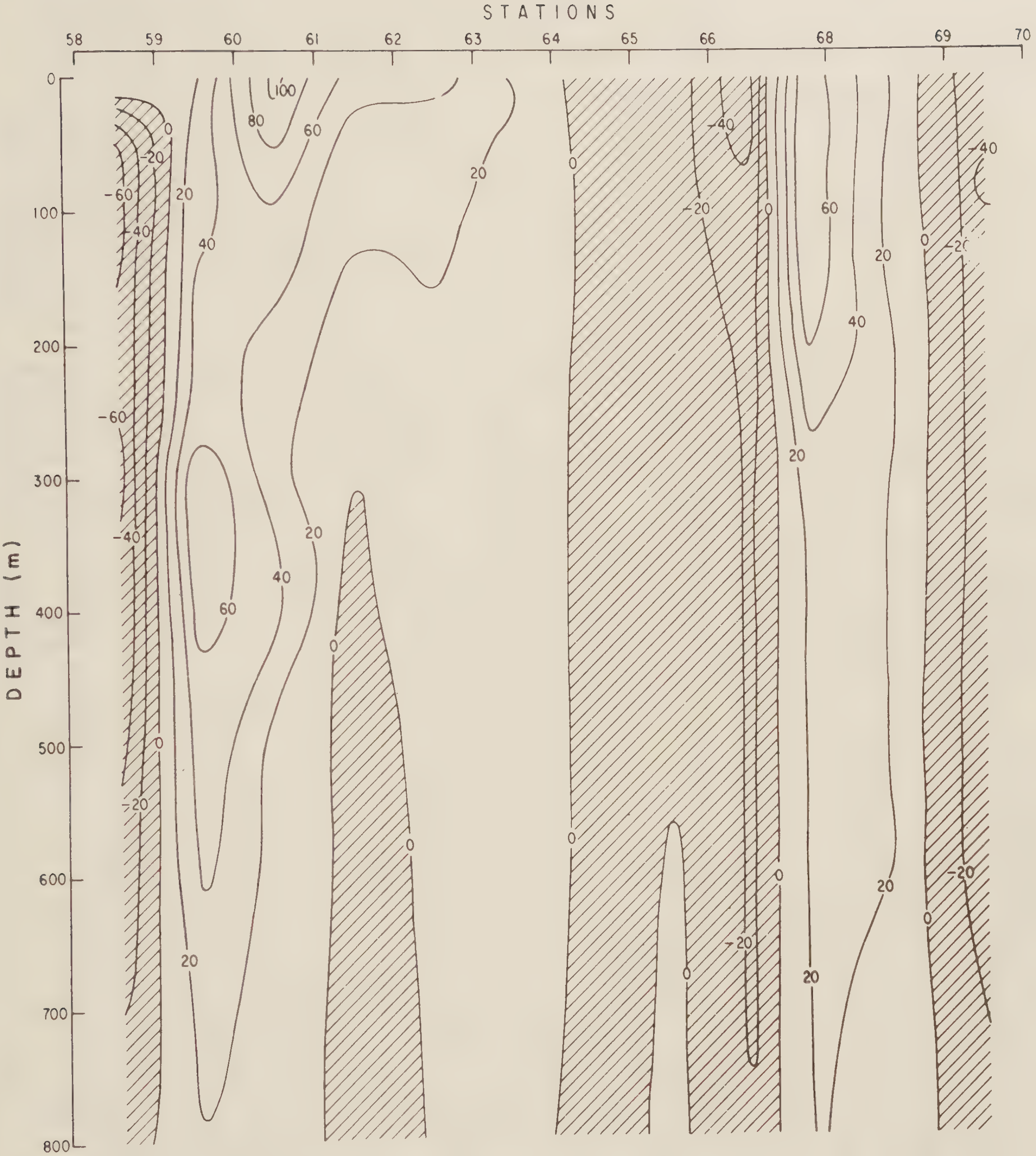

Fig. 2 Velocidades geostróficas (cm/s) a 60°00' long. W. Ref. 1 000 db

3. CIRCULACION

Las distribuciones verticales de la componente zonal de las velocidades geostróficas calculadas, siguen en líneas generales un mismo patrón en todas las secciones analizadas. Su característica principal es la sucesión alternada de corrientes y contracorrientes de gran extensión vertical, esto es, movimiento hacia el oeste y este, respectivamente. En el Océano Atlántico cerca de las Antillas, a los 60°00'W (Fig. 2) esta alternancia es la más evidente. Allí aparecen dos porciones de la sección en donde el flujo se dirige hacia el oeste: un ramal principal en la parte sur, de gran extensión e intensidad, que ocupa desde los 11°00' hasta los 12°40'N y uno secundario al norte, entre los 13°40' y 14°20'N. En el primero, las aguas superficiales alcanzan velocidades superiores a 100 cm/s cerca de los 11°30'N, donde se encuentra el eje de la corriente. Este eje está más cercano al continente a mayor profundidad, de manera que a 300 m aparece un núcleo intermedio de velocidades superiores a 60 cm/s, cerca de los 11°10'N. A profundidades mayores de 300 m el eje permanece a una misma latitud, alcanzando velocidades de 40 cm/s a los 600 m. En el ramal secundario el eje de la corriente aparece cerca de los 13°40'N. Aquí, las máximas velocidades hasta los 200 m de profundidad son del orden de 60 cm/s. Estos dos ramales de flujo posiblemente corresponden a las zonas de mayor influencia de las corrientes de Guayana y norecuatorial, al menos para el lapso de las observaciones. Las contracorrientes, destacadas en las gráficas por las partes sombreadas, se localizan al sur de 11°00', entre 12°40' y 13°40', y al norte de 14°20'N. La primera de éstas es la más fuerte y presenta velocidades superiores a 60 cm/s en dos núcleos situados a 100 y a 300 m de profundidad. La posición relativa de los núcleos de máxima velocidad y la proximidad a la Isla de Tabago permiten indicar que esta contracorriente devuelve gran parte de las aguas que son transportadas hacia el oeste en el ramal sur antes descrito. Las velocidades en los ejes de las otras contracorrientes son de alrededor de 40 cm/s. En adición a ellas, puede observarse una contracorriente de importancia relativamente pequeña a profundidades mayores de 300 m, cerca de los 11°50'N. Al comparar estos resultados con los de Fukuoka (1971) y Mazeika (1973), se pueden apreciar coincidencias generales en la localización y velocidad de las corrientes y contracorrientes, con la excepción más importante de la contracorriente observada cerca de Tabago, la cual no se menciona en estos trabajos posiblemente por no disponer los autores de observaciones en el área.

Las secciones verticales del interior del Mar Caribe muestran una mayor complejidad en la circulación, debido principalmente al efecto de las islas y a la presencia de giros ciclónicos y anticiclónicos. Con el fin de facilitar la interpretación de las corrientes en los cortes verticales, se presenta además la topografía dinámica de la superficie del mar, referida también a 1 000 db (Fig. 3). En esta gráfica se puede observar que la penetración de las aguas atlánticas al Caribe se efectúa principalmente por dos regiones: entre Granada y San Vicente y al norte de Santa Lucía. Estas dos bandas continúan fluyendo separadamente hacia el oeste, de manera relativamente complicada, tal como lo indica Fukuoka (1965). Aguas provenientes del noreste, las cuales no aparecieron a los 60°00' long. W, entran aparentemente por el Paso de Dominica y constituyen una importante contribución al flujo del eje norte de la Corriente del Caribe. Lamentablemente, por no disponer de datos oceanográficos de zonas más próximas a las islas, no es posible confirmar con verdadera certeza los detalles del flujo en los pasos interinsulares. No obstante, según puede deducirse de la sección meridional de 62°00'W (Fig. 4) la distribución vertical de las velocidades geostróficas corrobora muchos aspectos de la circulación descrita. Cerca del continente, la corriente que se dirige hacia el oeste no se extiende más allá de los 13° de latitud y su alcance vertical es de sólo 150 m, con velocidades apenas superiores a 40 cm/s. En las capas inferiores, el movimiento del agua es en la dirección contraria, a velocidades relativamente pequeñas (aproximadamente de 10 cm/s). Esta drástica reducción de la rama sur de la corriente del Caribe es probablemente ocasionada por una desviación del flujo hacia el talud continental, cerca de la Isla de Granada, con lo cual parte de ella no queda cubierta por la sección, además del retraimiento que ocurre cerca de Tabago. Entre 13°40' y 14°10'N se encuentran las aguas superiores de la rama septentrional de la corriente del Caribe, donde se alcanzan velocidades de 60 cm/s. Por debajo de estas se observa una contracorriente de velocidad relativamente moderada, pero de gran extensión vertical. La parte inferior de la corriente se encuentra situada más al sur, con su eje a los 13°30'N. La corriente de mayor importancia en esta sección es la que se observa al norte de los 14°30'N, donde se observan velocidades superiores a 80 cm/s en las capas superficiales y a 20 cm/s a los 550 m de profundidad. Estas aguas son las que aparentemente han penetrado al Caribe por el Paso de Dominica, según se sugiere antes. La contracorriente de mayor significación en este perfil vertical, se observa entre los 13° y 13°30'N, aproximadamente, pero su velocidad y dimensiones no son de gran magnitud.

La Fig. 5 muestra la distribución de las velocidades geostróficas calculadas para el meridiano de 63°00'W. Aquí se destacan, entre otros aspectos, un fortalecimiento de la rama sur de la Corriente del Caribe y el efecto de meandros en la circulación que dan lugar a que los ejes de las corrientes crucen repetidamente la sección. Estos últimos se pueden observar más claramente en la topografía dinámica de la superficie del mar. La rama norte de la corriente penetra a la sección entre 13°20' y 13°50'N, posteriormente describe un giro anticiclónico y se dirige hacia el este, cruzando de nuevo la sección entre 13°50' y 14°20'N. Finalmente da un giro ciclónico, se une con las aguas que supuestamente penetran por el Paso de Dominica y regresa hacia el oeste. También la rama sur de la corriente del Caribe describe giros de sentido similar entre los 12° y 13°N.

En el meridiano de 63°45'W (Fig. 6), la circulación adquiere una relativa simplicidad, apareciendo dos sectores bien definidos de movimiento hacia el oeste, los cuales corresponden a las ramas norte y sur de la corriente del Caribe. La del sur presenta una menor extensión vertical, debido quizás a la desviación parcial de sus aguas hacia el este con las contracorrientes, como puede inferirse también de la Fig. 3. La rama septentrional aparece aquí como una corriente de gran desarrollo horizontal y vertical. La zona intermedia, ocupada por la contracorriente, muestra velocidades de más de 80 cm/s en su núcleo principal situado entre 13° y 13°20'N.

En la topografía dinámica de la superficie del mar aparece una fuerte curvatura de tipo ciclónico en las isolíneas del norte de la Isla de Margarita. En la sección vertical de los 64°30'W (Fig. 7), se observa una contracorriente de apreciable desarrollo vertical al sur de 12°15'N, la cual corresponde precisamente a la parte sur de la curvatura ciclónica del flujo geostrófico. Estas características confirman los detalles de la circulación oceánica del Caribe suroriental descritas por Febres Ortega (1972) y Febres Ortega y Herrera (1975). En esos trabajos señalamos que la contracorriente costera de Venezuela

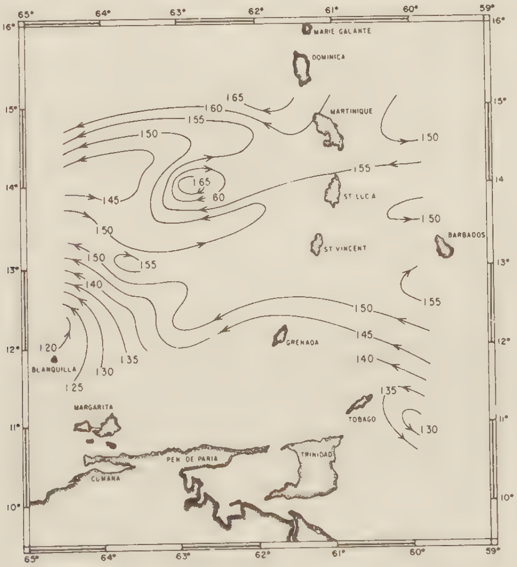

Fig. 3 Topografía dinámica de la superficie del mar (metros dinámicos)
Ref. 1 000 db

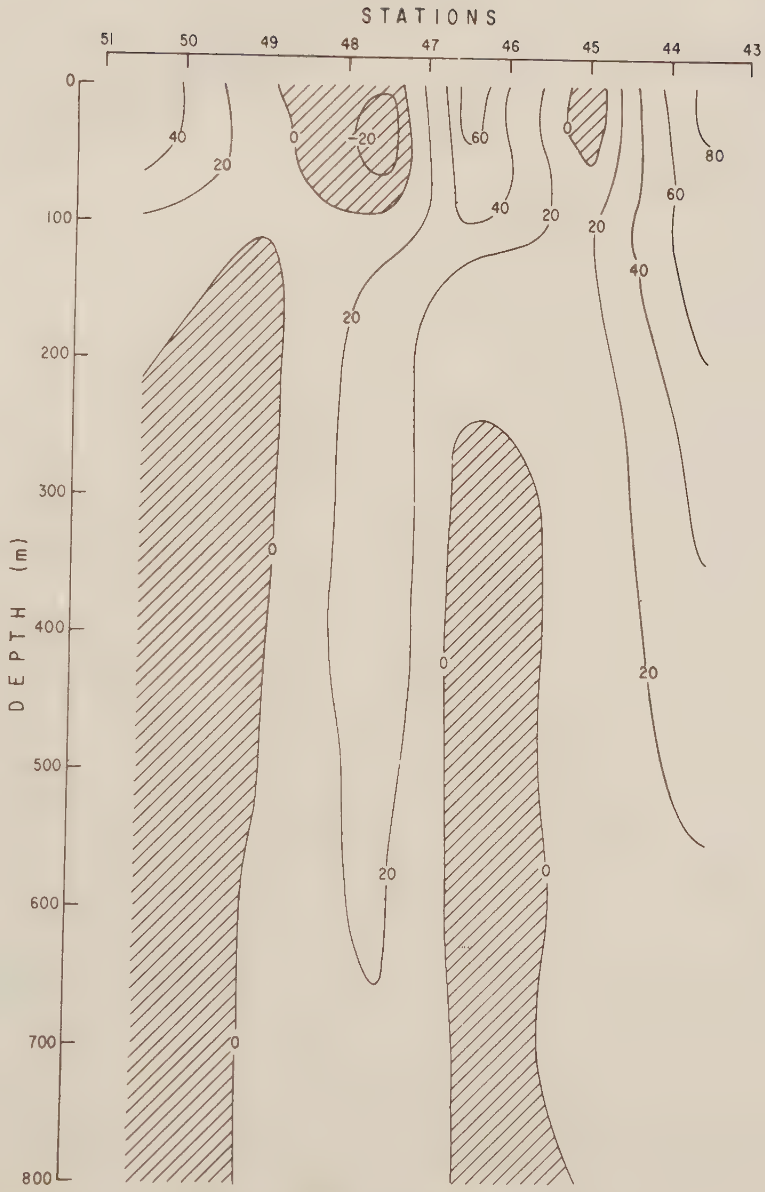

Fig. 4 Velocidades geostróficas (cm/s) a 62°00' long. W. Ref. 1 000 db

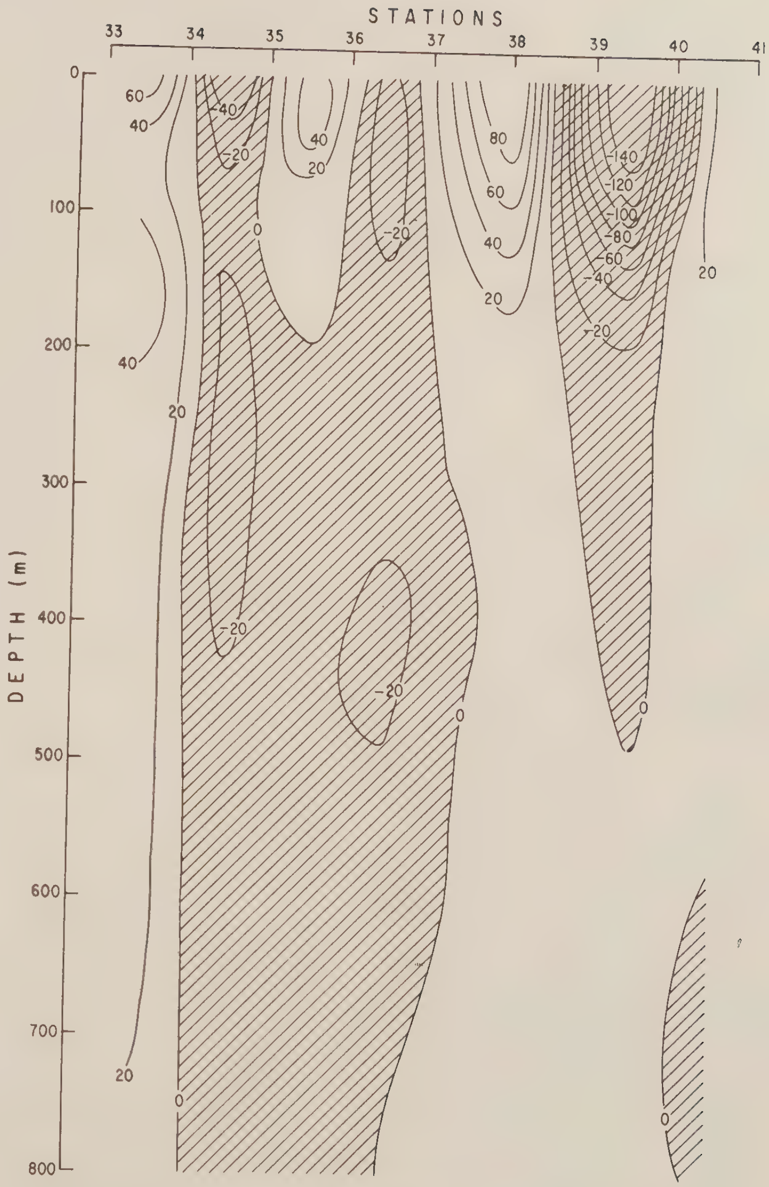

Fig. 5 Velocidades geostróficas (cm/s) a 63°00' long. W. Ref. 1 000 db

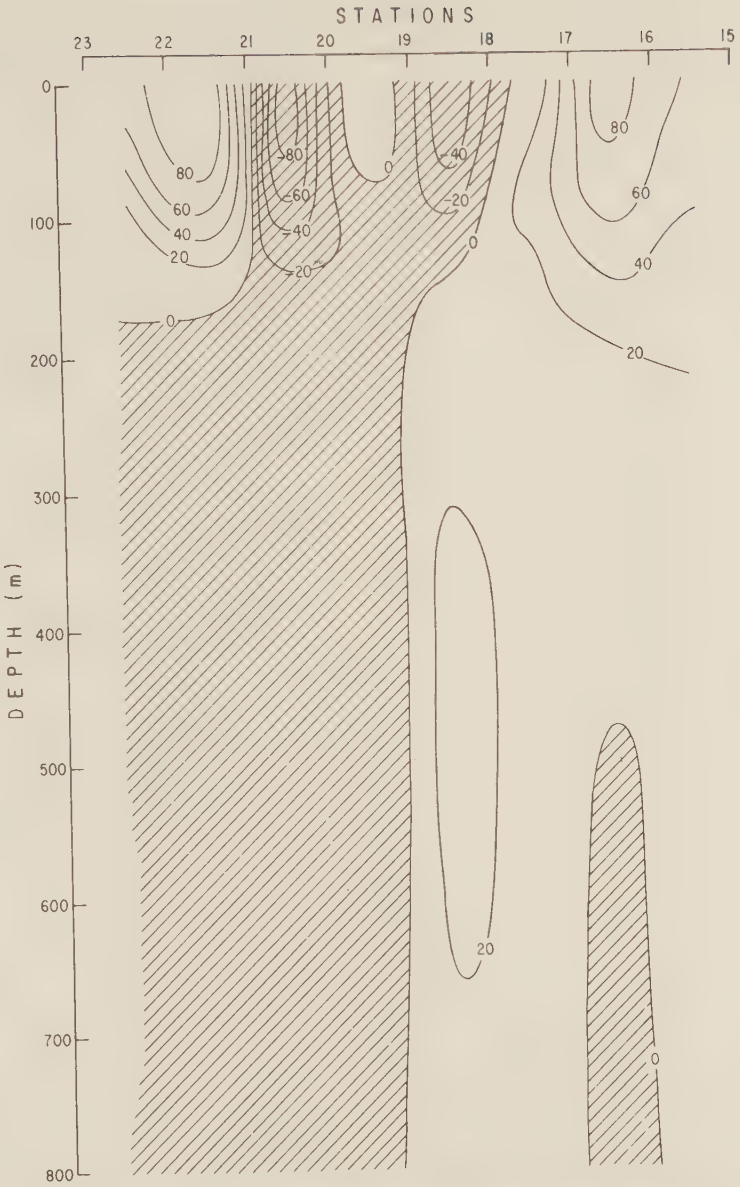

Fig. 6 Velocidades geostróficas (cm/s) a 63°45' long. W. Ref. 1 000 db

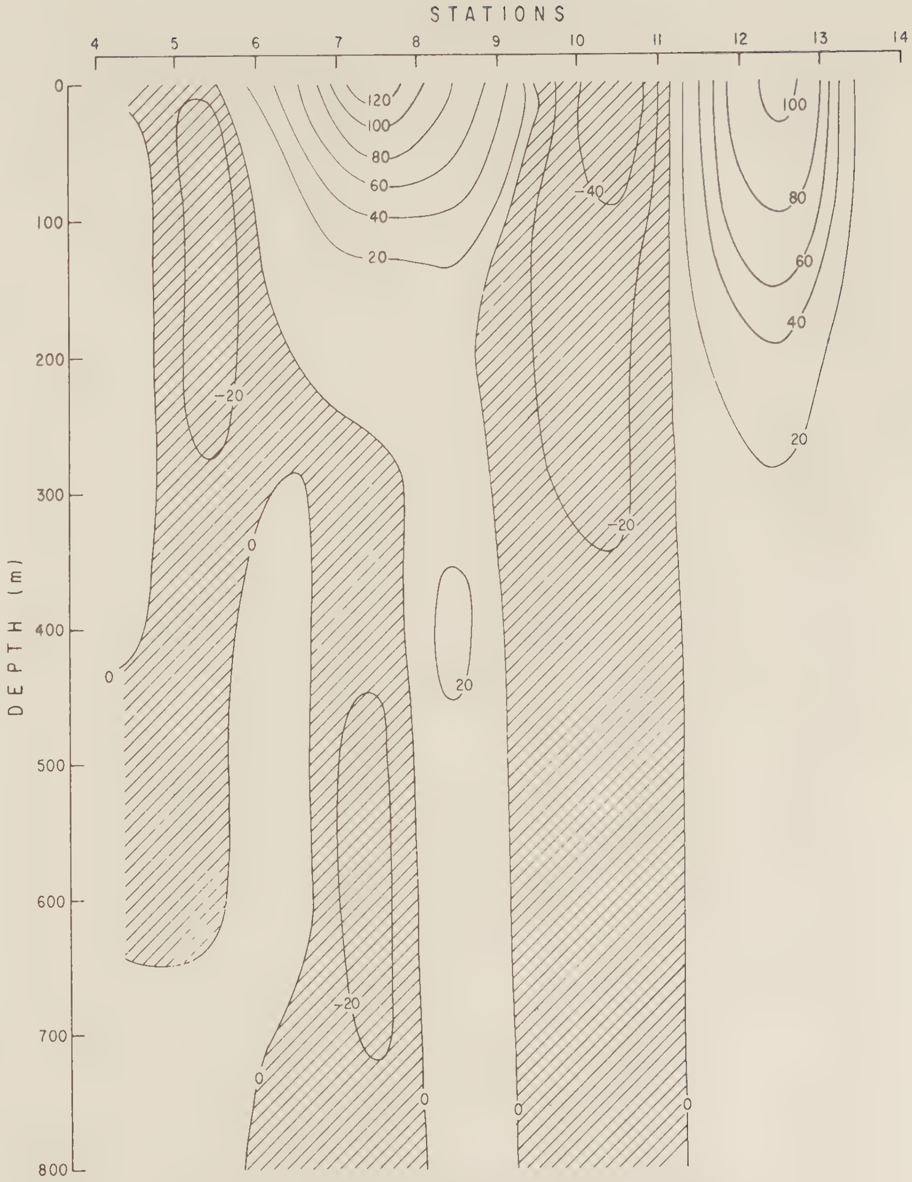

Fig. 7 Velocidades geostróficas (cm/s) a 64°30' long. W. Ref. 1 000 db

está asociada a la parte sur de un giro ciclónico, cuyo centro se localiza a los 67°W, unos 130 km al norte de este país. A esas conclusiones puede agregarse, que el extremo oriental del giro ciclónico y, por ende, de la contracorriente costera se encuentra entre 64°30' y 63°45'W, ya que en este último meridiano no hay evidencias de su existencia.

Por el norte de la contracorriente costera, la circulación es muy similar a la descrita en las otras secciones. No obstante, el eje sur de la Corriente del Caribe aparece situado un poco más al norte, alcanzando 12°50' de latitud en los 200 m superiores de la columna de agua y 13°10'N, en las capas inferiores. Las velocidades son mayores que en la sección precedente, debido en parte a la adición de las aguas de la contracorriente costera. Igualmente, la rama norte alcanza velocidades superiores, alimentada aparentemente por la contracorriente que se observa cerca de los 14°N. Nuestros resultados se diferencian del perfil vertical de Gordon (1967) para los 74°W, porque en éste no se encuentra una contracorriente de magnitud significativa en las capas superiores de la porción central del Mar Caribe. Esto pone de manifiesto que posiblemente la contracorriente no sea contínua a lo largo del Caribe oriental, sino que se restringe a las proximidades de las Antillas, donde parece integrar un giro ciclónico, como se infiere de la topografía dinámica.

Por otra parte, es importante destacar el hecho de que la distribución de altura dinámica muestra curvaturas similares para los dos ejes de la corriente del Caribe. Esto es, las aguas de ambos ejes se desvían ligeramente hacia el sur al sobrepasar el arco antillano y luego adquieren la fuerte curvatura anticiclónica y ciclónica antes referida. Según Veronis (1966), este tipo de meandros en la circulación oceánica tiene una relación íntima con la influencia que el relieve del fondo ejerce sobre la columna de agua en movimiento, como consecuencia de la conservación de la vorticidad potencial. En el aspecto regional, Fukuoka (1965) y Leming (1968) señalaron que el arco de las Antillas puede generar ondas en las corrientes. Más aun, Fukuoka (1965) sugiere que también la cordillera submarina de las Aves (entre 63° y 64°W) puede generar oscilaciones similares e inclusive señala que la longitud de onda de los meandros producidos por estos accidentes del fondo podría ser de unos 100 km. Coincidentemente, los meandros que aparecen en nuestras observaciones alcanzan una longitud de onda de magnitud semejante.

4. TRANSPORTE

Todas las mediciones anteriores del transporte de masa de agua a través de los pasos interinsulares de las Antillas Menores y en secciones orientadas meridionalmente en la cercanía de estas islas, tanto en el Caribe como en el Atlántico, coinciden aproximadamente en la magnitud que asignan al flujo dirigido hacia el oeste. Los cálculos de Gordon (1967) sobre el transporte geostrófico a través de seis secciones verticales del Mar Caribe, arrojan un promedio de 31 Sv para los meses de invierno (1 Sverdrup= 1 Sv = 10^6 m^3/s), con una dispersión de los valores de cerca de 10 Sv. El promedio correspondiente a sus dos secciones más próximas a las Antillas, 64°30' y 68°30'W, es de 29,5 Sv. Mediciones posteriores analizadas por Mazeika (1973) dan un transporte geostrófico de 29 Sv para el invierno de 1969, entre la Isla de Tabago y los 18°N. Para el propósito de nuestro trabajo es importante señalar que sus cálculos, para el verano del mismo año, dan apenas un transporte total de 22 Sv entre Tabago y 17°N.

Las mediciones directas de las corrientes efectuadas en los pasos principales de las Antillas Menores durante marzo y abril de 1970 por Stalcup y Metcalf (1972), dieron un promedio del transporte total cercano a los 27 Sv. Este flujo de agua ocurrió en su casi totalidad por los Pasos de Santa Lucía, San Vicente y Granada. En contraste con nuestras observaciones, el transporte por el Paso de Dominica fue casi despreciable en comparación con el de los otros pasos. Estos autores hacen énfasis sobre las diferencias obtenidas entre los cálculos geostróficos hechos en base a datos tomados en febrero de 1970, durante el crucero oceanográfico ATLANTIS 56, y sus mediciones directas. Según ellos, las corrientes geostróficas para tres secciones hechas a través del Paso de Granada dieron un transporte neto de 2 a 4 Sv hacia el este, mientras que las observaciones directas hechas de uno o dos meses después, mostraron en todas las ocasiones un transporte neto hacia el oeste. De igual manera, las corrientes geostróficas y las corrientes observadas directamente en los otros pasos interinsulares presentaron diferencias muy significativas.

Stalcup y Metcalf (1972) señalaron, en tal sentido, que las diferencias detectadas pueden obedecer, entre otras causas, a los efectos friccionales y del relieve del fondo sobre las corrientes. Consideramos probable, sin embargo, que la falta de simultaneidad de las observaciones, en presencia de variaciones temporales importantes en la circulación, tales como las que caracterizan esta región, de lugar a estas discrepancias.

Nuestra descripción del transporte geostrófico del sureste del Caribe y del Atlántico, cerca de las Antillas, se fundamenta en los valores calculados para segmentos significativos de las secciones meridionales observadas, así como en líneas aproximadamente zonales. Este método permite obtener detalles adicionales sobre la circulación y además, establecer un balance del flujo sobre la red de estaciones de observación. Estos resultados están resumidos en la Fig. 8, en la cual las flechas indican la dirección del transporte neto y las cifras, en su punto de aplicación, su magnitud en Sv. La sección hecha a lo largo del meridiano de 60°W no se unió a la red por encontrarse relativamente lejos del perfil más próximo y debido a que las Islas de las Antillas interferirían en esa simple integración. El transporte neto a través de esta sección es de sólo 11 Sv, aunque sin embargo, entre las estaciones 59 y 63 (11° y 12°20'N, respectivamente) pasan 26,3 Sv de los cuales 14,2 Sv se regresan hacia el este cerca de Tabago. Para cubrir este aparente déficit en el transporte de agua hacia el Caribe, es necesario que ocurra un flujo importante en esa dirección a latitudes mayores de 14°40'N, donde no alcanzaron las observaciones de esta sección. Esta posibilidad es evidente en la topografía dinámica de la superficie del mar. A los 62°00'W, el transporte hacia el oeste entre los 13°20' y 15° de latitud es de 21,5 Sv. Más al sur, el transporte neto es muy pequeño (0,1 Sv) y dirigido hacia el este. Esto último obedece a que la contracorriente subyacente descrita para este sector transporta un volumen de agua ligeramente superior al del flujo superficial que se desplaza desde el Atlántico con el eje sur de la Corriente del Caribe. El flujo neto a través de toda esta sección vertical es, por lo tanto, practicamente similar al calculado por Mazeika (1973) para la misma época del año.

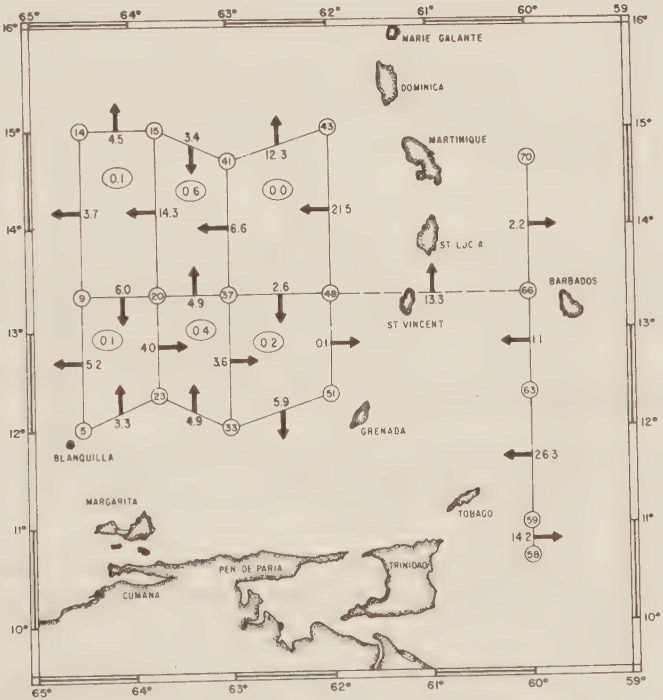
65°
64°
63°
62°
61°
60°
59
16°
15°
14°
13°
12°
11°
10°
MARIE GALANTE
DOMINICA
MARTINIQUE
ST LUC A
ST VINCENT
BARBADOS
GRENADA
TOBAGO
TRINIDAD
BLANQUILLA
MARGARITA
PEN DE PARIA
CUMANA
14
15
41
43
70
9
20
37
48
66
5
23
33
51
63
59
58
4.5
3.4
12 3
0.1
0 6
0 0
3.7
14.3
6.6
21 5
2.2
6.0
4.9
2.6
13.3
0 1
0 4
0 2
4 0
3.6
0 1
1 1
5 2
3.3
4.9
5.9
26 3
14 2

Fig. 8 Transporte de masa de agua (en Sv) a través de los segmentos indicados (0-1 000 db). Agosto de 1972

En la sección correspondiente a los 63°00'W, el transporte hacia el oeste entre las latitudes extremas de la serie de observaciones, alcanza solamente a 3 Sv. Este descenso en la magnitud del volumen transportado se debe a que gran parte de las aguas observadas en la sección precedente, se desvían hacia el norte, entre las estaciones 41 y 43 y hacia el sur, entre las estaciones 33 y 51. En este perfil se puede ver que la magnitud del flujo de aguas en la contracorriente situada entre los dos ejes de la Corriente del Caribe es bastante apreciable, dando lugar a que entre las estaciones 33 y 37 el transporte sea de 3,6 Sv hacia el este.

A los 63°45'W, el transporte neto de la Corriente del Caribe se incrementa de nuevo, alcanzando unos 10 Sv. Este crecimiento es ocasionado por la advección de aguas desde el norte y sur, entre las estaciones 15 y 41 y las estaciones 23 y 33, respectivamente. Entre este meridiano y el de 64°30'W, parte de las aguas escapan hacia el norte (4,5 Sv) y otras se desplazan más al sur de los 13°20'N, donde también convergen las aguas de la contracorriente costera de Venezuela, proporcionando así un mayor desarrollo del eje sur de la Corriente del Caribe.

Con el fin de demostrar la confiabilidad que permiten los datos oceanográficos utilizados, hemos puesto en la Fig. 8 cifras encerradas entre elipses, las cuales representan las cantidades necesarias (Sv) para obtener un balance del transporte geostrófico en cada polígono de la red. En términos relativos, estas diferencias, que representan excesos de agua, son tan pequeñas que permiten concluir que los efectos friccionales en las secciones estudiadas no ocasionan efectos importantes. De no ser así, la mayor proximidad a las islas provocaría desajustes en el balance de aguas de cada polígono. No obstante, en zonas aún más cercanas a las islas, es posible que los efectos friccionales sean realmente considerables, tal como lo señalan Stalcup y Metcalf (1972). Por último, es importante destacar que entre 60° y 62°W, las corrientes deben tener un fuerte componente hacia el norte. En efecto, para que se obtenga un balance del transporte geostrófico, es necesario que entre las estaciones 48 y 66 se desplazen hacia el norte cerca de 13,3 Sv, como se indica en la figura. Esta posibilidad se deduce también de los cálculos dinámicos hechas para capas subyacentes, los cuales no se incluyen en este trabajo por razones de espacio. En adición a estos, la distribución de la salinidad superficial para el lapso junio-noviembre analizada por Wüst (1964), demuestra la factibilidad de tal movimiento. Así mismo, las topografías dinámicas y la información sobre deriva de botellas trazadoras presentadas por Brucks (1968), en base a datos tomados en agosto de 1965, noviembre de 1966 y febrero de 1967, entre Barbados y el Arco de las Antillas, constituyen una valiosa comprobación de la existencia de un fuerte componente hacia el norte en las corrientes de esta zona.

5. REFERENCIAS

Brucks, J.T., The current east of the Windward Islands, West Indies. In Unesco/FAO
1971 Symposium on Investigations and Resources of the Caribbean Sea and Adjacent Regions, Willemstad, Curaçao, 18-26 Nov. 1968. Paris, Unesco, pp. 31-5

Febres Ortega, G., Isanosteric analysis of the eastern Caribbean waters during winter.
1972 Bol.Inst.Oceanogr.Univ.Oriente, 11(1):19-34

__________, Circulación oceánica y estratificación de las masas de agua superiores al
1974 norte de la Guayana. Cuadernos Azules, No. 5 Com. Org. III Conf. N.U. sobre el Derecho del Mar, Caracas.

Febres Ortega, G. y L.E. Herrera, Interpretación dinámica de algunas características
1975 oceanográficas de la Fosa de Cariaco, Mar Caribe. Bol.Inst.Oceanogr.Univ. Oriente, 14(1):3-30

Fuglister, F.C., Annual variations in current speeds in the Gulf Stream system. J.Mar.
1951 Res., 10(1):119-27

Fukuoka, J., Hydrography of the adjacent sea. 2. Some characteristics of oceanographical
1965 conditions in the Caribbean, especially in the region adjacent to Venezuela. Bol.Inst.Oceanogr.Univ.Oriente, 4(2):234-45

__________, The meandering of the ocean current east of Guiana. Bol.Inst.Oceanogr.Univ.
1971 Oriente, 10(1):25-8

Fukuoka, J., Coastal upwelling and sinking in the Caribbean Sea, especially about the
1971a existence of the undercurrent. In Fertility of the sea, edited by J. Costlow. New York, Gordon and Breach, pp. 123-42

Gordon A.L., Circulation of the Caribbean Sea. J.Geophys.Res., 72(24):6207-23
1967

Leming, T.D., Eddies west of the southern Lesser Antilles. In Unesco/FAO Symposium on
1971 Investigations and Resources of the Caribbean Sea and Adjacent Regions, Willemstad, Curaçao, 18-26 Nov. 1968, Paris, Unesco, pp. 113-20

Mazeika, P.A., Circulation and water masses east of the Lesser Antilles. Dtsch.Hydrogr.Z.,
1973 26(2):49-73

Pillsbury, J.E., The Gulf Stream, methods of the investigation and results of the research.
1890 Rep.U.S.Coast Geod.Surv., (1890), Append. 10

Stalcup, M.C. and W.G. Metcalf, Current measurements in the passages of the Lesser Antilles.
1972 J.Geophys.Res., 77(6):1032-49

Stalcup, M.C., W.G. Metcalf y M. Zemanovic, Current measurements in the Lesser Antilles.
1971 Woods Hole Oceanogr.Inst.Ref., (71-51) (Unpubl.)

Veronis, G., Rossby waves with bottom topography. J.Mar.Res., 24(3):339-49
1966

Wüst, G. and A. Gordon, Statification and circulation in the Antillean Caribbean basins.
1964 Part 1. Spreading and mixing of the water types with an oceanographic atlas. New York, Columbia University Press, 201 p.

DIVERGENCIA ANEMOGENICA HORIZONTAL DE LAS AGUAS SUPERIORES DE VENEZUELA ORIENTAL, MAR CARIBE

por

L.E. HERRERA y G. FEBRES ORTEGA[1]
Instituto Oceanográfico, Universidad de Oriente, Cumaná, Venezuela

CONTENIDO

1. INTRODUCCION
2. PRESENTACION DEL PROBLEMA
3. TRATAMIENTO DEL PROBLEMA
4. DISCUSION
5. AGRADECIMIENTOS
6. REFERENCIAS

Resumen

El campo de corrientes generadas por el viento y la divergencia horizontal de la velocidad fueron calculados, bajo condiciones simuladas de vientos, utilizando la teoría de Ekman para corrientes puras de deriva en un océano de profundidad finita. La región estudiada está localizada al norte de las penínsulas Araya y Paria, en donde los Vientos Alisios del Noreste muestran un componente oriental predominante todo el año. En nuestros cómputos se utilizó lo siguiente: a) Vientos del Este con celeridades de 4, 8, 12 y 16 m/s; b) Esfuerzo cortante del viento calculado mediante la ley del cuadrado de la velocidad; c) Coeficiente de arrastre en aumento lineal con el viento; d) Coeficiente de viscosidad turbulenta constante en profundidad y variable con la celeridad del viento; e) Area dividida en cuadrados de 5 millas náuticas por lado y con profundidad media calculada de los sondeos disponibles; f) Esquema de diferencias finitas para el cálculo de la divergencia. El campo superficial de las corrientes y la distribución horizontal de la divergencia son presentados para cada celeridad del viento empleada en los cálculos. A medida que aumenta la profundidad de influencia friccional, en relación a la profundidad del fondo, los vectores de la corriente tienden a alinearse con el viento. Los cambios sucesivos en el campo de corrientes son claramente observables. Las figuras de la divergencia horizontal de la velocidad muestran la aparición y desarrollo de tres zonas de divergencia en la superficie: cerca de la costa, a comienzos del talud continental y a sotavento del Banco de Los Testigos, con convergencias intercaladas. Estos resultados concuerdan con las características de la surgencia costera, de inicios del talud continental e inducida por islas que se presentan en la región.

Abstract

The wind-generated current field and the horizontal velocity divergence were calculated, under simulated wind conditions, employing Ekman's theory for pure drift currents in a finite depth ocean. The region studied is located north of the Araya and Paria peninsulas, where the northeast trades exhibit a dominant eastern component throughout the year. For our computations, the following were used: a) East winds with speeds of 4, 8, 12 and 16 m/s; b) Wind stress calculated by means of the square law; c) Drag coefficient in linear increase

---

[1] Actualmente en INTECMAR, Universidad Simón Bolívar, Caracas, Venezuela

with the wind; d) Eddy viscosity coefficient constant with depth and variable with wind speed; e) Array of grids, 5 nautical miles per side, with a mean depth assigned from available soundings; f) Finite difference scheme for calculating the divergence. The surface current field and the horizontal divergence distribution are present for each of the wind speeds used in the calculations. As the depth of frictional influence increases in magnitude, relative to ocean depth, the current vectors tend to align with the wind. The sequential changes in the current field are thus clearly observable. The surface velocity divergence charts show the appearance and development of three distinct divergence zones: near the coast, in the slope region, and on the leeward side of Los Testigos Bank. These results agree with the characteristics of coastal, slope, and island-induced upwelling known to occur in this region.

1. INTRODUCCION

En el análisis de flujos bidimensionales, los componentes cinemáticos del gradiente de la velocidad pueden ser usados para determinar los movimientos diferenciales de una porción del fluido en el plano horizontal. La divergencia horizontal de la velocidad permite, además, hacer inferencias acerca del movimiento vertical del fluido, mediante la aplicación del principio de conservación de la masa. En un fluido incompresible, la condición de no divergencia es satisfecha, de allí que la ecuación de continuidad pueda escribirse:

$$\frac{\partial w}{\partial z} = -\left(\frac{\partial u}{\partial x} + \frac{\partial v}{\partial y}\right) , \qquad (1)$$

lo que equivale a decir que, en un fluido de densidad constante no afectado por fenómenos de evaporación o de precipitación, el volumen neto de agua que penetra a (sale de) una columna vertical del fluido es una medida de la tasa a la cual el agua sale de (penetra a) esa columna debido a los movimientos verticales inducidos por convergencias (divergencias) en la superficie.

Teóricamente, los movimientos verticales en la columna de fluido pueden ser estimados mediante la integración vertical de la ecuación de continuidad, desde la superficie hasta una profundidad dada, si se conoce bien el campo de la velocidad en los contornos. Este enfoque ha sido empleado con algún éxito en Meteorología, gracias a la red mundial de estaciones que proporcionan datos continuos en escala sinóptica. Las aplicaciones oceanográficas son más limitadas por falta de una cobertura comparable en el espacio y en el tiempo y, además, porque los movimientos verticales en los océanos son tres o cuatro órdenes de magnitud menores que los movimientos horizontales, mientras que los gradientes verticales de la velocidad generalmente son menores en un orden de magnitud a los gradientes horizontales. Estos factores magnifican las fallas propias del método. En este trabajo, sólo se presenta la distribución superficial de la divergencia de la velocidad generada por los vientos, para una región del margen continental de Venezuela en donde se producen procesos estacionales de surgencia.

2. PRESENTACION DEL PROBLEMA

En los océanos pueden producirse movimientos ascendentes de masas de agua, en diversas escalas de tiempo y espacio, de acuerdo a la transitoriedad, intermitencia o permanencia del mecanismo generador, y a la extensión de su distribución geográfica. La designación de surgencia *sensu stricto* es reservada convencionalmente para aquellos movimientos ascendentes de "duración y extensión mínimas mediante los cuales aguas provenientes de capas subsuperficiales son transportadas a capas superficiales y removidas del área de surgencia por flujos horizontales" (Smith, 1968). En la mayoría de los casos, la surgencia es una consecuencia directa del esfuerzo cortante del viento sobre la superficie del mar, el cual genera una divergencia horizontal de la velocidad e induce flujos compensatorios de aguas subyacentes.

La surgencia de origen anemogénico puede ser explicada en base a la teoría de Ekman (1905), quien demostró que la acción de un viento uniforme, sobre la superficie de un mar homogéneo e infinitamente profundo, causa un transporte neto de masa de agua 90° *cum sole* con la dirección del esfuerzo cortante. La surgencia más intensa se produce cuando un viento que sopla paralelo a la línea costera transporta masas de agua mar afuera, en dirección normal a la costa, con el subsiguiente desarrollo de una línea de divergencia y el reabastecimiento de la capa superficial por aguas surgidas de estratos inferiores. En los procesos de surgencia costera, la satisfacción de los requisitos de continuidad lleva a la formación de una línea de convergencia más allá de la línea de divergencia, así como a la compensación del transporte hacia altamar, en la capa de Ekman, mediante un flujo hacia la costa a niveles inferiores. Hay otros factores diferentes de los vientos que también ocasionan movimientos verticales de masas de agua, tales como la separación o el encuentro de corrientes horizontales, la topografía del fondo, la presencia de islas y los gradientes isopícnicos en zonas frontales. En general, las divergencias y convergencias superficiales pueden ser identificadas como áreas de surgencia y de hundimiento, respectivamente, cualquiera sea su origen.

La capa superior de los océanos responde en forma relativamente rápida al acoplamiento friccional con los vientos. Shaffer (1972) estima que el campo de la velocidad dependiente del tiempo alcanza sus valores estacionarios uno o dos días después de iniciados los vientos, y presume que la surgencia resultante debe llegar a su desarrollo pleno en igual tiempo. Sin embargo, no es fácil correlacionar la magnitud y persistencia de los vientos con el campo de surgencia generado. Mientras los vientos soplen sobre la superficie, en una dirección apropiada, el transporte vertical de masas de agua prosigue. Una vez que la acción eólica cesa, las aguas surgidas tienden a hundirse de nuevo, lo que a menudo origina inversiones termohalinas. No obstante, las condiciones existentes antes del evento de surgencia no se restablecen de inmediato, ya que el ascenso de aguas subyacentes ocasiona una inclinación de las isolíneas en dirección normal al litoral.

En regiones con frecuentes eventos de surgencia se desarrolla un fuerte gradiente horizontal de la densidad, perpendicular a la costa, debido al ajuste baroclínico del campo de la masa. Bajo condiciones estacionarias, un mar baroclínico puede sustentar una corriente a lo largo de la costa, con superposición en la capa de Ekman de una corriente mantenida por el viento. Una característica típica del Mar Caribe, aún en períodos sin procesos de surgencia, es el ascenso que presentan las superficies isopícnicas hacia el sur. Al cesar la surgencia, las pendientes de estas superficies se tornan cada vez menores debido a procesos de mezcla, transferencia vertical de calor y advección de masas de agua que, de modo gradual, tienden a restaurar un estado de equilibrio en la estructura vertical de las aguas superiores. Un estimado del cambio estacional que experimentan las pendientes, puede inferirse de la correspondiente migración vertical de las isopicnas que es de unos 100 m en aguas venezolanas (Ljöen y Herrera, 1965).

Las características esenciales del sistema de surgencia del Mar Caribe suroriental son conocidas, gracias a investigaciones realizadas por diversos autores desde 1960. En general, en la costa norte de Suramérica, la surgencia se concentra en dos áreas localizadas frente a Venezuela y Colombia, respectivamente. El sistema de surgencia de Venezuela es el de mayor intensidad y menor extensión. El origen anemogénico de estos movimientos ascendentes ha sido establecido con certeza. En el Mar Caribe suroriental, los Vientos Alisios alcanzan sus velocidades más altas y su desarrollo vertical máximo en una banda relativamente estrecha (12^{o}-13^{o} latitud N). La intensidad de los vientos superficiales decrece hacia el norte y sur de dicha banda. Por esta razón, se desarrollan sendas zonas de divergencia y convergencia al sur y al norte del eje de vientos más fuertes, respectivamente.

El sistema de surgencia de Venezuela presenta una estacionalidad marcada. El mayor transporte vertical de agua se produce en invierno y comienzos de la primavera, con surgencia ocasional a fines de la primavera y comienzos del verano, y una ausencia virtual de movimientos ascendentes a fines de verano y en otoño. Cerca de la mitad del transporte de Ekman hacia el norte, está constituido por aguas surgidas de unos 90 a 175 m de profundidad, entre la costa y 150 km mar afuera. Las corrientes que penetran al Mar Caribe sufren una deflección hacia el norte, lo cual contribuye a intensificar la zona de divergencia generada por los vientos. La zona de surgencia está orientada en una dirección WNW, en su parte más septentrional, prácticamente paralela al curso que sigue la Corriente del Caribe en esta región. También hay evidencias claras de la existencia de una contracorriente dentro y por debajo de la zona de transición.

Al igual que en otros lugares, la temperatura es el mejor indicador de la surgencia en aguas venezolanas, con un descenso estacional del orden de $5^{o}C$. La salinidad también es un indicador confiable, ya que la capa intermedia de salinidad máxima de origen subtropical migra hacia la superficie en la época de surgencia, llegando a interceptarla en las áreas donde el fenómeno es más intenso (Febres Ortega y Herrera, 1975). Más tarde, la salinidad comienza a disminuir gradualmente por la advección, a partir del mes de junio, de aguas de baja salinidad relativa. La intersección de la superficie isanostérica de 400 cl/t con la superficie del mar puede servir de criterio para delinear la extensión horizontal del área de surgencia. No obstante, en la descripción de los procesos de surgencia es preciso examinar la distribución superficial de las propiedades cinemáticas - aún a través de un modelo simulado tan sencillo como el presente - como paso previo a un enfoque tridimensional más sofisticado de este fenómeno en particular y de la dinámica de las aguas costeras venezolanas, en general.

3. TRATAMIENTO DEL PROBLEMA

Nuestra área de estudio está comprendida entre las penínsulas de Arya y Paria (Venezuela) y 11°40' latitud N, y entre las longitudes 63°55' W y 61°50' W. Sus características batimétricas principales se muestran en la Fig. 1. La plataforma continental es amplia, con una distancia media de unos 90 km entre la costa e inicios del talud continental. En su parte oriental, la plataforma desciende rápidamente a más de 75 m en el eje del Valle Submarino de Carúpano, orientado paralelo a la costa, a profundidades de más de 110 m a 61°50' longitud W y de menos de 25 m al norte del Banco de Cubagua. La plataforma tiene una profundidad media de 66 m y se hace más somera de este a oeste. Al norte del Valle de Carúpano, la curva de 50-m circunda un ancho banco submarino que incluye las islas Los Testigos, Los Frailes y Margarita. El talud continental se encuentra al norte de 11°30' latitud N y está orientado en dirección paralela a la costa.

Los Vientos Alisios soplan con una persistencia notable en el Mar Caribe suroriental, pero su intensidad disminuye entre los 12°00' latitud N y el litoral. Esta distribución latitudinal de los vientos es conducente a la formación de una divergencia en el campo de las corrientes al sur del eje principal, es decir, en nuestra área de estudio. Los autores (Herrera y Febres Ortega, 1975, 1975a) han demostrado que los vientos están circunscritos, en su mayor parte, a direcciones entre el NNE y SSE, con un componente este predominante todo el año. Las direcciones medias entre ENE y NNE dominan el campo de flujo de diciembre a julio, y las comprendidas entre SE y SSE son más frecuentes de agosto a noviembre. Los componentes del norte están asociados a los vientos más fuertes del este, especialmente entre febrero y abril cuando la temporada de surgencia se halla en su apogeo. Los componentes del sur aparecen cuando la Zona de Convergencia Intertropical avanza hacia su posición más norteña y la celeridad de los Vientos Alisios declina.

Hemos señalado asimismo que la temperatura media mensual de las aguas superficiales en Puerto Sucre (Cumaná) muestra una alta correlación con los vientos medios mensuales en nuestra Estación Meteorológica de San Luis (Cumaná), según la regresión lineal siguiente:

$$\overline{T} = 32{,}10 - 1{,}91\,\overline{V}_a\,, \qquad (2)$$

en donde la temperatura (T) está dada en °C y la celeridad del viento (V_a) en m/s. Las temperaturas más bajas se observan con vientos fuertes provenientes de direcciones entre el ENE y NNE, mientras que las más altas están asociadas a vientos más calmos del este con un componente menor del sur.

La consistencia de estos resultados nos permitió seleccionar arbitrariamente, para los cómputos, vientos del este con celeridades de 4, 8, 12 y 16 m/s. El esfuerzo cortante del viento fue calculado mediante la siguiente ecuación:

$$\tau = \rho_a C_D |V_a| V_a\,, \qquad (3)$$

en donde τ = esfuerzo cortante del viento (dinas/cm^2); ρ_a = densidad del aire (se tomó $1{,}25 \times 10^{-3}$ g/cm^3); C_D = coeficiente de arrastre (no dimensional); y V_a = velocidad del viento. Se adoptó la suposición de Deacon (1962) de un coeficiente de arrastre en aumento lineal con el viento, a saber:

$$C_D = (1{,}10 + 0{,}04\,\overline{V}_a) \times 10^{-3} \qquad (4)$$

Se asumió que el coeficiente de viscosidad turbulenta (A) era constante en profundidad y variable con la celeridad del viento, de acuerdo a la relación derivada por Neumann

(Neumann y Pierson, 1966) en base a determinaciones de Thorade (1914) y de Schmidt (1917), esto es:

$$A = 0{,}1825 \times 10^{-4} V_a^{5/2} \qquad (5)$$

La profundidad de influencia friccional fue calculada a continuación, mediante la relación:

$$D = \pi A^{1/2} (\rho\omega \text{ sen } \Phi)^{-1/2} \qquad (6)$$

en donde ρ = densidad media del agua de mar (se tomó 1,025 g/cm^3); ω = velocidad angular de la Tierra ($7{,}292 \times 10^{-5}$ rad/s); y Φ = latitud.

El área de estudio fue dividida en una retícula de 270 cuadrados, de cinco millas náuticas por lado, con una profundidad media asignada a cada cuadrado en base a los sondeos disponibles. Los componentes horizontales de la velocidad fueron calculados para cada cuadrado, empleando la teoría de Ekman (1905) para corrientes puras de deriva en un océano de profundidad finita. En este sentido, se utilizaron las ecuaciones siguientes:

$$u = \alpha \text{ senh } b\zeta \cos b\zeta - \beta \cosh b\zeta \text{ sen } b\zeta \qquad (7)$$

$$v = \alpha \cosh b\zeta \text{ sen } b\zeta + \beta \text{ senh } b\zeta \cos b\zeta \qquad (8)$$

en donde las constantes (α) y (β) y la variable (b) están dadas por:

$$\alpha = \frac{\tau D}{A\pi} \frac{\cosh bd \cos bd + \text{senh } bd \text{ sen } bd}{\cosh 2bd + \cos 2bd} \qquad (9)$$

$$\beta = \frac{\tau D}{A\pi} \frac{\cosh bd \cos bd - \text{senh } bd \text{ sen } bd}{\cosh 2bd + \cos 2bd} \qquad (10)$$

$$b = \left(\frac{\rho\omega}{A} \text{sen}\Phi \right)^{1/2}$$

y en donde los únicos símbolos nuevos son (u,v) = componentes de la velocidad en las direcciones (x,y); ζ = d-z; y (d) = profundidad del fondo. Una vez obtenidos los componentes del campo de corrientes generadas por el viento, se procedió a computar la divergencia horizontal de la velocidad por medio de un sencillo esquema de diferencias finitas.

4. DISCUSION

De acuerdo a su definición (6), la profundidad de influencia friccional (D) es una función del coeficiente de viscosidad turbulenta (A) y de la latitud (Φ). La influencia de esta última es menor ($< 4\%$), debido a la estrechez de la banda latitudinal estudiada. El efecto de la viscosidad es mucho mayor, ya que se ha asumido una dependencia directa de (A) con respecto a la celeridad del viento. (Si se combinan las relaciones (5) y (6), se puede observar que $D \propto V_a^{5/4}$.) En las latitudes bajo consideración, la profundidad de influencia friccional oscila entre valores de 61,8-64,1 m para un viento de 4 m/s y de 349,3-362,3 m para una celeridad de 16 m/s. En este sentido, debe recordarse que la profundidad media de la plataforma continental en el área estudiada es de 66 m. Para profundidades de d = 0,5D o mayores, la dirección de la corriente superficial generada por el viento es esencialmente la misma que para un océano infinito, esto es 45° a la derecha del vector viento, en el Hemisferio Norte. Sin embargo, a medida que la razón d/D se hace menor, el ángulo entre el viento y la corriente también decrece. Por ello, el incremento de la profundidad de influencia friccional - resultante de aumentos en la celeridad del viento - trae consigo una tendencia de las corrientes superficiales a alinearse con el viento.

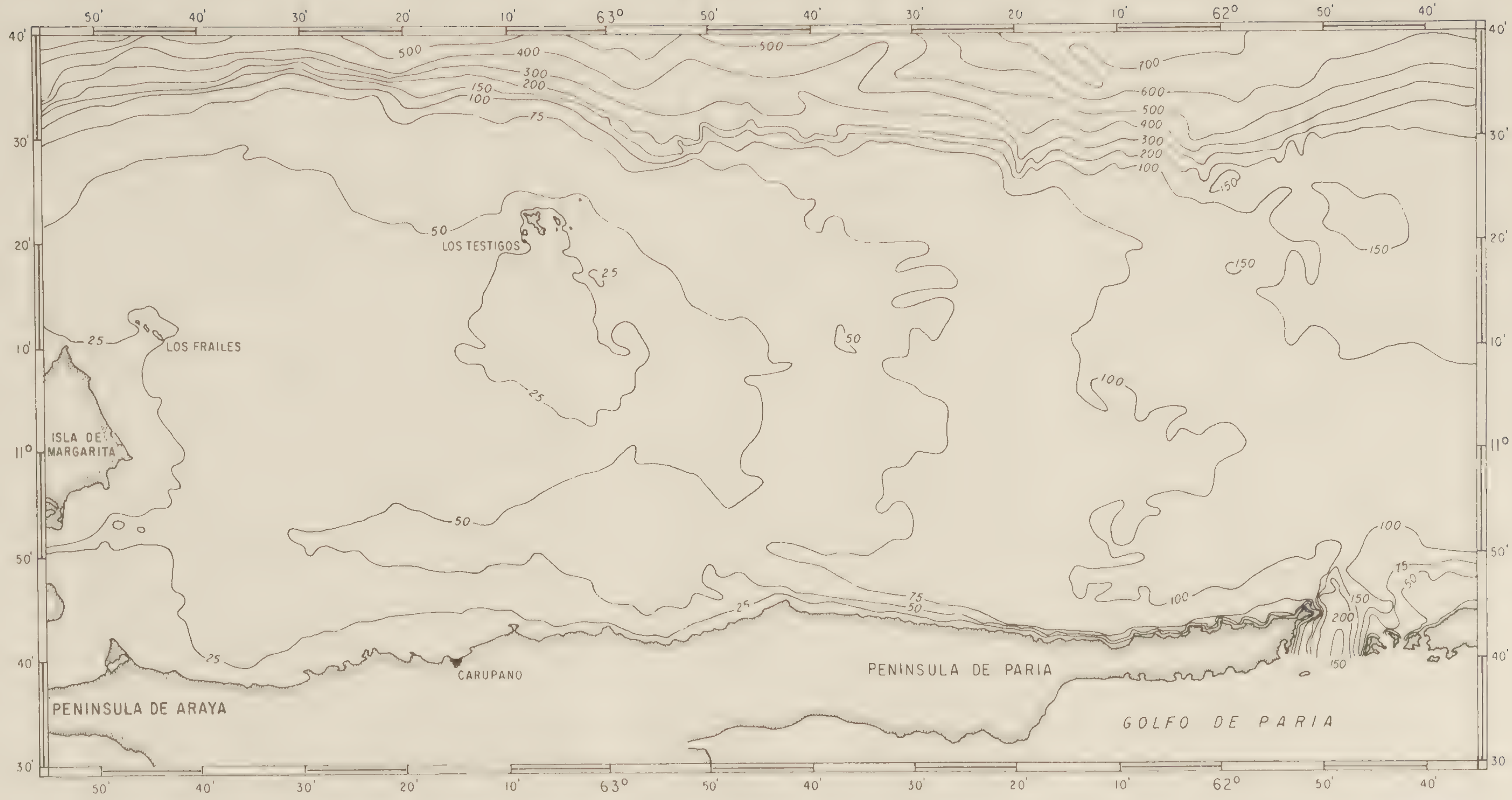
LOS TESTIGOS
LOS FRAILES
ISLA DE MARGARITA
CARUPANO
PENINSULA DE ARAYA
PENINSULA DE PARIA
GOLFO DE PARIA
63°
62°
11°

Fig. 1 Principales rasgos batimétricos de la plataforma continental y de la parte superior del talud continental del oriente de Venezuela, Mar Caribe

Los resultados principales de este trabajo aparecen ilustrados por las Figs. 2-5, en las cuales se presentan las distribuciones del campo superficial de las corrientes generadas por el viento (gráfica superior) y de la divergencia horizontal de la velocidad (gráfica inferior), para cada una de las velocidades de viento usadas en los cálculos. En la preparación de las distribuciones superficiales de la divergencia de la velocidad se han empleado unidades de $10^{-6}seg^{-1}$, y en las de las corrientes se sobrepuso la escala apropiada. La Fig. 2 corresponde a un viento este de 4 m/s. La profundidad de influencia friccional para esta celeridad varía entre 61,8 y 64,1 m. El campo de corrientes es bastante uniforme y los gradientes de la velocidad son de baja magnitud. La mayoría de los vectores de corrientes forman un ángulo de cerca de 45° con el viento y sus magnitudes son de unos 6,2 cm/s 4,4 cm/s). Los cambios mayores de velocidad se observan en las aguas someras (<25 m) del Banco de Los Testigos y, en menor grado, al oeste de Carúpano y al este de la Isla de Margarita Las zonas de divergencia y convergencia no muestran mayor definición, excepto en las cercanías de Los Testigos, pero se las diferencia con facilidad. Existen zonas de divergencia ligera al este y sureste de Los Testigos y a unos 10°45' N; 63°40' W, es decir, al este del Morro de Chacopata. En la parte sur del Banco de Los Testigos se encuentra una zona de convergencia.

A medida que aumenta la velocidad del viento, el campo de corrientes se torna más complejo, tal como lo ilustra la Fig. 3. Con un viento de 8 m/s, los valores de (D) oscilan entre 146,9 y 152,3 m para la banda latitudinal involucrada en este estudio. Por consiguiente, los vectores de corrientes, para aquellos cuadrados con profundidades medias inferiores a 75 m, muestran distintos grados de desviación con respecto a la situación típica de aguas profundas (corrientes hacia el noroeste de 11,6-11,8 cm/s; $u,v \sim 8,2-8,4$ cm/s). A medida que se acercan al Banco de Los Testigos, las corrientes provenientes del este empiezan a disminuir en intensidad y a girar ciclónicamente, hasta alcanzar una orientación casi zonal en las partes más someras del Banco. Más hacia el oeste, las celeridades aumentan de nuevo y los vectores señalan hacia el WNW. Al sur del Banco, el ángulo entre la corriente y el viento disminuye en forma gradual de este a oeste. La zona de divergencia principal se encuentra en las cercanías de Los Testigos, especialmente en su lado de sotavento donde llega a valores superiores a $8 \times 10^{-6}seg^{-1}$. Las isolíneas tienen forma bilobulada y reflejan la tendencia de la zona de divergencia a propagarse zonalmente. Frente a la costa, aproximadamente entre Morro de Chacopata y Carúpano, se desarrolla una segunda zona de divergencia de menor intensidad. Intercalada entre las zonas de divergencia, y ocupando las porciones sur y sureste del Banco de Los Testigos, se halla una zona de convergencia con valores extremos del orden de $-5 \times 10^{-6}seg^{-1}$.

En la Fig. 4 se presentan las distribuciones superficiales de las corrientes y de la divergencia, para un viento este de 12 m/s. La profundidad de influencia friccional varía entre 243,8 y 252,9 m a esta celeridad, lo cual implica que el campo de corrientes sufre su mayor distorsión en áreas con profundidades menores de unos 125 m. Las condiciones características de aguas profundas (corrientes de 17,6-17,8 cm/s; $u,v \sim 12,4-12,6$ cm/s) están restringidas a una extensión cada vez menor, debido a la intensificación y esparcimiento progresivos del efecto friccional. La mayor parte de los vectores de corrientes comprendidos dentro de la curva de 50 m están dirigidos esencialmente hacia el oeste. La magnitud de las corrientes llega a un mínimo en el Banco de Los Testigos pero, una vez transpuesto éste, aumenta de nuevo hacia la Isla de Margarita. El Valle Submarino de Carúpano ejerce un efecto notable sobre las corrientes, y los vectores localizados en su eje proporcionan el mejor ejemplo del cambio gradual, en dirección y magnitud, que experimentan las corrientes de este a oeste. Los rasgos básicos de la distribución de la divergencia son semejantes a los detectados a una celeridad de viento de 8 m/s, pero aparecen más definidos y con algunas variaciones en la disposición relativa de la divergencia bilobulada cercana a Los Testigos, la divergencia costera y la convergencia intercalada entre ambas. La divergencia costera muestra muy pocos cambios, pues aún ocupa un área alargada y paralela a la costa por más de 60 millas náuticas, y su valor máximo es de unos $4 \times 10^{-6}seg^{-1}$. La zona de convergencia se encuentra inmediatamente después, extendida hacia el norte en el lado de barlovento de Los Testigos y al noreste de la Isla de Margarita, pero ligeramente disminuida en intensidad. La característica más importante que se observa en la Fig. 4 es, sin embargo, el apreciable crecimiento zonal de la zona de divergencia principal, al norte de la latitud de Testigo Grande. En la vecindad de Los Testigos las principales isolíneas están cerradas, pero las situadas en el sector noroccidental están abiertas en su mayoría. Los valores más elevados ($>9 \times 10^{-6}seg^{-1}$) se hallan en el lado de sotavento de Los Testigos.

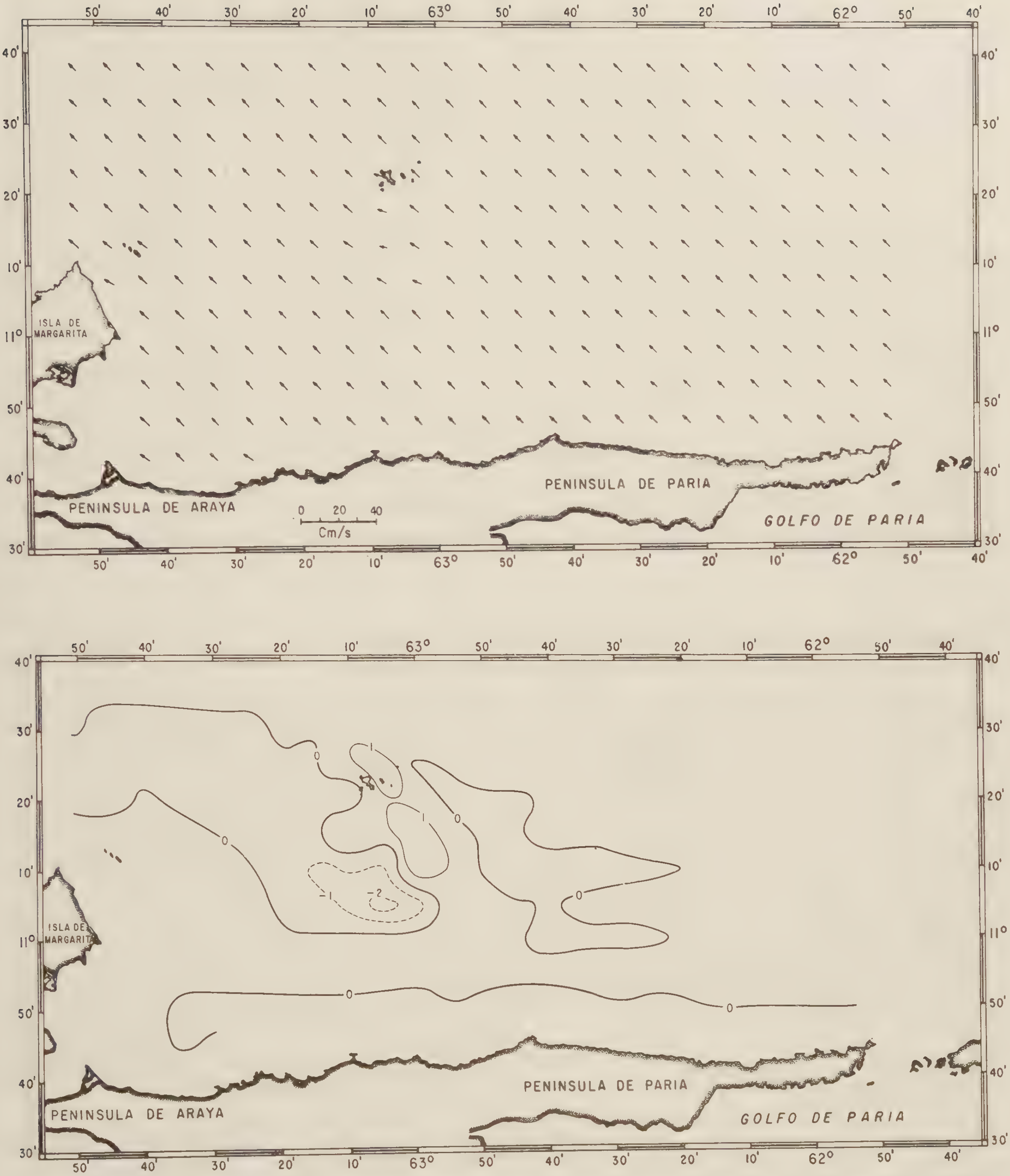
ISLA DE MARGARITA
PENINSULA DE ARAYA
PENINSULA DE PARIA
GOLFO DE PARIA
0 20 40
Cm/s
63°
62°
11°
0
1
-1
-2

Fig. 2 Distribuciones del campo superficial de las corrientes (arriba) y de la divergencia horizontal de la velocidad (abajo), para un viento del Este de 4 m/s

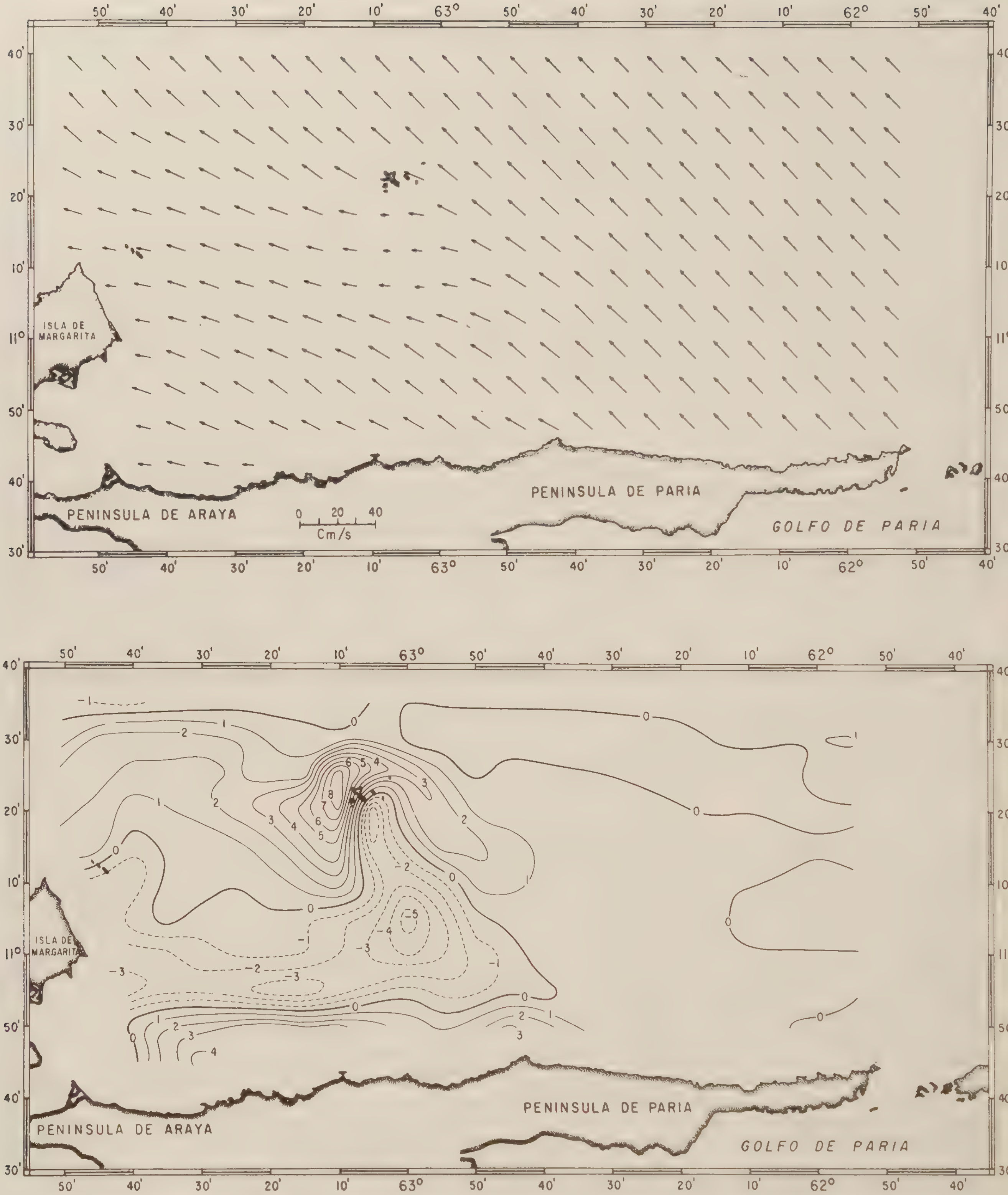
50' 40' 30' 20' 10' 63° 50' 40' 30' 20' 10' 62° 50' 40'
40' 30' 20' 10' 11° 50' 40' 30'
ISLA DE MARGARITA
PENINSULA DE ARAYA
PENINSULA DE PARIA
GOLFO DE PARIA
0 20 40
Cm/s
-1 0 1 2 3 4 5 6 7 8 -2 -3 -4 -5

Fig. 3 Distribuciones del campo superficial de las corrientes (arriba) y de la divergencia horizontal de la velocidad (abajo), para un viento del Este de 8 m/s

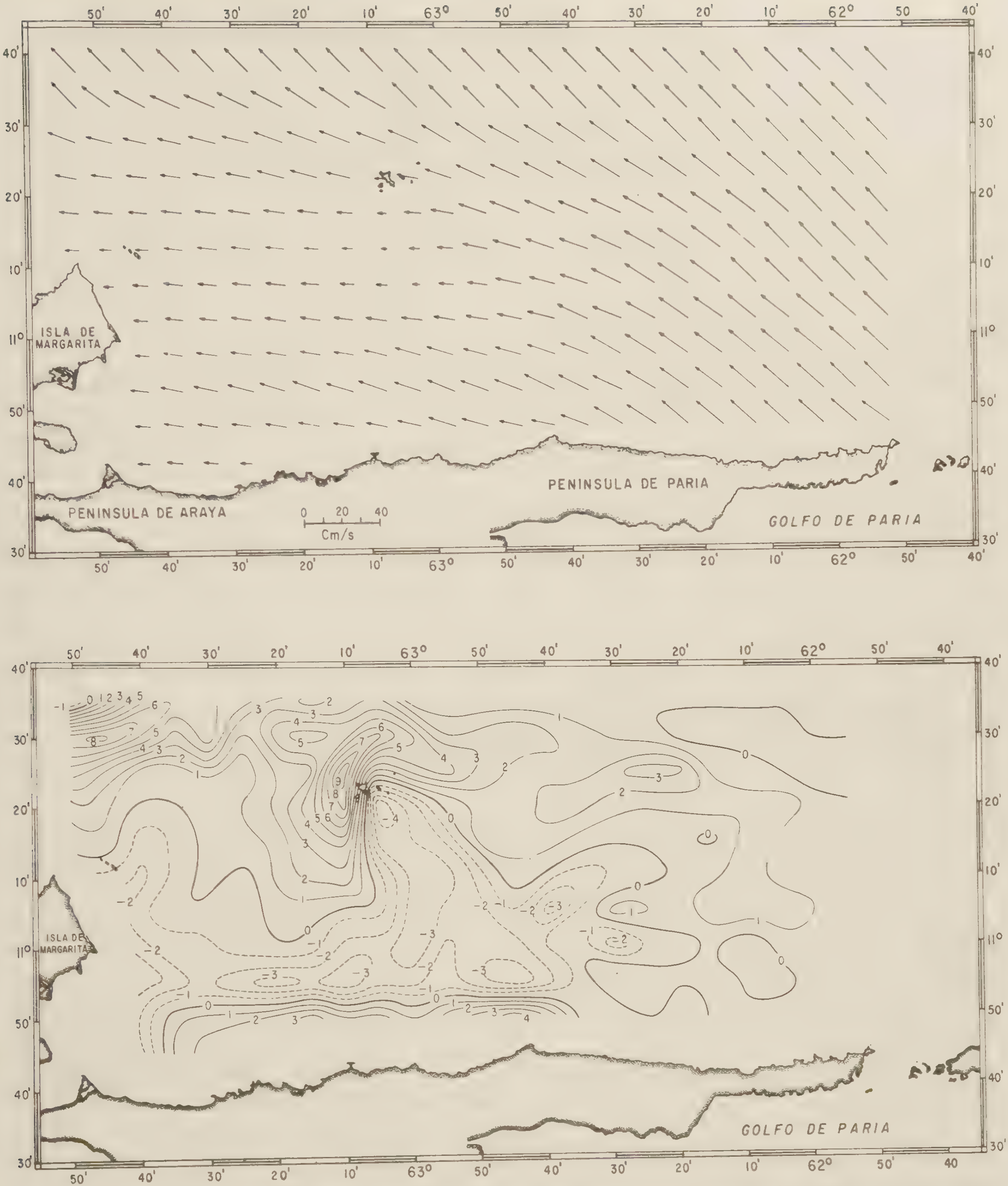
50'
40'
30'
20'
10'
63°
62°
11°
ISLA DE MARGARITA
PENINSULA DE ARAYA
PENINSULA DE PARIA
GOLFO DE PARIA
0 20 40
Cm/s

Fig. 4 Distribuciones del campo superficial de las corrientes (arriba) y de la divergencia horizontal de la velocidad (abajo), para un viento del Este de 12 m/s

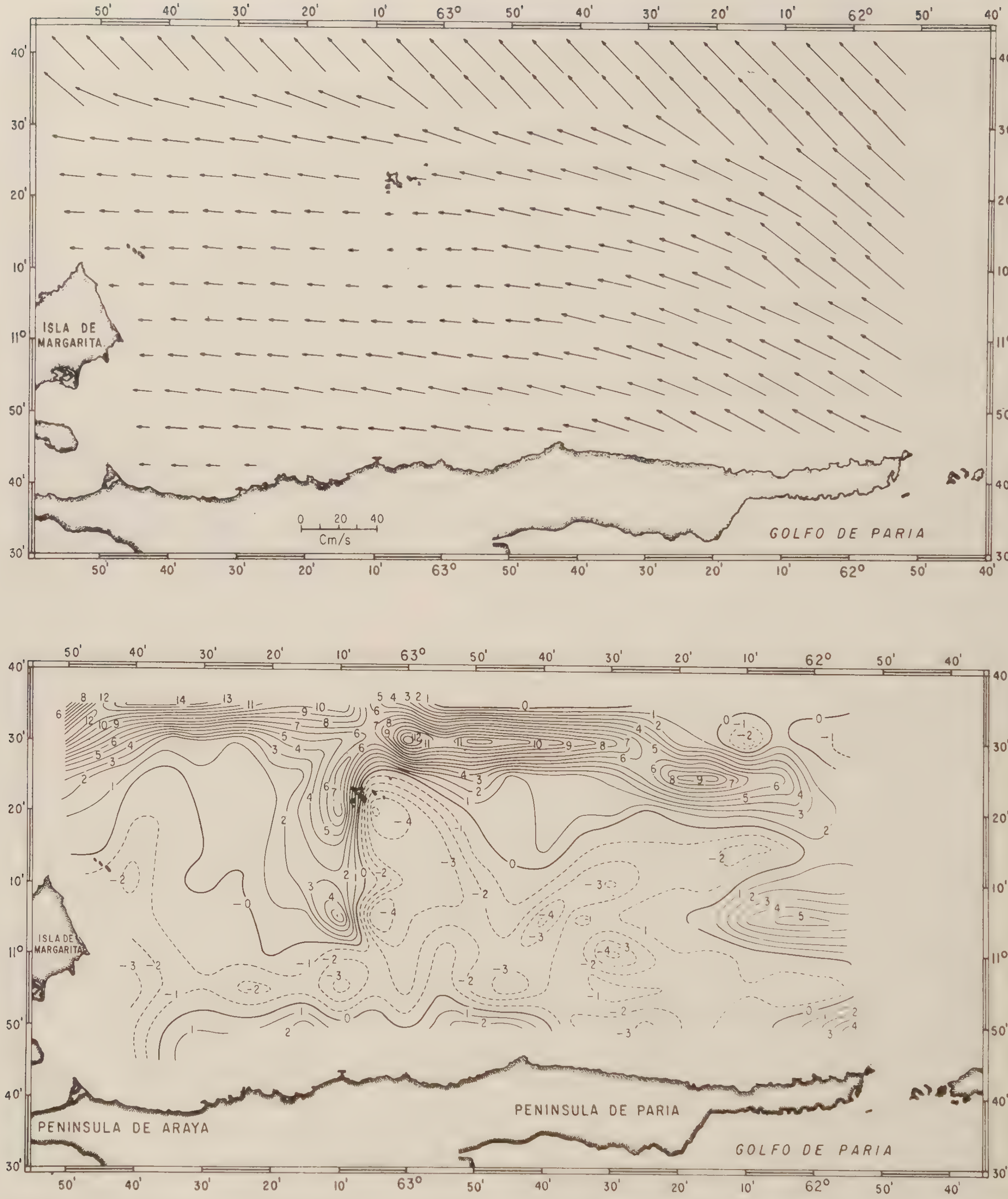
50'
40'
30'
20'
10'
63°
62°
11°
0 20 40
Cm/s
ISLA DE MARGARITA
GOLFO DE PARIA
PENINSULA DE PARIA
PENINSULA DE ARAYA

Fig. 5 Distribuciones del campo superficial de las corrientes (arriba) y de la divergencia horizontal de la velocidad (abajo), para un viento del Este de 16 m/s

La velocidad más alta considerada en este estudio fue de 16 m/s. En la Fig. 5 se ofrecen las distribuciones superficiales para esta velocidad que, obviamente, representan la etapa más avanzada de desarrollo cinemático. La profundidad de influencia friccional oscila entre 349,3 y 362,3 m, de allí que el campo de corrientes se desvíe de la situación característica de aguas profundas (corrientes de 24,1-24,3 cm/s; u,v~17, 1-17,2 cm/s) en toda la plataforma continental. Sobre el talud continental, los vectores de corrientes tipifican a las aguas profundas, en dirección y magnitud; entre el borde de la plataforma y 100 m se observa un ligero cambio en dirección, pero la celeridad permanece casi igual; entre 100 y 50 m la magnitud decrece un tanto, pero el ángulo entre la corriente y el viento es mucho menor; a menos de 50 m la corriente es muy lenta y casi zonal, especialmente en el Banco de Los Testigos. El efecto del Valle de Carúpano es muy conspicuo, ya que la profundidad de su eje varía desde más de 100 m a menos de 25 m. El cambio más abrupto en el campo de corrientes se produce a ambos lados del borde de la plataforma, por la mayor pendiente del fondo en la parte superior del talud. En esta región se producen los valores más altos de la divergencia ($>10^{-5}$seg^{-1}), tal como lo refleja la cercanía entre isolíneas. Se puede hablar entonces de una divergencia de inicios del talud, ya que el eje de máxima divergencia sigue ese contorno batimétrico. Al oeste de 63° W, los valores de la divergencia aumentan desde el sur hasta el borde del área de estudio, en donde queda abierto el núcleo principal. La tasa más rápida de dicho aumento se observa entre 63°25' W y 63°35' W, mientras que las isolíneas están más espaciadas a ambos lados. Entre 63°20' W y la longitud media de Testigo Grande, las isolíneas se propagan al sur, circundan dos núcleos menores a 11°05' N y 11°25' N – a lo largo del meridiano 63°10' W – regresan al norte y, finalmente, giran al oeste. Esta es claramente una divergencia superficial inducida por las islas y se halla acoplada a la divergencia de inicios del talud. Al este de 63° W, la banda de divergencia no está expuesta en su lado norte, sus isolíneas son cerradas y los valores máximos se hallan en tres núcleos separados; además, el eje de divergencia máxima muestra una inclinación ESE a partir de 62°30' W. Hay otro núcleo de divergencia, con su centro a 11°05' N; 62°05' W, asociado a la forma de "S" que allí tiene la curva de 100 m. La divergencia costera es ahora menos intensa y sus valores máximos se encuentran en puntos discretos, incluyendo la esquina suroriental del área estudiada. Se puede decir que hay una única zona de convergencia, amplia y de magnitud menor a la de las divergencias adyacentes. Los valores y gradientes mayores de la convergencia se encuentran en el lado debarlovento de Los Testigos. En esta zona, al igual que al este de la Isla de Margarita, la convergencia es atribuible principalmente al apilamiento de agua causado por el flujo zonal medio, mientras que en otras partes parece estar vinculada a transportes de masa de agua en dirección normal.

La Fig. 6 ha sido preparada para intentar atribuir un significado físico a las descripciones cinemáticas, en términos de procesos oceánicos reales. En ella se ofrecen las distribuciones meridionales de la profundidad media, del componente E-W de la corriente media y de la divergencia horizontal de la velocidad, para una celeridad de viento de 16 m/s. Los perfiles del fondo fueron obtenidos de las profundidades medias asignadas a los distintos cuadrados y, por ende, son más suaves que los del océano real. Las corrientes fueron promediadas de los valores a ambos lados de la sección escogida y sólo se presenta el componente E-W pues se considera que basta para explicar la variabilidad del campo de flujo. La sección a lo largo de 63°30' W está suficientemente alejada de Los Testigos, de modo que los efectos de estas islas son insignificantes. De sur a norte, el fondo desciende hacia el Valle de Carúpano y luego se hace más somero y plano hasta el borde de la plataforma. Las corrientes más fuertes (~20 cm/s) se producen en la zona donde se inicia el talud, con un máximo secundario (~14 cm/s) en el Valle de Carúpano, valores de poco más de 10 cm/s a mitad de la plataforma, y una disminución progresiva hacia el litoral. En la distribución de la divergencia se distingue una zona máxima en los inicios del talud, valores pequeños cerca de la costa, y una convergencia intercalada a mitad de plataforma. La sección a lo largo de 63°10' W atraviesa el Banco de Los Testigos por el lado de sotavento, lo cual confiere al fondo la silueta de un domo, con su punto más somero a 11°15' N. Las corrientes superficiales decrecen en forma apreciable sobre las aguas someras de mediados de la plataforma pero, por lo demás, el flujo zonal es similar al de la sección anterior. Entre 10°51' N y 11°01' N, se encuentra una zona de convergencia, al norte de la cual hay una ancha región en donde la divergencia del lado de sotavento de Los Testigos se fusiona con la divergencia de inicios del talud. La sección a 63°05' W corta el Banco de Los Testigos por su lado debarlovento

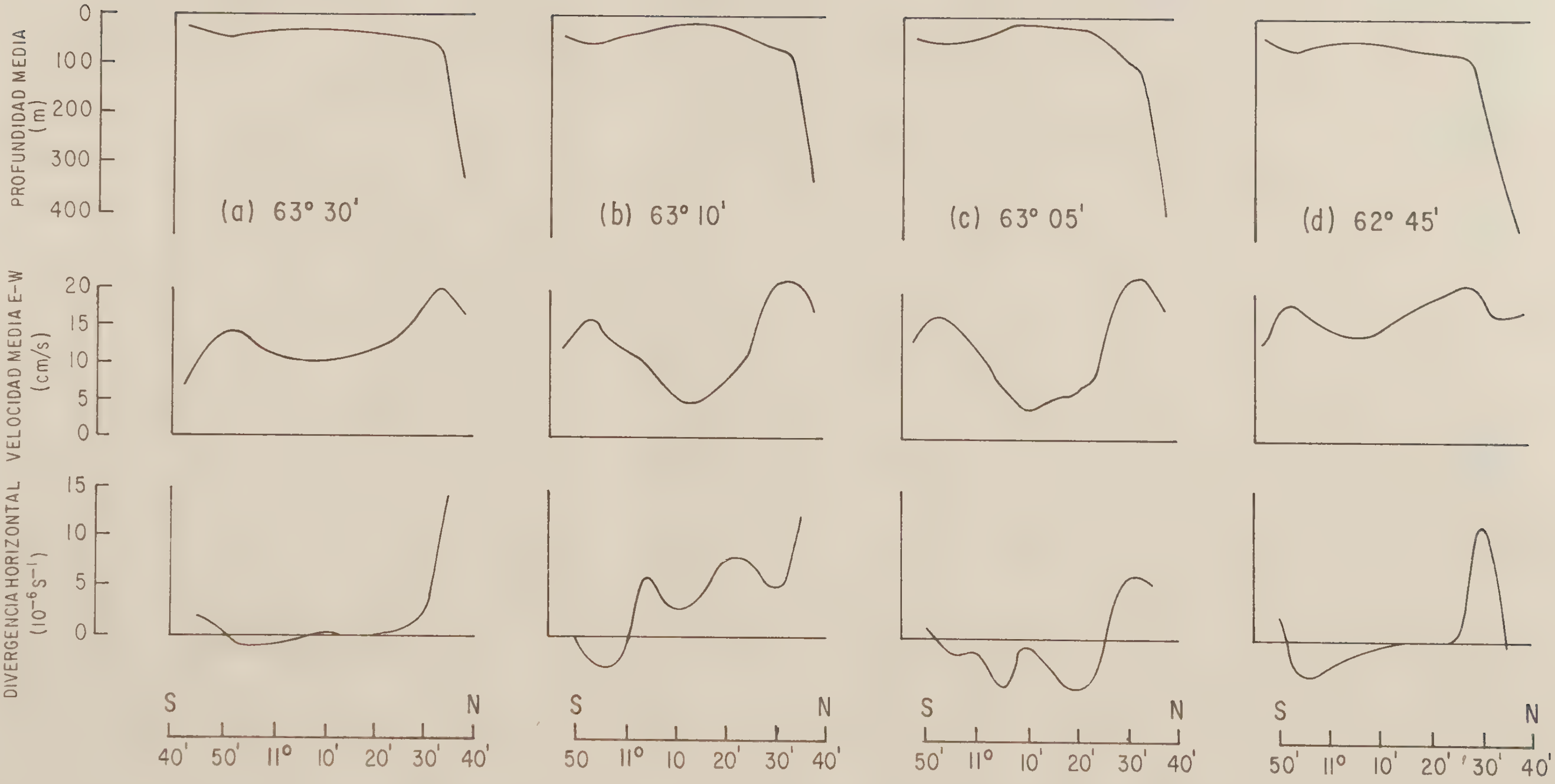

Fig. 6 Distribuciones meridionales de la profundidad media, del componente E-W de las corrientes medias y de la divergencia horizontal de la velocidad, a lo largo de las longitudes 63°30' W, 63°10' W, 63°05' W y 62°45' W

y la configuración del fondo, al igual que la distribución de las corrientes, son visiblemente similares a las de la sección a 63°10' W. Sin embargo, la distribución de la divergencia difiere notablemente, ya que la zona de convergencia intercalada se une a la que aparece en el lado debarlovento de Los Testigos. La divergencia de inicios del talud no alcanza valores tan elevados como en las secciones restantes. La sección a lo largo de 62°45' W es la menos afectada por Los Testigos, debido a encontrarse aguas arriba y a buena distancia de esas islas. Las corrientes exhiben los mismos rasgos cualitativos, pero su magnitud no es menor de 13 cm/s en ningún lugar y los máximos del Valle de Carúpano e inicios del talud alcanzan a 18 y 21 cm/s, respectivamente. La divergencia costera es seguida por una zona de convergencia y, más al norte, por la divergencia de inicios del talud. En esta última, el máximo está completamente encerrado, tal como lo indica el descenso de la curva hacia una divergencia de cero.

La deflección que sufren las corrientes al penetrar al Mar Caribe, intensifica la banda de divergencia y la orienta en sentido WNW, es decir, en dirección similar a la que se evidencia en nuestra Fig. 5. Las Figs. 15 y 16 de Ljöen y Herrera (1965), muestran el alineamiento WNW de las isolíneas, a 0 y 20 m de profundidad, durante la temporada de surgencia de abril de 1963. Los rasgos cinemáticos superficiales también concuerdan con los movimientos verticales de las aguas de la región. El desarrollo de zonas de divergencia y convergencia en los lados de sotavento y barlovento de las islas, respectivamente, indican el ascenso de aguas al oeste del Banco de Los Testigos y su hundimiento al este del mismo. Nuestros resultados coinciden cualitativamente con los obtenidos por Hart y Currie (1960) y Bang (1971), en sus investigaciones de la Corriente de Benguela, al igual que con el tratamiento teórico de Hill y Johnson (1974). Así, se puede indentificar una zona interior de surgencia discontinua (nuestra banda de surgencia costera), la cual es confirmada por las observaciones de aguas más frías en sectores de las penínsulas de Araya y Paria (Fukuoka, 1965; Griffiths y Simpson, 1972). Más hacia el norte, se encuentra una amplia región de convergencia, seguida por la banda principal de divergencia en donde se producen intensos procesos estacionales de surgencia. En lo que respecta a la circulación de las masas de agua, se han identificado la corriente a lo largo de la costa y la contracorriente por debajo del borde de la plataforma continental (Febres y Herrera, 1975, 1978).

5. AGRADECIMIENTOS

Nuestra sincera gratitud al Sr. Isaías Velásquez por sus excelentes ilustraciones y al Sr. Adonay Pernía por sus reproducciones fotográficas.

6. REFERENCIAS

Bang, N.D., 1971 The southern Benguela Current region in February, 1966. Part 2. Bathythermography and air-sea interactions. Deep-Sea Res., 18:209-24

Deacon, E.L., 1962 The drag of the wind on the sea. In Proceedings of the Symposium on Mathematical Hydrodynamical Methods of Physical Oceanography, Hamburg. Mitt. Inst.Meereskd.Univ.Hamb., (1):385-98

Ekman, V.W., 1905 On the influence of the Earth's rotation on ocean currents. Ark.Mat.Astron. Fys., 2:1-53

Febres Ortega, G.A. y L.E. Herrera, 1975 Interpretación dinámica de algunas de las características oceanográficas de la Fosa de Cariaco, Mar Caribe. Bol.Inst.Oceanogr.Univ.Oriente, 14(1):3-29

__________, 1978 Circulación y transporte de masa de agua en el Caribe Suroriental. FAO Fish. Rep., (200) Suppl.

Fukuoka, J., 1965 Coastal upwelling near Venezuela. 1. Year to year change of upwelling. Bol.Inst.Oceanogr.Univ.Oriente, 4(2):223-33

Griffiths, R.C. y J.G. Simpson, Afloramiento y otras características oceanográficas de las
1972 aguas costeras del nordeste de Venezuela. Proyecto MAC-PNUD-FAO. Ser.Recurs. Explot.Pesq.Invest.Pesq.Minist.Agric.Cría, Venez., (2):72 p.

Hart, T.J. y R.I. Currie, The Benguela Current. Discovery Rep., (31):123-298
1960

Herrera, L.E. y G.A. Febres Ortega, Seasonal variations of the Eastern Venezuela upwelling
1975 system. Paper presented to the Third International Symposium on Upwelling Ecosystems, Kiel, 25-28 August 1976, sponsored by the Institut für Meereskunde an der Universität Kiel

__________, Procesos de surgencia y de renovación de aguas en la Fosa de Cariaco, Mar
1975a Caribe. Bol.Inst.Oceanogr.Univ.Oriente, 14(1):31-44

Hill, R.B. y J.A. Johnson, A theory of upwelling over the shelf-break. J.Phys.Oceanogr.,
1974 4:19-26

Ljøen, R. y L.E Herrera, Some oceanographic conditions of the coastal waters of Eastern
1965 Venezuela. Bol.Inst.Oceanogr.Univ.Oriente, 4:7-50

Neumann, G. y W.J. Pierson, Principles of physical oceanography. Englewood Cliffs, New
1966 Jersey, Prentice-Hall, 545 p.

Schmidt, W., Wirkungender ungeordneten Bewegungen im Wasser der Meere und Seen. Ann.Hydrogr.
1917 Marit.Meteorol., 45:367-81, 431-46

Shaffer, G., A theory of time-dependent upwelling induced by a spacially- and temporally-
1972 varying wind with emphasis on the effects of a seabreeze-land breeze cycle. Kiel.Meeresforsch., 28:139-61

Smith, R.L., Upwelling. Oceanogr.Mar.Biol., 6:11-46
1968

Thorade, H., Die Geschwindigkeit von Triftströmingen und die Ekman'sche Theorie. Ann.Hydrogr.
1914 Marit.Meteorol., 42:375

A DESCRIPTION OF THE CIRCULATION OBSERVED IN THE EASTERN GULF OF MEXICO DURING CICAR SURVEY MONTH II, MAY 1972

by

W.J. MERRELL, JR.
NSF/IDOE
Washington D.C., 20550, U.S.A.

J.M. MORRISON and W.D. NOWLIN, JR.
Department of Oceanography
Texas A. & M. University
College Station, Texas 77843, U.S.A.

R.L. MOLINARI
NOAA/AOML
Miami, Florida 33149, U.S.A.

I.H. BROOKS and R. YAGER
Nova University
Dania, Florida 33004, U.S.A.

CONTENTS

1. INTRODUCTION
2. CIRCULATION PATTERN
3. WATER MASSES, VERTICAL DISTRIBUTIONS
4. TRANSPORT
5. ACKNOWLEDGEMENTS
6. REFERENCES

Abstract

During CICAR Survey Month II, May 1972, a coordinated effort to describe the circulation in the eastern Gulf of Mexico was made by four independent research groups. Repeated crossings of the CICAR Standard Sections at the Yucatan Strait and the Straits of Florida were made, while other data were collected within the Gulf.

The Loop Current, entering the Gulf through the Yucatan Strait, was observed to penetrate only as far north as 25°N. A large anticyclonic ring, with radius of at least 210 km, is known to have separated from the Loop during April and was centred at approximately 26°30'N and 87°W.

The distributions of temperature, salinity, dissolved oxygen, silicate and phosphate are related to the current régime and water masses present within the eastern Gulf of Mexico.

For both Straits, calculations of volume transport from the sea surface to the isopycnal $\sigma_t = 27.0$ (approximately 400 to 500 m) were made. The transports through the Florida Straits were determined by the direct method using dropsondes. Geostrophic transports were referenced to directly measured surface velocities within the Yucatan Straits. When averaged over one month these transport estimates (with error of ± 10 percent) agreed well and gave a mean value of $22 \times 10^6 m^3 sec^{-1}$.

During the month, three sections were occupied across the Loop Current within the Gulf of Mexico. One of these sections was repeated four times. Geostrophic transport estimates were made relative to the bottom, or the greatest depth sampled on a section. These crossings gave an average value of $30 \times 10^6 m^3 sec^{-1}$ for the Loop Current within the Gulf of Mexico. The average transport above $\sigma_t = 27.0$ mg cm^{-3} was $24 \times 10^6 m^3 sec^{-1}$.

Calculations of the geostrophic transport of the anticyclonic ring were also made relative to 1 000 db. The average transport was 29 x $10^6 m^3 sec^{-1}$ for two crossings of the ring. Above σ_t = 27.0 mg cm^3, the average ring transport was 23 x$10^6 m^3 sec^{-1}$.

Resumen

En mayo de 1972, segundo mes de las ICCRA, cuatro grupos independientes de investigadores trabajaron coordinadamente para describir la circulación de las aguas en la parte oriental del Golfo de México, recorriendo repetidamente las secciones-tipo de las ICCRA del Estrecho de Yucatán y de los Estrechos de la Florida, al mismo tiempo que recogían otros datos dentro del Golfo.

Se observó que la corriente circular que penetra en el Golfo por el Estrecho de Yucatán sólo llegaba, al norte, hasta los 25°N. Se sabe que en el mes de abril se separó un amplio remolino anticiclónico, de al menos 215 km de radio, que se localizó a 26°30'N y 87°O, aproximadamente.

La distribución de temperaturas, salinidad, oxígeno disuelto, silicatos y fosfatos se relaciona con el régimen de corrientes y las masas de aguas de la parte oriental del Golfo de México.

Se calculó, para ambos estrechos, el transporte volumétrico desde la superficie del mar a la isopicna σ_t = 27,0 (400 a 500 m, aproximadamente). Los transportes por los Estrechos de la Florida se determinaron directamente, utilizando sondas de caída libre. Los transportes geostróficos se compararon con las velocidades superficiales dentro de los Estrechos de Yucatán, medidas directamente: los promedios mensuales de estos cálculos de las velocidades de transportes - con un error de ± 10 % - concuerdan bien, dando un valor medio de 22 x $10^6 m^3 seg^{-1}$.

Durante el mes se hicieron tres secciones transversales de la corriente circular, dentro del Golfo de México, repitiéndose una de ellas cuatro veces. Se hicieron cálculos del transporte geostrófico con relación al fondo o al punto de muestreo de máxima profundidad en una de las secciones. Estos recorridos dieron un valor medio de 30 x $10^6 m^3 seg^{-1}$ para lo corriente circular dentro del Golfo de México; el transporte medio anterior, σ_t = 27,0 mg cm^{-3} fue de 24 x $10^6 m^3 sec^{-1}$.

Se hicieron también cálculos del transporte geostrófico del remolino anticiclónico con respecto a 1 000 db: para dos recorridos del remolino, el transporte medio fue de 29 x $10^6 m^3 seg^{-1}$. Por encima de σ_t = 27,0 mg cm^{-3}, el transporte medio fue de 23 x $10^6 m^3 seg^{-1}$.

1. INTRODUCTION

During CICAR Survey Month II, May 1972, a major field programme was conducted in the eastern Gulf of Mexico. The basic objective of this coordinated effort was to monitor the Loop Current and the currents in the Yucatan and Florida Straits simultaneously. This paper presents a summary of some of the data collected by scientists from the Atlantic Oceanographic and Meteorological Laboratories (AOML) of the National Oceanic and Atmospheric Agency (NOAA), the State University System Institute of Oceanography (SUSIO) of Florida, Nova University and Texas A. & M. University.

Fig. 1 illustrates the cruise coverage and the four sections which were selected for repeated observations. Transports across sections in the Florida Straits and surface velocities in the Yucatan Straits were determined by dropsondes deployed from Nova aircraft. Scientists aboard NOAA's R/V VIRGINIA KEY collected STD and XBT observations during 15 crossings of the Yucatan Strait. In the Florida Straits, Nova's R/V GULFSTREAM completed 16 dropsonde and STD sections at the longitude of Key West. Within the Gulf, scientists aboard SUSIO's R/V BELLOWS and Texas A. & M. University's R/V ALAMINOS surveyed the Loop Current region with STD, XBT and nutrient observations. Moreover, the ALAMINOS occupied one standard section within the Gulf four times during May. The University of Miami and the Instituto de Geofísica of the Universidad Nacional Autónoma de México also conducted cruises in the region during May. However, their observations are not used in this overview.

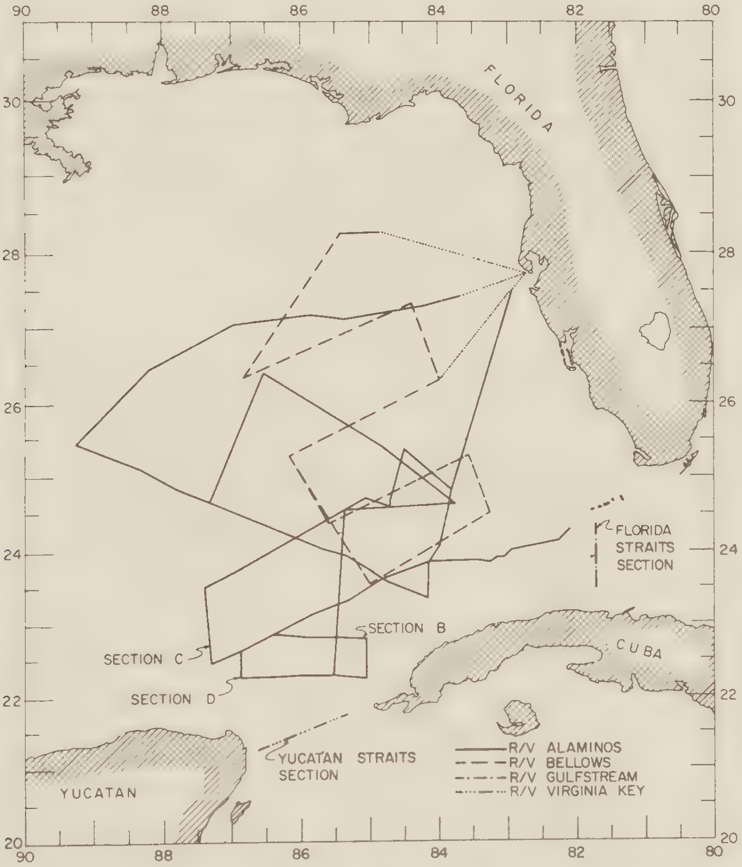

Fig. 1 Combined cruise tracks for the R/V ALAMINOS, R/V BELLOWS, R/V GULFSTREAM and R/V VIRGINIA KEY for the 1972 field programme

The original data may be found in technical reports distributed by the various institutions or be obtained upon request from the scientists involved. The data collected from the ALAMINOS have been distributed as Data Report 73-10T of the Texas A. & M. Research Foundation (Morrison, Merrell and Nowlin, 1973). Molinari (1974) has distributed the data from the R/V VIRGINIA KEY and R/V BELLOWS as a NOAA technical memorandum.

Several papers have already been written using data collected during CICAR Survey Month II. Brooks and Niiler (1975) reported on simultaneous measurements of the current and density fields of the Florida Current at the section between Key West, Florida, and Matanzas, Cuba. Molinari and Yager (1976) have described the average hydrographic conditions of a section across the Yucatan Straits. Morrison and Nowlin (1976) relate the nutrient and dissolved oxygen concentrations in the eastern Gulf to the Loop Current and anticyclonic current rings. They also give some estimates of the variability of both the property distributions and relative geostrophic flow within a period of a few weeks. We intend here to summarize and interrelate much of this information and to add some additional information.

2. CIRCULATION PATTERN

The major features of the current régime of the eastern Gulf of Mexico are the Loop Current (which is comprised of the Yucatan Current and its downstream extension through the Gulf and into the Florida Straits) and the anticyclonic rings which separate from this current. The topography of any isothermal surface between about 10° and 22°C has been shown repeatedly to be a good indicator of the geostrophic current régime in the eastern Gulf of Mexico.

In the spring of 1972, the circulation pattern of the eastern Gulf of Mexico was changing rapidly. A vertical section of temperature along an ALAMINOS section through the Gulf during March is presented in Fig. 2. These data indicate that between 25 March and 27 March 1972 the Loop Current extended well into the Gulf and that no detached ring was present. This picture had changed considerably by May. The repetitive nature of the cruise tracks of the four research vessels involved in CICAR Survey Month II allow us to illustrate (Figs. 3, 4 and 5) the circulation pattern as indicated by the 22°C isothermal surface, for three separate periods during May.

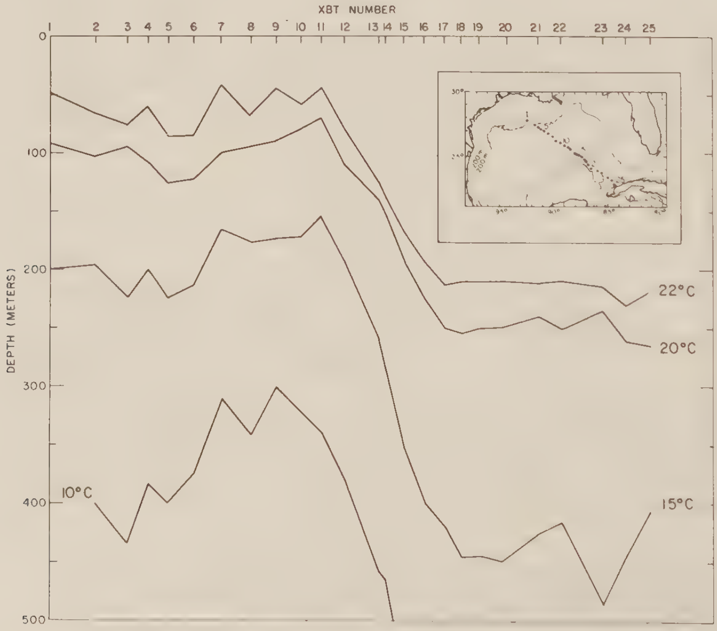

Fig. 2 Vertical section of temperature (°C) for an ALAMINOS section through the Gulf of Mexico in March 1972. The insert shows the position of the XBTs used in constructing this section

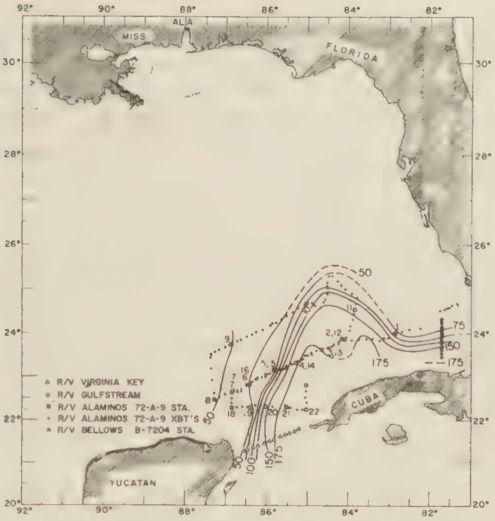
92°
90°
88°
86°
84°
82°
30°
28°
26°
24°
22°
20°
MISS
ALA
FLORIDA
CUBA
YUCATAN
50
75
100
150
175
R/V VIRGINIA KEY
R/V GULFSTREAM
R/V ALAMINOS 72-A-9 STA.
R/V ALAMINOS 72-A-9 XBT'S
R/V BELLOWS B-7204 STA.

Fig. 3 Depth of 22°C isotherm within the eastern Gulf of Mexico using data collected from 2 to 8 May 1972

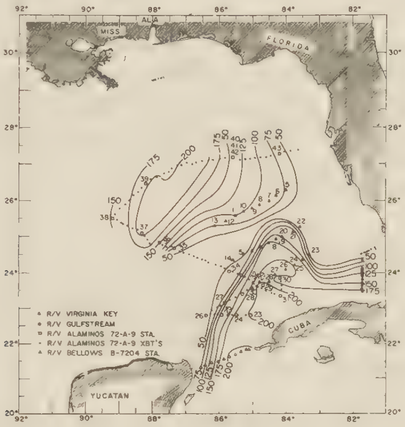
92°
90°
88°
86°
84°
82°
30°
28°
26°
24°
22°
20°
MISS
ALA
FLORIDA
CUBA
YUCATAN
50
75
100
125
150
175
200
R/V VIRGINIA KEY
R/V GULFSTREAM
R/V ALAMINOS 72-A-9 STA.
R/V ALAMINOS 72-A-9 XBT'S
R/V BELLOWS B-7204 STA.

Fig. 4 Depth of 22°C isotherm within the eastern Gulf of Mexico using data collected from 8 to 13 May 1972

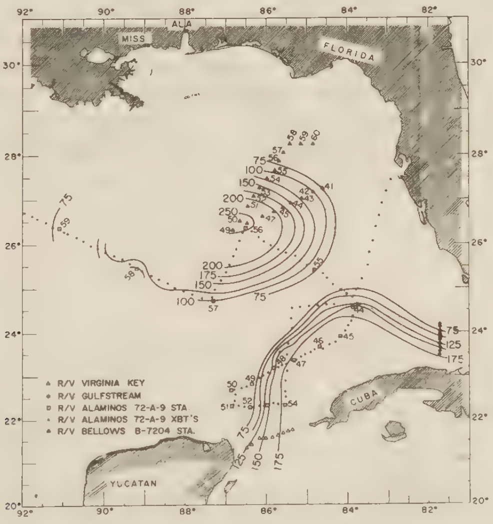
92°
90°
88°
86°
84°
82°
30°
28°
26°
24°
22°
20°
MISS
ALA
FLORIDA
CUBA
YUCATAN
75
100
125
150
175
200
250
R/V VIRGINIA KEY
R/V GULFSTREAM
R/V ALAMINOS 72-A-9 STA
R/V ALAMINOS 72-A-9 XBT'S
R/V BELLOWS B-7204 STA.

Fig. 5 Depth of 22°C isotherm within the eastern Gulf of Mexico using data collected from 16 to 21 May 1972

Some details of the changes in the circulation pattern during May are indicated by comparison of the three figures. The Loop Current did not extend quite as far to the north in the third time period as it did in the first two periods. The observed portion of the detached ring became symmetrical between the second and third observation periods.

3. WATER MASSES, VERTICAL DISTRIBUTIONS

The traditional method of identifying water masses is through the use of temperature-salinity (T-S) relationships. A composite of T-S curves for the eastern Gulf of Mexico is presented in Fig. 6, constructed from STD data collected with the R/V BELLOWS. The principal features are the extreme in salinity associated with the presence of Antarctic Intermediate Water and Subtropical Underwater. Antarctic Intermediate Water is indicated by the salinity minimum near 6.3°C of 34.84-34.88 °/oo and Subtropical Underwater is depicted by the salinity maximum near 22.5°C. This maximum varies from values of 36.75 °/oo within waters bounded by the Loop Current (Caribbean-type) to 36.40 °/oo for waters within the Gulf and outside of the Loop Current (Gulf-type water).

The distributions of temperature and salinity across the Loop Current can best be seen in vertical sections (Fig. 7, from Morrison and Nowlin, 1976). Fig. 7a is a vertical section of temperature constructed from STD and XBT observations taken during the ALAMINOS' first crossing of section C. Isotachs of relative geostrophic speed are presented in the background. This section shows two areas of intense temperature gradients which correspond to the inflow and outflow of the Loop Current. As one would expect, assuming geostrophy and a rather uniform T-S relationship, the regions of greater isotherm slope correspond to the greater current speeds. However, one should remember that section C is not perpendicular to the current (especially the inflow) so we cannot infer maximum speeds from this section. We note that the areas of intense current are relatively narrow and the Loop Current is a transition zone between the relatively warm Caribbean waters and the colder Gulf waters.

Fig. 7b shows values of salinity along the section. The salinity maximum (greater than 36.6 °/oo at 200 m) associated with the Subtropical Underwater delineates the extent of the Caribbean waters. The minimum associated with the Antarctic Intermediate Water occurs at about 700-900 m with the greater depths found at the centre of the Loop reflecting the mass adjustments associated with the current régime.

Other parameters may also be used to depict the distribution of water masses within the Gulf. Vertical distributions of dissolved oxygen, silicate and phosphate for two stations characterizing Caribbean Water (Sta. 36) and Gulf Water (Sta. 33) are presented in Fig. 8. The dissolved-oxygen concentrations show the very distinct differences between these two water masses. Within the Caribbean-type waters a relative maximum of dissolved oxygen is found at approximately 300 m. This maximum denotes the presence of 18°C Sargasso Sea water within the Caribbean-type water (Morrison and Nowlin, 1976). Because of mass field adjustments caused by the Loop Current, the main oxygen minimum occurs at increasing depth as the current is traversed from Gulf Water to Caribbean Water. Distributions of silicate and phosphate are less useful than oxygen for delineating water mass in the Gulf of Mexico. The main features of these distributions are the maxima of silicate and phosphate associated with Antarctic Intermediate Water.

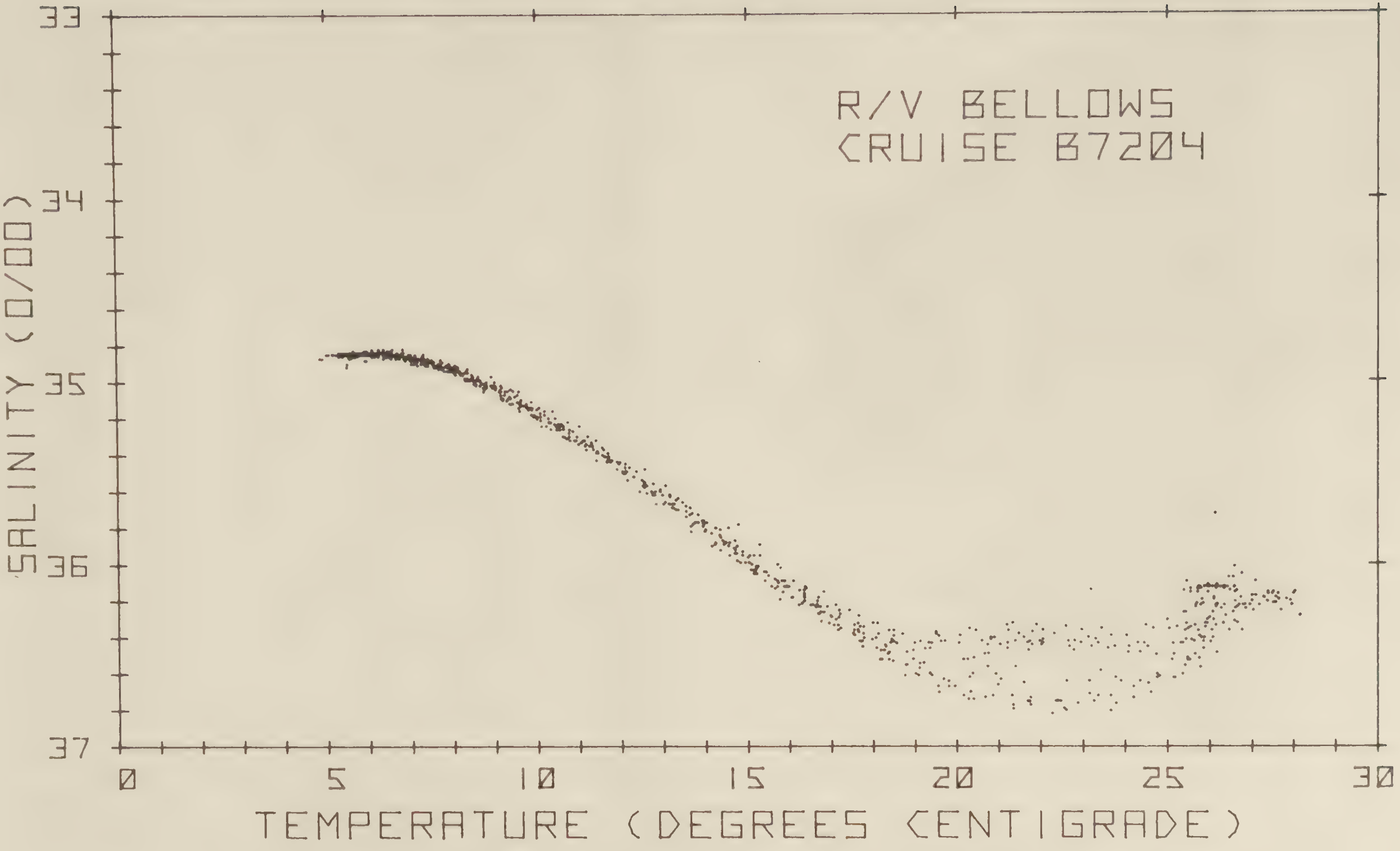

Fig. 6 Temperature-salinity diagram for the eastern Gulf of Mexico using data collected with the R/V BELLOWS during May 1978

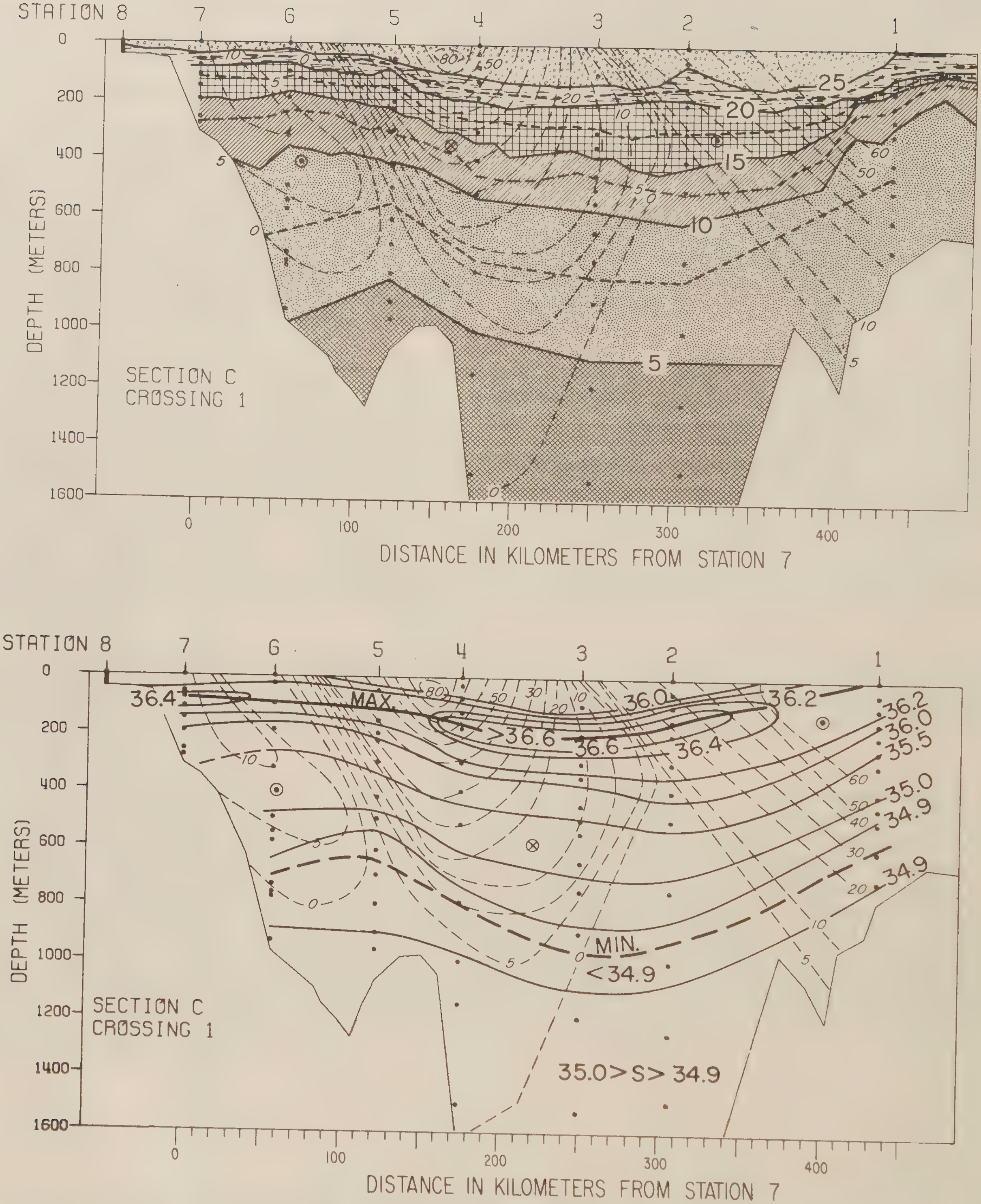

Fig. 7 Vertical sections of: (a) temperature (°C) and (b) Salinity (°/oo) for crossing of section C with superimposed isotachs of relative geostrophic speed (cm/sec). These sections were constructed from ALAMINOS data (after Morrison and Nowlin, 1976)

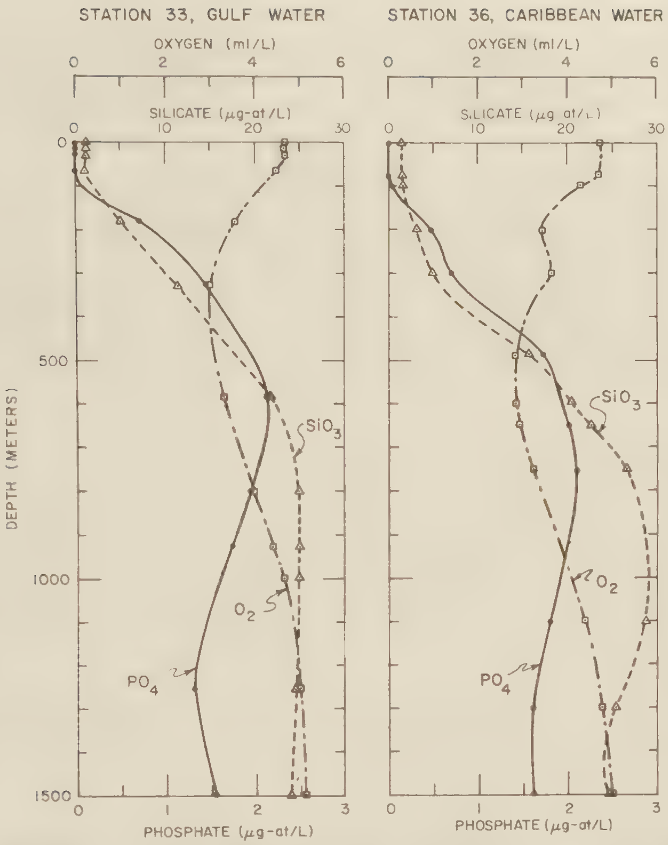

Fig. 8 Vertical distribution of dissolved oxygen (ml/l), silicate (ug-at/l) and phosphate (µg-at/l) for a station within Gulf-type water (ALAMINOS Sta. 33) and a station within Caribbean-type water (ALAMINOS Sta. 36)

4. TRANSPORT

We present in Fig. 9 the volume transport through different sections within the eastern Gulf of Mexico. Downstream distance from the Yucatan Straits is the ordinate and the date of observation is the abscissa. Molinari and Yager (1976) referenced transports in the Yucatan Straits to direct velocity measurements at the surface. Owing to data quality problems, the transport is presented as an average for four periods during May. Morrison and Nowlin (1976) calculated transports for three sections through the Loop Current. These transports were referenced to the deepest observation on each section. The transports through the Florida Straits were determined by the direct method using dropsondes (Brooks and Niiler, 1975). They chose the $\sigma_t = 27.0$ mg cm^{-3} density surface as an arbitrary bottom. Their ensemble averaged transport for May and June is roughly 75 percent of the transport noted by Richardson and Niiler (1969) for the entire water column during the same months in 1966. As the transport values at the Florida Straits were only available down to the $\sigma_t = 27.0$ mg cm^{-3} density surface, all transports given in Fig. 9 are for geostrophic flow between the sea surface and this density surface.

An examination of Fig. 9 shows that, in spite of different procedures and data quality problems, the transports are rather consistent over the observed spatial and temporal scales. The average transports between the surface and $\sigma_t = 27.0$ mg cm^{-3} are 22.3 x 10^{6}m^{3}sec^{-1} at the Yucatan Straits, 24.2 x 10^{6}m^{3}sec^{-1} for the Loop Current and 21.4 x 10^{6}m^{3}sec^{-1} at the Florida Straits. This agreement is remarkable when one considers that the transports calculated for the two Straits may be low, since those sections stopped about 35 km from Cuba and probably do not capture the entire flow. These values yield an average transport between the surface and $\sigma_t = 27.0$ mg cm^{-3} of approximately 23 x 10^{6}m^{3}sec^{-1} for the Loop Current during May 1972.

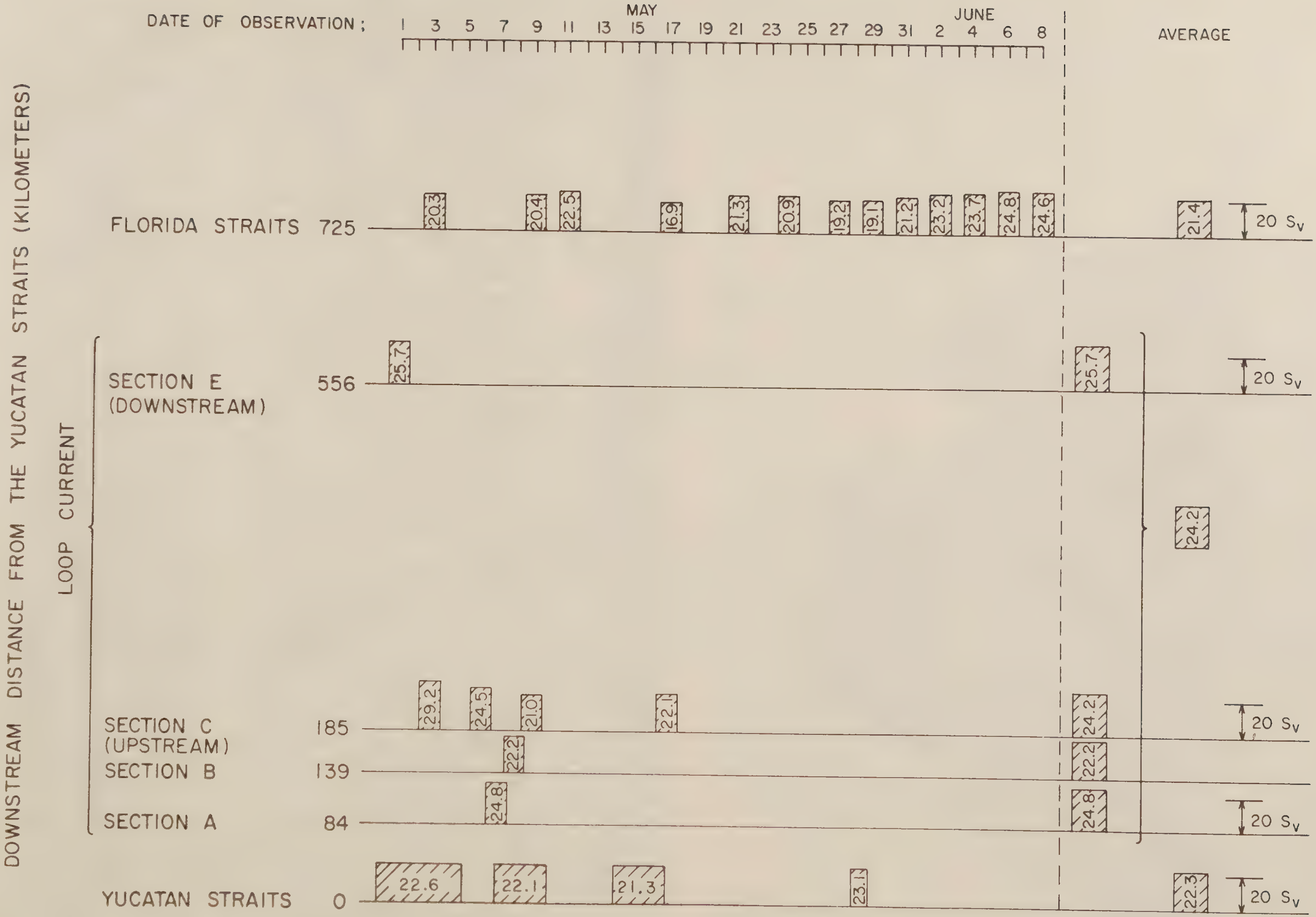

Fig. 9 Relative geostrophic transport (in units of $10^6 m^3 sec^{-1}$) above $\sigma_t = 27.0$ mg cm^{-1} for sections across the Loop Current during May and June 1972

There is some evidence of a slight increase of transport at the Florida Straits late in the record (June) which may correspond to the annual buildup of the Florida Current to a maximum in summer. Otherwise, within observational accuracies, the transports show no trends with time or downstream distance.

Morrison and Nowlin (1976) report that the total average transport of the Loop Current during May 1972, where the deepest observation on each section was used as the reference, was 30 x $10^6 m^3 sec^{-1}$. This agrees well with transport estimates given for this current where a variety of methods of referencing were used. Nowlin and Hubertz (1972) estimated the geostrophic transport within the upper 1 350 db to be 30 x $10^6 m^3 sec^{-1}$. Nowlin and McLellan (1967) calculated a geostrophic transport of 30 x $10^6 m^3 sec^{-1}$ within the upper 1 000 db. Schmitz and Richardson (1968) gave an average transport value of 29.6 x $10^6 m^3 sec^{-1}$ through the Florida Straits using the dropsonde method.

Transports were also calculated for the detached ring using data collected aboard R/V BELLOWS where 1 000 m was chosen as the reference level. For two crossings, the net transports between the surface and 1 000 m were 32.0 x $10^6 m^3 sec^{-1}$ and 26.7 x $10^6 m^3 sec^{-1}$. The average transport is 29.3 x $10^6 m^3 sec^{-1}$ which compares quite well with the transport of the parent Loop Current. The average volume transport between the surface and σ_t = 27.0 x $10^6 m^3 sec$ is 23.1 x $10^6 m^3 sec$, which agrees with this layer during May 1972.

5. ACKNOWLEDGEMENTS

This work was supported by the Office of Naval Research.

6. REFERENCES

Brooks, I.H. and P.P. Niiler, The Florida Current at Key West: Summer 1972. J.Mar.Res., 1975 21:83-92

Molinari, R.L., Data from the NOAA ship VIRGINIA KEY and the SUSIO ship BELLOWS collected 1974 during CICAR Survey Month II. NOAA Tech.Memo., (ERL AOML-22):153 p.

Molinari, R.L. and R.E. Yager, Upper layer hydrographic conditions at the Yucatan Strait 1977 during May 1972. J.Mar.Res., 35(1):11-20

Morrison, J.M. and W.D. Nowlin, Jr., Repeated nutrient, oxygen and density sections through 1977 the Loop Current. J.Mar.Res., 35(1):105-28

Morrison, J.M., W.J. Merrell, Jr. and W.D. Nowlin, Jr., The waters of the eastern Gulf of 1973 Mexico as observed during May 1972: I. Data collected aboard the R/V ALAMINOS. College Station, Texas A. & M. University, Department of Oceanography, Ref. (73-10-T):330 p.

Niiler, P.P. and W.S. Richardson, Seasonal variability of the Florida Current. J.Mar.Res., 1973 31(3):144-67

Nowlin, W.D., Jr. and J.M. Hubertz, Contrasting summer circulation patterns for the eastern 1972 Gulf. In Contributions on the physical oceanography of the Gulf of Mexico edited by L.R.A. Capurro and J.L. Reid. Houston, Gulf Publishing Co., pp. 119-37

Nowlin, W.D., Jr. and H.J. McLellan, A characterization of the Gulf of Mexico waters in 1967 winter. J.Mar.Res., 25:29-59

Schmitz, W.J. and W.S. Richardson, On the transport of the Florida Current. Deep-Sea Res., 1968 15:679-94

WATER EXCHANGE BETWEEN THE ATLANTIC OCEAN AND THE CARIBBEAN SEA

by

W.G. METCALF
Woods Hole Oceanographic Institution
Woods Hole, Massachusetts 02543 U.S.A.

CONTENTS

1. INTRODUCTION
2. MATERIAL AND METHOD
3. RESULTS
4. SUMMARY
5. ACKNOWLEDGEMENT
6. REFERENCES

Abstract

The water exchange between the Atlantic Ocean and the Caribbean Sea through the various major passages among the Antilles Islands is discussed in terms of the distribution of water properties and, in some cases, the pressure fields. Various layers in the water column are defined on the basis of salinity, dissolved oxygen and dissolved silicate as related to the potential temperature (θ). At a depth of about 700 m in the Anegada-Jungfern Passage a shallow inflow changes to a deeper outflow.

At sill level in several passages the current frequently alternates between inflow and outflow. Of a total of approximately 30 Sv ($\times 10^6 m^3 sec$) leaving the Caribbean through the Yucatan Channel, the greatest part enters through the more southerly passages of the Lesser Antilles. The Anegada-Jungfern Passage may serve as an escape valve for water of less than 6°C which enters through various passages but cannot escape through the main exit due to the shallow depths of the Florida Straits.

Resumen

Se discute el intercambio de aguas entre el Océano Atlántico y el Mar Caribe a través de diversos pasos importantes de las islas Antillas, en función de la distribución de las propiedades del agua y, en algunos casos, de los campos de presiones. Se definen varios estratos de la columna de agua, basándose en la salinidad y en el silicato y oxígeno disueltos, referidos a la temperatura potencial (θ). Las aguas someras que entran en el paso de Anegada-Jungfern, a 700 m, aproximadamente, de profundidad, salen a mayor profundidad.

En varios pasos, a nivel de los umbrales, la corriente cambia frecuentemente de sentido: la mayor parte del volumen total aproximado de 30 Sv($\times 10^6 m^3 seg$) de agua que sale del Caribe por el Canal de Yucatán, entra por los pasos meridionales de las pequeñas Antillas. El paso Anegada-Jungfern podría actuar como una válvula de escape de las aguas que, a menos de 6°C, entran por diversos pasos, pero que, a causa de la poca profundidad de los estrechos de la Florida, no pueden salir por la salida principal.

1. INTRODUCTION

The Caribbean work covered in this report started with a cruise in 1970 to the southeastern approaches to the Caribbean Sea aboard the R/V ATLANTIS II. Major cruises were also made in 1972 and 1974 aboard the R/V KNORR interspersed with some smaller cruises. The primary field observations were hydrographic stations and current observations. As shown in Fig. 2, the stations were occupied along both sides of the Antilles Arc, and current meters were moored in several of the deeper passages. Direct current measurements of short duration were made in some of the other passages.

The basic plan for the hydrographic station programme was to sample the water column from surface to bottom along the continental slope in deep enough water to get below the controlling depth of the nearby channels. The stations were spaced roughly 8 km apart across the ends of the channels and between 16 and 24 km apart abreast the islands of the Lesser Antilles. Stations were not occupied in regular sections alongside the large islands of Puerto Rico, Hispaniola and Cuba.

2. MATERIAL AND METHODS

Moored current meters were placed on or near the sills of Grenada Passage, Jungfern Passage and Windward Passage for periods of time ranging up to three months. Direct measurements of currents were made in the St. Vincent Passage, St. Lucia Passage and the Dominica Channel. Reports of much of this work have appeared in the scientific press over the past few years.

One of the main uses to which the hydrographic station data have been put has been the comparison of the water columns on the two sides of the Antilles Arc on the basis of the distribution of temperature, salinity, dissolved oxygen and dissolved silicate using various distinctive features in the water column to identify the several water types found in this area. In many respects, this method borrows heavily from the "Kernschicht" or "Core Method" developed by Wüst and used by him in his classic work on Caribbean circulation (Wüst, 1963 and 1964). Various identifiable layers or "cores" have here been used to look at the water movement between individual stations or in small sections of closely spaced stations across a number of the Antillean Passages rather than look at the broad Caribbean-wide circulation as Wüst has done. By using discrete sets of data gathered within a relatively short period of time by a single group of observers and analysed by uniform techniques throughout, one is able to discern circulation features on a much finer scale than is possible when using much larger numbers of data gathered over a much longer time scale by many different groups of observers using diverse analytical techniques. It should be kept in mind that this finer scale may reflect temporary or transient conditions rather than long term averages.

In dealing with these data, the basic assumption is made that if the water in a given layer is flowing from one region to another, there will be a discernable continuity in the distribution of properties. That is, if the water in a layer at one end of a passage is markedly different from that in the same layer at the other end in the various property interrelationships, it is to be inferred that the water in this layer is not flowing through this channel, at least at the time of the observations. (It is, of course, necessary that the observations be as synoptic as possible to lend validity to this line of reasoning.)

The reverse of this argument is a little more difficult to support without corroborating evidence. That is, if the water types at opposite ends of a passage are very similar, the water may well be flowing through that channel, but this is not necessarily proof that this is the case.

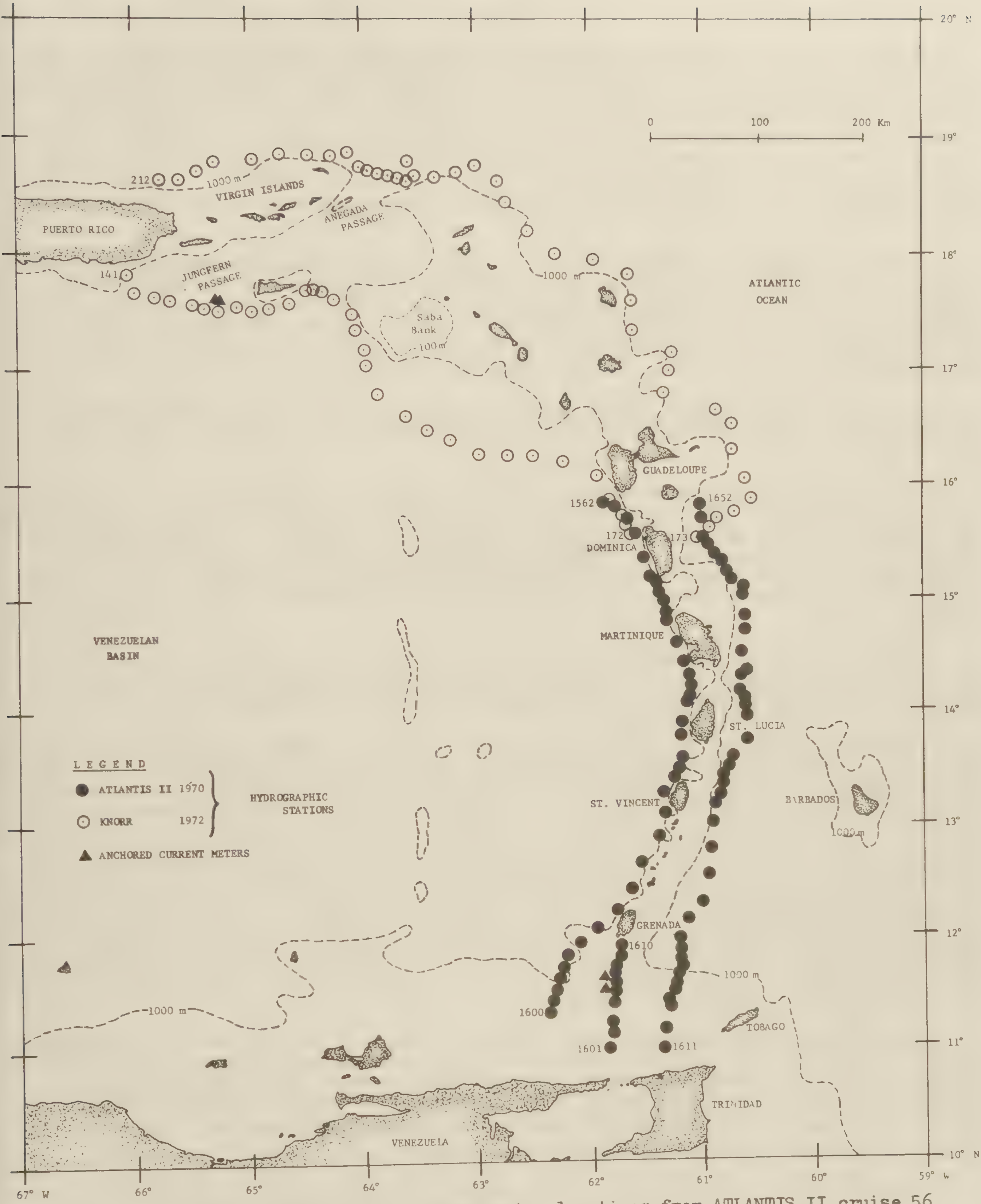
20° N
19°
18°
17°
16°
15°
14°
13°
12°
11°
10° N
67° W
66°
65°
64°
63°
62°
61°
60°
59° W
0
100
200 Km
PUERTO RICO
VIRGIN ISLANDS
ANEGADA PASSAGE
JUNGFERN PASSAGE
212
141
1000 m
Saba Bank
100 m
ATLANTIC OCEAN
GUADELOUPE
1562
1652
172
173
DOMINICA
MARTINIQUE
ST. LUCIA
ST. VINCENT
BARBADOS
GRENADA
1610
1600
1601
1611
TOBAGO
TRINIDAD
VENEZUELA
VENEZUELAN BASIN
LEGEND
● ATLANTIS II 1970
⊙ KNORR 1972
HYDROGRAPHIC STATIONS
▲ ANCHORED CURRENT METERS

Fig. 1 Hydrographic stations and current meter locations from ATLANTIS II cruise 56 (1970) and KNORR cruise 25 (1972)

Another factor to be kept in mind is that certain modifications may take place as the water moves, especially in the case of strong flow through a narrow passage which will probably be accompanied by turbulent mixing. Such a situation would very likely have the effect of blunting or partially eroding away a maximum or minimum core so that it would be less extreme at the downstream end. There is no conceivable way in which a subsurface maximum core of a conservative property could be increased in the course of flowing through a passage. In other words, if the core, whether it be a maximum or a minimum, is slightly less extreme at one end of a channel than at the other, the less extreme end must necessarily be the downstream end.

Stalcup and Metcalf (1972) reported on the direct current measurements carried out during the 1970 cruise. On that cruise, two moorings were placed near the middle of the Grenada Passage with two temperature-recording current meters on each. The recording instruments were 50 and 250 m above the bottom at each site. At the northern site, the current at both levels moved into the Caribbean. At the southern one, the current flowed out of the Caribbean for the first 3 weeks of observations and then turned to flow in.

In the St. Vincent and St. Lucia Passages and the Dominica Channel, current meters were lowered from the ship, sometimes throughout a tidal cycle. Also, free-fall current meters were employed.

In all four of the passages studied, the net flow was into the Caribbean, but in all cases the tidal signal was strong with occasional periods of outflow occurring at some levels. The averages computed by Stalcup *et al.* (1972) showed approximately 10 Sv (x $10^6 m^3 sec$) of inflow in both the Grenada and St. Vincent Passages, 6 Sv in the St. Lucia Passage and a little more than 1 Sv in the Dominica Channel. In the latter case, the flow was so strongly tidal that there is some question as to whether or not there is really any appreciable net inflow.

In other words, of a total of about 34 Sv leaving the Caribbean-Gulf of Mexico area via the Florida Straits (Niiler and Richardson, 1973) roughly 75 percent of the flow can be accounted for in the four southern major passages through the Lesser Antilles.

The station data used in Table 1 and in some of the graphs that follow were from opposite ends of the Anegada-Jungfern Passage and thus are most typical of that specific area. Details can be expected to differ somewhat in other regions. At the deeper levels (below the Antarctic Intermediate Water) the features listed in the table are primarily Atlantic Ocean characteristics. The corresponding layers inside the Caribbean are either missing or at least greatly modified despite the fact that with a sill depth of 1 815 m (Stalcup and Metcalf, 1973) the passage is approximately 1 000 m deeper than the Antarctic Intermediate Water in this area. The observations used are from those stations making up the Antlantic and Caribbean sections for which the geostrophic currents have been computed (see Fig. 2). The information derived from the relationships between the potential temperature and the other observed properties have been correlated with the geostrophic flow layer by layer in an attempt to demonstrate the consistencies or inconsistencies, as the case may be, between the observed distribution of properties and the theoretical currents.

The question of just which stations to choose in carrying out the dynamic computations is not an easy one. The sections across both ends of the passage were some distance from the passage itself and extended well beyond any reasonable delineation of the "entrance". To choose a portion of the longer section which gives the most "realistic" answer according to preconceived ideas of what the flow "should be" has its obvious drawbacks.

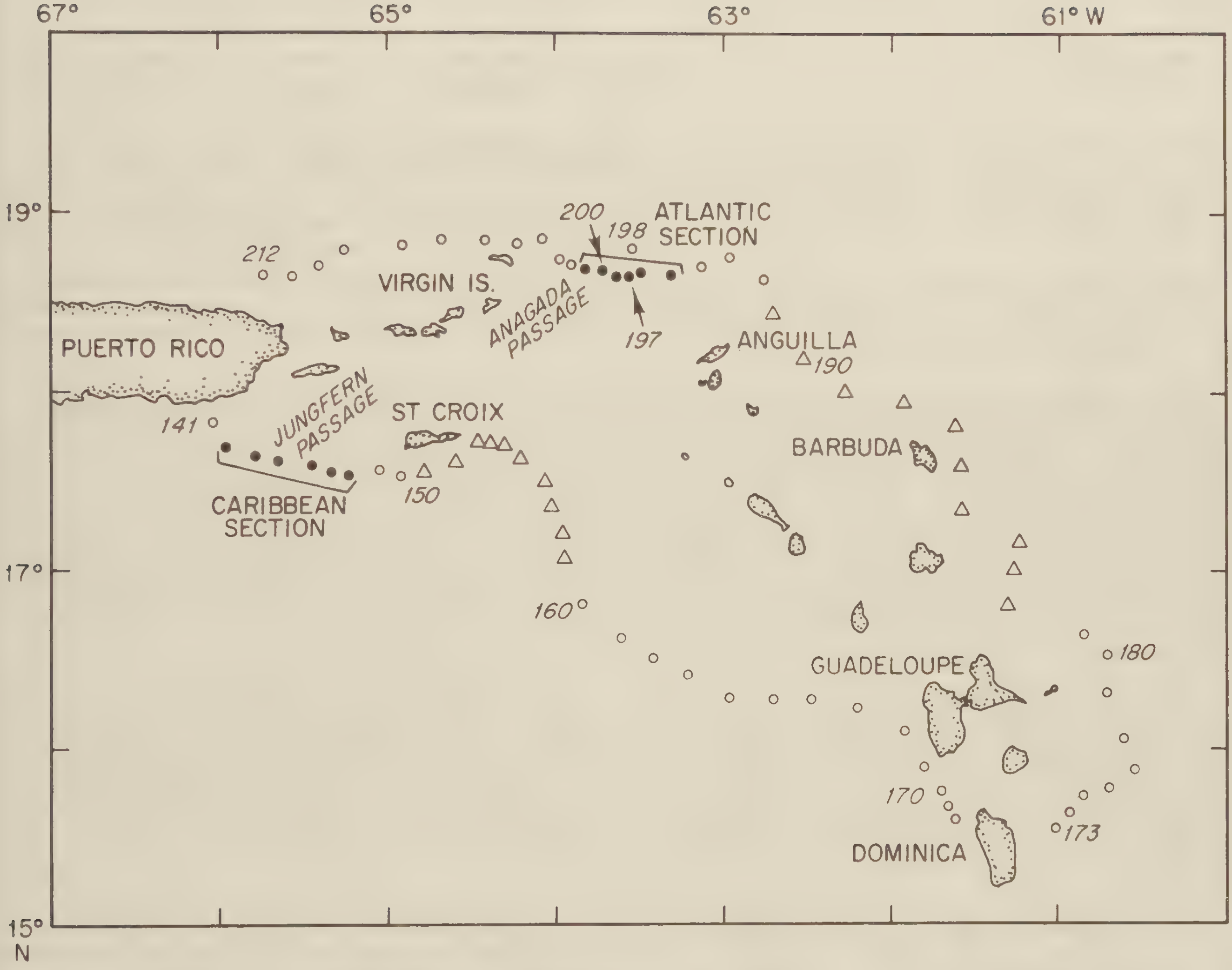
67°
65°
63°
61° W
19°
17°
15° N
212
200
198
ATLANTIC SECTION
VIRGIN IS.
ANAGADA PASSAGE
197
PUERTO RICO
ANGUILLA
190
JUNGFERN PASSAGE
ST CROIX
141
BARBUDA
CARIBBEAN SECTION
150
160
GUADELOUPE
180
170
173
DOMINICA

Fig. 2 Chart of Anegada-Jungfern Passage area showing hydrographic stations occupied on KNORR cruise 25, March-April 1972. Closed circule show Atlantic and Caribbean sections across to the passage for which geostrophic currents were computed and comparison of distribution of properties made. Δ's are those stations east of the passage entrance used in constructing Fig. 6 and discussed in text (from Metcalf, 1976)

TABLE I

Selected layers in the water column

Approximate depth range (m)	Approximate potential temperature range (°C)	Identifying feature	Water type of major feature
0 - 200	27 - 20	Shallow salinity maximum	Sub-tropical Underwater
200 - 400	20 - 14	Oxygen maximum	18° water
400 - 700	14 - 8	Oxygen minimum	Tropical Atlantic Central Water
700 - 1 100	8 - 5	Salinity minimum & silicate maximum	Antarctic Intermediate Water
1 100 - 1 600	5 - 4	Salinity maximum[a/] & decreasing silicate[a/]	North Atlantic Deep Water (upper part)
1 600 - 1 800	< 4	Decreasing salinity[a/] silicate minimum[a/]	North Atlantic Deep Water (lower part)

a/ These features are typically found in the Atlantic and are either missing or are greatly modified in the Caribbean

The computed geostrophic flow is very sensitive to the depth chosen for the reference level, and the basis for choosing this level has never been established to universal satisfaction. On the Jungfern Sill itself we had current meters measuring the flow near the bottom for over a month, and the records showed great variations in both speed and direction at frequencies including seiche periods, semi-diurnal and diurnal tidal periods, and longer periods of the order of days or weeks (Sturges, 1970; Stalcup, Metcalf and Johnson, 1975). There is, of course, much uncertainty as to how rapidly and completely the pressure fields respond to this type of change. In a restricted channel in which seiche and tidal forces provide much of the energy, some of the flow may simply be in response to a hydraulic head which is probably quite inadequately reflected in the pressure field.

Defant (1961) speculated that in a graph in which dynamic height differences between two stations are plotted against pressure, the portion of the curve showing the least gradient might be most closely associated with the level of least motion. Defant may have summed it up best when he wrote (1961/p. 494) "It should be stressed that the choice of such a (reference) surface is always more or less subjective, and such assumptions can only be made plausible by giving proper weight to all the different viewpoints which are in question."

In the present model the 600 decibar surface has been chosen as the reference level. (In this area, the 600 decibar surface is usually within 2 or 3 m of the 600 m level, and for present purposes they are considered to be essentially identical.) This choice of level was based on the following major considerations:

(1) this level fell within the general area of the minimum gradient in the pressure differences between the dynamic heights of adjoining stations in both the Atlantic and Caribbean sections;

(2) it is fairly close to the level (700 m) described by Sukhovey and Metal'nikov (1968) where they found by direct measurements that the current reversed itself from Caribbean inflow in the shallow layers to outflow in the deeper layers;

(3) the computations based on this level yielded results which appeared reasonable from what is known of the currents both at the surface and at the bottom on the Jungfern Sill.

A lack of synopticity in the observations, especially in areas where large variations are common, can blur the picture considerably. In fact, in the case of a long passage such as this one, the variations which normally are found at both ends would probably produce a confusing picture even if the observations were synoptic.

In Table II, the computed geostrophic currents for the various layers in the two hydrographic station sections are listed. The layers will be considered one at a time, and the relationship between the computed currents and the distribution of properties will be discussed.

3. RESULTS

3.1 0 to 200 metre Layer ($\theta = 27^{\circ}-20^{\circ}C$)

Strictly speaking the surface water could be considered a separate water type. It will not be dealt with at great length but it can be said that the surface salinity at the Caribbean end more closely resembles that at the Atlantic end than it does that found at the nearby Caribbean stations off to the east of the passage.

The Pilot Charts (U.S.N. Oceanographic Office, 1969) indicate a surface current setting primarily to the west in both the Atlantic and Caribbean in the general vicinity of the Anegada-Jungfern Passage throughout the year.

Of the 12 monthly charts, only the April one has an arrow in the passage itself signifying a current of unspecified velocity flowing into the Caribbean through this passage 25 to 50 percent of the time. Dietrich (1939) shows a similar current arrow representing a velocity of between 0 and 10 n mi/day (0-21 cm/sec) into the Caribbean along the axis of the passage. Wüst (1964) on the other hand, shows current arrows pointing roughly to the northwest indicating a surface flow more or less out of the Caribbean at a broad angle to the axis of the passage. The computed geostrophic currents in the upper 30 m of the Atlantic and Caribbean sections, based on a reference level of 600 decibars, show velocities of 12.1 and 9.2 cm/sec, respectively, directed into the Caribbean, just about the middle of Dietrich's velocity range.

Below the surface, the upper 200 m layer includes the salinity maximum which Wüst (1964) has called the Sub-tropical Underwater. This apparently is formed by surface evaporation in the sub-tropical Atlantic and spreads widely throughout much of the tropical North Atlantic Ocean and into the Caribbean Sea. In the particular area of this study, the salinity maximum is usually found at a depth of 125 to 175 m. As is seen in Figs. 3, 4 and 5 the θ-S, θ-O_2 and θ-silicate curves in the upper 200 m (above 20°C) for the two sets of stations at opposite ends of the channel are very similar, suggesting relatively unrestricted flow at this level. (The "braided rope" effect in Fig. 5 is an artifact resulting from the rounding off of the silicate values to the nearest whole microgram-atom/l.) For this upper 200 m layer of the water column, the average computed velocities were 12.3 and 8.7 cm/sec of Caribbean inflow across the Atlantic and Caribbean sections, respectively. The corresponding volume transports were 1.38 Sv across each section.

3.2 200 to 400 metre Layer ($\theta = 20^{\circ}-14^{\circ}C$)

In the θ-S diagram (Fig. 3) this layer takes in the upper half of the long straight portion of the curve. This water can be considered Tropical Atlantic Central Water, having θ-S characteristics intermediate between the more saline North Atlantic Central Water and the less saline South Atlantic Central Water (Sverdrup, Johnson and Fleming, 1942). The two sets of θ-S curves show a good deal of overlap, but on the whole the Atlantic observations favour the saltier side. This is taken to indicate that the flow at this level is not quite as free as that in the layer above where the overlap of the two sets of curves was more complete. The saltier Atlantic water coming through the passage between 200 and 400 m mixes at the Caribbean end with slightly less saline water which comes into the Caribbean through some of the more southern passages.

The difference between the Atlantic and Caribbean waters in this layer is more clearly apparent in the $\theta.O_2$ diagram (Fig. 4). The distinguishing feature of this layer is the oxity maximum associated with the 18° Water described by Worthington (1959) as forming in the northern Sargasso Sea in late winter and appearing as a wedge of high oxity water throughout a wide area of the Sargasso Sea at all seasons. Observations from further south along the Antilles Arc (Metcalf, Stalcup and Zemanovic, 1973) show that the oxity maximum in the Atlantic fades out before reaching the more southern passages, and the Anegada-Jungfern Passage is the only one through which any appreciable amount of this water appears to enter the eastern Caribbean. The lower oxity in this layer at the Caribbean end of the passage plus the relatively high silicate (Fig. 5) both are in line with the θ-S picture in suggesting that the flow is not as great as in the shallow layer. This conclusion receives support from the geostrophic computations which show velocities of 5.8 and 5.5 cm/sec into the Caribbean in the Atlantic and Caribbean sections, respectively. The corresponding volume transports are .65 and .87 Sv into the Caribbean.

TABLE II

Geostrophic current velocities and volume transports in various layers at the Atlantic and Caribbean ends of the Anegada-Jungfern Passage based on the 600 decibar reference level

Layer (m x 100)	Temp. range (°C)	Atlantic Section			Caribbean Section		
		Av. vel. (cm/sec)	Dir.[a]	Vol. transp. (Sv)	Av. vel. (cm/sec)	Dir.[a]	Vol. transp. (Sv)
0-2	27-20	12.3	Inflow	1.38	8.7	Inflow	1.38
2-4	20-14	5.8	Inflow	.65	5.5	Inflow	.87
4-7	14-8	0.6	Inflow	.06	0.8	Inflow	.20
7-11	8-5	0.5	Outflow	.11	0.7	Outflow	.22
11-16 11-12[b]	5-4	0.8	Outflow	.36	1.0	Outflow	.84
12-13		0.7	Outflow		0.8	Outflow	
13-14		0.6	Outflow		0.6	Outflow	
14-15		2.8	Outflow		12.5	Outflow	
15-16		6.8	Outflow		13.9	Outflow	
16-18	<4	5.5	Outflow	.23	4.8	Inflow	.06 (1 600-1 700 m only)
			Total inflow	2.09			2.51
			Total outflow	.70			1.06
			Net inflow	1.39			1.45

[a] Inflow indicates a flow into the Caribbean Sea

[b] Because of the large velocity gradients between 1 100 and 1 600 m, the velocities are listed for 100 m increments

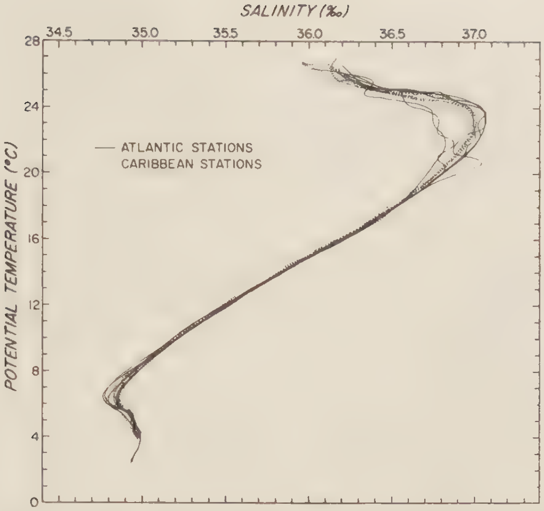

Fig. 3 Potential temperature-salinity curves comparing conditions at opposite ends of the Anegada-Jungfern Passage (from Metcalf, 1976)

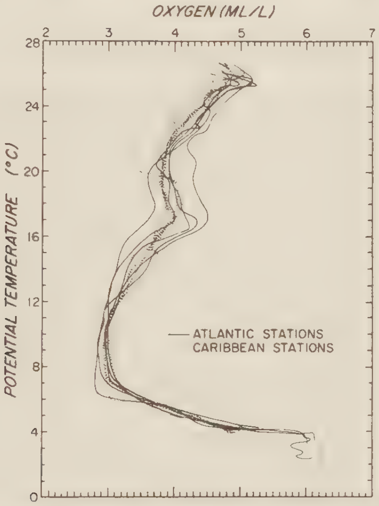

Fig. 4 Potential temperature-oxity curves comparing conditions at opposite ends of the Anegada-Jungfern Passage (from Metcalf, 1976)

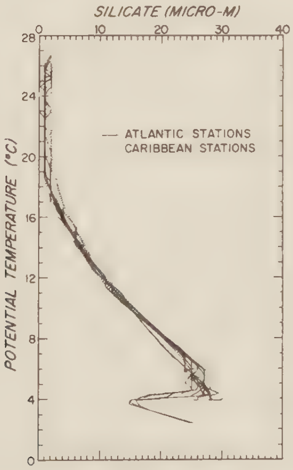

Fig. 5 Potential temperature-silicate curves comparing conditions at opposite ends of the Anegada-Jungfern Passage (from Metcalf, 1976)

3.3 400 to 700 metre Layer (θ = 14°-8°C)

This layer, also a part of the Tropical Atlantic CentralWater, shows a continuation of the long straight portion of the θ-S curve (Fig. 3) mentioned in connexion with the layer immediately above it. The most pronounced features between 400 and 700 m is the oxity minimum layer (see Fig. 4) This feature is found as a very low oxity tongue extending out from the western bulge of Africa at roughly 15° north latitude and is present very widely throughout the Atlantic Ocean (Sverdrup et al., 1942). Other than this feature, there is very little that can be said about this layer on the basis of the distribution of properties. The conditions inside and outside the Caribbean are very similar - a situation which has led in other layers to the assumption of unrestricted flow. However, other considerations discussed earlier have led to the adoption of the 600 m level as the reference level for the geostrophic computations.

It naturally follows from placing the reference level within this layer that the geostrophic flow across both the Atlantic and Caribbean sections would be small. The computed currents were into the Caribbean with velocities of less than 1 cm/sec in both sections. The volume transports were 0.06 Sv and 0.20 Sv for the Atlantic and Caribbean sections, respectively. Considering the uncertainties inherent in the methods used, it is felt that these transport figures are of limited significance and that the net water flow through the passage in the 400 to 700 m layer is essentially zero.

3.4 700 to 1 100 metre Layer (θ = 8°-5°C)

This layer takes in the salinity minimum core that is the identifying feature of the Antarctic Intermediate Water[1] which sinks below the surface at the Antarctic convergence (Sverdrup et al., 1942). The silicate maximum at a very slightly lower temperature and correspondingly greater depth also can be traced to this convergence. In the South Atlantic, Fuglister (1960) shows the salinity core to be below 34.24 °/oo at 32° South Latitude. To the north, the core becomes gradually modified through mixing, and at 16°N the minimum is shown by Fuglister (1960) to be just under 34.70 °/oo close to the Antilles. Salinity profiles presented by Metcalf, Stalcup and Zemanovic (1971) and bathymetric data from Stalcup, Metcalf and Zemanovic (1971) show that the salinity minimum core lies very close to the sill depth of the deeper passages through the Antilles Arc south of the Anegada-Jungfern region. The Caribbean profiles of Fuglister (op. cit.) show the lowest salinities in this layer in the eastern Caribbean transects to be in the southern half of the Venezuelan Basin.

In Fig. 3, the broad range of salinity minimum observations at each end of the Anegada-Jungfern Passage is quite enlightening. The salinity profiles presented by Metcalf et al. (1973, their Fig. 6) show that the salinity in the minimum core in the Atlantic increases from south to north. In the area near the entrance to the Anegada Passage, these values are mostly in the mid-34.80's. Near the centre of the Atlantic section at Station 200 the salinity falls as low as 34.763 °/oo and it is believed that this represents outflow from the Caribbean. In the Caribbean salinity profile of Metcalf et al. (1973, their Fig. 5) the salinity minimum core in the area near the entrance to the Jungfern Passage shows values mostly in the mid-34.70's. A value as high as 34.860 °/oo was found at Station 146, representing inflowing Atlantic Water. Inshore, the wide range of salinity values in the minimum core at both ends indicates both inflow and outflow in this layer.

Although not giving as clear a picture as the θ-S diagram, both the θ-O_2 and the θ-Silicat curves (Figs. 4 and 5) indicate a complicated circulation pattern in this layer. In both diagrams, the wide spread of both the Atlantic and the Caribbean envelopes suggest both inflow and outfow in this layer. (Outflow shows clearly in the vertical profiles presented by Metcalf et al., 1973 and their Figs. 8 and 10.)

1/ This is referred to by Wüst (1963) as Sub-Antarctic Intermediate Water

The suggestion was made by Pillsbury (1890) that water in the Anegada-Jungfern Passage flows into the Caribbean along the western side of the channel and out at the eastern. In the present data, however, both the higher salinity in the inflow from the Atlantic and the lower salinity in the outflow from the Caribbean were found near the centre stations of the sections across the ends of the channel. It is more probable that the current is not limited to the sides of the channel but rather that frequent reversals in direction of the flow in the main channel account for the observed distribution of water properties rather than the pattern of flow proposed by Pillsbury.

The question of to what degree or at what rate the geopotential topography adjusts to changing situations is particularly bothersome in an area like this, confined as it is by the local geography. It is felt intuitively that the rate of adjustment of the pressure field probably is slow enough to smooth out short term periodic changes such as tidal or seiche factors and internal waves. For longer period fluctuations there would presumably be more complete adjustment, but at what point this becomes important is difficult to ascertain. In the present case, the geostrophic transport across both sections was a small outflow of 0.11 and 0.22 Sv for the Atlantic and Caribbean sections, respectively, with corresponding velocities of 0.5 and 0.7 cm/sec. No particular claim is made as to whether this represents a long or short term average or merely was the case at the time the observations were made. It is simply pointed out that the distribution of properties shows that inflow as well as outflow occurs in this layer of the water column.

3.5 1 100 to 1 600 metre Layer ($\theta = 5.0^{\circ}-4.0^{\circ}C$)

In this layer the transition is completed on the Atlantic side of the Antilles Arc from the low salinity-high silicate core of the Antarctic Intermediate Water to the high salinity-low silicate core of the North Atlantic Deep Water. On the Caribbean side of the island chain the situation is very different. In the scatter diagrams of Fig. 6, the θ-S and θ-Silicate relationships below 8°C are shown for 10 stations from KNORR cruise 25 on either side of the Antilles Arc well to the southeast of the entrances of the Anegada-Jungfern Passage. The point of this selection is to demonstrate the situation in both the Atlantic and the Caribbean away from the immediate influence of any interchange of water below about 5.5°C which might be taking place through the only passage in the Antilles Arc deep enough to permit it.

In the scatter diagrams it can be seen that a small hiatus exists between the Atlantic and Caribbean salinity points in the 5.5° to 4° range (thus extending up somewhat into the layer above). This was also noted by Sturges (1965) and Worthington (1966) who took it to be evidence of an absence of Caribbean inflow in this layer. Sturges further hypothersized outflow on the basis of the pressure gradients below 7 000 m. An even wider hiatus is found in the silicate scatter diagram - a situation also remarked upon by Richards (1958) as well as Worthington (1966).

There is no passage into the eastern Caribbean other than the Anegada-Jungfern which is deep enough to permit an exchange of water in this temperature range between the Atlantic and Caribbean, and it is apparent from the diagrams that there is no single water type on the Atlantic side of the Antilles Arc that can be considered the progenitor of the Caribbean water of this temperature. It follows that the Caribbean water in this layer must be formed within the Caribbean Sea itself, apparently from the mixing of the waters above and below it each of which is of Atlantic origin. For lack of a better term, this might be called Caribbean Mid-Water and can be considered a distinct water type.

In the θ-S and θ-Silicate diagrams for the sections of hydrographic stations across the ends of the Anegada-Jungfern Passage (Figs. 3 and 5) no such marked hiatuses exist. In fact, both the Atlantic and the Caribbean observations show the characteristic patterns of the Caribbean Mid-Water from about 5.5° all the way down to just above 4°C. This can only mean that Caribbean Mid-Water is flowing out of the Caribbean through this passage.

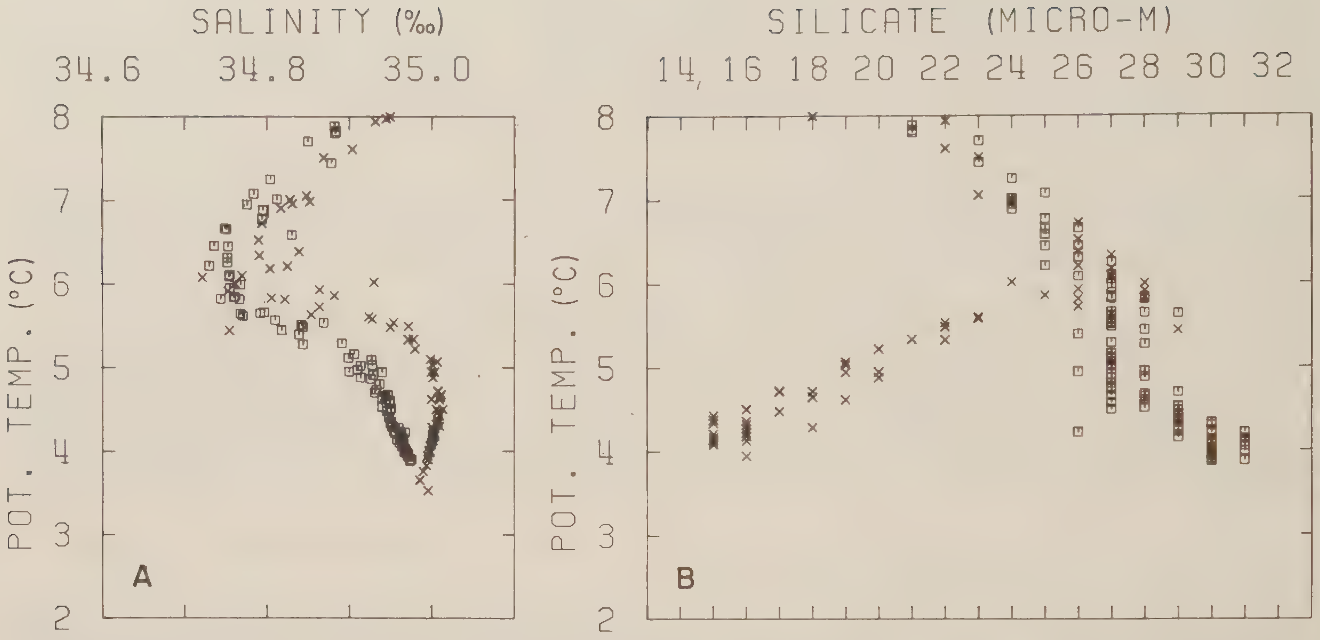

Fig. 6 Potential temperature-salinity (left) and -silicate (right) scatter diagrams from Caribbean (□) and Atlantic (✕) stations lying east of the entrances to Anegada-Jungfern Passage. Hiatus between the two sets of observations below 5.5°C are discussed in text (from Metcalf, 1976)

The role played by the Caribbean Mid-Water in the circulation of the Caribbean Sea may be an important one. Worthington (1971) pointed out that no water colder than 6°C leaves the Caribbean through the Florida Straits, and he further remarked that "water which does not leav the Caribbean cannot enter it in large quantities". Yet water below 6°C has been observed entering the Caribbean through the more southerly passages through the Antilles Arc (Stalcup et al., 1972) and especially through the Anegada-Jungfern Passage itself (Sturges, 1970 and 1975; Stalcup et al., 1975). It would appear that at least a portion of this deep cold inflow may mix with layers above it to form the Caribbean Mid-Water which leaves the Caribbean at this intermediate depth through the Anegada-Jungfern Passage.

This conjecture receives support from the computed geostrophic currents which show outflow in both the Atlantic and Caribbean sections with volumes of 0.36 and 0.84 Sv, respectively. Because the velocity gradient with depth is great, and the cross section of the channel decreases rapidly with depth, the average velocity for the layer as a whole is not very meaningful. Table 2 lists the computed velocities by 100 m depth increments. Velocities as high as 13.9 cm/sec were computed.

3.6 1 600 to 1 800 metre Layer ($\theta = < 4.0^\circ C$)

Although this layer is only 200 m thick, it is an important layer in the circulation picture and has received considerable attention in the recent past in connexion with studies of deep water renewal in the Caribbean basin (see Sturges, 1970 and 1975; Ross and Mann, 1971; Stalcup et al., 1975). It is in this layer that direct current measurements were made at 8 and 58 m above the bottom on the sill of the Jungfern Passage (sill depth 1 815 m) at the time the hydrographic station observations discussed in this report were being made (Stalcup et al., 1975) thus providing an independent check on the currents to compare with those derived from the geostrophic computations.

In the Atlantic section the salinity, which reached a small maximum in the layer above this as the core of the North Atlantic Deep Water, diminishes in the $<4.0^\circ$C layer while the silicate rises sharply as the proportion of Antarctic Bottom Water increases with decreasing temperature. As with the layer above, the situation in the Caribbean is quite different. The potential temperature does not go below 3.88°C in the Caribbean section, and the deep salinity at about 34.97 $^\circ/oo$ is only 0.01 or 0.02 $^\circ/oo$ lower than that in the Atlantic at corresponding temperatures. It is the deep silicate in the Caribbean that most clearly distinguishes it from the Atlantic, being generally >30 µg-atoms/l while the Atlantic water of the same temperature is about half that amount. Richards (1958) pointed to the high silicate concentrations in the deep Caribbean as being indicative of very slow renewal of the deep water.

In the Caribbean section, the single pair of stations representing this layer extended to only 1 700 m, so the deep computations are not complete. The current records mentioned above show the current to be increasing with depth in the 50 m layer immediately above the bottom at the time the hydrographic stations were occupied. Those records showed Caribbean inflow of roughly 20 cm/sec on 1 April 1972 when the hydrographic stations were occupied. The geostrophic computations show an inflow of 4.8 cm/sec with a volume transport of 0.06 Sv in the 1 600-1 700 m layer, and it should be emphasized that this probably represents less than half of the total geostrophic flow in this section.

During 10 April 1975 the current meters registered outflow from the Caribbean of roughly 3-5 cm/sec, and the Atlantic hydrographic stations occupied on that day show a geostrophic outflow of 5.5 cm/sec between 1 600 and 1 800 m with a corresponding volume transport of 0.23 Sv. As was described earlier, it is uncertain whether or not the geopotential topography can adjust rapidly enough to the current changes at tidal frequencies to give meaningful computed currents. It is encouraging, however, to note that the computations in these cases yield currents that are at least in the same direction as the observed flow, and in one of the two cases the velocities are essentially identical. In the other case, the velocities are at considerable variance, but it is felt that this is no more than is to be expected considering the roughness of the method.

The θ-S and θ-O_2 observations in the $<4^\circ$C range, unlike those in the 4-5°C range, give no indication of the flow in either direction through this passage. A single station in the Caribbean section (Sta. 143) shows a slight decrease in silicate below 4°C which is probably a small indication of an inflow of Atlantic water here. Stalcup *et al.* (1975) found that the low silicate values originating in the Atlantic could not be detected more than about 8 km inside the Caribbean from the Jungfern Sill even during periods when the inflow on the sill of close to half a knot was being recorded by the current meters on the sill.

4. SUMMARY

This review of the recent work we have done on the Atlantic-Caribbean water exchange is necessarily a qualitative one to a great extent. Until the time comes when large numbers of current meters can be placed throughout the water columns in all the major passages and left in place for periods of time of a year or more, relatively little quantitative information can be obtained. This would be a terribly expensive programme. Nevertheless, we feel that the approach taken here of correlating a small number of direct current measurements with the distribution of water properties and pressure fields has significantly advanced our understanding of the circulation of the Caribbean area as a whole, and has supplied rough figures concerning the magnitude of the flow.

It looks as if the major part of the water leaving the Caribbean via the Yucatan Channel has entered through the southeastern passages through the Lesser Antilles. The Anegada-Jungfern Passage, though the deepest and one of the widest of the passages, appears to be of relatively minor importance in the overall Caribbean circulation leading to the formation of the Florida Current. Its chief contribution to Caribbean circulation is, it is believed, its controlling role in the renewal of the deep water in the two main eastern basins (Colombian and Venezuelan). Its other important role is that of an escape valve which may account for the fact that a considerable amount of water below 6°C enters the Caribbean through several passages but cannot be found leaving it through the Yucatan Channel and the Florida Straits. This water forms a layer called the Caribbean Mid-Water - a distinct water type which as far as these data show escapes only through this passage. The actual volume of this flow ranges from roughly 0.5 to 1.0 Sv, but it is quite possible, of course, that this may be a highly irregular flow. The present data shed little light on this question.

Portions of this work are included in a paper entitled "Caribbean-Atlantic water exchange through the Anegada-Jungfern Passage" by W.G. Metcalf which has recently been accepted for publication in the Journal of Geophysical Research (copyrighted by American Geophysical Union).

This research was sponsored by the National Science Foundation under Grants DES 71-00262 (formerly GA 27939) and OCE 75-19729.

5. ACKNOWLEDGEMENT

This paper was previously published in Journal of Geophysical Research Vol.81 6401-09 pp. A version was previously published as Atlantic Water Exchange through the Anegada-Jungfern Passage.

6. REFERENCES

Defant, A., Physical oceanography. London, Pergamon Press, Vol.1:729 p.
1961

Dietrich, G., Das Amerikanische Mittelmeer. Z.Ges.Erdkd.Berl., 1939(3-4):108-30
1939

Fuglister, F.C., Atlantic Ocean Atlas of temperature and salinity profiles and data from
1960 International Geophysical Year, 1957-58. Atlas Ser.Woods Hole Oceanogr.Inst., (1)

Metcalf, W.G., Caribbean-Atlantic water exchange through the Anegada-Jungfern Passage.
1976 J.Geophys.Res., 81:640-1

Metcalf, W.G., M.C. Stalcup and M.E. Zemanovic, Hydrographic station data from ATLANTIS II
1971 Cruise 56 to the southeastern approaches to the Caribbean Sea, February-April 1970. Woods Hole Oceanogr.Inst.Ref., (71-13):179 p. (Unpubl.MS)

__________, Hydrographic station data, Caribbean Sea, KNORR Cruise 25. Woods Hole
1973 Oceanogr.Inst.Ref., (73-10):135 p. (Unpubl.MS)

Niiler, P.O. and W.S. Richardson, Seasonal variability of the Florida Current. J.Mar.Res.,
1973 31(3):144-67

Pillsbury, J.E., The Gulf Stream, methods of the investigation and results of the research.
1890 Rep.U.S.Coast Geod.Surv., (1890) Append.10

Richards, F.A., Dissolved silicate and related properties of some western North Atlantic
1958 and Caribbean waters. J.Mar.Res., 17:449-65

Ross, C.K. and C.R. Mann, Oceanographic observations in the Jungfern Passage and over the
1971 sill into the Venezuelan Basin, February, 1968. In Unesco/FAO Symposium on Investigations and Resources of the Caribbean Sea and Adjacent Regions, Willemstad, Curaçao, 18-26 November 1968. Paris, Unesco, pp. 171

Stalcup, M.C. and W.G. Metcalf, Current measurements in the passages of the Lesser Antilles.
1972 J.Geophys.Res., 77(6):1032-49

Stalcup, M.C. and W.C. Metcalf, Bathymetry of the Sills for the Venezuela and Virgin Islands
1973 Basins. Deep-Sea Res., 20(8):739-42

Stalcup, M.C., W.G. Metcalf and R.G. Johnson, Deep Caribbean inflow through the Anegada-
1971 Jungfern Passage. J.Mar.Res., 33 Suppl.:15-35

Stalcup, M.C., W.G. Metcalf and M. Zemanovic, Current measurements in the Lesser Antilles.
1971 Woods Hole Oceanogr.Inst.Ref., (71-51) (Unpubl.MS)

Sturges, W., Water characteristics of the Caribbean Sea. J.Mar.Res., 23(2):147-62
1965

__________, Observations of deep water renewal in the Caribbean Sea. J.Geophys.Res.,
1970 75(36):7602-10

__________, Mixing of renewal water flowing into the Caribbean Sea. J.Mar.Res.,
1975 33 Suppl.:117-30

Sukhovey, V.F. and A.P. Metal'nikov, The deep-sea water exchange between the Caribbean
1968 Sea and Atlantic Ocean. Oceanology, 8:159-64

Sverdrup, H.U., M.W. Johnson and R.H. Fleming, The oceans, their physics, chemistry and
1942 general biology. New York, Prentice-Hall Inc., 1087 p.

U.S. Naval Oceanographic Office, Atlas of Pilot Charts of Central American waters and South
1969 Atlantic Ocean. Publ.U.S.Naval Oceanogr.Off., (106)

Worthington, L.V., The 18° Water in the Sargasso Sea. Deep-Sea Res., 5:297-305
1959

__________, Recent oceanographic measurements in the Caribbean Sea. Deep-Sea Res.,
1966 13:731-9

__________, Water circulation in the Caribbean and its relationship to the North Atlantic
1971 circulation. In Unesco/FAO Symposium on Investigations and Resources of the
Caribbean Sea and Adjacent Regions, Willemstad, Curaçao, 18-26 November 1968,
Paris, Unesco, pp. 181

Wüst, G., On the stratification and circulation in the cold water sphere of the Antillean-
1963 Caribbean basins. Deep-Sea Res., 10:165-87

Wüst, G. and A. Gordon, Stratification and circulation in the Antillean-Caribbean Basins.
1964 Part 1. Spreading and mixing of the water types with an oceanographic atlas.
New York, Columbia University Press, 201 p.

TIDES IN THE GULF OF MEXICO AND CARIBBEAN SEA

by

H.O. MOFJELD[1]
Atlantic Oceanographic and
Meteorological Laboratories
Miami, FL 33149
U.S.A.

M. WIMBUSH[2]
Physical Oceanography Laboratory
NOVA University
Diana, FL 33004
U.S.A.

CONTENTS

1. BACKGROUND
2. INSTRUMENTATION
3. OBSERVED TIDES
4. LOW-FREQUENCY PRESSURE CONTINUUM
5. DISCUSSION
6. ACKNOWLEDGEMENTS
7. REFERENCES
APPENDIX

Abstract

Offshore pressure gauges were deployed in the Gulf of Mexico and the Caribbean Sea to measure tides and bottom pressure continua. The observations, in the Gulf of Mexico, indicate that it has a Helmholtz resonance with a period of 1.6 d. While the lack of confidence limits on theoretical cotidal charts hinders the comparison between theories and observations, the latter tend to support a model with direct astronomical forcing. The observations in the Caribbean Sea verify the general features of the theoretical cotidal charts. At a six-month-long station in the eastern Caribbean, bottom pressure fluctuations with 4 to 5 d period are coherent and in phase with atmospheric waves in the Easterlies. Inverse barometer compensation appeared less complete in this semi-enclosed sea, spanned by weather systems, than in the open ocean. An appendix gives corrections to the response method of tidal analysis, the procedure for converting the results to harmonic constants with error estimates, and tables of analytical results.

---

[1] Present address: Pacific Marine Environmental Laboratory, Environmental Research Laboratory, National Oceanic and Atmospheric Administration, Seattle, WA 98105, U.S.A.

[2] Present address: Graduate School of Oceanography, University of Rhode Island, Kingston, RI 02881, U.S.A.

Resumen

Se colocaron indicadores de presión en alta mar en el Golfo de México y Mar Caribe para medir las mareas y los continuos de presión al fondo. Las observaciones indican que el Golfo de México tiene una resonancia del tipo Helmholtz con un período de 1,6 días. La ausencia de límites de confianza en cartas teóricas de mareas dificulta la comparación de teorías y observaciones, pero los datos tienden a apoyar un modelo de regulación astronómica directa. Las observaciones en el Mar Caribe confirman los rasgos generales de la cartas teóricas. En una estación en el Caribe oriental ocupada durante seis meses, las oscilaciones de presión al fondo con un período de 4-5 días, coincidieron con las ondas atmosféricas en los vientos alisios de levante. En este mar semi-encerrado, atraversado integramente por sistemas atmosférios, la compensación barométrica inversa es aparentemente más débil que en el océano abierto. Un apéndice del trabajo incluye (i) correcciones al método de regresión (response method) de análisis de mareas, (ii) el procedimiento utilizado para convertir los resultados en constantes armónicas con estimación de los errores, y (iii) tablas de resultados analíticos.

1. BACKGROUND

To test theoretical models for tides and free oscillations in the Gulf of Mexico and the Caribbean Sea, offshore pressure observations were made (Fig. 1 and Table I) during 1971 to 1973 as part of the Cooperative Investigation of the Caribbean and Adjacent Regions (CICAR). Subsequent observations in 1974 are also considered.

1.1 Gulf of Mexico

Coastal observations (Zetler and D. Hansen, 1972) indicate that the daily tides dominate the western and northern Gulf of Mexico, even though the semi-daily tides are favoured both by co-oscillation with the Atlantic and by direct astronomical forcing. In these regions, the daily amplitudes and phases are relatively constant, and the phases are nearly opposite (180° difference in phase) to the corresponding phases in the western Atlantic and the eastern Caribbean Sea. The transition in phase occurs in the vicinity of amplitude nodes in the Straits of Florida and the Yucatan Channel.

According to Marmer (1954) a resonance of the gulf with a period near the daily tidal band causes the anomalously large daily tides. Platzman (1972) developed a theoretical model of the Gulf with realistic bathymetry and, using a resonance iteration technique, found a Helmholtz resonance with 0.88 d period and a spatial distribution similar to the daily tides. By assumption, this model requires surface elevation nodes in the Straits of Florida and in the Yucatan Channel. K. Hansen (1974) used a Lanczos process to compute resonances (free oscillations) in the combined Gulf of Mexico-Caribbean Sea system with nodes required in the Straits of Florida and at the Antilles. The lowest gravitational resonance has a period (1.04 d) near the daily tidal band but lacks a node in the Yucatan Channel; the next highest resonance has a node in the channel but has a period (0.67 d) nearer the semi-daily band. The mismatch of period and spatial distributions may be caused by the node at the Antilles not seen in the daily tides.

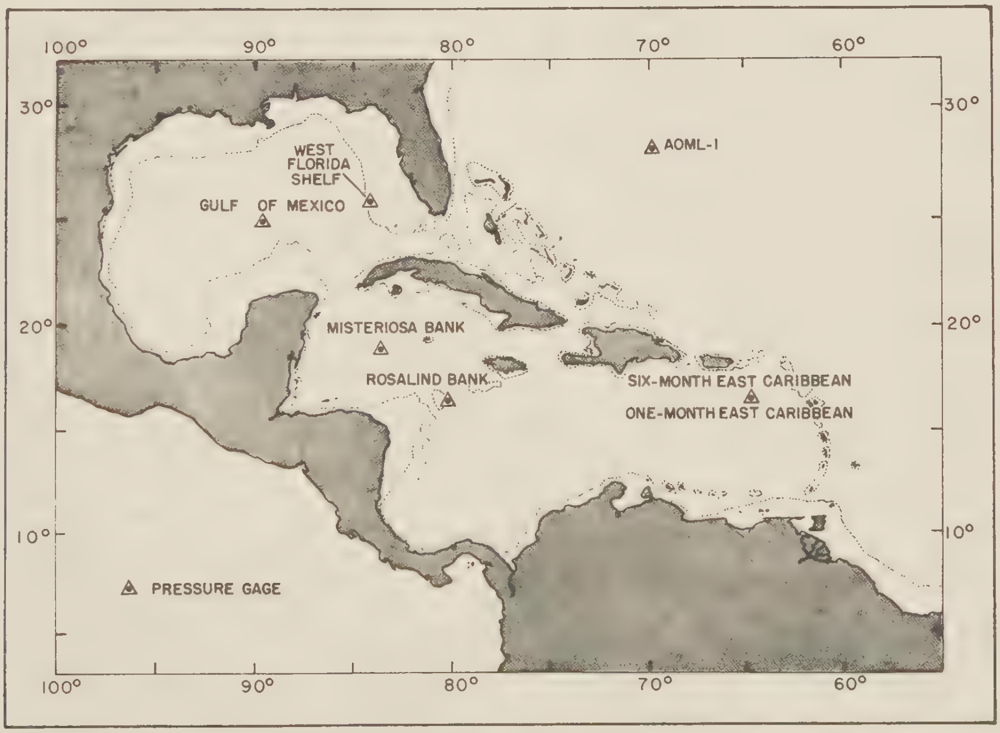

Fig. 1 Chart showing bottom pressure gauge and current meter stations in the Gulf of Mexico and Caribbean Sea. Also shown is the AOML-1 station in the western Atlantic Ocean

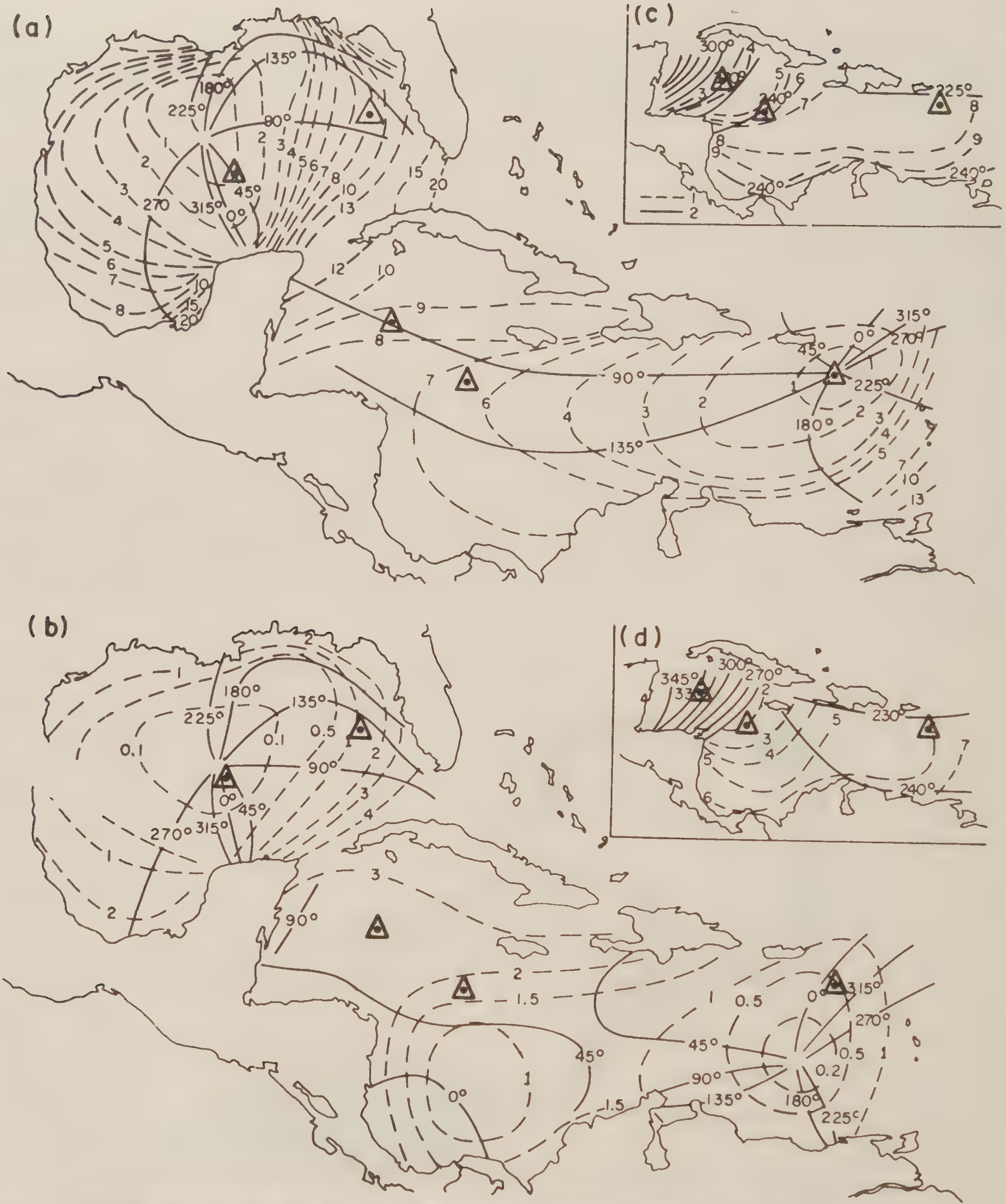
(a)
135°
180°
225°
80°
2
3
4
5
6
7
8
10
13
15
20
45°
0°
315°
270
12
10
9
8
7
6
4
3
2
1
90°
135°
45°
0°
315°
270
225°
180°
10
13
(c)
300°
4
5
6
7
240°
225°
8
9
240°
1
2
(b)
2
1
180°
225°
135°
0.1
0.5
2
90°
3
4
0°
45°
270°
315°
2
3
90°
1.5
0.5
45°
0°
1
1.5
90°
135°
180°
225°
315°
270°
0.2
(d)
345°
300°
270°
2
3
4
5
6
230°
7
240°

Fig. 2 Cotidal charts for the Gulf of Mexico and Caribbean Sea from the theoretical model by Michaelov, Melishko and Shcheveleva (1969). Cophase lines (solid) give the Greenwich phase lag in degrees; co-amplitude lines (dashed) give amplitudes in centimetres (a) semi-daily M_2 tide, (b) semi-daily S_2 tide, (c) daily K_1 tide, (d) daily O_1 tide

TABLE II

Standard deviation of harmonic constants from successive 29-d harmonic analyses at nearby shore and bottom-mounted tide stations

	Magueyes Island[a/] (17°58.3N, 67°02.8W)				Six-month east Caribbean (16°32.5N, 64°52.9W)			
	Mean		Standard Dev		Mean		Standard Dev	
	H (cm)	G (deg)	H (cm)	G (deg)	H (cm)	G (deg)	H (cm)	G (deg)
N_2	0.40	52.0	0.34	66.1	0.58	128.4	0.07	5.5
N_2	0.70	52.5	0.34	38.0	0.51	155.5	0.10	13.4
S_2	0.71	348.0	0.30	30.4	1.36	45.4	0.24	10.4
K_1	7.92	233.3	0.73	5.6	8.68	232.7	0.21	1.1
O_1	5.36	227.3	0.30	3.4	6.24	227.2	0.22	1.2

[a/] From Zetler and Cummings (1972)

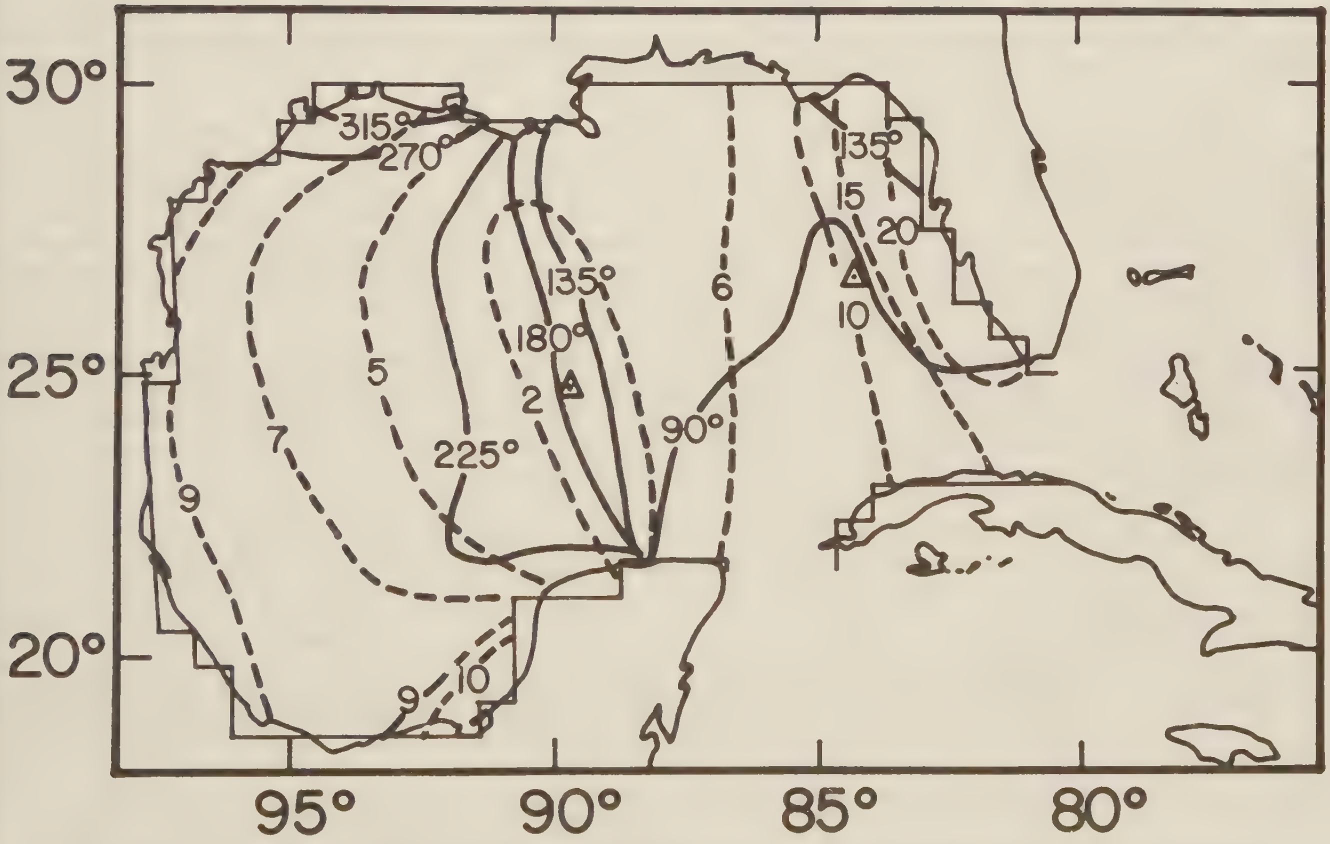

Fig. 3 Semi daily M_2 cotidal chart for the Gulf of Mexico from the theoretical model by Grijalva (1971). Cophase lines (solid) give the Greenwich phase lag in degrees; co-amplitude lines (dashed) give amplitudes in cm

TABLE I

Bottom pressure stations

Station	Latitude	Longitude	Depth (m)	Starting	Ending
Misteriosa Bank	18°52.9 N	83°48.3 W	22	15 July 71	13 Aug 71
Rosalind Bank	16°36.5 N	80°20.2 W	31	15 July 71	14 Aug 71
East Caribbean					
One-month	16°30.1 N	64°54.7 W	3 768	15 Sept 71	19 Oct 71
Six-month	16°32.5 N	64°52.9 W	3 990	17 May 72	9 Nov 72
Central Gulf of Mexico	24°46.1 N	89°38.9 W	3 461	11 Oct 72	18 Jan 73
West Florida Shelf	26°42.4 N	84°15.0 W	154	6 April 74	18 Nov 74

Theoretical work on daily tides *per se* in the Gulf of Mexico is limited to a model by Grace (1932) of K_1 tide. The model, which uses a small number of constant depth sections, correctly predicts a slowly varying K_1 tide in the western Gulf of Mexico but incorrectly predicts a large amplitude gradient across the Yucatan Channel.

Several models exist for the semi-daily tides in the Gulf of Mexico. Using W. Hansen's method (1952, 1962), Michaelov, Melishko and Shcheveleva (1969) computed cotidal charts (Fig. 2) for the combined Gulf of Mexico-Caribbean Sea system. Their model has a 40' grid spacing in the Gulf, uses realistic bathymetry and neglects non-linearities, friction, and direct astronomical forcing. Observed coastal harmonic constants are used as boundary conditions. Because of an apparent singularity at the critical latitude of the daily tides, these authors did not compute the daily tides in the Gulf of Mexico.

Also using W. Hansen's (1952, 1962) method, Grijalva (1971) computed the M_2 tide in the Gulf (Fig. 3). His model, which has a 30' grid spacing and includes friction and direct astronomical forcing of the water (but not the sea bed) specifies the surface elevation only at the Straits of Florida and the Yucatan Channel. Grijalva attributed the lack of an amphidromic point in his model to direct astronomical forcing.

Earlier theoretical work on tides in the Gulf is summarized by Zetler and D. Hansen (1970) while earlier work on resonances (free oscillations) is summarized by K. Hansen (1974).

1.2 Caribbean Sea

In the eastern Caribbean Sea, coastal and island observations show that the daily tides are relatively uniform with southward increases in phase consistent with those in the Atlantic. The amplitudes decrease slowly toward the west, decreasing more rapidly in the western Caribbean to apparent nodes in the Yucatan Channel. In the same region, there is a rapid increase in the daily phases. Michaelov *et al.* (1969) modelled the daily K_1 and O_1 tides in the Caribbean Sea on a 1° grid using the same assumptions they made for the Gulf. Their cotidal charts (Fig. 2) reproduce the general features of the daily tides in the Caribbean Sea.

The rapid, counter-clockwise increase in semi-daily phases and the small semi-daily amplitudes indicate that each semi-daily tide forms an amphidromic system in the eastern Caribbean. The semi-daily tides increase in amplitude toward the Yucatan Channel where they dominate the tidal régime. To test the M_2 model (Fig. 2) for the Caribbean Sea by Michaelov et al. (1969), the one-month east Caribbean station (Fig. 1 and Table I) was occupied at the theoretical M_2 amphidromic point. The resulting pressure series was analysed by Zetler and Cummings (1972) who found a small but non-zero, M_2 amplitude. The latter authors concluded from a study of successive 29-day series from nearby Magueyes Island that a 29-day series obtained near an amphidromic point might not yield an accurate harmonic constant for that constituent. The six-month east Caribbean station was therefore occupied, and results from that series are reported in this paper.

1.3 Low Frequency Pressure Continuum

Superimposed on the tidal signal in the open ocean is a bottom pressure continuum which is not well understood. At frequencies below the daily tidal band the continuum is thought to be associated with time-dependent geostrophic currents and atmospherically induced fluctuations. For the western Atlantic Ocean, Brown et al. (1975) found that the bottom pressure spectrum resembled the atmospheric pressure spectrum at low frequencies, but the bottom pressure and local atmospheric pressure were found to be only marginally coherent. The connexion between bottom pressure and atmospheric pressure is therefore more complex than a simple deviation from the inverse barometer compensation.

If the Gulf of Mexico has a resonance near the daily tidal band as proposed by Marmer (1954) it should be apparent in the bottom pressure continuum; the pressure spectra in the Gulf and the western North Atlantic should differ markedly near 1 cpd.

As discussed by Riehl (1954) the weather in the Caribbean Sea region is dominated by waves in the Easterlies that have periods of 4 to 5 d. It is interesting to speculate about the response of the semi-enclosed Caribbean Sea to forcing by these waves.

2. INSTRUMENTATION

The pressure series from the Caribbean Sea and from the central Gulf of Mexico station were obtained using Filloux (1970) deep-sea tide gauges. The gauges have metal Bourdon tube pressure transducers exposed to the full oceanic pressure. Intercomparison studies reported by the SCOR Working Group No. 27 (1975) and by Zetler et al. (1975) show that these gauges have a precision of at least 0.5 cm H_2O (relative to the mean), once a trend is removed from the data. The trend, due to creep in the Bourdon tubes, follows the logarithmic law proposed by Lomnitz (1956, 1957) and discussed by Jeffreys (1970). The long-term creep diverges from the Andrade's 1/3 power law proposed by Filloux (1970). Spurious shifts in the apparent background pressure occurred in the records from Misteriosa and Rosalind banks (Fig. 1). These shifts may be due to tilting of the gauges, as observed in laboratory tests; on the bottom, the tilting could be produced by wave-induced erosion around the instrument base. The analyses were limited to sections of record for which the background pressure was stable.

The pressure record from the West Florida shelf station was obtained with a pressure-temperature gauge described by Wimbush (1977). It used a 250-psi Vibrotron pressure sensor and a thermistor temperature sensor (to correct for a slight temperature sensitivity of the Vibrotron). Outputs of these sensors were integrated over the full sampling interval (1/8h); the sensitivity of the system is limited by Vibrotron noise, which is very small compared with the tidal signal.

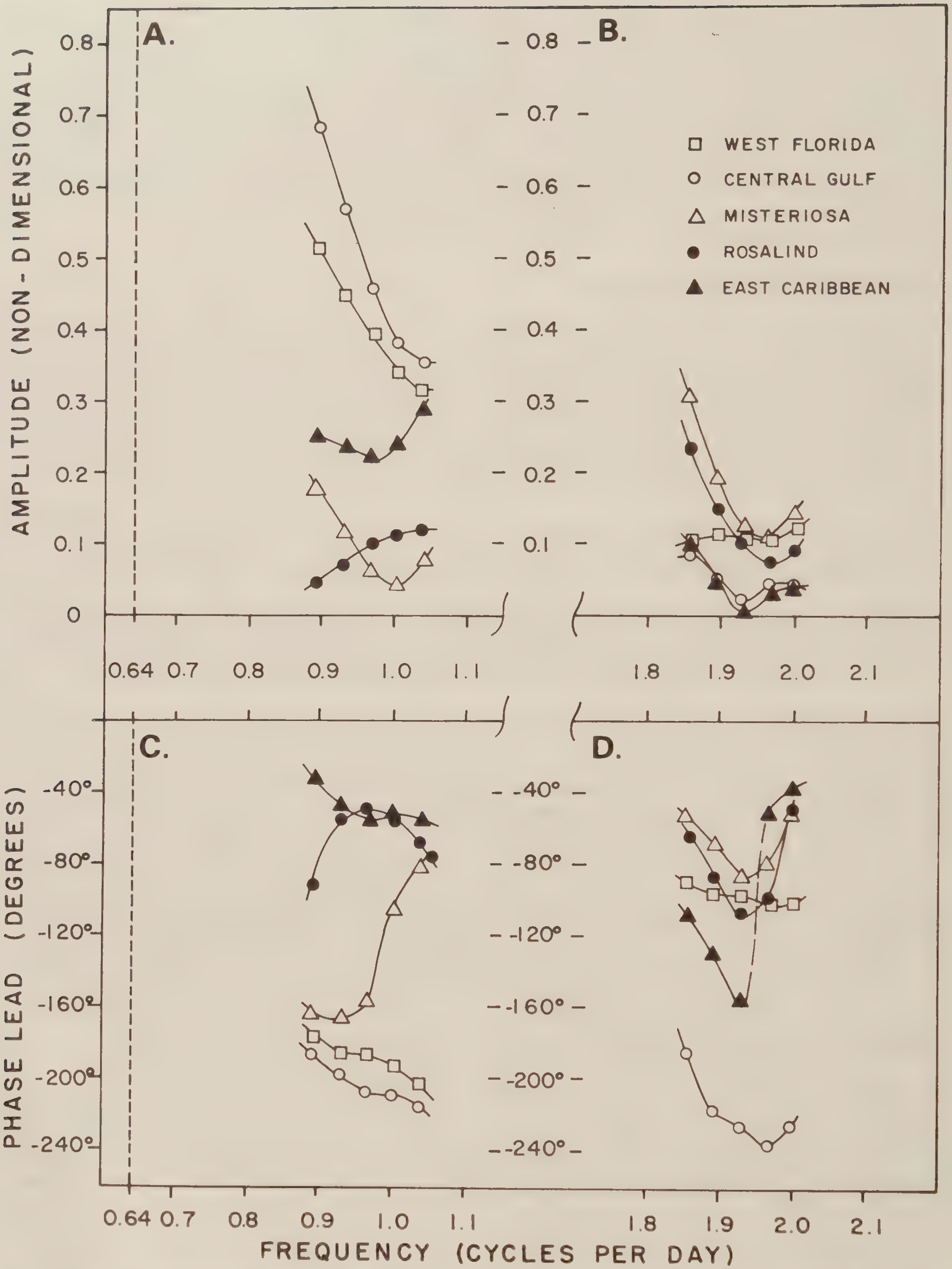

Fig. 4 Tidal admittance amplitudes computed from the bottom pressure records for the daily (A) and semi-daily (B) tidal bands and the corresponding phase leads (C) and (D). Tables of the admittances in standard form are given in the Appendix

3. OBSERVED TIDES

3.1 Accuracy of Harmonic Constants

Tidal harmonic constants were obtained from the pressure series using the response method. Results are given in the Appendix with a description of the method. The accuracy of observed harmonic constants is limited by length of record and by relative intensity of non-tidal continuum plus instrument noise within the tidal bands. For the records under discussion, the non-tidal pressure continuum is the primary source of error. The spectrum of the pressure continuum typically rises appreciably around the major tidal lines, due to the phase - incoherent internal tide. Cusps around the minor lines are buried in the background.

In the deep ocean one would expect less weather-induced fluctuation of bottom pressure than at coastal sea level stations. To compare the scatter in harmonic constants from nearby deep and shallow stations, successive 29-d analyses were done on the six-month east Caribbean bottom pressure record and a sea-level record from Magueyes Island, 280 km away, analysed by Zetler and Cummings (1972). Table II gives the means and standard deviations of the harmonic constants from these records.

Another error estimate uses the continuum spectru, integrated over the appropriate tidal band. This estimate, which is described in the Appendix, can be obtained from series that are too short for successive analyses. Standard deviations in Tables III and IV were obtained from the spectra.

TABLE III

Comparison of theoretical and observed harmonic constants at the central Gulf of Mexico and West Florida Shelf stations

	Michaelov, Melishko and Shcheveleva (1969)		Grijalva (1971)		Observed	
Central Gulf of Mexico station (24°46.1N, 89°38.9W)						
	H (cm)	G (deg)	H (cm)	G (deg)	H (cm)	G (deg)
M_2	1.0	45	~1.5	170	1.30±0.07	225.8±3.1
S_2	0.03	45	-	-	1.5 ±0.08	130.0±3.1
K_1	-	-	-	-	14.10±0.30	28.5±1.2
O_1	-	-	-	-	14.90±0.31	18.9±1.2
West Florida Shelf station (26°42.4N, 84°15.0W)						
	H (cm)	G (deg)	H (cm)	G (deg)	H (cm)	G (deg)
M_2	8.0	110	11	88	6.74±0.07	97.1±0.6
S_2	1.3	125	-	-	3.51±0.04	102.5±0.6
K_1	-	-	-	-	12.56±0.16	12.4±0.7
O_1	-	-	-	-	11.73±0.15	5.2±0.7

3.2 Gulf of Mexico

The measured K_1 and O_1 tides (Table III) at the central Gulf of Mexico station have at least twice the amplitudes of the corresponding tides in the western Atlantic. Although the K_1 amplitude in the western Atlantic is 1.24 times the O_1 amplitude and the astronomical K_1 forcing is 1.41 times the O_1 forcing, the O_1 amplitude exceeds the K_1 amplitude in the central Gulf. Hence, the admittance (response per unit forcing) is significantly larger at lower frequencies (Fig. 4). K_1 and O_1 harmonic constants are comparable with coastal values in the western Gulf, as given by Zetler and D. Hansen (1972). The observations support Marmer's (1954) contention that the Gulf has a resonance near the daily tidal band. The increasing admittance with decreasing frequency indicates that the resonance has a frequency below (longer period than) the daily tidal band. Further evidence for the resonance is given in the section on the low frequency continuum.

Since the model by Grace (1932) disagrees significantly with coastal values, no comparison was made between the K_1 measured at the central Gulf of Mexico station and this theory. The measured K_1 and O_1 values are consistent with the spatial distribution of the Helmholtz resonance computed by Platzman (1972), although the period is longer than the theoretical value.

The earlier K_1 and O_1 phases at the West Florida Shelf station (Fig. 4) relative to the central Gulf of Mexico station indicate that there is some progressive component to the daily tides near the Straits of Florida due to an unknown mixture of dissipation, direct forcing and propagation to or from the Caribbean Sea. The smaller daily amplitudes (Fig. 4) are consistent with nodes in the Straits of Florida.

The observed M_2 amplitude at the central Gulf of Mexico station agrees with the model of Michaelov et al. (1969) and the model of Grijalva (1971). For M_2 phase, the closer agreement of observations with the latter model tends to confirm Grijalva's contention that direct M_2 astronomical forcing is important in this small M_2 amplitude region of the Gulf.

Michaelov et al. (1969) also computed a theoretical distribution for S_2 (Fig. 2 and Table III) using coastal observations as boundary conditions and neglecting direct forcing. The S_2 tide is a superposition of gravitations and radiational tides. Assuming that the 0.9-cm amplitude[1] found by Zetler (1971) at Key West, Florida (24°34N, 81°48W) is characteristic of the radiational S_2 tide along the Gulf Coast, the radiational S_2 dominates the boundary conditions for the S_2 model. The discrepancy between the theoretical and observed S_2 harmonic constants (Table III) is then principally due to the neglect in the theory of nearshore wind and atmospheric pressure forcing.

At the West Florida Shelf station, the theoretical M_2 tides agree reasonably well with the measured values. This result could be expected because both theories (Table III) use nearby observed values as boundary conditions. The discrepancies may be due to tidal variation across the Shelf, which is unresolved by the models.

3.3 Caribbean Sea

The observed daily tides (Table IV) verify the general features of the K_1 and O_1 cotidal charts (Fig. 2) for the Caribbean Sea presented by Michaelov et al. (1969). The theory underestimates the daily amplitudes by about 10 percent at the eastern stations. Theoretical phases at the eastern stations have K_1 less than O_1 by 4 percent while observed phases have

---

1/ This amplitude is relatively small compared with others along the United States East Coast, as reported by Zetler (1971)

TABLE IV

Comparison of theoretical harmonic constants from Michaelov, Melishko and Shcheveleva (1969) and observed harmonic constants in the Caribbean Sea

Eastern Caribbean Sea								
	Six-month station ($16^{\circ}32.5N$, $64^{\circ}52.9W$)				One-month station ($16^{\circ}30.1N$, $64^{\circ}54.7W$)			
	Theoretical		Observed		Theoretical		Observed[a]	
	H (cm)	G (deg)	H (cm)	G (deg)	H (cm)	G (deg)	H (cm)	G (deg)
M_2	0	-	0.52±0.03	155.8±3.7	0	-	0.64	153
S_2	0.5	350	1.30±0.08	43.7±3.7	0.5	0	1.24	49
K_1	7.8	228	8.82±0.11	232.9±0.7	7.8	228	9.27	235
O_1	6.0	232	6.24±0.08	227.2±0.7	6.0	232	6.62	230

Western Caribbean Sea								
	Theoretical		Observed		Theoretical		Observed	
	H (cm)	G (deg)	H (cm)	G (deg)	H (cm)	G (deg)	H (cm)	G (deg)
M_2	8.7	88	7.88±0.46	84.2±3.3	6.5	105	6.63±0.35	107.0±3.0
S_2	2.6	60	3.89±0.23	55.9±3.3	1.7	50	2.51±0.13	55.6±3.0
K_1	$\leqslant 3$	280	1.58±0.19	284.3±7.0	5.0	243	4.33±0.28	235.3±3.7
O_1	$\leqslant 1$	320	3.06±0.37	347.0±7.0	2.0	250	1.89±0.12	235.5±3.7

[a] From Zetler and Cummings (1972) obtained from a 29-day harmonic analysis; no standard deviations given

K_1 greater than O_1 by 5 percent. The observed K_1 tide also lags the O_1 tide at the nearby Magueyez Island station (Zetler and Cummings, 1972) and other coastal stations in the Caribbean Sea (U.S. Department of Commerce, 1942). The discrepancies are due to errors in the boundary conditions or to mislabelling of the cotidal charts, because the uniformity of the tides in the eastern Caribbean precludes significant errors arising from inadequate dynamics in the model.

In the western Caribbean, the observations (Table IV) show the decrease in daily tidal amplitudes and rapid increase in daily phase lags (Fig. 2) predicted by Michaelov *et al.* (1969). The discrepancies between the theoretical and observed daily tides at the western Caribbean station arise from errors in the model's boundary conditions and, to a lesser extent, the influence of noise on observed harmonic constants from short records obtained at shallow stations.

The model by Michaelov *et al.* (1969) for the M_2 and S_2 tides in the Caribbean Sea predicts small amplitudes at the eastern Caribbean stations. Small semi-daily amplitudes are observed at these stations. As suggested for the M_2 and S_2 tides in the Gulf of Mexico, the

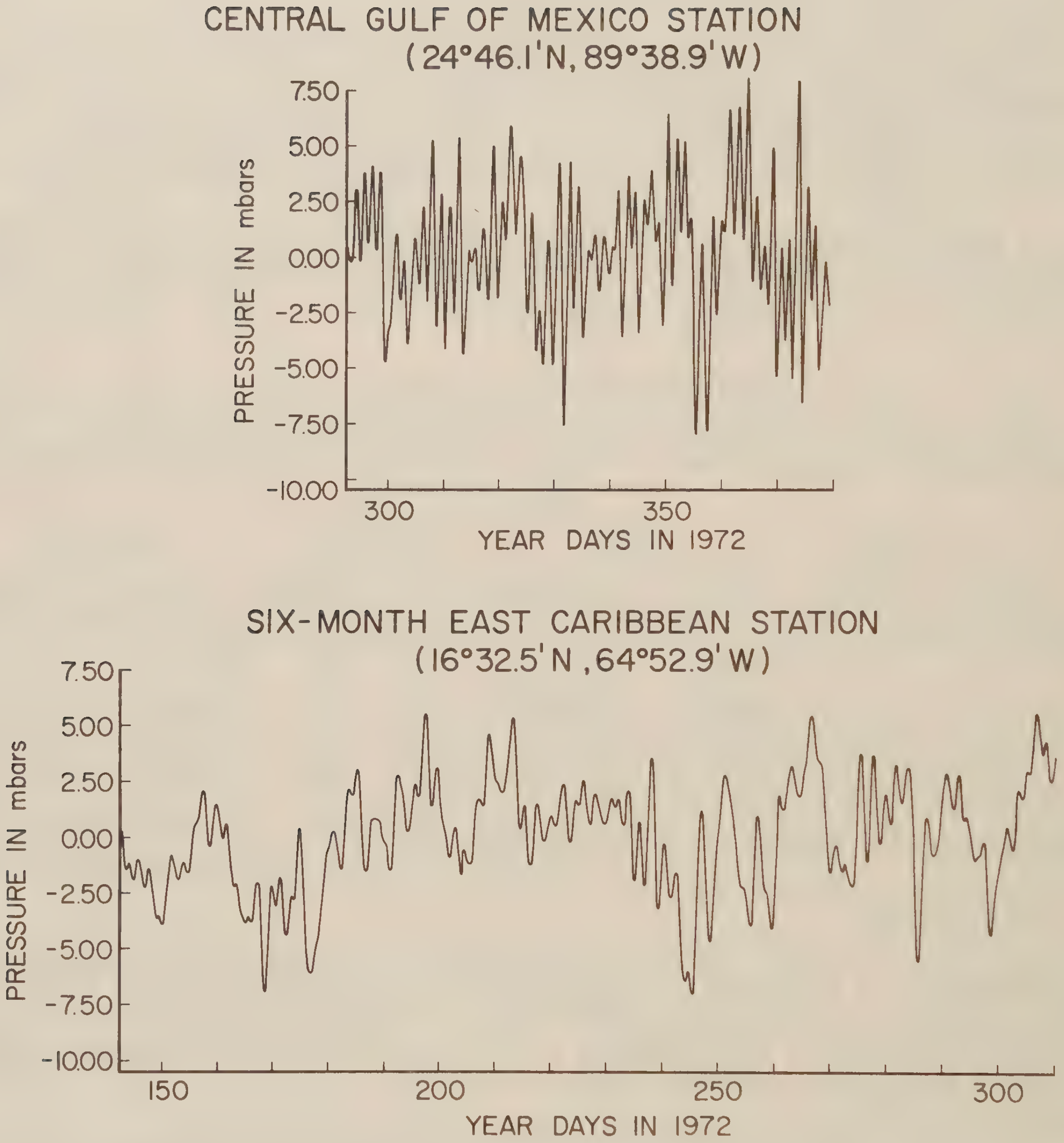

Fig. 5 Low-passed pressure records at the central Gulf of Mexico and six-month east Caribbean stations showing the pressure fluctuations in millibars at frequencies below the daily tidal band. The instrumental drift has been removed by subtracting a least-squares fitted logarithmic trend from each record. Note the rapid fluctuations in the central Gulf of Mexico record as contrasted with the lower frequency fluctuations at the east Caribbean station

difference between the theory and observation near a theoretical amphidrome may be due to directly forced tides and to radiational S_2 tide. The anomalous jump in semi-daily admittance phase (Fig. 4) at the six-month east Caribbean station may be due to the relative importance of the radiational S_2 tide near amphidromes of the gravitational, semi-daily tides. If the record were longer (years) the radiational admittance could be computed separately and the computed gravitational admittance might then appear smoother.

The six-month record is sufficiently long and the background noise sufficiently low to allow an analysis of the ter-daily M_3 tide arising from the C_3^3 gravitational potential. As given in Table E, the M_3 tide (0.12 cm, 48.1°G) is distinct from non-linearly generated lines in the ter-daily band.

4. LOW-FREQUENCY PRESSURE CONTINUUM

The records from the central Gulf of Mexico and the six-month east Caribbean stations are sufficiently long to permit a study of the low frequency, bottom pressure continuum. Shown in Fig. 5 are low-passed pressure series; the corresponding spectra are given in Fig. 6 together with the spectrum at the western Atlantic AOML-1 station discussed by Brown *et al.* (1975).

4.1 Gulf of Mexico

The Central Gulf of Mexico spectrum (Fig. 6) diverges from the AOML-1 spectrum at frequencies above 0.24 cpd, exhibiting an increase in spectral energy with higher frequency and forming a broad peak centred at about 0.64 cpd (period = 1.56 d)1/. After a dip centred at 0.8 cpd this spectrum rises toward the daily tidal band. The total pressure variance between 0.049 and 0.805 cpd at the Central Gulf of Mexico Station (8.81 mbar^2) is three times the corresponding variance at the western Atlantic AOML-1 station (2.64 mbar^2). The low frequency pressure continuum observed in the Gulf reinforces the contention that the Gulf has a resonance with a frequency slightly below the daily tidal band.

4.2 Caribbean Sea

The pressure spectrum (Fig. 5) at the six-month east Caribbean station follows the general trend of the western Atlantic AOML-1 spectrum. The pressure variances between 0.046 and 0.805 cpd are 2.64 and 2.48 mbar^2, respectively. The major differences between the spectra are the pronounced peak around 0.22 cpd (4.5-d period) and its overtone seen in the Caribbean. Since the weather in this region is dominated by waves in the Easterlies with 4 to 5-d period, the bottom pressure peaks may be atmospherically forced.

A simultaneous atmospheric pressure record2/ from St. Croix, V.I. (17°42N, 64°44W) 130 km north and slightly east of the bottom pressure station (16°33N, 64°53W), was obtained from the National Climatic Center. The autospectra, squared coherence and relative phase of the two records are shown in Fig. 7. Taking the 0.15-cpd spectral estimates as the bases of the 0.2-cpd peaks, the corresponding amplitudes are 0.5 and 4.0 mbar for the bottom pressure and atmospheric pressure fluctuations, respectively, giving an amplitude ratio of 0.13. The fluctuations are coherent because the peak in squared coherence stands well above the 95 per-cent confidence value for rejection of the null hypothesis (i.e., that the coherence is due to random chance).

1/ The spectrum from the West Florida Shelf station likewise contains a significant peak at 1.60 d

2/ The following comparison was suggested by a reviewer

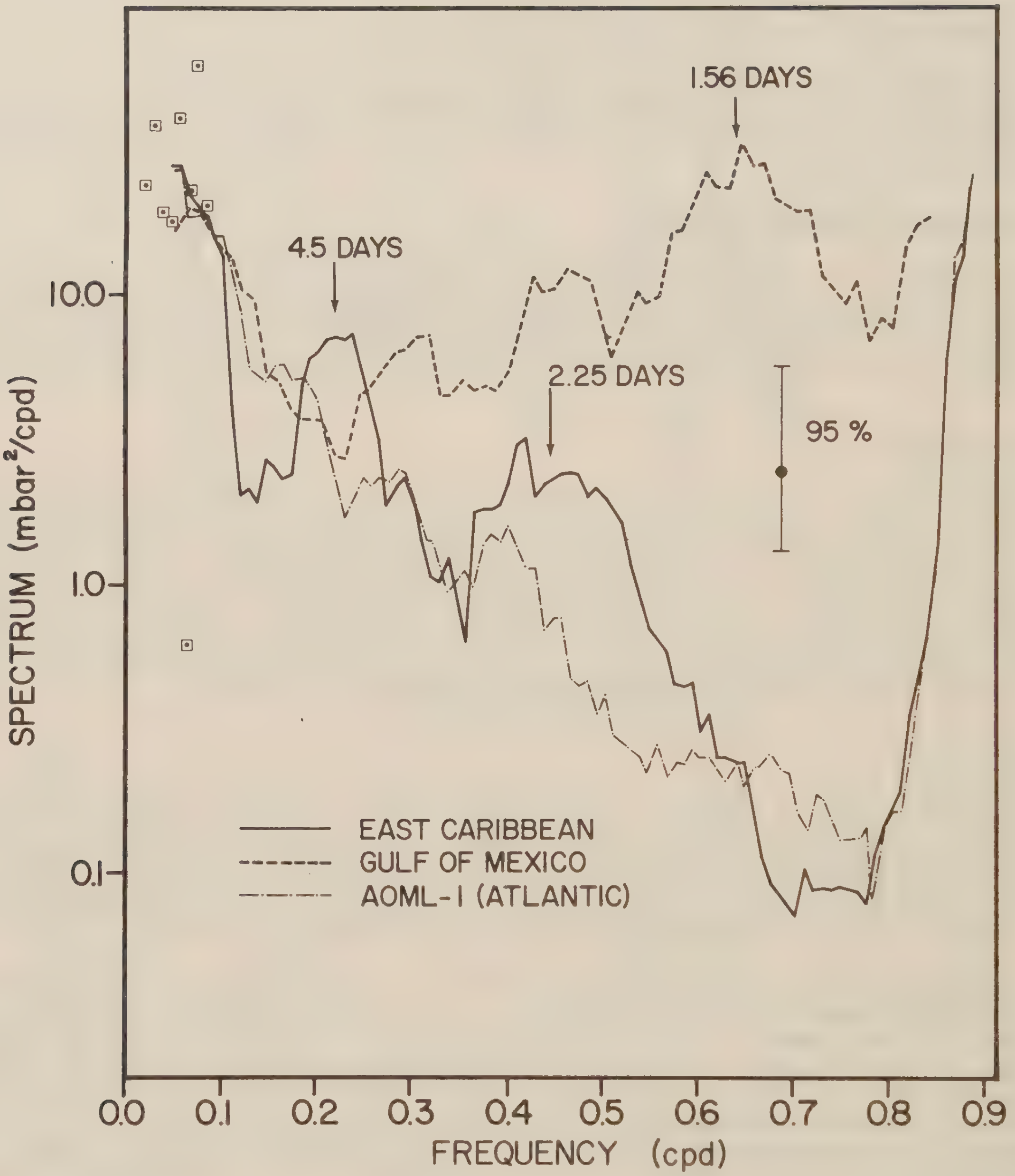

Fig. 6 Spectra of bottom pressure below the daily tidal band for the six-month east Caribbean, central Gulf of Mexico and AOML-1 (Atlantic) stations. The pressure records were cosine-tapered over the first and last 10 percent and Fourier-transformed to give primitive spectral estimates that have been smoothed with a seven point (14 degrees of freedom) box car average. The isolated points in the upper left corner are primitive spectral estimates for the east Caribbean record at and below the fortnightly frequency. Note the overall similarity between the AOML-1 and East Caribbean spectra and the peaks in the latter at 4.5 and 2.25-d periods. In contrast, the central Gulf of Mexico spectrum rises at frequencies above 0.2 cpd to a peak at 0.64 cpd (1.56 d period)

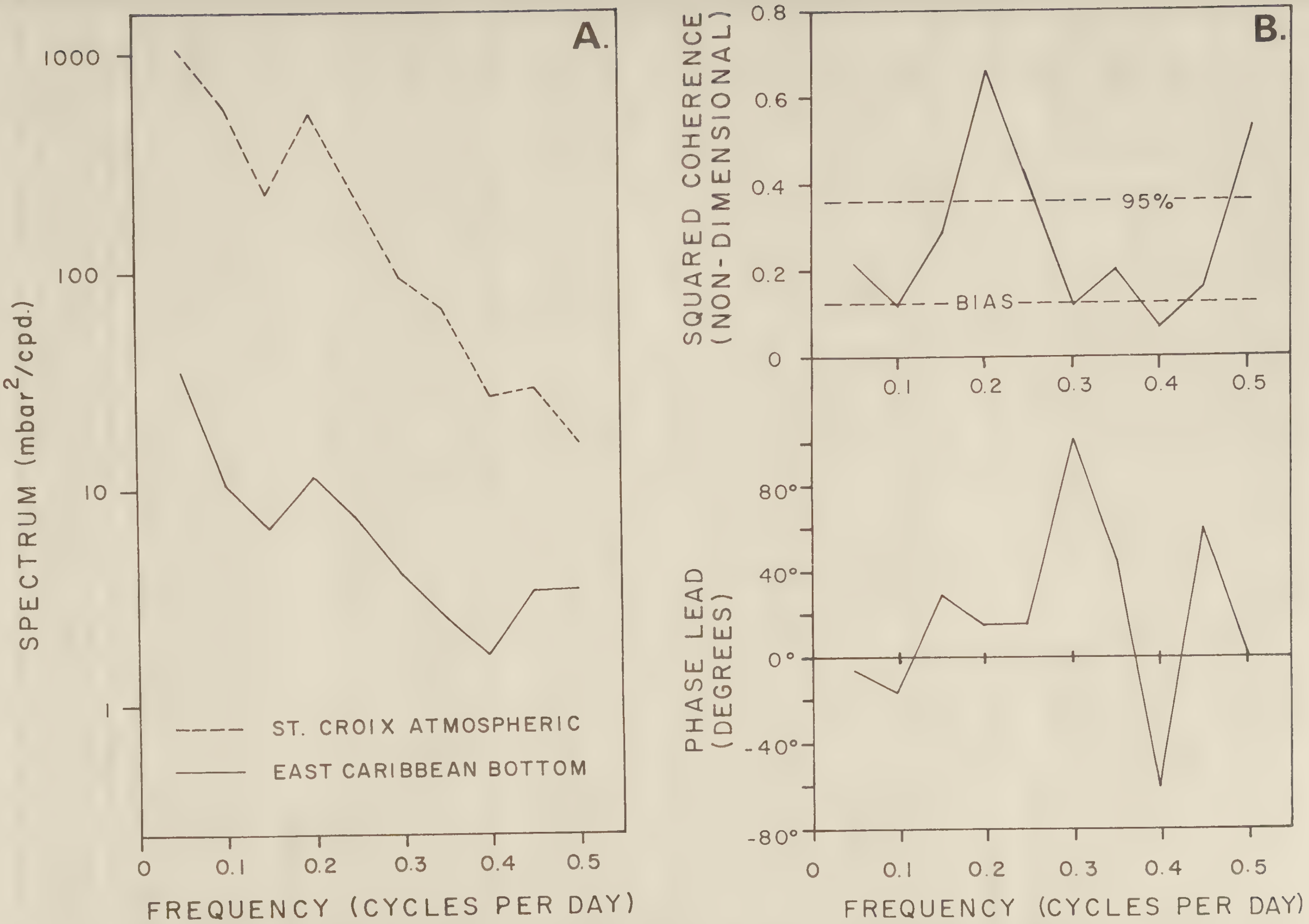

Fig. 7 Comparison of bottom pressure at the six-month east Caribbean station (16°33N, 64°53W) with atmospheric pressure at nearby St. Croix, V.I. (17°42N, 64°44W). The peaks in the autospectra (A) at 0.2 cpd are coherent (B) with the bottom pressure leading the atmospheric pressure by 15° at 0.2 cpd. Daily-averaged pressures were used with a 0.5-cpd Nyquist frequency

The bottom pressure fluctuations lead the atmospheric fluctuations to the north by 15 percent, or 4.5 h for a 0.22-cpd frequency. This is consistent with the northwestward propagation of the waves in the Easterlies as reported by Riehl (1954). He states that the waves propagate at 12 to 15 knots (6 to 8 m/sec^{-1}) while the observed 4.5 h phase lead gives a propagation speed of about 8 m/sec^{-1}, assuming that the waves propagate with a $315^{\circ}T$ heading. The 4 to 5-d bottom pressure fluctuations observed at the six-month east Caribbean station are coupled strongly and in phase with atmospheric wave. This is in contrast to the low-frequency, bottom pressure fluctuations in the western Atlantic where the bottom and atmospheric fluctuations are marginally coherent. A possible explanation for the different behaviour is that the inverse barometer compensation is less complete in the semi-enclosed Caribbean Sea, where weather patterns span the basin and where water exchange is hindered by narrow, shallow passes.

5. DISCUSSION

The original purpose of this study was to test tidal models with offshore observations. By themselves, the few stations are not sufficient to provide empirical tidal charts or even to indicate whether particular features such as amphidromic points exist in a given region. When conflicting theories predict distinctly different behaviour, an isolated station should discriminate between the theories. For example, the observed M_2 phase at the Central Gulf of Mexico station favours the model by Grijalva (1971) which includes direct astronomical forcing, over the model by Michaelov et al. (1969) which is forced only by co-oscillation. However, it might be possible to reconcile the latter model with observations by changing boundary conditions or grid spacing. The results of tidal models are traditionally given as a single chart of amplitude and phase for a given constituent. No reliability estimates are given based on a set of numerical experiments to determine the sensitivity of the model to reasonable ranges of parameters, uncertain bathymetry and numerical limitations. Confidence limits on the theoretical distributions are needed, just as they are for observations.

Although the daily tides dominate the Gulf of Mexico, the apparent critical-latitude singularity in the equations of motion prevented Michaelov et al. (1969) from computing the daily tidal charts for the Gulf. This singularity is removable and the daily tides in the Gulf can be computed by alternate numerical schemes.

Zetler and Cummings (1972) suggested that extensive observational searches for amphidromic points are unprofitable and report the recommendation by the Scientific Committee on Ocean Resources (SCOR) Working Group No. 27 on Tides in the Open Ocean that emphasis should be placed on regions of maximum constituent amplitude. Such a search would also be unprofitable because the constituent amplitudes and phases vary little over large areas around these maxima. The observations should be made to discriminate between theories. The basic limitation on observational offshore tide programmes is no longer the accuracy and endurance of tide gauges but rather the cost of obtaining the pressure records.

6. ACKNOWLDEGEMENTS

Many people have contributed significantly to the research presented in the paper. The authors wish to thank the National Ocean Survey's Engineering Development Laboratory and J.J. Falkenhoff in particular for both the design of arrays and assistance in the NOAA field programme. Within AOML, F.A. New did much of the initial checkout and modification work on the Filloux gauges. B.J. Culverhouse, D.F. Pashinski and R.S. Jennings worked with EDL and F.A. New on the array preparation and field work and were essential to the success of the project. R.B. Starr suggested the shallow water stations in the western Caribbean Sea. D.F. Jones designed and fabricated the arrays for those stations and supervised their installation. N.M. Targett was of considerable assistance in the laborious reading of pressure gauge records and the subsequent data processing. Useful advice was readily given by J.H. Filloux whose gauges have proved to be excellent instruments for open-sea bottom pressure studies.

The NOAA work was sponsored by the National Science Foundation under the agreement AG-253 for NOAA participation in the International Decade of Ocean Exploration. The Nova University work was supported by NOAA (PO 015150340) and by the National Science Foundation (Grant GA34149).

7. REFERENCES

Brown, W. et al., MODE bottom experiment. J.Phys.Oceanogr., 5:75-85
1975

Cartwright, D.E., W. Munk and B. Zetler, Pelagic tidal measurements - a suggested procedure
1969 for analysis. Trans.Am.Geophys.Union, 50:472-7

Cartwright, D.E. and A.C. Edden, Corrected tables of tidal harmonics. Geophys.J.R.Astron.
1973 Soc., 33:253-63

Filloux, J.H., Bourdon tube deep-sea tide gauges. In Tsunamis in the Pacific Ocean, edited
1970 by W.M. Adams. Honolulu, East-West Center Press, pp. 223-38

Grace, S.F., The principal diurnal constituent of tidal motion in the Gulf of Mexico. Mon.
1932 Not.R.Astron.Soc.Geophys.Suppl., (3):70-83

Great Britain, Her Majesty's Nautical Almanac Office, Explanatory supplement to the astrono-
1974 mical emphemeris and to the American ephemeris and nautical almanac. London,
HMSO, pp. 522-64

Grijalva, N., The M_2 tide in the Gulf of Mexico. Geofis.Int., Mex., 2:103-25
1971

Groves, G.W., Use of orthogonal functions for the analysis, prediction and study of the
1970 tide. Rep.Hawaii Inst.Geophys., (HIG-70-13):53 p.

Hansen, K.S., Calculations of normal modes for the Americal mediterranean seas. Univ.
1974 Chicago Tech.Rep., (26):71 p.

Hansen, W., Gezeiten and Gezeitenstrome der halbtagigen M_2 in der Nordsee. Dtsch.Hydrogr.Z.,
1952 Erganzungsh. (1):46 p.

__________, Hydrodynamical methods applied to oceanographic problems. In Proceedings of
1962 the Symposium of Mathematical and Hydrodynamical Methods of Physical Oceanography.
Mitt.Inst.Meereskd.Univ.Hamb., (1):25-34

Jeffreys, H., The earth. Cambridge University Press, 525 p. 5th ed.
1970

Lomnitz, C., Creep measurements in igneous rocks. J.Geol., 64:473-9
1956

__________, Linear dissipation in solids. J.Appl.Phys., 28:201-5
1957

Marmer, H.A., Tides and sea level in the Gulf of Mexico. Fish.Bull.U.S.Fish Wildl.Serv.,
1954 55:101-18

Michaelov, U.S., V.P. Melishko and G.I. Shcheveleva, Estimation of the tides and tidal cur-
1969 rents in the Gulf of Mexico and Caribbean Sea. Tr.Gos.Okeanogr.Inst., 96:146-73

Munk, W.H. and D.E. Cartwright, Tidal spectroscopy and prediction. *Philosophical Trans.R.*
1966 *Soc.(A)*, 259:533-81

Platzman, G.W., Two-dimensional free oscillations in natural basins. *J.Phys.Oceanogr.*,
1972 2:117-38

Radok, R., W. Munk and J. Isaacs, A note on mid-ocean internal tides. *Deep-Sea Res.*,
1967 14:121-4

Riehl, H., Tropical meteorology. McGraw-Hill, 392 p.
1954

SCOR Working Group No. 27, An intercomparison of open sea tidal pressure sensors. *UNESCO*
1975 *Tech.Pap.Mar.Sci.*, (21):67 p.

U.S. Department of Commerce, Tidal harmonic constants, Atlantic Ocean including Arctic and
1942 Antarctic Regions, TH-1. Washington D.C., Government Printing Office, 139 p.

Wimbush, M., An inexpensive sea floor precision pressure recorder. *Deep-Sea Res.*, 24:493-7
1977

Zetler, B.D., Radiational ocean tides along the coasts of the United States. *J.Phys.Oceanogr.*
1971 1:34-8

Zetler, B.D. and R.A. Cummings, Tidal observations near an amphidrome. *Geophys.Surv.*,
1972 1:85-9

Zetler, B.D. and D.B. Hansen, Tides in the Gulf of Mexico. *In* Contributions on the physical
1972 oceanography of the Gulf of Mexico, edited by L.R.A. Capurro and J.L. Reid.
Houston, Texas, Gulf Publishing Co., Vol. 2:265-75

Zetler, B.D. *et al.*, MODE tides. *J.Phys.Oceanogr.*, 5:430-41
1975

APPENDIX

Tidal Analysis of the Pressure Records

The bottom pressure records were analysed for tidal components by the following procedure:

Each pressure record was first divided through by $\bar{\rho}g$ to convert it to units of sea level. In practice the mean density of the water column, $\bar{\rho}$, was taken as a constant for each record. Gravity, g, was taken to be 979 cm s^{-2}, a typical value for the region.

These sea level records were then analysed for tidal components by the response method of Munk and Cartwright (1966)[1]. In this method, spherical harmonic expansions of the tide-generating potential (computed from the known motions of earth, moon and sun) are fitted to the observed data in a least squares sense. Lags and leads of the potential functions may be introduced to allow for variations with frequency of response admittances of the ocean at the observation point. These admittances are then calculated by Fourier transformation of the weights representing the least squares fit.

For comparison with results from harmonic methods of tidal analysis, it is convenient to calculate amplitudes and phases of individual tidal lines in the spectrum. The amplitude $H(f)$ of a tidal line with frequency f is calculated by multiplying the admittance amplitude $R(f)$ by the amplitude of the tide-generating potential $H_{pot}(f)$. $H_{pot}(f)$ for the present historical period is given (in metres) in column 3, Table 1 of Cartwright and Edden (1973). The Greenwich phase $G(f)$ of the tidal line is calculated from the phase $\Phi(f)$ of the admittance (defined as in Munk and Cartwright, 1966) by the relation $G = m\pi - \Phi$, where m is the species number of the tidal line.

Errors in these tidal estimates are principally due to the incoherent noise in the spectral neighbourhoods of the tidal lines. Around each tidal line a cusp-like rise in noise spectrum is observed. This is thought to be caused by baroclinic tides, which derive their energy from the barotropic tide but are rendered incoherent by the variable density structure of the ocean (Radok, Munk and Isaacs, 1967). With this model, the noise variance in each tide constituent is proportional to the tidal variance of the constituent, with the result that the standard error is given by

$$\sigma = \left[\frac{\mu}{2\ell}\right]^{1/2} \sigma, \quad \mu \ll 1$$

relative to H itself or to one radian in G, where μ is the ratio of the residual to recorded variance (i.e., the proportion of the recorded variance that is non-tidal) and ℓ is the length of the record in months (i.e., length in days ÷ 27.322).

Tables A-E give the results of this analysis applied to the Gulf of Mexico and Caribbean bottom pressure records. The presentation follows the form recommended by Cartwright, Munk and Zetler (1969).

---

[1] The following corrections (many suggested by Cartwright, private communication) have been made to the formulae in Appendix A of this reference. In section b, $\bar{R}_o/\rho_o$ is replaced by $(\bar{R}_o/\rho_o)^2$ as proposed by Groves (1970). In sections d and e, $\omega_o = 0.4093197552 - 0.00022711096892\ T$; T^3 is replaced by T^2 in eq. A17; $-3me_o \sin(h_o-p_o)$ is added to the r.h.s. of eq. A18; $m = 0.048013258$; $-\ 3/2\ m^2\ e_o \cos\ (h_o-p_o)$ is added within $[\ ]$ of eq. A19. The Internal Astronomical Union 1964 astronomical constants were used throughout (see p. 492 ff of the Explanatory Supplement to the Astronomical Emphemeris and to the American Emphemeris and Nautical Almanac, 1974)

TABLE A

Station: Central Gulf of Mexico — 24°46.1N 89°38.9W, depth 3748 m,
1972 October 14, 1629 - 1973 January 17, 1135 GMT

Reference: $C_2^1(0,\pm2,\pm4)$, $C_2^2(0,\pm2,\pm4)$, C_3^3

Admittances (Station/Reference)					Principal harmonic constituents			
Interval 1 cpm (0.366011 cpd)								
Frequency (cpd)	Real	Imaginary	R	ϕ (deg)		Frequency (cpd)	H (cm)	G (deg)
0.8929346	-0.67828	0.07851	0.68281	173.40	(Q_1)	0.8932441	3.42	006.7
0.9295357	-0.53763	0.18376	0.56816	161.13	O_1	0.9295357	14.90	018.9
0.9661368	-0.40599	0.20743	0.45591	152.94				
1.0027379	-0.33624	0.18226	0.38246	151.54	(P_1)	0.9972621	4.76	028.4
1.0393390	-0.29605	0.19920	0.35683	146.06	K_1	1.0027379	14.10	028.5
Recorded variance: 304.43 cm^2							±2.1%	±1.2°
Residual variance: 0.95 cm^2								
1.8590714	-0.08469	0.00735	0.08501	175.04				
1.8956725	-0.04168	0.03133	0.05214	143.06	(N_2)	1.8959820	0.63	217.3
1.9322736	-0.01438	0.01481	0.02064	134.15	M_2	1.9322736	1.30	225.8
1.9688747	-0.02392	0.03446	0.04195	-124.77				
					(S_2)	2.0000000	1.50	130.0
2.0054758	-0.03112	-0.03120	0.04407	-134.92	K_2	2.0054758	0.35	134.9
Recorded variance: 1.98 cm^2							±5.4%	±3.1°
Residual variance: 0.04 cm^2								

TABLE B

Station: West Florida Shelf Break

26°42.4N 84°15.0W, depth 154 m
1974 April 7, 1845 - November 17, 1304 GMT

Reference: $C_2^1(0,\pm2,\pm4)$, $C_2^2(0,\pm2,\pm4)$, C_3^3

Admittances (Station/Reference) Interval 1 cpm (0.366011 cpd) Frequency (cpd)	Real	Imaginary	R	ϕ (deg)	Principal harmonic constituents	Frequency (cpd)	H (cm)	G (deg)
0.8929346	-0.51272	-0.03282	0.51377	-176.34	(Q_1)	0.8932441	2.58	356.5
0.9295357	-0.44564	0.04024	0.44745	174.84	O_1	0.9295357	11.73	005.2
0.9661368	-0.39082	0.05126	0.39417	172.53				
					(P_1)	0.9972621	4.24	011.2
1.0027379	-0.33265	0.07310	0.34058	167.60	K_1	1.0027379	12.56	012.4
1.0393390	-0.29103	0.12712	0.31758	156.40				
							±1.3%	±0.7°
Recorded variance: 161.98 cm^2								
Residual variance: 0.44 cm^2								
1.8590714	0.00019	-0.10838	0.10838	-89.90				
1.8956725	-0.01133	-0.11161	0.11218	-95.79	(N_2)	1.8959820	1.36	095.8
1.9322736	-0.01322	-0.10578	0.10660	-97.13	M_2	1.9322736	6.74	097.1
1.9688747	-0.02223	-0.10632	0.10862	-101.81				
					(S_2)	2.0000000	3.51	102.5
2.0054758	-0.02463	-0.11909	0.12161	-101.68	K_2	2.0054758	0.97	101.7
Recorded variance: 30.43 cm^2							±1.0%	±0.6°
Residual variance: 0.05 cm^2								

TABLE C

Station: Misteriosa Bank

18°52.9N 83°48.3W, depth 22m,
1971 July 23, 0001 - August 19, 1803 GMT

Reference: $C_2^1(0,\pm2)$, $C_2^2(0,\pm2)$

Admittances (Station/Reference)

Interval 1 cpm (0.366011 cpd)

Frequency (cpd)	Real	Imaginary	R	ϕ (deg)
0.8929346	-0.17160	-0.05025	0.17881	-163.68
0.9295357	-0.11351	-0.02627	0.11651	-166.97
0.9661368	-0.05585	-0.02316	0.06046	-157.48
1.0027379	-0.01062	-0.04155	0.04289	-104.34
1.0393390	0.01279	-0.07763	0.07868	-80.65

Recorded variance: 7.73 cm²
Residual variance: 0.24 cm²

Frequency (cpd)	Real	Imaginary	R	ϕ (deg)
1.8590714	0.18556	-0.24718	0.30908	-53.10
1.8956725	0.07245	-0.17620	0.19051	-67.65
1.9322736	0.01251	-0.12402	0.12465	-84.24
1.9688747	0.01819	-0.10151	0.10312	-79.84
2.0054758	0.08833	-0.11333	0.14368	-52.07

Recorded variance: 37.00 cm²
Residual variance: 0.25 cm²

Principal harmonic constituents

	Frequency (cpd)	H (cm)	G (deg)
(Q_1)	0.8932441	0.90	343.7
O_1	0.9295357	3.06	347.0
(P_1)	0.9972621	0.50	293.3
K_1	1.0027379	1.58	284.3
		±12%	±7°
(N_2)	1.8959820	2.30	067.8
M_2	1.9322736	7.88	084.2
(S_2)	2.0000000	3.89	055.9
K_2	2.0054758	1.15	052.1
		±5.8%	±3.3°

TABLE D

Station: Rosalind Bank

16°36.5N 80°20.25W, depth 31 m,
1971 July 22, 0000 - August 14, 1700 GMT

Reference: $C_2^1(0,\pm 2)$, $C_2^2(0,\pm 2)$

Admittances (Station/Reference)

Interval 1 cpm (0.366011 cpd)

Frequency (cpd)	Real	Imaginary	R	ϕ (deg)
0.8929346	-0.00116	-0.04676	0.04677	-91.42
0.9295357	0.04080	-0.05936	0.07203	-55.49
0.9661368	0.06519	-0.07721	0.10105	-49.82
1.0027379	0.06693	-0.09660	0.11752	-55.28
1.0393390	0.04566	-0.11351	0.12235	-68.09

Recorded variance: 13.84 cm²
Residual variance: 0.10 cm²

Frequency (cpd)	Real	Imaginary	R	ϕ (deg)
1.8590714	0.10425	-0.20902	0.23357	-63.49
1.8956725	0.01110	-0.14915	0.14956	-85.74
1.9322736	-0.03061	-0.10035	0.10491	-106.96
1.9688747	-0.01221	-0.07275	0.07377	-99.52
2.0054758	0.06247	-0.07210	0.09540	-49.09

Recorded variance: 22.95 cm²
Residual variance: 0.11 cm²

Principal harmonic constituents

	Frequency (cpd)	H (cm)	G (deg)
(Q_1)	0.8932441	0.24	270.9
O_1	0.9295357	1.89	235.5
(P_1)	0.9972621	1.42	234.0
K_1	1.0027379	4.33	235.3
		±6.4%	±3.7°
(N_2)	1.8959820	1.80	086.0
M_2	1.9322736	6.63	107.0
(S_2)	2.0000000	2.51	055.6
K_2	2.0054758	0.76	049.1
		±5.3%	±3.0°

TABLE E

Station: Six-Month East Caribbean

16°32.5N 64°52.9W, depth 3990 m
1972 May 20, 0000 - November 9, 1309 GMT

Reference: C_2^0, $C_2^1(0,\pm2,\pm4)$, $C_2^2(0,\pm2,\pm4)$, C_3^3, x_1^1

Admittances* (Station/Reference) Interval 1 cpm (0.366011cpd)					Principal harmonic constituents			
Frequency (cpd)	Real	Imaginary	R	ϕ (deg)		Frequency (cpd)	H (cm)	G (deg)
0.8929346	0.20989	-0.13665	0.25045	-33.07	(Q_1)	0.8932441	1.26	213.2
0.9295357	0.16164	-0.17448	0.23785	-47.19	O_1	0.9295357	6.24	227.2
0.9661368	0.12927	-0.17947	0.22118	-54.24				
					(P_1)	0.9972621	2.85	233.2
1.0027379	0.14436	-0.19082	0.23927	-52.89	K_1	1.0027379	8.82	232.9
1.0393390	0.16838	-0.23455	0.28873	-54.32				
							±1.3%	±0.7°
Recorded variance: 68.02 cm^2 Residual variance: 0.14 cm^2								
1.8590714	-0.03302	-0.09934	0.10468	-108.39				
1.8956725	-0.03047	-0.03710	0.04801	-129.40	(N_2)	1.8959820	0.58	129.7
1.9322736	-0.00748	-0.00336	0.00820	-155.82	M_2	1.9322736	0.52	155.8
1.9688747	0.02096	-0.02510	0.03270	-50.14				
					(S_2)	2.0000000	1.30	043.7
2.0054758	0.03184	-0.02444	0.04014	-37.51	K_2	2.0054758	0.32	037.5
Recorded variance: 1.35 cm^2 Residual variance: 0.07 cm^2							±6.4%	±3.7°
2.8984104	-0.10248	0.11420	0.15344	131.90	M_3	2.8984104	0.12	048.1
Recorded variance: 0.035 cm^2 Residual variance: 0.027 cm^2							±**%	±**°

* gravitational not radiational

** μ = (residual/recorded) variance = 0(1), formula inapplicable

AN OVERVIEW OF THE CAYMAN SEA-GULF OF MEXICO CIRCULATION BASED ON CICAR SURVEY MONTH AND OTHER DATA

by

R.L. MOLINARI
NOAA/AOML
Miami, Florida 33149, U.S.A.

CONTENTS

1. INTRODUCTION
2. SPATIAL AND TEMPORAL CHARACTERISTICS OF THE CAYMAN-GULF CURRENT
3. DYNAMICAL PROCESSES ACTIVE IN THE CAYMAN-GULF CURRENT
4. THE ROLE OF THE CAYMAN-GULF CURRENT IN THE NORTH ATLANTIC GYRE
5. SUMMARY
6. ACKNOWLEDGEMENTS
7. REFERENCES

Abstract

The Atlantic Oceanographic and Meteorological Laboratories (AOML) have participated in seven CICAR Survey Months (CSMs). AOML's involvement was designed to map synoptically the circulation in the Cayman Sea and Gulf of Mexico. The CSM concept was verified in the sense that the most complete and synoptic spatial coverage was obtained when the coordination between participants was extensive.

In this overview, CICAR Regional Data Centre and AOML data sets are combined to describe the current structure in the Cayman-Gulf basins. A current, continuous in structure referred to as the Cayman Gulf Current, but not in nomenclature, is tracked through the region. The west-flowing Cayman Current enters the Cayman Sea through the Jamaica-Honduras Passage. Surface velocities approaching 75 cm/sec have been measured in the mid-Cayman Basin south of the Cayman Ridge. In the region of the Yucatan Strait, the Cayman Current turns north to become the Yucatan Current. Threefold increases in the current speeds have been observed here by direct current measurements. In the Gulf of Mexico the CSM data support the hypothesis of an annual cycle in the northern penetration of the next current segment, the Loop Current, and demonstrate the dramatic year-to-year variability in the occurrence of a particular phase. The last segment of the system is located in the Straits of Florida, where accelerations comparable to those observed in the Yucatan Strait are measured, and the Florida Current is formed.

Dynamical studies indicate that the Cayman Gulf Current is not significantly affected by local forcing, but is instead a free inertial current along its entire length.

Resumen

Los laboratorios oceanográficos y meteorológicos del Atlántico (AOML) han participado en siete expediciones mensuales de las ICCRA, con objeto de hacer un mapa sinóptico de la circulación en el Mar del Caimán y el el Golfo de México. Pudo comprobarse la utilidad de estas expediciones, ya que cuando el trabajo de los participantes estuvo bien coordinado, se obtuvo la cobertura espacial más completa y sinóptica.

En esta recopilación, la serie de datos del Centro de Datos Regionales de las ICCRA y de los laboratorios oceanográfico y meteorológicos del Atlántico son utilizados combinadamente para describir la estructura de las corrientes en las cuencas del Golfo y del Mar del Caimán. Se siguió el curso a través de la región de una corriente de estructura continua conocida - aunque no en la nomenclatura - como corriente del Golfo-Mar del Caimán, que penetra en este mar, procedente del oeste, por el paso Jamaica-Hondura. En la mitad de la cuenca del Mar del Caimán, al sur del bajo del Caimán, se han medido velocidades superficiales que se aproximan a los 75 cm/seg. En la región del Estrecho de Yucatán, la corriente del Mar del Caimán, gira hacia al norte, convirtiéndose en la Corriente de Yucatán, habiéndose observado, mediante mediciones directas de esta corriente, que su velocidad llega a triplicarse. Los datos obtenidos durante las expediciones de las ICCRA apoyan la hipótesis de la existencia de un ciclo anual para la penetración septentrional del segmento inmediato de corriente, la corriente circular, y ponen de manifiesto la forma tan espectacular con que varía de un año a otro una determinada fase. Por último, el sector final del sistema está situado en los Estrechos de la Florida, donde se han medido aceleraciones comparables a las observadas en el Estrecho de Yucatán y en el lugar donde se forma la Corriente de la Florida.

Estudios dinámicos indican que la corriente del Golfo de Caimán no está en forma significativa affectada por fuerzas _in_ _loco_ si no que ella es una corriente de inercia a lo largo de su entera longitud.

1. INTRODUCTION

Observational studies conducted during the field phase of the Cooperative Investigation of the Caribbean and Adjacent Regions (CICAR) have resulted in a significant increase in the quantity of data available for the study of the circulation in the Cayman Sea and the Gulf of Mexico. Many of these field programmes were conducted during the CICAR Survey Months (CSMs). The CSMs were instituted in an effort to coordinate ship schedules so as to obtain maximum spatial coverage of an area in the shortest time.

Data collected during CSM-I, July-August, 1971 resulted in the 20°C topography given in Fig. 1. The data collected by ships from several nations and institutions provide a spatial grid not available from single-ship operations. Temperature surfaces in this region reflect the geostrophic current régime, with large gradients correlated with intense geostrophic currents. For instance, Ichiye (1962) has found a good correlation between temperature patterns at 100 and 200 m and the dynamic height field relative to 1 000 m.

A band of large gradients can be tracked as a continuous feature from the Jamaica-Honduras Passage to the Straits of Florida. Although this continuity suggests a single current, the feature has been studied in the past on a regional basis, and several portions of the flow have acquired distinct names. The established nomenclature for these currents, with one exception, are as given in Fig. 1:

(1) the Cayman Current, previously referred to as the Caribbean Current (Emilsson, 1971) which extends from the Jamaica-Honduras Passage to the Yucatan Peninsula;
(2) the Yucatan Current which flows along the Yucatan Peninsula and Campeche Bank from approximately 18°N to 24°N;
(3) the Loop Current which is the anticyclonic northern extension of the Yucatan Current;
(4) the west Florida Current which flows along the west Florida Shelf when the Loop Current extends deep into the Gulf of Mexico, and
(5) the Florida Current which exits the Gulf of Mexico through the Straits of Florida.

The name Cayman-Gulf Current will be used when referring to the continuous flow comprised of these segments. Three questions relating to the Cayman-Gulf Current will be addressed. These questions, listed in order of increasing difficulty, are:

(1) What are the spatial and temporal characteristics of the Cayman-Gulf Current?
(2) What are the dynamical forces which drive this flow?
(3) What relation, if any, does this flow bear to the general circulation of the North Atlantic?

CSM and other data as well as results already published are presented to summarize our state of knowledge pertaining to these questions.

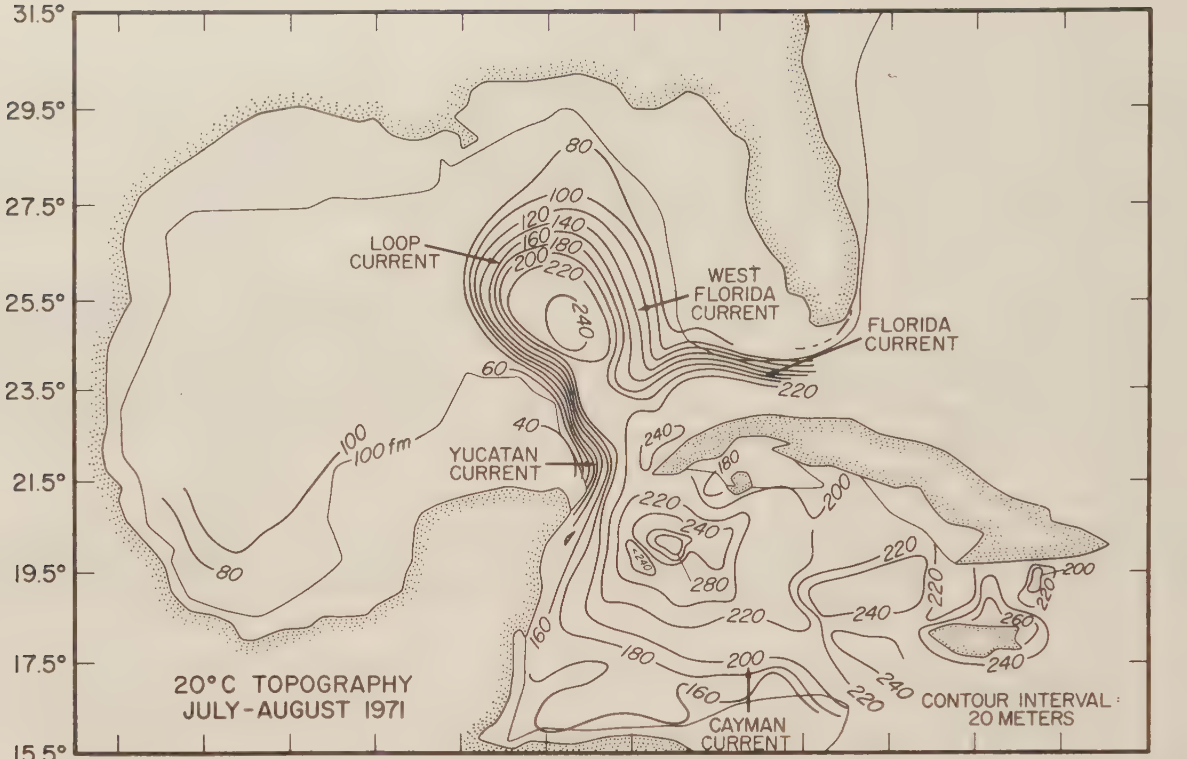

31.5°
29.5°
27.5°
25.5°
23.5°
21.5°
19.5°
17.5°
15.5°
97.5°
95.5°
93.5°
91.5°
89.5°
87.5°
85.5°
83.5°
81.5°
79.5°
77.5°
75.5°
73.5°
LOOP CURRENT
WEST FLORIDA CURRENT
FLORIDA CURRENT
YUCATAN CURRENT
CAYMAN CURRENT
100 fm
20°C TOPOGRAPHY
JULY-AUGUST 1971
CONTOUR INTERVAL: 20 METERS

Fig. 1 The 20°C isothermal surface observed during CICAR Survey Month I, July-August 1971. The nomenclature for the segments of the Cayman-Gulf Current are also given

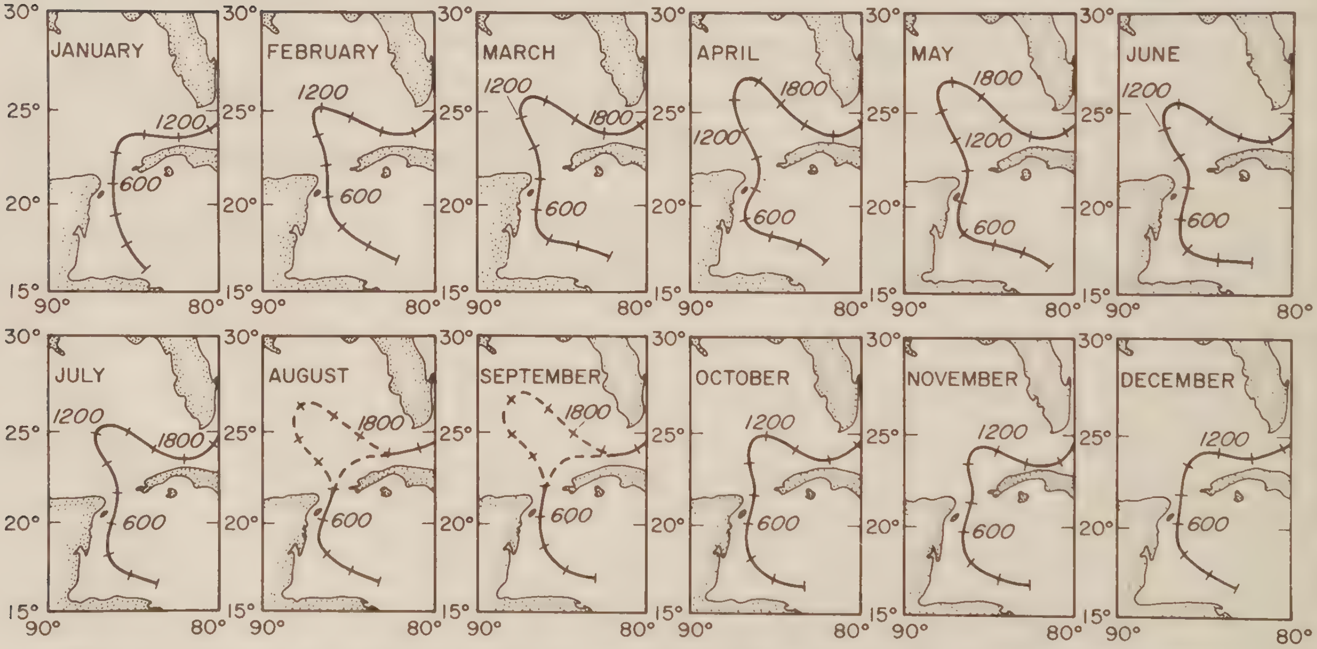

JANUARY
FEBRUARY
MARCH
APRIL
MAY
JUNE
JULY
AUGUST
SEPTEMBER
OCTOBER
NOVEMBER
DECEMBER
600
1200
1800
30°
25°
20°
15°
90°
80°

Fig. 2 Monthly mean axes of the Cayman-Gulf Current. The path lines represent the axes of the maximum temperature gradients at 150 m as given by Robinson (1973). Tick marks along the axes denote 200 km intervals

2. SPATIAL AND TEMPORAL CHARACTERISTICS OF THE CAYMAN-GULF CURRENT

Climatological temperature data compiled by Robinson (1973) were used to determine the monthly mean axes of the Cayman-Gulf Current given in Fig 2. The pathlines represent the axes of the maximum temperature gradients at 150 m. These gradients are assumed coincident with the core of the current. As two distinct regions of large gradients were indicated by the climatological temperature data, two axes are drawn in the Gulf of Mexico during August and September.

The monthly paths of the Cayman-Gulf Current which were measured from the 150 m isobath in the Jamaica-Honduras Passage to 80°W in the Straits of Florida apparently vary with an annual cycle. If the southernmost segments of the two axes given for August and September are overlooked, the longest paths are found in the spring and summer and the shortest in autumn and winter. Both the Cayman Sea and Gulf of Mexico segments of the total path are longer in the spring and summer.

Although synoptic representations of the Cayman Sea portion of the Cayman-Gulf Current have been obtained (see Parr, 1937; Cochrane, 1968 or Molinari, 1975) the data were insufficient to determine if an annual cycle existed in the current location. The axes of Fig. 2 indicate that during the spring and summer the Cayman Current has a larger westerly component in the southern basin which accounts for the paths being longer than those observed in the fall and winter.

An annual cycle has been suggested for the Gulf of Mexico portion of the Cayman-Gulf Current. Leipper (1970) proposed that the Loop Current intrudes north into the Gulf of Mexico during the spring; then, as either a loop or an eddy detached from the loop spreads to the west, it finally recedes to a minimum intrusion in the winter. This cycle has also been observed both in a recent synoptic study (Maul, 1975) and in another climatological study of the eastern Gulf of Mexico circulation (Whitaker, 1971).

The data presented here are distributed in time in order to permit a revaluation of the annual cycles discussed above. Temperature and surface drifter data were collected during seven quasi-synoptic time periods: October 1970, July-August 1971, May 1972, May-June 1975, August 1975, October-November 1975 and February 1976. These periods coincided with CICAR Survey Months, except for the October 1970 and August 1975 periods.

The topography of the 20°C isothermal surface is used to depict the large-scale circulation patterns. Surface drifter data collected during several of the experiments are also presented. These Lagrangian drifter data are presented in an Eulerian framework in the sense that the time series of drifter positions are converted to speeds and contoured as a steady-state Eulerian field. The Lagrangian speed data were smoothed first by a technique in which successive groups of speed values were fitted to a polynomial curve (Molinari and Kirwan, 1975).

The 20°C surfaces, Figs. 1 and 3-8, illustrate the large year-to-year variability which exists in the circulation pattern for a particular month. For instance, although the April-May 1972 and May-June 1975 path lengths of the Cayman-Gulf Current (as indicated by axes of the maximum slopes along the 20°C surface) are similar, the circulation patterns are decidedly different (Figs. 3 and 4) in that the 1972 Cayman Current veers to the south before turning north at the Mexican coast. While (although the data are not conclusive) the 1975 pattern suggests that the veering did not occur ; Cochrane (1968) observed a similar southerly deflection during May 1966, but not in May 1968.

The most dramatic differences in the circulation patterns are observed in the anticyclonic eddies found south and north of the Yucatan Channel. In 1975 the eddy south of Cuba (Fig. 4) is significantly smaller and more intense than in 1972 (Fig. 3). In the Gulf of Mexico, a detached eddy was located north of the Cayman-Gulf Current in 1972 but not in 1975. The depression which appears in the 20°C surface at 87.5°W and 27.5°N in 1975 surrounds water which does not have the T-S relationship characteristic of eddies detached from the Loop Current. The 1972 eddy separated from the Loop Current in April and had kinematic properties similar to the main flow (Merrell et al., 1976).

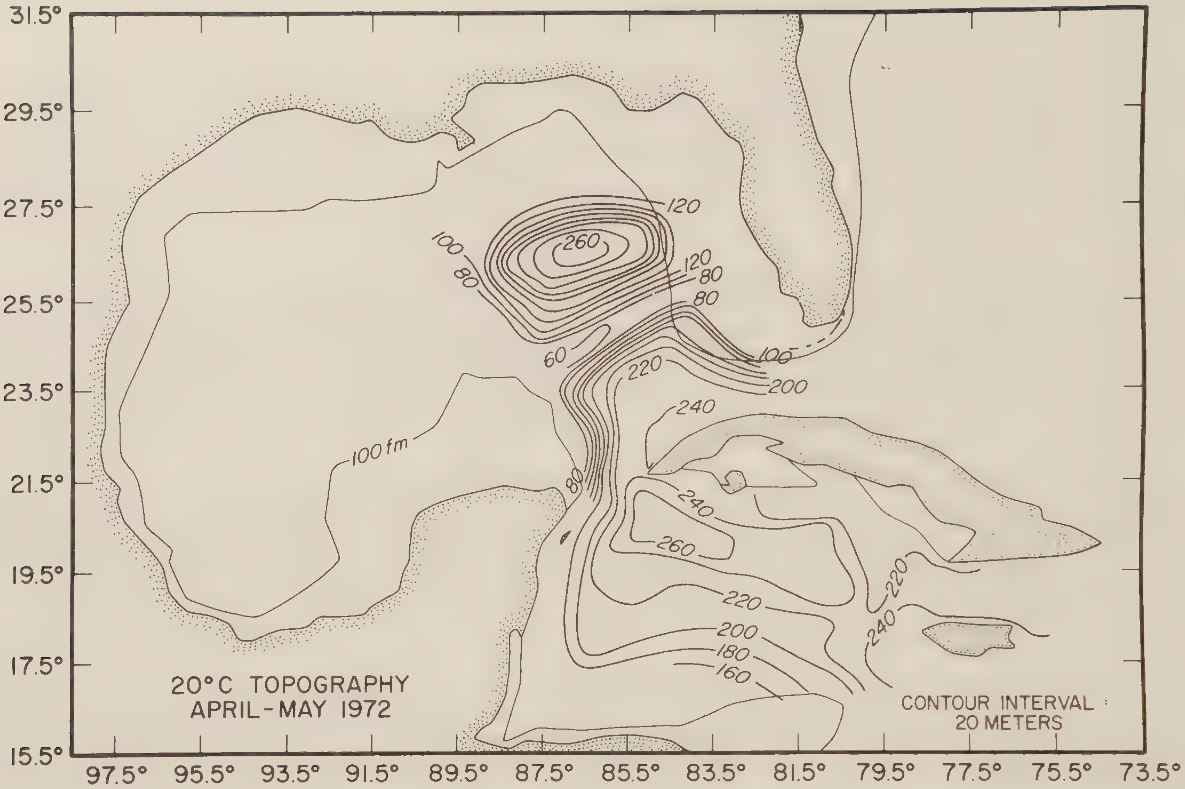
31.5°
29.5°
27.5°
25.5°
23.5°
21.5°
19.5°
17.5°
15.5°
97.5°
95.5°
93.5°
91.5°
89.5°
87.5°
85.5°
83.5°
81.5°
79.5°
77.5°
75.5°
73.5°
120
260
100
80
120
80
80
60
100
200
220
240
100 fm
80
240
260
220
200
180
160
220
240
20°C TOPOGRAPHY
APRIL-MAY 1972
CONTOUR INTERVAL
20 METERS

Fig. 3 The 20°C isotherm surface observed during CICAR Survey Month II, April-May 1972

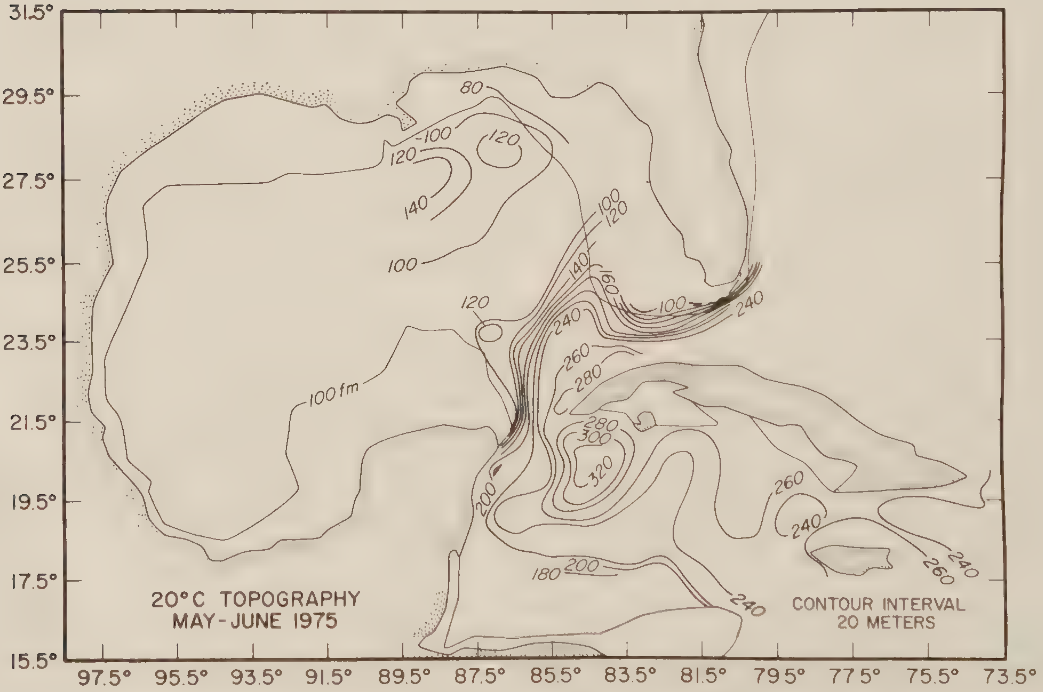
31.5°
29.5°
27.5°
25.5°
23.5°
21.5°
19.5°
17.5°
15.5°
97.5°
95.5°
93.5°
91.5°
89.5°
87.5°
85.5°
83.5°
81.5°
79.5°
77.5°
75.5°
73.5°
80
100
120
120
140
100
100
120
140
160
100
240
120
240
260
280
100 fm
280
300
320
200
260
240
240
260
180
200
240
20°C TOPOGRAPHY
MAY-JUNE 1975
CONTOUR INTERVAL
20 METERS

Fig. 4 The 20°C isothermal surface observed during May-June 1975

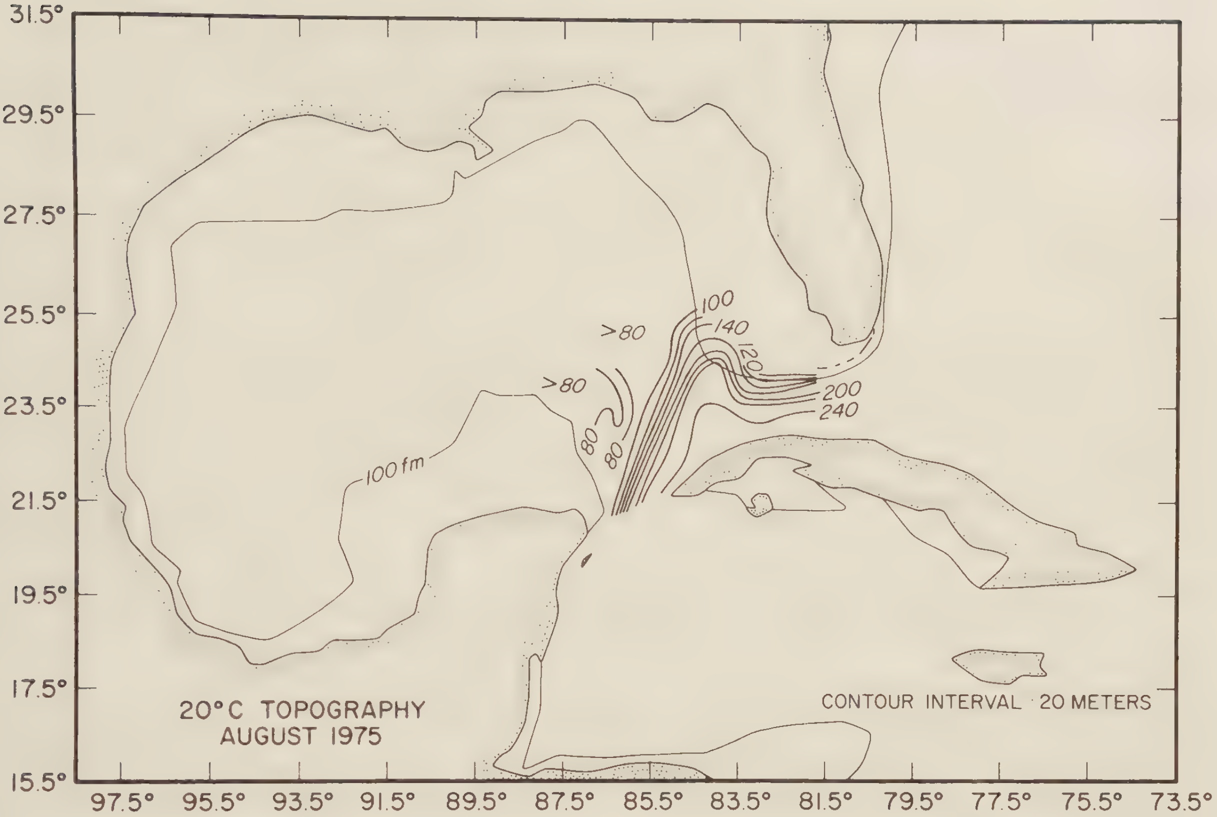
20°C TOPOGRAPHY
AUGUST 1975
CONTOUR INTERVAL 20 METERS
100 fm
>80
>80
80
80
100
140
120
200
240
31.5°
29.5°
27.5°
25.5°
23.5°
21.5°
19.5°
17.5°
15.5°
97.5°
95.5°
93.5°
91.5°
89.5°
87.5°
85.5°
83.5°
81.5°
79.5°
77.5°
75.5°
73.5°

Fig. 5 The 20°C isothermal surface observed during August 1975

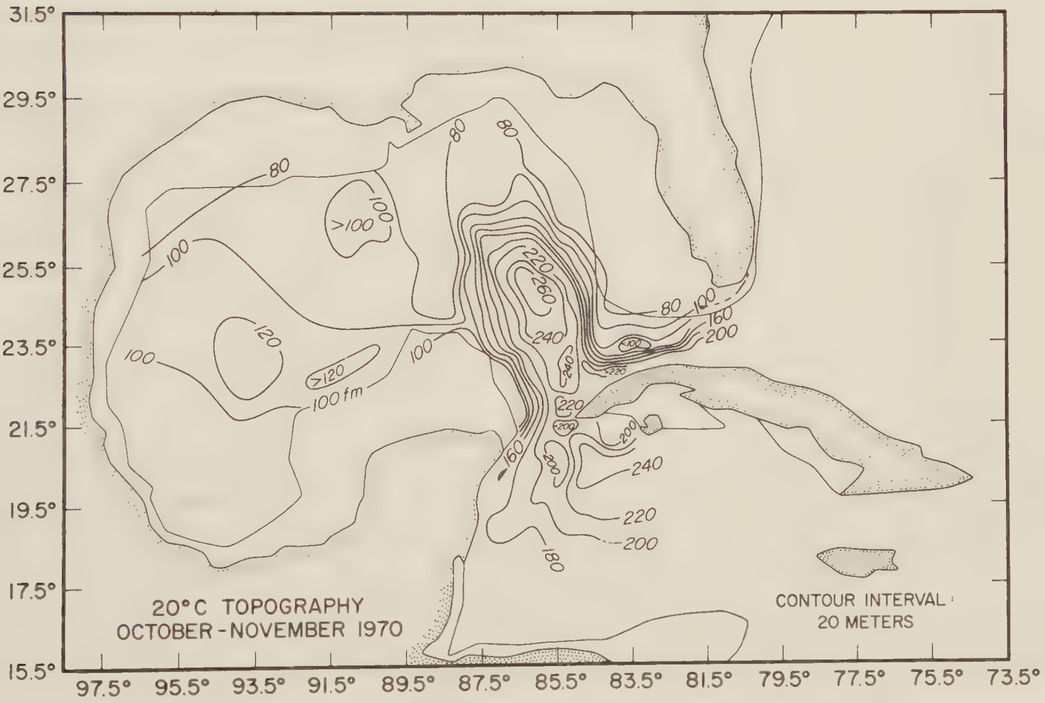
20°C TOPOGRAPHY
OCTOBER-NOVEMBER 1970
CONTOUR INTERVAL
20 METERS
80
80
80
>100
100
100
120
100
>120
100 fm
100
220
260
240
240
220
200
80
100
160
200
100
220
200
240
160
200
220
200
180
31.5°
29.5°
27.5°
25.5°
23.5°
21.5°
19.5°
17.5°
15.5°
97.5°
95.5°
93.5°
91.5°
89.5°
87.5°
85.5°
83.5°
81.5°
79.5°
77.5°
75.5°
73.5°

Fig. 6 The 20°C isothermal surface observed during October–November 1970

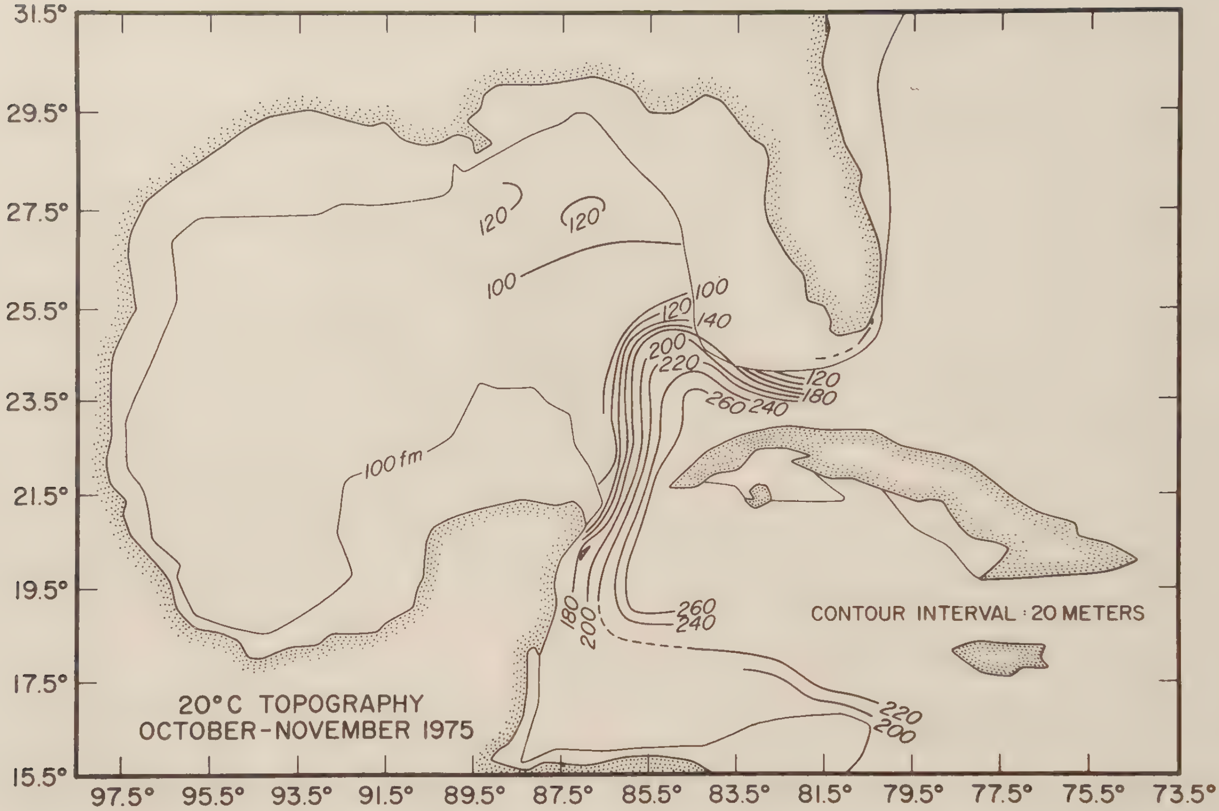
31.5°
29.5°
27.5°
25.5°
23.5°
21.5°
19.5°
17.5°
15.5°
97.5°
95.5°
93.5°
91.5°
89.5°
87.5°
85.5°
83.5°
81.5°
79.5°
77.5°
75.5°
73.5°
120
120
100
100
120
140
200
220
120
180
260
240
100 fm
180
200
260
240
CONTOUR INTERVAL : 20 METERS
220
200
20°C TOPOGRAPHY
OCTOBER-NOVEMBER 1975

Fig. 7 The 20°C isothermal surface observed during October-November 1975

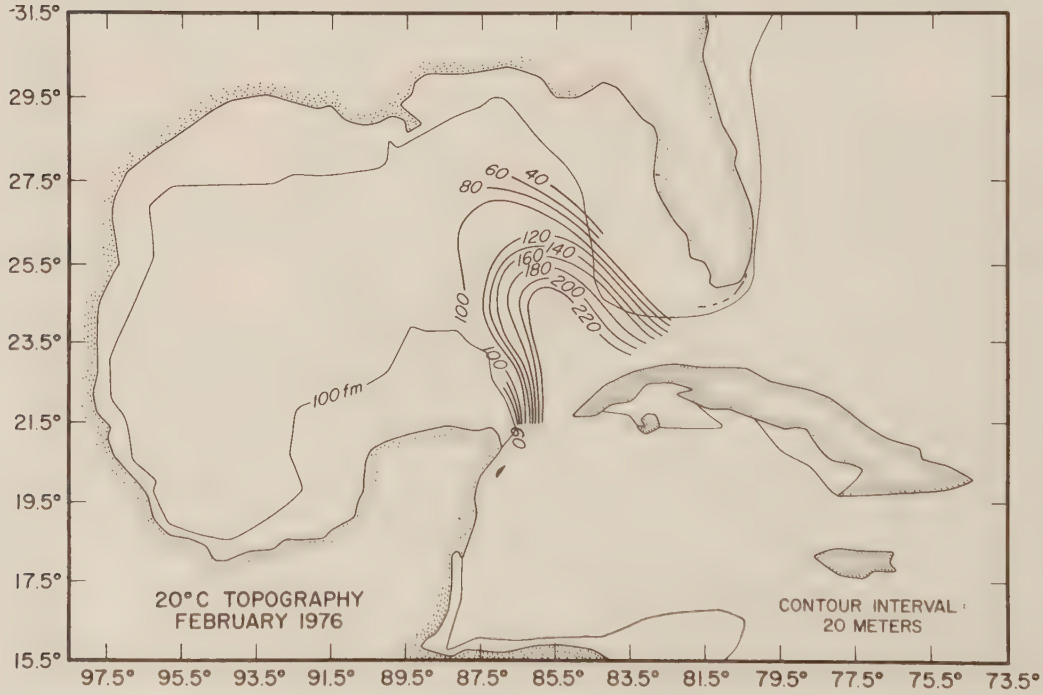
31.5°
29.5°
27.5°
25.5°
23.5°
21.5°
19.5°
17.5°
15.5°
97.5°
95.5°
93.5°
91.5°
89.5°
87.5°
85.5°
83.5°
81.5°
79.5°
77.5°
75.5°
73.5°
60
40
80
120
140
160
180
200
220
100
100
100 fm
60
20°C TOPOGRAPHY
FEBRUARY 1976
CONTOUR INTERVAL
20 METERS

Fig. 8 The 20°C isothermal surface observed during February 1976

Nowlin and Hubertz (1972) observed a detached eddy in June 1967 and a well-developed loop indicative of a pre-separation pattern in June 1966. The small penetration of the Loop Current in 1975 suggests that an eddy had already detached, and indeed Leckegis (1976) observed a separation in February 1975, the earliest time in the year when such an event has been documented.

The summer (Figs. 1 and 5) and autumn (Figs. 6 and 7) 20°C surfaces further demonstrate the large year-to-year seasonal variability in the path length of the Loop Current. During both cases the intrusion during 1975 was considerably less than that observed in the other years.

Cochrane (1976) has shown that the Yucatan Current as it leaves the Yucatan Channel at approximately 22°N has two preferred directional modes. In the west mode, observed during August 1971 (Fig. 1), the current flows to the northwest, while in the east mode, observed during August 1976 (Fig. 5), the current flows to the northeast. The Loop Current intrusion is deeper in the west mode. The existence of two regions of large gradients in August and September (Fig. 2) indicate that the direction of the climatological Yucatan Current during these months has the same two preferred modes at 22°N.

Maul (1975) indicated that eddy separations occurred in November 1970 and late August 1971. The large meanders found in the West Florida Current during both years (Figs. 1 and 6) apparently are precursors to a detachment event (Cochrane, 1972).

The February 1976 20°C surface (Fig. 8) shows what prior to February 1975 (Leckegis, 1976) was observed as a typical wintertime intrusion of the Loop Current (Nowlin, 1972 and SUSIO, 1975).

Perhaps the most remarkable feature of the data from May 1975 through February 1976, combined with data recently collected in May and August 1976, is the absence of the usual intrusion cycle of the Loop Current. Instead, the apex of the Loop Current remained at approximately the same latitude, 25.5°N from May-June 1975 through February 1976 (Figs. 4,5, 7 and 8). The apex intruded somewhat to 26.5°N by May 1976 (not shown) but remained at this latitude until August 1976 (also not shown). Thus, from May 1975 to August 1976 no large intrusion of the Loop Current intrusion was observed.

In addition to these temporal changes in the spatial characteristics of the Cayman-Gulf Current, temporal changes in the intensities of various segments of the current have been observed. For instance, the sea-surface speeds of the Yucatan Current and the Florida Current apparently vary with an annual period. Mean monthly, ship-drift data indicate that the maximum speeds of the Yucatan Current occur in June and the minimum speeds in November (Cochrane, 1965). In addition, when the flow is most intense, the core of the current is usually observed farther west in the Yucatan Channel than when the flow is weak (Molinari and Cochrane, 1972). The maximum surface speeds of the Florida Current as given by ship-drift reports occur in July and the minimum in November (Fuglister, 1951). However, when fitted by an annual harmonic, a long series of directly measured volume transports in the Straits of Florida exhibit a maximum transport in June (Niiler and Robinson, 1973).

Although the path of the Cayman-Gulf Current varies widely, as shown by the 20°C surfaces, the distribution of speed along the axis of the current remains much the same regardless of path. The surface drifters were launched in the current axis which was located by the thermal field. In all four experiments (Figs. 9 to 12) the drifters decelerated as they entered the anticyclonic turns in both the Cayman Sea and Gulf of Mexico and accelerated as they left these turns. Significant accelerations occur in the Yucatan Straits (Figs. 10 and 11) and the Straits of Florida (Fig. 10). These accelerations are also indicated in all the thermal fields in these regions (Figs. 1 and 3-8) by the large increase in the temperature gradients.

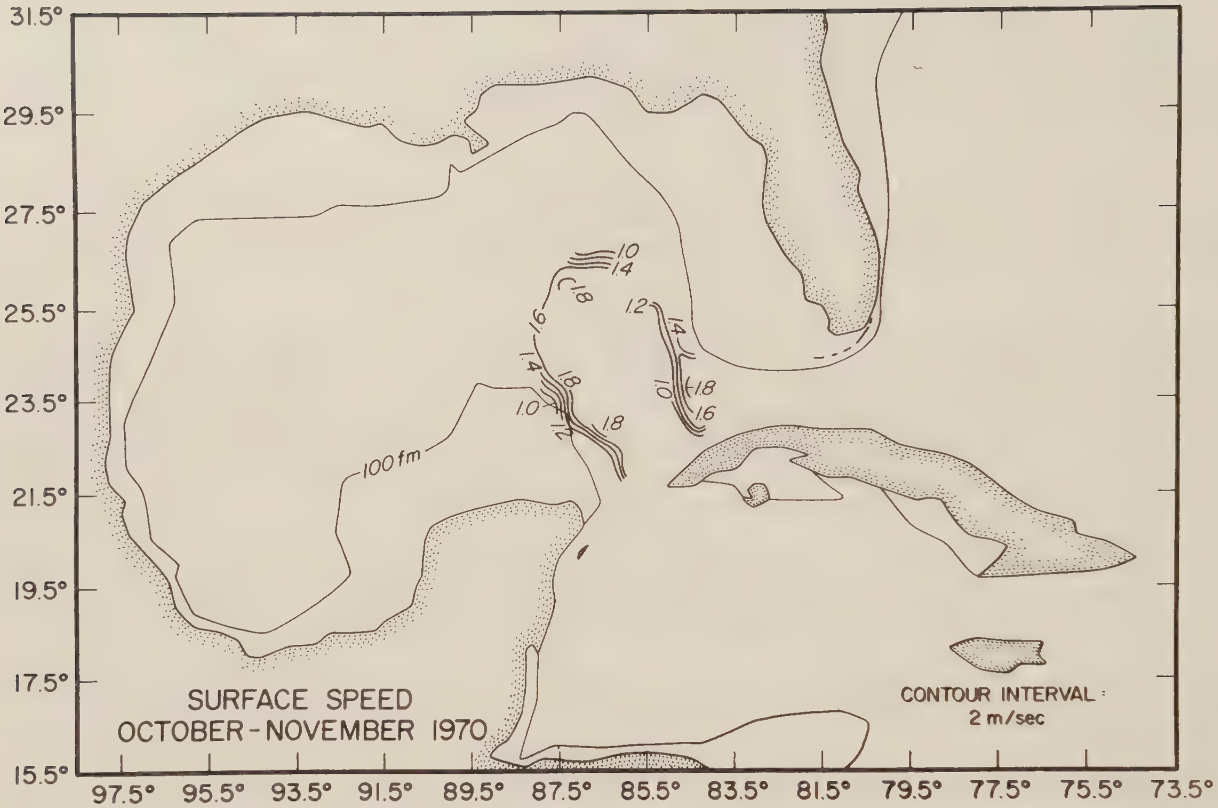
31.5°
29.5°
27.5°
25.5°
23.5°
21.5°
19.5°
17.5°
15.5°
97.5°
95.5°
93.5°
91.5°
89.5°
87.5°
85.5°
83.5°
81.5°
79.5°
77.5°
75.5°
73.5°
1.0
1.4
1.8
1.6
1.4
1.8
1.0
1.2
1.8
1.2
1.4
1.0
1.8
1.6
100 fm
SURFACE SPEED
OCTOBER-NOVEMBER 1970
CONTOUR INTERVAL:
2 m/sec

Fig. 9 The distribution of surface current speeds determined from surface drifters (see text) during October–November 1970

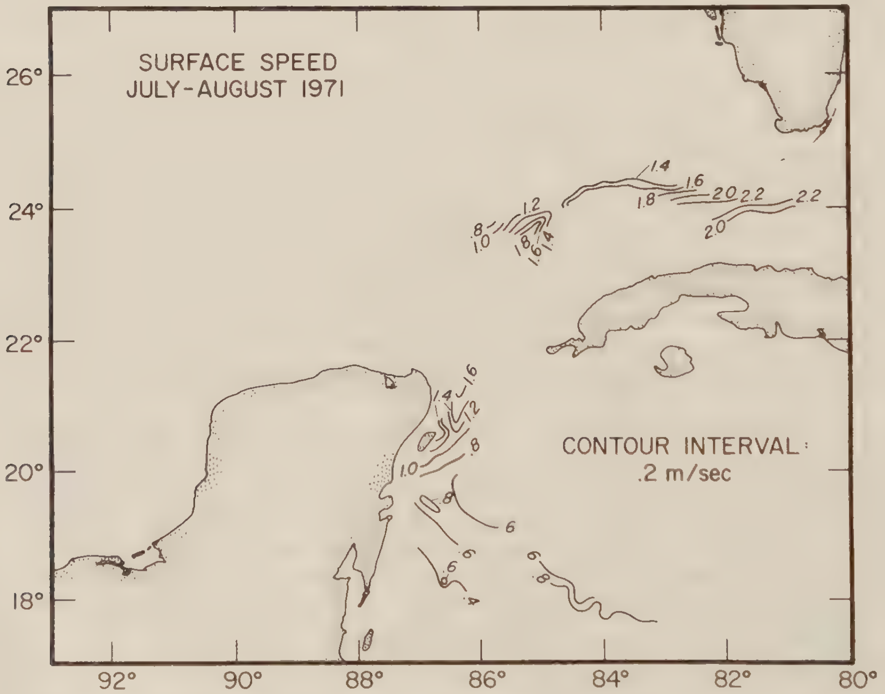
SURFACE SPEED
JULY-AUGUST 1971
26°
24°
22°
20°
18°
92°
90°
88°
86°
84°
82°
80°
1.4
1.6
1.8
2.0
2.2
2.2
2.0
1.2
.8
1.0
1.8
1.6
1.4
1.6
1.4
1.2
.8
1.0
.8
.6
.6
.6
.4
.6
.8
CONTOUR INTERVAL:
.2 m/sec

Fig. 10 The distribution of surface current speeds determined from surface drifters (see text) during July–August 1971

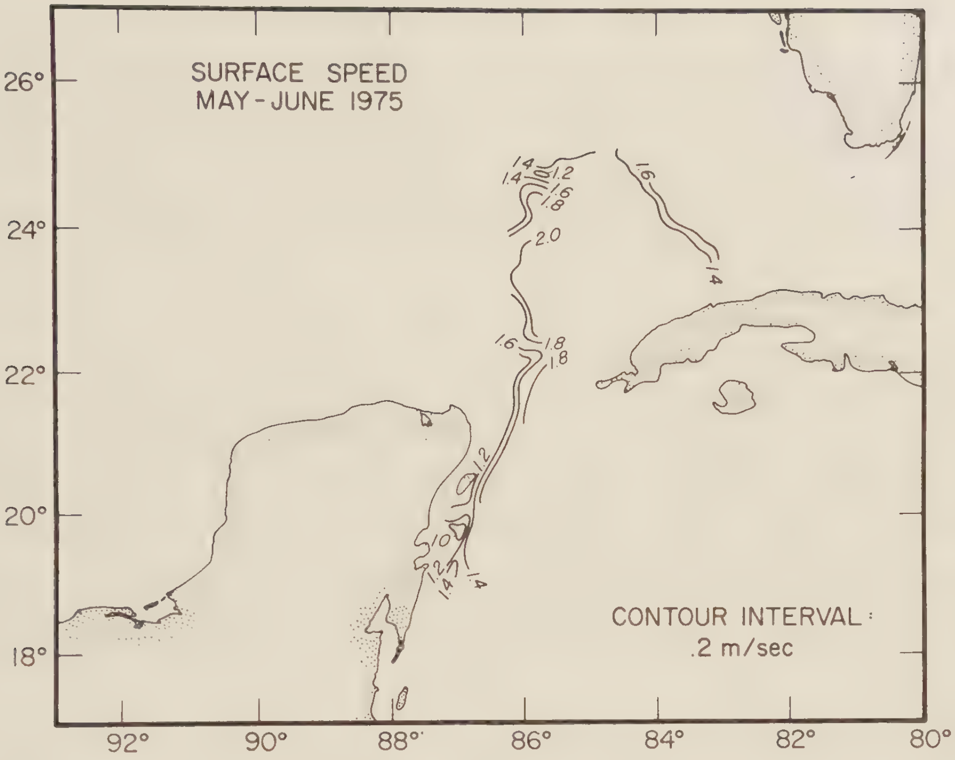
SURFACE SPEED
MAY-JUNE 1975
CONTOUR INTERVAL:
.2 m/sec
26°
24°
22°
20°
18°
92°
90°
88°
86°
84°
82°
80°
1.4
1.2
1.6
1.8
2.0
1.0

Fig. 11 The distribution of surface current speeds determined from surface drifters (see text) during May-June 1975

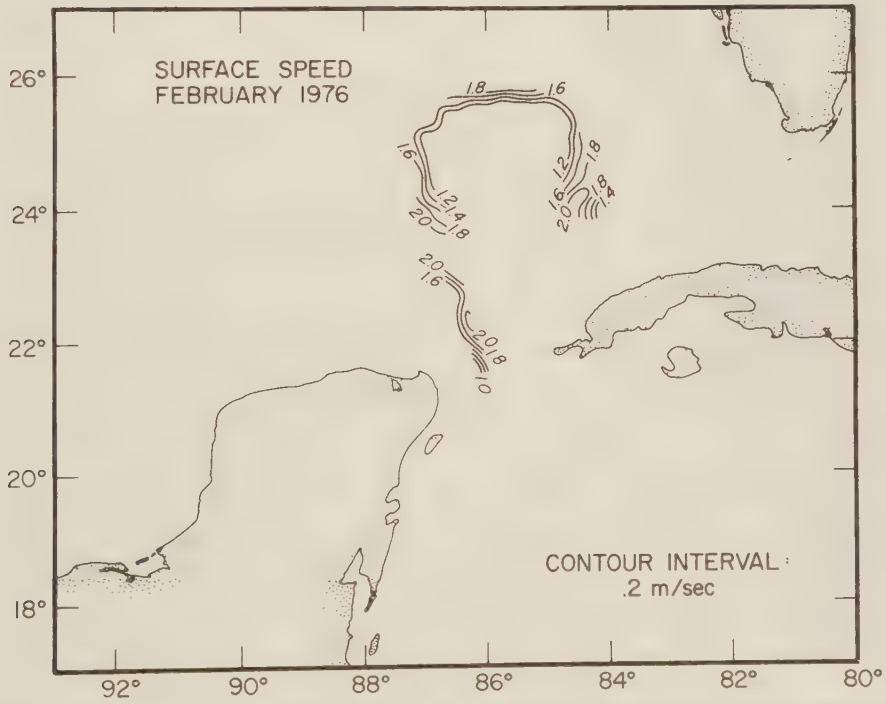
SURFACE SPEED
FEBRUARY 1976
CONTOUR INTERVAL:
.2 m/sec
26°
24°
22°
20°
18°
92°
90°
88°
86°
84°
82°
80°
1.8
1.6
1.2
1.4
2.0
1.0

Fig. 12 The distribution of surface current speeds determined from surface drifters (see text) during February 1976

3. DYNAMICAL PROCESSES ACTIVE IN THE CAYMAN-GULF CURRENT

The causes of the observed temporal and spatial variability of the Cayman-Gulf Current and the documented fluctuations of the Yucatan and Florida Currents have not been determined. However, there are indications that these phenomena are related to local and distant wind-fields. Fuglister (1951) found that the Caribbean Current near the Lesser Antilles varies with an annual cycle which he correlated with the local wind-stress cycle in this region. The phases of the Yucatan and Florida Current cycles relative to the phase of the Caribbean Current cycle are such as to suggest a downstream propagation of the annual cycle.

The fluctuations in the intensities of the Florida and Yucatan Currents have been correlated with the winds over the mid-Atlantic and Cayman Seas. Stommel (1965) found in two out of three case studies that an increase in the transport of the Florida Current occurred during the time of a breakdown in the strength of the Bermuda-Azores high. The breakdown, according to Stommel, increases the Ekman transport through the Lesser Antilles and eventually through the Straits of Florida. Emilsson (1971) proposed that the intensity of the Yucatan Current is modulated by the wind-field over the Cayman Sea. When the winds are strong with a large west or northwest component the resulting Ekman drift causes an outflow through the Windward Passage, thereby reducing the transport through the Yucatan Straits.

An additional wind effect on the Cayman-Gulf Current was proposed by Parr (1937) and Gordon (1967). Their data indicate that the Cayman Current flowed against the internal pressure gradient in the Cayman Sea. The energy required for this "uphill" flow was provided by the wind-field.

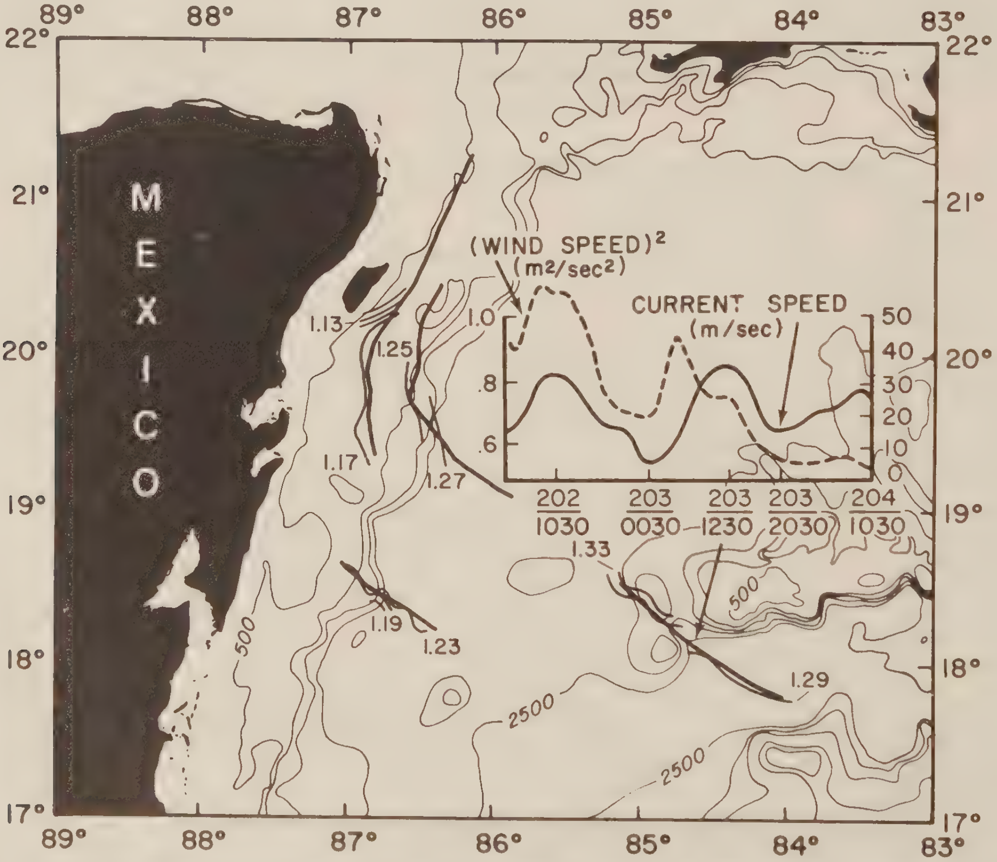

Fig. 13 Centre-of-mass trajectories for buoy clusters deployed during July 1971. The trajectories are superimposed on the dynamic topography of the sea-surface computed relative to 600 m. The insert gives the current speed and wind speed squared functions-vs-time for the indicated trajectory

The surface drogue trajectories and speeds shown in Fig. 13 indicate that in mid-basin the drifters did not decelerate as they moved against the pressure gradient. A description of the drogues and the possible errors due to positioning accuracy, wind effects, etc. are given by Molinari and Kirwan (1975). The downstream component of the wind speed squared (Fig. 13, insert) and the drogue speeds are coherent over the initial part of this trajectory, suggesting that the wind is putting energy into the current to cause the cross gradient flow. This area is one of the two regions where Gordon (1967) proposed that the largest input of energy by the wind occurs. However, as the flow along this trajectory is geostrophic to within 10%, and the deceleration equivalent to the downstream pressure gradient is negligible, of the order 10^{-7}m/sec^2 (Molinari, 1976), the effect of the wind during this period was probably small and limited to the upper layers.

The cause of the temporal variability of the Cayman Current has not been determined, but various proposals have been offered for the cause of the Loop Current cycle: Paskausky and Reid (1972) in a barotrophic numerical model, and Wert and Reid (1972) in a two-layer model. Both of these varied the cross-stream velocity structure at the Yucatan Straits while keeping the total transport into the gulf constant. The effect of this boundary condition is to vary with time the relative vorticity distribution at the input boundary. Both studies produced an annual cycle of Loop Current penetration similar to the cycle proposed by Leipper (1970). However, Maul (1975) suggested that the penetration of the Loop Current might be related to a difference in phase between the maximum transports through the Yucatan Straits and Straits of Florida. Cochrane (1965) has noted that a phase difference of approximately one month exists at least in the surface speeds of the Yucatan and Florida Currents.

The dynamics along the axis of the Cayman-Gulf Current are such that accelerations and decelerations occur in the same relative positions regardless of the path length of the current. Decelerations are observed in the anticyclonic turns at 19°N and 86°W (Fig. 10) and at the apex of the Loop Current (Figs. 9 to 12). Chew (1974) has proposed a kinematical argument that these accelerations are related to adjustments in the shear and curvature components of the relative vorticity which must occur in turning currents. In addition, decelerations are required in anticyclonic turns in which the flow is governed by the gradient relation between Coriolis and centripetal accelerations and pressure gradient forces such as observed in the Cayman Current (Molinari, 1976).

Cochrane (1962) suggested that the formation of the Yucatan Current could be explained in terms of the inertial boundary layer theory of Charney (1955). In this theory, a broad, slow, westward drift in the interior of the ocean is intensified to a narrow, intense, northward flowing boundary current by the action of the earth's rotation. The earth's rotation is modelled by a linear change in Coriolis parameter with latitude, the so-called Beta effect. Molinari (1975) in a numerical modelling study, and Molinari and Kirwan (1975) in an observational study present additional evidence to support this theory.

The results of Chew (1974) support the contention that potential vorticity was conserved along the Loop and Florida Currents during the October 1970 and August 1971 experiments (Figs. 9 and 10). Thus, the available evidence is consistent with the idea that the entire Cayman-Gulf Current is essentially a free inertial current with local forcing having a negligible influence.

4. THE ROLE OF THE CAYMAN-GULF CURRENT IN THE NORTH ATLANTIC GYRE

Ichiye (1969) has hypothesized that the Cayman Sea and Gulf of Mexico serve as a sink of negative relative vorticity for the North Atlantic gyre. A sink is necessary to ensure that absolute vorticity is conserved from 20°N to 30°N; and can be furnished by a source of positive relative vorticity due to friction at the boundary, and/or eddy detachment in the Gulf of Mexico and subsequent loss of negative relative vorticity.

The region obviously has an effect on the heat/salt budget of the North Atlantic since the eddies which detach from the Cayman-Gulf Current in the Gulf of Mexico remove a considerable amount of heat and salt from the North Atlantic gyre. This effect has not been studied extensively.

5. SUMMARY

The physical oceanographic data collected during CICAR significantly broadened the database on which to conduct studies of the region. Most of these data have been analysed in descriptive efforts to infer the current régimes and their temporal variability. The observational evidence portrays a continuous current flowing from the Jamaica-Honduras Passage to the Straits of Florida, with speeds along the axis of the flow ranging between 50 and 200 cm/sec

Some dynamical studies have been conducted, and the results of these studies indicate that the current is essentially inertial. That is, no significant external forces act on the current as it flows through the Cayman Sea and Gulf of Mexico. Thus the kinematics of the Cayman-Gulf Current is similar to that of other segments of the Gulf Stream system, and it should be considered the first leg of that portion of the North Atlantic gyre. Historically, the Yucatan Current has assumed this role. Many questions regarding the dynamics of the circulation in this region still remain to be answered. For instance, why is there so much variability in the year-to-year monthly current pattern? What is the role of bottom topography in establishing the current régime? What wind régimes contribute to establishing the current fields? Many of these questions will require studies farther upstream into the Caribbean Sea and the Atlantic Ocean in order to be answered. However, because of the importance of these currents to all aspects of the oceanography of the region, it is essential that studies continue to ensure that the questions are answered.

6. ACKNOWLEDGEMENTS

A large portion of the data presented in this discussion were collected aboard the NOAA vessels RESEARCHER and VIRGINIA KEY. The invaluable assistance of the officers and crew of these ships is gratefully acknowledged.

The work was supported in part by the Bureau of Land Management under BLM Interagency Agreement 08550-IA5-26.

7. REFERENCES

Chew, F., The turning process in meandering currents: a case study. *J.Phys.Oceanogr.*,
1974 4:21-57

Cochrane, J.D., The Yucatan Current. College Station, Texas A. & M. University, Department
1965 of Oceanography, Ref. (65-17T):20-7 (Unpubl.)

__________, The currents and waters of the eastern Gulf of Mexico and the western Caribbean
1968 Sea. College Station, Texas A. & M. University, Department of Oceanography,
Ref. (68-8T):19-28 (Unpubl.)

__________, Separation of an anticyclone and subsequent developments in the Loop Current
1972 (1969). *In* Contributions on the physical oceanography of the Gulf of Mexico
edited by L.R.A. Capurro and J.L. Reid. Houston, Gulf Publishing Co., pp. 91-106

__________, The configuration of the Gulf of Mexico Loop Current in relation to bathymetry
1976 and season. Paper submitted to the CICAR II Symposium sponsored by IOC, FAO,
Unesco and WMO, Caracas, Venezuela, July 12-16, 1976. Spanish abstract in progress
in marine research in the Caribbean and adjacent regions. CICAR II Symposium,
abstracts of submitted papers. Caracas, Venezuela, CICAR, p. 14

Emilsson, I., On the upper layer circulation in the Cayman Sea. *In* Unesco/FAO Symposium
1971 on Investigations and Resources of the Caribbean Sea and Adjacent Regions,
Willemstad, Curaçao, 18-26 November 1968. Paris, Unesco, pp. 53-60

Fuglister, F.C., Annual variation in current speeds in the Gulf Stream system. *J.Mar.Res.*,
1951 10:119-27

Gordon, A.L., Circulation of the Caribbean Sea. *J.Geophys.Res.*, 72:6207-23
1967

Ichiye, T., Circulation and water mass distribution in the Gulf of Mexico. *Geofis.Int.Mex.*,
1962 2:47-76

__________, Experiments on circulation of the Gulf of Mexico and the Caribbean Sea with
1969 a rotating tank. College Station, Texas A. & M. University, Ref. (69-17T):37 p.
(Unpubl.)

Legeckis, R., Present and planned satellite observations of the Gulf of Mexico and the
1978 Caribbean Sea. *FAO Fish.Rep.*, (200) Suppl.

Leipper, D.F., A sequence of current patterns in the Gulf of Mexico. *J.Geophys.Res.*,
1970 75:637-57

Maul, G., An evaluation of the use of the Earth Resources Technology Satellite for observing
1975 ocean current boundaries in the Gulf Stream system. *NOAA Tech.Rep.*, (ERL 335-
AOML 18):125 p.

Merrell, W.J. Jr. *et al.*, A detailed description of the circulation observed in the eastern
197 Gulf of Mexico during CICAR Survey Month II, May 1972. *FAO Fish.Rep.*, (200) Suppl.

Molinari, R.L., A comparison of observed and numerically simulated circulation in the Cayman
1975 Sea. *J.Phys.Oceanogr.*, 5:51:62

__________, The formation of the Yucatan Current based on observations of Summer 1971.
1976 *J.Phys.Oceanogr.*, 6:596-602

Molinari, R.L. and J.D. Cochrane, The effect of topography on the Yucatan Current. In
1972 Contributions on the physical oceanography of the Gulf of Mexico, edited by L.R.A. Capurro and J.L. Reid. Houston, Gulf Publishing Co., pp. 149-55

Molinari, R.L. and A.D. Kirwan, Calculations of differential kinematic properties from
1975 Lagrangian observations in the western Caribbean Sea. J.Phys.Oceanogr., 5:483-91

Niiler, P.P. and W.S. Richardson Jr., Seasonal variability of the Florida Current. J.Mar.
1973 Res., 31:144-67

Nowlin, W.D., Winter circulation patterns and property distributions. In Contributions on
1972 the physical oceanography of the Gulf of Mexico, edited by L.R.A. Capurro and J.L. Reid. Houston, Gulf Publishing Co., pp. 3-51

Nowlin, W.D. and J.M. Hubertz, Contrasting summer circulation patterns for the Eastern
1972 Gulf. Loop Current versus anticyclonic ring. In Contributions on the physical oceanography of the Gulf of Mexico, edited by L.R.A. Capurro and J.L. Reid. Houston, Gulf Publishing Co., pp. 139-48

Parr, A.E., A contribution to the hydrography of the Caribbean and Cayman Sea, based upon
1937 the observations made by the R/V ATLANTIS, 1933-1934. Bull.Bingham Oceanogr. Collect., 5:1-110

Paskausky, D.F. and R.O. Reid, A barotrophic prognostic numerical circulation model. In
1972 Contributions on the physical oceanography of the Gulf of Mexico, edited by L.R.A. Capurro and J.L. Reid. Houston, Gulf Publishing Co., pp. 163-76

Robinson, M.K., Atlas of monthly mean sea surface and sub-surface temperature and depth of
1973 the top of the thermocline Gulf of Mexico and Caribbean Sea. Scripps Inst. Oceanogr., Ref. (73-8): 105 p.

SUSIO, Compilation and summation of historical and existing physical oceanographic data from
1975 the eastern Gulf of Mexico. Coral Gables, State University System of Florida, Institute of Oceanography, Final Report to the Bureau of Land Management, Contract No. 08550-CT4-64

Stommel, H.M., The Gulf Stream: a physical and dynamical description. Berkeley, University
1965 of California Press, 248 p.

Wert, R.J. and R.O. Reid, A baroclinic prognostic numerical circulation model. In
1972 Contributions on the physical oceanography of the Gulf of Mexico, edited by L.R.A. Capurro and J.L. Reid. Houston, Gulf Publishing Co., pp. 177-209

Whitaker, R.E., Seasonal variations of steric and recorded sea level of the Gulf of Mexico.
1972 Masters thesis, Texas A. & M. University, Department of Oceanography, 109 p.

SOVIET INVESTIGATIONS OF THE DYNAMICS AND PROPERTIES OF THE WATERS OF THE CARIBBEAN SEA AND GULF OF MEXICO

by

B.A. NELEPO
Marine Hydrophysical Institute
Ukrainian S.S.R. Academy of Sciences
Sevastopol, U.S.S.R.

V.N. STEPANOV, R.P. BULATOV and
M.M. DOMANOV
Institute of Oceanology
Academy of Sciences of the U.S.S.R.
Moscow, U.S.S.R.

CONTENTS

1. INTRODUCTION
2. STRATIFICATION OF WATERS
3. WATER CIRCULATION
4. WATER EXCHANGE
5. WATER MASSES
6. REFERENCES

Abstract

Complex investigations in the American Mediterranean Sea were carried out as part of the CICAR programme by several scientific centres of the Soviet Union. The material obtained was used for studying hydrophysical and hydrochemical water properties, the artificial radioactivity, peculiarities of formation, spreading, and transformation of water masses, stratification and structure of the water, circulation, and water exchange with the ocean through straits.

The results of these circulatory investigations are of special interest in understanding the nature of the Caribbean Sea and Gulf of Mexico. The calculations of geostrophic currents showed that the main Caribbean current is much narrower than had been thought previously. To the south of it in the Caribbean Sea intensive cyclonic revolving of the waters was discovered, and to the north, a weak anticyclonic system. In the Gulf of Mexico, while the cyclonic transfer prevails, separate mesoscale rotations are traced. Such a system of circulation is preserved to the depth of approximately 1 000 m. Deeper, in correspondence with the bottom relief, weak independent rotations of water are being formed in separate deep-water hollows.

The water interchange through the straits was estimated together with possible transfer of substances, including radioactive nuclei of artificial origin.

The results obtained were published in two special volumes of collected articles. One of them, "Investigation of Caribbean Sea", was published in 1974 by Marine Hydrophysical Institute; the other, "Complex Investigations of Caribbean Sea, Gulf of Mexico 2" (IOAN works, vol. 100), was published by the Institute of Oceanology. In addition, the collected articles, "Chemical and Oceanographic Researches of Seas and Oceans", were published in 1975, including the work, based on generalization and analysis of all the compiled data concerning the American Mediterranean.

Resumen

Como parte de las ICCRA, varios centros científicos de la U.R.S.S. llevaron a cabo importantes investigaciones en aguas del Mediterráneo americano.

Con los materiales recogidos se estudiaron las propiedades hidrológicas e hidroquímicas del agua del mar; la radioactividad artificial; las peculiaridades de formación, dispersión y transformación de las masas de agua; la estratificación y estructura del agua, su circulación y el intercambio de agua con el océano a través de los estrechos.

Los resultados de estas investigaciones sobre la circulación de las aguas son del mayor interés para comprender la naturaleza del Mar Caribe y del Golfo de México. Los cálculos de las corrientes geostróficas muestran que la corriente principal del Caribe es mucho más estrecha de lo que hasta ahora se pensaba. Al sur de esta corriente, dentro del Mar Caribe, se descubrió una fuerte circulación ciclónica, y al norte, una débil circulación anticiclónica. En el Golfo de México, donde prevalece un transporte ciclónico, se han seguido los cursos de circulaciones medias aisladas: Este tipo de sistema de circulación se conserva a la profundidad aproximada de 1 000 metros. En aguas más profundas, en correspondencia con el relieve del fondo, se forman débiles circulaciones independientes.

Se calculó el intercambio de aguas a través de los estrechos, junto con el posible transporte de substancias, entre ellas los núcleos radioactivos de origen artificial.

Los resultados obtenidos se publicaron en dos volúmenes especiales de artículos seleccionados. Uno de ellos, "Investigation of Caribbean Sea" (Investigaciones sobre el Mar Caribe) fue publicado en 1974 por el Instituto de Hidrofísica Marina, y el otro "Complex Investigations of Caribbean Sea, Gulf of Mexico 2" (obras del IOAN, vol. 100), fue publicado por el Instituto de Oceanología. Además, los artículos seleccionados, "Chemical and Oceanographic Researches of Seas and Oceans" (Investigaciones químicas y oceanográficas de los mares y océanos), que se publicaron en 1975, incluyen la labor de generalización y análisis de todos los datos compilados relativos al Mediterráneo americano.

1. INTRODUCTION

The American Mediterranean Sea is one of the most specific and interesting basins of the World Ocean. This is due to distinctive features of its dynamics and to the Gulf Stream which originates from it. As is known, this current greatly affects not only the Atlantic Ocean. Waters formed in the north of the Atlantic Ocean spread widely. The interest shown by the Soviet oceanologists in the research on the Caribbean Sea and the Gulf of Mexico is mainly associated with this. In addition, we strive to render assistance to the Latin-American States for studies of the nature and resources of the American Mediterranean.

Our research began during the Soviet-Cuban Expedition in 1964. In the seventies this research was continued in the CICAR programme. The results obtained were published in numerous articles and special collected papers. In addition, a general study of physio-chemical properties and dynamics of waters of the Caribbean Sea and the Gulf of Mexico has been conducted based on all oceanographic data accumulated so far (Stepanov *et al.*, 1975).

2. STRATIFICATION OF WATERS

In the American Mediterranean Sea a tropical type of thermohaline stratification is found which is typical of the adjacent areas of the open ocean (Stepanov, 1974). Especially strong layering of waters is characteristic of this type (Fig. 1). This is associated with a very significant vertical change in temperature and, hence, in density, with the presence of extremely high salinity in the lower layer of surface waters and a well pronounced drop of all physio-chemical properties of the Intermediate Waters (exhibiting low salinity, low content of dissolved oxygen at the maximum phosphate concentration. Deep and Bottom Waters are fairly uniform with respect to temperature, salinity and density. The oxygen content of the Deep and Bottom Waters is similar to that observed in the Surface Waters; while the concentrations of organic substances are comparable to those of the Intermediate Waters.

Studies of stratification were also performed using caesium-137 falling out from the atmosphere onto the ocean surface. In order to investigate its vertical variations, special methods were developed and employed. These utilized an anchored buoy containing sorbents which permit one to obtain an integral value of the radionuclide concentration over the entire period of the observation.

The analysis of the data obtained indicates that the stratification revealed by the tracer method is closely connected with other parameters and is especially well correlated with salinity (correlation coefficient is equal to 0.80-0.96). Maximum concentrations of radiocaesium are found at 200-300 m in the layer of extremely high salinity.

The collected data suggest the possibility of applying the model of the advective transport to the discussed region and forecasting the radionuclide content variations in sea water from variations in salinity.

The data obtained were also used to make a water balance estimate for the American Mediterranean Sea which proved to be fairly close to that determined by hydrophysical methods. The research performed also made it possible to determine distinctive features of radioactive contamination in the Caribbean and the Gulf of Mexico.

3. WATER CIRCULATION

The averaging of a large mass of initial data enabled one to gain an idea about geostrophical circulation in the upper 2 000 m of the Caribbean Sea and the Gulf of Mexico. The earlier knowledge was mainly confined to the circulation of Surface Waters.

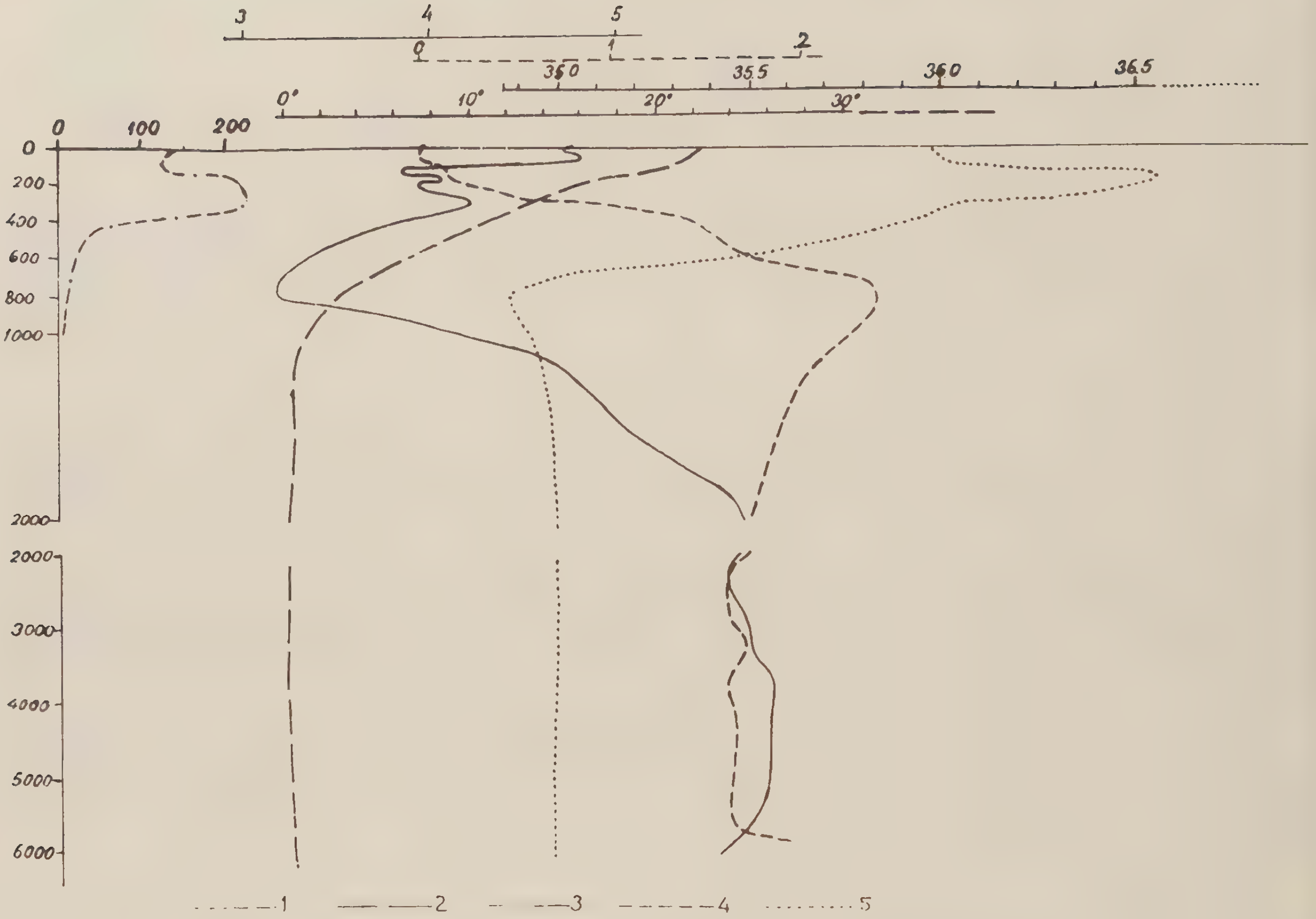

Fig. 1 Vertical change in radiocaesium (1), temperature (2), concentration of dissolved oxygen (3), content of phosphates (4), and salinity (5) in the middle part of the Caribbean Sea

The calculation of geostrophic currents was performed from a reference surface of 2 500 dbar. This is the maximum possible value from which the construction of charts of a dynamical relief over the entire American Mediterranean is permissible. According to these geostrophic calculations the Caribbean Current (the main flow of this sea carrying waters from east to west, see Fig. 2) turns out to be much more narrow than indicated by ship's drift records. It can be traced as an intensive flow in the middle part of the Caribbean. North of it, a weak anticyclonic gyre is encountered which is represented by several meso-scale eddies. In the southern part of the sea, an intensive cyclonic gyration of waters occurs which is divided into two gyres by a protruding continental prominence in the area of the Gulf of Maracaibo. The northern periphery of a cyclonic gyre is formed by the Caribbean Current: the southern one by the Colombian and Venezuelan Currents. Previously, only the first could be traced from ship's drift.

A clockwise system of the vertical water circulation (the Caribbean Current being its axis) has become apparent from the discovery of anticyclonic gyres in the northern part of the sea and cyclonic ones in the southern part. The system accounts for the mechanism of an active renewal of waters which is indicated by a high oxygen content in deep and bottom layers. With more intensive water gyration and cyclonic gyre the upward motions must be substantially more active than the downward flows which are excited by weak anticyclonic eddies. Balancing will arise due to an inflow of waters through the northern Antillean passages. The intensity of the Caribbean Current does not vary, in fact, all the way from the Antillean passages as far as the Yucatan Strait. In the water separating Central America from Cuba the velocity of water movement increases; from here the general flow of the American Mediterranean Sea is called the Yucatan Current. Flowing directly northward, in the Florida Straits latitude it turns abruptly eastward. This is attributed to an interaction between water circulation of the American Mediterranean and a north-tropical anticyclonic system of the open Atlantic (Stepanov, 1974). Making a loop which extends far to the north, the Yucatan Current proceeds toward the Florida Straits almost without changing its intensity. The Florida Current begins here.

Calculations performed by us generally confirmed the previous knowledge concerning the circulation of Surface Waters of the Gulf of Mexico and allowed one to understand the movement of intermediate and deep water masses. The picture proved to be very mixed. When cyclonic transport prevails in the Gulf periphery with a number of separate eddies of the same direction of rotation, a quasistationary anticyclonic gyre is located in the central part. The gyre extends from south-west to north-east. With such complicated horizontal circulation, numerous vertical movements occur which contribute to active water mixing in the Gulf of Mexico.

The calculations indicate that the system remains basically as far as an axis of intermediate waters in the Caribbean Sea and the Gulf of Mexico, i.e. in the upper 1 000 m (Fig. 3). Below this, like the situation characteristic of the entire World Ocean (Stepanov, 1974) a strong transformation of the circulation takes place due to pronounced weakening of the influence of zonal transport which predominates near the surface. The water exchange with the ocean remains only through the deepest straits, i.e. the Windward and Anegada Passages. Under conditions of a strongly broken bottom topography, very weak anticyclonic gyres (Fig. 3) are generated in troughs due to which downward motions favouring the mixing, should occur. The resulting sinking of waters with higher oxygen content is favourable to the development of oxidation processes, mineralization of organics and, hence, the accumulation of organic substances. We see just this in the character of the physio-chemical fields which is an evidence of the validity of the calculation of the geostrophical circulation of waters.

4. WATER EXCHANGE

When the transit transport of waters entering from the ocean through the Antillean Straits and then leaving through the Florida Strait is intensive, the water exchange plays a much more important role here than that in many other seas.

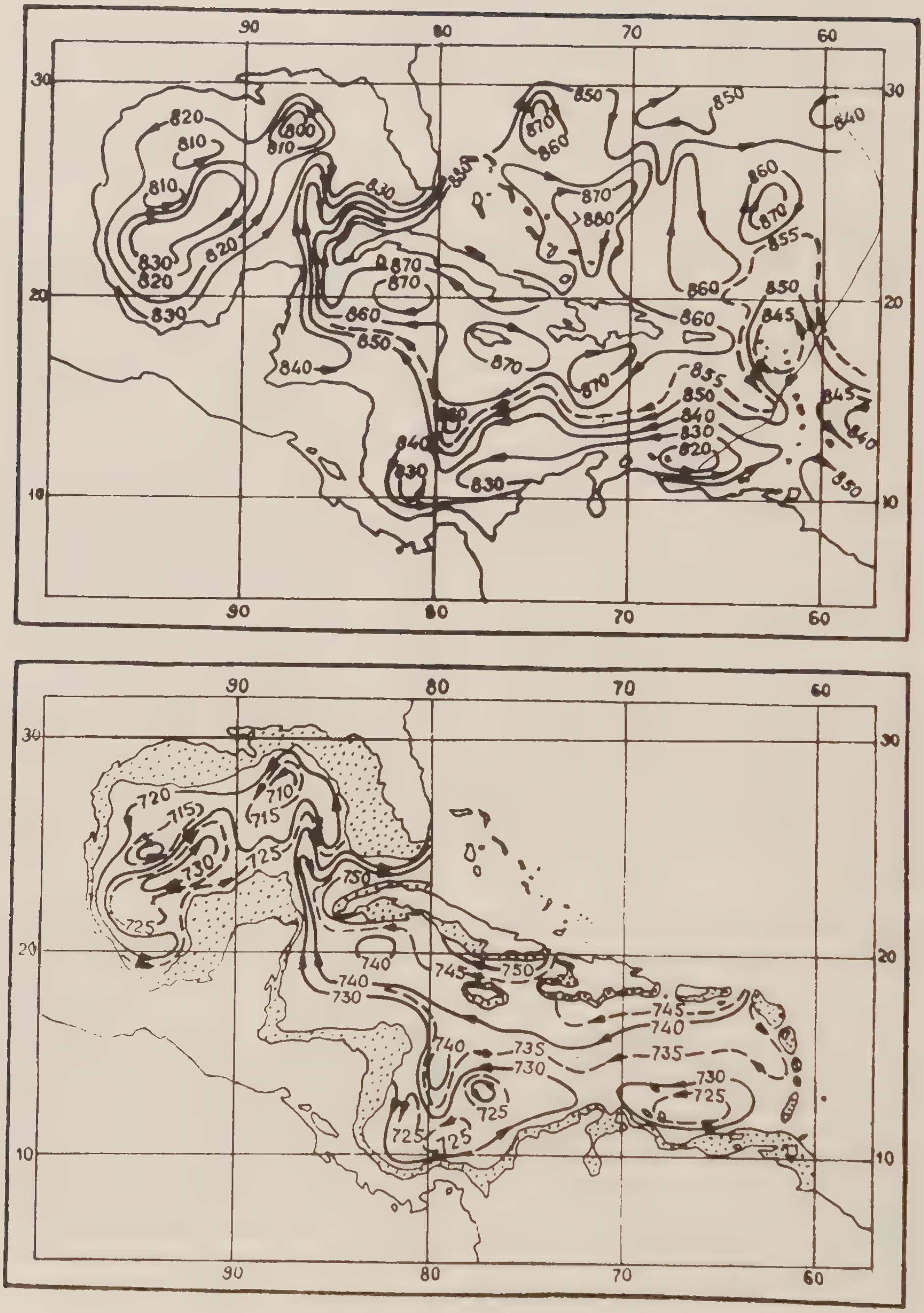
90
80
70
60
30
20
10
820
810
810
800
810
830
830
820
820
830
850
870
860
870
860
850
860
870
855
850
845
840
870
870
860
850
840
860
870
870
855
850
840
830
820
845
840
850
840
830
830
720
715
710
715
730
725
725
750
740
745
750
740
730
745
740
735
735
730
740
730
725
725
725
725

Fig. 2 Circulation of waters at the surface (above) and at a depth of 200 m (below) calculated from a reference surface of 2 500 m

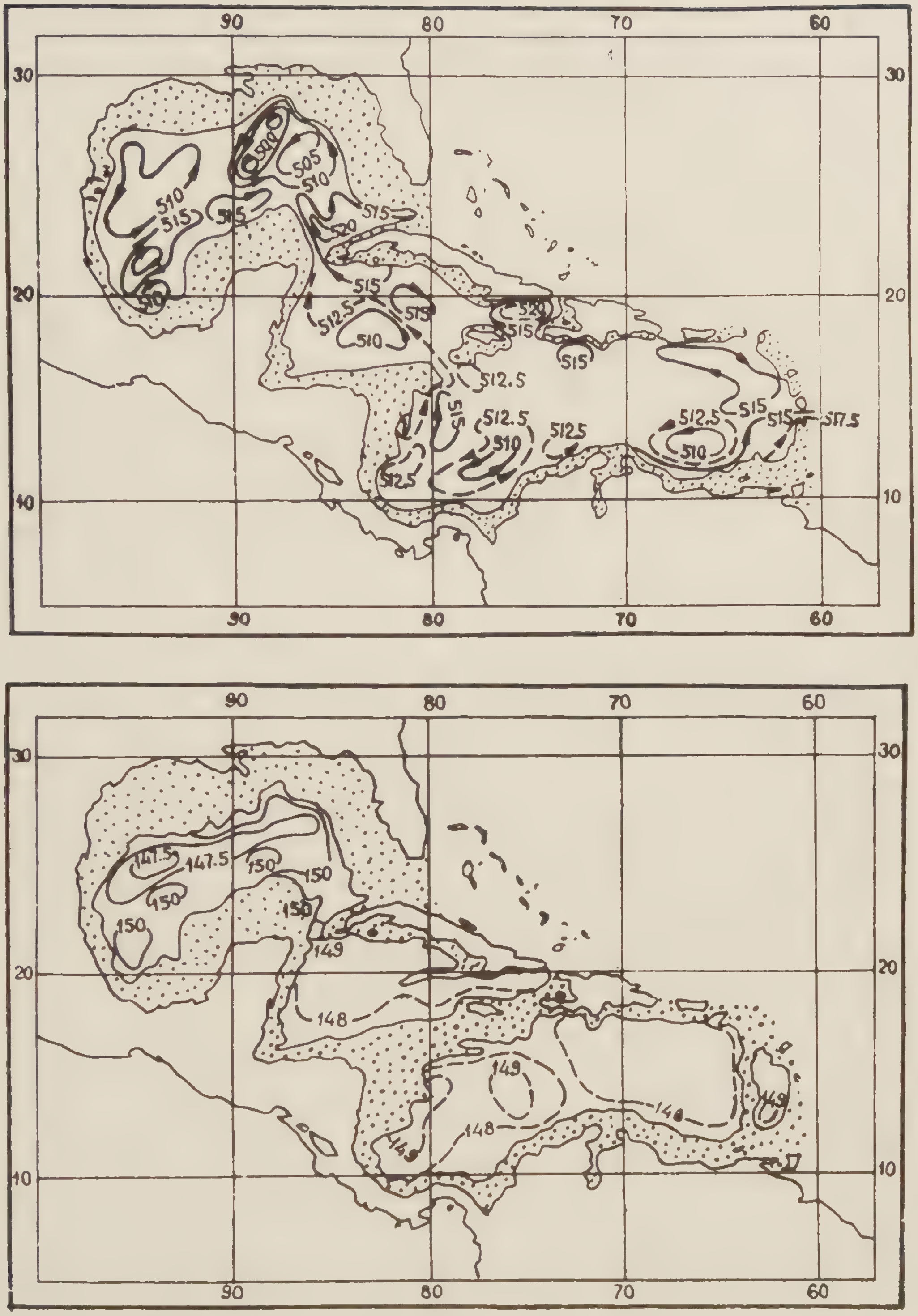
90
80
70
60
30
20
10
500
505
510
515
520
512.5
517.5
147.5
150
149
148

Fig. 3 Circulation of waters at a depth of 300 m (above) and at 2 000 m calculated from a reference surface of 2 500 m

The available estimates of the water exchange on the Florida Strait are most well-founded. They are obtained both from the instrumental measurements of currents and on the basis of calculations from indirect data (see Table I). Three quarters of all the Caribbean waters are flowing out through it into the ocean. The discharge through the Windward Passage is only 2 times less than that through the Florida Strait but the outflow is 6.5 times weaker. About one third of all waters entering the American Mediterranean is carried through this strait alone.

TABLE I

Evaluation of the water transport through the straits of the American Mediterranean Sea, in $10^6 m^3 sec$

Name of the strait	Inflow to the sea from the ocean		Outflow from the sea to the ocean
	from hydro-physical data	by the tracer method	
Florida Straits	0.7	-	26.0
Windward Passage	12.7	14.3	4.0
Mona Passage	1.9	2.0	0.3
Anegada Passage	2.3	18.7	4.7
Lesser Antillean Straits	(17.4)		-

The water exchange through the Mona Strait is of very little importance. The Anegada Passage is third with respect to the degree of importance in the total water exchange. However, with its significant section the available water transport values seem to be underestimated. We did not manage to gather any information on the amount of waters transported through the straits of the Lesser Antillean islands. It follows from the estimation of the total water exchange that such an inflow must be about a half of all inflowing oceanic waters in order to compensate for the discharge through the Florida Straits. This is evident from the estimation of the water exchange obtained by the tracer method.

5. WATER MASSES

The research carried out is based on the joint analysis of physical and chemical fields and the circulation of waters.

5.1 Surface Waters

Surface Waters refer to a tropical type, in accordance with the geographical position of the American Mediterranean Sea. They are characterized by high temperature and salinity, lower oxygen content, and minimum concentrations of organic substances. These waters are brought here by the Northern Trade Wind Current from the open part of the ocean and become somewhat transformed under the effect of distinctive features of local heat- and moisture-exchange. In addition, a relatively small amount of less saline equatorial waters, which is transported by the Guiana Current, flows into the southeastern part of the Caribbean Sea.

The lower boundary of Surface Waters in the regions with predominant upward flow can be traced approximately at a depth of 200 m and in places where water sinking prevails at 300-400 m. Like any other Surface Waters in the American Mediterranean Sea, they are divided into three layers: the homogenous surface layer, the transition layer, and, the lower or subsurface layer featuring extremely high salinity well pronounced for the low latitudes.

The high salinity which most markedly characterizes the subsurface layer occurs in the tropical latitudes of the open ocean. Physio-chemical fields are substantially transformed in this layer as compared with the surface one. The effect of heat, moisture, and gas exchange with the atmosphere is strongly limited and water circulation becomes the main factor in the formation of the fields. Apart from advection, under the influence of which the subsurface layer is formed, the role of vertical motion counts more and more. The temperature and oxygen content decrease in the areas where Intermediate Waters ascend, and, density and phosphate concentrations increase (Fig. 4). Sinking of Surface Waters has the opposite effect. The effect of vertical motions begins to show up clearly from the upper boundary of subsurface waters at a depth of 100 m. This is more strongly marked at 200 m. The phosphate content increases significantly since photosynthesis sharply reduces at these depths and consumption of organic salts practically ceases. These are mainly discharged due to the outflow to the surface layer in the places where upwelling of water prevails. However the phosphate concentration is slightly less in the American Mediterranean than that in the open ocean. Thus, the large reserves of nutrient salts are concentrated in the subsurface layer in the south of the Caribbean Sea, which leads to high biological productivity of water areas adjacent to the continent. In the rest of the area of the American Mediterranean Sea high biological productivity is characteristic only of the regions with well developed coastal shallow waters.

5.2 Intermediate Waters

Intermediate Waters are formed as a result of the mixing of two types of Intermediate Water masses entering from the ocean through the passages of the Antillean islands. One of them is formed in the subantarctic latitudes. One can easily trace these waters from the extremely low values of salinity and dissolved oxygen which occur at the maximum concentration of phosphates. The upper portion of the subantarctic waters situated above their core, where minimum salinity occurs, penetrates through the Lesser Antillean Passages. Another water type - an intermediate North Atlantic one - flows in only through the Greater Antillean Passages. Owing to higher salinity, these waters have greater density and therefore spread in the Caribbean Sea in the lower portion of the intermediate structure zone. Apart from higher salinity, their effect becomes apparent in the northern part of the sea as an increase in the oxygen content and as a decrease in the phosphate concentration.

Since stratification of organic compounds in the Caribbean is quite the same as in the ocean, the place from which Intermediate Waters come, it is interesting to evaluate the extent of the influence of the utilization of nutrients under conditions of the American Mediterranean Sea. This process turns out to be substantially active in the Caribbean Sea. Near the core of Intermediate Waters the concentration of phosphates (at 800-1 000 m) is by 25-50 percent higher than that in the adjacent regions of the open ocean. The field of phosphates is formed not only under the influence of the transit transport of oceanic waters but also in accordance with peculiarities of the local circulation.

The highest concentration of phosphates is encountered in the area of a cyclonic water circulation, the lowest in anticyclonic gyres (Fig. 5). This situation is common for the entire World Ocean. In the places with predominant downward motions, organic residues are carried downward. In those places where upwelling occurs, nutrients sink slowly which prolongs the period of nutrient utilization. Accordingly, maximum concentrations of phosphates occur in cyclonic systems. In the upper portion of the intermediate structural zone (at a depth of 500 m) the highest phosphate concentration, exceeding 2.0-2.5 µg-at/l, is observed in the southeastern Caribbean where cyclonic systems are situated. As one moves from here, their concentration decreases rapidly to values slightly less than 1 µg-at/l south of Cuba as a result of anticyclonic circulation of waters.

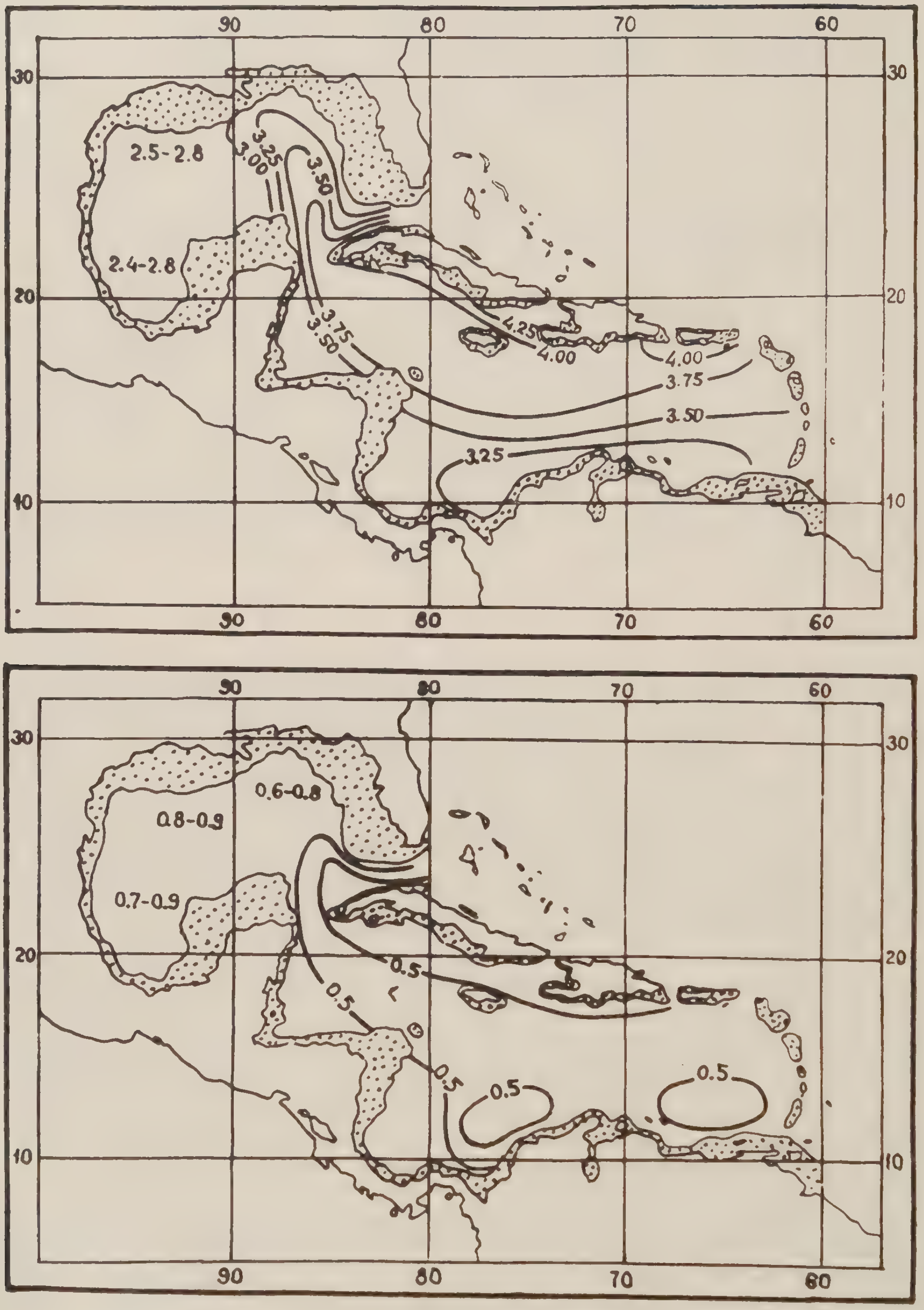
90
80
70
60
30
20
10
2.5-2.8
2.4-2.8
3.25
3.00
3.50
3.75
3.50
4.25
4.00
4.00
3.75
3.50
3.25
0.6-0.8
0.8-0.9
0.7-0.9
0.5
0.5
0.5
0.5
0.5

Fig. 4 Concentration of dissolved oxygen (above) and of phosphates (below) at a depth of 200 m

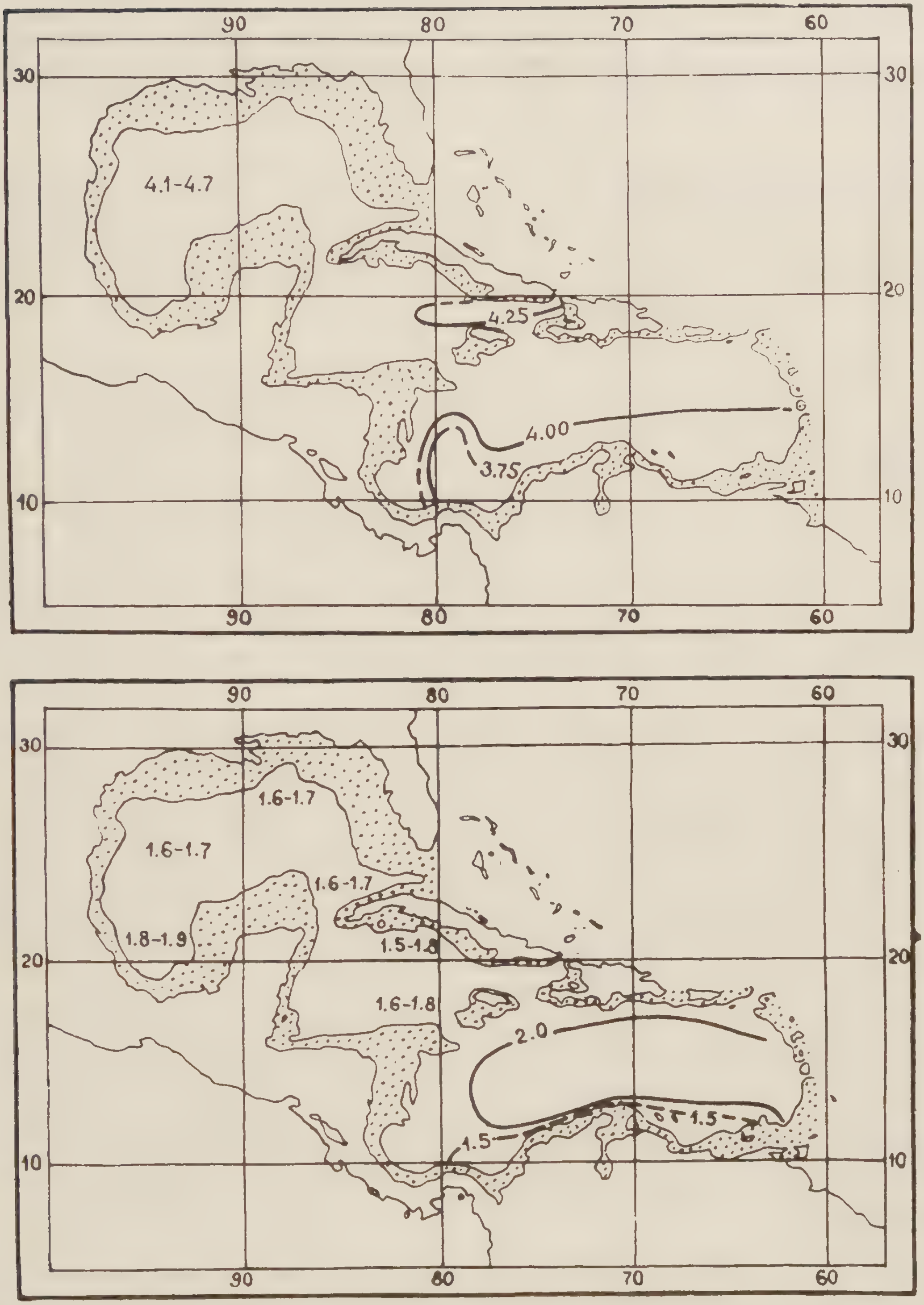
90
80
70
60
30
20
10
4.1-4.7
4.25
4.00
3.75
1.6-1.7
1.6-1.7
1.6-1.7
1.8-1.9
1.5-1.8
1.6-1.8
2.0
1.5
1.5

Fig. 5 Concentration of dissolved oxygen (above) and of phosphates (below) at 1 000 m depth

The field of dissolved oxygen reflects three important and distinctive features: (1) water rising in cyclonic systems in the south of the Caribbean Sea where its minimum concentration is encountered; (2) inflow of waters through the passages of the Greater Antillean islands which exhibit higher oxygen concentrations; and (3) spreading of the Caribbean water in the Gulf of Mexico with its higher oxygen content. Correspondingly, oxygen concentration in the western part of the Caribbean Sea is somewhat higher than that in the eastern part and in the Gulf of Mexico.

Dynamical and physio-chemical conditions vary significantly in the Lower Intermediate Waters. The Nicaragua Ridge almost completely divides the Caribbean Sea into two deepwater parts. The reconstruction of circulation takes place; very weak anticyclonic gyres arise within separate troughs. The passages of the Lesser Antillean islands and the Straits of Florida are partitioned off from 800-1 000 m. The water exchange is maintained but through the Anegada and the Windward Passages.

5.3 Deep Waters

The upper boundary of the Deep Waters can be traced from sill depth which limits the water exchange with the ocean; in the Caribbean Sea, mainly from 2 000 m, in the Gulf of Mexico, slightly higher, from 1 400-1 500 m. The properties of Deep Waters in the sea also differ essentially from those in the ocean. Like other very separated basins, the American Mediterranean Sea below sills limiting the water exchange is filled with waters with the same properties as those observed at a level of such underwater barriers. Therefore not only Deep but also Bottom Waters of the American Mediterranean Sea feature characteristics which are very close to each other and correspond to those observed in the ocean at a depth of about 1 000 m. Their temperature equals 4.1-4.2°C, salinity - 34.97-34.99 percent, density - 1.02780. In adjacent oceanic regions Deep Waters are colder, their temperature is slightly higher than 2°C; salinity is about 34.88 percent; density is approximately 1.0279.

The hydrochemical characteristics of Deep Waters are very different from those observed in the adjacent oceanic regions. This difference is manifest firstly in the concentration of phosphates. The phosphate concentration is very low in the deep waters of the ocean (of the order of 1.2-1.5 µg-at/l); in the Caribbean their average content reaches 1.5-2.0 µg-at/l. Their higher concentration as compared to that in the ocean points to the higher intensity of processing of organics in the American Mediterranean Sea. This is caused by dynamics of waters. On the contrary, the amount of dissolved oxygen is lower than that in the ocean. Its concentration is 4.7-5.0 ml/l in the sea; it reaches values close to oceanic ones (up to 5.5-6.0 ml/l) only in the western part of the Caribbean Sea where an especially large amount of North Atlantic water comes in.

From the analysis of physio-chemical properties of Deep Caribbean Waters one can conclude that they result from mixing of three water masses penetrating from the ocean: Lower Intermediate Subantarctic masses, Lower Intermediate North Atlantic masses and Upper Deep North Atlantic ones. The first of these enters, primarily, through the straits of Lesser Antillean islands and exerts the greatest influence on the southeastern part of the Caribbean Sea. Two other water types enter through the deepest straits: the Windward and Anegada Passages.

5.4 Bottom Waters

Bottom Waters are basically formed from Deep North Atlantic Waters penetrating through the deepest passages of the Windward and Anegada Straits; having greater density than that of local waters, they sink along the continental slope to the bottom of the Caribbean troughs. Their presence affects the higher oxygen content and salinity in Bottom Waters of the northern part of the Caribbean. Downward motions generated in the periphery of southern Caribbean cyclonic systems must play a fairly important rôle. Owing to them, Deep Waters flowing along the steep south American continental slope can sink to the bottom. The basic mass of the bottom Caribbean water seems to form in this manner. These waters enter the Gulf of Mexico through the Yucatan Strait.

Thermohaline properties of Bottom Waters are close to those of the Deep Waters from which they are mainly formed but their temperature is somewhat higher on account of the adiabatic effect. Hydrochemical characteristics are of particular interest. Saturation with oxygen is about 70-80 percent; in the absolute expression it varies on the average from 4.7-4.5 ml/l to 5.8 ml/l in separate deep-water troughs. Its decrease is discovered near the very bottom in some places which is associated with the intensive development of oxidation processes.

The most astonishing feature is an increase in concentration of phosphates from the upper boundary of Bottom Waters down to the bottom in the eastern Caribbean Sea (the Grenadian and Venezuelan Trenches). An increase in phosphate content in Bottom Waters seems to be attributed to sweeping away from the land (mainly, from islands) of large quantities of vegetation. During the Soviet expedition on board the AKADEMIK KURCHATOV trawls brought large amounts of almost intact vegetation from the bottom of deep trenches: algae and sea grass from their coastal areas as well as the leaves and twigs of terrestrial vegetation.

As a result of the high dynamics of waters, these materials are rather rapidly carried to the bottom. Here in the presence of high oxygen concentrations mineralization takes place, due to which higher concentrations of phosphate occur near the bottom.

Conducting of further research on the Caribbean Sea and the Gulf of Mexico by cooperative efforts of all states concerned will make it possible to extend studies of the nature and resources of these most interesting areas of the World Ocean.

6. REFERENCES

Domanov, M.M., B.A. Nelepo and V.N. Stepanov, (The role of circulation and stratification
1975 of waters in spreading of contamination of the Caribbean basin). Morsk.Gidrofiz. Issled., 69(2):187-97 (in Russian)

Morskoi Gidrofizicheskii Institut, (Investigations of the Caribbean Sea, 1974). Sevastapol,
1974 Morskoi Gidrofizicheskii Institut (in Russian)

Panfilova, S.G. and V.N. Stepanov, (On the variability of physico-chemical properties of
1975 waters of the American Mediterranean Sea). Dokl.Akad.Nauk SSSR, 222(2):459-61 (in Russian)

Rass, T.S. (ed.), (Hydrology, plankton and benthos communities of the Caribbean Sea and the
1975 Gulf of Mexico). Tr.Inst.Okeanol., 101:152 p. (in Russian)

__________, (Multiple investigations of the Caribbean Sea, the Gulf of Mexico and adjacent
1975a waters). Tr.Inst.Okeanol., 100:360 p. (in Russian)

Stepanov, V.N., (The world ocean. Dynamics and properties of waters). Moscow, Znanie,
1974 256 p. (in Russian)

Stepanov, V.N. *et al.*, (The formation of chemical and physical fields and dynamics of waters
1975 of the Caribbean Sea and Gulf of Mexico). *In* (Chemico-oceanographic investigations of seas and oceans.) Moscow, Nauka, pp. 79-110 (in Russian)

A COMPARISON OF SUMMER AND WINTER DRIFTER MOVEMENTS WITHIN THE AMERICAN MEDITERRANEAN

by

D.F. PASKAUSKY
Office of Naval Research, Code 481;
and Naval Ocean Research and
Development Activity, Code 211,
Arlington, Virginia 22217, U.S.A.

W.D. NOWLIN, JR.
Department of Oceanography
Texas A. & M. University
College Station, Texas 77843, U.S.A.

CONTENTS

1. A COMPARISON OF SUMMER AND WINTER SURFACE DRIFTER MOVEMENTS WITHIN THE AMERICAN MEDITERRANEAN
2. ACKNOWLEDGEMENTS
3. REFERENCES

Abstract

A total of 806 drifters were released at 33 stations in the Gulf of Mexico and Caribbean Sea during the period 6 June to 27 July 1974. Returns from 46 drifters (5.7%) representing 21 (64%) of the stations have been received. This compares well with a 7.4% drifter return from 64% of the stations in the same area at which 1 015 drifters were released during the autumn and winter of 1973.

A net westward drift through the Caribbean Sea and into the Gulf of Mexico was indicated by the drifter returns for both winter and summer releases. Some of the drifters released at Caribbean stations were found on the east coast of Florida (after only two months) and others were found along the northern shore of the Gulf of Mexico (after ten months) indicating dispersion in the flow through the Yucatan Straits.

In contrast to the winter deployment, no returns were recorded from summer releases within the Gulf of Mexico (except for those released near the Yucatan Channel) until early winter. Two possible seasonal variations can be seen by comparing the winter and summer drifter movements in the Caribbean: (1) the summer drift speeds were slightly faster than the winter speeds and (2) the flow at the eastern Antilles splits, with a northward flowing portion by-passing the Caribbean in the summer.

Resumen

Del 6 de junio al 27 de julio de 1974 se lanzaron, en el golfo de México y Mar del Caribe, 806 objetos a la deriva, de los cuales se recuperaron 46 (el 5,7 por ciento), pertenecientes a 21 estaciones (el 64 por ciento). Durante el otoño e invierno de 1973, se lanzaron, en la misma zona, 1 015 objetos a la deriva, de los cuales se recogieron el 7,4 por ciento, pertenecientes al 64 por ciento de las estaciones.

La recuperación de los objetos que se lanzaron en el invierno y el verano ponen de manifiesto la existencia de un claro movimiento de hacia occidente en el Mar Caribe y en el Golfo de México. Algunos de los que se lanzaron a la deriva en las estaciones del Caribe se encontraron en la costa oriental de Florida - al cabo de sólo dos meses - y otros a lo largo de la costa septentrional del Golfo de México, al cabo de diez meses, lo que indica una dispersión de las aguas que fluyen por los estrechos de Yucatán.

En contraste con los lanzamientos invernales, de los objetos lanzados durante el verano en el Golfo de México no se recuperó ninguno hasta principios del invierno (salvo los que se lanzaron cerca del canal de Yucatán). La comparación de los movimientos de arrastre invernales y estivales en el Caribe pone de manifiesto dos posibles variaciones estacionales: (1) las velocidades de arrastre estivales fueron ligeramente mayores que las invernales y (2) el flujo en la parte oriental de las Antillas se divide, fluyendo una parte hacia el norte durante el verano, sin pasar por el Caribe.

1. A COMPARISON OF SUMMER AND WINTER SURFACE DRIFTER MOVEMENTS WITHIN THE AMERICAN MEDITERRANEAN

During the period between 6 June and 27 July 1974 a total of 806 drifters were released from the TEXAS CLIPPER at 33 stations in the American Mediterranean. The locations of these summer stations and of 36 stations at which 1 015 surface drifters were released from the R/V ALAMINOS between 25 October and 11 December 1973 is shown in Fig. 1. The drifters, which consist of a yellow plastic disk 18 cm in diameter with a 55 cm red plastic stem, are imprinted with an offer of a reward of U.S.$ 1 in English and Spanish.

As of 1 January 1976, 46 drifters (5.7%) from 21 stations (64%) had been recovered; this compares to returns from 7.4% of the drifters representing 64% of the 36 winter stations (Murphy _et al._, 1975).

Locations of drifters recovered on the east coast of Florida and the Florida Keys (identified by the number of the stations where the drifter was released) are shown in Fig. 1 for releases during the winter of 1973 and summer of 1974. As expected, both releases indicate that the surface waters move from the eastern Antilles to and through the Yucatan Straits and thence out of the Gulf of Mexico through the Florida Strait.

During the winter the fastest net drift speed (shortest water route divided by the time until found) from mid-Caribbean to the east coast of Florida was 0.40 m sec^{-1} as reported by Murphy _et al._ (1975), while during the summer the fastest net drift speed was 0.53 m sec^{-1}. Net drift speeds for a few selected returns are presented in Table I. Since true path length and time on the beach are unknown, the summer net drift speeds presented in Table I, which are somewhat faster than the winter speeds may only indicate that more people are on the beaches in the summer. In any case, the summer drift speeds in Table I are rough estimates of the net drift through the Caribbean.

Although no returns were reported from the winter deployment stations near the Virgin and Leeward Islands, it is noteworthy that the summer returns (see Fig. 2, stations 10 and 11) indicate a north-westerly flow between these islands and along the eastern edge of the Bahama Islands. Since the Murphy _et al._ (1975) paper was published, one drifter from station 15 (see Fig. 1a) was found on the east coast of Abaco Island in the Bahama Islands.

Stations 16, 17, and 18 in the central Caribbean had returns from both the western shores of the Caribbean and the eastern shore of Florida. An indication of dispersion in the flow through the Yucatan Straits is seen in the returns from stations 19, 20, and 23. A drifter released on 10 July 1974 at station 19 was found at South Padre Island, Texas (on the northwest shore of the Gulf of Mexico) on 28 March 1975 while a drifter launched at station 20 on 11 July 1974 (see Fig.1) was found at Sebastian, Florida, on 22 October 1974. Station 23 (release date 16 July 1974) was even more interesting since one drifter was found in West Biscayne Bay, Florida, on 2 February 1975, and another was found on Padre Island, Texas, on 17 May 1975.

In the Gulf of Mexico there were two returns from station 33 (release date 26 July 1974); one on the east coast of Florida on 4 October 1974 and one on the west coast of Florida on 11 January 1975. The remainder of the Gulf of Mexico station returns shown on Fig. 2 were found between 28 December 1974 (station 26) and 31 May 1975 (station 30). Thus the movement seems to be slower during summer in the Gulf of Mexico. Two possible seasonal variations can be seen by comparing the winter and summer drifter movements in the Caribbean: (1) the summer drift speeds were slightly faster than the winter speeds and (2) the flow at the eastern Antilles splits, with a northward flowing portion by-passing the Caribbean in the summer.

A continuing programme of drifter releases now underway in the Gulf of Mexico should give additional insight into the seasonal variability of the net surface drift in the American Mediterranean.

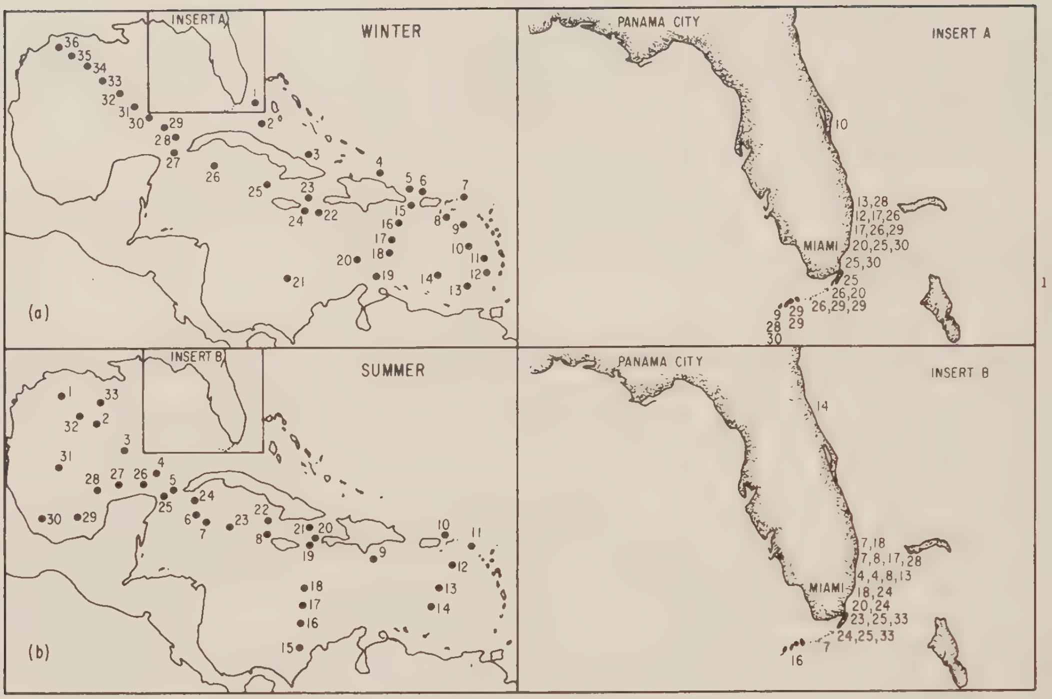
INSERT A
WINTER
(a)
PANAMA CITY
INSERT A
MIAMI
13,28
12,17,26
17,26,29
20,25,30
25,30
25
26,20
26,29,29
INSERT B
SUMMER
(b)
PANAMA CITY
INSERT B
MIAMI
7,18
7,8,17,28
4,4,8,13
18,24
20,24
23,25,33
24,25,33
15

Fig. 1 Locations and numbers of stations at which drifters were released during (a) winter 1973 and (b) summer 1974. Locations of drifter recoveries on the Florida Keys and east coast (indicated by release station numbers) are shown in the inserts

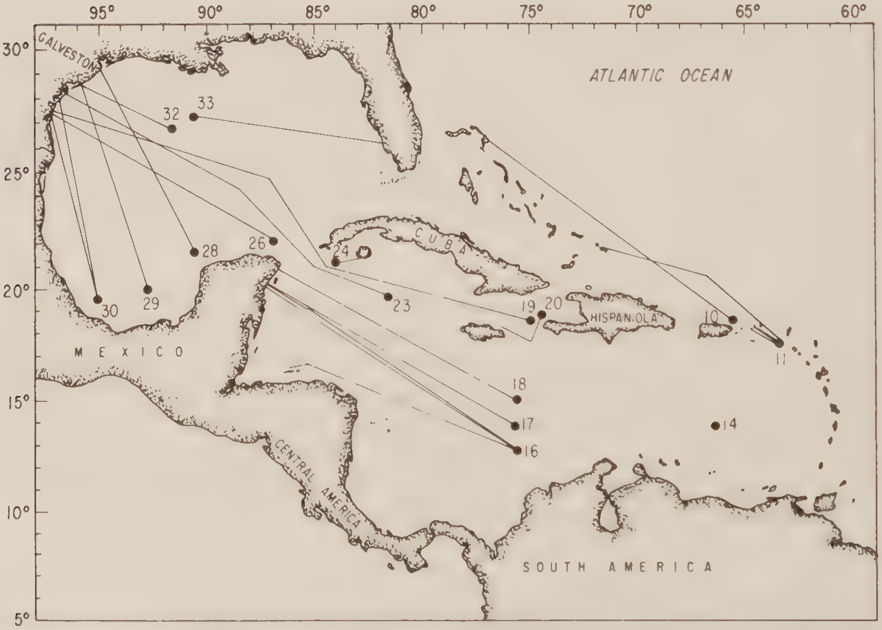
95°
90°
85°
80°
75°
70°
65°
60°
30°
25°
20°
15°
10°
5°
GALVESTON
ATLANTIC OCEAN
CUBA
HISPANIOLA
M E X I C O
CENTRAL AMERICA
S O U T H A M E R I C A

Fig. 2 Drifter returns from the summer 1974 release found at locations other than the Florida Keys and east coast

TABLE I

Calculation of maximum net drift speed (shortest water route divided by the time until found) for selected drifter returns

Station	Recovery Location	Distance travelled (km)	Time until found (days)	Advance speed ($m\ sec^{-1}$)
18	Yucatan, Mexico	1 700	35	0.56
17	Cocoa Beach, Florida	3 100	68	0.53
16	Honduras	1 400	63	0.26
14	St. Augustine, Florida	4 800	116	0.48
25	Florida Keys	850	18	0.55
10	Abaco Island, Bahamas	975	77	0.15

2. ACKNOWLEDGEMENTS

Acknowledgement is made to the crew on the TEXAS CLIPPER in the summer of 1974 for their help in releasing the drifters and to Don Murphy of the University of Connecticut for logging the drifter returns.

3. REFERENCE

Murphy, D.L. *et al.*, Movement of surface drifters in the American Mediterranean.
1975 *J.Phys.Oceanogr.*, 5:549-51

LA VELOCIDAD DEL SONIDO EN LA REGION SUROCCIDENTAL DEL GOLFO DE MEXICO

por

F. RUIZ RENTERIA
Instituto de Geofísica
Universidad Nacional Autónoma de México
México, D.F.

CONTENIDO

1. INTRODUCCION
2. CALCULO Y DISTRIBUCION DE LA VELOCIDAD DEL SONIDO
3. LOCALIZACION DE LA CAPA PROFUNDA DE V.S. MINIMA
4. CORRECCIONES PARA ECOSONDEOS
5. DISCUSION Y CONCLUSIONES
6. REFERENCIAS

Resumen

La velocidad del sonido es presentada y discutida a base de datos oceanográficos recabados durante 3 cruceros CICAR en la región suroccidental del Golfo de México efectuados por el buque oceanográfico VIRGILIO URIBE de la Marina de México.

Para el cálculo de la velocidad del sonido se empleó la fórmula de Wilson. Con fines de comparación también se usó la fórmula recientemente propuesta por Del Grosso, la que rindió resultados muy similares a los obtenidos por la fórmula de Wilson.

Partiendo de la fórmula de Wilson se desarrolla un procedimiento que permite determinar la profundidad de la velocidad mínima del sonido (canal sonoro profundo) y se presenta la topografía de la capa de velocidad mínima, la que se halla normalmente entre 800 y 1 000 m en la región investigada.

Basada en estos datos recientes y específicos para la región, se elabora una tabla para corrección de ecosondeos aplicable para las dos escalas comúnmente usadas en ecosondas comerciales (1 500 m/s y 800 br/s). Esta tabla difiere ligeramente de la presentada por Matthews en el año 1939 para esta región.

Abstract

The velocity of sound has been determined on the basis of oceanographic data collected during 3 CICAR cruises of the Mexican Navy research vessel VIRGILIO URIBE in the southwestern Gulf of Mexico. Computations were carried out by means of the Wilson formula. A recent formula proposed by Del Grosso was also used for comparison, giving very similar results.

A procedure for detection of the depth of the velocity minimum (deep sound channel) based on the Wilson formula, is presented as well as the topography of this layer, normally found in this area between 800 and 1 000 m.

The recent and specific oceanographic data are also used for an echo sounding corrections table that can be applied to the two scales commonly used on commercial echo sounders (1 500 m/s and 800 fm/s). Those corrections differ only slightly from those given by D.J. Matthews in 1939 for this region.

1. INTRODUCCION

Durante el otoño de 1970, primavera de 1971 y otoño de 1971, se realizaron tres cruceros oceanográficos en la región suroccidental del Golfo de México, con el fin de efectuar estudio de oceanografía física con motivo del proyecto CICAR, para los cuales se usó el navío oceanográfico de la Marina Mexicana VIRGILIO URIBE. Los tres cruceros, denominados COSMA 70-12, COSMA 71-10 y COSMA 71-22 respectivamente, se desarrollaron con, más o menos, el mismo derrotero y en cada uno se ocuparon alrededor de 55 estaciones, cuya situación fue aproximadamente la misma(Fig. 1).

Las estaciones consistieron básicamente en hidrocalas estandard entre 0 y 1 500 m de profundidad, con niveles de muestreo en 2, 25, 50, 75, 100*, 150, 200, 250*, 300*, 400, 500*, 600, 800, 1 000*, 1 200 y 1 500* m, donde los asteriscos indican nivel con termómetro no protegido; cuando el fondo estaba por encima de los 1 500 m los niveles se ajustaban de manera que el ultimo quedara lo más cercano posible a éste. La temperatura se corrigió por medio de gráficas especialmente diseñadas para este efecto (Emilsson, 1954), y la salinidad se midió con un salinómetro de inducción marca Beckman. Otros estudios se hicieron, que no tienen interés directo para el presente trabajo.

Los datos obtenidos, en lo que a velocidad del sonido en el mar concierne, se procesaron con ayuda del computador Burroughs 6 700 de la UNAM (Universidad Nacional Autónoma de México) mediante un programa similar al llamada "Station Data Computer (Dinger, 1970) usado por el NODC (National Oceanographic Data Center). Los datos resultantes de este proceso se usaron para elaborar una distribución del parámetro en cuestión en la región suroccidental del Golfo de México, en forma de transectos para las estaciones del año antes mencionadas, así como también para situar la capa profunda de mínima velocidad y, por último, aprovechando la existencia de estos datos, recientes y específicos del Golfo de México, se calculó una tabla para corrección de ecosondeos con el objeto de compararla con la elaborada por Matthews (1939).

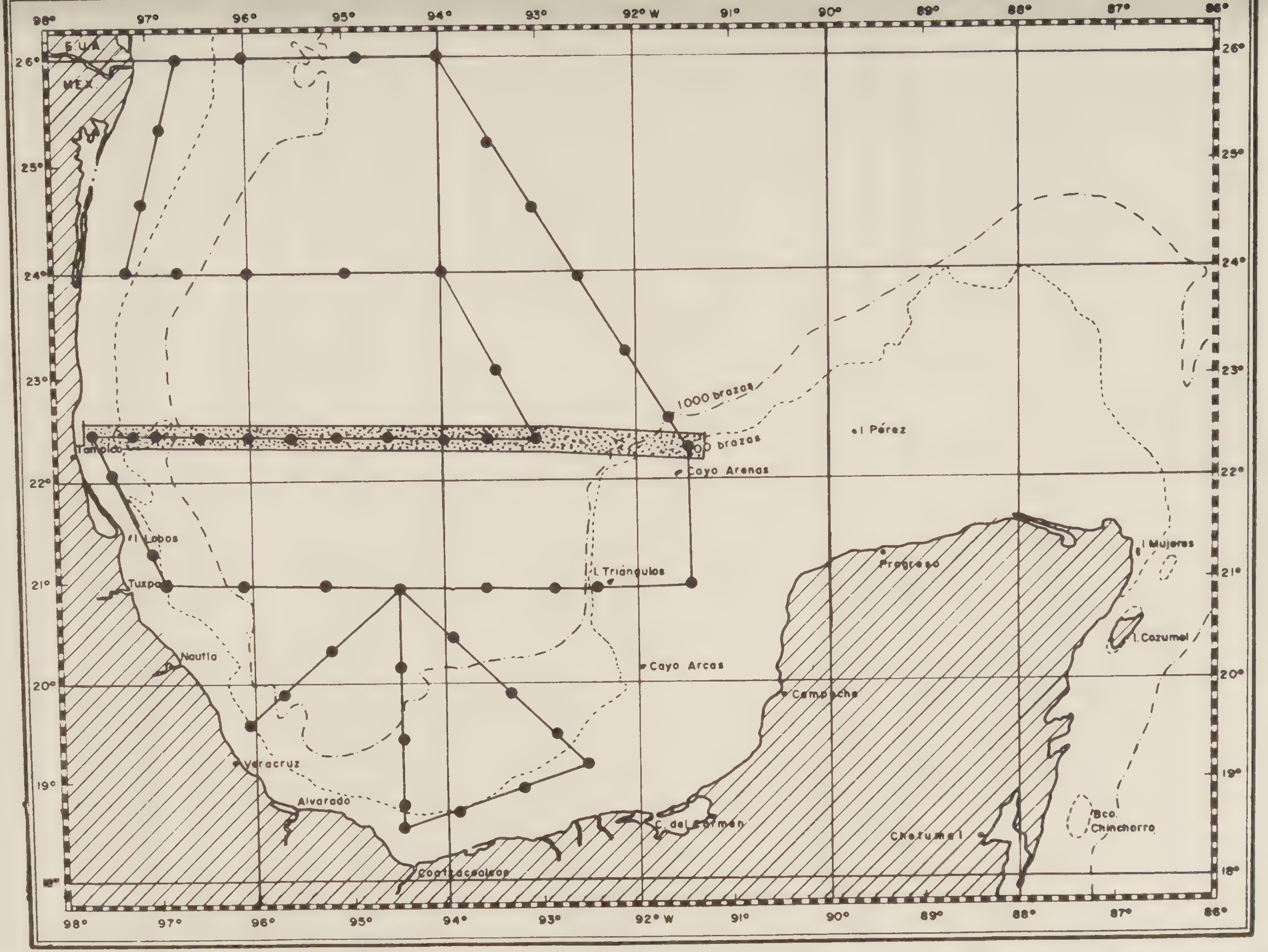
E.U.A.
MEX.
Tampico
I. Lobos
Tuxpan
Nautla
Veracruz
Alvarado
Coatzacoalcos
C. del Carmen
Campeche
Cayo Arcas
I. Triángulos
Cayo Arenas
1000 brazos
brazos
I. Pérez
Progreso
I. Mujeres
I. Cozumel
Chetumal
Bco. Chinchorro
98°
97°
96°
95°
94°
93°
92° W
91°
90°
89°
88°
87°
86°
26°
25°
24°
23°
22°
21°
20°
19°
18°

Fig. 1 Red de estaciones en el Golfo de México, que sirvió de base para este trabajo. Esta red se usó en tres ocasiones
Crucero C 70-12 del 31/10/70 al 13/11/70
Crucero C 71-10 del 24/5/71 al 9/6/71
Crucero C 71-22 del 27/10/71 al 10/11/71
El área punteada señala el transecto Tampico-Cayo Arenas

2. CALCULO Y DISTRIBUCION DE LA VELOCIDAD DEL SONIDO

Para el cómputo se usa la ecuación de Wilson (1960):

$$V = 1449{,}14 + V_S + V_T + V_P + V_{STP} \tag{1}$$

en donde:

$$\begin{aligned}
V_T &= 4{,}5721T - 4{,}4532x10^{-2}T^2 - 2{,}6045x10^{-4}T3 + 7{,}9851x10^{-6}T^4 \\
V_P &= 1{,}6027x10^{-1}P + 1{,}0268x10^{-5}P2 + 3{,}5216x10^{-9}P^3 - 3{,}3603x10^{-12}P^4 \\
V_S &= 1{,}39799(S - 35) + 1{,}69202x10^{-3}(S - 35)^2 \\
V_{STP} &= (S - 35)(-1{,}1244x10^{-2}T + 7{,}7711x10^{-7}T^2 + 7{,}7016x10^{-5}P - 1{,}2943x10^{-7}P^2 \\
&\quad + 3{,}1580x10^{-8}PT + 1{,}5790x10^{-9}PT^2) + P(-1{,}8607x10^{-4}T + 7{,}4812x10^{-6}T^2 \\
&\quad + 4{,}5283x10^{-8}T^3) + P^2(-2{,}5294x10^{-7}T + 1{,}8563x10^{-9}T^2) + P^3(-1{,}9646x10^{-10}T)
\end{aligned}$$

S es salinidad en $^{\circ}/oo$, T temperatura en $^{\circ}C$ y P es presión en kg/cm^2. Posteriormente se prueba con la fórmula recién obtenida por Del Grosso (1974):

$$V = V_{000} + V_T + V_S + V_P + V_{STP} \tag{2}$$

donde

$$\begin{aligned}
V_{000} &= 1402{,}392 \\
V_T &= 0{,}501109398873x10^{1}T - 0{,}550946843172x10^{-1}T^2 + 0{,}221535969240x10^{-3}T^3 \\
V_S &= 0{,}132952290781x10^{1}S + 0{,}128955756844x10^{-3}S^2 \\
V_P &= 0{,}156059257041x10^{0}P + 0{,}244998688441x10^{-4}P^2 - 0{,}883392332513x10^{-8}P^3 \\
V_{STP} &= -0{,}127562783426x10^{-1}TS + 0{,}635191613389x10^{-2}TP + 0{,}265484716608x10^{-7}T^2P^2 \\
&\quad - 0{,}265484716608x10^{-7}T^2P^2 - 0{,}159349479045x10^{-5}TP^2 + 0{,}522116437235x10^{-9}TP^3 \\
&\quad - 0{,}438031096213x10^{-6}TP^3 - 0{,}161674495909x10^{-8}S^2P^2 + 0{,}968403156410x10^{-4}T^2S \\
&\quad + 0{,}485639620015x10^{-5}TS^2P - 0{,}340597039004x10^{-3}TSP
\end{aligned}$$

la que rinde resultados que difieren a lo más en 0,6 m/s con los producidos por la ecuación de Wilson para los primeros 250 m de profundidad, 0,5 a 0,4 m/s para los siguientes 250 m y, máximo, 0,3 m/s para profundidades comprendidas entre 500 y 1 500 m.

La distribución de la velocidad del sonido (V.S.) se presenta mediante transectos, uno escogido como típico de entre nueve, para cada crucero (Figs. 2, 3 y 4). Este tiene aproximadamente la misma situación en los tres casos (Fig. 1), extendiéndose desde Tampico hasta Cayo Arenas.

3. LOCALIZACION DE LA CAPA PROFUNDA DE V.S. MINIMA

La suavidad de las curvas verticales de la V.S. en las estaciones oceanográficas estudiadas, hace muy insegura la determinación de la profundidad del valor mínimo mediante inspección visual de las mismas, por lo que se hizo necesaria la elaboración de un método analítico de localización de la mencionada profundidad.

Derivemos la ecuación de Wilson (1) con respecto a la profundidad (Z); los puntos de la curva vertical, donde $dV/dZ = 0$, corresponden a valores máximos o mínimos de V.S., uno de los cuales serían el mínimo profundo que deseamos situar. Así tenemos que:

$$\frac{dT}{dZ} = - \frac{\left(\frac{d\,V_P}{d\,P} + \frac{\partial V_{STP}}{\partial P}\right) \frac{dP}{dZ} + \left(\frac{d\,V_S}{d\,S} + \frac{\partial V_{STP}}{\partial S}\right) \frac{dS}{dZ}}{\frac{d\,V_T}{d\,T} + \frac{\partial V_{STP}}{\partial T}} \qquad (3)$$

Esta expresión representa las condiciones que debe cumplir el gradiente vertical de la temperatura en una estación oceanográfica para que exista un valor crítico en la curva vertical de velocidad del sonido; que dicho valor sea precisamente el mínimo profundo se logrará confinando los valores de salinidad, temperatura y presión (profundidad) a los siguientes rangos:

$800\ \text{m} < Z < 1\,000\ \text{m}$

$34{,}3\ ^{o}/oo < S < 34{,}7\ ^{o}/oo$

$4{,}6^{o}C < T < 5{,}3^{o}C$

valores que en un muy alto porcentaje de las estaciones efectuadas enmarcan al mínimo.

En vías de convertir (3) en una fórmula práctica se hace necesario substituir las derivadas por diferencias finitas:

$$\frac{\Delta T}{\Delta Z} = - \frac{\left(\frac{\Delta V_P}{\Delta P} + \frac{\Delta V_{STP}}{\Delta P}\right) \frac{\Delta P}{\Delta Z} + \left(\frac{\Delta V_S}{\Delta S} + \frac{\Delta V_{STP}}{\Delta S}\right) \frac{\Delta S}{\Delta Z}}{\frac{\Delta V_T}{\Delta T} + \frac{\Delta V_{STP}}{\Delta T}} \qquad (4)$$

Los valores de la diferencia de V_S, V_T, V_P y V_{STP} respecto de S, T y P se obtienen directamente de las tablas de Wilson (Horne, 1969) promediando sobre los rangos deseados. $\Delta P/\Delta Z$ y $\Delta S/\Delta Z$ se obtienen de los datos de las estaciones promediando en los mismos rangos y promediando además para todas las estaciones; la substitución en (4) nos da:

$$\frac{\Delta T}{\Delta Z} = -\ 0{,}0041^{o}C/m$$

para averiguar en qué profundidad se cumple esta igualdad, se construyen curvas de $\Delta T/\Delta Z$ contra Z calculando $\Delta T/\Delta Z$ mediante valores observados en cada estación (Fig. 4a).

La profundidad del mínimo obtenida por medio de la interpolación gráfica se presenta en los transectos (Figs. 2, 3 y 4), así como en mapas topográficos de la capa profunda de mínima V.S. para cada uno de los 3 cruceros aquí tratados (Figs. 5,6 y 7).

4. CORRECCIONES PARA ECOSONDEOS

Se calcula una corrección aditiva de la forma:

$$Z_r = Z_e + Q$$

donde Z_r representa la profundidad real, Z_e la lectura o profundidad dada por la ecosonda y Q la corrección. De esta manera, Q estará dado por:

$$Q = Z_r\ (1 - V_e(\overline{1/V})) \qquad (5)$$

en la que V_e es el doble del factor de escala de la ecosonda y $(\overline{1/V})$ es el promedio de los inversos de los valores de V.S. conocidos. El uso de este promedio se hace necesario debido a que dichos valores se conocen como función de la profundidad; se evalúa como:

$$\overline{1/V} = \frac{1}{Z_r}\int_0^{Z_r} \frac{dZ}{V} = \frac{1}{Z_r}\sum_0^j \left(\frac{Z_{n+1} - Z_n}{2}\right)\left(\frac{1}{V_{n+1}} - \frac{1}{V_n}\right)$$

donde la integral se aproxima sumando trapezoides.

Con ésto, un programa para computadora, alimentado con valores de V.S. en profundidades estandard de cada estación de las situadas en un área determinada del Golfo, ejecuta las siguientes funciones:

- interpolación, mediante 3 puntos, de la V.S. cada 5 m hasta la profundidad estandard máxima, de la estación;
- integración numérica mediante suma de trapecios de 5 m de altura, hasta profundidades múltiplos de 100 m y cada 100 m hasta las siguientes profundidades (hasta donde hay datos) para cada estación de un área del Golfo: 100, 200, ... 1 500 m;
- obtención de la corrección para los dos tipos de ecosondas comerciales (820 br/s y 800 br/s),(1 500 m/s y 1 463 m/s) cada 100 m en las profundidades mencionadas;
- cálculo del promedio, desviaciones estandard y media en un mismo nivel para todas las estaciones del área.

Hace lo mismo para uno o varios paquetes de estaciones, las que se dividieron en áreas con el objeto de detectar y, en caso afirmativo, delimitar, zonas de iguales correcciones en la parte suroccidental del Golfo de México.

Es de hacerse notar que la corrección obtenida con (5) es la cantidad que es necesario adicionar a una profundidad real para conocer la lectura dada por una ecosonda; una gráfica Z_e contra Q permite interpolar el valor de la corrección buscada cuando Z_e es un múltiplo entero de 100, desde 100 hasta 1 500 m.

Los datos revelan que, dentro de los límites fijados por la desviación estandard, la región suroccidental del Golfo de México se puede considerar como un área homogénea y sin variación estacional en lo que respecta a la corrección para ecosondeos. El Cuadro I muestra los resultados obtenidos, así como los logrados por Matthews (1939).

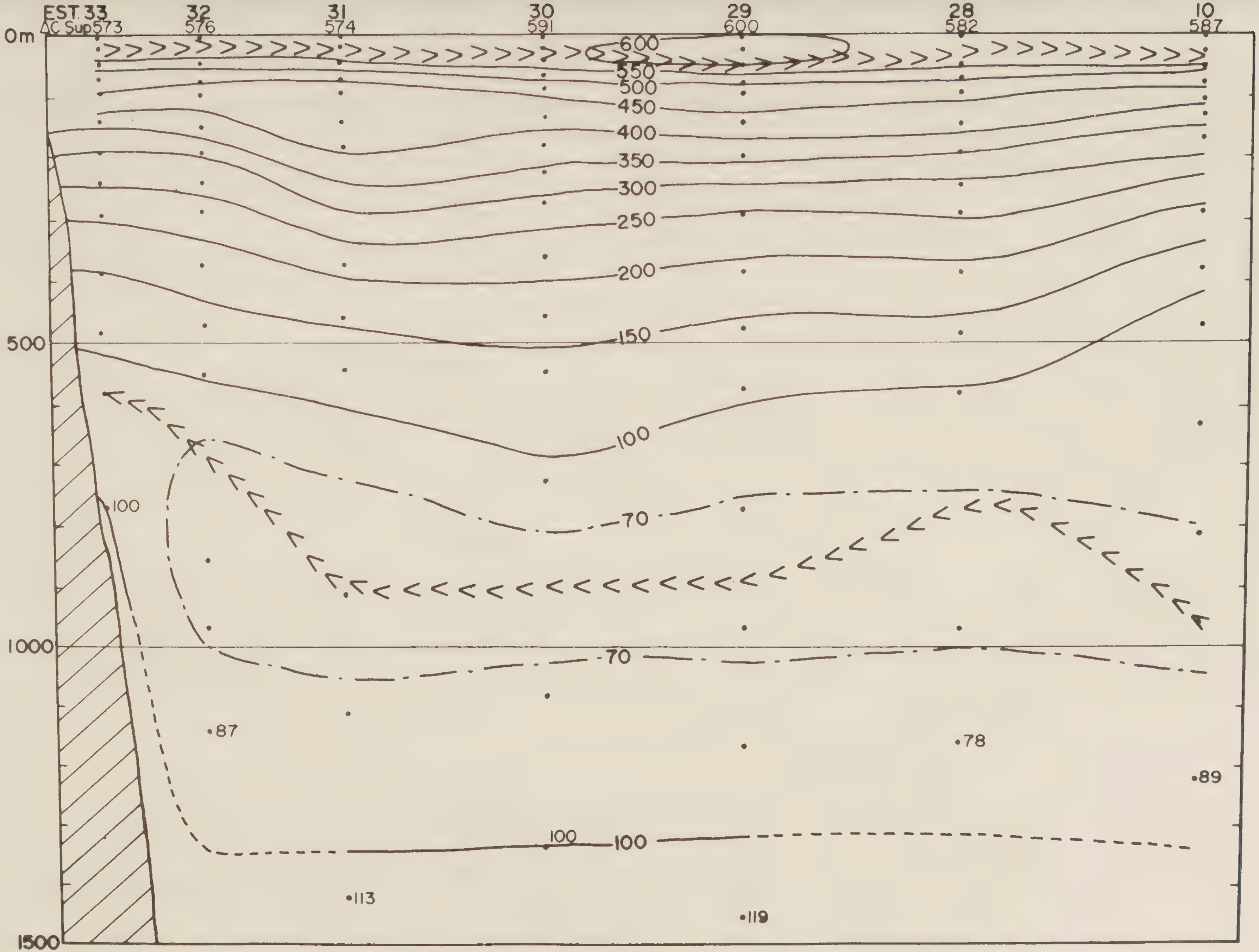

Fig. 2 Distribución de la velocidad del sonido. Transecto Tampico-Cayo Arenas, 7/11/70 al 8/11/70. Los números expresan anomalías en dm/seg sobre 14 000 dm/seg
(V(dm/seg) = (V - 1 480) x 10)
> : capa de máxima
< : capa de mínima

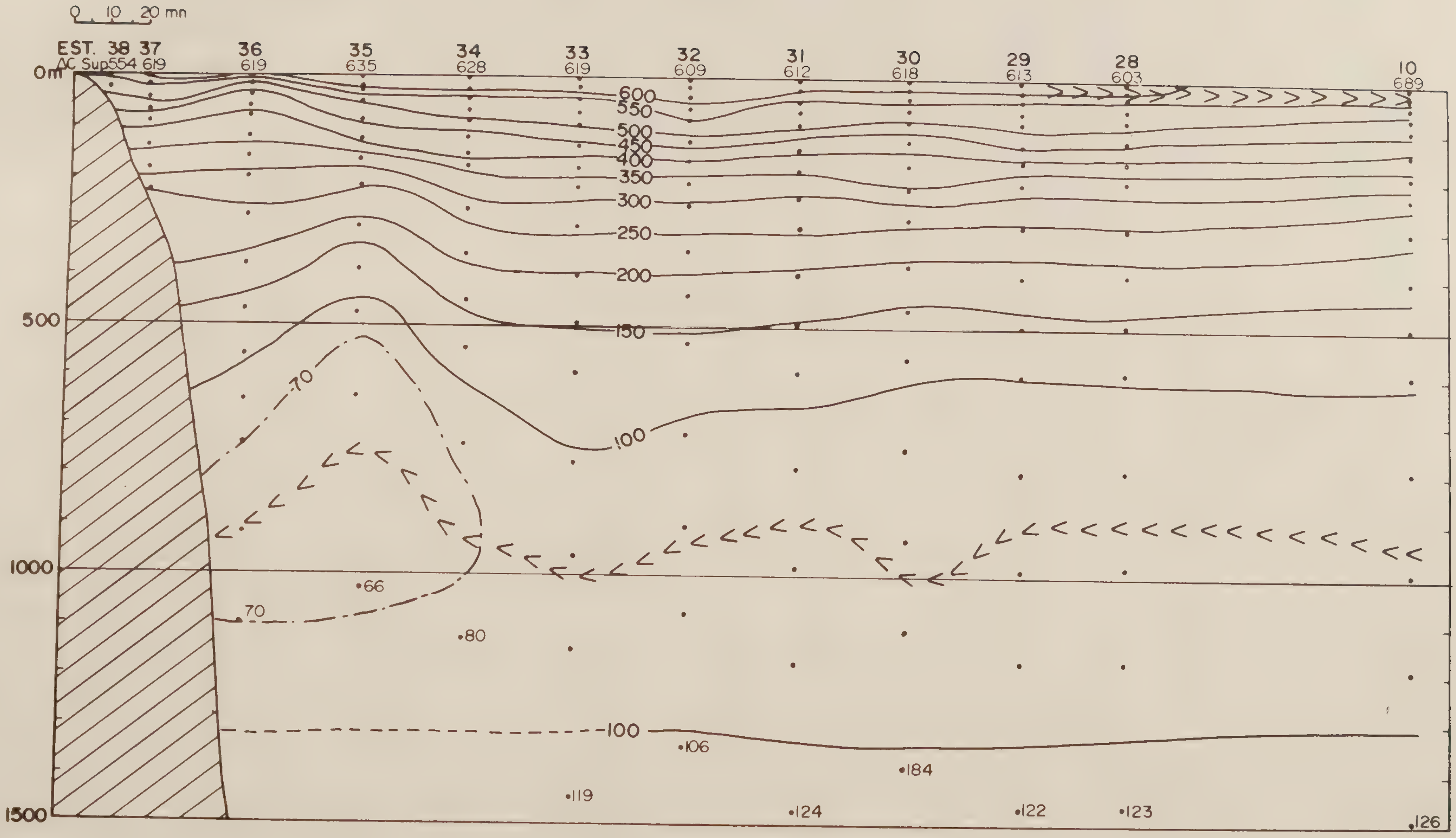

Fig. 3 Distribución de la velocidad del sonido. Transecto Tampico–Cayo Arenas. 1/6/71 al 3/6/71. Para simbología ver Fig. 2

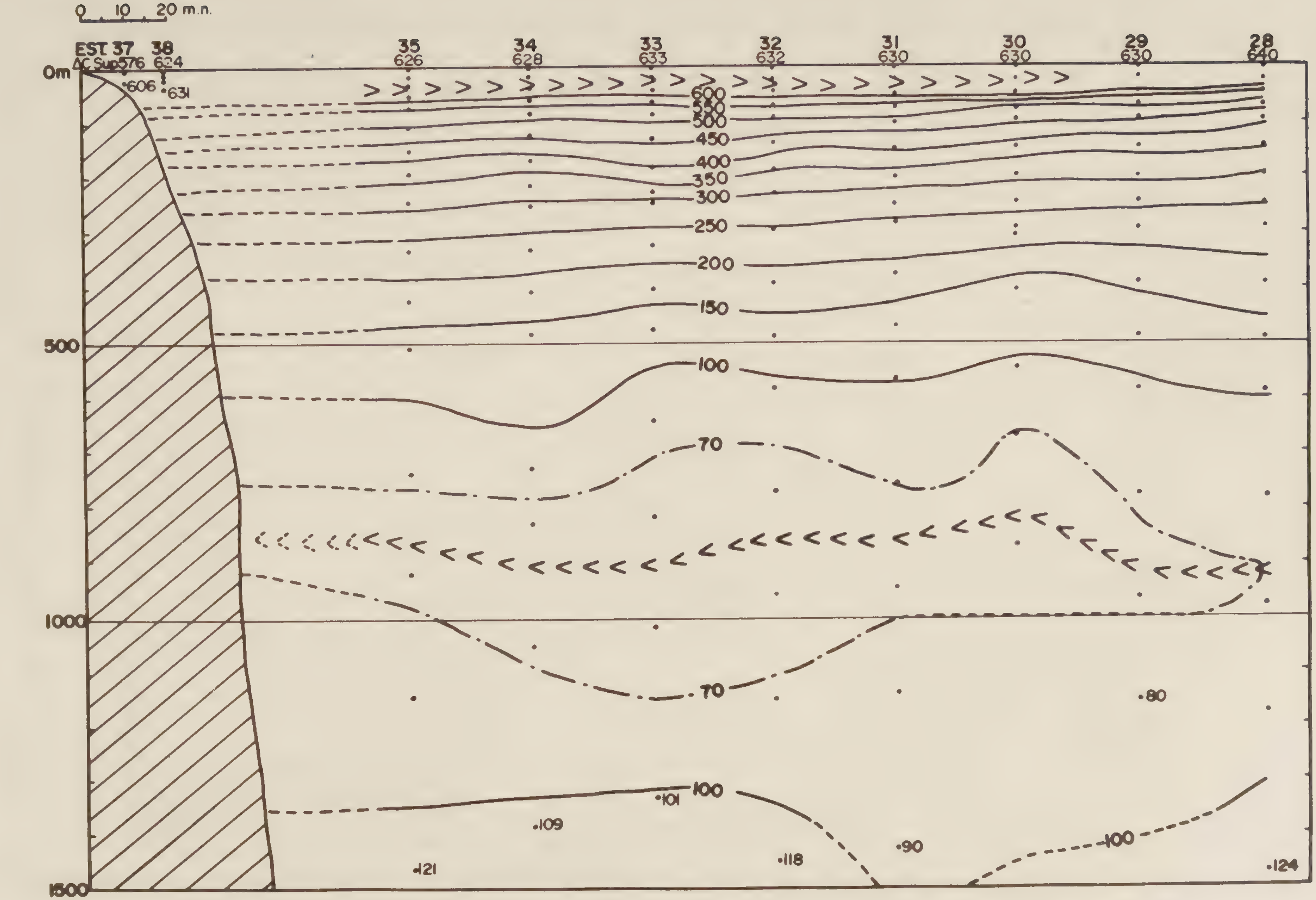

Fig. 4a Distribución de la velocidad del sonido. Transecto Tampico-Cayo Arenas, 3/11/71 al 6/11/71. Para simbologia ver Fig. 2

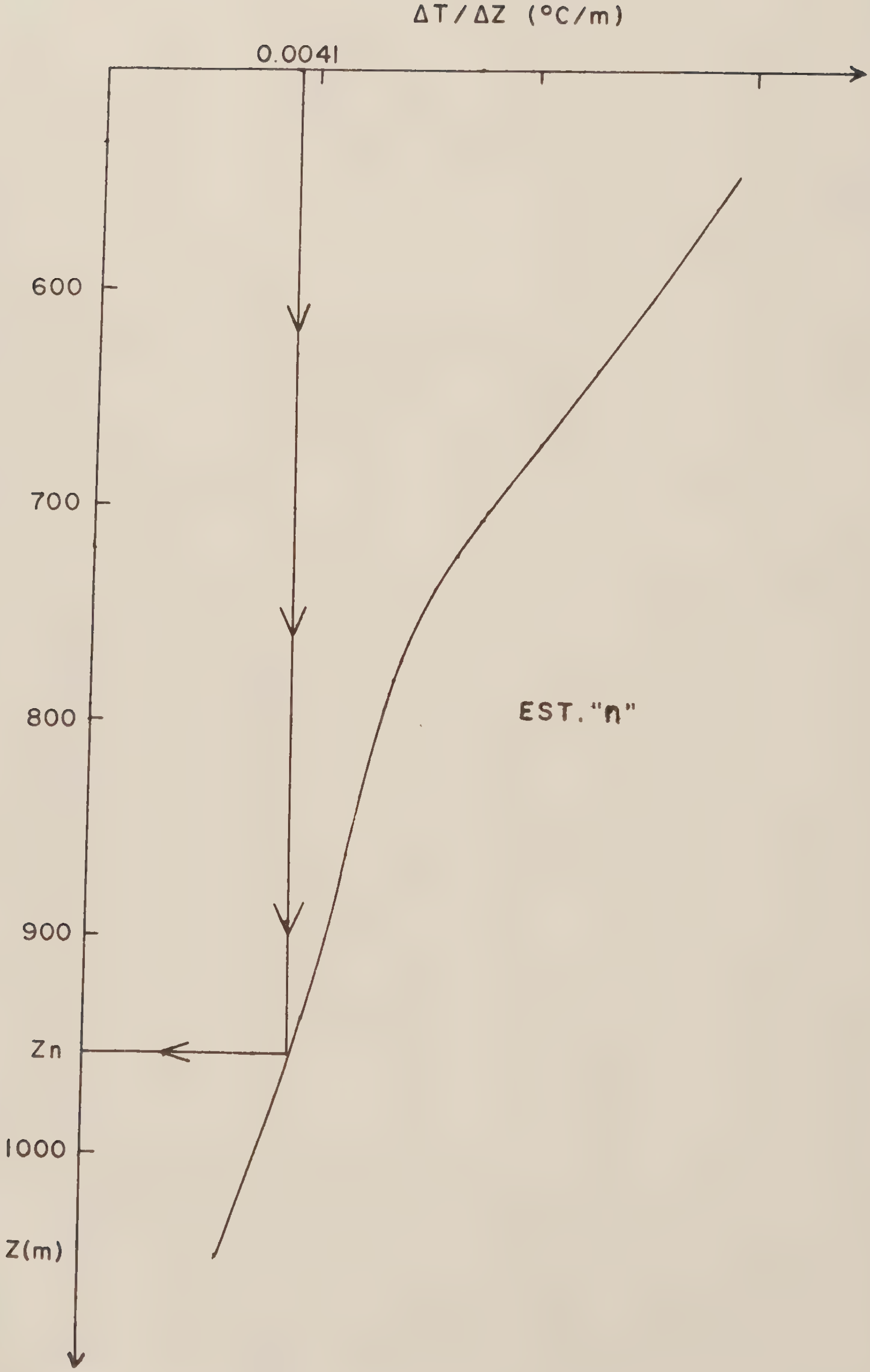

Fig. 4b Gráfica usada para determinar la profundidad (Z_n) de la V.S. mínima en una estación oceanográfica

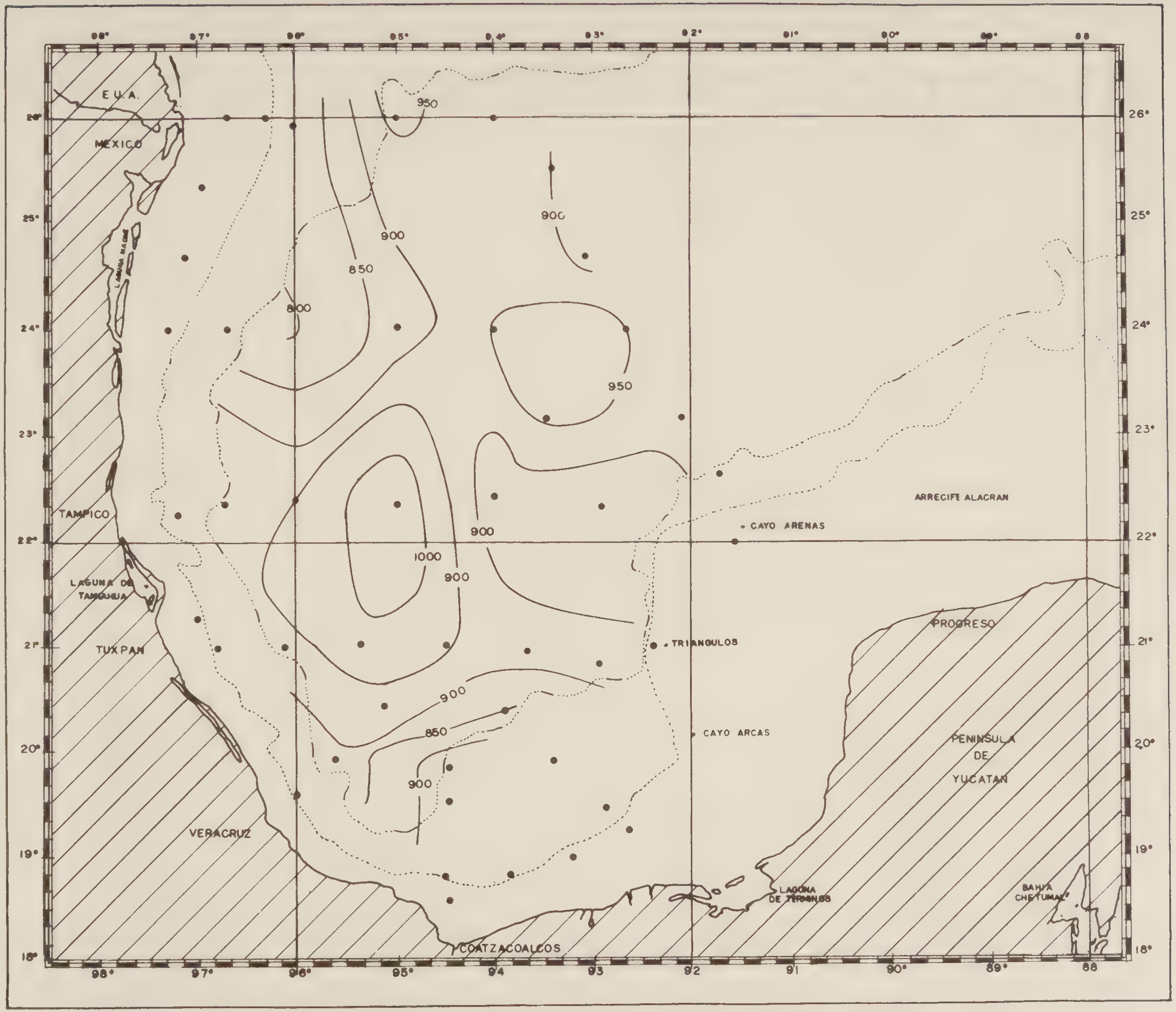
E.U.A.
MEXICO
LAGUNA MADRE
TAMPICO
LAGUNA DE TAMIAHUA
TUXPAN
VERACRUZ
COATZACOALCOS
LAGUNA DE TERMINOS
PENINSULA DE YUCATAN
PROGRESO
BAHIA CHETUMAL
ARRECIFE ALACRAN
CAYO ARENAS
TRIANGULOS
CAYO ARCAS
950
900
850
800
1000
98°
97°
96°
95°
94°
93°
92°
91°
90°
89°
88
26°
25°
24°
23°
22°
21°
20°
19°
18°

Fig. 5 Topografía del mínimo vertical de la velocidad del sonido, en ocasión del Crucero C 71-10

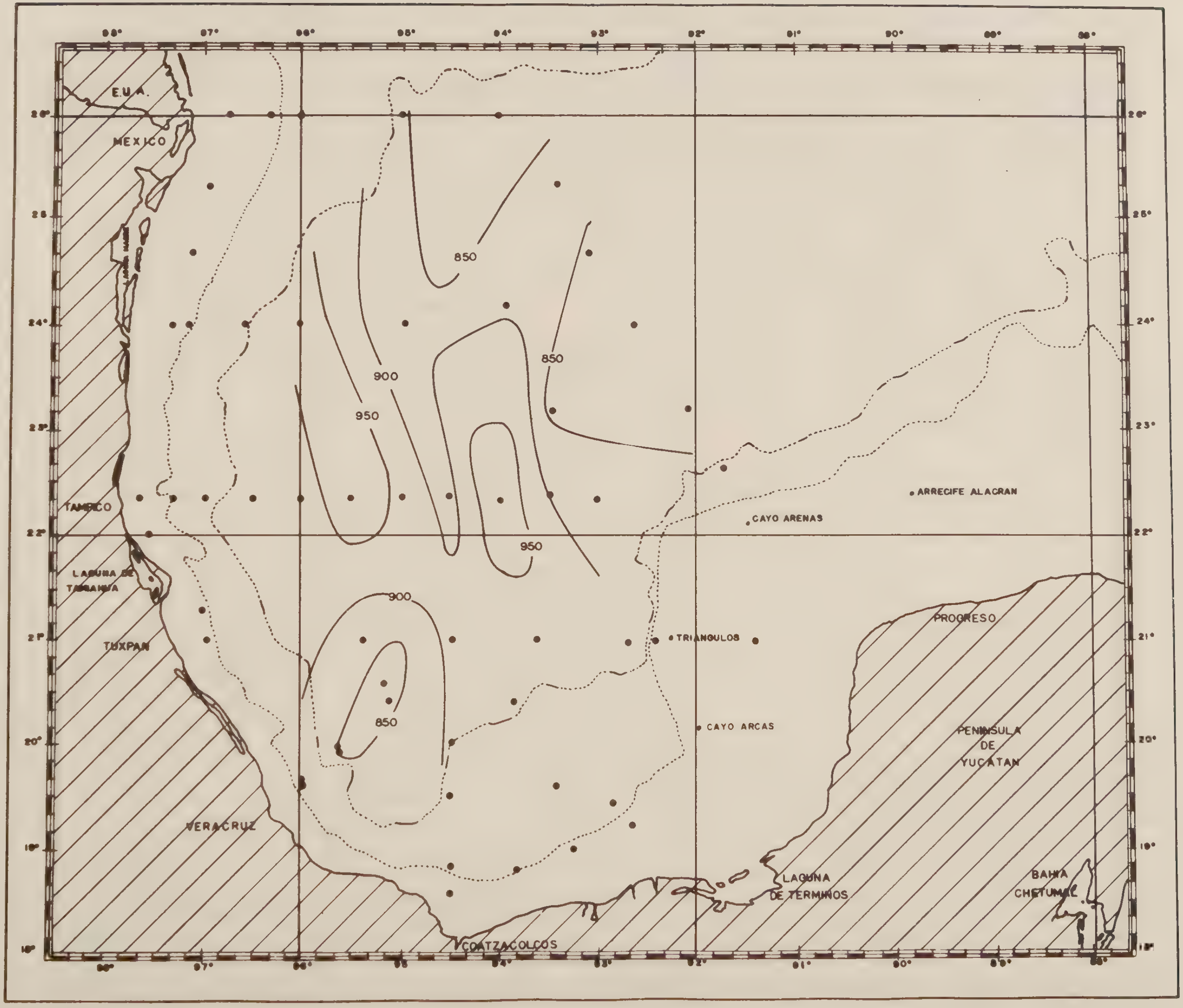
98°
97°
96°
95°
94°
93°
92°
91°
90°
89°
88°
26°
25°
24°
23°
22°
21°
20°
19°
18°
E.U.A.
MEXICO
TAMPICO
LAGUNA DE TAMIAHUA
TUXPAN
VERACRUZ
COATZACOLCOS
LAGUNA DE TERMINOS
BAHIA CHETUMAL
PENINSULA DE YUCATAN
PROGRESO
ARRECIFE ALACRAN
CAYO ARENAS
TRIANGULOS
CAYO ARCAS
850
850
900
950
950
900
850

Fig. 6 Topografía del mínimo vertical de la velocidad del sonido, en ocasión del Crucero C 71-10

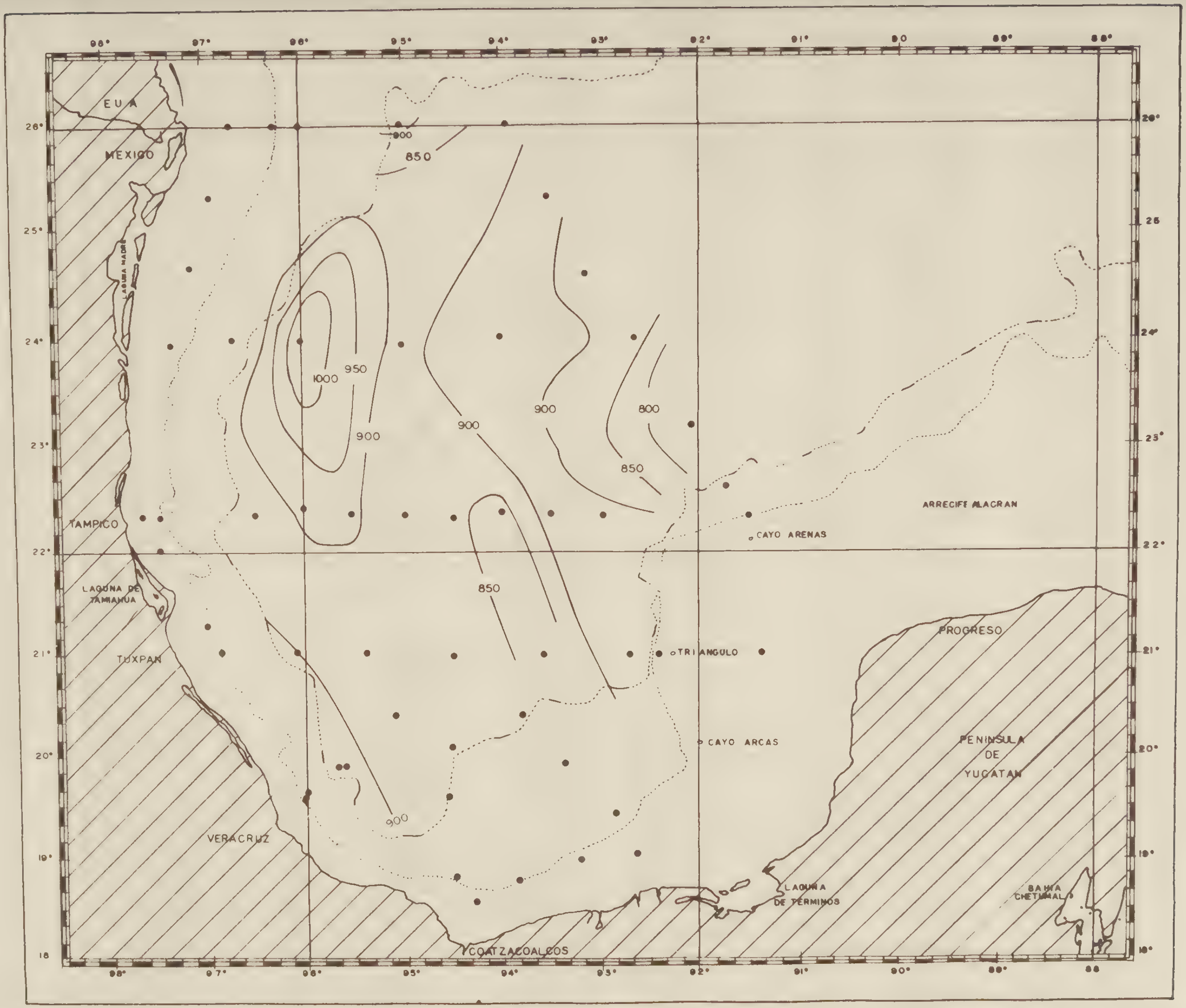
98°
97°
96°
95°
94°
93°
92°
91°
90
89°
88°
26°
25°
24°
23°
22°
21°
20°
19°
18
E U A
MEXICO
LAGUNA MADRE
TAMPICO
LAGUNA DE TAMIAHUA
TUXPAN
VERACRUZ
COATZACOALCOS
LAGUNA DE TERMINOS
BAHIA CHETUMAL
PENINSULA DE YUCATAN
PROGRESO
ARRECIFE ALACRAN
CAYO ARENAS
TRIANGULO
CAYO ARCAS
900
850
1000
950
900
900
900
800
850
850
900

Fig. 7 Topografía del mínimo vertical de la velocidad del sonido, en ocasión del Crucero C 71-22

5. DISCUSION Y CONCLUSIONES

La discrepancia entre los valores de V.S. obtenidos mediante la fórmula de Wilson por un lado y los de la fórmula de Del Grosso por el otro, no tiene mayores consecuencias sobre los resultados de este trabajo.

Los transectos de V.S. aquí presentados muestran gradientes, en lo general, muy homogéneos; los correspondientes a los cruceros 71-10 y 71-22 (primavera y otoño de 1971), señalan que la V.S. decrece desde 1 540 m/s a 1 495 m/s en los primeros 500 m de profundidad. Por otro lado, en ocasión del crucero 70-12 (otoño de 1970) el mismo intervalo presenta un decrecimiento que va desde 1 535 m/s hasta 1 495 m/s. Esta diferencia de 4 m/s en relación con el otoño de 1971, es consecuencia del intenso enfriamiento que sufrió la capa superficial durante el otoño de 1970.

Por otra parte, los transectos correspondientes a los cruceros efectuados en la misma temporada en años distintos (otoño, 1970 y 1971), presentan máximos intermedios en la capa superficial; es de suponerse que tales máximos sean un fenómeno estacional provocado por enfriamiento de la capa de superficie por los vientos fríos de la época.

Por debajo de los 500 m los gradientes son suaves (ver Figs. 2, 3 y 4), tanto que la velocidad decrece desde 1 495 m/s hasta un mínimo de más o menos 1 486 m/s, situado entre 800 y 1 000 m de profundidad, para volver a aumentar hasta 1 494 m/s en el extremo de la profundidad observada.

En la capa de 500 a 1 500 m, los transectos muestran grandes irregularidades, tanto espaciales como temporales, en la distribución de V.S. y en la situación del mínimo profundo (canal sonoro). Estas aparentes fluctuaciones pueden ser reales, pero no se excluye la posibilidad de que sean producidas en las gráficas por la gran distancia vertical entre los puntos de observación en esta capa.

En cuanto al método de localización de la profundidad del mínimo valor profundo de V.S. en la vertical desarrollado aquí, conviene hacer una evaluación de su certidumbre. Los principales errores podrían deberse a la substitución de derivadas por diferencias finitas y al uso de promedios. Añadiéndole factores de compensación por dichos errores, la ecuación (4) se vería así:

$$\frac{\Delta T}{\Delta Z} \pm C_1 = - \frac{\left(\frac{\Delta V_P}{\Delta P} + \frac{\Delta V_{STP}}{\Delta P} \pm C_2\right)\left(\frac{\Delta P}{\Delta Z} \pm C_3\right) + \left(\frac{\Delta V_S}{\Delta S} + \frac{\Delta V_{STP}}{\Delta S} \pm C_4\right)\left(\frac{\Delta S}{\Delta P} + C_5\right)}{\frac{\Delta V_T}{\Delta T} + \frac{\Delta V_{STP}}{\Delta T} \pm C_6}$$

Evaluados y substituídos los C's se tiene:

$$\frac{\Delta T}{\Delta Z} = - 0{,}0041 \pm 0{,}0008^{\circ}C/m$$

lo cual significa que el gradiente vertical de temperatura que en la región estudiada provoca un mínimo en V.S. se conoce con una certeza de $\pm$ 0,0008°C/m, valor que, llevado a las gráficas "$\Delta T/\Delta Z$ - Z" da el rango de certidumbre en la determinación de la profundidad. Esto nos permite concluir que, mediante el método descrito, se puede situar la profundidad de la capa profunda de mínima V.S. dentro de un rango de 100 m, que representa una mejora de hasta 100 m con respecto a la simple apreciación visual de la curva vertical de V.S.

Existe otra fuente de incertidumbre que depende del método observacional, el cual sólo puede apreciar fenómenos de macroestructura, debido a la separación de los niveles de muestreo (hasta 200 m en profundidades alrededor del mínimo), pero, debido a la falta de datos sobre estructura media y fina en el Golfo de México, no es posible elucubrar mucho sobre el tema. Lo más que se puede decir es que, usando gradientes de temperatura obtenidos en el Pacífico Norte (Gregg et al., 1973) el rango de incertidumbre se ampliaría hasta 200 m.

En conclusión, con los datos actuales se puede decir que la profundidad de la capa profunda de mínima velocidad del sonido en el suroeste del Golfo de México se conoce con un margen de incertidumbre de ± 50 m; el que el margen sea éste podría ser la causa de la irregularidad y falta de semejanza de los mapas topográficos presentados (Figs. 5, 6 y 7). Se perfila, por lo tanto, la necesidad de conocer la estructura de la velocidad del sonido con mayor precisión, ya sea mediante el uso de mallas de muestreo más cerradas, o registros continuos así como también la necesidad de conocer la estructura fina del Golfo.

Por lo que se refiere a las correcciones para ecosondeos, se concluye que, dentro de ciertos límites de precisión (± 1 m) el Golfo de México suroccidental se presenta como un área uniforme y estacionaria, y que las diferencias entre las correcciones presentadas por Matthews y las encontradas en el presente trabajo, están dentro del límite establecido.

CUADRO I

Correcciones para ecosondeos en la región suroccidental del Golfo de México. Comparación con la Tabla de Matthews, ∂ es la desviación **estandard**, W(m/s) = 1/(1/V), V_e en m/s

Prof. m	W	V_e 1 500	V_e 1 463	∂	Matthews 1 500	Matthews 1 463
100	1 534,4	2	5	0		
200	1 526,2	3	8	0	3	9
300	1 520,0	4	12	1		
400	1 514,9	4	14	1	4	14
500	1 510,8	4	16	1		
600	1 507,4	3	18	1	3	18
700	1 504,3	2	19	1		
800	1 502,4	1	22	1	1	21
900	1 500,8	1	23	1		
1 000	1 499,5	0	24	1	-2	24
1 100	1 498,4	-1	27	1		
1 200	1 497,4	-2	28	1	-3	27
1 300	1 496,8	-3	30	1		
1 400	1 496,3	-3	32	1	-5	31
1 500	1 496,1	-4	33	1		

6. REFERENCIAS

Del Grosso, V.A., 1974 New equation for the speed of sound in natural waters (with comparisons to other equations). J.Acoust.Soc.Am., 56(4):1084

Dinger, C., 1970 Computer programs in oceanography. Publ.Natl.Oceanogr.Data Cent.(Catal.Ser.), (C-5):82 p.

Emilsson, I., 1954 On the correction of the reversing thermometers and construction of graphs for total correction. Bol.Inst.Oceanogr., S.Paulo, 5(1-2):71-81

Gregg, M.C., C.S. Cox y P.W. Hacker, 1973 Vertical microstructure measurements in the central North Pacific. J.Phys.Oceanogr., 3(4):458-69

Horne, R.A., 1969 Marine chemistry. The structure of water and the chemistry of the hydrosphere. Nueva York, Wiley-Interscience, pp. 524-8

Matthews, D.J., 1939 Tables of the velocity of sound in pure water and in sea water for use in ecosounding and in sound-ranging. Londres, Hydrographic Department Admiralty

Wilson, W.F., 1960 Equation for the speed of sound in sea water. J.Acoust.Soc.Am., 32(10):1357

CIRCULACION DEL AGUA EN EL SUROESTE DEL GOLFO DE MEXICO

por

A.M. VAZQUEZ DE LA CERDA
Dirección General de Oceanografía y Señalamiento Marítimo
Secretaría de Marina, México

Resumen

El Gobierno mexicano ha efectuado campañas oceanográficas sistemáticamente en el suroeste del Golfo de México con el B/O VIRGILIO URIBE en ocho cruceros hechos desde octubre de 1970 hasta noviembre de 1971. La información de estos cruceros forma la base de una nueva descripción más detallada de la circulación del Golfo. Todos los cruceros son discutidos a través de la anomalía geopotencial y de la superficie topográfica isotérmica de 15°C. la cual se aproxima al modelo de flujo geostrófico. Los resultados confirman el dominio de un remolino de circulación anticiclónica en el oeste del Golfo. La circulación en su lado oeste tiene una velocidad geostrófica un poco mayor de lo que la información de las cartas piloto sugieren. Debido a que aparentemente es invariable su presencia en el oeste del gran remolino anticiclónico el nombre de Remolino Mexicano Anticiclónico se propone para esta forma. Su promedio de volumen en transporte geostrófico es aproximadamente de 10 millones de metros cúbicos por segundo. Una región ciclónica encontrada en la parte central u oeste de la Bahía de Campeche está en forma permanente. Algunas veces es fuerte y aparentemente cerrada. Otra región ciclónica en el noroeste de la Laguna de Tamihaua puede ser una forma periódica. Una intrusión hacia el sur de una cresta en geopotencial es encontrada al oeste del Banco de Campeche y ella está algunas veces conectada con el Remolino Mexicano Anticiclónico. Esta es, aparentemente, una forma permanente también.

Abstract

The Mexican Government surveyed the southwestern Gulf of Mexico systematically from the R/V VIRGILIO URIBE in eight cruises made from October 1970 to November 1971. Data from these cruises form the basis of this new and more detailed description of the circulation there. All cruises are discussed through the geopotential anomaly and the use of the 15°C isothermal surface topography, which approximates the geostrophic flow pattern. The results confirm the dominance of the anticyclonic eddy circulation in the western Gulf. The circulation of its west side has somewhat higher geostrophic velocity than Pilot Chart information suggests. Because of the apparently invariable presence in the west of a large anticyclonic eddy, the name Mexican Anticyclonic Eddy is proposed for this feature. Its average geostrophic volume transport is approximately 10 million cubic metres per second. A cyclonic region found in the central or western Bay of Campeche seems to be a permanent feature. At times it is strong and apparently closed. Another cyclonic region in the northeast of Tamihaua Lagoon may be a recurring feature. A southward intrusion of a ridge in geopotential is found west of the Campeche Bank and is sometimes connected with the Mexican Anticyclonic Eddy. It is, apparently, a permanent feature also.

Desde 1970, el Gobierno mexicano, a través de la Secretaría de Marina y algunas instituciones de investigación, ha realizado investigaciones en el oeste del Golfc a bordo del buque de la Armada de México B/O CADETE VIRGILIO URIBE, OSM (1970 y 1971). Datos obtenidos durante cruceros de oceanografía física fueron procesados en el Instituto de Geofísica, Universidad Nacional Autónoma de México y en la Dirección General de Oceanografía y Senalamiento Marítimo, Secretaria de Marina. Estos cruceros cubrieron la parte oeste del Golfo en un promedio de dos semanas cada uno. Asimismo el Instituto Nacional de Pesca, Secretaría de Industria y Comercio, en el B/O URIBE efectuó cruceros en el suroeste del Golfo (Granados *et al.*, 1972). La combinación de estos cruceros en 1970 y 1971, junto con uno realizado por la Universidad de Texas A&M en la parte central del Golfo, dan una imagen muy completa de la circulación de las aguas en el Golfo de México (Cuadro I).

En noviembre de 1970, se realizó el primer crucero de oceanografía física por el B/O URIBE (Fig. 1). Se puede observar la mitad aproximadamente de un remolino anticiclónico localizado en la parte norte del Banco de Campeche. Los valores indican anomalía en geopotencial en centímetros dinámicos. El cálculo de volumen de transporte geostrófico da un valor de 6,5 x $10^6 m^3/seg^{-1}$. Es probable que el valor sea un poco mayor que el obtenido. Una intrusión en el Banco de Campeche al oeste está marcada como una extensión hacia el sur del remolino anticiclónico. En la parte sur de la Bahía de Campeche se nota una región ciclónica y probablemente sea un remolino ciclónico pero los datos de anomalía dinámica no lo alcanzan a indicar.

CUADRO I

Cruceros oceanográficos

Fecha	Buque	Crucero	Profundidad (m) en las observaciones		Localizacion
21.10-3.11.70	ALAMINOS	70-A-14	82[a/]	1 200	Golfo Central
31.10-13.11.70	URIBE	COSMA 70-12	53	1 500	Golfo Occidental
14.1-23.1.71	URIBE	COSMA 71-02	15	500	Golfo Sudoccidental
27.4-11.5.71	URIBE	COSMA 71-08	50	500	Golfo Sudoccidental
24.5-9.6.71	URIBE	COSMA 71-10	57	1 500	Golfo Occidental
19.7-31.7.71	URIBE	COSMA 71-14	44	500	Golfo Sudoccidental
4.8-3.9.71	URIBE	COSMA 71-16	75[b/]	1 500	Golfo Sud
7.10-18.10.71	URIBE	COSMA 71-20	43	500	Golfo Sudoccidental
27.10-10.11.71	URIBE	COSMA 71-22	57	1 500	Golfo Occidental

a/ 21 calas con termómetros reversibles y 61 STDs

b/ Estaciones adicionales se efectuaron en el oeste del Mar Caribe (Emilsson, 1971)

Para mayo-junio de 1971 (Fig. 2) el análisis de los datos indicó que el centro del remolino anticiclónico se había desplazado más hacia el oeste del Golfo. Su forma es un tanto irregular y tiene un volumen de transporte geostrófico de 8,7 x $10^6 m^3/seg^{-1}$. Hay una región ciclónica desde las costas de Texas que se prolonga hacia el centro del Golfo. Nuevamente se marca una intrusión hacia el sur en el oeste del Banco de Campeche unida al remolino anticiclónico principal. La región ciclónica en la Bahía de Campeche se encuentra más hacia el oeste. Correspondiendo al mismo crucero, en la Fig. 3 en una ampliación cerca de la Laguna de Tamiahua se observa el extremo suroeste del remolino anticiclónico. Asimismo las flechas indican los vectores de corriente obtenidos en las mediciones de Electro Kinetógrafo Geomagnetíco (GEK) (Bravo, 1972), que confirma la circulación de las aguas. Se observa también el obstáculo topográfico submarino que hace cambiar la dirección de la corriente, formando un remolino ciclónico al noreste de la Laguna de Tamiahua.

En el crucero de agosto de 1971 (Fig. 4) solamente se tienen datos en la Bahía de Campeche; sin embargo se puede observar la parte sur del remolino anticiclónico encontrándose en la parte oeste del Golfo y también la intrusión en la parte oeste del Banco de Campeche. El valor del volumen de transporte geostrófico es de 2,7 x $10^6 m^3/seg^{-1}$, que no representa el total de la circulación anticiclónica.

Para noviembre de 1971 (Fig. 5), la circulación del remolino anticiclónico se ha incrementado y también se ha desplazado hacia el norte. El valor del volumen de transporte geostrófico es 12,4 x $10^6 m^3/seg^{-1}$, el mayor encontrado en esta serie de cruceros. La velocidad en el oeste del remolino anticiclónico excede de un nudo. También se marca el remolino ciclónico en la Bahía de Campeche, pero ahora se encuentra desplazado hacia el oeste; además tiene conexión con la parte central del Golfo. La intrusión anticiclónica al oeste del Banco de Campeche está separada del remolino anticiclónico.

La secuencia de los nueve cruceros a través de la topografía de 15°C que se asemeja a la configuración de geopotencial es presentada de la Fig. 6 a la Fig. 9.

En el mes de noviembre de 1970 el crucero del B/O URIBE y el del B/O ALAMINOS (Fig. 6A) concuerdan perfectamente ya que son quasi-sinópticos. Se pueden observar todas las características del Golfo de México a partir de la parte oeste de la corriente de Lazo hacia el oeste. Las profundidades de la topografía estan dadas en metros. La corriente de Lazo alcanza profundidades hasta de 450 metros. Dos regiones ciclónicas están localizadas entre el norte del Banco de Campeche y la desembocadura del Río Mississippi. Estas regiones fueron reportadas por Whitaker (1971) en sus cartas mensuales. El gran remolino anticiclónico localizado al oeste del Golfo tiene algunas extensiones. La primera al norte del Banco de Campeche (Cochrane, J.D., comunicación personal) que ha sido reportada anteriormente, siguiendo la topografía en la parte oeste del Banco de Campeche, está otra intrusión. En la Bahía de Campeche se marca un remolino ciclónico cerrado. También se marca otro remolino ciclónico al oeste del gran remolino anticiclónico.

En enero de 1971 (Fig. 6B), no obstante estar muy espaciadas las estaciones en la Bahía de Campeche, es posible representar una región ciclónica en el suroeste del Banco de Campeche.

En abril-mayo de 1971 (Fig. 7A), muestra nuevamente la región ciclónica en el suroeste de la Bahía de Campeche. La región anticiclónica en forma de intrusión se encuentra al oeste del Banco de Campeche, probablemente se ha desplazado hacia el oeste.

El crucero mayo-junio de 1971 (Fig. 7B) ha sido discutido anteriormente, mostrando el remolino anticiclónico en el oeste del Golfo, así como las regiones ciclónicas en su periferia, es decir el de la Bahía de Campeche y el que se encuentra al noreste de la Laguna de Tamiahua.

Para julio de 1971 (Fig. 8A) la intrusión en la Bahía de Campeche se ha desplazado más hacia el oeste, dividiendo la región ciclónica en dos partes y también la región anticiclónica en dos partes. Probablemente la región ciclónica del sur esté conectada con la indicada más al centro del Golfo.

En agosto de 1971, Fig. 8B indica que la región anticiclónica está situada más al norte y claramente separada en dos partes. La región ciclónica en la Bahía de Campeche tiene una extensión hacia el norte; también la intrusión está presente en el oeste del Banco de Campeche.

En octubre de 1971 (Fig. 9A), la configuración es muy similar a la de agosto.

Para noviembre de 1971 (Fig. 9B) se muestra claramente como el remolino anticiclónico ha incrementado su valor y se ha desplazado más al norte cerca de la costa de México. La región ciclónica cruza el Golfo del suroeste hacia el noreste, y es muy posible que estas características se hayan desarrollado antes. Ahora la intrusión al oeste del Banco de Campeche está separada completamente del remolino anticiclónico.

La salinidad en la superficie del mar en los cruceros también da una buena información para localizar el remolino anticiclónico (figuras no mostradas en la presente contribución) ya que su centro muestra valores de mayor concentración de salinidad.

El resultado del análisis de los cruceros confirma el dominio de una circulación anticiclónica en la parte oeste. Esto sugiere que el eje de la corriente en el lado oeste del remolino anticiclónico está aproximadamente a 160 km de la costa de México, y normalmente su velocidad (geostrófica) sea un poco más de un nudo, siendo mayor de lo que sugiere la información de las cartas piloto (1955); posiblemente el flujo esté ocultado en parte por la dirección del viento. En ninguno de los cruceros el remolino anticiclónico ocupó completamente la parte oeste del Golfo. Este fué circundado por algunas regiones ciclónicas las cuales le dieron una forma irregular en su periferia. En base a los datos discutidos y a la información de otros cruceros, hay más regiones anticiclónicas usualmente entre la principal en el oeste del Golfo y el formado en el centro del Sistema de la Corriente de Lazo en el Este.

La circulación en la parte central y oeste del Golfo es siempre menor que la Corriente de Lazo, segmento del Sistema de la Corriente del Golfo.

Algunas veces, como sucedió en noviembre de 1971, al análisis indicó una depresión de geopotencial que atravesó el oeste del Golfo y hubo dos regiones anticiclónicas. Ninguno de los cruceros indicó un remolino anticiclónico relativamente pequeño en el oeste. Debido a la presencia invariable del gran remolino anticiclónico en el oeste del Golfo, el nombre de Remolino Anticiclónico Mexicano es propuesto para esta formación característica.

La Corriente de Lazo es separada a menudo del resto del Golfo por una circulación ciclónica a lo largo de su flanco izquierdo (oeste) como es ilustrado en el crucero de octubre-noviembre de 1970 (Fig. 6A). Esta situación es sugerida por los promedios mensuales obtenidos por Whitaker (1971). Dicha circulación ciclónica ha sido encontrada en cruceros subsecuentes. Esta configuración es encontrada aparentemente más a menudo que la mostrada por Nowlin y McLellan en el invierno de 1962. La Corriente de Lazo, por esta razón, parece no estar conectada directamente con la circulación en el oeste. Esto puede tomarse en cuenta por la rareza con la cual la salinidad en todos los niveles de la Corriente de Lazo se encuentre en el oeste.

Las características generales del Remolino Anticiclónico Mexicano en los cruceros, son las siguientes: el centro en comparación con sus alrededores tiene mayor profundidad a una superficie isanostérica dada; el centro del remolino anticiclónico tiene altos valores de salinidad con respecto a su periferia y mayor concentración de oxígeno disuelto en la periferia que en el centro. El promedio de transporte del volumen geostrófico es aproximadamente de 10 millones de metros cúbicos por segundo, el cual corresponde aproximadamente a 1/3 de transporte del volumen de la Corriente de Lazo.

Una intrusión hacia el sur con un valor alto en geopotencial a lo largo del Banco de Campeche estuvo presente en cada uno de los cruceros discutidos, es decir de octubre-noviembre de 1970 a noviembre de 1971. Nowlin y McLellan (1967) también indicaron que estuvo presente en marzo de 1962. Parece ser que ésta es una formación característica permanente. De octubre-noviembre de 1970 hasta mayo-junio de 1971 la intrusión hacia el sur fué una extensión del Remolino Anticiclónico Mexicano dominante en el oeste del Golfo. Desde agosto hasta el final de la serie de cruceros analizados es decir hasta noviembre de 1971 la intrusión fué una parte separada del Remolino Anticiclónico Mexicano. Sus características generales fueron alta salinidad y baja concentración de oxígeno disuelto. La intrusión implica un flujo a lo largo del extremo oeste del Banco de Campeche, el cual es de esperarse si consideramos que la corriente está dirigida por la topografía del fondo marino.

La circulación ciclónica encontrada en la Bahía de Campeche fué observada en todos los cruceros analizados, excepto en enero por la poca información que se tuvo en ese mes. El Atlas de Cartas Piloto (1955) lo muestran en enero, marzo, abril, noviembre y diciembre. Es probable que ésta sea una formación permanente, pero que no cubre toda la Bahía de Campeche como lo presentan las Cartas Piloto. Debido a que la intrusión está siempre presente, el remolino ciclónico se encuentra en la parte oeste de la Bahía de Campeche. Algunas veces el remolino ciclónico está conectado a traves de una baja presión con la parte norte. El remolino ciclónico siempre tuvo relativamente baja salinidad y alta concentración de oxígeno disuelto.

En noviembre de 1970, en la topografía de 15°C fué observada una región ciclónica al noreste de la Laguna de Tamiahua. En mayo-junio la región ciclónica fué observada nuevamente en la estructura termo-halina y confirmada por las mediciones hechas con el GEK (Bravo, 1972) (Fig. 3). Sin embargo en agosto y noviembre de 1971 el Remolino Anticiclónico Mexicano estuvo muy cerca de la costa y aparentemente el remolino ciclónico al noreste de Tamiahua estuvo ausente. Es probable que esta región ciclónica sea una formación característica periódica.

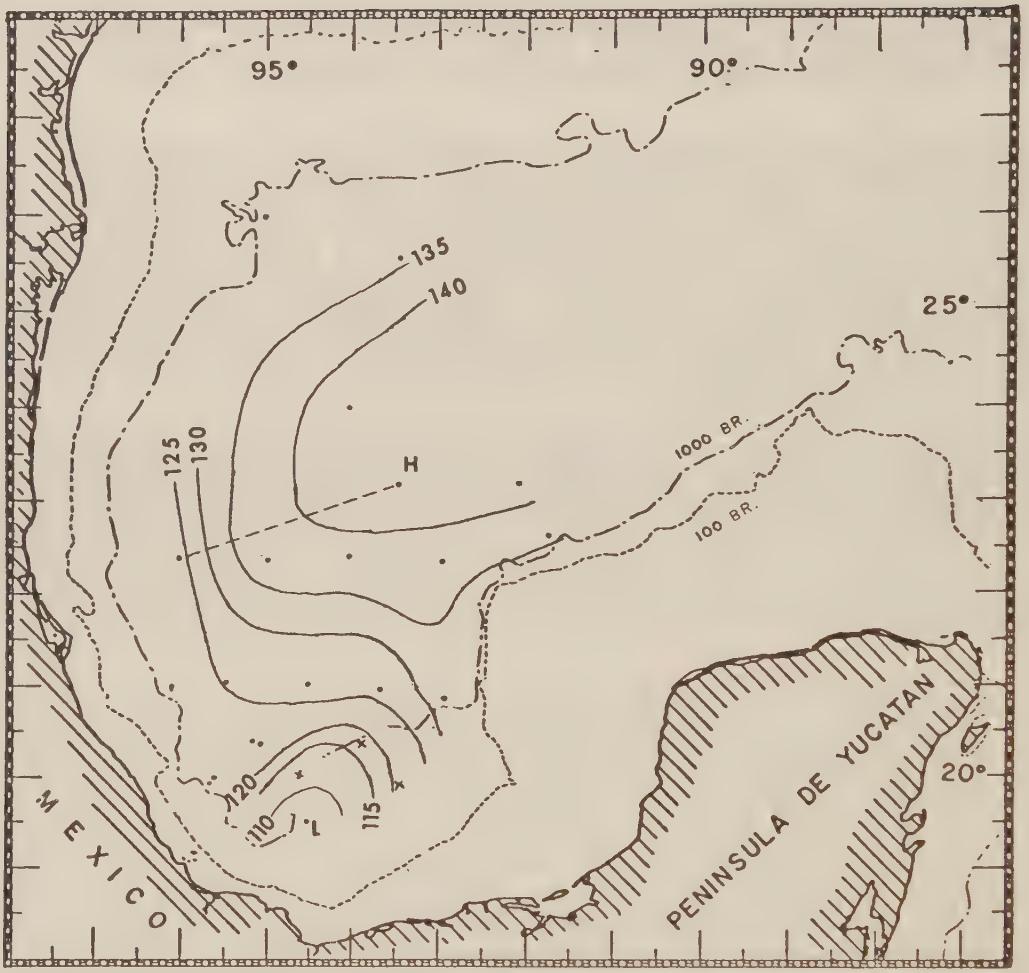
95°
90°
25°
20°
135
140
125
130
H
1000 BR.
100 BR.
120
110
L
115
MEXICO
PENINSULA DE YUCATAN

Fig. 1 Anomalía geopotencial (en centímetros dinámicos) de la superficie del mar relativa a 1 200 decibares. Noviembre de 1970 (COSMA 70-12). x indica alguna extrapolación. Volumen de transporte geostrófico entre las estaciones conectadas con una línea discontinua (- - -) ha sido determinado

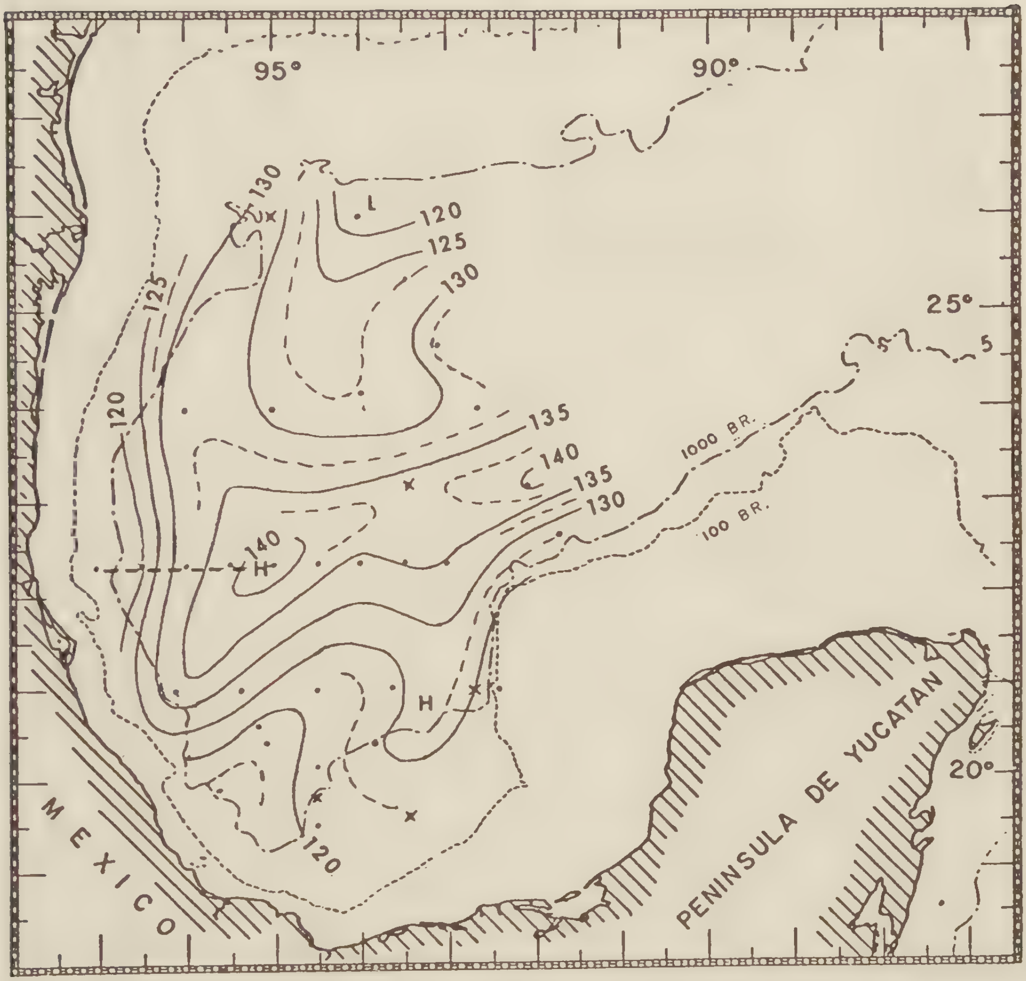
95°
90°
25°
20°
130
120
125
130
125
120
135
140
135
130
140
120
H
L
H
1000 BR.
100 BR.
5
M E X I C O
PENINSULA DE YUCATAN

Fig. 2 Anomalía geopotencial (en centímetros dinámicos) de la superficie del mar relativa a 1 200 decibares, mayo-junio de 1971 (COSMA 71-10). x indica alguna extrapolación. Volumen de transporte geostrófico entre las estaciones conectadas con una línea descontinua (- - -) ha sido determinado

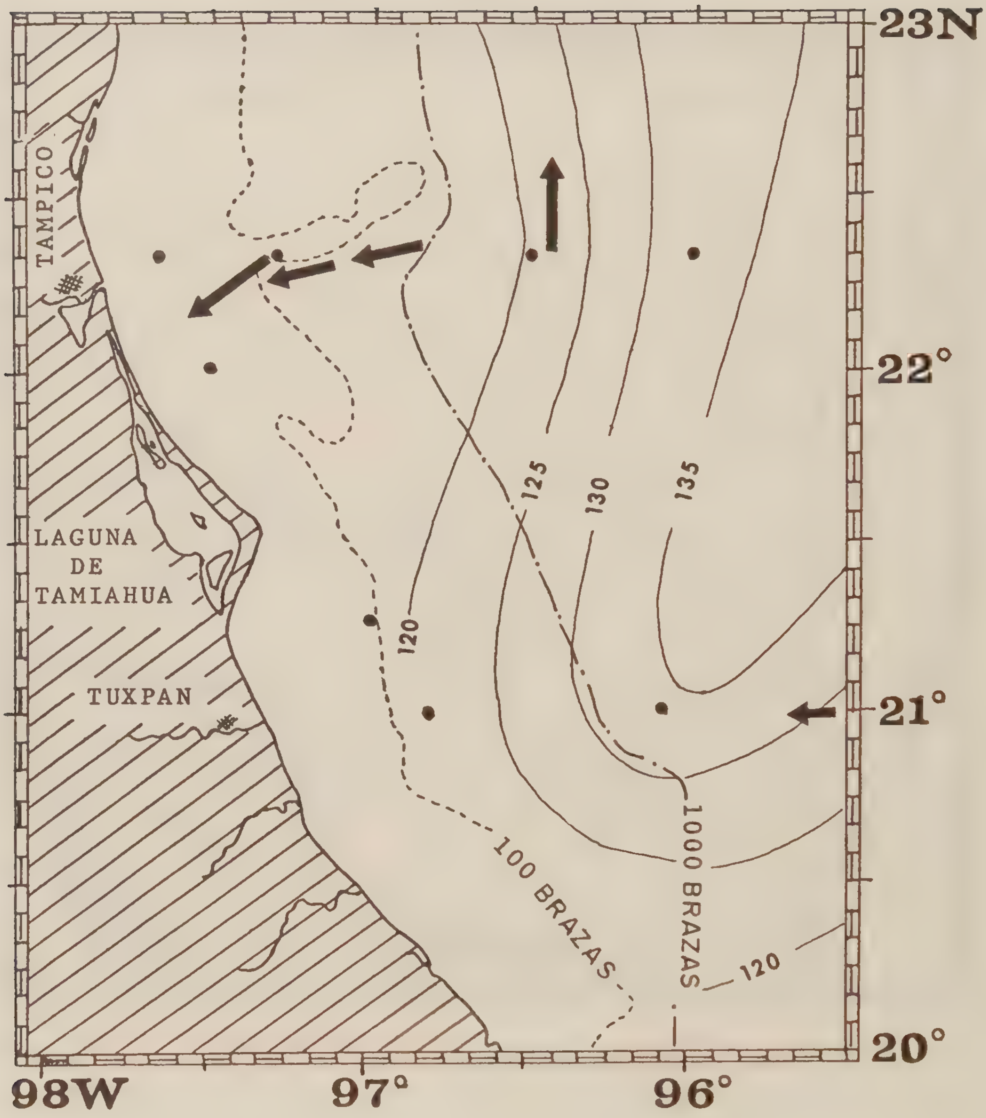
23N
22°
21°
20°
98W
97°
96°
TAMPICO
LAGUNA
DE
TAMIAHUA
TUXPAN
125
130
135
120
120
100 BRAZAS
1000 BRAZAS

Fig. 3 Proximidades de la Laguna de Tamiahua. Anomalía geopotencial (en centímetros dinámicos) de la superficie del mar relativa a 1 200 decibares. Las flechas significan el vector resultante de las mediciones GEK, mayo-junio 1971 (COSMA 71-10)

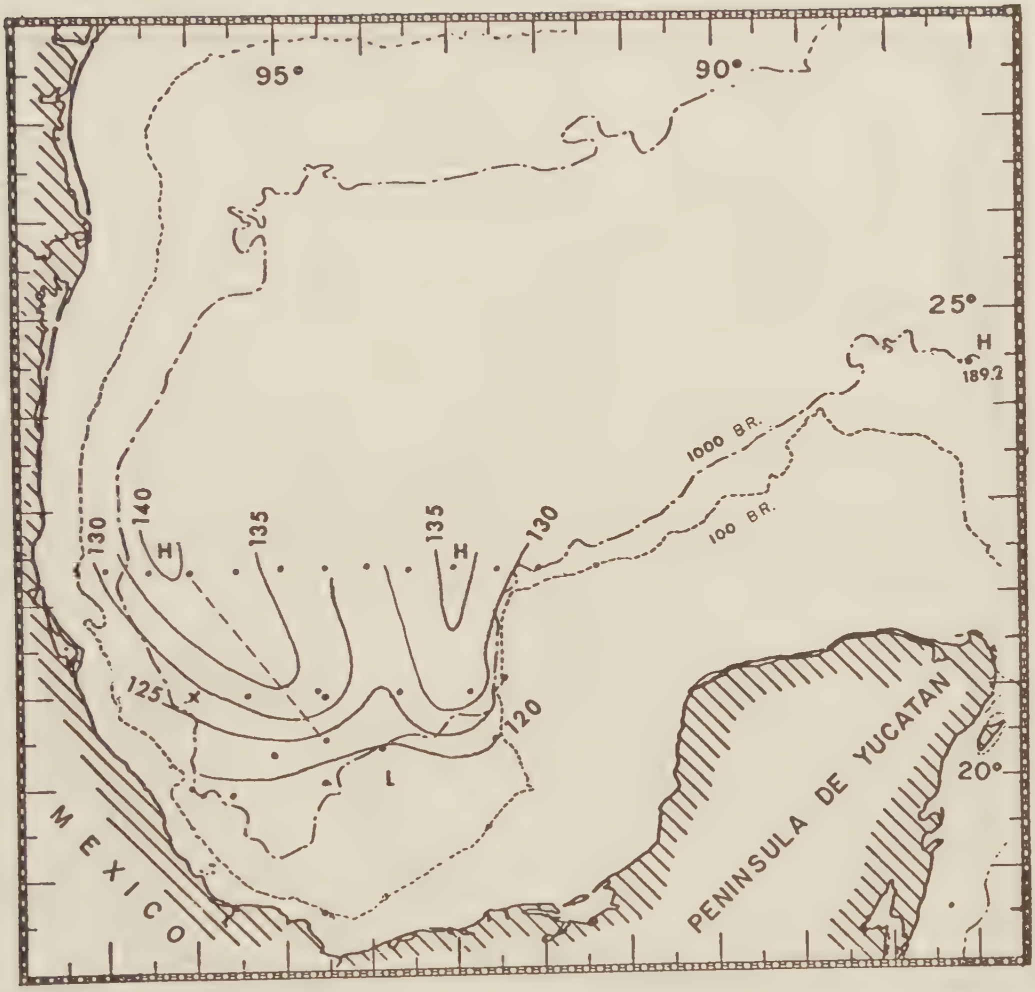
95°
90°
25°
H
189.2
1000 BR.
100 BR.
130
140
H
135
135
H
130
125
x
120
L
20°
MEXICO
PENINSULA DE YUCATAN

Fig. 4 Anomalía geopotencial (en centímetros dinámicos) de la superficie del mar relativa a 1 200 decibares, agosto de 1971 (COSMA 71-16). x indica alguna extrapolación. Volumen de transporte geostrófico entre las estaciones conectadas con una línea descontinua (- - -) ha sido determinado

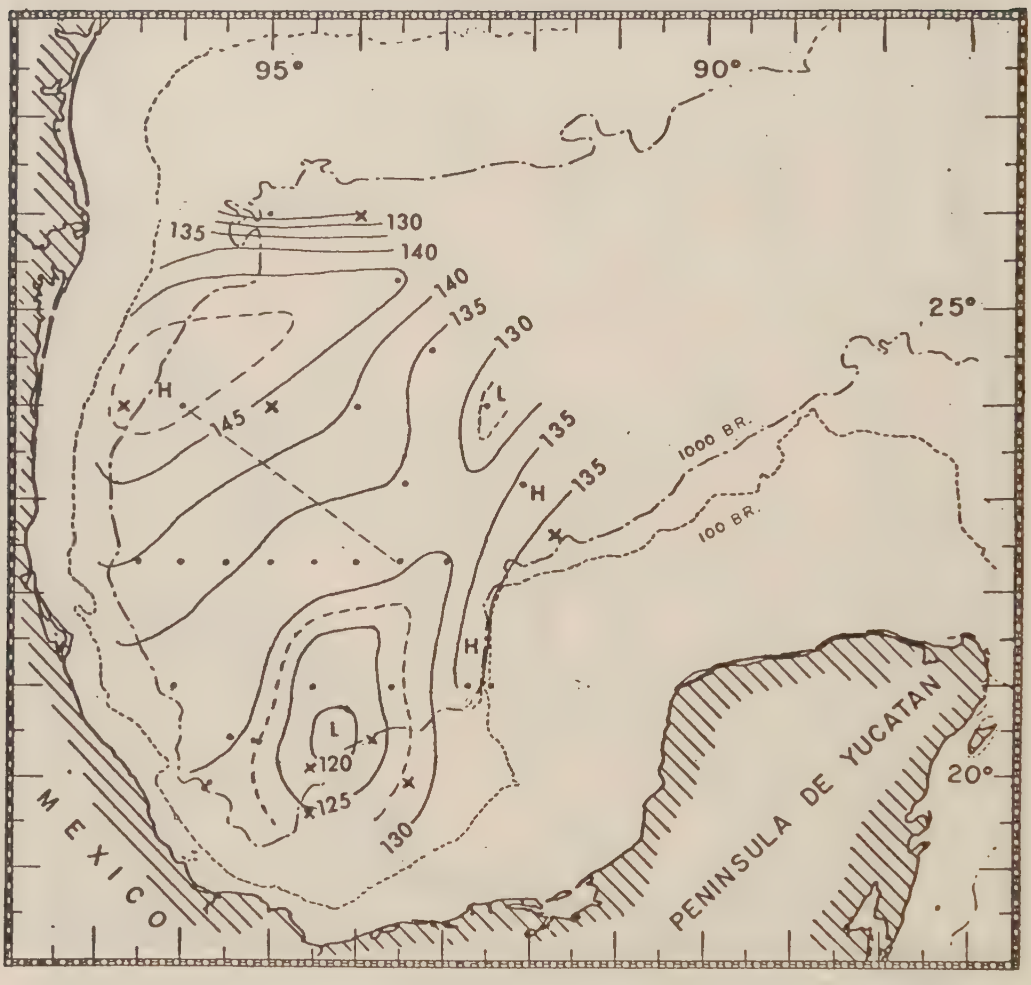
95°
90°
25°
20°
130
135
140
140
135
130
145
H
L
135
135
H
1000 BR.
100 BR.
H
L
120
125
130
MEXICO
PENINSULA DE YUCATAN

Fig. 5 Anomalía geopotencial (en centímetros dinámicos) de la superficie del mar relativa a 1 200 decibares, noviembre de 1971 (COSMA 71-22). x indica alguna extrapolación. Volumen de transporte geostrófico entre las estaciones conectadas con una línea descontinua (- - -) ha sido determinado

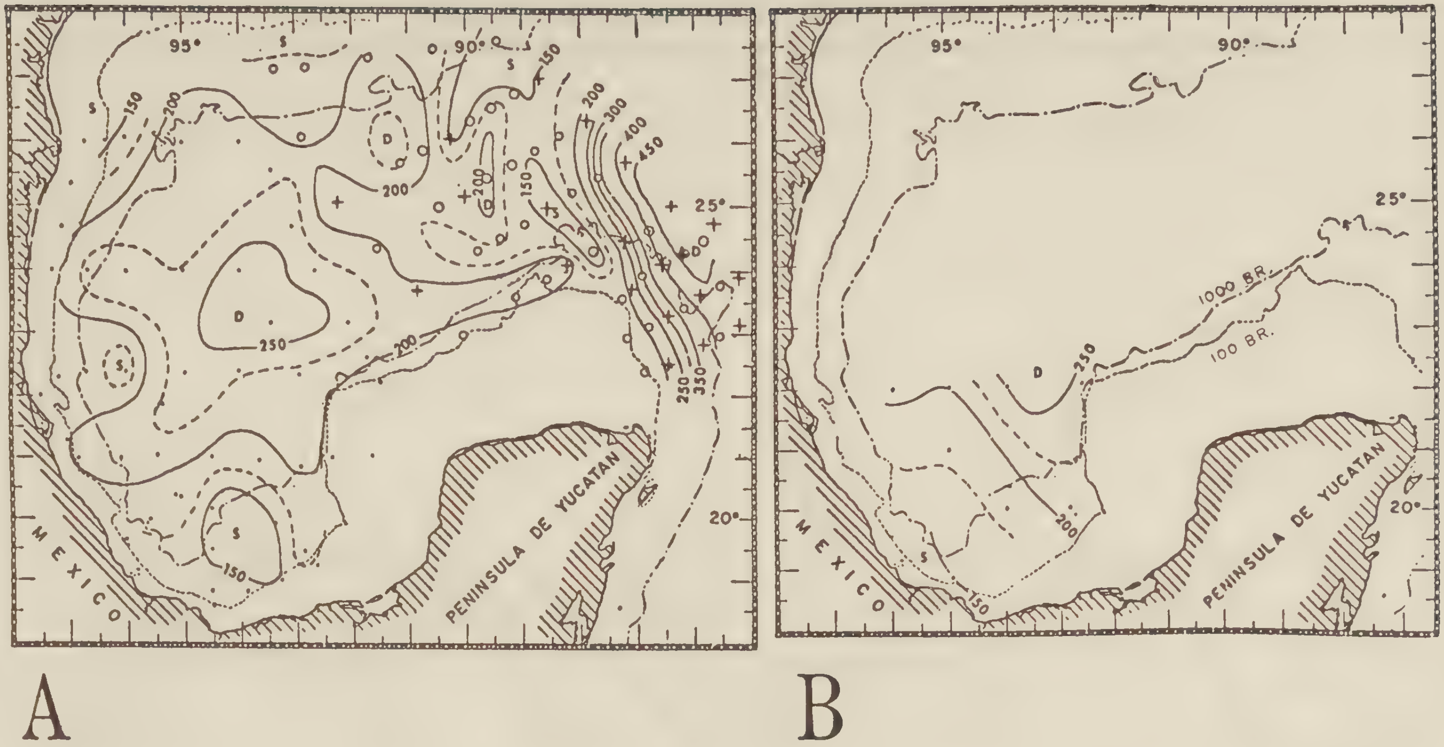
A
95°
90°
25°
20°
S
D
150
200
250
300
350
400
450
MEXICO
PENINSULA DE YUCATAN
B
95°
90°
25°
20°
1000 BR.
100 BR.
D
250
200
150
S
MEXICO
PENINSULA DE YUCATAN

Fig. 6 Topografía (en metros) de la superficie isotérmica de 15°C: A, octubre-noviembre de 1970 (COSMA 70-12) y 70-A-14; (+) indica cala de botellas Nansen y (o) indica un STD tomado por el B/O ALAMINOS (21 de octubre al 3 de noviembre 1970) y (•) indica cala de botellas Nansen tomadas por el URIBE (31 de octubre al 13 de noviembre de 1970). B, enero de 1971 (COSMA 71-02)

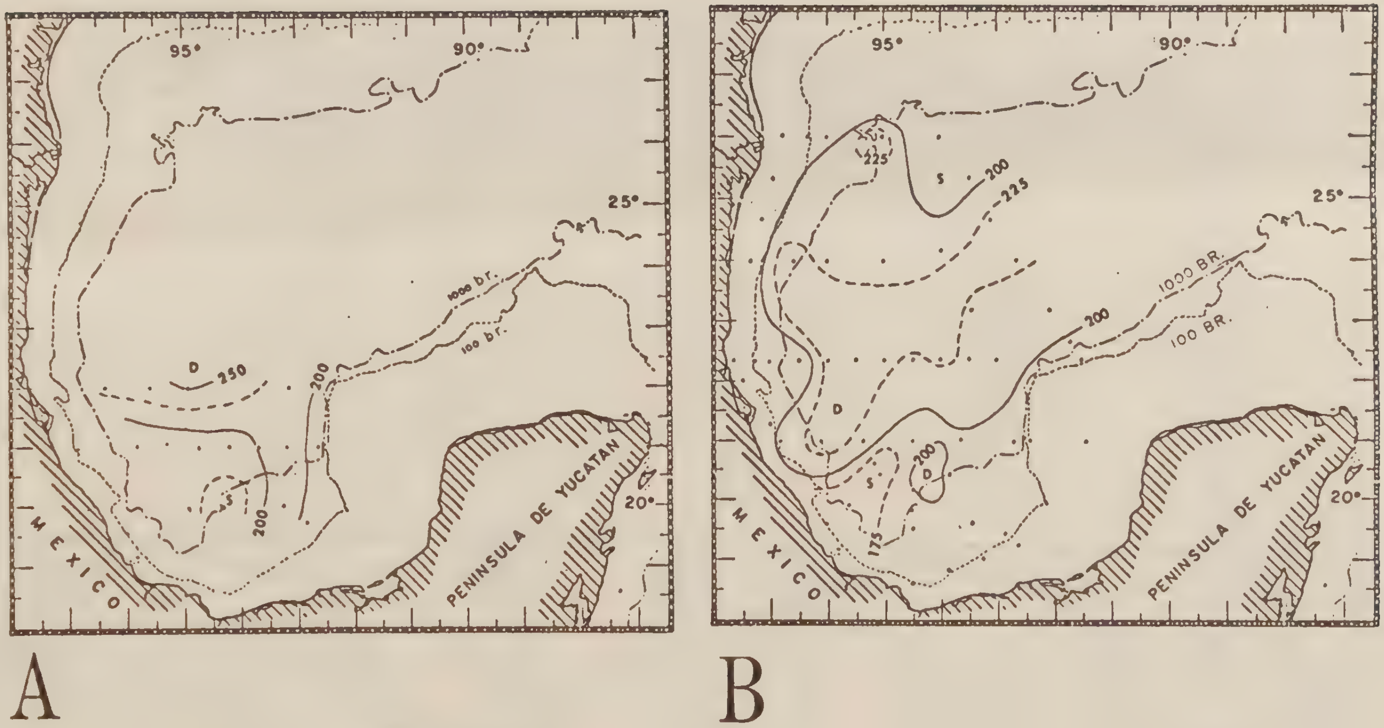
95°
90°
25°
20°
MEXICO
PENINSULA DE YUCATAN
1000 br.
100 br.
D
250
200
S
200
A
95°
90°
25°
20°
S
200
225
225
200
1000 BR.
100 BR.
D
200
D
S
175
MEXICO
PENINSULA DE YUCATAN
B

Fig. 7 Topografía (en metros) de la superficie isótermica de 15ºC:
A, abril-mayo 1971 (COSMA 71-08)
B, mayo-junio 1971 (COSMA 71-10)

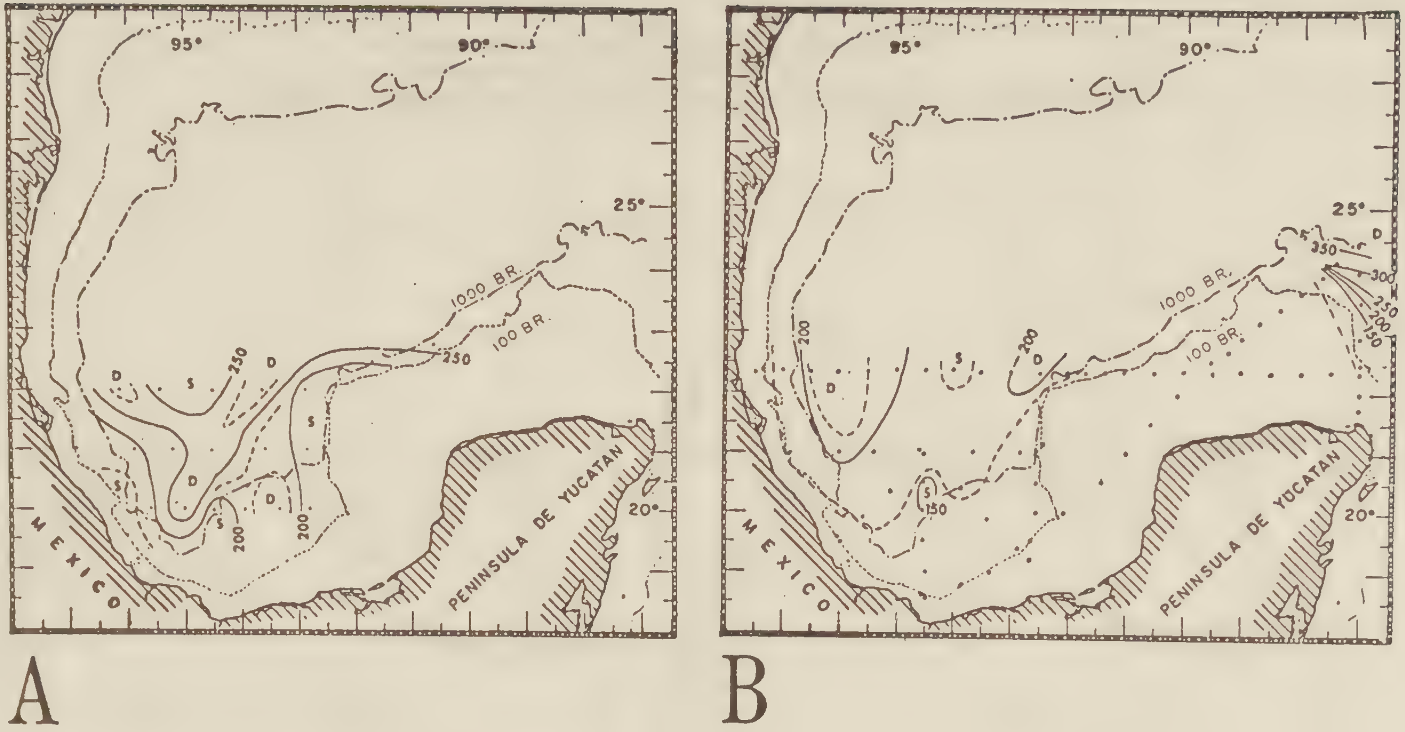
A
95°
90°
25°
20°
1000 BR.
100 BR.
250
200
D
S
MEXICO
PENINSULA DE YUCATAN
B
95°
90°
25°
20°
1000 BR.
100 BR.
350
300
250
200
150
D
S
MEXICO
PENINSULA DE YUCATAN

Fig. 8 Topografía (en metros) de la superficie isotérmica de 15°C:
A, julio de 1971 (COSMA 71-14)
B, agosto de 1971 (COSMA 71-16)

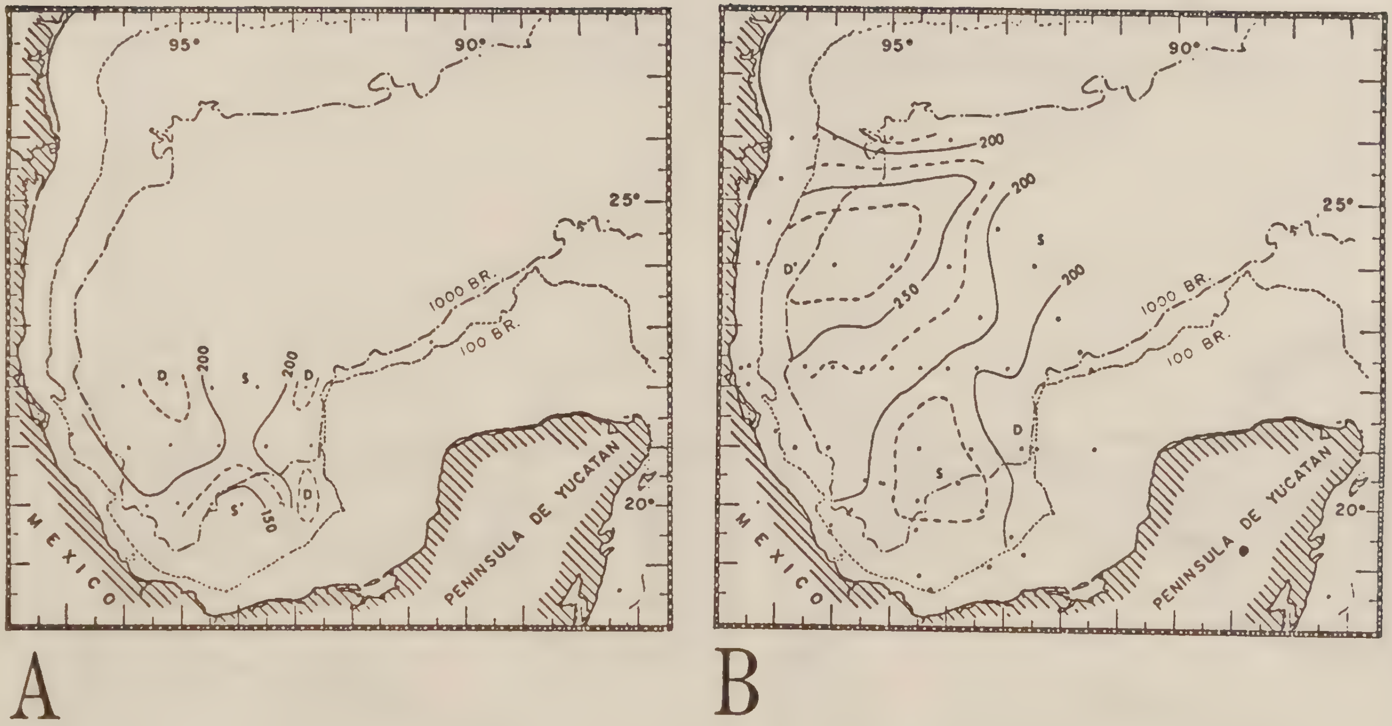
95°
90°
25°
20°
1000 BR.
100 BR.
200
150
250
D
S
MEXICO
PENINSULA DE YUCATAN
A
B

Fig. 9 Topografía (en metros) de la superficie isotérmica de 15°C:
A, octubre de 1971 (COSMA 71-20)
B, noviembre de 1971 (COSMA 71-22)

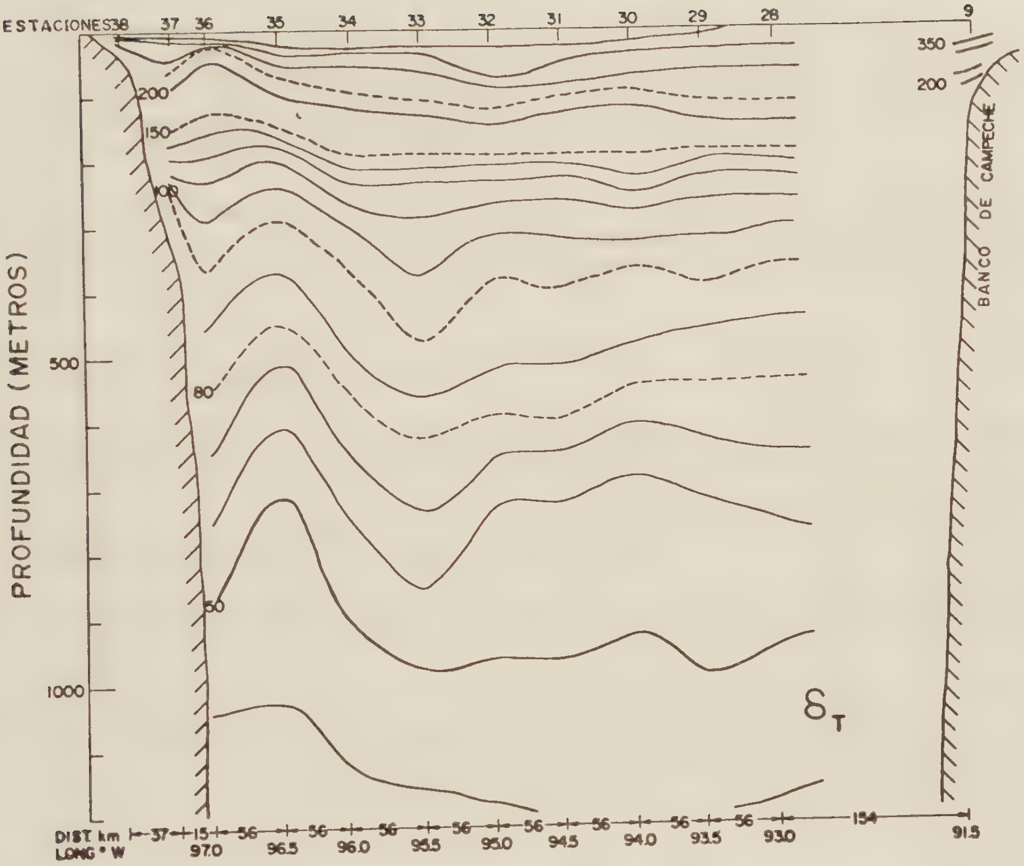

Fig. 10 Volumen específico (en centilitros por tonelada). Transecto a través del remolino anticiclónico en mayo-junio de 1971 (COSMA 71-10). Exageración vertical 500:1

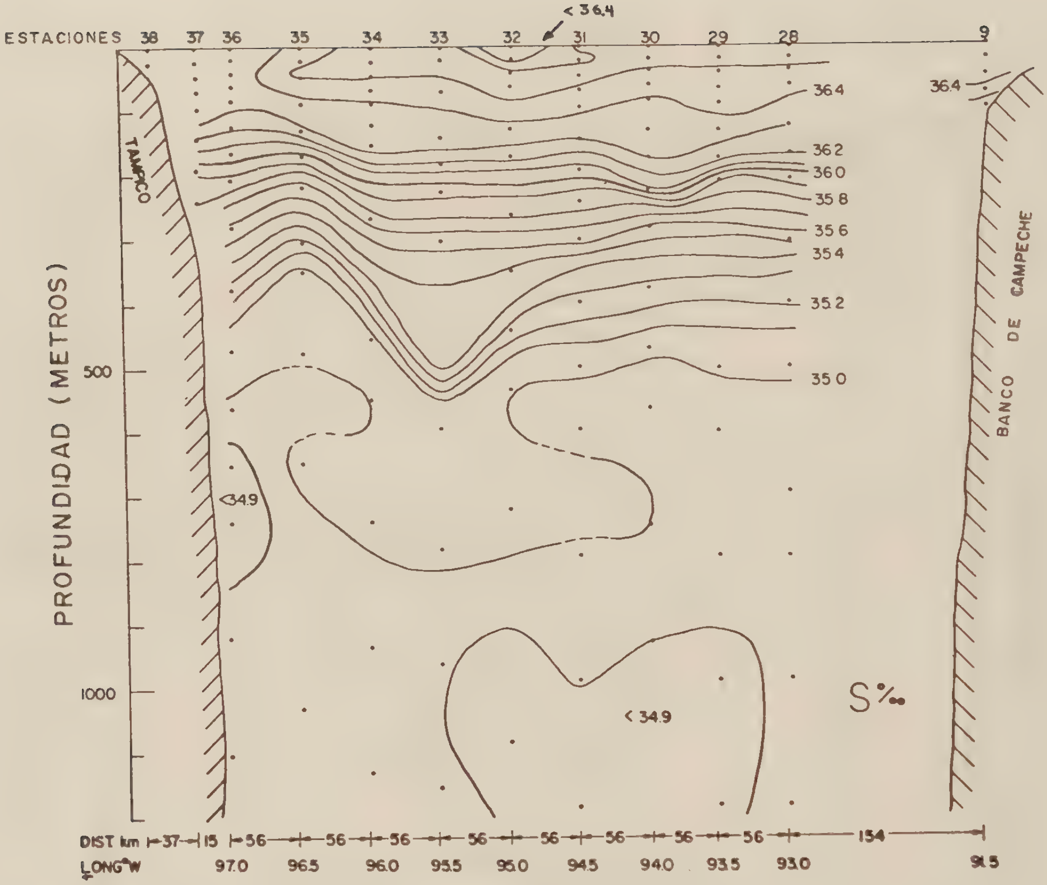

Fig. 11 Salinidad (partes por mil). Transecto a través del remolino anticiclónico en mayo-junio 1971 (COSMA 71-10). Exageración vertical 500:1

REFERENCIAS

Bravo, C.J.L., Observaciones de las corrientes mediante el electrocinetógrafo geomagnético
1972 "GEK". Tesis Profesional, Universidad Nacional Autónoma de México, 112 p.

Granados G., J.L., J.M. Robles P. y E.E. Villanueva U., Informe de datos oceanográficos del
1972a crucero VU/71-02. Reporte de ciencias marinas, no. 2 (NP). México, D.F., Dirección General de Oceanografía y Señalamiento Marítimo, Departamento de Ciencias Marinas, Sub-Secretaría de Pesca, Instituto Nacional de Pesca, 48 p.

__________, Informe de datos oceanográficos del crucero VU/71-08. Reporte de ciencias
1972b marinas, no. 4 (NP). México, D.F., Dirección General de Oceanografía y Señalamiento Marítimo, Departamento de Ciencias Marinas, Sub-Secretaría de Pesca, Instituto Nacional de Pesca, 95 p.

__________, Informe de datos oceanográficos del crucero VU/71-14. Reporte de ciencias
1972c marinas, no. 7 (NP). México, D.F., Dirección General de Oceanografía y Señalamiento Marítimo, Departamento de Ciencias Marinas, Sub-Secretaría de Pesca, Instituto Nacional de Pesca, 81 p.

__________, Informe de datos oceanográficos del crucero VU/71-20. Reporte de ciencias
1972d marinas, no. 4 (NP). México, D.F., Dirección General de Oceanografía y Señalamiento Marítimo, Departamento de Ciencias Marinas, Sub-Secretaría de Pesca, Instituto Nacional de Pesca, 84 p.

Nowlin, W.D., Jr. and H.J. McLellan, A characterization of the Gulf of Mexico waters in
1967 winter. J.Mar.Res., 25(1):29-59

Oceanografía y Señalamiento Marítimo, Reporte de cruceros de 1970. México, Dirección
1971 General de Faros e Hidrografía, Secretaría de Marina, 30 p.

__________, Reporte de cruceros de 1971. México, Dirección General de Oceanografía y
1972 Señalamiento Marítimo, Secretaría de Marina, 74 p.

U.S. Naval Oceanographic Office, Atlas of Pilot Charts: Central American waters and South
1955 Atlantic Ocean. Washington, D.C., U.S. Government Printing Office, 8 p.

Whitaker, R.E., Seasonal variations of steric and recorded sea level of the Gulf of Mexico.
1971 M.S. Thesis, Texas A & M University, College Station, 110 p.

PHYSICAL OCEANOGRAPHY IN THE WATERS OFF SURINAM AND FRENCH GUIANA DURING 1970-1971

by

M.P. VISSER
Royal Netherlands Meteorological Institute
De Bilt, Netherlands

CONTENTS

1. INTRODUCTION
2. THE WATER COLUMN
3. BOTTOM WATER AND NORTH ATLANTIC DEEP WATER
4. SUBANTARCTIC INTERMEDIATE WATER
5. SUBTROPICAL INTERMEDIATE WATER
6. SURFACE WATER
7. REFERENCES

Abstract

Observations on ocean dynamics, hydrographic properties and transparency of the surface water were carried out during autumn 1970 and spring 1971 off the Surinam coast to about 10°North (research ship LUYMES and during autumn 1970 in adjacent Brazilian waters (research ship ALMIRANTE SALDANHA).

Subtropical Intermediate Water, characterized by a strong salinity maximum, is found to occur at depths between tens and hundreds of metres. The core of Sub Antarctic Intermediate Water is found to have its axis between 700 and 850 m, North Atlantic deep water between 1 500 and 2 500 m and bottom water below 2 500 m.

In the cold water sphere,especially the Sub Antarctic Intermediate Water, characterized between the boundaries σ_t = 27.3 - 27.4 is found to be in a large scale "turbulent" motion along the continental slope, the dimensions of eddies being of the order of 100 km. In an Oxygen-Salinity diagram the North Atlantic deep water can be distinguished in an upper and middle water mass, gradually changing into bottom water. This bottom water is found to stick close to the representation of Wüst in the O-S diagram.

In the warm water sphere the Sub-Tropical Intermediate Water is found to move in two separate gyres. One of them off the coast of Surinam and French Guiana, the other off Brazil. The waters of these two are distinguished from each other by their temperature-oxygen relation, according to work by Metcalf and Stalcup.

In the surface water seasonal influences are found in the salinity distribution resulting from northeastern and southeastern trades respectively. A very strong current shear is found across the layer between the surface and the halocline. Large-scale movements of this water have been traced by some drift bottle experiments; recoveries of the bottles have only been reported from the Americas. An estimate is made of the fresh water discharge of the Amazon River passing along the coast. There are no indications to support an intermittency of the "fresh water" flow.

Resumen

Durante el otoño de 1970 y la primavera de 1971 se hicieron observaciones acerca de la dinámica oceánica, propiedades hidrográficas y transparencia del agua superficial, frente a la costa de Surinam, hasta 10°N aproximadamente (buque de investigación LUYMES) y durante el otoño de 1970, en las aguas brasileñas adyacentes (buque de investigación ALMIRANTE SALDANHA).

El Agua Subtropical Intermedia, caracterizada por una fuerte salinidad, se encuentra a profundidades entre decenas y centenas de metros y su eje del Agua Subtropical Intermedia se halla entre los 700 y los 850 m; el del Agua Profunda del Atlántico Norte, entre los 1 500 y los 2 500 m, y el del Agua del Fondo, por debajo de los 2 500 m.

La capa fría, especialmente el Agua Subantártica Intermedia, caracterizada entre los límites $\sigma_t = 27{,}3 - 27{,}4$, se halla en un estado de movimiento "turbulento" en gran escala a lo largo del talud continental, y la dimensión de los remolinos es de 100 km aproximadamente. En un diagrama Oxígeno-Salinidad, en el Agua Profunda del Atlántico Norte puede distinguirse una masa superior y otra media, que se convierte gradualmente en Agua de Fondo. Este Agua de Fondo se encuentra muy cerca de la representación de Wüst en el diagrama O-S.

En la capa caliente se ha observado que el Agua Subtropical Intermedia se desplaza en dos giros separados; uno frente a la costa de Surinam y la Guayana Francesa, y otro frente a la costa del Brasil. Las aguas de estos dos giros se distinguen por su relación temperatura-oxígeno, según el trabajo de Metcalf y Stalcup.

En lo que respecta a la salinidad, el agua superficial sufre las influencias estacionales de los alisios del nordeste y del sudeste, respectivamente. A través de la capa, entre la superficie y la haloclina hay un gradiente muy fuerte de corrientes. Se han seguido los movimientos en gran escala de esta agua haciendo mediante algunos experimentos con botellas flotantes, que han sido recuperadas en las Américas. Se hace una estimación de la descarga de agua dulce de el Río Amazonas que fluye a lo largo de la costa. No hay indicios que apoyen una intermitencia del flujo de "agua dulce".

1. INTRODUCTION

The goal of our physical oceanographic investigations in the "adjacent regions" of CICAR was in the first place to get some more insight into the movement of less saline water along the coast of South America, the current pattern, its dependency on season and the influence of rivers. By different methods and using different tracers (salinity, drift bottles) the surface waters were surveyed during a couple of weeks, in both spring and in autumn. In the meantime, information was collected on the movements of the "Sub-tropical Intermediate Water", closely connected with the surface water mass, and both belonging to the "warm water sphere".

Investigations of the deeper water masses of the so-called "cold water sphere" were mainly set up to support the chemical research in these waters. However, during the processing of the data it was found to be of more than marginal interest from the physical point of view.

Time and area of the investigations were autumn 1970 and spring 1971, off the Surinam coast to about 10° North (research ship LUYMES, Fig.1). Also we have to thank the Brazilian Navy for making additional observations in the waters bordering Brazil on the basis of the arrangements in the CICAR framework (research ship ALMIRANTE SALDANHA).

2. THE WATER COLUMN

The column of water from surface to bottom is composed of the following water masses (Fig. 2):

1. surface water under influence of the run-off of the continent, sun's radiation and the atmosphere, with salinities between 36 and 30 °/oo, even 21 °/oo occasionally. and at its lower boundary, at depths of between 50 and 100 m bounded by a very shallow halocline, not at the same depth as the thermocline;

2. the saline Sub-tropical Intermediate Water from the northern or southern sub-tropics, with its axis at depths of between 80 and 200 m or greater;

3. the cold Sub-Antarctic Intermediate Water has its axis at depths of between 700 and 850 m. It will be found off the continental shelf; North Atlantic deep water is found at the next lower stage with some higher salinity; gradually changing into bottom water with lower salinity and low temperature.

In the sections which follow we shall give some attention to all mentioned water types, from bottom to surface.

3. BOTTOM WATER AND NORTH ATLANTIC DEEP WATER

It was proven that the bottom water being characterized by the potential temperature $\theta < 5^{\circ}C$ for the relevant dozen of deep stations, shows a θ , S diagram that closely resembles the characteristics found by Wüst (1964). Also according to the method of Wüst (1933), the amount of Antarctic Water in the Bottom Water turns out to be 35% at a distance of about 45 m from the bottom, where he gives 32-40%. However, using silicate as a tracer these percentages become higher. This will be illustrated by van Bennekom in his lecture.

It is interesting that in looking at the relation between salinity and oxygen content we get a continuous and smooth picture for both the Bottom Water and the overlaying North Atlantic Deep Water (Fig.3). The characteristics of this picture also make it possible to distinguish the Upper North Atlantic Deep Water (salinity maximum, the so-called Mediterranean Water) and the Middle North Atlantic Deep Water (oxygen maximum); the latter gradually changing into the Bottom Water with lower oxygen content and lower salinity than the North Atlantic Deep Water masses. (The original names have been used here: Upper, Middle and Lower North Atlantic Deep Water, of which the latter one is not of interest here).

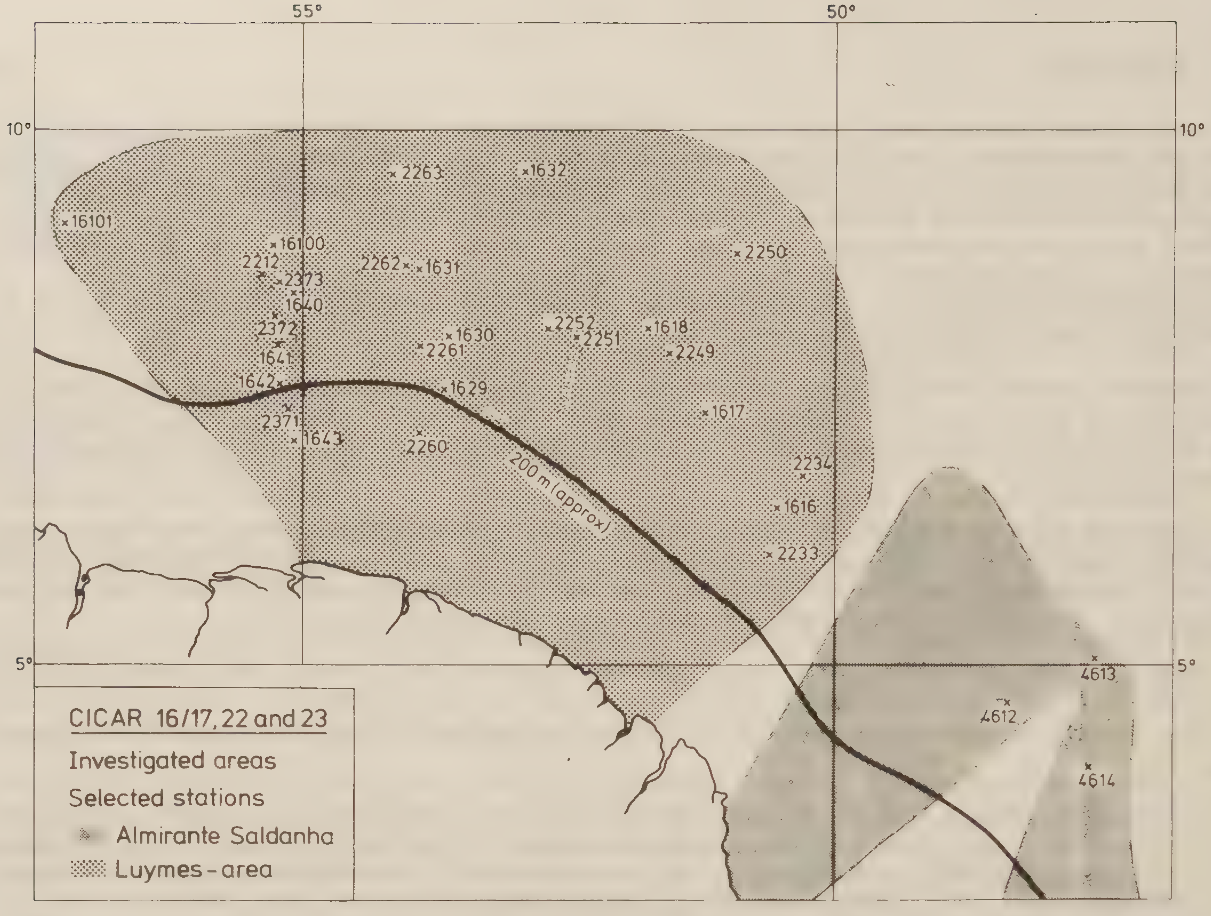
55°
50°
10°
10°
5°
5°
2263
1632
16101
16100
2212
2373
1640
2262
1631
2250
2372
1641
1630
2261
2252
2251
1618
2249
1642
1629
2371
1643
2260
1617
200 m (approx)
2234
1616
2233
4613
4612
4614
CICAR 16/17, 22 and 23
Investigated areas
Selected stations
Almirante Saldanha
Luymes-area

Fig. 1 CICAR 16/17, 22 and 23: areas investigated by LUYMES and ALMIRANTE SALDANHA: selected stations

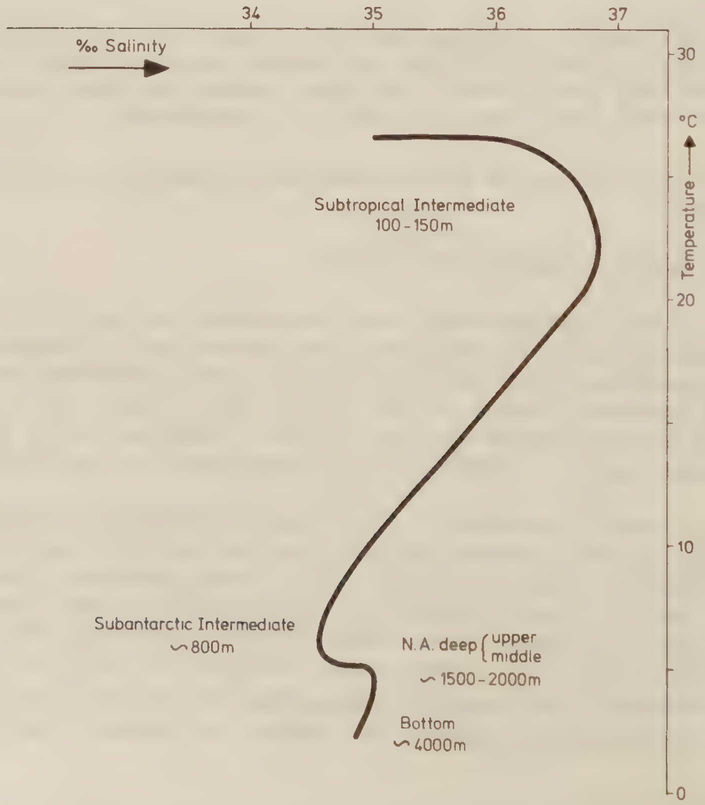

Fig. 2 North Atlantic water masses off Surinam (schematic)

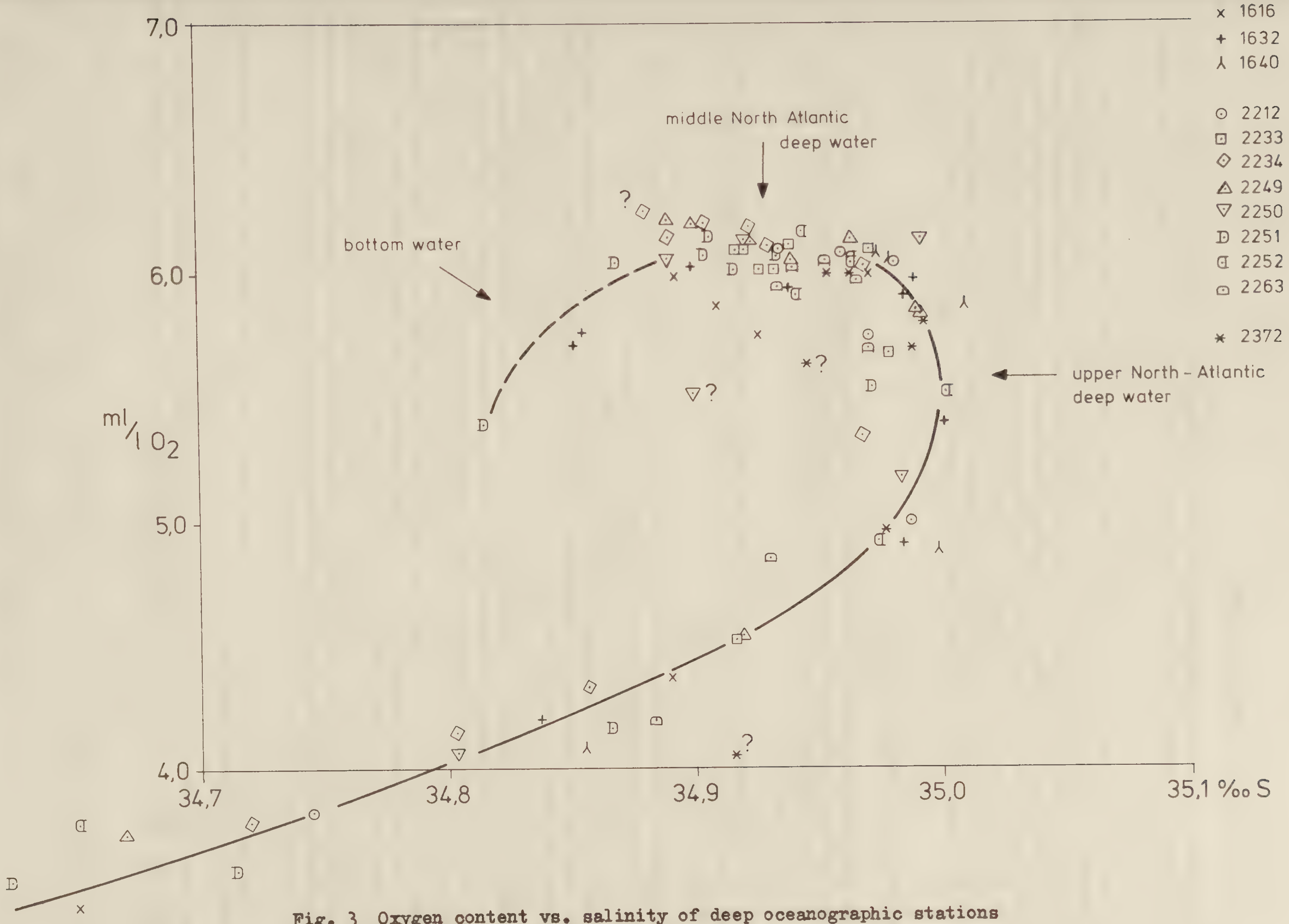

Fig. 3 Oxygen content vs. salinity of deep oceanographic stations during oceanographic stations during LUYMES cruises CICAR 16/17, 22 and 23

4. SUB-ANTARCTIC INTERMEDIATE WATER

The relatively cold water mass with vertical dimensions of several hundreds of metres, having its axis at depths 700-850 m originates at the southerly Sub-Antarctic convergence, at about 50° South.

If we stick to the level $\sigma_t = 27.30$ coinciding roughly with the nucleus of this water, it is extremely striking to see how it is situated in front of the continental slope. Fig. 4 and 5 give an idea of the depth-differences that occur and of inferred current directions connected with these variations. It is clear that a strong, large-scale eddying occurs. Wüst (1935) was already of the opinion that the spreading of the Antarctic Intermediate Water is coupled with bends, and certainly with returns, from the main movement along the South American continental slope, that are suggested here as well. The phenomenon seems to be in good agreement with recent Soviet research as well (Kort *et al.*, 1969, 1972).

5. SUB-TROPICAL INTERMEDIATE WATER

The warm and very saline waters that are found immediately over the Sub-Antarctic and below the surface layer come from sub-tropical regions. From these sources the water is brought to the Caribbean by the Sub-tropical Undercurrent (Wüst, 1964), which gives Wüst reason to the following:

> "....It is remarkable that by the deep-reaching gradient force of the Guyana Current, Sub-tropical high salinity water masses are also transported from the southern hemisphere to our concerned areas....".

This remark is based on earlier work of Defant, who reached this conclusion on the basis of Meteor observations from 1925 to 1927.

To get an idea of the movements of this water type, the method of isentropic analysis has been used by us, according to Montgomery (1938). We then have to look for one or more surfaces of constant "potential density" σ_θ, to get an insight into the movement of the water. Since the depth of this water mass never is more than a few hundreds of metres, it is allowed to take "density" σ_t instead of σ_θ. In earlier publications Montgomery advised to take $\sigma_t = 25.4$ as a good reference level, and we have done so since it coincides closely with the salinity-maximum. An example for a couple of stations has been shown (Fig. 6 and 7). Analysing the depth of this $\sigma_t = 25.4$ level of both LUYMES and ALMIRANTE SALDANHA data of autumn 1970 gives Fig. 8, showing two gyres (anti-cyclonic), one off the French Guyanian coast and one in a south easterly direction off the Brazilian coast. Note that the "ridge" between these two gyres has a depth (110 m) of only half that of both the "valleys" (180 m and 240 m) (Fig. 9). Inferred water movement is shown in Fig. 8. A very complex situation is created on the "ridge" off Cape Orange. We have the impression that the complex currents of the surface water (which sometimes made exact navigation very difficult during our CICAR cruises) are a direct result of this situation.

During spring 1971 a similar pattern was found, but not so complete as the foregoing, since only one ship was available.

Are both gyres of the same water type? In the case of the temperature-salinity relationship they can hardly be discerned. However, taking the temperature-oxygen relationship, they can (Fig. 10).

Thus, according to Metcalf and Stalcup (1967), it can safely be assumed that the Sub-tropical Intermediate Water of the eastern gyre is of southern origin, and that of the western gyre of northern sub-tropical origin. It is a striking detail that for some stations, i.e., those situated at the deepest point of both "pits" and on the connexion-line between them, this only holds for the waterlayer at about 200 m and deeper (10 ≈ 17°C). Discrimination is not possible for the shallower parts. Another difference between our work and

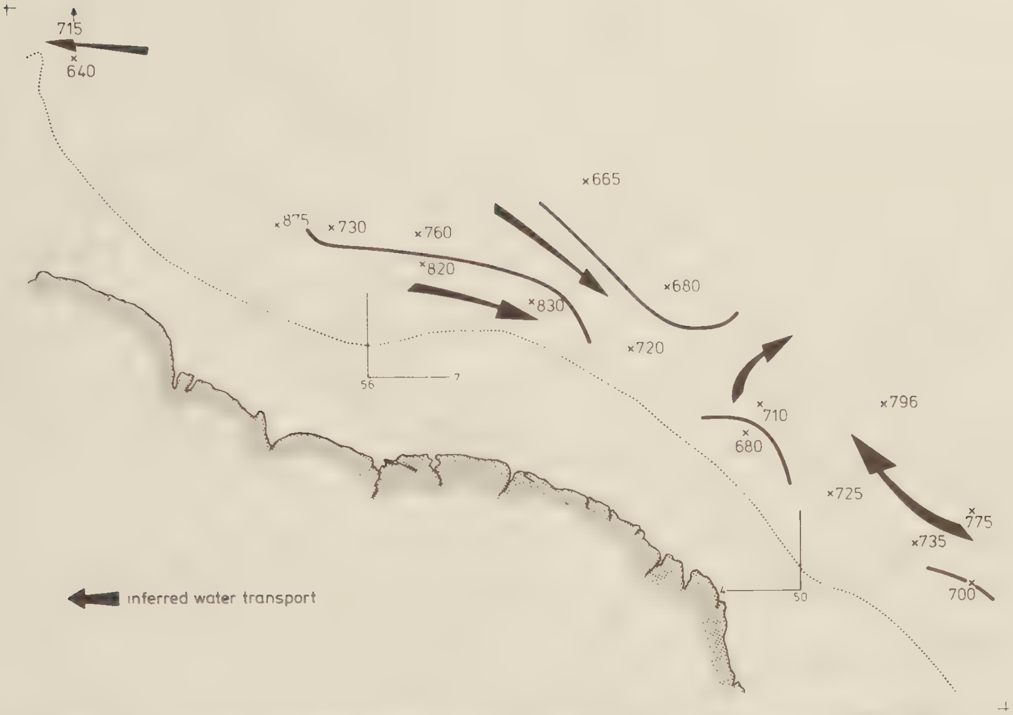
715
640
665
875
730
760
820
830
680
720
56
7
710
680
796
725
775
735
700
50
inferred water transport

Fig. 4 Depth in metres of the surface $\sigma_t = 27.3$, according to soundings by LUYMES, CICAR 16/17 and by ALMIRANTE SALDANHA cruise 46, autumn, 1970

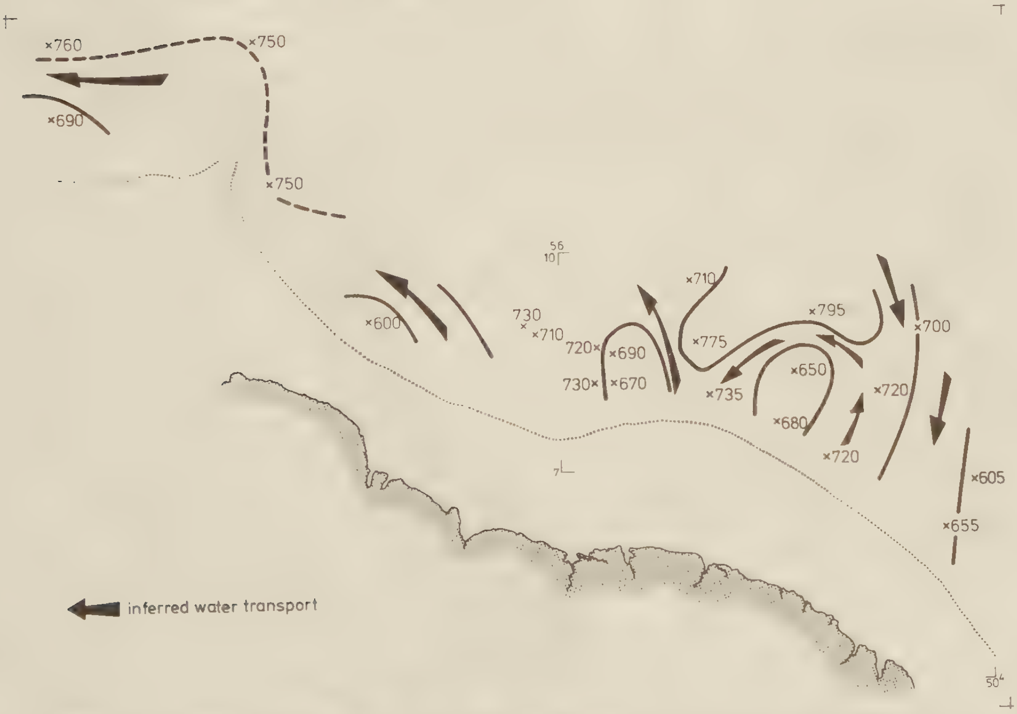
760
750
690
750
56
10
600
730
710
720
690
730
670
710
775
735
795
650
680
720
700
720
605
655
7
50
inferred water transport

Fig. 5 Depth in metres of the surface $\sigma_t = 27.3$, according to soundings by LUYMES, CICAR 22 and 23 spring, 1971

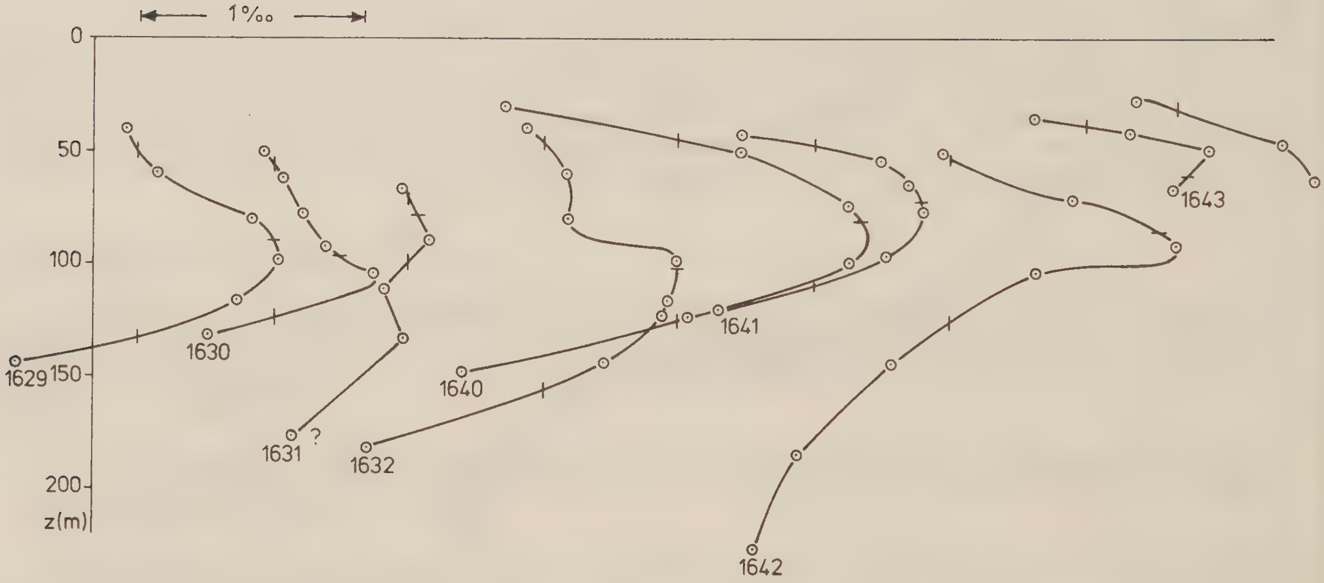

Fig. 6 Detailed salinity-depth relations; : salinity = 36.0, — : σ_t = 25.4

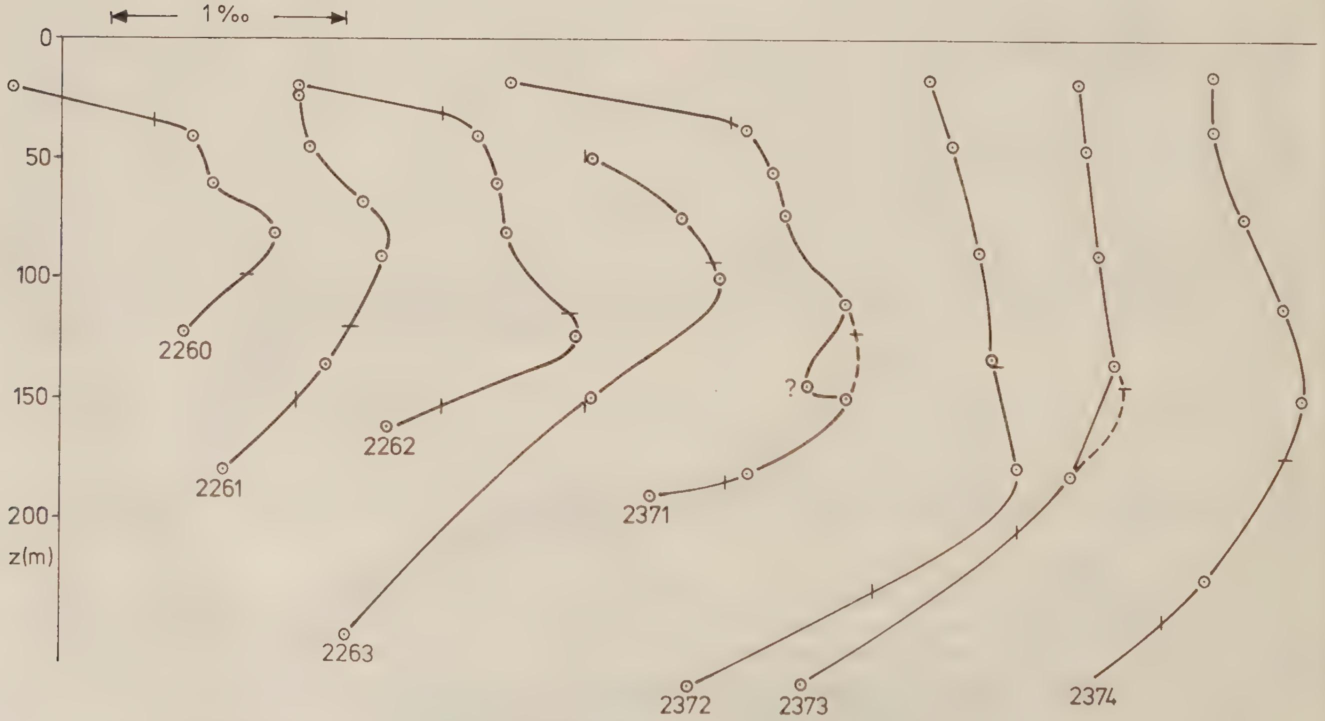

Fig. 7 Detailed salinity-depth relations; : salinity = 36.0, — : σ_t = 25.4

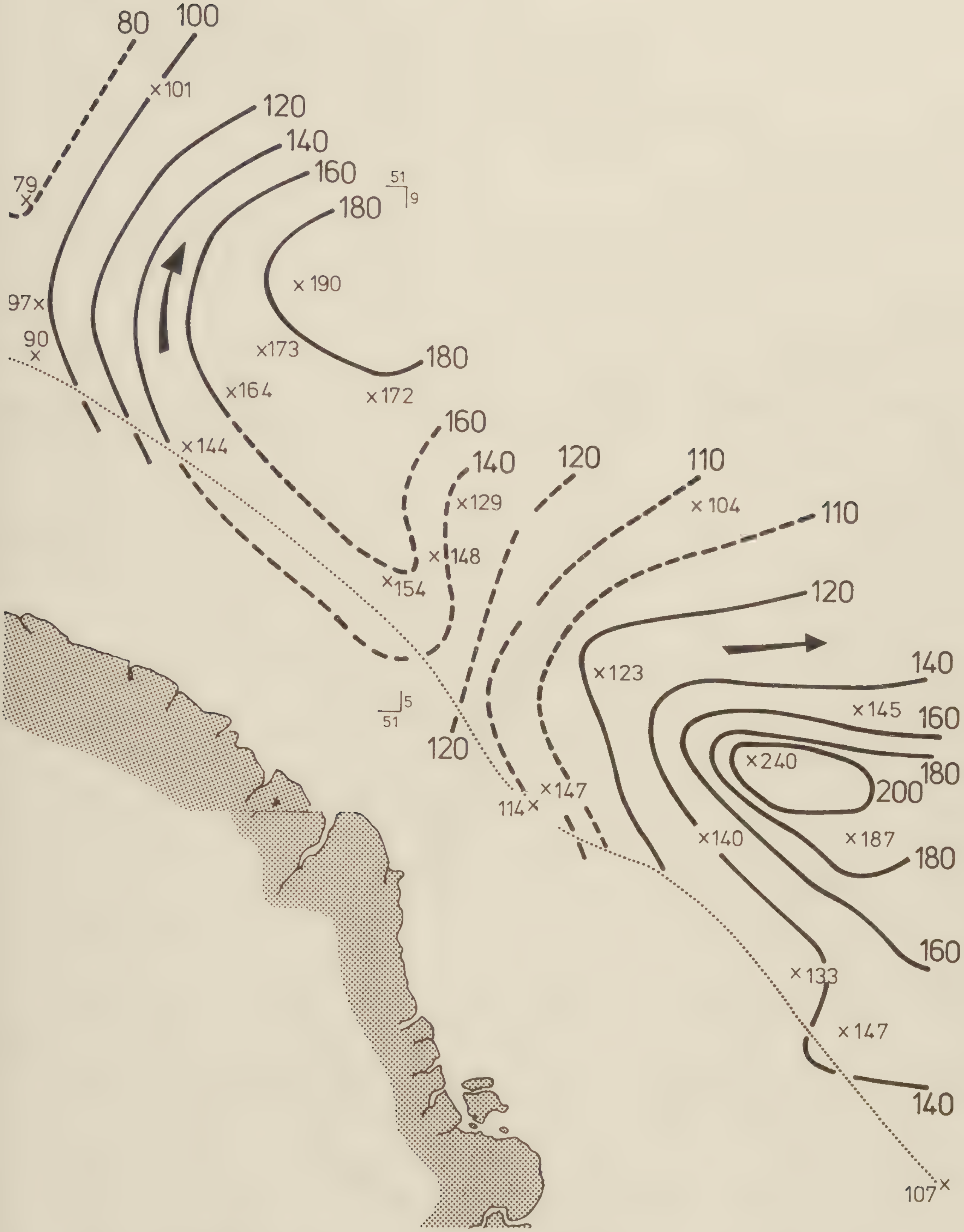
80
100
×101
120
140
160
180
51
9
79
×
×190
97×
90
×
×173
180
×164
×172
×144
160
140
120
110
×129
×104
110
×148
×154
120
×123
140
5
51
×145
160
120
×240
180
200
114×
×147
×140
×187
180
160
×133
×147
140
107×

Fig. 8 LUYMES CICAR 16/17 and ALMIRANTE SALDANHA cruise 46, autumn 1970.
Depth of the σ_t = 25.4 surface

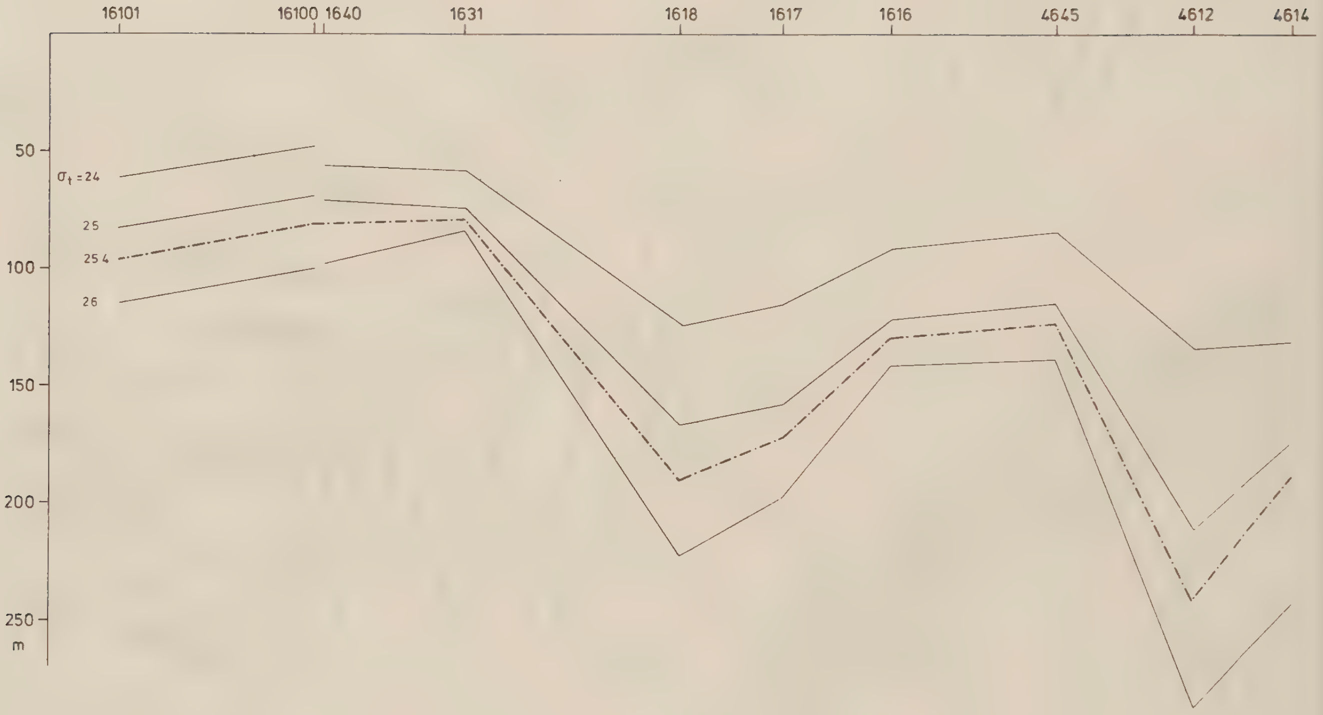

Fig. 9 Position of some σ_t surfaces during autumn 1970 along the coast from 57°W to 48°W

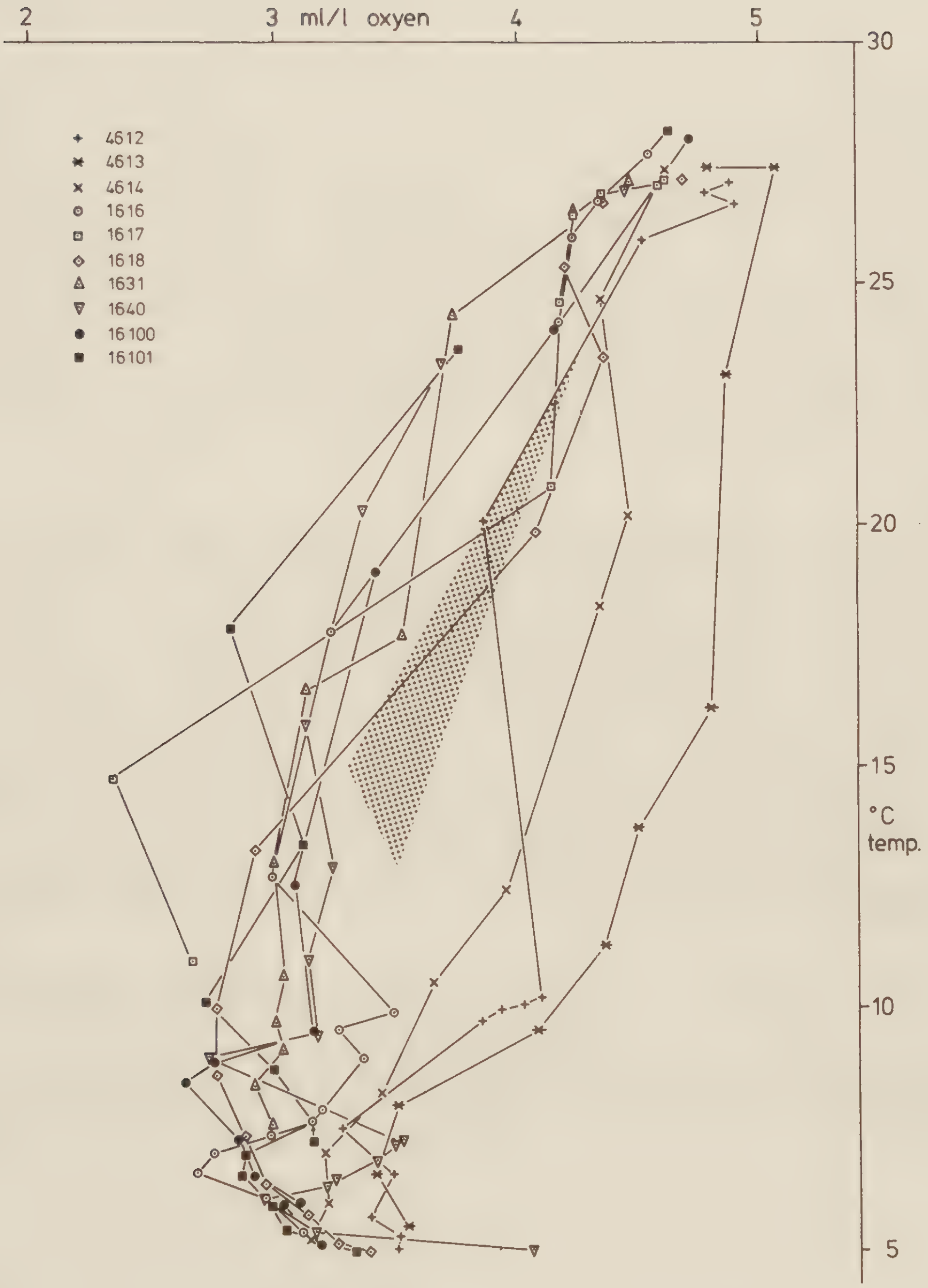

Fig. 10 T–O_2 diagram of the stations given in Fig. 9

that of Metcalf and Stalcup is that in our case the boundary between the gyres is situated a few hundreds of kilometres more to the west than has been the case in their investigations. These facts give partial support to their theory, and partially show the restrictions of it. Otherwise they are indications of the strong variability occurring in this part of the ocean, even perhaps to be considered as large-scale turbulence.

6. SURFACE WATER

The problems of the surface water are mainly the spreading of Amazon water in the ocean, interaction between these water types and the origin of the Equatorial Countercurrent. Many authors already have worked on these problems.

We found very strong variability both in time and in place for the surface salinity, supporting the idea of a large scale turbulent interaction between saline and more diluted waters. However, the main current of less saline waters along the coast seems to be uninterrupted. After a relatively rapid mixing of fresh water with ocean water the mixed water is transported into the Guiana current as a thin layer. As distance from the mouth of the Amazon increases, this layer increases in thickness and in salinity, since more ocean water becomes incorporated in it. The current profiles in this framework are striking: current speed at the surfaces 1.5 m/s or more, and less than 0.5 m/s at 20 m depth, this combined with 36°/oo salinity at 20 m depth diminishing to 20°/oo at the surface. This was observed on a position off Cape Orange near the Guyana-Brazilian Border. To the west, circumstances are less pronounced, as has been proven by some anchor stations at about 30 mi from the coast. (This material is/will be described in more detail in a couple of scientific reports of the Royal Netherlands Meteorological Institute by the authors (in alphabetical order) van Bennekom, Tijssen, van der Veen and Visser.)

7. REFERENCES

Kort, V.G., 1972 New data on the dynamic structure of the western boundary currents in the tropical Atlantic. *Rapp.P.-V.Réun.CIEM*, 162:276-9

Kort, V.G. *et al.*, 1969 New data on the western most boundary currents of the tropical Atlantic. *Dokl.Akad.Nauk.SSSR*, 188:677-80 (in Russian)

Metcalf, W.G. and M.C. Stalcup, 1967 Origin of the Atlantic equatorial undercurrent. *J.Geophys. Res.* 72:4959-75

Montgomery, R.B., 1938 Circulation in upper layers of southern north Atlantic deduced with use of isentropic analysis. *Pap.Phys.Oceanogr.Meteorol.*, 6(2)

Wüst, G., 1933 Schichtung und Zirkulation des Atlantischen Ozeans. *Wiss.Ergeb.Dtsch.Att.Exped. Meteor*, 6(1)

__________, 1935 Die Stratosphare des Atlantischen Ozeans. *Wiss.Ergeb.Dtsch.Att.Exped.Meteor*, 6(1)

__________, 1964 Stratification and circulation in the Antillean-Caribbean basins. Part I. Spreading and mixing of the water types. New York, Columbia University Press, 201 p.

HYDROLOGICAL CONDITIONS IN THE CENTRAL ZONE OF THE VENEZUELAN CARIBBEAN SEA, FEBRUARY 1975

by

D. VOLTOLINA
Fundación La Salle de Ciencias Naturales
Apdo 8150
Caracas, Venezuela

CONTENTS

1. INTRODUCTION
2. MATERIAL AND METHODS
3. RESULTS
4. CONCLUSIONS
5. ACKNOWLEDGEMENTS
6. REFERENCES

Abstract

The data of a 1975 February cruise in the zone limited by 66° and 70° W and between the mainland and the Venezuelan and Netherland's Antilles show that the area is characterized, in this season, by a general phenomenon of upwelling, affecting the whole coastal zone and a great part of the islands which enclose the basin.

Temperature and salinity isopleths show in fact a peculiar distribution, with lower sea surface temperatures distributed along the islands and nearshore. Surface salinity isopleths are almost normal approaching the coastline, changing their trends near to the coast, where they assume the same trend as the isothermal lines. This is due to subsurface waters, with low temperature and high salinity values which, moving westward, as generally described for the upper equatorial waters in the northern hemisphere, surface near to the islands and, as a consequence of their higher density, move southward, entering into the basin. Here they may show a tendency to sink, which is followed by a new upwelling upon arriving near the coast. Deeper waters, pertaining to the tropospheric level, show the same kind of distribution in the basin.

The density distribution maps suggest the presence of some eastward flowing counter currents caused by the vertical movements described above.

The same types of water described for the Caribbean Sea by various authors are readily identified from T-S diagrams. Some differences have been noted between this late-winter situation and the one previously described for another cruise, carried out during August 1974.

Resumen

Los datos tomados en febrero de 1975 durante una expedición oceanográfica a la zona comprendida entre los meridianos 66° y 70° oeste, las Antillas venezolanas y holandesas, y el continente muestran que toda ella se caracteriza, en esta estación, por un fenómeno de afloramiento que afecta a toda la bauda costera y a gran parte de las islas que rodean la cuenca.

Las isopletas de temperatura y salinidad tienen, en efecto, una distribución peculiar, con temperaturas de las aguas superficiales más bajas cerca de la costa y alrededor de las islas. Las isopletas de salinidad son casi normales a la costa, cambiando de sentido cerca de ella, en donde es análogo al de las isotermas.

Esto es debido a las aguas sub-superficiales, de baja temperatura y alta salinidad que, moviendose hacia el oeste, como ocurre, en general, con las aguas superiores ecuatoriales en el hemisferio norte, afloran a la superficie cerca de las islas y, a causa de su mayor densidad, se despl egan hacia el sur, penetrando en la cuenca. Una vez en ella, tienden a sumergirse, y después, cuando llegan cerca de la costa, de nuevo a aflorar.

Fenómenos parecidos se observan tambien en aguas más profundas, troposféricas, al entrar en la cuenca.

Los mapas de distribución de densidad revelan la presencia de algunas contracorrientes, con aguas que se despliegan hacia el este, originadas por los movimientos verticales ya mencionados.

Con diagramas T-S se reconocen facilmente los mismos tipos de aguas descritos por varios autores para el Caribe. Se han apreciado algunas diferencias entre esta situación, al final del invierno, y la descrita anteriormente durante otra expedición realizada el mes de agosto de 1974.

1. INTRODUCTION

Since 1960 the Fundación La Salle de Ciencias Naturales has been actively involved in a multidisciplinary study of the Venezuelan Caribbean Sea in order to evaluate the national fishing resources, the exploitation of which is mostly carried out by artisanal fishermen.

In the governmental plans, this utilization is to be rationally promoted in the limits of an official programme, for which a comprehensive study of the fishing resources and of the limits of the possibilities of their exploitation was warranted.

After a previous twelve years' study of the eastern zone, from the borders of British Guyana up to 66° W longitude, culminated with the publication of the first volume of the "Carta Pesquera de Venezuela" (Hno Ginés et al., 1972), the study continued in the central zone, from 66° to 70° W longitude, limited northerly by 12°30' N latitude, and southerly by the mainland.

In this area, some scientific expeditions were carried out during these years, mainly with geological and geomorphological aims or for exploratory fishing, while the hydrological conditions were studied with three cruises: in October 1973 (Voltolina, 1975), August 1974 (Voltolina, 1976a) and with a third one, the results of which are presented in this paper.

Other observations had been carried out previously in the same area, and made available at the opening CICAR Symposium by Aragno (1971), together with other data from the whole Venezuelan Caribbean Sea, and other data are being collected by means of some regular cruises in the same zone, mainly for hydrochemical and biological purposes.

The present paper deals with the basic hydrological features of the zone, as resulting from the data collected during an oceanographic cruise carried out, onboard the R/V LA SALLE, in the period 15 February - 5 March 1975 (Fig. 1)

For any other bibliographic reference to this zone, which has been studied by other scientists, chiefly utilizing the data collected in 1933-34 and 1954 by the R/V ATLANTIS, and in 1963 by the R/V CRAWFORD, or other data mainly collected by the Instituto Oceanográfico of the Universidad de Oriente, the reader should refer to Okuda et al. (1974), who made a complete revision of all the bibliographic references available for the zone. Because this research was supported by a Governmental agency, all the data, maps, figures, etc., as well as a comprehensive report on the cruise and its results, have been presented to the Sponsor (Voltolina, 1976b), and may not be given here in extenso.

2. MATERIALS AND METHODS

The samples were taken by means of reversing Nansen bottles at the standard depths mentioned in U.S. Navy Hydrographic Office (1952), with some slight modification for the upper levels, already mentioned in Voltolina (1976a).

All the bottles were equipped with two reversing thermometers and, beginning from 100 m down, with an unprotected one, for depth correction.

Salinity and oxygen were measured on board, by an inductively coupled salinometer and by Winkler titration according to Strickland and Parsons (1968). pH was also measured, but only part of the data have been used owing to some faults of the pH meter during the first part of the cruise and these data are not reported here.

The data were corrected, interpolated and tabulated with a Monroe 1860 4/4 desk calculator, and used to draw, by manual interpolation, the maps and sections presented in this paper.1/

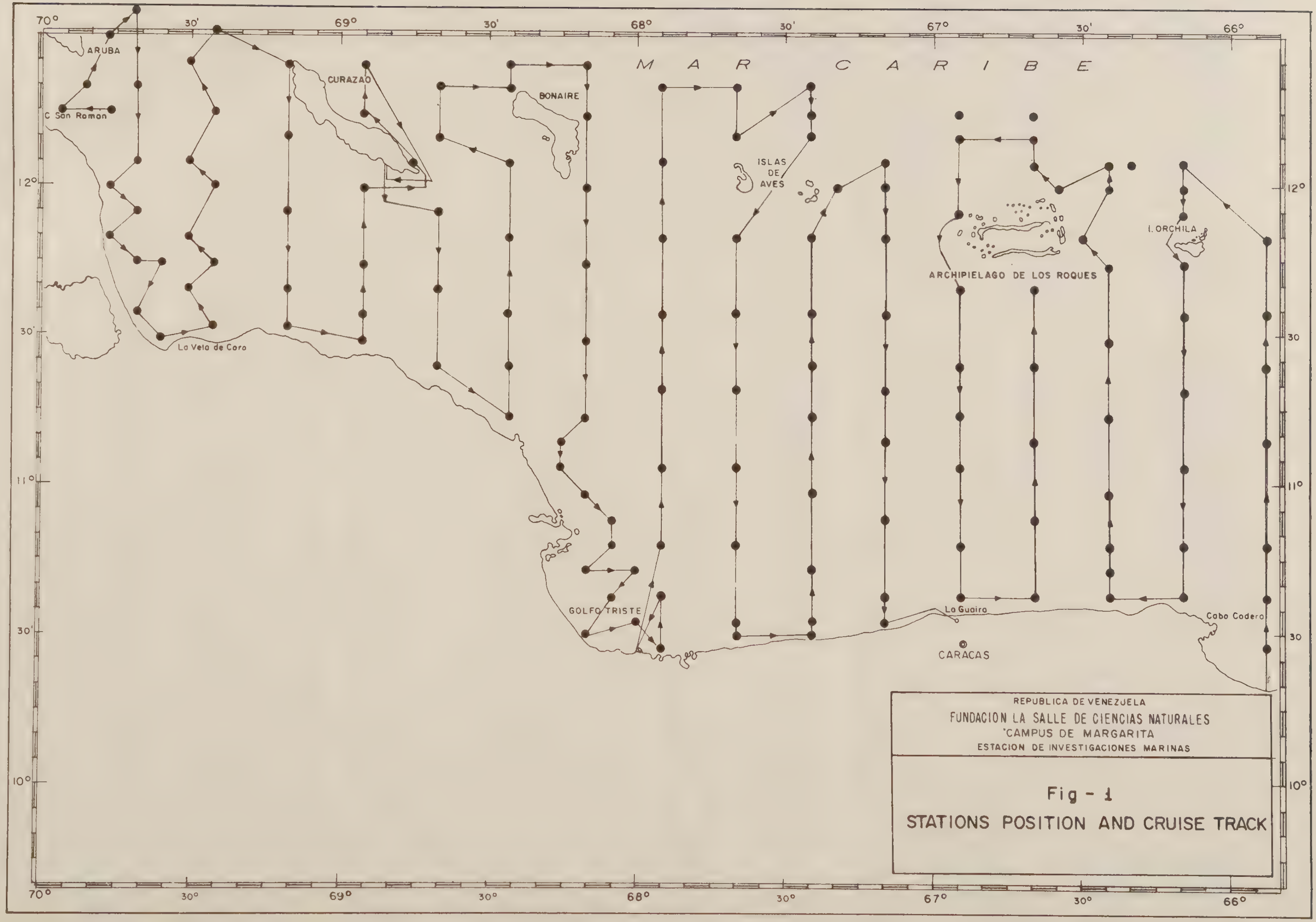
M A R C A R I B E
ARUBA
C San Roman
CURAZAO
BONAIRE
ISLAS DE AVES
ARCHIPIELAGO DE LOS ROQUES
I. ORCHILA
La Vela de Coro
GOLFO TRISTE
La Guaira
CARACAS
Cabo Codera
70°
30'
69°
30'
68°
30'
67°
30'
66°
12°
30'
11°
30'
10°
30
30°

REPUBLICA DE VENEZUELA
FUNDACION LA SALLE DE CIENCIAS NATURALES
"CAMPUS DE MARGARITA
ESTACION DE INVESTIGACIONES MARINAS

Fig - 1
STATIONS POSITION AND CRUISE TRACK

3. RESULTS

3.1 Temperature

If compared to the data of the previous expeditions (Voltolina, 1975, 1976a), the surface temperature was lower during this period, in the limits of the minimum values mentioned in Wüst (1964), for the whole Caribbean Sea and in U.S. Department of Commerce (1975), for the zone and the seasonal period investigated by ourselves. Its geographic distribution at 5 m depth is shown in Fig. 2a. In this it may be noted that almost the entire coastal zone is characterized by low temperature values. This, according to all the data on this area, demonstrates the presence of a phenomenon of upwelling, which is much more evident in the eastern part. In fact the lower temperatures are limited to a narrow coastal zone in the central and eastern part, where values of 23°-24°C may be found, whereas the greatest part of the basin is distinguished by waters of 25.5°C or higher. In the western part coastal temperatures are higher than the ones mentioned for central and eastern coastal waters, which demonstrates that the phenomenon does not have the same intensity throughout the whole area.

The northerly chain of islands, which closes the basin, complicates the distribution of the isotherms. It is still evident that this northern area also exhibits a phenomenon of upwelling, immediately followed by sinking when the waters enter the basin.

A small coastal zone of the area named Golfo Triste, is somehow an exception to this general phenomenon, showing temperatures higher than the average. There is evidence that the upwelling here is limited by approximately the 100 m isobath, and that the waters of the inner part of the Gulf are thus isolated from the general circulation in the zone.

This situation, complicated in proximity of the islands, continues approximately unchanged until the depth of 100 m (Fig. 2b). At this depth the lower temperatures are separated from the coast in the eastern part by a narrow zone of warmer waters which is caused by a change in the trend of the isotherms. The isotherms tend upward approaching the coast in the upper levels, while at this depth they tend downward when reaching the stations closest to the coastline, as appears in Fig. 3.

Apart from this difference, probably caused by the piling up of the waters of lower temperature and higher density near the coast, the 100 m horizon is not too different, in its general meaning, from the one of 5 m presented in Fig. 2a.

In the central part of the basin, south of Las Aves Islands, a large sinking phenomenon is easily recognizable from the high temperature values of a peleciform area which tends south-eastward, almost merging to a small area located southwest of the Los Roques Archipelago.

Through a series of gradual changes which could be better appreciated in the series of vertical sections presented elsewhere (Voltolina, 1976), the thermal situation evolves from the one described before to the deeper ones.

Already at 200 m, the low values of temperature present near the islands demonstrate the presence of another phenomenon of upwelling which affects waters deeper than the ones surfacing near the coast. It is in fact evident, from Fig. 3, that at approximately this depth the upwelling of intermediate or deep waters begins. The bottom topography causes the waters to reach the upper levels and enter the basin. Once in the basin they sink again and return to approximately their original depth.

The geographic distribution of temperature in all the following layers continues almost identically. In general, low temperatures are to be found near the islands, alternating with zones of warmer waters. The coastal zone exhibits low temperatures, while the central part of the basin is characterized by relatively warmer waters.

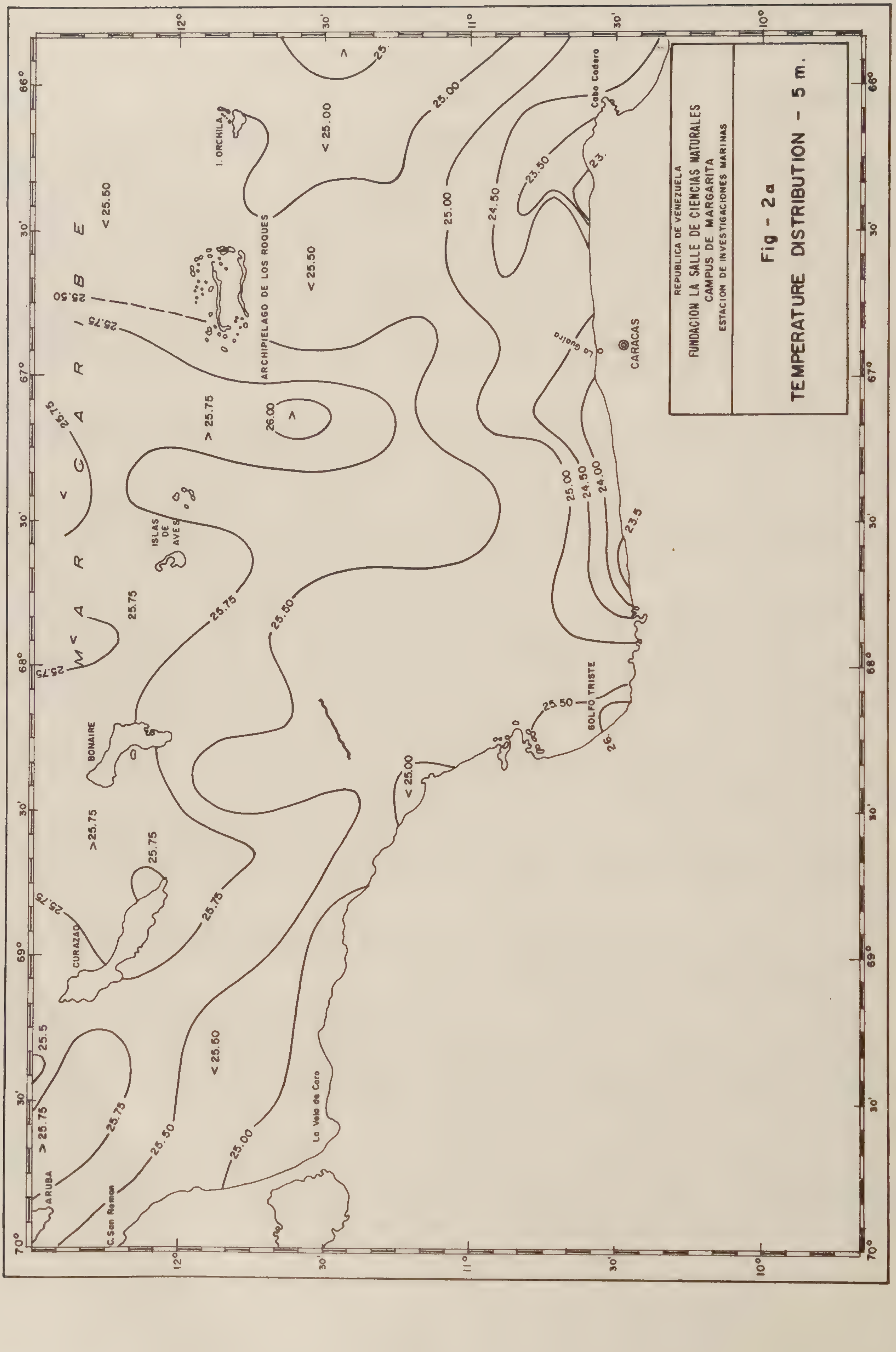
REPUBLICA DE VENEZUELA
FUNDACION LA SALLE DE CIENCIAS NATURALES
CAMPUS DE MARGARITA
ESTACION DE INVESTIGACIONES MARINAS
MAR CARIBE
ARUBA
CURAZAO
BONAIRE
ISLAS DE AVES
ARCHIPIELAGO DE LOS ROQUES
I. ORCHILA
C. San Roman
La Vela de Coro
GOLFO TRISTE
La Guaira
CARACAS
Cabo Codera
70°
69°
68°
67°
66°
30'
12°
11°
10°
25.00
25.50
25.75
26.00
24.50
24.00
23.50
23.5
23.
25.5
26.
25.
< 25.00
< 25.50
> 25.75
< 25.75

Fig - 2a

TEMPERATURE DISTRIBUTION - 5 m.

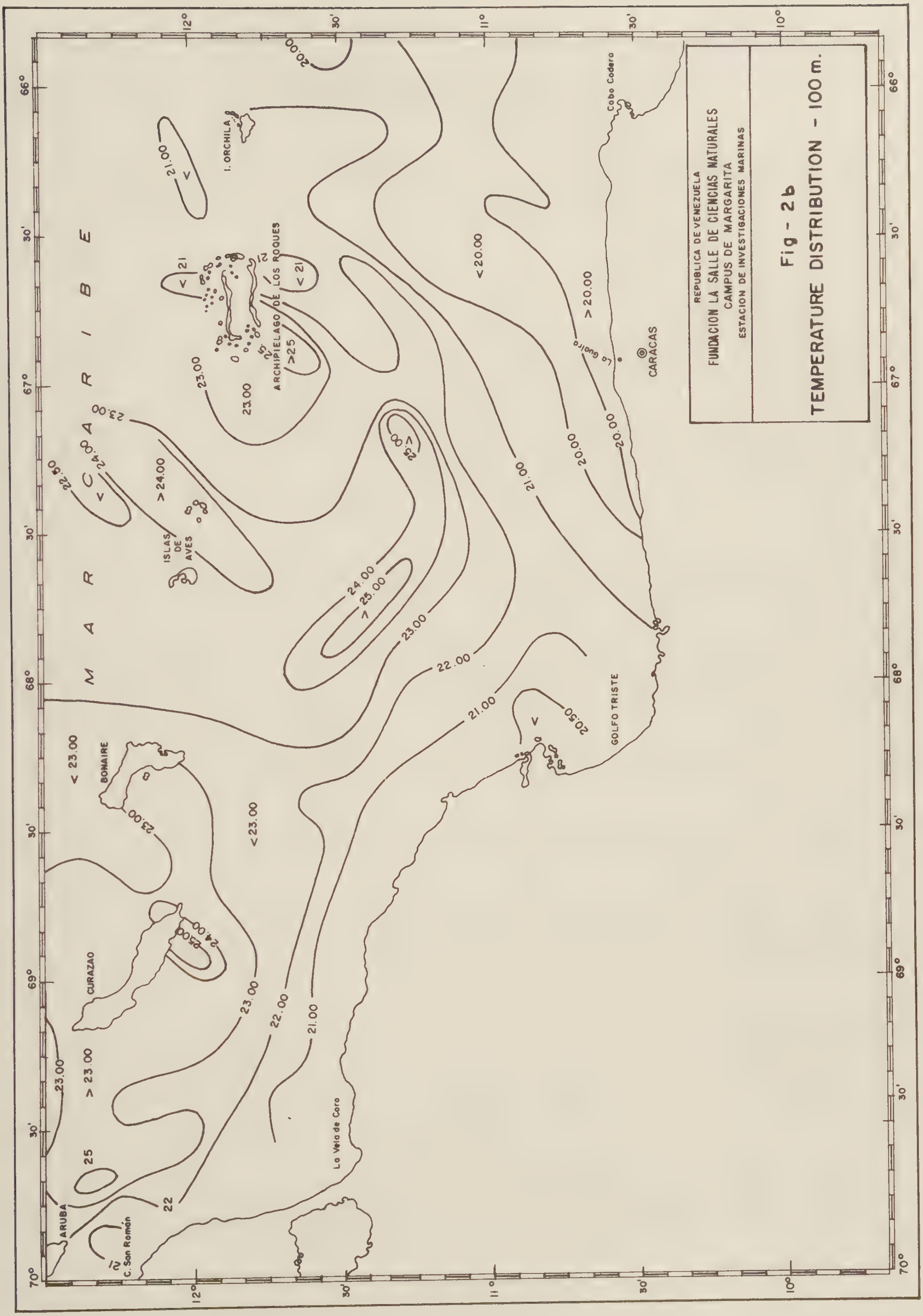
M A R C A R I B E
ARUBA
C. San Román
CURAZAO
BONAIRE
ISLAS DE AVES
ARCHIPIELAGO DE LOS ROQUES
I. ORCHILA
La Vela de Coro
GOLFO TRISTE
La Guaira
CARACAS
Cabo Codera
70°
69°
68°
67°
66°
30'
12°
11°
10°
25
22
23.00
> 23.00
22.00
21.00
25.00
24.00
< 23.00
23.00
> 24.00
22.50
< 24.00
> 25.00
24.00
< 25
23.00
> 25
< 21
< 21
21.00
20.00
< 20.00
> 20.00
20.50
22.00
21.00

REPUBLICA DE VENEZUELA
FUNDACION LA SALLE DE CIENCIAS NATURALES
CAMPUS DE MARGARITA
ESTACION DE INVESTIGACIONES MARINAS

Fig - 2b
TEMPERATURE DISTRIBUTION - 100 m.

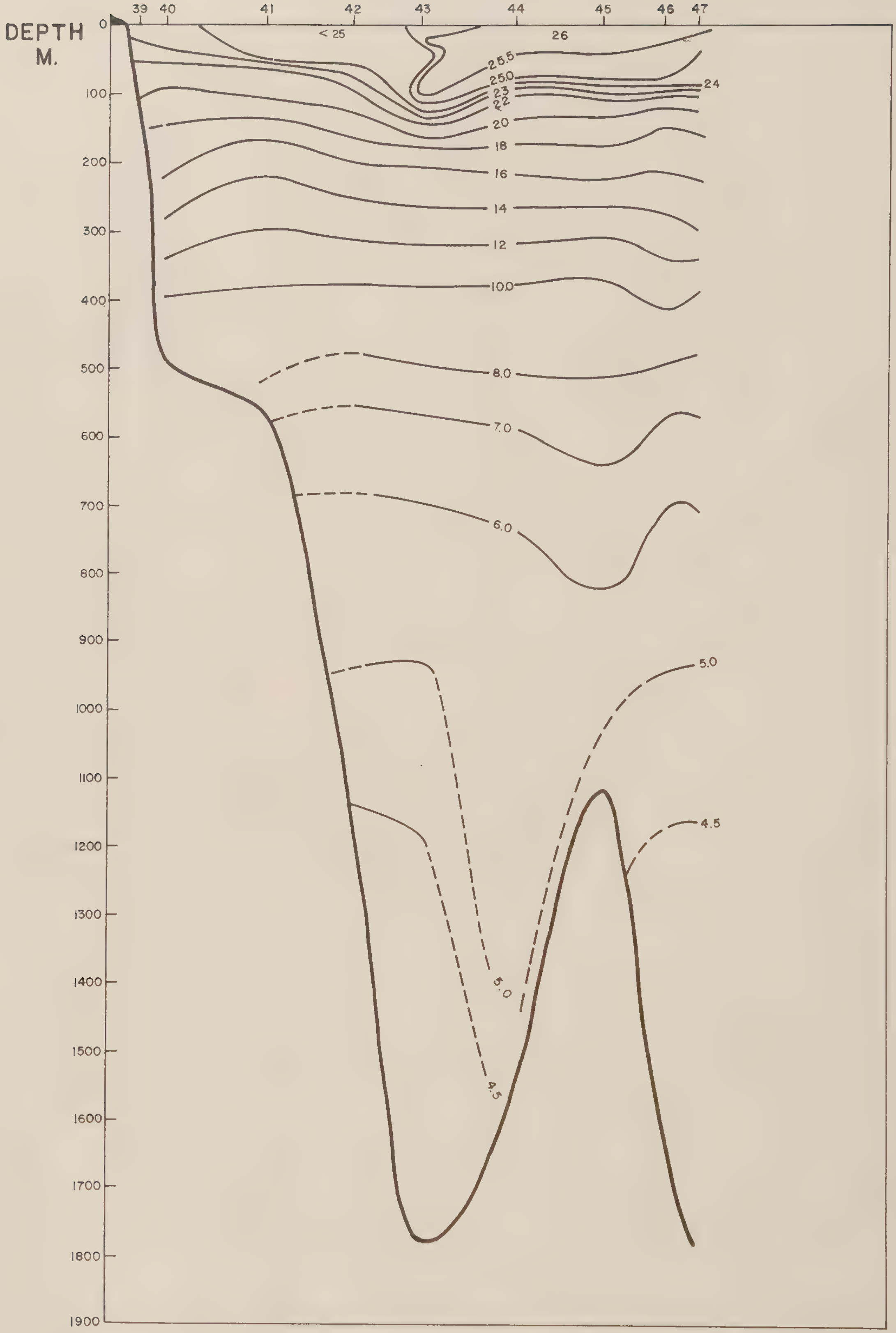

Fig. 3 Vertical temperature distribution along transect 6

This shows that in almost the entire area a sequence of upwelling and sinking is present, which is easily recognizable in Fig. 3, by the trend of the isothermal lines, and which is also evident from the distribution of the other hydrological parameters, as seen in the following sections.

Also, some thermic inversion has been noted; one inversion is represented in Fig. 3. These phenomena are generally due to the northward movement of the coastal surface waters, caused by wind stress (Fukuoka, 1963) or to local cooling of surface waters, as discussed in Voltolina (1976).

3.2 Salinity

Salinity distribution at the depth of 5 m is shown in the upper part of Fig. 4.

From this, a general correspondence to temperature distribution at the same depth appears evident. As a matter of fact, salinity values increase more or less regularly in the western and central parts of the basin, going from the northern to the southern stations. This is due to the subtropical underwaters surfacing near the coast, a subsurface layer of high salinity, whose values are higher in this zone than those mentioned by many authors who have been working in the Caribbean, as Parr (1937), Wüst (1964) and many others. As a matter of fact, the average salinity mentioned in the literature for this layer is about 36.85 percent; while our data indicate salinities ranging from 37.0 to 37.3 percent, which are confirmed in U.S. Department of Commerce (1975).

This difference becomes even more striking in the eastern part, south of the Los Roques Archipelago. Here we found a 20 mile wide belt with salinities ranging from 37.3 to 37.4 percent which extended from the above mentioned Archipelago, down to the coast.

Also, practically the entire eastern zone shows a very peculiar distribution of isohalines, which are normal to the coastline. This partially coincides with the trend demonstrated by some isothermal lines at the same depth and in the same zone, which also show a tendency to run normal to the coast in their northern portion and to then change their trend when approaching the coastline.

The same kind of geographical distribution described for the central and western zones, continues to a depth of about 50 m.

Below this depth, the higher values of salinity are located in the central part of the basin, or near the islands, while the coastal zone exhibits waters of lower salinity (Fig. 4b, salinity at 100 m).

This kind of distribution is readily understood from Fig. 5, which shows a transverse section of the basin. This indicates that the high salinity layer upwells near the islands and, after limited sinking in the central part of the basin, surfaces near the coast, thus giving an explanation for the kind of distribution for the upper layers represented in Fig. 4.

From the same section it appears evident that the same sequence of vertical movements is followed by the deeper layers, which are characterized by lower salinity values.

As a consequence, relatively low salinities are present in the 100 m horizon in the zones near the islands and the coast, while the central part of the basin is distinguished by the high salinities of the Subtropical Underwater.

This kind of distribution continues to a depth of about 300 m or deeper, at least in some restricted zone. Below this depth, salinity distribution becomes more regular and may be easily deduced from Fig. 5.

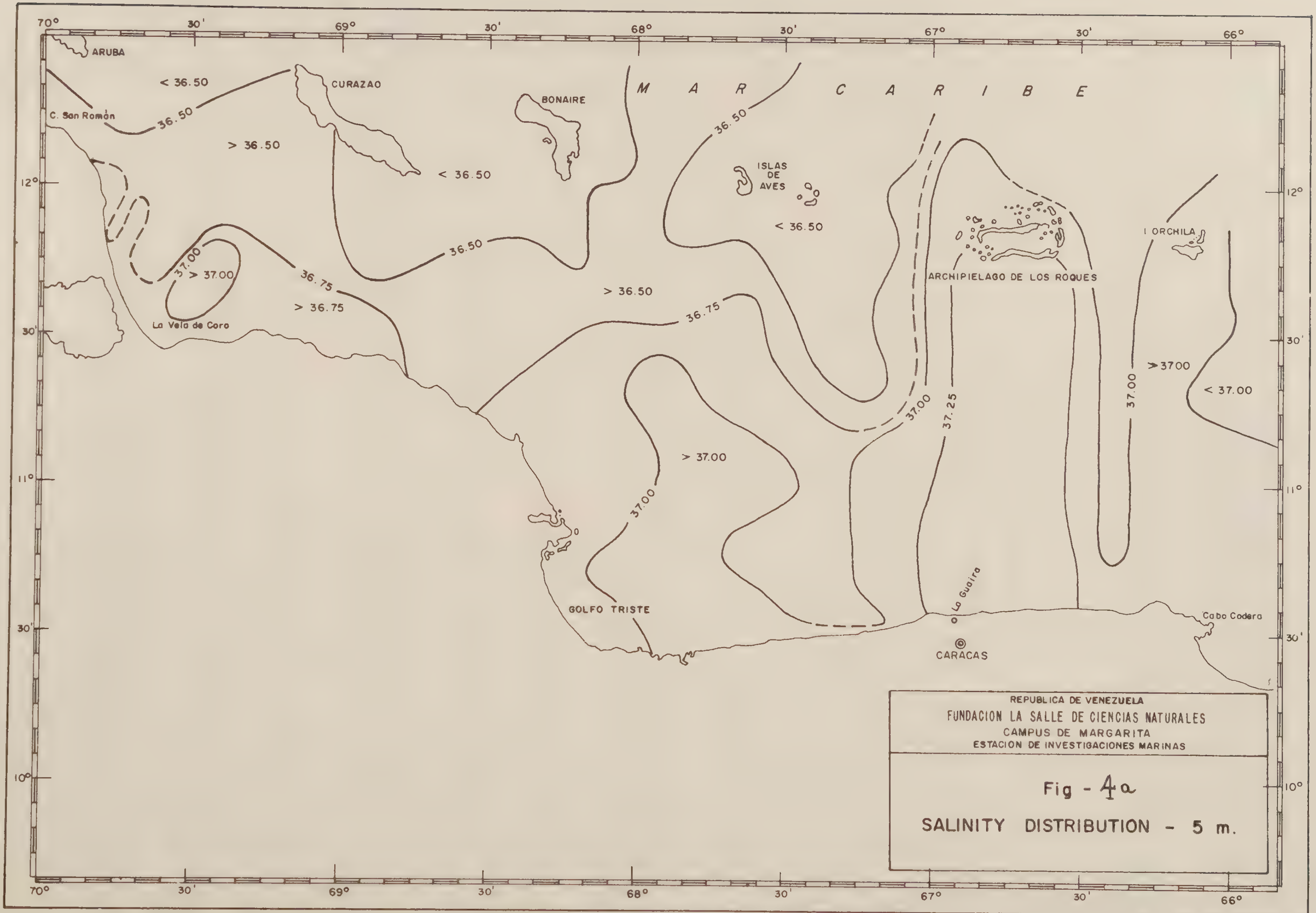
70°
30'
69°
30'
68°
30'
67°
30'
66°
12°
30'
11°
30'
10°
ARUBA
C. San Román
< 36.50
36.50
> 36.50
CURAZAO
< 36.50
BONAIRE
M A R C A R I B E
36.50
ISLAS DE AVES
< 36.50
37.00
> 37.00
La Vela de Coro
36.75
> 36.75
36.50
> 36.50
36.75
> 37.00
37.00
GOLFO TRISTE
37.00
37.25
ARCHIPIELAGO DE LOS ROQUES
I. ORCHILA
37.00
> 37.00
< 37.00
La Guaira
CARACAS
Cabo Codera

REPUBLICA DE VENEZUELA
FUNDACION LA SALLE DE CIENCIAS NATURALES
CAMPUS DE MARGARITA
ESTACION DE INVESTIGACIONES MARINAS

Fig - 4a

SALINITY DISTRIBUTION - 5 m.

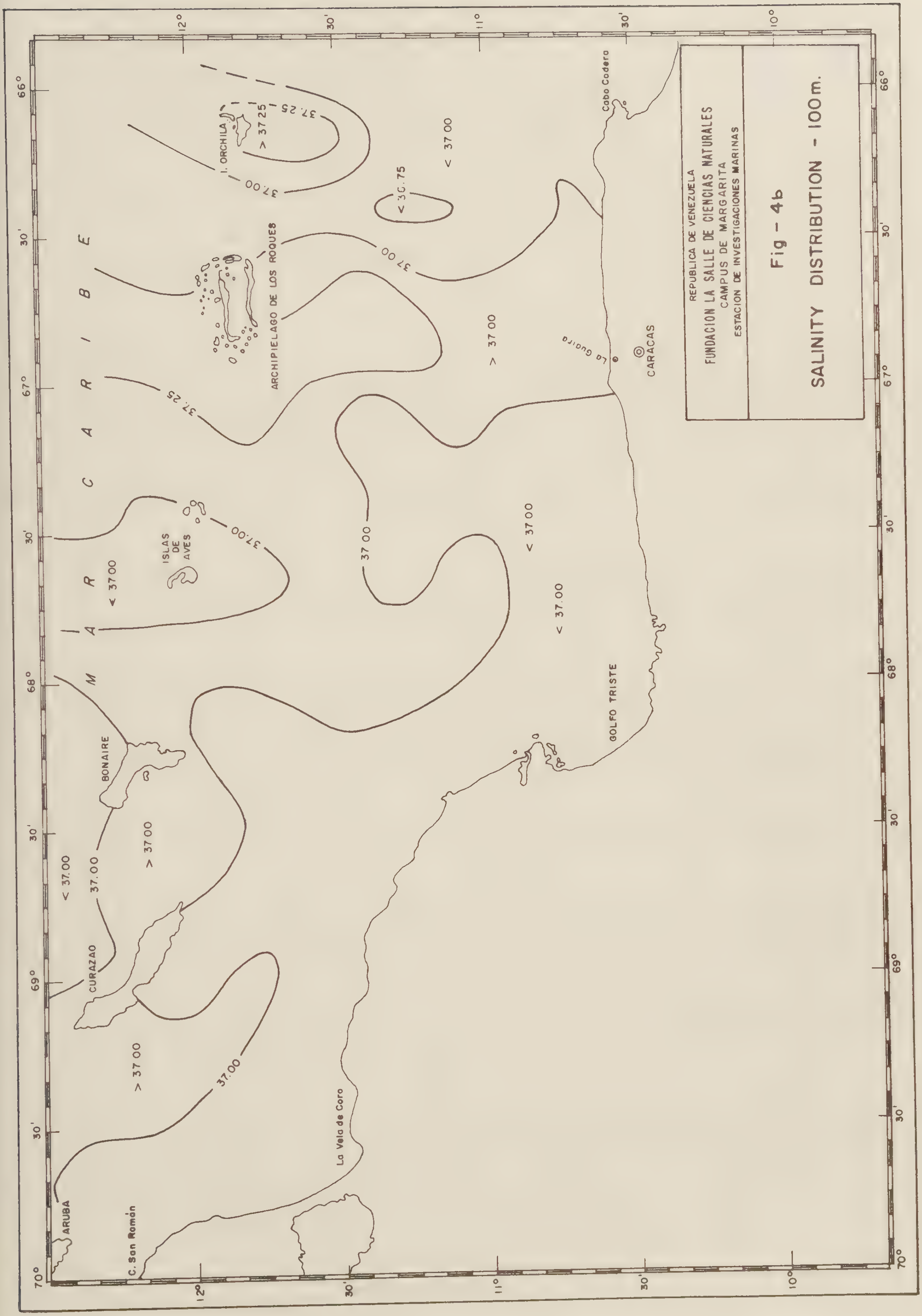

REPUBLICA DE VENEZUELA
FUNDACION LA SALLE DE CIENCIAS NATURALES
CAMPUS DE MARGARITA
ESTACION DE INVESTIGACIONES MARINAS

Fig - 4b

SALINITY DISTRIBUTION - 100m.

M A R   C A R I B E
I. ORCHILA
ARCHIPIELAGO DE LOS ROQUES
ISLAS DE AVES
BONAIRE
CURAZAO
ARUBA
C. San Román
La Vela de Coro
GOLFO TRISTE
La Guaira
CARACAS
Cabo Codera
37.25
> 37.25
37.00
< 37.00
< 36.75
> 37.00
12°
11°
10°
30'
66°
67°
68°
69°
70°

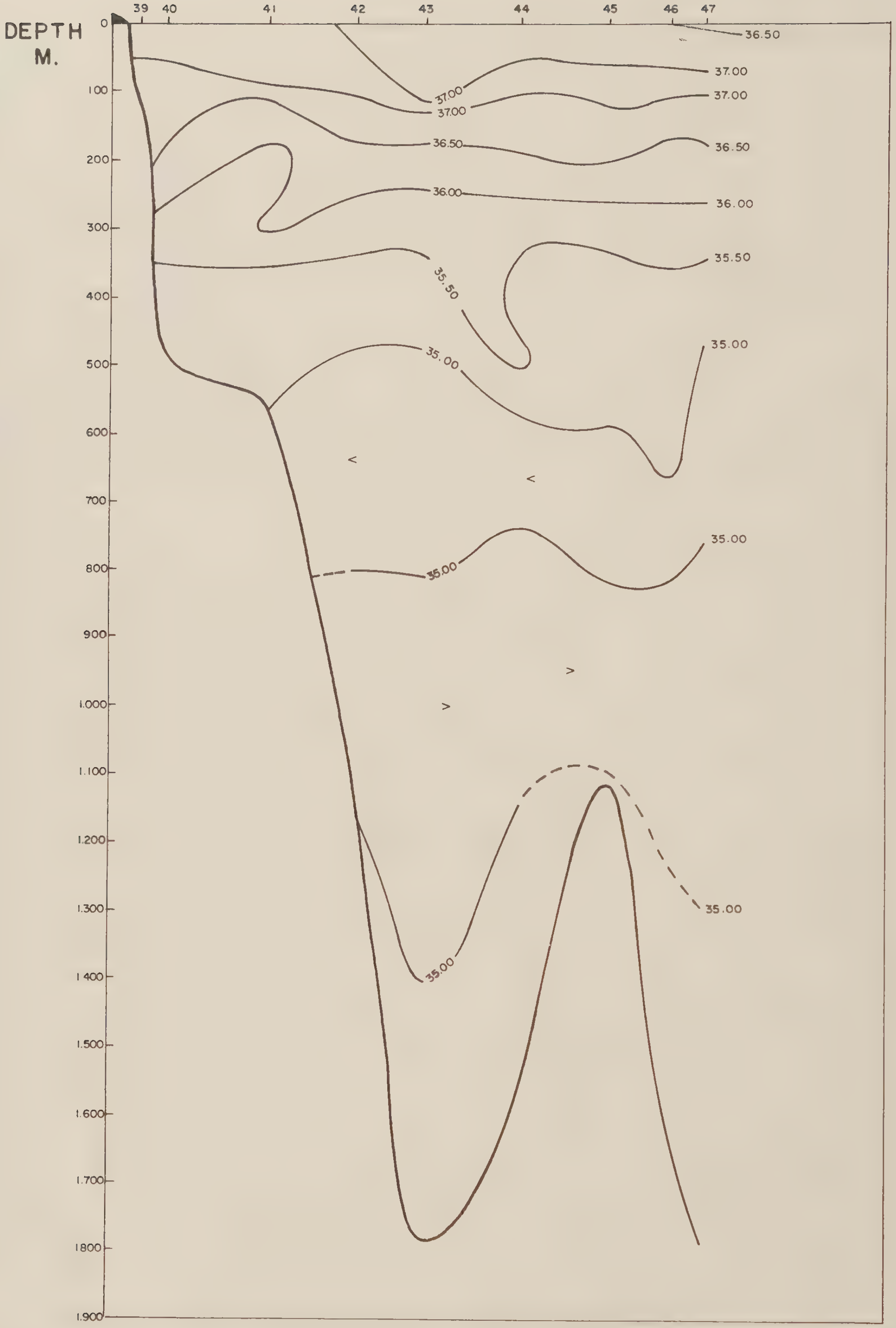

Fig. 5 Vertical salinity distribution along transect 6

The eastern part, if examined through the same kind of vertical sections, does not present any difference in the general trend of the isohalines. Only the absolute values of salinity are higher than in the rest of the basin, at least for the upper and intermediate layers. The surface layer of low salinity, typical of the Caribbean Sea (see section on T-S diagrams), is completely or almost completely absent.

Upwelling and sinking are present, as in the other zones, but may not be deduced by our maps, due to the thickness of the Subtropical Underwaters and to the rather slight differences in the horizontal salinity distribution.

As to the origin of the various water types, this will be discussed in the section dedicated to T-S diagrams.

3.3 Sigma-t

The geographic distribution of this parameter shows a clear relationship to the ones exposed previously for temperature and salinity. As a matter of fact, examining Fig. 6 which shows the geographic distribution of Sigma-t at the same depths of the Figs. 2 and 4, we find a notable correspondence among them. As a consequence density isopleths of the 5 m level show the same tendency to run more or less parallel to the coast in the central and western parts, with higher values in the southern stations than in the offshore ones. In the eastern zone they tend to follow the same trend demonstrated by the isothermal lines, running normal to the coast in their northern part and parallel to it in their southern portion.

At 100 m, the situation is similar to the trend described before. It may be noted further that at this depth higher values did not occur at the more coastal stations. Instead, in the eastern zone the values were lower than those from the stations in the central part of the basin.

This kind of distribution, so similar to the ones of temperature and salinity, is easily understood by observing Fig. 7 which shows the vertical distribution of the isopycnal lines in a vertical section normal to the coast. From this, it appears that a double upwelling exists; the first one relative to sub-surface waters which, from an average depth of 75-125 m in the offshore stations, appear at the surface near to the coast. These waters show, in some sections, a sinking phenomenon when they enter into the basin.

The tendency to surface near to the coast generally ceases with the isopycnal lines 26.5 or 27.0 which, probably due to the piling up of sub-surface waters, show instead a downward trend.

The second upwelling affects deeper waters and is especially evident north of the islands. Here it appears evident that the waters pertaining to the tropospheric and intermediate layers, as defined by Mamayev (1975), and even deeper than these, reach upper levels and enter into the basin, where they sink to their original depths.

This sequence of vertical movements is also accompanied, following the general theories, by horizontal movements (currents), which should be better studied by dynamic methods. However, we have used the data presented here to draw a tentative currents system which will be checked with the results of the dynamic computations in progress.

To this end we made the perhaps too simplicistic assumption that a downward trend of the isopycnal lines in the vertical sections corresponds to a movement with an eastward component; while a westward current is present when the isopycnal lines tend upward . That is to say that a zone of lower density south of an isopycnal line of higher value will demonstrate an eastward movement in our maps.

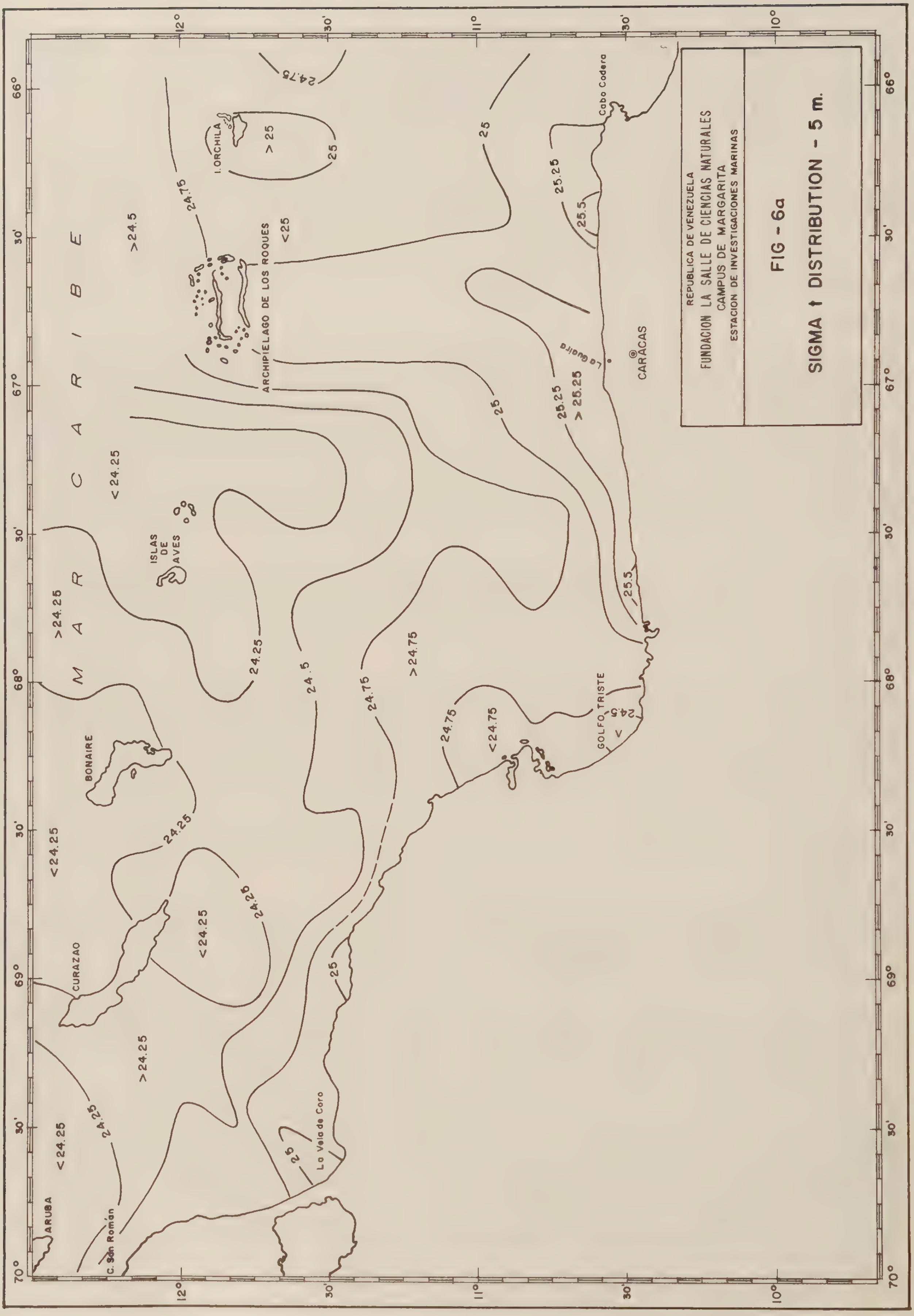

REPUBLICA DE VENEZUELA
FUNDACION LA SALLE DE CIENCIAS NATURALES
CAMPUS DE MARGARITA
ESTACION DE INVESTIGACIONES MARINAS

FIG - 6a

SIGMA t DISTRIBUTION - 5 m.

MAR CARIBE
ARUBA
C. San Román
CURAZAO
BONAIRE
ISLAS DE AVES
ARCHIPIELAGO DE LOS ROQUES
I. ORCHILA
Cabo Codera
La Guaira
CARACAS
GOLFO TRISTE
La Vela de Coro
66°
67°
68°
69°
70°
30'
12°
11°
10°
< 24.25
24.25
> 24.25
24.5
> 24.5
24.75
> 24.75
< 24.75
25
> 25
< 25
25.25
> 25.25
25.5

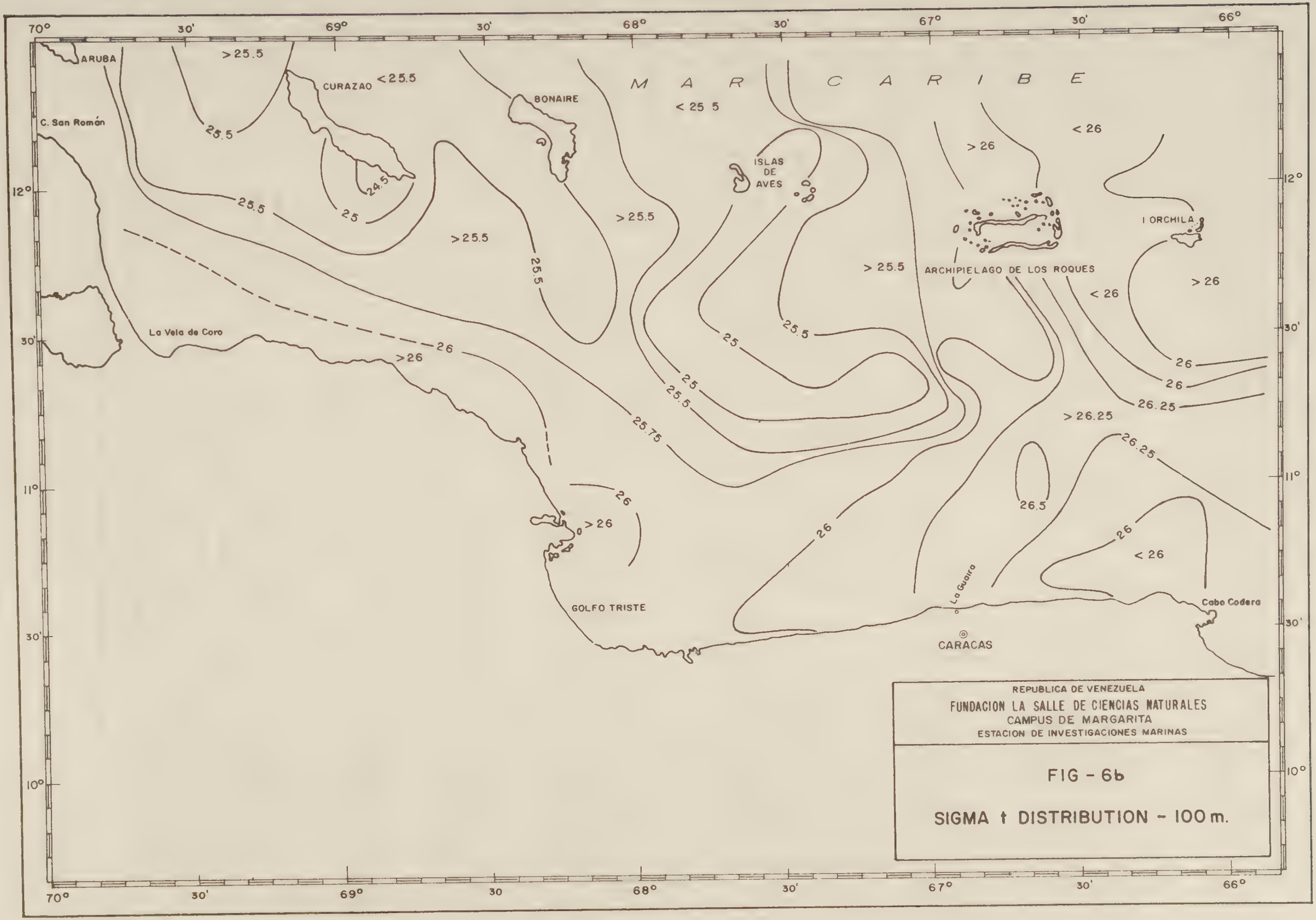
70°
30'
69°
30'
68°
30'
67°
30'
66°
12°
30'
11°
30'
10°
30
MAR CARIBE
ARUBA
C. San Román
CURAZAO
BONAIRE
ISLAS DE AVES
ARCHIPIELAGO DE LOS ROQUES
I ORCHILA
La Vela de Coro
GOLFO TRISTE
La Guaira
CARACAS
Cabo Codera
> 25.5
< 25.5
25.5
24.5
25
< 25 5
> 25.5
> 26
< 26
26
26.25
> 26.25
26.5
25.75

REPUBLICA DE VENEZUELA
FUNDACION LA SALLE DE CIENCIAS NATURALES
CAMPUS DE MARGARITA
ESTACION DE INVESTIGACIONES MARINAS

FIG - 6b

SIGMA t DISTRIBUTION - 100 m.

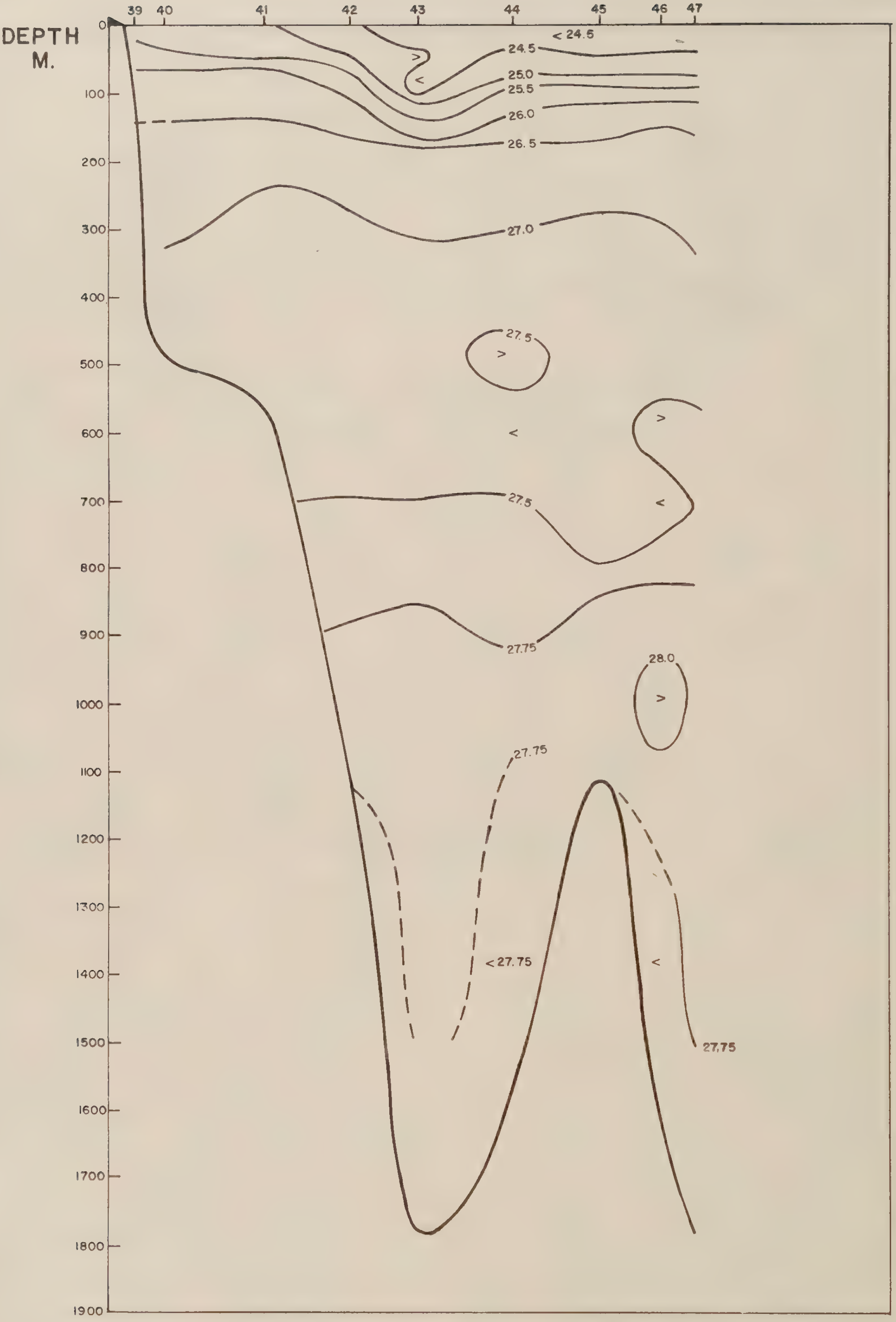

Fig. 7 Vertical Sigma-t distribution along transect 6

Following this, it becomes evident that surface waters generally go westward, north of the islands and near the coast. Due to the fact that the rate of sinking is rather limited, the presence of an eastward current may not be deduced from our maps, at least up to a depth of 100–125 m. At this depth, counter currents begin to appear south of Las Aves Islands and between Aruba and Bonaire.

At greater depths, a double counter current may be found south of the islands and near to the coast, due to the downward trend of the isopycnal lines. This system, which is complicated by the great number of passages between the islands, can then be seen in simpler terms. The waters upwell and enter the basin because their density is higher than that of the water at that level. Once in the basin the waters tend to sink and thereby change direction. As they approach the coast the waters surface and then sink again. The implication is that there will be new changes in the direction of the currents which originate from this series of vertical movements.

In this period counter currents are less evident at the upper levels, due to the rather limited rate of sinking of the Subtropical Underwaters , while it is more evident at deeper levels, affecting a great part of the basin as is indicated in Fig. 8, where Sigma-t distribution is given for the 300 m level.

As was previously indicated, this is only a tentative scheme which will be defined better by the results of dynamic computations. Nevertheless, the results not only agree with the ones of a previous cruise (Voltolina,1977), but are also in accordance with the general theories on this area (see e.g. Fukuoka,1963; Okuda,1974); the map by Febres on surface and geostrophic currents along the Venezuelan coast (Hno Ginés et al.,1972), and with many direct observations of current velocities and directions in this zone (British Admiralty Chart 1966 (1960), states "... inshore and in the vicinity of the off lying islands counter currents of up to 2 knots can be expected.").

3.4 T-S diagrams

These diagrams have not only been used for a better identification of the various water types present in the zone, but also to verify the various vertical movements described in the preceding sections. By using a different symbol for any depth and by marking every station, it has been possible to demonstrate that the same water type was present at different depths in the different stations of the same transect, giving further evidence of vertical movements in the zone.

This method was employed before, and some examples which are relevant to this zone have been published by the author (Voltolina,1975, 1977). Further, all the diagrams from this cruise have been presented elsewhere (Voltolina,1976), and may not be given here for the reasons stated in the note to the section: Materials and Methods.

Here, only a general T-S diagram for a single section will be given (Fig. 9), in order to identify the various water types present in the basin; for these we shall use the same terms used by Wüst (1964) and by Okuda (1974).

The first water type which may be described by the observation of this diagram, corresponds to Wüst's Surface Waters (SW). This is typical of offshore stations and was characterized in this period by temperatures of 25-26°C or slightly higher, with salinities ranging from 36 to 36.6 percent. Its extension is rather limited and it becomes at least partially mixed with the following Subtropical Underwater (SU). This constitutes, in the Caribbean, a subsurface layer of high salinities and of variable thickness and depth. As already mentioned, its salinity concentration is higher in the upper levels than the one mentioned by the authors working in the Caribbean (in many cases higher than 37 percent).

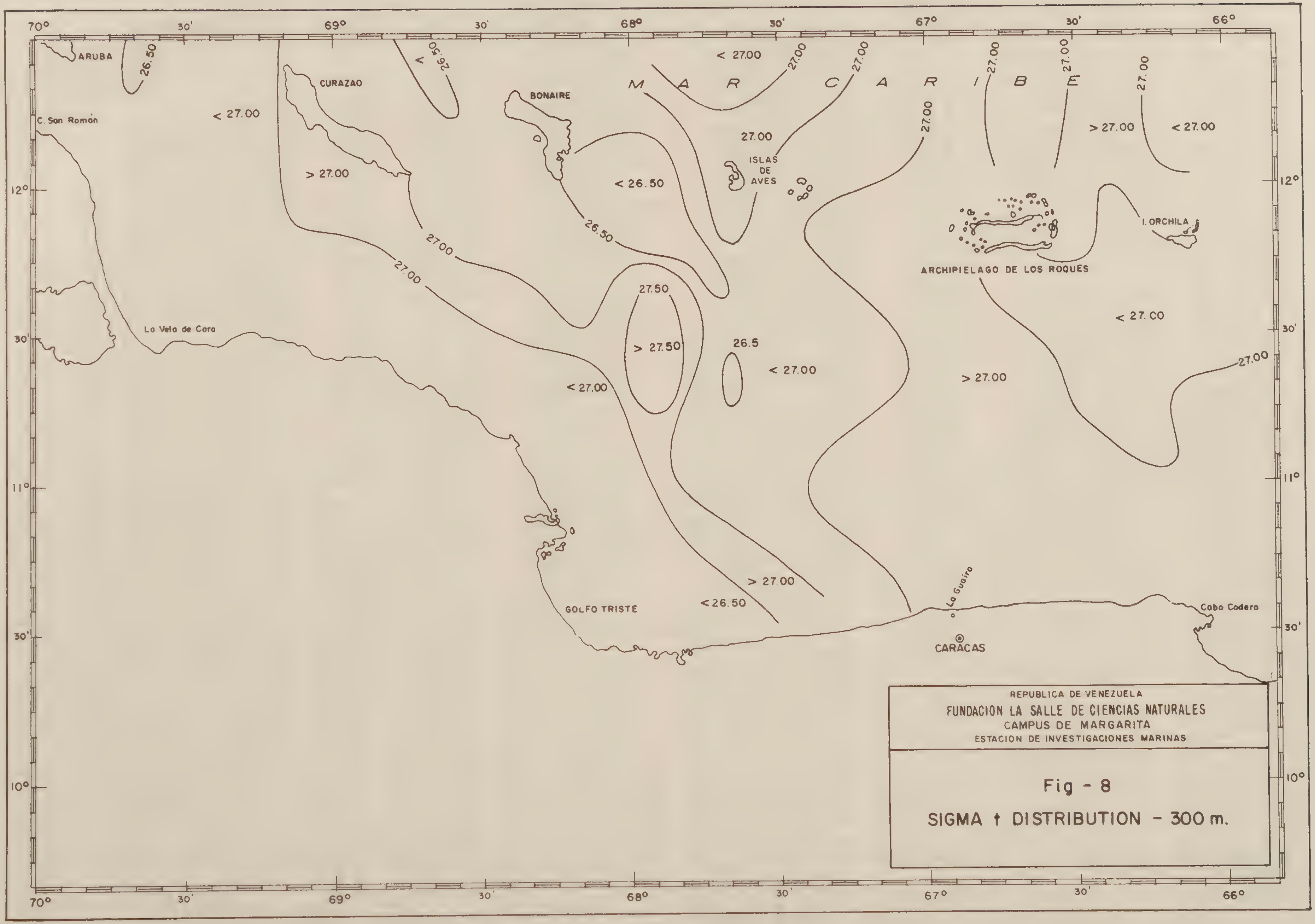
70°
30'
69°
30'
68°
30'
67°
30'
66°
12°
30'
11°
30'
10°
M A R C A R I B E
ARUBA
C. San Román
CURAZAO
BONAIRE
ISLAS DE AVES
ARCHIPIELAGO DE LOS ROQUES
I. ORCHILA
La Vela de Coro
GOLFO TRISTE
La Guaira
CARACAS
Cabo Codera
26.50
< 27.00
> 27.00
< 26.50
27.00
26.50
27.50
> 27.50
26.5
< 27.00
> 27.00
< 27.00
< 26.50
> 27.00
< 27.C0
27.00

REPUBLICA DE VENEZUELA
FUNDACION LA SALLE DE CIENCIAS NATURALES
CAMPUS DE MARGARITA
ESTACION DE INVESTIGACIONES MARINAS

Fig - 8

SIGMA t DISTRIBUTION - 300 m.

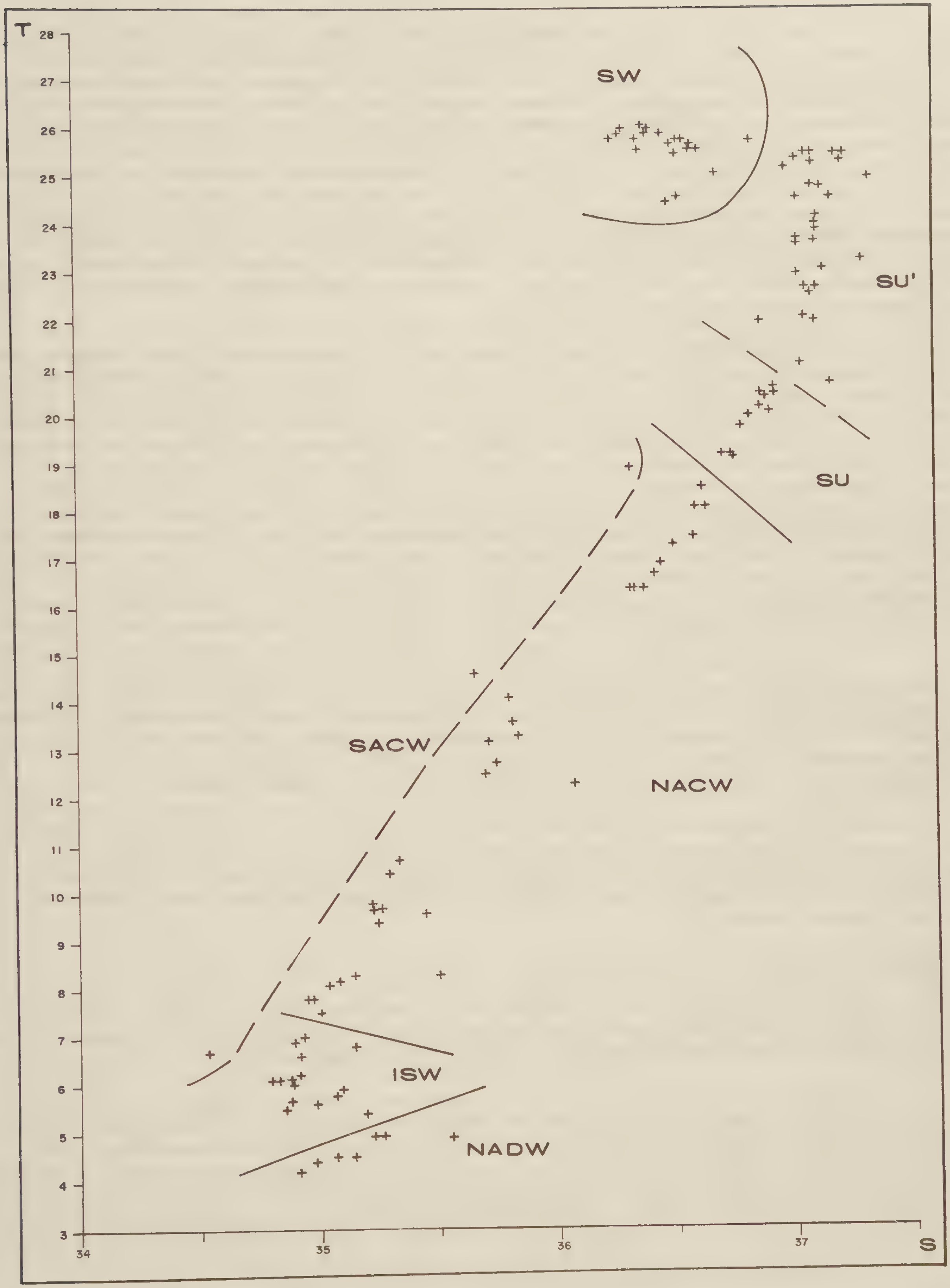

Fig. 9 T-S diagram from transect 6

In the southern part of the Caribbean this kind of water cannot be found deeper than 125-150 m, and in this zone it also affects large surface coastal areas, owing to the upwelling phenomenon already described. In general, its higher salinity concentrations have been found at the surface and in zones where it has evidently been subjected to long exposure to meteorological action, due to the fact that it presents high temperatures. It seems probable therefore that these high salinities are the result of the action of both wind and atmospheric temperature, which favour evaporation and, consequently, high salinity. It has been stated by Colón (1960), that sea surface evaporation is higher in autumn and winter. This high evaporation rate could, together with the absence of rain and rivers, explain the high salinities of part of the Subtropical Underwater. In the diagram we decided to separate this kind of water into two sections: SU and SU'. The first is applicable to deeper layers; the second to waters which have been subject to the action of atmospheric agents, usually to surface levels.

Below the Subtropical Underwater a transition zone may be noted, with temperatures and salinities progressively lower; this will be discussed later. The third Wüst water type, Intermediate Subantarctic Waters (ISW), is characterized by temperatures of 5-7°C and by salinities of 35 percent or lower. This water is present in a rather thick layer, at a depth of 600-800 m, having its core located at an average depth of 700 m. This was defined by Wüst as an intermediate minimum salinity layer, which corresponds to our data. Salinity values tend to increase below this layer, showing concentrations higher than 35 percent at great depths. This indicates the presence of a fourth type of water, North Atlantic Deep Water (NADW). For the Caribbean Wüst mentions also the term Caribbean Bottom Waters, leaving the difference between the two types indefinite. According to Okuda (1974), who finds that "Caribbean Bottom Waters maintain the characteristics of the North Atlantic Deep Waters", we shall use this last term, as it defines waters of salinities slightly higher than 35 percent, with temperatures of about 4°C, which in our case range from 4 to 5°C.

The waters with decreasing temperature and salinity in the transition zone are, after Sverdrup et al. (1942) and Mamayev (1975), of North Atlantic origin, and should be termed North Atlantic Central Waters (NACW). Only in some diagrams it has been possible to recognize the presence of waters of South Atlantic Origin (South Atlantic Central Waters - SACW), whose temperature and salinity values are lower for a same Sigma-t value.

In a previous cruise this transition zone, though mostly affected by North Atlantic waters, showed a clear presence of waters coming from the South Atlantic, well separated from the other water masses (Voltolina,1976). This was not the case for this cruise. The South Atlantic Central Waters, where present, were usually mixed and partially identified with the adjacent waters.

3.5 Oxygen

The geographical distribution of oxygen concentration at the depths of 5 and 100 m is shown by the maps of Fig. 10. The maps show characteristics which make it possible to compare oxygen distribution with the distributions of the other parameters.

It is relatively difficult, however, to deduce the phenomena which were previously seen from the simple examination of these maps. This is because the oxygen distribution is modified, at least in the upper levels, by various factors. It is not possible, for instance, to relate high oxygen concentrations to the upwelling of subtropical underwaters, which are characteristically well oxygenated because Surface Waters are also characterized by high concentrations of oxygen. This is due in part to biological activity (as in the small south-eastern zone, for instance, with more than 5 cm^3/l phytoplankton bloom); in part due to the fact that oxygen absorption is favoured by the strong winds blowing during this period.

Nevertheless, from Fig. 11 it appears clear that surfacing waters are characterized by oxygen concentrations ranging from 3.5 to 4.5 cm^3/l, while Surface Waters, or the waters that have already reached the surface due to upwelling, have a higher oxygen concentration (4.5 cm^3/l or more).

This explains the oxygen distribution at 5 m of Fig. 10, in which we may now attribute the concentrations of less than 4.5 cm^3/l, to a recent upwelling. The relationship is complicated by the kind of factors previously discussed and this becomes more evident at the level of 100 m. From comparison of the vertical sections of oxygen and salinity, we may realize that the waters of the SU' type, having salinities greater than 37 percent, are also characterized by higher oxygen concentrations (4 cm^3/l or more); while those of the SU type (salinity of 36.5-37 percent) have oxygen concentrations of 3.5-4 cm^3/l.

Referring these data to Fig. 10, we can then state that upwelling occurs in the zones characterized by oxygen concentrations of less than 4 cm^3/l, while higher oxygen concentrations may indicate the presence of Surface Waters or of waters which have already been subject to the action of meteorological agents.

At greater depths, concentrations lower than 3 cm^3/l may occur in connexion with the intermediate minimum salinity layer. This is also characterized (Wüst, 1964; Okuda, 1974) by an intermediate oxygen minimum.

Below this layer an inverse trend is evident, with values gradually increasing with the depth, almost reaching concentrations of 5 cm^3/l at depths higher than 1 800-2 000 m.

4. CONCLUSIONS

The data presented in the previous sections permit a general description of the hydrological conditions of the zone investigated by our programme and a general scheme of its circulation.

The hydrological structure is not much different from the ones described for other seasonal situations, which demonstrates that at least the first 200-300 m is basically ruled by the trade winds, as already demonstrated by various authors (see e.g., Fukuoka, 1963; Gordon, 1967). These winds blow, though with differing intensity, during the whole year (Contreras, 1969). This explains why this basin is characterized by the same phenomena in any seasonal situation, differing only in their intensity and extension.

The characteristics of Surface Waters are quite different from the ones described for previous expeditions, but this causes only local or minor changes to the general hydrology of the zone.

We have consequently observed the same phenomenon of upwelling, near the coast and near the islands, involving both Subsurface and Intermediate Waters, and a sinking one in the central part of the basin.

From this, we have deduced a general scheme of circulation which comes from these changes in vertical movements. It consists for Surface Waters in an undulating current going westward, with an eastward component in the central part of the basin, due to sinking motion of the waters south of the islands. At deeper levels two counter currents have been detected, in connexion with sinking of Intermediate and Deep Waters along the coast and along the chain of islands which enclose the basin.

T-S diagrams have been used to investigate the origins of the various water masses. From these, it has been possible to recognize all the water types described for the Caribbean Sea by various authors and to confirm that, during this season, South Atlantic Waters represent a minor fraction of the Atlantic Central Waters. The latter constitute a core, about 400 m thick, between the Subtropical Underwaters and the Antarctic Intermediate Waters.

We are now trying to make a quantitative evaluation of the data presented; this, together with the hydrochemical and biological data which are being collected at present, will permit us to evaluate the potential biological productivity of the zone, which constitutes the main purpose of our programme.

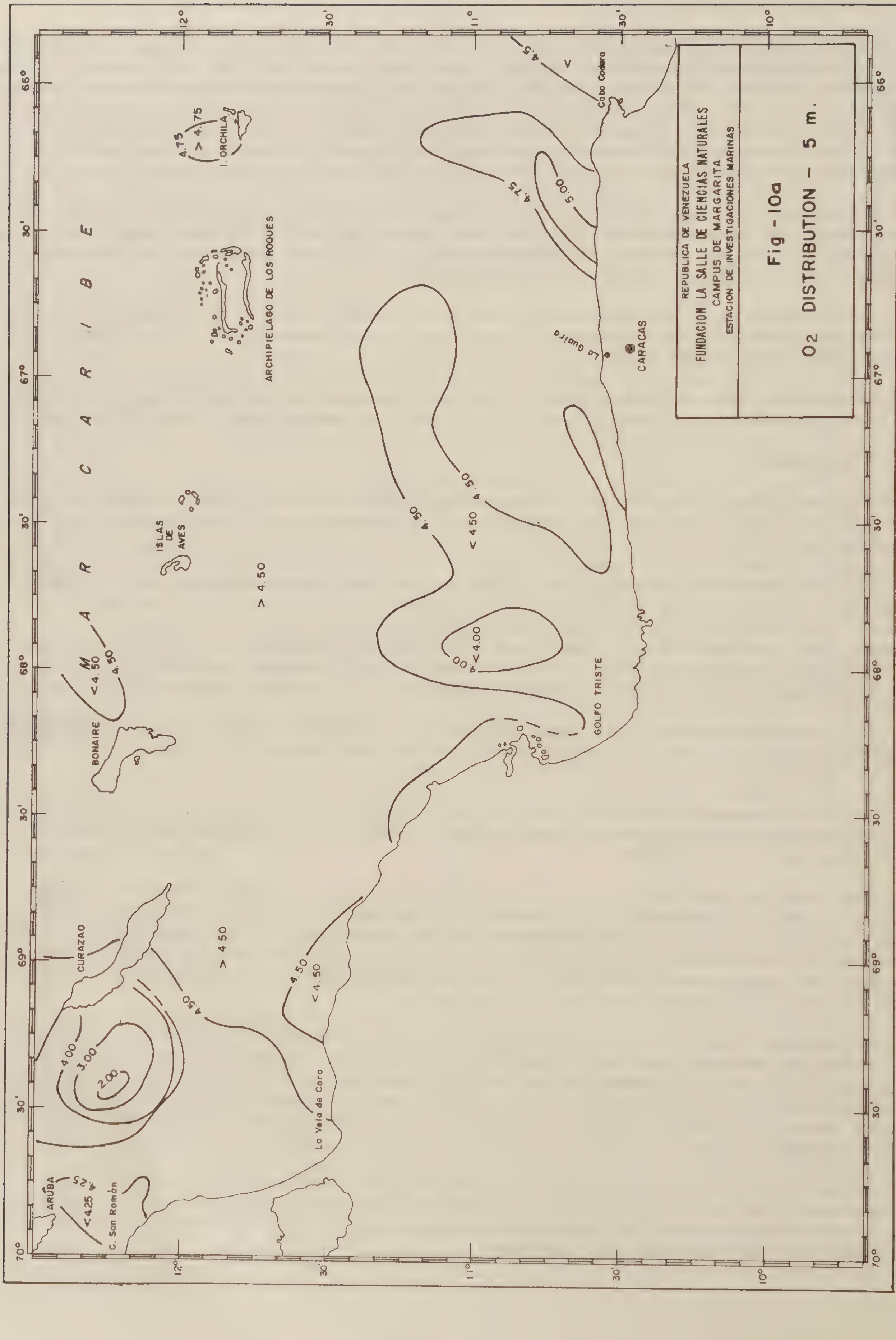

REPUBLICA DE VENEZUELA
FUNDACION LA SALLE DE CIENCIAS NATURALES
CAMPUS DE MARGARITA
ESTACION DE INVESTIGACIONES MARINAS

Fig - 10a

O_2 DISTRIBUTION - 5 m.

M A R C A R I B E
ARUBA
C. San Román
CURAZAO
BONAIRE
ISLAS DE AVES
ARCHIPIELAGO DE LOS ROQUES
I. ORCHILA
Cabo Codera
La Guaira
CARACAS
GOLFO TRISTE
La Vela de Coro
4.25
< 4.25
4.00
3.00
2.00
4.50
> 4.50
< 4.50
4.75
> 4.75
5.00
< 4.00
4.5
12°
30'
11°
10°
66°
67°
68°
69°
70°

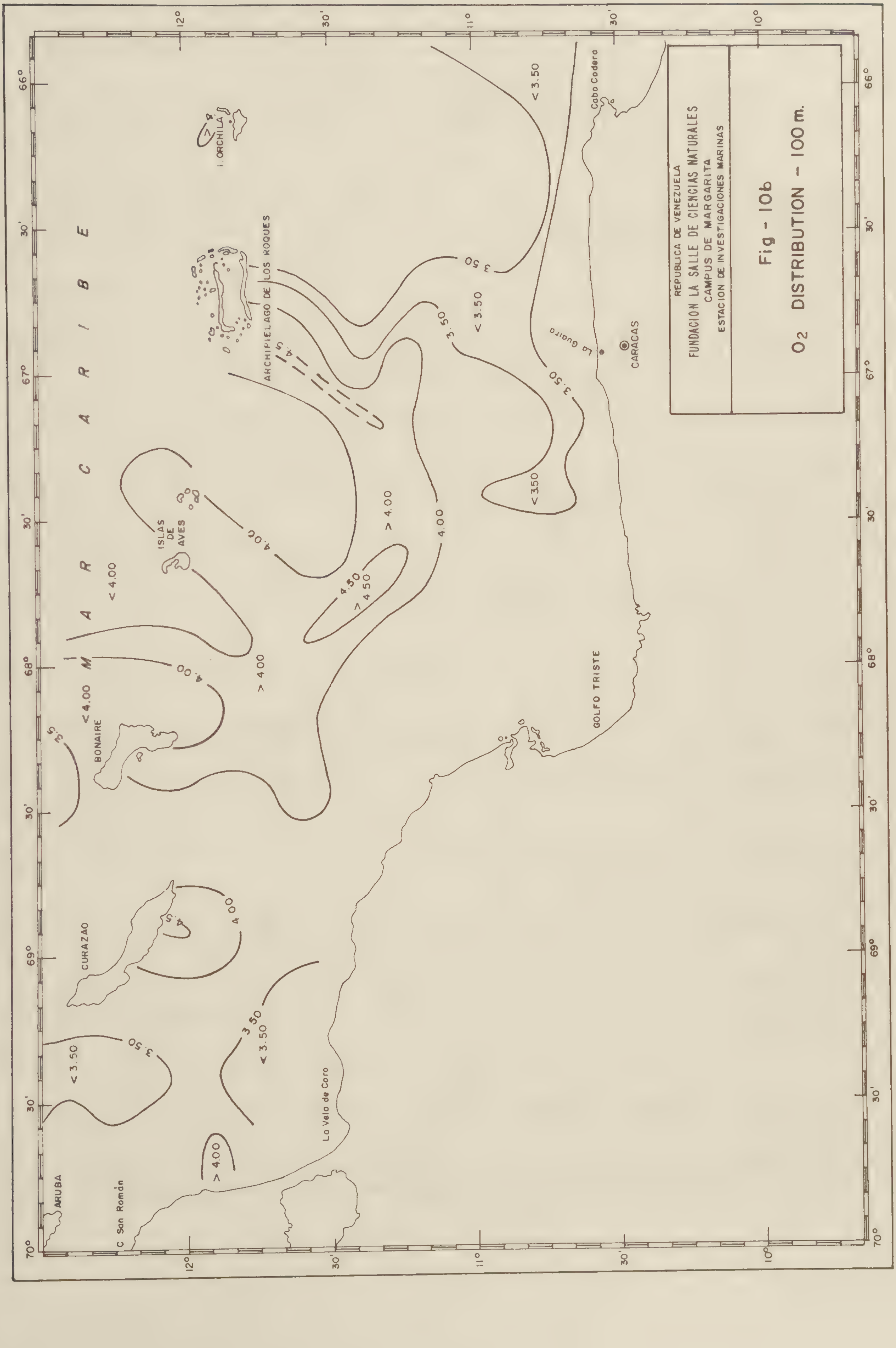

REPUBLICA DE VENEZUELA
FUNDACION LA SALLE DE CIENCIAS NATURALES
CAMPUS DE MARGARITA
ESTACION DE INVESTIGACIONES MARINAS

Fig - 10b

O_2 DISTRIBUTION - 100 m.

MAR CARIBE
I. ORCHILA
ARCHIPIELAGO DE LOS ROQUES
ISLAS DE AVES
BONAIRE
CURAZAO
ARUBA
C San Román
La Vela de Coro
GOLFO TRISTE
La Guaira
CARACAS
Cabo Codera
< 3.50
3.50
< 3.50
3.50
< 3.50
4.5
4.00
> 4.00
4.50
> 4.50
< 4.00
4.00
> 4.00
< 4.00
3.5
4.00
4.5
3.50
< 3.50
3.50
< 3.50
> 4.00
12°
30'
11°
30'
10°
66°
30'
67°
30'
68°
30'
69°
30'
70°

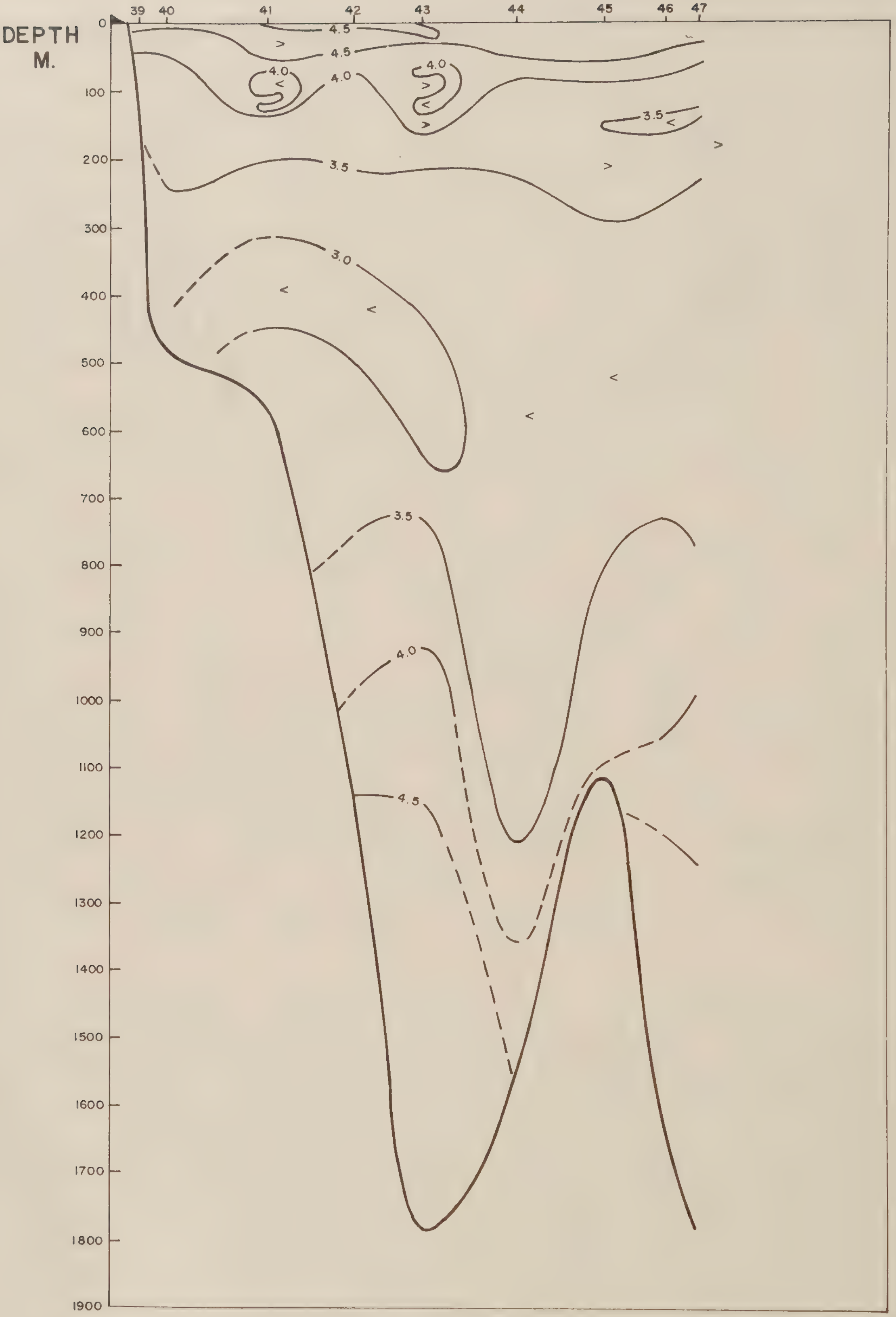

Fig. 11 Vertical distribution of oxygen concentration along transect 6

5. ACKNOWLEDGEMENTS

The writer wishes to acknowledge to his wife, Anna Lia, her invaluable help during the whole duration of this investigation. Her continuous and dedicated cooperation in data elaboration and correction have made possible the extension of the present paper, which I gratefully dedicate to her.

The continuous encouragement of Hno Ginés, President of the Fundación, the constant support of Mr. Hector Mandazen, the cooperation of Luis M. Iriarte and José A. Salazar in data correction and elaboration and of Miss María Isabel Nuñez in drawing all the figures presented in this paper, are also gratefully aknowledged.

6. REFERENCES

Aragno, F.J., Dinámica del Mar Caribe en la costa Venezolana. In Unesco/FAO Symposium on
1971 investigations and resources of the Caribbean Sea and Adjacent Regions, Willemstad, Curaçao, 18-26 November 1976. Paris, Unesco, pp. 13-26

Colón, F.A., On the heat balance of the troposphere and water body of the Caribbean Sea.
1960 Rep.Natl.Hurricane Res.Proj., (41)

Contreras, A., Resumen climatológico de la Estación climatológica de Punta de Piedras,
1969 Estado Nueva Esparta, 1962-67. Mem.Soc.Cienc.Nat.La Salle, 29:146-69

Fukuoka, J., Un análisis de las condiciones hidrográficas del Mar Caribe. Mem.Soc.Cienc.
1963 Nat.La Salle, 23:43-55

Gordon, A.L., Circulation of the Caribbean Sea. J.Geophys.Res., 72:6207-23
1967

Great Britain, Admiralty South America, North Coast. Tortuga to Cabo la Vela. London,
1960 H.M.S.O., Chart (1966)

Hno, G. et al., Carta pesquera de Venezuela. 1. Areas de nororiente y Guayana. Monogr.
1972 Fund.La Salle Cienc.Nat., (16):328 p.

Mamayev, O.I., Temperature-Salinity analysis of world ocean waters. Elsevier Oceanogr.
1975 Ser., 11:374 p.

Okuda, T. et al., Revisión de los datos oceanograficos en el Mar Caribe Suroriental,
1974

Parr, A.E., A contribution to the hydrography of the Caribbean and Cayman Seas. Bull.
1937 Bingham Oceanogr.Collect., 5(4):1-110

Strickland, J.D.H. and T.R. Parsons, A practical handbook of seawater analysis. Bull.Fish.
1968 Res.Board Can., (167):311 p.

Sverdrup, H.U., M. Johnson and R. Fleming, The oceans, their physics, chemistry and general
1942 biology. Englewood Cliffs, N.Y., Prentice Hall, 1087 p.

U.S. Department of Commerce, Temperature, salinity, oxygen and phosphate in waters off
1975 eastern Central America and northern South America. Key Oceanogr.Rec.Doc., 4

U.S. Naval Hydrographic Office, Processing oceanographic data. Publ.U.S. Naval Hydrogr.
1952 Off., (614)

Voltolina, D., Evidencia de afloramientos en las aguas costaneras de Venezuela. In
1975 Memorias del primero Simposio latinoamericano sobre oceanografía biológica.
Mexico, pp. 363-74

__________, Condiciones hidrológicas en la zona central del Mar Caribe Venezolano.
1976 Febrero 1975. Caracas, Fundación La Salle, (Internal rep.)

__________, Condiciones hidrológicas en la zona central del Caribe Venezolano. In
1977 Memorias del secundo Simposio latinoamericano sobre oceanografía biológica.
Cumaná, Universidad de Oriente, vol.2:235-57

Wüst, G. and A. Gordon, Stratification and circulation in the Antillean Caribbean basin.
1964 Part 1. Spreading and mixing of the water types with an oceanographic atlas.
New York, Columbia University Press, 201 p.

CHEMICAL OCEANOGRAPHY: SUMMARY OF CICAR RESULTS AND RECOMMENDATIONS FOR THE FUTURE

by

D.K. ATWOOD
NOAA/AOML
Miami, Florida 33149, U.S.A.

CONTENTS

1. INTRODUCTION
2. RIVER INPUTS AND EFFECTS
3. CARIACO TRENCH
4. DEEP BASIN WATERS
5. SUSPENDED MATERIAL
6. UPPER WATERS
7. OTHER PROGRESS
8. RECOMMENDATIONS
9. ACKNOWLEDGEMENTS
10. REFERENCES

Abstract

This Symposium has demonstrated that much progress has been made since 1969 concerning knowledge of the marine chemistry of the Caribbean. The area of river inputs and effects has received considerable attention during CICAR; a major share of the efforts were directed toward the effects of the Amazon River. Work presented during this Symposium included: nutrient contributions from the Amazon to the Guyana shelf waters; effects of both the Orinoco and Amazon outflows upon suspended clays, carbonates and organic matter in the eastern Caribbean and adjacent western Atlantic; and the lack of inorganic processes which remove dissolved silica in the estuaries and nearshore water of both the Amazon and Mississippi Rivers. Less is known about the Orinoco and Magdalena Rivers' contributions. Notable progress has been made toward understanding the processes occurring within the Cariaco Trench since the beginning of CICAR. Extensive progress has been made describing the suspended matter in the Caribbean and the mechanisms by which it diffuses. Progress has also been made in the study of the upper circulation of the Caribbean and Gulf of Mexico. The American Mediterranean is a defined marginal sea composed of a series of interconnected basins with both oceanic and terrestrial inputs. Future research should be designed to utilize this unique situation for the study of marine chemical processes. More work needs to be done in defining the physical oceanography of the region so that the chemical oceanographer can plan his experiments and interpret his data with greater ease. The question of river inputs will have to be addressed in greater detail, especially for the Orinoco and Magdalena Rivers. Understanding of anthropogenic inputs is necessary before any meaningful pollution monitoring can be initiated. Elucidating the role played by micronutrients, such as phosphates and nitrates, in the American Mediterranean will be an area of considerable future progress. The effect of catastrophic events such as hurricanes upon marine chemical processes has been almost completely neglected. The need for interdisciplinary seminars which focus on reasonably sized geographic areas is clearly indicated.

Resumen

Este simposio ha puesto de manifiesto los notables progresos realizados desde 1969 por la química marina del Caribe. En los coloquios de las ICCRA se dedicó considerable atención a la cuestión de los materiales de acarreo de los ríos, y a sus efectos, especialmente los causados por el río Amazonas. Entre los trabajos presentados al simposio figuraban: contribución, en elementos nutrientes, del Amazonas a las aguas de la plataforma continental de Guyana; efectos de las descargas de los ríos Orinoco y Amazonas sobre las arcillas, carbonatos y materias orgánicas en suspensión en el Caribe oriental y en el Atlántico occidental adyacente, y ausencia de procesos inorgánicos que eliminen la sílice disuelta en los estuarios y en las aguas litorales de los ríos Amazonas y Mississippi. Las contribuciones de los ríos Orinoco y Magdalena son menos conocidas. Desde que empezaron las ICCRA se conocen mucho mejor los procesos que ocurren en la fosa submarina Cariaco; la descripción de las materias de suspensión en el Caribe, y de sus mecanismos de difusión, es un progreso importante; también ha progresado el estudio de la circulación superior en el Caribe y en el Golfo de México. El Mediterráneo americano es un mar marginal, compuesto de una serie de cuencas interconectadas, con materiales de acarreo oceánicos y terrestres. Deben hacerse futuras investigaciones, a fin de que esta situación única pueda servir al estudio de los procesos químicos marinos. La definición de la oceanografía física de la región requiere más trabajo, para que el oceanógrafo químico pueda planificar sus experimentos e interpretar sus datos con mayor facilidad. Las descargas fluviales tienen que ser estudiadas más detalladamente en particular las de los ríos Orinoco y Magdalena. Para poder iniciar la observación de contaminaciones importantes hay que comprender el fenómeno de las descargas antropogénicas. El esclarecimiento de la función que desempeñan los micronutrientes, como los fosfatos y los nitratos, en el Mediterráneo americano, es una cuestión cuyo estudio progresará considerablemente en el futuro. Se ha prestado muy poca atención a los efectos de fenómenos catastróficos, como los huracanes, sobre los procesos químicos marinos. Se indica claramente la necesidad de seminarios interdisciplinarios que se centren en el estudio de zonas geográficas de una extensión razonable.

1. INTRODUCTION

Status of knowledge in 1968–69: At the start of CICAR, or prior to the beginning of the field phase, a reasonable baseline of chemical oceanographic knowledge had at least begun to exist concerning the Caribbean and adjacent regions. The effects of the Amazon River outflow on the ecology close to the discharge had been investigated. Ryther, Menzel and Corwin, 1967, demonstrated that the low phosphate and nitrate content of the outflow resulted in the lowering of productivity in the nearby ocean waters even though large amounts of dissolved silicate were available. The distribution of dissolved silicate and other nutrients in the Caribbean, as they related to the adjacent North Atlantic, had been described (Richards, 1958). The suggestion had been made that the modeling of dissolved silicate distribution in the Cariaco Trench might develop an understanding which would allow us to approach the problems regarding the extent of renewal in the deep Grenada, Venezuela, and Colombia Basins (Metcalf, 1969). The chemistry of the Cariaco Trench had been described in some detail (Richards and Vacarro, 1956; Redfield, Ketchum and Richards, Volume II, The Sea), and an idea of the frequency of overturn or renewal of the bottom water of that trench had been postulated. The suspended matter in the water column had been considered, and a knowledge of mineral sources and transport in the Caribbean and Gulf of Mexico was developing (Jacobs and Ewing, 1969).

Since a knowledge of the dynamics of ocean systems is essential if a chemical oceanographer is to intelligently interpret his numbers, it is also pertinent to consider some of the physical oceanographic knowledge, which was available to us at the start of CICAR, as well as certain landmark results in that field which occurred during CICAR. In 1969, we were fortunate to have the Wüst and Gordon (1964) monograph on stratification and circulation in the Caribbean, which contained the existing knowledge about Caribbean water masses and their sources. We also had the 1966 paper by Gordon that used Metcalf's 1958 CRAWFORD 17 sections (Metcalf, 1959), along with others, to describe what was known at that time about the dynamics of the system. These data were of significant utility in planning chemical oceanographic research.

Since 1969, the progress in our knowledge of the marine chemistry of the Caribbean has increased at a rapid rate. Much of this progress has been demonstrated at this Symposium. The following includes not only the results presented here, but also papers published elsewhere during that time and work which is now in process or being prepared for publication. In inventorying these latter categories, I have relied heavily upon information from colleagues present at the Symposium, and I have attempted to discuss these results in general categories below.

2. RIVER INPUTS AND EFFECTS

This area has received considerable attention during CICAR; a major share of the efforts were directed toward the effects of the Amazon River. This is understandable in view of the vast amount of water which this river discharges, i.e., between 20 and 30 percent of the freshwater input to the Atlantic Ocean. During this Symposium Bennekom and Tijssen (1977) presented results concerning nutrient contributions from the Amazon to the Guyana shelf waters and their effect upon primary productivity in that area. Betzer et al. (1977) have demonstrated the significant effects of both the Orinoco and Amazon outflows upon suspended clays, carbonates and organic matter in the eastern Caribbean and adjacent western Atlantic. Fanning and Pilson (1973) have demonstrated the lack of inorganic processes which remove dissolved silica in the estuaries and nearshore water of both the Amazon and Mississippi Rivers, and Milliman and Boyle (1975) have described the biological uptake of dissolved silica in the Amazon Estuary. Work carried out by Edmond within the Amazon Estuary and River during 1976 should yield more knowledge on this important source area. Stevens and Brook (1972) have demonstrated the effect of Amazon discharge upon the salinity and silicate relationships near Barbados, and Froelich and Atwood (1977) have described its effects on the salinity/silicate structure of the upper 400 m of the eastern Caribbean. They have postulated that 68 percent of the seasonal freshwater inputs to the Caribbean are from the Amazon, and that these effects are noticeable as far west as Jamaica. Elsewhere, Carder and Schlemmer

(1973) have described nepheloid material found in the subtropical underwater in the Gulf of Mexico which is probably Amazonian in origin. Gibbs (1970, 1972, 1976) has described the water chemistry of the Amazon River itself, particularly the mechanisms by which it transports elements and sediment to the nearby North Atlantic Ocean.

Less is known about the Orinoco River's effects, and still less is known about the Magdalena River's contributions.

3. CARIACO TRENCH

Since its discovery by Worthington in 1954 and the description of its chemistry by Richards and Vacarro (1956), the Cariaco Trench has intrigued chemical oceanographers because of the anoxic processes occurring within it. Notable progress has been made toward understanding the processes occurring within this trench since the beginning of CICAR. Fanning and Pilson (Fanning, 1972) developed a model for the trench which describes its sulphate, phosphate and silicate distributions. In a paper submitted to this conference, Jeffrey and Gershey (1977) demonstrated that organic matter within the trench was not enriched, but that its composition was different by comparison to that of a nearby oxygenated basin. Okuda (1977), in another CICAR-II paper, described the nutrient, oxygen and temperature relationships of the upper waters of the trench and adjacent areas. Additional work on samples of deep trench waters which were collected by R/V TRIDENT during 1974, work which is now in progress, should do much to increase our understanding of anoxic processes.

4. DEEP BASIN WATERS

The first CICAR Symposium (1968) included important discussions of the deep hydrography of Caribbean basins, notably Worthington's (1971) discussion of the potential temperature regime at the Windward and Jungfern sills. Extensive progress has been made in this area during CICAR. Stalcup et al. (1975) and Sturges (1975) have succeeded in quantifying the sporadic inflow over the Jungfern sill from the Atlantic to the deep Venezuelan basin as being about $50 \times 10^3 m^3$sec. Froelich and Atwood (1974) demonstrated that this inflow was also evidenced by parcels of low silicate water near the Puerto Rico serial station (17°36'N, 67°00'W). Atwood et al. (1977), in a paper presently in press, have demonstrated that this inflow creates a gradient in deep dissolved silicate concentrations across the entire Venezuela Basin which is commensurate to the amount of net inflow measured. Fanning (1976), in a paper presented to the CICAR-II Symposium, described the flux of silicates from deep Caribbean and Gulf of Mexico basin sediments and postulated that this flux controls deep silicate concentrations. Using this result, he postulated the following residence times or flushing rates for the major basins: Venezuela and Colombian, 200 years; Cayman, 30 years; Gulf of Mexico, 100 years. Papers presently in preparation by Stalcup and Metcalf on data collected from R/V KNORR at the Windward sill in 1974 (Metcalf et al., 1974) should contribute extensively to our knowledge concerning input to deep basins of the western Caribbean.

5. SUSPENDED MATERIAL

Besides the work mentioned above, which describes suspended matter of Amazon and Orinoco origin, other extensive progress has been made. Bassin et al. (1972) described the suspended matter in the Caribbean Sea, and Ichiye et al. (1972) described the mechanisms by which it diffuses. Betzer et al. (1977) described seasonal patterns in suspended calcium carbonate during the wet and dry seasons within the eastern Caribbean.

6. UPPER WATERS

Significant progress made in the study of upper circulation of the Caribbean and Gulf of Mexico, which was described in the physical oceanographic sessions of the CICAR-II Symposium, is of invaluable aid to chemical oceanographers. The eastern Caribbean inputs and flows are beginning to be understood as is the movement of water out of the Caribbean to the Gulf of Mexico and the transport of these waters to the western Gulf in loop-derived eddies. Chemical contributions to this progress have included the description by Kimard et al. (1974) of 18° Sargasso Sea Water in the eastern Caribbean and Berberian and Starr's (1977) use of nutrient/salinity relationships to describe circulation in the Cayman Sea and Gulf of Mexico.

7. OTHER PROGRESS

The distribution of dissolved organics has received little attention anywhere, and CICAR has been no exception to this neglect. During the first CICAR Symposium, Linnenbon and Swinnerton (1971) described C_1 to C_4 dissolved hydrocarbons in the Caribbean and the influence of diurnal variations on their distribution. More recently, Brooks and Sackett (1973) described the distribution of these substances in the Gulf of Mexico and demonstrated that these have extensive anthropogenic sources, e.g.: seaport activities, refineries, and offshore petroleum production operations. Botello et al. (1977), at this conference, described efforts to obtain baseline data on organic occurrences in undisturbed coastal lagoons prior to development near the Mexican coast, and Cedeño Fermín (1977) described the distribution of dissolved carbohydrates in the eastern Caribbean and Gulf of Paria. Jimenez et al. (1977) described large surface active molecules in the eastern Caribbean which affect algal adhesion.

Trace and heavy metal distributions in the Caribbean and Gulf of Mexico have received even less attention. One paper in this conference by Forester et al. (1977) described initial investigations of the occurrence of the first few transition metals, i.e., cadmium, and certain radionuclides in Caribbean waters and plankton.

In the first CICAR Symposium, Andersen (1970, 1971) described work on strontium/chlorinity ratios in the Caribbean and postulated that these ratios might be specific for various water cores. Since that time, Atwood et al. (1973) have demonstrated that there is no such variability in Ca/Cl% and Mg/Cl% ratios. Yet a possibility does exist for Sr/Cl% even though methods which were accurate and precise enough to test this hypothesis were not then available. Isotope dilution methods now available for analysis of Sr should allow for such testing.

8. RECOMMENDATIONS

The American Mediterranean is especially suited to the study of numerous basic chemical oceanographic problems. It is a defined marginal sea composed of a series of interconnected basins with both oceanic and terrestrial inputs. Future research should be designed to use this unique situation in the study of marine chemical processes. It is especially relevant that the physical oceanography of the system be quite well defined in order to allow the chemical oceanographer to plan his experiment and interpret his data with greater ease. We have made considerable progress in this area, especially in the western Caribbean, the Gulf of Mexico, and the passages of the Greater and Lesser Antilles; but more needs to be done. The terrigenous inputs to the system come mostly from four major rivers: the Amazon, Orinoco, Magdalena and Mississippi. Of these, only the Amazon input has been investigated to any degree, and surprisingly, more is known about the inputs from the Amazon and the Orinoco than the Mississippi inputs. Very little is known about the Magdalena inputs even though this river has the greatest potential of the four for transporting suspended material to the deep Caribbean basins. Pulido (1969) of Colombia reported 17 cable breaks near the Magdalena delta over a 26-year period, indicating extensive turbidite inputs. The four rivers drain a variety of terrains. These terrains vary drastically in the extent of their anthropogenic inputs; an understanding of this is necessary before any meaningful pollution monitoring can be initiated.

We should not only address ourselves to the problems of these river inputs, but also to the entire problem of sources and fluxes within the Caribbean, particularly the different chemistries of the deep basins and the processes controlling them. This should include studies of the rates of dissolution of various particulate matter in surface waters, particularly silicate and the extent of remineralization occurring throughout the water column and in the sediments.

Although we are beginning to understand the distribution of dissolved silica in the American Mediterranean, as well as the processes controlling it, we know very little about marine chemical processes in which other micronutrients such as phosphate and nitrate, which are much more important to living resources, play a role. This should be considered in future programmes. However, in this subject area, as in all chemical processes, an effort must be included to understand the effect of the biosphere on the physical chemical system and vice versa. For example, there are currently no comprehensive data on primary production in the open Caribbean Sea.

One aspect which has been almost completely neglected from a chemical standpoint is the effect of catastrophic events such as hurricanes, a meteorological feature unique to the area. Hurricanes have extensive effects on water movement, flushing of shelves and coastal regions and movement of shelf sediments. To study the effects of these events would require local quick response vessels and extensive international coordination.

One of the programmes suggested for IOCARIB by the Puerto Rico meeting of experts is a dynamical chemical model of the American Mediterranean. In concept, this is a vast programme which could be never-ending. It is important to note, however, that such a model is a goal, not a programme itself. Steps toward this goal can be taken in manageable pieces. In approaching this goal, investigators should pay particular attention to the four major river systems, interbasin differences and the processes causing them, the restricted circulation within basins, and the impact of both suspended and bottom sediment on basin water chemistry. A proposed study of the Orinoco outflow and its effects on the southeastern Caribbean and Gulf of Paria might be considered as one of the first "manageable" steps. Similar programmes should be generated for the Magdalena and Mississippi outflows as well as other parts of the system, such as the Venezuela and Guajira upwellings.

The need for interdisciplinary seminars which focus on reasonably sized geographic areas in developing such programmes is clearly indicated.

9. ACKNOWLEDGEMENTS

The author gratefully acknowledges the suggestions and assistance of Drs. Peter R. Betzer, Kent A. Fanning, Neil R. Andersen and Mark Wimbush.

10. REFERENCES

Andersen, N.R., J.D. Gassaway and W.E. Maloney, The relationship of the strontium/chlorinity 1970 ratio to water masses in the tropical Atlantic Ocean and Caribbean Sea. Limnol. Oceanogr., 15:467-72

Andersen, N.R. and J.R. Jadamec, Strontium and barium distributions in the Caribbean Sea. 1971 In Unesco/FAO Symposium on Investigations and Resources of the Caribbean Sea and Adjacent Regions, Willemstad, Curaçao, 18-26 Nov.1968. Paris, Unesco, pp.15-22

Atwood, D.K., P.N. Froelich and W.F. Kinard, Temporal and depth study of alkaline earth 1973 chlorinity ratios in seawater at a single station south of Puerto Rico. Limnol. Oceanogr., 18:771-83

Atwood, D.K. et al., Deep silicate content as evidence of the extent of renewal of 1978 Venezuela Basin Water. Submitted to Deep-Sea Res.,

Bassin, N.J., J.E. Harris and A.H. Bouma, Suspended matter in the Caribbean Sea: a 1972 gravimetric analysis. Mar.Geol., 12:M1-M5

Bennekom, A.J. van and S.B. Tijssen, Nutrients on and off the Guyana shelf related to 1978 upwelling and Amazon outflow. FAO Fish.Rep., (200)Suppl.

Berberian, G.A. and R.B. Starr, The circulation of the Cayman Sea and the Gulf of Mexico
1978 as deduced from nutrient distributions. FAO Fish.Rep., (200)Suppl.

Betzer, P.R. et al., The sources, movements, and reactions of suspended clays, carbonates,
1976 and organic matter in the eastern Caribbean Sea during the wet and dry seasons. Proceedings of CICAR-II Symposium on Progress in Marine Research in the Caribbean and Adjacent Regions, Caracas, Venezuela, 12-16 July 1976

Betzer, P.R. et al., Seasonal patterns in suspended calcium carbonate concentrations during
1977 the dry and wet seasons in the eastern Caribbean. In Fate of fossil fuel CO_2 in the atmosphere/ocean system, edited by N.R. Andersen. New York, Plenum Press

Botello, A.V., E. Hicks and E.F. Mandelli, Estudios preliminares sobre los niveles de algunos
1978 contaminantes en la Laguna de Terminos, Campeche, México. FAO Fish.Rep., (200) Suppl.

Brooks, J.M. and W.M. Sackett, Sources, sinks and concentrations of light hydrocarbons in
1973 the Gulf of Mexico. J.Geophys.Res., 78:5248-58

Carder, K.L. and F.C. Schlemmer, III, Distribution of particles in the surface waters of
1973 the eastern Gulf of Mexico: an indicator of circulation. J.Geophys.Res., 78: 6286-99

Cedeño Fermín, G., Carbohidratos disueltos en aguas de la región nor-oriental de Venezuela.
1978 FAO Fish.Rep., (200)Suppl.

Fanning, K.A., Studies on dissolved silica at the boundaries of the ocean system. Ph.D.
1972 Thesis, Graduate School of Oceanography, University of Rhode Island, Kingston, R.I., U.S.A.

__________, Dissolved silica in the American Mediterranean. FAO Fish.Rep., (200)Suppl.
1978

Fanning, K.A. and M.E.Q. Pilson, The lack of inorganic removal of dissolved silica during
1973 river-ocean mixing. Geochim.Cosmochim.Acta, 37:2405-15

Forster, W.O. et al., Radionuclide and trace element associations with plankton and possible
1976 vertical transport mechanisms in the Caribbean. FAO Fish.Rep., (200)Suppl.

Froelich, P.N. and D.K. Atwood, New evidence for sporadic renewal of Venezuela Basin water.
1974 Deep-Sea Res., 21:969-75

__________, Influence of the Amazon and Orinoco River discharge on surface salinity and
1978 dissolved silicate concentration in the Caribbean Sea. FAO Fish.Rep., (200) Suppl.

Gibbs, R.J., Circulation in the Amazon River Estuary and adjacent Atlantic Ocean. J.Mar.
1970 Res., 28:113-23

__________, Water chemistry of the Amazon River. Geochim.Cosmochim.Acta, 36:1061-6
1972

__________, Amazon River sediment transport in the Atlantic Ocean. Geology, 4:45-8
1976

Gordon, A.I., Circulation of the Caribbean Sea. J.Geophys.Res., 72:6207-23
1967

Ichiye, T., N.J. Bassin and J.E. Harris, 1972 Diffusivity of suspended matter in the Caribbean Sea. *J.Geophys.Res.*, 77:6576-88. (See also correction to paper, *J.Geophys.Res.*, 78:3631 (1973); Comments on paper by S. Eittreim, P.E. Biscaye and A.I. Gordon, *J.Geophys.Res.*, 78:640-3 (1973); Reply to comments by T. Ichiye, *J.Geophys.Res.*, 78:6404-5 (1973))

Jacobs, M.B. and M. Ewing, 1969 Mineral source and transport in waters of the Gulf of Mexico and Caribbean Sea. *Science, Wash.*, 163:805-9

Jeffrey, L.M. and R.M. Gershey, 1978 Organic matter in the Cariaco Trench. *FAO Fish.Rep.*, (200) Suppl.

Jiménez Velez, B. *et al.*, 1978 Adhesion enhancing organics in the eastern Caribbean Sea. *FAO Fish.Rep.*, (200)Suppl.

Kinard, W.F., D.K. Atwood and G.S. Giese, 1974 Dissolved oxygen as evidence for 18°C Sargasso Sea water in the eastern Caribbean Sea. *Deep-Sea Res.*, 21:79-82

Linnenbom, V.J. and J.W. Swinnerton, 1971 Distribution of low molecular weight hydrocarbons and excess molecular nitrogen in the Cariaco Trench. *In* Unesco/FAO Symposium on Investigations and Resources of the Caribbean Sea and Adjacent Regions, Willemstad, Curaçao, 18-26 Nov.1968. Paris, Unesco, pp.125-30

Metcalf, W.G., 1959 Oceanographic data from the Caribbean Sea; CRAWFORD cruise 17, February-March 1958 for the International Geophysical Year of 1957-58. *Woods Hole Oceanogr.Inst.Ref.*, (59-9) (Unpubl.MS)

__________, 1969 Dissolved silicate in the deep North Atlantic. *Deep-Sea Res.*, 16 Suppl.: 139-45

Metcalf, W.G., M.C. Stalcup and M.E. Zemanovic, 1974 Hydrographic stations data Caribbean Sea ATLANTIS II cruise 78 and KNORR cruise 37. *Woods Hole Oceanogr.Inst.Ref.* (74-90) (Unpubl.MS)

Milliman, J.D. and E. Boyle, 1975 Biological uptake of dissolved silica in the Amazon River Estuary. *Science, Wash.*, 189:995-7

Okuda, T., 1978 Condiciones hidroquímicas de las aguas superiores de la Fosa de Cariaco y âreas adyacentes. *FAO Fish.Rep.*, (200)Suppl.

Pulido, E.R., 1969 Las obras de bocas de Ceniza, Colpuertos, Puertos de Colombia. Bogotá, Colombia, Impreso en Italgraf, 100 p.

Redfield, A.C., B.H. Ketchum and F.A. Richards, 1963 The influence of organisms on the compositio of seawater. *In* The sea, edited by M.N. Hill. New York, Wiley Interscience, vol.2:26-77

Richards, F.A., 1958 Dissolved silicate and related properties of some western North Atlantic and Caribbean waters. *J.Mar.Res.*, 17:449-65

Richards, F.A. and R.F. Vaccaro, 1956 The Cariaco Trench, an anaerobic basin in the Caribbean Sea. *Deep-Sea Res.*, 3:214-28

Ryther, J.H., D.W. Menzel and N. Corwin, 1967 Influence of the Amazon River outflow on the ecology of the western tropical Atlantic. 1. Hydrography and nutrient chemistry *J.Mar.Res.*, 25:69-83

Stalcup, M.C., W.G. Metcalf and R.G. Johnson, 1975 Deep Caribbean inflow through the Anegada-Jungfern Passage. *J.Mar.Res.*, 33 Suppl.:15-35

Stevens, D.M. and A.L. Brooks, Identification of Amazon River water at Barbados, West
1972 Indies, by salinity silicate measurements. Mar.Biol., 14:345-8

Sturges, W., Mixing of renewal water flowing into the Caribbean Sea. J.Mar.Res., 33
1975 Suppl.:117-30

Worthington, L.V., Water circulation in the Caribbean Sea and its relationship to North
1971 Atlantic circulation. In Unesco/FAO Symposium on Investigations and Resources of the Caribbean Sea and Adjacent Regions, Willemstad, Curaçao, 18-26 Nov.1968. Paris, Unesco, pp.181-91

Wüst, G. and A. Gordon, Stratification and circulation in the Antillean-Caribbean basins.
1964 Part 1. Spreading and mixing of the water types with an oceanographic atlas. New York, Columbia University Press, 201 p.

GYPSUM - ORGANIC INTERACTIONS IN TROPICAL SEAWATER
II. IDENTIFICATION OF PRECIPITATION INHIBITING ORGANICS

by

M.J. BARCELONA and D.K. ATWOOD
Marine Sciences Department
University of Puerto Rico
Mayaguez, Puerto Rico 00708

CONTENTS

1. INTRODUCTION
2. CHARACTERIZATION OF INHIBITING ORGANICS
3. CONCLUSIONS
4. ACKNOWLEDGEMENTS
5. REFERENCES

Abstract

Studies of gypsum ($CaSO_4.2H_2O$) precipitation disclose that it is at least 1 000 times more sensitive than the calcium carbonate system to organic inhibition of nucleation and crystallization. Model compounds, particularly surface active compounds, successfully inhibit gypsum precipitation at sub-ppm levels. Strong calcium ligands at 10 to 100 times the above concentrations show no effect. The results strongly suggest absorptive poisoning of gypsum crystal nuclei. The inhibiting organics have been extracted from seawater, separated into neutral and free acid fractions, and the free acid fraction shown to be more active.

The free acids associated with gypsum recently precipitated from seawater have a longer mean chain-length than those present in seawater. Gypsum samples from a salina show a branched, saturated C_{22} acid in high concentration among the free acids associated with it.

Resumen

Los estudios de la precipitación del yeso ($CaSO_4.2H_2O$) muestran que es al menos mil veces más sensible que los carbonatos cálcicos a la inhibición orgánica de la nucleación y de la cristalización. Con sus compuestos, en particular los compuestos activos de superficie, se consigue inhibir la precipitación del yeso a niveles inferiores a partes por mil. En fuertes grupos coordinadores del calcio, de diez a cien veces superiores a las concentraciones anteriores, no se ha observado ningún efecto. Los resultados indican claramente un posible envenenamiento por adsorción de los núcleos cristalinos del yeso. Se han extraido del agua del mar los materiales orgánicos inhibidores, separándolos en su fracción neutra y en su fracción de ácidos libres, y se ha observado que esta última fracción es más activa.

Los ácidos libres asociados a yeso recientemente precipitado del agua del mar tienen una longitud media de cadena mayor que la de los ácidos presentes en el agua del mar. En muestras de yeso de una salina se ha observado un C_{22} ácido saturado, ramificado, y en fuerte concentración entre los ácidos libres a él asociados.

1. INTRODUCTION

Dissolved organic compounds in seawater have been shown to affect the chemistry of major ionic constituents, notably that of Ca^{++}. The work of Chave (1965), Chave and Schmalz (1966), Chave and Suss (1970) and Meyers and Quinn (1971), has demonstrated that surface active compounds associate with clay minerals and with the calcium sites in carbonates. Kitano and Hood (1965) attempted to model these interactions by addition of known naturally-occurring compounds to calcium bicarbonate solutions. They were able to demonstrate that certain organics affected the rate of carbonate precipitation and thus allowed slow precipitation of the stable form, calcite, or more rapid formation of the unstable aragonite, or vaterite, in solutions that contained 1 000 to 10 000 mg of organic material per litre. At such levels, the addition of an organic acid, i.e. citric acid, will also disturb alkalinity and pH. Both of these parameters are fundamental to discussions of carbonate equilibria.

However, two facts seem clear: (1) calcium carbonate is apparently supersaturated in the ocean's surface water yet precipitates directly only in a few scattered environments, and, (2) authigenically precipitated carbonates have organic coatings. Our interest in the role of organics in the marine chemistry of calcium led us to the study of gypsum precipitation. Gypsum is the first major salt to precipitate from evaporating seawater. The influence of organic compounds on its solubility and precipitation behaviour have potential application to the problems of seawater desalination (Shaffer, 1967); the suitability of gypsum as a structural material (Komatsu, Yano and Katada, 1968), and, the removal of by-product gypsum in the production of super-phosphate fertilizers (J. Kepinski and Z. Szyroki, 1970).

The study of gypsum precipitation from seawater is simplified compared to the study of calcium carbonate precipitation since there is only one stable crystalline form at near-ambient temperatures; and there is no direct gaseous equilibrium or pH sensitivity involved. Preliminary work (Barcelona, Tosteson and Atwood, 1976) disclosed that chloroform extractable organics slowed or completely inhibited gypsum precipitation in artificially Ca^{++} saturated seawater.

The above workers developed a rapid titration technique which consisted of timed additions of suitable volumes (0.1-0.5 ml) of 5 M $CaCl_2$ solution to 25 ml of stirred seawater in an Erlenmeyer flask - cuvette combination. Simultaneous to the Ca^{++} addition, the percent transmittance of the sample could be read at 600 nm. The transmittance (or adsorbance) readings were then plotted versus Ca^{++} concentration. At the onset of gypsum precipitation a rapid decrease in solution transmittance occurred. The plot of percent T (or adsorbance) versus Ca^{++} added would then follow a positive sloped line. This line was extrapolated back to the concentration axis to permit quantitation of the Ca^{++} requirement to bring on precipitation. Changes in Ca^{++} requirements were interpreted as indicating the presence of more or less precipitation inhibiting organic material in the seawater. By extracting the seawater with certain solvents they were able to shift the curve toward less Ca^{++} requirement. The extent of this shift was a function of the solvent used. The most effective solvents were chloroform and di-ethyl ether.

Statistical evidence concerning the reliability of the technique for indicating changes in inhibiting organic content is contained in Fig. 1. In this figure, the results of a least-squares fit of the titration data (adsorbance vs. Ca^{++} added) on five samples from each of two locations are portrayed before and after extraction. The sample locations are shown in Fig. 2. Error bars at the 95 percent confidence level are included in Fig. 1. Fig. 1 shows that significant differences in the amount of Ca^{++} required to initiate gypsum precipitation exist between samples of subsurface seawater taken from nearshore or offshore locations as well as for the same sample before and after chloroform extraction. It is clear that the differences in the amount of Ca^{++} required before and after extraction of seawater samples are significantly greater than these standard deviations. From their oxidizability and relative solubility in seawater, chloroform and di-ethyl ether, we deduced that the precipitation inhibiting organics were lipid compounds, somewhat polar, and of less than 500 amu molecular weight. Yields of chloroform extractable material ranged from 0.05-0.10 mg/l offshore from the University of Puerto Rico Department of Marine Sciences (DCM) Marine Station in La Parguera and were as high as 1.50 mg/l in a known polluted area such as Mayaguez Bay or Guanica Bay (see Fig. 2).

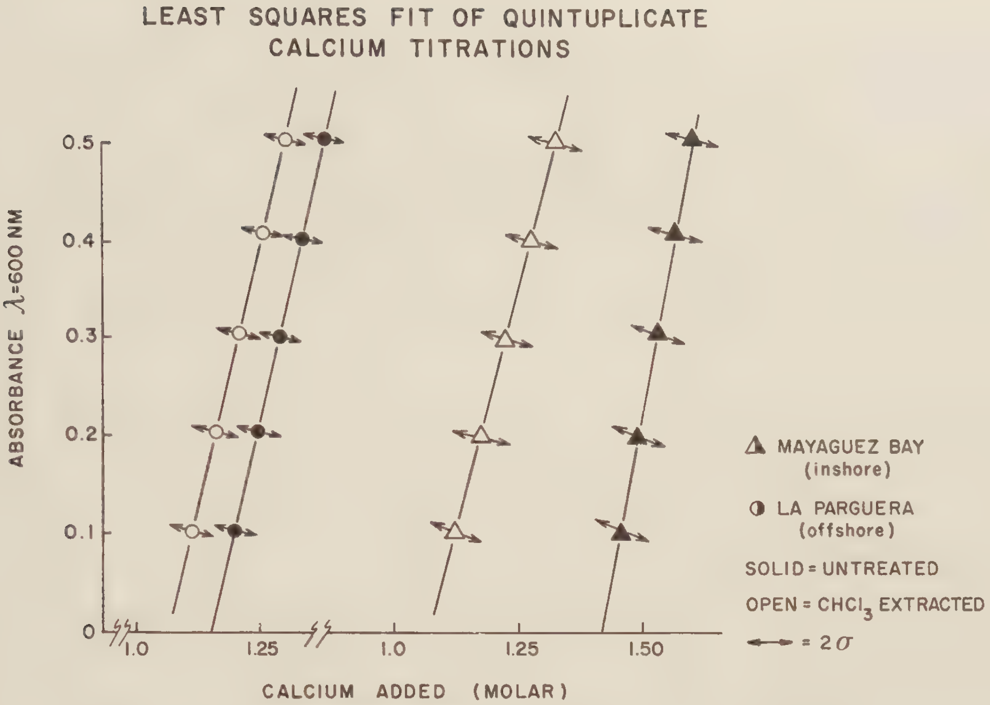

Fig. 1 Least squares fit of quintuplicate titrations

Adsorbance for timed additions of 5 M $CaCl_2$ to unextracted (solid figures) and extracted (open figures) seawater samples versus calcium concentration added. Samples are from Mayaguez Bay (triangle) and from near La Parguera, Puerto Rico, U.P.R. Marine Station (circles)

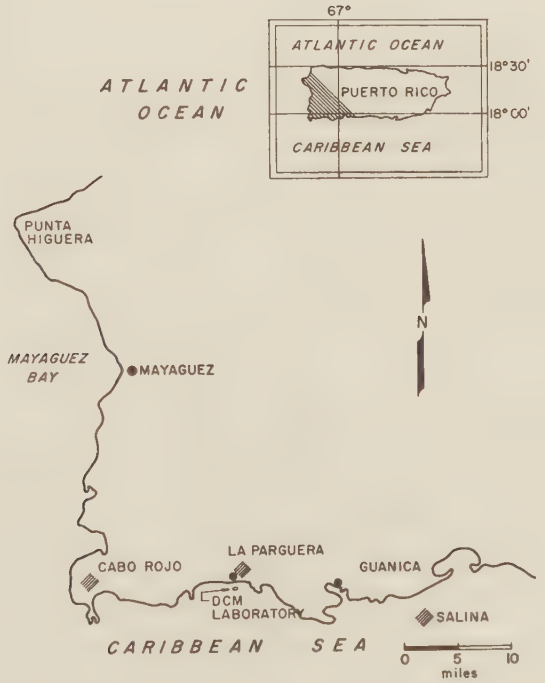
67°
ATLANTIC OCEAN
PUERTO RICO
18°30'
18°00'
CARIBBEAN SEA
ATLANTIC OCEAN
PUNTA HIGUERA
MAYAGUEZ BAY
MAYAGUEZ
N
CABO ROJO
LA PARGUERA
GUANICA
DCM LABORATORY
SALINA
CARIBBEAN SEA
0
5
10
miles

Fig. 2 Map of sampling sites

Inset of Puerto Rico as a reference to enlarged map of southwestern Puerto Rico showing sampling sites for water and gypsum samples (Scale 1:326 856 at 18°N)

2. CHARACTERIZATION OF INHIBITING ORGANICS

2.1 Effect of Synthetic Organics

In order to get an idea of the range of organics which are possibly involved in the inhibition, a series of addition experiments were performed using "model" organic compounds. Compounds selected include: strong Ca^{++} complexers (glycylglycine, Na_2 EDTA, pyruvate), general lipids (C_{12} - C_{18} fatty, succinic, malic and glutamic acids) and compounds which have either been identified in seawater, or which we felt were possible pollutant types (mannitol, inositol, glycerol, glucose, dextrose, citrate, glycolate, formate, acetate, Tergitol ^{R}, and Triton X-100 ^{R}).

Organic compounds were added in microlitre aliquots (20-30 µl) as aqueous solutions (10^{-2} to 10^{-5} M) to 25 ml of filtered seawater. The resulting organic concentrations were in the parts-per-billion[1/] and low parts-per-million range, thus within the limits we might expect for organics in coastal water. After from 5 to 15 min of agitation, a 5 ml volume of 5 M $CaCl_2$ solution was rapidly pipetted into the seawater solution and a timer was started. This addition results in a total calcium concentration of 0.84 M and the precipitation occurs within 10-20 min. The solution's transmittance was then monitored with time as described in the introduction. In this and the experiments described below, this technique was shown to be less tedious and more precise than the titration by addition of excess calcium ion as described by Barcelona et al. (1976). The above modification provides an analogous decrease in the percent transmittance as nucleation gives way to precipitation of gypsum crystals. In plotting the resulting data we continue to extrapolate the vertical line representing the decrease in transmittance back to the time (x) axis and, instead of excess Ca^{++} requirements, quantitate lag-time or time to onset of precipitation. All samples to which organics were added are compared to the average lag-time measured without organic addition (using triplicate samples).

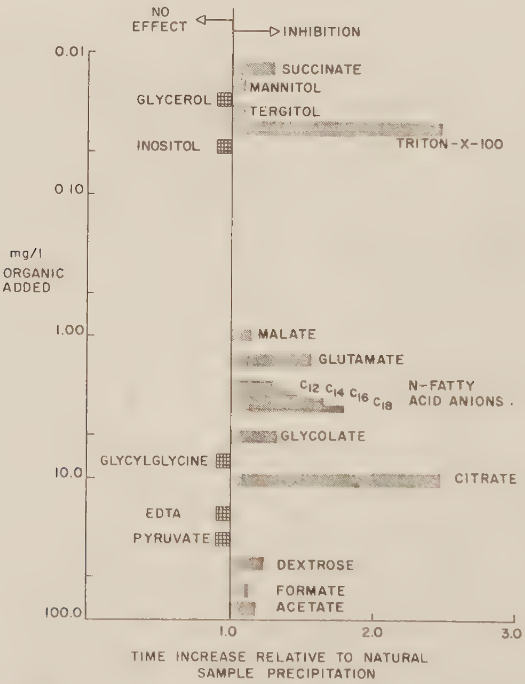

Fig. 3 Precipitation inhibition as a function of model organics

Concentration of model organics added as a function of relative increase in lag-time to gypsum precipitation. Lag-times are relative to that of untreated samples

---

[1/] Billion, in U.S. usage, equals a thousand million

Fig. 3 gives the results of these experiments. For each organic reagent added the relative increase in time to the onset of gypsum precipitation is shown as a function of the amount of that reagent added. Results plotted are the average of three runs compared to the same blank. The results indicate that certain organics can affect the rate of gypsum precipitation from seawater and at believable concentrations. The most successful organics give us a clue to the possible mechanism of inhibition as well as how to separate natural inhibitory compounds from the chloroform extractibles. We note that:

(1) di-acids, polyhydroxy compounds, and alcohols seem to be most active in inhibiting gypsum precipitation;

(2) the combination of the two functional groups, i.e. polyprotic-hydroxy acids does not materially improve the activity;

(3) inhibiting activity is not a function of calcium ion complexing tendency as strong ligands have no effect, even at concentrations in excess of 10 mg/l, and,

(4) fatty acid anions at 3-5 mg/l are effective inhibitors of gypsum precipitation. The more active anions were those of longer chain length. This leads us to postulate a surface adsorption mechanism which causes delayed nucleation of gypsum crystals.

2.1.1 Effect of natural organics

Since the effect of specific types of trace organics has been established by these laboratory experiments, it is logical to attempt identification of similarly active compounds in natural seawater. The effect of extraction on inhibition of gypsum precipitation indicates that the inhibiting compounds can be removed from the system. However, the amounts of organic materials present in seawater are minimal, particularly in the tropics and we must process large volumes of water to get enough material even to allow determination of individual classes of compounds.

2.1.2 Collection of samples

In the following discussion we will refer to several sample sites in southwestern Puerto Rico which are shown in Fig. 2. The UPR Marine Station at La Parguera is located at least 10 miles from sources of industrial pollution, but does have numerous shoreline outfalls of domestic sewage. Water samples were also collected from Guanica Bay which lies east of the Marine Station. The bay is quite enclosed and only flushed by tidal circulation. It is subjected to large inputs of pollutant organics and inorganics from a large sugar mill, a fertilizer factory, and domestic sewage from approximately 15 000 inhabitants of the city of Guanica. Samples near La Parguera were taken offshore, and in Guanica at the mouth of the bay and 1 km offshore. Water was collected from a depth of 2 m in a 10 l pyrex vessel which traverses the surface in both directions closed. A gasoline engine-powered wooden boat was used.

Gypsum samples from two salinas were collected as well. Botoncillo Salt Works near La Parguera is erratically operational owing to the area's unseasonal rains. It has a variable population of brine shrimp and scattered blue green algal mats in deposit ponds which have a salinity of less than 150 per mille. The second salina sampled is in a more arid part of southwestern Puerto Rico and is run by Cabo Rojo Enterprises. Here, the brine shrimp densely populate the water in ponds of less than 200 per mille salinity. This salina also has a very extensive algal mat in its deposit ponds, and the operation is more efficient than at the Botoncillo facility because the area receives < 25 cm of rainfall per year (Cabo Rojo Enterprises' estimate). One to two kg of gypsum samples were collected from these two salinas by shovel, after scraping off overlying NaCl. The samples were examined by optical microscopy and sulphate contents were analysed gravimetrically (as $BaSO_4$) to ensure a gypsum content of > 96 percent.

2.1.3 Separation of natural organics from seawater

The experiments described below were designed to identify the more active fraction in the chloroform extractible matter from seawater. Three 10-l samples were collected from a depth of 2 m offshore from the University of Puerto Rico's Marine Station in La Parguera. The samples were filtered (Whatman No. 54 at < 635 mm Hg vacuum) within 30 min after collection. Five ml of 5 M $CaCl_2$ were rapidly added to a 25 ml aliquot of each sample in turn and the precipitations monitored as described above. Eight litres of each remaining sample were twice extracted with chloroform in a pyrex vessel. Agitation was provided by an electrically driven glass rod and teflon paddle. Gypsum precipitation was similarly initiated and monitored in an aliquot of each sample after extraction.

The chloroform extracts obtained from these samples were individually taken to dryness in a rotary evaporator (Rotovap R, Buchi, Rinco Instruments) at 40°C and < 635 mm Hg vacuum. The residues were redissolved in chloroform to 10 ml volume. Five millilitres of the total extract were used for experiments in which total organics were added to seawater. The remaining 5 ml were separated into neutral and free-acid fractions according to the scheme in Fig. 4, which also reviews the preceding sample treatment.

The neutral fractions generally showed colour (pale yellow) and showed visible light adsorption at 650-680 nm. The acid fractions were colourless, represented 64 percent ± 20 percent of the total extract and showed an adsorption maximum at 283 nm. Spectra were measured in $CHCl_3$ versus $CHCl_3$ reference with a Beckman DB scanning spectrophotometer). These neutral and free-acid fractions were also used in addition experiments described below to determine their effects on gypsum precipitation.

In the addition experiments a microlitre syringe was used to add the necessary total extract, free-acid or neutral fraction to the flask-cuvette combination. The chloroform solvent was first evaporated in a stream of filtered nitrogen prior to addition of 25 ml of filtered, extracted seawater. After mixing, 5 ml or 5 M $CaCl_2$ solution was rapidly added. In each case precipitation lag-times were compared to those observed for the untreated sample without organic addition. All samples were done in triplicate.

2.1.4 Results of addition of various natural organic fractions to seawater

The results of the total extract, free-acid and neutral fractions additions to extracted seawater are shown in Fig. 5 as the average of three runs. In this figure the relative percent increase in precipitation lag-time is plotted versus the particular type of addition made. Additions were made at integral multiples of a sample's original total organic neutral or free-acid content based on the fact that first we extracted a known volume of seawater and the sample used for the precipitation experiment was 25 ml. The addition of organics extracted from natural seawater to extracted seawater results in a very nearly the same lag-time observed in an untreated sample. A definite inhibitory effect is noted for addition of up to twice the original amount present prior to extraction. However, addition of greater than that amount does not greatly increase the lag-time to precipitation. The 'plateau' in activity indicated may be interpreted in terms of an adsorptive mechanism of delayed nucleation. Once the available sites of organic inhibition have been saturated, further addition may be expected to cause little or no increased times. Since Fig. 5 illustrates that the free-acid fraction is active in inhibiting gypsum precipitation and is nearly twice as active as the neutral fraction, we concentrated our efforts on the free-acid fraction in further work.

SCHEME OF SAMPLE TREATMENT IN ACTIVE-FRACTION EXPERIMENTS

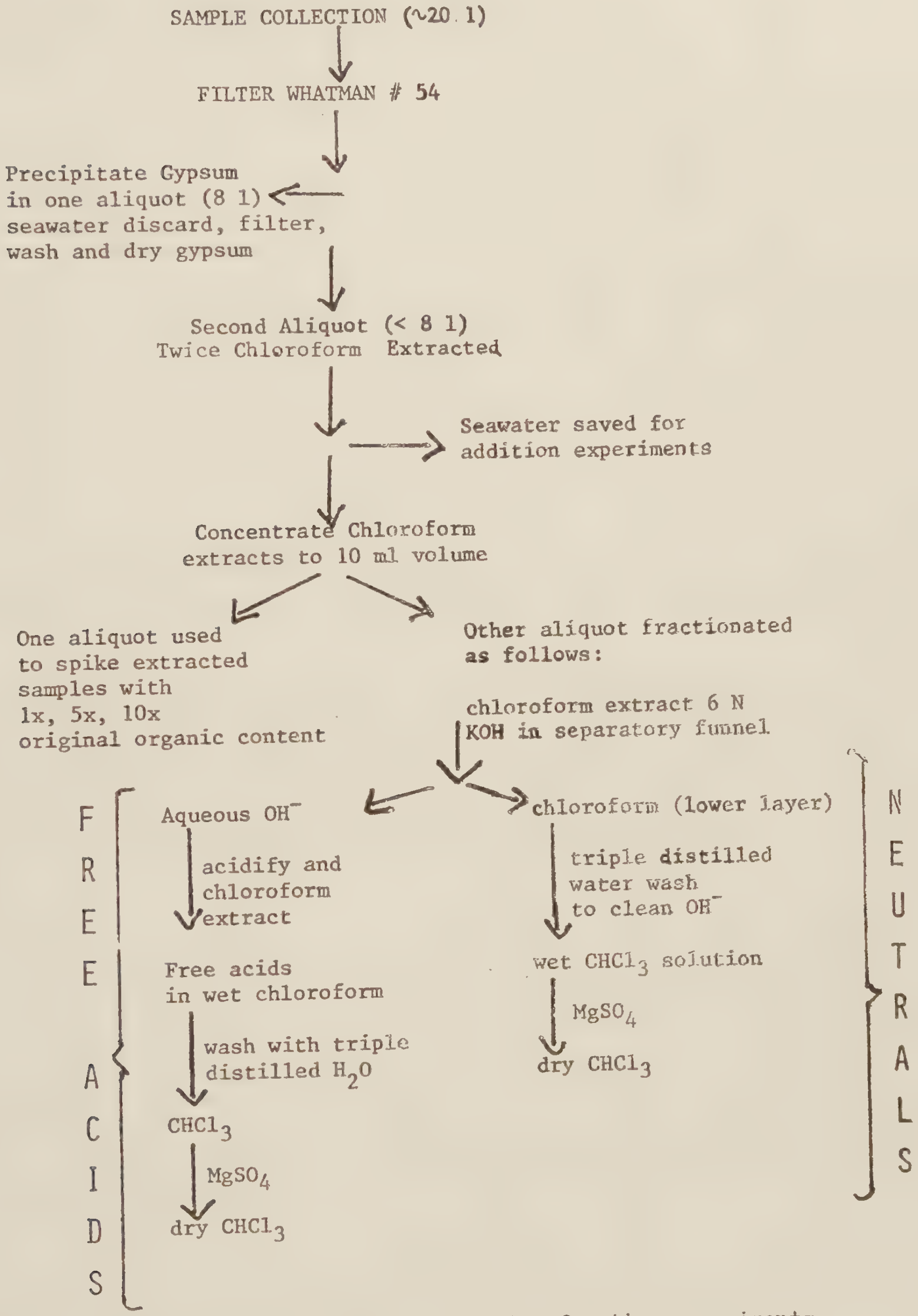
SAMPLE COLLECTION (~20 l)
FILTER WHATMAN # 54
Precipitate Gypsum in one aliquot (8 l) seawater discard, filter, wash and dry gypsum
Second Aliquot (< 8 l) Twice Chloroform Extracted
Seawater saved for addition experiments
Concentrate Chloroform extracts to 10 ml volume
One aliquot used to spike extracted samples with 1x, 5x, 10x original organic content
Other aliquot fractionated as follows:
chloroform extract 6 N KOH in separatory funnel
Aqueous OH$^-$
acidify and chloroform extract
Free acids in wet chloroform
wash with triple distilled H_2O
$CHCl_3$
$MgSO_4$
dry $CHCl_3$
chloroform (lower layer)
triple distilled water wash to clean OH$^-$
wet $CHCl_3$ solution
$MgSO_4$
dry $CHCl_3$
FREE ACIDS
NEUTRALS

Fig. 4 Scheme of sample treatment in active-fraction experiments

Scheme of sample collection and treatment for addition of natural organics to seawater. The figure includes the fractionation scheme of chloroform extracts as well

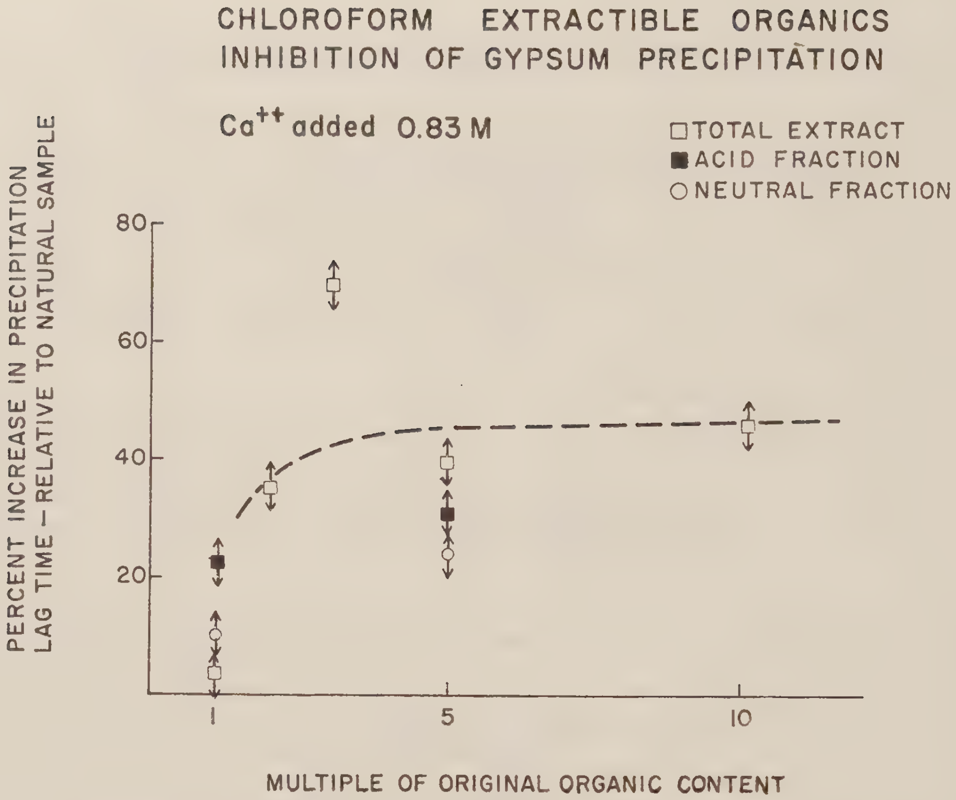

Fig. 5 Percent increase in precipitation lag-time as a function of multiple additions of organics

Percent increase in lag-time to gypsum precipitation versus the multiples of original organic content added. Results are plotted for addition of total extractible organics (open squares), free-acid fraction (solid squares), and neutral fraction (open circles), to extracted samples. All lag-time increases are relative to untreated samples. Multiples of organic content added were determined by dilution in sample of a known volume from total extract or fraction solutions.

2.1.5 Characteristics of active free acids

Our intent was to separate and characterize the major components of the free acid mixture from the following sources: (1) seawater; (2) gypsum precipitated from seawater in the laboratory, and, (3) gypsum recently deposited in the salinas.

We postulate adsorptive inhibition of gypsum crystal nucleation for the delayed precipitation in the presence of these organics. Presumably then, the organics should remain with the precipitated solid. The salina samples should provide us the best chance of isolation of the active compounds since gypsum is available there in large amounts. Since the separation and analysis of non-volatile fatty acids from seawater and minerals has been well described (Parker, 1969; Meyers and Quinn, 1971; Meyers, Quinn and Marshall, 1974) the techniques will be only briefly outlined here. Nine 20-l seawater samples were collected near Guanica Bay and filtered as described before. Two aliquots (8 litres each) were taken from each sample. One was chloroform extracted and the extract concentrated as before. The other was Ca^{++} saturated (using chloroform - extracted 5 M $CaCl_2$), agitated for 48 h and the solid then allowed to settle. The mother liquor was decanted and the gypsum collected on a glass fibre filter (Gelman AE).

The gypsum samples ($\sim$0.3 g/l) were washed twice with cold methanol and air dried. They were then dissolved in a minimal volume of hot (60°C) 5 percent HCl and the resulting solutions were twice extracted with chloroform. Three samples of gypsum from each salina were taken as described previously. The crystals were crushed in a mortar and pestle and sieved to pass 200 mesh. They were then washed twice with portions of chloroform and methanol, and air dried. They were finally dissolved in hot 5 percent HCl, as were the laboratory precipitates, and similarly extracted.

The concentrated extracts from the seawater, the gypsum precipitated from seawater in the laboratory, and the salina precipitates were fractionated as described in Fig. 4. The neutral fractions were saponified and saved for future analyses. The free-acid fractions were evaporated to dryness (60°C) in scrupulously clean culture tubes that had teflon-lined screw caps. Solvent and procedural blanks as well as $C10$, C_{12}, C_{14}, C_{16}, C_{18}, C_{20} fatty acid standards were similarly treated. The samples, blanks and standards were esterified in 14 percent BF_3/MeOH, at 100°C for ten minutes, hexane extracted, evaporated to 1 ml volume and dried with $MgSO_4$. The methyl esters were analysed by GLC using a Varian 2700 gas chromatograph with N_2 carrier gas, and with electrolytic H_2 (Elhygen, Varian Assoc.) and filtered compressed air supplied to the flame ionization detector. The stainless steel column was 1.6 m x 3.1 mm packed with 3 percent SE-30 on 100/200 mesh Varaport 30. The runs were temperature programmed, after two minutes isothermal at 100°C, at a rate of 10°C/min to 280°C. Standards and blanks were run at least twice at the beginning, once at intervals of 5 samples and at the end of analytical periods. Retention time analysis was used to identify the fatty acids in samples relative to the standards.

Unequivocal analysis is very difficult for organics in the marine environment. At all times we have attempted to maintain compounds in their natural state, thus the solvent extraction and fractionation were performed under mild conditions. However, the quantitative esterification using BF_3/MeOH is known to cause rearrangements in unsaturated, hydroxy or epoxy acids (Morrison and Smith, 1964).

We are fortunate to have uncovered a pattern in the free-acid results that narrows the avenue of search for the active compounds. The weight percentages of free-fatty acids at each carbon number were computed for all samples. The results for the seawater acids were averaged to obtain an average weight percent at each carbon number per sample. The acids associated with the laboratory-precipitated gypsum were similarly treated. Table 1 contains the following data: the mean carbon number based on the weight percent at each carbon number analysed, the standard error of this mean (S_x), the standard deviation (S) and the variance (S^2). Additional values calculated from previously published data are included for comparison. A significant difference seems to exist with longer chained acids being associated with the gypsum precipitates that were extracted from seawater. To test rigorously whether this trend is real we calculated the probability of observed differences in mean carbon number arising by chance on a total sample basis using a simple T test. The numbers of samples involved were $N = 9$ for the seawater samples, $N = 9$ for the precipitated gypsum samples and $N = 6$ for the salina samples. Intercomparison of the seawater analyses with those of any of the solid samples disclosed that the probability of the differences in mean carbon number arising by chance is < 0.05. Furthermore, the mean carbon number of the acids associated with laboratory precipitated gypsum is statistically undistinguishable from that found in the salinas. Thus it seems that of the fatty acids in seawater, the longer chained ones are most apt to inhibit gypsum precipitation. The C_{19} - C_{22} free fatty acids in the salina samples were most heavily centred at $\sim C_{22}$. This designation is approximate as our retention time versus carbon number calibrations are accurate to ±1 carbon number (n) for $(n) > 20$.

The component eluted at n-C_{22} fatty acid ester was the best candidate for further characterization. Thin layer chromatography, on Sil Gel G (2 percent $AgWO_3$) developed ascending in n-hexane/di-ethyl ether/acetic acid 70/30/2 v/v/v, was utilized to establish whether the $\sim C_{22}$ component travelled with its saturated homologs, indicating that it, too, is saturated.

TABLE I

Results of free fatty-acid assay of marine samples

Sample	Location	Mean Carbon Number ± S_x	S	S^2	Average Concentration	% of Extractables	Ref.
Seawater	Guanica Bay, PR	16.89 ± 0.20	1.96	3.8	4.1 µg/l	1	a
Gypsum	Precipitated from above seawater	19.57 ± 0.30	2.98	8.8	13 mg/kg	84	a
Gypsum	Botoncillo Salina La Parguera, PR	20.76 ± 0.24	2.43	5.9	6 mg/kg	70	a
Gypsum	Cabo Rojo Salina Cabo Rojo PR	21.64 ± 0.16	1.15	5.3	19 mg/kg	50	a
Seawater (sub-surface)	Grand Cayman	15.21 ± 0.21	2.12	4.5	...	...	b
Seawater (sub-surface ?)	Surface 25°18'N, 85°18'W	16.56 ± 0.17	1.66	2.8	...	...	c
Zooplankton	Galveston Bay	17.72 ± 0.22	2.06	4.2	...	...	c

a = this work
b = Meyers (1975)
c = Slowey, Jeffrey and Hood (1962)

To establish the nature of the carbon chain involved, a urea adduction was performed on the methyl esters. Both fractions, the normal (adducted into urea crystals) and branched (excluded by urea crystals) were re-injected. The component of interest (~ C_{22}) only appeared in the urea excluded or branched fraction. The fraction eluting at this retention time was recovered in a combination KBr disk die/GC fraction collector (Barnes Engineering) and subsequently investigated by IR spectrometry.

The infra-red spectrum showed the following strong absorptions: C-H stretch (2 925-2 855 cm^{-1}); CH_3-CH_2-ester $R-\overset{O}{\overset{\|}{C}}-O-R$ stretch-bend (1 730-1 715 cm^{-1}), and, CH_3-wag-split indicating extensive methyl branching (1 360-1 380 cm^{-1}). From this information we conclude that the major free acids in the salina gypsum are long chain, branched saturated fatty acids. A sample of the GLC eluate of ~ C_{22} has been submitted for mass spectral analysis and results are not yet available.

3. CONCLUSIONS

Natural organics that inhibit the precipitation of gypsum in artificially saturated systems have been extracted from seawater. The effect of addition of known organics to seawater indicates that these active compounds may be fatty-acid anions. Natural chloroform-extractable organic matter from seawater has been separated into free acid and neutral fractions based on solubility in aqueous base. The free acid fraction has proven to be more active in inhibiting gypsum precipitation than its neutral counterpart. C_{14} to C_{22} fatty acids are demonstrably present in seawater, in gypsum precipitated from seawater in the laboratory and in gypsum collected in salt works. The mean chain lengths of the n-fatty acids associated with gypsum precipitation are slightly longer (C_{20}-C_{22}) than those separated from seawater (~ C_{17}). One component of the fatty-acid mixture from gypsum precipitated by solar evaporation of seawater has been characterized as a branched, saturated C_{22} acid. Its presence in the gypsum of the more biologically productive of the two salinas sampled may be linked to components of brine shrimp lipid tissue.

If the inhibiting activity of trace organics could be enhanced it may aid in the control of scaling in boilers of desalination plants. The efficient production and utilization of gypsum as a by-product in the solar sea salt industry may depend on the elimination of neighboring sources of surface-active organic materials.

4. ACKNOWLEDGEMENTS

This work has been supported by the Comité de Investigaciones of the University of Puerto Rico, Recinto Universitario Mayaguez. The authors would like to express their thanks to Ms. Helen Becker for typing the manuscript, and to Ms. Evangelina Fradera de Hernandez for drawing the figures. Further thanks are due to Dr. Michael Reck, Department of Humanities, University of Puerto Rico, Rio Piedras, for translating the Japanese reference.

5. REFERENCES

Barcelona, J.J., T.R. Tosteson and D.K. Atwood, Study of organic-calcium interactions: gyp-
1976 sum precipitation in tropical surface waters. Mar.Chem., 4:89-92

Chave, K.E., Carbonates: association with organic matter in surface seawater. Science, Wash.,
1965 148:1723-4

Chave, K.E. and R.F. Schmalz, Carbonate-seawater interactions. Geochim.Cosmochim.Acta,
1966 30:1037-48

Chave, K.E. and E. Seuss, Calcium carbonate saturation in seawater: effects of dissolved
1970 organic matter. Limnol.Oceanogr., 15:633-7

Kepinski, J. and Z. Szroki, Effect of surface active agents on the rate of growth and shape
1970 of gypsum crystals in the manufacture of 'wet-phosphoric' acid. Pr.Nauk Wyzsz. Szk.Ekon.Wroclaw, 23:123-8

Kitano, Y. and P.W. Hood, The influence of organic material on the polymorphic crystalliza-
1965 tion of calcium carbonate. Geochim.Cosmochim.Acta, 29:29-41

Komatsu, M., S. Yano and K. Kotada, The influence of organic matters on the gypsum produced
1968 from sea-salt. Sekko To Sekkai (Gypsum and Lime), 97:18-24

Meyers, P.A., Dissolved fatty acids in seawater from a fringing reef and a barrier reef at
1976 Grand Cayman. Limnol.Oceanogr., 21:315-9

Meyers, P.A. and J.G. Quinn, Fatty acid-clay mineral association in artificial and natural
1971 seawater solutions. Geochim.Cosmochim.Acta, 35:628-32

Meyers, P.A., J.G. Quinn and N. Marshall, A method for analysis of fatty acids in coral.
1974 Limnol.Oceanogr., 19:846-8

Morrison, W.R. and L.M. Smith, Preparation of fatty acid methyl esters and dimethyl-acetals
1964 from lipids with boron fluoride-methanol. J.Lipid Res., 5,(4):600-8

Parker, P.L., Fatty acids and alcohols. In Organic geochemistry, methods and results, edited
1969 by G.E. Eglinton and M.T.J. Murphy. New York, Springer-Verlag, chapter 14:357-73

Shaffer, L.H., Solubility of gypsum in seawater and seawater concentrates at temperatures from
1967 ambient to 65°C. J.Chem.Eng.Data, 12(2):183-9

Slowey, J.F., L.M. Jeffrey and D.W. Hood, The fatty acid content of ocean water. Geochim.
1962 Cosmochim.Acta, 26:607-16

NUTRIENTS ON AND OFF THE GUYANA SHELF RELATED TO UPWELLING AND AMAZON OUTFLOW

by

A.J. VAN BENNEKOM and S.B. TIJSSEN
Netherlands Institute for Sea Research
P.O. Box 59, Texel
The Netherlands

CONTENTS

1. INTRODUCTION
2. METHODS
3. CHEMISTRY OF THE OCEANIC WATER COLUMN
4. COASTAL UPWELLING
5. CHEMISTRY OF AMAZON PLUME
6. ACKNOWLEDGEMENTS
7. REFERENCES

Abstract

The distribution of PO_4-P and H_4SiO_4 in a 2 300 km long section from the Guyana Basin to the Venezuela Basin is related to the watermasses present in the vertical profile. Silicate content distinguishes deep waters in two basins while alternating maxima and minima in phosphate slightly below the core layer of Sub-Antarctic Intermediate Water are related to the transport velocity in that layer. The various surveys show frequent upwelling on the Guyana shelf especially near 55°W. The upwelling water comes from depths of 70 to 140 m, the upper part of the thermocline, where the nutrient concentrations are only slightly higher than in surface waters. Upwelling cannot fully explain the nutrient distribution because the concentrations increase toward the coast. In the turbid nearshore zone a characteristic water type with high salinity, low oxygen and high silicate content is found near the bottom. Probably, part of the phosphate mineralized from plankton remains,and accumulated by the current pattern, is inorganically absorbed on the suspended minerals.

The Amazon River has higher nutrient concentrations than the typical surface water in the tropical Atlantic. Phosphate, nitrate and variable part of the silicate are quickly consumed by primary production. Amazon outflow, upwelling and nearshore mineralization give a basis for understanding the complicated pattern of primary productivity on the Guyana shelf, discussed by Cadée (1975) from results obtained during the same cruises.

Resumen

La distribución de fosfatos y silicatos en una sección de 2 300 km de longitud que va desde la cuenca de Guyana a la cuenca venezolana, depende de las masas de agua situadas en su vertical. Las aguas profundas de ambas cuencas se distinguen por su contenido en silicatos, mientras que los máximos y mínimos de contenido de fosfatos, que se observan ligeramente debajo de la capa central de las aguas subantárticas intermedias, dependen de la velocidad de transporte en esa capa.

En varios reconocimientos se han observado frecuentes afloraciones en la plataforma continental de Guyana, especialmente cerca de los 55° O. El agua aflora procede de profundidades de 70 a 140 m, que es la parte superior de la termoclina, donde las concentraciones

de nutrientes son sólo ligeramente superiores a las de las aguas superficiales. El afloramiento no explica totalmente la distribución de nutrientes, porque las concentraciones aumentan hacia la costa. En la zona costera túrbida las aguas próximas al fondo se caracterizan por su elevada salinidad, gran contenido de silicatos y bajo contenido de oxígeno: es probable que parte del fosfato mineralizado de los restos de plancton acumulados por las corrientes sea absorbido inorgánicamente por los minerales en suspensión.

El río Amazonas tiene concentraciones de nutrientes superiores a las de las aguas superficiales tipicas del Atlántico tropical. Los fosfatos, nitratos, y una parte variable de silicatos, son rápidamente consumidos por la producción primaria. Las descargas del Amazonas, los afloramientos, y la mineralización cerca de la costa pueden servir de base para comprender el complicado sistema de productividad primaria en la plataforma continental de la Guyana, como explica Cadée en sus publicaciones (1975), basándose en los resultados obtenidos durante los mismos cruceros.

1. INTRODUCTION

The work on which this paper is based was carried out during two surveys of the Dutch Navy Vessel H.R.M.S. LUYMES in September, October and November 1970 and March and April 1971. The two surveys will be called the October and the March survey. The area is shown in Fig. 1; most of the work was done off Surinam and French Guiana, but also in both years several stations were occupied near the Windward Islands.

In October 1970 the Brazilian research vessel ALMIRANTE SALDANHA on our request carried out a survey on and off the Brazilian continental shelf between the Oyapok and the Amazon rivers. Although this ship could not go into the Amazon River itself, this cooperation with the Brazilian Navy greatly enlarged the investigated area. We would like to acknowledge this cooperation as well as the unrestricted use of the data.

2. METHODS

Hydrocasts were taken with N.I.O. propylene waterbottles equipped with protected and unprotected reversing thermometers. BTs were taken regularly and served very well to complete and refine vertical temperature profiles. All analyses were made onboard ship. Salinity was measured on an inductive salinometer (Autolab Industries, Sydney). Dissolved oxygen samples were determined by the Winkler technique, using a modification described by Carritt and Carpenter (1966). After settling of the precipitate part of the supernatant, liquid was sucked off and titration performed in the sampling bottle. Dissolved orthophosphate-phosphorus was analysed according to Murphy and Riley (1962). In turbid coastal waters, filtration (0.45 µ membrane filter) was necessary, even then turbidity blanks were often appreciable. The reactive silicate method published in Strickland and Parsons handbook (1968) was applied. The yellow molybdate complex was allowed 10 ± 1 minutes to form (Fanning and Pilson, 1973). Nitrite analyses were performed as described by Strickland and Parsons (1968). Nitrate + nitrite was determined according to the procedures described by Wood et al. (1967) and Nehring (1968) with some minor modifications. The method introduced by Koroleff (1970) was applied in the ammonia determination. All extinctions were measured in 4 cm cells on a Unicam SP 600 spectrophotometer.

3. CHEMISTRY OF THE OCEANIC WATER COLUMN

We will briefly discuss the different water masses of the tropical Atlantic from the section shown in Fig. 1. Fig. 2A shows the salinity structure. From 4 000 to the bottom at 4 700 m we have relatively low salinities, 34.8-34.9 °/oo and low temperatures, 1.74-2.20°C, typical for a high percentage of Antarctic Bottom Water. This is flowing from the Brazilian Basin and spreading as a thin layer close to the bottom at least as far as 30°N according to the work of Amos et al. (1971) near Bermuda. From 4 000 m up to 1 500 m the salinity increases very gradually. In these water masses, the middle and upper North Atlantic Deep Waters, phosphate, nitrate and oxygen also change very little with depth (see Table I). The maximum salinities of the upper North Atlantic Deep Water are just over 35 °/oo in the Antilles Arc region. Further up in the water column, the salinities decrease until, at 700 to 800 m, the minima characteristic for Sub-Antarctic Intermediate Water are reached. These waters also flow into the Caribbean through the deep passages between the Antilles. The core of Antarctic Intermediate Water is eroded: 34.5 °/oo salinity is found near the Amazon and 34.75 °/oo salinity off Caracas.

Above this, the Subtropical Intermediate Waters are found with maximum salinities at 80 to 130 m depth, maxima of just over 37 °/oo salinity near the Windward Islands and barely 36.3 °/oo salinity in the eastern part of the region. East of about 52°W a pronounced salinity maximum is absent, this was noted by Metcalf (1968). Metcalf and Stalcup were the first to identify two types of Subtropical Intermediate Water, different in oxygen content. Visser (1976) has demonstrated that these two water masses meet each other off French Guiana.

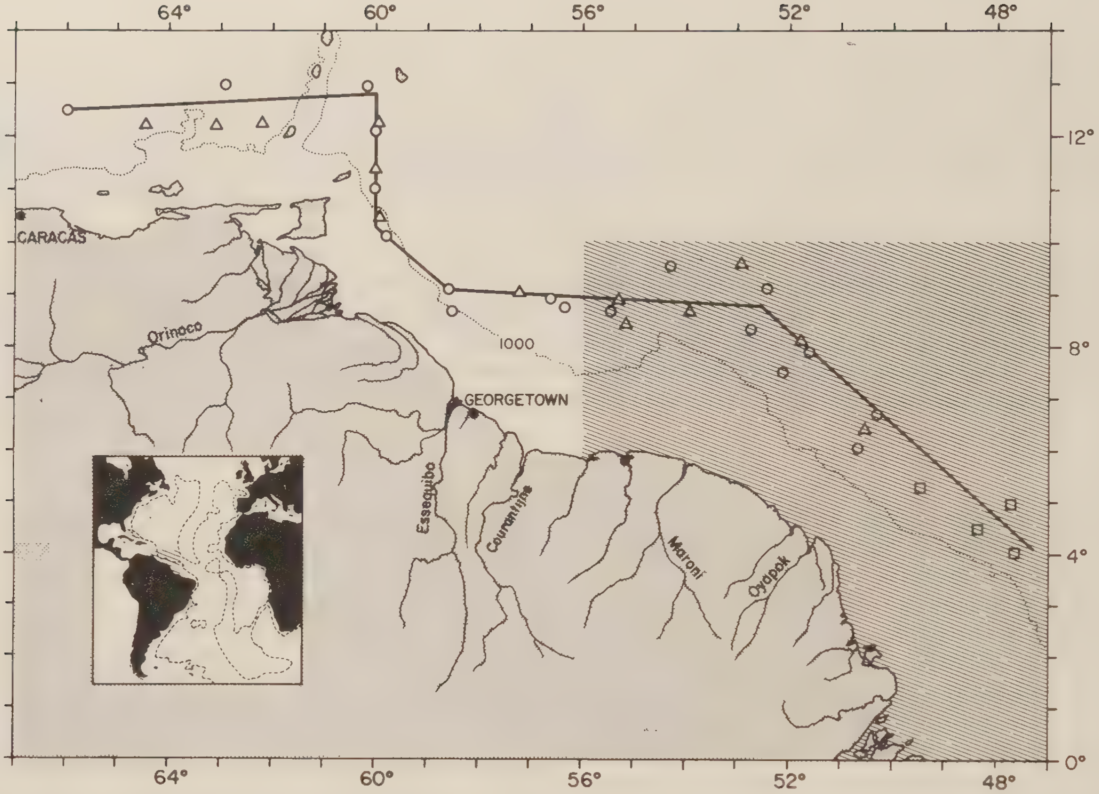

Fig. 1 Deep water stations on a section from the Guyana Basin to the Venuzuela Basin samples September-October 1970 (△ Neth. st., □ Braz. st.) and March-April 1971 (○, Neth. st.).
Shaded: main area of investigations
......: 1 000 m isobath

Finally, at the surface layer, very shallow (4 to 10 m) and very sharp (up to 3 $^{o}/_{oo}$ salinity/m) haloclines are found in the Amazon plume, even at a distance of 1 000 km from the river mouth (Fig. 10). A few more details will be mentioned from the phosphate and silicate profiles in the same section. The phosphate section (Fig. 2B) shows a faint minimum at 2 000 m and maxima associated with the core of Sub-Antarctic Intermediate Water. Looking more closely, this maximum is seen to consist of a series of alternating maxima of up to 2.55 and minima of about 2.1 µM. The same phenomena have been found by Clowes (1938) and Deacon (1933) from the DISCOVERY expedition into the southern Atlantic and were attributed to seasonal differences in phosphate content near 50°S where the Sub-Antarctic Intermediate Waters sink from the surface. The pattern of maxima and minima in our stations is also found in nitrate to a lesser extent but not in silicate, salinity or oxygen. Alternating maxima and minima are also present in the observed phosphate distribution.

If the average distance between two maxima - 600 km - is covered in one year, we find an average velocity in the core layer of 2 cm/sec, somewhat less than the 2.5 to 5 cm/sec calculated by Clowes and Deacon with the same method and the 4 cm/sec independently derived by Wüst (1949) from dynamic calculations for the tropical Atlantic north of the equator.

The silicate section in Fig. 2C gives very high values near the bottom (up to 70 µM). This provides further evidence for the presence of Antarctic Bottom Water. The salinity-silicate relationship for our stations add to the rapidly accumulating evidence (Spencer, 1972; Mann, 1973 and others) that silicate can be used as a quantitative tracer in the deep Atlantic waters. With the salinity-silicate relationship we find that the deepest water in the Guyana Basin contains about 50 percent Antarctic Bottom Water (van Bennekom and Visser, in preparation). There is a pronounced difference in silicate content of the layers between 1 000 and 2 500 m in the Atlantic and the Caribbean, first noted by Richards (1958), the silicate minima associated with the North Atlantic deep waters are not found in the Caribbean. This is shown in more detail in Fig. 3 where silicate is given against sigma-t for stations on both sides of the Windward Islands. (Sigma-t is chosen because both salinity and temperature have extremes in the depth interval concerned.) Atlantic and Caribbean waters differ below 900 m, the depth of the St. Vincent Passage. Apparently the deeper St. Lucia and Dominica Passages further north do not have great influence, compatible with the current measurements of Stalcup and Metcalf (1972). One observation at the northernmost Atlantic station shows water of Caribbean type at 1 000 m, indicating the possibility of a slight transport of deep water out of the Caribbean through these northern passages.

Comparison of nutrient profiles with the characteristic salinity profiles shows that extremes of nutrients and salinity do not coincide in the tropical Atlantic. An example is given in Fig. 4. The phosphate maximum is found about 50 m deeper and the silicate maximum about 200 m deeper than the Sub-Antarctic Intermediate core layer. More examples are given in Table I.

A thorough discussion of tropical Atlantic nutrient and salinity profiles is outside the scope of this paper since they do not concern the Caribbean. However, these features become more understandable when it is realized that the typical water masses of the tropical Atlantic are not pure water types but in their turn mixtures of water types with a changing composition in north-south direction as well as vertically.

TABLE I

Oxygen, AOU (µg-at/l^{-1}) and nutrient (µM) values at characteristic depths in the Guyana Basin
Ranges are given for all stations with depth < 100 m

	Depth	S °/oo	T°C	O_2	AOU	PO_4-P	NO_3-N	H_4SiO_4	n
Surface		20–36.2	26–29			0–0.1	< 0.05	60–1.3	
S.I.W.	106±35	36.2–37	20–26	245–413		0–0.75	0.1–6.8	1–5	40
max. AOU	610±200				350±20				21
max. NO_3-N	715±200						22±2		7
min. S °/oo	735±120	34.60±0.06	5.54±0.6						21
max. PO_4-P	770±150					2.33±0.25			17
max. H_4SiO_4	860±100							29.5±2.5	18
max. S °/oo	1 560±350	34.984±0.02	4.28±0.7						13
min. H_4SiO_4	1 730±200							16±2	11
min. PO_4-P	1 840±250					1.13±0.15			11
min. AOU	1 970±350				115±6				13
min. NO_3-N	2 300±300						14.3±0.6		3
max. depth	4 675	34.815	1.74	480	207	1.74	16.5	69	1

NH_4-N in the surface layer had an average of 1.2 µM and a range of 0.04–1.6 in the S.I.W.

4. COASTAL UPWELLING

From current profiles during a full tidal cycle, movement of shelf bottom water toward the coast was found in April by Eisma (1967, 1971) between 54° and 56°W. This was also found during our surveys in March and October, but only west of 54°W. The residual currents have a southerly component of -7 to 13 cm sec^{-1}. In the same, fairly small region, upwelling was also deduced by Mazeika (1973) from the distribution of surface temperatures in autumn.

During our March and October surveys, nearshore surface waters off Surinam were about 2°C colder than those offshore and more to the east (see Fig. 5). The vertical sections of temperature given in Fig. 7 show an upward slope of isotherms toward the coast, especially between 54° and 55°W. The temperature patterns are sometimes continuous, but often isolated cold water cells are found near the coast. Apparently the upwelling is not a continuous process. The water in the cold cells to which we shall return later is either the remnant of a previous upwelling at that longitude or has been transported parallel to the coast from a nearby position with continuous upwelling. The recurving coastline of South America between 51° and 57°W makes an offshore movement of surface waters by the easterly trade winds probable only west of 53°W. The complicated current patterns outside the shelf edge influence the source of upwelling waters. Owing to the pronounced haloclines and the surface salinity maxima in the thermocline, the vertical stability of the water column is fairly high and turbulence occurs in horizontal gyres. Current velocities are up to 4 knots in the shallow, wind-driven Amazon plume and 1 to 2 knots in the core of the Subtropical Intermediate Waters (Goulet and Ingham, 1971 and Mazeika, 1973).

Mazeika suggests that piling up against the Antilles Arc effects a southward deflection in the North Equatorial Current, detectable as a tongue of high salinity, directed toward the coast near 56°W. This high salinity water causes part of the Guyana Current to recurve as shown by Metcalf (1968). From the work of Mazeika (1973), Metcalf (1968) and Visser (1976) it is clear that the area of transition between low-oxygen North Atlantic waters and high-oxygen waters of the Guyana Current changes seasonally. In January and February it is found at about 52°W, in March at 53° to 54°W, in May and June east of 48°W, in July and August east of 51°W and from October to December again at 52° to 53°W.

The waters of the high-oxygen type have a lower specific gravity, presumably they are forced upward against the tongue of high salinity. This causes a bulge in the upper part of the thermocline, as can be seen in Figs. 5C and D. The position of this bulge must influence the characteristics of the upwelling water and, in our opinion, warrants a closer investigation. The possible influence of the Amazon plume on these processes has been a subject of much speculation. Because of the large short-term fluctuations, synoptic pictures of this plume are virtually lacking, but it seems plausible that the plume water moves as a completely separate layer under wind influence, dissipating a considerable part of this wind stress, which then cannot act on the subsurface Guyana Current. According to Oltman (1967) in May and June the Amazon discharge is at its maximum and in spring the plume is closer to the coast because the dominant direction of the wind is shifted to northeast in this period. This might well, in a somewhat indirect way, cause the eastward shift in the transition between waters of North and South Atlantic origin in this period.

Nutrients and oxygen in a section with continuous upwelling are shown in Figs. 6A-H. The upwelling water originates in the upper part of the thermocline; therefore nutrient levels are low. Salinity and temperature in the shelf bottom water are about constant, all changes in nutrients must be the result of in situ processes on the shelf. The preservation of higher nutrient and lower oxygen values in the nearshore bottom water can be qualitatively understood by considering the optical properties of these waters (Visser, 1972). Particularly in the near coastal region, the Guyana Current carries much, very fine, suspended matter. This confines the euphotic zone to 6 m, less than the upper half of the water layer. Low oxygen values and high nutrient concentration caused by decomposition of plankton remains cannot be counteracted by primary production until this water layer is mixed or advected into more favourable light conditions. Some PO_4-P, NO_2-N and NO_3-N and much silicate are produced, while much oxygen is consumed. The consumption of oxygen and the production of silicate are confined to limited regions and well correlated with one another (see Fig. 8). These areas also coincide approximately with the areas of high primary productivity observed by Cadée (1975) in measurements at the same stations (Fig. 12). Especially in October (Fig. 12) two areas of relatively high productivity were present, one - in the east - in the Amazon plume with salinities of 30 °/oo (see below) and another in the west with salinities of more than 35 °/oo (see Fig. 11A). A direct influence of the Amazon plume is absent in the latter area; this is presumably related to upwelling. In March (Fig. 12C) the productive areas in high and low salinity regions overlap each other (see Fig. 11D); in each case diatoms were the main component of the phytoplankton.

In situ production of nutrients on the shelf was already mentioned. To make more quantitative statements, the source depth of the upwelling must be known. This depth was estimated for the October cruise in the following way (see Fig. 9). Nine nearshore bottom water samples below a thermocline were available; they had a narrow range in salinity (36.21 to 36.32 °/oo salinity) and in temperature (23.22 to 24.26°C). Off the shelf edge, water with these characteristics is not found at a uniform depth. As mentioned earlier there is a "western" profile with a pronounced salinity maximum and a shallow thermocline and an "eastern" profile with a deeper thermocline and without a pronounced salinity maximum. (Incidently, the separation between the thermocline and the very shallow halocline is also visible in profiles of the "eastern" type). In order to get as small depth ranges as possible, we assumed that during upwelling the shelf bottom water is not becoming colder or more saline. In the case that upwelling water originated in the west, it comes from 70 to 75 m and for an eastern origin 120 to 140 m is the source depth. In both cases the source concentrations of oxygen (320 to 360 µg-at l^{-1}), phosphate (0.25 µM) and silicate (3 µM) were hardly different. This is compatible with the water movements suggested earlier, namely that water of eastern origin is forced upward and backward by the tongue of high salinity of western origin.

Comparison of these source values with the average concentrations and ranges in the cold water cells is given in Table II.

TABLE II

Oxygen, phosphate and silicate on the Guyana shelf, September and October 1970

	O_2, µg-at/l^{-1}	H_4SiO_4, µM	PO_4-P, µM
Cold water cells	170 (67-272)	15 (7-26)	0.48 (0.3-0.85)
Shelf edge	340 (320-360)	3	0.25
Difference	170	12	0.23

Phosphate and silicate are produced and oxygen is consumed in the ratio 1:52:730. The normal relation for mineralization of plankton is 1:16:273 (Richards, 1958). One explanation for the very low amounts of phosphate might be that the mineralizing organic matter is of humic acid type, low in phosphate. However, these compounds are refractory and mineralization in the coastal zone must be a fairly rapid process: notwithstanding a high mean primary productivity of 0.9 gC m^{-2} day^{-1} (Cadée, 1975) even the surface waters are, on the average, undersaturated with respect to oxygen. A more likely explanation is inorganic absorption of phosphate on the very fine suspended material. Starting with the normal ratio, a consumption of 170 µg-at l^{-1} of oxygen means a production of 0.62 µM PO_4-P. About half of this amount would then be absorbed on the suspended clay. Such processes have been found by Pomeroy *et al.* (1965) while Gessner (1960) in experiments with Varzea soils from the Amazon region found that phosphate was absorbed from the water at concentrations of 0.3 µM.

Determinations of organic carbon and phosphate in the same suspended material are lacking. Van Bennekom and Eisma (unpublished observations) found about 350 µg total phosphorus/gram suspension in the coastal zone off Surinam and Tjoe-Awie (1975) found 6.5 mg organic carbon/gram fine grained bottom sediment off Guyana. This would give a ratio of organic carbon over phosphorus of about 20, whereas 40 is normal for organic material of marine origin. Tjoe-Awie (1975) also found that a substantial part of the particulate nitrogen is bound inorganically to the clay minerals. The suggested process in which suspension from the Amazon River is enriched in phosphorus, advected from the ocean by upwelling and kept there by the accumulative current pattern, needs further investigation in our opinion. It might well influence the fertility of the soil in the young coastal plains.

5. CHEMISTRY OF AMAZON PLUME

Fig. 10 shows the salinity distribution from observations within a period of two weeks together with characteristic vertical profiles. To delineate the structure of the plume, bottle spacings of about 1 m proved essential. The plume-like distribution over a larger area (observations over a period of 6 weeks) is shown in Fig. 11. In March, April, September, October and November no isolated lenses of brackish water, such as reported by Ryther et al. (1967), were encountered. In both cruises the plume left the coast, in October near the Oyapok and in March near the Maroni River, some 300 km more to the west. Also in both cases, eastward transport of brackish water was found at 9°N. In the surface layer a correlation exists between salinity and reactive silicate (Fig. 11, see also Fig. 2C), indicating riverine origin of the fresh water. Points from samples taken near the mouths of the Guyanese rivers fell above the envelopes in the salinity-silicate graphs. The contribution of local rainfall, suggested by Neumann (1969), must be small. Through a 180-km wide section (Fig. 10) off French Guiana 80 000 to 200 000 m^{3}sec^{-1} is transported with a velocity of at least 50 cm sec^{-1} and this would mean a rainfall of 15 to 40 cm/sec.

As already mentioned, Cadée found a high primary productivity 500-1 000 mgC m^{-2} day^{-1} in the Amazon plume, especially in the southeastern region (Fig. 12), where salinities in the surface layer were about 20 °/oo S in March and 29 °/oo in October. In these waters the oxygen saturation percentages were up to 130 percent in March and up to 129 percent in October. When the plume moves offshore, primary production quickly diminishes. According to Ryther et al. (1967) it may even become smaller than in surrounding ocean waters. In any event phosphate (0.4 µM) and nitrate (3 µM) concentrations in the Amazon River as given by Gibbs (1972) are higher than in surface ocean waters, so when the high sediment load of the estuaring region has settled we may expect stimulation of phytoplankton growth. Already at 20 °/oo S when sea water and river water are mixed in about equal proportions the PO$_4$-P and NO$_3$-N levels are hardly enhanced relative to surface ocean water. (Of course absence of these nutrients in the dissolved state does not mean the impossibility of phytoplankton growth; new nutrients might become available by recycling, and NH$_4$-N is also present.)

Extrapolation of silicate-salinity graphs back to zero salinity gives silicate concentrations of 20-50 µM in March 1971 (Fig. 11F), 35-60 in April 1971 (not shown), 90 in June 1969 (van Bennekom, unpublished observation), 90 in June 1974 (Milliman and Boyle, 1975), 130 in October and 70 in November 1970 (Fig. 11C). Reactive silicate concentrations in the Amazon are given by Oltman, 1967 (115-150 µM), Gibbs, 1972 (a yearly average of 187 µM and a range of 152-207) and Milliman and Boyle, 1975 (130 for early June). In any case appreciable amounts of reactive silicate are removed upon mixing of Amazon water into the ocean, the average amount seems to be rather larger than the 25 percent given by Milliman and Boyle (1975) in the order of 25 M tons SiO$_2$. Diatoms play an important role in this removal, the large removal in March and April might be due to higher nutrient concentrations in tropical rivers associated with flooding in the beginning of the wet season.

In the coastal zone, also release of reactive silicate occurs. A numerical example, given with appropriate reserve, will bring some insight as to the quantities involved. A layer of 10 m above the bottom in an area of 20 000 km^2 contains about 10 µM more reactive silicate than adjacent areas (in total an extra amount of 100 000 tons SiO$_2$, see Fig. 8A).

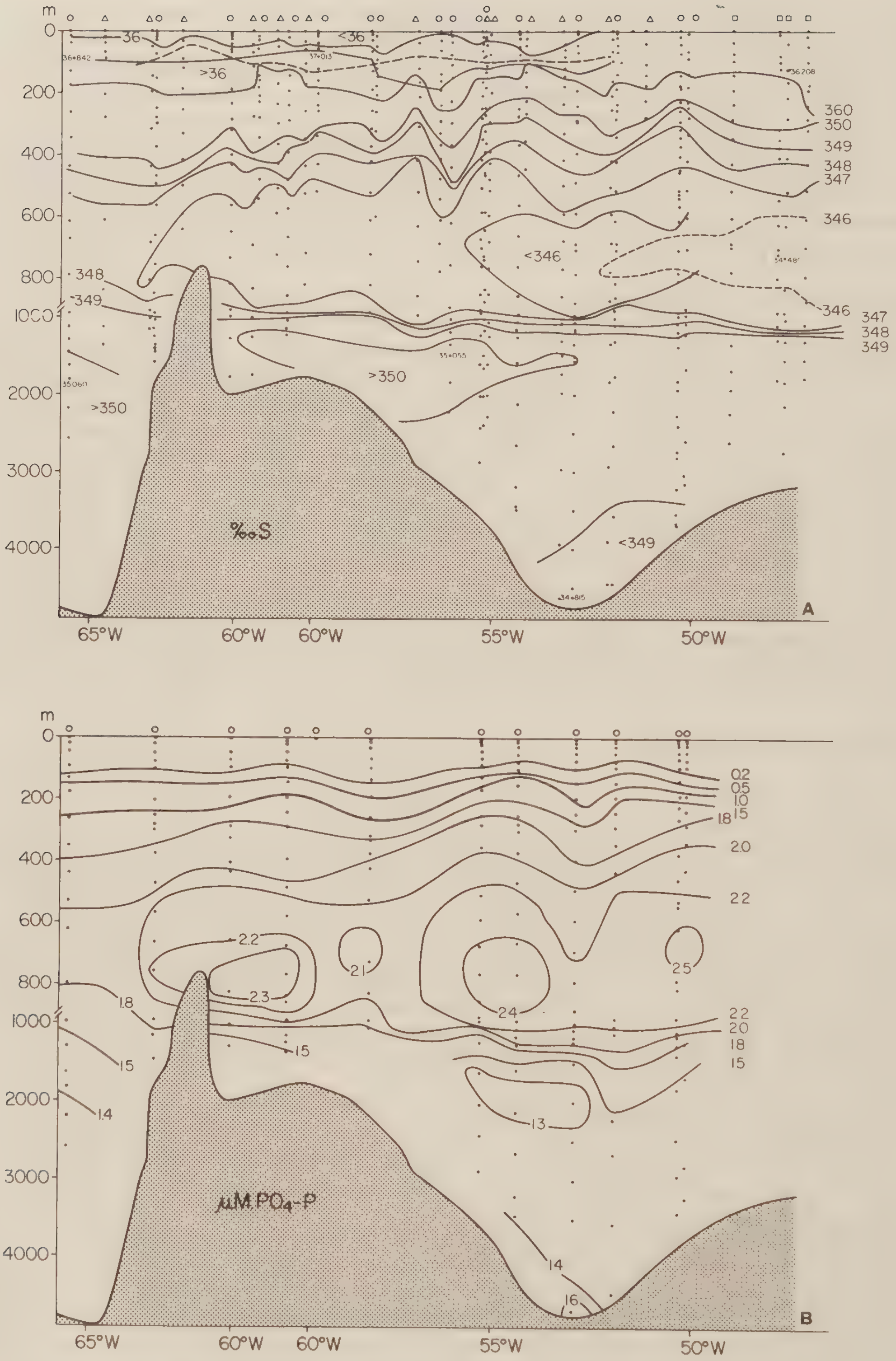

Fig. 2 Distributions of salinity, reactive silicate and soluble orthophosphate in the section of Fig. 1

A:- - - - - - - - 34.6 (1970)

—— —— Sub-Antarctic Intermediate Water core (1970)

36.842 ———— 37.013 ———— Sub-Antarctic Intermediate Water core (1971)

(extreme values are given in small digits)

B: 1971 distribution

C: 1970 + 1971 distribution, - - - - 1970 only

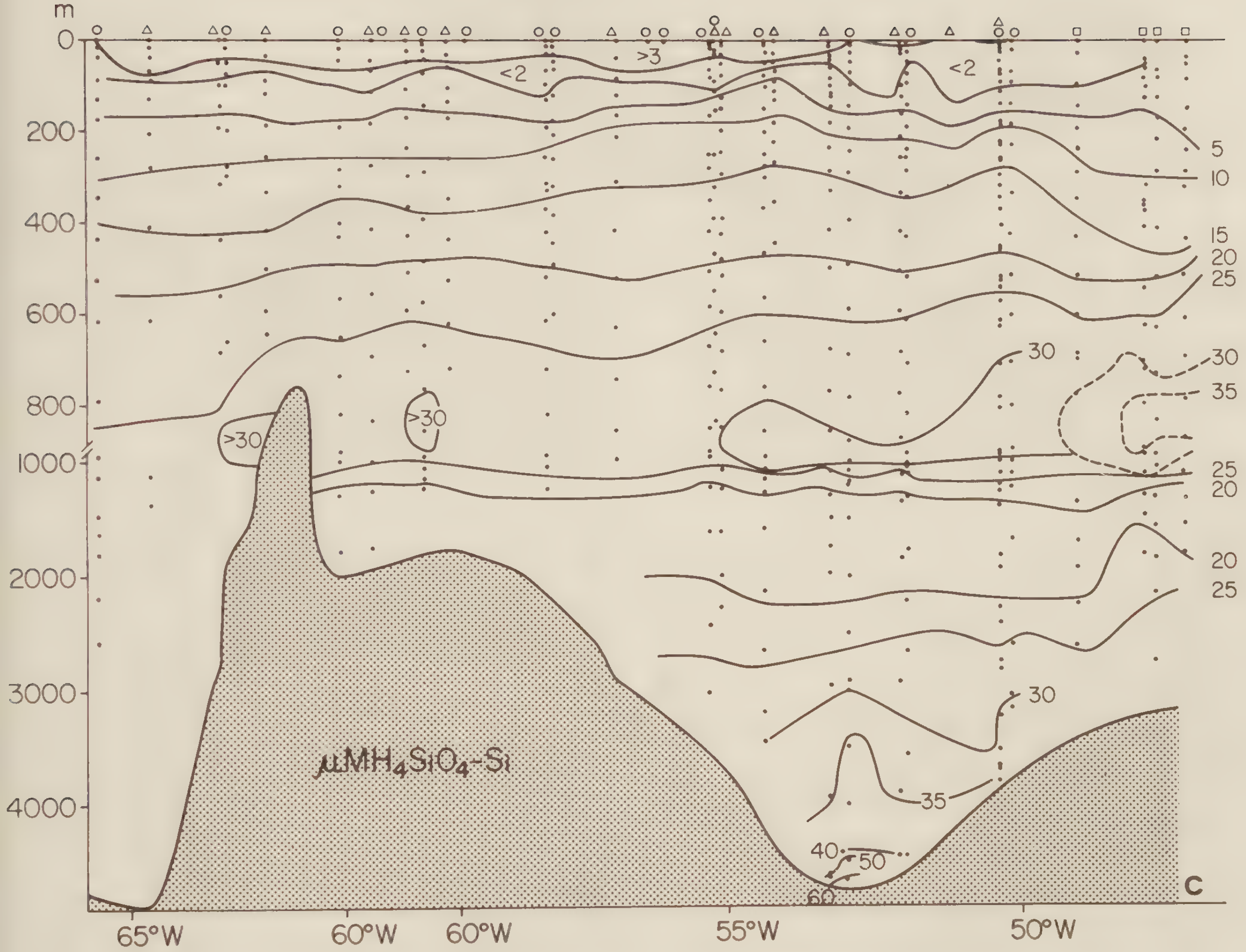

With a residence time of about a week, estimated from residual current velocities in this bottom layer, this would mean the release of 5 million tons of SiO_2 per year, about 10 per cent of the Amazon discharge. The same type of phenomena - removal by diatoms and partial resolution in areas of accumulation - were also found by van Bennekom *et al.* (1974) in the estuary of the Rhine. It might well be a general phenomenon in which case the amount of reactive silicate reaching the oceans is substantially less than that leaving the rivers.

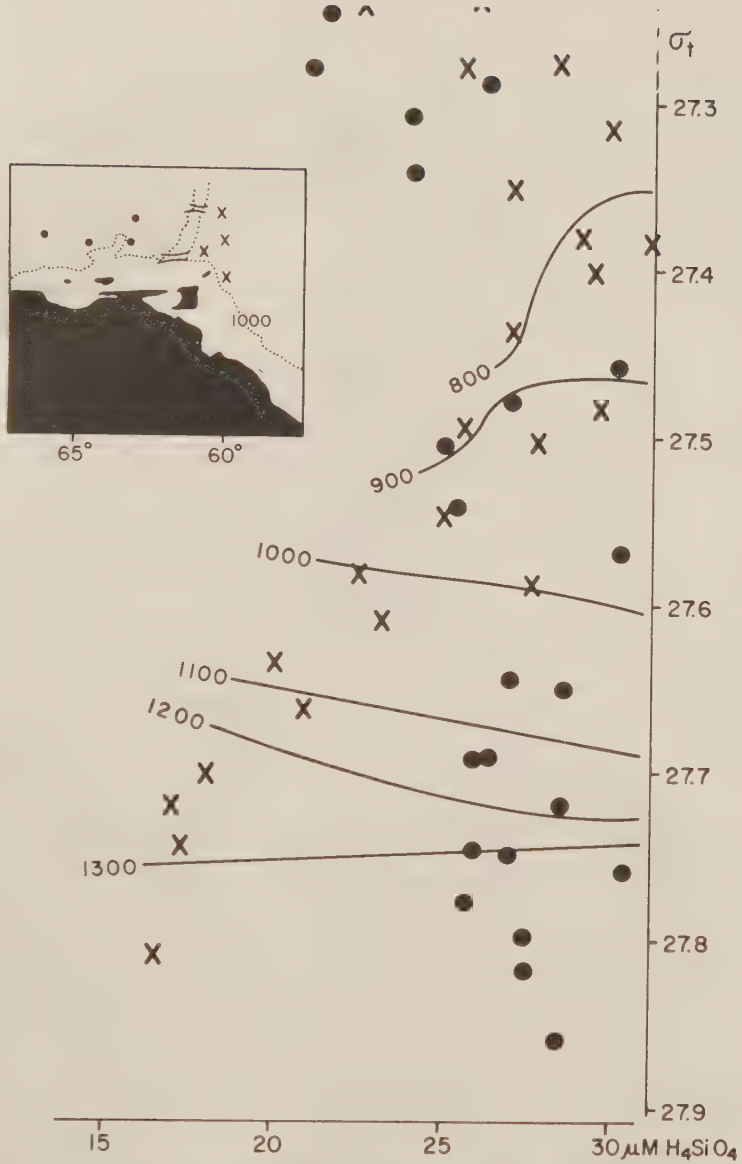

Fig. 3 Relations between sigma-t, depth in metres and reactive silicate west and east of the St. Vincent and Grenada Passages in the Antilles Arc

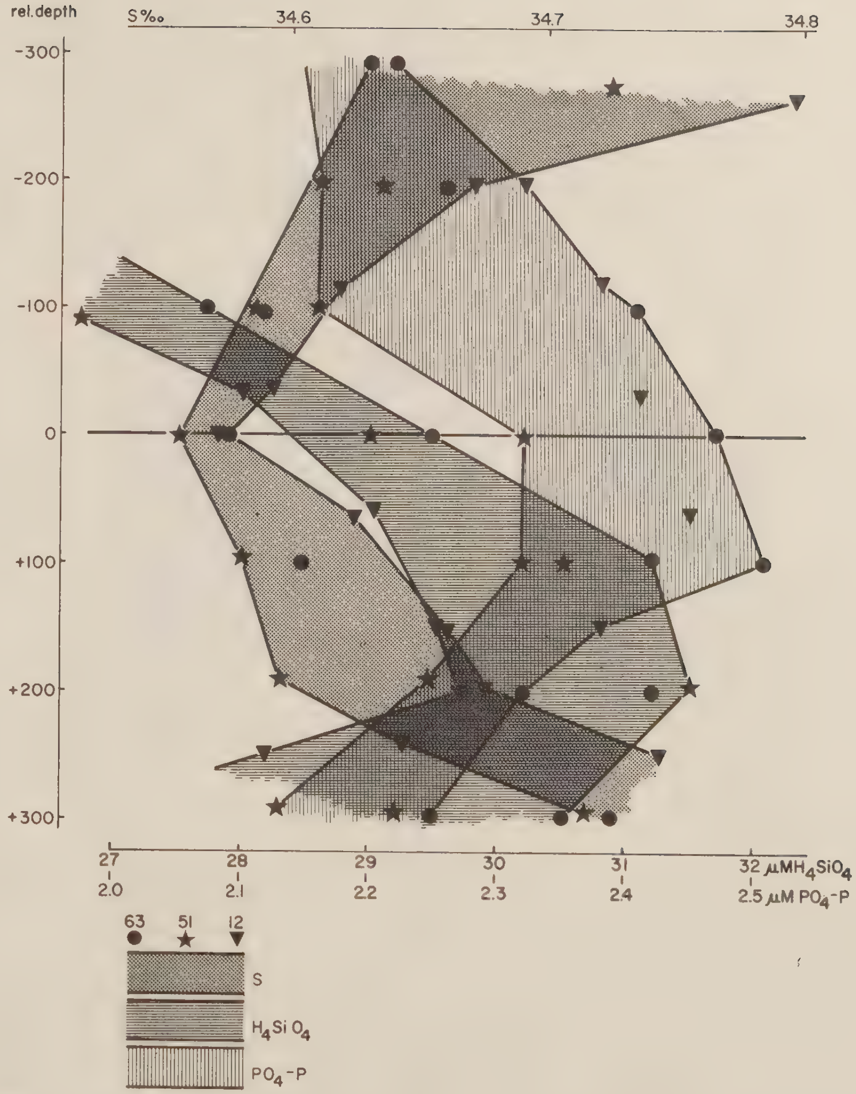

Fig. 4 Relative levels of minimum salinity, maximum reactive silicate and maximum soluble orthophosphate in the core of the Sub-Antarctic Intermediate Water at some representative stations
Station position and time:
12: 08°40'N, 55°24'W; 16 March 1971
51: 09°08'N, 52°28'W; 26 March 1971
63: 09°37'N, 54°12'W; 28 March 1971

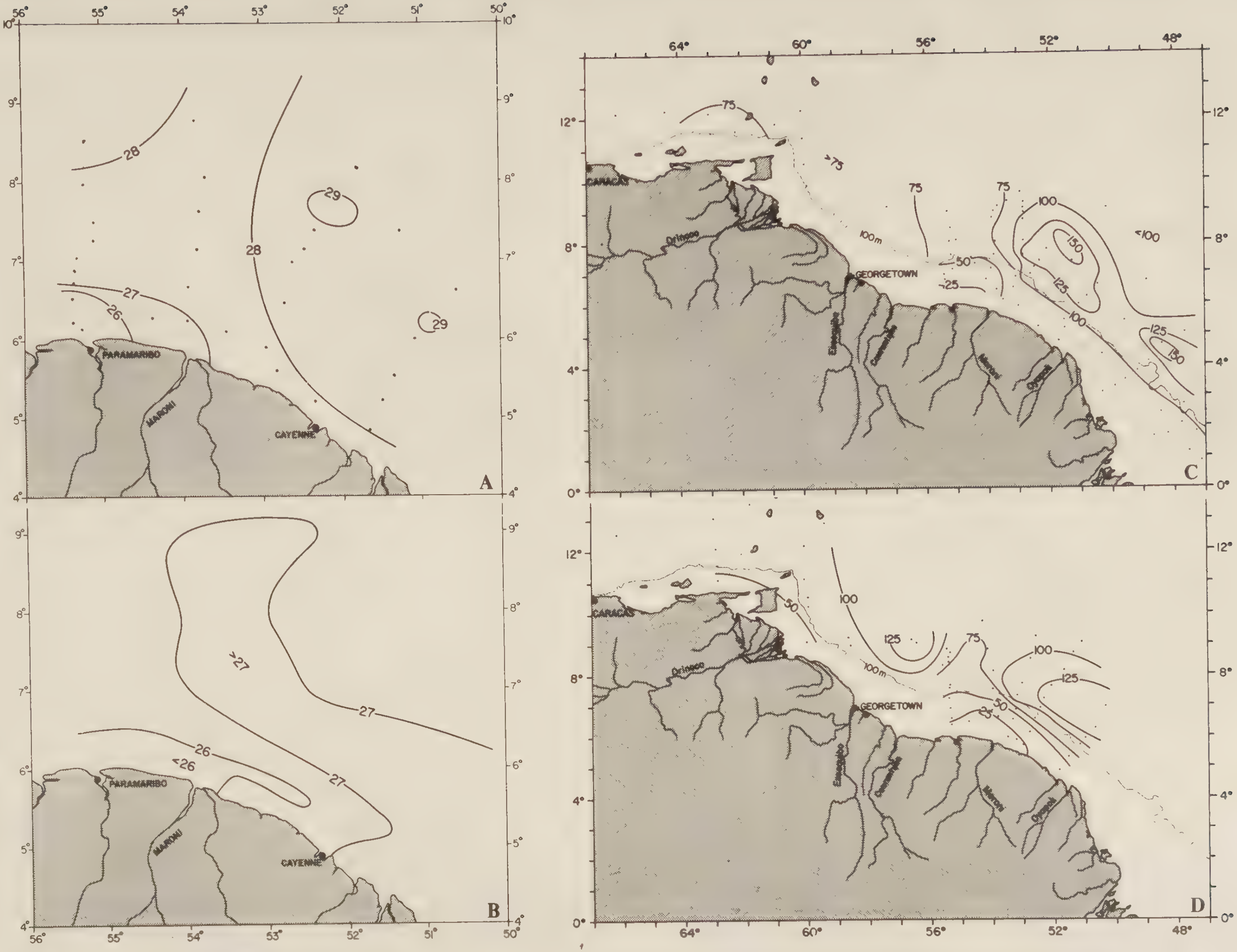
A
B
C
D
28
29
27
26
>27
<26
75
>75
100
<100
125
150
50
25
100m
PARAMARIBO
CAYENNE
MARONI
GEORGETOWN
CARACAS
Orinoco
Essequibo
Corentyne
Maroni
Oyapock

Fig. 5 Surface temperature distribution (A and B; °C) and depth of the 24°C isotherm (C and D; m)
A and C: 1970 observations
B and D: 1971 observations

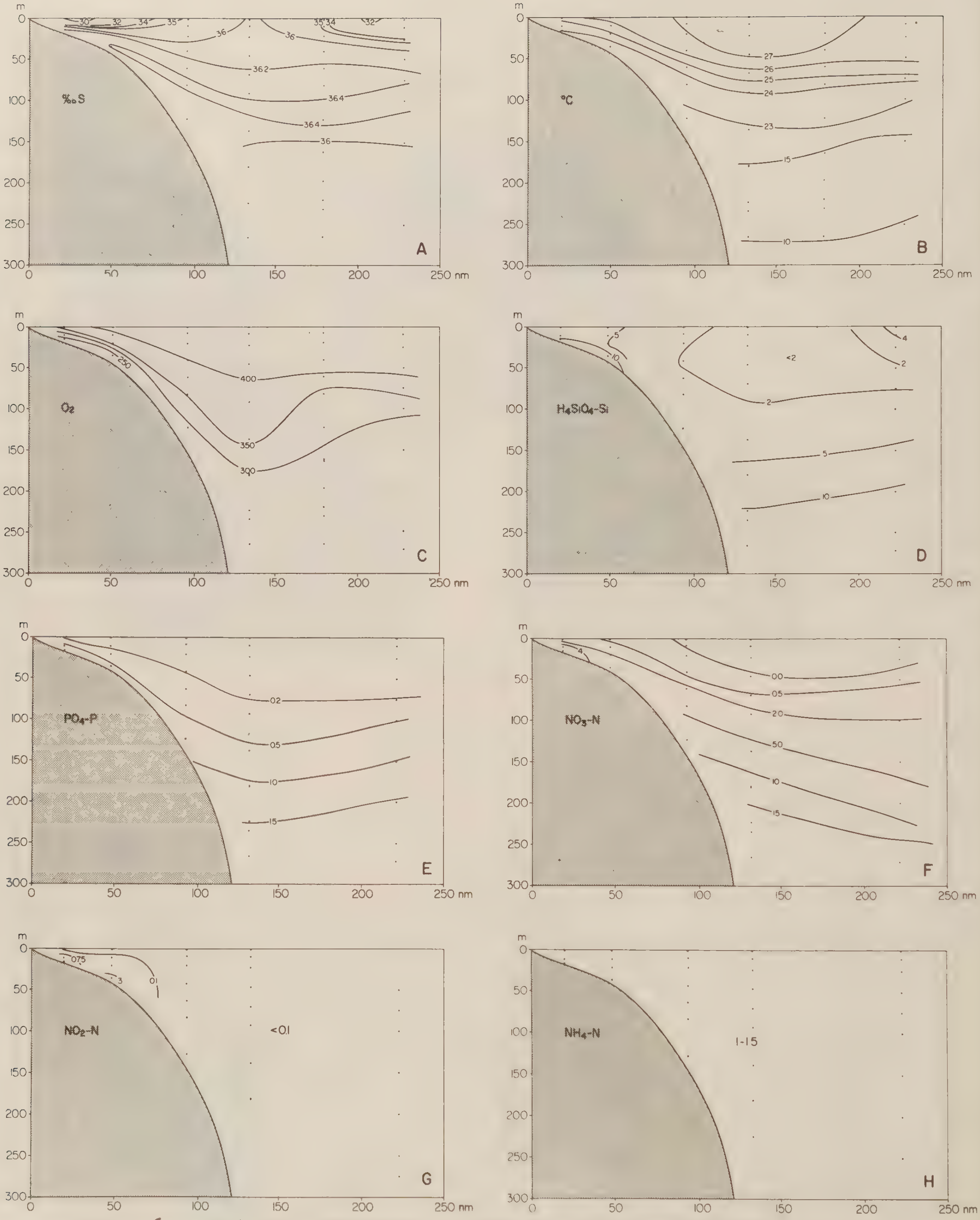

Fig. 6 Salinity, temperature, oxygen and nutrient distributions in a N-S section at 54°W in March 1971
C-H: µg-at l^{-1}

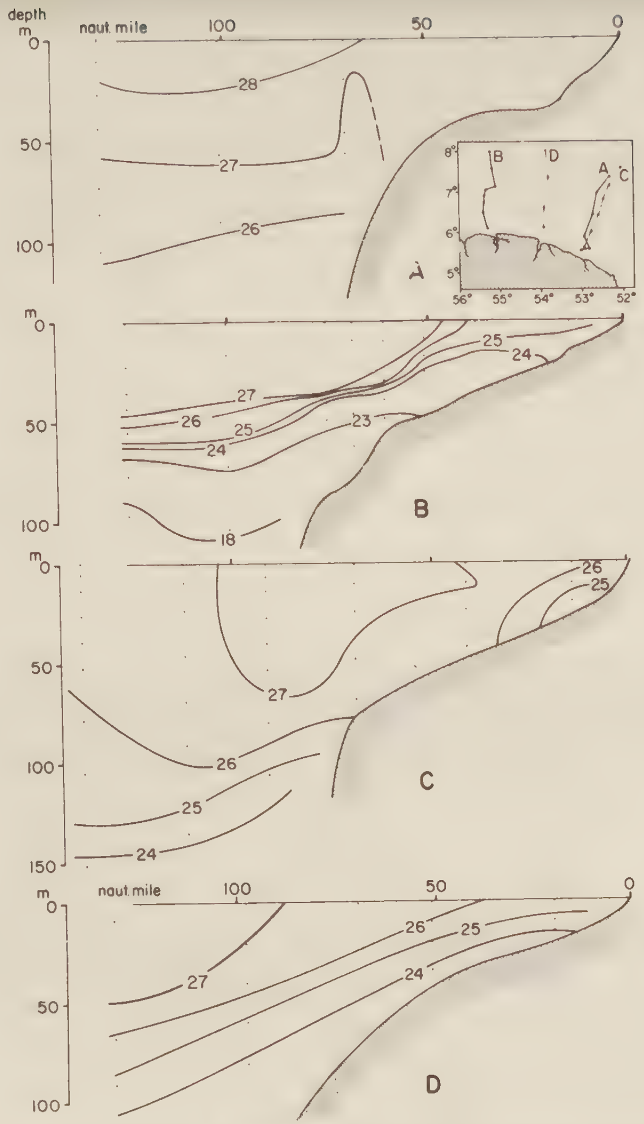

Fig. 7 Temperature distributions on the Guyana Shelf (°C)
A and B: 1970 observations
C and D: 1971 observations

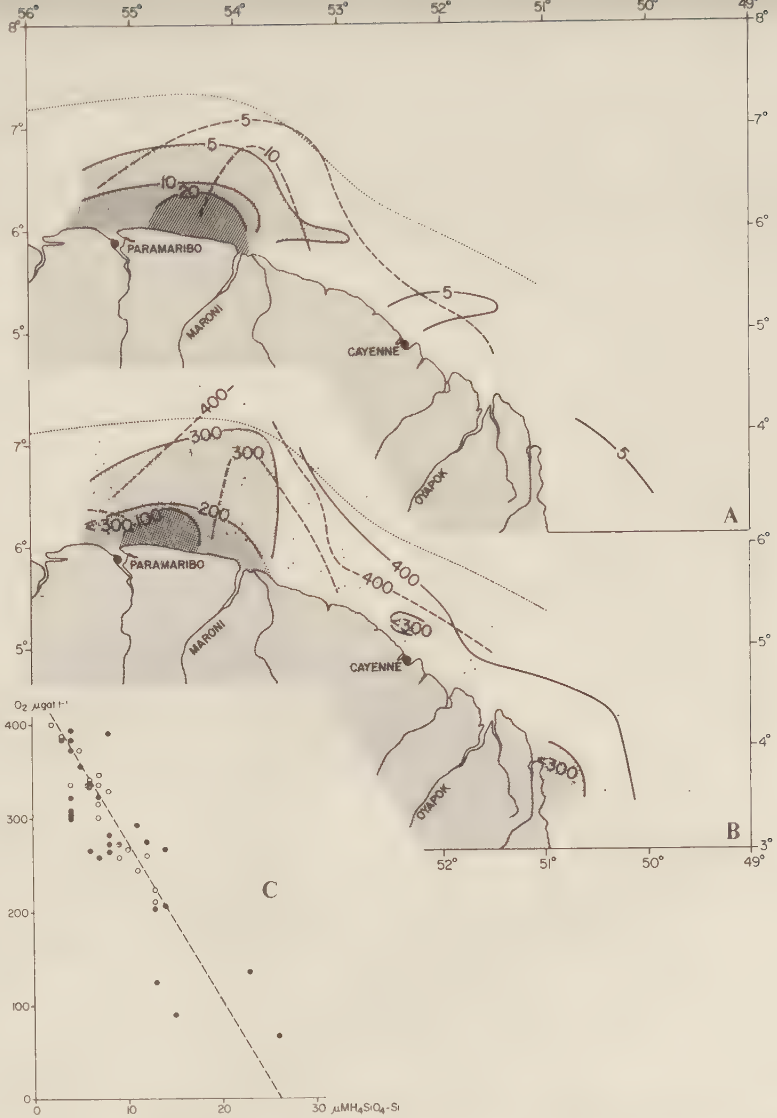
56°
55°
54°
53°
52°
51°
50°
49°
8°
7°
6°
5°
4°
3°
PARAMARIBO
CAYENNE
MARONI
OYAPOK
5
10
20
A
400
300
200
100
B
O₂ µgat l⁻¹
µMH₄SiO₄-Si
C

Fig. 8 Oxygen and silicate conditions in the bottom water layer on the Guyana Shelf.
reactive silicate in µM (A)
dissolved oxygen in µg-at l^{-1} (B)

A and B: ——— and shaded, September–October 1970
- - - - - March 1971
••••••• shelf edge

C: ● September–October 1970 and ○ March 1971

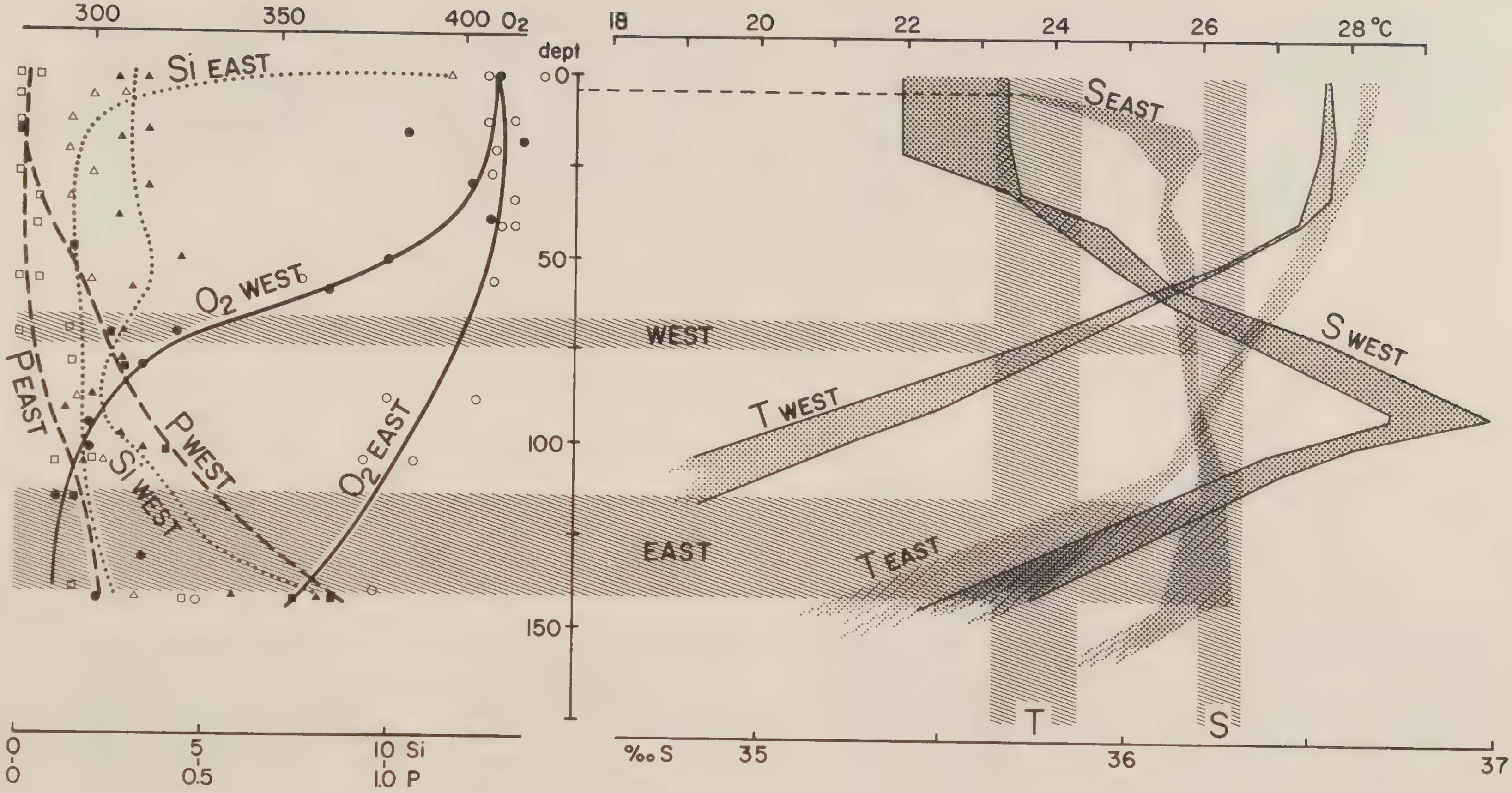

Fig. 9 Estimation of source water, oxygen and nutrient values. PO_4–, H_4SiO_4– and oxygen-profiles, and salinity (S) and temperature envelopes for selected stations on the outer shelf edge, 55°15'W–53°30'W (West) and 53°30'W–51°W (East) on the Guyana Shelf in 1970; shaded columns T and S: temperature and salinity ranges found in the shelf bottom water under upwelling conditions.

- - - - - - - - - - - PO_4-profiles) ■ □)
. . . . H_4SiO_4-profiles) ▲ West and △) East
———————— oxygen-profiles) ● ○)

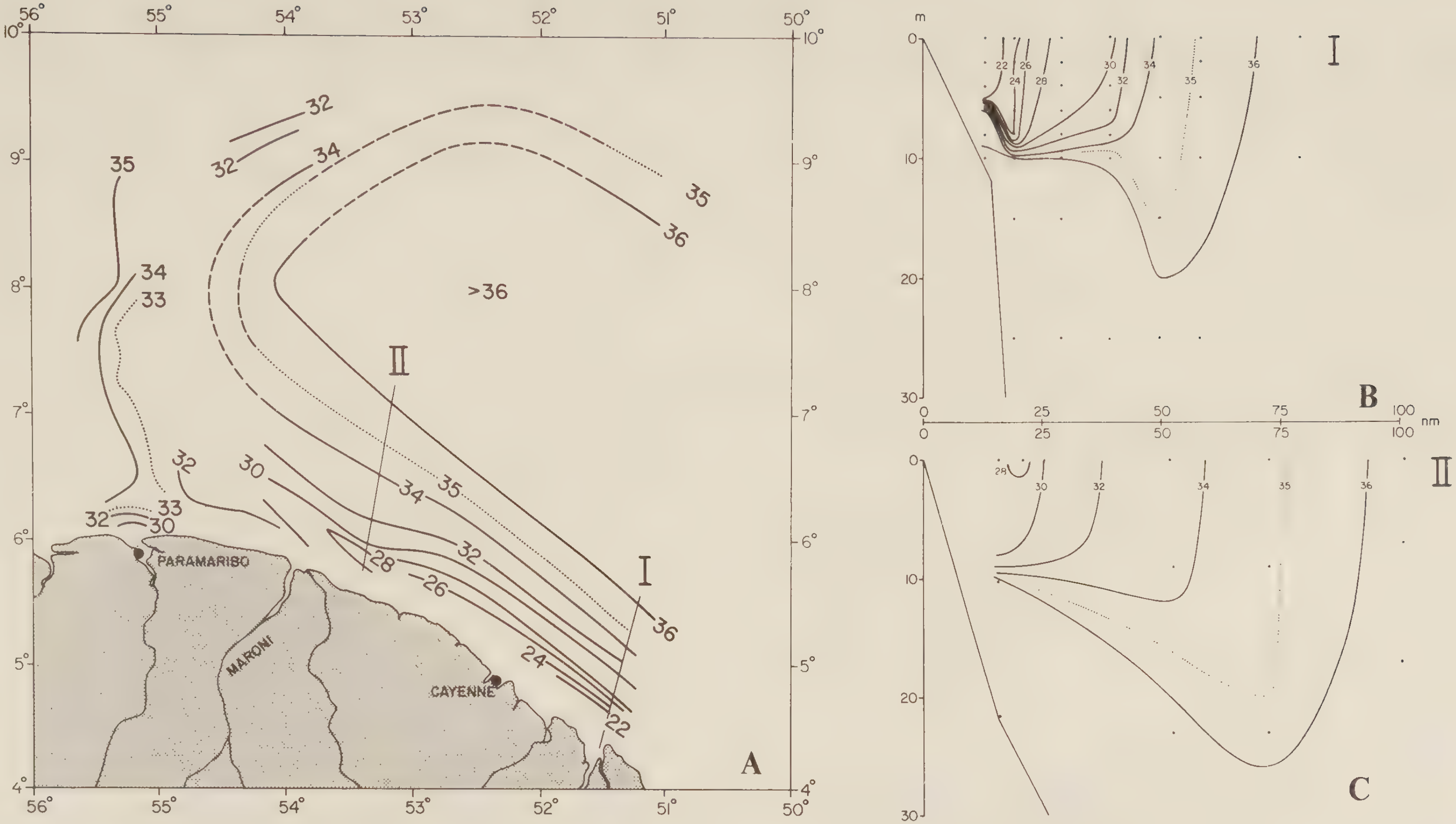
A
B
C
I
II
>36
PARAMARIBO
CAYENNE
MARONI
56°
55°
54°
53°
52°
51°
50°
10°
9°
8°
7°
6°
5°
4°
m
nm
0
25
50
75
100
10
20
30
22
24
26
28
30
32
33
34
35
36

Fig. 10 Schematic surface salinity distribution (A) and salinity depth distributions (B and C), 16-29 March 1971
Lines I and II in A: positions of sections B and C
---- --- ----: estimated

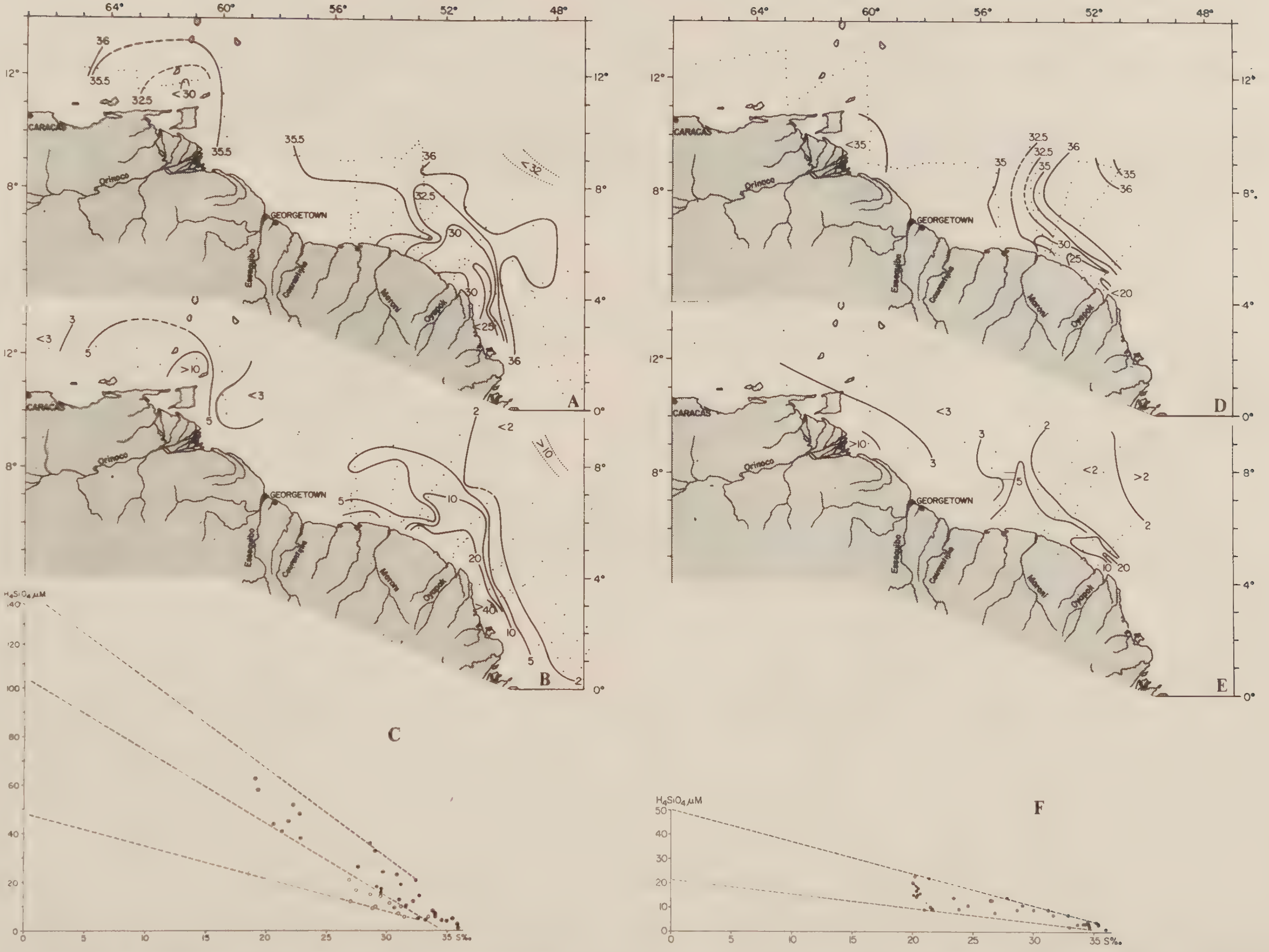
A
B
C
D
E
F
64°
60°
56°
52°
48°
12°
8°
4°
0°
CARACAS
GEORGETOWN
Orinoco
Essequibo
Corantijne
Maroni
Oyapock
36
35.5
32.5
<30
30
<25
<32
<35
35
25
<20
<3
3
5
>10
<2
2
10
20
40
>2
H4SiO4 µM
35 S‰

Fig. 11 Surface salinity (A and D), surface reactive silicate concentration (B and E) and reactive silicate versus salinity graphs (C and F)

A, B, C: { ——— ● } 24 September–8 October 1970

{ ·············· ○ } 22-29 October, 1970

D, E. F: March 1971

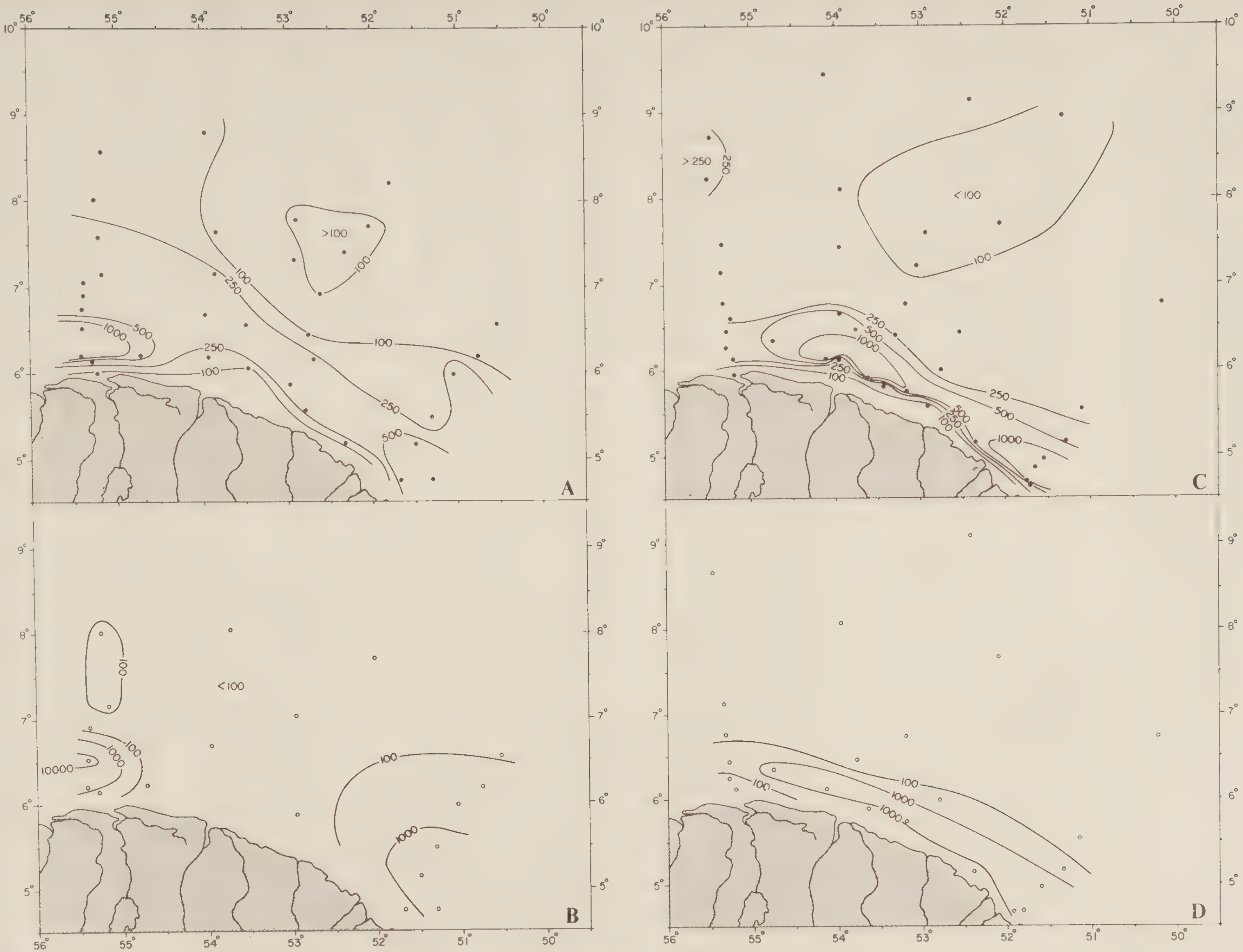
A
B
C
D
>100
<100
>250
100
250
500
1000
10000
56°
55°
54°
53°
52°
51°
50°
10°
9°
8°
7°
6°
5°

Fig. 12 Estimated in situ primary production (A and C, mgC m^{-2} day^{-1}) and phytoplankton cell numbers (B and C, ml^{-1})
A and B: 24 September–9 October 1970
C and D: 16–31 March 1971
(Cadée, 1975 with permission of the Netherlands Journal of Sea Research)

6. ACKNOWLEDGEMENTS

The field work for this study was a cooperative effort of the Royal Netherlands Meteorological Institute (KNMI) and the Netherlands Institute for Sea Research (NIOX). The many discussions with our colleagues K. van der Veen and M.P. Visser of KNMI and G.C. Cadée, W. Helder and E.C. Tjoe-Awie of NIOZ are gratefully acknowledged, as well as the help of H.F.J. van Voorst, M.W. Manuels and J.J.A. van Weereld in the chemical determinations, and the skill of the reprographic department of NIOZ in making the drawings.

Special thanks are due to the Royal Dutch Navy for the fruitful cooperation and to the officers and crew of H.R.M.S. LUYMES for invaluable support at sea; to the Brazilian Navy, officers and crew of Noc. ALMIRANTE SALDANHA for carrying out, at our request, the work on and off the Brazilian continental shelf. We received many valuable suggestions from the two hydrographic officers, F.C. Baumeier and T.R. Deelder.

We also thank the Netherlands Organization for the Advancement of Pure Research (ZWO) for financial support.

7. REFERENCES

Amos, A.F., A.L. Gordon and E.D. Schneider, Water masses and circulation patterns in the
1971 region of the Blake-Bahama Outer Ridge. Deep-Sea Res., 18:145-65

van Bennekom, A.J. et al., The seasonal cycles of reactive silicate and diatoms in the Dutch
1974 Wadden Sea. Neth.J.Sea Res., 8:174-207

Cadée, G.C., Primary production off the Guyana coast. Neth.J.Sea Res., 9:128-43
1975

Carritt, D.E. and J.H. Carpenter, Comparison and evaluation of currently employed modifi-
1966 cations of the Winkler method for determining dissolved oxygen in sea water. J.Mar.Res., 24:286-318

Clowes, A.J., Phosphate and silicate in the Southern Ocean. Discovery Rep., (19):120 p.
1938

Deacon, G.E.R., A general account of the hydrology of the South Atlantic Ocean. Discovery
1933 Rep., (7):173-238

Eisma, D., Oceanographic observations on the Surinam Shelf. Spec.Publ.Hydrogr.Newsl., Neth.,
1967 (5):21-53

Eisma, D. and A.J. van Bennekom, Oceanographic observations on the eastern Surinam Shelf
1969 Spec.Publ.Hydrogr.Newsl., Neth., (6):25-30

Fanning, K.A. and M.E.Q. Pilson, On the spectrophotometric determination of dissolved silica
1973 in natural waters. Anal.Chem., 45:136-40

Gessner, F., Untersuchungen über den phosphathaushalt der Amazonas. Int.Rev.Ges.Hydrobiol.,
1960 45:339-45

Gibbs, R.J., Water chemistry of the Amazon River. Geochim.Cosmochim.Acta, 36:1061-6
1972

Goulet, J.E. and M.C. Ingham, The shallow layer of high salinity in the Southwestern tropical
1971 Atlantic Ocean. Bull.Mar.Sci., 21:716-32

Koroleff, F., Direct determination of ammonia in natural waters as indophenol blue.
1970 Inf.Technol.Methods Seawat.Anal.ICES, (3):19-22

Mann, C.R., A.R. Coote and D.M. Garner, The meridional distribution of silicate in the
1973 Western Atlantic Ocean. Deep-Sea Res., 20:791-801

Mazeika, P.A., Circulation and water masses east of the Lesser Antilles. Dtsch.Hydrogr.Z.,
1973 26:51-73

Metcalf, W.G., Shallow currents along the Northeastern coast of South America. J.Mar.Res.,
1968 26:232-43

Milliman, J.D. and E. Boyle, Biological uptake of dissolved silica in the Amazon River
1975 estuary. Science Wash., 189:995-7

Murphy, J. and J.P. Riley, A modified single solution method for the determination of phosphate in natural waters. Anal.Chim.Acta, 27:31-6
1962

Nehring, D., Some remarks on the determination of nitrate and ammonia in sea water. ICES
1968 Interlab.Rep., (2):16-7

Neumann, G., Seasonal salinity variations in the upper strata of the Western tropical
1969 Atlantic Ocean. 1. Sea surface salinities. Deep-Sea Res., 16, Suppl.:165-77

Oltman, R.E., Reconnaissance investigations of the discharge and water quality of the
1967 Amazon. In Atas do Simpósio sôbre a Biota Amazonica, Vol. 3, Limnologia,
pp. 163-85

Pomeroy, L.R., E.E. Smith and C.M. Grant, The exchange of phosphate between estuarine water
1965 and sediment. Limnol.Oceanogr., 10:167-72

Richards, F.A., Dissolved silicate and related properties of some western North Atlantic
1958 and Caribbean waters. J.Mar.Res., 17:449-65

Ryther, J.H., D.W. Menzel and N. Corwin, Influence of the Amazon River outflow on the ecology
1967 of the western tropical Atlantic. 1. Hydrography and Nutrient Chemistry. J.Mar.
Res., 25:69-83

Stalcup, M.C. and W.G. Metcalf, Current measurements in the passages of the Lesser Antilles.
1972 J.Geophys.Res., 77:1032-49

Strickland, J.D.H. and T.R. Parsons, A practical handbook of seawater analysis. Bull.Fish.
1968 Res.Board Can., (167):65-70, 77-80

Tjoe-Awie, E.C., Report on sedimentological investigations as part of the CICAR programme
1975 1970-1972. 1. A reconnaissance survey of bottom sediments in the Amazon's mouth
region. Publ.Rep.Neth.Inst.Sea Res., (1975-19):1:51

Visser, M.P., Over de troebelheid van de Atlantische Oceaan voor de kust van Suriname en
1972 Frans Guyana. Sci.Rep.Neth.Meteorol.Inst., (72-7):65 p.

__________, Physical oceanography in the waters off Surinam and French Guyana during 1970-
1978 1971. FAO Fish.Rep., (200) Suppl.

Wood, E.D., F.A.J. Armstrong and F.A. Richards, Determination of nitrate in seawater by
1967 cadmium-copper reduction to nitrite. J.Mar.Biol.Assoc.U.K., 47:23-31

Wüst, G., Die Kreisläufe der atlantischen Wassermassen, ein neuer Versuch raümlicher
1949 Darstellung. Forsch.Fortschr., 25:285-9

THE CIRCULATION BETWEEN THE CAYMAN SEA AND THE GULF OF MEXICO AS DEDUCED FROM NUTRIENT DISTRIBUTIONS

by

G.A. BERBERIAN and R.B. STARR
NOAA/AOML
Miami, Florida 33149, U.S.A.

CONTENTS

1. INTRODUCTION
2. DATA COLLECTION AND FIELD PROCEDURES
3. LABORATORY ANALYSES
4. OBSERVATIONS AND DISCUSSION
5. CONCLUSIONS
6. ACKNOWLEDGEMENTS
7. REFERENCES

Abstract

Analyses of dissolved oxygen, nitrate, phosphate and silicate from samples collected by the U.S. National Oceanic and Atmospheric Administration's (NOAA) Atlantic Oceanographic and Meteorological Laboratories (AOML) during 1970, 1971 and 1972 in the Cayman Sea and eastern Gulf of Mexico indicate that relative nutrient concentrations can be used to define the deep flow regime of these seas. Results are in agreement with previous findings that the surfaces of the Gulf of Mexico and Cayman Sea have very low nutrient content. However, at depth, the main northward flow through the Yucatan Channel is characterized by relatively high nutrient values and near bottom oxygen values exceeding 5 ml/l, which, together with temperature and salinity, imply this bottom water to be of North Atlantic Deep Water origin. A counterflow at the bottom along the western side of the Yucatan Channel can be distinguished by relatively low oxygen and nutrients. Additionally, nutrient-oxygen data suggest that upwelling occurs at times along the western side of the Yucatan Channel.

Resumen

El análisis del oxígeno disuelto, y de los nitratos, fosfatos y silicatos contenidos en las muestras recogidas por los Laboratorios de Oceanografía y Meteorología Atlántica (AOML) del Organismo Nacional Oceánico y Atmosférico de los Estados Unidos (NOAA) durante 1970, 1971 y 1972 en el Mar del Caimán y en la parte oriental del Golfo de México, indican que las concentraciones correspondientes de nutrientes pueden utilizarse para definir el régimen de las corrientes profundas de esos mares. Los resultados obtenidos coinciden con los anteriores en que las aguas superficiales del Golfo de México y del Mar del Caimán tienen muy bajo contenido de nutrientes; sin embargo, las aguas profundas de la corriente principal hacia el norte, a través del canal de Yucatán, se caracterizan por sus valores relativamente elevados en nutrientes y por valores de oxígeno superiores a 5 ml/l cerca del fondo, los cuales, unidos a la temperatura y a la salinidad, permiten suponer que estas aguas de fondo procederían de las aguas profundas del Atlántico norte. Las secciones del fondo hechas a lo largo de la parte occidental del Canal de Yucatán se caracterizan por un contenido relativamente bajo de oxígeno y de nutrientes. Además, los datos sobre el oxígeno y los nutrientes indican que a veces se producen afloramientos a lo largo de la parte occidental del Canal de Yucatán.

1. INTRODUCTION

Recent advances in the automated analyses for the marine micronutrients such as nitrate, nitrite, silicate and phosphate have permitted the processing of sufficient amounts of data to evaluate them as possible tracers of water circulation. This is particularly useful where the weak gradients of temperature and salinity make these parameters marginal for such purposes. As part of the U.S. participation in the CICAR during the years 1970, 1971 and 1972, more than 3 000 water samples at depths from the surface to over 2 000 m deep from more than 300 oceanographic stations in the Caribbean and Gulf of Mexico have been collected by the Atlantic Oceanographic and Meteorological Laboratories of NOAA and analysed for nutrients, temperature, salinity and dissolved oxygen. It is apparent from these analyses that, with the exception of nitrite, the distributions and concentrations of these nutrients can be useful in helping to describe ocean circulation.

The temperature structure of these seas is quite well known and will not be discussed here. This presentation will be limited to describing the distribution of nutrients, salinity and dissolved oxygen along sections which are important to the understanding of the circulation between the Cayman Sea (the northwestern Caribbean Sea) and the eastern Gulf of Mexico. Our discussion will centre around sections across or immediately south of the Yucatan Channel which were occupied in 1970, 1971 and 1972 (Fig. 1). Concurrent with this discussion of the Yucatan Channel sections and the Cayman Sea circulation, nutrient relationships in the main northward flow through the channel and in variable (but significant) southward counterflow will be presented.

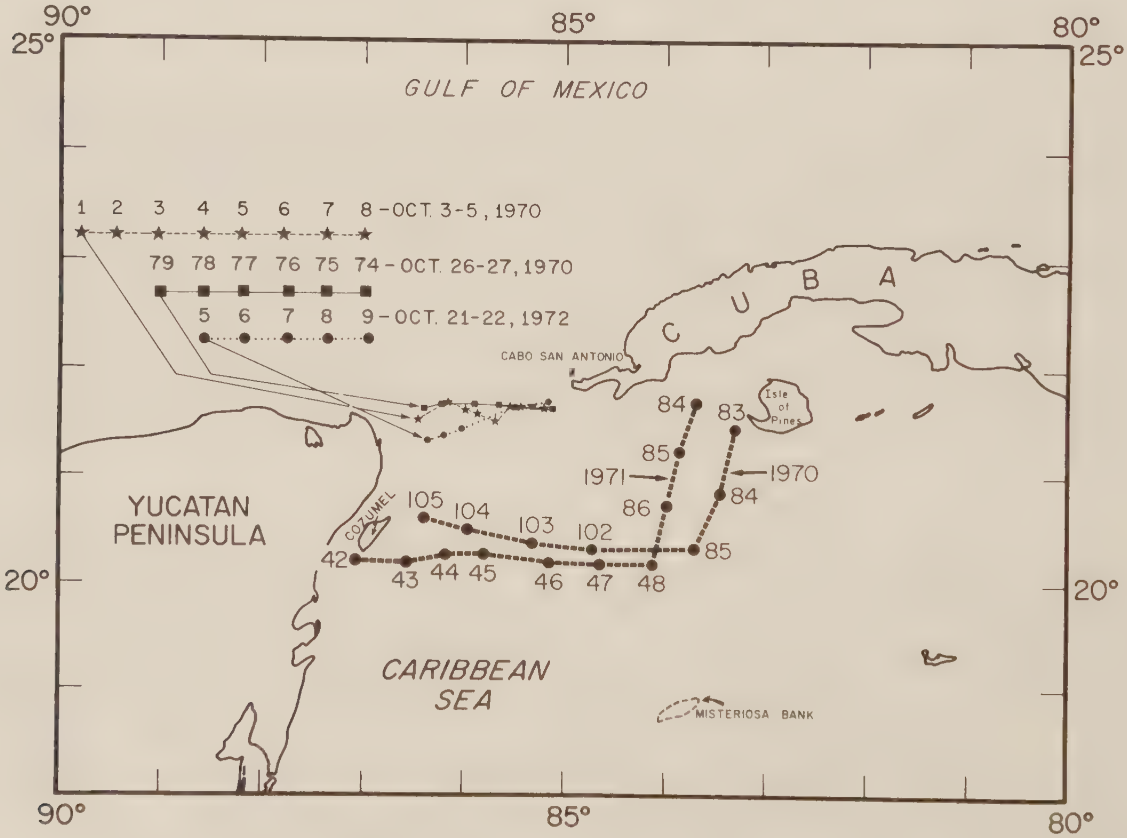
90°
85°
80°
25°
25°
GULF OF MEXICO
1 2 3 4 5 6 7 8 - OCT. 3-5, 1970
79 78 77 76 75 74 - OCT. 26-27, 1970
5 6 7 8 9 - OCT. 21-22, 1972
C U B A
CABO SAN ANTONIO
Isle of Pines
84
83
85
1971
1970
86
84
85
YUCATAN PENINSULA
COZUMEL
105
104
103
102
42
43
44
45
46
47
48
20°
20°
CARIBBEAN SEA
MISTERIOSA BANK
90°
85°
80°

Fig. 1 Location of stations in the Yucatan Channel area

2. DATA COLLECTION AND FIELD PROCEDURES

Data from the following cruises are reported on in this paper: Cruise 1, October to November, 1970; Cruise 2, July to August, 1971; Cruise 3, October to November, 1972. During each cruise, except on stations 1 to 8 across the Yucatan Channel in early October, 1970, temperature and salinity were measured at each station by means of a Plessey model 9006 STD with attached General Oceanics Rosette Multi-Sampler rigged with standard 1.7 l Niskin bottles. Stations 1 to 8 were obtained by oceanographic casts with Nansen bottles. Water samples with the Rosette Multi-Sampler were collected at specified temperatures and depths chosen to sample maximum and minimum physical and chemical properties of the water column as seen in historical oceanographic data. These were analysed for salinity, oxygen and nutrient concentration. Salinity measurements were completed aboard ship using a Beckman inductive salinometer. The samples for dissolved oxygen were drawn first in order to minimize atmospheric contamination and temperature-induced changes. Sample analysis was conducted on board ship using modified Winkler titration method described by Strickland and Parsons (1968).

Approximately 200 to 300 ml aliquots were collected in polyethylene bags (Whirl-Paks), or polyethylene bottles, frozen immediately and returned to AOML Laboratories for nutrient analyses.

3. LABORATORY ANALYSES

The nutrient samples were analysed for dissolved inorganic nitrate (NO^{-}_{3}-N), nitrite (NO^{-}_{2}-N), orthophosphate ($PO^{\equiv}_{4}$-P), and silicate ($SiO^{=}_{4}$-Si), with a four-channel Technicon AutoAnalyzer.

The analytical procedures used in the analysis for nitrate and nitrite are described by Armstrong et al. (1967). Essentially, the orthophosphate is the procedure described by Grasshoff (1965) and the silicate procedure is described by Strickland and Parsons (1968). The water used for standardization, blank determination and wash between samples is filtered Gulf Stream seawater obtained from the surface of the Straits of Florida. The detection limits and precision of analysis for the four nutrients are listed below in Table I.

TABLE I

Operational characteristics of the nutrient-analyses system

Parameter	Range and detection limit µg-at/l	Coefficient of variation (95% confidence level) % at µg-at/l
NO_3-N/l	0.50 - 50.0	0.17 at 15.00
NO_2-N/l	0.10 - 20.0	1.20 at 3.20
PO_4-P/l	0.05 - 20.0	1.60 at 0.64
SiO_4-Si/l	0.50 - 50.0	0.97 at 25.00

4. OBSERVATIONS AND DISCUSSION

In all cases, across the Yucatan Channel, the Subtropical Underwater is characterized by the highest salinities (36.75‰) in the water column, by dissolved oxygen values generally less than 4 ml/l, by phosphate and silicate concentrations usually below their detection limits, and nitrate about 5 µg-at/l. The Antarctic Intermediate Water is distinguished by the lowest salinities (34.85‰) in the water column, by oxygens between 3 and 4 ml/l, phosphates greater than 1.5 µg-at/l, nitrates of 30 to 35 µg-at/l, and silicates of 20 to 25 µg-at/l. Upper North Atlantic Deep Water is typified by salinities very close to 35.00‰, by dissolved oxygens greater than 5 ml/l, by phosphates of approximately 1.0 µg-at/l, nitrate between 20 and 25 µg-at/l, and silicate between 15 and 20 µg-at/l.

With respect to the three sections taken directly across the Yucatan Channel (Fig. 2 through 10), the one obtained on NOAA-CARIB during October, 1972 (Fig. 2, 3 and 4) appears to be in most agreement with the distribution of properties described by Richards (1958) and Howlin and McLellan (1967). Geostrophic current computations performed on this section show a general strong, baroclinic flow to the north, even at depth (Fig. 2). An exception to this, apparent in this figure, is a possible very weak southerly counterflow at depth along the western side of the bottom as seen in the current meter data of Hansen and Zetler (1972). The computed maximum velocity occurs at the surface along the western side of the channel and amounts to 79 cm/sec (1.5 knots). Along the Cuban side of the channel, the flow appears less, while the least flow is in the centre of the channel.

The salinity structure, also shown in Fig. 2, supports these interpretations as it is typical of the salinity values seen in the Caribbean Sea (Wüst, 1964). The Subtropical Underwater as defined here by the 36.75‰ isohaline is concentrated along the west side of the channel, while the Antarctic Intermediate Water below 34.90‰ crosses most of the section. Probable Upper North Atlantic Deep Water with a salinity of 35.00‰ is indicated at the bottom.

The near-surface phosphate, nitrate and silicate values (Fig. 3 and 4) exemplify the low nutrient values seen in these waters throughout the Caribbean and Gulf of Mexico. At the bottom, phosphate values below 1.5 µg-at/l, nitrates under 25 µg-at/l, and silicates from 17 to 20 µg-at/l are associated with the possible deep counterflow. These values are in agreement with the distributions of Richards (1958) and Metcalf (1969), which suggest that, compared to the 1970 results discussed below, the counterflow was insignificant at this time. This conclusion is in agreement with the lack of shear noticed when occupying the western stations of this section compared to 1970. The upward tilt of nutrient isopleths toward the west side of the Yucatan Channel is not great enough to suggest upwelling at the time this section was taken.

In contrast to the regularity shown by the 1972 observations, the Yucatan sections resulting from the October, 1970 work suggest a very different flow regime. Concurrent current meter observations were obtained at the same time as these stations. These have been reported by Hansen and Zetler (1972) and confirm that a south-flowing current was in existence at the bottom of the Yucatan Channel during this period.

There is some evidence of this flow in the computed geostrophic current section (Fig. 5). The calculated velocities for 1970 also show a considerably stronger surface current along the west side of the channel than was observed in 1972. The indicated baroclinic flow on the east side of the channel was very much less than in 1972, while a surface countercurrent is suggested in the vicinity of Station 5. In accordance with these observations, it was noted during the occupation of these stations that the ship drifted rapidly northward on Station 2, and experienced a high wire angle due to very strong shear at depth, while at Station 5 it did not drift at all. At Station 8, the ship drifted southward in a counterflow around Cabo San Antonio, but an additional station closer inshore would be required to define this in Fig. 5.

The concurrent salinity distribution shown in this figure is somewhat more irregular than in 1972 with the Subtropical Underwater shifted to the east side of the channel. Additionally, the core of the Antarctic Intermediate Water, as defined by the 34.85‰ isohaline, is absent or virtually absent and relatively little water of 35.00‰ salinity is present. This suggests less flow of these waters north through the Yucatan Channel at this time.

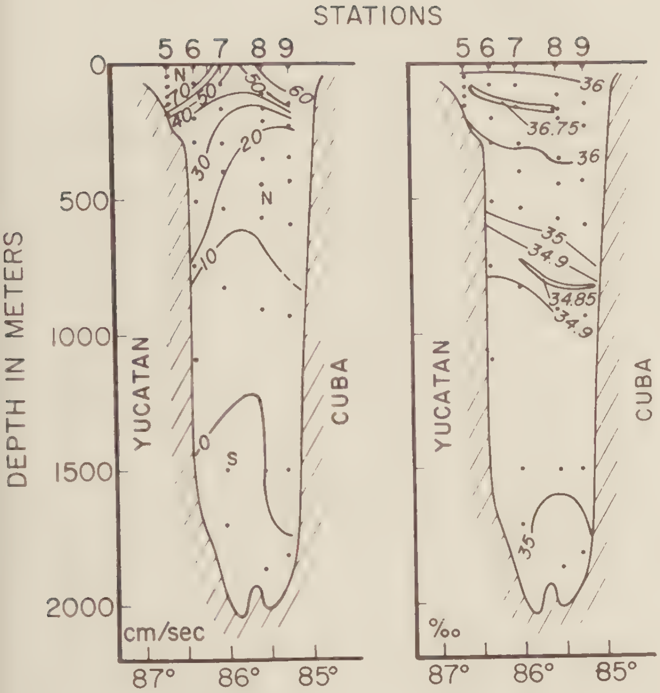

Fig. 2 Isotachs of current velocity relative to 1 700 m depth and salinity distribution, Yucatan Channel, 21-22 October 1972

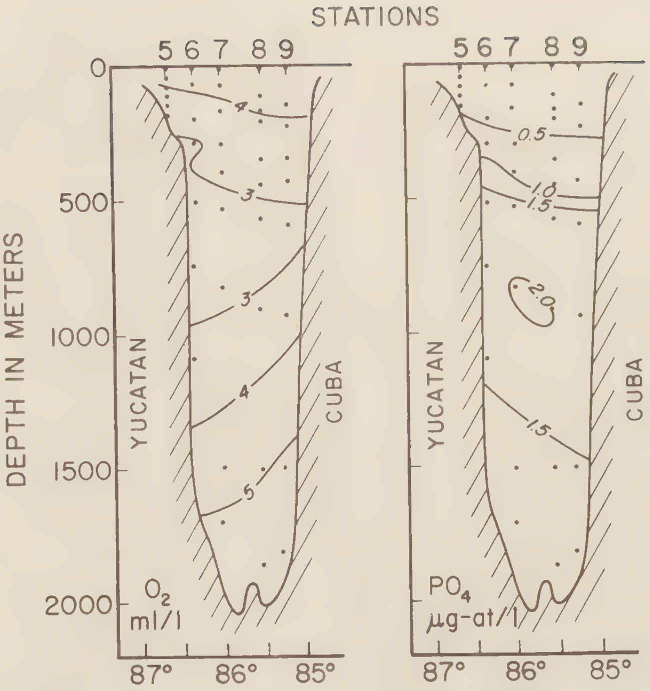

Fig. 3 Regular nutrient distribution, Yucatan Channel, 21-22 October 1972

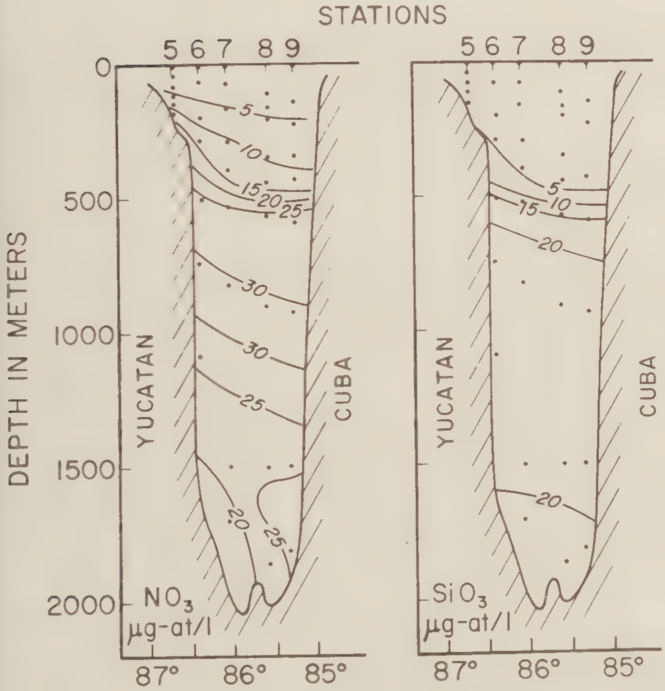

Fig. 4 Regular nutrient distribution, Yucatan Channel, 21-22 October 1972

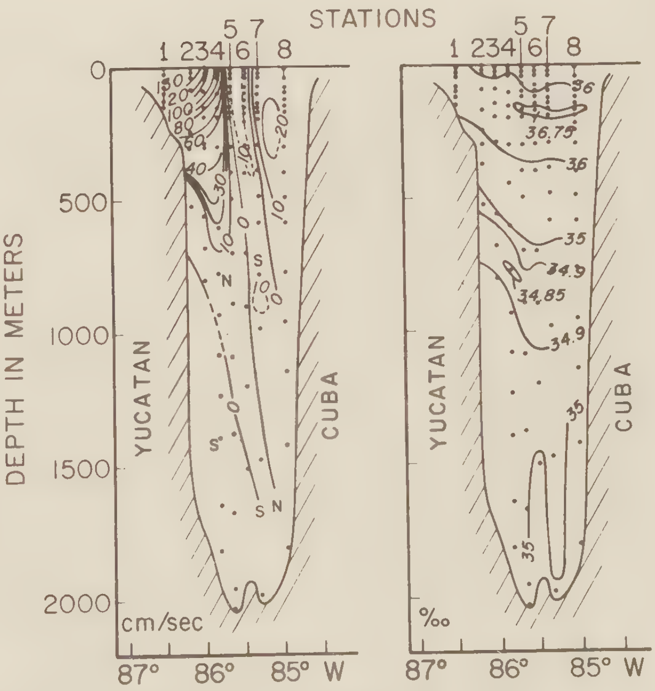

Fig. 5 Isotachs of current velocity relative to 1 700 m depth and salinity distribution, Yucatan Channel, 3-5 October 1970

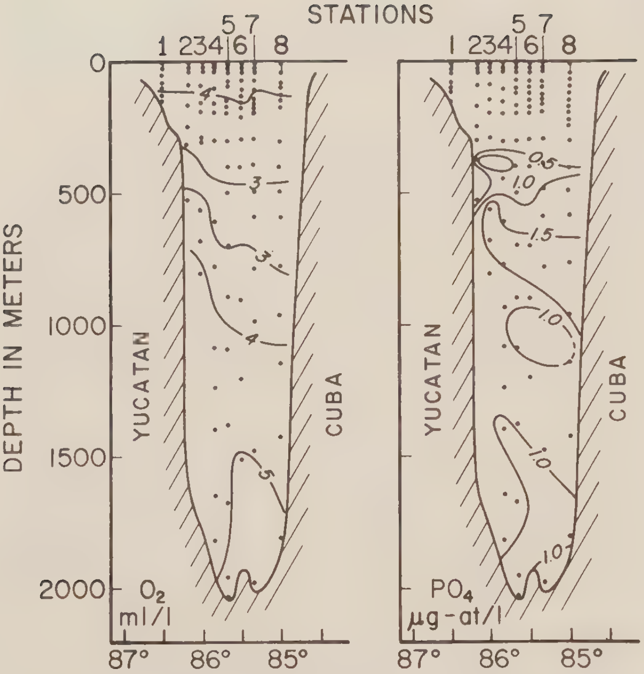

Fig. 6 Anomalous nutrient distribution,
Yucatan Channel, 3-5 October 1970

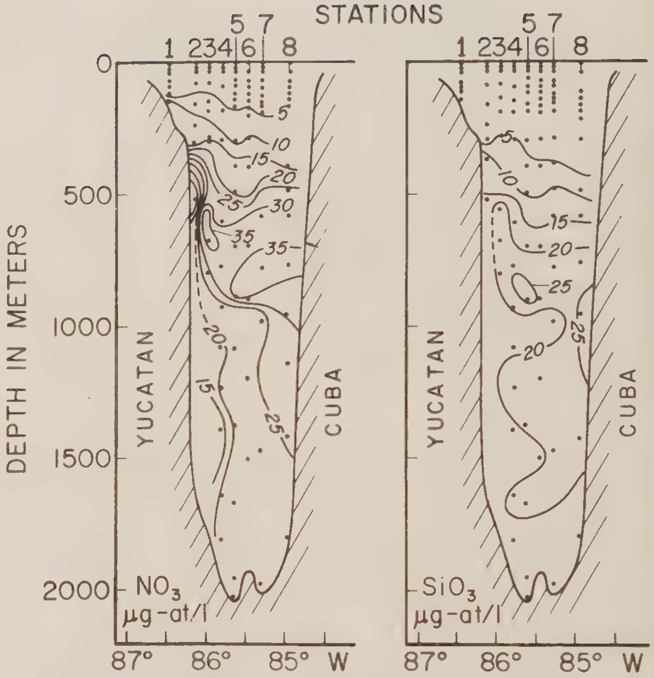

Fig. 7 Anomalous nutrient distribution,
Yucatan Channel, 3-5 October 1970

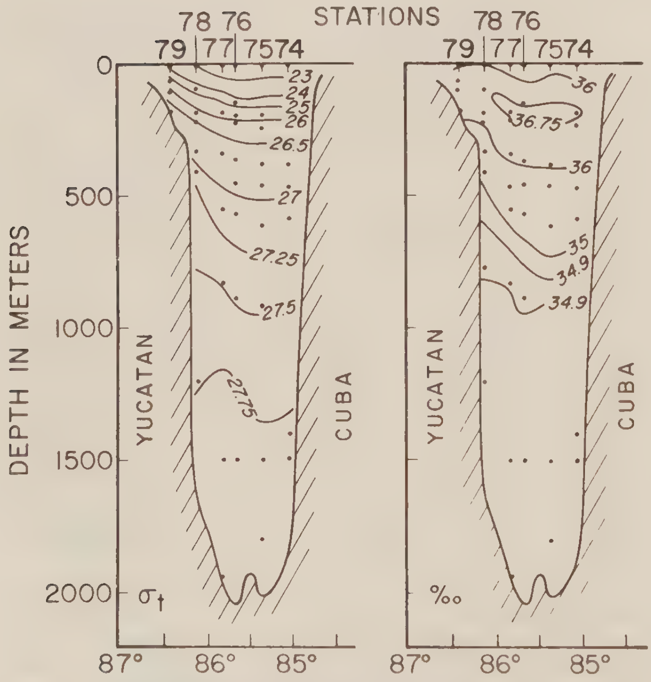

Fig. 8 Density and salinity distributions,
Yucatan Channel, 26-27 October 1970

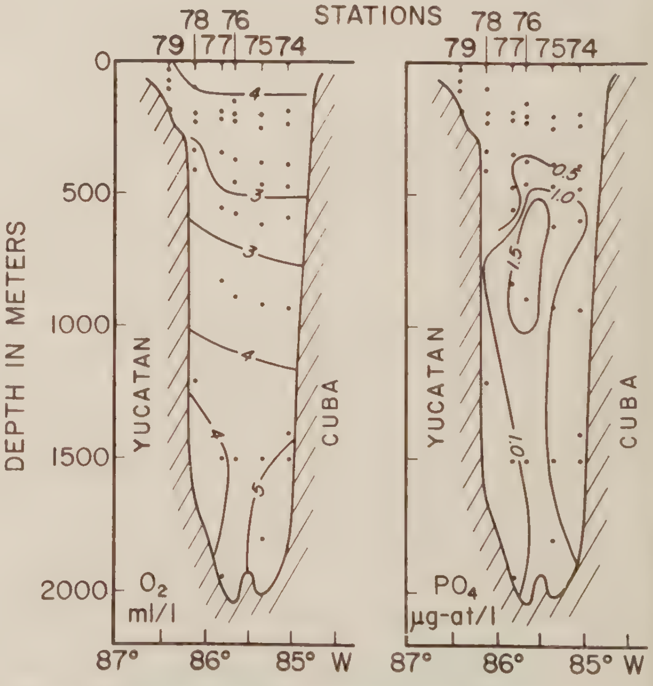

Fig. 9 Anomalous nutrient distribution,
Yucatan Channel, 26-27 October 1970

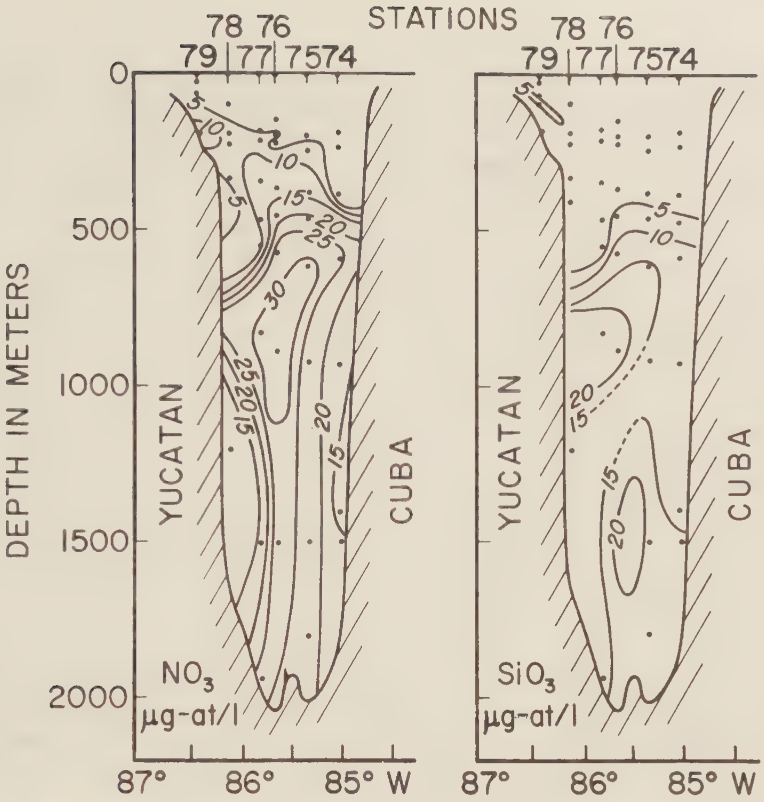

Fig. 10 Anomalous nutrient distribution, Yucatan Channel, 26-27 October 1970

The irregular oxygen-phosphate-nitrate-silicate distributions shown in Fig. 6 and 7 illustrate some of the variability associated with this variation of the flow regime. These data are consistent with the current structure and the salinity distribution already discussed. High nitrate, silicate and phosphate are evident in the main northward flowing current between 500 and 1 000 m depth; while the indicated south flowing bottom water along the Yucatan side has dissolved oxygen values lower than seen previously: phosphates of about 1.0 μg-at/l, nitrates as low as 15 μg-at/l, and silicates again under 20 μg-at/l.

A second 1970 occupation of this line of stations occurred in late October (Fig. 8, 9 and 10). While this section is in general agreement with the first crossing, several significant differences are apparent. The salinity distribution is characterized by a very large core of Subtropical Underwater indicating strong northward flow at shallow depth, but no Antartic Intermediate Water as defined by core salinities of 34.85‰ or less. Additionally, there is no 35.00‰ salinity at the bottom so that the flow of Upper North Atlantic Deep Water at these depths is indicated as being minimal. The density structure and current meter record (Hansen and Zetler, 1972) support a continuing southward bottom counterflow. The dissolved oxygen of this bottom counterflow is now mostly below 4 ml/l, while the phosphate is still close to 1.0 μg-at/l, the nitrate is again in the 15 μg-at/l range, and silica is down to 10 to 12 μg-at/l. Upwelling along the western side of the Yucatan Channel is suggested by the higher than normal near-surface nitrate and silicate values and low oxygens in these figures.

In conjunction with the 1970 Yucatan Channel sections, a line of stations was taken in October-November, 1970 from Cozumel to the vicinity of the Isle of Pines (Fig. 1). This line is important because it crosses an anticyclonic gyre which seems to be a persistent feature between Yucatan Channel and Misteriosa Bank (Molinari, 1975; Hazelworth and Starr, 1975), and because it can be compared to a line of stations (Fig. 1) occupied in 1971 when the threat of a hurricane prevented the taking of the Yucatan Channel section samples. In 1970, the salinity distribution, shown in Fig. 11, agrees with that of the Yucatan Channel section. The 36.75‰ isopleth of the Subtropical Underwater defines the rim of the gyre while the deepening of the lower 34.90‰ isopleth at Station 102 indicates the centre of the gyre. Although there is an appreciable amount of Upper North Atlantic Deep Water as expressed by the 35.00‰ isopleth, very little of the 34.85‰ Antarctic Intermediate Water is evident here, in agreement with the Yucatan Channel sections. The phosphate, nitrate and silicate plots (Fig. 12, 13 and 14) define the gyre very distinctively, particularly the high values associated with the Antarctic Intermediate Water. The nutrient values, as illustrated by silicate (Fig. 14), are low in the centre of the gyre relative to those reported for these depths by Richards (1958, 1960) and Metcalf (1969).

In comparison to the salinity and nutrient distributions in the 1970 section, those of the 1971 section portray a more strongly developed gyre centred on Station 47 and a relatively strong southeasterly flow centred on Station 86 (Fig. 15). This flow is apparently composed of the eastern arm of the gyre and flow from around Cabo San Antonio (Emilsson, 1971; Molinari, 1975; Hazelworth and Starr, 1975). According to their dynamic topography and our geostrophic current computations (Fig. 15), the main northward flow occurs as a broad stream between Stations 42 and 45, while the flow between Stations 45 and 47 is the western arm of the gyre (Hazelworth and Starr, 1975).

The salinity distribution shown in Fig. 16 differs from 1970. The Subtropical Underwater defined by the 36.75‰ isohaline is missing in the rim of the gyre but is seen in the centre and along the Cuban Shelf where mixing is not so intense. The rim of the gyre is conspicuously defined at depth by the large blobs of Antarctic Intermediate Water with a salinity less than 34.85‰. No Upper North Atlantic Deep Water, defined by a salinity of 35.00‰, is seen in this section in 1971.

The dissolved oxygen (Fig. 17) has a surprisingly thin O_2 minimum layer and a very strong gradient in it with an O_2 maximum at 500 m near Cuba. Since this station was near the broad, southern Cuban Shelf and out of the main stream of the flow around Cabo San Antonio, this high oxygen water may originate from the South Cuba Shelf as a result of sinking of high density water (Emilsson, Tapens and Godoy, 1971). The maximum nutrient values are seen here associated with very little flow as shown by phosphate, nitrate and silicate (Fig. 18, 19 and 20). At depth on the eastern and northern stations, the low nutrient values are again in disagreement with earlier findings (Richards, 1958, 1960; Metcalf, 1969); while the low nitrate value at 500 m at the station next to Cuba supports the surface source for this water postulated in the oxygen discussion.

5. CONCLUSIONS

Nutrient values associated with the interchange of water between the Cayman Sea and Gulf of Mexico exhibit characteristics that enable nutrients to be used as tracers of the circulation. Near-surface values of nutrients in these seas are characteristically too low to be useful as tracers, but below 300 to 400 m phosphate, nitrate and silicate distributions appear to be closely related to the circulation pattern. In the Yucatan Channel, high nutrient values are associated with Antarctic Intermediate Water and then decrease roughly 20 percent with depth to values characteristic of Upper North Atlantic Deep Water except in the bottom counterflow where dissolved oxygen is about 1.0 ml/l lower than Upper North Atlantic Deep Water, phosphate ranges around 1.0 μg-at/l, nitrate ranges from less than 15 to 20 μg-at/l, and silicate is less than 20 μg-at/l. In these three Yucatan Channel sections it appears that oxygen and nitrate values are the most definitive indicators of the counterflow. However, because of the indicated variability of this flow, this might not always be the case. It is difficult to make comparisons with historical data because of the lack of nutrient values from this area, particularly nitrate.

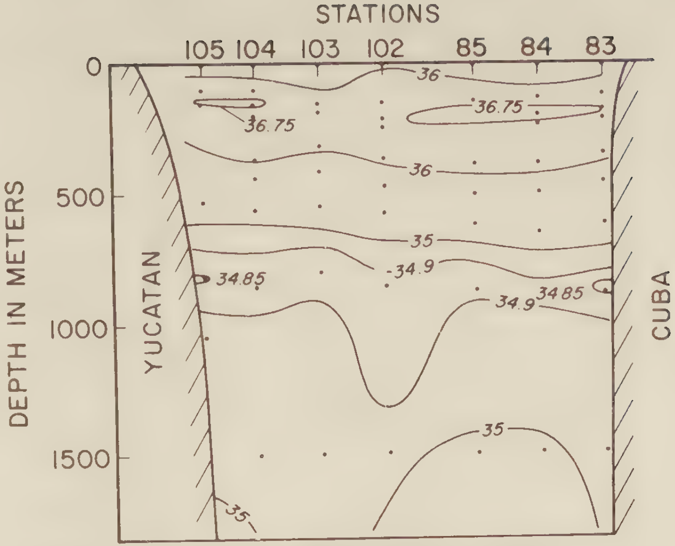

Fig. 11 Salinity distribution (‰)
south of Yucatan Channel,
28 October to 2 November 1970

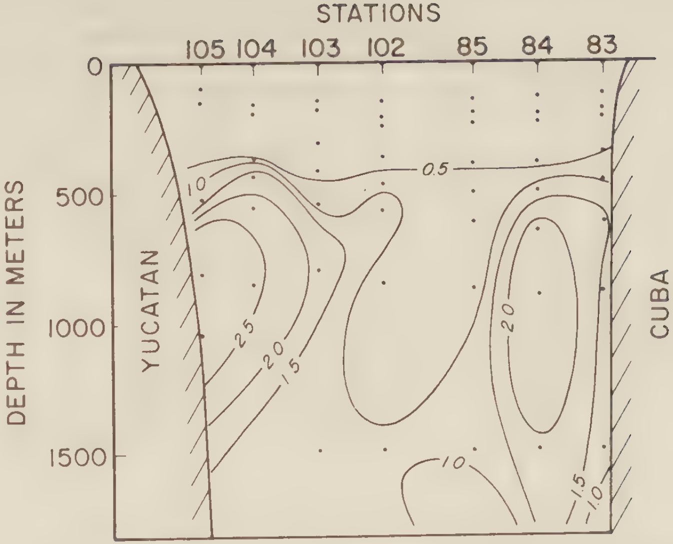

Fig. 12 Phosphate distribution (µg-at/l)
south of Yucatan Channel,
28 October to 2 November 1970

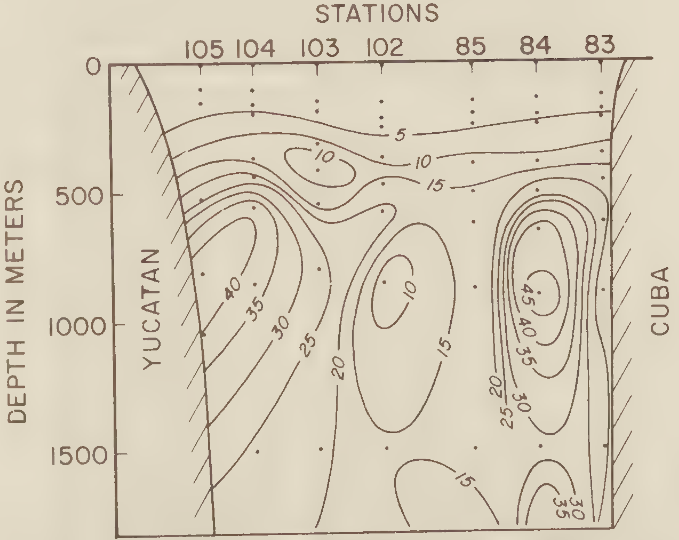

Fig. 13 Nitrate distribution (µg-at/l)
south of Yucatan Channel,
28 October to 2 November 1970

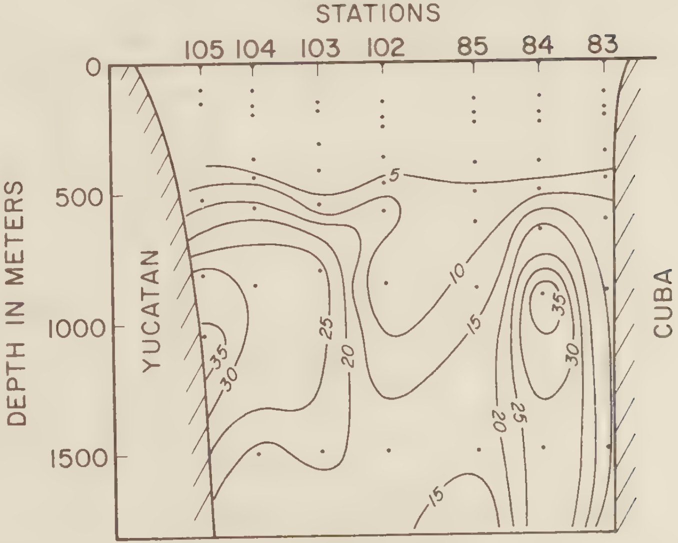

Fig. 14 Silicate distribution (µg-at/l)
south of Yucatan Channel,
28 October to 2 November 1970

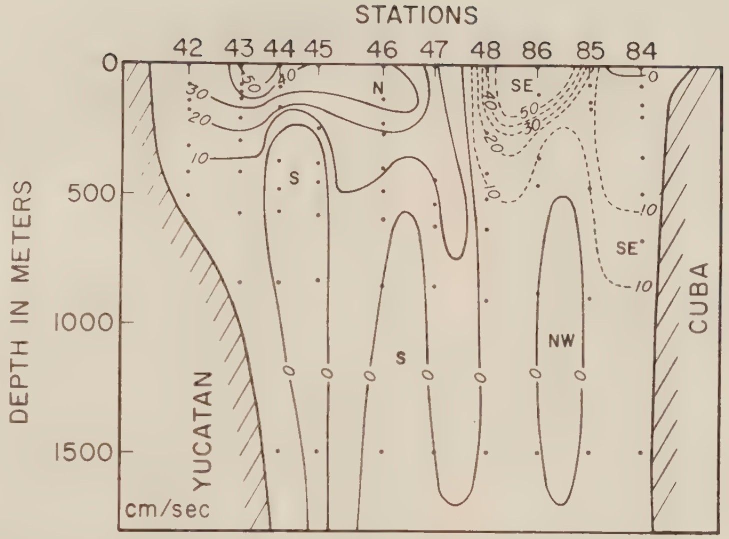

Fig. 15 Isotachs of current velocity (cm/sec) relative to 1 800 m depth, south of Yucatan Channel, 29 July to 30 August 1971

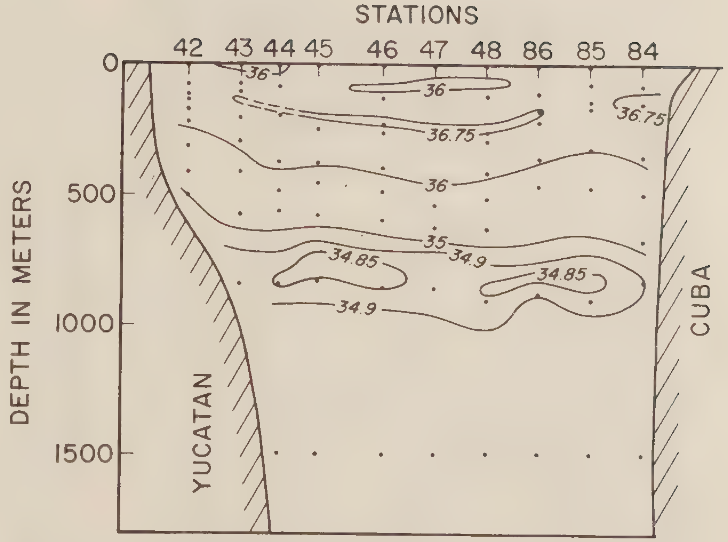

Fig. 16 Salinity distribution (‰) south of Yucatan Channel, 29 July to 30 August 1971

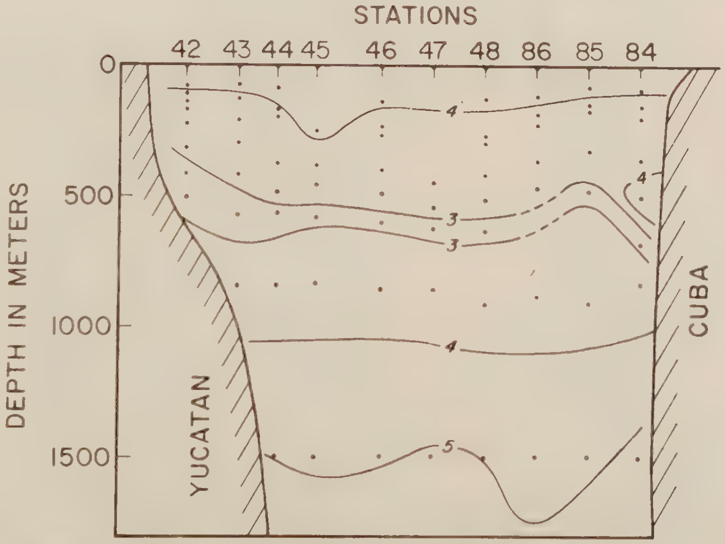

Fig. 17 Oxygen distribution (ml/l) south of Yucatan Channel, 29 July to 30 August 1971

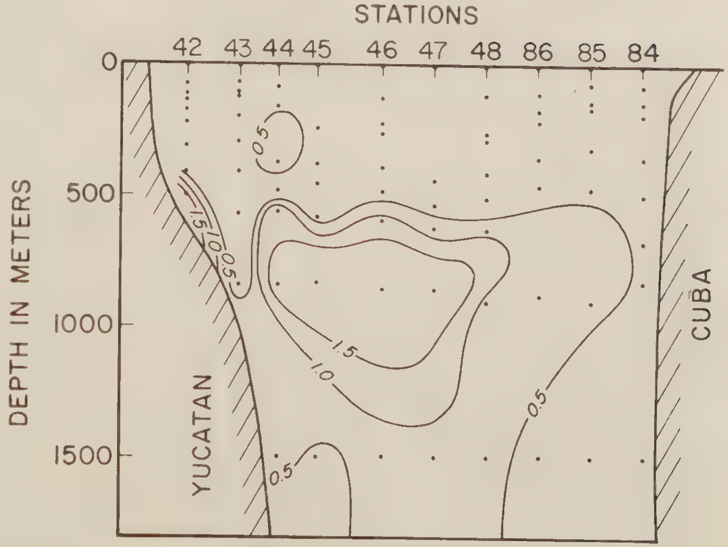

Fig. 18 Phosphate distribution (μg-at/l) south of Yucatan Channel, 29 to 30 August 1971

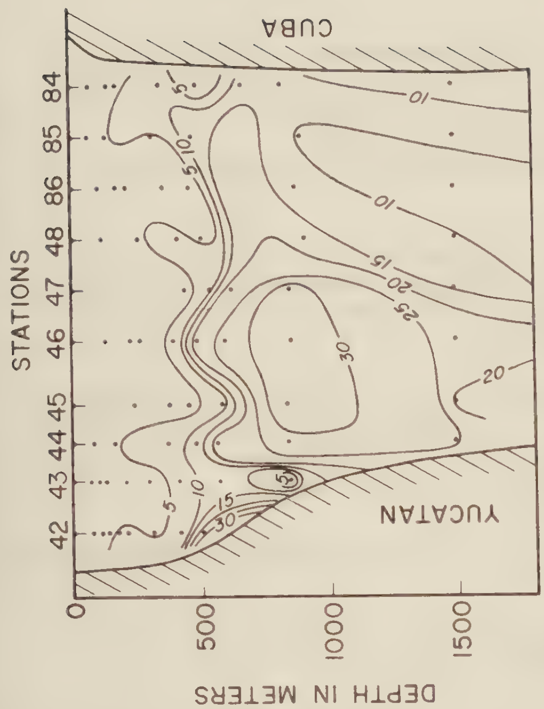

Fig. 19 Nitrate distribution (µg-at/1) south of Yucatan Channel, 28 July to 30 August 1971

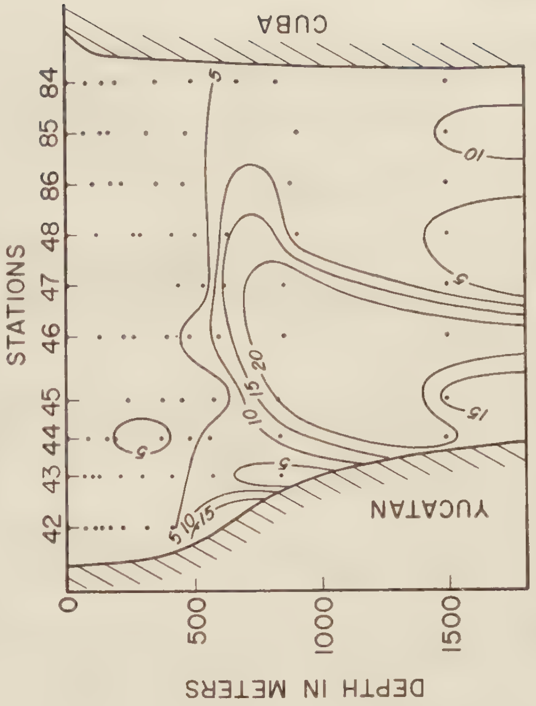

Fig. 20 Silicate distribution (µg-at/1) south of Yucatan Channel, 28 July to 30 August 1971

Comparing the sections across Yucatan Channel and to the south in the Cayman Sea with one another indicates that the nutrient distributions, the associated salinity structure and the flow determinations are quite variable with time, although there is consistency in the major features. The October, 1972 Yucatan Channel section has the most normal nutrient structure with the least indication of southerly flow at the bottom or at the surface around Cabo San Antonio. Supporting current calculations indicate a strong baroclinic flow through the Yucatan Channel at the surface from the Cayman Sea to the Gulf of Mexico, particularly along the western side and, a probably intermittent, but definable, counterflow along the bottom on the Yucatan Peninsula side. Additionally, a variable southerly, though possibly continuous, surface flow is evident around Cabo San Antonio. The anticyclonic gyre crossed by the Cayman Sea sections has a prominent nutrient signature and seems to be a permanent feature between Misteriosa Bank and Yucatan Channel.

6. ACKNOWLEDGEMENTS

The authors express their thanks to the officers and crew of the R/V DISCOVERER for the long and diligent hours they devoted to collecting these data. Thanks are also due to John Hazelworth of AOML for data processing for the geostrophic current computations. The work was funded in part by the National Science Foundation under International Decade of Exploration grant AG-253. We would also like to thank Mr. Robert Carrodus and his group for all the illustrations in this paper.

7. REFERENCES

Armstrong, F.A.J., C.R. Stearns and J.D.H. Strickland, The measurement of upwelling and 1967 subsequent biological processes by means of the Technicon Auto Analyzer and associated equipment. Deep-Sea Res., 14:381-9

Emilsson I., Note on the countercurrent in the Yucatan Channel and the Western Cayman Sea. 1971 Geofis.Int., Mex., 11:139-49

Emilsson, I., J. Tappanes and J. Godoy, Aspectos hidrográficos de la plataforma sur de 1971 Cuba. In Unesco/FAO Symposium on Investigations and Resources of the Caribbean Sea and Adjacent Regions, Willemstad, Curaçao, 18-26 November 1968. Paris, Unesco, pp. 64-71

Grasshoff, K., Automatic determination of fluoride, phosphate and silicate in sea water. 1965 In Technicon Fifth International Symposium, Automation in analytical chemistry, held in London, October 13, 1965. Tarrytown, New York, Mediad Inc., Publ. No.65-P76E, pp. 304-7

Hansen, D.V. and B.D. Zetler, Deep currents in the Yucatan Strait. Trans.Am.Geophys.Union, 1972 53:392 (Abstr.)

Hazelworth, J.B. and R.B. Starr, Oceanographic conditions in the Caribbean Sea during the 1975 summer of 1971. NOAA Tech.Memo., (ERL 344-AOML 20):144 p.

Metcalf, W.G., Dissolved silicate in the deep North Atlantic. Deep-Sea Res., 16 Suppl.: 1969 139-45

Molinari, R.L., A comparison of observed and numerically simulated circulation in the Cayman 1975 Sea. J.Phys.Oceanogr., 5:51-62

Nowlin, W.D. Jr. and H.J. McLellan, A characterization of the Gulf of Mexico waters in 1967 winter. J.Mar.Res., 25:29-59

Richards, F.A., Dissolved silicate and related properties of some western North Atlantic 1958 and Caribbean waters. J.Mar.Res., 17:449-65

__________, Some chemical and hydrographic observations along the north coast of South 1960 America. 1. Cabo Tres Puntas to Curaçao, including the Cariaco Trench and Gulf of Cariaco. Deep-Sea Res., 7:163-82

Strickland, J.D.H. and T.R. Parsons, A practical handbook of sea water analysis. Bull.Fish. 1968 Res.Board Can., (167):311 p.

Wüst, G. and A. Gordon, Stratification and circulation in the Antillean-Caribbean basins. 1964 Part 1. Spreading and mixing of the water types with an oceanographic atlas. New York, Columbia University Press, 201 p.

ESTUDIOS PRELIMINARES SOBRE LOS NIVELES DE ALGUNOS CONTAMINANTES EN LA LAGUNA DE TERMINOS, CAMPECHE, MEXICO

por

A.V. BOTELLO, E. HICKS y E.F. MANDELLI[1]
Centro de Ciencias del Mar y Limnología (U.N.A.M.)
Apartado Postal 70-305
México 20, D.F. México

CONTENIDO

1. INTRODUCCION
2. MATERIALES Y METODOS
3. RESULTADOS Y DISCUSION
4. CONCLUSIONES
5. REFERENCIAS

Resumen

La elección de la Laguna de Terminos se hizo en base a su condición natural aparentemente inalterada, que serviría como un patrón de comparación con otras zonas ya afectadas por procesos humanos. Los estudios realizados incluyeron la determinación de algunos contaminantes en aguas, organismos y sedimentos.

Los resultados indicaron concentraciones relativamente bajas de nitrógeno y fósforo de fuentes inorgánicas. Durante la época de lluvias se notó un ligero incremento de estas substancias sin alcanzar concentraciones que impliquen eutroficación incipiente.

Las concentraciones de metales pesados pueden ser consideradas como valores naturales, mostrando ligeras variaciones estacionales.

Los niveles de n-parafinas en invertebrados y fanerógamas marinas representan valores naturales no afectados por la presencia de hidrocarburos fósiles. Lo mismo ocurre con los hidrocarburos aromáticos policíclicos.

Finalmente, el análisis de n-parafinas en los sedimentos permitió detectar zonas de diferente concentración natural de estos compuestos y zonas en donde es evidente la presencia de hidrocarburos fósiles debido a actividades portuarias.

---

[1] Unesco/PNUD

Abstract

Terminos Lagoon was chosen for this study because it is apparently unpolluted and can therefore provide a useful comparison with other areas already affected by human activities. The study included measurements of various pollutants in the water, organisms and sediments.

The results showed fairly low concentrations of inorganic nitrogen and phosphorous. There was a slight increase during the rainy season, but not to levels suggesting incipient entrophication.

The heavy metal concentrations can be considered to be natural background values, showing only small seasonal variations.

Hydrocarbon concentrations in organisms also appear to be at natural levels, but in the sediments there is some spatial variation, indicating the effect of passing vessels in some areas.

1. INTRODUCCION

Existe la necesidad de comenzar con estudios básicos sobre los niveles de contaminantes presentes en zonas costeras y estuarinas. En el caso particular de México, el cual cuenta con 1 156 000 hectáreas de lagunas costeras y zonas estuarinas, esta inquietud adquiere especial interés.

Entre las lagunas costeras de México, la Laguna de Términos, reviste gran importancia debido a su potencial biológico-pesquero; además de ser una zona que aún en la actualidad ha sido muy poco afectada por las diversas actividades humanas.

El interés del presente estudio radica en la condición que presenta la citada laguna, la cual puede ser considerada como un modelo de un área en etapa de preindustrialización. Esta condición natural inalterada permite utilizarla como patrón de comparición natural inalterada permite utilizarla como patrón de comparación con otras lagunas costeras del Golfo de México, en donde la influencia de las actividades humanas no permiten determinar con certeza los valores básicos de substancias naturales y artificiales potencialmente consideradas como contaminantes.

La Laguna de Términos, se encuentra localizada en el litoral del Golfo de México, entre los meridianos 91°15' y 92°00' de longitud oeste y los paralelos 18°25' y 19°00' de latitud norte, con una longitud de 70 km y 28 km de ancho, estando limitada al norte por la Isla del Carmen. Es una laguna somera con una profundidad máxima de 4,50 m (Phleger y Ayala-Castañares, 1971). Tres grandes ríos descargan sus aguas en la laguna y son: el Palizada, Chompin y Candelaria, los cuales forman parte de la red hidrológica del Río Usumacinta. En el presente estudio se consideraron como contaminantes potenciales la presencia de hidrocarburos aromáticos organoclorados, hidrocarburos parafínicos, hidrocarburos aromáticos policíclicos y algunos metales pesados en organismos indicadores. Con respecto a la calidad de las aguas se hizo un estudio de la distribución de las substancias nutrientes para identificar posibles fuentes de eutroficación.

Estos estudios son los primeros que se realizan en forma sistemática en las lagunas del litoral mexicano y es la parte inicial de un proyecto nacional que el Centro de Ciencias del Mar y Limnología de la Universidad Nacional Autónoma de México, tiene programade para zonas costeras del Golfo de México y el Pacífico.

2. MATERIALES Y METODOS

La zona de estudio fué dividida en 12 sectores comprendidos cada uno dentro del área que corresponde a 10 minutos de latitud y 10 minutos de longitud. En el área lagunar incluyendo las bocas, se establecieron 27 estaciones de nuestreo planeadas y distribuídas para obtener datos representativos de la hidrografía lagunar (Fig. 1).

Las substancias nutrientes disueltas en el agua ($N\text{-}NO_2^- + NO_3^-$, $N\text{-}NH_3 + NH_4^+$ y $P\text{-}PO_4^{-3}$), se analizaron siguiendo los métodos y recomendaciones de Strickland y Parsons (1968).

Los metales pesados Cd, Cu y Zn, presentes en invertebrados se determinaron por medio de espectrofotometría de absorción atómica y conforme a las técnicas publicadas por la FAO (1975), el Pb por medio de la técnica de Pagenkopf et al. (1972), y el Hg según Uthe et al. (1970).

Los hidrocarburos aromáticos organoclorados se analizaron por cromatografía de gases, según la técnica de Zitko (1971).

Los hidrocarburos parafínicos y los aromáticos policíclicos fueron analizados siguiendo los métodos empleados por Clark y Blumer (1967), y la técnica desarrollada por Onuska et al. (1975) y por medio de cromatografía de gases-espectrometría de masas.

3. RESULTADOS Y DISCUSION

3.1 Nutrientes

Las variaciones de los parámetros hidroquímicos se presentan en el Cuadro I.

Con respecto a los compuestos de nitrógeno inorgánico, en la Laguna de Términos como en casi todas las lagunas litorales, las fuentes más importantes son los compuestos de amonio y amoníaco, siguiendo en orden de importancia los nitratos y nitritos.

Del análisis del cuadro se observa que el amonio y amoníaco son los más abundantes de los compuestos nitrogenados, aumentando considerablemente durante el mes de julio, por lo que se considera que este incremento se debe al aporte de los ríos, que se suma a los procesos de regeneración in situ.

La concentración de nitritos y nitratos en la columna de agua fué más baja que la del amonio y amoníaco durante el ciclo hidrológico y su distribución dentro de la columna líquida del área lagunar, se mantuvo muy homogénea.

La concentración de los compuestos de fósforo ($P\text{-}PO_4^{-3}$) se mantuvo baja y estable, durante el período de estudio; los valores oscilaron entre 0,10 y 0,26 µg.at/l, sin presentarse una diferencia estadística significativa.

Aunque no se conoce con certeza la contribución de compuestos de fósforo por los ríos que descargan en el vaso lagunar, se considera que un alto porcentaje de los mismos son producto de su regeneración in situ.

3.2 Hidrocarburos aromáticos organoclorados

En el Cuadro II se observan las concentraciones de insecticidas y BPCs, contenidos en Crassostrea virginica proveniente de los bancos ostrícolas de Laguna de Términos.

De los insecticidas el p′ - p′ DDE fué el más abundante con una concentración promedio de 0,007 ppm (peso húmedo) y en tanto el p′ - p′ DDT, el o′ - p′ DDT, el p′ - p′ Methoxichlor y el Dieldrin, se presentaron en concentraciones menores a 0,001 ppm (peso húmedo) y los BPCs con un valor promedio de 0,0046 ppm.

Estos valores se consideran significativamente bajos al ser comparados con los límites de tolerancia en alimentos permitidos, por la U.S. Food and Drug Administration. Por lo tanto, se infiere que la presencia de estos compuestos en Crassostrea virginica es el resultado del acarreo de los mismos y que son derivados de la incipiente actividad agrícola que se desarrolla en las áreas cercanas a la laguna o que bien pueden ser transportados por la atmósfera (Duce et al., 1974; Harvey y Steinhaver, 1974), a partir de áreas con alta actividad industrial y agrícola.

3.3 Metales pesados

Con respecto a los metales pesados presentes en Crassostrea virginica, las concentraciones de éstos, se anotan en el Cuadro III. Se puede ver que el Pb y Hg no tienen variaciones significativas, en tanto el Zn, Cu y Cd presentan un incremento notable en el análisis correspondiente al mes de noviembre, lo cual sugiere un aumento de estos elementos en el medio donde se desarrollan los ostiones, debido a que el caudal de los ríos que desembocan a la laguna aumenta considerablemente y en consecuencia el material aportado contiene apreciables concentraciones de estos metales. Asimismo, al compararse los resultados obtenidos con los valores límites de tolerancia en alimentos se ve que la concentración de éstos permanece baja, considerándolos como niveles naturales en un área libre de interacción con actividades humanas.

3.4 Hidrocarburos parafínicos y aromáticos policíclicos

Las concentraciones de los hidrocarburos parafínicos, están sumarizadas en el Cuadro IV, y éstos varían en relación con el organismo en que se presentan.

Así en fanerógamas marinas el valor promedio es de 10,9 ppm, en algas bénticas de 8,7 ppm y en invertebrados (Crassostrea virginica) de 5,7 ppm (peso húmedo).

Los valores del CPI o Carbon Preference Index (Cooper y Bray, 1963) van de 1,2 a 1,4 los cuales concuerdan con los encontrados por esos autores para organismos marinos.

En los sedimentos la concentración de n-parafinas se presenta en un rango de 6 a 28 ppm (peso húmedo) con un valor medio de 13,5 ppm, correspondiendo a la estación de muestreo no. 1, los valores más altos (28 ppm). En el correspondiente cromatograma (Fig. 2) se observa la presencia de parafinas con bajo peso molecular, además de los hidrocarburos Pristano y Fitano, lo cual indica que esa zona se encuentra ligeramente contaminada por la acción del hombre, debido a las actividades portuarias y al constante tránsito de embarcaciones pesqueras.

La menor concentración de n-parafinas (6 ppm) se presentó en sedimentos provenientes de la estación de muestreo no. 27 (Fig. 3), lo que es debido en parte al efecto de las corrientes marinas provenientes del Golfo de México y que penetran en la laguna a través de esta región (Phleger y Ayala-Castañares, 1971; Mandelli y V. Botello, 1974), las cuales no permiten la sedimentación de organismos y de material orgánico, por lo que la producción natural de hidrocarburos biogénicos se ve reducida a un mínimo (Blumer, 1965; Han et al., 1968).

El CPI presenta un valor promedio de 3,8, lo cual confirma la predominancia de las parafinas de carbono impar y este valor está dentro del rango (2,4 a 5,5) reportado para otras regiones (Cooper y Bray, 1963; Clark y Blumer, 1967).

En Crassostrea virginica además de hidrocarburos parafínicos se analizó el contenido de hidrocarburos aromáticos policíclicos (PAHs) los cuales se presentaron en una concentración de 3,1 ppm (peso húmedo) de la cual 0,049 ppm corresponde a los Benzopirenos.

En el Cuadro V las concentraciones de hidrocarburos se comparan con los obtenidos por Ehrhardt (1972) para esta misma especie proveniente de zonas contaminadas (Bahía de Galveston, EE. U U.) y si bien los datos de ese autor son un caso extremo de contaminación, nos brindan la oportunidad de contrastarlos con los obtenidos en una zona que se considera inalterada.

Con respecto a los Benzopirenos, los datos contenidos en el Cuadro V no son estrictamente comparables, debido a que en este trabajo son reportados como Benzopirenos totales incluyendo al 3,4 Benzopirenos con actividad carcinogenética y otros isómeros no activos. El dato comparativo de Cahnmann y Kuratsume (1957) se incluye como referencia de una zona portuaria contaminada y se refiere exclusivamente al isómero activo (3,4 Benzopireno).

4. CONCLUSIONES

Los datos presentados en este trabajo nos brindan información básica sobre el comportamiento de las substancias nutrientes en la columna de agua de la laguna. Las variaciones en cuanto a la concentración de éstas se relacionan principalmente con la regeneración interna de las mismas.

Los resultados obtenidos a través de este estudio muestran que la Laguna de Términos se mantiene como un medio ambiente estuarino oligotrófico.

En cuanto a las concentraciones de hidrocarburos aromáticos organoclorados, hidrocarburos parafínicos y aromáticos policíclicos, se mantienen en niveles bajos cuando son comparados con zonas contaminadas.

CUADRO I

Valores medios de nutrientes integrados para la columna de agua de Laguna de Términos, Campeche, México

MUESTREO	$N-NO_2^- + NO_3^-$ µg at/l	$N-NH_3 + NH_4^+$ µg at/l	$P-PO_4^{-3}$ µg at/l
III-1974	0.17	5.40	0.20
V-1974	0.28	4.98	0.10
VII-1974	0.22	25.08	0.12
IX-1974	1.35	4.30	0.17
XI-1974	0.62	1.26	0.26
II-1975	0.28	3.23	0.19

CUADRO II

Insecticidas y BPCs residuales en *Crassostrea virginica*, de Laguna de Términos, Campeche, México

INSECTICIDAS	ppm (PESO HUMEDO)	LIMITES DE TOLERANCIA EN ALIMENTOS ppm (1)
p'-p' DDE	0.004-0.011 (0.007)	0.5-7.0
p'-p'DDT+o'-p'DDT	< 0.001	
p'-p' METHOXICHLOR	< 0.001	——
DIELDRIN	< 0.001	0.03-0.3
BPC's	0.018-0.074 (0.046)	2.0

(1) U.S. Food and Drug Administration.

CUADRO III

Valores medios de metales pesados en tejidos de *Crassostrea virginica*, Laguna de Términos, Campeche, México

FECHA DE COLECTA	METALES PESADOS ppm (PESO HUMEDO)				
	Hg	Cd	Pb	Cu	Zn
VII-1974	———	0.83	0.25	26.5	84.2
IX-1974	0.035	0.74	———	22.4	74.8
XI-1974	0.044	1.07	0.27	35.3	158.2
II-1975	0.053	0.79	0.25	21.3	87.3
LIMITES DE TOLERANCIA EN ALIMENTOS	0.50	10	0.50	50	100

CUADRO IV

Concentración de n-parafinas en organismos y sedimentos de Laguna de Términos, Campeche, México

MATERIAL	CPI(1)	n-PARAFINAS ppm PESO HUMEDO
FANEROGAMAS MARINAS	1.2	9.7 - 12.7 (10.9)
ALGAS BENTICAS	1.4	(8.7)
INVERTEBRADOS	1.2	3.3 - 8.4 (5.7)
SEDIMENTOS	3.8	6 - 28 (13.5)

(1) CPI Cooper y Bray, 1963.

CUADRO V

Concentración de hidrocarburos en tejidos de *Crassostrea virginica*, de Laguna de Términos, comparados con valores para la misma especie de zonas contaminadas

HIDROCARBUROS	ANALISIS	ppm (peso húmedo)	PROCEDENCIA
n-Parafinas	CG/EM	5.7	Laguna de Términos, Campeche México (Este trabajo)
HAP's	CG/EM	3.1	
Benzopirenos	CG/EM	0.049	
n-Parafinas	CG/EM	104	Bahía de Galveston, Texas U. S. A. Ehrhardt (1972)
HAP's	CG/EM	132	
3,4 Benzopireno	UVE	0.010 - 0.020	Norfolk, Virginia, U.S.A. Cahnmann y Kuratsune (1957)

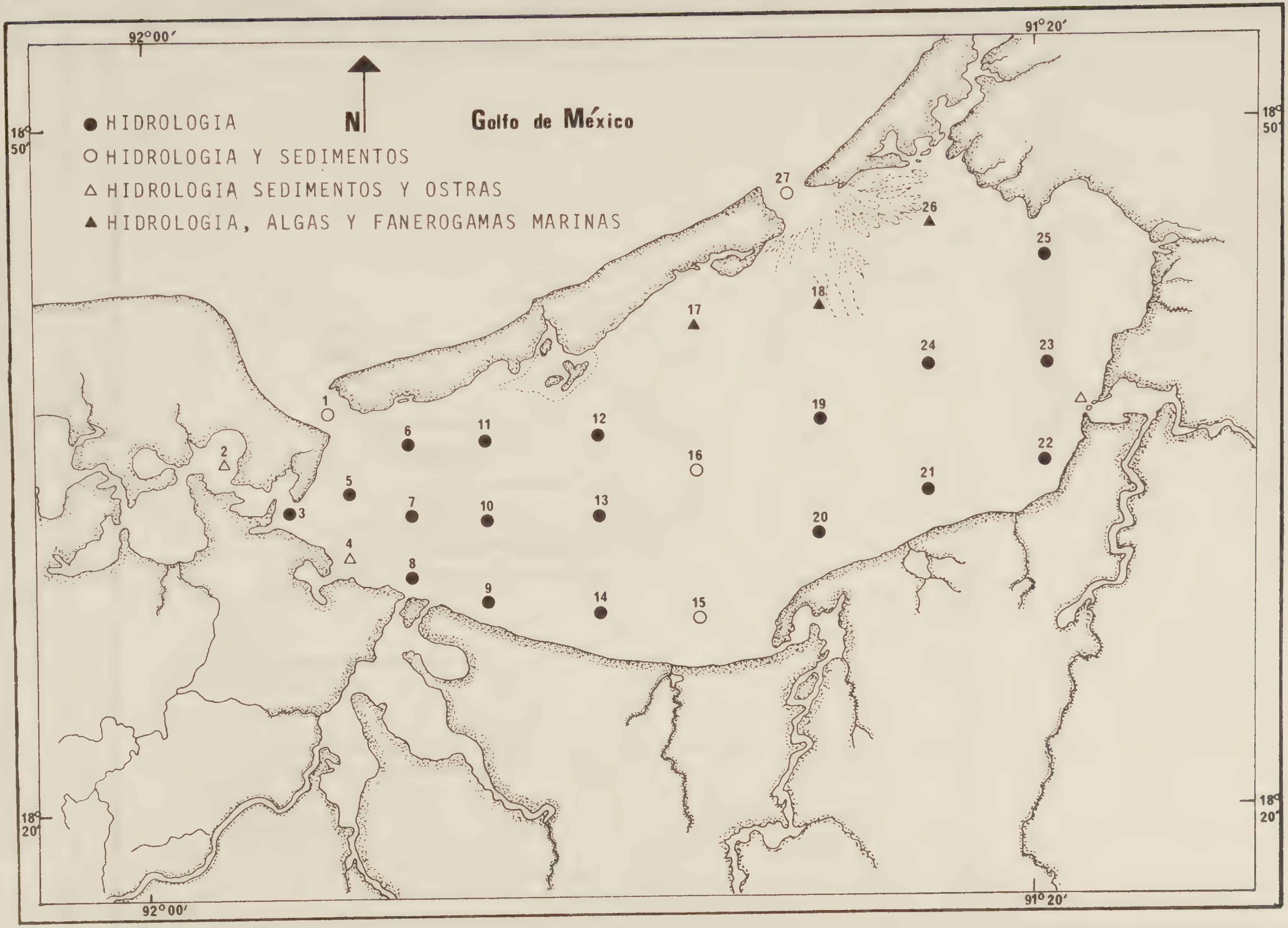
● HIDROLOGIA
○ HIDROLOGIA Y SEDIMENTOS
△ HIDROLOGIA SEDIMENTOS Y OSTRAS
▲ HIDROLOGIA, ALGAS Y FANEROGAMAS MARINAS
N
Golfo de México
92°00′
91°20′
18° 50′
18° 20′
1
2
3
4
5
6
7
8
9
10
11
12
13
14
15
16
17
18
19
20
21
22
23
24
25
26
27

Fig. 1 Localización de las estaciones de muestreo en la Laguna de Términos, Campeche, México

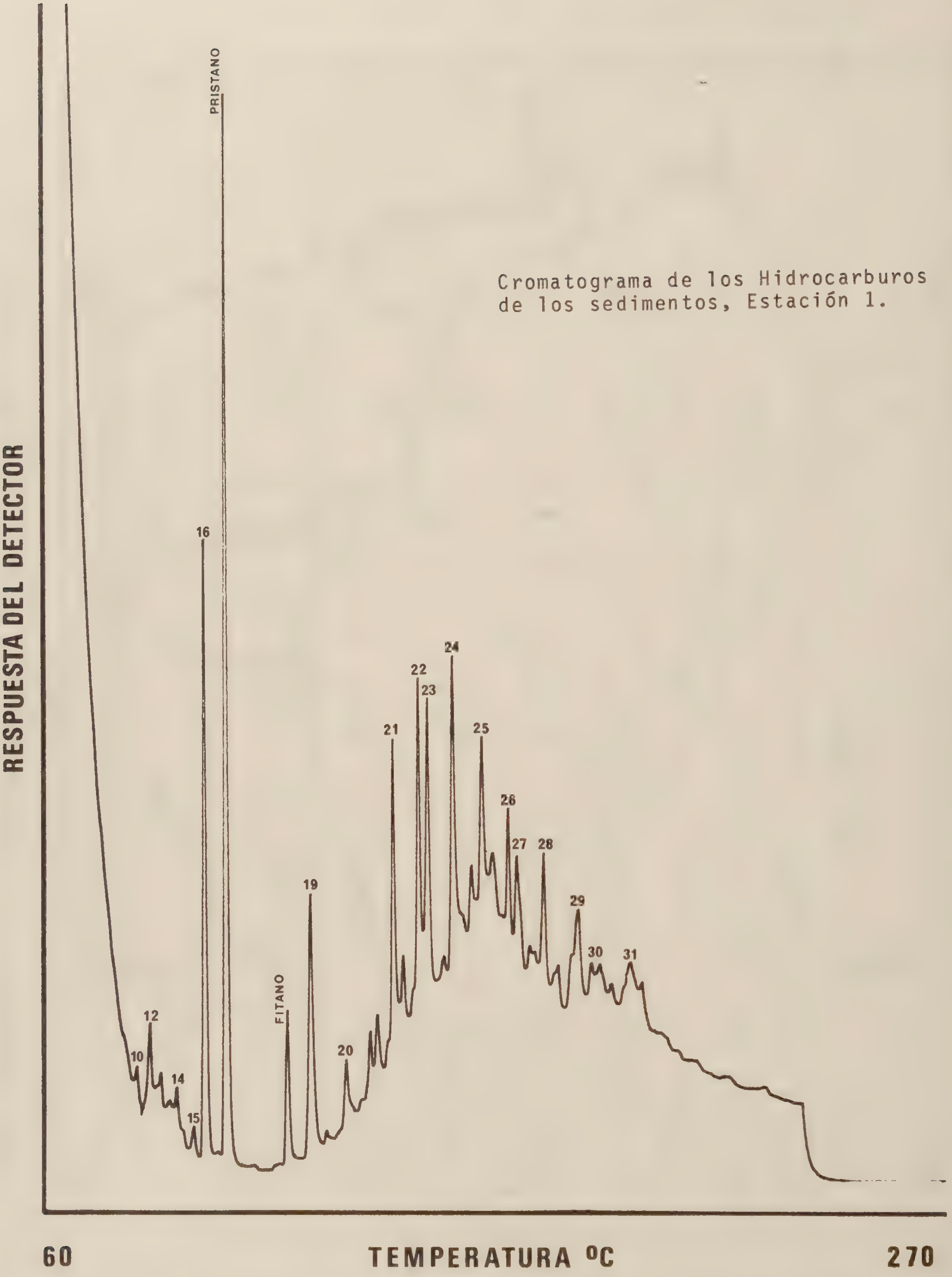
Cromatograma de los Hidrocarburos
de los sedimentos, Estación 1.

Fig. 2 Cromatograma de las n-parafinas presentes en sedimentos
de la estación de muestreo no. 1

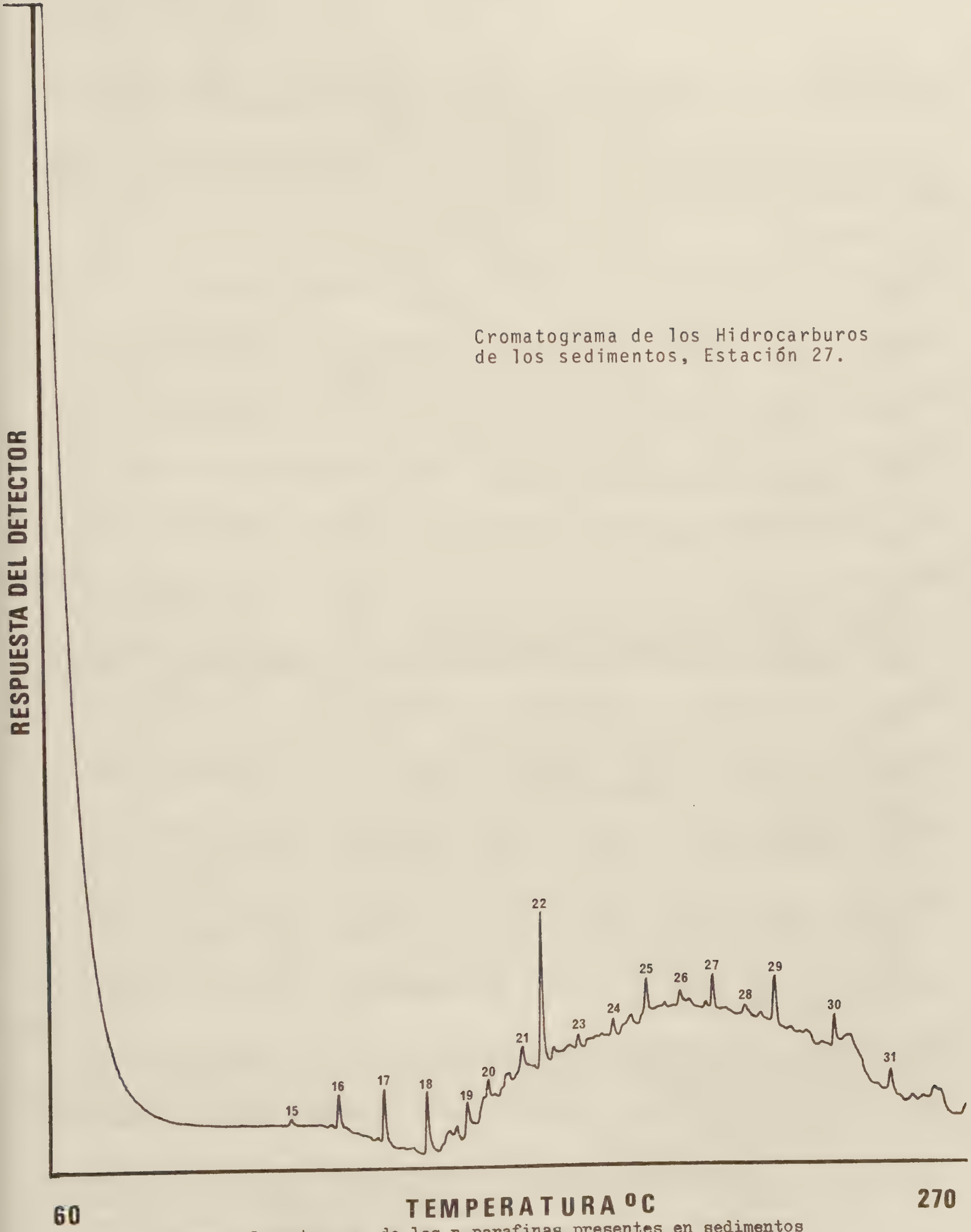
Cromatograma de los Hidrocarburos de los sedimentos, Estación 27.

Fig. 3 Cromatograma de las n-parafinas presentes en sedimentos de la estación de muestreo no. 27

Los metales pesados también se mantienen en concentraciones muy bajas y presentan una variación estacional, incrementándose con el aporte de los ríos principalmente durante la época de lluvias.

Debido a ésto, se considera a la Laguna de Términos como un ecosistema lagunar libre de alteraciones y que puede tomarse como un patrón de comparación con otras zonas ya afectadas por los procesos de industrialización y urbanización.

5. REFERENCIAS

Blumer, M., Organic pigments: their long fate. Science, Wash., 149:722-6
1965

Cahnmann, H.J. y M. Kuratsune, Determination of polycyclic aromatic hydrocarbons in
1957 oysters collected in polluted water. Anal.Chem., 29:1312-7

Clark, C.R. y M. Blumer, Distribution of n-parafins in marine organisms and sediment.
1967 Limnol.Oceanogr., 12:79-87

Cooper, J.E. y E.E. Bray, A postulated role of fatty acids in petroleum formation.
1967 Geochim.Cosmochim.Acta, 27:1113-27

Duce, R.A., G.J. Quinn y T.L. Wade, Residence time of non-methane hydrocarbons in the
1974 atmosphere. Mar.Pollut.Bull., 5:59-61

Erhardt, M., Petroleum hydrocarbons in oysters from Galveston Bay. Environ.Pollut.,
1972 3:257-71

FAO, Manual of methods in aquatic environment research. Part 1. Methods for detection,
1975 measurement and monitoring of water pollution. FAO Fish.Tech.Pap., (137):238 p.

Han, L.T., On the formation of hydrocarbons by marine bacteria. In Petroleum microbiology,
1968 by J.B. Davis. New York, Elsevier

Harvey, G.R. y W.G. Steinhaver, Atmospheric transport of polychlorobiphenyls to the
1974 North Atlantic, Atmos.Environ., 8

Mandelli, F.E. y A.V. Botello, A study of variables related to the water quality of
1975 Terminos Lagoon and adjacent coastal areas, Campeche, Mexico.

Onuska, I.F., et al., The determination and identification of polyaromatic hydrocarbons
1975 in oysters from the Gulf of Mexico, CCIW, Ontario, Canada. Unpublished report.

Pagenkopf, G.K., D.R. Newman y R. Woodriff, Lead determination using graphite furmance.
1972 Anal.Chem., 44:2248-52

Phleger, F.B. y A. Ayala-Castañares, Processes and history of Terminos Lagoon, Mexico.
1971 Am.Assoc.Pet.Geol.Bull., 55(12):2130-40

Strickland, D.H. y T.R. Parsons, A practical handbook of seawater analysis. Bull.Fish.
1968 Res.Board Can., (167):311 p.

Uthe, J.F., A.J. Armstrong y M.P. Stainton, Mercury determination in fish by wet digestion
1970 and flameless atomic absorption spectrophotometry. J.Fish.Res. Board Can.,
27(4):805-11

Zitko, V., Polychlorinated biphenyls and organochlorine pesticides in some freshwater
1971 and marine fishes. Bull.Envir.Contam.Toxicol., 6(5):464-70

CARBOHIDRATOS DISUELTOS EN AGUAS DE LA REGION NORORIENTAL DE VENEZUELA

por

G. CEDEÑO FERMIN
Instituto Oceanográfico, Universidad de Oriente
Cumaná, Venezuela

CONTENIDO

1. INTRODUCCION
2. AREA DE ESTUDIO
3. METODOS DE ANALISIS Y MUESTREO
4. RESULTADOS Y DISCUSION
5. CONCLUSIONES
6. REFERENCIAS

Resumen

En este trabajo es presentada la distribución de carbohidratos disueltos en la región nororiental de Venezuela. Se hicieron muestreos en los golfos de Paria, Cariaco y Santa Fé y en la zona comprendida entre la costa nororiental de Venezuela y los 13°00' de latitud norte y 61°00' y 64°31' de longitud oeste. Se usó el método de fenol-ácido sulfúrico para determinar las concentraciones.

En el Golfo de Paria se muestreó en la época de sequía y lluvia desde 1972 a 1974, observándose una mayor concentración de carbohidratos en el período de sequía, al sur de la Península de Paria (5 mg/l) y costas de Trinidad (8 mg/l). La distribución de superficie y fondo en el Golfo de Cariaco se caracterizó por ser más elevada hacia la parte norte (3 mg/l). En el Golfo de Santa Fé durante el año 1974, la concentración escasamente sobrepasó los 2 mg/l y la parte más interna del Golfo presentó los máximos valores. La zona comprendida entre la costa nororiental y los 13° de latitud norte, presentó tres áreas de mayor concentración (≃3 mg/l): al norte de la Península de Paria hasta los 11°40', perfil correspondiente a 63°30' de longitud oeste y este de Margarita.

De las investigaciones realizadas se observó una relativa uniformidad en la distribución de carbohidratos, máximos en la capa de termoclina. El Golfo de Paria presentó las mayores fluctuaciones y los valores más elevados de carbohidratos disueltos.

Abstract

In this paper the distribution of dissolved carbohydrates in the waters of northeastern Venezuela is presented. Samples were collected in the gulfs of Paria, Cariaco and Santa Fé and in the area between the Venezuelan coast and 13°00'N lat. and between 61°00' and 64°30'N long. The phenol sulfuric acid method was used to determine concentrations.

In the Gulf of Paria, the samples were taken during the dry and rainy seasons from 1972 to 1974. A greater concentration of carbohydrates was observed during the dry season south of the Paria Peninsula (5 mg/l) and off the Trinidad coast (8 mg/l). In the Gulf of Cariaco both on the sea surface and bottom the distribution was characterized by higher values towards the north (3 mg/l). In the Gulf of Santa Fé, during 1974, the concentration

was slighty above 2 mg/l with the highest value in the inner part of the gulf. The zone between the coast and 13°00'N lat. showed three areas of maximun concentrations (≃3 mg/l): north of Paria up to 11°40' lat., along east and west of Margarita Island.

Our results show a relative uniformity in the distribution of carbohydrates in the mixed layer, with an increase at the termocline. The Gulf of Paria had the greatest fluctuations and the highest values in the concentrations of dissolved carbohydrates.

1. INTRODUCCION

La información sobre la materia orgánica disuelta en el agua de mar es escasa y es realmente difícil obtener conclusiones acerca de la distribución de sus componentes. La importancia de la materia orgánica es evidente por la influencia que ejerce en la distribución y crecimiento de muchos organismos. Newell (1965) sugirió la utilización activa del material orgánico por animales bentónicos y Parsons (1962) usando substratos radioactivos demostró que el consumo heterotrófico del material orgánico soluble podría ser explicado en término de la cinética de consumo, lo cual implica que el consumo activo de compuestos metabolizados es una función de su concentración en el medio. Parsons y Seki (1970) mencionan dos procesos naturales, los cuales contribuyen a la formación de los compuestos orgánicos disueltos y particulados en el medio acuático. El primero de esos procesos involucra la descomposición de plantas y animales, para liberar compuestos solubles y sustancias más refractarias que son descompuestas posteriormente por la acción bacteriana. Un segundo proceso incluye la formación del material orgánico por liberación de productos extracelulares por organismos vivientes. Menzel y Ryther (1970) indicaron que descargas fluviales y precipitaciones podrían contribuir a la acumulación de material orgánico en el agua de mar. Duursna (1963) propuso que el nivel de materia orgánica disuelta puede ser usado como índice de la productividad primaria midiendo su tasa de acumulación. Dentro de esa gama de compuestos orgánicos disueltos en el agua de mar se encuentran los carbohidratos, los cuales pueden servir como fuente de energía para muchas reacciones bioquímicas. Acerca de la distribución de los carbohidratos disueltos en el agua de mar, Collier et al. (1950,1953) encontraron concentraciones de 0,5 mg/l en el Golfo de México, Lewis y Raskestraw (1955) reportaron valores hasta 7,9 mg/l en aguas costeras de San Diego (California). Walsh (1965) encontró valores de 0,4 a 3,17 mg/l en Cape Cod y Handa (1966-67) estudió la distribución en el Oceáno Indico, Kuroshio y área adyacentes, reportando valores de 0,19 a 0,66 mg/l.

En el presente trabajo se reporta un estudio sobre la distribución de los carbohidratos disueltos en aguas de la zona nororiental de Venezuela.

2. AREA DE ESTUDIO

Como muestra la Fig. 1, el área de estudio comprende los golfos de Cariaco, Santa Fé y Paria y la región al norte del Estado Sucre.

El Golfo de Cariaco, situado en la región nororiental de Venezuela se limita al norte por la Península de Araya; es de forma elíptica y con profundidad promedia de 50 m. Por su entrada en forma de silla y de profundidad 25 m, penetran las aguas del Mar Caribe. Kato (1961) determinó que los vientos alisios al sacar las aguas superficiales en los primeros meses del año, producían una surgencia, la cual influye notablemente en las características bioquímicas del Golfo.

El Golfo de Santa Fé, se localiza al sureste del margen de la Depresión Oriental de Fosa de Cariaco. Presenta forma de V, su entrada es ancha y de profundidad promedio 70-80 m que se reduce gradualmente hacia el interior. La forma amplia de la entrada permite una renovación constante de sus aguas. En el Golfo desembocan pequeños ríos, que contribuyen muy poco a las condiciones hidroquímicas de sus aguas. Okuda (1975), determinó tres períodos de surgencia que corresponden a los meses de enero a abril con baja temperatura y oxígeno y alta concentración de nutrientes, el segundo de junio a agosto con penetración de agua subtropical, el tercero de septiembre a noviembre que corresponde a la época de menor intensidad con alta temperatura y oxígeno y bajo contenido de nutrientes.

El Golfo de Paria situado entre la Isla de Trinidad y la costa oriental de Venezuela, se comunica al norte con el Mar Caribe por la Boca de Dragón y al sureste con el Atlántico por la Boca de Serpiente. Presenta profundidad promedio de 20 m y en él desembocan numerosos ríos, principalmente el Orinoco, el cual contribuye notablemente a la circulación general y a la modificación de las características hidroquímicas.

La región norte del Estado Sucre se extiende desde la costa norte del mismo hasta los 13° lat. norte y desde los 61° a los 63°30' lat. oeste. La región cubre la plataforma continental de Venezuela, la cual en el oriente es muy extensa y se extiende más allá de la isla de los Testigos, hasta los 11°30' lat. norte. La surgencia es característica de esta zona, lo cual contribuye a la modificación de las condiciones hidroquímicas.

3. METODOS DE ANALISIS Y MUESTREO

Los carbohidratos disueltos fueron determinados por el método de fenol ácido sulfúrico descrito por Handa (1966), la concentración (mg/l) expresada en términos equivalentes de D-glucosa, y las muestras fueron tomadas en botellas Nansen y Niskin.

La recolección de las muestras en el Golfo de Cariaco se efectuó en el mes de febrero de 1972, mientras que en el Golfo de Santa fé, durante el año 1974 se realizaron observaciones mensuales en las estaciones del perfil central y áreas adyacentes (estaciones 4 y 13). En la región norte del Estado Sucre, el muestreo se hizo en secciones meridionales, durante el crucero LS 7402 (marzo-abril) a bordo del buque LA SALLE, en el año 1974. En el Golfo de Paria se tomaron las muestras en la época de sequía y lluvia desde el año 1972 a 1974 en los cruceros LS 7202 (abril), y LS 7206 (noviembre), LS 7301 (abril), LS 7302 (agosto) y LS 7403 (septiembre).

4. RESULTADOS Y DISCUSION

4.1 Golfo de Cariaco

La Fig. 2 muestra la distribución vertical de los carbohidratos disueltos en las estaciones situadas en la entrada y parte central del Golfo de Cariaco. Se observan concentraciones máximas ($\simeq$2 mg/l) cercanas a la termoclina, capa generalmente abundante en material orgánico; luego se nota un ligero aumento en la cercanía de la interfase agua-sedimentos. Roa y Ottmann (1961), encontraron valores relativamente altos (8,9 por ciento) de carbono orgánico para esta zona, lo cual está muy relacionado con la abundancia de los carbohidratos.

La distribución horizontal de superficie y fondo (Fig. 3) se caracterizó por altas concentraciones ($\simeq$3 mg/l) hacia la parte norte del golfo, siendo las concentraciones del fondo más altas, quizás debido a una mayor influencia de la materia orgánica de los sedimentos marinos.

4.2 Golfo de Santa Fé

La variación de los carbohidratos disueltos en el Golfo de Santa Fé es mostrada en las Figs. 4 y 5. La estación 4 situada en áreas adyacentes al golfo presenta una distribución uniforme con predominio de las isolíneas de 0,5. Valores más altos se observan en los meses de febrero, junio y septiembre. La estación 13 cercana a la entrada, muestra una distribución irregular con concentraciones máximas de 4 mg/l en los meses de enero, marzo a julio y noviembre. Las estaciones 7 y 8 a la entrada del golfo muestran una distribución vertical uniforme interrumpida por núcleos de alta concentración entre 5-20 m y 40-60 m, los cuales predominan en los meses de marzo a abril junio y noviembre.

Las estaciones 9 y 10 presentan valores altos en los meses de marzo a junio y septiembre entre 20 y 30 m. En la parte más profunda del golfo (estaciones 11 y 12) las concentraciones más bajas corresponden a los primeros meses del año (enero a abril).

En general, en el Golfo de Santa Fé predominan las isolíneas de 0,5 y 1, y valores máximos se observan a profundidades de 5 a 30 m. Okuda (1975) señala tres períodos de surgencia para el Golfo de Santa Fé, comprendidos en los meses de enero a abril, junio a agosto y septiembre a noviembre, lo cual se relaciona notablemente con los meses señalados como de mayor concentración de carbohidratos disueltos.

4.3 Area norte del Estado Sucre

La distribución de superficie y fondo de carbohidratos (Fig. 6), durante el crucero LS 7402 presenta similitudes en la conformación de sus isolíneas y muestran tres zonas de mayor concentración (4 mg/l), las cuales están localizadas al norte de la Península de Paria (correspondiente a la plataforma continental), oeste de la Isla de Margarita y perfil correspondiente a los 63°30' de longitud oeste. Estas zonas son señaladas por Okuda y Gómez (1964) por poseer altos valores de carbono orgánico especialmente el oeste de la Isla de Margarita, la cual presentó 5,03 por ciento de carbono orgánico, igualmente la plataforma continental al norte del Estado Sucre, mostró valores mayores de 0,5 por ciento de carbono orgánico. Zonas con menor concentración de carbohidratos están localizadas después de los 12° de lat. norte.

En esta área se diferencian claramente dos regiones: la primera que corresponde a la plataforma, con valores de 3 mg/l y la segunda con concentraciones menores de 0,5 mg/l que comprende la región oceánica.

4.4 Golfo de Paria

La distribución horizontal característica del año 1972 es mostrada en la Fig. 7, en la cual podemos observar que durante el crucero del mes de abril (LS 7202), correspondiente al período de sequía, se presentan concentraciones de hasta 8 mg/l, en la parte central del golfo, oeste y noroeste de Trinidad y Boca de Dragón. El fondo muestra una distribución semejante, pero con valores altos hacia el sur de la Península de Paria. En el mes de noviembre (LS 7206) se aprecian bajas concentraciones, (<1 mg/l) tanto en las capas superficiales como en las de fondo.

En el año 1973 (LS 7301) la distribución en el fondo y superficie (Fig. 8) muestra máximos valores hacia el noroeste de Trinidad (>8 mg/l) y sur de la Península de Paria, Hacia el centro del golfo los valores no sobrepasan a 1 mg/l. En el mes de agosto (LS 7302) los valores más altos se localizan hacia el sur de la Península de Paria. Tanto en la superficie como en el fondo los valores no sobrepasan 1 mg/l.

En 1974 (Fig. 9), durante el mes de septiembre (LS 7403) se observan bajas concentraciones hacia el centro del golfo (≃0,5 mg/l), mientras que hacia la parte oeste se nota un aumento.

En general la distribución en el Golfo de Paria muestra dos áreas de mayor concentración; al oeste de Trinidad y al sur de la Península de Paria, y una zona de menor concentración correspondiente a la parte central. Esta distribución está estrechamente relacionada con los valores de carbono orgánico encontrados por Bonilla (1975), en donde delimita zonas similares en abundancia de materia orgánica, y señala para la parte oeste de Trinidad 1-1,5 por ciento de carbono orgánico y para el sur de la Península de Paria 1-2 por ciento, en tanto que la parte central del golfo tiene su contenido menor (0,5 por ciento).

Durante los primeros meses del año (período de sequía) los carbohidratos son más abundantes que en los últimos meses (período de lluvias), lo cual podría estar relacionado con la abundancia de organismos del plancton marino.

5. CONCLUSIONES

De acuerdo a los análisis realizados se encontró una notable relación entre la termoclina, capa dinámicamente estable y rica en material orgánico, y la concentración máxima de los carbohidratos; igualmente es notoria la influencia de los sedimentos marinos en la distribución de los carbohidratos pues zonas de alta concentración de carbono orgánico guardan una relación directa con la abundancia de estos compuestos orgánicos.

La mayoría de las áreas estudiadas corresponden a zonas costeras, y el Golfo de Paria muestra la concentración más elevada, quizás por el aporte de materia orgánica descargada por los numerosos ríos que desembocan en el golfo. En la zona norte del Estado Sucre, en la parte que corresponde al área más oceánica se encontraron las concentraciones más bajas en virtud de la poca variación de los procesos biológicos y bioquímicos que allí se desarrollan.

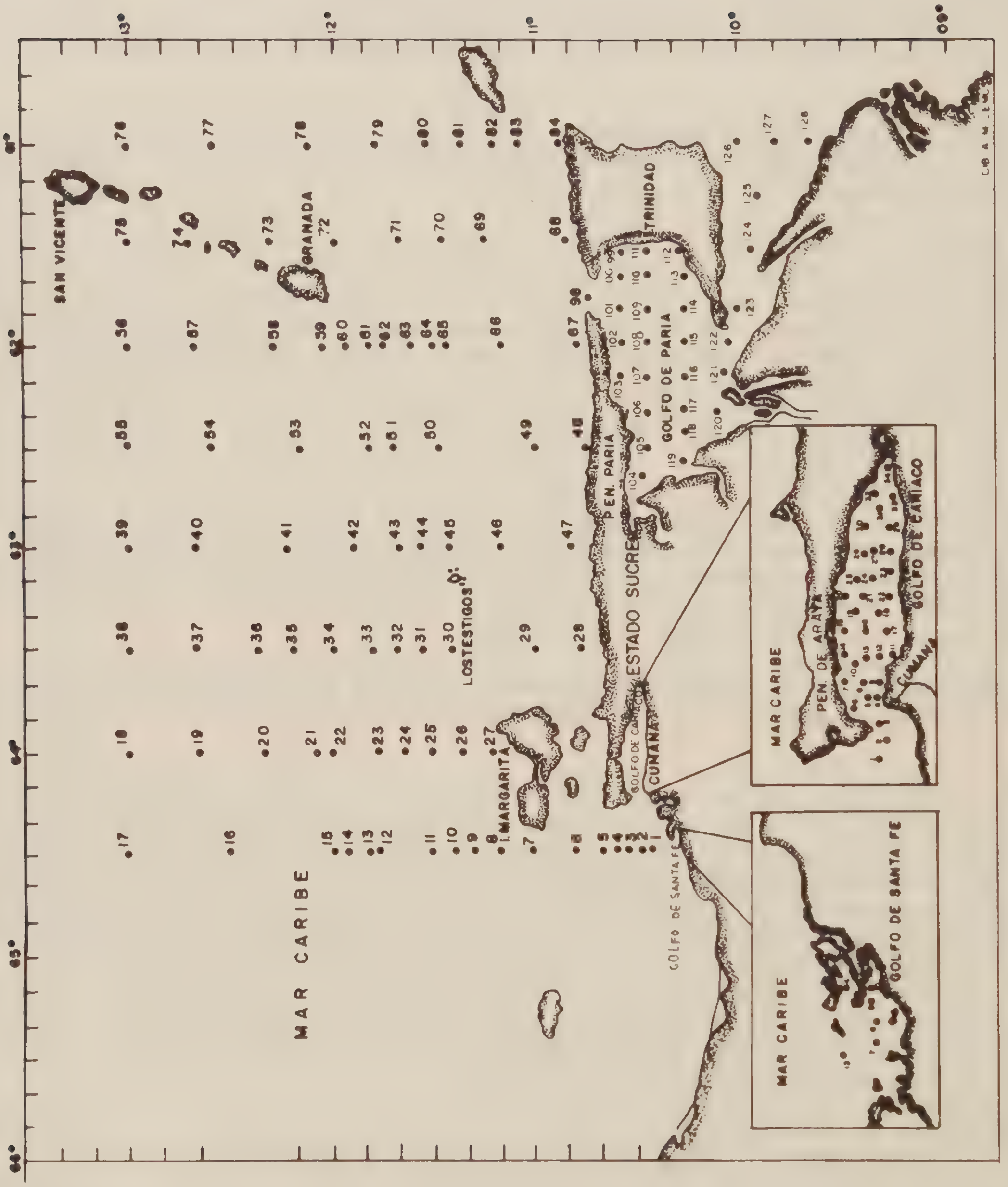
MAR CARIBE
SAN VICENTE
GRANADA
TRINIDAD
MARGARITA
LOS TESTIGOS
ESTADO SUCRE
PEN. PARIA
GOLFO DE PARIA
GOLFO DE CARIACO
CUMANA
GOLFO DE SANTA FE
MAR CARIBE
PEN. DE ARAYA
GOLFO DE CARIACO
CUMANA
MAR CARIBE
GOLFO DE SANTA FE
13°
12°
11°
10°
09°
61°
62°
63°
64°
65°
66°

Fig. 1 Mapa de la zona estudiada

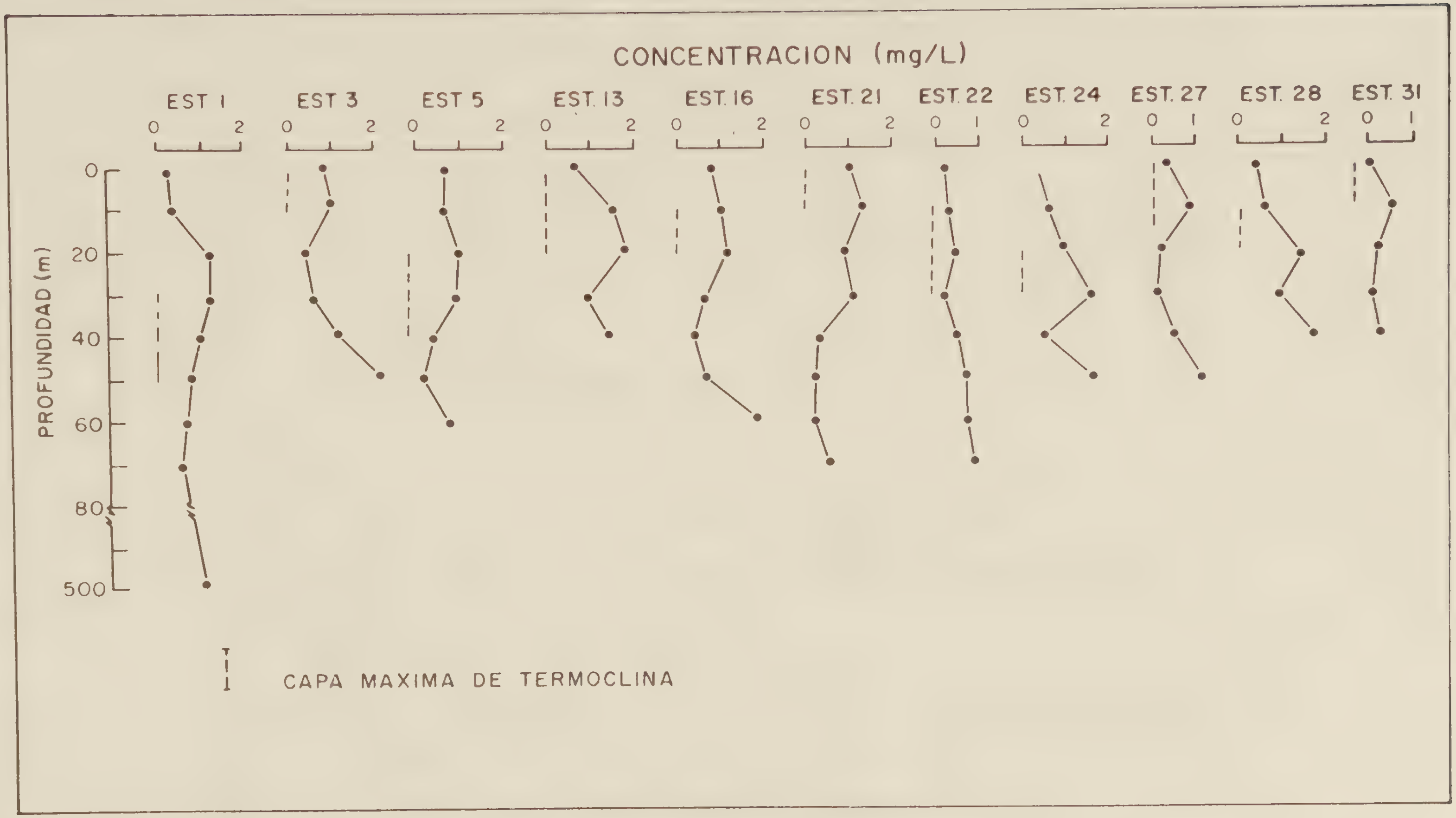

Fig. 2 Distribución vertical de carbohidratos en el Golfo de Cariaco

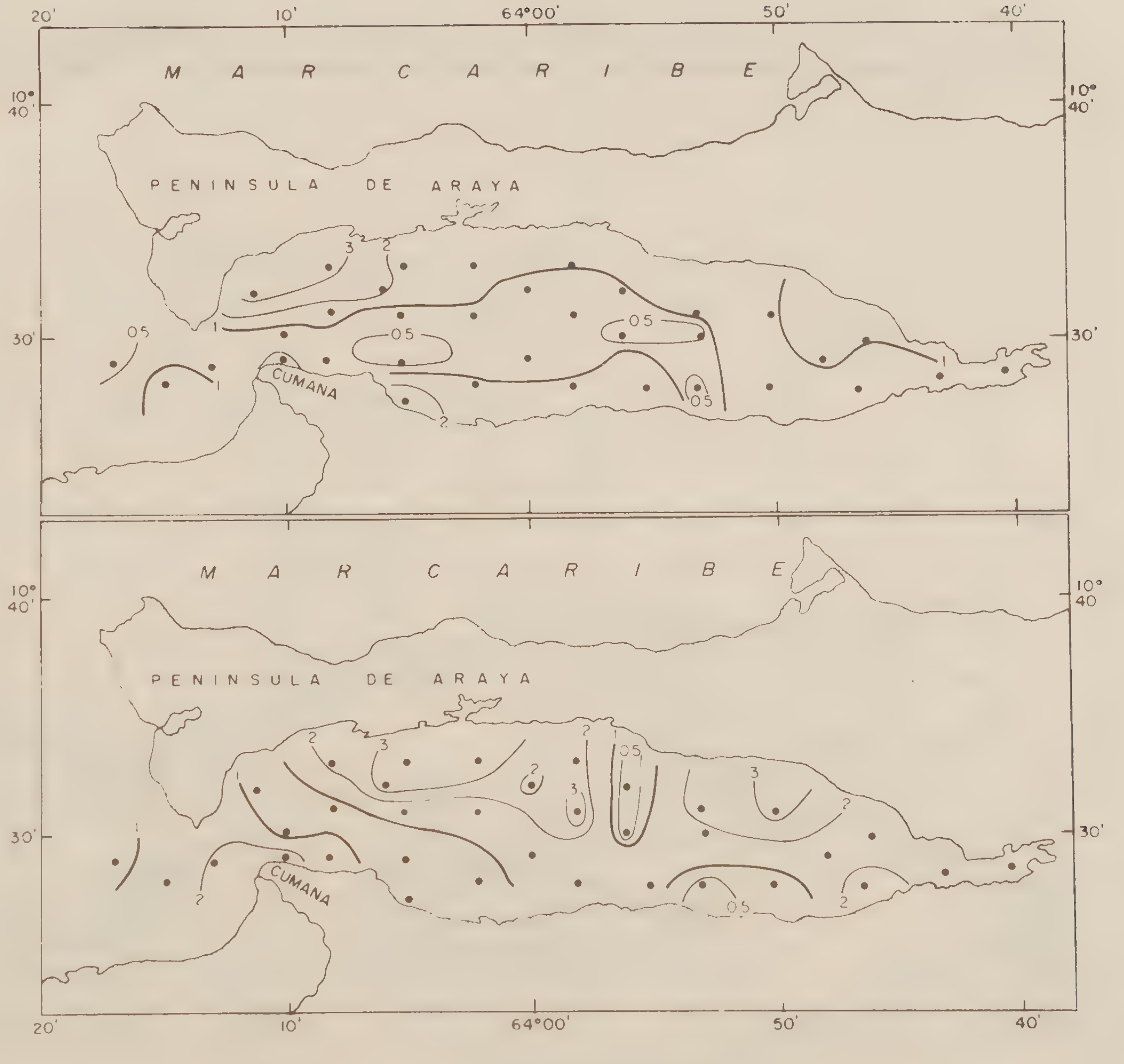
MAR CARIBE
PENINSULA DE ARAYA
CUMANA
20'
10'
64°00'
50'
40'
10° 40'
30'
0.5
1
2
3

Fig. 3 Distribución horizontal de superficie y fondo en el Golfo de Cariaco

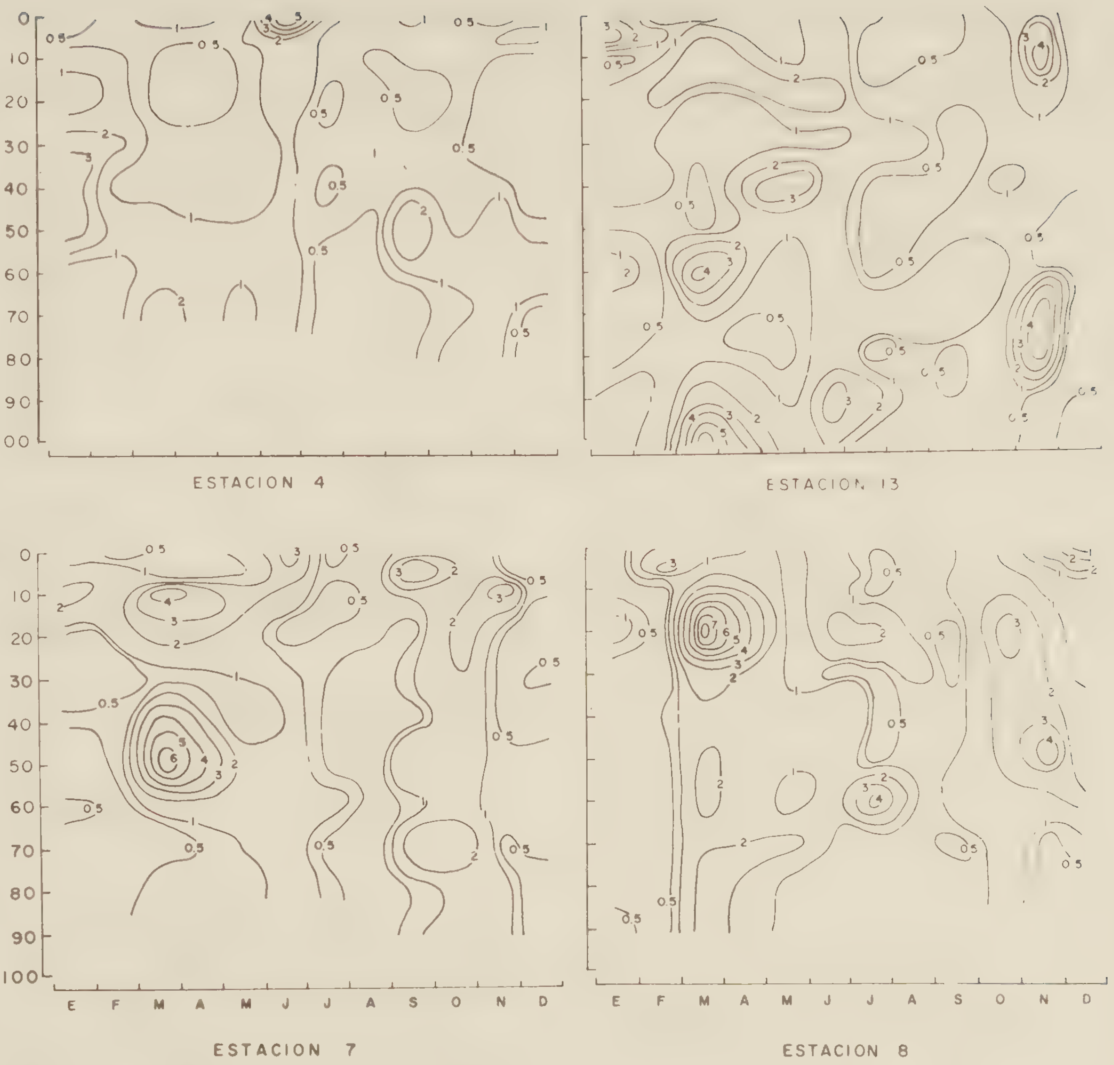

Fig. 4 Carbohidratos disueltos en el Golfo de Santa Fé (est. 4-13, 7 y 8)

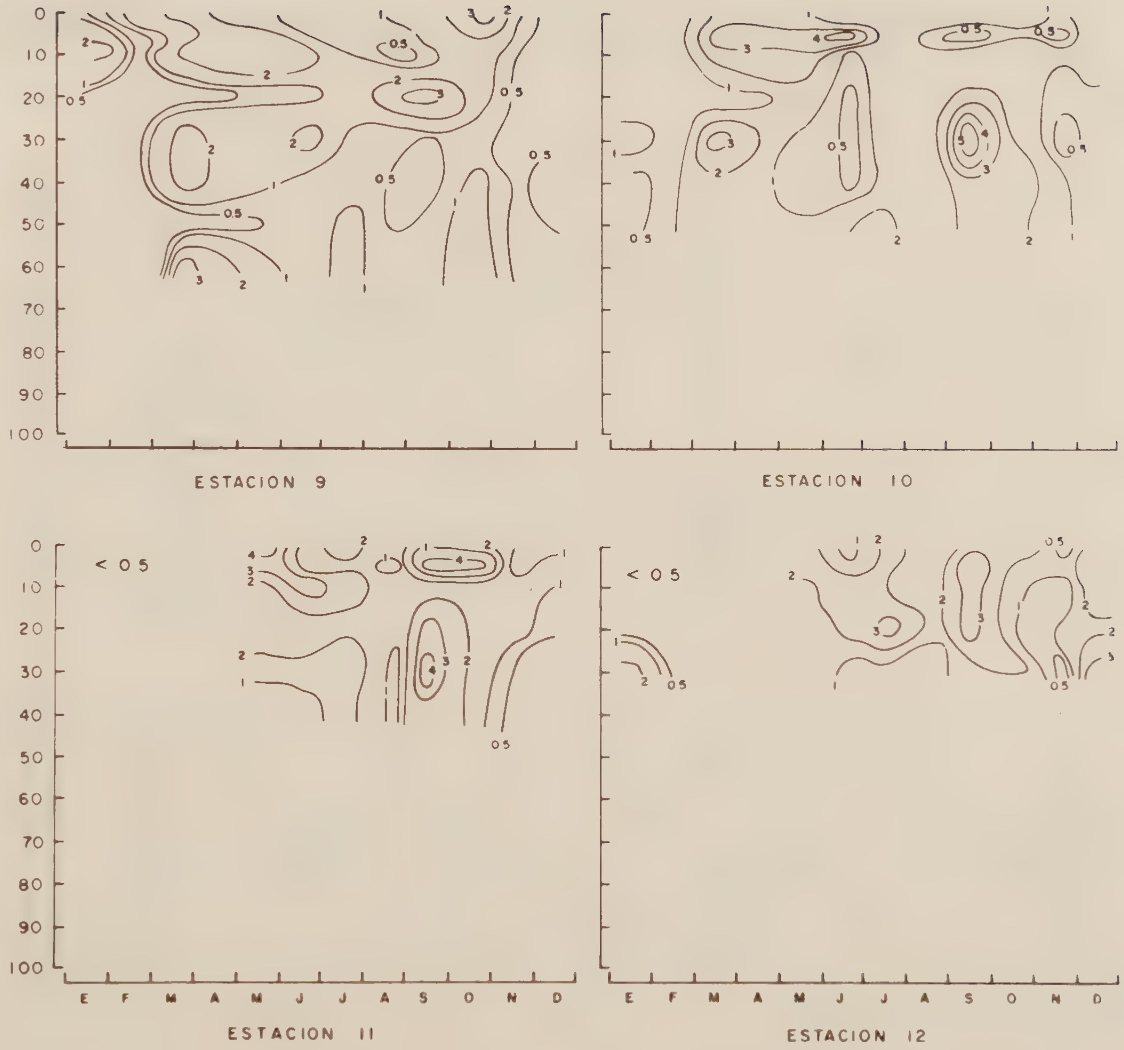

ESTACION 9

ESTACION 10

ESTACION 11

ESTACION 12

Fig. 5 Carbohidratos disueltos en el Golfo de Santa Fé (est. 9, 10, 11 y 12)

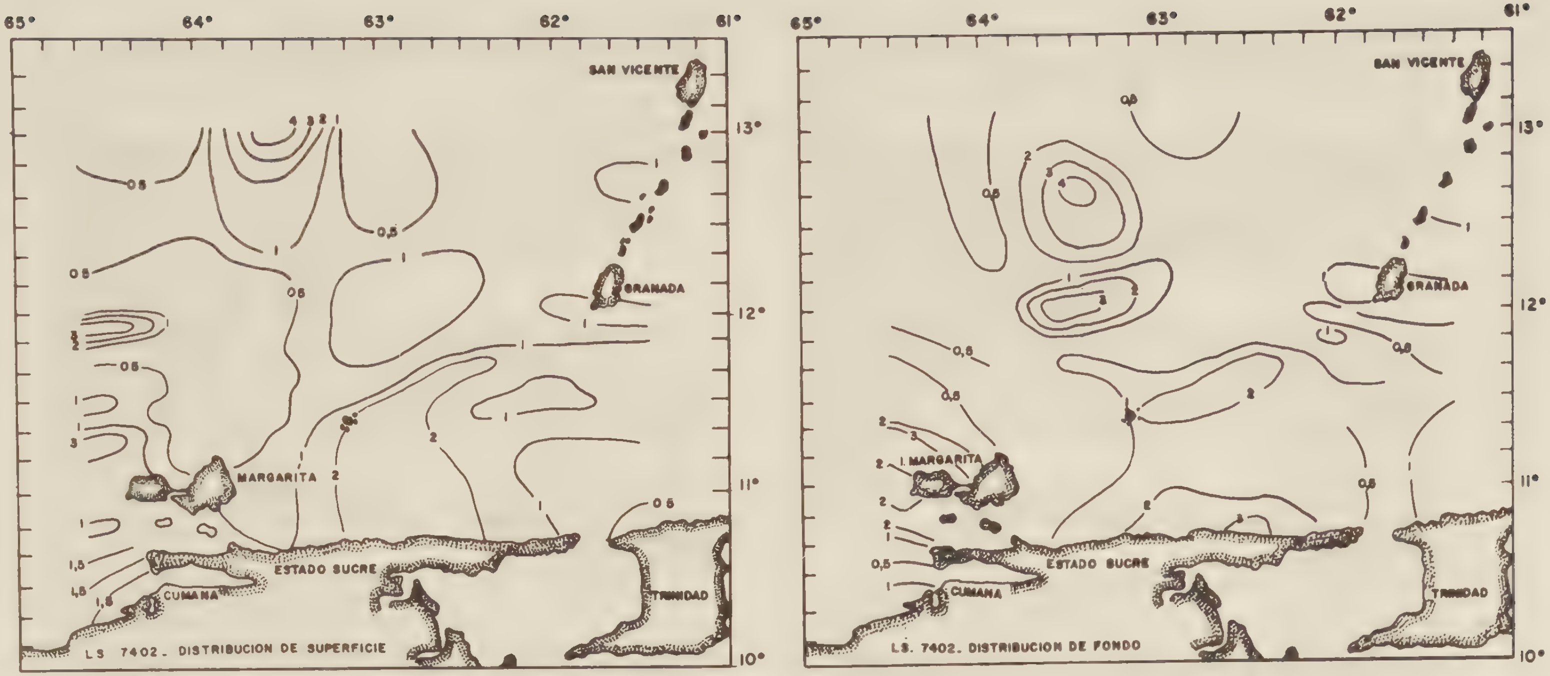
65°
64°
63°
62°
61°
13°
12°
11°
10°
SAN VICENTE
GRANADA
MARGARITA
ESTADO SUCRE
CUMANA
TRINIDAD
LS 7402. DISTRIBUCION DE SUPERFICIE
L.S. 7402. DISTRIBUCION DE FONDO
0,5
1
1,5
2
3
4

Fig. 6 Carbohidratos disueltos en el norte del Estado Sucre

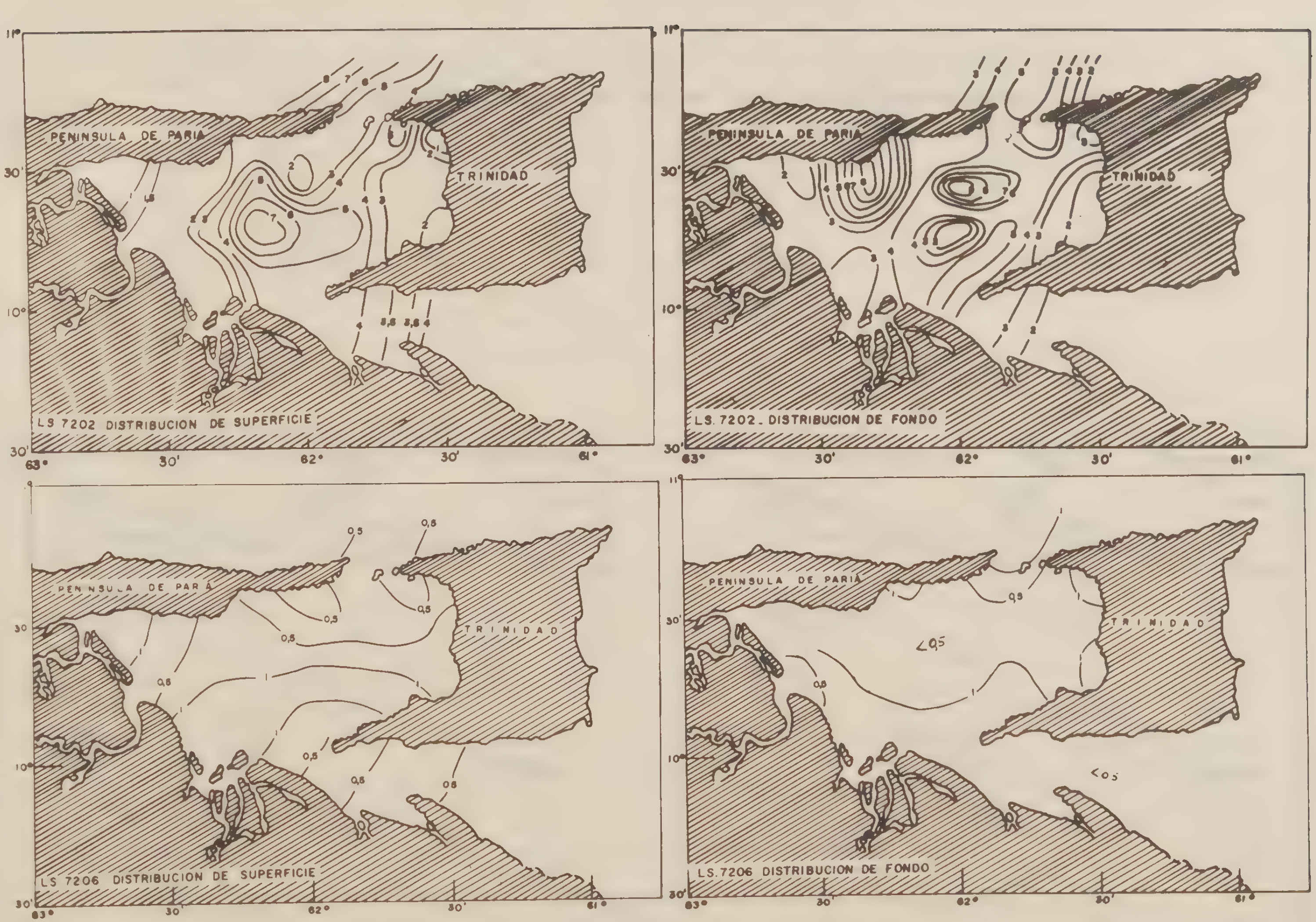
PENINSULA DE PARIA
TRINIDAD
LS 7202 DISTRIBUCION DE SUPERFICIE
LS. 7202. DISTRIBUCION DE FONDO
LS 7206 DISTRIBUCION DE SUPERFICIE
LS. 7206 DISTRIBUCION DE FONDO
11°
30'
10°
63°
62°
61°
<0,5
0,5
0,8
1

Fig. 7 Carbohidratos disueltos en el Golfo de Paria 1972

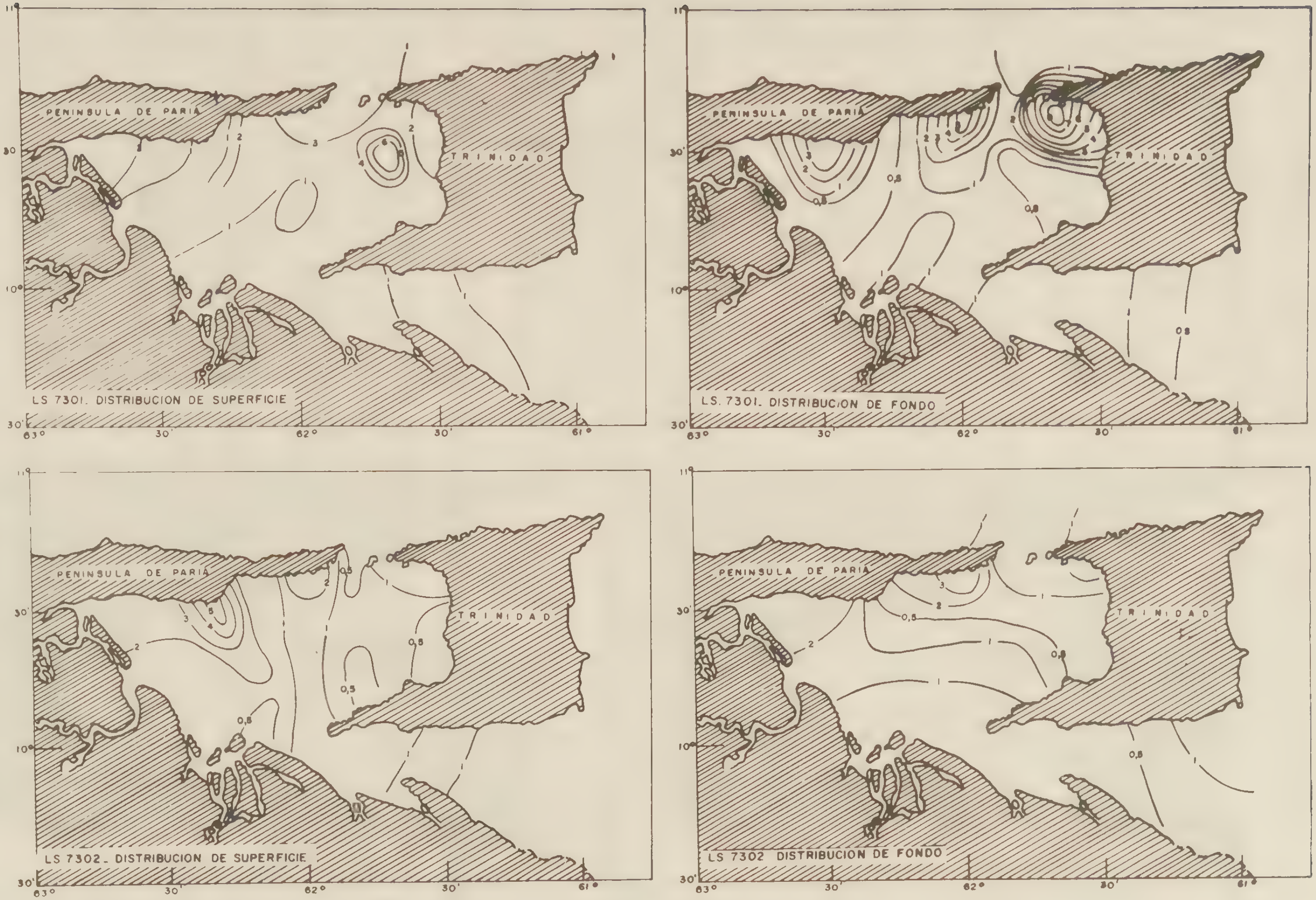
LS 7301. DISTRIBUCION DE SUPERFICIE
LS. 7301. DISTRIBUCION DE FONDO
LS 7302. DISTRIBUCION DE SUPERFICIE
LS 7302 DISTRIBUCION DE FONDO
PENINSULA DE PARIA
TRINIDAD
11°
30'
10°
63°
62°
61°
0,5
0,8
1
2
3
4
5
6

Fig. 8   Carbohidratos disueltos en el Golfo de Paria 1973

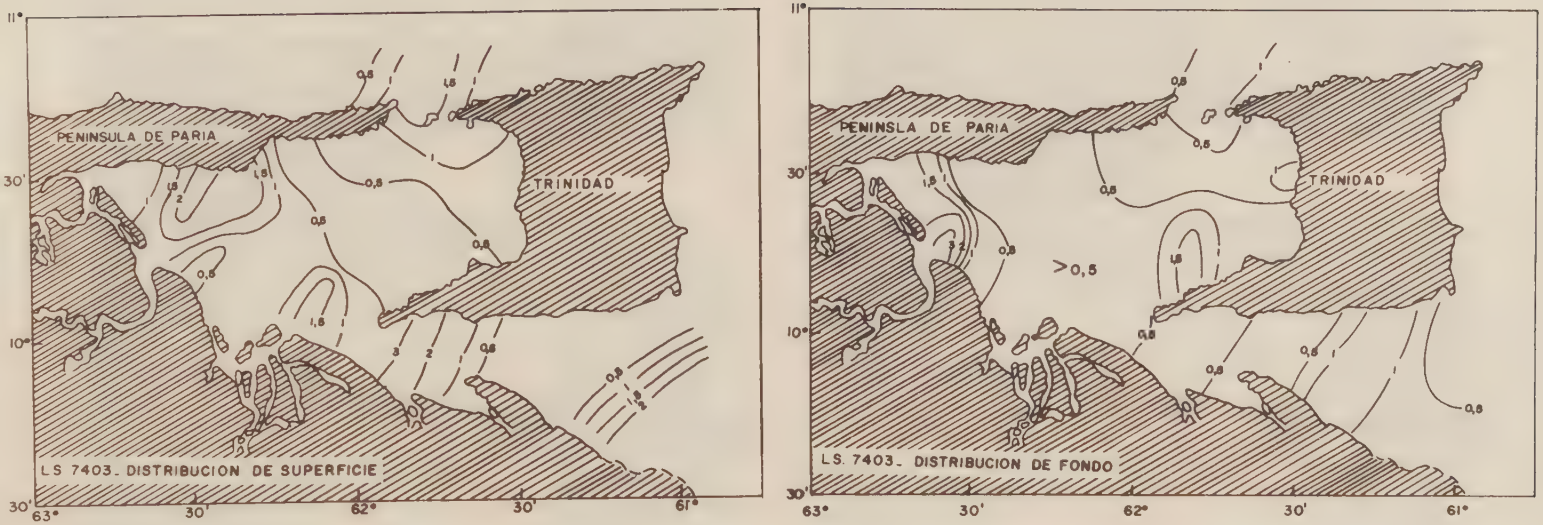
PENINSULA DE PARIA
TRINIDAD
LS 7403_ DISTRIBUCION DE SUPERFICIE
0,5
1,5
2
3
11°
30'
10°
30'
63°
30'
62°
30'
61°
PENINSLA DE PARIA
TRINIDAD
LS. 7403_ DISTRIBUCION DE FONDO
>0,5
1,5
3
2
0,5

Fig. 9 Carbohidratos disueltos en el Golfo de Paria 1974

6. REFERENCIAS

Bonilla, (in press)

Collier, A., On the significance of organic compounds in sea water. Trans.Am.Wildl.Conf., 1953 18:463-8

Collier, A., S. Ray y W. Magnitzky, A preliminary note on naturally ocurring organic sub- 1950 stances in sea water affecting the feeding of oyster. Science, Wash., 111:2876

Duursma, E.K., The production of dissolved organic matter in the sea, related to the primary 1963 production of organic matter. Neth.J.Sea Res., 2:85-94

Handa, N., Distribution of dissolved carbohydrates in the Indian Ocean. J.Oceanogr.Soc. 1966 Jap., 22(2):16-22

Hande, V., The distribution of the dissolved and particulate carbohydrates in Kuroshio and 1967 its adjacent areas. J.Oceanogr.Soc.Jap., 23(3):115-23

Kato, K., Oceanochemical studies on the Gulf of Cariaco. 1. Chemical and hydrographical 1961 observations in January 1961. Bol.Inst.Oceanogr.Univ.Oriente., 1:49-72

Lewis, G.J. y N.W. Rakestram, Carbohydrates in sea water. J.Mar.Res., 14:253-8 1955

Menzel, D.W. y J.H. Ryther, Distribution and cycling of organic matter in the ocean. Occas. 1970 Publ.Inst.Mar.Sci.Univ.Alaska, (1):31-54

Newell, R., The role of detritus in the nutrition of two marine deposit feeders, the proso- 1965 branch Hydrobia ulvae and the bivalve Macoma baltica. Proc.Zool.Soc. Lond., 144:25-45

Okuda, T., Características hidroquímicas del Golfo de Santa Fé y áreas adyacentes. Bol. 1975 Inst.Oceanogr.Univ.Oriente, 14(1-2):251-68

Okuda, T. y J.R. Gómez, Distribución del carbono y nitrógeno orgánico de los sedimentos en 1964 la región nororiental de Venezuela. Bol.Inst.Oceanogr.Univ.Oriente, 3(1-2):91-105

Parsons, T.R. y J.D.H. Strickland, On the production of particulate organic carbon by hetero- 1962 trophic processes in sea water. Deep-Sea Res., 8:211-22

Parsons, T.R. y H. Seki, Importance and general implications of organic matter in the aquatic 1970 environments. Occas.Publ.Inst.Mar.Sci.Univ.Alaska, (1):1-27

Roa, Morales P. y F. Ottmann, Primer estudio topográfico y geológico del golfo de Cariaco. 1961 Bol.Inst.Oceanogr.Univ.Oriente, 1(1):5-20

Walsh, G.E., Studies on dissolved carbohydrate in Cape Cod waters. 1. General survey. 1965 Limnol.Oceanogr., 10:570-6

DISSOLVED SILICA AND THE AMERICAN MEDITERRANEAN[1]

by

K.A. FANNING
Department of Marine Science
University of South Florida
St. Petersburg, Florida 33701

Abstract

The bathymetry of the American Mediterranean system shows it to be composed of three basic parts: the eastern Caribbean, the western Caribbean, and the Gulf of Mexico. Dissolved silica, as well as other nutrients, traces the processes occurring in the deep water of this system. Although separated from each other by the Jamaica-Nicaragua Rise, both the eastern and western Caribbean appear to be well-mixed and uniform below their respective controlling sill depths. However the deep eastern Caribbean is enriched in silica compared to its renewal water while the deep western Caribbean is not. Interstitial silica profiles and flux measurements on cores indicate that diffusive fluxes from the sediments of the eastern Caribbean provide its deep enrichment. However, interstitial silica profiles from the western Caribbean suggest equally large silica fluxes from its sediments. Therefore, the time of contact between deep water and the bottom seems to be less in the western Caribbean. The deep Gulf of Mexico is perhaps not as well-mixed as the Caribbean, but some enrichment in silica apparently occurs after its renewal water flows through the Yucatan Strait. Interstitial silica profiles in the Gulf show strong gradients which could drive a flux out of the bottom. Finally, details of the mixing across the sills of the system are easily seen from closely spaced silica measurements.

Resumen

El Mediterráneo americano estaría compuesto, según la batimetría, de tres partes fundamentales: el Caribe oriental, el Caribe occidental y el Golfo de México. Los procesos que se desarrollan en las aguas profundas de este sistema pueden conocerse por el contenido en sílices disueltos de esas aguas, así como de otros nutrientes. Aunque el Caribe oriental y el occidental están separados por la elevación Jamaica-Nicaragua, las aguas de ambos están bien mezcladas y son uniformes debajo de sus respectivos umbrales de control de profundidad. Sin embargo, las aguas profundas del Caribe oriental son ricas en sílices, en comparación con las aguas renovables, mientras que las aguas profundas del Caribe occidental no lo son. Los perfiles de las sílices intersticiales y las mediciones de los flujos en los centros indican que este enriquecimento de las aguas profundas se debe a flujos de difusivos procedentes de los sedimentos del Caribe oriental; pero, los perfiles de las sílices intersticiales del Caribe occidental indican flujos igualmente importantes de sílices procedentes de sus sedimentos. Por consiguiente, las aguas profundas del Caribe occidental estarían en contacto con el fondo menos tiempo. Las aguas profundas del Golfo de México tal vez no estén tan bien mezcladas como las del Caribe, pero después que sus aguas renovables fluyen a través del Estrecho de Yucatán, se enriquecen algo en sílices. Los perfiles de las sílices intersticiales del Golfo muestran fuertes gradientes, que podrían revelar la existencia de un flujo procedente del fondo. Las mediciones del contenido de sílices, hechas a cortas distancias, permiten observar fácilmente los detalles de las mezclas que se producen a través de los umbrales del sistema.

---

[1] Abstract only submitted

DISSOLVED SILICATE AND SALINITY STRUCTURE OF THE UPPER WATERS OF THE VENEZUELA BASIN, CARIBBEAN SEA

by

P.N. FROELICH, JR.
Graduate School of Oceanography
University of Rhode Island
Kingston, Rhode Island 02882, U.S.A.

D.K. ATWOOD
Department of Marine Sciences
University of Puerto Rico
Mayaguez, Puerto Rico 00708, U.S.A.

CONTENTS

1. INTRODUCTION
2. SUBTROPICAL UNDERWATER
3. SURFACE WATERS
4. REFERENCES

Abstract

The Subtropical Underwater undergoes fluctuations in its core strength and lateral location within the Venezuela Basin. These variations may be related to changes in the Caribbean Current, the relative importance of different passes as entrance ways for the SUW into the Caribbean, mixing with seasonal low-salinity surface water, and seasonal and longer term meteorological influences on evaporation/precipitation excesses in the source region.

Amazon River water contributes about 65 percent and equatorial rainfall about 35 percent to the freshwater causing seasonal salinity depressions in surface waters of the eastern Caribbean.

Resumen

Las aguas profundas subtropicales de la cuenca venezolana están sujetas a fluctuaciones de su fuerza central y emplazamiento lateral, fluctuaciones que pueden atribuirse a cambios en la corriente del Caribe, a la importancia relativa de diferentes pasos como vías de entrada de estas aguas profundas tropicales al Caribe, a la mezcla con aguas superficiales de baja salinidad, y a las influencias meteorológicas durante las estaciones, o durante períodos más breves, sobre las diferencias entre la evaporación y la precipitación en la región original.

La disminución de la salinidad, durante las estaciones, de las aguas superficiales del este del Caribe es debida en parte a las aportaciones de agua dulce del río Amazonas (un 65 por ciento, aproximadamente) y en parte a las precipitaciones ecuatoriales (el 35 por ciento aproximadamente).

1. INTRODUCTION

The waters in the upper several hundred metres of the Venezuela Basin undergo seasonal variations in salinity, temperature, and dissolved silicate. This paper will present some of the results of our studies at the University of Puerto Rico concerning these fluctuations and discuss some of their probable causes. We will limit ourselves to a discussion of the surface mixed layer and the Subtropical Underwater.

The data presented here were collected during the PESCA program of the University of Puerto Rico at a monthly serial hydrographic station 35 km south of La Parguera, Puerto Rico in the Venezuela Basin (17°38'N, 67°00'W) and on a transect south of this station along 67°W between La Parguera, Puerto Rico and La Guaira, Venezuela (Fig. 1). The serial station marks the northernmost station of the transect line. The transect has been occupied about three times per year since 1972. The serial station has been occupied at least once a month since 1969.

A discussion of data collection and analytical techniques has appeared elsewhere (Froelich, 1973; Froelich and Atwood, 1974) and will not be repeated here.

2. SUBTROPICAL UNDERWATER

The Subtropical Underwater (SUW) is formed in the eastern Sargasso Sea at about 25°N. In these desert latitudes, surface salinities exceed 37.5 per mille owing to an evaporation rate which far surpasses the rate of precipitation (Wüst and Gordon, 1964). This salty, warm water slides under the fresher, warmer and lighter equatorial water to the south to form the core of the SUW. The core of the SUW enters the Venezuela Basin through the main passes in the Lesser Antilles, and appears as a salinity maximum at about 150 m, 22-24°C in the northern Venezuela Basin (Fig. 2).

Figs. 3 and 4 show temperature and salinity time series at the serial station for the years 1971-73. Salinity values in the SUW core (125-175 m) range from as high as 36.99 per mille to less than 36.7 per mille. Dissolved silicate values in the core of the SUW display a minimum, varying from about 0.8 µM to 1.3 µM (Fig. 5). Three major episodes of salinity higher than 36.9 per mille coincide with three major episodes of silicates less than 1.0 µM. The two parameters are evidently gauging the same fluctuations.

Figs. 6, 7 and 8 are temperature, salinity and silicate sections respectively along the 67° PESCA transect for June, 1972. The core of the Subtropical Underwater was most pronounced at about 16°N and 175 m deep (Fig. 7). The maximum salinity in the core layer here was 37.08 per mille, significantly higher than the highest salinity recorded at the serial station during the period 1971-73. The silicate minimum (Fig. 8), with values less than 1.5 µM, mirrors the structure of the SUW salinity maximum.

Figs. 9, 10 and 11 are temperature, salinity and silicate sections respectively, along the same transect in October, 1972. Salinities in the entire core of the SUW were much reduced (Fig. 10). Salinities exceeded 36.9 per mille only at 15°N, station 2625. Silicate values here, also, are below 1.5 µM (Fig. 11).

In March/April, 1973 (Figs. 12, 13 and 14), the high salinity, low silicate core of the SUW was very strong across the entire basin (Figs. 13 and 14). Salinities of 37.03 per mille existed at stations 2655 and 2656, between 14°N and 15°N and a tongue of water with salinities higher than 36.9 per mille stretches from the north end of the basin to about 13°N.

It is apparent from these data that the SUW is characterized by a silicate minimum which displays variations coincident with salinity variations. The low silicate characteristic is produced in the nutrient-depleted Sargasso Sea, source region for the SUW.

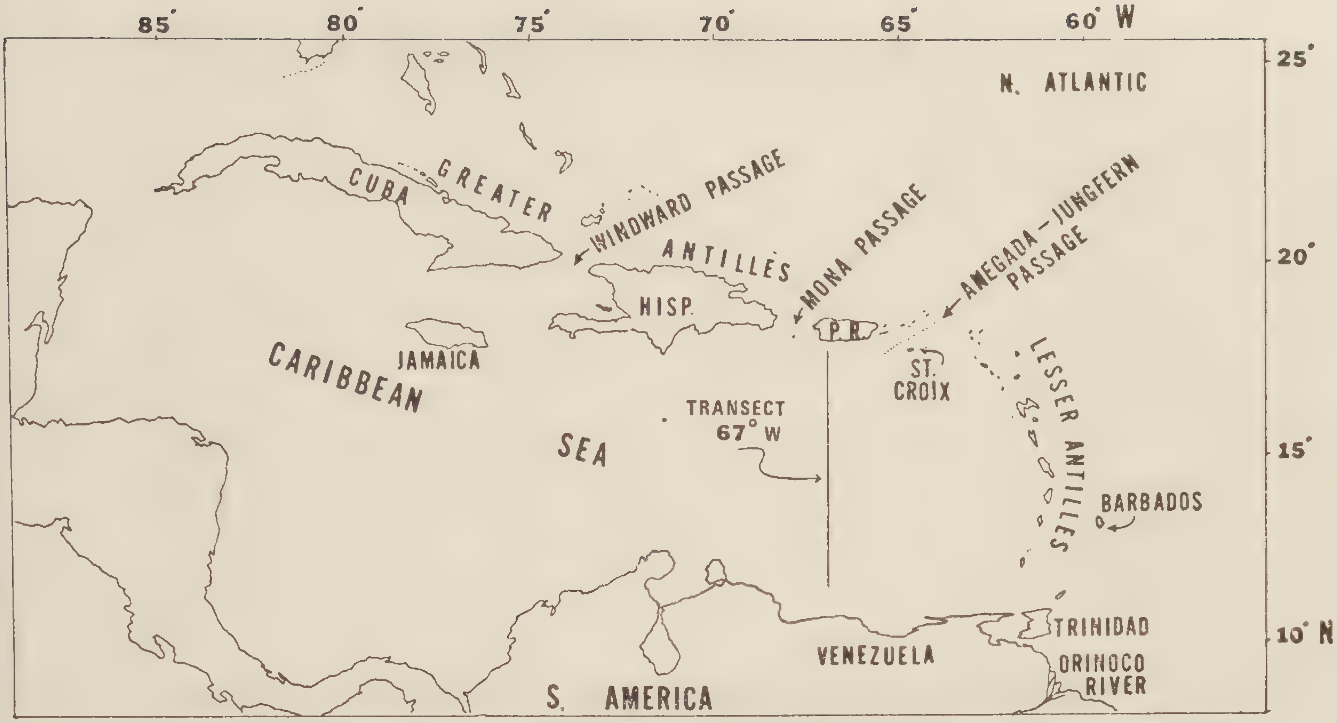
85°
80°
75°
70°
65°
60° W
25°
20°
15°
10° N
N. ATLANTIC
CUBA
GREATER
WINDWARD PASSAGE
ANTILLES
HISP.
MONA PASSAGE
P.R.
ANEGADA-JUNGFERN PASSAGE
JAMAICA
CARIBBEAN
SEA
TRANSECT 67° W
ST. CROIX
LESSER ANTILLES
BARBADOS
TRINIDAD
VENEZUELA
ORINOCO RIVER
S. AMERICA

Fig. 1 Map of the Caribbean Sea, showing location of Venezuela transect. The Puerto Rico serial station is at the northern end of this transect, 35 km south of Puerto Rico

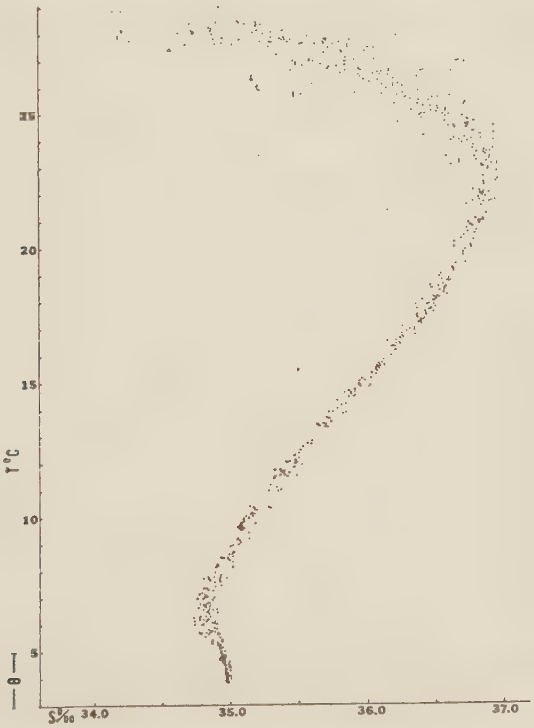

Fig. 2 TS diagram of 1971-73 data at P.R. serial station

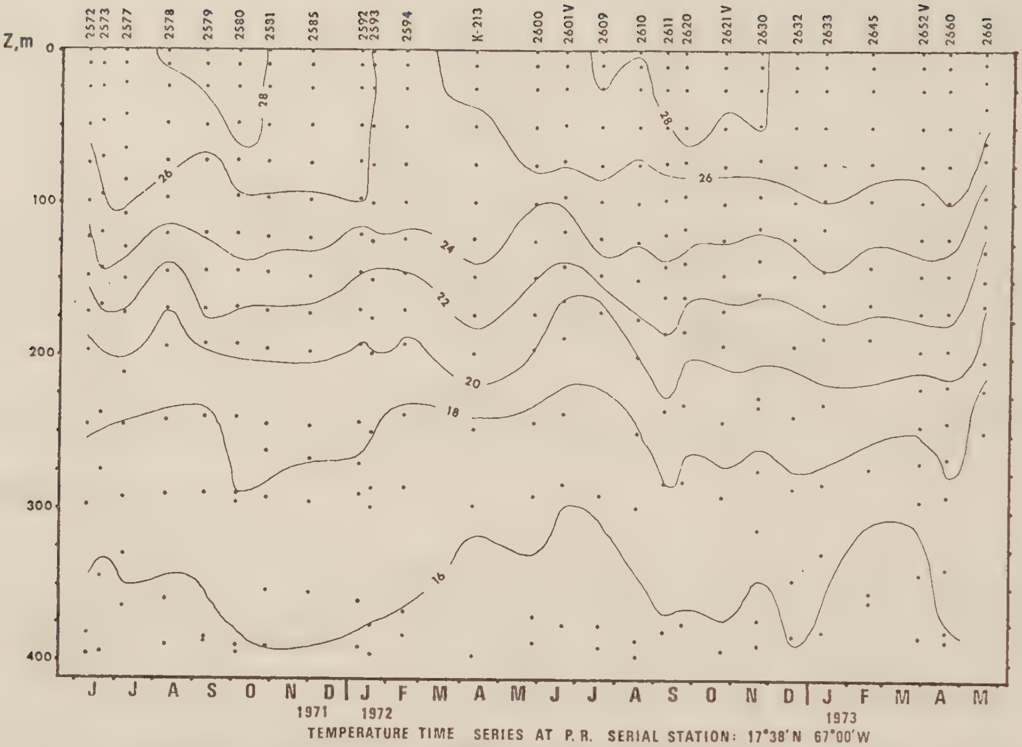

Fig. 3 Temperature time series at serial station

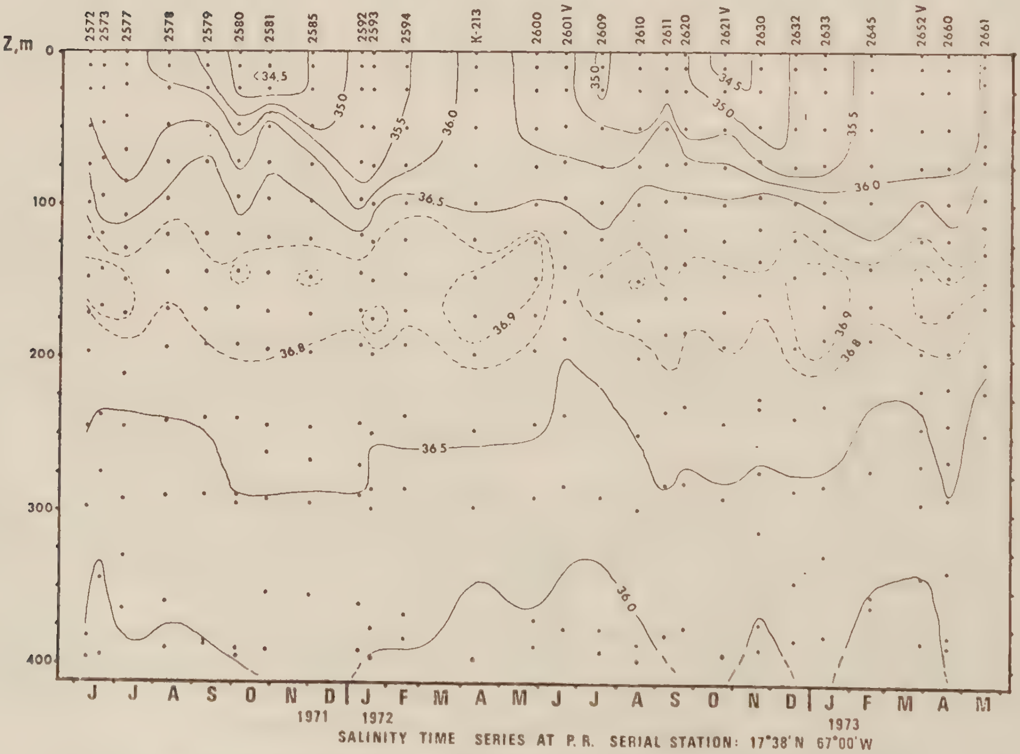

Fig. 4 Salinity time series at serial station

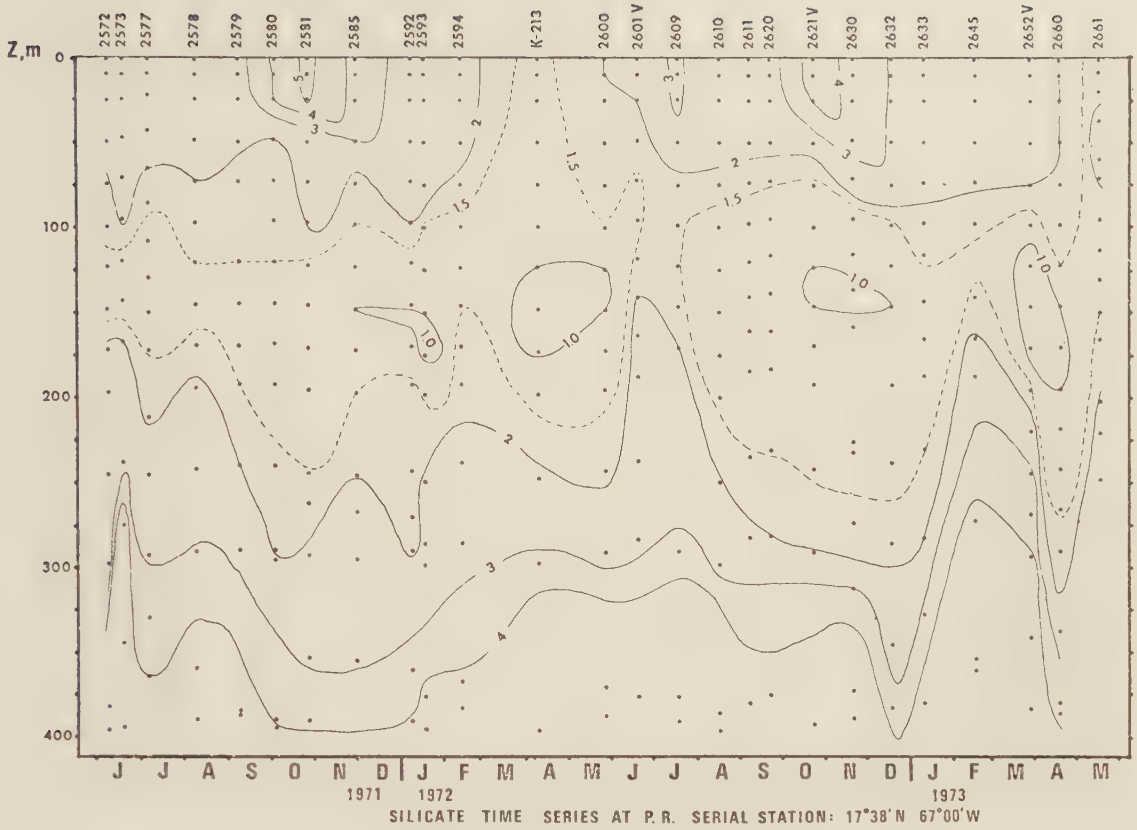

Fig. 5 Silicate time series at serial station

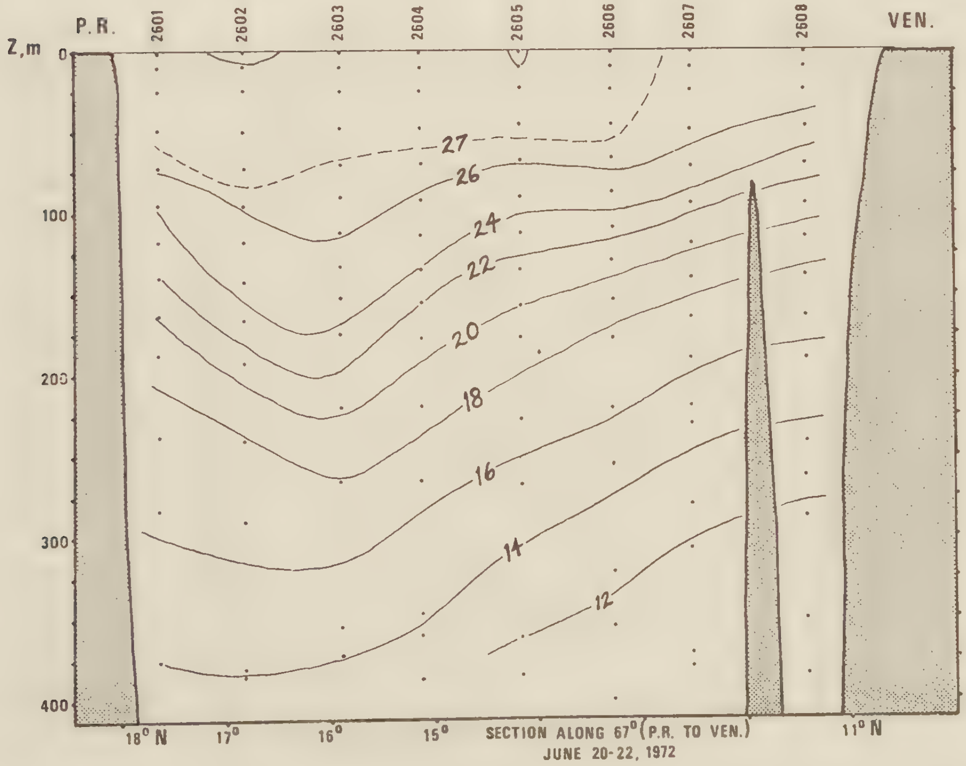

Fig. 6 Temperature section, Venezuela transect: June 20-22, 1972

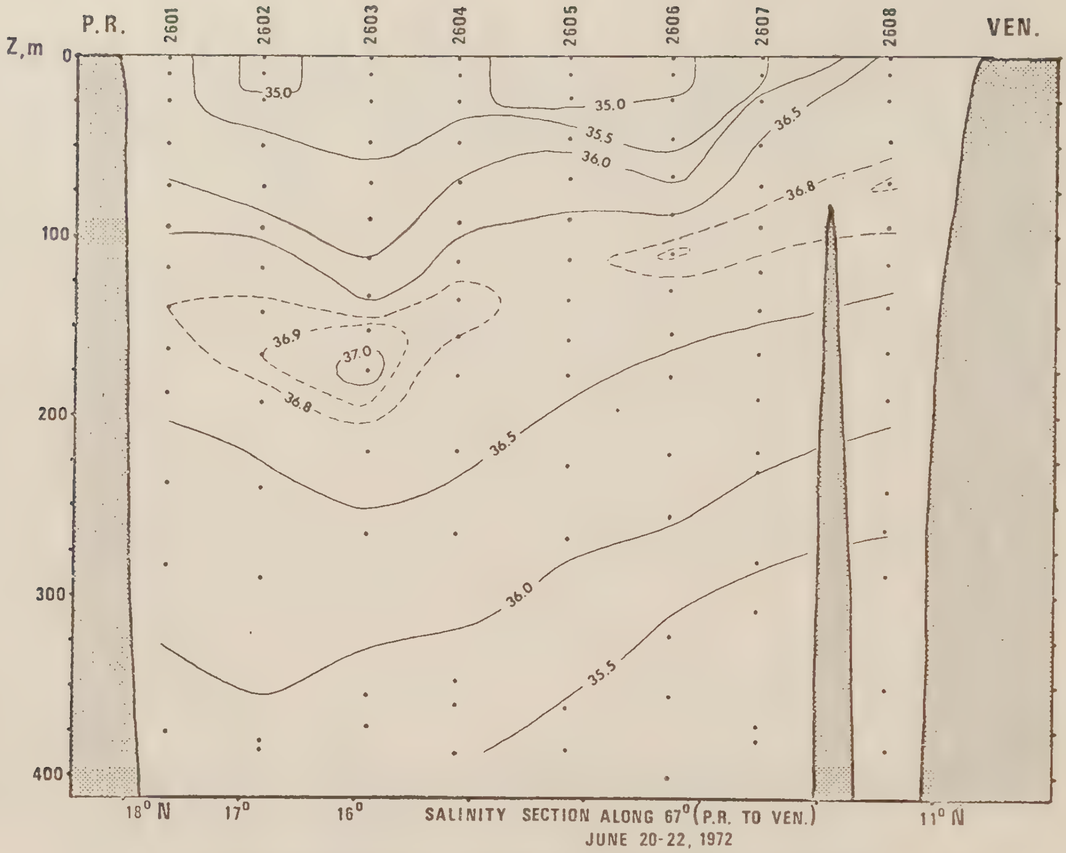

Fig. 7 Salinity section, Venezuela transect: June 20–22, 1972

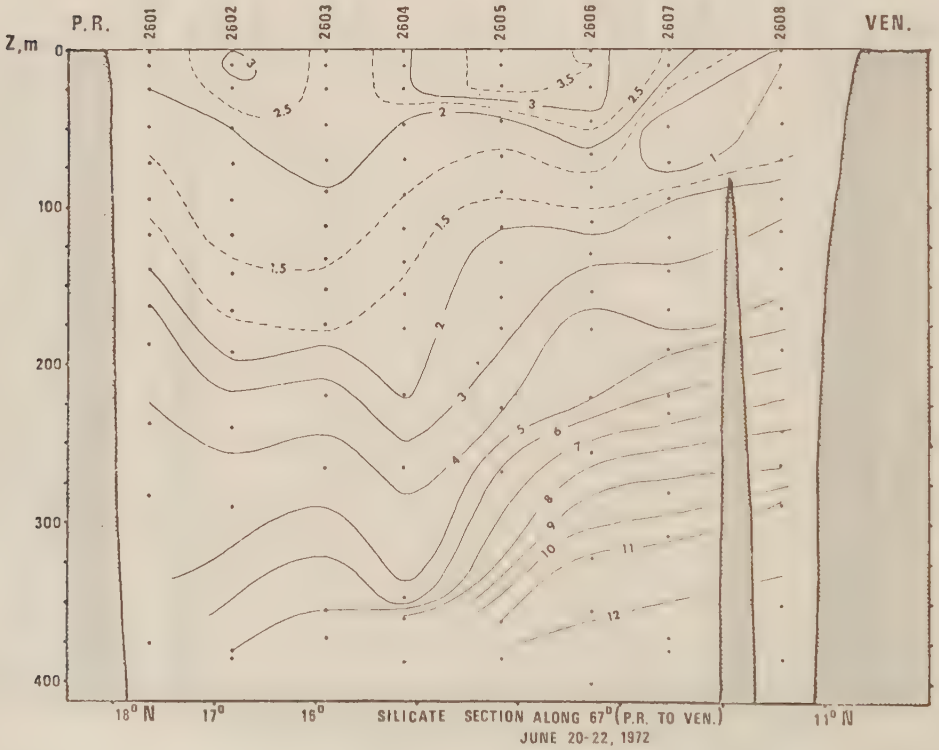

Fig. 8 Silicate section, Venezuela transect: June 20–22, 1972

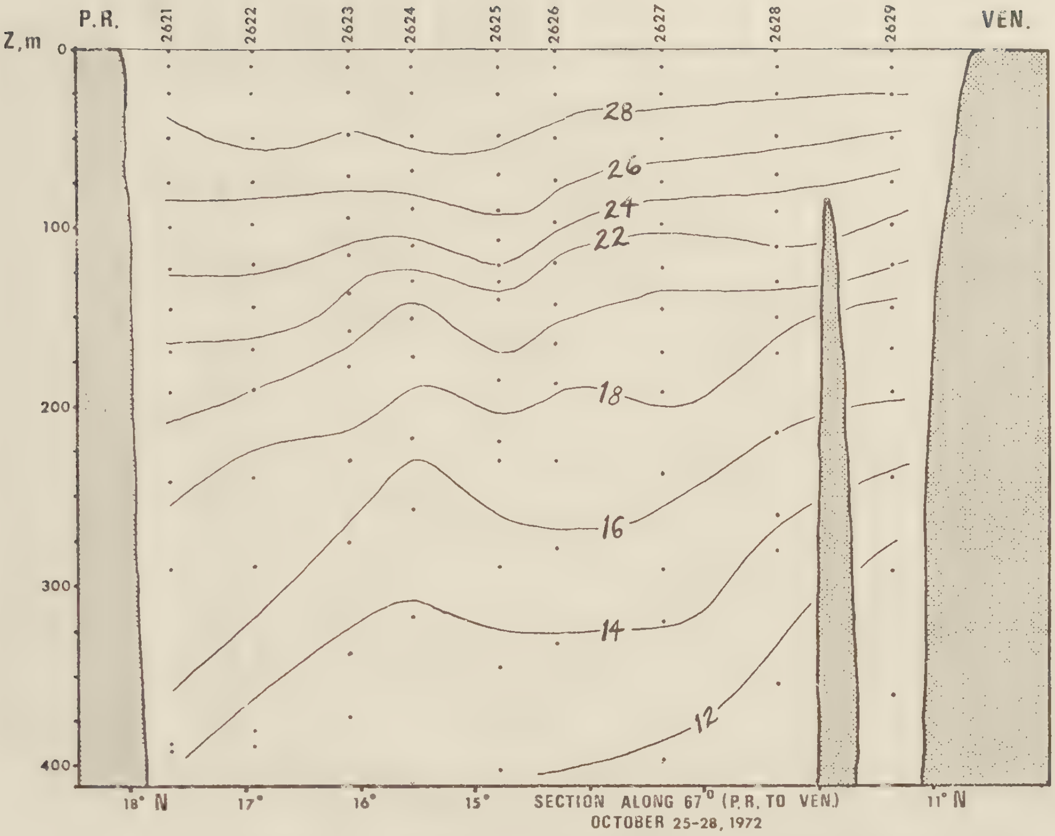

Fig. 9 Temperature section, Venezuela transect: October 25-28, 1972

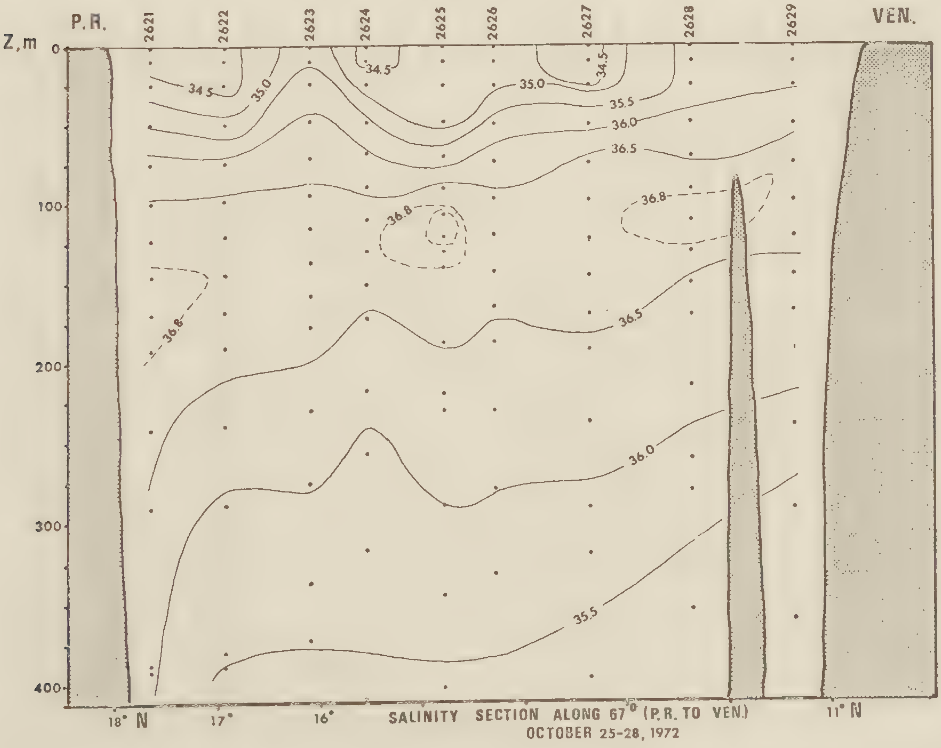

Fig. 10 Salinity section, Venezuela transect: October 25-28, 1972

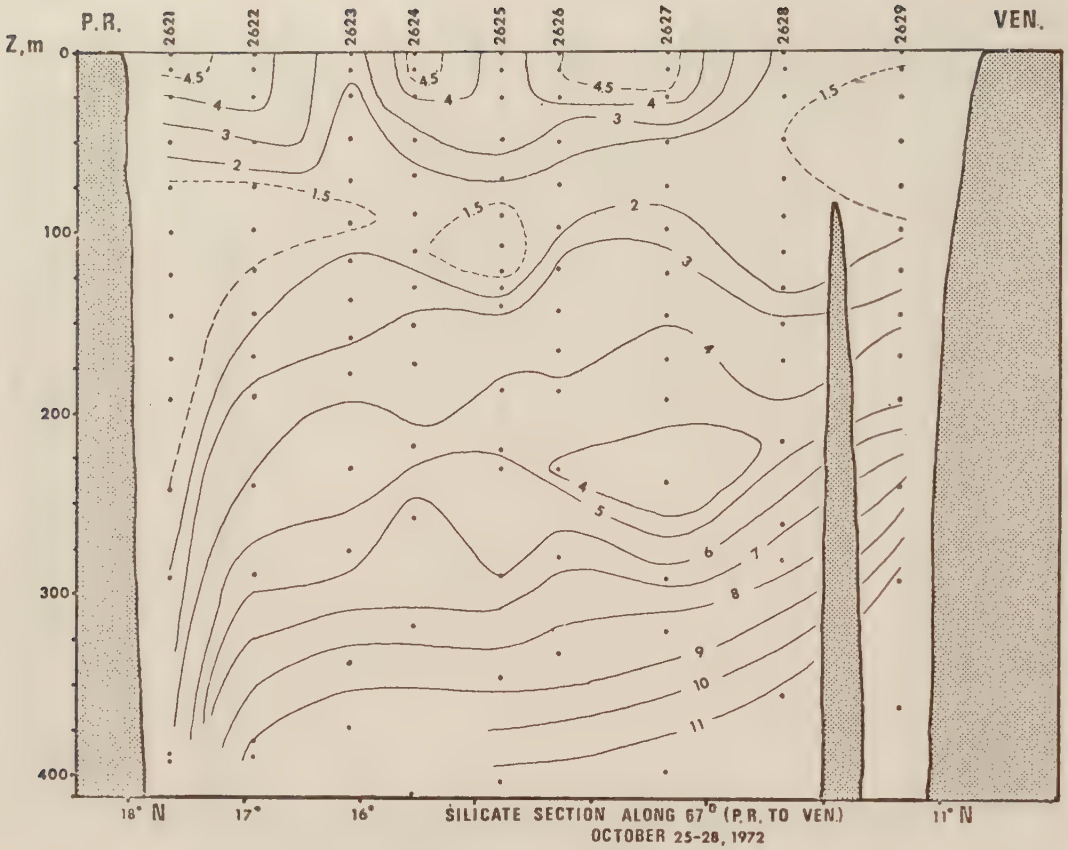

Fig. 11 Silicate section, Venezuela transect: October 25-28, 1972

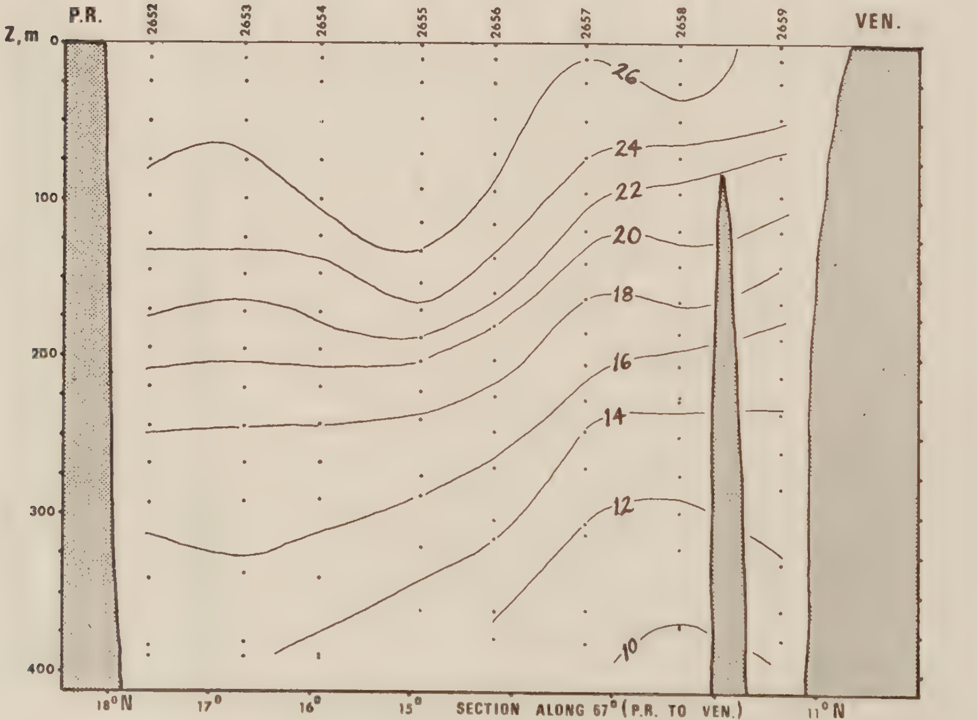

Fig. 12 Temperature section, Venezuela transect: March 29-April 1, 1973

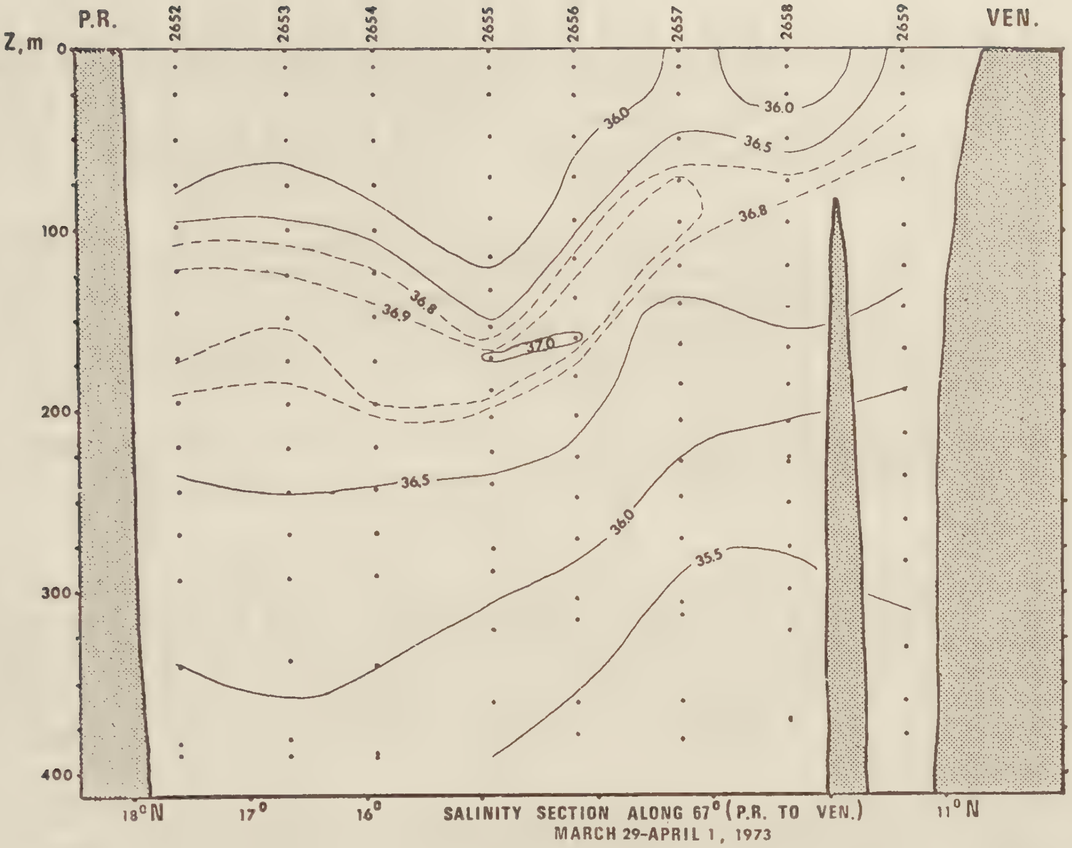

Fig. 13 Salinity section, Venezuela transect: March 29-April 1, 1973

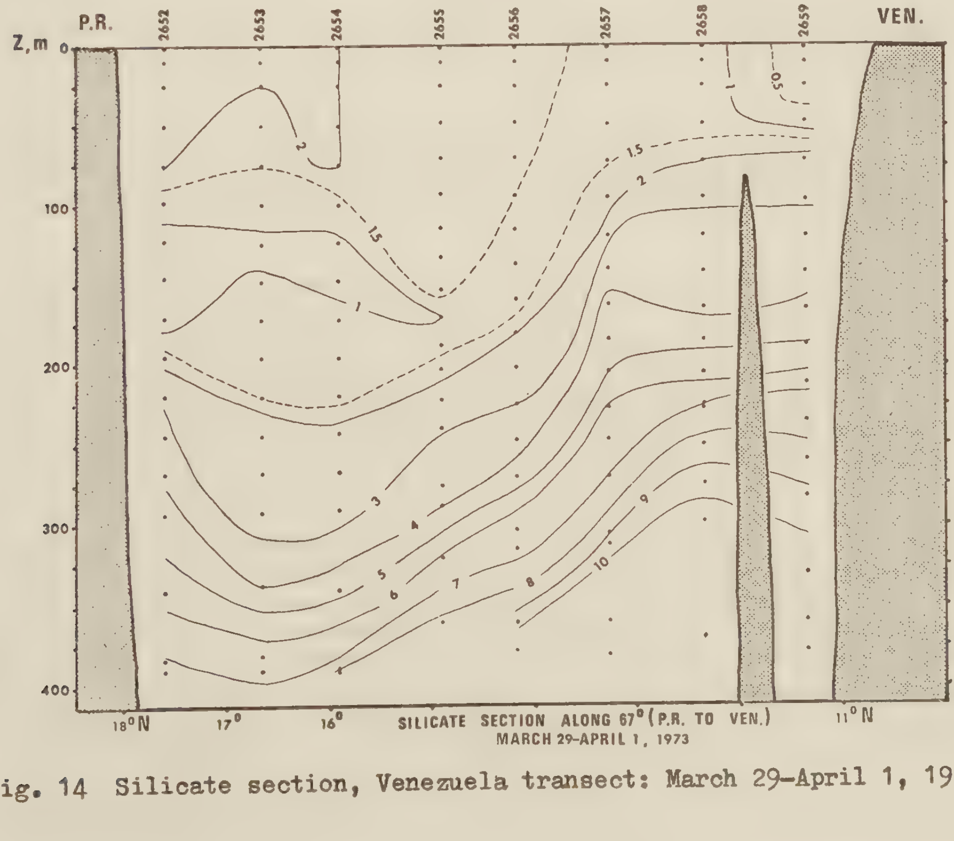

Fig. 14 Silicate section, Venezuela transect: March 29-April 1, 1973

A variety of possible explanations can be put forth to explain the observed temporal and spatial fluctuations in the SUW. Comparison of Figs. 7 and 6, 10 and 9, and 13 and 12 suggests that the lateral position of the highest salinity core of the SUW occurs at the centre of anticyclonic eddies. Therefore one could argue that the position and strength of the SUW reflect the changing current structure of the Caribbean Current and its associated eddies and countercurrents.

Variations in meteorological conditions at the source area could also be responsible for seasonal or longer term fluctuations. The core of the SUW may also reflect the varying importance with time of different passages through the Lesser Antilles as primary corridors of inflow for the SUW. In addition, there is a dependence of SUW salinities on surface salinities, suggesting that seasonal surface salinity variations are reflected as deep as the SUW due to vertical mixing.

Any or all of these causes are undoubtedly responsible for the observed fluctuations in the core of the Subtropical Underwater.

3. SURFACE WATERS

We can next consider salinity variations in the surface mixed layer. Salinity fluctuations have been observed for years in the Caribbean surface waters and have been related to local seasonal rainfall, rainfall over the northern tropical Atlantic, and outflow from the Orinoco and Amazon Rivers (Beer et al., 1968; Fancher, 1973; Steven and Brooks, 1972; Gade, 1961; Wüst and Gordon, 1964). We will attempt to show that these salinity depressions are primarily the result of Amazon and Orinoco River outflow which enters the Caribbean seasonally.

At the Puerto Rico serial station, surface salinities approach a minimum value in late October and early November (Fig. 4). High surface salinities occur in April/May. This seasonal pattern has been repeated consistently from at least 1969 to the present and is strong evidence for periodic seasonal fluctuations. Values of dissolved silicate in the surface waters are high during the low salinity intrusions and low during high salinities (Fig. 5). An inverse relationship of this type is exactly what we would expect if the low salinity intrusions are caused at least in part by silicate-rich fresh water runoff.

However, for a number of years, we suspected that we were seeing the result of local runoff from Puerto Rico rather than Amazon river water. After all, the serial station is only 35 km south of western Puerto Rico, and it could be argued that the station was being influenced by local drainage. We were also aware that the monthly average rainfall curve for Puerto Rico accurately mirrored the surface salinity changes, further suggesting a local effect.

A number of lines of evidence convinced us that the salinity depressions were not a local phenomenon. First of all, the 67°W sections show surface salinities across the entire basin in March/April higher than 35.8 per mille (Fig. 13) and dissolved silicate values less than 2.1 µM (Fig. 14). There was thus not a trace of low salinity surface water inside the Venezuela Basin during late spring. By June/July the low salinity silicate-rich surface water was first beginning to appear in the central Venezuela Basin much before its appearance at the serial station (Figs. 7 and 8). By October/November, pockets of low-salinity, silicate-rich surface water occur in the central basin as well as near Puerto Rico (Figs. 10 and 11).

These surface salinity excursions are, indeed, occurring across the entire Venezuela Basin and are not connected to local precipitation and runoff effects. Our suspicions that the Amazon River was responsible were strengthened again, mainly because of its enormous flow volume (equal to about 30 percent of the total river flow into the Atlantic) and its position 'upstream' from the Caribbean. The currents feeding into the eastern Caribbean originate in the North Equatorial and Guiana Current systems (Wüst and Gordon, 1964; Gordon, 1967) (Fig. 15). The fluvial output from the Amazon is periodically carried far offshore by a complex pattern of currents northeast of Brazil, and becomes embedded in the Guiana Current system (Cochrane, 1965; Metcalf and Stalcup, 1967; Metcalf, 1968). Water of Amazon origin has been observed in lenses discontinuous with low salinities nearer the Amazon far off the Brazilian coast (Böhnecke, 1936; Ryther et al., 1967; Calef and Grice, 1967; Gibbs, 1970) as far north as Barbados (Landis, 1971).

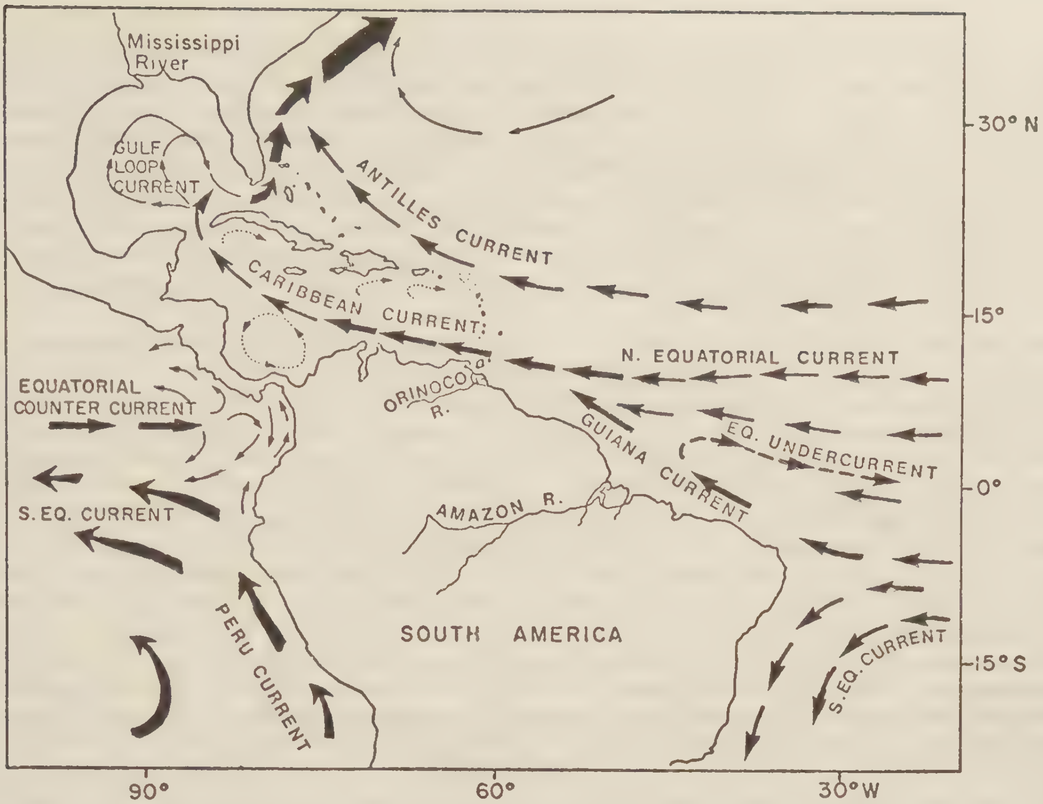
Mississippi River
GULF LOOP CURRENT
ANTILLES CURRENT
CARIBBEAN CURRENT
N. EQUATORIAL CURRENT
EQUATORIAL COUNTER CURRENT
ORINOCO R.
EQ. UNDERCURRENT
GUIANA CURRENT
S. EQ. CURRENT
AMAZON R.
SOUTH AMERICA
PERU CURRENT
S. EQ. CURRENT
30° N
15°
0°
15° S
90°
60°
30° W

Fig. 15 Map of general currents of Equatorial Atlantic and Caribbean

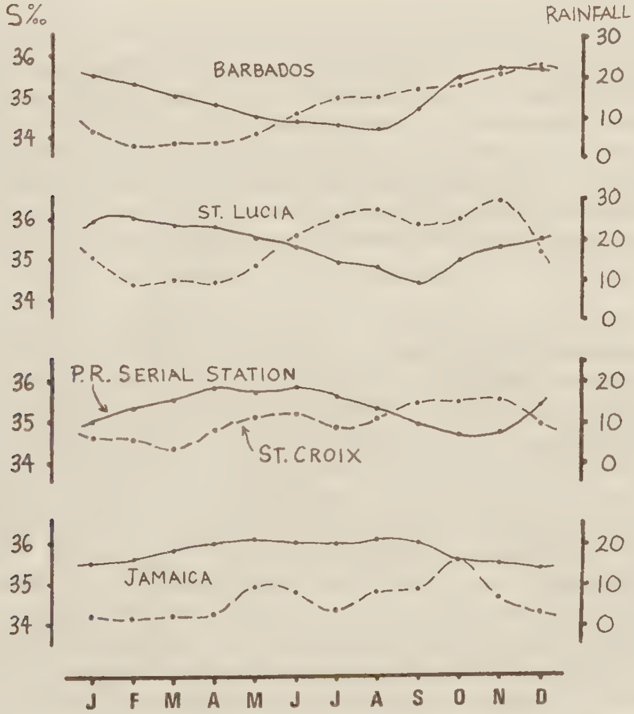

Fig. 16 Monthly march of salinities (solid lines) and rainfall (dashed lines) at selected sites. Barbados salinity data from Barbados serial station: Lewis et al. (1962), Beers et al. (1968), Steven and Brooks (1972). St. Lucia salinities from C & GS Publication 31-1 (1965). Jamaica salinity data from Jamaica serial station: Beers et al. (1968). All other rainfall data from H.O. Publication Nos. 21, 22 and 23 (1963, 1967)

Maximum Amazon runoff occurs during May, June, and July (Oltman, 1968; Davis, 1964; Gibbs, 1970), yet Neumann (1969) finds that seasonal surface salinities along the northeast coast of Brazil are related to local precipitation and runoff (maximum in March and April) rather than Amazon runoff. Evidently the Amazon outflow does not heavily influence coastal Brazil, but is instead diverted into the open ocean where its waters are mixed into the tropical Atlantic surface waters and swept westward with the general circulation around and through the Caribbean. This may not always be the case: both Gibbs (1976) and van Bennekom (this volume) have recently observed the Amazon plume to extend northwestward from the mouth of the river along the continental shelf before turning offshore.

Surface waters enter the Caribbean from the area directly south and southeast of the Lesser Antilles (Gordon, 1967; Febres-Ortega, 1970) where large lenses of Amazon river water have been observed. Low salinity surface water then proceeds through the Caribbean in a seasonal manner each year. Fig. 16 displays average monthly rainfall and surface salinity data for selected sites in the Caribbean. The salinities at all sites (except St. Lucia) were obtained from offshore serial stations, presumably uninfluenced by local runoff. Rainfall data are from nearby sites of minimum orographic ('island') effects (except Jamaica) in an attempt to best represent open oceanic rainfall. Minimum salinities occur at Barbados during August, St. Lucia in September, Puerto Rico in October and November, and Jamaica in December. The difference between maximum and minimum salinities at each site decreases downstream in the same direction (Barbados to Jamaica). These data suggest a slow migration and downward mixing of low salinity water through the Caribbean from east to west with the prevailing currents. The rainfall curves for each of these locations clearly demonstrate the discontinuity of surface salinity and rainfall everywhere except at Puerto Rico. Thus local precipitation is not a primary cause of surface salinity changes. Some fresh water is undoubtedly contributed by the Orinoco, particularly in the southern Venezuela Basin (Gade, 1961; Betzer, this volume), even though the outflow is only about one sixth that of the Amazon. The silicate-rich riverwater is also of course diluted with silicate- and salt-free rainfall both by direct precipitation on the sea surface and by advection of rain-freshened surface water into the area.

We can place limits on the relative volumes of river water and rainwater causing these salinity depressions by making use of the relationship between salinity and silicate, and by devising a simple model similar to the two-point mixing models generally applied to estuaries. In our model, however, we must account not only for biological removal of silica, but also for dilution of the entire system by silica- and salt-free rainwater. Rain is never considered in estuarine mixing, since the volume of rain falling directly on the surface of the estuary is usually miniscule when compared to the total runoff and river input. In our proposed open ocean system, however, rainfall directly on the sea surface is important and must be considered.

We have defined the surface mixed layer to be the upper homogeneous layer of surface water whose salinity is constant within 0.1 per mille and whose silicate concentration is constant within 0.2 µM. A least-squares regression of silicate versus salinity was then computed for all surface mixed layer data that we collected from 1971 to 1973, including serial stations, 67°W transects, and several STD casts taken from the R/V DISCOVERER during NOAA/CARIB (Fig. 17). Results reveal a surprisingly close relationship, which, among other things, suggests that silicate is remarkable conservative over the salinity range between 34.0 per mille and 36.5 per mille. This is due to the very low phosphate and nitrate concentrations in the surface Caribbean, causing very low levels of productivity (Richards, 1958). Ryther et al. (1967) observed that lenses of Amazon river water off the coast of Brazil, though high in silicate, were depleted in other nutrients and, therefore, actually depressed the productivity of the surrounding already inpoverished sea. Biological removal of dissolved silicate is probably insignificant in the Caribbean. Inorganic silicate removal is insignificant in estuaries (Fanning and Pilson, 1973; Boyle et al., 1974) and probably unimportant in the open ocean.

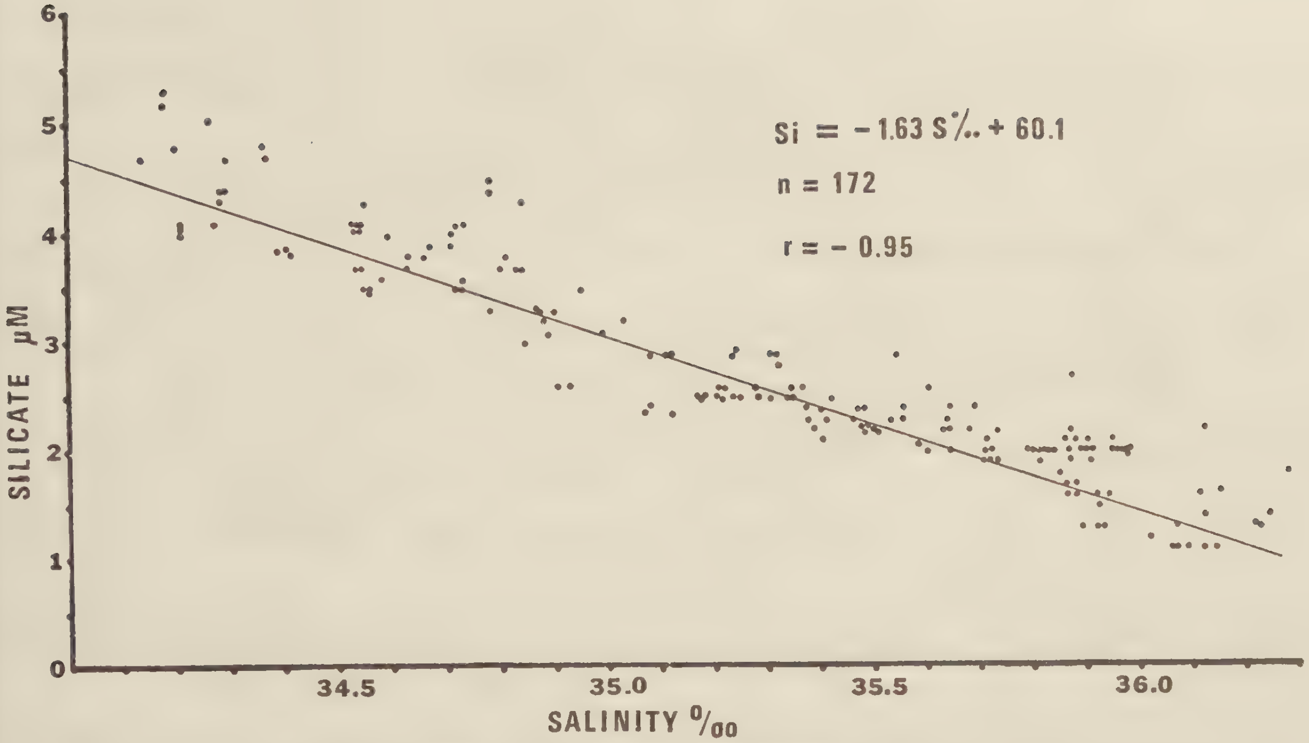

Fig. 17 Scatter diagram of silicate versus salinity for surface mixed layer, Venezuela Basin. Regression line and equation fitted by least-squares method

The regression equation in Fig. 17 would indicate that at the freshwater tie-point (S ‰ = 0), one could expect silicate value of about 60 µM. This is about one half to one third the value normally reported for the silicate concentration of Amazon river water (Gibbs, 1972; Milliman and Boyle, 1975). Therefore, at least one half to one third of the freshwater contributing to the salinity depressions is composed of Amazon river water. It cannot be less, unless rain is dumping dissolved silica onto the surface of the tropical Atlantic. The remainder must be composed of rainwater. If there is biological removal of silicate within the Amazon estuary or in the open ocean, then the relative proportion of Amazon contribution must be even higher, as we shall see.

Milliman and Boyle (1975) have measured dissolved silicate and salinity in the Amazon estuary over a salinity range of 0-30 per mille. We have reproduced part of their results in Fig. 18. They found Amazon river water to have a silicate concentration of 125-135 µM. Between salinities of 0 per mille and 6 per mille, silicate appeared to be conserved, following the upper mixing line. Between 6 per mille and 10 per mille, about 25 percent of the riverine silicate was removed by diatoms, as indicated by high percentages of diatom frustules in the suspended load over this salinity range. Above 10 per mille, silicate again appeared to be conservative, but followed a lower dilution line (solid lower line in Fig. 18).

By comparison, the regression line computed from our mixed layer data is shown on Fig. 18 as a dashed line (extrapolation of our regression line between 34.0 and 36.5 per mille). The data points scattered about this line were collected by Ryther et al. (1967) in a lense of Amazon water about 400 km from the mouth of the Amazon River.

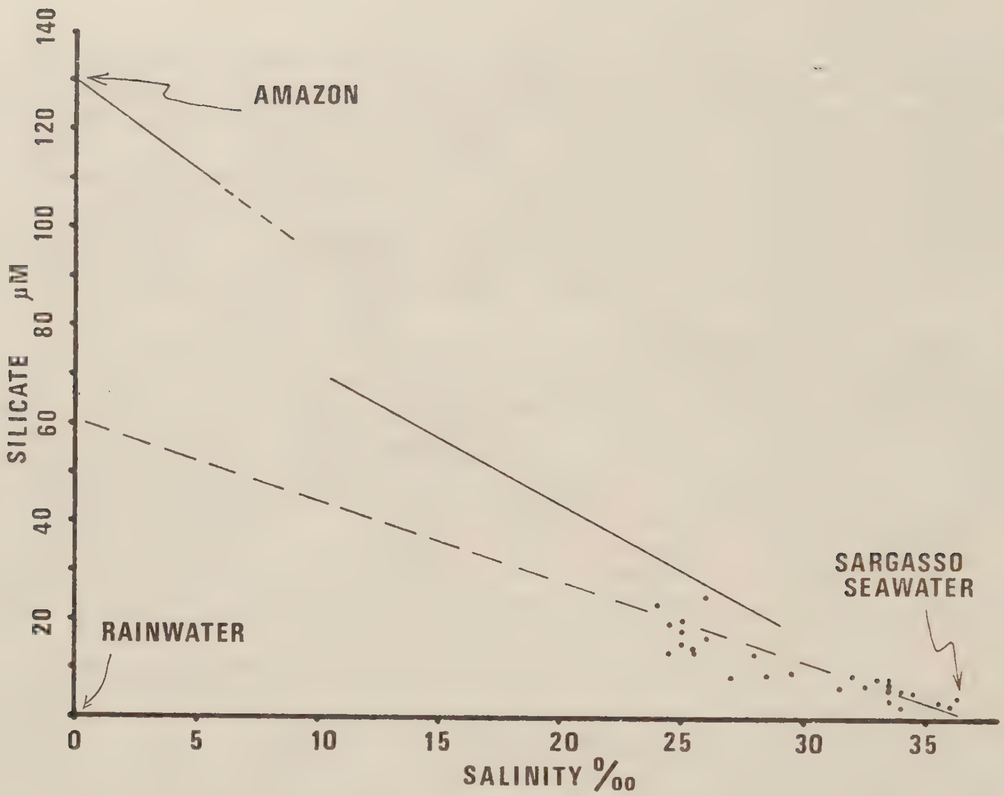

Fig. 18 Three point mixing diagram (see text). Upper solid lines from Milliman and Boyle (1975). Dashed line extrapolation of regression on Fig. 16. Data points from Ryther et al. (1967)

Apparently, after leaving the estuary and travelling some hundreds of kilometres offshore, the Amazon water has either lost more silicate to biological removal, or been diluted by some silicate-free freshwater source, such as rain, or rain-freshened surface sea water.

It is more likely that the Amazon water has encountered and partially mixed with equatorial low-salinity water. The Meteor Atlas (Böhnecke, 1936) shows equatorial low salinity water intruding into this area during the late summer, in a position where it could encounter and mix with these fresh Amazon lenses. In fact, we suspect that the large degree of scatter in Ryther's et al. (1967) data is due not to analytical error, but to incomplete mixing of these two fresh surface waters, causing a heterogeneous distribution of silicate and salinity. As this mixture of low-salinity water continues northwestward into the Caribbean, mixing and stirring more completely as it travels, its salinity is increased by mixing with the underlying SUW, until at Puerto Rico the silicate-salinity relationship is fairly smooth.

If this picture is correct, then our mixing diagram in Fig. 18 tells us that about 65 percent of the fresh water seasonally entering the Caribbean is of Amazon (and Orinoco) origin. The other 35 percent is from rain, presumably rain that falls over the northern equatorial current system during the northern rainy season. Since the outflow of the Amazon plus Orinoco Rivers (about 200 x $10^3 m^3 sec^{-1}$) contributes 65 percent of the total freshwater influx, then the influx from rain (35 percent) must be about 100 x $10^3 m^3 sec^{-1}$. This volume of rain falling into an area of the tropical North Atlantic approximately 40° by 10° (the area of the North Equatorial Current system) would be the equivalent of about 70 cm of rain per year. Neumann and Pierson (1966) give the average annual excess of precipitation over evaporation in the equatorial North Atlantic between 0° and 10°N as about 67 cm y^{-1}. This good agreement supports the basic contention of the model that the major proportion of the fresh water influx causing seasonal salinity depressions in the eastern Caribbean derives from the mouths of rivers, principally the mouth of the Amazon.

4. REFERENCES

Beer, J.R., D.M. Steven and J.B. Lewis, Primary productivity in the Caribbean Sea off
1968 Jamaica and the tropical North Atlantic off Barbados. Bull.Mar.Sci., 18:86-104

Böhnecke, G., Temperatur, Salzegehalt und Dichte an der Oberfläche des Atlantischen Ozeans.
1936 1. Wiss.Ergebn.Dtsch.Atl.Exped.Meteor., 5(1):186 p.

Boyle, E. et al., On the chemical mass-balance in estuaries. Geochim.Cosmochim.Acta,
1974 38:1719-28

Calif, G.W. and G.D. Grice, Influence of the Amazon River outflow on the ecology of the
1967 western tropical Atlantic. 2. Zooplankton abundance, copepod distribution, with remarks on the fauna of low-salinity area. J.Mar.Res., 25:84-92

Cochrane, J.D., Equatorial currents of the western Atlantic. College Station, Texas A & M
1965 University, Progress Report Ref. (65-17T):6-19

Davis, L.C., The Amazon's rate of flow. Nat.Hist., 73:15-9
1964

Fancher, J.E., Seasonal changes of sea level of the Caribbean Sea as examined at a single
1971 station. Masters thesis, Department of Marine Sciences, University of Puerto Rico at Mayaguez, Puerto Rico, 51 p.

Fanning, K.A. and M.E.Q. Pilson, The lack of inorganic removal of dissolved silica during
1973 river-ocean mixing. Geochim.Cosmochim.Acta, 37:2405-15

Febres-Ortega, A., Currents and waters of the upper 1200 meters of the eastern Caribbean
1970 Sea during winter. Masters thesis, Department of Physical Oceanography, Texas A. & M. University, College Station, 48 p.

Froelich, P.N., Dissolved silicate in the Venezuela Basin of the Caribbean Sea. Masters
1973 thesis, Department of Marine Sciences, University of Puerto Rico at Mayaguez, Puerto Rico, 62 p.

Froelich, P.N. and D.K. Atwood, New evidence for sporadic renewal of Venezuela Basin Water.
1974 Deep-Sea Res., 21:969-75

Gade, H.G., On some oceanographic observations in the south-eastern Caribbean Sea and the
1961 adjacent Atlantic Ocean with special reference to the influence of the Orinoco River. Bol.Inst.Oceanogr.Univ.Oriente, 2:287-342

Gibbs, R.J., Circulation in the Amazon River estuary and adjacent Atlantic Ocean. J.Mar.Res.,
1970 28:113-23

__________, Water chemistry of the Amazon River. Geochim.Cosmochim.Acta, 36:1061-6
1972

__________, Amazon River sediment transport in the Atlantic Ocean. Geology, 4:45-8
1976

Gordon, A.J., Circulation of the Caribbean Sea. J.Geophys.Res., 22:6207-23
1967

Landis, R.C., Early BOMEX results of sea surface salinity and Amazon River water. J.Phys.
1971 Oceanogr., 1:278-81

Metcalf, W.G., Shallow currents along the northeastern coast of South America. J.Mar.Res.,
1968 26:233-43

Metcalf, W.G. and M.C. Stalcup, Origins of the Atlantic equatorial undercurrent. J.Geophys.
1967 Res., 72:4959-75

Milliman, D. and E. Boyle, Biological uptake of dissolved silica in the Amazon River estuary.
1975 Science, Wash., 189:995-7

Neumann, G., Seasonal salinity variations in the upper strata of the western tropical Atlantic Ocean.
1969 1. Sea surface salinities. Deep-Sea Res., 16 Suppl.:165-77

Neumann, G. and W.J. Pierson, Principles of physical oceanography. Englewood Cliffs, N.J.,
1966 Prentice-Hall, Inc., 545 p.

Oltman, R.E., Reconnaissance investigations of the discharge and water quality of the Amazon
1968 River. Circ.U.S.Geol.Surv., (552):16 p.

Richards, F.A., Dissolved silicate and related properties of some Western North Atlantic
1958 and Caribbean waters. J.Mar.Res., 17:449-65

Ryther, J.H., D.W. Menzel and N. Corwin, Influence of the Amazon River outflow on the ecology
1967 of the western tropical Atlantic. 1. Hydrography and nutrient chemistry. J.Mar.
Res., 25:69-83

Steven, D.M. and A.L. Brooks, Identification of Amazon River water at Barbados, West Indies,
1972 by salinity and silicate measurements. Mar.Biol., 14:345-8

Wüst, G. and A. Gordon, Stratification and circulation in the Antillean-Caribbean basins,
1964 Part 1. Spreading and mixing of the water types with an oceanographic atlas.
New York, Columbia University Press, 201 p.

RADIONUCLIDE AND TRACE ELEMENT ASSOCIATIONS WITH PLANKTON AND POSSIBLE VERTICAL TRANSPORT MECHANISMS IN THE CARIBBEAN

by

W.O. FORSTER
ERDA
Washington, D.C.
U.S.A.

D.P. KHARKAR
L.F.E.
California
U.S.A.

K.K. TUREKIAN and J. THOMSON
Yale
Connecticut
U.S.A.

CONTENTS

1. INTRODUCTION
2. ANALYTICAL METHODS
3. RESULTS
4. DISCUSSION
5. REFERENCES

Abstract

Plankton collected from the Caribbean during an NSF-IDOE study, 1971-1972, show strong association of certain trace elements and various radionuclides when compared to the sea water. Normalizing several trace elements and radionuclides to mixed layer concentrations of biologically important species indicates various sorption mechanisms. Depth distributions indicate the dominant vertical transport mechanisms for several trace elements and various radionuclides from the mixed to the deep layers is from biota debris.

Resumen

El plancton recogido en el Caribe durante un estudio del NSF-IDOE, 1971-1972, muestra cuando se compara con el agua de mar, una marcada asociación de ciertos oligo-elementos y de varios radionúclidos. La normalización de varios oligo-elementos y radionúclidos a concentraciones de capas mixtas de especies biológicamente importantes pone de manifiesto diversos mecanismos de sorción. Las distribuciones de profundidad indican que para varios oligo-elementos y radionúclidos, el transporte vertical dominante desde las capas mixtas a las capas profundas, es de restos de fauna y flora.

1. INTRODUCTION

The principal objective of this study was to evaluate the extent of pollution in the Caribbean from human activities on its perimeter. However, it was envisioned that the trace element and radionuclide data collected on these cruises would be useful to better understand the mechanisms controlling and the rates of material transfer throughout this important basin. Generally, trace element and radionuclide distribution patterns are a complex function of the rates and pathways of introduction to the basin, removal by advective processes and the extent of removal by biological and geochemical sorption processes. An important first step in the understanding of these complex interactions between the species of concern and the water column is the collection and analysis of a reliable time series distribution pattern, of which this is only a beginning. It is fortunate to have coincident radioactive and trace element data as the natural radioactive decay of Pb^{210} (22 y) and Po^{210} (138 da) combined with disequilibria between such parent-daughter relationships can provide unique insights into the time rate of such biogeochemical processes. These two natural daughters of U^{238} have short enough half lives to have sufficient activities in the sea yet long enough for measurable radioactive disequilibria to be maintained by the oceanic process of concern. Finally, these tracers are supported by in situ decay of the parent which allows an accurate measure of the initial source term. This latter advantage is not realized in the case of Pb^{210} in the mixed layer as most of this activity is from atmospheric Rn^{222}. However, these three advantages have allowed many authors to effectively use uranium daughters to better understand the following variety of oceanographic processes. Students of K.K. Turekian at Yale University, such as Thomson et al. (1975) determined the accumulation of various metals in and their release from the sediments of Long Island Sound, while L.K. Benninger (1975) used the uranium series radionuclides as tracers of geological processes in Long Island Sound; at Lamont Laboratory, Broeker and Bender (1972) determined the age of marine strandlines in connexion with paleoclimatic studies and, also, made vertical diffusivity estimates from GEOSECS data in the North Atlantic by Trier, Broecker and Feely (1972); Craig, Krishnaswami and Somayajulu (1973) showed radioactive disequilibrium in the deep sea of Pb^{210} relative to Ra^{226} could be as much as 75 percent, suggesting that stable lead is also quickly removed from the water column by adsorption onto sinking particles; the Ph.D. Thesis of Bacon (1975) at Woods Hole showed the general utility of Ra^{226} -Pb^{210} -Po^{210} disequilibria to indicate scavenging efficiencies; another student, R.C. Schedit, made use of uranium and thorium daughters in prospecting for dense mineral deposits along the west coast: and finally calculations of alpha dose to marine organisms from Po^{210} exposures were made by Folsom and Beasley (1972). Thus the utility of Pb^{210} and Po^{210} to aid in understanding short period exchanges has been well established.

2. ANALYTICAL METHODS

Mixed plankton and sea water samples were collected daily during two NSF-IDOE sponsored cruises investigating the extent of pollution in the Caribbean Sea. Plankton samples were separated and either preserved by formalin for later identification or freeze-dried onboard ship for later stable element and radionuclide analysis. Approximately 40 stations were sampled and the plankton results reported here are from collections at alternate stations along the cruise tracts shown in Fig. 1.

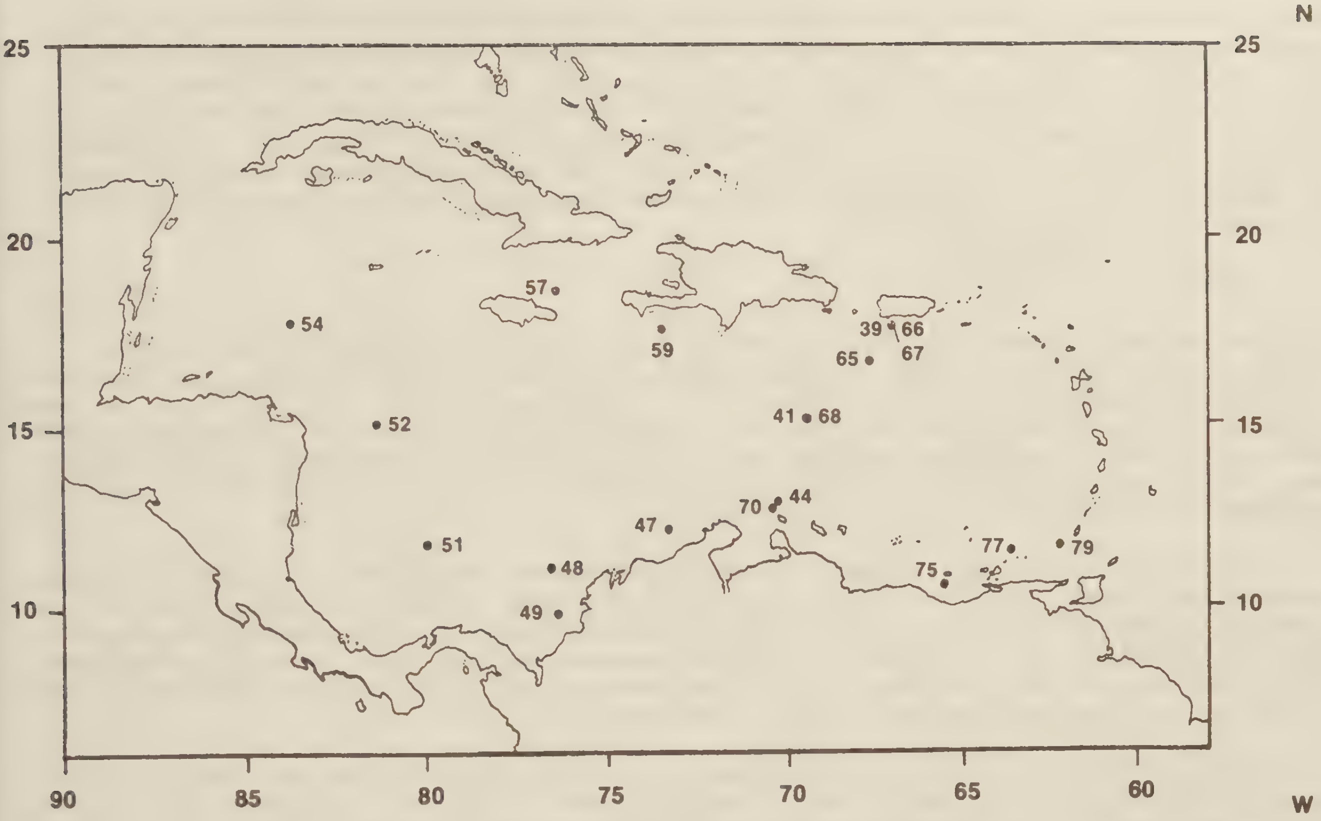

Fig. 1 Sampling sites in Caribbean waters

Stable element analyses of the sea water and plankton samples were carried out by both atomic absorption spectrometry and neutron activation technique. Elements determined by both methods show comparable results. For atomic absorption analysis duplicate 500 mg freeze-dried plankton samples were dissolved in perchloric-nitric acid mix and subsequently boiled to dense white fumes in a water bath. Three reagent blanks and replicate orchard leaf standards were processed along with the plankton to ensure a common matrix between the sample and standards. The following absorptivities (absorbance/ppm) were determined for each trace element: Cr (.038), Mn (.040), Fe (.033), Co (.017), Ni (.016), Cu (.026), Zn (.154), Cd (.132) and Pb (.006). For neutron activation analysis, clean-room handling techniques were used to seal sample and standards in quartz ampules and then irradiated in a Triga III reactor over an integrated flux of 10^{18} neutrons cm^{-2}. The fast neutron flux was calculated from the $Ni^{58}(n,p)Co^{58}$ reaction, while the thermal flux was estimated from the $Co^{59}(n,\alpha)Co^{60}$ reaction. Standards from NBS such as orchard leaves, tuna fish and bovine liver were also irradiated with the plankton. After a three-week cooling period, the gamma ray spectrum of each sample was analysed and the trace element concentrations were calculated by spectrum stripping.

Sea water samples were immediately frozen onboard ship. Later, in the laboratory, total species analysis was carried out by coprecipitation of the trace elements with iron chloride titrated slowly to a pH of 9.3 with ammonia. Separan was added after settling for 24 hours; the precipitate was filtered, dissolved in dilute hydrochloric acid and analysed in a manner similar to the plankton samples. The concentration factor was 400-fold over the concentration in the sea water.

The radiochemical analysis was carried out for $U^{234,238}$, $Th^{228,232}$, $Ra^{226,228}$, Pb^{210} and Po^{210}, but only the latter three species were of sufficient activity to be meaningful. A nitric acid solution of the dried homogenized plankton was repeatedly oxidized with perchloric and hydrofluoric acid until a clear acid solution was present. Polonium was plated onto silver discs and counted for several days by alpha spectrometry with silicon surface barrier detectors. Lead was separated by precipitation with chromate at pH 5, and was filtered and dried on a lucite planchette for beta counting the five-day Bi^{210} daughter on a thin mylar window proportional system. $Radium^{226}$ was determined by counting the four-day daughter Rn^{222} in ZnS (Ag) coated cells. Chemical yields were determined by adding gamma tracers during the original acid dissolution step. Detector efficiencies were well known for these isotopes. Counting errors are generally less than 5 percent for Ra^{226} and Po^{210} and less than 10 percent for Pb^{210}.

3. RESULTS

The results obtained with these radioactive and stable techniques for the plankton samples are shown in Tables I and II respectively. The average activity levels in the plankton increases approximately 20-fold from Ra^{226} to Pb^{210} and from Pb^{210} to Po^{210}. The decay constants for these three radionuclides are 0.00043, 0.0032 and 1.83 y^{-1} respectively, which shows an effective equilibrium activity rate of 74 and 57 between the above pairs of daughters. This shows both Pb^{210} and Po^{210} have an increased activity over that calculated from supported Ra^{226} and Pb^{210} at equilibrium values.

Table II lists the trace element composition of these same plankton samples. The mean concentration ranges from a low of 3 ppm for cobalt to over 300 ppm for iron. This two orders of magnitude change for this variety of trace elements is considered narrow, since some trace elements are in the water at concentrations less than parts per billion[1/] and have little known biological functions, while other elements are in the water at hundreds of parts per billion and are known to be critical in metabolic processes.

Table III lists the trace element composition of both the east and west basins of the Caribbean as determined by atomic absorption techniques. Only zinc and nickel have mean concentrations greater than 1 ppb[1/] which are 5.2 and 1.1 ppb respectively; copper, cobalt, chrome and cadmium had mean concentrations of 0.8, 0.7, 0.5 and 0.2 ppb in sequence. The surface waters of the western basin had significantly higher concentrations of chrome, copper and zinc compared to the eastern basin while the opposite is true for cobalt, nickel and cadmium. The radionuclides also show significant activity difference in each basin as Po^{210} is similar to chrome, copper and zinc with greater activity in the western basin; Ra^{226} and Pb^{210} had greater activities in the eastern basin, similar to cobalt, nickel and cadmium.

4. DISCUSSION

The concentrations of trace elements and radionuclides in marine plankton are a function of the concentration of the particular species in the surrounding water, and the degree of enrichment through metabolic processes relative to this available supply. The subsequent fate of these chemical species depends upon their release properties during the transformation of the planktonic debris during its descent through the water column and ascent through trophic levels. These aspects of the trace element and radionuclide redistributions by mixed plankton are addressed.

4.1 Geographic variations

This study found significant geographical differences in several trace element concentrations and radionuclide activities throughout the Caribbean. Fig. 2 shows the trace element concentrations in surface waters of both basins of the Caribbean. The incoming water from the Guiana Current does not have a reliable characteristic composition of these species, and the short term, local biogeochemical processes dictate a rather variable surface water pattern. Adequate radionuclide data are not available to make basin comparisons similar to the trace element relationships although it appears from plankton concentrations that the incoming Guiana Current generally has greater Ra^{226} and Pb^{210} activities.

1/ Parts per thousand million in U.S. usage

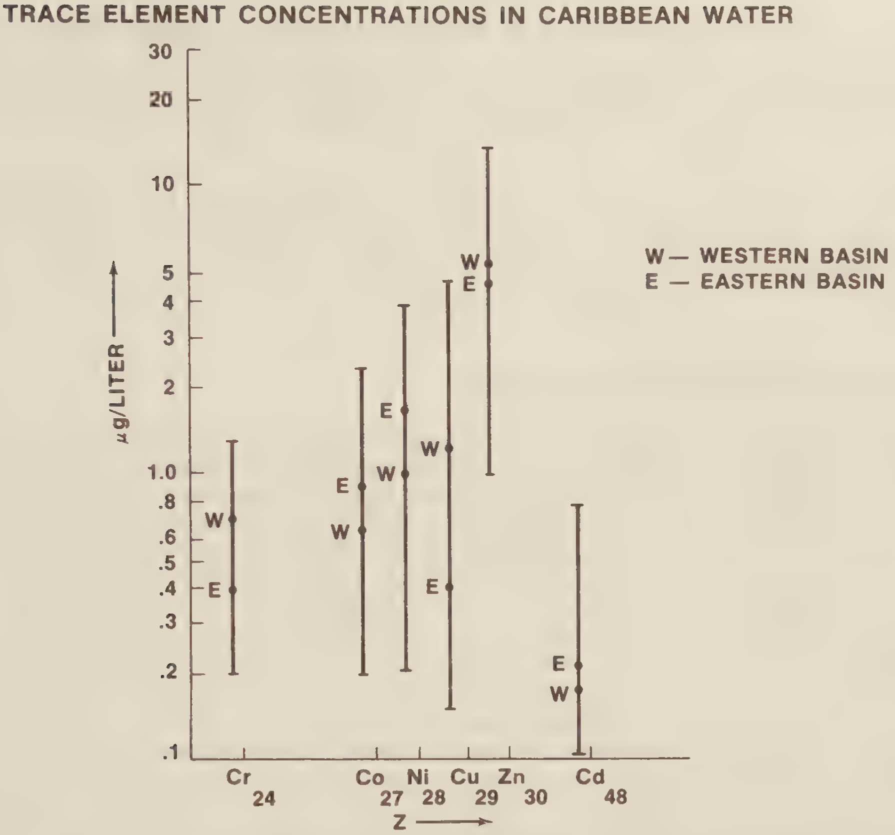

Fig. 2 Ranges of trace elements in Caribbean plankton

4.2 Concentration Factors

Table IV shows the estimated radionuclide concentration factors in mixed plankton based on the previous activities of sea water from the North Atlantic. Trace element concentration factors are also included for these same plankton, but in this case the concentration factors are for plankton and water from the same locations. Both zinc and copper appear to be concentrated to a greater degree (up to 10^5 x) by these plankton than by other transition metals. Of the radionuclides radium-226 is concentrated by plankton the least and is equivalent to cobalt concentration factors; Pb^{210} concentration is between that of zinc and cadmium. Po^{210} is concentrated the most and exceeds the value for copper by six fold. It cannot be determined from these analyses whether the concentration factors which were observed represent passive physical-chemical sorption, or active biological uptake, assimilation and retention. However, both Ra^{226} and Pb^{210} concentration factors in Caribbean plankton are similar to those synthetic fibre-scavenging efficiencies obtained by Krishnaswami et al. (1972) for these same three radionuclides. One might assume that a certain base level of these species is concentrated by each organism through passive sorption processes which vary with size and charge characteristics, but that the significant increases in concentrations primarily occur through biological mechanisms.

An illustration of the importance of the different biological concentration mechanism can be made with the data in Table V which summarize four stations' trace element concentrations in plankton collected by nets of two different mesh sizes. It is assumed the finer mesh (#20) net would contain a higher ratio of primary producers than would the larger mesh (#6) net. Therefore, the ratio of trace element concentrations in each net should be some indication if the mineral species is metabolically involved in the lower trophic level organisms. This is based on two assumptions: (1) the herbivores in the larger meshed net will have much less surface area for adsorption, and (2) in order to transfer the mineral species from the primary producers to the herbivores the trace element will probably be metabolically involved at the primary level. The data in Table V show only two mineral species; copper and cadmium are more concentrated in the coarse net samples than in the fine net samples. Manganese, iron, cobalt and nickel are allunder-represented in these samples of larger organisms.

The composition of the net contents at these various stations are described in Table VI. Copepods dominate the catch at all stations, sometimes accounting for 90 percent of the biomass. The filter-feeding calanoids are ubiquitous and represent the greatest fraction of the herbivores. Euphasiids are the only other major contribution to the biomass at several stations.

4.3 Transfer of Materials in the Water Column

Estimates of the transfer of surface radioactivity and trace elements through the water column for surface radioactivity and trace elements through the water column for possible uptake by benthic organisms can be made by contrasting the concentrations of these mineral species in epipelagic and benthic organisms. The trace element data shown in Table VII were obtained from benthic collections from these same cruises and were analysed in the same manner as that described for the plankton samples. The trace elements that are biologically active and associated with suspended material in the upper water column appear to be transported to depths for subsequent uptake by benthic organisms. This is shown by benthos/plankton ratios which are greater than one for manganese, iron, cobalt, nickel and cadmium. The more soluble species of copper and chromium show benthos/plankton ratios less than those which would indicate a rapid recycling of these species in the mixed layer. It is possible that benthic organisms receive the greatest portion of these trace elements from the substrate on which they live and that therefore no simple relationship to the trace element composition of the waters above can be demonstrated. However, for four of these trace elements shown in Table VIII the mixed surface waters are depleted in cobalt, nickel, zinc and cadmium as compared with deeper waters by values of up to 50 percent. This would mean the benthos organisms not only have a greater concentration of these trace elements available from the water column but also have additional sources in the sediments.

4.4 Variability for Trace Element and Radionuclide Data

In order to evaluate the precision of the data collected on these cruises ratios of range/means were determined for the trace elements and radionuclides for the plankton and water samples wherever available. These results are displayed in Table IX. A low ratio would indicate a high precision within a set of samples, for example a value of three indicates a reasonably narrow range for trace element variability for both the plankton and the sea water samples. The data show both copper and zinc are quite variable in plankton samples.

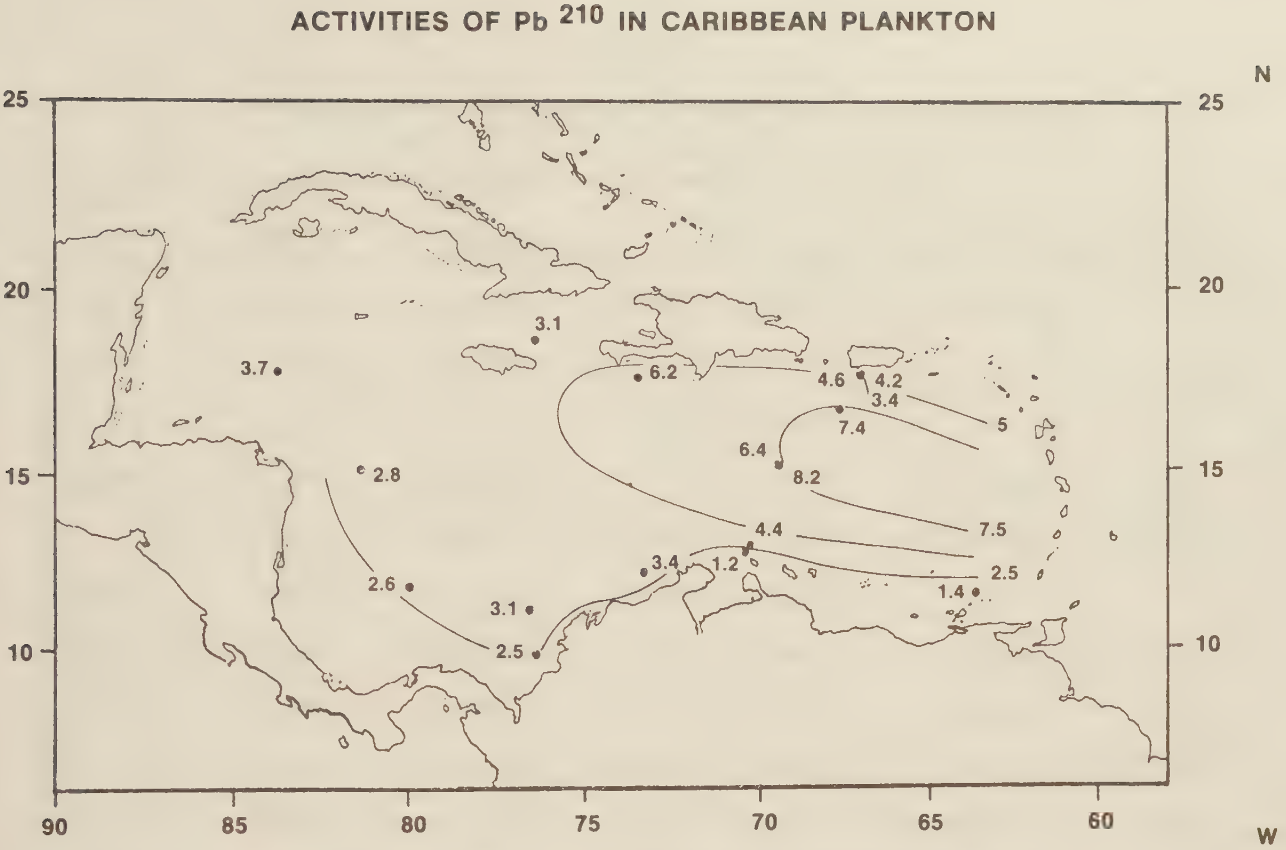
ACTIVITIES OF Pb 210 IN CARIBBEAN PLANKTON
N
W
25
20
15
10
90
85
80
75
70
65
60
3.1
3.7
6.2
4.6
4.2
3.4
5
7.4
6.4
8.2
2.8
4.4
7.5
3.4
1.2
2.5
1.4
2.6
3.1
2.5

Fig. 3 Trace element concentrations in Caribbean Water

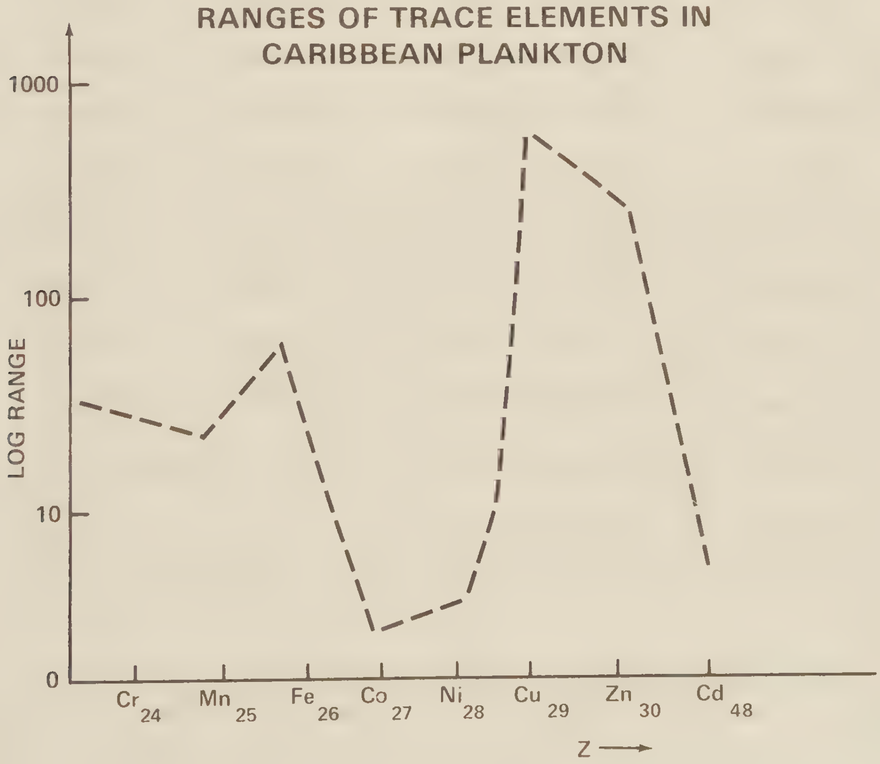

Fig. 4 Lead-210 distributions in the Caribbean

TABLE I

Concentration of radioactive nuclides in Caribbean plankton

Station	Date	Location	^{226}Ra dpm/g	^{210}Pb dpm/g	^{210}Po dpm/g
39	21 Nov 71	17°54'N, 66°55'W	0.29±0.02	4.5±0.3	90±4
41	22 Nov 71	15°15'N, 68°17'W	0.14±0.01	6.4±0.5	61±2
44	23 Nov 71	12°58'N, 70°4' W	0.28±0.02	4.4±0.4	68±3
47	24 Nov 71	12°9' N, 73°10'W	0.27±0.02	3.4±0.4	52±2
48	25 Nov 71	11°8' N, 76°28'W	0.15±0.01	3.1±0.3	
49	26 Nov 71	9°56'N, 76°20'W	0.13±0.01	2.5±0.2	64±2
51	29 Nov 71	11°50'N, 79°58'W	0.14±0.01	2.6±0.2	54±2
52	30 Nov 71	15°3' N, 81°21'W	0.16±0.01	2.8±0.3	73±2
54	1 Dec 71	17°52'N, 83°41'W	0.14±0.01	3.7±0.3	
57	2 Dec 71	18°39'N, 76°16'W	0.13±0.01	3.1±0.3	81±3
59	6 Dec 71	17°41'N, 73°22'W	0.15±0.02	6.2±0.5	101±4
65	11 Jan 72	16°51'N, 67°34'W	0.20±0.02	7.4±0.5	
66	21 Jan 72	17°53'N, 66°55'W	0.20±0.03	4.2±0.4	73±3
67	21 Jan 72	17°54'N, 66°55'W	0.63±0.04	3.4±0.4	71±3
68	22 Jan 72	15°15'N, 68°14'W	0.16±0.02	8.2±0.5	72±3
70	23 Jan 72	12°46'N, 70°11'W	0.33±0.02	1.2±0.2	31±1
75	25 Jan 72	10°41'N, 65°28'W	0.84±0.04	2.3±0.3	74±1
77	26 Jan 72	11°36'N, 63°36'W	0.15±0.01	1.4±0.2	33±1
79	26 Jan 72	11°40'N, 62°11'W	1.10±0.04	10.2±0.6	114±5

TABLE II

Concentrations of selected trace elements in Caribbean plankton (µg/g-dry)

Station	Date	Location	Cr	Mn	Fe	Co	Ni	Cu	Zn	Cd
39	21 Nov 71	17°54'N, 66°55'W	10.0	6.9	50	2.0	6.1	25	145	3.2
41	22 Nov 71	15°15'N, 68°17'W	5.0	6.9	35	2.0	6.1	36	178	6.6
44	23 Nov 71	12°58'N, 70°4' W	5.0	3.5	40	2.1	6.1	61	85	6.9
47	24 Nov 71	12°9' N, 73°10'W	-	12.0	18	2.1	6.1	89	-	6.9
48	25 Nov 71	11°8' N, 76°28'W	40.0	10.5	135	2.0	6.1	25	-	9.3
49	26 Nov 71	9°56'N, 76°20'W	-	10.5	20	6.0	12.2	25	118	5.7
51	29 Nov 71	11°50'N, 79°58'W	-	12.0	55	2.1	6.1	94	103	7.1
52	30 Nov 71	15°3' N, 81°21'W	-	5.2	25	2.1	6.1	20	68	6.4
54	1 Dec 71	17°52'N, 83°41'W	-	3.5	25	2.0	9.2	17	50	7.8
57	2 Dec 71	18°39'N, 76°16'W	-	5.2	50	2.0	12.2	59	80	4.5
59	6 Dec 71	17°41'N, 73°22'W	20.0	10.0	65	4.0	6.1	164	-	6.1
65	11 Jan 72	16°51'N, 67°34'W	11.0	11.5	115	-	13.2	585	942	6.6
66	21 Jan 72	17°53'N, 66°55'W	-	16.7	186	-	13.2	55	1 537	5.4
67	21 Jan 72	17°54'N, 66°55'W	-	4.2	39	-	7.8	124	905	7.2
68	22 Jan 72	15°15'N, 68°14'W	1.3	14.6	175	-	7.8	155	3 787	10.4
70	23 Jan 72	12°46'N, 70°11'W	-	4.2	162	-	10.6	13	119	5.8
75	25 Jan 72	10°41'N, 65°28'W	-	4.2	51	-	7.9	78	120	7.6
77	26 Jan 72	11°36'N, 63°36'W	4.0	4.2	51	-	7.9	680	345	7.6
79	26 Jan 72	11°40'N, 62°11'W	1.3	20.8	145	-	13.2	163	200	7.6
Range			1.3 to 40.0	3.5 to 28.6	39 to 3 300	2.0 to 6.0	6.1 to 24.0	13 to 1 570	85 to 3 787	3.2 to 10.4
Mean			9.5	17.4	377	3.0	9.3	150	297	5.3
[R/M]			4.1	1.0	8.2	0.8	2.1	10.5	12.7	1.4

TABLE III

Trace element concentrations in Caribbean water (µg/L)

Western Basin (41 samples)	Cr	Co	Ni	Cu	Zn	Cd
Range	0.3 to 1.5	0.1 to 1.6	0.2 to 1.4	0.2 to 4.6	1.3 to 12.5	0.05 to 0.78
Mean	0.7	0.6	1.0	1.3	5.5	0.19
[R/M]	1.8	2.7	1.2	3.3	2.0	4.0
Eastern Basin (47 samples)	**Cr**	**Co**	**Ni**	**Cu**	**Zn**	**Cd**
Range	0.2 to 1.04	0.2 to 2.3	0.3 to 3.8	0.2 to 0.8	0.8 to 10.5	0.09 to 0.69
Mean	0.4	0.9	1.2	0.4	4.8	0.25
[R/M]	2.1	2.3	2.8	1.5	2.2	2.4

TABLE IV

Radionuclide and trace element concentration factors in Caribbean plankton

	Cr	Co	Ni	Cu	Zn	Cd	Ra^{226}	Pb^{210}	Po^{210}
Mean plankton (unit/g)	9.5	3.0	9.3	150	297	5.3	0.27	4.3	70
Mean surface waters (unit/L)	0.6	0.8	1.1	0.9	5.2	0.2	0.06	0.11	0.70
Concentration factors ($x10^3$)	15.8	3.8	8.5	167	57.1	26.5	4.5	39.1	1 000

TABLE V

Trace element concentrations in Caribbean plankton relative to net sizes

Stations	Net size	Cr	Mn	Fe	Co	Ni	Cu	Zn	Cd
67	6	-	4.2	39	-	7.8	124	905	7.2
	20	-	69	3 690	-	15.8	92	153	4.1
44	6	5	3.5	40	2.1	6.1	61	85	6.9
	20	10	27.5	240	6.0	13.3	39	-	6.6
47	6	-	12	18	2.1	6.1	89	-	6.9
	20	10	86	147	4.0	21.3	36	202	4.8
48	6	40	10.5	135	2.0	6.1	25	-	9.3
	20	5	36	105	4.0	9.2	47	-	6.6
Average ratio	$\left[\frac{20}{6}\right]$	-	9-0	-	2.3	2.3	0.9	-	0.7

TABLE VI

Percent composition of Caribbean plankton

Stations	Calanoids	Cyclopoids	Euphisiids	Eggs	Diatoms	Snail larvae	Chaetognaths	Hyperia	Cumace
39									
41	65	25	T	-	-	T	T	-	-
44									
47	75	10	T	-	-	T	-	-	-
48	60	-	-	T	20	-	15	-	-
49	15	15	15	-	-	20	T	-	-
51									
52									
54	60	10	T	-	-	T	1	-	-
57	60	-	-	-	-	T	T	-	-
59	70	T	T	-	-	T	T	-	-
65	75	T	-	T	-	-	-	15	15
66									
67									
68	60	T	10	-	-	-	-	-	T
70	80	T	2	T	T	-	-	-	T
75	90	-	-	T	T	T	-	-	
77	50	25	-	T	T	T	-	-	T
79	80	10	-	T	T	-	-	-	T

All samples were collected with a mesh #6 net except stations #75 and #79 which were collected with a mesh #20 net

T = Trace amounts

TABLE VII

Mean trace element concentrations in Caribbean benthos and plankton (µg/g-dry)

	Cr	Mn	Fe	Co	Ni	Cu	Cd
Benthos (31 species)	1.7	24.2	720	27	1 510	15.9	8.7
Plankton (mixed)	9.5	17.4	377	3	9.3	150	5.3
Ratio [benthos/plankton]	0.2	1.4	1.9	9.0	160	0.1	1.6

TABLE VIII

Trace element depth distributions in Caribbean waters (µg/l)

Stations	Mean surface/mean deep	Co	Ni	Zn	Cd
44		$\frac{0.4}{1.0}$	-	$\frac{6.0}{8.0}$	-
48		$\frac{0.5}{0.8}$	$\frac{0.5}{1.2}$	-	$\frac{0.1}{0.4}$
52		$\frac{0.5}{0.8}$	$\frac{1.0}{1.2}$	$\frac{3.0}{5.5}$	$\frac{0.15}{0.25}$
66		$\frac{0.6}{0.8}$	$\frac{1.0}{2.5}$	$\frac{6.0}{8.0}$	$\frac{0.25}{0.35}$
68		-	$\frac{6.0}{7.5}$	$\frac{4.0}{5.5}$	-
Mean ratio	$\frac{\text{surface}}{\text{deep}}$	0.6	0.7	0.7	0.5

TABLE IX

Radionuclide and trace element variability in Caribbean plankton and sea water

	Cr	Co	Ni	Cu	Zn	Cd	Ra^{226}	Pb^{210}	Po^{210}
Plankton	4.1	0.8	2.1	10.5	12.7	1.7	4.0	2.1	1.2
Sea water	2.4	2.9	3.3	5.2	2.2	3.5	-	-	-

Variability = range/mean

5. REFERENCES

Bacon, M.P., Applications of disequilibria in the study of marine geochemical processes.
1975 Ph.D. Thesis MIT-WHOI program

Benninger, L.K.
1975

Broecker, W.S. and M.L. Bender, Age determination on marine strandlines. In Calibration
1972 of hominoid evolution, edited by W.W. Bishop and J.A. Moller. Edinburgh, Scottish Academic Press

Craig, H., K. Krishnaswami and B.L.K. Somayajulu, Radioactive disequilibria in the deep sea.
1973 Earth Planet.Sci.Lett., (17):295

Folsom, T.R. and T.M. Beasley, Contributions from Alpha emitter, Po^{210}, to the natural
1973 radiation environment of the marine organisms. In Radioactive contamination in the marine environment. IAEA Proc.Ser., (STI/PUB/313):625-32

Thomson, J., K.K. Turekian and R.J. McCaffrey, The accumulation of metals in and release
1975 from sediments of Long Island Sound. In Estuarine research, edited by L.E. Cronin. New York, Academic Press

Trier, R.M., W.S. Broecker and H.W. Feeley, Radium-228 geosecs profiles. Earth Planet.Sci.
1972 Lett., 1972

ORGANIC MATTER IN THE CARIACO TRENCH

by

L.M. JEFFREY
Department of Oceanography
Texas A&M University

R.M. GERSHEY
Institute of Marine Sciences
University of Alaska, Seward

CONTENTS

1. INTRODUCTION
2. PROCEDURES
3. RESULTS AND DISCUSSION
4. SUMMARY
5. REFERENCES

Abstract

Comparison of detailed profiles of dissolved and particulate organic carbon in the water column of the anoxic Cariaco Trench and an oxygenated station in the Caribbean Sea of similar depth indicated that there was no enrichment of dissolved or suspended organic matter in the anoxic water. Comparison of the compositions of the organic concentrates obtained by adsorption on charcoal from the anoxic and oxygenated stations revealed that the organic matter from 1 000 metres in the anoxic station was richer in organic carbon, nitrogen and sulphur but poorer in oxygen than that from the same depth at the oxygenated station. Sulfhydryl groups were detected in the organic matter from the anoxic zone only. It appears that the oxidation processes in the Cariaco Trench modify the dissolved organic matter in the water column, but do not lead to enhanced preservation. Apparently most of the oxidation of the organic matter occurs in the upper oxygenated zone of the basin.

Stable carbon isotope composition of the dissolved, the particulate, and the sedimentary organic matter of both the anoxic and oxygenated stations indicated typical marine organic σ^{13}C values. However, the anoxic sediments and interstitial water were much more enriched in organic matter, apparently because of the high sedimentation rate in this area.

Resumen

La comparación de los perfiles detallados de carbón orgánico, disueltos o en partículas, de la columna de agua del foso submarino anóxico Cariaco y de una estación oxigenada del Caribe de profundidad análoga, muestra que el agua anóxica no está enriquecida con materias orgánicas disueltas o en suspensión. La comparación de los componentes de los concentrados orgánicos obtenidos por adsorción en estaciones anóxicas y oxigenadas revela que la materia orgánica de la estación anóxica a 1 000 m de profundidad era más rica en carbón orgánico, en nitrógeno y en azufre, pero más pobre en oxígeno que la de la estación oxigenada a la misma profundidad. Grupos de sulfidrilos sólo se detectaron en la materia orgánica de la zona anóxica. Los procesos de oxidación que ocurren en el foso submarino Cariaco modifican, al parecer, la materia orgánica disuelta en la columna de agua, pero sin activar la conservación. Casi toda la oxidación de la materia orgánica se produce en la zona superior oxigenada de la cuenca.

La composición en isótopos estables del carbono de la materia orgánica sedimentaria, en partículas o disuelta, tanto de la estación anóxica como de la oxigenada, daba valores típicos marinos (σ^{13} C) de materia orgánica, mientras que los sedimentos anóxicos y las aguas intersticiales eran mucho más ricas en materia orgánica, al parecer, a causa del alto grado de sedimentación en esta zona.

1. INTRODUCTION

The general opinion one forms from a survey of the literature concerning anoxic basins is that reducing conditions (associated with low redox potentials) favour the preservation of organic matter. Indeed, several workers have found anoxic sediments which are enriched in organic carbon (Gucluer and Gross, 1964; Orr and Grady, 1967; Richards and Vaccaro, 1956; Smith, 1954; Zsolnay, 1971). However, there is little evidence to support the notion that the quantity of organic matter in the water column of anoxic basins is greater than the amount found in comparable oxygenated ocean water. Analyses for dissolved organic carbon concentrations on samples from the Black Sea indicated that there was an increase in concentration of organic carbon with depth (Deuser, 1971). Solvent extraction of the anoxic waters of Lake Nitinat, Vancouver Island and subsequent analysis of the extracts by thin layer chromatography indicated the presence of mercaptans and a generally less polar nature for the dissolved organic matter (Adams, 1968). These data are not conclusive, however, and additional data comparing the amounts and characteristics of organic matter of anoxic water to that of otherwise similar oxygenated water are lacking.

Work done by Orr and Gaines (1975) on an anoxic basin in the Pettaquamscutt River (Rhode Island) revealed that the rate of oxidation of organic matter by sulphate reduction in sediments can be quite high in reducing environments where sulphate is abundant. Their results suggest that perhaps too much emphasis has been placed on the importance of reducing environments in determining the amount of organic matter present in such systems. Thus, reducing environments may have more effect on the nature of the surviving organic matter than on the amount present.

The primary objective of this research was to compare the concentrations of both dissolved and particulate organic carbon in the water column of the anoxic Cariaco Trench with the concentrations in the oxygenated waters of the nearby Caribbean Sea. This comparison was made in order to determine if organic carbon had accumulated to a greater degree in the anoxic trench.

Another objective was to determine if any differences existed, in a qualitative sense, between the dissolved organic matter of the anoxic water of the trench and that of the waters of the Caribbean. In order to determine the chemical characteristics of the dissolved organic matter, gram-size samples were needed. These quantities of material were isolated by adsorption on charcoal columns, utilizing the deep sea pumping system described by Jeffrey *et al.* (1973). Sea water was pumped continuously from various depths, filtered, acidified, and passed through activated charcoal columns.

The final objective was to compare the organic carbon content and the stable carbon isotope composition of the sediments with the suspended organic matter from the oxic and anoxic waters to further clarify the nature of organic carbon cycling in anoxic marine environments.

2. PROCEDURES

2.1 Sample collection sites

The Cariaco Trench (Fig. 1) is a shallow basin off the Venezuelan Coast in which anoxic conditions exist below the sill depth of about 150 m. The depression is divided into eastern and western basins by a ridge whose depth is between 800 and 850 m, the maximum depth of the depression is 1 400 m. Samples were obtained from this area and the immediate surrounding area of the Caribbean Sea during an October cruise 72-A-16 (Leg II) of the R/V ALAMINOS at the stations indicated on Fig. 1. Gram-size samples of organic matter were collected at station 4 within the trench where anoxic conditions prevail and at station 6 on the north side of the sill where oxic conditions prevail. Both samples were collected from a depth of 1 000 m.

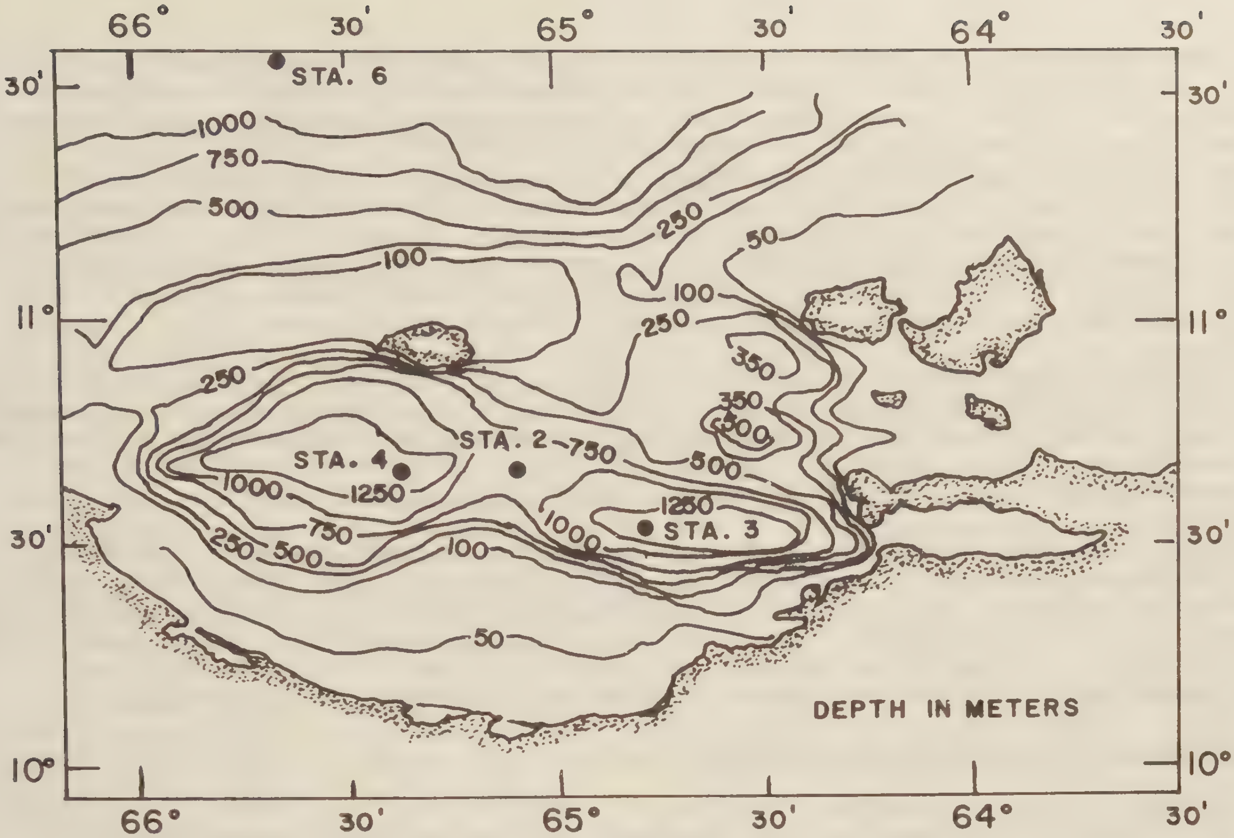

Fig. 1 Map of Cariaco Trench

2.2 Hydrographic properties

The salinities of the water samples obtained from Nansen bottle casts were determined using a Bisset Berman inductive salinometer. Temperature readings were obtained from reversing thermometers attached to the Nansen bottles.

The standard method of Strickland and Parsons (1968) was used for the determination of dissolved oxygen. It is a modification of the classic Winkler titration in which the dissolved oxygen reacts with divalent manganese to form hydroxides which in turn liberate an amount of iodine equivalent to that of the original oxygen when acidified in the presence of iodide. The iodine was titrated with standardized thiosulphate solution.

Hydrogen sulphide was measured in the water samples taken within the trench using the method of Cline (1969) with minor modifications in sample handling technique.

2.3 Dissolved and particulate organic carbon concentrations

Organic carbon was determined according to the wet combustion method of Menzel and Vaccaro (1964) as modified by Fredericks and Sackett (1970). Profiles of DOC and POC were determined at stations 4 and 6. Samples were analysed in 10 ml ampoules that had been combusted at 500°C for 12 hours to remove any organic contamination. Glass fibre filters with a pore size of 0.3 micron were used for POC after combustion in the same manner as the ampoules.

Water samples were collected in 5-l Nisken bottles spaced 50 to 100 m apart and extending to the bottom of the water column. Two 1-l aliquots were transferred to acid washed holding bottles. Using a vacuum pump, water was drawn from the holding bottles through an in-line filter and then into a 125-ml Erlenmeyer flask, the excess water flowing into a 3-l suction flask which served as a trap to protect the vacuum pump. Three samples of 10 ml each of the filtered water from the 125-ml Erlenmeyer flask were introduced into the ampoules with a 10-ml glass syringe for triplicate determination of DOC. To the ampoules were than added 0.2 g of potassium persulphate and 0.25 ml of 6 percent phosphoric acid. For the determination of POC, the filters were folded and placed in ampoules with forceps, and 5 ml of distilled water were added, followed by the persulphate and phosphoric acid.

All ampoules were purged with purified oxygen for approximately 6 min before being sealed on an apparatus designed by Fredericks (1964). The sealed ampoules were than heated in an oven at 100°C for at least 24 hours in order for the organic carbon to be oxidized by the persulphate. The foregoing sampling and sealing procedures were carried out at sea and the sealed ampoules were returned to the land-based laboratory for analysis.

The tops of the ampoules were crushed on a specially designed apparatus (Fredericks, 1964) and the carbon dioxide flushed out with purified nitrogen. The carbon dioxide was quantified on a Beckman non-dispersive infra-red analyser connected to a strip chart recorder equipped with a disk integrator. The amount of CO_2 was calculated from the peak area on the recorder chart. Calibration was achieved by measuring the amount of CO_2 produced from a known amount of sodium carbonate solution injected into 25 percent phosphoric acid.

2.3 Adsorption of organic matter on charcoal

In order to isolate gram-size quantities of organic matter from stations 4 and 6 (see Fig. 1), 13 000 l of filtered, acidified sea water were pumped over charcoal columns. This was accomplished through the use of the continuous flow, deep water pumping system of Jeffrey *et al.* (1973).

Three large pyrex columns (5 ft x 3 in internal dimension) were each filled with approximately 2 kg of activated charcoal (700°C for 6 hours under an atmosphere of nitrogen) and sea water was simultaneously pumped through them from three depths (30, 300, and 1 000 m) through polyethylene tubing and 0.3 micron fibre glass filters with a diameter of 29.3 cm. The pH of the water was adjusted between 2.0 and 3.0 by injecting 50 percent (v/v) hydrochloric acid/seawater through stainless steel needle valves located in the water line immediately before the columns. The acid was contained in a 5-gal stainless steel tank which was pressurized to 50-60 psi by means of compressed air.

The pH of the water exiting from the columns was monitored every 15 to 30 min and adjustments of the needle valves made as required to compensate for the changes in pH caused by variations in flow rate through the filters.

2.4 Desorption of the adsorbed organic matter

Of the six charcoal columns processed on the cruise, only the two containing the organic matter collected at 1 000 m at stations 4 and 6 were used in this study. Both sample columns were eluted first with approximately 10 column volumes (20 l) of distilled water to remove the bulk of salt and acid from the charcoal. The columns were then eluted with 6 to 7 column volumes of each of the following solvents: methanol, acetone, chloroform:methanol (2:1) and 1.0 M ammonium carbonate solution. The organic solvents used were 'distilled in glass' grade obtained from Burdick and Jackson (Muskegon, Michegan).

The column washes were concentrated by evaporating the solvents on a rotary evaporator at reduced pressure (4 cm Hg) and at temperatures ranging from 40° to 50°C. The solvents were condensed in the evaporator and reused for subsequent column washes. The ammonium carbonate fractions were dried at 60°C in a circulating-air oven or freeze dried. The final volume for all of the fractions thus eluted from the column was approximately 250 ml.

3. RESULTS AND DISCUSSION

3.1 Salinity and temperature distribution

The temperature and salinity profiles for stations 4 and 6 are given in Figs. 2 and 3 respectively.

Within the trench (western basin), the temperature decreased from surface values, in the range of 28°C, to about 18°C at 150 m. From 400 m to the bottom at 1 300 m, the temperature was very constant, ranging between 16.93° and 17.08°C. The profile for station 6 outside of the trench is similar to that of station 4 above the sill depth but the temperature continued to decrease at greater depths, falling to 4.12°C at 1 500 m. The lowest temperature found in the trench was 16.93°C at 800 m. This is somewhat higher than the minimum temperature (16.88°C) found by Richards et al. (1956) and many indicate a warming trend.

The isolation of the water mass in the trench is further demonstrated by the distribution of salinity. The surface salinity was found to be 36.07 per mille and increased to a maximum of 36.77 per mille at 100 m. From this depth the salinity decreased to 36.23 per mille at 800 m and remained near this value to the bottom. In the Caribbean north of the sill, the salinity distribution was similar to that of the trench to a depth of 150 m but steadily decreased to 35.00 per mille at depth.

The distribution of salinity reported here is essentially the same as that reported by Richards et al. (1956). The temperature and salinity distributions at stations 2 and 3 (located on the ridge and eastern basin respectively) were found to be very nearly the same as those for station 4.

3.2 Dissolved oxygen and sulphide

The oxygen content of the trench water was near saturation (4.5 ml/l) near the surface and decreased regularly with depth until it could no longer be detected by the Winkler titration at depths from 375 m to 400 m (Fig. 4).

Sulphide was first detected at 250 m in a concentration of 0.6 µg-atoms/l sulphide sulphur. The concentration of sulphide increased rapidly with depth to a maximum of 18.8 µg-atoms/l at 1 200 m (Fig. 5). At station 3, in the eastern basin of the trench, a slightly higher level of sulphide was found to occur at 1 300 m (25 µg-atoms/l).

These data are somewhat different from those reported by Richards et al. (1956). A profile of sulphide sulphur taken by Richards in the same general area of the trench shows an increase of sulphide to a maximum value of 30 µg-atoms/l at 800 m, below which a constant concentration was found to the bottom. Sulphide was first detected at a depth of 475 m.

3.3 Organic carbon of the water column

The distributions of both dissolved and particulate organic carbon (DOC and POC respectively) were determined for both stations 4 and 6.

Fig. 5 shows the profiles of dissolved organic carbon concentrations for the two stations. At both stations high surface values (1.0 mgC/l) were found to decrease rapidly with depth until concentrations in the range of 0.6 mgC/l were reached near 200 m. Below this depth, the amount of DOC remained relatively constant to the bottom in both areas.

Therefore, the Cariaco Trench showed no accumulation of organic matter in the water column in contrast to the results of Deuser (1971) who reported an increase in dissolved organic carbon with depth of from 1 to 6 mgC/l in the anoxic zone of the Black Sea. Apparently the residence time of about 100 years (Richards et al, 1956; Deuser, 1973) for the water of the Cariaco Trench is too short for the accumulation of dissolved organic matter. The residence time for the water of the Black Sea is estimated to be at least one order of magnitude greater than that of the Cariaco Trench (Deuser, 1971; Deuser, 1973).

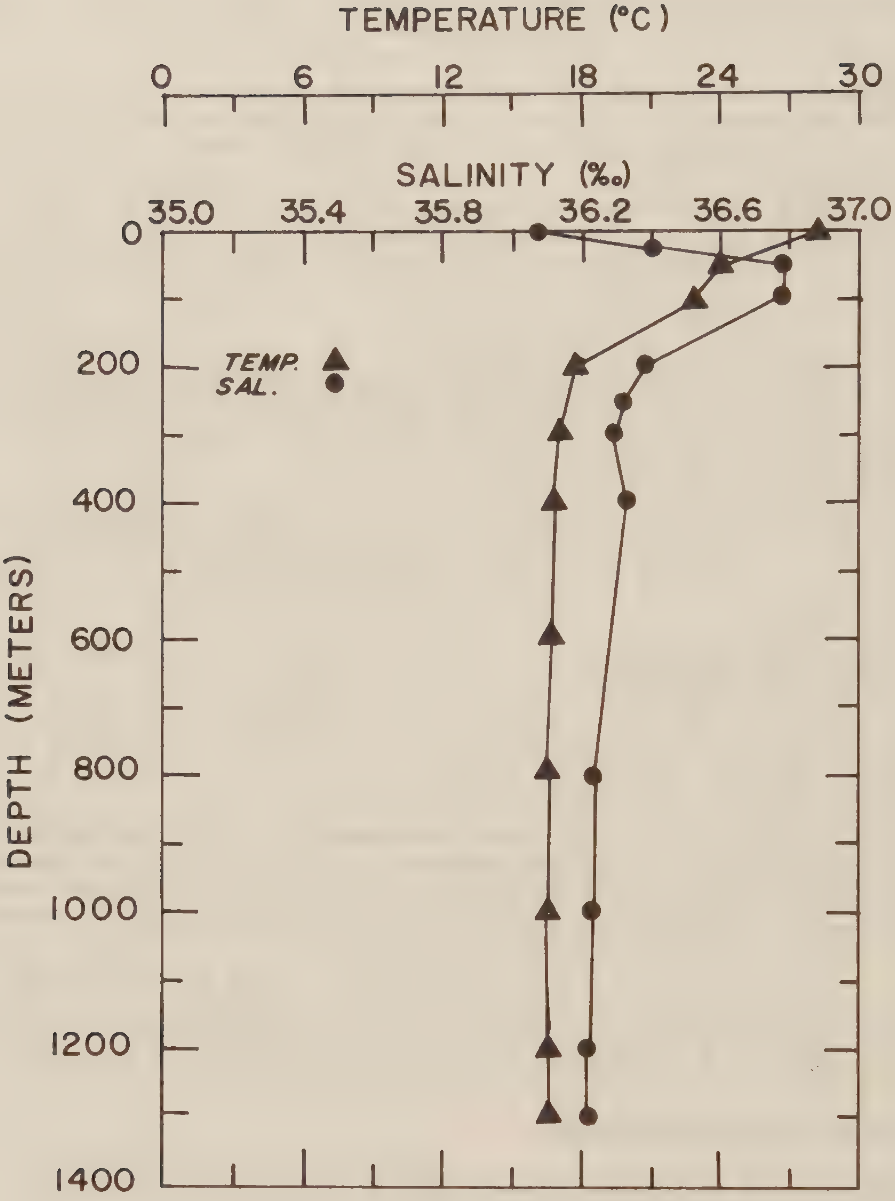

Fig. 2 Temperature and salinity profiles for station 4 (10°38'N; 65°24'W), October 1972

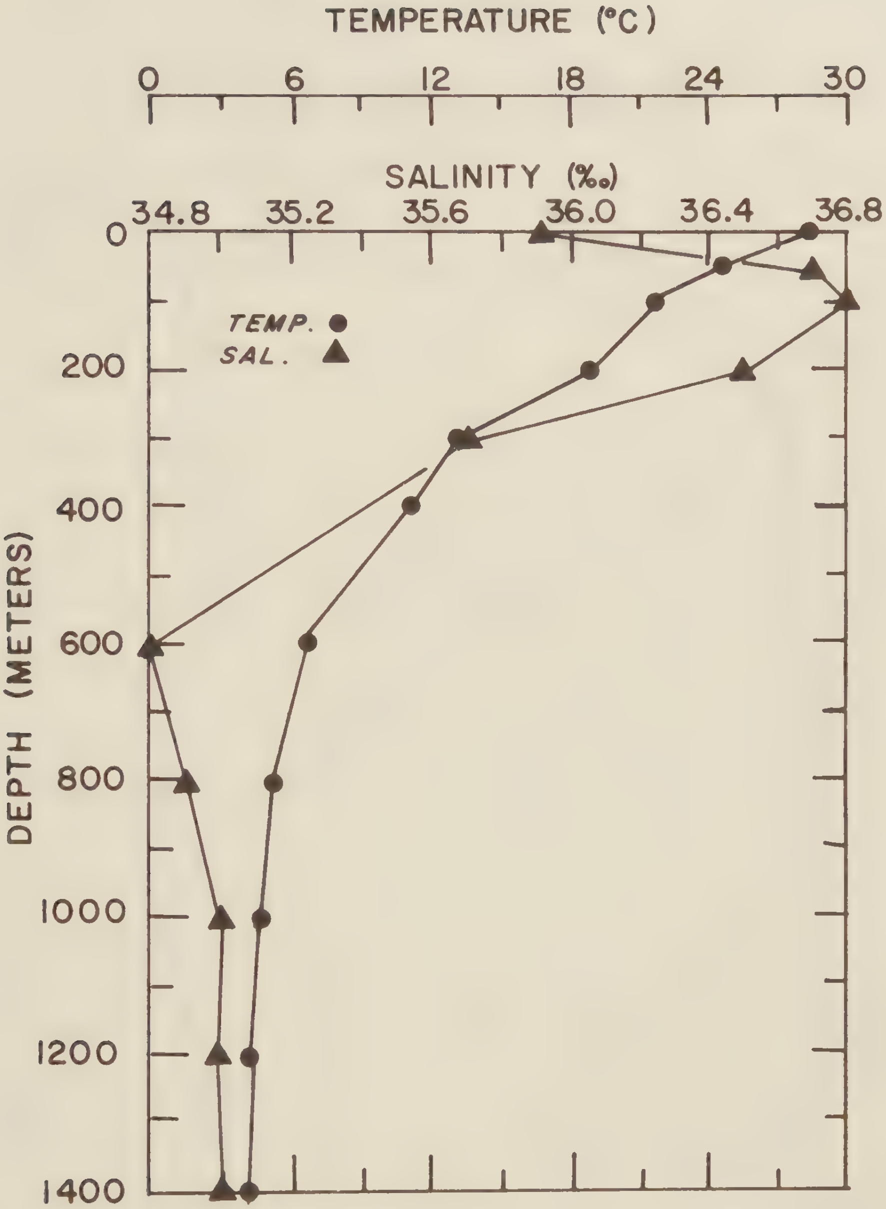

Fig. 3 Temperature and salinity profiles for station 6 (11°37'N; 65°38'W), October 1972

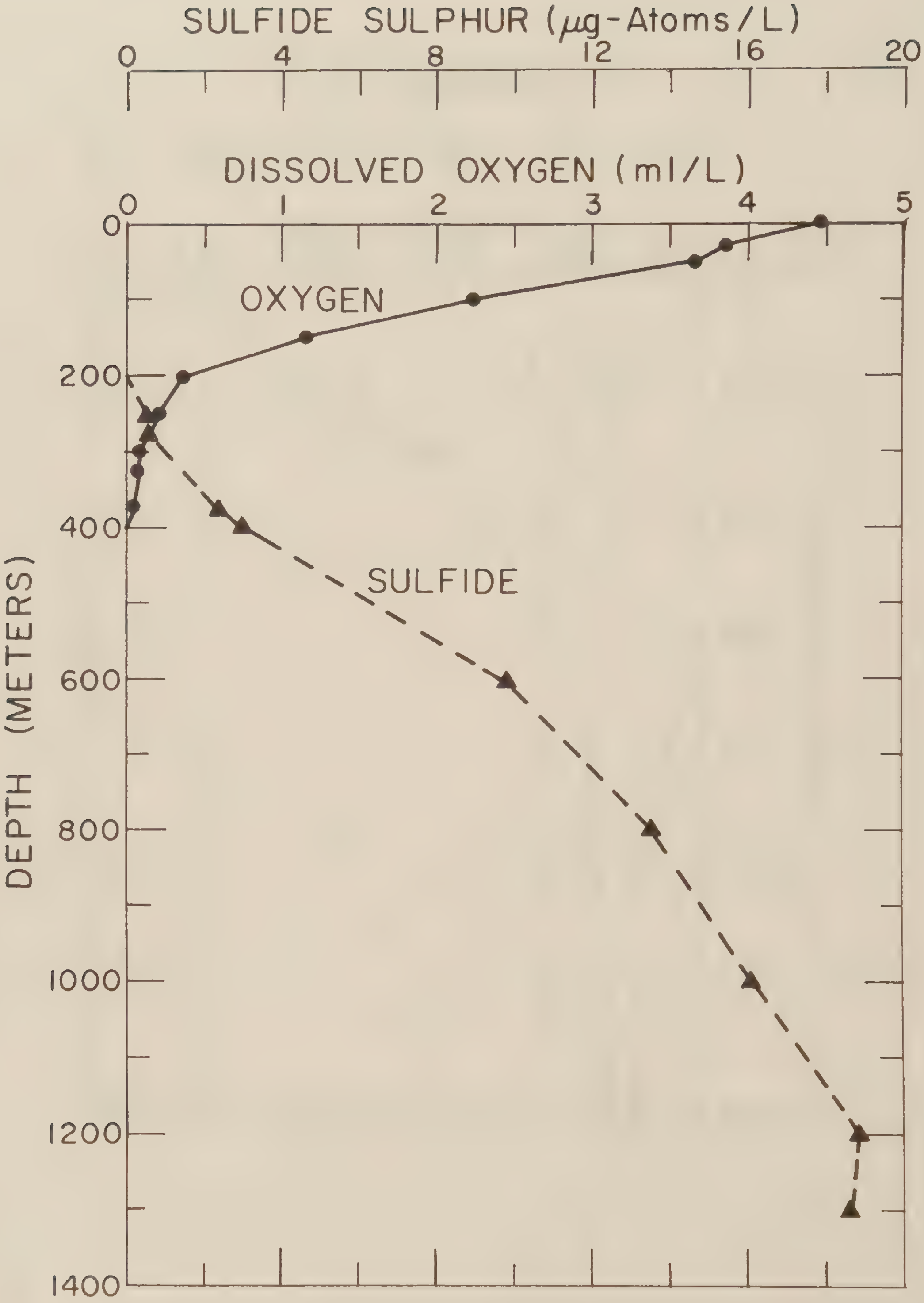

Fig. 4 Distributions of sulphide sulphur and dissolved oxygen as a function of depth for station 4 (10°38'N; 65°24'W), October 1972

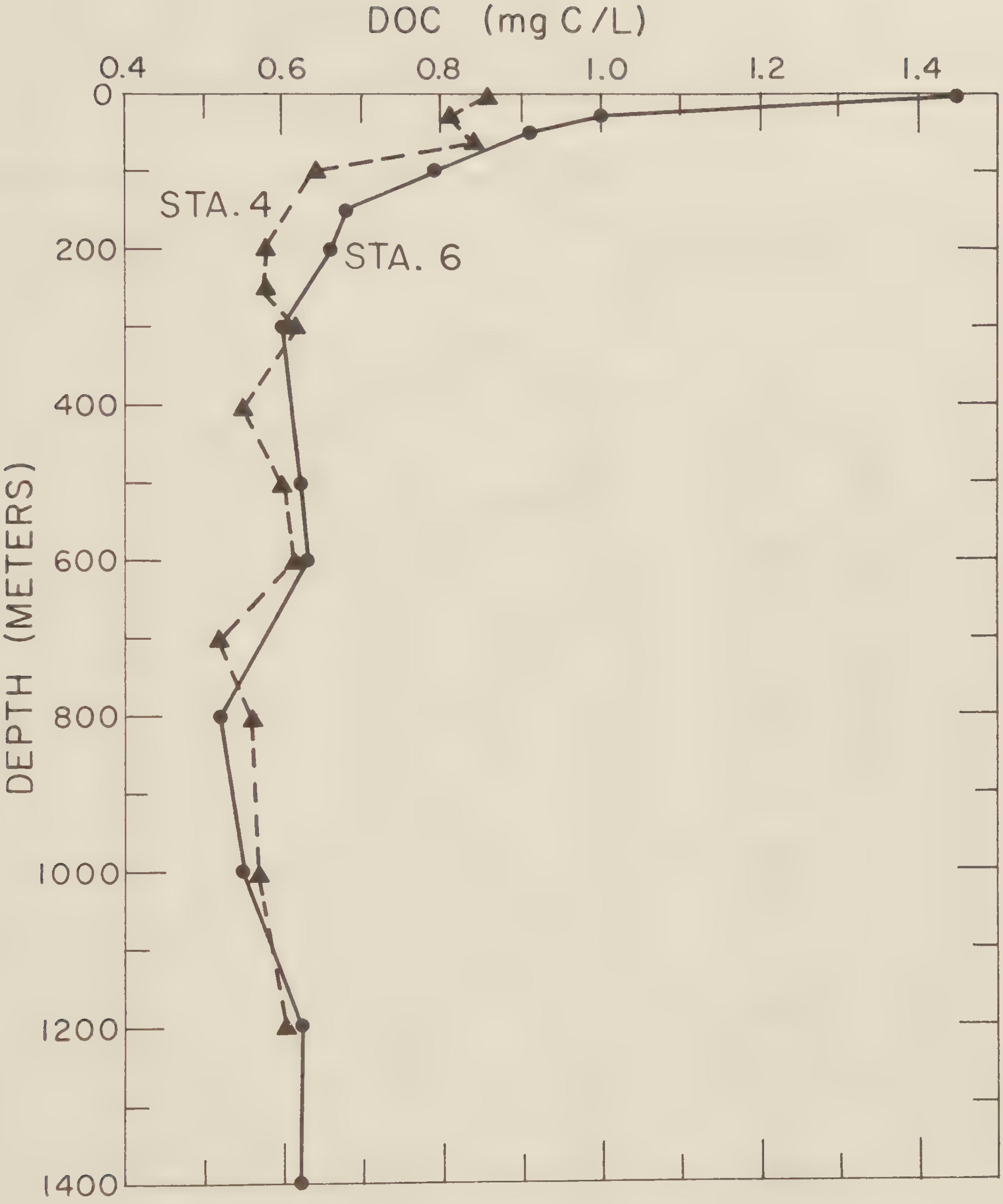

Fig. 5 Distribution of dissolved organic carbon (DOC) as a function of depth for station 4 (10°38'N; 65°24'W) and station 6 (11°37'N; 65°38'W), October 1972

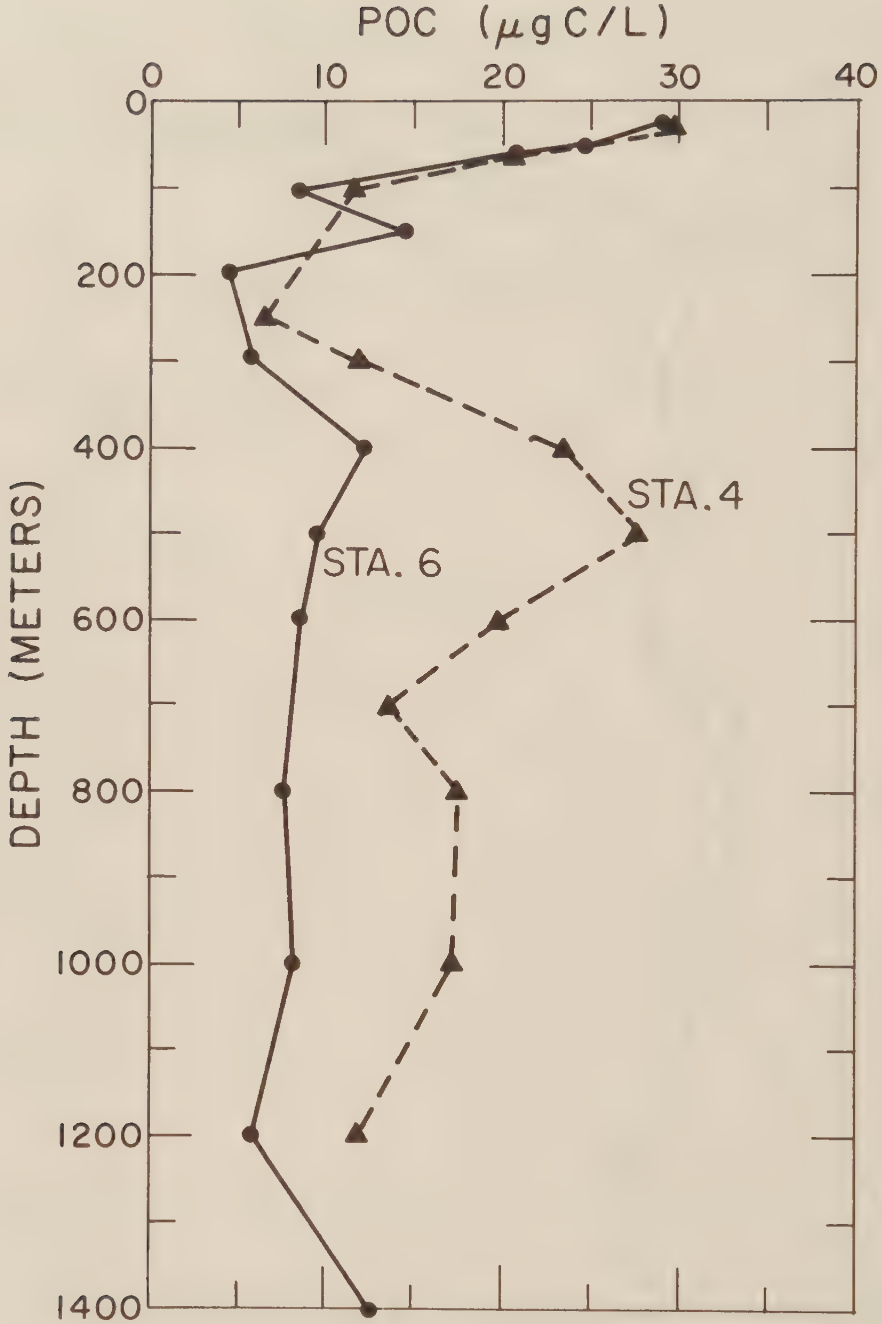

Fig. 6 Distribution of particulate organic carbon (POC) as a function of depth for station 4 (10°38'N; 65°24'W) and station 6 (11°37' N; 65°38'W) October 1972

There is a slight difference between the profiles of particulate organic carbon for stations 4 and 6 (Fig. 6). Concentrations of POC in the range of 30 µgC/l were found in surface waters while the amount of POC dropped off sharply to a minimum of approximately 5 µgC/l at 200 m at both stations. The profile for station 6 shows an increase of POC to about 10 µgC/l at 500 m, below which depth the value remains at this constant level to the bottom. The profile for station 4, on the other hand, indicates that a maximum of 30 µgC/l occurs at 500 m below which the concentration drops to approximately 20 µgC/l and remains so to the bottom. Thus the amount of POC at depth in station 4 is roughly twice that of station 6.

3.4 Organic carbon in the sediments and suspended matter

The organic carbon content of two cores, one from the Cariaco Trench and one from the surrounding Caribbean Sea, was determined and stable carbon isotope ratios were obtained for this organic matter. The data for the two cores are presented in Table I.

TABLE I

Organic carbon and $\sigma^{13}C$ of sediments

Station	Section (cm)	Carbon (%)	$\sigma^{13}C$ (‰)
4	0–10	3.77	-20.2
4	10–20	4.16	-19.8
4	20–30	4.15	-20.0
4	30–40	3.90	-20.2
4	40–50	3.92	-20.4
4	50–60	3.44	-20.3
4	60–70	4.36	-19.9
4	70–80	4.21	-20.3
4	80–90	3.74	-20.7
4	90–100	3.94	-20.4
4	100–110	4.20	-20.4
4	110–120	3.68	-20.6
4	120–130	2.94	-20.1
4	140–150	3.99	-20.4
6	0–10	1.52	-19.1
6	10–20	1.41	-19.1
6	20–30	1.28	-20.0
6	30–40	1.01	-19.8
6	40–50	1.08	-19.7
6	50–60	1.23	-19.9
6	60–70	1.30	-19.7
6	70–80	1.42	-19.9
6	80–90	1.53	-19.9
6	90–100	1.61	-19.8
6	100–110	1.18	-

It is evident that, in the interval studied (0-150 cm), the percentage of organic carbon shows no increasing or decreasing trend in either case. However, the percentage for the anoxic station is significantly higher than that of the oxic station with values of 3.77 percent compared to 1.52 percent (first 10 cm). In comparison, most pelagic sediments contain 0.3 to 1.0 percent organic carbon (Parker, 1967; Hobson and Menzel, 1969; Niino, 1969). However, several authors have reported higher percentages of organic carbon in sediments collected from various anoxic basins. Richards and Vaccaro (1956) have reported 4 percent organic carbon in the Cariaco Trench, and Gucluer and Gross (1964) have found up to 7 percent organic carbon in sediment from the anoxic part of the Saanich Inlet. In the oxygenated parts of the inlet, on the other hand, the sediments contained only 1-2 percent organic carbon. Deuser (1971) reported an average value of 4 percent for organic carbon in the sediments of the anoxic Black Sea.

The values reported here are in agreement with those of Richards and Vaccaro (1956), but are lower than those found in the Saanich Inlet and many other near-shore basins. The fact that these environments receive large amounts of organic material from terrestrial sources and have high sedimentation rates may explain the high organic content of the sediments there and detracts from the usefulness of comparisons with the Cariaco Trench.

Thus the increased amount of organic material in the sediments of the Cariaco Trench as compared to the oxygenated Caribbean Sea may be an indication that the reducing conditions existent in the anoxic zone lead to a preservation of organic matter. This conclusion, however, must not be accepted without reservation.

The sediments of the Cariaco Trench were laid down at the remarkable rate of 50 $cm/10^3/y$ (Heezen *et al.*, 1958). This deposition rate is more than an order of magnitude greater than those found in most ocean areas. If one assumes that the sediments obtain their organic composition from sinking particulate matter and that the particulate matter of the trench is of approximately the same composition as that of other waters, it becomes quite clear that the oxidation rate of organic matter at the sediment/water interface in the trench must be very high in order to maintain the organic matter at 4 percent of the sediment composition. Even if only a small fraction of the suspended organic matter settles out to form sediments, the oxidation rate of organic matter in the trench must be greater than or at least comparable to oxidation rates in oxic zones.

Further evidence that organic oxidation rates in the trench are of a considerable magnitude is given by the isotopic data of the particulate organic carbon and sedimentary organic carbon. A $\sigma^{13}C$ value of -23.3 per mille was found for the particulate organic carbon of the Cariaco Trench, while the $\sigma^{13}C$ value for the organic carbon of the sediments was found to be -20.2 per mille for the first 10 cm (-20.3 per mille averaged over 150 cm). This discrepancy in $\sigma^{13}C$ between particulate carbon and sedimentary organic carbon was also found in the nearby Caribbean at station 6 (POC $\sigma^{13}C$ = -23.2 per mille; sedimentary carbon $\sigma^{13}C$ = -19.1 per mille) and shows up in many other areas (Eadie and Jeffrey, 1975).

The enrichment of $\sigma^{13}C$ in the sediments is thought to be the result of biological activity at the sediment/water interface. Therefore, the $\sigma^{13}C$ values of the trench organic matter suggest that oxidation of organic matter is indeed occurring in the anoxic environment to the extent that the isotope fractionation observed is no less than in 'ordinary' sediments.

3.5 Adsorption of dissolved organic matter on charcoal

A total of 13 442 l of seawater from 1 000 m was passed over a charcoal column at station 4. Using the difference in DOC values for the column influent and effluent, a total of 6.0 g of organic carbon was adsorbed by the charcoal. This corresponds to an adsorption efficiency of 74 percent. At the end of the pumping period, the column was capped and stored at 10°C for subsequent analysis.

At station 6, 13 876 l of sea water from 1 000 m were pumped over a charcoal column. The amount of organic material adsorbed and the efficiency of this operation were calculated in a similar manner as at station 4. Thus a total of 6.8 g of organic carbon were isolated with a corresponding efficiency of 82 percent.

Several explanations for the incomplete adsorption of organic matter by charcoal can be postulated. Among these would be: (1) loosely bound compounds could have been slowly eluted from the column during the pumping operation; (2) flow channelling may have occurred; (3) some compounds may have no affinity for charcoal, and, (4) the pH was not at all times optimum for adsorption.

The adsorption efficiencies reported here are both within the range (70–95 percent) found by Jeffrey (1969) for deep sea water samples taken from the Gulf of Mexico.

3.6 Recovery of adsorbed organic material

Each of the columns was eluted with a series of organic solvents after approximately two months of cold storage. After each of the solvent extracts had been concentrated to a volume of less than 300 ml, 1-ml aliquots were taken and dried under a stream of nitrogen. The organic matter was then analysed for carbon and the amount of organic carbon in each fraction calculated. A summary of these data is presented in Table II.

TABLE II

Recovery of organic matter from charcoal

Station	Fraction	Wt of organic matter (g)	C (%)	Wt of carbon (g)	% of total on column
4	MeOH-1	0.826	45.7	0.38	6.3
4	MeOH 3-14	1.476	45.7	0.67	11.2
4	Acetone	0.724	52.6	0.38	6.3
4	$CHCl_3$/MeOH	1.058	51.2	0.54	9.0
4	$(NH_4)_2CO_3$	9.860	12.0	1.18	19.7
4	Not eluted				47.5
6	MeOH-1	0.520	35.9	0.19	2.8
6	MeOH 3-14	3.260	24.5	0.80	11.7
6	Acetone	3.300	45.1	1.49	21.8
6	$CHCl_3$/MeOH	5.360	47.6	2.55	37.4
6	$(NH_4)_2CO_3$	14.980	11.2	1.67	24.5
6	Not eluted				1.8

Incomplete recovery of organic matter was obtained for anoxic station 4 which had a desorption efficiency of 53 percent. For station 6, desorption efficiency was 98 percent with an overall recovery efficiency of 39 percent. The range of percentage recovery found by Jeffrey (1969) was from 67 percent to 98 percent for samples taken in the Gulf of Mexico. Perhaps an important source of error is the measurement of the volume of sea water pumped through the columns. The flow meters used may have been correct only to ± 10 percent. Other causes for a low recovery rate might include: (1) the presence of irreversible adsorption sites on the charcoal; (2) the loss of volatile compounds during the processing of the column; (3) the loss of fine charcoal particles with adsorbed organic matter during the pumping operation, and, (4) the material in the column may require additional solvents of lower (or higher) polarity than the elutants used.

The second and fourth of the possibilities given above are dependent upon the nature of the adsorbed organic matter. Thus the low recovery rate for the organic matter from the anoxic Cariaco Trench may be an indication that the qualitative aspects of this material are different from those of organic matter from the Caribbean Sea and Gulf of Mexico.

Table II shows the percentages of total organic carbon recovered by each solvent. For the material collected in the Cariaco Trench, the major amount of carbon was eluted with methanol while the greater portion of the organic matter for station 6 was removed from the charcoal column by chloroform/methanol. This information seems to indicate that the organic matter of the anoxic environment is more polar in nature than that of the oxygenated environment, in contrast to the findings of Adams et al. (1968). Upon further investigation of the data it is seen that 47.5 percent of the organic matter from the trench was not eluted by the series of solvents used, while only 1.8 percent of the organic matter was left on the charcoal column in the case of station 6. The significant portion of the organic matter which was not eluted in the case of station 4 could be non-polar material strongly adsorbed on the charcoal which requires a 'stronger' solvent for its removal, such as hexane or benzene.

3.7 Elemental analysis of recovered organic material

The solvent eluted organic matter was analysed for carbon, hydrogen, nitrogen and sulphur. The results of these analyses are given in Table III.

TABLE III

Elemental analyses of recovered organic matter

Station	Fraction	%C	%N	C/N	%S	%H	Total
4	MeOH	45.7	4.34	12.3	0.52	6.11	56.6
4	Acetone	52.6	1.69	36.3	1.54	6.38	62.2
4	$CHCl_3$/MeOH	51.2	2.03	29.4	1.57	6.48	61.2
4	Average	48.3	3.27	17.2[a]	0.97	6.25	58.8
6	MeOH	26.2	2.2	13.8	0.41	5.12	33.8
6	Acetone	45.1	1.7	31.9	0.27	5.24	52.0
6	$CHCl_3$/MeOH	47.6	1.5	37.0	0.00	5.99	55.0
6	Average	40.4	1.8	26.2[a]	0.20	5.55	47.8

[a] Ratio of weighted averages of %C and %N corrected to read in atoms

The organic material of the anoxic water had a higher carbon, nitrogen, hydrogen and sulphur content than the organic matter from aerobic station 6. The weighted average of the sum of these elements for the three solvent fractions was found to be 58.8 percent in the case of station 4 and 47.8 percent for station 6. Consequently, the organic matter from the anoxic environment contains a smaller percentage of other elements (primarily oxygen, some phosphorus and halogens) than that of the oxygenated environment. This may be interpreted to mean that the organic matter of the anoxic zone is less highly oxidized than that of the Caribbean Sea. This material is also less oxidized than organic matter collected from deep water at the Yucatan Straits and Sigsbee deep areas of the Gulf of Mexico (Jeffrey, 1969).

The C/N ratios (calculated on an atomic basis) for the combined solvent washes of the charcoal columns for station 4 and station 6 were found to be 17.2 and 26.2 respectively (Table III. It should be noted that these ratios (as well as all of the elemental data) were calculated on an amount of material which represents only 39 percent and 81 percent of the dissolved organic carbon in the original sea water. These ratios may be compared with other samples and with each other, however, since the isolation methods employed in all cases were the same as far as it was possible to duplicate them.

The C/N ratios reported by Jeffrey (1969) were in the range of 17.6 at 1500 m in the Yucatan Straits area to 20.0 at 692 m in the Sigsbee deep area. These values are comparable to the ratios reported here but both sets of data are considerably different from the C/N ratios of cold North Atlantic Deep Water (2.5 to 6.0; Duursma, 1961). However, Duursma also found high C/N ratios (in the range of 20 and above) in the warm waters of the Gulf Stream in the North Atlantic and concluded that the decomposition of organic matter in warm waters proceeds differently from that in cold water in that organic nitrogen compounds are more completely decomposed.

With respect to the Cariaco Trench, the C/N ratio of 17.2 may indicate that the conditions there are more favourable for the preservation of the nitrogen-containing compounds in the water column as compared to the oxygenated environment of the open Caribbean. The difference between the C/N ratios is not great, but the hypothesis is further supported by the higher percentage of nitrogen in the organic material isolated from the anoxic environment.

The average percentage of sulphur (both inorganic and organic) in the organic matter isolated by charcoal adsorption was 1.0 percent for the anoxic station and 0.2 percent for station 6. The highest concentrations of sulphur in the organic matter from station 4 were found in the relatively non-polar acetone and chloroform/methanol fractions and were both in the range of 1.5 percent.

3.7 Sulfhydryl compounds

There was evidence that organically bound sulphur was present in all three solvent fractions for the Cariaco Trench material. Spot tests for thiols (-SH group) and tests for evolution of hydrogen sulphide upon pyrolysis were performed on the samples from both environments. The results of these analyses are given in Table IV. The organic material from the anoxic zone gave a positive test for the presence of the sulfhydryl group while that of the oxic zone gave a negative test. Hydrogen sulphide, detected by lead acetate paper, was split off upon pyrolysis of the three samples which gave a positive test for thiols; while those which gave a negative test for the sulfhydryl group did not split off hydrogen sulphide. Elemental sulphur 'blanks' were run in these tests and gave negative results in both cases. Positive responses to both tests were given by mercapto acetic acid and octadecylmercaptan.

The positive test for the sulfhydryl group which was observed for the organic matter from the Cariaco Trench could have resulted from any number of compounds produced by the process of anaerobic decomposition. Compounds of both polar (Reid, 1968) and non-polar (Duursma, 1965) character are formed under such conditions and are present in the trench; as evidenced by the positive test for the sulfhydryl group in the methanol, acetone and chloroform/methanol fractions.

TABLE IV

Result of spot tests for organic sulphur (Feigel and Anger, 1966)

Station	Fraction	Precipitation of Cuprous Salts	Evolution of H_2S upon pyrolysis
4	$CHCl_3$/MeOH	+	+
4	Acetone	+	+
4	MeOH	+	+
6	$CHCl_3$/MeOH	–	–
6	Acetone	–	–
6	MeOH	–	–

4. SUMMARY

The distributions of both dissolved and particulate organic carbon showed high surface values (from 0.86 to 1.45 mgC/l for DOC and from 29.1 to 29.4 µgC/l for POC) which decreased with depth to a combined value in the area of 0.62 mgC/l. These profiles of DOC and POC indicated that no accumulation of dissolved organic matter in the anoxic zone of the water column has occurred in contrast to the findings of Deuser (1971) who reported an increase in dissolved organic carbon with depth from 1 to 6 mgC/l in the anoxic zone of the Black Sea. The residence time of the water of the Black Sea was estimated to be about 1 000 years, while that of the trench in the order of 100 years (Deuser, 1971). The fact that increased values for DOC are not observed in the trench may also be an indication that the reducing nature of the system has little effect on the rate of oxidation of DOC and POC even if the oxidation process itself is of a quite different nature than that of oxic zones.

The organic carbon content of the first 10 cm of a gravity core taken in the western basin of the trench was 3.77 percent. This value is much higher than most pelagic sediments (from 0.3 percent to 1.0 percent) and higher than that figure for sediments in the nearby Caribbean (1.5 percent). At first glance, these data appear to suggest that organic matter in the sediments is not being oxidized as efficiently as in oxygenated environments. However, if one considers the fact that the sedimentation rate is very high in the trench and that the suspended matter contains 20 percent organic matter (Feely, personal communication), the oxidation rate in the sediment in this environment is likely to be proceeding at an appreciable rate. In addition, there is evidence that the Cariaco Trench may have a large input of organic carbon from the euphotic zone which has a primary productivity of 2.3 gC/m^2/day as compared to 0.26 gC/m^2/day in the nearby Caribbean (Curl, 1960). These data suggest that the higher percentage of organic matter in the sediment of the anoxic zone may be the result of an increased input rather than a decreased oxidation rate.

The $\sigma\,^{13}C$ value of –20.2 per mille for the sediments of the Cariaco Trench is essentially the same as found for the oxic station in the Caribbean (–19.9 per mille). At both stations the $\sigma\,^{13}C$ for the POC was in the area of –23.3 per mille. The difference in $\sigma\,^{13}C$ between suspended carbon and sedimentary carbon reflects the diagenetic activity at the sediment/water interface. It appears, then, that the same amount of activity that takes place in the sediments of the Caribbean is occurring in the Cariaco Trench.

Gram-size quantities of organic matter were isolated by adsorption on charcoal with an efficiency of 74 percent for the Cariaco Trench and 82 percent for the station in the open Caribbean. This material was eluted from the columns with a series of organic solvents with efficiencies of 53 percent and 98 percent for the anoxic and oxic stations respectively. Incomplete recovery of the adsorbed organic matter from the anoxic station may be an indication that the material remaining on the column requires a more non-polar solvent for its removal thus implying that the organic matter from the trench possesses a more non-polar character than that of the material from the oxygenated station.

Elemental analyses of the isolated organic matter revealed that the material from the anoxic water had higher percentages of carbon, hydrogen, nitrogen and sulphur and less oxygen than organic matter collected from the oxygenated zone. In addition, a lower C/N ratio and higher percentages of nitrogen and sulphur were observed for the organic matter from the reducing zone.

These data may be interpreted to mean that the soluble organic material from the trench is less highly oxidized and contains more nitrogen containing compounds. This evidence suggests that the oxidation of nitrogen compounds under anoxic conditions proceeds somewhat more slowly than in oxygenated systems. Further evidence that the products of oxidation under anoxic conditions may differ qualitatively from products produced in aerobic systems was given by tests which indicated the presence of the sulfhydryl group in the isolated organic matter of the trench.

In order to more fully understand the nature of the oxidation processes occurring in this environment it would be helpful to determine the budget for organic carbon. Future work in this area might include more studies of the primary productivity of the trench and the nearby Caribbean in addition to investigations of various other sources of carbon. A need for more work on the fractionation and characterization of the isolated organic matter of the water column and sediments is also indicated.

5. REFERENCES

Adams, D.D. and F.A. Richards, Dissolved organic matter in an anoxic fjord, with special
1968 reference to the presence of mercaptans. Deep-Sea Res., 15:471-81

Cline, J.D., Spectrophotometric determination of hydrogen sulfide in natural waters. Limnol.
1969 Oceanogr., 14:454-8

Curl, H. Jr., Primary production measurements in the north coastal waters of South America.
1960 Deep-Sea Res., 7:183-9

Deuser, W.G., Organic carbon budget of the Black Sea. Deep-Sea Res., 18:995-1004
1971

__________, Cariaco Trench: oxidation of organic matter and residence time of anoxic
1973 water. Nature, Lond., 242:601-3

Duursma, E.K., Dissolved organic carbon, nitrogen and phosphorus in the sea. Neth.J.Sea
1961 Res., 1:1-141

__________, The dissolved organic constituents of sea water. In Chemical oceanography,
1965 edited by J.P. Riley and G. Skirrow. New York, Academic Press, vol.1:433-77

Eadie, B.J. and L.M. Jeffrey, $\delta^{13}C$ analyses of oceanic particulate organic matter. Mar.
1973 Chem., 1:199-209

Feigl, F. and V. Anger, Spot tests in organic analysis. Amsterdam Elsevier, 616 p.
1966

Fredericks, A.D., A method for the determination of dissolved organic carbon in sea water
1964 by gas chromatography. M.S. Thesis, Texas A&M University, College Station, 96 p.

Fredericks, A.D. and W.M. Sackett, Organic carbon in the Gulf of Mexico. J.Geophys.Res.,
1970 75:2199-206

Gucluer, S.M. and M.G. Gross, Recent marine sediments in the Saanich Inlet, a stagnant
1964 marine basin. Limnol.Oceanogr., 9:359-69

Heezen, B.C., et al., Bull.Geol.Soc.Am., 69:1579-89
1958

Hobson, L.A. and D.W. Menzel, The distribution and chemical composition of particulate
1969 organic matter in the sea and sediments off the east coast of South America.
Limnol.Oceanogr., 14:159-63

Jeffrey, L.M., A method for isolation of dissolved organic matter from sea water and some
1969 chemical characteristics of the isolated material. Ph.D. Dissertation, Texas
A&M University, College Station, 152 p.

Jeffrey, L.M., A. Fredericks and E. Hillier, An inexpensive deep sea pumping system.
1973 Limnol.Oceanogr., 18:336-40

Menzel, D.W. and R. Vaccaro, The measurement of DOC and POC in sea water. Limnol.Oceanogr.,
1964 9:138-42

Niino, H., K.O. Emery and Chul Min Kim, Organic carbon in sediments of the Japan Sea. J.
1969 Sediment Pet., 39:1390-8

Orr, W.L. and A.G. Gaines, Observations on the rate of sulfate reduction and organic matter
1975 oxidation in the bottom waters of an estuarine basin: the upper basin of the
Pettaquamscutt River (Rhode Island). Adv.Organic Geochem., 1975

Orr, W.L. and J.R. Grady, Perylene in basin sediments off southern California. Geochim.
1967 Cosmochim.Acta, 31:1201-9

Parker, P.L., Fatty acids in recent sediments. Contrib.Mar.Sci., 12:245-9
1967

Parker, P.L. and J.A. Calder, Stable carbon isotope ratio variations in biological systems.
1970 Occas.Publ.Inst.Mar.Sci.Univ.Alaska, (1):107-27

Reid, E.M., Organic chemistry of bivalent sulfur. New York, Chemical Publishing, 539 p.
1968

Richards, F.A., Anoxic basins and fjords. In Chemical oceanography, edited by J.P. Riley
1965 and G. Skirrow. New York, Academic Press, vol.1:611-43

__________, The enhanced preservation of organic matter in anoxic marine environments.
1970 Occas.Publ.Inst.Mar.Sci.Univ.Alaska, (1):399-411

Richards, F.A. and R.F. Vaccaro, The Cariaco Trench, an anoxic basin in the Caribbean Sea.
1956 Deep-Sea Res., 3:214-28

Smith, P.J. Jr., Studies on the origin of petroleum: occurrence of hydrocarbons in recent
1954 sediments. Bull.Am.Assoc.Pet.Geol., 38:377-404

Strickland, J.D.H. and T.R. Parsons, A practical handbook of seawater analysis. Bull.Fish.
1968 Res.Board Can., (167):311 p.

Zsolnay, A., Diagenesis as a function of redox conditions in nature: comparative survey of
1971 certain organic and inorganic compounds in an oxic and anoxic Baltic basin.
Kiel.Meeresforsch., 27:135-65

CONDICIONES HIDROQUIMICAS DE LAS AGUAS SUPERIORES DE LA FOSA DE CARIACO Y AREAS ADYACENTES

por

T. OKUDA
Instituto Oceanográfico
Universidad de Oriente
Cumaná, Venezuela

CONTENIDO

1. INTRODUCCION
2. ORIGEN DE LOS DATOS UTILIZADOS
3. AREAS DE ESTUDIO
4. RESULTADOS
5. AGRUPACION DE LAS AGUAS DE ORIGEN COMUN
6. COMPARACION DE LAS CARACTERISTICAS QUIMICAS ENTRE TRES GRUPOS DE AGUA
7. REFERENCIAS

Resumen

Algunos aspectos hidrográficos y químicos de las aguas superiores de la Fosa de Cariaco y áreas circundantes fueron estudiados de acuerdo a datos recolectados durante nuestras expediciones, en los años entre 1965 y 1975. Las condiciones hidrográficas en las áreas costeras de Venezuela nororiental dependen principalmente de la surgencia estacional de las aguas subyacentes causada por los vientos alisios. Las variaciones estacionales de los parámetros hidroquímicos en la Fosa de Cariaco y áreas adyacentes muestran características similares entre sí (Okuda et al. 1968, 1969 y 1975). La correlación entre la temperatura y otros parámetros (oxígeno, AOU - utilización aparente de oxígeno, P-fosfato y N-nitrato) en las áreas estudiadas fue generalmente muy buena. Se observó que la magnitud de los coeficientes de dicha correlación parece coincidir con la intensidad de la surgencia en las áreas de estudio. Aunque las áreas de afuera y dentro de la Fosa de Cariaco no presentan una diferencia apreciable en los valores de los parámetros hidroquímicos, se observa una alteración significativa de estos valores en los Golfos de Santa Fé y Cariaco. Se pudo observar que mientras en el Golfo de Cariaco las concentraciones de fosfato aumentaban, por el contrario en el Golfo de Santa Fé disminuían y las concentraciones de nitrato no presentaban variación; igualmente la reducción de los valores de oxígeno muestra una alteración similar en ambos golfos. Debido a esto, se encuentra una elevada razón O/P en el Golfo de Santa Fé y una baja razón N/P en el Golfo de Cariaco.

Abstract

Some hydrographical and chemical aspects of the upper waters of the Cariaco Trench and surrounding areas were studied on the basis of data collected during our expeditions in the years between 1965 and 1975. The hydrographical conditions in the coastal areas of northeastern Venezuela depend mainly on the seasonal upwelling of subsurface waters caused by the trade winds. Seasonal variations of hydrochemical parameters in the Cariaco Trench and adjacent areas show similar characteristics (Okuda et al. 1968, 1969 and 1975). There

is a good correlation between temperature and other parameters (oxygen, AOU - apparent oxygen utilization, phosphate-P and nitrate-N) in the areas studied. It is observed that the magnitude of coefficients of the said correlation seems to agree with the intensity of the upwelling in the areas studied. Even though the areas outside and inside the Cariaco Trench do not show an appreciable difference in the values of hydrochemical parameters, there is a significant change of these values in the Gulf of Santa Fé and the Gulf of Cariaco. It could be observed that while in the Gulf of Cariaco the concentrations of phosphate increase, in the Gulf of Santa Fé they decrease, and the concentrations of nitrate present no significant variation and also the reduction of oxygen values shows a similar change in both the gulfs. By this reasoning it appears that there is a high ratio of O/P in the Gulf of Santa Fé and a low ratio N/P in the Gulf of Cariaco.

1. INTRODUCCION

De acuerdo con los datos oceanográficos obtenidos por la R/V ATLANTIS en 1933 y 1934, Parr (1937) indicó la posible existencia de la surgencia en el área sureste del Mar Caribe. Richards (1960) discutió la presencia de la surgencia intensa en la costa oriental de Venezuela. Posteriormente, varios investigadores observaron el mismo fenómeno y llegaron a la conclusión de que las condiciones hidrográficas de las aguas superiores en las costas surorientales del Mar Caribe, varían dependiendo de la intensidad de la surgencia, la cual está estrechamente relacionada con el régimen de los vientos alisios (Fukuoka, 1963; Fukuoka et al., 1963, 1965; Ljoen y Herrera, 1965; Gordon, 1967; Okuda et al., 1969; Febres, 1974; Okuda y Benitez, 1974).

Okuda (1975) observó una buena correlación entre la temperatura y los parámetros químicos en el Golfo de Santa Fé y la depresión oriental de la Fosa de Cariaco, indicando que la variación y distribución de estos parámetros en estas áreas probablemente estén controladas simplemente por factores comunes para ambas regiones, principalmente la intensidad de la surgencia. En el mismo trabajo, sin embargo, Okuda (1975) encontró que la razón O/P en el Golfo de Santa Fé es muy elevada, en comparación con la observada en la Depresión Oriental de la Fosa de Cariaco. Esto quizás significa una diferencia marcada en la actividad bioquímica entre ambas áreas.

Ampliando las zonas de estudio, en este trabajo, se trata de hacer una comparación de las características hidroquímicas en las áreas fuera de la Fosa de Cariaco (desde el borde norte hasta 12°N), dentro de la Fosa de Cariaco (Depresión Oriental y Occidental), el Golfo de Santa Fé y el Golfo de Cariaco, con el fin de observar una posible alteración de las características químicas de las aguas, mientras se transportan desde el área fuera de la Fosa de Cariaco hacia el área más cercana de la costa.

2. ORIGEN DE LOS DATOS UTILIZADOS

Los datos utilizados en este trabajo fueron obtenidos en las expediciones hidroquímicas realizadas por el Departamento de Oceanografía Química del Instituto Oceanográfico, durante el período de 1965 a 1975. Las áreas y el origen de los datos correspondientes son como siguen:

1. Fuera de la Fosa (22 estaciones con 157 muestras en total): GQ-65, LS-7001, LS-7101, LS-7105, LS-6703, LS-6705 y LS-7204.

2. Depresión Occidental (21 estaciones, con 131 muestras en total): GQ-65, GQ-66, LS-7001, LS-7101, LS-7105 y LS-7204.

3. Depresión Oriental (29 estaciones, con 198 muestras en total): GQ-65, GQ-66, LS-7001, LS-7105 y LS-7204.

4. Golfo de Santa Fé (24 estaciones, con 134 muestras en total): datos mensuales desde agosto de 1972 a abril de 1975.

5. Golfo de Cariaco (21 estaciones, con 135 muestras en total): GQ-66, GQ-69 y GQ-70.

En este trabajo, se emplearon los datos de temperatura, oxígeno disuelto, utilización aparente de oxígeno (AOU), P-fosfato y N-nitrato.

3. AREAS DE ESTUDIO

La Fosa de Cariaco está situada dentro del borde continental de Venezuela, en el área suroriental del Mar Caribe. Su borde norte está separado de la parte profunda del Mar Caribe por una cresta submarina, que se extiende desde la Isla de Margarita hasta Cabo Codera. La comunicación entre el Mar Caribe y la Fosa de Cariaco se realiza aproximadamente a una profundidad de 150 m al norte de Cabo Codera (en la parte oeste de la fosa). Debido a esto se obstaculiza el intercambio de las aguas subyacentes con el Mar Caribe. En la fosa,

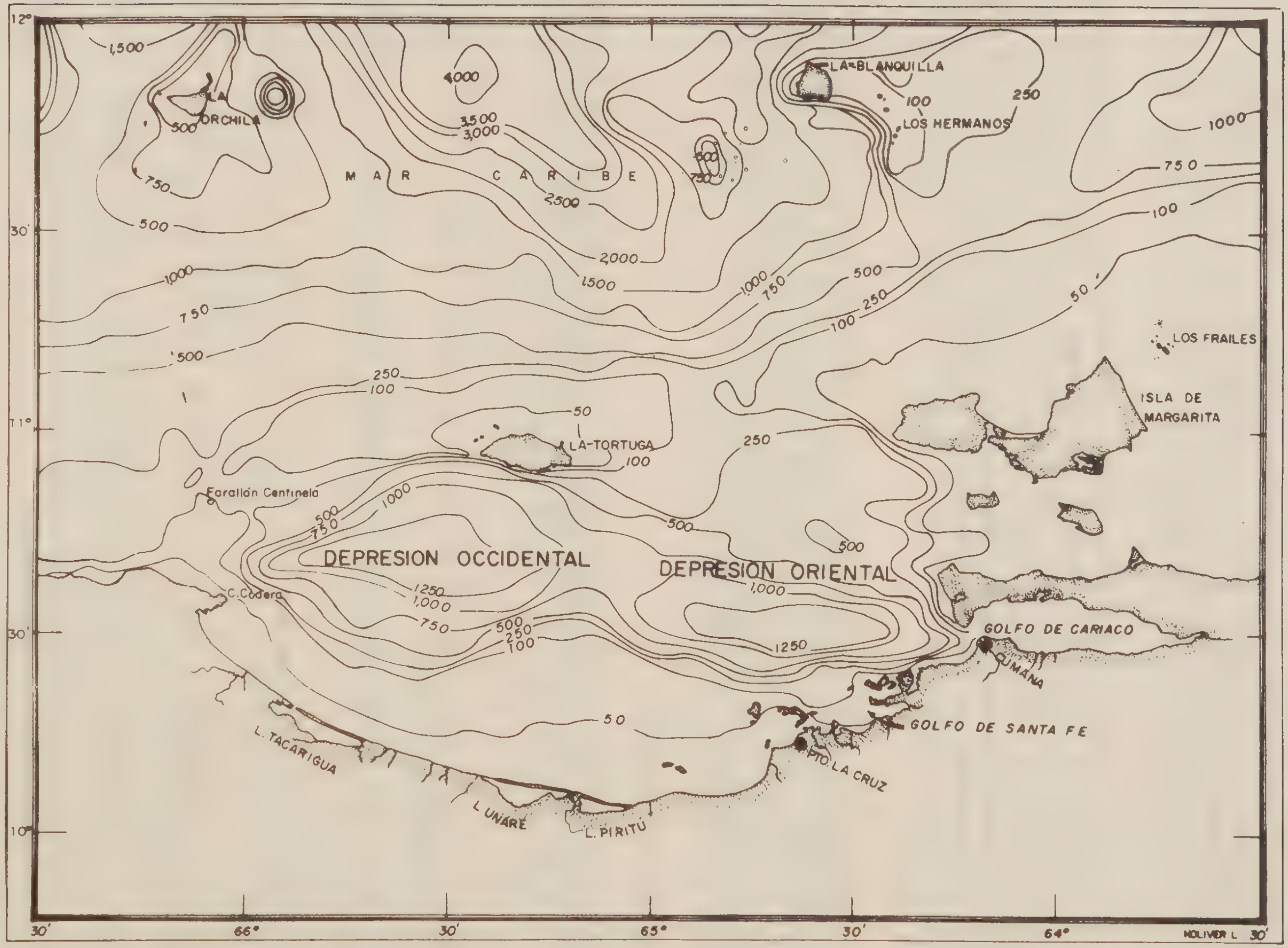
LA ORCHILA
LA BLANQUILLA
LOS HERMANOS
LOS FRAILES
ISLA DE MARGARITA
MAR CARIBE
LA TORTUGA
Farallón Centinela
C. Codera
DEPRESION OCCIDENTAL
DEPRESION ORIENTAL
GOLFO DE CARIACO
CUMANÁ
GOLFO DE SANTA FE
PTO. LA CRUZ
L. TACARIGUA
L. UNARE
L. PIRITÚ
1,500
500
750
4000
3,500
3,000
2,500
2,000
1,500
1000
100
250
50
1,000
1250
12°
30'
11°
10°
66°
65°
64°
HOLIVER L

Fig. 1   Mapa de la Fosa de Cariaco y áreas adyacentes

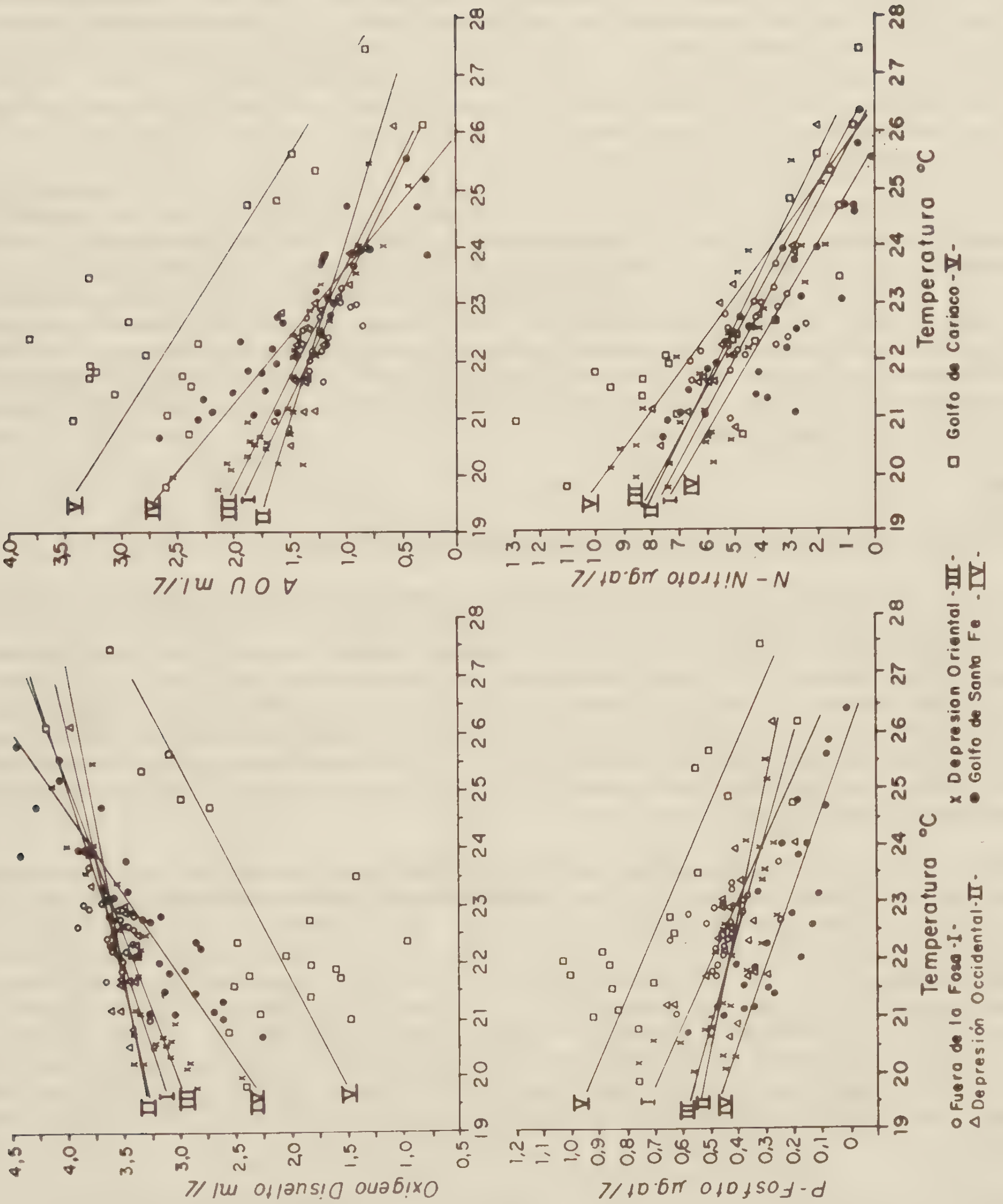

Fig. 2 Correlación entre temperatura y parámetros químicos

se encuentran dos depresiones, las cuales están situadas al este y oeste (Depresiones Oriental y Occidental), separándolas un umbral submarino de aproximadamente 900 m de profundidad. Ambas depresiones poseen una profundidad máxima alrededor de 1 400 m (Fig. 1).

El Golfo de Santa Fé está localizado en la parte sureste del márgen de la Depresión Oriental de la Fosa de Cariaco. Desde el talud en el márgen suroriental de la Depresión oriental, la isobata de 100 m se introduce hacia la entrada del Golfo de Santa Fé, presentando una profundidad de 70-80 m en la entrada y de 60-70 m en el centro, disminuyendo gradualmente hacia el interior, hasta una profundidad de 20-30 m. La entrada del Golfo es más ancha y se reduce progresivamente hacia el interior presentando forma de V. Por eso, esta situación geográfica facilita el intercambio de las aguas en el Golfo. En la parte sureste del golfo, desembocan pequeños ríos, pero estos aportes afectan muy poco las condiciones hidrográficas de esta área (Okuda, 1975).

El Golfo de Cariaco, se encuentra situado en la parte este del borde de la Depresión Oriental de la Fosa de Cariaco. Está separado de dicha depresión por un umbral submarino de 60-70 m de profundidad, localizado a la entrada del golfo. Una característica geográfica del Golfo de Cariaco es que su entrada es muy angosta y posee una profundidad menor que la parte central del mismo (aproximadamente 90 m de profundidad). Esta condición afecta la circulación y renovación de las aguas del golfo. En la entrada del golfo desemboca el río Manzanares el cual descarga unos 500 a 600 millones de toneladas de agua anual. Sin embargo, la influencia del río Manzanares en las condiciones hidrográficas del golfo es probablemente pequeña, debido a que los vientos soplan predominantemente del noreste y del este, provocando un flujo superficial hacia el oeste.

4. RESULTADOS

4.1 Relación entre la Temperatura y los Parámetros Hidroquímicos

En el área costera tropical, donde se presenta la surgencia, la aparición de baja temperatura en las capas superficiales se origina principalmente por las aguas subyacentes que afloran y posiblemente no es por el efecto del enfriamiento atmosférico. En general, la temperatura es responsable de las variaciones de la densidad en las aguas de la costa cercana a la Fosa de Cariaco, debido a la poca variación de la salinidad en comparación con el cambio de la temperatura. Además, la forma de la distribución y la variación de los parámetros químicos muestran bastante similitud a la de la temperatura, y no presenta una diferencia notable en la distribución espacial de estos parámetros en comparación con su variación estacional (Okuda *et al.*,1968; Okuda, 1975).

Para observar una alteración espacial de los parámetros químicos, la Fig. 2 presenta una correlación entre la temperatura y dichos parámetros en las áreas fuera y dentro de la Fosa de Cariaco, los Golfos de Santa Fé y de Cariaco. Los valores en esta figura son los promedios de la columna de agua; entre 10 m y el fondo en los golfos de Santa Fé (aprox. 50 m) y de Cariaco (aprox. 60 m) y entre 10 m y la profundidad observada correspondiente a una temperatura mayor de 19°C en las áreas fuera y dentro de la Fosa de Cariaco (aproximadamente 100-150 m de profundidad). Debido a que la temperatura mínima en los golfos fue superior a 19°C, se calculó el promedio de la columna de agua para las áreas de la Fosa (el exterior y el interior) como se mencionó más arriba. Para evitar posibles efectos de la atmósfera, los datos superficiales fueron excluidos en el cálculo del promedio de la columna de agua.

Las líneas expresadas en la Fig. 2 están basadas en las ecuaciones del Cuadro I, calculadas por el método del mínimo cuadrado.

En general, los valores de las áreas de fuera (I) y dentro (II y III) de la Fosa de Cariaco se presentan más agrupados. Los valores del oxígeno disuelto y la AOU en los dos golfos (IV y V) se alejan considerablemente de los tres grupos arriba mencionados; especialmente se nota una desviación en el Golfo de Cariaco, apreciándose más bajas concentraciones de oxígeno disuelto y más alta AOU en comparación con otras áreas. También se observa la misma tendencia en el Golfo de Santa Fé, en la región de temperatura menor de 23°C aproximadamente.

En cuanto a la relación entre la temperatura y el fosfato, igualmente se observa una desviación del grupo del Golfo de Cariaco de los otros cuatro grupos, apreciándose los valores notablemente elevados del contenido de fosfato en el Golfo de Cariaco. Los valores de fosfato del Golfo de Santa Fé se presentan más aproximados a los de las otras tres áreas de fuera y dentro de la fosa, aunque sus valores son ligeramente inferiores a los de estas tres áreas. Por otro lado, la relación de la temperatura y el nitrato nuestra relativamente poca desviación entre las distintas áreas.

La desviación observada de los valores de oxígeno disuelto, AOU y fosfato en los dos golfos desde las áreas fuera y dentro de la fosa, es probablemente debido a la diferencia en las características de las reacciones bioquímicas entre los dos grupos y el calentamiento del agua mientras se desplaza hacia la costa.

De acuerdo con los coeficientes de correlación (Cuadro I), la relación entre la temperatura y los parámetros químicos presenta generalmente una buena correlación entre ambas variables, a pesar de que algunas de las áreas de fuera de la Fosa y el Golfo de Cariaco muestran una correlación no muy buena. Es interesante observar que los coeficientes de correlación entre la temperatura y los parámetros químicos muestran, en forma general, un incremento desde fuera de la Fosa hasta el Golfo de Santa Fé, en el orden indicado en el Cuadro I (excepto en algunos casos). En el Golfo de Cariaco, la magnitud de los coeficientes de correlación entre la temperatura, oxígeno y AOU corresponden al área entre fuera de la fosa y la depresión occidental, y los mismos coeficientes para la relación entre temperatura, fosfato y nitrato se observan entre la Depresión Oriental y el Golfo de Santa Fé. Este orden del incremento de los coeficientes de correlación parece coincidir con el de la intensidad de surgencia en las áreas de estudio.

4.2 Correlación entre el Fosfato, la AOU y el Nitrato

La correlación entre las concentraciones de fosfato, AOU y nitrato en las cinco áreas se presenta en la Fig. 3. Los valores en este gráfico son los promedios de la columna de agua, que fueron empleados en la Fig. 2. A pesar de que se observa cierta dispersión de los valores, se aprecia generalmente una buena correlación entre el fosfato y los otros dos parámetros. No se nota una desviación sistemática de los valores entre las cinco áreas estudiadas, como se ha observado en la relación entre la temperatura - oxígeno disuelto, AOU y fosfato en la Fig. 2.

Las siguientes correlaciones entre el fosfato, AOU y nitrato en las cinco áreas fueron calculadas según el método de mínimo cuadrado:

CUADRO II

Correlaciones entre fosfato, AOU y nitrato

Area	AOU (ml/l) - P (μg. at/l)	r	N (μg. at/l) - P (μg. at/l)	r
I	AOU = 1,56 P + 0,49	0,741	N = 6,32 P + 1,71	0,520
II	AOU = 1,08 P + 0,02	0,451	N = 8,53 P + 1,66	0,610
III	AOU = 2,77 P + 0,22	0,735	N =14,00 P - 0,52	0,946
IV	AOU = 3,74 P + 0,45	0,803	N =14,00 P + 0,09	0,855
V	AOU = 2,77 P + 0,64	0,749	N =11,80 P - 2,03	0,798

r: coeficiente de correlación; I = fuera de la Fosa de Cariaco; II = Depresión Occidental; III = Depresión Oriental; IV = Golfo de Santa Fé; V = Golfo de Cariaco

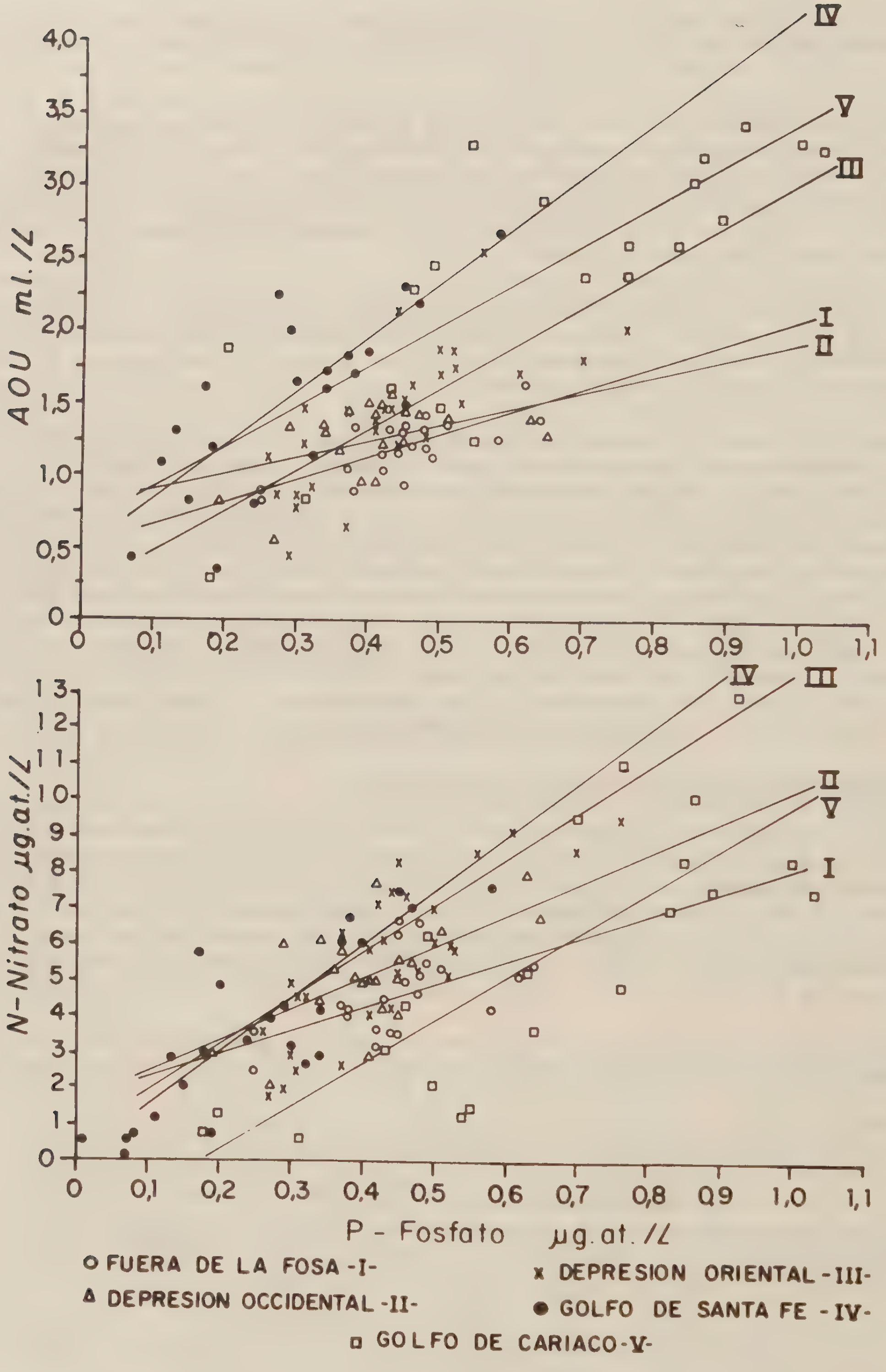

Fig. 3 Correlación entre fosfato - AOU y nitrato

CUADRO I

Correlaciones entre la temperatura
Parámetros químicos

Area	O_2(ml/l) - Temp.(°C)	r	AOU(ml/l) - Temp.(°C)	r
Fuera de la Fosa - I	O_2 = 0,166 T - 0,16	0,594	AOU = - 0,245 T + 6,70	- 0,736
Depresión Occidental - II	O_2 = 0,093 T - 1,46	0,741	AOU = - 0,168 T + 5,02	- 0,839
Depresión Oriental - III	O_2 = 0,190 T - 0,78	0,847	AOU = - 0,259 T + 7,11	- 0,899
Golfo de Santa Fé - IV	O_2 = 0,346 T - 4,53	0,894	AOU = - 0,429 T + 11,1	- 0,918
Golfo de Cariaco - V	O_2 = 0,269 T - 3,83	0,682	AOU = - 0,347 T + 10,4	- 0,770

Area	P=(µg.at/l) - Temp.(°C)	r	N(µg.at/l) - Temp.(°C)	r
Fuera de la Fosa - I	P = - 0,093 T + 2,53	- 0,585	N = - 1,10 T + 29,2	- 0,578
Depresión Occidental - II	P = - 0,043 T + 1,37	- 0,517	N = - 1,01 T + 27,9	- 0,866
Depresión Oriental - III	P = - 0,057 T + 1,69	- 0,627	N = - 1,12 T + 30,1	- 0,789
Golfo de Santa Fé - IV	P = - 0,073 T + 1,91	- 0,839	N = - 1,20 T + 31,0	- 0,849
Golfo de Cariaco - V	P = - 0,093 T + 2,77	- 0,763	N = - 1,50 T + 39,7	- 0,831

r: Coeficiente de correlación

Como se observa en el Cuadro II, las áreas de la Depresión Oriental y los Golfos de Santa Fé y Cariaco muestran una buena correlación entre el fosfato, AOU y nitrato en comparación con las otras dos áreas.

De acuerdo con estas correlaciones, se obtienen las siguientes relaciones por átomo:

Fuera de la Fosa de Cariaco - I	O: N: P = 183: 8,0:1
Depresión Occidental - II	O: N: P = 170: 10,2:1
Depresión Oriental - III	O: N: P = 267: 13,5:1
Golfo de Santa Fé - IV	O: N: P = 373: 14,1:1
Golfo de Cariaco - V	O: N: P = 304: 9,8:1

Se observa una diferencia marcada en las relaciones elementales O/P y N/P entre las distintas áreas. Los dos golfos muestran la razón O/P elevada en comparación con las áreas de fuera y dentro de la fosa. Entre las últimas tres áreas, la razón O/P en la Depresión Oriental fue algo superior a la de otras áreas. Richards y Vaccaro (1965) encontraron un valor de 235 para la razón O/P en las capas superiores de la Fosa de Cariaco. Este valor es aproximadamente igual a la razón O/P obtenida en la Depresión Oriental en este trabajo.

En general, los valores de la razón N/P en estas áreas son inferiores a un valor (15) considerado como la razón N/P normal en el agua de mar, especialmente para el área de fuera de la fosa, la Depresión Occidental y el Golfo de Cariaco, los cuales muestran valores muy bajos.

5. AGRUPACION DE LAS AGUAS DE ORIGEN COMUN

En las secciones anteriores, las características hidroquímicas en la Fosa de Cariaco y áreas adyacentes fueron comparadas en base a los valores promedios de las columnas de agua. Sin embargo, para obtener una mejor información sobre posibles alteraciones de las características hidroquímicas de las aguas, debido a su transporte desde el área de fuera de la Fosa de Cariaco hacia el área más cercana a la costa, sería más efectivo analizar el cambio de las características hidroquímicas de las aguas del mismo origen.

Por este motivo, utilizando todos los datos empleados para el cálculo de los promedios de las columnas de agua de las secciones anteriores en cada área respectiva, se calculó los valores promedios de la salinidad correspondientes al intervalo de cada 0,5°C de temperatura entre 19,0 y 29,5°C. La Fig. 4 presenta el diagrama de temperatura-salinidad de las cinco áreas de estudio, el cual fue elaborado en base a los promedios de salinidad obtenidos en la forma arriba mencionada y sus respectivas temperaturas.

Se observa que a la temperatura inferior de aproximadamente 21°C, no se presenta gran diferencia en la salinidad entre las distintas áreas; especialmente se nota esta evidencia en la temperatura menor de 20°C. En la zona mayor de 24°C, se aprecia una marcada diferencia entre las cinco áreas de estudio.

De acuerdo con estas observaciones, y por conveniencia se separaron tres grupos de agua que posiblemente son de orígenes comunes:

GRUPO A: Aguas que poseen una temperatura mayor de 24°C y una salinidad menor de 36,7 por mil (agua superficial)

GRUPO B: Aguas que poseen una temperatura entre 21°C y 24°C, y una salinidad mayor de 36,7 por mil (agua subtropical)

GRUPO C: Aguas que poseen una temperatura inferior de 21°C y una salinidad menor de 36,7 por mil (agua situada por debajo del núcleo de agua subtropical).

En la Fig. 4 se observa una variación apreciable de la salinidad, presentándose los valores más bajos en el área fuera de la fosa, mientras que hacia los golfos aumenta considerablemente. Esta baja salinidad observada en las aguas superficiales en el área fuera de la fosa es debido a la influencia de las aguas originadas por el aporte de los ríos sudamericanos. La salinidad relativamente alta encontrada en los dos golfos indica que estas áreas no son afectadas significativamente por las aguas aportadas por los ríos de Suramérica. En el Grupo B, aunque se observa muy poca dispersión en la salinidad entre las cinco áreas los dos golfos todavía muestran una salinidad más elevada que las otras tres áreas. Esto quizás indica que el agua subtropical ocupa con mayor frecuencia las áreas de los golfos debido a la surgencia.

6. COMPARACION DE LAS CARACTERISTICAS QUIMICAS ENTRE TRES GRUPOS DE AGUA

De acuerdo con los tres grupos de agua antes indicados, se recopilaron todos los datos químicos del agua en las cinco áreas ya señaladas. La Fig. 5 muestra los promedios de los parámetros químicos de los tres grupos, así como el total de las respectivas áreas.

En general, se observa una marcada semejanza en las concentraciones de los parámetros químicos y las razones N/P y O/P entre las Depresiones Occidental y Oriental de la Fosa de Cariaco, con excepción de una pequeña diferencia en la razón N/P en el Grupo A (agua superficial). Además, no se encuentra una diferencia apreciable en los valores de los parámetros químicos entre fuera y dentro de la Fosa de Cariaco en los Grupos A y B; sin embargo, se presenta cierta alteración de dichos valores en el Grupo C entre ambas áreas, apreciándose una reducción del oxígeno disuelto, un aumento de la AOU, el fosfato, el nitrato, las razones N/P y O/P en el área dentro de la fosa.

Los valores promedios de estos parámetros en los dos golfos (Santa Fé y Cariaco) varian en mayor grado que los de las áreas arriba mencionadas, aunque la forma de alteración es distinta en cada uno. Estos golfos muestran una marcada reducción del oxígeno disuelto, un aumento de la AOU y muy poco cambio de la concentración del nitrato; sin embargo, en cuanto a los valores de fosfato, ambos golfos presentan una relación opuesta, es decir, el contenido de fosfato en el Golfo de Santa Fé se reduce mientras que en el Golfo de Cariaco aumenta considerablemente. Esta evidencia causó el incremento de la razón O/P en Santa Fé y por el contrario, la reducción de la razón N/P en Cariaco.

De acuerdo con la relación entre la temperatura y el oxígeno disuelto (igualmente la AOU), podría esperarse valores más elevados de fosfato en el Golfo de Santa Fé, así como valores más altos de nitrato para ambos golfos. En el caso del Golfo de Santa Fé, la razón N/P presenta un valor aproximado a la razón (15) que se encuentra normalmente en el agua oceánica, por lo tanto, la causa de baja concentración de fosfato y nitrato es quizás debida a la formación de nitrógeno y fósforo orgánico por la actividad bioquímica.

En el caso del Golfo de Cariaco, la razón O/P muestra un valor normal, pero la razón N/P presenta un valor muy inferior al que podría esperarse. También, se nota una elevada concentración de fosfato en el Golfo de Cariaco. Esto quizás sea debido a la situación geográfica de dicho golfo, el cual posee una entrada angosta con una profundidad menor que la parte central del golfo, dando lugar posiblemente a que se produzcan los siguientes fenómenos en esta área de acuerdo con el sistema de los vientos. El agua subtropical (Grupo B) y aguas más bajas del núcleo del agua subtropical (Grupo C) que contienen alta concentración de fosfato y nitrato, penetran por encima del umbral submarino a la entrada y se desplazan hacia el interior del golfo. Mientras estas aguas se mueven hacia el interior de esta área, posiblemente el fosfato y el nitrato se transforman a la forma orgánica a través de la actividad fotosintética. Luego, esta materia orgánica transformada se precipita al fondo. Las aguas superficiales del golfo que contienen baja concentración de fosfato y nitrato, se desplazan hacia el exterior del mismo, a través de la capa superficial. Por este proceso, podemos esperar una acumulación del nitrógeno y el fósforo en el golfo. Sin embargo, en el Golfo de Cariaco, el nitrato desaparece, formándose luego el nitrógeno molecular debido al proceso de desnitrificación que ocurre comúnmente, en especial, en la época de menor intensidad de la surgencia. Este último fenómeno sería la causa de los valores bajos de la razón N/P en el Golfo de Cariaco.

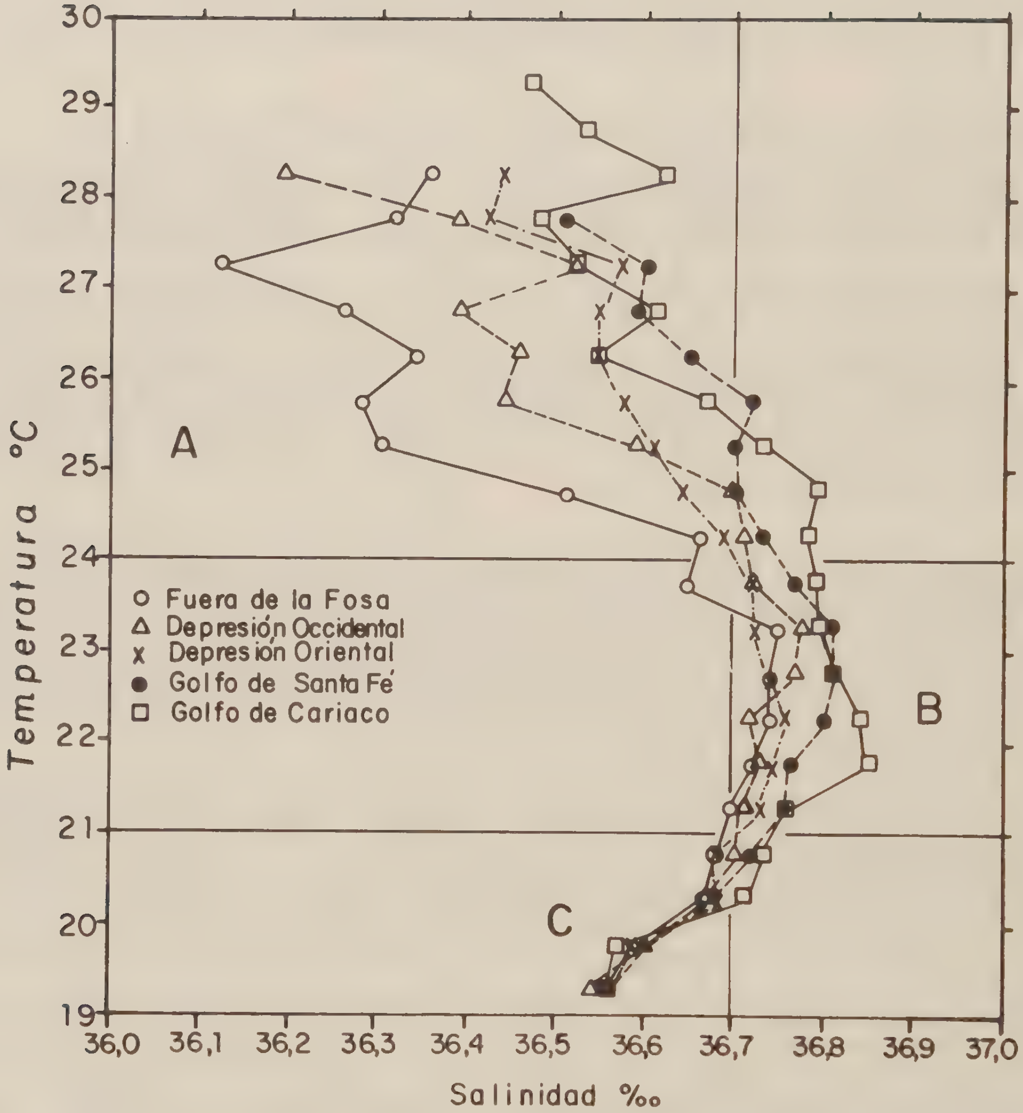

Fig. 4 Diagrama de temperatura-salinidad

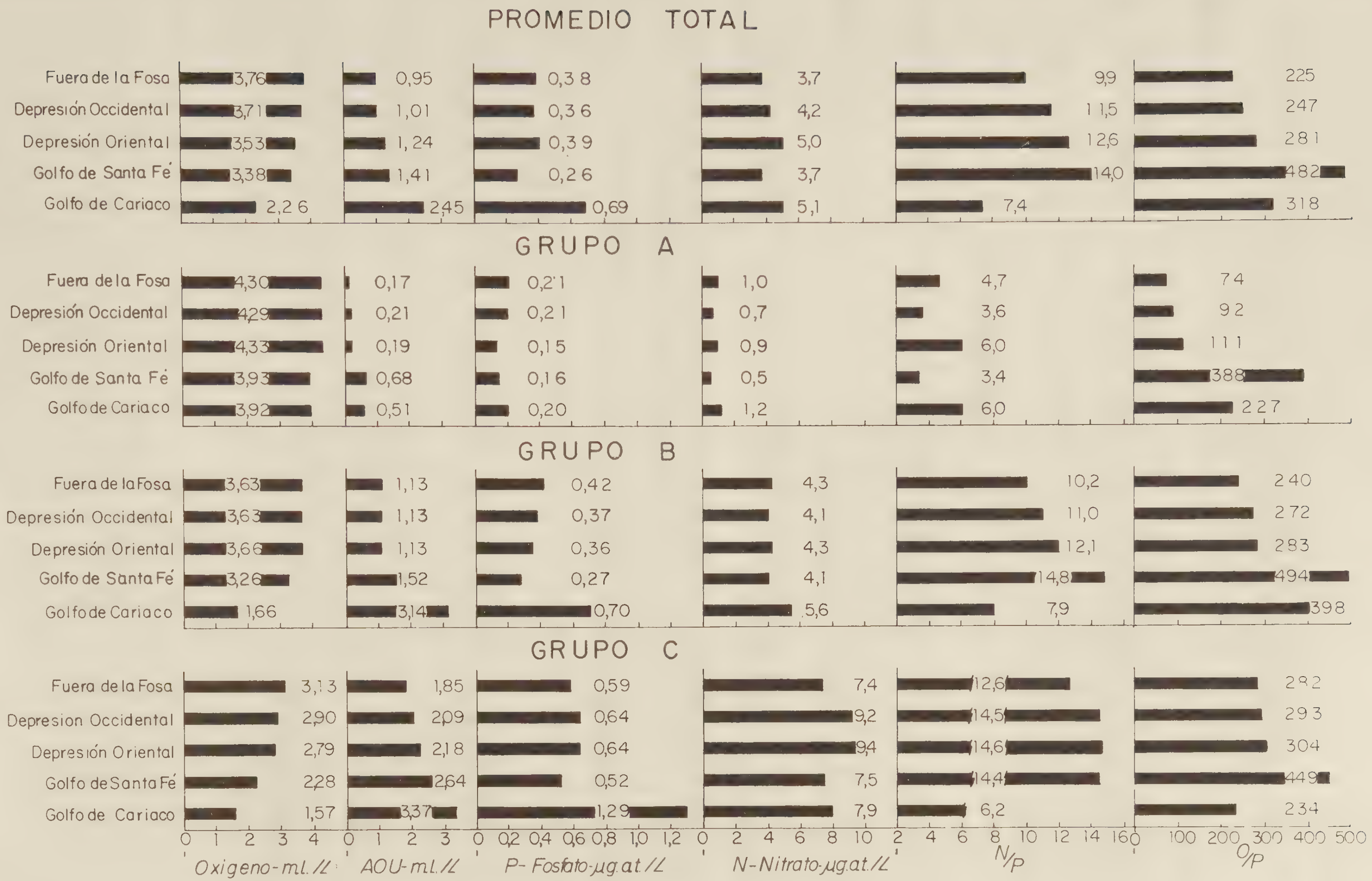

Fig. 5 Promedios de los parámetros químicos de los tres grupos de agua

7. REFERENCIAS

Febres Ortega, G.A., Circulación de las aguas superiores de la Fosa de Cariaco en abril
1974 de 1974. Bol.Inst.Oceanogr.Univ.Oriente, 13(1-3):79-86

Fukuoka, J., Un análisis de las condiciones hidrográficas del Mar Caribe. Mem.Soc.Cienc.Nat.
1963 La Salle, 23(64):43-55

__________, Hydrography of the adjacent sea. (2). Some characteristics of oceanographical
1965 conditions in the Caribbean Sea, especially in the region adjacent to Venezuela.
Bol.Inst.Oceanogr.Univ.Oriente, 4(2):234-45

Fukuoka, J. y A. Ballester, Un análisis de las condiciones hidrográficas del Mar Caribe.(3).
1963 Mem.Soc.Cienc.Nat.La Salle, 23(65):132-42

Gordon, A.L., Circulation of the Caribbean Sea. J.Geophys.Res., 72(24):6207-23
1967

Ljoen, R. y L.E. Herrera, Some oceanographic conditions of the coastal waters of eastern
1965 Venezuela. Bol.Inst.Oceanogr.Univ.Oriente, 4(1):7-50

Okuda, T., Características hidroquímicas del Golfo de Santa Fé y áreas adyacentes. Bol.Inst.
1975 Oceanogr.Univ.Oriente, 14(2):251-68

Okuda, T. y J. Benitez A., Condiciones hidrográficas de las capas superiores en la Fosa
1974 de Cariaco y áreas adyacentes durante la época lluviosa. Bol.Inst.Oceanogr.
Univ.Oriente, 13(1-2):147-62

Okuda, T., J. Benitez y E. Fernández, Vertical distributions of inorganic and organic
1969 nitrogen in the Cariaco Trench. Bol.Inst.Oceanogr.Univ.Oriente, (1-2):28-34

Okuda, T., B.R. Gamboa y A.J. García, Seasonal variation of hydrographic conditions in the
1969 Cariaco Trench. Bol.Inst.Oceanogr.Univ.Oriente, 8(1-2):21-7

Okuda, T. et al., Condiciones hidrográficas y químicas en la Bahía de Mochima y la Laguna
1968 Grande del Obispo desde 1964 a 1966. Bol.Inst.Oceanogr.Univ.Oriente, 7(3):7-37

Parr, A.E., A contribution to the hydrography of Caribbean and Cayman Seas, based upon
1937 the observations made by the research ship ATLANTIS 1933-34. Bull.Bingham
Oceanogr.Collect., 5(4):1-110

Richards, F.A., Some chemical and hydrographic observations along the north coast South
1960 America.I. Cabo Tres Puntas to Curaçao including the Cariaco Trench and the
Gulf of Cariaco. Deep-Sea Res., 7(3):163-82

Richards, F.A. y R.F. Vaccaro, The Cariaco Trench; an anaerobic basin in the Caribbean Sea.
1956 Deep-Sea Res., 3(3):214-28

ADHESION ENHANCING ORGANICS IN THE EASTERN CARIBBEAN SEA

by

B. JIMENEZ VELEZ, T.R. TOSTESON, B.R. ZAIDI,
R.S. TSAI and D.K. ATWOOD
Department of Marine Sciences
University of Puerto Rico, CAAM
Mayaguez, Puerto Rico

CONTENTS

1. INTRODUCTION
2. MATERIALS AND METHODS
3. RESULTS
4. DISCUSSION
5. ACKNOWLEDGEMENTS
6. REFERENCES

Abstract

The organic composition and surface activity of macromolecular material extracted from seawater samples taken in the Eastern Caribbean Sea have been examined. The extracted materials were tested for their adhesion-enhancing activity by determining their effect on the adhesion of marine phytoplankton cells to glass surfaces. The test materials were recovered from seawater samples collected along a 67°W transect between Venezuela and Puerto Rico. Sampling was designed to collect materials in Caribbean Surface Water (CSW) at depths of 10 m and 50 m and in the high salinity core of the Subtropical Underwater (SUW).

The results of this study indicate that the materials recovered from samples of the Subtropical Underwater enhance the adhesion of the phytoplankton cells to glass surfaces. This activity was present in this water mass at 67°W transect stations from Puerto Rico to Venezuela. The materials recovered from the mixed surface layer samples showed the presence of adhesion-enhancing activity; however, this activity was not uniformly distributed along the 67°W transect.

The adhesion enhancement activity appears to be associated with the organic carbon and nitrogen contents in the recovered materials. The concentration, carbon and nitrogen contents and the adhesion-enhancement activity of the materials recovered from samples of the surface water during the daylight were significantly greater than was found with the materials recovered from samples taken at night. The relationship between this phenomenon and the production of adhesion-enhancing substances by marine micro-organisms is discussed.

Resumen

Se ha examinado la composición orgánica y la actividad superficial de las sustancias macromoleculares de muestras de agua del mar tomadas en el Caribe oriental. La activación de la adherencia de los materials recogidos fue comprobada determinando su efecto sobre la adherencia de las células del fitoplancton marino a las superficies vítreas. Los materials ensayados procedían de muestras de agua del mar tomadas a lo largo del meridiano 67°O, entre Venezuela y Puerto Rico. El objeto del muestreo era recoger materiales en las aguas superficiales del Caribe (CSW), a profundidades de 10 y 50 m, y en el centro del agua submarina subtropical (SUW), que es muy salino.

Los resultados de este estudio indican que los materiales de las muestras de aguas submarinas tropicales activan la adherencia de las células del fitoplancton a las superficies vítreas. Esta actividad pudo observarse en esta masa de agua, en las estaciones del meridiano 67°O situadas entre Puerto Rico y Venezuela. En los materiales de las muestras tomadas en la capa superficial mixta pudo observarse la existencia del fenómeno de activación de la adherencia, aunque esta actividad no estaba distribuida uniformemente a lo largo del meridiano 67°O.

La activación de la adherencia aparece asociada al contenido de carbono orgánico y de nitrógeno de los materiales recogidos. La concentración, el contendio de carbono y de nitrógeno, y la acción de la adherencia de los materiales de las muestras recogidas en las aguas superficiales eran notablemente mayores en los materiales de las muestras tomadas durante el día que en los de las muestras tomadas durante la noche. Se discute la relación entre este fenómeno y el de la producción, por los microorganismos marinos, de substancias que activan la adherencia.

1. INTRODUCTION

High molecular weight, organic materials that enhance the adhesion of micro-algal cells to glass surfaces have been isolated from seawater samples taken off the south coast of Puerto Rico since 1972. These materials were found both in the Caribbean Surface Water (CSW) and associated with the Subtropical Underwater (SUW) at depths from approximately 100 m to 150 m (Tosteson, Atwood and Tsai, 1976). Other investigators suggested that surfactants found in seawater were derived in part from the extracellular products released by phytoplankton and macro-algae (Fogg, 1952; Hoyt, 1970; Thomas, 1971; Samuel and Fogg, 1971). The exudates of planktonic algae and marine bacteria contain a high molecular weight, organic material that affects the adhesion of these micro-organisms to glass surfaces (Tosteson and Corpe, 1975). The effect of these "surface active" materials is evidenced by the fact that they promote an increase in the adhesion of these cells to glass and their aggregation to one another.

2. MATERIALS AND METHODS

The seawater samples examined in this study were obtained on transects along 67°W between Puerto Rico and Venezuela. These transects run from approximately 20 m south of Puerto Rico (latitude 17°36'N) to a point approximately 40 mi off the north coast of Venezuela (latitude 11°22'N). The transects consisted of the series of eight evenly spaced hydrographic stations shown in Fig. 1. The water samples employed in this study were collected in October 1974 and again in February 1975. The exact locations of these stations are given in Table I.

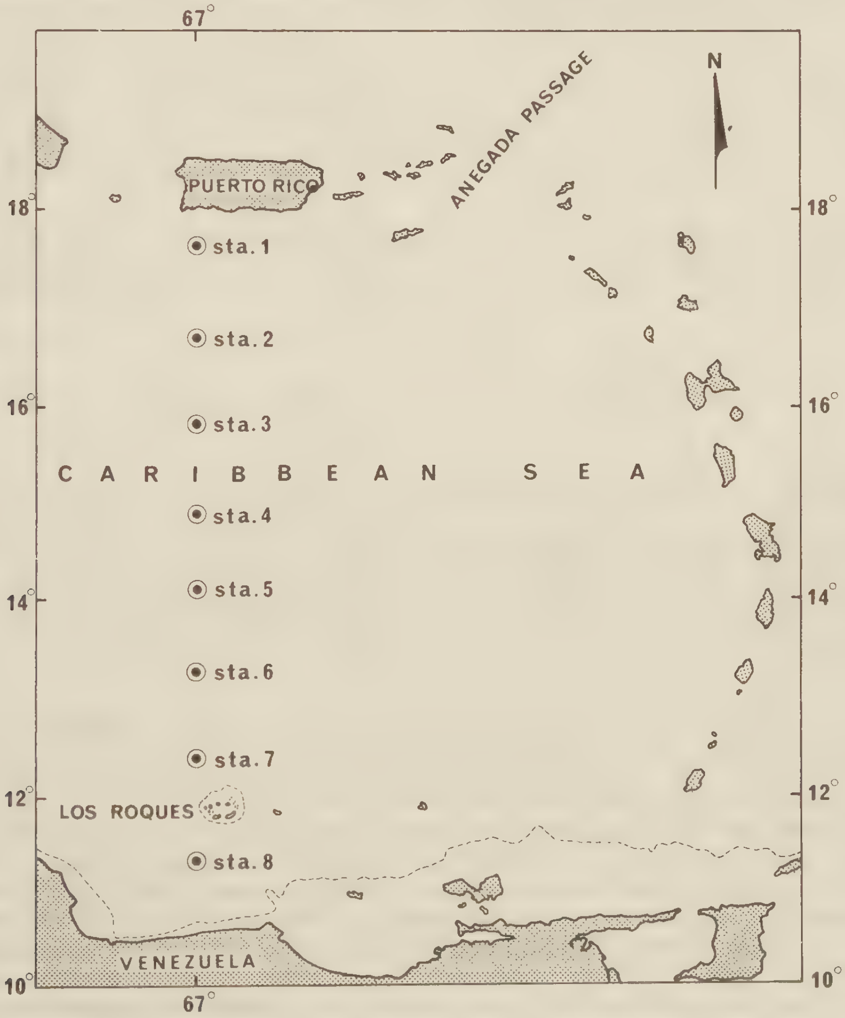

Fig. 1 Location of transects and hydrographic stations

TABLE I

	Crawford Station	Hydrographic Station	Latitude (north)	Fractional distance from Puerto Rico to Venezuela
October 1974	2717	1	17°38'	0.05
	2719	3	15°50'	0.30
	2720	4	14°50'	0.43
	2721	5	14°03'	0.54
	2722	6	13°16'	0.65
	2723	7	12°24'	0.76
	2724	8	11°22'	
February 1975	2728	1	17°36.7'	0.05
	2729	2	16°39.5'	0.18
	2730	3	15°49.5'	0.30
	2731	4	14°54.5'	0.42
	2732	5	14°10.5'	0.52
	2733	6	13°18'	0.64
	2734	7	12°25'	0.76
	2735	8	11°23'	0.90

Seawater samples were collected using Niskin bottles (30 l). Sample depths were obtained by comparing the salinity of the sample to the salinity-temperature profile for the station at the time of sampling. The vertical sampling schedule was essentially designed to examine two discrete water masses: (1) Caribbean Surface Water (at depths of 0 to 70 m) and (2) the Subtropical Underwater (at approximate depths of 100 m to 175 m depending on the latitude).

The water samples were stored in large Cubi containers and refrigerated until transferred to the laboratory where they were filtered (millipore filters, pore size 0.45 micron) to remove the particulate matter. The milliport filters were carefully rinsed and soaked in distilled water for some hours prior to their use. The high molecular weight materials in the filtered water samples were concentrated by the addition of dry Sephadex gel (G-50). Procedures of this nature have been reported elsewhere (Sirotkina et al., 1974). In the work reported here the excluded high molecular weight materials were generally concentrated from 10 to 20 times, depending on the original starting volume of the sample (12-16 l). The concentrated solution of high molecular weight materials was desalted by thorough dialysis against distilled water from 10 to 15 times sample volume. These preparations were freeze-dried and the resulting material weighed and stored for subsequent experimentation.

A series of blank solutions consisting of distilled water and artificial seawater (Kester *et al.*, 1967) was passed through the entire system employed, i.e., Niskin bottle, storage container, millipore filters, Sephadex gels, dialysis and freeze-drying. The material recovered from these blank samples was stored for later analysis.

The materials recovered from selected samples were analysed for their organic carbon, nitrogen and hydrogen contents. The organic carbon was determined from wet samples (Dohrman Envirotec) and the carbon, nitrogen and hydrogen contents of dry material were determined using a Carbon, Hydrogen and Nitrogen Analyzer (Hewlitt Packard). All samples were analysed in triplicate. The organic carbon, hydrogen and nitrogen contents of the materials recovered from the blank solutions processed in the system were also determined.

The micro-algal species used to evaluate the surface adhesion activity of the recovered materials was the marine *Chlorella vulgaris* (Beijerinck). The effect of the test substances on the adhesion of these cells to glass surfaces was assessed. This procedure has been employed previously to study the adhesion of these planktonic algal cells to glass surfaces (Zaidi and Tosteson, 1972; Tosteson, Zaidi and Hale, 1973; Tosteson and Zaidi, 1974; Tosteson and Corpe, 1975; Tosteson, Atwood and Tsai, 1976).

3. RESULTS

High molecular weight materials recovered from 527 l of seawater were examined in the course of this study. A total of 378 duplicate adhesion assays was made employing the high molecular weight materials recovered from the respective seawater samples. The control duplicate adhesion assays carried out during the period of testing were divided into seven groups. The average number of cells adhered to the glass surfaces in the control assays was 14.8 ± 2.8 (S.E.) x 10^4. The average coefficient of variation ($S/\bar{x}$) was $0.14 \pm .02$ (S.E.). Significant deviations from this control value ($3.5 \times S$, $p < .01$) indicate that any value of cells adhered $48 \pm 7\%$ different than these controls is significant.

The concentrations of the recovered high molecular weight materials, expressed in terms of the original volume from which they were extracted in the samples taken at an average depth of approximately 50 m at the transect stations is given in Table II.

TABLE II

Materials recovered from 50 metre depth samples

Station[a]	Depth (m)	Original concentration of recovered materials (mg/l)[b]		Adhesion activity	
		October	February	October	February
1	49	17.9^{D}[c]	2.4^{D}[c]	+	+
2	48	-	49.4^{L}	-	+
3	48	1.5^{D}	2.3^{D}	+	+
4	44	22.5^{L}	2.1^{D}	+	+
5	47	6.1^{L}	9.0^{L}	+	0
6	45	92.9^{L}	38.9^{L}	0	0
7	47	57.5^{L}	6.8^{D}	0	+
8	47	8.7^{D}	34.3^{L}	+	+

[a] See Fig. 1

[b] Blank solutions 3.5 ± 1.2 mg/l

[c] D = dark station; L = light station

Those preparations having significant adhesion enhancement activity are indicated on the table. Thus in both October 1974 and February 1975 the materials recovered from these seawater samples in the south-central region of the transect (stations 6 and 7 in October and 5 and 6 in February) had no significant adhesion enhancement activity. As can be seen in Table II the concentrations of recoverable material varied considerably from station to station on both occasions.

The concentrations of the recovered materials and their respective adhesion enhancement activities in the samples taken of the Subtropical Underwater at four of the transect stations (stations 1, 5, 7, and 8) in October and February are shown in Table III.

TABLE III

Materials recovered from SUW samples

Station[a]	Depth (m)	Original concentration of recovered materials (mg/l)[b]		Adhesion activity	
		October	February	October	February
1	147-185	5.5^{D}[c]	5.6^{D}[c]	+	+
5	109-131	19.8^{D}	4.2^{L}	+	0
7	77-101	4.7^{L}	4.1^{D}	+	+
8	82-101	5.7^{D}	5.4^{L}	+	+

a/ See Fig. 1

b/ Bland solutions 3.5 ± 1.2 mg/l

c/ D = dark station; L = light station

The materials recovered in October showed adhesion enhancement activity at all four of the stations examined whereas the materials extracted from the SUW at station 5 in February showed no activity. This station is in the centre of the Caribbean. The concentrations of the recoverable high molecular weight material in these water samples did not vary as markedly as those seen in the seawater samples taken at approximately 50 m. In general the recoverable material in the SUW samples was less than that seen in the samples from 50 m.

The variability in the concentrations of recoverable high molecular weight material in those samples of CSW (50 m) appeared to depend upon whether the respective station was sampled during the night or during the day. The average concentration of recoverable material in the samples taken at the seven stations occupied during the night was 5.6 ± 2.2 (S.E.) mg/l, while the average concentration in those samples taken at the eight stations occupied during the day was 38.8 ± 10.0 (S.E.) mg/l. The difference in these means can be shown to be significant ($p < 0.01$). Qualitatively the variability in concentrations of recoverable material in the CSW samples taken in October 1974 was similar to that seen in the same samples taken in February 1975. This similarity is also seen in the pattern of adhesion-enhancement activity found with the recovered materials on these two transects.

The distribution of the high molecular weight material recovered from the samples taken at a depth of 50 m between Puerto Rico and the north coast of Venezuela is illustrated in Fig. 2. The data obtained from both the October 1974 and the February 1975 samples are presented in this figure as a function of the fractional distance of the respective stations from Puerto Rico to Venezuela. Note the distinct difference between stations sampled in daylight and in darkness.

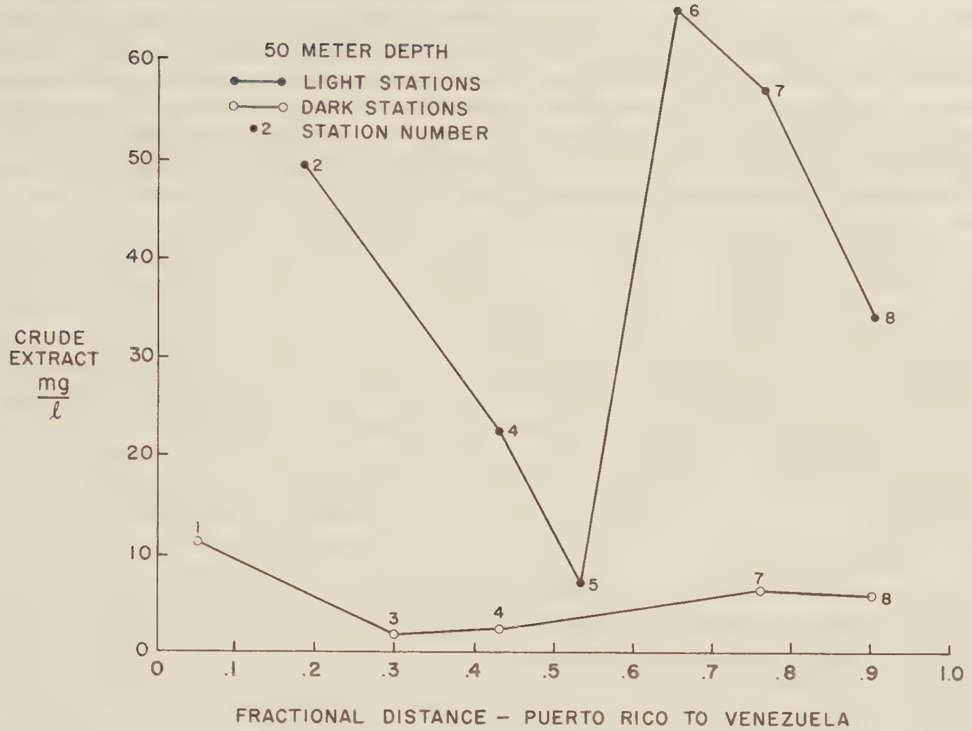

Fig. 2 The distribution of high molecular weight material recovered from the samples taken at a depth of 50 m between Puerto Rico and the north coast of Venezuela

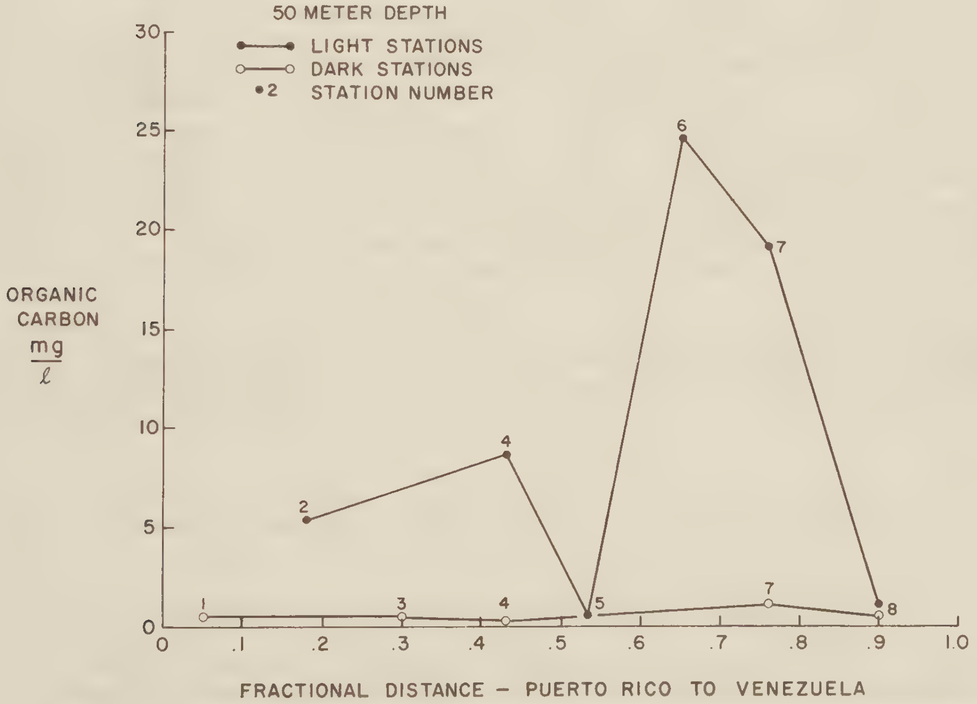

Fig. 3 The distribution of organic carbon recovered from the samples taken at a depth of 50 m between Puerto Rico and the north coast of Venezuela

The organic carbon contents of the recovered materials from the 50 m samples show a distribution similar to that of the total crude extract. Fig. 3 illustrates this relationship. The carbon contents of the materials extracted from stations occupied during the daytime in both the northern and southern portions of the transect are significantly greater than the carbon contents found in the materials recovered from samples taken at stations occupied during the night. It is of interest to note the high carbon values found in the southern portion of the transect (stations 6 and 7) in the light of the fact that these materials did not exhibit adhesion enhancement activity (see Table II).

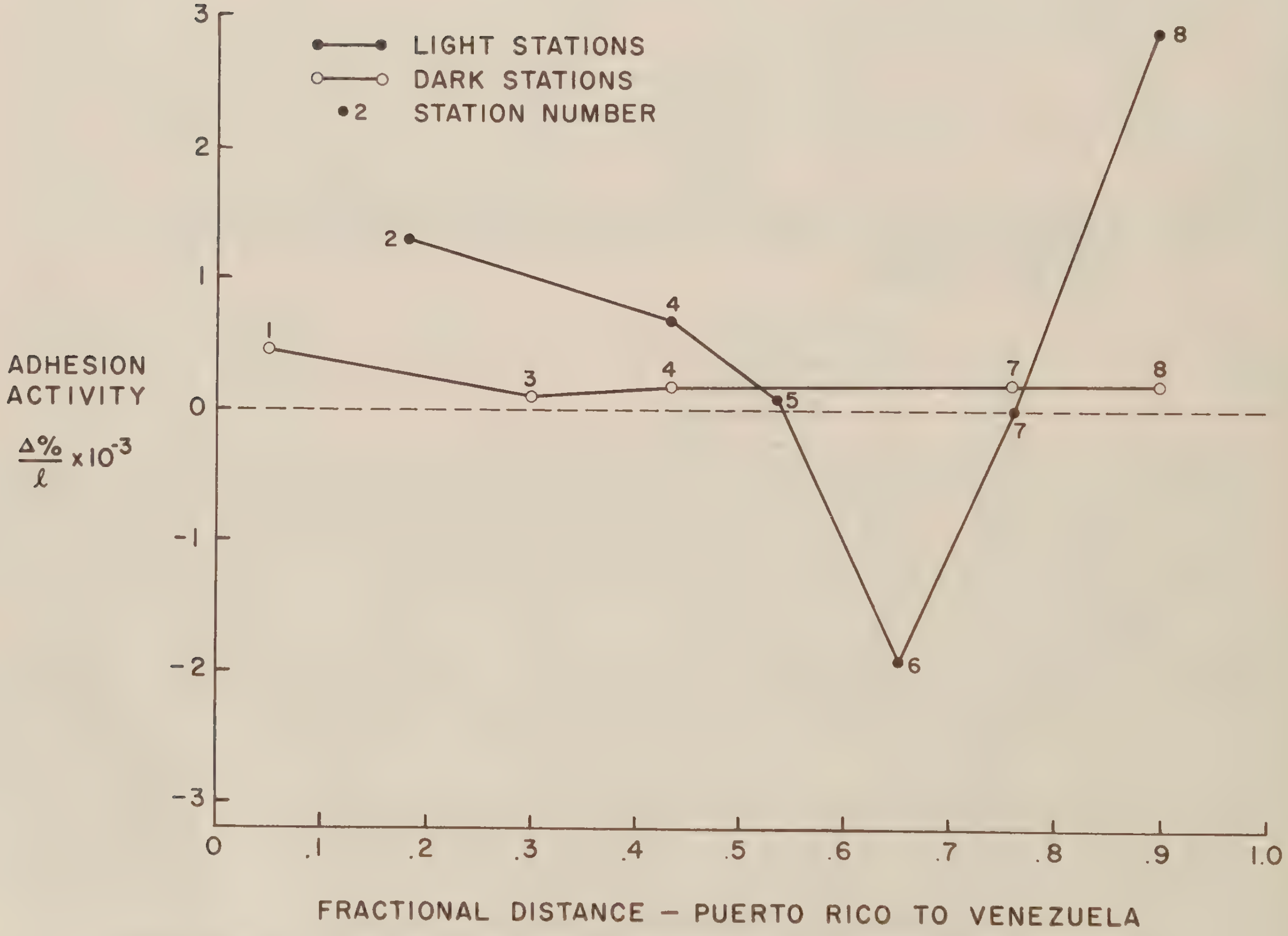

Fig. 4 The distribution of enhancement activity in the samples taken at a depth of 50 m between Puerto Rico and the north coast of Venezuela

The distribution of adhesion-enhancement activity in the samples taken at a depth of 50 m along the transect is illustrated in Fig. 4. In general the adhesion enhancement or inhibitory activity of the materials recovered is expressed in terms of the percent increase (or decrease) in the number of cells attached to glass surfaces in the presence of the test materials, as compared to the number adhered in the absence of these materials (adhesion assay controls). This enhancement or inhibition, when significant (± 48% of the respective control value) can be expressed in terms of the concentration of the particular test material employed. Thus a "specific activity" (Δ%/mg) can be calculated for the active crude material recovered in each of the samples examined in this study. In any particular sample the product of this "specific activity" and the concentration of recovered high molecular weight material will give the activity associated with a litre of the original sample (Δ%/l). Fig. 4 shows the distribution of this activity found in stations taken during the day as compared to those taken at night. The adhesion enhancement activity associated with materials recovered from "light" stations in the northern portion of the transect was significantly greater than that found in the northern "dark" stations. In the southern portion of the transect, "light" stations 6 and 7 yielded material that was markedly inhibitory (station 6) or had no significant effect (station 7) on the adhesion. It is of interest to note that stations 6 and 7 were those at which the samples contained an unusually high organic carbon content. However, the most pronounced adhesion enhancement activity was found in the final "light" station of the southern portion of the transect (station 8).

The average distribution of the concentrations of organic carbon and nitrogen contents and adhesion activities of the materials recovered from samples taken at a depth of 50 m at stations occupied during the day and night at the northern and southern portions of the transect are compared in Table IV. Samples taken at stations occupied during the day yielded amounts of materials that were on the average significantly greater in all of the parameters tested at both the northern and southern portions of the transect than the amounts of materials obtained from samples taken at stations occupied during the night. The "dark" stations in the northern portion of the transect were similar to those taken at night in the southern portion. In the "light" stations taken in the southern portion of the transect the concentration and the organic carbon contents of the crude recovered material were greater than those found in the materials recovered from the daytime stations in the northern portion of the transect. However, the organic nitrogen and the adhesion activity were less in the southern as compared to the northern "light" stations. In the southern stations occupied during the day, stations 6 and 7 had inhibitory and/or no effect on the adhesion of the test cells, whereas the materials obtained from the sample taken at station 8 had an elevated adhesion enhancement activity. Thus the average value of the adhesion activity in the southern "light" stations is somewhat misleading. The high average carbon contents of these materials is due to the organic carbon found in the materials taken at stations 6 and 7 (see Fig. 3). Both of these stations were inactive with respect to adhesion. This inactivity is associated with the low average organic nitrogen contents found in these samples.

Table V compares the average concentrations, organic carbon and nitrogen contents, and the adhesion activities of the materials recovered from samples of the SUW at stations occupied during the night as compared to the daytime. These differences, while suggestive, are not statistically significant.

TABLE IV

Materials recovered from 50 m depth samples

		Dark stations	Light stations
Northern stations (4)	Crude extract (mg/l)	5.24 (5)	39.95 (2)
	Carbon (mg/l)	0.323	7.035
	Nitrogen (mg/l)	0.021	0.410
	Activity (Δ %/l)	180	980
Southern stations (3)	Crude extract (mg/l)	6.6 (2)	55.9 (4)
	Carbon (mg/l)	1.300	17.357
	Nitrogen (mg/l)	0.030	0.028
	Activity (Δ %/l)	177	442

Blank solutions: Crude extract 3.5 ± 1.2 mg/l
Carbon 0.1 ± .03 mg/l
Nitrogen .017 ± .005 mg/l

TABLE V

Materials recovered from SUW samples

	Dark stations	Light stations
Crude extract (mg/l)	8.11 (5)	4.75 (3)
Carbon (mg/l)	2.481(4)	0.303(3)
Nitrogen (mg/l)	0.074(4)	0.030(3)
Activity (Δ %/l)	351 (5)	46 (4)

Blank solutions: Crude extract 3.5 ± 1.2 mg/l
Carbon 0.1 ± .03 mg/l
Nitrogen .017 ± .005 mg/l

4. DISCUSSION

The distribution of adhesion enhancement activity on the transect between Puerto Rico and Venezuela appears to be similar in those samples taken in October 1974 and February 1975. In the Caribbean Surface Water (CSW) there appear to be two areas of adhesion enhancement activity; one associated with the northern and another with the southern portion of the transect. In the central and south central portion of the transect the high molecular weight materials recovered from samples of this water mass either showed no activity or inhibited the adhesion of the test cells to glass surfaces (Table II).

The surface samples taken during the day had a greater concentration of high molecular weight material and a significantly greater adhesion enhancement effect/unit weight on both occasions when the transect was occupied. The exception to this occurred in the central and south central portions of the transect, where the recovered material was either inactive or significantly inhibitory. At one of the stations in the southern portion of the transect (station 6), the materials isolated from a daytime sample of the CSW had a significant inhibitory effect on the adhesion of the test cells; the materials isolated from the SUW at the same station showed adhesion enhancement activity. Thus, vertical movements of active material must be accompanied by horizontal displacements driven by ocean currents.

To this point, it is significant that the major westward advection of surface waters in the eastern Caribbean occurs in the south central portion (between 12° and 14°N) and flows in this area are largely restricted to the upper 100 m where velocities of greater than 70 cm/sec have been observed (Gordon, 1967; Atwood, Polifka and Duncan, 1975). Geostrophic calculations using data collected during the October 1974 and February 1975 transects generally confirm this advection (Atwood and Duncan, in preparation).

The role of cellular exudates in promoting microbial productivity has been suggested by a number of investigators (Hale and Tosteson, 1975; Nalewajko, Dunstall and Shear, 1976). At least a portion of the cellular exudates of marine bacteria and phytoplankton are high molecular weight organics that promote the adhesion and aggregation of micro-algal cells (Tosteson and Corpe, 1975). The effect of this phenomenon on the growth and productivity of these populations is not clear at this time. However, alterations in the surface properties of cells have been associated with the initiation of cell division (Edelman, 1976). Thus the adhesion and/or aggregation of micro-algal cells might well be a factor in the control of the growth of these populations.

The high molecular weight, adhesion enhancing material isolated from the cultures of marine bacteria and micro-algae, and from seawater samples taken off the south coast of Puerto Rico appears to be organic in nature (Tosteson and Corpe, 1975; Tosteson, Atwood and Tsai, 1976). The active material appears to be only a small percentage of the crude material (1%, wt./wt.).

The existence of areas of inhibition and inactivity in the south central region of the eastern Caribbean suggests the presence of specific inhibitory substances. The inactivity of the adhesion-enhancing materials has been reported to be inhibited by certain low molecular weight sugars (Tosteson and Zaidi, 1974). The relation between the reported inhibitory effect of low molecular weight sugars and these high molecular weight materials is at present being investigated. Whether or not this activity is due to a particular compound or a group of compounds has yet to be demonstrated. Also, whether or not the active material in the CSW and SUW is the same or changes within the same water mass is not clear at this point. At present we are working to answer these questions.

5. ACKNOWLEDGEMENTS

Funds for this project were provided by the Department of Marine Sciences, the Comité de Investigaciones, the University of Puerto Rico (Mayaguez) and the Economic Development Administration of the Commonwealth of Puerto Rico. The authors wish to thank Mrs. Vangie Hernández for her illustrations.

6. REFERENCES

Atwood, D.K., J.R. Polifka and C.P. Duncan, Temporal variations in current transport in the 1975 eastern Caribbean Sea. Paper presented at the Associated Island Marine Laboratories of the Caribbean Meeting, St. Croix, Virgin Islands, 2-5 May 1975

Edelman, M., Surface modulation in cell recognition and cell growth. Science, 192:218-26 1976

Fogg, G.E., The production of extracellular nitrogenous substances by a blue-green alga. 1952 Proc.R.Soc.Ser.B., 139:372-97

Gordon, A.I., Circulation of the Caribbean Sea. J.Geophys.Res., 72(4):6207-23 1967

Hale, D.R. and T.R. Tosteson, Interaction of marine microbial populations. In Proceedings of the 11th Meeting of the Association of Island Marine Laboratories of the Caribbean, 1975 (in press)

Hoyt, J.W., High molecular weight substances in the sea. Mar.Biol., 7:93-9 1970

Kester, D.R. et al., Preparation of artificial seawater. Limnol.Oceanogr., 12:176-9 1967

Nalewajko, C., T.G. Dunstall and H. Shear, Kinetics of extra-cellular release in axenic 1976 algae and in mixed algal-bacterial cultures: significance in estimation of total (gross) phytoplankton excretion rates. J.Phycol., 12:1-5

Samuel, S., N.M. Shah and G.E. Fogg, Liberation of extra-cellular products of photosynthesis 1971 by tropical phytoplankton. J.Mar.Biol.Assoc.U.K., 51:793-8

Sirotkina, I.S., et al., Use of cellulose sorbents and sephadexes in the systematic analysis 1974 of organic matter in natural water (MS)

Thomas, J.P., Release of dissolved organic matter from natural populations of marine phyto- 1971 plankton. Mar.Biol., 11:311-23

Tosteson, T.R. and W.A. Corpe, Enhancement of adhesion of the marine Chlorella vulgaris by 1975 polymers from the sea and exudates from microbial cultures. Can.J.Microbiol., 21:1025-31

Tosteson, T.R. and B.R. Zaidi, Surface active macromolecules in the marine environment: a sugar specific, lectin like activity. In Proceedings of the 4th Symposium on Food and Drugs from the Sea (in press)

Tosteson, T.R., D.K. Atwood and R.S. Tsai, Surface active organics in the Caribbean Sea. 1976 In Oceans '76, Second Annual combined conference sponsored by the Marine Technology Society and the Institute of Electrical and Electronics Engineering. Washington, D.C., Marine Technology Society and Institute of Electrical and Electronics Engineering, pp. 13C1-13C7

Tosteson, T.R., B.R. Zaidi and D.R. Hale, Surface active organics in the Caribbean Sea. In Proceedings of the Tenth Meeting of the Association of Island Marine Laboratories of the Caribbean (in press)

Zaidi, B.R. and T.R. Tosteson, The differential adhesion of Chlorella vulgaris during the 1972 cell cycle. Proc.Int.Seaweed Symp., 7:323-8

A NEPHELOID LAYER ASSOCIATED WITH THE GUIANA CURRENT

by

K.L. CARDER, S.I. McCLELLAND
and P.R. BETZER
University of South Florida
St. Petersburg, Florida 33701

D.R. KESTER
University of Rhode Island
Kingston, Rhode Island 02881

CONTENTS

1. INTRODUCTION
2. BACKGROUND
3. EXPERIMENTAL PROCEDURES
4. RESULTS AND DISCUSSION
5. SUMMARY
6. ACKNOWLEDGEMENTS
7. REFERENCES

Abstract

Light-scattering, suspended, particulate matter, and particle size distribution measurements were taken along the Guyanan and Venezuelan shelves during autumn 1974. A near-bottom nepheloid layer was found along the entire study area. It was generally about 30 m thick and at least 50 nautical miles wide for a transect of the shelf just to the south of the Orinoco River. The landward portion of the nepheloid layer could not be described since ship operations were restricted to beyond the 12-mile territorial limit.

The offshore waters were clear (SPM = 10 µg/l; $\beta 45 = 0.01$ m^{-1} steradian^{-1}) while the nepheloid waters were extremely turbid (SPM = 1 903 µg/l; $\beta 45 = 0.35$ m^{-1} steradian^{-1}). Relationships between light-scattering and SPM values were developed to provide additional SPM data points from the light-scattering profiles. The rate of sediment transport by the Guiana Current nepheloid layer was estimated to be 0.75 to 1.30 short tons/sec or about 7 percent to 12 percent of the average rate at which sediment is delivered to the oceans by the Amazon River.

Resumen

En el otoño de 1974, se midió, en las aguas de las plataformas continentales de Guyana y de Venezuela, la dispersión de la luz y la distribución de las partículas de materia en suspensión, y de sus tamaños, encontrándose, a lo largo de la zona de estudio, en una sección transversal de la plataforma continental situada al sur exactamente del río Orinoco, una capa nefeloide cerca del fondo, que tenía, por lo general, unos 30 m de espesor y, por lo menos, 50 millas náuticas de anchura. No pudo describirse la parte hacia tierra de la capa nefeloide, porque los barcos no podían operar más allá del límite territorial de 12 millas.

Las aguas costeras eran claras (PS = 10 µg/l; $\beta 45 = 0{,}01$ m^{-1} esteradianes^{-1}), mientras que las aguas nefeloides eran sumamente turbias (PS = 1 903 µg/l; $\beta 45 = 0{,}35$ m^{-1} esteradianes^{-1}). Se estudiaron las relaciones entre los valores de la dispersión de la luz y de la PS a fin de proporcionar nuevos datos de la PS basados en los perfiles de dispersión de la luz. Se calculó que la velocidad a que transporta los sedimentos la capa nefeloide de la corriente de Guyana sería de 0,75 a 1,30 toneladas cortas por segundo, es decir, del 7 al 12 por ciento, aproximadamente, de la velocidad media a la que el río Amazonas transporta los sedimentos a los océanos.

1. INTRODUCTION

The transport of particles of mainly Amazon and Orinoco origin into the deep Caribbean Sea has been estimated by van Andel (1967) to be as great as 95 million tons annually. This estimate was based largely on deltaic sediment thicknesses and not on direct observations. The Amazon-derived materials found near the Orinoco River contain generally coarser particles (van Andel, 1967) than do those of Orinoco origin. One of the aims of TRIDENT Cruise TR 158 to the southeast entrances to the Caribbean Sea was to attempt to identify differences, e.g. mineralogic, optical, size, chemical, in particulate matter from these major river sources.

The purpose of this paper is to report the distribution and transport of suspended particles along the Guyanan and Venezuelan shelves in order to evaluate the contribution that nepheloid layers make in transporting eastern-derived sediments (probably from the Amazon) into the Caribbean Sea.

2. BACKGROUND

The area of study is shown in Fig. 1. It extends from Guyana into the southeastern corner of the Caribbean Sea. The major sources of detrital suspended material to the area are the Amazon and Orinoco Rivers, with only minor amounts being supplied by the coastal rivers (Reyne, 1961). The major transport mechanisms for sediments from the east include the Guiana Current on the outer shelf and wave-driven, longshore currents nearshore (Gibbs, 1974). Vast migrating mudbanks have been reported along the coast of Guyana (Demerara Coastal Investigations, 1962), and a line of demarcation between highly turbid nearshore waters and clearer shelf waters was sharply visible about two miles from shore near Georgetown, Guyana during TRIDENT Cruise TR 158. Waves and a large tidal range (of about 2 m near the Orinoco) contribute to the turbulent energy available to suspend this nearshore sediment component, estimated to be from 150 to 200 million tons annually (Demerara Coastal Investigations, 1962).

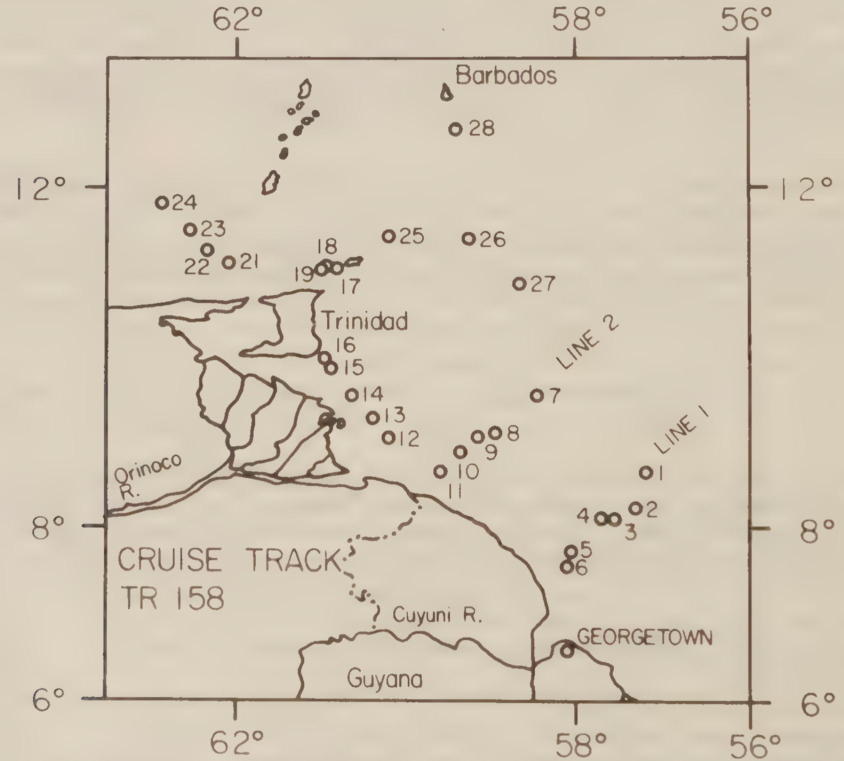

Fig. 1 Study area and station locations for TRIDENT Cruise TR 158

The transport of sediment along the outer shelf is generally poorly known. This may be due in part to the complicated circulation along the northeast South American shelf, especially near the Amazon River. In this region the oxygen-rich North Brazilian Coastal Current curves east to make up much of the Equatorial Under-Current (Metcalf and Stalcup, 1967; Cochrane, 1968). At this point, the Amazon River effluent might be expected to be carried to considerable distances offshore and the North Equatorial Current to move southward toward the coast to contribute to the formation of the Guiana Current (Metcalf, 1968). This would explain the presence of a brackish water lens well off the continental shelf north of the Amazon with relatively high salinities found closer to shore as described in Ryther et al. (1967).

Such circulation patterns would suggest that, aside from the transport of particles by the longshore currents, the Guiana Current could be relatively free of particles of Amazon origin except when the brackish water lens is present or when shelf sediments are suspended in a near-bottom nepheloid layer.

3. EXPERIMENTAL PROCEDURES

TRIDENT Cruise TR 158 (see Fig. 1) departed from Georgetown, Guyana, 15 October 1974 and was terminated in Bridgetown, Barbados. Of special interest in this report are the two cross-shelf transects (Stations 1 to 11) taken upstream (southeast) of the Orinoco River which permitted us to make geostrophic estimates of the velocity field across the Guiana Current. Both STD (salinity and temperature versus depth) and hydrobottle lowerings were made on these sections. In situ measurements of oxygen versus depth were made with a Backman MINOS oxygen sensor interfaced with a Bissett-Berman 9040 STD system using a single conductor electrical cable. In deep water, hydrocasts were made using eight 30-l Niskin bottles (for SPM samples) and 15 5-l Niskin bottles (with reversing thermometers) interspersed. Light-scattering determinations were made on all samples.

Particles were filtered from the 30-l samples using a closed, gravity-driven system (see Betzer et al., 1974) for SPM suspended particulate matter) determinations. The filters were pre-tared Nuclepore^R (45-mm diameter pads with .4 µm pore diameter) filter pads and were placed in falcon tubes and desiccated before weighing with a six-place balance at a shore-based laboratory.

Samples were drawn from each of the bottles for light-scattering determinations, which were performed using a Brice Phoenix (model 2000) light-scattering photometer at an angle of 45°. For the purposes of this paper these measurements were used to interpolate between SPM values so as to provide increased spatial resolution. Correlation coefficient values of better than 0.9 have been reported for comparisons between optical and SPM data (e.g. Biscaye and Eittreim, 1974; Carder et al., 1974). However, the linear coefficients change with the particle type and distribution in the ocean, so interpolation between known SPM points using a linear optical function with variable coefficients is preferable to using a fixed relationship for all samples.

In order to calculate geostrophic velocities for TR 158 both the hydrographic and STD data were needed since STD lowerings were not performed at the shallow stations (<100 m of depth). At hydrographic stations, temperature values were available only on the 5-l bottles; thus, linear interpolation and extrapolation were used to complete the data set.

A level of no motion was needed for each station in order to determine geostrophic velocities. Various methods exist for this determination: e.g., Dietrich(1937), Hidaka (1940), and Defant (1941). Current meter velocities were not available so the zero reference level was determined by other means. For the outer station pairs of Lines 1 and 2 (Stations 1 and 2, and 7 and 8), the level was taken to be the deepest standard depth because, according to the method of Defant (1941), the dynamic depth profile was nearly constant there. A secondary reference level was 600 m where the dynamic depth profile was also constant. For the next shoreward station pair, the velocity at the deepest standard depth was taken to be the same as that already found at the corresponding depth of the next seaward station pair. This procedure was performed for each station pair of each line.

The northwest transport values of water and suspended sediment for the lines were determined by overlaying respective SPM (P) and geostrophic velocity (V) cross-sections, resulting in a number of solenoids. For the i^{th} solenoid, its area (A_i) and values of P_i and V_i were determined. Then the transport of water T_w and of particulates T_p were calculated as follows:

$$T_w = \sum_{i=i}^{n} V_i A_i \ (m^3/sec),$$

$$T_p = \sum_{i=i}^{n} P_i V_i A_i \ (g/sec);$$

where V_i, A_i and P_i are in units of m/sec, m^2 and g/m^3, respectively.

4. RESULTS AND DISCUSSION

The distributions of salinity, temperature, current speed (component normal to Lines 1 and 2), and turbidity are presented in Figs. 2-11 for Lines 1 and 2. A number of the distribution characteristics will be pinpointed and discussed below.

The lowest salinity values (34 per mille) found on the two shelf transects were observed at Station 1 (Fig. 2), more than 100 nautical miles offshore. These values appear to be at the edge of a large lens of low-salinity water, undoubtedly of Amazon origin. Ryther et al. (1967) reported a lens of low-salinity water in nearly the same location and they attributed its origin to the Amazon River. This water was reported to be low in nutrients (except silica), to be low in phytoplankton in comparison to adjacent offshore waters and to be separated from the coast by a productive upwelling region. A glance at Fig. 3 confirms that geostrophic upwelling was centred at Station 5 during TR 158, and the light-scattering (Fig. 5) and SPM (Fig. 6) data show the lens (Station 1) to be low in suspended particles. These findings are in accordance with an Amazon River origin for this low-salinity water. No water of less than 35 per mille salinity was found on Line 2, but a surface lens of reduced salinity (35.2 per mille) was found near the coast (Fig. 7). This water was also very turbid (Fig. 11), probably originating from a local coastal river such as the Cuyuni River.

Lenses of warm water (T>28°C, Line 1; T>27.6°C, Line 2) mark the high-speed core of the Guiana Current (Figs. 4 and 9) moving northwestward, and turbid nepheloid layers (Figs. 6 and 11) mark the portions of the shelf where the highest currents (Figs. 4 and 9) interacted with the shelf sediments. A current reversal was found just below the Subtropical Underwater (S 36.7 per mille) which itself was quite low in particles. A current reversal was also found between Stations 8 and 9, with the southeastward-flowing offshore water much less turbid than the northwestward flowing inshore water. Rather complicated circulation patterns are reported to be prevalent in this region (Neumann, 1960; Metcalf, 1968; Cochrane, 1968; Febres, 1973 and Mazeika, 1973), with eddies often providing current reversals offshore.

The surface current speeds found in the Guiana Current were a little higher than those reported by Neumann (1960) to be in the 20-40 cm/sec range, but he provided no values for water shallower than 600 m where our velocity maxima occurred. The fact that the shelf regions where near-bottom turbidity maxima occurred also were regions where maximum near-bottom currents were found is good evidence that the technique used to provide reference speeds for sections shallower than the reference depth, 600 m, was adequate for this set of data. Ideally, current meters moored on the shelf would be best suited to the determination of shelf currents.

The transport rates of water and suspended particulate matter through the sections of Lines 1 and 2 are summarized in Table I and compared to the water and sediment discharge rates of the Amazon and Orinoco Rivers. An estimate of the sediment transported by longshore currents along the Guyana coastline is also provided (after Demerara Coastal Investigation, 1962).

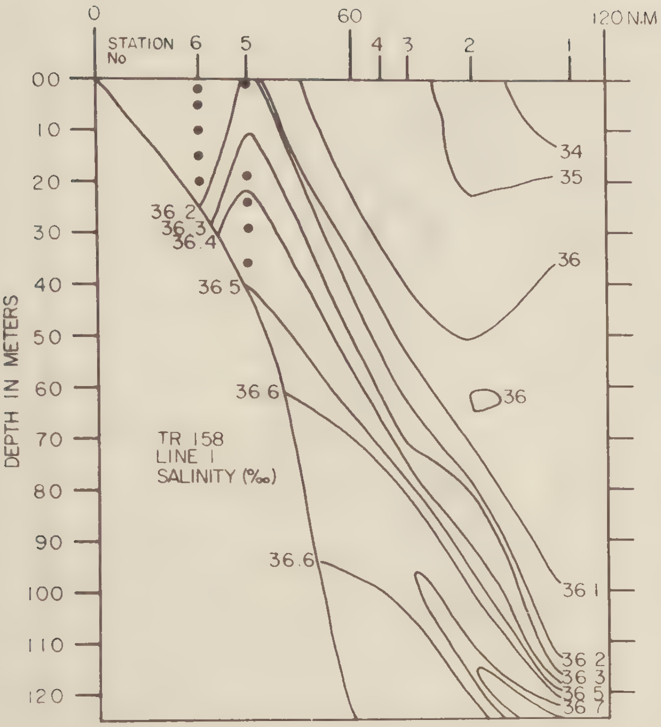

Fig. 2 Salinity section along Line 1

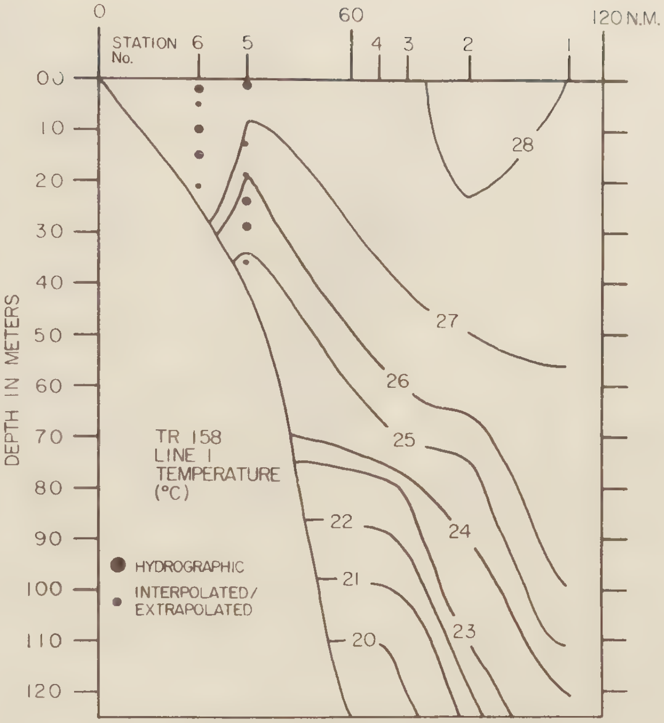

Fig. 3 Temperature section along Line 1

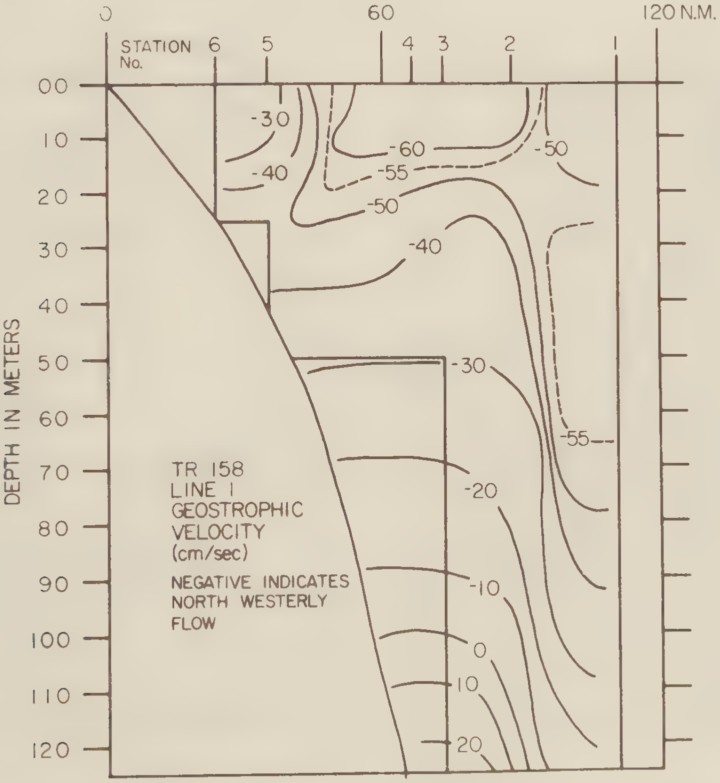

Fig. 4 Geostrophic flow field along Line 1

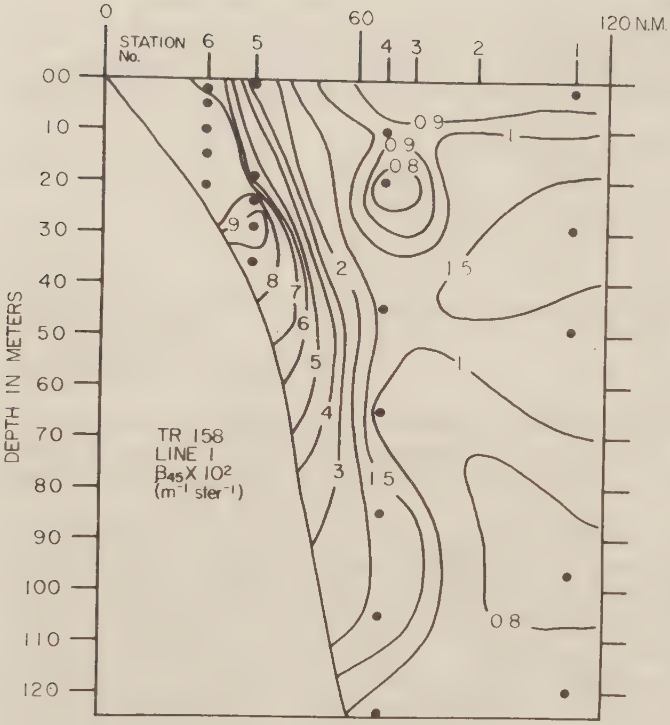

Fig. 5 Volume scattering function (β45) along Line 1

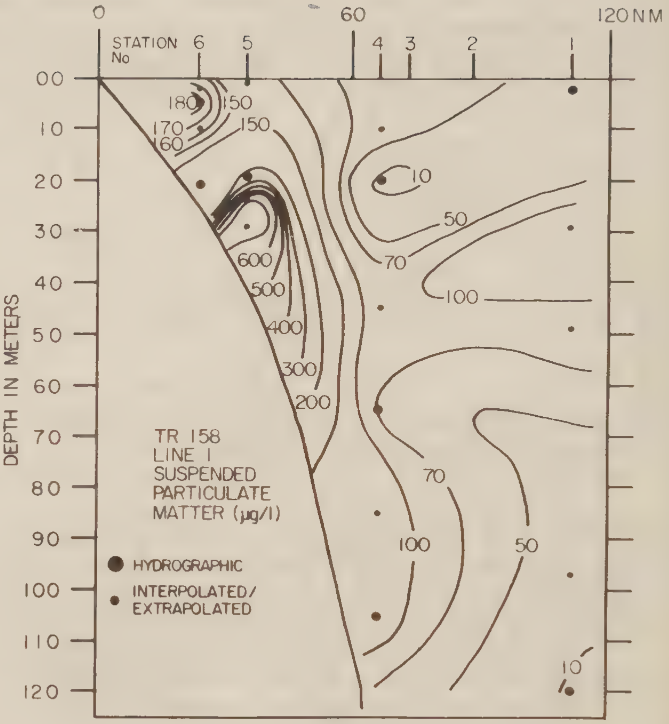

Fig. 6 Suspended particulate matter with optical interpolations along Line 1

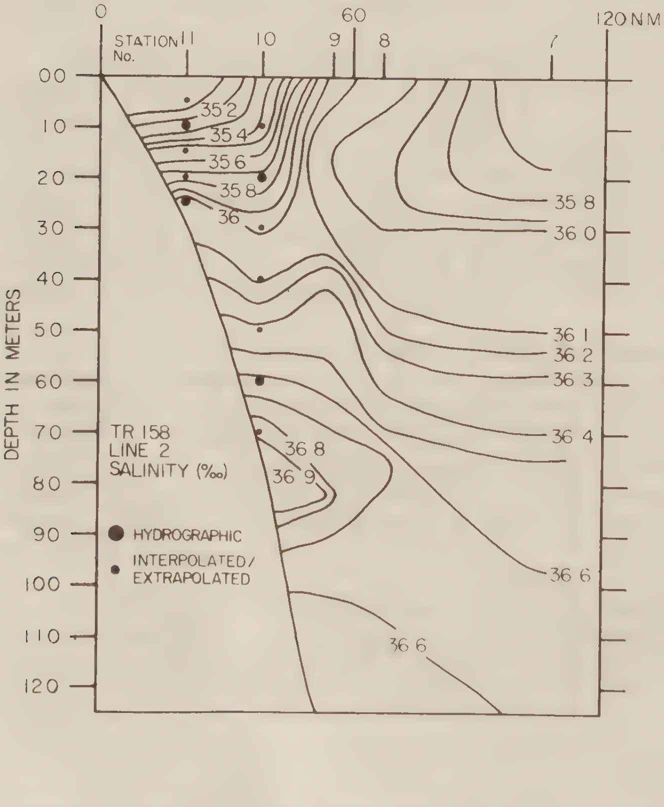

Fig. 7 Salinity section along Line 2

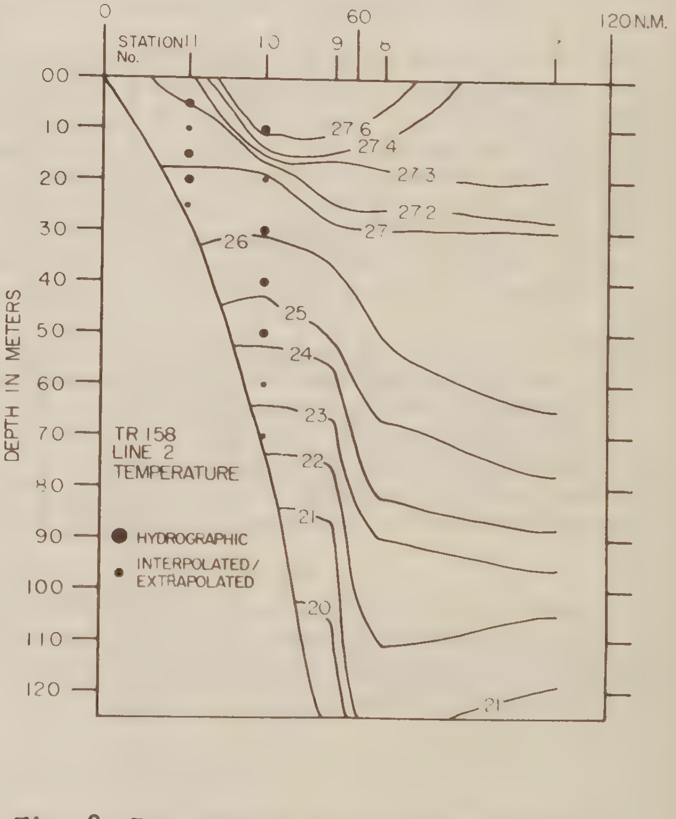

Fig. 8 Temperature section along Line 2

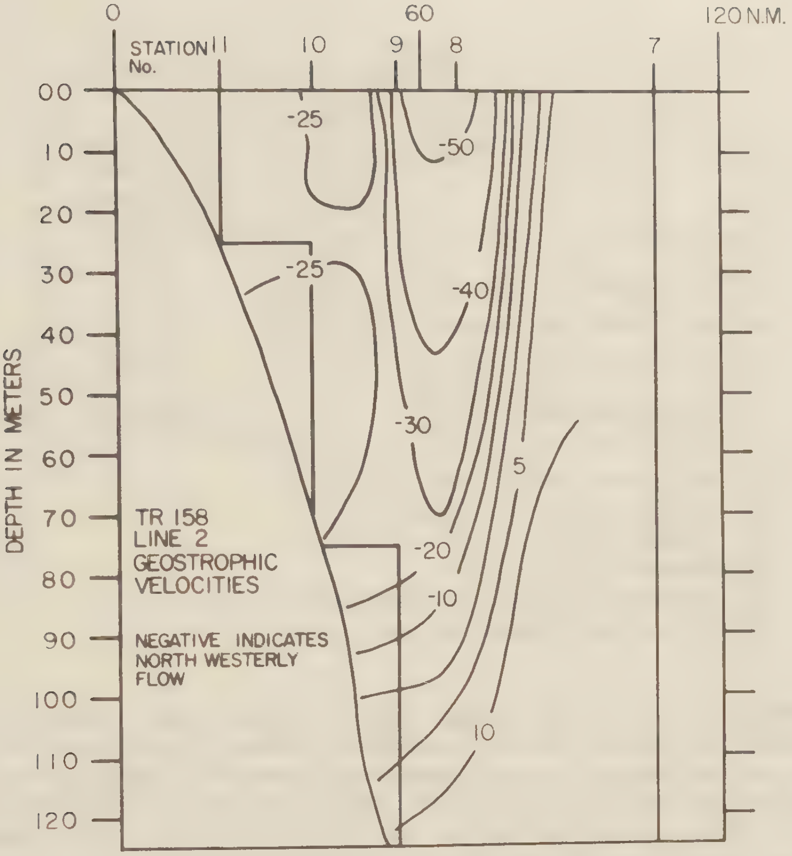

Fig. 9 Geostrophic flow field along Line 2

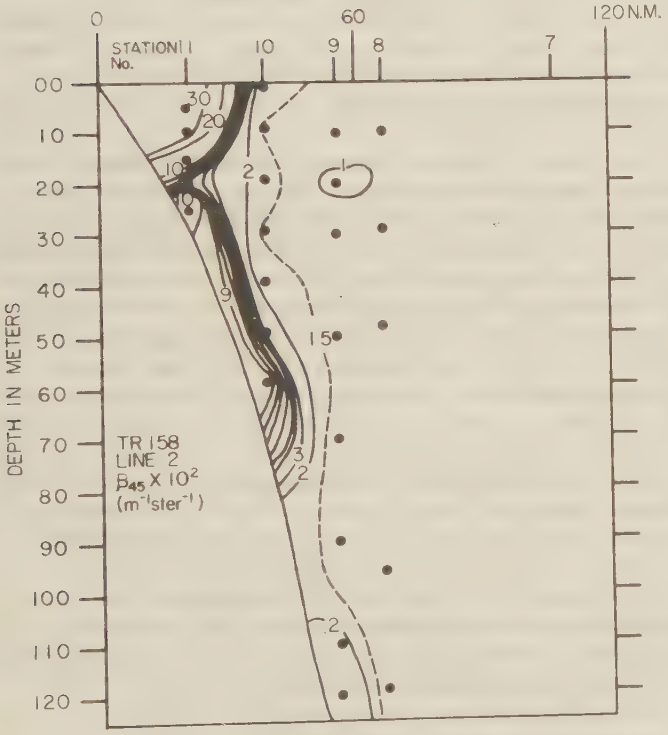

Fig. 10 Volume scattering function (β45) along Line 2

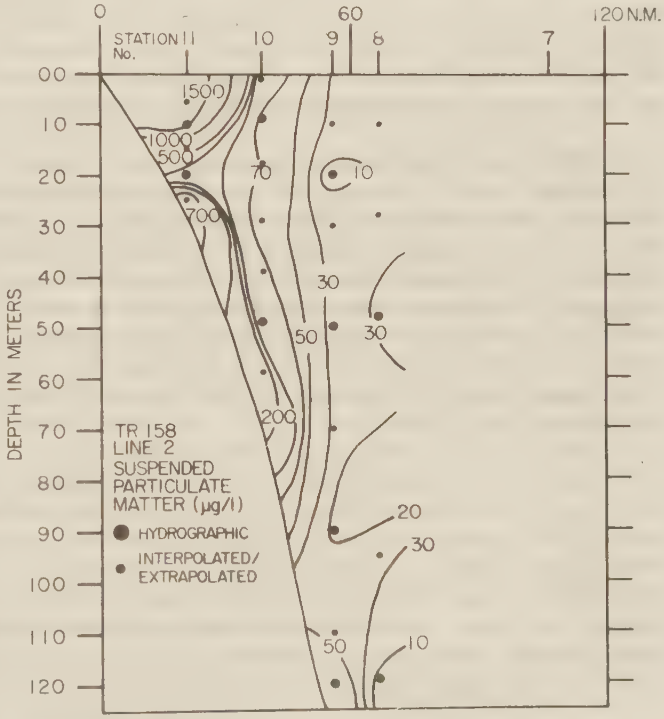

Fig. 11 Suspended particulate matter with optical interpolations along Line 2

TABLE I

Transport rates

	Water (sv.) [a]	Sediments (tons/sec)
Guiana Current (Line 1)	5.20	1.30
Guiana Current (Line 2)	1.80	0.75
Orinoco River discharge	0.017[b]	2.74[d]
Amazon River discharge	0.17[c]	11.00[c]
Longshore Current[f]		4.8-6.3[e]

a/ Sverdrup = $10^6 m^3/sec$
b/ Keller, 1962
c/ Gibbs, 1965
d/ Sánchez, 1950
e/ Demerara Coastal Investigation, 1962
f/ Based upon annual average

The volume transport rate for the Guiana Current across Line 1 was 4 times the rate across Line 2. Whether this variation was caused by spatial or temporal differences between the two locations is not certain. It could have been caused by both, since large-scale eddies (e.g.,60-180 n.mi diameter) are often found off the Guyana shelf (see Mazeika, 1973; Febres, 1974; Neumann, 1960). These transport values are from 6 percent to 17 percent of the mean annual flow-out of the Caribbean through the Yucatan Channel.

The mass transport rate of sediment carried by the Guiana Current decreased by only about 40 percent in going from Line 1 to Line 2. The nearly ten-fold increase in SPM values for the inshore station of Line 2 over those for the inshore station of Line 1 (Figs. 11 and 6) is the main reason that the percentage decrease in sediment transported is not as large as the percentage decrease in water transported by the Guiana Current.

The suspended sediment transport rates of the Guiana Current along the shelf were from 12 percent to 27 percent of the rate attributed to longshore currents. These numbers are probably conservative since no bedload contributions are included in the Guiana Current numbers. These rates of sediment transport represent 7 percent and 12 percent of the mean annual sediment discharge rate of the Amazon River and 27 percent and 47 percent of the mean annual sediment discharge rate of the Orinoco River. Including the sediment transport rate attributed to the longshore currents, the sediment transport rate along the Guyanan and Venezuelan shelf is from 50 percent to 69 percent the average sediment discharge rate for the Amazon River and from 227 percent to 302 percent the average sediment discharge rate for the Orinoco River.

Based upon the sediment distribution around Trinidad, most of the suspended sediment arriving from the southeast as well as the sediment derived from the Orinoco distributaries are either deposited in the Gulf of Paria or on the shelf north of Trinidad and Venezuela (van Andel, 1967). Practically no deposition occurs on the Atlantic shelf adjacent to Trinidad. Thus the material delivered from the southeast by the longshore current and the nepheloid layer must be deposited adjacent to the Orinoco delta, enter the Gulf of Paria, or pass through the channel between Tobago and Trinidad. Investigating this latter possibility will provide some insight into the relative importance of these two routes.

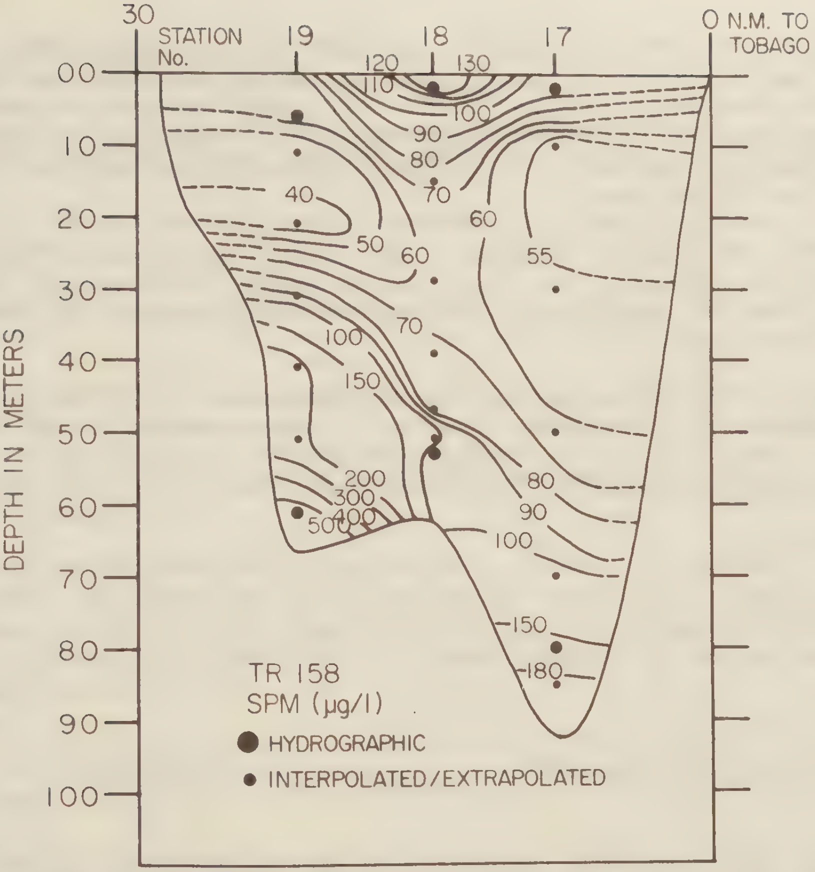

Fig. 12 Suspended particulate matter with optical interpolations on a line between Trinidad and Tobago

A cross-section of SPM was made across the passage between Tobago and Trinidad using optical interpolations between measured SPM values (Fig. 12). Unfortunately, the section did not approach as close to Venezuela as desired, leaving a portion of the passage with undetermined turbidity. The dotted lines were used to extrapolate turbidity values into this region so that an approximation to the suspended sediment transported through this passage could be made. Combining these data with an average current speed of from 1 to 2 knots (the U.S. Hydrographic Office reports its speed at the sea surface to be from 2 to 4 knots in 'Sailing Directions') provides a conservative estimate of the sediment transport rate through this passage of 0.56 to 1.12 tons/sec. These rates are from 43 percent to 149 percent of the rates determined for the nepheloid layer transported by the Guiana Current.

Since practically the entire sediment transport through the Tobago-Trinidad passage can be accounted for by the near-bottom nepheloid layer, then most of the sediment transported by the longshore current and discharged by the Orinoco River must enter the Gulf of Paria. This is in general agreement with the conclusions of van Andel (1967).

5. SUMMARY

(1) The transport of water and suspended particles by the Guiana Current was calculated for two shelf transects across the Guyanan and Venezuelan shelves.

(2) The transport rate of water by the Guiana Current was determined to be 1.8 and 5.2 Svs. (based upon geostrophic calculations) across the two transect lines, or from 6 percent to 17 percent the mean annual flow-out of the Caribbean through the Yucatan Channel.

(3) The transport rate for suspended sediment by the Guiana Current was calculated to be 0.75 and 1.3 tons/sec respectively across the two transect lines. These values are 7 percent and 12 percent of the mean annual sediment discharge rate for the Amazon River, 27 percent and 47 percent of the rate for the Orinoco River, and in the range of 12 percent to 27 percent of the rate attributed to longshore currents along the Guyana coast.

(4) Together, the sediment transport rates by the Guiana Current and the longshore current were estimated to range from 50 percent to 69 percent the mean annual discharge rate for the Amazon River and from 277 percent to 302 percent the rate of the Orinoco River.

(5) Practically the entire sediment transport through the Tobago-Trinidad passage can be accounted for by upstream measures of the transport of the near-bottom nepheloid layer. Thus, most of the sediment transported by the longshore current as well as that discharged by the Orinoco River must enter the Gulf of Paria.

6. ACKNOWLEDGEMENTS

The work reported in this paper was supported by the Office of Naval Research: Contract N00014-72-A-0363-0001 to the University of South Florida and by contract N00014-68-A-0215-0003 to the University of Rhode Island.

7. REFERENCES

van Andel, T.H., The Orinoco delta, J.Sediment.Pet., 37(2):297-310
1967

Betzer, P.R., K.L. Carder and D.W. Eggimann, Light-scattering and suspended particulate
1974 matter on a transect of the Atlantic Ocean at 11°N. In Suspended solids in water, edited by R. Gibbs. New York, Plenum, pp. 295-314

Biscaye, P.E. and S.L. Eittreim, Variations in benthic boundary layer phenomena: Nepheloid
1974 layer in the North American Basin. In Suspended solids in water, edited by R. Gibbs. New York, Plenum, pp. 227-60

Carder, K.L., P.R. Betzer and D.W. Eggimann, Physical, chemical, and optical measures of
1974 suspended particle concentrations: their intercomparison and application to the west African shelf. In Suspended solids in water, edited by R. Gibbs. New York, Plenum, pp. 173-93

Cochrane, J.D., Currents and waters of the eastern Gulf of Mexico and western Caribbean, of
1968 the western tropical Atlantic Ocean, and of the eastern tropical Pacific Ocean. Progress Report Ref. 68-8T for ONR project NR-083-036. College Station, Texas A & M University, 38 p.

Demerara Coastal Investigations, Report on siltation of Demerara Bar Channel and coastal
1962 erosion in British Guiana. Delft, Netherlands, Hydraulics Laboratory, 240 p.

Dietrich, G., Die "dynamische" Bezugsflache, ein Gegenwartsproblem der dyn. Ozeanographie.
1937 Ann.Hydrogr.Marit.Meteorol., 65:506-19

Defant, A., Die absolute Topographie des physikalischen Meeresniveaus und der Druckflächen,
1941 sowie die Wasserbewegungen im Atlantischen Ozean. Wess.Ergebn.Dtsch.Atl.Exped. Meteor., 6(2):191-260

Febres Ortega, G., Circulación oceánica y estratificación de las masas de agua superiores al
1974 norte de la Guayana, Publicaciones de la Comisión Organizadora de la III Conferencia de la Naciones Unidas Sobre Derecho Del Mar, 1-27

Gibbs, R.J., The geochemistry of the Amazon river basin, Ph.D. Thesis, University of
1965 California, San Diego, 96 p.

Gibbs, R., The suspended material of the Amazon shelf and tropical Atlantic Ocean. In
1974 Suspended solids in water, edited by R. Gibbs. New York, Plenum, pp. 203-10

Hidaka, K., Absolute evaluations of oceanic currents in dynamic calculations. Proc.Imp.
1940 Acad.Jap., 15(8)

Keller, R., Gewässer und Wasserhaushalt des Nestlandes. Leipzig, 520 p.
1962

Mazeika, P.A., Circulation and water masses east of the Lesser Antilles. Dtsch.Hydrogr.Z.,
1973 26(2):49-73

Metcalf, W.G. and M.C. Stalcup, Origin of the Atlantic Equatorial Undercurrent. J.Geophys.
1967 Res., 72(20):4959-75

Neumann, G., Evidence for an equatorial undercurrent in the Atlantic Ocean. Deep-Sea Res.
1960 6:328-34

Reyne, A., On the contribution of the Amazon River to accretion of the coast of the Guianas.
1961 Geol.Mijnbouw, 40:219-26

Ryther, J.H., D.W. Menzel and N. Corwin, Influence of the Amazon River outflow on the ecology
1967 of the western tropical Atlantic. 1. Hydrography and nutrient chemistry.
J.Mar.Res., 25(1):69-83

Sanchez, F.K., Algunas consideraciones con respecto a la determinación del acarreo solido y
1950 su magnitud en algunos ríos de Venezuela. Rev.Col.Ing.Venez., 177:28-9

LATE CENOZOIC PALEOCEANOGRAPHY OF THE PANAMA, COLOMBIA AND VENEZUELA BASINS

by

LLOYD D. KEIGWIN, JR.
Graduate School of Oceanography, University of Rhode Island
Kingston, Rhode Island 02881, U.S.A.

CONTENTS

1. INTRODUCTION
2. METHODS
3. RESULTS
4. DISCUSSION
5. CONCLUSIONS
6. ACKNOWLEDGEMENTS
7. REFERENCES

Abstract

Plankton foraminifera of Pliocene and Pleistocene age have been examined in Deep Sea Drilling Project (DSDP) Sites of the Panama Basin (Pacific Ocean) and Colombia and Venezuela Basins (Atlantic Ocean) to determine biogeographic and paleoceanographic features that might assist in timing the separation of Atlantic and Pacific tropical planktonic faunas, and hence, the development of the Panama Isthmus. Previous studies have suggested a Late Miocene to Middle Pliocene occurrence of this event. Percent abundance of the cool-water planktonic foraminifera *Neogloboquadrina pachyderma* (Ehrenberg), and the frequency oscillations of its cooler, sinistral phenotype are useful in this regard. The Early Pliocene of the Panama Basin (DSDP 157) and the Colombia Basin (DSDP 154A) contain abundant sinistral *N. pachyderma*. The sinistral form is about half as abundant in the Early Pliocene of the more eastern Caribbean (DSDP 148 and 149, Venezuela Basin), and only the dextral phenotype is present in the more northern Panama Basin (DSDP 158). This biogeographic distribution suggests that there was an exchange of surface waters between these sites in the Early Pliocene and that the Isthmus of Panama was not yet fully developed.

Resumen

En los lugares de la cuenca panameña (Océano Pacífico) y de las cuencas de Colombia y de Venezuela (Océano Atlántico) indicados por el Proyecto de exploración de mares profundos (DSDP) se han examinado foraminíferos planctónicos del plioceno y pleistoceno, a fin de determinar las características biogeográficas y paleoceanográficas que podían contribuir a determinar la época de separación de las faunas planctónicas tropicales del Atlántico y del Pacífico y, por consiguiente, de la formación del istmo de Panamá, que según estudios anteriores se habría producido en un período comprendido entre el mioceno superior y mediados del plioceno. La abundancia, en tanto por ciento, de los foraminíferos planctónicos de agua fría, *Neogloboquadrina pachyderma* (Ehrenberg), y las frecuentes oscilaciones de su fenótipo sinixtrorso, más frío, son útiles a este respecto. Los sedimentos del plioceno inferior de la cuenca panameña (DSDP 157) y de la cuenca colombiana (DSDP 154A) contienen en abundancia el *N. pachyderma* sinixtrorso, mientras que en los sedimentos del plioceno

inferior de la parte más oriental del Caribe (DSDP 148 y 149, cuenca venezolana) abunda mucho menos, aproximadamente la mitad, y en la parte más septentrional de la cuenca panameña (DSDP 158) sólo se encuentra el fenótipo dextrorso. Basándose en esta distribución biogeográfica, puede afirmarse que hubo un intercambio de aguas superficiales entre estos lugares durante el plioceno inferior, y que el istmo de Panamá no se había formado todavía completamente.

1. INTRODUCTION

Deep Sea Drilling Project (DSDP) Site 157 was located in the Panama Basin on the Carnegie Ridge to help determine the oceanographic history of the basin (Heath and van Andel, 1973; Fig. 1). DSDP 154A was located in the Colombia Basin (Fig. 1) to record oceanographic effects of the Late Cenozoic closing of the Panama Isthmus and to provide a complete Late Cenozoic type section for micropaleontological work (Edgar *et al.*, 1973). Studied together, both sites are useful in determining paleoceanographic change brought about by the completion of the Panama land bridge. The final stages of the tectonic separation of the tropical Atlantic and Pacific Oceans was recently thought to have occurred in the Late Miocene or earliest Pliocene (Whitmore and Stewart, 1965; Woodring, 1966; Kaneps, 1970; Emiliani *et al.*, 1972; Parker, 1973; Casey *et al.*, 1975; Rosen, 1975; and Keigwin, 1976), but a more recent detailed biogeographic study has placed it in the middle of the Pliocene (Saito, 1976). Based on his study of coiling direction changes in the planktonic foraminiferal genus *Pulleniatina* (Cushman) from paleomagnetically dated piston cores in the Atlantic, Pacific and Indian Oceans, Saito (1976) suggests that the tropical marine connexion across the isthmus was severed about 3.5 million years (MY) ago.

DSDP 157 is a normal pelagic carbonate sequence, but DSDP 154A consists of two lithologic units: a normal pelagic carbonate sequence 153 m thick abruptly overlying a terrigenous-pyroclastic turbidite sequence (Fig. 2). Shipboard workers (Edgar *et al.*, 1973) suggested that the change in sedimentary regime was due to the uplift of the site which they associated with the block faulting marking one step in the closure of the isthmus. This study is part of a larger biogeographic study of the eastern tropical Pacific and western tropical Atlantic. This paper will demonstrate that the Colombia and Venezuela Basins share Early Pliocene faunal elements (sinistral *N. pachyderma*) with the cooler part of the Panama Basin.

2. METHODS

The procedures followed in washing and counting planktonic foraminifera are outlined elsewhere (Keigwin, 1976). Samples were chosen at approximate 3 m intervals (Site 154A) and 4.5 m intervals (Site 157), equal to a time spacing of about 60 000 years. Site 154A was more intensively sampled below 123 m (Fig. 2) and only Early Pliocene samples were examined from Sites 148 and 149. The large gaps between samples are due to either drilling disturbance of the section or incomplete core recovery (Edgar *et al.*, 1973; van Andel *et al.*, 1973).

3. RESULTS

The Early Pliocene sediments of both the Panama and the Colombia Basins are marked by an interval of abundant *N. pachyderma* (Fig. 2). In the lowest pelagic sample of Site 154A (at 153 m, just above the terrigenous turbidite) this species is numerically insignificant, but within the overlying 10 m the abundance rises to about 20 percent of the planktonic foraminiferal fauna and then abruptly returns to low levels. A similar occurrence is seen in Site 157 with a maximum abundance of more than 30 percent of the fauna. Within this interval in each basin the specimens are about 90 percent sinistral and the rest of the fauna shows no other evidence of temperate latitude or cool-water affinity. Throughout the remainder of Site 154A, *N. pachyderma* remains dextral and is a minor faunal element with the exception of an interval of minor abundance near the Pliocene-Pleistocene boundary (Fig. 2). In the Panama Basin this species is never again as abundant higher in the section as it is in the Early Pliocene, although there are some sinistral specimens in the later part of the Pleistocene (Keigwin, 1976).

In the Venezuela Basin (Fig. 1) the lowest Early Pliocene sample of each site (Site 148, core 27, section 6, 137-140 cm; Site 149, core 11, section 6, 100-102 cm) examined contains sinistral *N. pachyderma*. In each of these two samples this phenotype comprises 11 percent of the planktonic foraminifera and in overlying samples becomes numerically insignificant.

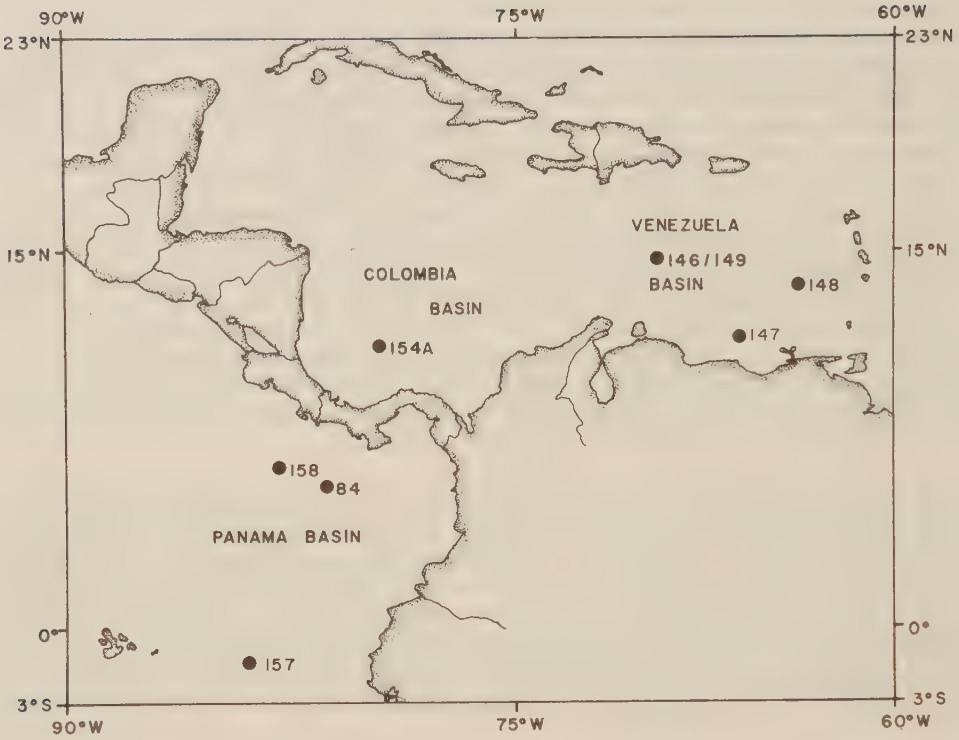
90°W
75°W
60°W
23°N
15°N
0°
3°S
VENEZUELA BASIN
146/149
148
147
COLOMBIA BASIN
154A
158
84
PANAMA BASIN
157

Fig. 1 Location of DSDP sites referred to in this study

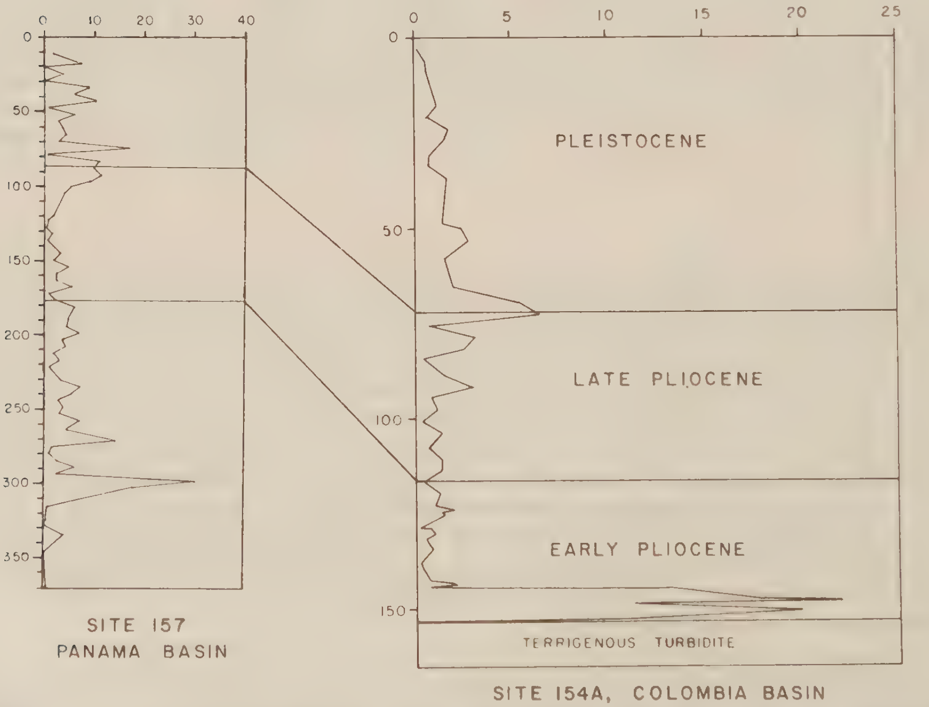

Fig. 2 Percent abundance of the planktonic foraminifera *N. pachyderma* (horizontal axis) versus depth down-core in metres (vertical axis) for DSDP Sites 157 and 154A. Note scale difference between the two sites

4. DISCUSSION

In the sedimentary sections of all three basins examined (Fig. 1), the interval with abundant sinistral N. pachyderma occurs just below a shift in coiling direction preference of the planktonic foraminiferal genus Pulleniatina from sinistral to dextral (Keigwin, in preparation). Saito (1976) concludes that this shift in Pulleniatina coiling occurred simultaneously in the Atlantic, Pacific and Indian Oceans at about 3.5 MY ago. Therefore, this acme zone of sinistral N. pachyderma in the Panama, Colombia and Venezuela Basins is somewhat older.

At the same level in Site 158 on the Cocos Ridge in the Panama Basin (Fig. 1), N. pachyderma is entirely dextral (Keigwin, 1976). At Site 157 the occurrence of the cooler-water form is attributed to increased activity of the Peru-Chile Current, possibly upwelling, and northward displacement of a higher latitude fauna. At Site 158 the presence of dextral specimens probably reflects increased upwelling, perhaps in association with the Costa Rica Dome (Wyrtki, 1964). Kennett and Vella (1975) have shown that in the Early Pliocene of the southwest Pacific the sinistral phenotype ranged into warmer waters compared with the modern ocean, but it is still probably useful as a marker of cool waters.

At the oral presentation of this work I suggested the Colombian Current as a possible means of introduction of sinistral N. pachyderma into the Colombia Basin. This swift, shallow north-flowing current is derived from the Peru-Chile Current and presently becomes an eddy in the Panama Bight (Stevenson, 1970). In the absence of the Panama Isthmus, it could have flowed directly toward the location of Site 154A. This interpretation must be reevaluated for two reasons. First, I have since found sinistral N. pachyderma in the Venezuela Basin (Sites 148 and 149). It seems unlikely that the Colombia Current, if it did indeed enter the Caribbean before the final closure of the isthmus, would carry Pacific faunal elements as far east as the Venezuela Basin. Secondly, a sedimentological and seismic reflection study of the Venezuela Basin suggests that from the Cretaceous to the Early Miocene, strong westward currents swept along the northern coast of South America and into the Pacific (Holcombe and Moore, 1977).

The significance of sinistral N. pachyderma in the Early Pliocene of the Caribbean is enigmatic. It is probable that this phenotype reflects cool water temperature at this time. This population probably was not introduced to the Colombia and Venezuela Basins by westward flowing currents because it is more abundant in the Colombia Basin (20 percent) than in the Venezuela Basin (11 percent). This population may reflect local upwelling conditions. Sinistral N. pachyderma occur rarely in the coldest Pleistocene intervals of DSDP Site 147 in the Cariaco Trench (Fig. 1), and there its presence is thought to be due to coastal upwelling (Rogl and Bolli, 1973). Finally, there may be some unknown reason for a regional proliferation of sinistral phenotypes with enough surface water communication from the Pacific to the Caribbean to maintain a breeding population. This possibility is supported by the eastward decrease in maximum percent abundance from about 30 percent to about 20 percent to 11 percent, from the Panama Basin to the Colombia Basin to the Venezuela Basin.

5. CONCLUSIONS

Sinistral N. pachyderma, which is only found in the coolest part of the Panama Basin in the Early Pliocene, is also found in the Colombia and Venezuela Basins. In each basin this occurrence is dated as somewhat older than 3.5 MY, the date given by Saito (1976) for the final closure of the marine connexion between the tropical Atlantic and Pacific Oceans. It seems likely that there was some exchange of surface waters from the Pacific to the Caribbean to maintain this inferred cool-water population.

6. ACKNOWLEDGEMENTS

I thank the Deep Sea Drilling Project for readily making samples available for my study and J.P. Kennett for his financial support. This research was supported by National Science Foundation Grant DES-74-19370 (Geological Oceanography) to J.P. Kennett.

7. REFERENCES

Casey, R.E., K.J. McMillen and M.A. Baeur, Evidence for and paleoceanographic significance
1975 of relict radiolarian populations in the Gulf of Mexico and Caribbean. *In* Abstracts with Programs, Geological Society of America Annual Meeting, Salt Lake City, pp. 1022-3

Edgar, N.T. *et al.*, Initial reports of the Deep Sea Drilling Project. Vol.15. Washington,
1973 D.C., U.S. Government Printing Office, 1137 p.

Emiliani, C., S. Gartner and B. Lidz, Neogene sedimentation on the Blake Plateau and the
1972 emergence of the Central American Isthmus. *Paleogeogr.Paleoclimat.Paleoecol.*, 11:1-10

Heath, G.R. and T.H. van Andel, Tectonics and sedimentation in the Panama Basin: geologic
1973 results of Leg 16, Deep Sea Drilling Project. *In* Initial reports of the Deep Sea Drilling Project. by T.H. van Andel. Vol. 16. Washington, D.C., U.S. Government Printing Office, pp. 899-913

Holcombe, T.L. and W.S. Moore, Paleocurrents in the eastern Caribbean: geologic evidence
1977 and implications. *Mar.Geol.*, 23:35-56

Kaneps, A.G., Late Neogene biostratigraphy (planktonic foraminifera), biogeography, and
1970 depositional history. PhD Thesis, Columbia University, New York, 185 p.

Keigwin, L.D. Jr., Late Cenozoic planktonic foraminiferal biostratigraphy and paleoceanography
1976 of the Panama Basin. *Micropaleontology*, 1976

Kennett, J.P. and P. Vella, Late Cenozoic planktonic foraminifera and paleoceanography at
1973 DSDP Site 284 in the cool subtropical South Pacific. *In* Initial reports of the Deep Sea Drilling Project. by J.P. Kennett *et al.* Vol. 15. Washington, D.C., U.S. Government Printing Office, pp. 769-99

Parker, F.L., Late Cenozoic biostratigraphy (planktonic foraminifera) of tropical Atlantic
1973 deep-sea sections. *Rev.Esp.Micropaleontol.*, 5(2):253-89

Rogl, F. and H.M. Bolli, Holocene to Pleistocene planktonic foraminifera of Leg 15, Site 147
1973 (Cariaco Basin (Trench), Caribbean Sea) and their climatic interpretation. *In* Initial reports of the Deep Sea Drilling Project. by N.T. Edgar *et al.* Vol. 15. Washington, D.C., U.S. Government Printing Office, pp. 553-616

Rosen, D.E., A vicariance model of Caribbean biogeography. *Syst.Zool.*, 24(4):431-64
1975

Saito, T., Geologic significance of coiling direction in the planktonic foraminifera
1976 *Pulleniatina*. *Geology*, 4(5):305-9

Stevenson, M., Circulation in the Panama Bight. *J.Geophys.Res.*, 75:659-72
1970

van Andel, T.H. *et al.*, Initial reports of the Deep Sea Drilling Project. Vol. 16.
1973 Washington, D.C., U.S. Government Printing Office, 949 p.

Whitmore, F.C.J. and R.H. Stewart, Miocene mammals and Central American seaways. *Science,*
1965 *Wash.*, 148(3667):180-2

Woodring, W.P., The Panama land bridge as a sea barrier. *Proc.Am.Philos.Soc.*, 110(6):
1966 425-33

Wyrtki, K., Upwelling in the Costa Rica Dome. *Fish.Bull.U.S.Fish Wildl.Serv.*, 63(2):355-72
1964

MARINE GEOLOGY RESEARCH ON THE COLOMBIAN CARIBBEAN SHELF

by

A. KLINGEBIEL
Institut de Géologie du Bassin d'Aquitaine
Bordeaux, France

G. VERNETTE
Misión Técnica Francesa
Escuela Naval
Cartagena, Colombia

CONTENTS

1. INTRODUCTION
2. SEDIMENTS FROM CARTAGENA AREA
3. SEDIMENTS FROM MAGDALENA PRODELTA AREA
4. SEDIMENTS FROM THE SHELF NORTH OF PUNTA GALERA
5. CONCLUSION
6. ACKNOWLEDGEMENTS

Abstract

A preliminary mineralogical and lithological study of sediment cores originating from the marine geology cruise carried out on the Colombian shelf between Cartagena Bay and the Magdalena delta, lead to the distinction of three sedimentary provinces and to a hypothesis concerning sediment distribution in this coastal area of the Caribbean Sea.

Resumen

En el mes de Junio, 1975, científicos franceses y columbianos hicieron investigaciones de geología marina a bordo del buque oceanográfico francés LE NOROIT, en la plataforma continental comprendido entre el delta del río Magdalena y la bahía de Cartagena. Según un estudio mineralógico y litológico preliminar de los nucleos de los sedimentos, se pueden distinguir tres provincias de sedimentación y formular una hipótesis sobre la distribución de los sedimentos en la costa colombiana del mar Caribe.

1. INTRODUCTION

During June 1975, a geological survey of the Caribbean shelf of Colombia was carried out by French and Colombian scientists, cooperating on board the French oceanographic vessel LE NOROIT.

Three studies were included in this research programme:

(1) sediments distribution between the Cartagena Bay and the Magdalena delta;

(2) recognition of eventual coastal forms and accumulations corresponding to old Quaternary low sea levels encountered in other countries, and

(3) prospection of sediments facies, belonging to such accumulations.

Three morphologically different sites of the shelf were investigated by this cruise:

(1) an irregular shelf in front of Cartagena Bay;

(2) a wide and flat shelf, north of Punta Galera, and

(3) the Magdalena prodelta, prograding directly on the slope.

The 12 piston cores (Kullemberg type) brought up from these sites were described and sampled in the Centro Nacional de Investigaciones Oceanográficos of the Escuela Naval in Cartagena. Sample analyses were conducted in the Institut de Géologie du Bassin d'Aquitaine of Bordeaux University (France).

The preliminary results of these studies are given below:

2. SEDIMENTS FROM CARTAGENA AREA

We shall compare one core taken in the bay with one from the slope outside the bay.

2.1 Core No. 75101 (water depth: 25 m; core length: 2.40 m)

This core was taken from the main channel in the middle of the straits between Castillo Grande and the Escuela Naval. It shows (Fig. 2) a 2 m thick, sorted sequence: sand and sandy clay with wood pieces followed by black yellowish silty clay and, on the top, a fine black clay with some shell debris. The finest sand fraction (50–100 microns) displays, from base to top, a decrease of quartz and dark mineral content; mica is present in every level and shell detritus and microfauna tests (mostly benthic foraminifera) increase in the upper part of the sequence. These fossils are scarce in the lower sand layer and more numerous in the upper clays (25–30 percent) in which they represent almost the entire coarse fraction. Clay minerals are montmorillonite (70 percent), illite (10 percent), and kaolinite + chlorite (20 percent). A sorting study of the lower sand level indicates a bed load transport. Upper clays result from suspension transport and deposition in a quiet lagoon; they are mixed with a notable input of biogenic calcareous material.

This sequence may be evidence of a former period of fluvial sedimentation in the bay (while the sea level was 25 m lower than now), rather than of marine transgression (between 5 000 to 1 000 years B.P.). The bay was progressively invaded by marine waters and the higher sea level induced the development of benthic marine fauna in the bay, but reduced the input of fluvial sediments. At present, the finest suspended clays reach only to the centre of Cartagena Bay.

2.2 Core No. 75104 (water depth: 182 m; core length 3.00 m)

This core comes from the slope outside Cartagena Bay. All along this core we find a thick homogeneous dark grey clay with random shell debris (Fig. 3). One can observe that the quartz is scarce and fine; the coarse sand fraction (more than 160 microns) is composed exclusively of pelagic and benthic foraminifera. In two levels (3 m and 1.70 m beneath the sea bed) some of the foraminifera are filled with pyrite and associated with numerous pellets. Lime content is generally about 20 percent, but is somewhat less in the pyritic beds. Clay content increases from 50 percent to more than 60 percent from the bottom to the top of the core. Clay mineral association is about the same as in Cartagena Bay with slightly less smectite content.

3. SEDIMENTS FROM MAGDALENA PRODELTA AREA

Five cores (Fig. 1) coming from the Magdalena prodelta allow an initial study of the sediments observed at both sides of the river mouth. Core No. 74106 (water depth 118 m; core length 4.40 m) characterizes general sediment composition in this area (Fig. 4). As everywhere in this area, we find black, silty clays with some very thin sand layers, chiefly in the lower part of the core. The sand fraction is less than 10 percent and generally 5 percent of the sediment mass. Fine sand (50–100 microns) is composed of quartz, mica and dark minerals; medium sand (100–160 microns) contains chiefly mica; coarse sand (more than 160 microns) is exclusively composed of mica, without any biogenic particle. Clay mineral association is relatively homogeneous in this area, in which the most important variation seems to be mica abundance. Clay fraction shows a high kaolinite + chlorite and chlorite + vermiculite content, which is a characteristic of the terrigenous source of suspended sediments in this zone of the Colombian shelf.

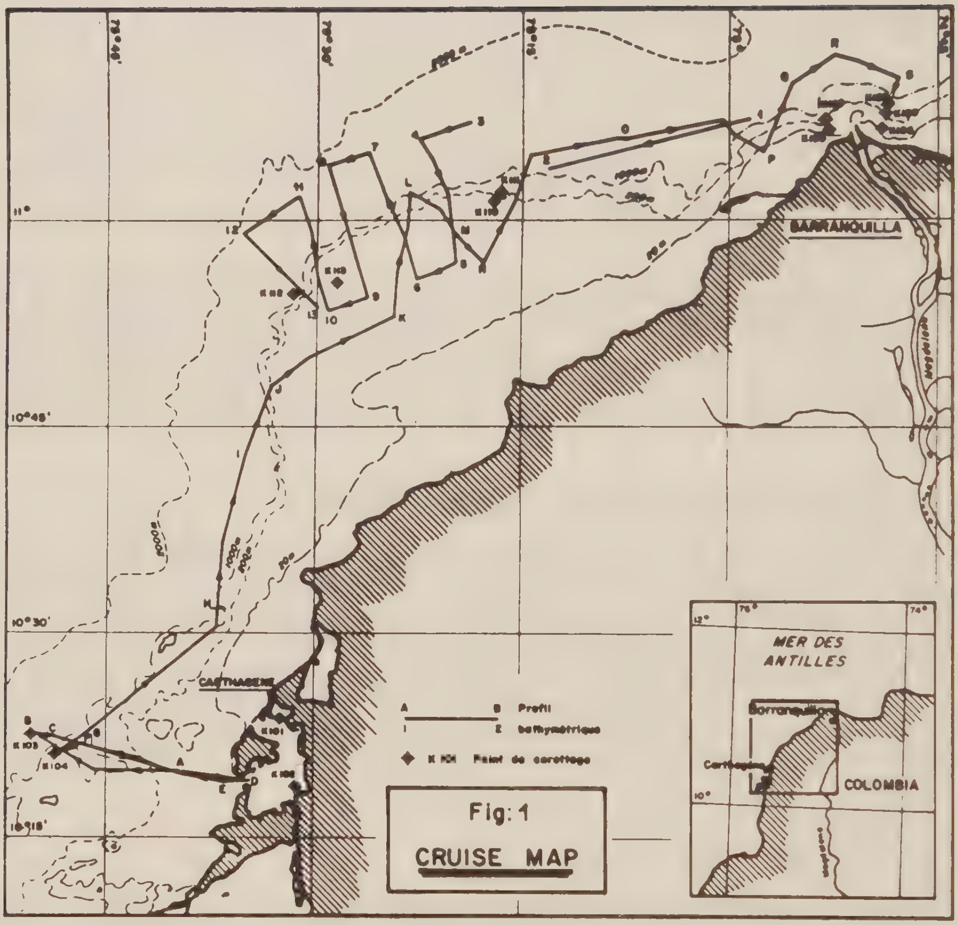
11°
10°45'
10°30'
10°15'
BARRANQUILLA
CARTHAGENE
A B Profil
1 2 bathymétrique
◆ K 101 Point de carottage
Fig: 1
CRUISE MAP
MER DES ANTILLES
Barranquilla
Cartagena
COLOMBIA

Fig. 1 Cruise map

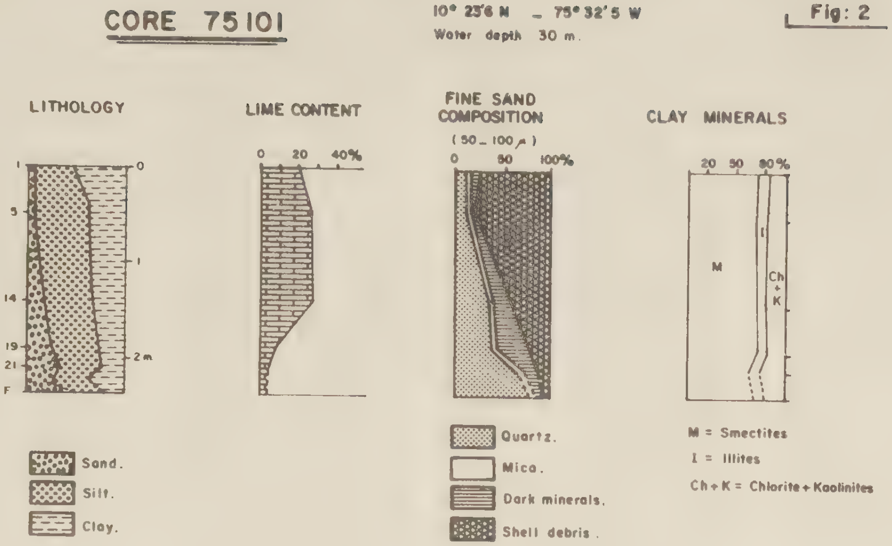
Fig: 2

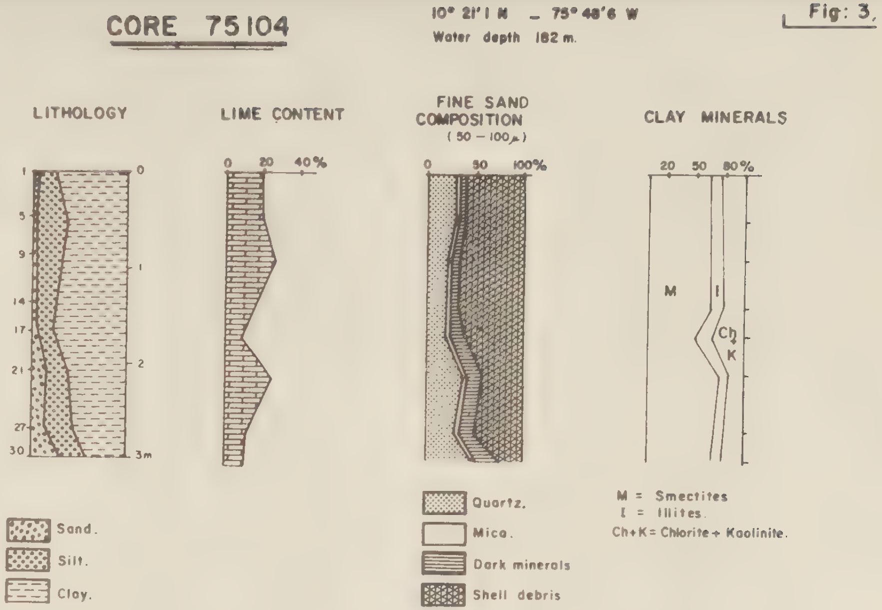
Fig: 3.

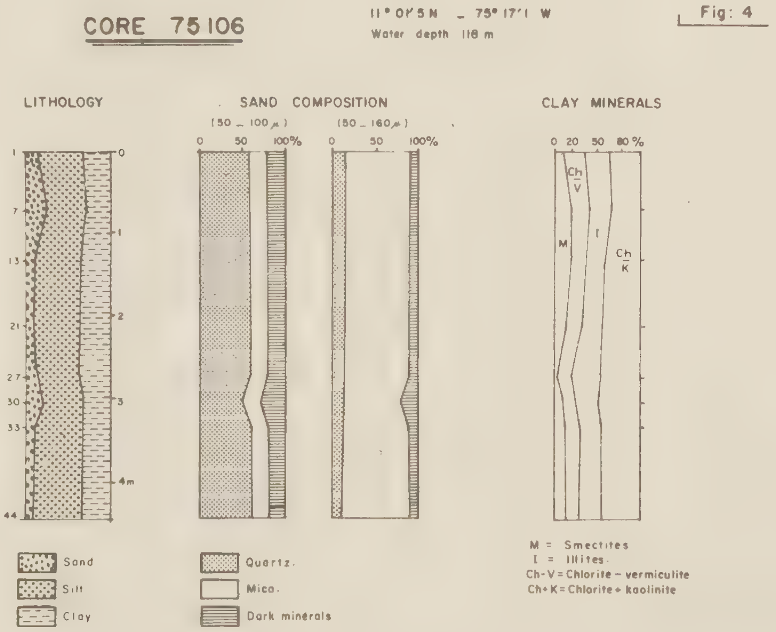
Fig: 4

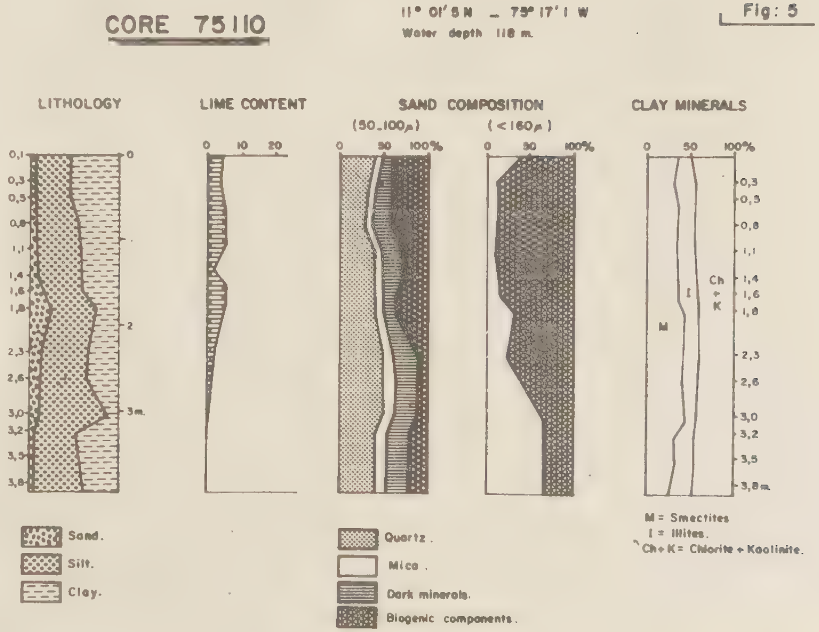
Fig: 5

Figs. 2 through 5, Core samples

4. SEDIMENTS FROM THE SHELF NORTH OF PUNTA GALERA

Four cores give data on sediment composition in the outer shelf and upper slope of this area. These cores are composed of black clays with various amounts of quartz sand, silt and biogenic components, both pelagic and benthonic organisms. Lithologic data do not allow any correlation between these cores in which we can observe irregular layering and numerous bioturbations. However, considering general lithologic composition we may use for example Core No. 75110 (water depth 118 m; core length 3.80 m). From base to top, this core is composed of a fine black clay (3.80–3.20 m), a brown dark clay with thin silty layers (at 3 m, and between 2 and 1.5 m) and a black homogeneous mud at the top.

Lime content, very small in the lower part of the core, increases to 5 percent between 3 and 1.80 m; its presence is determined by the biogenic supply from both planctonic and shelf benthonic fauna. The coarser sand fraction (more than 160 microns) contains only mica and biogenic debris.

The clay mineral association is intermediate between that found in Cartagena area and that from the Magdalena prodelta. The greater illite frequency and crystallinity comparatively to that from the prodelta area may be related to the longer oceanic transport of suspended matter issued from the river. From these data we can assume that most terrigeneous sediment supply originates from the Magdalena river; only the finest suspensates directly reach this area. Silt abundance seems to be the result of a long westward transport on the shelf where shells, silt and sands are deeply removed and mixed. Sorting studies show, from 1.80 m to the sediment surface, a decreasing sand content and an increasing amount of clay and pelagic fauna. The correlation of such a sequence with the holocene transgression needs a stratigraphic study which shall be done in the future.

5. CONCLUSION

Despite the development of some reef structures in this part of the Caribbean coast, shelf sediments are chiefly detritic. However sand deposits are scarce and located in old fluvial valleys such as the bottom of the Cartagena Bay channel. Marine deposits are composed of clays, silts and micas, mixed with various yet small amounts of biogenic calcareous particles. Sediment distribution is suggested by their composition which leads to the distinction of three sedimentary provinces:

(1) the Magdalena prodelta, covered only by terrigeneous suspended material coming from the large river plume. Sedimentation rate is probably very high;

(2) the Cartagena Bay area in which very fine terrigeneous sediments coming from the flat coastal plain, crossed by the 'Dique canal', biogenic components coming from the inner shelf and pelagic faunas are intermixed. Sedimentation rate seems to be irregular and related to morphological sites, and

(3) an intermediate area on the wide flat shelf north of Punta Galera where sediment supply is small and irregular. Fine sediments come from river suspensions and coarser particles are removed from biogenic accumulations on the shelf.

We hope that this first investigation shall be useful for building new research programmes leading to a detailed sediment map of the Colombian Caribbean coast.

6. ACKNOWLEDGEMENTS

This oceanographic cruise has been undertaken by the French Embassy in Colombia, the Centre National pour l'Exploitation des Océans (owner of the oceanographic vessel LE NOROIT) and by the Centro de Investigaciones Oceanográficas of the Escuela Naval in Cartagena, Colombia.

SUMMARY OF NOAA GEOLOGICAL-GEOPHYSICAL STUDIES DURING CICAR EXPEDITIONS

by

G. PETER
NOAA, ERL, MESA Program Office
Boulder, Colorado 80302

CONTENTS

1. INTRODUCTION
2. VENEZUELAN MARGIN, SOUTH CARIBBEAN FAULTS
3. RECENT MOVEMENTS ALONG THE 'DEAD-TRACES' OF TRANSFORM FAULTS
4. BARBADOS RIDGE
5. FRONTAL DEFORMATION
6. PLEISTOCENE-HOLOCENE SEDIMENTATION
7. REFERENCES

Abstract

The Atlantic Oceanographic and Meteorological Laboratories (AOML) of the National Oceanic and Atmospheric Administration (NOAA) have conducted marine geological and geophysical studies in the Caribbean area in the course of six expeditions between 1968 and 1972. These studies were concentrated on the Venezuela and Trinidad continental margins, on the Barbados Ridge complex, and on the Mid-Atlantic Ridge and the Demerara Abyssal Plain between the Barracuda and Vema fracture zones.

This paper presents the highlights of these studies in relation to the following topics:

(1) Venezuelan Margin, South Caribbean fault problem;
(2) Recent movements along the 'dead traces' of transform faults east of the Barbados Ridge;
(3) Structure of the Barbados Ridge;
(4) Frontal deformation of sediments: Barbados Ridge-Curacao Ridge, and
(5) Pleistocene-Holocene sedimentation event.

Resumen

Los Laboratorios Oceánicos y Meteorológicos del Atlántico del Organismo Nacional de Cuestiones Oceánicas y Atmosféricas han hecho estudios geológicos y geofísicos marinos en la zona del Caribe durante seis expediciones efectuadas entre 1968 y 1972. Los estudios versaron principalmente sobre los margenes continentales de Venezuela y Trinidad, el complejo de la cresta de Barbados, y la cresta de la metad del Atlántico y la meseta abisal de Demerara, entre las zonas de fractura de Barracuda y Vema.

En este trabajo se exponen los puntos más importantes de tales estudios, en relación con las cuestiones siguientes:

(1) El margen venezolano, el problema de la falla 'Caribe del Sur';

(2) Movimientos recientes a lo largo de las trazas muertas de las fallas de transformación al este de la cresta de Barbados;

(3) Estructura de la cresta de Barbados;

(4) Deformación frontal de sedimentos: el bajo de Barbados - bajo de Curaçao, y

(5) El fenómeno de sedimentación en el pleistoceno-holoceno.

1. INTRODUCTION

The Atlantic Oceanographic and Meteorological Laboratories (AOML) of the National Oceanic and Atmospheric Administration (NOAA) - a scientific agency within the U.S. Department of Commerce, under the auspices of CICAR investigations - conducted several marine geological and geophysical studies in the Caribbean area between 1968 and 1972.

These studies were directed toward understanding (1) the structure of the continental margin of Venezuela; (2) the structure of the continental shelf between South America and the Lesser Antilles Island Arc, with particular emphasis on the hypothetical 'South Caribbean Fault'; (3) the development of the Mid-Atlantic Ridge east of the Lesser Antilles Island Arc, and (4) the structure of the Barbados Ridge complex, including the influences of the east-west faults of the adjacent Atlantic on its development, and the geophysical evidences of the subduction process in its formation.

Geological-geophysical work was performed during the following cruises in the Caribbean area: an expedition for the purpose of tracing the El Pilar fault eastward from Trinidad and an expedition which studied the structural elements of the Barbados Ridge complex and their extension onto the South American continental shelf; one cruise devoted to the geological-geophysical study of the central Venezuelan continental shelf through examination of structural trends that extend into this area from the Lesser Antilles Island Arc and continental Venezuela; and two expeditions - one in which members of the Dirección de Geología, Ministerio de Minas e Hidrocarburos, Venezuela participated, and one in cooperation with the University of Durham, England, which studied the structure of the Barbados Ridge complex and the adjacent Atlantic Basin. On an additional expedition in the area, the NOAA-CARIB cruise, we assisted in the study of small-scale, local geological structures that were selected by the participating visiting scientists from various countries of the Caribbean area.

Most of the background research and our detailed results already have been published in the scientific literature. This summary is intended to provide only a brief description of the purpose of the NOAA/AOML CICAR related marine geological-geophysical studies, and will touch upon few of the interesting results of this work. The following topics will be discussed:

(1) Venezuelan margin, South Caribbean fault problem;

(2) Recent movements along the 'dead-traces' of transform faults east of the Barbados Ridge complex;

(3) Structure of the Barbados Ridge;

(4) Frontal deformation of sediments: Barbados Ridge-Curaçao Ridge, and

(5) Pleistocene-Holocene sedimentation event.

2. VENEZUELAN MARGIN, SOUTH CARIBBEAN FAULT

According to the now widely accepted plate tectonic interpretation of the Caribbean area of Molnar and Sykes (1969), a right-lateral strike-slip fault separates South America from the Caribbean plate (Fig. 1). The most likely locations for this hypothetical fault (Fig. 2) are: (1) the Venezuelan Basin-Curaçao Ridge contact; (2) the coast-line fault system, and (3) the El Pilar and the La Victoria faults located to the east and to the west of the Bay of Barcelona, respectively (Peter, 1972). Based on a 2 cm/y westward motion of South America (an average rate of opening of the Atlantic) and continuous movement for 50 million years (presumed initiation of subduction and the beginning of the formation of the Lesser Antilles Island Arc), approximately 1 000 km of strike-slip motion must have occurred along these faults.

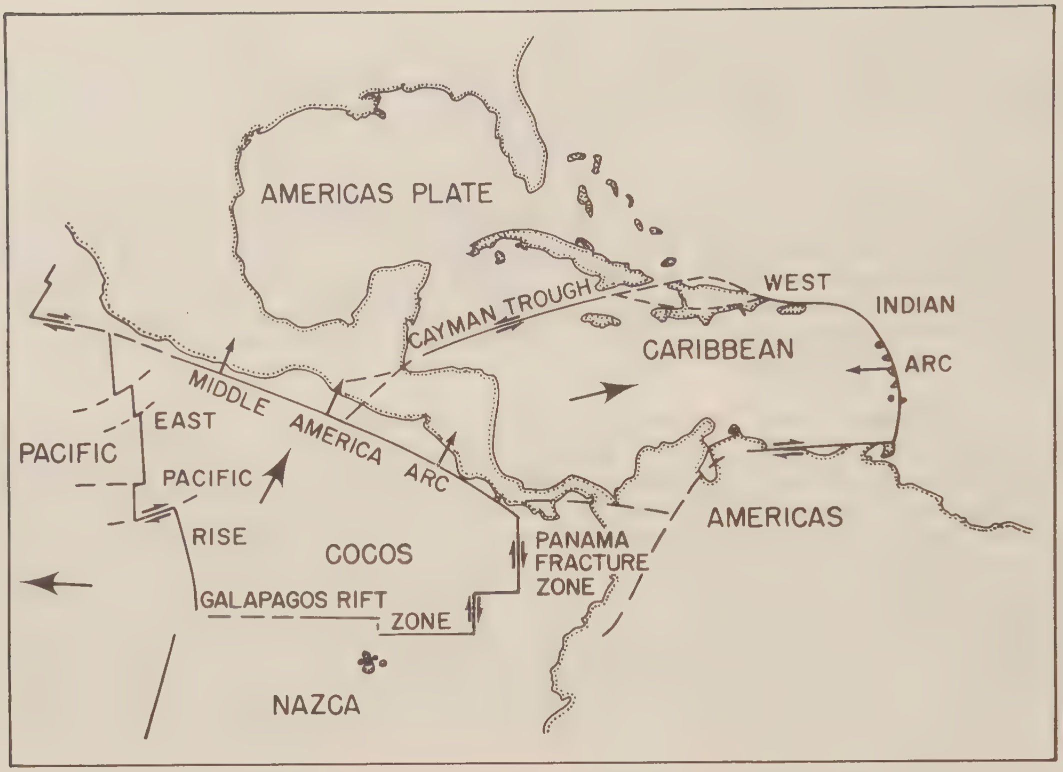
AMERICAS PLATE
CAYMAN TROUGH
WEST
INDIAN
ARC
CARIBBEAN
MIDDLE
AMERICA
ARC
EAST
PACIFIC
RISE
PACIFIC
COCOS
PANAMA
FRACTURE
ZONE
GALAPAGOS RIFT
ZONE
AMERICAS
NAZCA

Fig. 1 Distribution and relative motion of crustal plates around the Caribbean Sea (from Molnar and Sykes, 1969)

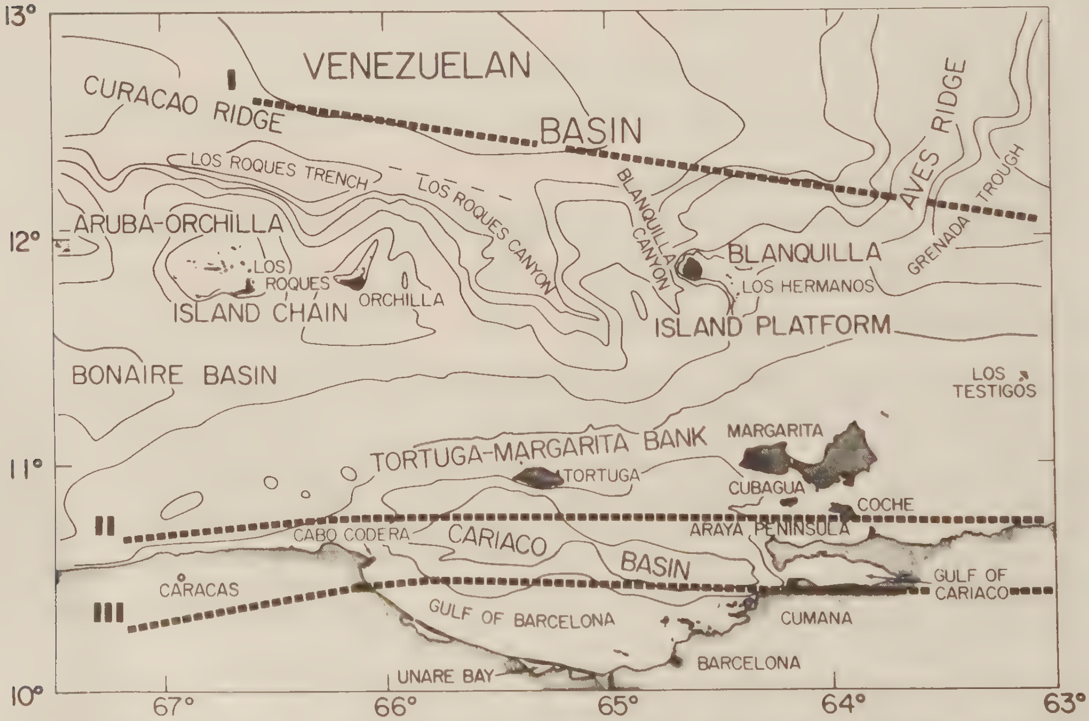
13°
12°
11°
10°
67°
66°
65°
64°
63°
I
II
III
VENEZUELAN
BASIN
CURACAO RIDGE
LOS ROQUES TRENCH
LOS ROQUES CANYON
BLANQUILLA CANYON
AVES RIDGE
GRENADA TROUGH
ARUBA-ORCHILLA
LOS
ROQUES
ORCHILLA
ISLAND CHAIN
BLANQUILLA
LOS HERMANOS
ISLAND PLATFORM
BONAIRE BASIN
LOS
TESTIGOS
TORTUGA-MARGARITA BANK
MARGARITA
TORTUGA
CUBAGUA
COCHE
ARAYA PENINSULA
CABO CODERA
CARIACO
BASIN
CARACAS
GULF OF
CARIACO
CUMANA
GULF OF BARCELONA
BARCELONA
UNARE BAY

Fig. 2 The three most likely locations of the 'South Caribbean Fault' illustrated along the north-central Venezuelan continental margin (from Peter, 1972)

Because recent reviews of the geology of the Caribbean Mountain System show that most of the major east-west oriented faults are high-angle normal faults rather than strike-slip faults (Bellizzia, 1972), and that, despite the maximum 15 km strike-slip along the El Pilar fault, dominant vertical motions are also associated with it (Salvador and Stainforth, 1968; Metz, 1968), the offshore fault systems seem to be the likely candidates for the 'South Caribbean fault'.

In summary, we believe that the following argue against large strike-slip displacements along the offshore fault systems as well: (1) the topographic continuity of the Aves Ridge into the Blanquilla Island platform (Peter, 1971); (2) the southwest extension of the Grenada Trough negative free-air gravity anomaly over the continental shelf (Talwani, 1966; Peter, 1971); (3) the uninterrupted continuity of the positive magnetic and gravity anomaly belt from Grenada to Los Testigos (Peter and Lattimore, 1971; Peter, 1972), and (4) the continuity of the large negative isostatic gravity anomaly belt (Fig. 3) from the Barbados Ridge into Trinidad and then to Venezuela (Bush and Bush, 1969).

To reconcile these observations with the requirements of the plate tectonics hypothesis for a 'South Caribbean Fault' and the need to accommodate several hundred kilometres of strike-slip motion, one may argue that there are several dozens of small faults offshore and within the Caribbean Mountain System with small, right-lateral, strike-slip motion, the aggregate of which correspond to the required displacement between the two plates. One may also assume that there are intra-crustal decollement surfaces that permit only a small fraction of the deeper plate motions to have surface manifestations, or that movements occur through creep and other forms of crustal deformation. The latter would, in essence, require a new type of plate margin, one that would allow a non-rigid behaviour of the plate margin. I believe that both intra-crustal decollement and plate margin deformation are reasonable assumptions, and have played a role in global tectonics. In the evolution of the Venezuelan continental margin there are suggestions of vertical tectonics and for considerable north-south deformation; no deformation is known, however, that appears to have been caused by hundreds of kilometres of right-lateral shear.

Another key observation of the geophysical investigations of the central Venezuelan continental margin was that the fault trends of the continental margin showed great similarities to those mapped within the Caribbean Mountain System (Peter, 1971;1972). A simplified fault map of the continental margin (Fig. 4) shows both east-west and northwest-southwest trending faults, some extending toward major faults on land. The extension of the El Pilar fault to the southern wall of the Cariaco Basin is clearly indicated, and there are strong suggestions that the controlling faults of the Los Roques canyon are related to the Urica fault. Just as on land, the east-west faults are offset by the northwest-southeast trending faults (see the offset of the east-west faults in the Cariaco Basin area), and there are clear indications on the seismic reflection records that many of these faults are currently active.

3. RECENT MOVEMENTS ALONG THE 'DEAD-TRACES' OF TRANSFORM FAULTS

The verification of the development of the Mid-Atlantic Ridge and the identification of the sea floor spreading magnetic anomaly bands east of the Barbados Ridge complex were key accomplishments of the NOAA/AOML 1971 and 1972 studies (Peter et al., 1973; Peter et al., 1974; Peter and Westbrook, 1976). The tentative identification of the magnetic anomaly lineations (Fig. 5) suggests that the Cenozoic development of the Mid-Atlantic Ridge in this area was practically identical to that of the rest of the North Atlantic.

The major magnetic offsets (transform faults) shown in Fig. 5 are also associated with topographic lineaments. The westward extension of these faults is especially well defined west of 56°W, where the flank of the Mid-Atlantic Ridge is buried and does not complicate the sea floor topography. Some of these major east-west trending fault lineaments are seen at approximately 15°20'N, 14°N, and 13°N (Fig. 6). A north-south oriented seismic reflection profile along 54°30'W (Fig. 7; line is located along the eastern edge of Fig. 6) clearly shows

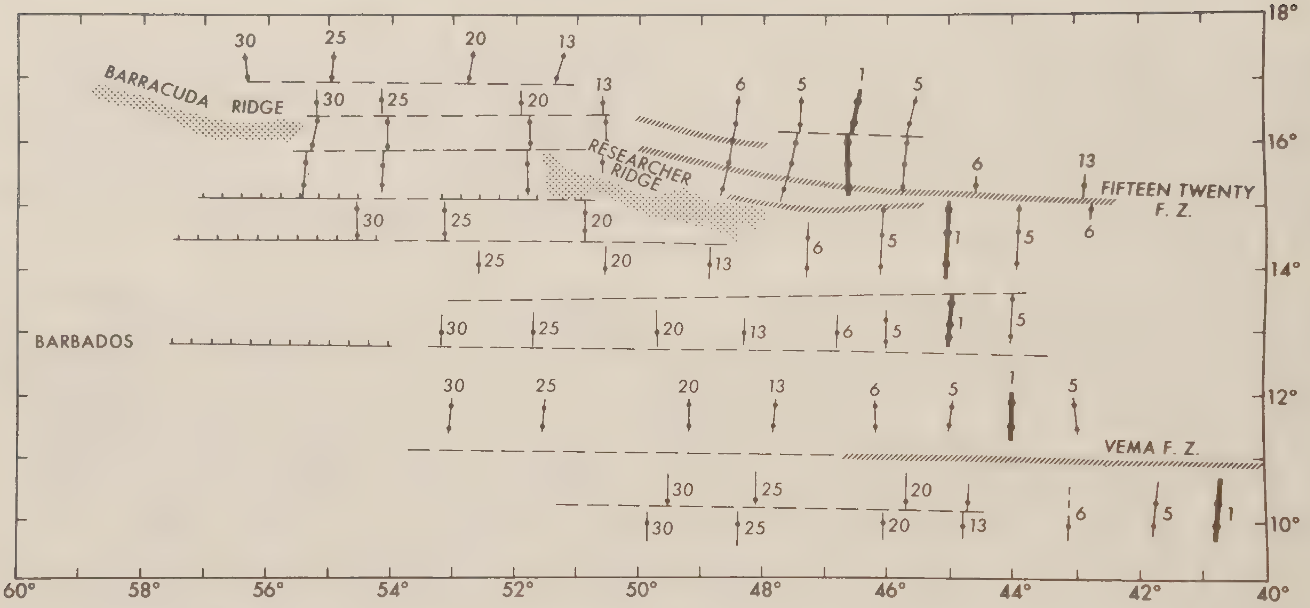

Fig. 5 Magnetic anomaly offset pattern east of the Lesser Antilles Island Arc (from Peter and Westbrook, 1976)

the 15°20'N fault (Collette and Rutten, 1972), and other major faults at 14°38'N and directly south of 13°N. Although a small step still exists on the sea floor, the trough created by the 15°20'N fault is already filled by acoustically transparent sediments; a similar trough at the 13°N fault is practically unfilled. In addition to these major faults, Fig. 8 illustrates a number of minor faults also in an area south of the Barracuda Ridge. The displacements of the reflecting horizons increase with depth, suggesting long-time tectonic activity; the steps on the sea floor suggest that this tectonic activity occurred in relatively recent time. As most faults seem to be associated with scarps or relatively steep basement slopes, it is reasonable to conclude that the origin of the tectonic activity is within the oceanic crust.

If our association of these currently active faults with the 'dead-traces' of transform faults is correct, one may conclude that either (1) the magnetic anomaly offsets may not be due entirely to transform faulting (first suggested by Ball and Harrison, 1970), or (2) these so-called 'dead-traces' of transform faults remain zones of weakness in the oceanic crust where they provide avenues for tectonic adjustments (Peter and Westbrook, 1976).

4. BARBADOS RIDGE

The Barbados Ridge complex is an outer sedimentary island arc that consists of a system of north-south and east-west oriented ridges, troughs, and other topographic lineaments. The north-south topographic elements are prominent from the continental shelf of South America northward to about 13°N; the area between 13°N and 14°N may be considered a transition zone and the east-west trending elements seem to be more abundant north of 14°N (Fig. 6).

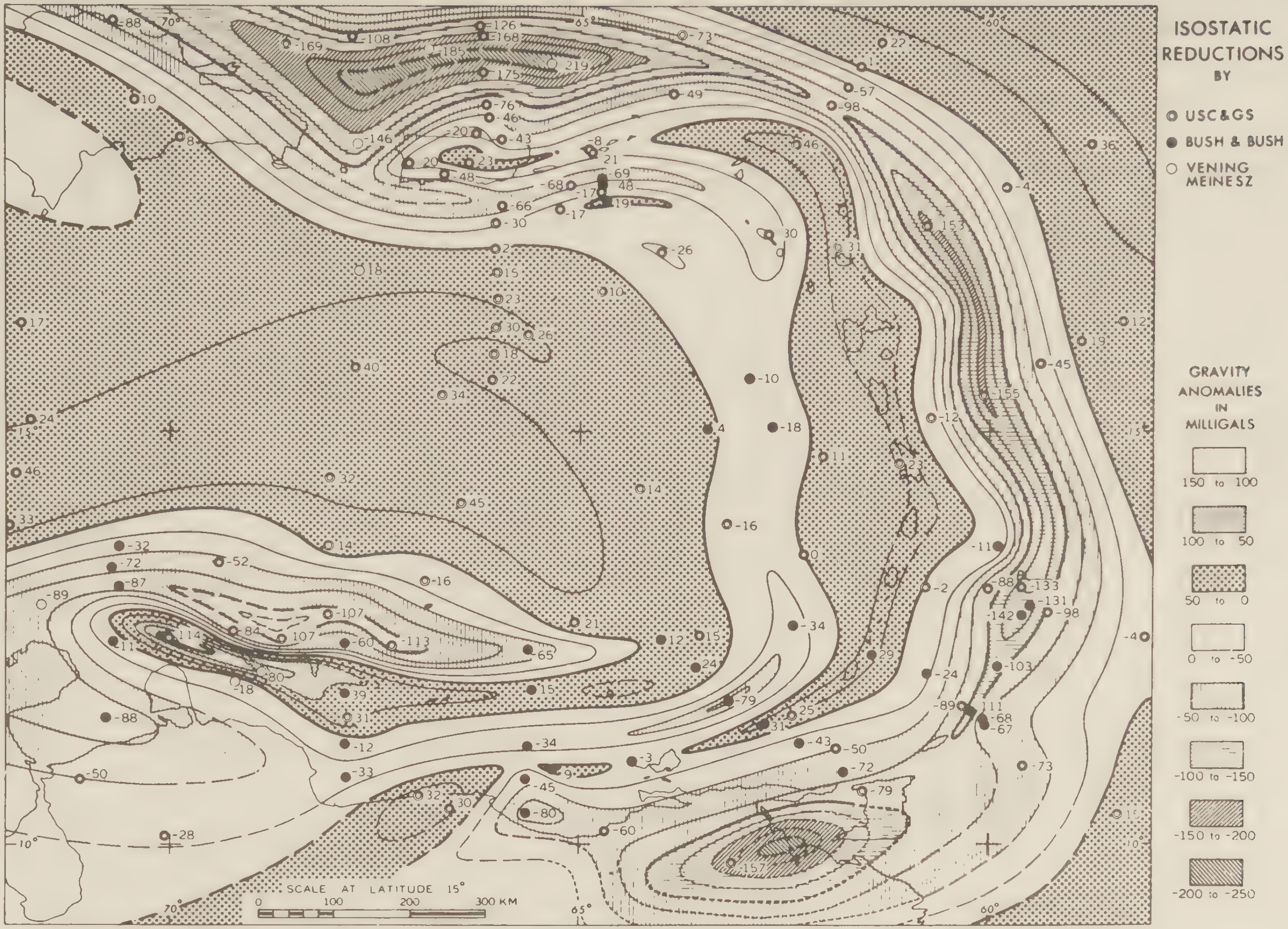
ISOSTATIC REDUCTIONS BY
USC&GS
BUSH & BUSH
VENING MEINESZ
GRAVITY ANOMALIES IN MILLIGALS
150 to 100
100 to 50
50 to 0
0 to -50
-50 to -100
-100 to -150
-150 to -200
-200 to -250
SCALE AT LATITUDE 15°
0 100 200 300 KM
70°
65°
60°
10°
15°

Fig. 3 Pratt-Hayford isostatic gravity map of the Lesser Antilles Island Arc, northern Venezuela, the Aves Ridge, and the Venezuelan Basin (from Bush and Bush, 1969)

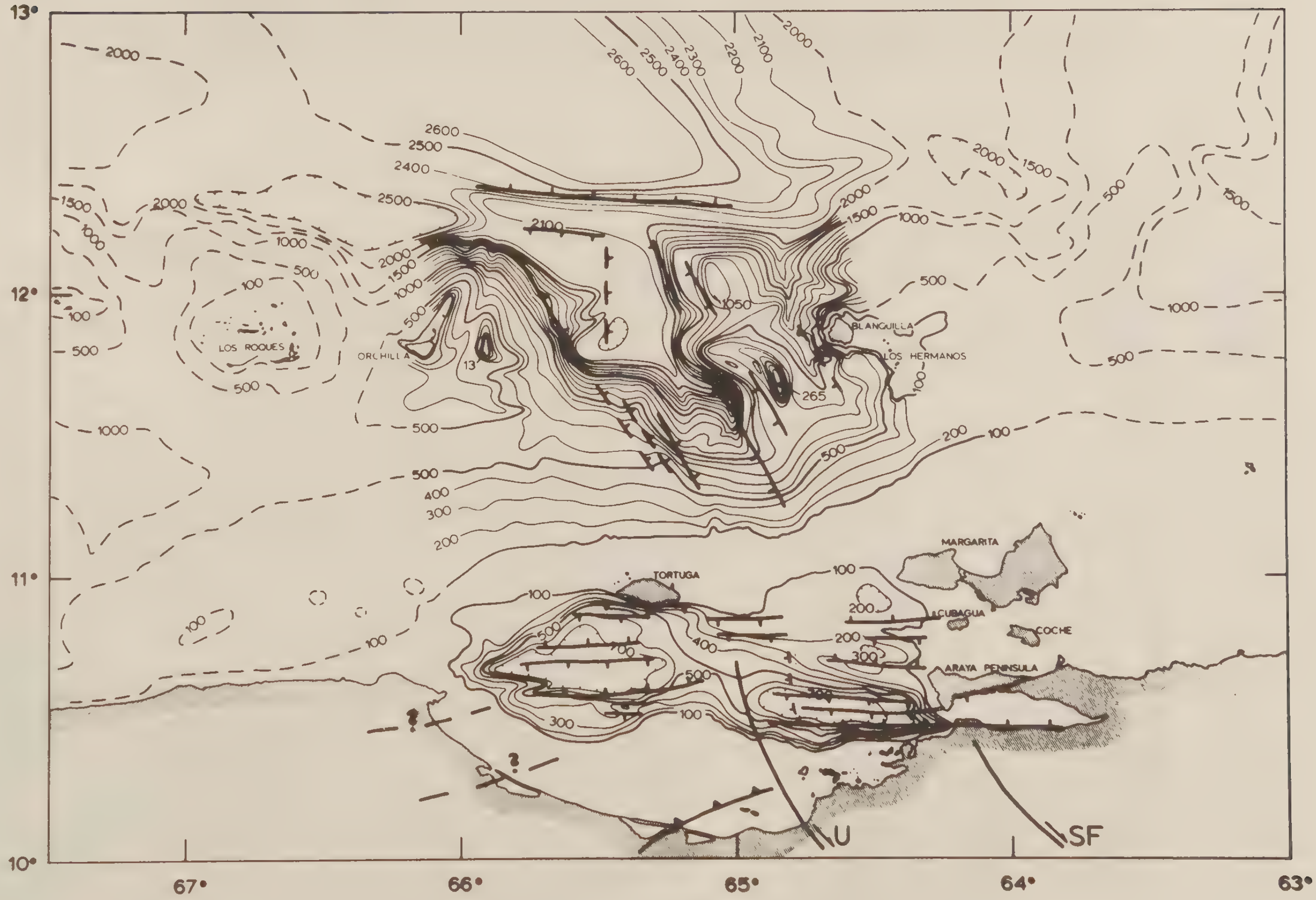
13°
12°
11°
10°
67°
66°
65°
64°
63°
LOS ROQUES
ORCHILLA
BLANQUILLA
LOS HERMANOS
MARGARITA
TORTUGA
CUBAGUA
COCHE
ARAYA PENINSULA
U
SF
2600
2500
2400
2300
2200
2100
2000
1500
1000
500
400
300
200
100
1050
265
13

Fig. 4 Principal faults of the continental margin off north-central Venezuela (from Peter, 1971; 1972). U = Urica fault; SF = San Francisco fault

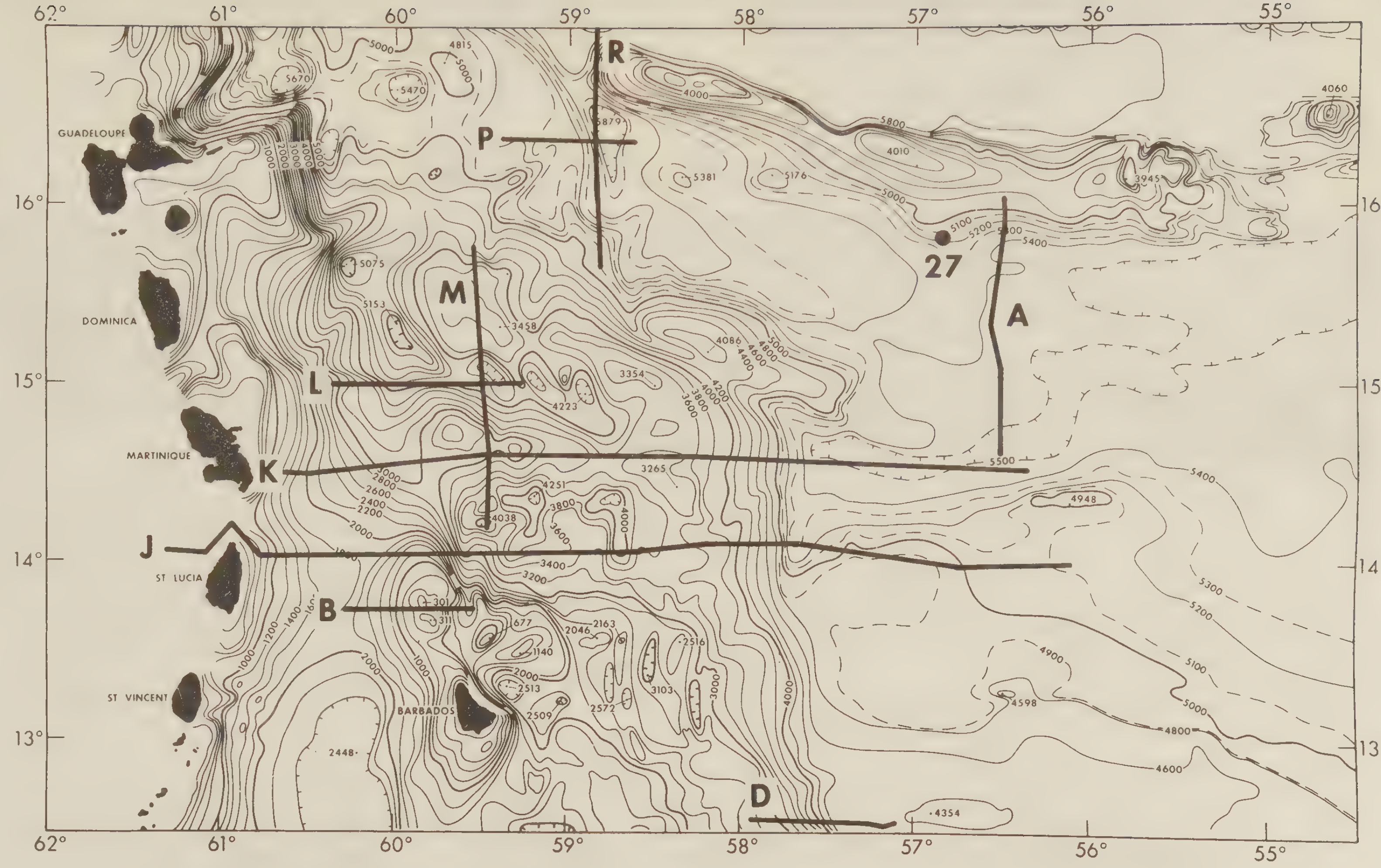
62°
61°
60°
59°
58°
57°
56°
55°
16°
15°
14°
13°
GUADELOUPE
DOMINICA
MARTINIQUE
ST LUCIA
ST VINCENT
BARBADOS
R
P
M
L
K
J
B
D
A
27
5000
4815
5670
5470
5879
4000
5800
4010
5381
5176
5000
3945
4060
5100
5200
5300
5400
5075
5153
3458
4086
4400
4600
4800
5000
3354
4223
4200
4000
3800
3600
5500
3265
4251
3800
4038
3600
4000
3400
3200
2000
2200
2400
2600
2800
3000
301
311
677
2163
2046
1140
2516
2000
2513
2509
2572
3103
3000
4000
1400
1200
1000
2000
1000
2448
4948
5400
5300
5200
5100
4900
4598
5000
4800
4600
4354

Fig. 6 Bathymetric map of the Barbados Ridge (BR) complex and the adjacent Atlantic sea floor (from Peter and Westbrook, 1976). Contours are simplified and at 200-m intervals over the BR complex; contour interval is 100 m at depths greater than 5 000 m

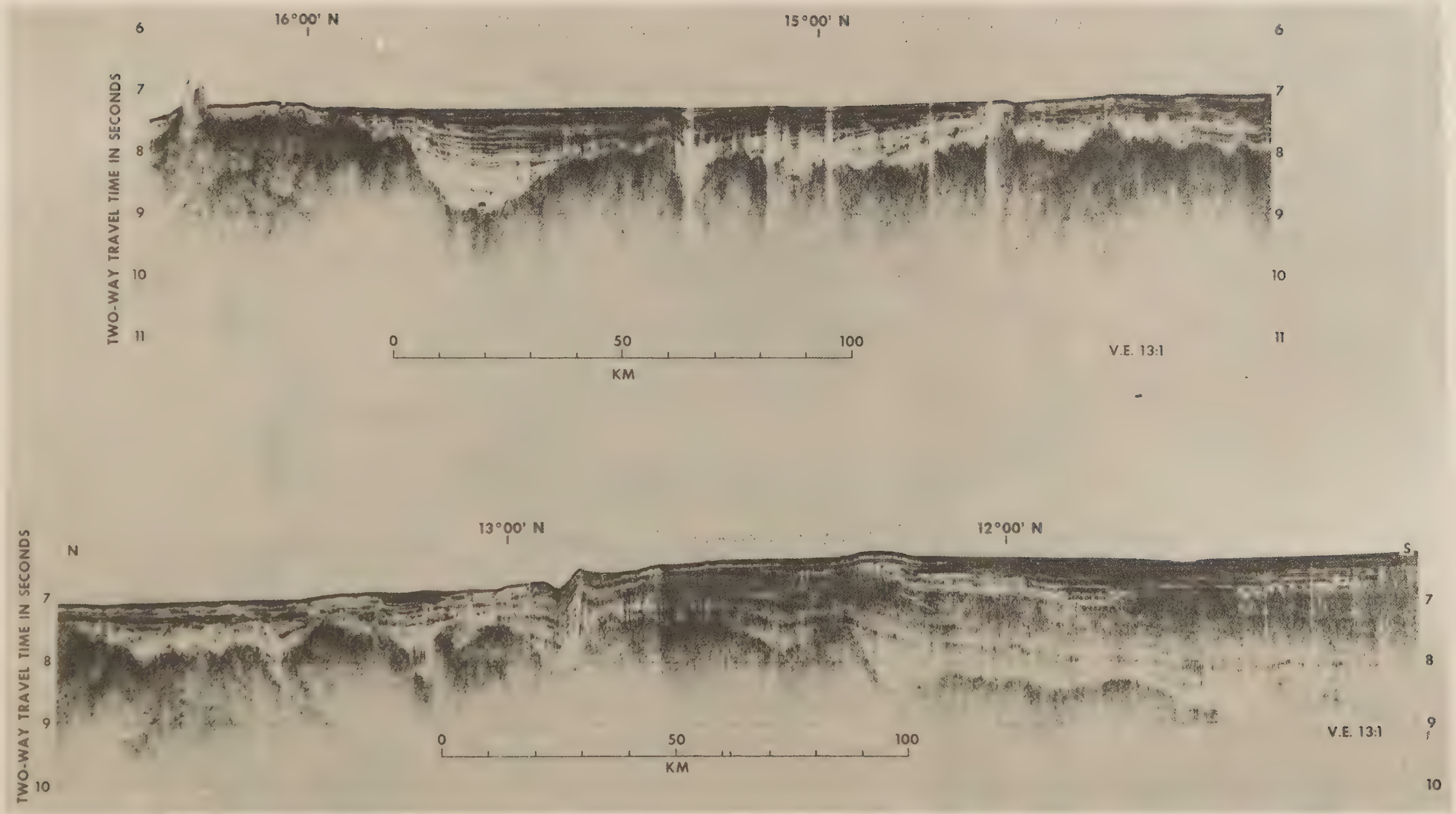

Fig. 7 North-south seismic reflection profile along 54°30'W, crossing the eastern vestiges of the Barracuda Ridge and the Demerara Abyssal Plain to the south of it (from Peter and Westbrook, 1976)

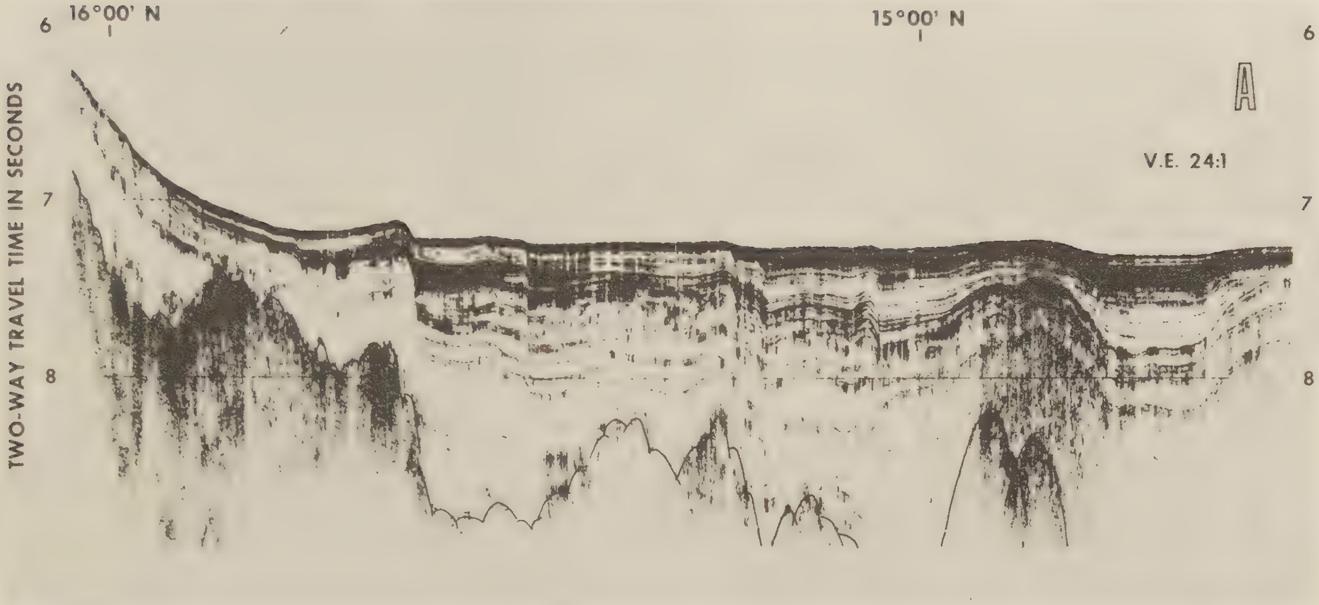

Fig. 8 Retouched photograph of north-south seismic reflection record along 56°30'W, directly to the south of the Barracuda Ridge (from Peter and Westbrook, 1976)

There are two conclusions that must be emphasized with regard to the structure of the Barbados Ridge complex: (1) the east-west topographic elements of the Barbados Ridge complex are related to the similarly oriented fault systems of the adjacent Atlantic Basin, which appear to extend under the complex westward to the volcanic arc, and have influenced its development, and (2) the tectonic activity responsible for the elevation of the Barbados Ridge complex has been influenced by these east-west faults, and although relatively recent uplifts occurred throughout the entire complex, some of the internal tectonic activity is younger (more recent) north of 14°N.

Although the east-west topographic lineaments are quite obvious on the bathymetric map, the most significant discontinuity located at 14°N is well reflected also on the Bouguer anomaly map (Fig. 9). It is represented by a band of low Bouguer anomalies that extend from about 56°W (over the Atlantic Basin) to a point southeast of Martinique, and another band of relatively high Bouguer anomalies that reach westward to Sta. Lucia.

Owing to the abrupt termination of the major north-south oriented, island-arc related, topographic (and structural) trends at 14°N, the 1 000 m drop in the average depth to the north of this point and the drastic change in other geophysical characters, Westbrook (1973, 1975) considered 14°N to be the northern terminus of the 'true' Barbados Ridge. Peter and Westbrook (1976) presented an alternate interpretation that proposes a three-part division of the Barbados Ridge complex: (1) from the South American shelf to 14°N; (2) from 14°N to about 16°N (the actual northern boundary of this unit trends northwest-southeast, and extends from 15°N to 16°10'N), and (3) from 16°N to the Puerto Rico Trench. The amount of uplift each sub-unit has received is progressively less toward the north with no uplift of the northernmost unit. The centre unit has apparently suffered major internal deformation during the Pleistocene-Holocene.

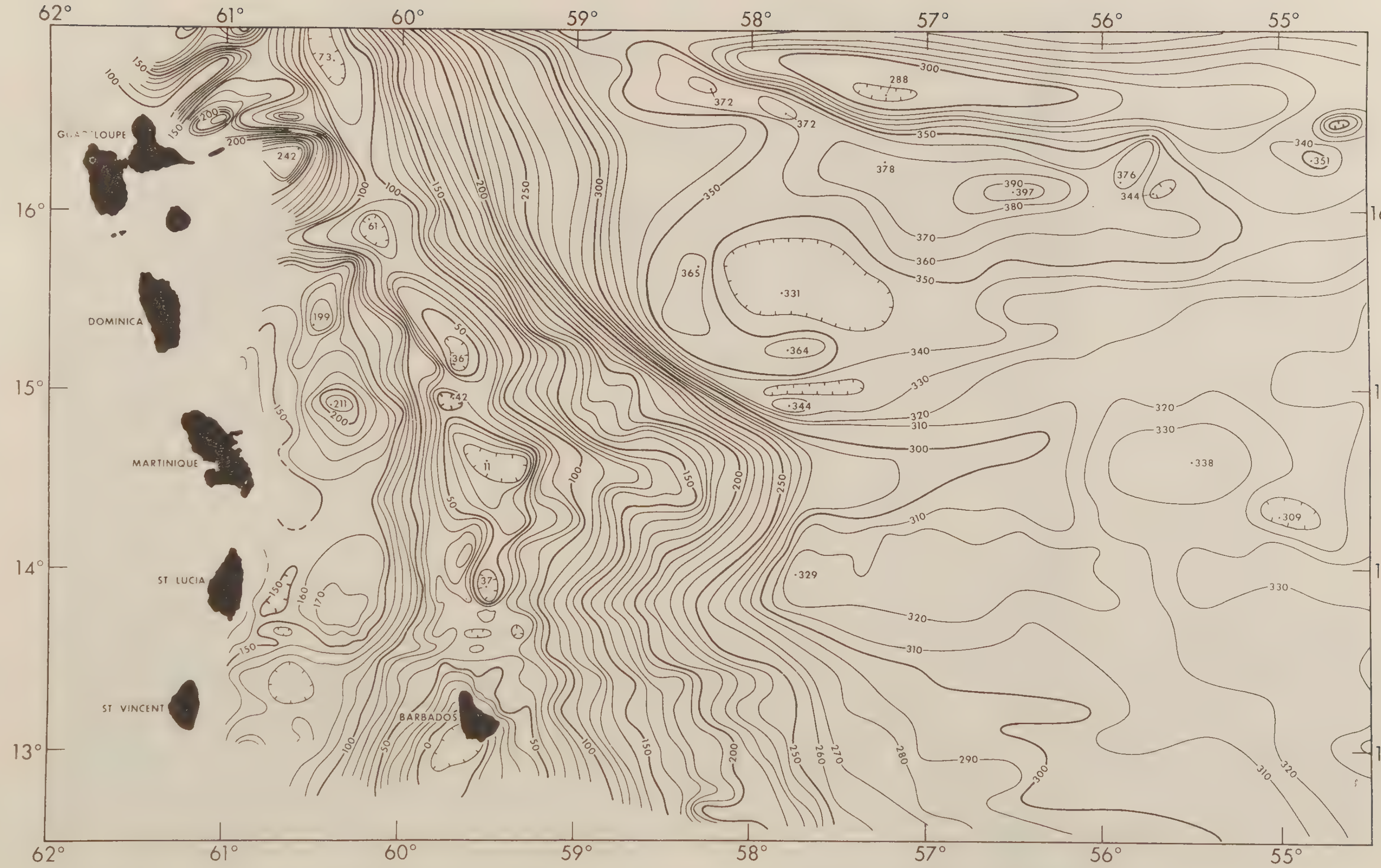
62°
61°
60°
59°
58°
57°
56°
55°
16°
15°
14°
13°
GUADELOUPE
DOMINICA
MARTINIQUE
ST LUCIA
ST VINCENT
BARBADOS

Fig. 9 Bouguer gravity anomaly map over the Barbados Ridge complex and the adjacent Atlantic sea floor (from Peter and Westbrook, 1976)

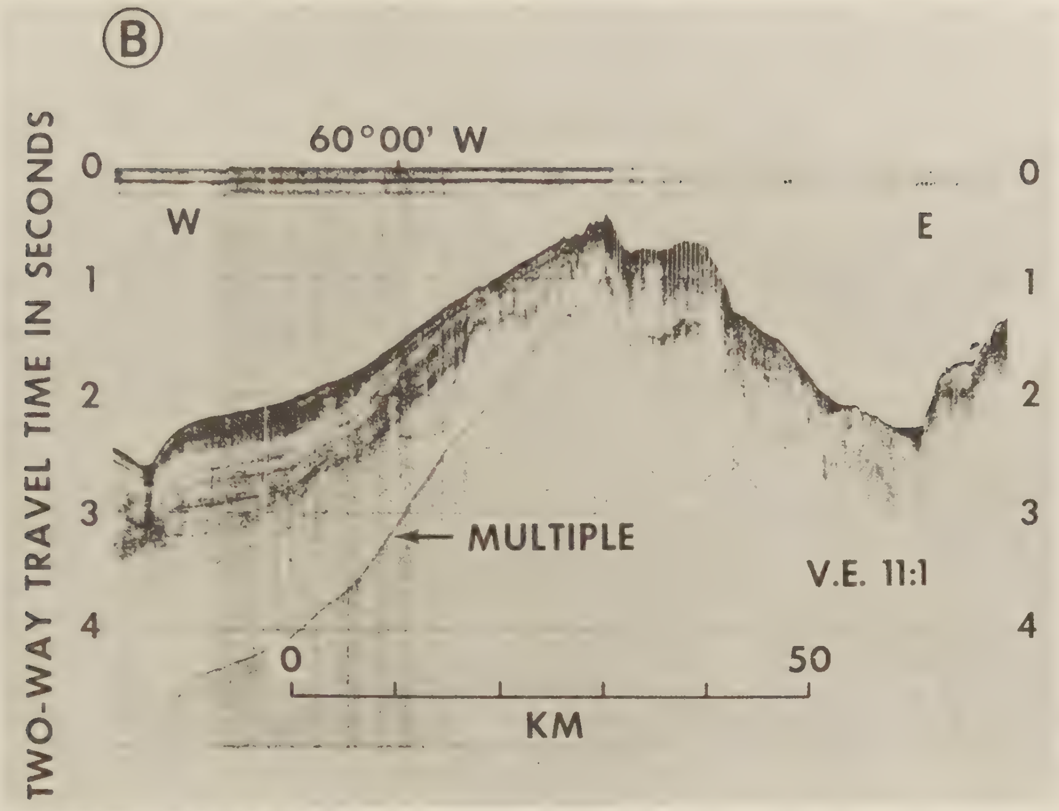

Fig. 10 Photograph of seismic reflection record B (from Peter and Westbrook, 1976). For location see Fig. 6

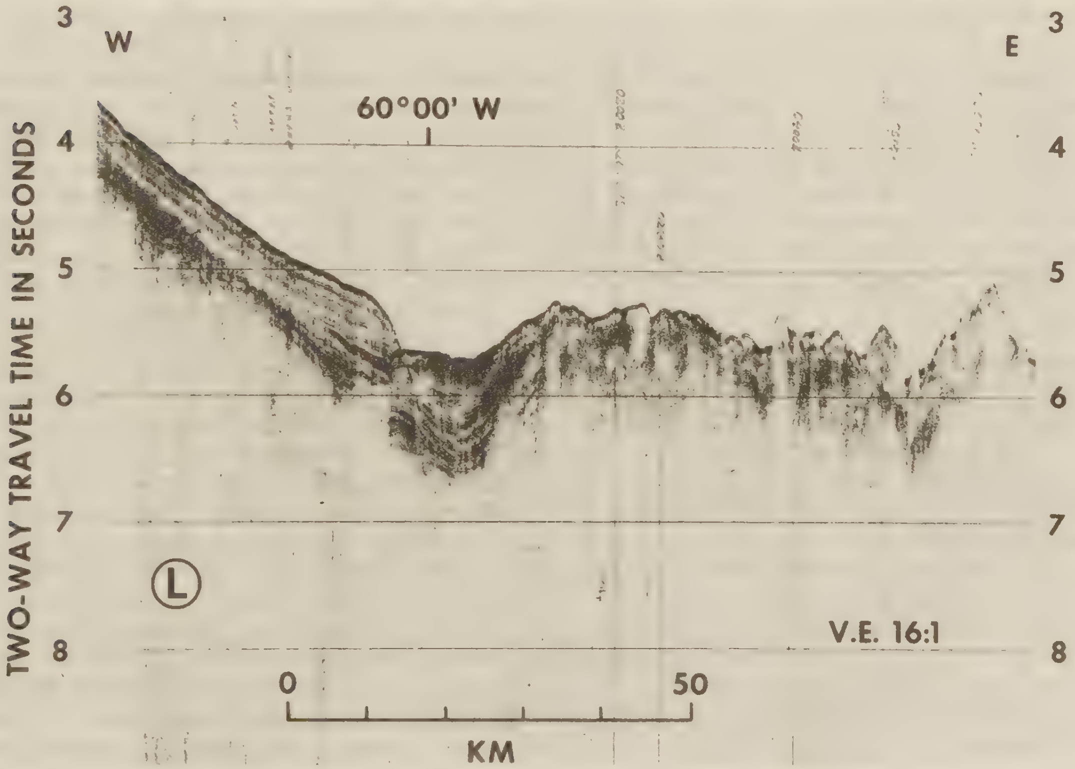

Fig. 11 Photograph of seismic reflection record L (from Peter and Westbrook, 1976). For location see Fig. 6

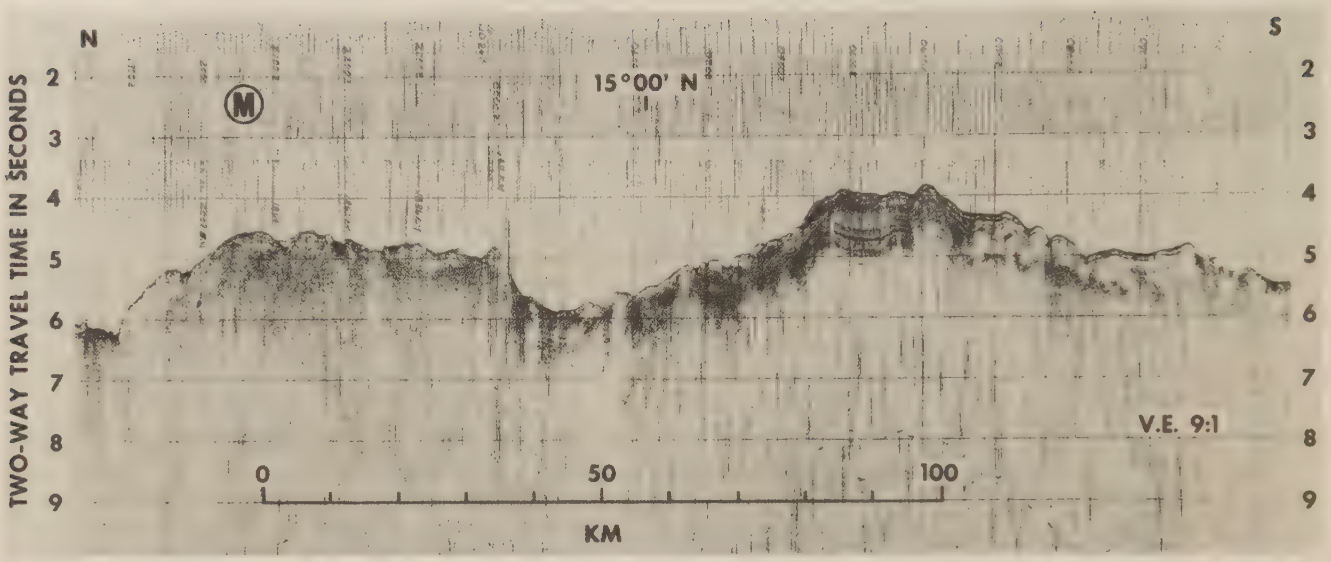

Fig. 12 Photograph of seismic reflection record M (from Peter and Westbrook, 1976). Stratified sediments on top of hill south of 50°N are the same as those shown on record L below the graben of the Lesser Antilles Trench. For location see Fig. 6

The reasons for which we believe that the internal tectonic disturbances of the Barbados Ridge complex are younger north of 14°N are twofold: (1) the topography of the Lesser Antilles Trench is much more youthful looking than its structural equivalent, the Tobago Trough, and (2) the upper one kilometre of sediments of the Tobago Trough pinch out against the western flank of the Barbados Centre Ridge (Fig. 10), whereas the upper one kilometre of sediments in the Lesser Antilles Trench is upfolded and faulted onto the Centre Ridge (a hilly area considered to be the northern equivalent of the Centre Ridge to the east of the graben) (Figs. 11 and 12), suggesting that faulting in this area was more recent (Peter and Westbrook, 1976).

5. FRONTAL DEFORMATION

It has been established with reasonable certainty that at the axis of mid-oceanic ridges new crust is being generated and, if the extrapolation of spreading rates for the magnetic anomaly age determinations is valid, then this process has been active since the Mesozoic. Similar activity in the Paleozoic or earlier times is a good possibility, but it is much harder to demonstrate. It is clear that thousands of kilometres of Mesozoic and older oceanic crust had to plunge back into the mantle to give way to the younger crust, unless the Earth had undergone a large expansion in size in the past 200 million years. Plate tectonics dogma denies the physical possibility of Earth-expansion, and claims that all the new crust that has has been generated along mid-oceanic ridges has pushed an equal area of old crust back into the mantle. One of the aims of our work in the Barbados Ridge complex area was to investigate the surface manifestations of the hypothetical subduction zone there by checking the detailed geology and geophysics of the upper part of the crust where it supposedly plunges into the mantle.

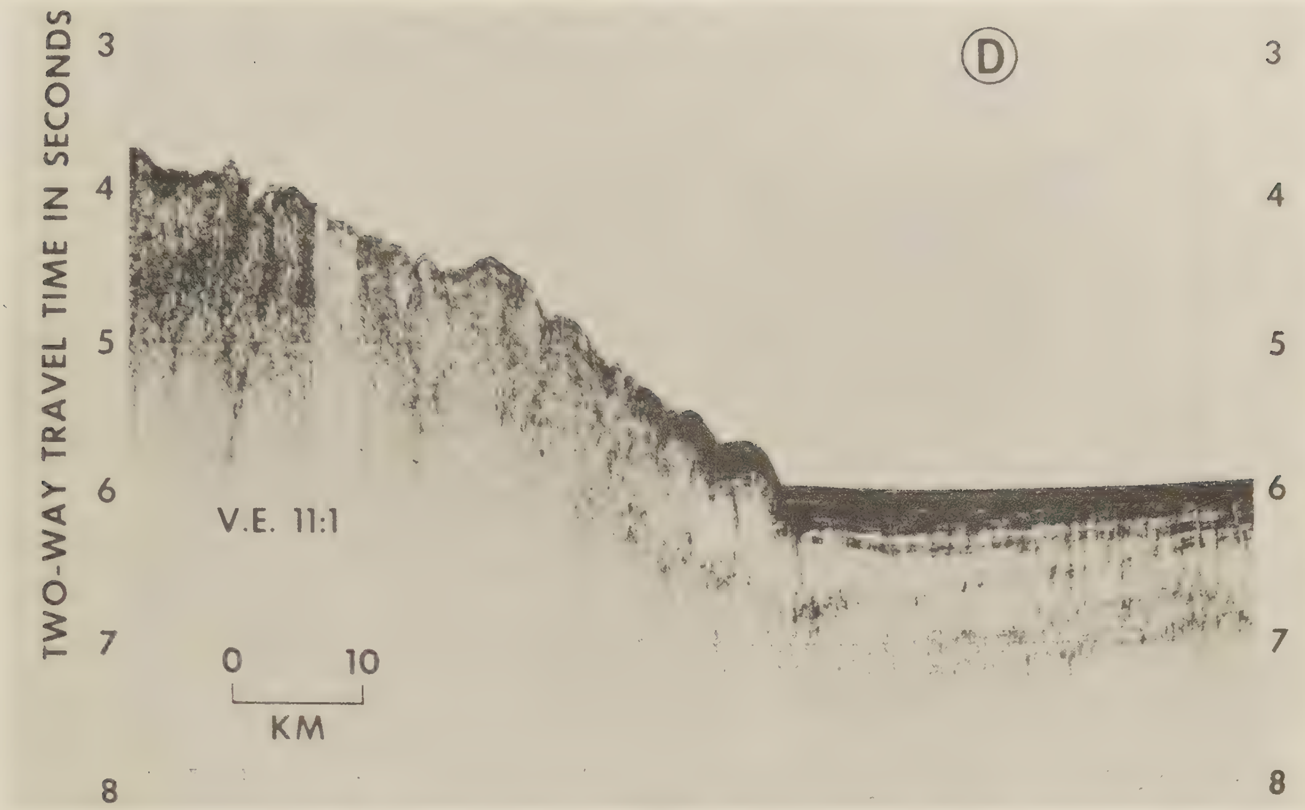

Fig. 13 Photograph of seismic reflection record D (from Peter and Westbrook, 1976). For location see Fig. 6

Two seismic reflection lines illustrate what happens to the upper kilometre of the Atlantic Basin sediments. Line D (Fig. 13), southeast of Barbados shows the uplift of the sediments at the toe of the Barbados Ridge complex. The well-stratified upper sedimentary horizons are progressively thinner as they are uplifted some 300 m along two faults. These faults are high-angle normal or reverse faults, and are apparently caused by the uplift of the Barbados Ridge complex, with an accompanying near 10-km eastward extension of the toe. The profile does not show any obvious deformation of the upper one kilometre of sediments although, admittedly, even a 500-m horizontal deformation would be hard to detect at this vertical exaggeration. With a continuous westward movement of the sea floor, however, horizontal deformation, not the vertical uplift, should be the most prominent. Whether the vertical uplift has been caused by isostasy (a logical assumption considering the large negative isostatic gravity anomaly belt associated with this area), or is due to the sediments added to the base of the Barbados Ridge complex as a result of subduction scraping off the sediments from the Atlantic sea floor, cannot be determined. As isostasy is a physical reality, and no obvious sign of horizontal deformation was found, I believe this uplift was caused by isostasy.

In contrast to the case above, on line P (Fig. 16) north of the elevated parts of the Barbados Ridge complex, the Atlantic crust and the over 1 km of sediments overlying the basement gently dip westward beneath a sediment pile, characterized by incoherent seismic reflections. The acoustically incoherent sediment pile, just like the acoustically similar sediments on the toe of the Barbados Ridge complex have been referred to as 'scraped off' sediments of the Atlantic (Chase and Bunce, 1969; Bunce et al., 1970). It is my contention that if such a scraping process would operate here, then not only the overlying sediment pile but also at least the upper, unconsolidated sediments of the Atlantic sea floor should be disturbed. It appears unlikely that the mostly unlithified sediments of the Atlantic would underthrust a 1-km to 2-km thick sediment pile to some 40 km without themselves suffering any noticeable internal deformation.

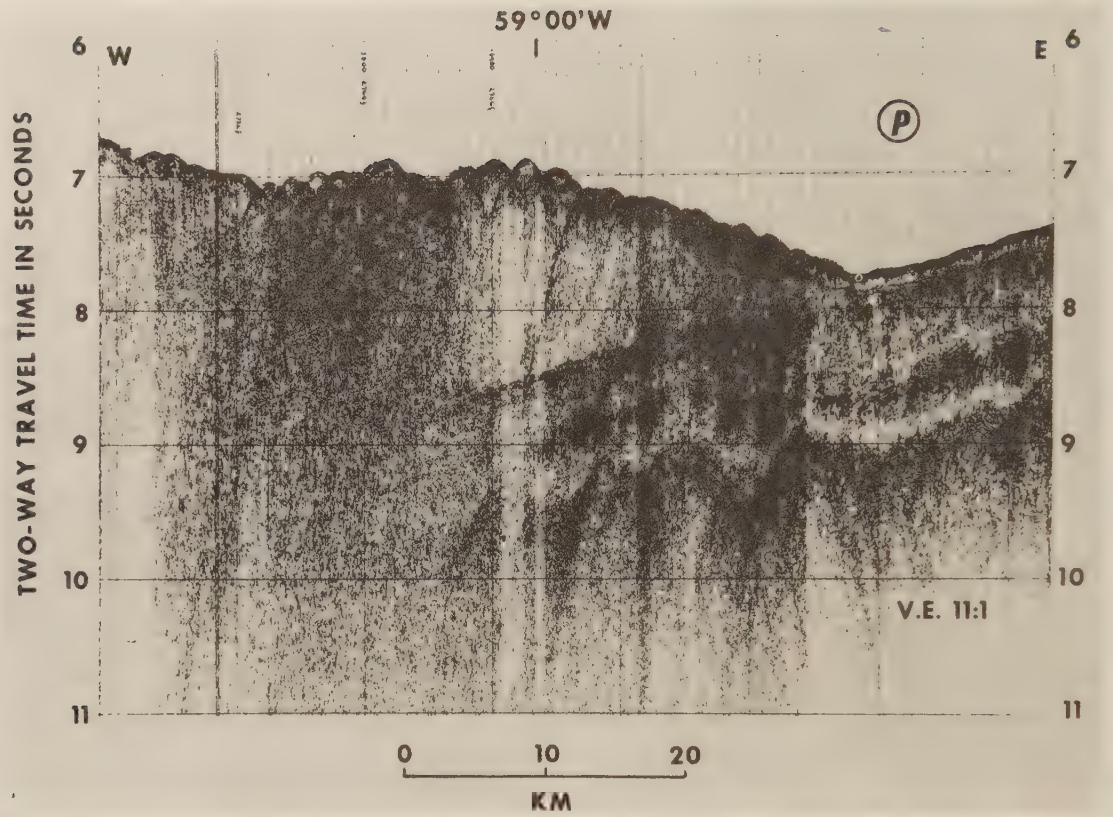

Fig. 14 Photograph of seismic reflection record P (from Peter and Westbrook, 1976)

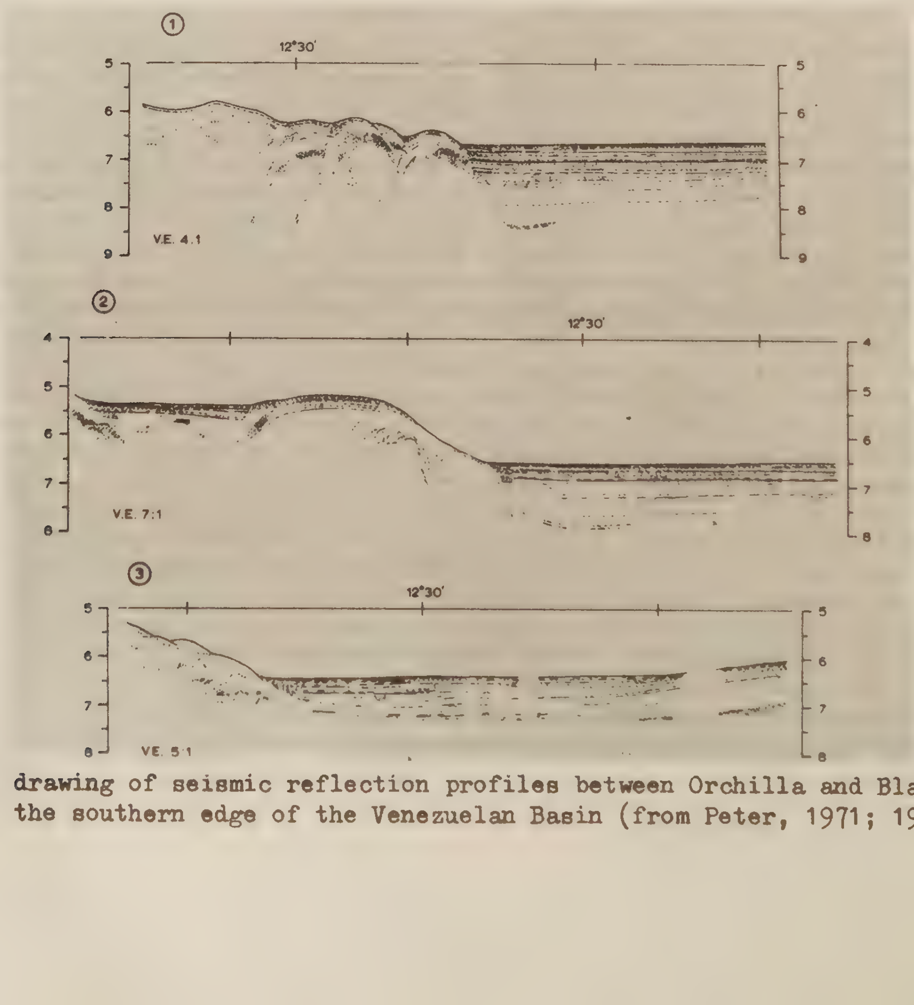
①
12°30'
5
6
7
8
9
V.E. 4:1
②
12°30'
4
5
6
7
8
V.E. 7:1
③
12°30'
5
6
7
8
V.E. 5:1

Fig. 15 Line drawing of seismic reflection profiles between Orchilla and Blanquilla islands over the southern edge of the Venezuelan Basin (from Peter, 1971; 1972)

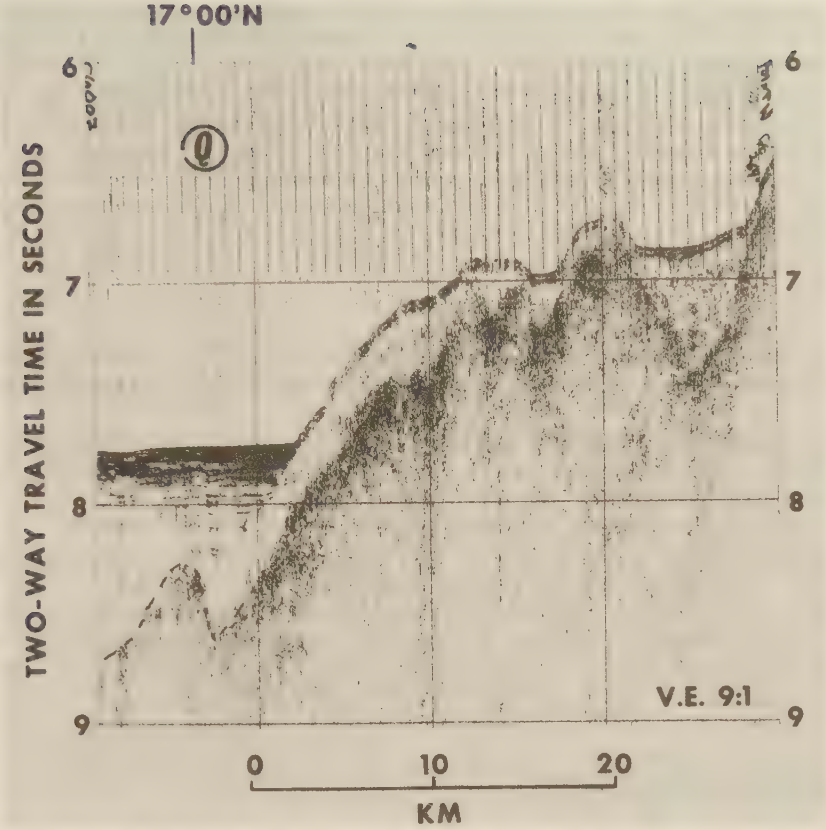

Fig. 16 Photograph of a seismic reflection record over the northwestern edge of the Barracuda Abyssal Plain. (North is to the right.)

As an alternate explanation to that required by plate tectonics, it is suggested that: (1) the upper sedimentary horizon (the strong upper reflector on Line P) is an unconformity rather than a thrust surface, and (2) the overlying sediments are not scrapings of the Atlantic sea floor but slump- and current-derived sediments that originated mostly from the adjacent island arc and simply piled up on top of the Atlantic sea floor sediments.

The Venezuelan Basin—Curaçao Ridge deformation front is illustrated on three profiles located between 64°W and 65°W, off the area of the Los Roques canyon (Fig. 15). These profiles suggest a lack of conformity between the sediments of the toe of the Curaçao Ridge and those deposited in the Venezuelan Basin. These results are to be expected as most plate tectonic interpretations require only a Cretaceous subduction zone in this area. Yet the USGS-IDOE data (1972) and a multi-channel seismic reflection line by Talwani et al. (1976) indicate the folding of the stratified horizontal sediments and their uplift at the toe of the Curaçao Ridge in an area some 200 km to the west of these profiles. Again, subduction was cited to explain the phenomena, in this case requiring that this margin be characterized not only by a transform fault, but also by subduction (despite the fact that there is no present volcanism or Benioff zone in this area). As an alternate explanation, I suggest that isostatic uplift of the Curaçao Ridge would cause a similar deformation of the highly stratified sediments.

6. PLEISTOCENE-HOLOCENE SEDIMENTATION

As most of our studies were directed toward understanding the structure of the Atlantic sea floor adjacent to the Barbados Ridge complex, an interesting byproduct of our efforts was discovering the extent of the enormous amounts of sediments that have been deposited in the area in the Pleistocene and Holocene. Sediments with thicknesses in excess of 1 000 m were found in the Vema fracture zone (van Andel et al., 1971), where deep sea drilling stopped at 480 m in middle Pleistocene sediments (JOIDES, 1969). The origin and extent of these sediments within the Demerara Abyssal Plain were discussed by Heezen et al. (1964) and Damuth and Fairbridge (1970).

Our results suggest that these sediments are not only distributed throughout the Demerara Abyssal Plain, but found their way around the Barracuda Ridge and also filled the Barracuda Abyssal Plain. A north-south seismic reflection record taken near the western end of the Barracuda Abyssal Plain (Fig. 16) shows highly stratified, turbidite-like sediments covering the acoustically transparent sediments of the Atlantic sea floor (Schubert and Peter, 1973; Schubert, 1974). Because the thickness of the acoustically transparent layer is essentially the same below the turbidites as above them on the sloping Atlantic sea floor, we infer that these turbidites are also part of the Pleistocene-Holocene sedimentation event that covered the area to the south.

REFERENCES

Andel, Tj.H. van, R.P. Von Herzen and J.D. Phillips, The Vema fracture zone and the tectonics 1971 of transverse shear zones in oceanic crustal plates. Mar.Geophys.Res., 1:261-83

Ball, M.M. and C.G.A. Harrison, Origin of the Gulf and Caribbean and implications regarding 1970 ocean ridge extension, migration and shear. Trans.Gulf Coast Assoc.Geol.Soc., 19:287-94

Bellizzia, A.G., Sistema Montanoso del Caribe, borde sur de la placa Caribe es una cordillera 1972 aloctona? Trans.Carib.Geol.Conf., 6:247-58

Bunce, E.T. et al., The Lesser Antilles Arc and the eastern margin of the Caribbean Sea. 1970 In The sea, edited by A.E. Maxwell. New York, Wiley-Interscience, vol.4.Pt.2: 359-85

Bush, S.A. and P.A. Bush, Isostatic gravity map of the eastern Caribbean region. Trans. 1969 Gulf Coast Assoc.Geol.Soc., 19:281-5

Chase, R.L. and E.T. Bunce, Underthrusting of the eastern margin of the Antilles by the 1969 floor of the western North Atlantic Ocean, and origin of the Barbados Ridge. J.Geophys.Res., 74:1413-20

Collette, B.J. and K.W. Rutten, Crest and fracture zone geometry of the mid-Atlantic ridge 1972 between 10° and 16°N. Nature, Lond., 237:131-4

Damuth, J.E. and R.W. Fairbridge, Equatorial Atlantic deep-sea sands and ice-age aridity 1970 in tropical South America. Bull.Geol.Soc.Am., (81):189-206

Heezen, B.C., R.D. Gerard and M. Tharp, The Vema fracture zone in the Equatorial Atlantic. 1964 J.Geophys.Res., 69:733-9

JOIDES (Joint Oceanographic Institutions Deep Earth Sampling Program), Deep sea drilling 1969 Leg 3 and Leg 4. Geotimes, 14:13-6

Metz, H.L., Geology of the El Pilar fault zone, State of Sucre, Venezuela. Trans.Carib. 1968 Geol.Conf., 4:293-8

Molnar, P. and L.R. Sykes, Tectonics of the Caribbean and Middle America regions from focal 1969 mechanisms and seismicity. Bull.Geol.Soc.Am., (80):1639-84

Peter, G., Geology and geophysics of the Venezuelan continental margin between Blanquilla 1971 and Orchilla islands. Ph.D. Dissertation, George Washington University, Washington, D.C., 206 p. (unpubl. MS)

__________, Geologic structure offshore north-central Venezuela. Trans.Carib.Geol.Conf., 1972 6:283-94

Peter, G. and R.K. Lattimore, Geophysical investigation of the Venezuelan continental margin.
1971 Trans.Am.Geophys.Union, 52:251

Peter, G. and G.K. Westbrook, Tectonics of the southwestern North Atlantic and the Barbados
1976 Ridge complex. Am.Assoc.Pet.Geol.Bull., 61

Peter, G., C. Schubert and G.K. Westbrook, NOAA-IDOE Caribbean-Atlantic geotraverse.
1974 Geotimes, 19:12-5

Peter, G. *et al.*, Development of the mid-Atlantic ridge east of the Lesser Antilles island
1973 arc. Nature Phys.Science, 245:129-31

Salvador, A. and R.M. Stainforth, Clues in Venezuela to the geology of Trinidad, and vice
1968 versa. Trans.Carib.Geol.Conf., 4:31-40

Schubert, C., Seafloor tectonics east of the northern Lesser Antilles. Abstr.Carib.Geol.
1974 Conf., 7:62-3

Schubert, C. and G. Peter, Sea floor tectonics west of the Barracuda Ridge. Trans.Am.
1973 Geophys.Union, 54:326

Talwani, M., Gravity anomaly belts in the Caribbean. *In* Continental margins and island
1966 arcs. Pap.Geol.Surv.Can., (66-15):177

Talwani, M. *et al.*, Multi-channel seismic study in the Venezuelan Basin and the Curaçao
1976 Ridge. Trans.Am.Geophys.Union, 57:266

USGS-IDOE, USGS-IDOE Leg 4 Venezuelan Borderland. Geotimes, 17:19-21
1972

Westbrook, G.K., Crust and upper mantle structure in the region of Barbados and the Lesser
1973 Antilles. Ph.D. Dissertation, University of Durham, England, 228 p. (unpubl. MS)

__________, The structure of the crust and upper mantle in the region of Barbados and the
1975 Lesser Antilles. Geophys.J.R.Astron.Soc., 43:42 p.

QUATERNARY MARINE TERRACES OF LA BLANQUILLA ISLAND, NORTHEASTERN VENEZUELAN OFFSHORE

by

C. SCHUBERT
Centro de Ecología
Instituto Venezolano de Investigaciones Científicas
Apartado 1827
Caracas 101, Venezuela

CONTENTS

1. INTRODUCTION
2. GEOMORPHOLOGY
3. BLANQUILLA FORMATION
4. ACKNOWLEDGEMENTS
5. REFERENCES

Abstract

A sequence of reef limestones, called the Blanquilla Formation, crops out on La Blanquilla island. This formation consists of three marine terraces (from youngest to oldest): Limestone Terrace 1; Limestone Terrace 2, and Limestone Terrace 3, whose elevations above sea level are 7-10 m, 11-15 m, and 25 to over 30 m, respectively. The Blanquilla Formation lies unconformably above the basement of the island, which consists of the Garantón Trondhjemite of Paleocene age. At the base of the limestone there is a basal conglomerate consisting of igneous and metamorphic rock and limestone. All these terraces contain fossils, particularly corals, which show evidence of progressively greater diagenetic alteration with age. Limestone Terrace 2 contains two facies: an external coralline facies and an internal arenaceous facies. The age of the La Blanquilla Formation is inferred by comparison with similar sequences on other Caribbean islands (La Orchila and Barbados), whose ages have been determined radiometrically. In addition, tentative correlations are made with Aruba, Curaçao, Bonaire, Jamaica, and Cuba. From these comparisons, the age of the Blanquilla Formation is Pleistocene.

Resumen

En la isla de La Blanquilla aflora una serie de calizas arrecifales denominada formación Blanquilla, compuesta de tres terrazas marinas, que son, de la más joven a la más vieja: la terraza caliza 1, la terraza caliza 2, y la terraza caliza 3, y cuyas elevaciones sobre el nivel del mar son, respectivamente, de 7 a 10 m, de 11 a 15 m y de 25 a más de 30 m. La formación Blanquilla no se conforma al basamento de la isla, que está compuesta del trondhyemita Garantón, del paleoceno. En la base de la formación hay un conglomerado basal de rocas ígneas y metamórficas y de caliza: todas estas terrazas contienen fósiles, especialmente corales, en los que se observan indicios de una creciente alteración diagenética a causa de la edad. La terraza caliza 2 tiene dos caras, una cara externa coralina y otra interna arenosa. La edad de La Blanquilla se infiere por comparación con series análogas situadas en estas islas del Caribe, cuyas edades se han determinado por radiometría (La Ochila y Barbados). Se han hecho, además, correlaciones provisionales con Cuba, Curaçao, Bonaire, Jamaica y Cuba: basándose en estas comparaciones, la formación Blanquilla es del período pleistoceno.

1. INTRODUCTION

La Blanquilla island is located, together with the Los Hermanos islands, on a shallow submarine platform near the southern end of Aves Ridge (Fig. 1). It is situated approximately 100 km northwest of Margarita Island, and the platform is separated from La Orchila Island (approximately 160 km west of La Blanquilla) by the Los Roques submarine canyon (Maloney, 1971). The geographic coordinates of La Blanquilla are: 11°50'N lat., 64°35'W long.; its shape is that of a quadrant (90°); its diameter is approximately 10 km (Zuloaga, 1953); and its elevation reaches more than 30 m above sea level. The area of the island is 52.5 km^2 (Vila, 1967). It is a low, flat island, whose eastern part is made up of several levels of marine terraces and its western part consists of low hills in which the Garantón Trondhjemite crops out (Fig. 2). Recently Peter (1972) described in detail the submarine morphology between La Blanquilla and La Orchila, and presented structural maps based on submarine geophysical data. In them he interpreted Los Roques Canyon as a northwest trending graben.

The physiography of La Blanquilla was described by Zuloaga (1953); that author and Maloney (1971) described the geology in general terms, particularly the sedimentary rocks. The igneous rocks were described and analysed by Schubert and Moticska (1973), and Santamaría and Schubert (1974). These rocks consist of trondhjemite with a basic quartz-diorite front in the northwestern part of the island. These plutonic rocks were intruded by pegmatitic dikes and veins. The trondhjemite was described originally as biotite granodiorite and quartz-diorite by Rutten (1931,1940). Zuloaga (1953) refers to it as the La Blanquilla Granite; Maloney (1971) introduced the name Garantón Granodiorite and established its type locality around Garantón bay. Later, Schubert and Moticska (1973) made detailed petrographic analyses of the igneous rocks of La Blanquilla and formally defined the Garantón Trondhjemite. Santamaría and Schubert (1974) made geochemical and geochronological studies, including potassium/argon (K/Ar) dating on feldspar and biotite: (1) of the Garantón Trondhjemite which gave ages of 64 ± 3.5 and 62 ± 3.5 m.y. B.P., and (2) of the pegmatite which gave ages of 64 ± 3.4 and 62 ± 3.4 m.y. B.P. These radiometric ages suggest a Paleocene age for the Garantón

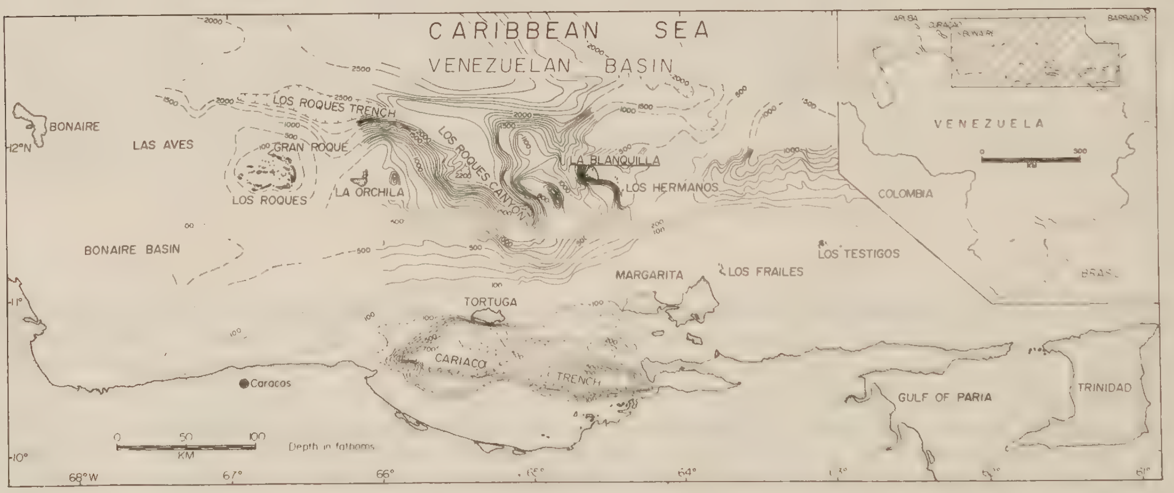
CARIBBEAN SEA
VENEZUELAN BASIN
LOS ROQUES TRENCH
LOS ROQUES CANYON
BONAIRE
LAS AVES
GRAN ROQUE
LOS ROQUES
LA ORCHILA
LA BLANQUILLA
LOS HERMANOS
BONAIRE BASIN
LOS TESTIGOS
MARGARITA
LOS FRAILES
TORTUGA
CARIACO TRENCH
Caracas
GULF OF PARIA
TRINIDAD
VENEZUELA
COLOMBIA
12°N
11°
10°
68°W
67°
66°
64°
KM
Depth in fathoms

Fig. 1 Index map

Trondhjemite. A K/Ar analysis of a granodiorite sample dredged from Aves Ridge (J. Sutter, personal commun. in Santamaría and Schubert, 1974) gave an age of 65 m.y. B.P.; this result, plus the submarine topographic evidence, supports the hypothesis that La Blanquilla island represents the southernmost outcrop of Aves Ridge.

2. GEOMORPHOLOGY

On La Blanquilla Island there are two types of morphology. These originate from the contrast between the two types of rock that crop out on its surface. The two types of morphology are gentle, rounded hills and nets of shallow arroyos on the Garantón Trondhjemite, and, horizontal terraces on reef limestones and associated beach rock, which surround the trondhjemite nucleus.

All of the northern Venezuelan coast and the islands along it are located within a relatively arid belt (Wilhelmy, 1954; Lahey, 1973). This belt results from the relative aridity of the trade winds which blow from the east-northeast almost all year long and the relatively low temperature of the southern Caribbean sea water (in general from 0.5 to 1°C less than sea water north of the islands). Annual rainfall is 150 mm on La Orchila Island; 512 mm on Margarita Island, and 267 mm on Coche Island (south of Margarita) (Walter and Medina, 1971). These are the stations closest to La Blanquilla and they illustrate the relative aridity which characterizes the belt (there are no weather stations on La Blanquilla). According to Wilhelmy (1954), the well-developed hydrographic nets on Aruba, Curaçao, and Bonaire could not have been developed under present-day climatic conditions, characterized by low rainfall. This author concluded that they must have been formed during more humid times (pluvials); but the correlation between these times and glacial or interglacial epochs has not been resolved yet (Zonneveld, 1968). Sedimentary analyses of cores from the bottom of the Caribbean Sea indicate that the provenance areas were, in general, more arid during the temperature minima than during the temperature maxima (Bonatti and Gartner, 1973). In any case, the system of arroyos in western La Blanquilla Island, located in the same arid belt as the Netherlands Leeward Islands, probably represents a remnant of erosion under conditions more humid than those today.

On the rest of La Blanquilla there are three levels of terraces which represent times of reef growth and planation, and which are at present above sea level (a.s.l.). These three terraces are at following elevations a.s.l.: 7 m to 10 m (Limestone Terrace 1), 11 m to 15 m (Limestone Terrace 2), and 25 m to slightly above 30 m (Limestone Terrace 3) (Fig. 2). The surface of these terraces is horizontal, although there is a slight upward grade from the coast inward. A cliff marks the edge of the terraces, with a variable elevation: 7 m to 10 m for the Limestone Terrace 1 cliff; 1 m to 1.5 m for the Limestone Terrace 2 cliff; and 1 m to 10 m for the Limestone Terrace 3 cliff. Along the cliff of Limestone Terrace 1, a wave-cut notch is being developed. In addition, within this cliff there is evidence of former sea level or island stands, such as submarine caves and wave-cut notches. Along this cliff there is evidence of wave erosion such as semicircular inlets produced by the collapse of the terrace or natural bridges.

3. BLANQUILLA FORMATION

The sedimentary rocks of La Blanquilla Island consist exclusively of reef limestones with subordinate quantities of calcarenite and beach rock. These rocks crop out in a sequence of three terraces (Fig. 2) in the eastern half of the island and in a smaller surface around the southern and western edge of it.

The existence of coral formations on La Blanquilla was mentioned by most of the authors referred to in the introduction and others (Sievers, 1898; Lowe, 1911; Rutten, 1931, 1940); they did not, however, describe or analyse them (except Rutten 1940 who mentioned some coral identifications by H. Gerth). Zuloaga (1953) described the morphology of the limestone in general and included a peleontological list (identifications by J.G. Marks and L. Weingeist); based on the latter he postulated a Pleistocene to Recent age for the limestone. This list included several species of corals, equinoderms, pelecypods, gastropods, and foraminifera.

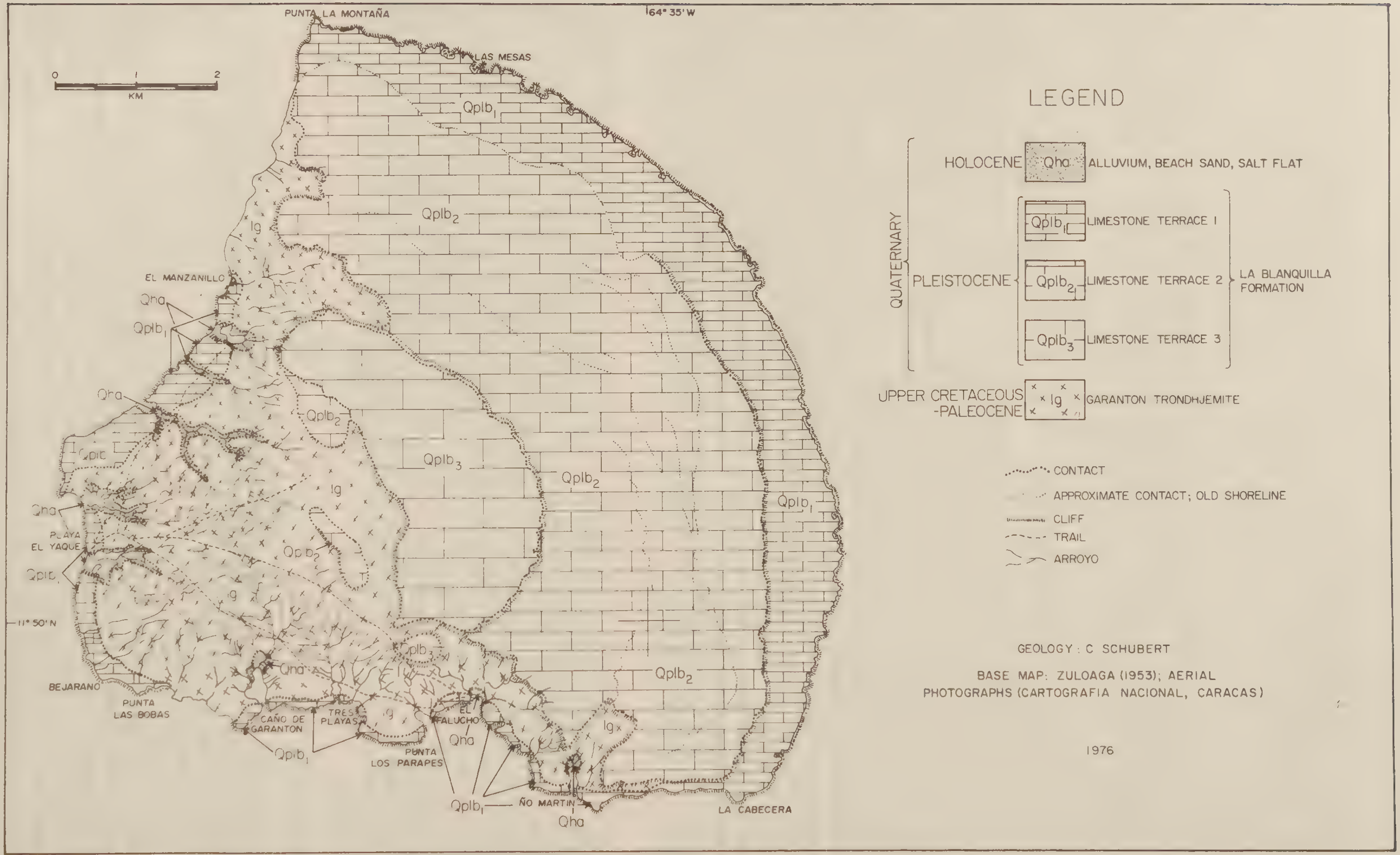
LEGEND
QUATERNARY
HOLOCENE
Qha
ALLUVIUM, BEACH SAND, SALT FLAT
PLEISTOCENE
Qplb$_1$
LIMESTONE TERRACE 1
Qplb$_2$
LIMESTONE TERRACE 2
Qplb$_3$
LIMESTONE TERRACE 3
LA BLANQUILLA FORMATION
UPPER CRETACEOUS -PALEOCENE
lg
GARANTON TRONDHJEMITE
CONTACT
APPROXIMATE CONTACT; OLD SHORELINE
CLIFF
TRAIL
ARROYO
GEOLOGY: C SCHUBERT
BASE MAP: ZULOAGA (1953); AERIAL PHOTOGRAPHS (CARTOGRAFIA NACIONAL, CARACAS)
1976
0
1
2
KM
PUNTA LA MONTAÑA
64° 35' W
LAS MESAS
EL MANZANILLO
PLAYA EL YAQUE
11° 50' N
BEJARANO
PUNTA LAS BOBAS
CAÑO DE GARANTON
TRES PLAYAS
PUNTA LOS PARAPES
EL FALUCHO
ÑO MARTIN
LA CABECERA

Fig. 2 Geological map of La Blanquilla Island, Venezuela

Finally, Maloney (1971) described the limestone of La Blanquilla with more detail and proposed the name La Blanquilla Formation for it. This author mentioned the existence of two terraces with a contrasting fossiliferous content: the lower one rich and the upper one poor in them. For this reason, he postulated the name 'Falucho Member' for the lower terrace limestone. In addition, he repeated the faunal list of Zuloaga (1953). In the present report the name Blanquilla Formation is formally defined; the name Falucho Member is not retained because the fossiliferous contrast, the base of its original definition, does not exist throughout the limestone sequence. The Blanquilla Formation consists of three well defined terraces with a progressively greater diagenetic alteration with age. Due to this diagenesis, the fossiliferous content is apparently less in the oldest terrace.

Fig. 3 shows a section through the central part of La Blanquilla island in an east-west direction. In it the relationship between the marine terraces and the island basement is shown.

3.1 Limestone Terrace 3

Limestone Terrace 3 is the oldest of the sedimentary formations of La Blanquilla. It crops out in the central and highest part of the island, unconformably above the Garantón Trondhjemite in the western part, and in contact with Limestone Terrace 2 in the eastern part (Figs. 2 and 3). The surface of the terrace is horizontal and is frequently broken by ancient karstic structures (principally dolines). The colour of the limestone is light tan, but on the surface it weathers to bluish grey. The edge of the outcrop is marked by a cliff whose elevation varies between 1 m and 10 m. In general, the cliff is low along the contact with Limestone Terrace 2. This contact is irregular and much weathered. Above the contact with the Garantón Trondhjemite there is a small basal conglomerate of igneous and metamorphic rocks (for example, amphibolite probably derived from the Los Hermanos islands, 15 km southwest of La Blanquilla) (Maloney, 1971; Schubert and Moticska, 1973).

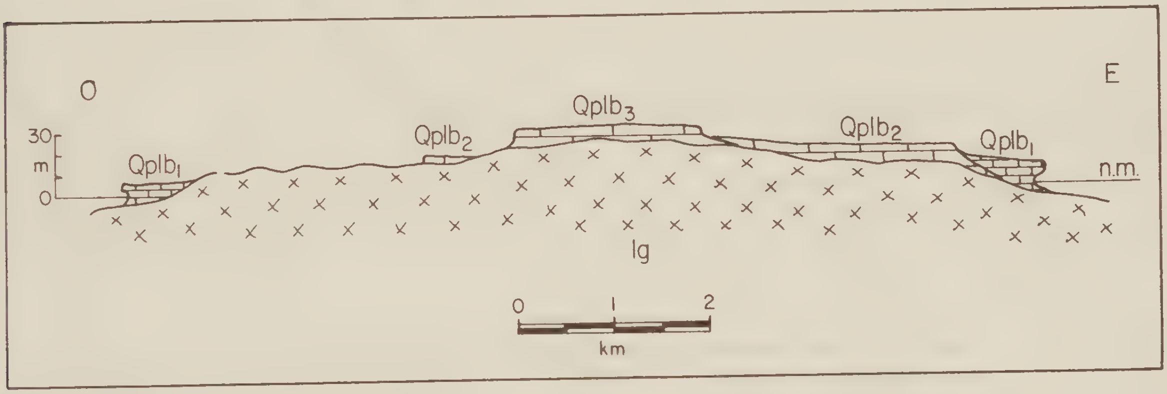

Fig. 3 East-west geological section across the central part of La Blanquilla.
The symbols are the same as in Fig. 2

The limestone consists of amorphous microcrystalline masses and masses of calcite crystals. The latter were derived from the recrystallization of the original calcium carbonate (aragonite). In some places remnants of corals and less frequently marine shells can still be recognized. Among the corals collected, the following were identified: Diploria sp., Montastrea cavernosa, and Solenastrea bournoni (?). All these specimens show clear diagenetic effects in the recrystallization of the original aragonite to calcite. In these corals only their external structure is recognizable; almost all of the internal structure (such as the columella and septae) has disappeared through solution and recrystallization.

The thickness of Limestone Terrace 3 is variable, ranging from 2 m to 6 m. This was observed along the contact with the Garantón Trondhjemite.

3.2 Limestone Terrace 2

Limestone Terrace 2 crops out in the northern and eastern parts of La Blanquilla, east of the outcrop area of Limestone Terrace 3 (Figs. 2 and 3). In addition, there are two small outcrops west of Limestone Terrace 3, one isolated and the other in contact with it. Limestone Terrace 2 is the intermediate terrace (in age and elevation) and is the most extensive: it covers approximately one third of the island. Its surface is horizontal, with a very slight inclination ($<1^{\circ}$) from the central part of the island to the coast. Its base lies unconformably on the Garantón Trondhjemite. Along the contact area with Limestone Terrace 3 it is probable that it lies over part of the latter's edge. The external edge of Limestone Terrace 2 consists of a low cliff (up to 1.5 m high), located between 0.5 km and 1 km from the coast, except at the southeastern end of the island. Along this cliff it is in contact with Limestone Terrace 1. In the rest of the outcrops, the cliff lies on trondhjemite. As in the case of Limestone Terrace 3, the contact with the trondhjemite consists of a basal conglomerate of igneous rocks and limestone. Linear structures can be observed on the surface of Limestone Terrace 2 (especially on aerial photographs), which are parallel to the general curvature of the outcrop (Fig. 2). These probably represent ancient shorelines. In addition, there are numerous karstic structures.

Limestone Terrace 2 consists of two facies: a fossiliferous facies along the external edge and an arenaceous facies in the inner part, near the contact with Limestone Terrace 3. The fossiliferous facies lies within an outer belt approximately 1 km wide, from the outward cliff. It is composed of a light tan limestone (grey in weathered surfaces), similar to the limestone of Limestone Terrace 3, but with fewer quantities of calcite. The corals are less altered and are relatively easy to recognize in outcrop. Among them, the following were identified: Acropora palmata, Diploria labyrinthiformis, Montastrea sp., and a probable specimen of Solenastrea. Diagenetic alteration is clearly recognizable, although it has progressed to a lesser extent than in Limestone Terrace 3. In addition to their external structures, remnants of their internal structures can still be recognized, in particular the columella and septae. The arenaceous facies crops out in the internal belt of Limestone Terrace 2. It consists of calcareous conglomerate, calcarenite, and calcilutite, and lesser amounts of calcareous sandstone and sandstone. Occasionally fossiliferous zones (coquinoid rock) are found which contain marine shells (gastropods, pelecypods).

The external fossiliferous facies represents a former reef which extended along the La Blanquilla coast. The arenaceous facies represents the reef lagoon and beach deposits. The lack of sections through the arenaceous facies did not permit a detailed sedimentological analysis; all observations had to be made on the surface of the terrace. The thickness of Limestone Terrace 2 can only be estimated from the outcrops in contact with the Garantón Trondhjemite; it varies between 1.5 or 2 m and probably 5 m.

3.3 Limestone Terrace 1

Limestone Terrace 1 represents the youngest limestone on La Blanquilla. This limestone crops out along the border of almost the entire island (Figs. 2 and 3), forming a narrow terrace and a 7 m to 10 m cliff. It is best developed in the northern and eastern parts of the island where it forms a continuous cliff which is being actively eroded by the waves. The surface of the terrace is horizontal and many karstic structures are found (dolines, etc.) along with collapse structures caused by wave erosion. Within the cliff which marks the external border of the terrace there is substantial evidence of former wave erosion, such as submarine caves, natural bridges and wave-cut notches. The base of the terrace lies unconformably on the Garantón Trondhjemite. Just above this contact there is a basal conglomerate of up to 1.5 m thickness, composed of trondhjemite, other igneous rocks, and limestone, in addition to lesser quantities of metamorphic rocks, probably derived from the Los Hermanos Islands or intermediate zones (Schubert and Moticska, 1973).

The best and most accessible outcrops of Limestone Terrace 1 are located between El Falucho and La Cabecera (Fig. 2), along the southeastern coast of the island. Fig. 4 shows two typical sections of this terrace in which the stratification marked by different coral species is evident. This can be interpreted as resulting from environmental conditions during deposition of the limestone; or due to variation in sea level during that deposition. In the sections, there is a modern wave-cut notch, an earlier one approximately at 1.5 m to 2 m a.s.l. and older ones at higher elevations.

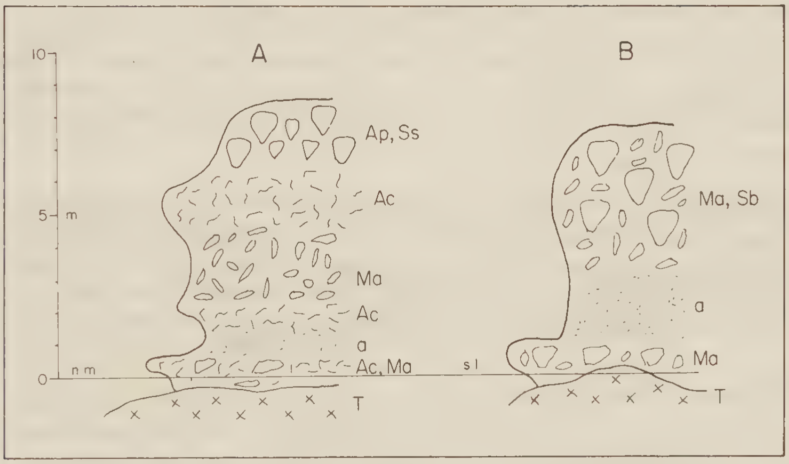

Fig. 4 Stratigraphic sections of Limestone Terrace 1, La Blanquilla Island: (A) first bay east of El Falucho (Fig. 2); (B) second bay east of El Falucho (Fig. 2). Symbols are: a – calcarenite; Ac – *Acropora cervicornis*; Ap – *A. palmata*; Ma – *Montastrea annularis*; Sb – *Solenastrea bournoni*; Ss – *Siderastrea siderea*, and T – Garantón Trondhjemite

The limestone of Limestone Terrace 1 is very fossiliferous; it consists of fragments of corals of different species, stratified and horizontal. In addition, there are numerous corals in growth position. The latter are of special importance for radiometric dating because they represent corals which were living at the time of, or shortly before, limestone formation. Several of these corals in growth position were carefully collected for geochronologic analyses. There are also subordinate layers of calcarenite (Fig. 4), which include fragments of marine shells and corals. Among the corals collected, the following were identified: Acropora cervicornis, A. palmata, Colpophylia natans, Diploria sp., Montastrea annularis, M. cavernosa, Siderastrea siderea, Solenastrea bournoni, and S. sp. Among the corals found in growth position, all belong to the genus Montastrea. As expected, the diagenetic alteration of Limestone Terrace 1 is much less than in the other terraces, which is evidence of its younger age. The internal structure of the corals is easily recognized and in great part they conserve their original mineralogy (aragonite).

The thickness of Limestone Terrace 1 is variable, but in general it varies between 5 m and 10 m.

3.4 Age and tentative correlation

The age of the Blanquilla Formation can be estimated by comparison with other limestone sequences in the Caribbean region. On the islands of Aruba, Curaçao, and Bonaire, for example, occurs a sequence of five Pleistocene outcrop terraces which are progressively older from lowest to highest (de Buisonjé, 1964, 1974), of Pleistocene age. On La Orchila, there is a marine terrace at elevations between 1 m and 3 m a.s.l. (Schubert and Valastro, 1976), whose age was determined radiometrically as Sangamon (approximately 131 000 years B.P., as determined by the $^{230}Th/^{238}U$ method). This age correlates rather well with radiometric ages determined on the terrace sequence of Barbados (Mesollela et al., 1969; Matthews, 1973). In particular, the La Orchila terrace correlates radiometrically with Terrace 3 of Barbados. Assuming that the lower terraces (preserved best) represent a general episode of limestone formation during the Sangamon Interglacial, then Limestone Terrace 1 of La Blanquilla would be equivalent to the Lower Terrace of Aruba, Curaçao and Bonaire, the marine terrace of La Orchila, and Terrace 3 of Barbados. In addition, it could be equivalent to Terrace 1 of Jamaica (Cant, 1973; Horsfield, 1975), and the First Terrace (Primera Terraza) of the Matanzas-Habana region of Cuba (Shanzar et al., 1975).

In order to quantify these correlations, a series of carefully collected samples from the terraces of Curaçao and La Blanquilla are being analysed at present, with the collaboration of the U.S. Geological Survey (Denver, Colorado, U.S.A.). The results of these analyses will give a firmer basis for defining the chronology and correlations of these terraces with other sequences of marine terraces in the Caribbean Sea and elsewhere.

4. ACKNOWLEDGEMENTS

I thank the Oficina Nacional de Pesca, in particular the Oficina de Investigaciones Pesqueras of Cumaná, for transport to La Blanquilla and assistance there. Juan Urich kindly cooperated in the coral identifications. Maraven Company generously prepared the petrographic thin sections. Finally, I would like to thank Raúl Merecuana in a very special way for his assistance in the field work.

5. REFERENCES

Bonatti, E. and S. Gartner, Caribbean climate during Pleistocene ice ages. Nature,Lond., 1973 244:563-611

Cant, R.V., Jamaica's Pleistocene reef terraces. Geol.Mijnbouw, 52:157-60 1973

de Buisonjé, P.H., Marine terraces and subaeric sediments on the Netherlands Leeward Islands,
1964 Curaçao, Aruba and Bonaire, as indicators of Quaternary changes in sea level and
climate. 1 and 2. Proc.K.Akad.Wet.Amsterdam (B), 67:60-79

__________, Neogene and quaternary of Aruba, Curaçao and Bonaire. Uitg.Natuurwet.Studiekr.
1974 Suriname, 78:293 p.

Horsfield, W.T., Quaternary vertical movements in the greater Antilles. Bull.Geol.Soc.Am.,
1975 86:933-8

Lahey, J.F. On the origin of the dry climate in northern South America and the southern
1973 Caribbean. In Coastal deserts. Their natural and human environments, edited by
D.H.K. Amiran and A.W. Wilson. Tucson, University of Arizona Press, pp. 75-90

Lowe, P.R.A., A naturalist on desert islands. London, Witterby Co.
1911

Maloney, N.J., Geology of La Blanquilla island with notes on Los Hermanos islands, eastern
1971 Venezuela. Proc.Carib.Geol.Conf., 5:91-5

Matthews, R.K., Relative elevation of Late Pleistocene high sea level stands: Barbados uplift
1973 rates and their implications. Quaternary Res., 3:147-53

Mesollela, K.J. et al., The astronomical theory of climatic change: Barbados data. J.Geol.,
1969 77:250-74

Peter, G., Geology and geophysics of the Venezuelan continental margin between Blanquilla
1972 and Orchila islands. NOAA Tech.Memo., (ERL 226-AOML 6): 82 p.

Rutten, L., On rocks from the Venezuelan islands between Bonaire and Trinidad and on some
1931 rocks from northwestern Venezuela. Proc.K.Akad.Wet.Amsterdam, 34:1101-10

__________, New data on the smaller islands north of Venezuela. Proc.K.Akad.Wet.Amsterdam,
1940 43:820-7

Santamaría, F. and C. Schubert, Geochemistry and geochronology of the southern Caribbean -
1974 northern Venezuela plate boundary. Bull.Geol.Soc.Am., 85:1085-98

Schubert, C. and P. Moticska, Reconocimiento geológico de las islas venezolanas en el Mar
1973 Caribe, entre Los Roques y Los Testigos (Dependencias Federales). 2. Islas orientales y conclusiones. Acta Cient.Venez., 24:19-31

Schubert, C. and S. Valastro, Quaternary geology of La Orchila island, central Venezuelan
1976 offshore, Caribbean Sea. Bull.Geol.Soc.Am.,(87)

Shanzer, E.V., O.M. Petrov and G. Franco, Sobre formaciones costeras del Holoceno en Cuba,
1975 las terrazas pleistocénicas de la región Matanzas-Habana y los sedimentos vinculados a ellas. Ser.Geol.Acad.Cien.Cuba, (21):26 p.

Sievers, W., Die Inseln vor der Nordküste von Venezuela. Globus, 74:163-5, 291-4, 302-7
1898

Vila, M.A., Aspectos geográficos de las Dependencias Federales. Caracas, Corporación Venezo-
1967 lano Fomento, 112 p.

Walter, H. and E. Medina, Caracterización climática de Venezuela sobre la base de climadiagramas de estaciones particulares. Bol.Soc.Venez.Cienc.Nat., 29:211-40
1971

Wilhelmy, H. Die Klimamorphologische und pflanzengeographische Entwicklung des Trockengebietes am Nordrand Südamerikas seit dem Pelistozän. Erde, Berl., 6:244-73
1954

Zonneweld, J.I.S., Quaternary climatic changes in the Caribbean and N. South America. Eiszeitalter.Geoenw., 19:203-8
1968

Zuloaga, G., La Blanquilla y Los Hermanos. Bol.Acad.Cienc.Fís.Mat.Nat.Caracas, (49):46 p.
1953

LATE QUATERNARY CALCIUM CARBONATE DISSOLUTION HISTORY, WESTERN GULF OF MEXICO

by

R.C. THUNELL
Graduate School of Oceanography
University of Rhode Island
Kingston, Rhode Island

CONTENTS

1. INTRODUCTION
2. PHYSIOGRAPHIC AND OCEANOGRAPHIC SETTING
3. METHODS OF INTERCORE CORRELATION
4. PALEOCLIMATOLOGY
5. CHRONOLOGY
6. SEDIMENTATION RATES
7. CALCIUM CARBONATE DISSOLUTION
8. CONCLUSIONS
9. REFERENCES

Abstract

Calcium carbonate dissolution has been studied in eighty piston cores from the western Gulf of Mexico taken at depths ranging from 965 m to 3 630 m. The degree of dissolution throughout the cores was determined by studies of foraminiferal test fragmentation, benthic foraminiferal abundance, calcium carbonate concentration, and various relationships between solution susceptible and solution resistant planktic foraminiferal species. A dissolution or 'preservation' curve was produced for each core by subjecting these variables to a principal component analysis. This is a multivariate statistical technique that explains the variation in the observed data in terms of independent and artificial variables called principal components. The paleoclimatic history recorded in these cores is similar to those defined previously in the Gulf of Mexico and the Caribbean. Two megascopically distinct ash layers and well defined planktic foraminiferal subzones permit precise intercore correlation of dissolution horizons. All cores demonstrate intense dissolution during several of these subzones, especially during the early-middle Y glacial episode, X1 interglacial episode, and W1 glacial episode. Other less consistent dissolution horizons exist in various cores. Sedimentation rates increase while calcium carbonate concentrations decrease during glacial episodes, suggesting increased dilution by terrigenous materials. Despite this, glacial episodes demonstrate greater dissolution and worse preservation of foraminiferal tests. Therefore, increased dissolution of calcium carbonate during glacial episodes must be a function of some mechanism that more than compensates for the increased rate of burial by terrigenous sediments. Dissolution is particularly enhanced in the shallower depths, indicating that conventional open ocean dissolution processes are not responsible for the observed effects. A shoaling of the lysocline andoxidation of organic matter may be the primary mechanisms controlling the dissolution of calcium carbonate in the western Gulf of Mexico.

Resumen

Se estudia la disolución del carbonato cálcico en las aguas de la parte occidental del Golfo de México, utilizando ocho testigos de émbolo, a profundidades de 965 a 3 630 metros. El grado de disolución en los testigos se determinó estudiando la fragmentación experimental de foraminíferos la abundancia de foraminíferos bénticos, la concentración de carbonato cálcico y las relaciones entre las especies foraminíferas plácticas susceptibles o resistentes a la solución. Para cada testigo se trazó la curva de disolución o de 'conservación', sometiendo estas variables a un análisis de sus principales componentes, que es un procedimiento estadístico de múltiples variables que explica la variación de los resultados obtenidos en función de variables independientes y artificiales denominadas componentes principales. La historia paleoclimática registrada por estos testigos es análoga a la ya definida para el Golfo de México y el Caribe. Dos estratos volcánicos megascópicamente diferentes, y zonas foraminíferas plácticas bien definidas permiten precisar la correlación, entre los testigos, de los horizontes de disolución. En todos los testigos se observó una intensa disolución durante varias de estos subperíodos, especialmente durante el episodio glaciarico, el episodio interglaciarico X1 y el episodio glaciarico W1. En varios testigos se observaron también otros horizontes de disolución menos consistentes. Durante los episodios glaciaricos, las velocidades de sedimentación aumentan, mientras que las concentraciones de carbonato del calcio disminuyen, lo que indica una mayor disolución de materiales terrígenos. No obstante, en las glaciaciones se observa una mayor disolución y una peor conservación de los foraminíferos experimentales; por consiguiente, la mayor disolución de carbonato cálcico durante los episodios glaciaricos tiene que depender de algún mecanismo que compense sobradamente la mayor velocidad de enterramiento de los sedimentos terrígenos. La disolución se intensifica particularmente en las aguas poco profundas, lo que indica que los efectos observados no pueden atribuirse a los procesos convencionales de disolución en los mares abiertos. Uno de los mecanismos principales que regulan la disolución del carbonato cálcico en la parte occidental del Golfo de México podría ser la anoxidación lisoclina de la materia orgánica a menores profundidades.

1. INTRODUCTION

Alteration of calcareous microfaunal assemblages by calcium carbonate dissolution has been recognized since the earliest investigations of deep-sea sediments (Murray and Renard, 1891). Despite much recent effort and consequent better understanding of dissolution processes (Olausson, 1965; Berger, 1968, 1970; Broecker, 1971; Gardner, 1975), some controversy still exists concerning the relationship between Quaternary glacial-interglacial episodes and variations in the degree of dissolution. Cyclic carbonate concentration patterns in the equatorial Pacific were originally observed by Arrhenius (1952) and again reported by Hays et al. (1969). Arrhenius (1952) concluded that carbonate accumulation rates are primarily controlled by productivity, whereas Berger (1973) associates carbonate minimum levels with enhanced interglacial dissolution. This latter hypothesis has been supported by the subsequent work of Thompson and Saito (1974). Difficulty arises when trying to apply this dissolution hypothesis to Atlantic sediments. Olausson (1965, 1971) has reported that in the Atlantic, carbonate maximum levels correspond with intergla ials and carbonate minimum levels with glacials. Gardner (1975) has observed enhanced dissolution during glacial episodes in equatorial Atlantic deep-sea cores; a direct contrast to the earlier findings of Berger (1973). The present discussion focuses on carbonate dissolution in deep-sea Quaternary sediments of the western Gulf of Mexico and in particular attempts to determine whether dissolution was enhanced during glacial or interglacial episodes.

In order to make accurate paleoecological or paleoclimatic interpretations, it is necessary to differentiate between faunal changes that result from climatic or related environmental changes and those superimposed by dissolution. Dissolution does not modify an assemblage in a uniform manner due to the differential susceptibility of each species (Berger, 1968). Most of the resistant species tend to be warm-water forms and therefore a dissolution modified assemblage would normally have a warmer or more equatorial appearance compared with the original assemblage (Berger, 1968). A well defined biostratigraphic zonal scheme for the Gulf of Mexico (Kennett and Huddlestun, 1972) is employed in this study to accurately place the dissolution history within a stratigraphic and paleoclimatic framework, and to facilitate intercore correlation of dissolution horizons. The eight cores, collected during TRIDENT Cruise 126, evaluated in this study were taken from the western Gulf of Mexico (Fig. 1) and range in depth from 965 m to 3 630 m.

2. PHYSIOGRAPHIC AND OCEANOGRAPHIC SETTING

Detailed bathymetric and geomorphologic studies of the Gulf of Mexico have been carried out by Uchupi (1967) and Bergantino (1971). The traverse of eight cores examined in this study extends from the continental shelf adjacent to the Mexican Ridge System at a depth of 965 m, across the ridge system and onto the abyssal plain to a depth of 3 630 m. The ridge system acts as a partial barrier to the transport of terrigenous sediments from the continental shelf area into deeper parts of the Gulf of Mexico. Cores located in the abyssal plain seaward of this ridge system probably derive most of their terrigenous components from material carried through the Campeche Canyon. Quaternary sediment patterns for this area have been described in detail by Bouma (1971), Davies (1971), and Sweet and Bouma (1971).

Physical oceanographic characteristics of the Gulf of Mexico have been examined by Leiper (1970) and Nowlin (1971). The general circulation pattern consists of a Loop Current which flows northwestward from the Yucatan Straits affecting the central and eastern gulf. This Loop Current is an extension of the Yucatan Current which flows clockwise through the central gulf and through the Florida Straits (Nowlin, 1971). Unlike the eastern gulf, the western gulf undergoes strong seasonal changes with a well defined winter flow pattern and highly variable summer pattern caused by eddies drifting into the western gulf.

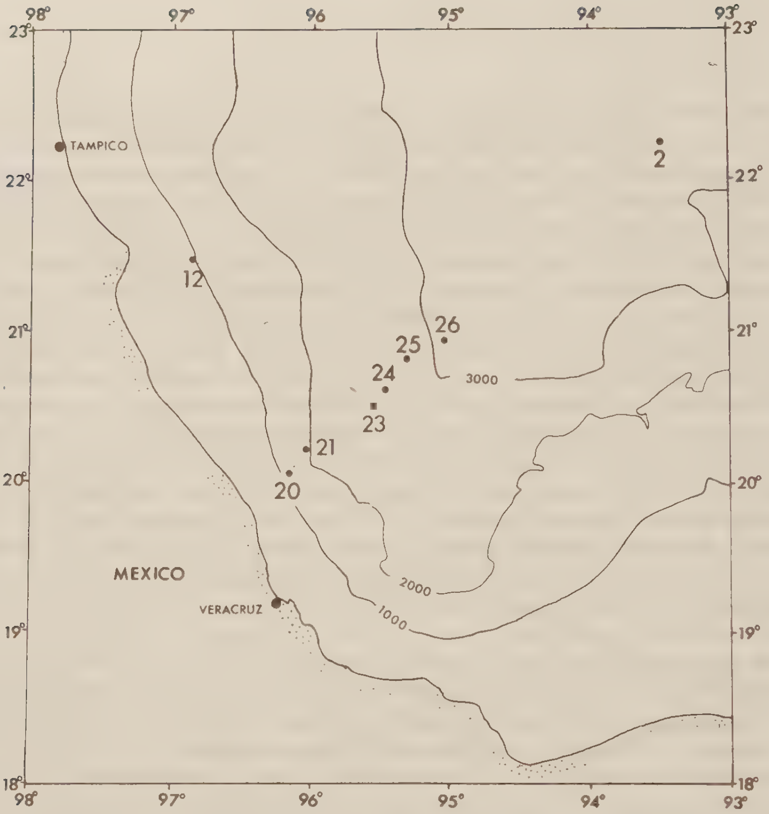
98°
97°
96°
95°
94°
93°
23°
22°
21°
20°
19°
18°
TAMPICO
VERACRUZ
MEXICO
2
12
20
21
23
24
25
26
3000
2000
1000

Fig. 1 Location of cores used in this study

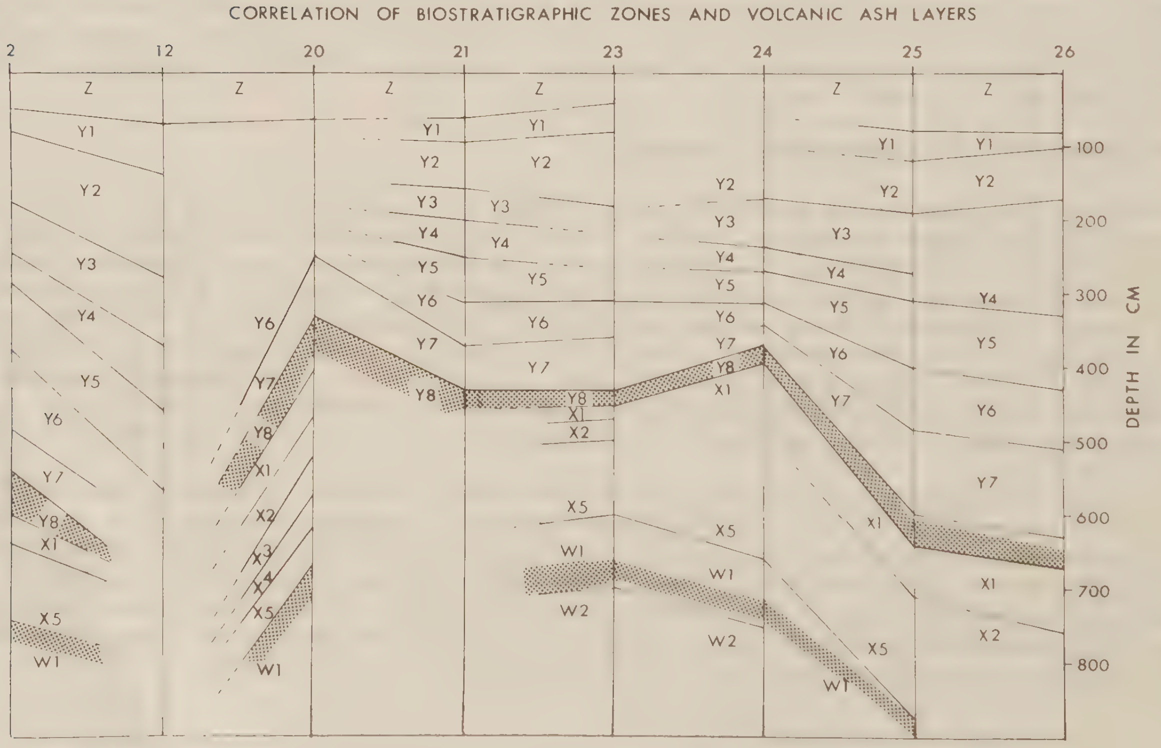

Fig. 2 Intercore correlation of biostratigraphic zones and volcanic ash horizons for cores used in this study from the western Gulf of Mexico. Stipled sections represent ash layers. Core length is indicated in centimetres

3. METHODS OF INTERCORE CORRELATION

3.1 Biostratigraphy

Species frequency patterns of planktonic foraminifera provide the most accurate method for intercore correlation in this study. The basic biostratigraphic framework is the Ericson and Wollin (1968) zonal scheme, which is based on the consistent presence or absence of the *Globorotalia menardii* complex (*G. menardii menardii*, *G. menardii tumida* and *G. menardii flexuosa*). These zones, designated Q-Z in order of decreasing age, generally represent alternating glacial and interglacial episodes. The more precise intercore correlation required is based on the Kennett and Huddlestun (1972) planktonic foraminiferal subzonations (Fig. 2). Kennett and Huddlestun (1972) recognized 18 distinct planktonic foraminiferal subzones within the Gulf of Mexico Quaternary sequence, ranging from zone V through zone Z. These zones are based primarily on the frequency distribution of eight planktonic foraminiferal species or species complexes.

In the cores studied, zones W-Z (approximately 170 000 years B.P. to the present) are represented (Fig. 2). The warm stages, zones X and Z, are marked by the consistent presence of the *G. menardii* complex, while the W and Y cold stages are marked by the absence of the *G. menardii* complex. Two subzones are recognized within the W; five subzones within the X; eight subzones within the Y; and two subzones within the Z (Fig. 2) (Kennett and Huddlestun, 1972). These subzones are biostratigraphic divisions which do not necessarily reflect climatic change, although the faunal oscillations that mark them also often suggest climatic control.

3.2 Volcanic Ash Distribution

Two megascopically distinct ash horizons are recognized in the late Quaternary sequence of the western Gulf of Mexico. Since a volcanic eruption is considered to be an instantaneous geologic event, these isochronous time planes, in conjunction with the previously described biostratigraphic framework, provide the basic means for intercore correlation in this study. The two prominent ash layers occur within the W1 subzone and the Y8 subzone (Fig. 2).

The W1 subzone was recovered in 5 of the 8 cores, with all five containing the associated ash layer. The W1 ash layer varied in thickness from approximately 30 cm to 50 cm. Abundant ash is dispersed immediately above and below the layer due to bioturbation. The Y8 ash layer, although not as thick as the W1 ash layer (generally 15-30 cm thick), is readily observed in 7 of the 8 cores (TR126-12 did not penetrate to Y8). The Y8 subzone is a very narrow biostratigraphic unit and in some cores (TR126-2, TR126-20, TR126-21, and Tr126-25) the associated volcanic ash greatly dilutes the planktonic foraminiferal content. Ewing *et al.* (1958) previously found this ash layer to be dispersed over a large part of the Gulf of Mexico and associated it with the X-Y boundary. Less consistent traces of volcanic ash also occurred in some cores in the Y6 and the early X, but the ash does not allow for consistent intercore correlation.

4. PALEOCLIMATOLOGY

4.1 Procedures

In this study the paleoclimatic history of the western Gulf of Mexico was determined for approximately the last 150 000 years by examining sediments recovered through most of the W glacial episode. The consistent presence or absence of the *G. menardii* complex was used to define the interglacial and glacial boundaries respectively. Detailed paleoclimatic changes reflected in the frequency variation of all planktonic foraminifera have been interpreted using a principal component analysis. This analysis is a multivariate statistical technique that explains the variation in the observed data in terms of independent variables called principal components (Malmgren and Kennett, 1972). The components are ranked according to the amount of variance they incorporate, and in this study the first component is interpreted as reflecting temperature changes. A more detailed explanation of the use of principal component analysis in paleoclimatic studies of the Gulf of Mexico is given by Malmgren and Kennett (in preparation). By using this 'total fauna' analysis, both solution susceptible and solution resistant species are employed in the construction of paleoclimatic curves and should partially compensate for bias introduced into the paleoclimatic interpretation by calcite dissolution.

4.2 Paleoclimatic Interpretation

Detailed paleoclimatic curves have been constructed by Kennett and Huddlestun (1972) based on the relative frequencies of temperature sensitive species found in planktonic foraminiferal assemblages of the Gulf of Mexico. From these 'total fauna' curves, a standard climatic curve was generated for the Gulf of Mexico. This generalized curve demonstrates a close relationship between the V-Z zonations of Ericson and Wollin (1968) and the inferred glacial-interglacial episodes.

The technique employed in this study allows for rapid, yet accurate paleoclimatic reconstructions from well-preserved faunas. The variability in the down core frequency of all planktonic foraminifera produces a principal component curve that is interpreted as reflecting climatic changes in the western Gulf of Mexico during approximately the last 150 000 years. The climatic curves produced by this technique exhibit a close correspondence to the climatic curve of Kennett and Huddlestun (1972) and the Caribbean oxygen isotope curve of Emiliani (1971) (Fig. 3). Similarity between the Kennett and Huddlestun (1972) curve and the curves produced in this study is expected since the two techniques group the foraminiferal species similarly. Instead of assuming all forms to be equally 'cold' or 'warm', Kennett and Huddlestun (1972) were able to classify certain species as being 'marginally warm' or 'marginally cold'. Likewise, the principal component analysis assigns a coefficient that varies in sign and magnitude to each individual species depending on that species particular temperature preference.

The relationship between the more important climatic changes and their associated planktonic foraminiferal zones have been discussed elsewhere (Kennett and Huddlestun, 1972). In several cores technical problems such as the implosion of piston core liners resulted in the loss of certain core sections and prevented sampling at 20 cm intervals. This resulted in the loss of detail for those particular portions of the paleoclimatic record.

The terms glacial and interglacial can only be loosely applied to the W and Y zones, and to the X and Z zones respectively. This is because certain climatic episodes within these zones are intermediate between fully glacial and fully interglacial maxima. In particular, the Y7 subzone in the Gulf of Mexico is intermediate between the maximum cooling of the Y zone and the maximum warming of the X zone. Conversely, for the Caribbean climatic record, the section equivalent to the Y7 is actually placed within the X 'interglacial' episode (Emiliani, 1971).

5. CHRONOLOGY

The Broecker and van Donk (1970) time scale, based on Pa^{231} and Th^{230} dates for Caribbean cores, has been employed in this study. A close correlation between major climatic events exists for oxygen isotope curves previously developed for the Caribbean (Emiliani, 1971) and the foraminiferal curves established in this study (Fig. 3). Therefore, by indirectly dating the primary climatic events, the climatic history of the western Gulf of Mexico is placed within a proper chronologic framework. Biostratigraphic zones and small scale climatic events superimposed on the broad glacial-interglacial episodes are dated by using sedimentation rates calculated between previously dated time horizons (Broecker and van Donk, 1970; Kennett and Huddlestun, 1972). Since no core had a complete W sequence, the oldest climatic event that can be dated by correlation is the W-X boundary or termination II (Broecker and van Donk, 1970) at 127 000 years B.P. Therefore, the maximum age of the complete climatic sequence obtained in this study is approximately 150 000 years B.P.

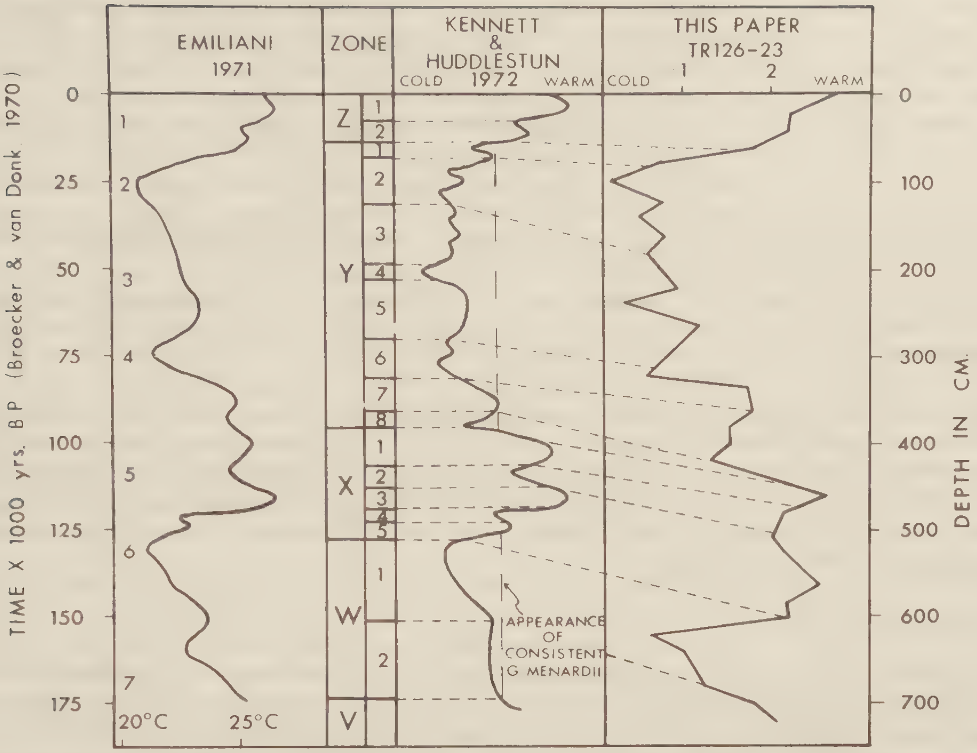

Fig. 3 Comparison of Late Quaternary paleoclimatic curves. For all curves, cold is to the left, and warm is to the right. Emiliani (1971) paleoclimatic curve and associated stages (1-7) based on oxygen isotope analysis of Caribbean deep-sea cores. Kennett and Huddlestun (1972) biostratigraphic zonations and paleoclimatic curve based on faunal analysis of western Gulf of Mexico deep-sea cores. Paleoclimatic curve for core TR126-23 form this study generated by principal component analysis. Time scale of Broecker and van Donk (1970) is plotted on the left, and core length is plotted on the right.

6. SEDIMENTATION RATES

Consistent sedimentation rates of approximately 5 cm/1 000 years were calculated for 7 of the 8 cores for the past 11 000 years (Z interglacial). A higher rate of approximately 7 cm/1 000 years was calculated for the Z interglacial episode in core TR126-25. Prior to the Z-Y boundary, sedimentation rates vary between approximately 3 and 8 cm/1 000 years and appear to be partially related to water depth.

The shallowest core (TR126-12), located on the continental shelf at a depth of 965 m, has a sedimentation rate of approximately 8 cm/1 000 years for the last glacial episode (11 000 years B.P. to 90 000 years B.P.). This high sedimentation rate can best be explained by the proximity to the Mexican coast. Lowered sea levels during the Y glacial episode and greater discharge down the slope of the shelf probably resulted in increased input of terrigenous materials.

Cores taken at depths of from 1 315 m to 2 550 m (TR126-20, TR126-21, TR126-23, TR126-24) and located within the Mexican Ridge province, demonstrate fairly consistent sedimentation rates of approximately 4-5 cm/1 000 years throughout their entire length (zones X-Z). Only one core (TR126-24) had a higher sedimentation rate of approximately 7 cm/1 000 years during the X interglacial episode. These rather uniform rates probably result from restriction of terrigenous material transport from the shelf region by the Mexican Ridge System. Although terrigenous input onto the shelf region may increase during glacial episodes, the ridge system effectively inhibits the seaward movement of this material and prevents any significant glacial increase in sedimentation rates.

relative abundance throughout each core. It is important that each of these curves be interpreted only as representing possible dissolution horizons since fluctuations in all of the species percentages may reflect responses to various environmental conditions other than dissolution. Both the susceptible group and the resistant group include warm and cold water species in order to help minimize the effects of frequency changes caused by climatic effects.

Fluctuations in the frequency of G. ruber is considered to be a particularly good dissolution indicator because of low resistance to dissolution (Berger, 1970) and lack of any distinct temperature preference in the Gulf of Mexico (Kennett and Huddlestun, 1972). Since this species is the major faunal component in Gulf of Mexico sediments, significant decreases in the abundance can most likely be interpreted as the result of dissolution and not a reaction to climatic change. An inverse relationship between G. ruber frequency and N. dutertrei frequency is expected.

N. dutertrei is a highly solution-resistant form and has been used previously as a dissolution indicator (Kennett and Huddlestun, 1972). However, variation in the frequency of this species may reflect a response to environmental effects (Ruddimen, 1971) other than dissolution. To differentiate between these two alternative processes, comparisons are made between fluctuations of N. dutertrei and other species with known environmental preferences, such as G. sacculifera and G. inflata.

7.2 Results and Discussion

In an attempt to quantify the effects of dissolution, each core was examined with respect to the previously described solution parameters to identify the timing and magnitude of the dissolution intervals (Figs. 4 and 5). Intercore correlation, using biostratigraphic zonation, makes it possible to determine geographic continuity of dissolution horizons between cores. To evaluate the dissolution history within each biostratigraphic subzone, each of the four parameters must be considered individually and collectively to differentiate between other possible contributing factors besides dissolution.

Changes in benthonic foraminiferal abundance for each core are plotted as a ratio of the abundance of benthonic to planktonic foraminifera (Fig. 4). When extremely low percentages of benthonic foraminifera occur, an increase of only several individual specimens can result in high fluctuations of the benthonic to planktonic ratio. A general decrease in benthonic percentage occurs with increasing water depth, and all cores except TR126-2 display sufficiently high percentages of benthonic foraminifera needed to use a ratio method. For core TR126-2, a variation of only 5 specimens produces a 50 percent change in the benthonic to planktonic ratio, and therefore the ratio is not an acceptable dissolution indicator for this core. Maximum benthonic abundances in the remaining cores vary between 13 percent (TR126-26) and 55 percent (TR126-12) of the total fauna. The benthonic to planktonic ratio in these cores indicate most intense and consistent dissolution in the early-middle part of the Y zone (Y5, Y6, Y7), the end of the X zone (X1), and the end of the W zone (W1).

Fragmentation of planktonic foraminiferal tests is an obvious qualitative characteristic of a sample that has undergone dissolution. A quantitative interpretation of fragmentation, however, is difficult because a single test can break into any number of increasingly smaller fragments. Furthermore, fragments caused by dissolution cannot be differentiated from those due to simple mechanical breakage from bioturbation. The fragment to whole test ratio for each core (Figs. 4 and 5) indicates enhanced dissolution during the early-middle Y zone (Y5, Y6, Y7), the X1 subzone, and possibly the W1 subzone. The amount of fragmentation, when considered as a percentage of the sum of whole tests plus fragments, varied between 5 percent and 70 percent.

The down core frequency distribution of G. ruber displays major decreases throughout much of the Y zone (Y2, Y3, Y5, Y6, Y7), the X1 zone, and the W1 subzone (Figs. 4 and 5). However, changing water mass characteristics as well as dissolution may be responsible for these observed decreases. It is inferred that the decrease in G. ruber associated with the early-middle Y zone (Y5, Y6, Y7), the X1 subzone and the W1 subzone result from dissolution, since these zones correspond with the zones suggested by the other dissolution parameters. In the late Y zone (Y2, Y3), decreases in G. ruber may be associated with changes in water mass properties such as temperature, salinity, or nutrient content.

Cores located seaward of the Mexican Ridge System (TR126-25, TR126-26, TR126-2) and on the abyssal plain (2 760 m to 3 630 m) are marked by higher sedimentation rates (approximately 7-8 cm/100 years) during the Y glacial episode. Since the Mexican Ridge System is apparently effective in blocking terrigenous sediment transport from the west, another region must serve as the source for this increased input. This material may be derived from the coastal region to the south and transported to the abyssal plain through the Campeche Canyon by turbidity flows and bottom currents.

7. CALCIUM CARBONATE DISSOLUTION

7.1 Dissolution Parameters

Four basic components of deep-sea sediments were examined in order to identify dissolution horizons in the Gulf of Mexico for the last 150 000 years: (1) degree of foraminiferal test fragmentation; (2) benthonic foraminiferal abundance; (3) total calcium carbonate concentration, and (4) relationships between solution susceptible and solution resistant species. Under certain conditions, each of these parameters may be partially or completely regulated by other environmental mechanisms (i.e. changes in productivity, noncalcareous dilution) rather than dissolution factors.

Increased fragmentation of fossil assemblages has been directly related to dissolution (Berger, 1970), possibly enhanced by bottom water turbulence (Edmond, 1974). Calcium carbonate dissolution is a selective process that enhances the test preservation of thick-walled planktonic foraminifera and benthonic foraminifera (Berger, 1973). The possibility also exists that fragmentation may be partially due to simple mechanical breakage during bioturbation. This second possibility is assumed to be only a minor contributor to the total amount of fragmentation, except where tests have been weakened due to dissolution.

Benthonic foraminiferal abundance in deep-sea sediments is a useful indicator of dissolution for two reasons: in general, benthonics are approximately three times more resistant to dissolution than planktonics (Berger, 1973), and, benthonic abundances in the Gulf of Mexico are fairly low below 2 000 m (Phleger, 1951). However, changing bottom water conditions may also cause variations in benthonic abundance. For example, increased bottom water temperatures may allow the migration of certain shallow dwelling species into deeper habitats. Berger (1973) attempted to calculate the loss of foraminifers to dissolution based on three assumptions: (1) the initial benthonic to planktonic ratio is constant through time; (2) the initial benthonic to planktonic ratio is only effected by dissolution and not productivity, and, (3) benthonic foraminifera are not susceptible to dissolution. From these assumptions, the percentage of foraminifers lost to dissolution can be derived from: $L = 1 - Bo/B$ where L is the percentage of lost foraminifera, Bo is the initial benthonic percentage, and B is the final benthonic percentage (Berger, 1973). This relationship can only predict a general value change since the basic assumptions are almost certainly faulty. In this study, both benthonic and planktonic foraminiferal fragments were observed indicating that benthonics are indeed susceptible to dissolution and that the third assumption listed above is false. The loss of benthonic foraminifera to dissolution results in an L value lower than that predicted by the initial assumptions.

Variations in calcium carbonate concentrations are directly related to productivity and noncalcareous dilution, as well as dissolution. Several workers (Ruddimen, 1971; Hays and Perruzza, 1972) consider variations in detrital clay input to be the controlling factor for the distribution of calcium carbonate in the equatorial Atlantic. High clay concentrations (60-80 percent) suggest that dilution may also be the primary determinant of calcite concentrations in the Gulf of Mexico. Equations derived to calculate the percentage of calcium carbonate lost to dissolution (Berger, 1971) cannot be applied in this study because of the extremely high proportion of noncalcareous sediment components.

Foraminiferal dissolution index curves for each core used in this study were constructed based on the frequency ratio of four solution resistant species (G. crassaformis, G. truncatulinoides, G. inflata, and N. dutertrei) to four solution susceptible species (G. ruber, G. bulloides, G. sacculifera, and O. universa). The particular species in each grouping were selected according to Berger's (1970) solution susceptibility ranking and their

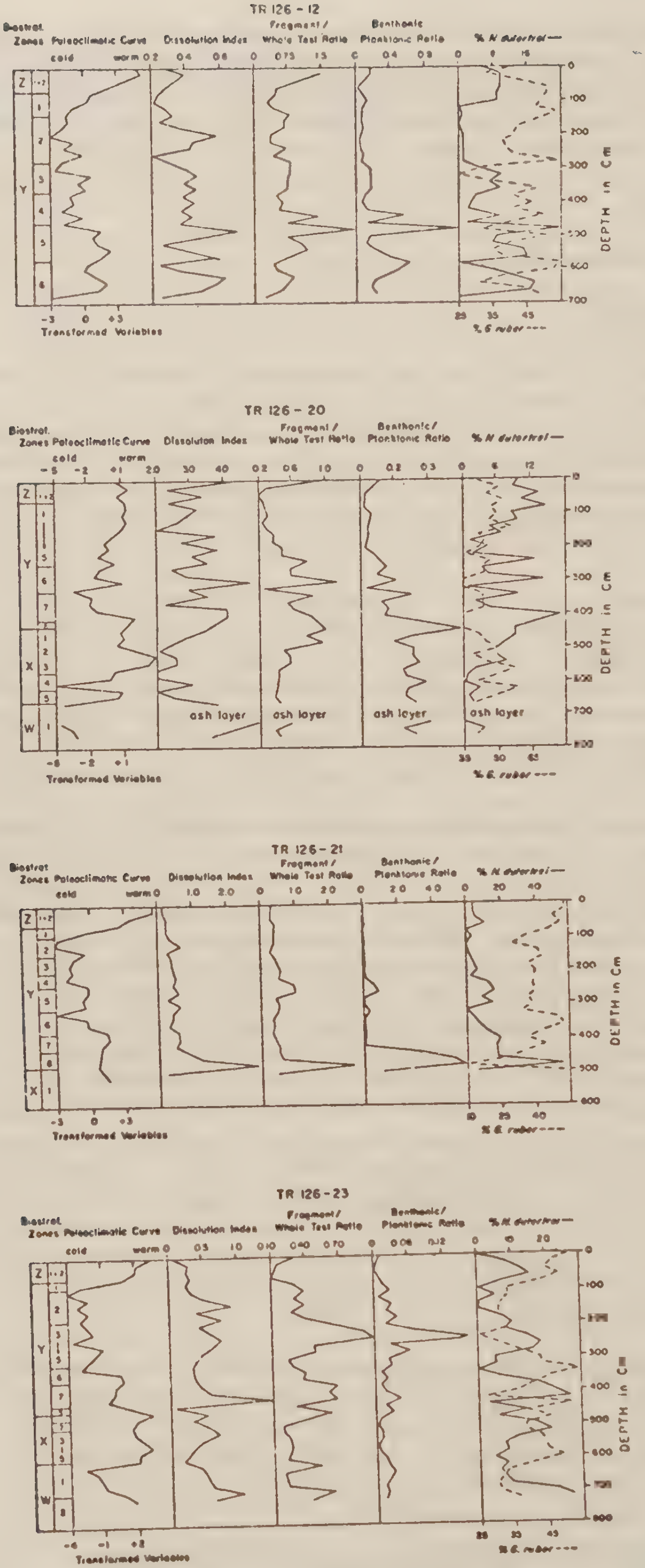

Fig. 4 Paleoclimatic curves derived by principal component analysis and dissolution parameters for cores TR126-12, TR126-20, and TR126-23. The biostratigraphic zones were defined by Ericson and Wollin (1968) and Kennett and Huddlestun (1972). Core length is plotted in centimetres

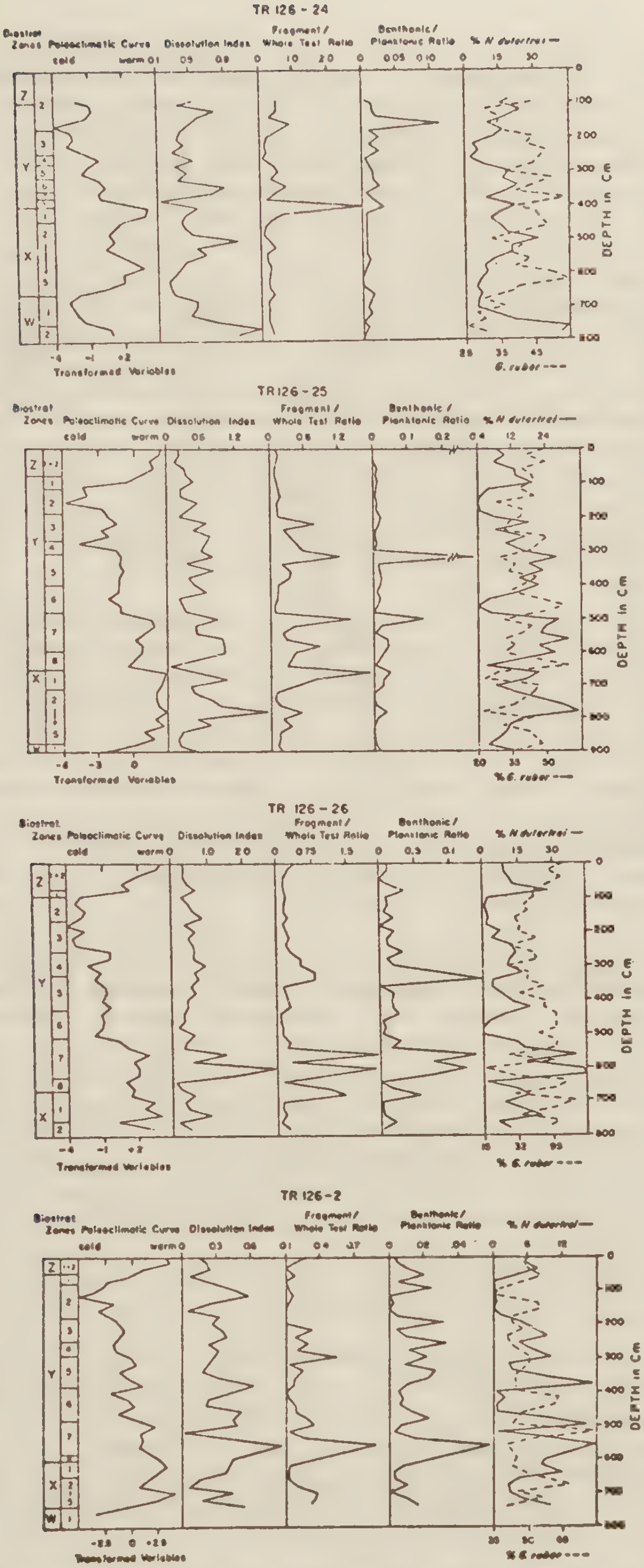

Fig. 5 Paleoclimatic curves derived by principal component analysis and dissolution parameters for cores TR126-24, TR126-25, TR126-26, and TR126-2. The biostratigraphic zones were defined by Ericson and Wollin (1968) and Kennett and Huddlestun (1972). Core length is plotted in centimetres

N. dutertrei frequency increases occur during the early-middle Y zone (Y3, Y5, Y6, Y7), the X1 subzone, and the W1 subzone (Figs. 4 and 5), are well correlated with the subzones indicated by the other dissolution parameters. The down core frequency fluctuations of *N. dutertrei* and *G. ruber* are compared (see Figs. 4 and 5) in order to evaluate the extent of the expected inverse relationship. During intervals marked by the lack of dissolution, *N. dutertrei* and *G. ruber* generally display a random distribution with respect to each other. However, during intervals of dissolution, these two species show a strong inverse relationship because of their contrasting susceptibility to solution. *N. dutertrei* also exhibited distinct frequency increases during the Y1 glacial subzone and the Z interglacial zone. However, since the other parameters do not reinforce the possibility that this is caused by dissolution, the increase in abundance during this glacial-interglacial transitional period is probably a response to an environmental stimulus other than dissolution. In particular, it has been proposed (Ruddiman, 1971) that *N. dutertrei* responds primarily to changes in salinity rather than temperature fluctuations. Kennett and Shackleton (1975) have shown that the melting of the Laurentide ice sheet and subsequent outpouring of fresh water into the Gulf of Mexico between about 15 000 and 12 000 years B.P. caused a significant decrease in surface salinities throughout the Gulf. If this is true, the observed increase in *N. dutertrei* during the Y1 subzone may have resulted from a salinity decrease in surface waters of the Gulf at the end of the last glacial episode.

Calcium carbonate concentration proved to be an ambiguous parameter for identifying specific intervals of dissolution due to overall low concentrations (15 percent to 44 percent) (Fig. 6). Thompson and Saito (1974) also found it difficult to correlate calcium carbonate fluctuations and observed foraminiferal dissolution cycles because of high calcite concentrations in western equatorial Pacific sediments. Calcium carbonate percentage curves (Fig. 6) for western Gulf of Mexico cores however indicate a general trend of decreased calcite content during the early-middle Y zone, and higher concentrations during the Z zone, the X zone, and the upper Y zone. Each curve in Fig. 6 has been divided into a carbonate 'positive' or 'maximum' side and a carbonate 'negative' or 'minimum' side based on the median calcite percentage value of each core. A fairly consistent relationship in the distribution of calcium carbonate exists in the cores examined.

Noncarbonate dilution is considered by some workers to be the principal controlling factor for calcite concentrations in equatorial Atlantic sediments (Ruddiman, 1971; Hays and Perruzza, 1972), but it must be assumed that dissolution has also had some effect. A model that assumes dilution to be the only variable cannot account for the uniform glacial-interglacial sedimentation rates calculated for cores TR126-20, TR126-21, TR126-23, and TR126-24. Uniform sedimentation rates in these cores can best be explained as a balance between increased noncalcareous dilution and enhanced calcite loss to dissolution during the Y glacial episode. The increase in Y glacial sedimentation rates in cores TR126-2, TR126-12, TR126-25 and TR126-26 would be even greater if it were not for calcite loss through dissolution. These two independent factors, dilution and dissolution, appear to respond in unison to produce the observed variations in calcium carbonate content. In the western Gulf of Mexico, the dissolution parameters other than calcite content indicate that intensified dissolution during the early Y glacial episode reduces calcareous sediment accumulation rates.

Only the two cores taken from the shallowest depths, TR126-12 (965 m) and TR126-20 (1 315 m), indicate enhanced dissolution during the Z interglacial episode (Fig. 4). Diagenetic combustion of organic material and subsequent liberation of CO_2 to the sediments can result in increased dissolution at shallow water depths (Berger, 1970; Huang and Goodell, 1970). The organically-induced increase in the corrosiveness of the shelf waters may be independent of glacial-interglacial episodes and result in the observed dissolution pattern in shallow regions.

The Y glacial episode is marked by fairly large temperature variations throughout the zone (Emiliani, 1971). Most of the biostratigraphic subzones can be considered as fully glacial, however, as previously stated, the Y7 subzone is intermediate between fully glacial and fully interglacial conditions. Subzones Y5, Y6, and Y7 appear to be the periods of most intense and consistent dissolution, thus indicating that dissolution has occurred over a range of climatic conditions. Therefore, all of the observed dissolution during the Y glacial episode should not be interpreted as occurring during fully glacial conditions.

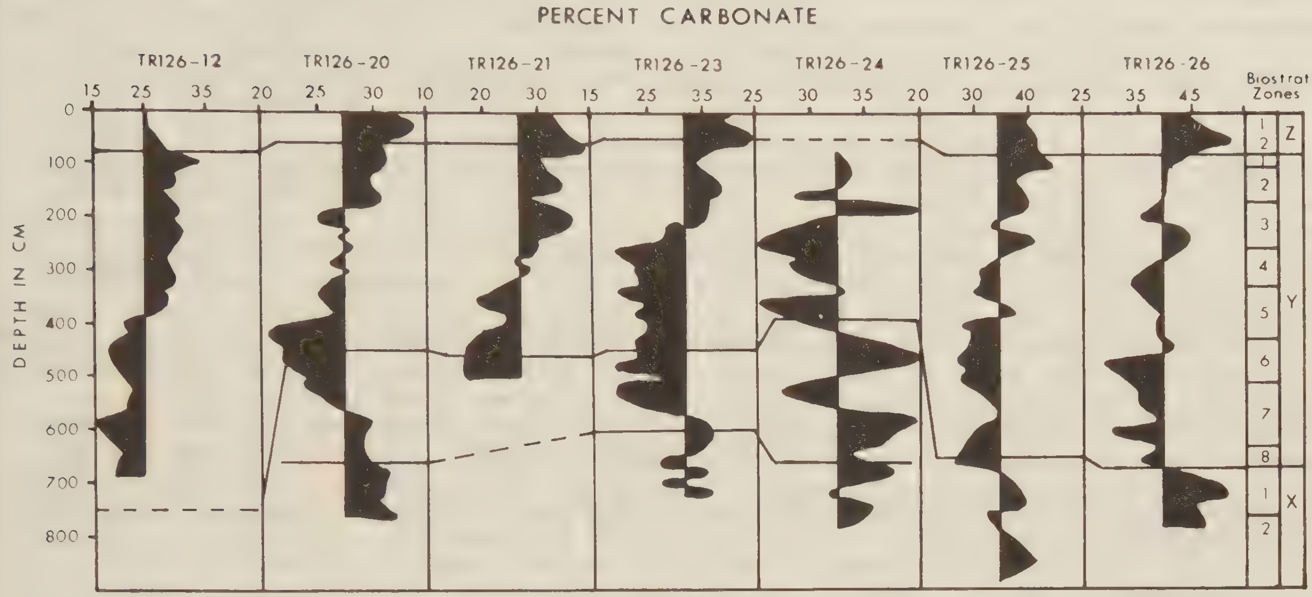

Fig. 6 Calcium carbonate concentrations for all cores used in this study. Each curve is divided about its median carbonate concentration. Note the generally high concentrations in the Z zone and upper Y zone, low concentrations in the lower Y zone and upper X zone, and high concentrations in the lower X zone. The biostratigraphic zones were defined by Kennett and Huddleston (1972). Core length is plotted in centimetres.

Thus, each of the dissolution parameters used in this study display, to a varying extent, an overall down core trend toward increased dissolution during the Y glacial episode. Dissolution horizons are consistently observed during the early-middle Y zone (particularly subzones Y5, Y6, and Y7), the X1 subzone, and the W1 subzone in cores which reached sediment of this age. Other less consistent dissolution intervals also exist throughout each core. Gardner (1975) also observed increased dissolution during glacial episodes of equatorial Atlantic sediments based on parameters similar to those used in this study. This finding is opposite that proposed by Berger (1973) for the equatorial Pacific and North Atlantic. Thompson and Saito (1974) have supported Berger's (1973) hypothesis of intensified interglacial dissolution based on observed foraminiferal dissolution cycles in the equatorial Pacific. The discrepancy in these findings suggests that dissolution may be a function of local water mass characteristics.

If it is assumed that dissolution is essentially a post-depositional process (Berger and Piper, 1972), rapid burial during periods of increased noncalcareous dilution should inhibit dissolution and ensure better test preservation. In the western Gulf of Mexico, this is not the case. Better test preservation and reduced dissolution occur during the interglacial episodes when sedimentation rates are generally lower relative to the Y glacial episode. Conversely, fragmentation increases and preservation is poor during the Y glacial episode in spite of generally higher sedimentation rates. This observation supports the hypothesis that carbonate dissolution during glacial episodes is a function of certain water mass properties that more than compensate for increased dilution by terrigenous sediments.

The controlling mechanisms for increased dissolution during the Y glacial episode in the western Gulf of Mexico are by no means clear. Philippi (1910) was one of the first workers to associate calcium carbonate dissolution with the flow of 'corrosive' Antarctic Bottom Water, while other workers have associated the upper depth limit of this bottom water mass with the lysocline (Berger, 1970). Edmond (1974) considers the advective or turbulent motions of carbon dioxide in rich bottom water to be the primary mechanism responsible for accelerated dissolution. However, there are two reasons why this region may not be controlled by such conventional mechanisms: dissolution is observed at very shallow depths (less than 1 000 m), and the western Gulf lacks any active bottom circulation (Wüst, 1964).

A shoaling of the lysocline and a decomposition of organic material may work simultaneously in controlling carbonate dissolution in the western Gulf of Mexico. Berger (1970) has shown that a shallow lysocline can be expected in highly productive, near shore areas. The delivery of large amounts of organic material to the sea floor near the continent should result in dissolution at abnormally shallow depths (Berger, 1970). In this region of the western Gulf of Mexico, organic material is derived from both continental runoff and overlying productivity. As oxidation occurs, pH is lowered through the release of carbon dioxide and other acidic products, making pore water more corrosive to calcite. The observed increase in dissolution during parts of the Y glacial episode in the western Gulf may reflect increased organic input from exposed continental margins during low sea level stands. The organic material, like the terrigenous sediment, may be concentrated in the near shore end of the traverse due to the seaward restriction of material transport by the Mexican Ridge System. This inferred dispersal pattern of organic material and the existence of a shallow lysocline may thus account for the observed dissolution at all core sites, with particular intensification in the shallower region.

8. CONCLUSIONS

The analysis of certain dissolution parameters in deep-sea sediment cores from the western Gulf of Mexico provides several indications:

(1) Dissolution is enhanced during glacial rather than interglacial episodes. In particular, the early-middle Y zone (Y5, Y6, Y7), the X1 subzone, and the W1 subzone are marked by consistent dissolution over the entire region.

(2) Evaluation of as many dissolution parameters as possible, both individually and collectively, must be made in order to minimize the effects of environmental factors other than dissolution. Foraminiferal test fragmentation and benthonic foraminiferal abundance appear to be the most consistent parameters that react to carbonate dissolution. Generally low calcite concentrations prevent the recognition of individual dissolution horizons but show a general trend toward decreased calcite accumulation rates during the early-middle part of the Y glacial episode.

(3) Terrigenous dilution and carbonate dissolution may work contemporaneously to control the distribution of calcite in this region.

(4) Cores located near the shallowest end of the traverse (TR126-12 and TR126-20) display the most intense dissolution. In the remaining cores dissolution appears to be of a consistent intensity.

(5) Dissolution at all depths makes it difficult to invoke the conventional bottom water dissolution hypothesis. Instead, dissolution may be induced by a shoaling of the lysocline and the decomposition of organic material, the input of which may be enhanced during glacial low stands of sea-level.

9. REFERENCES

Arrhenius, G., Sediment cores from the East Pacific. Rept.Swed.Deep-Sea Exped., 5:227 p.
1952

Bergantino, R.N., Submarine regional geomorphology of the Gulf of Mexico. Bull.Geol.Soc.
1971 Am., (82):741-52

Berger, W.H., Planktonic foraminifera: selective solution and paleoclimatic interpretation.
1968 Deep-Sea Res., 15:31-43

__________, Planktonic foraminifera: selective solution and the lysocline. Mar.Geol.,
1970 8:111-38

__________, Sedimentation of planktonic foraminifera. Mar.Geol., 11:325-58
1971

__________, Deep-Sea carbonates: Pleistocene dissolution cycles. J.Foramin.Res., 3:187-
1973 95

Berger, W.H. and D.J.W. Piper, Planktonic foraminifera: differential settling, dissolution,
1972 and redeposition. Limnol.Oceanogr., 17:275-87

Bouma, A.H., Cyclic sedimentation patterns in deep Gulf of Mexico sediments. In TAMU
1971 results from USNS Kane 1969 Expedition, edited by A.H. Bouma, W.R. Bryant and D.K. Davies. College Station, Texas A&M University, pp. 82-97

Broecker, W.S., Calcite accumulation rates and glacial to interglacial changes in oceanic
1971 mixing. In The late Cenozoic glacial ages, edited by K.K. Turekian. New Haven, Conn., Yale University, pp. 239-65

Broecker, W.S. and J. van Donk, Insolation changes, ice volumes, and the O^{18} record in
1970 deep-sea cores. Rev.Geophys.Space Phys., 8:169-98

Davies, D.K., Deep-sea sands and silts in the Gulf of Mexico. In TAMU results from USNS
1971 Kane 1969 Expedition, Gulf of Mexico, edited by A.H. Bouma, W.R. Bryant and D.K. Davies. College Station, Texas A&M University, pp. 6-36

Edmond, J.M., On the dissolution of carbonate and silicate in the deep ocean. Deep-Sea Res.,
1974 21:455-80

Emiliani, C., The last interglacial: Paleotemperatures and chronology. Science, Wash.,
1971 171:571-3

Ericson, D.B. and G. Wollin, Pleistocene climates and chronology in deep-sea sediments.
1968 Science, Wash., 162:1227-34

Ewing, M., D.B. Ericson and B.C. Heezen, Sediments and topography of the Gulf of Mexico.
1958 In Habitat of oil, edited by L.G. Weeks. Tulsa, Oklahoma, American Association of Petroleum Geologists, pp. 995-1053

Gardner, J.V., Late Pleistocene carbonate dissolution cycles in the eastern equatorial
1975 Atlantic. In Dissolution of deep-sea carbonates, edited by W.V. Sliter, A.W.H. Bé and W.H. Berger. Spec.Number Cushman Found.Foramin.Res., (13):129-41

Hays, J.D. and A. Perruzza, The significance of calcium carbonate oscillations in eastern
1972 equatorial Atlantic deep-sea sediments for the end of the Holocene warm interval. Quaternary Res., 2:355-62

Hays, J.D. et al., Pliocene-pleistocene sediments of the equatorial Pacific: their paleo-
1969 magnetic, biostratigraphic, and climatic record. Bull.Geol.Soc.Am., 80:1481-514

Haung, T.C. and H.G. Goodell, Sediments and sedimentary processes of the eastern Mississippi
1970 core, Gulf of Mexico. Am.Assoc.Pet.Geol.Bull., 54:2070-100

Kennett, J.P. and P. Huddlestun, Late Pleistocene paleoclimatology, foraminiferal biostrati-
1972 graphy and tephrochronology, western Gulf of Mexico. Quaternary Res., 2:38-69

Kennett, J.P. and N.J. Shackleton, Laurentide ice sheet meltwater recorded in Gulf of
1975 Mexico deep-sea cores. Science, Wash., 188:147-50

Leiper, D.F., A sequence of current patterns in the Gulf of Mexico. J.Geophys.Res., 75:
1970 637-57

Malmgren, G. and J.P. Kennett, Biometric analysis of phenotypic variation: Globigerina
1972 pachyderma (Ehrenberg) in the South Pacific Ocean. Micropaleontology, 18:241-8

Molnia, B.F., A rapid and accurate method for the analysis of calcium carbonate in small
1974 samples. J.Sediment.Pet., 44:589-90

Murray, J. and A.F. Renard, Report on deep-sea deposits based on the specimens collected
1891 during the voyage of H.M.S. CHALLENGER in the years 1872 to 1876. In Report on the scientific results of the voyage of the H.M.S. CHALLENGER. London, H.M.S.O., 525 p.

Nowlin, W.D., Water masses and general circulation of the Gulf of Mexico. In Oceanology
1971 International, February 28, 1971, 33 p.

Olausson, E., Evidence of climatic changes in north Atlantic deep-sea cores, with remarks
1965 on isotope paleotemperature analysis. Prog.Oceanogr., 3:221-52

__________, Quaternary correlations and the geochemistry of oozes. In Micropaleontology
1971 of the oceans, edited by B.M. Funnel and W.R. Riedel. Cambridge, Cambridge University Press, pp. 375-98

Philippi, E., Die grundproben der Deutschen Sudpolar Expedition 1901-1903. Deutsch,
1910 Sudpolar Expedition 1901-1903, vol.2:411-616

Phleger, F., Ecology of foraminifera, northwest Gulf of Mexico. Part 1. Foraminifera
1951 distribution. Mem.Geol.Soc.Am., (46):88 p.

Ruddiman, W.F., Pleistocene sedimentation in the equatorial Atlantic. Stratigraphy and
1971 faunal paleoclimatology. Bull.Geol.Soc.Am., 82:283-302

Sweet, W.E. and A.H. Bouma, Composite sediment 4D map of the Gulf of Mexico. In TAMU
1971 Results from the USNS Kane 1969 Expedition, Gulf of Mexico, edited by A.H. Bouma, W.R. Bryant and D.K. Davies. College Station, Texas A&M University, pp. 98-120

Thompson, P.R. and T. Saito, Pacific pleistocene sediments: planktonic foraminiferal
1974 dissolution cycles and geochronology. Geology, 1974:333-5

Uchupi, E., Bathymetry of the Gulf of Mexico. Trans.Gulf Coast Assoc.Geol.Soc.Annu.Meet.,
1967 (17):161-72

THE ROLE OF THE ATMOSPHERIC BOUNDARY LAYER IN AIR-SEA INTERACTION PROCESSES IN THE TROPICS

by

E. AUGSTEIN
Max Planck Institüt für Meteorologie
Hamburg
Federal Republic of Germany

CONTENTS

1. INTRODUCTION
2. THE VERTICAL STRUCTURE OF THE MARINE ATMOSPHERIC BOUNDARY LAYER
3. THE GOVERNING PROCESSES IN THE ATMOSPHERIC BOUNDARY LAYER
4. CONCLUSIONS
5. REFERENCES

Abstract

The vertical structure of the marine atmospheric boundary layer is determined by the dynamic and thermodynamic effects of the sea surface on the large-scale atmospheric flow. Depending upon the strength and direction of the mean vertical atmospheric motion and the heat, moisture and momentum exchange at the sea interface,up to 5 distinct sublayers develop. The top region is generally marked by a temperature inversion, where small-scale motions are suppressed. As the governing turbulent and convective processes (which vary with height) are closely coupled, most of the variations initiated at any level immediately propagate through the entire layer. Rather strong modifications of this kind are due to changes in cloud convection which are mostly forced by the large-scale field of motion or by radiational effects. It can be shown that the sensible heat flux at the sea surface actively amplifies cloud convection while evaporation passively reacts to cloud activity. With respect to the atmospheric energy cycle the trade wind boundary layer acts as a channel in which the sensible and latent heat gained from the ocean is accumulated and transported into the Inter-Tropical Convergence Zone (ITCZ). Here, and occasionally in tropical disturbances, the latent heat is released in deep cumulus clouds and by this it very effectively maintains the Hadley circulation. In the ITCZ, and in disturbances, intensive vertical cloud mixing prevents the formation of a low level inversion and consequently the top of the atmospheric boundary layer is not as clearly defined as in undisturbed trades.

Resumen

Se determina la estructura vertical de la capa atmosférica que limita con el mar, por medio de los efectos dinámicos y termodinámicos de la superficie del mar sobre el flujo atmosférico en gran escala. Pueden formase hasta cinco subcapas diferentes, según la fuerza y dirección del movimiento medio atmosférico vertical, y del calor, humedad e intercambio de cantidad de movimiento en la cara común aire-mar. La región superior se distingue generalmente por una inversión de temperatura, con supresión de los pequeños movimientos escalares. Como los procesos convectivos y turbulentos - que pueden variar con la altura - están estrechamente relacionados, casi todas las variaciones iniciadas a un determinado nivel se propagan immediatamente por toda la capa. Modificaciones bastante intensas de este tipo se deben a los cambios en la convección de las nubes, causados casi todos ellos, por el campo de movimientos en gran escala, o por los efectos de las radiaciones. Puede observarse que el flujo de calor sensible en la superficie del mar amplifica activamente la convección nu-

bosa, mientras que la evaporación reacciona pasivamente a la actividad de las nubes. En lo que respecta al ciclo de energía atmosférica, la capa límite de vientos alisios actúa como un canal que acumula el calor latente y sensible recogido del océano, y lo transporta a la zona de convergencia intertropical. En esta zona y, ocasionalmente, en las perturbaciones tropicales, el calor latente se disuelve en nubes profundas cumuliformes, gracias a las cuales mantiene muy eficazmente la circulación Hadley. En la citada zona de convergencia intertropical, y en las perturbaciones, la mezcla intensa de nubes verticales impide la formación de una inversión de bajo nivel y, por consiguiente, la parte superior de la capa límite atmosférica no está definida tan claramente como en los vientos alisios no perturbados.

1. INTRODUCTION

Global annual energy budget considerations (Budyko,1956; Albrecht 1960) have proven the tropics and subtropics to be regions of energy surplus and the moderate and polar latitudes to be areas of energy deficit. In order to balance these differences considerable meridional heat transports are necessary. These are achieved by the large-scale atmospheric circulation and by ocean currents. In this context it may be emphasized that even in the tropics the atmosphere is principally a net heat sink due to long-wave back-radiation while the solid earth and the oceans are radiatively warmed. Therefore, in order to produce the actually observed state thermal energy must be transferred across the underlying boundary into the atmosphere. These required vertical heat fluxes are carried out by long wave radiation, heat conduction and - especially over the oceans - by evaporation.

The two latter processes, heating and moistening of the air from below, together with the frictional effect of the hydrodynamical rough surface,initiate and amplify small-scale perturbations of the large-scale atmospheric flow. Thus, the air motion becomes turbulent and consequently the layer resistance with respect to vertical fluxes of physical and chemical properties is diminished compared to a pure laminar flow. Similar boundary effects are observed in the ocean. The regions where such perturbations detectably modify the field of motion in the air and the water are defined as atmospheric boundary layer and oceanic mixed layer, respectively.

From these descriptive considerations one may suspect already that the air-sea interaction processes are closely related to the flow characteristics on both sides of the interface, i.e., on the turbulence structure of the boundary layers of the two media. A comprehensive treatment of the exchange mechanisms at the sea surface should therefore be based on a simultaneous study of the oceanic mixed layer and the atmospheric boundary layer. But since the relaxation time of the two boundary layers is different with respect to several processes it is occasionally justifiable to treat only one of them in detail and to describe the other one rather crudely. This assumption is more or less realistic for studies of the undisturbed trade wind boundary layer. In this case the ocean may be considered as an infinite heat source. Since such situations have been investigated carefully by experiments and model computations in the past we will mainly concentrate on the undisturbed trade wind flow in the subsequent discussion. Increased insight into the disturbed state is to be expected from the GATE[1] data, gathered during the international field work in 1974.

2. THE VERTICAL STRUCTURE OF THE MARINE ATMOSPHERIC BOUNDARY LAYER

2.1 Temperature, Water Vapour and Wind Distribution

Basic information about the atmospheric structure in the trades has been published by V. Ficker (1936) and Reger (1927) using the observations of the METEOR-Expedition conducted from 1925 to 1927. A more detailed description of the vertical static structure of the trade wind boundary layer, which is still valid, was given by Bunker *et al.* (1950) on the basis of air-craft measurements over the Caribbean Sea. Since then numerous experiments have been carried out in various parts of the tropical oceans during different times of year. On the basis of this material, we are able to present a comprehensive description of the mean vertical distribution of temperature, humidity and the wind vector in the lower tropical atmosphere over the ocean. A careful examination of the data suggests that it is quite suitable to relate the various observed vertical profiles to a low-level air mass trajectory of the Hadley circulation.

---

[1] GATE = GARP Atlantic Tropical Experiment

2.2 The Transports of Energy and Momentum in the Atmospheric Boundary Layer

At present the most comprehensive investigations of the boundary layer transports still originate from the volume budget computations which are compiled from gust probe aircraft measurements at higher altitudes and by detailed buoy observations near the sea surface. While the budget method allows only for a distinction between grid scale and sub-grid scale processes, the other quoted measurements provide some insight into the spectral resolution of the smaller scales of motion.

In accordance with the BOMEX results of Holland and Rasmussen (1973), Yanai et al. (1973), and Betts (1975), Augstein et al. (1973) and Augstein and Wagner (1975) have derived from ATEX budget studies that in undisturbed trades:

(1) the trade inversion and the transition layer are penetrated by large-scale downward mass flow;

(2) the large-scale water vapour and sensible heat transport is consequently downward throughout the entire boundary layer;

(3) the turbulent and convective fluxes of water vapour are directed upward from the sea surface to the inversion where they more or less terminate, and

(4) the turbulent and convective sensible heat flux is upward (decreasing with height) in the mixed layer and downward (increasing with height) in the cloud layer.

In the ITCZ region, the small-scale fluxes have the same direction as in the trades, but they reach upward to the 400 mb- or even 300 mb-level. This behaviour is well documented by the observational results in Fig. 5. In this graph the mean profiles of the potential temperature θ, the equivalent potential temperature θ_E and the vertical distribution of the small-scale fluxes of water vapour plus liquid water $F_{(q+1)}$ and sensible heat-neglecting condensation and evaporation $F_{(\theta-1)}$ are portrayed for undisturbed trades (full lines) and for the transition region between the trades and the ITCZ (dashed, dotted and dash-dotted curves). Note, in all cases considerable vertical transports are present in the mixed layer where the vertical gradients of potential temperature and specific humidity practically vanish. Furthermore, Brümmer (1976) has derived from ATEX measurements (Fig. 6) that horizontal momentum is transported downward where the vertical gradient of the respective wind component is zero. And the flux becomes even countergradient in the upper part of the mixed layer. These findings, together with the results of aircraft gust probe measurements of Bean et al. (1972) during BOMEX and Pennell and Le Mone (1974) near Puerto Rico, indicate the importance of convection for the vertical mixing also in the subcloud layer.

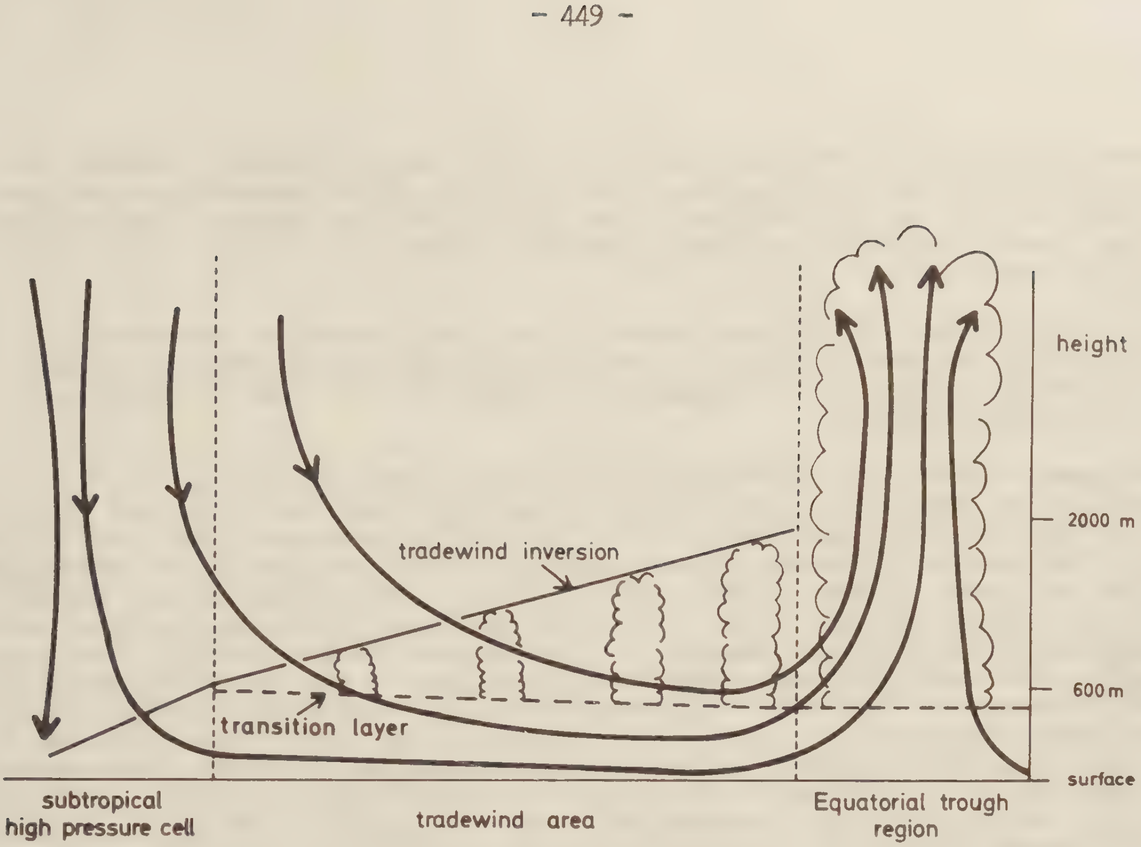

Fig. 1 Scheme of the trade wind flow

The result of this compilation may be sketched in a very general way as portrayed in Fig. 1. On the large scale the lower atmosphere is governed by subsidence from the subtropical high through the trade wind belts until very close to the Inter-Tropical Convergence Zone (ITCZ) where the horizontal divergence of the flow changes to convergence. In the subsidence region the trade inversion, which increases downstream, tops the atmospheric boundary layer, while no distinct upper limit can be detected in the convective régime of the ITCZ or in disturbances. Within the Hadley cell we may roughly distinguish between three regions: (1) the nearly cloudless subtropical high pressure areas with its core over the eastern parts of the oceans; (2) the trade wind belts with gentle low-level winds and mostly non-precipitating shallow convection, and (3) the convectively very active Inter-Tropical Convergence Zone, where the two hemispherical circulation systems merge in the lower troposphere. More or less representative mean vertical profiles of temperature and specific humidity of the three regions are reproduced in Figs.2 and 3. In the eastern parts of the oceans over the upwelling cold-water regions a rather shallow mixed layer develops which is capped by a strong temperature inversion. In this layer the moisture distinctly decreases with height (Fig. 2). Further downstream in the undisturbed trades the low-level atmosphere is subdivided into five sub-layers as shown by the full lines in Fig. 3. Starting from below we find first the statical,unstable surface layer reaching upward to about 80 m height. Further upward the profiles gradually change into the well-mixed layer. At about 600 m above the sea surface a stable layer with discontinuous temperature and humidity variations marks the transition between the mixed layer and the overlying conditionally unstable cloud layer. The boundary layer is topped by the trade inversion where the temperature increases while the moisture content decreases with height. For convenience the dry adiabat and the saturation adiabat are also indicated by the dashed and dotted curves in Fig. 3. Near the ITCZ (dashed profiles of Fig. 3) the cloud layer has become thicker and the inversion is less pronounced. The dotted lines represent convectively active parts of the convergence zone where the mixed layer depth is especially shallow. The cloud layer is nearly wet adiabatically stratified. It reaches upward beyond the 700 mb level. The profiles of Fig. 3 which are mainly based on measurements during ATEX[1] 1969 agree fairly well with results of BOMEX[2] (Holland and Rasmussen, 1973), the Caribbean Sea data of Bunker et al. (1950), observations over the Pacific Ocean of Riehl et al. (1951), Neiburger et al. (1961) and Holland (1975) and the findings of Bunker (1968) over the Indian Ocean and of Riehl and Augstein (1974) in the Southeast Asia Monsoon.

A very thin molecular layer right above the sea surface should be introduced as a further sub-régime of the boundary layer. Clauss et al. (1970) and McAlister and McLeish (1969) have shown observationally for the atmosphere as well as for the ocean that such layers exist in light wind conditions.

The dynamic effect of the hydrodynamical rough sea surface is reflected in the vertical distribution of the wind vector. The momentum budget considerations of Charnock et al. (1956), Holland and Rasmusson (1973) and Brümmer (1976) lead to the conclusion that individual acceleration in the trade wind boundary layer is negligibly small compared to the pressure gradient force, the Coriolis force and the surface friction; while measurements of Estoque (1971) and model calculations of Mahrt (1972) confirm the importance of air mass accelerations near the Equator where the horizontal components of the Coriolis force are small. The variation of the geostrophic wind (the thermal wind) with height, due to the intensive vertical mixing, is largely determined by the horizontal gradient of the sea surface temperature. Since the mean horizontal gradients of the surface pressure and the sea surface temperature are at least qualitatively similar within the whole Hadley régime, some features of the vertical wind distribution of the ATEX profiles in Fig. 4 are typical for the entire oceanic trade wind region. The thermal wind (increasing west wind with height) caused by the ITCZ-directed horizontal temperature gradient largely balances the low-level wind shear caused by surface friction. The net effect is a nearly shear-free flow in the mixed layer between 50 m and 500 m height. Within the cloud layer the vertical shear increases and no distinct changes occur at the trade inversion. A low-level weak wind maximum is mostly observed in the upper part of the mixed layer below cloud base. Brümmer et al. (1974) have found from different experiments that a slight veering of about 6 degrees in the lowest 500 m of the atmosphere appears to be typical for the trades. The averaged ATEX profiles in Fig. 4 indicate an additional veering up to 15 degrees within the cloud layer.

The vertical structures of the thermodynamic properties and of the field of motion result as a net effect of generation, dissipation and transports of heat, water vapour and momentum. Therefore, the mean profiles of temperature, specific humidity, and wind components provide us with a certain amount of information about the governing processes within the various subregions of the atmospheric boundary layer.

---

[1] ATEX = Atlantic Trade Wind Experiment

[2] BOMEX = Barbados Oceanographic and Meteorological Experiment

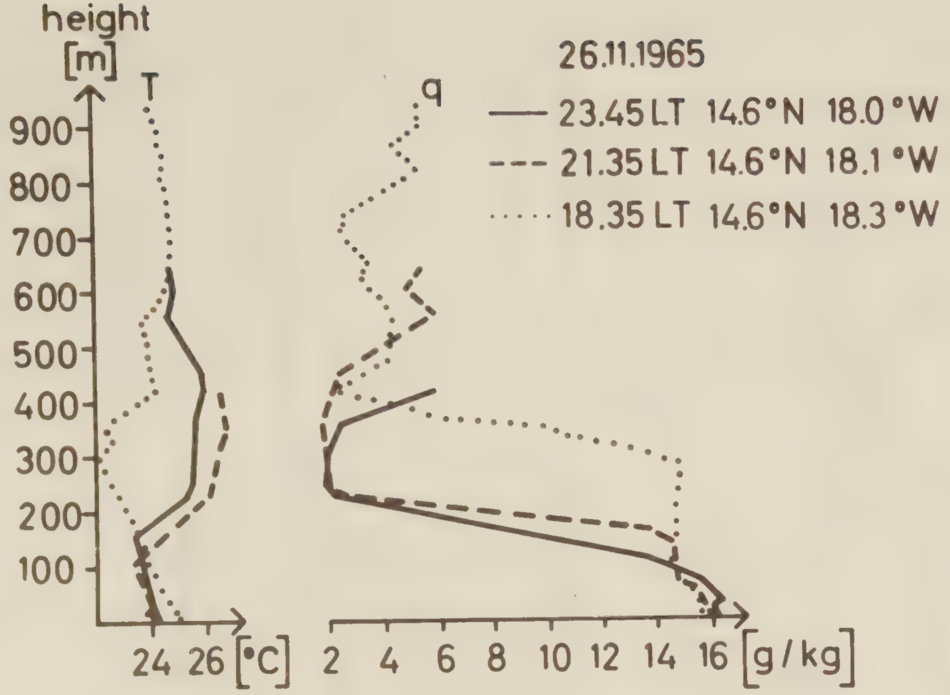

Fig. 2 Profiles of temperature T and specific humidity q measured near the coast of West Africa

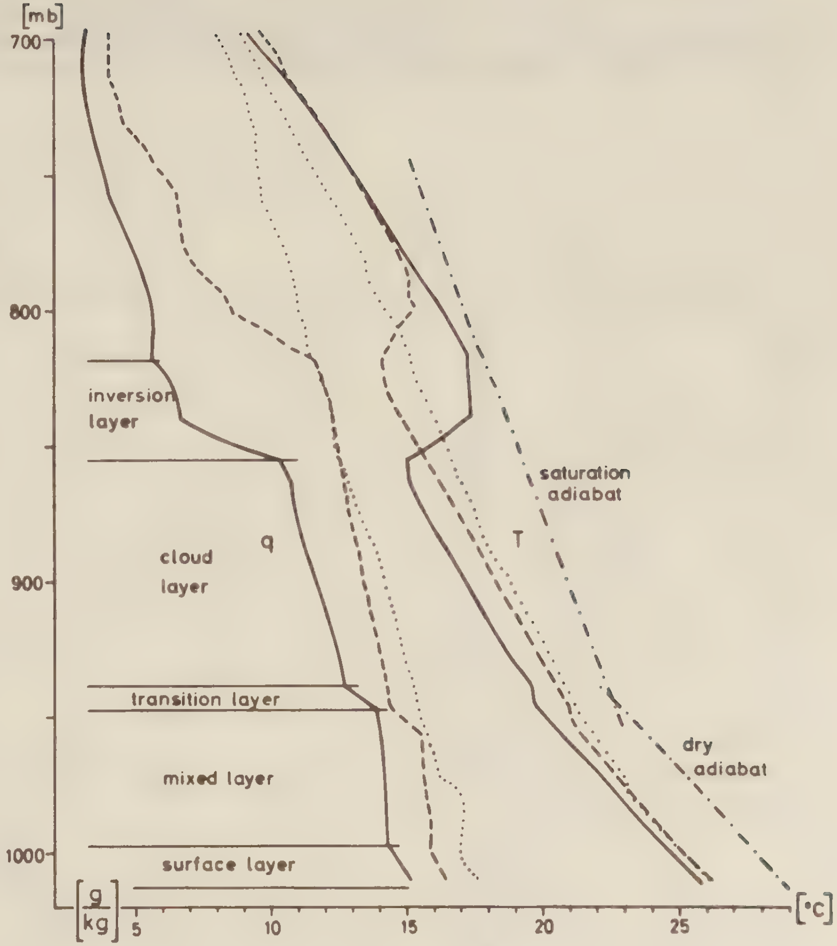

Fig. 3 Mean temperature (T) and specific humidity (q) profiles measured during ATEX. Undisturbed trades: full lines, fringes of the ITCZ: dashed and dotted lines

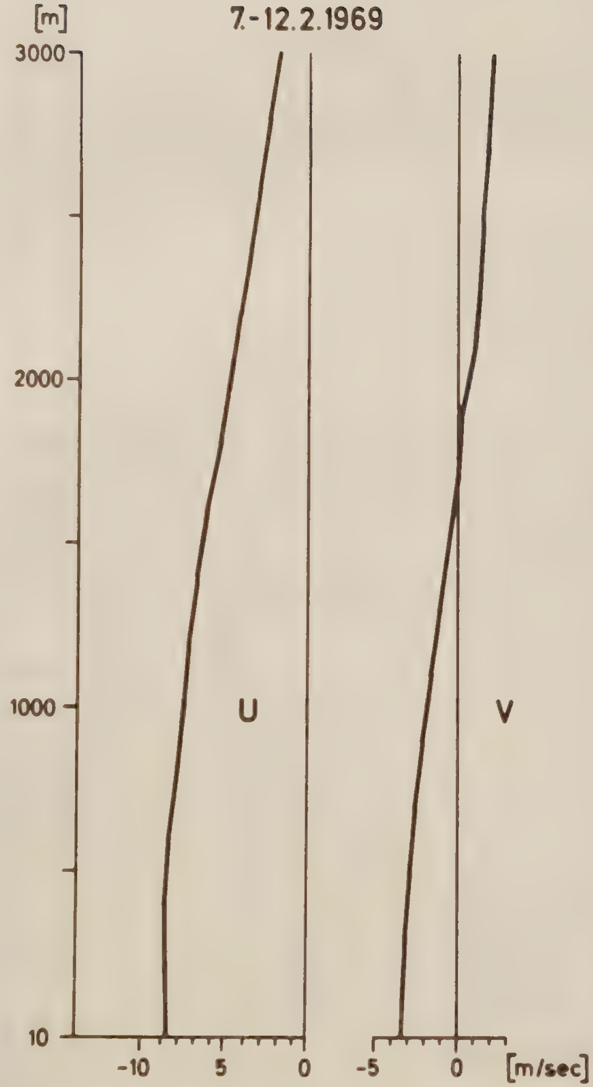

Fig. 4 Mean profiles of the zonal (U) and meridional (V) wind component during ATEX

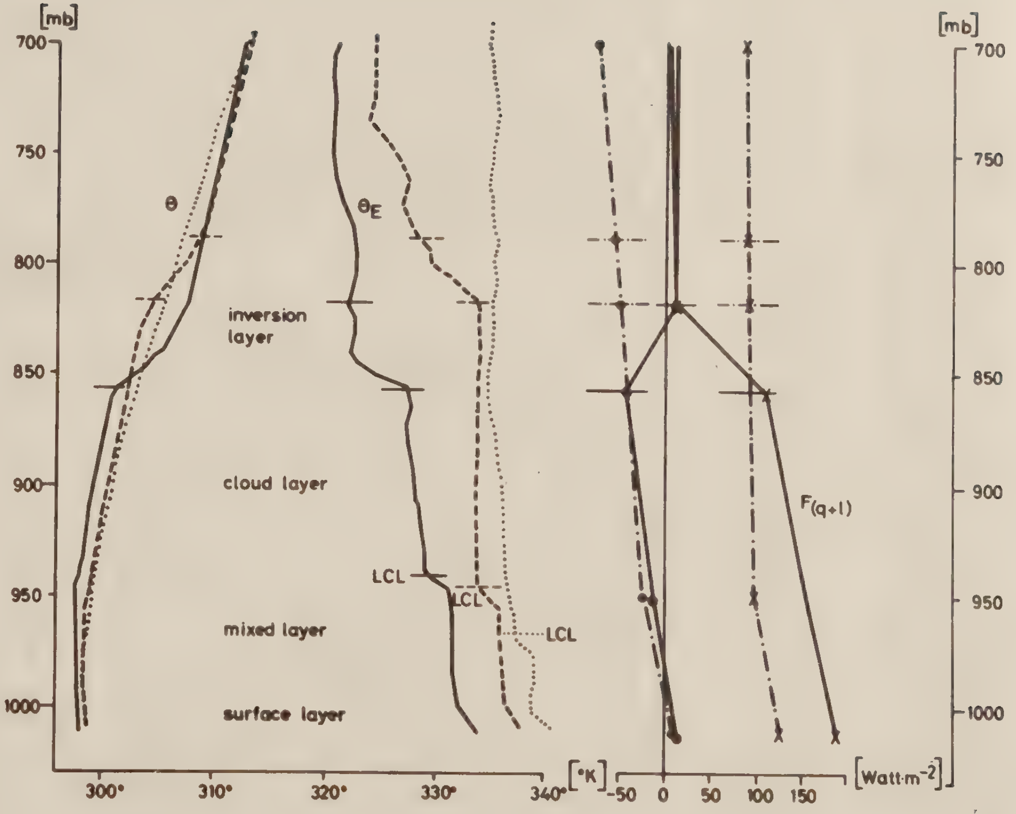

Fig. 5 Mean profiles of potential temperature θ, equivalent potential temperature θ_E and the fluxes of sensible heat $F_{(\theta - 1)}$ and latent heat $F_{(q + 1)}$ without accounting for evaporation.
Full lines: undisturbed trade wind conditions, broken lines: disturbed conditions. LCL = lifting condensation level

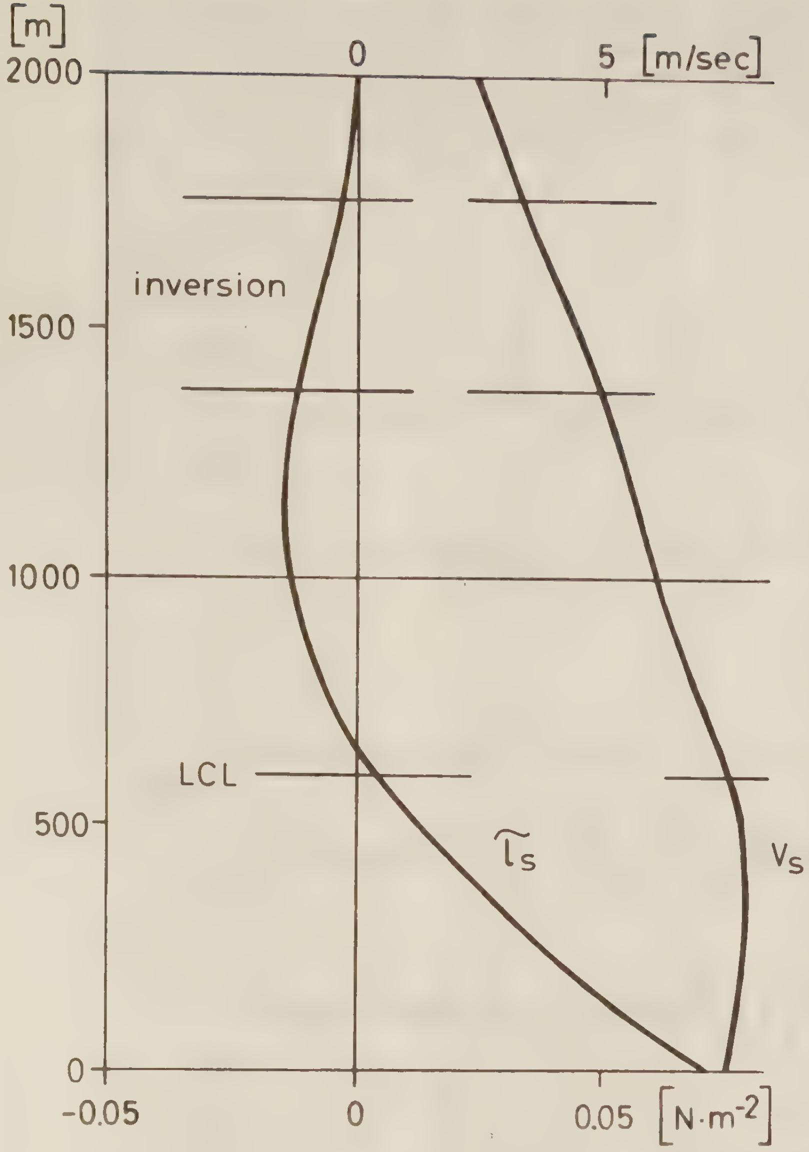

Fig. 6 Vertical flux of momentum τ_S and the related wind component V_S after Brümmer (1976). Subscript S indicates the coordinate parallel to the surface wind

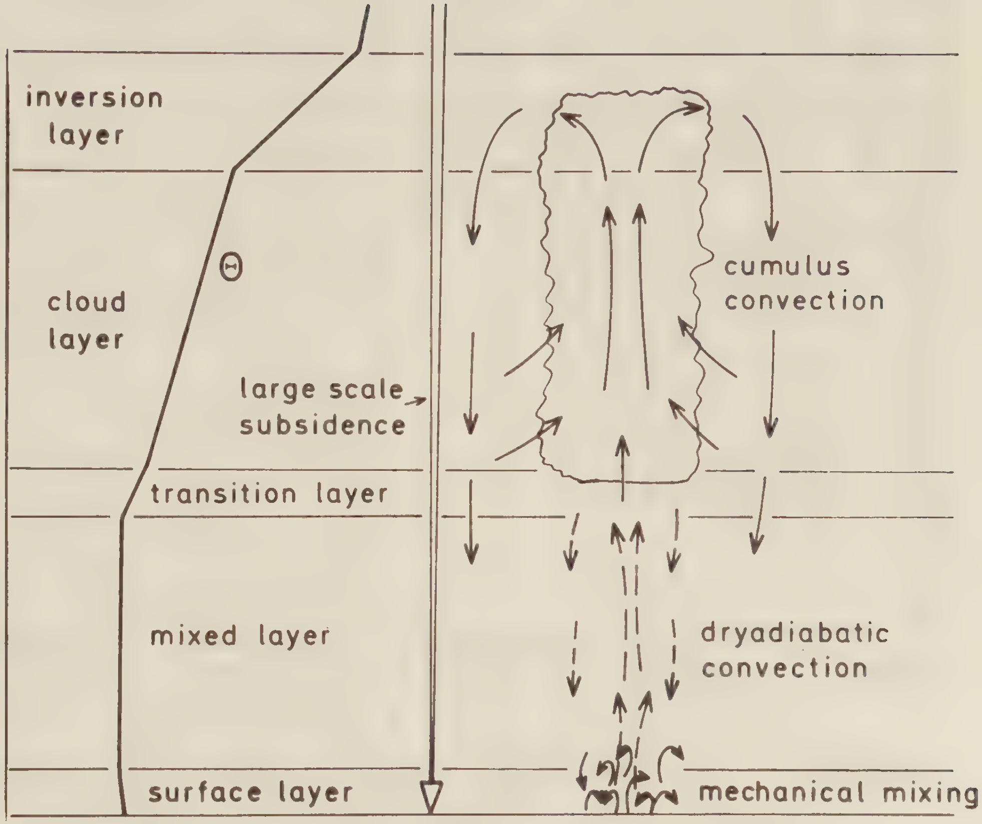
inversion layer
cloud layer
Θ
large scale subsidence
transition layer
mixed layer
surface layer
cumulus convection
dryadiabatic convection
mechanical mixing

Fig. 7 Scheme of processes in the atmospheric boundary layer related to the profile of the potential temperature θ

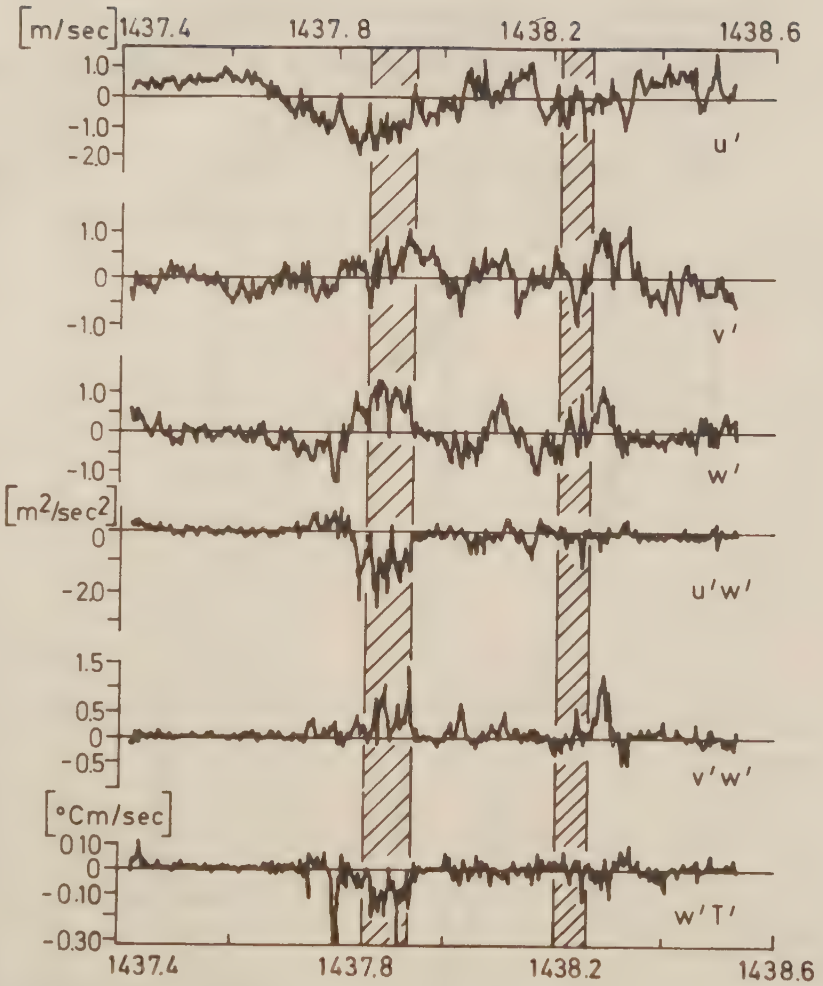

Fig. 8 Crosswind aircraft measurements of the fluctuations of the three wind components U', V', W', the momentum fluxes U'W', V'W' and the heat flux W'T' at 531 m height. Abscissa: time. Shaded areas: below clouds. After Le Mone and Pennell (1976)

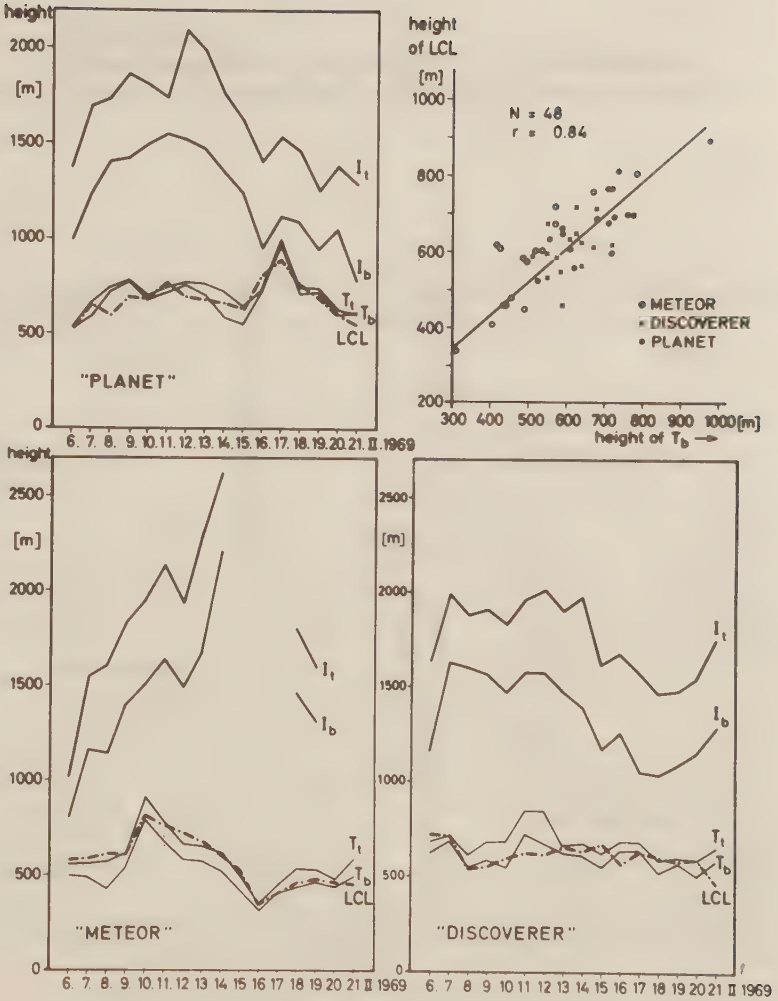

Fig. 9 The boundaries of the trade inversion I_t, I_b and the transition layer T_t, T_b (full lines) and the height of the lifting condensation level of surface air (dashed and dotted) of the ATEX ships

3. THE GOVERNING PROCESSES IN THE ATMOSPHERIC BOUNDARY LAYER

3.1 Undisturbed Conditions

The mean profiles of temperature, water vapour and wind velocity combined with the height distribution of the vertical transports of energy and momentum suggest that the layered structure of the lower trade wind atmosphere is determined by a particular arrangement of the governing physical processes. Qualitatively, this probable relationship between the various layers and the dominant motions is sketched in Fig. 7. Principally, short- and long-wave radiation which as a net effect cause cooling in the entire atmospheric boundary layer should be included in this scheme. Although direct interaction between the relatively short living turbulent and convective motions and radiation can be neglected (Sasamori, 1972), indirect influences by radiatively caused slow changes of the mean static stability can clearly modify the small-scale field of motions as we will show.

In the non-precipitating trade wind belts, radiative cooling is compensated mainly by adiabatic warming of the large-scale subsiding air and, to a smaller extent, by sensible heat input from the ocean.

In this discussion we will concentrate on the coupling between the energy and momentum transfer through the sea surface and the transport mechanisms in the various parts of the atmospheric boundary layer. Spectra of temperature, humidity and wind component fluctuations as well as the relevant cross-spectra measured by Phelps and Pond (1971) and Wucknitz (1976) indicate that microscale turbulence is dominant in the surface layer transports. Aircraft measurements of Bean et al. (1972) suggest that with increasing height buoyancy driven, dry convection gains more and more importance. The buoyant motions lead to a formation of a well-mixed region above the shallow surface layer. The development of such a layer in a subsiding initially stable, stratified airflow with unstable conditions only at the lower boundary has been successfully described with the aid of similar model assumptions by Ball (1960), Lilly (1968), Carson (1973), Tennekes (1973) and Deardorff (1972). All of these authors imply that the buoyancy generated kinetic energy by heating and moistening of the air from below is totally (Ball, 1960) or partly (all the others) converted into potential energy through entrainment of potentially warmer air from above through the top of the mixed layer. In order to achieve this effect buoyant parcels are assumed to overshoot their level of equilibrium and by this force mass with smaller density downward. Thus, the top of the mixed layer is determined by a balance of the small-scale mass entrainment from below and the large-scale downward mass flow.

As soon as the most powerful convective plumes or bubbles penetrate to their condensation level clouds start to develop. This process has been simulated in a numerical grid point model recently by Sommeria (1976) and the physical process of single non-precipitating clouds has been described in detail by Betts (1973). Nevertheless, no sufficient concept presently exists for a satisfactory prognostic formulation of the cloud transport of heat, water vapour and momentum.

Although considerable progress has been achieved in this field by Arakawa and Schubert (1974) and Krishnamurti (1975) several questions are still open concerning momentum transport and cloud-to-cloud interaction.

Condensational warming increases the buoyancy of the water vapour saturated, ascending air parcels and small-scale kinetic energy is generated. Part of this kinetic energy is converted into potential energy when the cloud tops overshoot their level of equilibrium. The trade inversion forms where cumulus mixing balances large-scale sinking in such a situation. Measurements by Holland (1975) over the Pacific Ocean and, more recently, by Le Mone and Pennell (1976) near Puerto Rico (Fig. 8) clearly document that even updrafts of shallow trade cumuli originate from some depth in the mixed layer. Therefore, a compensating downward mass flux through cloud base level in the environment of the clouds will add to the large-scale subsidence. Consequently, increased cloudiness forces the stable transition layer further downward and this leads to a temporarily decreased possibility for new cloud formation. This close interrelation between the mass flux at cloud base and height of the transition layer is obvious from the significant correlation between the daily averages of the lifting condensation level (LCL) of surface air and the height of the transition layer during ATEX (Fig. 9). Further insight into the interaction between the various boundary layer processes can be gained from the study of diurnal variations in the quantities displayed in Fig. 10. The vertical entrainment velocity w_e at the inversion base has been determined as a residual of the large-scale mass transports and the height variation of the inversion is assumed to be a good indicator for cloud activity. As the large-scale subsidence did not vary diurnally mainly short-wave radiation was left as the basic trigger mechanism for the observed changes. In accordance with model computations of Hinzpeter (1968), the derived amplitude of the diurnal temperature wave increases with height from the sea surface up the trade inversion. Its phase relation coincides with that of the air-sea temperature difference in Fig. 10. Thus, static stability has a minimum in the early morning and a maximum in the afternoon. This obviously leads to the variation of cloudiness as represented by w_e. During the period of increased convective activity (big arrow) the transition layer has its minimum height while the trade inversion is forced upward; when convection is less pronounced (small arrow) the transition layer has its maximum height and the inversion migrates downward. Regarding the energy exchange at the sea surface, the sensible heat flux is modified by the radiative changes and it can directly amplify the 24-hourly convective cycle. In contrast to the sensible heat flux evaporation does not force the variation of cloudiness; it reacts upon the convective activity changes. In consistence with the earlier conclusions about the mass flux at cloud base level, we find that enhanced convection decreases the moisture content of the mixed layer (see Fig. 10) by the specific humidity variations at 10 m height. This drying effect causes an upward displacement of the LCL (negative feedback on convection) and an increase of evaporation at the sea surface (positive feedback on convection). Unfortunately, the insufficient humidity measurements obtained from the radiosondes during ATEX (Ostapoff et al., 1970) do not permit an exact quantitative investigation of the variation of the moisture fluxes at cloud base. However, if we assume that the moisture variation throughout the mixed layer is the same as that near the sea surface, where it should have a minimum value, the convective water vapour flux at cloud base would vary diurnally by about 30 percent. These examples suggest a very sensitive balance between the various processes in the atmospheric boundary layer, the exchange mechanisms at the air-sea interface, and the thermal and kinematic characteristics of the large-scale field even in a rather uniform air flow.

3.2 Disturbed Conditions

Disturbed conditions are generally related to a horizontally convergent flow in the lower atmosphere. This is true for the Inter-Tropical Convergence Zone as well as for tropical depressions and hurricanes. In such situations horizontal advection, in particular of water vapour, dominates the local input from below (Reed and Recker, 1971), but if a disturbance becomes stationary for some time, the strong absorption of the solar radiation within thick clouds and the effect of rainfall can considerably change the sea surface conditions and thus the air-sea energy exchange. From studies of the oceanic mixed layer, Ostapoff et al. (1973) have derived that under cloud clusters the ratio between sensible and latent heat flux can vary between 0.05 and 0.25. Preliminary GATE results of Emmitt (1976) support the assumption that updrafts in enhanced cumulus convection originate in the lower part of the mixed layer (Fig. 11), and Seguin and Garstang (1976) have provided evidence that deep clouds significantly modify the mixed layer. They have pointed out that the static stability is increased while the moisture content is decreased in the sub-cloud layer due to strong cloud convection. Cold downdrafts of precipitating clouds, as described by Zipser (1969), are well represented in the temperature records near the sea surface (Fig. 12). At present there is only scarce information available about interactions between the different processes in disturbed conditions, but the further evaluation of the GATE measurements will presumably help to answer most of the still open questions.

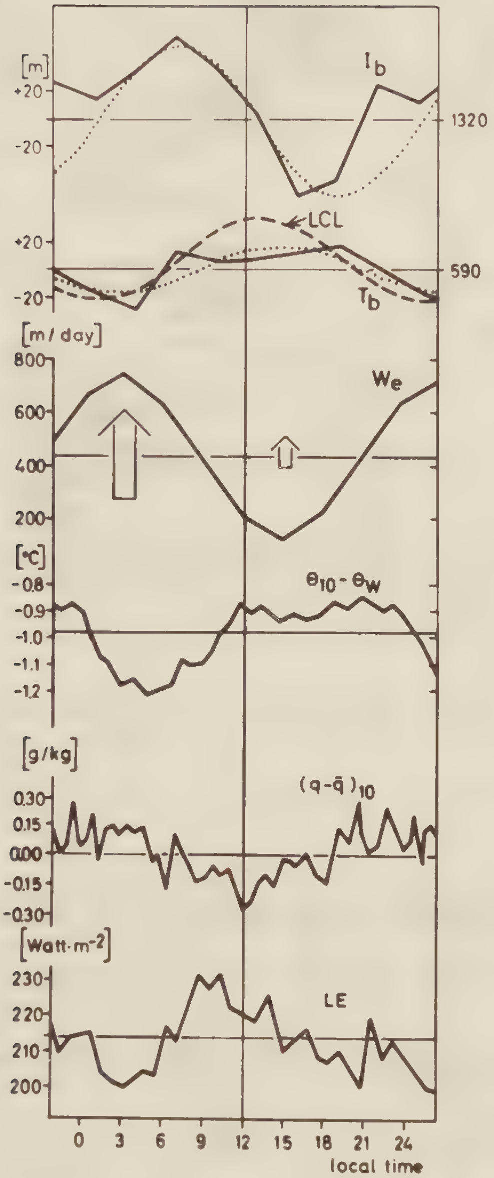

Fig. 10 Diurnal variations of the inversion base I_b, the base of the transition layer T_b, the lifting condensation level LCL, the residual entrainment velocity W_e at the inversion base, the air-sea temperature difference $\theta_{10} - \theta_W$, the specific humidity at 10 m height $(q - q)$ and the latent heat flux LE at 10 m height. Dotted curves indicate the first harmonic of the respective curves. Big arrow marks strong and small arrow marks weak convective activity

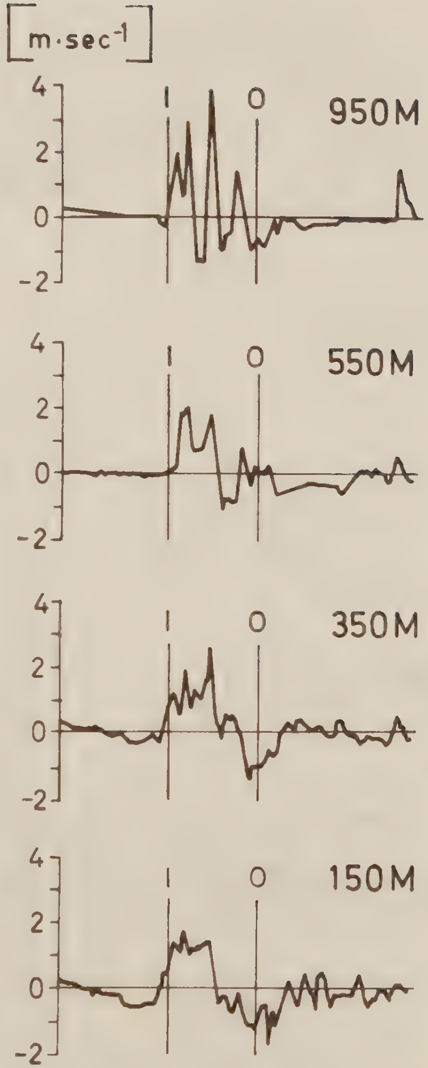

Fig. 11 Vertical motion measured during a cloud passage between I and O at various heights during GATE. After Emmitt (1976)

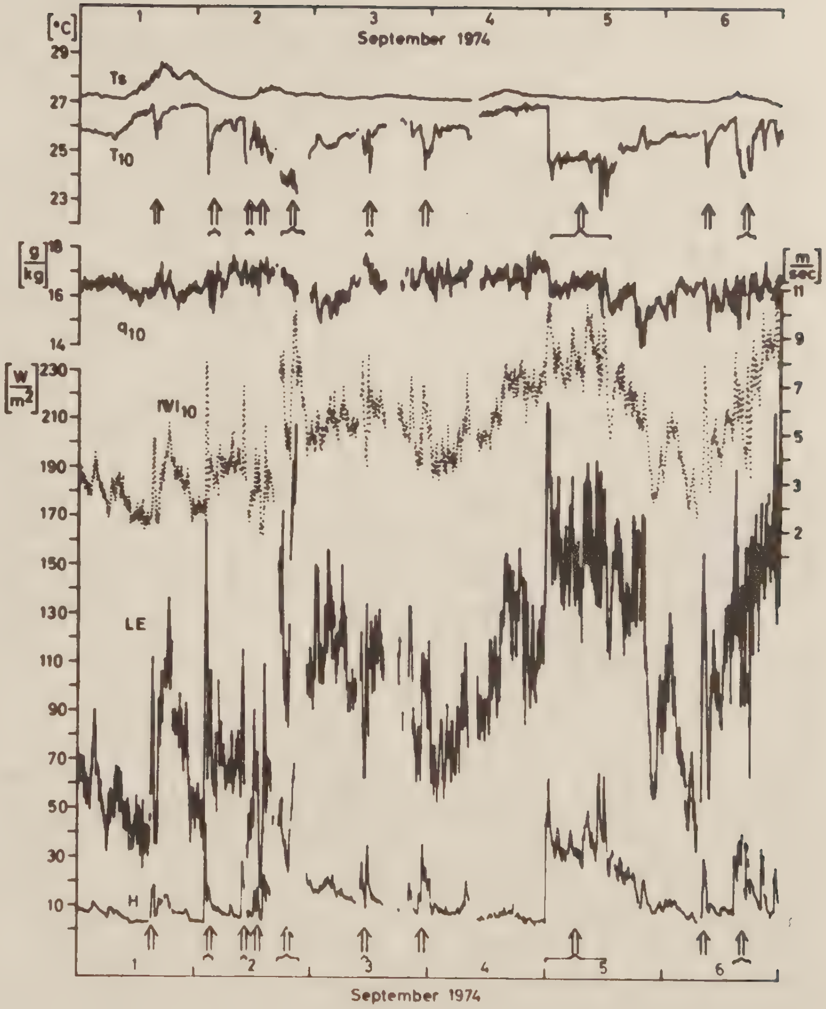

Fig. 12 Time series of sea surface temperature T_S, air temperature T_{10}, specific humidity q_{10}, wind speed $|W|_{10}$, latent (LE) and sensible (H) heat fluxes during GATE at RV METEOR. Arrows indicate times with rainfall. Subscript 10 refers to 10 m height

4. CONCLUSIONS

Previous theoretical and experimental studies have shown that the vertical structure of the maritime atmospheric boundary layer in low latitudes is determined by the characteristics of the large-scale flow and by the locally generated small-scale motions. The effect of both leads to a multilayered structure in the undisturbed trade wind regions. Due to this structure most of the water vapour transferred from the sea surface to the atmosphere is accumulated in the layer below the trade inversion and is transported downstream into the ITCZ. Here the low-level airflow converges and latent heat is released in the updrafts of deep cumulus clouds. This heating very effectively generates available potential energy which maintains the Hadley circulation. The importance of the air-sea energy exchange and of the boundary layer processes within this large-scale energy cycle of the atmosphere becomes immediately obvious.

5. REFERENCES

Albrecht, F., Jahreskarten des Warme- und Wasser-haushalts der Ozeane. Ber.Dtsch.Wetterd., 1960 66

Arakawa, A. and W. Schubert, Interaction of a cumulus cloud ensemble with the large scale 1964 environment. Part 1. J.Atmos.Sci., 31:674-701

Augstein, E. et al., Mass and energy transports in an undisturbed Atlantic trade wind flow. 1973 Mon.Weather Rev., 101:111

Augstein, E. and V. Wagner, Vertical coupling within the Hadley circulation over the Atlantic 1975 Ocean. Beitr.Phys.Atmos., 48:103-18

Ball, F.K., Control of inversion height by surface heating. Q.J.R.Meteorol.Soc., 86:483-94 1960

Bean, B.R. et al., An analysis of airborne measurements of vertical water vapour flux during 1972 BOMEX. J.Atmos.Sci., 29:860-9

Betts, A.K., Non-precipitating cumulus convection and its parameterization. Q.J.R.Meteorol. 1973 Soc., 99:178-96

Brummer, B., The kinematic, dynamics and kinetic energy budget of the Trade Wind flow over 1976 the Atlantic Ocean. Meteor Forschungeergeb.(B.Meteorol.Aeron.), (11)

Brummer, B., E. Augstein and H. Riehl, On the low level wind structure in the Atlantic trade. 1974 Q.J.R.Meteorol.Soc., 100:109-21

Budyko, M.I., Atlas teplovogo alansa zemnogo shara. Glavnaia Geofiz.Obs.Leningr., 1963 1963

Buneer, A.F., Turbulence and turbulent fluxes over the Indian Ocean. Tech.Rep.Woods Hole 1968 Oceanogr.Inst., (68-62)

Bunker, A.F. et al., Vertical distribution of temperature and humidity over the Caribbean 1950 Sea. Pap.Phys.Oceanogr.Meteorol., 1950:82 p.

Carson, D.J., The development of a dry inversion-capped convectively unstable boundary 1973 layer. Q.J.R.Meteorol.Soc., 93:450-67

Charnock, H.J., R.D. Francis and P.A. Sheppard, An investigation of wind structure in the trades. Philos.Trans.R.Soc., Lond.(A), 249:179-234

Clauss, E., H. Hinzpeter and J. Muller-Glewe, Ergibnisse von messungen des temperaturpro-
1970 fils der atmosphare nahe der grenzflache ozeanatmosphare. Meteor Forschungeergeb. (B. Meteorol.Aeron.), (5):85-9

Deardorff, J.W., Numerical investigation of neutral and unstable layers. J.Atmos.Sci.,
1972 29:91-115

Emmitt, G.D., Cumulus structure from near cloud base to the surface. Paper in preparation
1971 for J.Applied Meteorol.

Estoque, M.A., The planetary boundary layer over Christmas Island. Mon.Weather Rev.,
1971 (99):193-201

Ficker, H. von., Die passatinversion. Veröf.Meteorol.Inst.Univ.Berl., 1(4)
1936

Hinzpeter, H., Tagesperiodische Änderungen des oberflächennahen temperaturfeldes über dem Meer
1968 als Folge von Strahlungsquellen und -senken. Kiel.Meeresforsch., 24:1-13

Holland, J.Z., Characteristics of the lower atmosphere near Saipan, April 29 to May 16 1945.
1975 NOAA Tech., (EDS CEDDA 2):20 p.

Holland, J.Z. and E.M. Rasmussen, Measurements of atmospheric mass, energy momentum budgets
1973 over a 500 km square of tropical ocean. Mon.Weather Rev., 101:11-55

Le Mone, M.A. and W.T. Pennell, The relationship of trade wind cumulus distribution to sub-
1976 cloud layer fluxes and structure. Mon.Weather Rev., 104:524-39

Lilly, D.K., Models of cloud-topped mixed layers under a strong inversion. Q.J.R.Meteorol.
1968 Soc., 94:292-309

Mahrt, L., A numerical study of the influence of advective accelerations in an idealized
1972 low altitude, planetary boundary layer. J.Atmos.Sci., 29:1477-84

McAlister, E.D. and W. McLeish, Heat transfer in the top millimeter of the ocean. J.Geophys.
1969 Res., 74:3408-14

Neiburger, M., D.S. Johnson and C.W. Chien, Studies of the structure of the atmosphere over
1961 the eastern north Pacific. Berkeley, University of California Press, 94 p.

Ostapoff, F., Y. Tarbeyev and S. Worthem, Heat flux and precipitation estimates from oceano-
1973 graphic observations. Science, Wash., 180(4089):960-2

Ostapoff, F., W. Shinners and E. Augstein, Some tests on the radiosonde humidity error.
1970 NOAA Tech.Memo., (ERL 194-AOML 4):50 p.

Pennell, W. and M.A. Le Mone, An experimental study of turbulence structure in the fair-weathe
1974 weather trade wind boundary layer. J.Atmos.Sci., 31:1308-23

Phelps, G.T. and S. Pond, Spectra of temperature and humidity fluctuations and of the fluxes
1971 on moisture and sensible heat in the marine boundary layer. J.Atmos.Sci., 28:918-28

Reed, R.J. and E.E. Recker, Structure and properties of synoptic scale wave disturbances
1971 in the equatorial western Pacific. J.Atmos.Sci., 28:1117-33

Reger, J., Der sudostpassat. Beitr.Phys.Freien Atmos., 13:59-63
1927

Riehl, H. and E. Augstein, Surface interaction calculations over the Gulf of Tonkin.
1973 Tellus, 25(5):424-34

Riehl, H. et al., The northeast trade of the Pacific Ocean. Q.J.R.Meteorol.Soc., 77:598-626
1950

Sasamori, T., A linear harmonic analysis of atmospheric motion with radiative dissipation.
1972 J.Meteorol.Soc.Jap., 50:505-18

Seguin, W.R. and M. Garstang, Some evidence of the effects of convection on the structure
1976 of the tropical subcloud layer. J.Atmos.Sci., 33:660-6

Sommeria, G., Three-dimensional simulation of turbulent processes in an undisturbed trade
1976 wind boundary. J.Atmos.Sci., 33:216-41

Tennekes, H., A model for the dynamics of the inversion above a convective boundary layer.
1973 J.Atmos.Sci., 30:558-67

Wucknitz, J., Determination of turbulent fluxes of momentum and sensible heat from fluctuation
1976 measurements and the structure of wind field above waves at the tropical Atlantic during ATEX. Forschungeergeb.(B.Meteorol.Aeron.), (11)

Yanai, M., S. Espensen and J.H. Chu, Determination of tropical cloud clusters from large-
1973 scale heat and moisture budgets. J.Atmos.Sci., 30:611-27

Zipser, E.J., The role of organized unsaturated convective downdrafts in the structure and
1969 rapid decay of an equatorial disturbance. J.Appl.Meteorol., 8:799-814

A CLIMATIC HEAT BUDGET STUDY OF THE GULF OF MEXICO

by

P.C. ETTER[1]
Department of Oceanography
Texas A. & M. University
College Station 77843
Texas, U.S.A.

CONTENTS

1. INTRODUCTION
2. DATA AND AVERAGING
3. COMPUTATIONS AND RESULTS
4. ACKNOWLEDGEMENTS
5. REFERENCES

Abstract

Monthly and annual mean heat budgets are calculated for four regions covering the Gulf of Mexico. The radiation balance at the sea surface (Q_R) is based on direct measurements of incoming solar radiation, as presented by Löf, Duffie and Smith (1965). The evaporation rate (E), and consequently the latent heat flux (Q_E), is calculated by use of bulk-aerodynamic formulae on the basis of meteorological data dating from 1858 to 1971, as available from the National Climatic Center; the annual mean evaporation rate (E) for the Gulf of Mexico was found to be 204 centimetres per year, substantially higher than found in previous work. However, verification based on aerological data has been obtained from the evaporation-minus-precipitation (E-P) values of Cummings (1968) and good estimates of P. The sensible heat flux (Q_H) is calculated by use of Bowen's ratio. The rate of heat storage (Q_T) is calculated apparently for the first time directly by use of available bathythermograph (BT) data. Heat flux divergence due to ocean currents (Q_V), calculated as a residual in the heat budget equation, is small.

The monthly mean values of Q_R and Q_E+Q_H obtained in this study are greater than those found by Hastenrath (1968) for the entire Gulf of Mexico. The best agreement, based on annual averages, was found with Budyko (1963).

Resumen

Se calcula el equilibrio térmico medio mensual y anual de las cuatro regiones que cubren el Golfo de México. El balance de las radiaciones en la superficie del mar (Q_R) se basa en mediciones directas de la radiación solar incidente, de acuerdo con Löf, Duffie y Smith (1965). La velocidad de evaporación (E) y, por consiguiente, el flujo de calor latente (Q_E), se calcula por medio de fórmulas aerodinámicas globales, basadas en los datos meteorológicos tomados desde 1858 a 1971, y proporcionados por el Centro Nacional de Climatología; la velocidad media anual de evaporación (E) obtenida para el Golfo de México fue de 204 cm por año,

---

[1] Present affiliation: MAR, Incorporated, Rockville, MD 20852

notablemente mayor que la obtenida en trabajos anteriores; sin embargo, basándose en datos aerológicos, se han podido verificar los valores de Cummings (1968) para la evaporación-menos-precipitación (E-P), y buenas estimaciones para P. El flujo de calor sensible (Q_H) se calcula por medio del cociente de Bowen. La velocidad de almacenamiento de calor (Q_T) se calculó, al parecer por primera vez directamente, utilizando los datos batitermográficos (BT) conocidos. La divergencia del flujo térmico debida a las corrientes océanicas (Q_V), calculada como residuo de la ecuación de equilibrio térmico, es pequeña.

Los valores medios mensuales de Q_R y Q_E+Q_H obtenidos en este estudio son mayores que los obtenidos por Hastenrath (1968) para todo el Golfo de México. La mejor concordancia, basada en las medias anuales, fue la obtenida por Budyko (1963).

1. INTRODUCTION

A heat budget study of any oceanic region is a problem in balancing the thermal energy gains and losses at the sea surface with the thermal energy stored within and transferred through the water body.

The thermal energy budget of an oceanic water column of unit cross-sectional area may be expressed as:

$$Q_R = Q_A + Q_T + Q_V \quad (1)$$

where:

$$Q_R = Q_S - Q_B \quad (2)$$

$$Q_A = Q_E + Q_H \quad (3)$$

and where:

Q_S = net absorbed solar radiation at the sea surface

Q_B = effective back radiation at the sea surface

Q_R = radiation balance at the sea surface

Q_E = turbulent flux of latent heat

Q_H = turbulent flux of sensible heat

Q_A = net turbulent heat flux from the sea surface

Q_T = rate of heat storage

Q_V = heat flux divergence due to currents

Previous heat budget studies of the Gulf of Mexico have usually been confined to small regions and small time scales, or have directed attention to only certain terms in the heat budget equation in an attempt to refine empirical relations or measurement techniques. Only one known attempt has been made to examine the heat budget of the entire Gulf of Mexico on a climatic scale (Hastenrath, 1968). Since that time, advances in the estimation of radiative and turbulent fluxes have been made. Oceanographic problems such as accounting for sea-surface temperatures and salinities of the Gulf of Mexico clearly required more accurate and complete estimates of the heat-budget quantities for the Gulf of Mexico.

2. DATA AND AVERAGING

Solar radiation data were obtained from a report by Löf, Duffie and Smith (1965) (cited in de Jong, 1973). Löf et al. computed mean radiation levels based on data compiled from weather reports and summaries. For areas in which few or no radiation data were available, mean radiation levels were synthesized by use of sunshine-hours data and approximation formulae.

Meteorological and oceanographic data in summary form were obtained from the National Climatic Center (NCC) and the National Oceanographic Data Center (NODC) through reports by the U.S. Department of Commerce (1973) and the U.S. Naval Weather Service Command (1975). These data were averaged by month for various areas within the Gulf of Mexico. The meteorological data were collected between 1858 and 1971; the oceanographic data were collected over a much shorter period of time. However, to accommodate the data in this form, it was necessary to divide the Gulf of Mexico into areas of varying sizes to take into account the manner in which the data were divided in the original summary reports. To optimize spatial resolution, it was decided to combine the data into four areas that roughly approximated geographic quarters. These areas, hereafter called regions, are referred to as the northwest (NW), northeast (NE), southwest (SW) and southeast (SE) regions (Fig. 1).

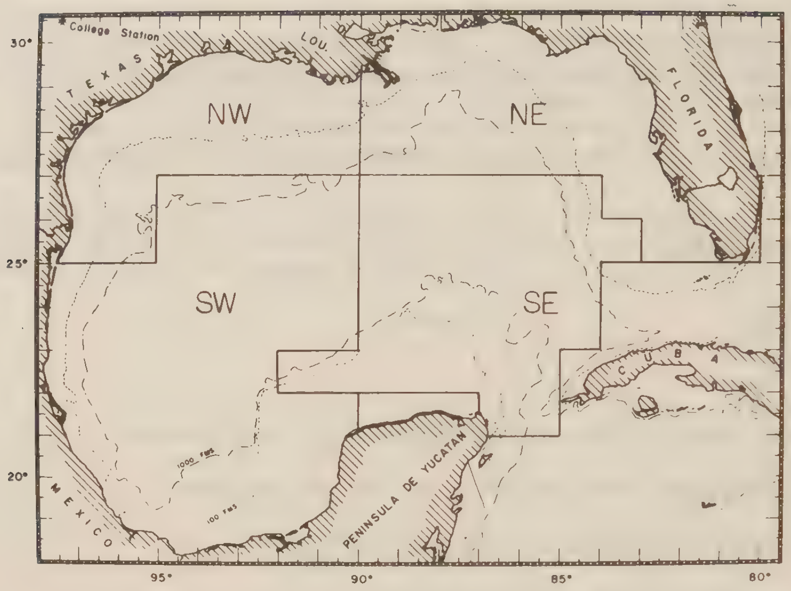
College Station
TEXAS
LOU.
FLORIDA
NW
NE
SW
SE
CUBA
PENINSULA DE YUCATAN
MEXICO
1000 fms
100 fms
30°
25°
20°
95°
90°
85°
80°

Fig. 1 Location of the four regions into which the Gulf of Mexico was divided. The regions are labelled as the northwest (NW), northeast (NE), southwest (SW) and southeast (SE) regions

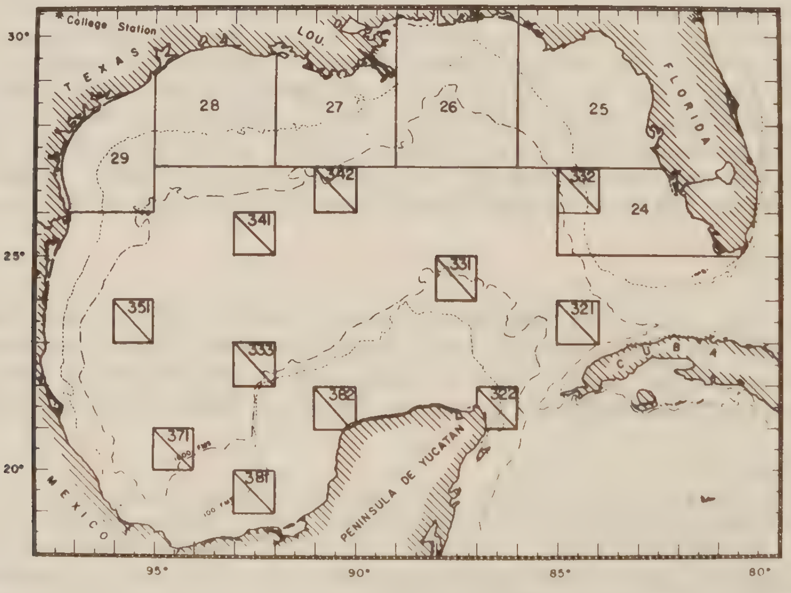
College Station
TEXAS
LOU.
FLORIDA
28
27
26
25
29
24
342
332
341
331
351
321
333
382
322
371
381
CUBA
PENINSULA DE YUCATAN
MEXICO
1000 fms
100 fms
30°
25°
20°
95°
90°
85°
80°

Fig. 2 Location of the subregions into which the meteorological data were divided. The subregions are numbered as they were in their respective reports. Hatched subregions were taken from a report by the U.S. Department of Commerce (1973)

The oceanographic data, consisting of temperature-versus-depth information, were taken from the report by the U.S. Department of Commerce (1973).

The meteorological data, based on ship observations, were taken from reports by the U.S. Department of Commerce (1973) and the U.S. Naval Weather Service Command (1975). The areas in these reports, hereafter called regions (Fig. 2), are numbered as they were in their respective reports. The subregions taken from the U.S. Department of Commerce report are hatched.

In computing monthly mean values for the entire Gulf of Mexico, the four regions were weighted as follows: NW - 16%, NE - 20%, SW - 39%, SE - 25%.

3. COMPUTATIONS AND RESULTS

3.1 The Radiation Balance at the Sea Surface (Q_R)

The radiation balance at the sea surface is comprised of the net absorbed solar radiation (Q_S) and the effective back radiation at the sea surface (Q_B).

The net absorbed solar radiation can be expressed as

$$Q_S = Q_I\,(1 - \alpha) \qquad (4)$$

where: Q_I = net solar radiation received on a horizontal plane at the sea surface

α = albedo of the surface of the ocean

Values of Q_I were taken from a report by Lőf, Duffie and Smith (1965) (cited in de Jong, 1973). These values, based largely on actual observations, are higher than previous findings (e.g., Black, 1955) which mainly relied on empirical relations. For values of the monthly mean albedo of the sea surface at a mean latitude of 25°N, reference was made to the work of Payne (1972).

The effective back radiation at the sea surface can be expressed as:

$$Q_B = Q_{Bo}(1 - c'C) \qquad (5)$$

where: Q_{Bo} = back radiation at the sea surface under cloudless skies

C = cloud cover (in percent)

c' = dimensionless coefficient = 0.0061

The value of the coefficient c' was taken from Table IX of Budyko (1974), at a mean latitude of 25°N. For values of Q_{Bo}, reference was made to the work of Reed and Halpern (1975). In this work, Reed and Halpern found that the formula for Q_{Bo} developed by Anderson (1954), based on data collected over Lake Heffner, yielded the best comparison with actual measurements. James (1966) has constructed a nomograph based on Anderson's formula, and this nomograph was used to determine the values of Q_{Bo}. This method gives much lower values than the nomograph in Sverdrup, Johnson and Fleming (1942), p. 111. However, a comparison with in situ measurements indicates that the nomograph of Sverdrup et al. gives excessively high values of Q_{Bo}. To compare the results obtained in each of the four regions a graph has been constructed showing the annual variations of Q_R (Fig. 3). The annual mean spatial distribution of Q_R is shown in Fig. 4.

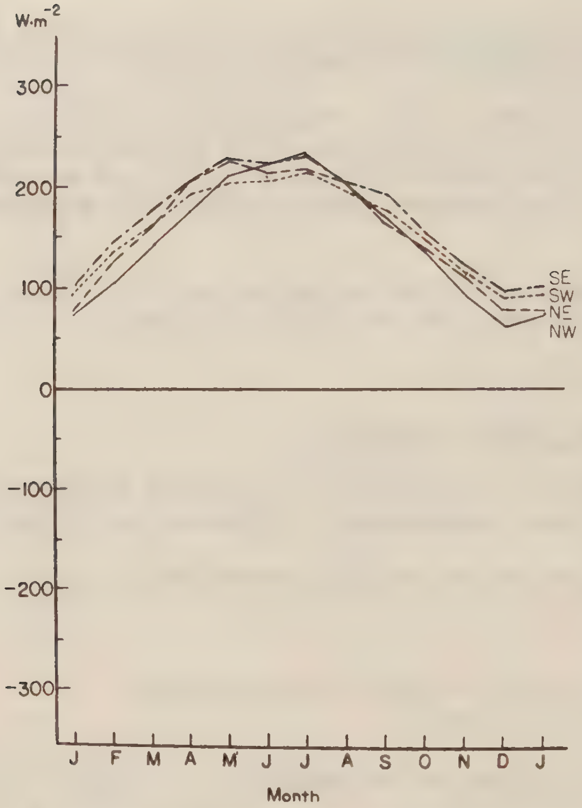

Fig. 3 Annual variation of the radiation balance at the sea surface (Q_R) in the NW, NE, SW and SE regions

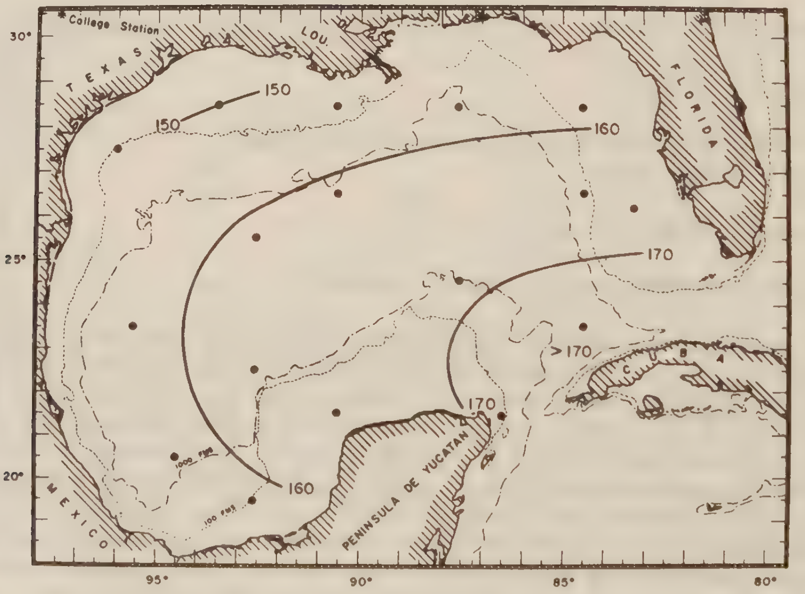
College Station
TEXAS
LOU.
FLORIDA
MEXICO
PENINSULA DE YUCATAN
CUBA
150
150
160
160
170
170
>170
1000 fms
100 fms
30°
25°
20°
95°
90°
85°
80°

Fig. 4 Annual mean distribution of the radiation balance at the sea surface (Q_R), in Watts per square metre

3.2 The Net Turbulent Heat Flux from the Sea Surface (Q_A)

The net turbulent heat flux from the sea surface is composed of the turbulent flux of latent heat (Q_E) and the turbulent flux of sensible heat (Q_H). In numerous developments e.g., Roll (1965), it has been shown that the turbulent flux of latent heat can be expressed as:

$$Q_E = LE = L \left[\frac{0.621\ \rho_a}{p_a} c_E (e_s - e_a)\ W \right] \qquad (6)$$

and that the turbulent flux of sensible heat can be expressed as

$$Q_H = \rho_a c_{pa} c_H (T_s - T_a)\ W \qquad (7)$$

where: L = latent heat of vaporization

E = rate of evaporation

ρ_a = density of air

p_a = atmospheric pressure (in millibars)

c_E = dimensionless coefficient of latent heat transfer

c_{pa} = specific heat of air at constant pressure

c_H = dimensionless coefficient of sensible heat transfer

W = wind speed (at 10-metre level)

T_s = temperature of air at the sea surface

T_a = temperature of air (usually measured at a height of 10 metres above the sea surface)

e_s = saturation vapour pressure of air at temperature T_s (in millibars)

e_a = vapour pressure of air at temperature T_a (in millibars)

Equations (6) and (7) are generally referred to as bulk-aerodynamic formulae. Alternatively, if c_E and c_H are equal, the turbulent flux of sensible heat (Q_H) may be determined from the turbulent flux of latent heat (Q_E) through use of the Bowen ratio (R) as

$$Q_H = RQ_E \qquad (8)$$

where:

$$R = \frac{c_{pa}\ p_a}{0.621\ L} \left(\frac{T_s - T_a}{e_s - e_a} \right) \qquad (9)$$

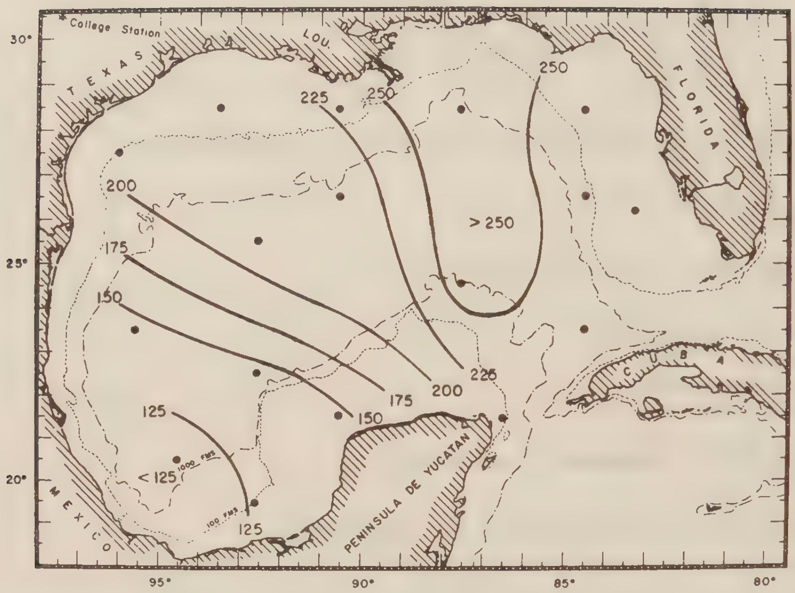
College Station
TEXAS
LOU.
FLORIDA
MEXICO
PENINSULA DE YUCATAN
CUBA
250
225
250
> 250
200
175
150
225
200
175
150
125
< 125
125
1000 FMS.
100 FMS.
30°
25°
20°
95°
90°
85°
80°

Fig. 5 Annual distribution of the evaporation rate (E), in centimetres per year

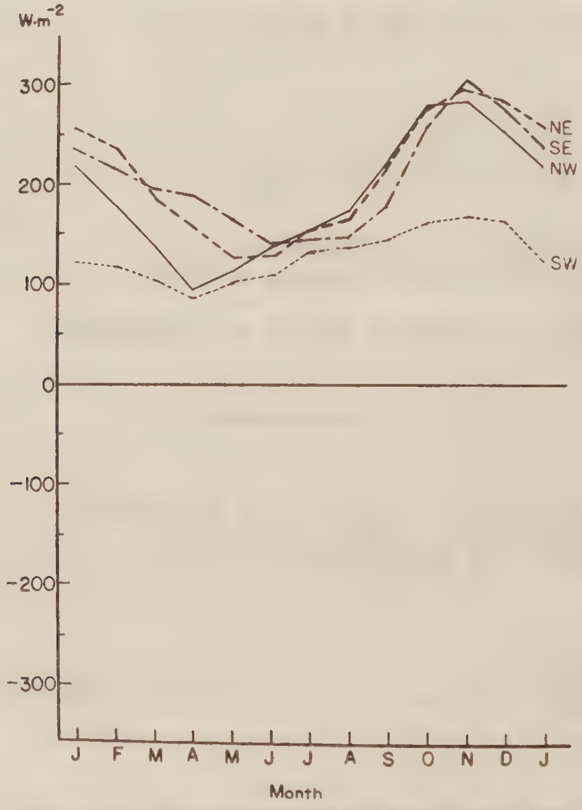

Fig. 6 Annual variation of the net turbulent heat flux from the sea surface (Q_A) in the NW, NE, SW and SE regions

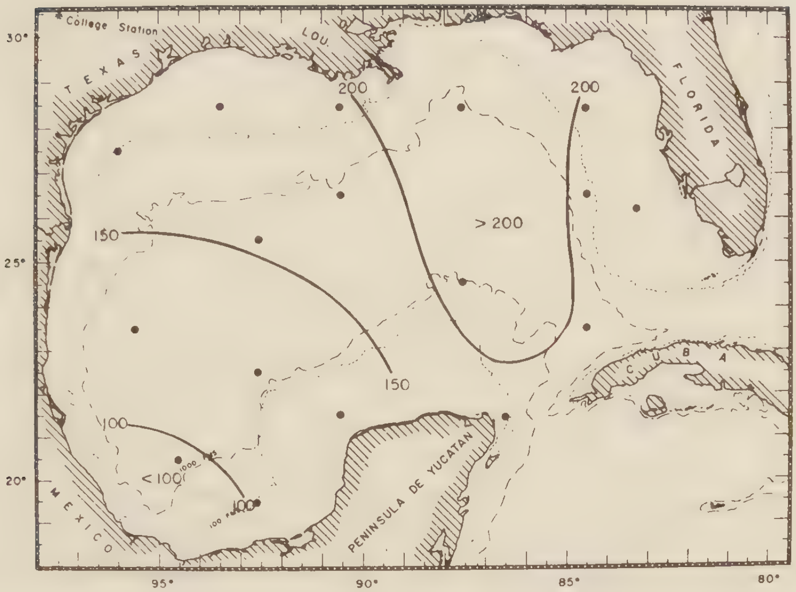
College Station
TEXAS
LOU.
FLORIDA
CUBA
MEXICO
PENINSULA DE YUCATAN
200
200
> 200
150
150
100
< 100
100
1000
30°
25°
20°
95°
90°
85°
80°

Fig. 7 Annual mean distribution of the net turbulent heat flux from the sea surface (Q_A), in Watts per square metre

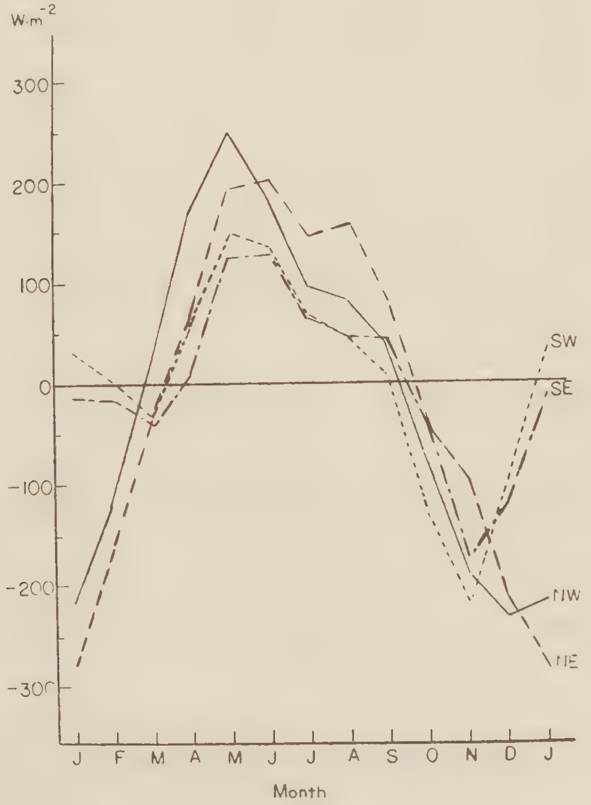

Fig. 8 Annual variation of the rate of heat storage (Q_T) in the NW, NE, SW and SE regions

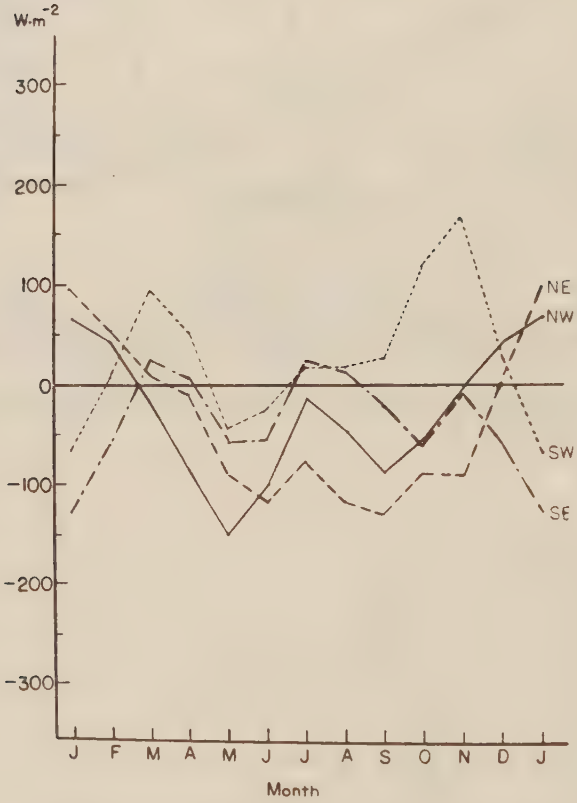

Fig. 9 Annual variation of the heat flux divergence due to currents (Q_V) in the NW, NE, SW and SE regions

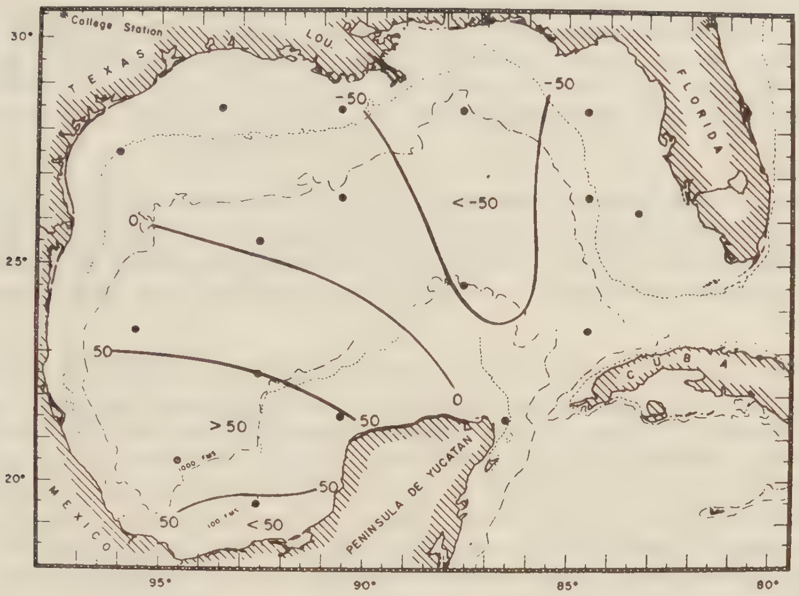
College Station
TEXAS
LOU.
FLORIDA
MEXICO
PENINSULA DE YUCATAN
CUBA
-50
-50
< -50
0
0
50
50
> 50
50
50
< 50
1000 fms
100 fms
30°
25°
20°
95°
90°
85°
80°

Fig. 10 Annual mean distribution of the heat flux divergence due to currents (Q_V), in Watts per square metre

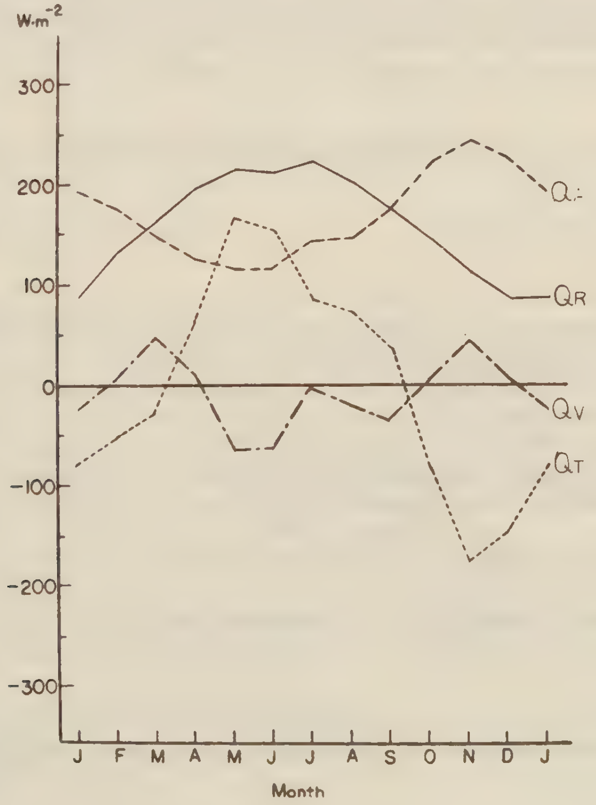

Fig. 11 Annual variation of the radiation balance at the sea surface (Q_R), the net turbulent heat flux from the sea surface (Q_A), the rate of heat storage (Q_T), and the heat flux divergence due to currents (Q_V) for the entire Gulf of Mexico

One of the most difficult problems encountered in this study was the determination of c_E and c_H. The work of Bunker (1975) seemed to be the most comprehensive study available at the time. Based on the findings of other workers, Bunker generated a table of values of c_E which depended on the wind speed and the air-sea temperature difference. He assumed that c_E and c_H were equal.

From a comparison of meteorological data collected by ships with data collected by research installations, Bunker found that the values of c_E and c_H should be increased by 10% when applied to ship data. This increase was apparently needed to compensate for the distortion of the air flow and modification of the temperature and humidity fields by ship structures.

In his work, Bunker applied his coefficients to individual observations. Since the sources of data used in this study presented only monthly mean values of observations, it was decided to use a constant value of c_E and c_H for each region as determined by the annual mean wind speed and air-sea temperature difference in each of the four respective regions of the Gulf of Mexico.

The problem of utilizing average values of observations instead of individual observations in the calculation of turbulent heat fluxes from the ocean has been discussed by many researchers. The objection raised to the use of average values is that covariations between parameters are ignored. Malkus (1962) performed a sample examination of data taken on a cruise in the Caribbean Sea in April 1946 to determine the difference between climatic averages of turbulent heat flux calculations based on 3-hourly ship observations and calculations using climatic mean values for the entire period. She found that the use of climatic mean values of observations would have underestimated both the evaporative and sensible heat fluxes by about 7%.

Therefore, in an attempt to compensate for the underestimation of heat fluxes due to the use of climatic averages of observations, the values of c_E and c_H were increased an additional 7% above the 10% increase recommended by Bunker. Consequently, in this study, the values of c_E and c_H determined from Bunker (1975) were multiplied by a factor of 1.177. These values, both uncorrected and corrected, are listed in Table I. The uncorrected values are in parentheses.

The rate of evaporation (E) was calculated by use of Eq.(6) in the form

$$E = \frac{0.621 \ \rho a}{p_a} c_E (e_s - e_a) W \qquad (10)$$

The saturation vapour pressure of air over sea water (e_s) was determined from the following relation given by Sverdrup et al. (1942, p.115):

$$e_s = (1-0.000537 \ S) \ e_d \qquad (11)$$

where: e_d = saturation vapour pressure of air over distilled water at temperature T_s

S = salinity of sea water in parts per thousand (o/oo)

For an average salinity of 35 o/oo, Eq. (11) reduces to

$$e_s = 0.98 \ e_d \qquad (12)$$

The annual mean spatial distribution of the evaporation rate over the Gulf of Mexico is presented in Fig. 5.

An independent verification of the evaporation rate of 204 centimeters per year for the entire Gulf of Mexico, as determined in this study, was obtained from the evaporation-minus-precipitation (E-P) values of Cummings (1968) and the precipitation (P) values of Möller (1951). Cummings calculated (E-P) values based on aerological data. For the entire Gulf of Mexico, he found an average (E-P) value of 118 centimetres of equivalent water depth per year. It was determined from Möller that the precipitation rate over the entire Gulf of Mexico was 85 centimetres per year. Combining this value with Cummings' (E-P) value yielded an evaporation rate of 203 centimetres per year, a value in excellent agreement with the rate determined from the bulk-aerodynamic formulae.

The turbulent flux of latent heat (Q_E) was calculated by Eq. (6) and the turbulent flux of sensible heat (Q_H) was calculated by Eq. (8). The net turbulent heat flux from the sea surface (Q_A), defined by Eq. (3), was determined for each of the four regions. The annual variations of Q_A for each of the regions are depicted in Fig. 6. This figure shows that all four regions have a maximum value of Q_A in November. The annual mean spatial distribution of Q_A is shown in Fig. 7. This figure shows the effect of the Loop Current in the eastern half of the Gulf of Mexico as a maximum in Q_A.

3.3 The Rate of Heat Storage (Q_T)

This term was obtained through use of the relationship

$$Q_T = \frac{\partial}{\partial t} H \qquad (13)$$

where:

$$H = \int_{-D}^{0} \rho_w \, c_{pw} \, T_w \, dz \qquad (14)$$

and where:

z = depth

T_w = water temperature at depth z

t = time

c_{pw} = specific heat of sea water at constant pressure

ρ_w = density of sea water

D = depth to which integration is carried out

Ideally, the depth (D) for these calculations should be at a depth where the thermal regime is no longer affected by fluctuations in meteorological factors. In practice, however, D can be chosen at a depth where fluctuations resulting from direct surface meteorological variations become small. Robinson (1973) found that the depth of the top of the thermocline in the Gulf of Mexico generally does not exceed about 100 metres. Since temperature versus depth data were usually available to depths of at least 200 metres, it was decided to use this latter depth for the calculation of Q_T.

Monthly values of the quantity H (H_i, i = 1,.....,12) were calculated through use of the temperature-versus-depth data in the report by the U.S. Department of Commerce (1973). The rate of heat storage for each month (Q_{T_i}, i = 1,.....,12) was then obtained by expressing Eq. (13) in the same manner as Pattullo (1957) as

$$Q_{T_i} = \frac{H_{i+1} - H_{i-1}}{2 \text{ months}} \qquad (15)$$

TABLE I

Values of the uncorrected and corrected coefficients of latent heat transfer (c_E) for each region (x 1 000)
Uncorrected values are in parentheses

NW	NE	SW	SE
(1.58)	(1.68)	(1.45)	(1.68)
1.86	1.98	1.71	1.98

TABLE II

Comparison of annual mean values of various components of the oceanic heat budget obtained in different studies encompassing the Gulf of Mexico. Values are in Watts per square metre

Heat Budget Component	Present Study	Hastenrath (1968)	Budyko (1963)	Jacobs (1951)
Q_R	162	114	159	—
Q_A	170	131 *	159	119
Q_V	-8 *	-17	0 *	—

* Determined as a residual

The annual variations of Q_T in each of the four regions are shown in Fig. 8. The value of Q_T obtained in each of the four regions was considered to be representative of the entire region, even though parts of a given region might be shallower than 200 metres. Thus, the rate of heat storage could not be spatially contoured over the Gulf of Mexico. It should be noted that an undetermined contribution to Q_T has been neglected by not considering the remainder of the water column.

3.3 Solution of the Oceanic Heat Budget Equation

By using the values of Q_R, Q_A and Q_T obtained earlier, the heat flux divergence due to currents (Q_V) can be determined as a residual in Eq. (1). Thus, Q_V actually represents the heat flux required to balance the oceanic heat budget at any given location and time. The annual variations of Q_V, calculated as a residual, are shown in Fig. 9 for each region. The annual mean spatial distribution of Q_V is shown in Fig. 10. This figure shows a centre of heat convergence in the area of the Loop Current in the eastern Gulf of Mexico.

A comparison of the annual mean variations of Q_R, Q_A, Q_T and Q_V for the entire Gulf of Mexico is presented in Fig. 11. These four curves represent the means of the respective curves in Figs. 3, 6, 8, and 9, weighted by the area of each region.

3.4 Comparison with Earlier Studies

To show how the present results compare with previous studies encompassing the Gulf of Mexico, a comparison of annual mean values of various heat budget components was made with the results of Jacobs (1951), Budyko (1963) (cited in Budyko, 1974) and Hastenrath (1968) in Table II. Components found as a residual are denoted by an asterisk. The annual mean values of Q_R and Q_A found in this study exceed those of previous studies; the best agreement between studies was found with Budyko (1963).

Upon closer comparison with the results of Hastenrath (1968), it was found that he underestimated both the radiation balance at the sea surface (Q_R) and the net turbulent heat flux from the sea surface (Q_A). Also, Hastenrath greatly underestimated the amplitude of the annual variation of the rate of heat storage (Q_T).

4. ACKNOWLEDGEMENTS

This paper is taken in part from a thesis submitted to Professor John D. Cochrane in partial fulfillment of the requirements for the degree of Master of Science in the Department of Oceanography at Texas A. & M. University.

5. REFERENCES

Anderson, E.R., 1954 Energy-budget studies. In Water-loss investigations: Vol. 1. Lake Heffner Studies Tech.Rep. U.S.Geol.Surv.Prof.No. 269. Washington, D.C., U.S. Government Printing Office, pp. 71-119

Black, J.N., 1955 The distribution of solar radiation over the earth's surface. Arch.Meteorol. Geophys.Biklimatol. (B), 7:165-89

Budyko, M.I., 1963 Atlas of the Heat Balance of the Earth. Glavnaia Geofiz.Obs., Leningr. 1963 69 charts

———, 1974 Climate and life. Int.Geophys.Ser., 18:508 p.

Bunker, A.F., 1975 Energy exchange at the sea surface of the western North Atlantic Ocean. Tech. Rep.Woods Hole Oceanogr.Inst., (WHOI-75-3):107 p. (Unpubl.MS)

Cummings, A.D., Climatological aspects of the balance of water vapor in the atmosphere
1968 overlying the Gulf of Mexico. M.S. Thesis on file at Texas A&M University, College Station, 50 p.

Hastenrath, S.L., Estimates of the latent and sensible heat flux for the Caribbean Sea
1968 and the Gulf of Mexico. *Limnol.Oceanogr.*, 13:322-31

Jacobs, W.G., Large scale aspects of energy transformations over the ocean. *In* Compendium
1951 of meteorology. Boston, Mass., American Meteorology Society, pp. 1057-70

James, R.W., Ocean thermal structure forecasting. SP-105, ASWEPS Manual. Vol.5. Washington,
1966 D.C., U.S. Navy Oceanographic Office

de Jong, B., Net radiation received by a horizontal surface at the earth. Delft University
1973 Press, The Netherlands, Delft, 51 p.

Löf, G.O.G., J.A. Duffie and C.O. Smith, World distribution of solar radiation. *Eng.Exp.Stn.*
1965 *Rep.Univ.Wis.*, (21)

Malkus, J.S., Interchange of properties between sea and air: large scale interactions. *In*
1962 The sea, edited by M.N. Hill. New York, Interscience, Vol.1:88-294

Moller, F., Vierteljahrskarten des Niederschlags für die ganze Erde. *Petermanns Geogr.Mitt.*,
1955 95:1-7

Patullo, J., The seasonal heat budget of the oceans. Ph.D. dissertation. University of
1957 California at Los Angeles, 104 p.

Payne, R.E., Albedo of the sea surface. *J.Atmos.Sci.*, 29:959-70
1972

Reed, R.K. and D. Halpern, Insolation and net long-wave radiation off the Oregon Coast.
1975 *J.Geophys.Res.*, 80:839-44

Robinson, M.K., Atlas of Monthly Mean Sea Surface and Subsurface Temperature and Depth of
1973 the Top of the Thermocline. Gulf of Mexico and Caribbean Sea. *Scripps Inst. Oceanogr.SIO ref.*, (73-8)

Roll, H.U., Physics of the marine atmosphere. *Int.Geophys.Ser.*, (7):426 p.
1965

Sverdrup, H.U., M.W. Johnson and R.H. Fleming, The oceans, their physics, chemistry, and
1942 general biology. Englewood Cliffs, Prentice-Hall, 1087 p.

U.S. Department of Commerce, NOAA, Environmental Data Service, Environmental conditions
1973 within specified geographical regions, offshore east and west coasts of the United States and in the Gulf of Mexico. Washington, D.C., U.S. Government. Printing Office

U.S. Naval Weather Service Command, Summary of synoptic meteorological observations. North
1975 American coastal marine areas (Revised). Atlantic and Gulf coasts. Vol.4. Asheville, N.C., National Climatic Center. (Available from the National Technical Information Service (NTIS), Springfield, Va.)

AIR-SEA INTERACTIONS DURING CONDITIONS OF SQUALLS AND DEEP CONVECTION

by

F. OSTAPOFF and S. WORTHEM
National Oceanic and Atmospheric Administration
Atlantic Oceanographic and Meteorological Laboratories
Sea-Air Interaction Laboratory
Miami, Florida, U.S.A.

CONTENTS

1. INTRODUCTION
2. THE ATMOSPHERE SURFACE LAYER RESPONSE
3. THE OCEANIC SURFACE LAYER RESPONSE
4. CONCLUSION
5. REFERENCES

Abstract

In September 1972 a mixed-layer experiment was conducted some 200 miles north of San Juan, Puerto Rico, as part of the CICAR programme in meteorology. Two MAMOS buoys were deployed, one of which was instrumented meteorologically. Air and water temperature, humidity, windspeed and radiation were observed and recorded at one-minute intervals. During passage of deep convective systems, a dramatic change in heat and momentum flux occurs associated with the circulation of those systems. In fact, the observations demonstrate the effects of up and down drafts generated within these deep convective cells on the thermodynamic properties of the surface layer resulting in an increase of sensible heat flux by an order of magnitude and latent heat flux by a factor of 2 to 4. Consequently, the Bowen ratio (sensible to latent heat flux) changes from about .10 for 'normal' tradewind conditions to .30-.35 under those disturbed conditions. Precipitation from these systems changes the static stability of the oceanic mixed layer and causes dramatic changes of temperature in the uppermost layer.

Resumen

Como parte del programa meteorológico de las ICCRA se realizó, en septiembre de 1972, un experimento en la capa de aguas mezcladas, a unas 200 millas al norte de San Juan de Puerto Rico. Se lanzaron dos boyas MAMOS, una de ellas dotada de instrumentos de medición meteorológica. Se observaron y registraron las temperaturas del agua y del aire, la humedad, la velocidad del viento y la radiación, a intervalos de un minuto. Durante el paso de sistemas de convección penetrante se produce un cambio drástico en el flujo de calor y en la cantidad d de movimiento, asociado a la circulación de esos sistemas. Las observaciones demuestran prácticamente los efectos de las corrientes ascendentes y descendentes engendradas dentro de las celdas de convección penetrante sobre las propiedades termodinámicas de la capa superficial, consistentes en que el flujo de calor sensible aumenta unas diez veces, y el flujo de calor latente, de dos a cuatro veces. Por consiguiente, el cociente de Bowen (flujo de calor sensible dividido por flujo de calor latente) cambia de 0,10 aproximadamente, en condiciones de vientos alisios 'normales', a 0,30-0,35, cuando se producen estas perturbaciones. Las precipitaciones originadas por estos sistemas cambian la estabilidad estática de la capa mixta oceánica, y originan drásticos cambios de temperatura en la capa superior.

1. INTRODUCTION

In this paper we would like to present some observations which will show the effects of atmospheric disturbances on the surface meteorological conditions and their effect on the upper ocean. Most of them were collected within the framework of CICAR. The data were obtained during the mixed-layer experiment, held north of San Juan, P.R. in September, 1971. A description of the instrumentation used during this experiment is given in another paper at the Symposium (Worthem and Ostapoff, 1976).

Much of what we know about the structure of the undisturbed atmosphere in the tropics has been described by Augstein *et al.* (1973) and Augstein *et al.* (1974), using the observations of the Atlantic Tradewind Expedition, 1969 (ATEX); and by Holland and Rasmussen (1973), using the data from the Barbados Oceanographic and Meteorological Experiment, 1969 (BOMEX).

2. THE ATMOSPHERE SURFACE LAYER RESPONSE

In order to understand the thermodynamic properties of the air near the ocean surface as they evolve during the passage of a squall line or deep penetrating convective system, Fig. 1 shows a schematic representation of the vertical structure of such systems, according to Zipser (1969). Moist, warm air of the mixed layer below cloud base will be drawn into the towering convective portion of the cloud, pumping moisture into the system and feeding the rain-producing part of the anvil. Associated with the precipitation, which can be of considerable magnitude, is the region of down-draft. Often, a gust front is produced under the the cloud and ahead of the cool and sometimes dry down-draft air. This air comes from a level above the cloud base (Betts, 1976) and is cooled by evaporation. But, its moisture content stays normally below that of the environmental air near the surface. The associated deep down-draft transport will reach the surface of the ocean (see Fig. 2).

Fig. 2 shows a time series of specific humidity, wind speed, air temperature, sea-air temperature difference and sea-surface temperature. The data was obtained at one-minute intervals at a height of six metres above the sea surface from a buoy (Worthem and Ostapoff, 1976). As seen from the sea surface temperature, the record was obtained during night time. Prior to the passage of a convective system at 0020 LT 2 October 1971, the atmospheric variables exhibit the normally found conditions over the tropical ocean: relative humidity, about 75 percent; air-sea temperature difference of about 1°C; wind speed about 6 m sec^{-1}. These values will give typical sensible heat flux of 30 cal $cm^{-1}d^{-1}$ and latent heat fluxes of 400 cal $cm^{-2}d^{-1}$ resulting in a Bowen ratio in the order of $B \approx .10$ (see Fig. 3).

At 0020 LT, and then again at 0500 LT during the experiment, deep convective systems passed over the buoy and its sensors. The gust front associated with the convective cloud is clearly evident in the wind record. Peak values of 15 m sec^{-1} were reached, and immediately both the relative humidity and specific humidity began dropping sharply indicating the arrival of the cold, dry, down-draft air. The air-sea temperature difference reached about 3.5°C in the first case and somewhat more than 5°C in the second case. This was due to the cold air in both cases, since the water temperature did not change noticeably as a result of these events. The first event lasted a half an hour; the second about one hour before the atmosphere began returning to large-scale, equilibrium environmental conditions.

In Fig. 3, the momentum and heat fluxes are presented for the time series shown in Fig. 2. The aerodynamic bulk formulas corrected for stability have been used to calculate the fluxes. The momentum and heat exchange rates changed considerably, as shown in Table I. The Bowen ratio increases with the size of the disturbance. It may reach mid-latitude values of about .30-.35 for large systems.

Table I

Momentum, sensible and latent heat flux estimates during undisturbed and disturbed conditions

Meteorological conditions	Momentum flux dyn cm^{-2}	Sensible heat flux cal cm^{-2} d^{-1}	Latent heat flux cal cm^{-2} d^{-1}	Bowen ratio
Undisturbed	.5	3	40	.08
Disturbed (1)	3.4	14	110	.13
Disturbed (2)	3.4	25	125	.20

3. THE OCEANIC SURFACE LAYER RESPONSE

As seen from Fig. 2, the ocean response to small-scale atmosphere disturbances as indicated by the sea surface temperature is hardly noticeable. This is not surprising because of the great heat capacity of water and the almost instantaneous mixing due to wave set-up.

However, if the other thermodynamic property of ocean water, salinity, is significantly altered, then the top layer of the ocean may respond differently, depending upon the stability conditions which may be set-up by heavy precipitation from individual convective systems or enormous river run-off during the rainy season, e.g., the Amazon River and Orinoco River. Detailed descriptions of the processes in the upper ocean under various stability conditions are given in the paper by Worthem and Ostapoff (1978).

How the stability can be changed by atmospheric events can be seen in Fig. 4 which shows a sequence of two-hourly temperature and salinity profiles obtained in the Inter-Tropical Convergence Zone (ITCZ) at approximately 4°N and 24°W in July 1972. Initially, the so-called oceanic mixed layer was indeed well mixed in temperature and salinity to about 60 m depth (to within the accuracy of the instrument which was an internally analogue recording STD device). Rain started at the time of the profile indicated by the precipitation symbol. It lasted for about 12 hours and amounted to about 18 mm as observed by the rain gauge on the ship. However, if the salt deficit in the top layer is solely attributed to local precipitation and not to other processes such as advection, then about 46 mm of rain water should have precipitated. This is somewhat more than twice what has been observed; but one should remember that reliable shipboard rain observations are notoriously difficult to obtain (Shinners, 1970). Further into the time series in Fig. 4, another brief shower occurred, again leaving its signature in the top layer of the ocean.

A wave-mixed layer developed to a depth of about 7-10 m as can be seen in Fig. 4. After the rain stopped, the low-salinity/low-temperature lens is diffused downward, probably by either turbulent diffusion or mixing caused by shear instability.

A closer look at the downward diffusion is presented in Fig. 5 which shows details of two successive temperature and salinity profiles, two hours apart. The heat and salt deficits are preserved and redistributed with time. Another example is given in Fig. 6, obtained in the Caribbean Sea southeast of Puerto Rico under a cloud cluster (see satellite picture in Fig. 7). In this case, the two profiles were taken one hour apart. These time series have been used to calculate the complete budget in the upper ocean and to derive precipitation information from salinity measurements for cases where advection can be neglected (Ostapoff *et al.*, 1973).

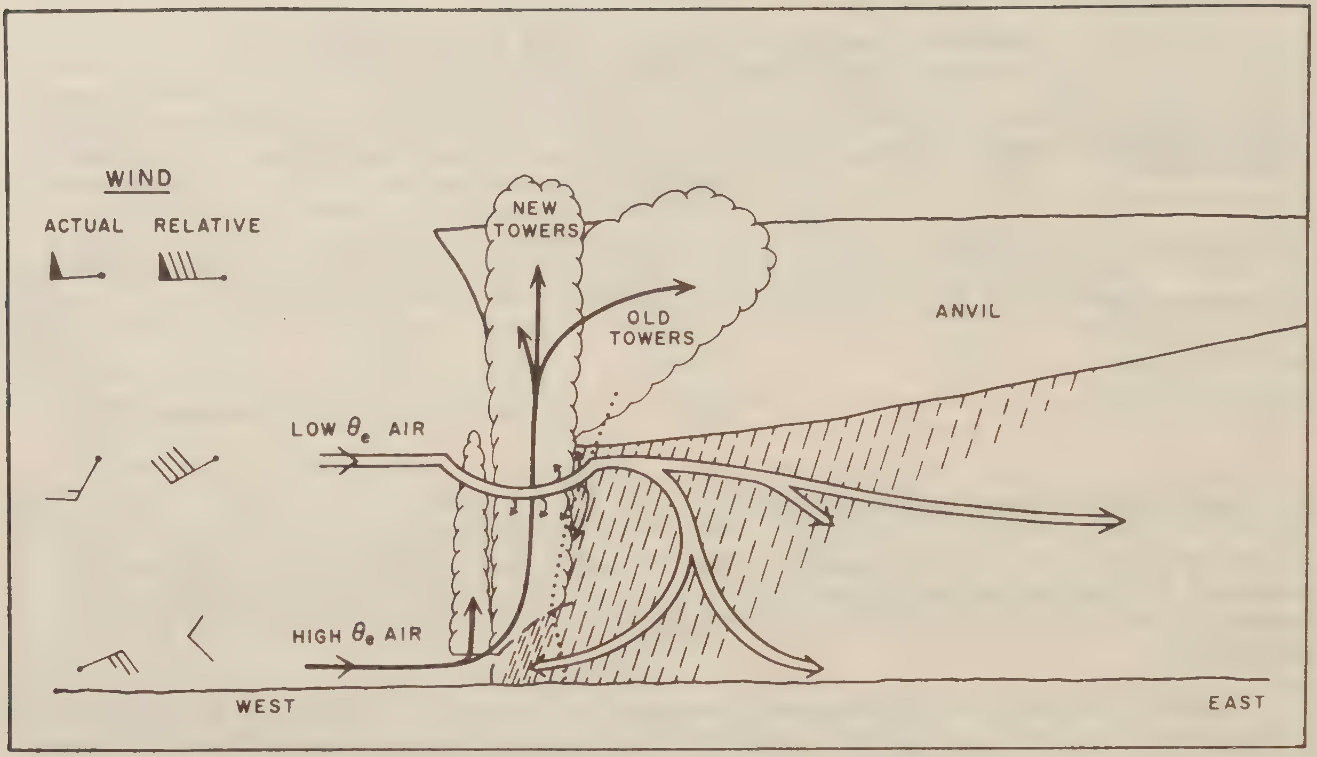
WIND
ACTUAL
RELATIVE
NEW TOWERS
OLD TOWERS
ANVIL
LOW θ_e AIR
HIGH θ_e AIR
WEST
EAST

Fig. 1 Schematic presentation of streamlines in convective cloud system according to Zipser (1969)

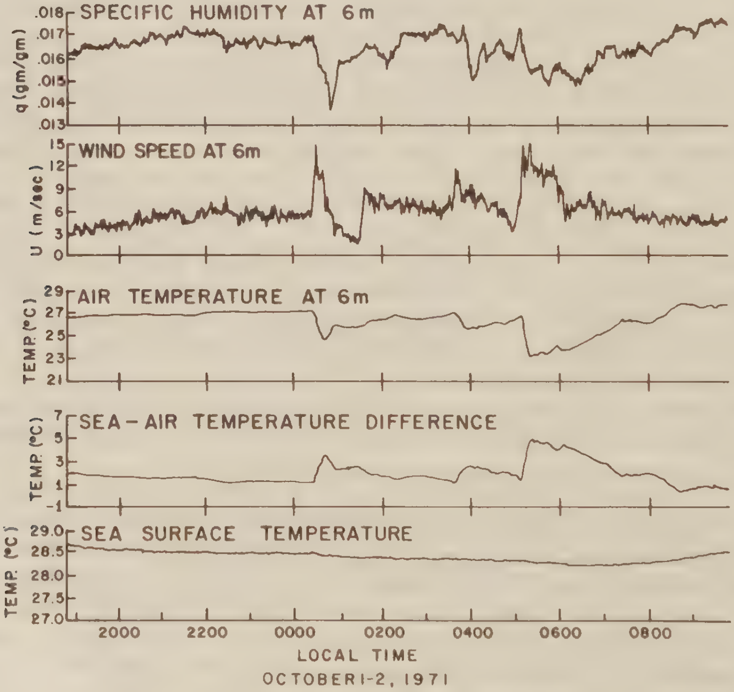

Fig. 2 Time series of specific humidity, wind speed, air temperature and sea-surface temperature during atmospheric deep convection events

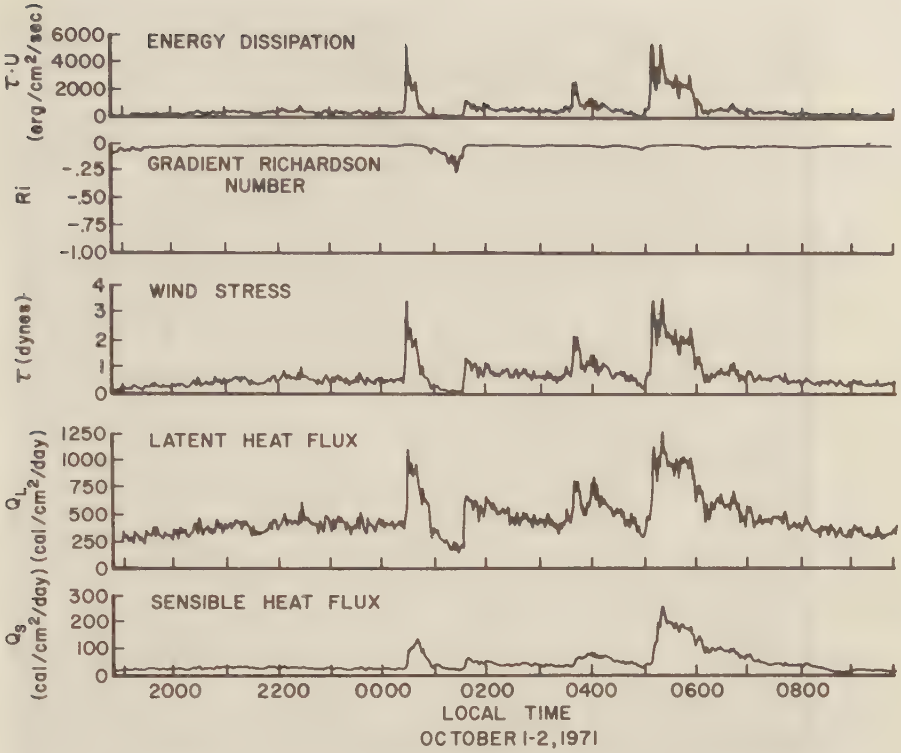

Fig. 3 Time series as in Fig. 2 for derived energy fluxes

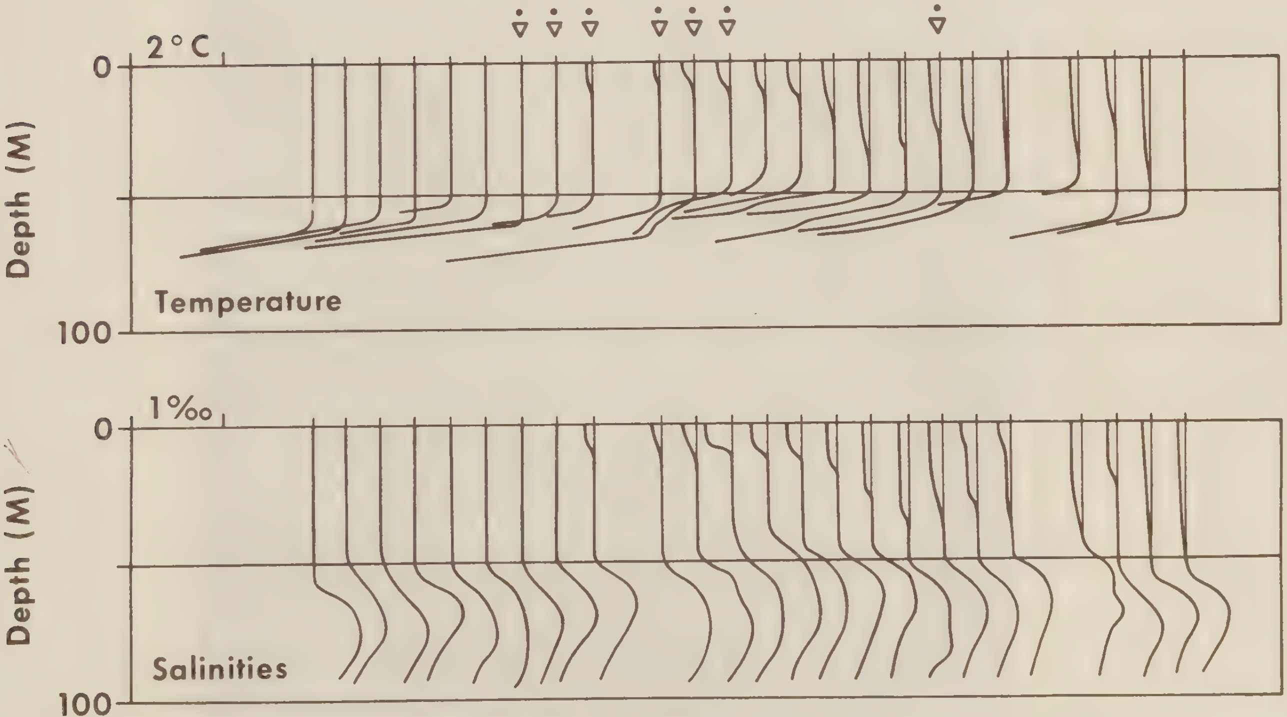

Fig. 4 Two-hourly time series of temperature (top) and salinity (bottom) profiles obtained during precipitation events

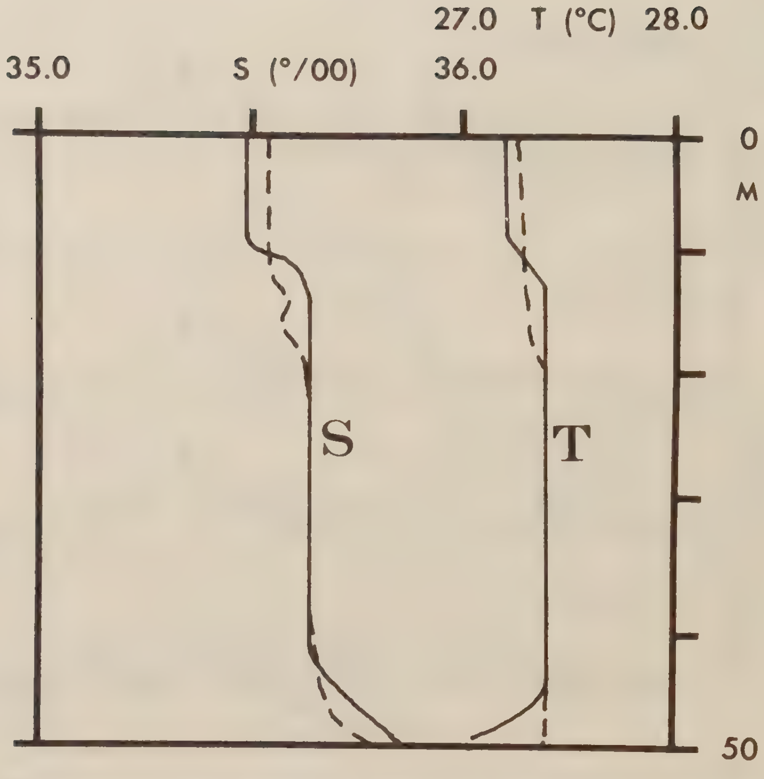

Fig. 5 Temperature and salinity profiles obtained two hours apart

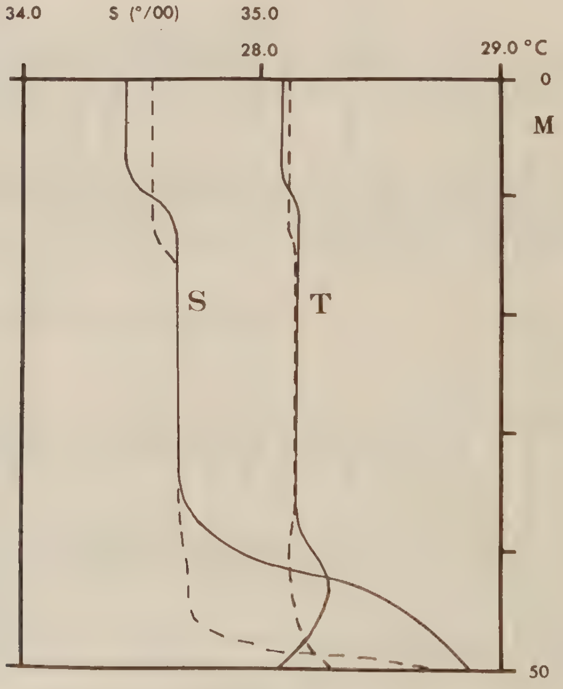

DISCOVERER 11.11.72

Fig. 6 Temperature and salinity profiles obtained one hour apart southeast of Puerto Rico

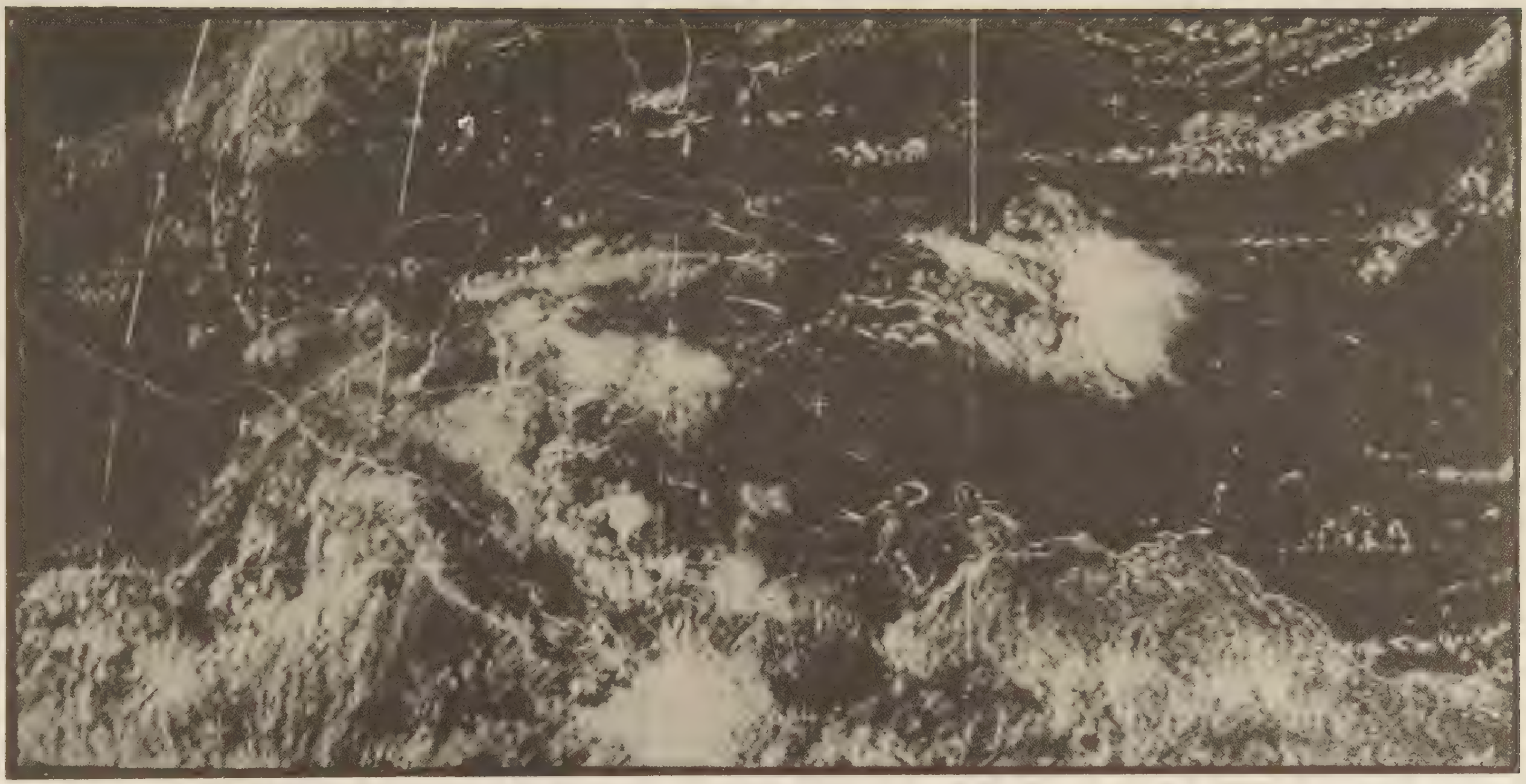

Fig. 7 Satellite photograph of cloud cluster southeast of Puerto Rico on 11 November 1972 when T-S profiles were obtained (see Fig. 6) during NOAA-Carib

4. CONCLUSION

The purpose of this paper is to show, with the aid of a few examples, how the lowest layers of the atmosphere and the upper layers of the ocean respond to a deep convection system. Indeed, it is shown that extreme down-draft conditions exist right down to the ocean surface for relatively large time scales, on the order of a half an hour. Then the enormously enhanced sensible and latent heat fluxes, generated by the down-draft conditions themselves, may feed back into these systems and quickly modify the near-surface layers. The large energy fluxes at the sea surface provide a source of heat and moisture flux into the boundary layer which tends to cause restoration of the large-scale environmental conditions.

It is also shown that precipitation plays an important role in the thermodynamics of the upper ocean mixed layer in determining and modifying the stability of this layer; thus allowing different processes to dominate the exchanges within the oceanic mixed layer and energy exchanges between the ocean and the atmosphere.

5. REFERENCES

Augstein, E., H. Schmidt and F. Ostapoff, 1974 The vertical structure of the atmospheric planetary boundary layer in undisturbed trade winds over the Atlantic Ocean. Boundary-Layer Meteorol., 6:129-50

Augstein, E. *et al.*, 1973 Mass and energy transports in an undisturbed Atlantic trade-wind flow. Mon.Weather Rev., 101(2):101-11

Betts, A.K., 1976 The thermodynamic transformation of the tropical sub-cloud layer by precipitation and down drafts. J.Atmos.Sci., 33(6):1008-20

Holland, J.Z. and E.M. Rasmusson, 1973 Measurements of atmospheric mass, energy and momentum budgets over a 500-kilometer square of tropical ocean. Mon.Weather Rev., 101:11-55

Ostapoff, F., Yu. Tarbeyev and S. Worthem, 1973 Heat flux and precipitation estimates from oceanographic observations. Science, Wash., 180:960-2

Shinners, W.W., 1970 Status of instrument development for specialized marine observations. Meteorol.Monogr., 11:294-301

Worthem, S. and F. Ostapoff, 1978 The response of the tropical North Atlantic to meteorological forcing functions. FAO Fish.Rep., (200) Suppl.

Zipser, E.J., 1969 The role of organized unsaturated convective down drafts in the structure and rapid decay of an equatorial disturbance. J.Appl.Meteorol., 8:799-814

TEMPORADA DE LLUVIAS EN LAS COSTAS VENEZOLANAS DURANTE EL AÑO 1975

por

M. PERDOMO de MATA y K. HUBSCHMAN
Departamento de Meteorología
Dirección de Hidrografía y Navegación
Comandancia General de la Marina
República de Venezuela

CONTENIDO

1. INTRODUCCION
2. MECANISMOS DE LA TEMPORADA LLUVIOSA EN VENEZUELA
3. LLUVIAS EN 1975
4. CONCLUSIONES
5. REFERENCIAS

Resumen

Hay varios procesos que pueden producir lluvias en las costas venezolanas. Usualmente se cree que el desplazamiento estacional de la Convergencia Intertropical es el factor más importante, especialmente por producir la precipitación durante la temporada de lluvias, pero un estudio de las lluvias y sus causas durante 1975 muestra que en ese año otros factores fueron más importantes.

Abstract

A number of processes may bring about rainfall in Venezuela. Seasonal movements of the Intertropical Convergence are usually thought to be the most important, especially in causing precipitation during the rainy season, but a study of rainfall and its causes during 1975 shows that in this year other factors were more important.

1. INTRODUCCION

El presente trabajo tiene por objeto hacer un breve estudio del mecanismo de la temporada lluviosa en las costas venezolanas durante el año 1975, comparándola con valores medios de precipitación para secuencias de varios años de registro contínuo.

Se tomaron como base los registros de precipitación de las estaciones meteorológicas de primer orden: Barcelona, Coro, Escuela Naval, Guiria, La Orchila, Maiquetía y Puerto Cabello, ubicadas a todo lo largo de la costa venezolana (Fig. 1).

Para comprender mejor las causas de la precipitación en las costas venezolanas, se describirá primero el mecanismo de la temporada lluviosa en Venezuela.

2. MECANISMO DE LA TEMPORADA LLUVIOSA EN VENEZUELA

La temporada lluviosa, que muchos erradamente denominan invierno y que no es tal, ya que paradógicamente coincide con el verano astronómico del hemisferio norte, al cual pertenece Venezuela; está comprendida entre los meses de mayo y noviembre (siete meses) y la seca entre diciembre y abril (cinco meses).

Esta temporada lluviosa está profundamente influenciada por la llamada Zona de Convergencia Intertropical, que no es más que la zona de separación o de convergencia entre los regímenes de vientos de los hemisferios norte y sur, alrededor de las bajas latitudes tropicales y cuyo desplazamiento sigue la variación anual de la declinación solar y el consecuente cambio latitudinal del sistema principal de presiones asociado; estando siempre ubicada sobre el cinturón de bajas presiones (Figs. 2 y 3) según Gray (1968). Esta zona de convergencia origina un ascenso en las masas de aire de las áreas adyacentes con el consecuente aumento de la nubosidad. Debido al ascenso de las masas de aire, la temperatura de las mismas desciende, produciendo inestabilidad. Al llevarse a cabo la condensación dentro de las nubes se origina la precipitación con mucha actividad atmosférica (Fig. 4). Este proceso ocurre a lo largo de toda la Zona de Convergencia Intertropical y es por lo tanto uno de los principales responsables de las precipitaciones en Venezuela.

La posición media de la Zona de Convergencia Intertropical es en julio (verano astronómico del hemisferio norte) 13° lat. norte pero puede variar entre 2° y 27°N, y en enero (verano astronómico del hemisferio sur) 4° lat. sur, pero puede variar entre 17°S y 8°N (Riehl, 1954).

Igualmente importante en la distribución de la precipitación en Venezuela es la llamada vaguada, que es un área prolongada de baja presión que indica una circulación ciclónica, en los niveles bajos de la atmósfera y que puede producir precipitación de cualquier tipo. Generalmente produce lloviznas y lluvia de diciembre a mayo y chaparrones y tormentas de junio a noviembre. Existe también la vaguada en la altura, que indica circulación ciclónica por encima de los 5 000 m.

Además de la Zona de Convergencia Intertropical y de la vaguada también influyen en nuestra temporada lluviosa las llamadas ondas del este, las cuales son perturbaciones tropicales asociadas con las bajas presiones y que se desplazan de este a oeste en la región de los vientos alisios, por lo tanto alcanzan nuestras costas y esto ocurre entre los meses de junio a septiembre, originando convergencia, inestabilidad y precipitaciones.

De menor influencia para nosotros pero de gran importancia por sus trágicas consecuencias son los ciclones y huracanes que son centros de muy baja presión con vientos muy fuertes (más de 120 km/h), localizados en áreas marítimas entre los 10° y 30° de lat. norte y sur, durante los meses de mayo a noviembre y cuyo desplazamiento sigue un rumbo inseguro, de ahí su difícil pronóstico. En realidad la frecuencia de los ciclones tropicales sobre nuestras costas es mínima y de muy poca contribución para nuestra temporada lluviosa.

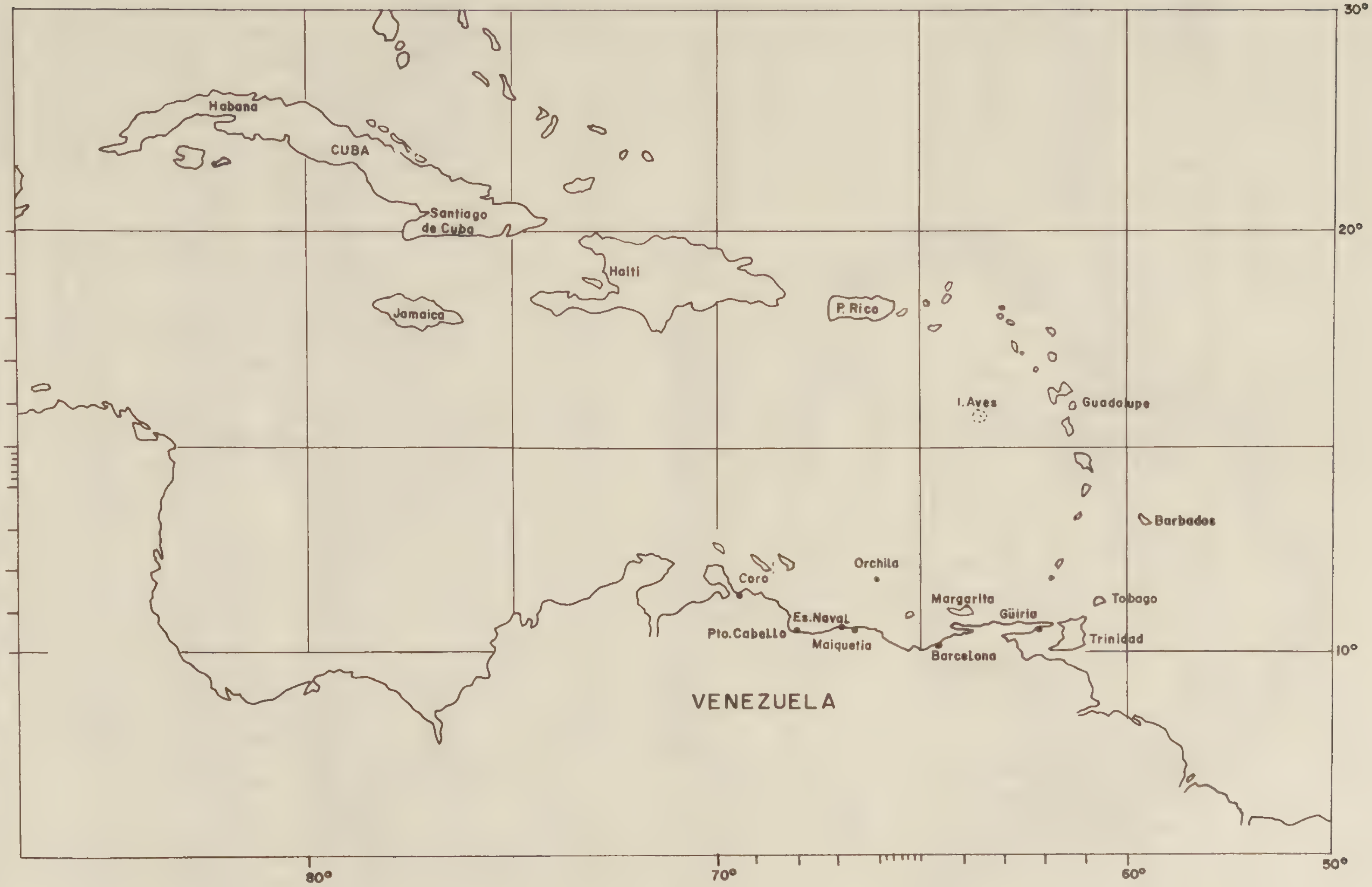
30°
20°
10°
80°
70°
60°
50°
Habana
CUBA
Santiago de Cuba
Jamaica
Haiti
P. Rico
I. Aves
Guadalupe
Barbados
Orchila
Coro
Es. Naval
Pto. Cabello
Maiquetia
Margarita
Güiria
Barcelona
Tobago
Trinidad
VENEZUELA

Fig. 1 Ubicación de las estaciones en la costa venezolana

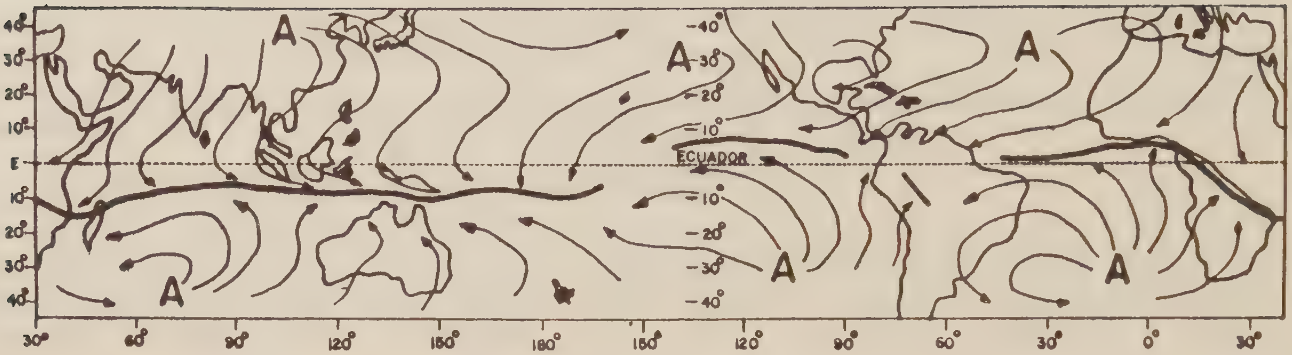
A
A
A
A
A
A
ECUADOR
40°
30°
20°
10°
E
10°
20°
30°
40°
-40°
-30°
-20°
-10°
-10°
-20°
-30°
-40°
30°
60°
90°
120°
150°
180°
150°
120°
90°
60°
30°
0°
30°

Fig. 2, Las flechas indican el flujo des viento idealizado en el mes de Enero. La línea gruesa representa la posición media de la Zona de Convergencia Intertropical para el mismo mes. La letra A significa centros de Alta Presión.

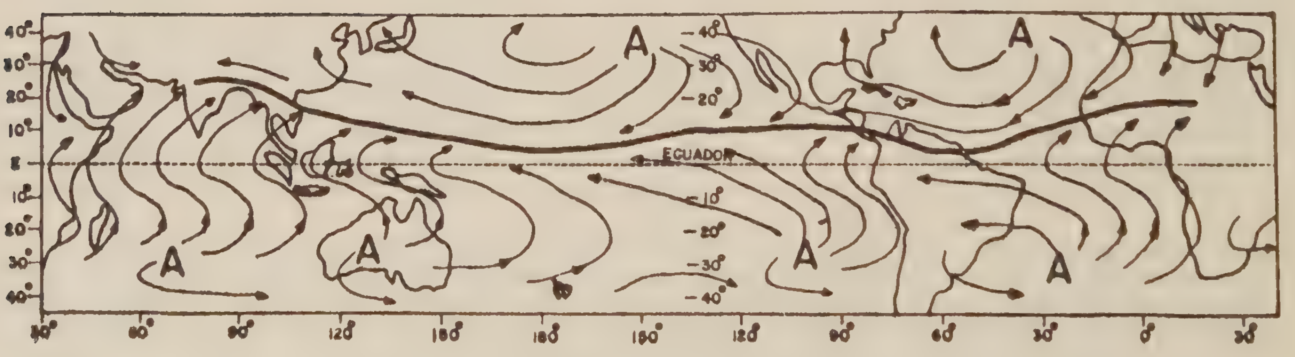
A
A
A
A
A
A
ECUADOR
40°
30°
20°
10°
E
10°
20°
30°
40°
-40°
30°
-20°
-10°
-20°
-30°
-40°
30°
60°
90°
120°
150°
180°
150°
120°
90°
60°
30°
0°
30°

Fig. 3, Flujo del viento idealizado en el mes de Julio. La línea gruesa representa la posición media de la Zona de Convergencia Intertropical para el mismo mes. La letre A significa centros de Alta Presión.

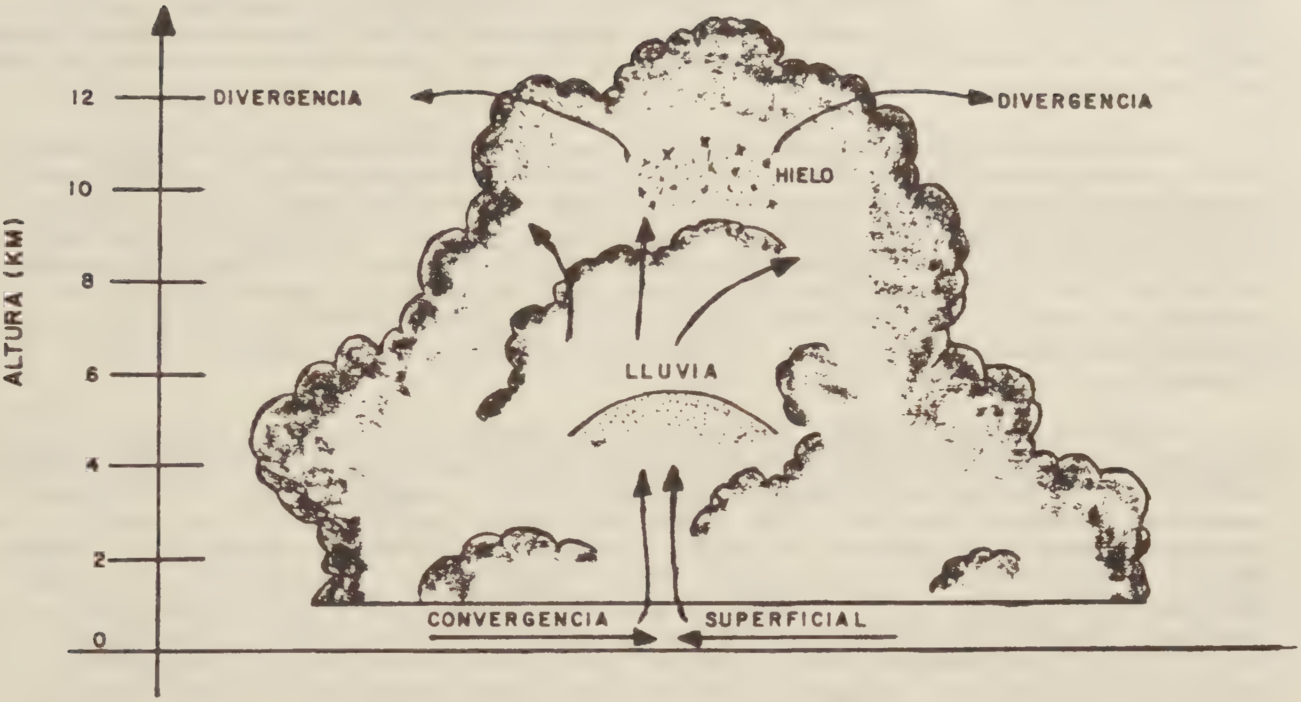

Fig. 4 Esquema de la generación de lluvia a partir de la convergencia superficial

Otra causa de precipitaciones dentro de la temporada lluviosa o de la seca, son las llamadas advecciones de aire polar modificado del hemisferio norte, que causan repentinos descensos de temperatura y precipitaciones muy intensas y de poca duración entre los meses de octubre a junio y que son, por lo tanto, las causantes de las precipitaciones que ocurren durante la temporada seca en las costas y en norte de Venezuela, aunque también contribuyen con la temporada lluviosa durante los meses de octubre, noviembre, mayo y junio. Debemos recordar el caso de fuertes lluvias registradas el 15 y 16 de febrero de 1951 (plena estación seca) ocasionadas por advección de aire polar modificado, causando inundaciones y tragedia desde Puerto Cabello hasta los Caracas.

Estas advecciones antes mencionadas también pueden provenir del hemisferio sur, ocasionando intensas precipitaciones al sur de Venezuela especialmente en los meses de agosto y septiembre y por lo tanto contribuyen con nuestra temporada lluviosa, aunque no ocurren con mucha frecuencia (Perdomo, 1968, 1969).

Para finalizar mencionaremos la influencia de los factores orográficos que contribuyen grandemente con la temporada lluviosa pero con características locales, restringida a sitios con relieve montañoso. El aire por el ascenso orográfico forma la lluvia en el lado de barlovento y en su descenso se transforma en aire seco produciendo el llamado "efecto Fohen".

Por todo lo anteriormente expuesto concluimos que la temporada de lluvias en Venezuela está influenciada por una gran cantidad de factores tanto orográficos como termodinámicos, que hacen muy difícil su pronóstico.

3. LLUVIAS EN 1975

A continuación se analizarán detalladamente las precipitaciones caídas en las estaciones meteorológicas antes mencionadas. Se analizará primeramente un cuadro comparativo entre la lluvia caída durante el año 1975 y la correspondiente a una secuencia de años, para cada estación, e igualmente se analizarán las precipitaciones acumuladas para los mismos períodos. En estos cuadros se nota claramente el déficit o exceso producido durante cada mes en cada estación, y en el caso de los cuadros de precipitación acumulada, el déficit o exceso a través del año.

Analizando los cuadros se deduce que los cuatro primeros meses del año 1975 fueron secos, comparándolos con las medias de precipitación correspondientes a las estaciones investigadas, debido principalmente a la influencia de una alta presión sobre el área. Las ligeras precipitaciones ocurridas en estos meses fueron ocasionados por vaguadas esporádicas en la media y alta troposfera y a advección de aire polar modificado proveniente del norte. La única anomalía fue la ocurrida en el mes de abril, específicamente en la estación Maiquetía el día 24, cuando cayeron 26,0 mm de precipitación, la cual fue originada por una vaguada en la altura, con su centro localizado sobre la costa central de Venezuela.

Durante la segunda quincena del mes de mayo, comenzó la temporada de lluvias en Venezuela en el año 1975. Sin embargo, comparando con las medias de períodos anteriores hubo déficit de precipitación durante los meses de mayo a agosto en casi toda la costa venezolana durante el año 1975. Las excepciones fueron Puerto Cabello y la Orchila y trataremos de describir brevemente las causas de estas precipitaciones anormales. En Puerto Cabello el día 7 del mes de mayo cayó un fuerte chaparrón que produjo 26,8 mm de precipitación en el término de 1½ h, y que fue producto de una vaguada en la altura, la cual permaneció durante varios días sobre el área, causando en total 51,0 mm, durante los 17 y 17 y 23. Esta vaguada también ocasionó precipitaciones en Guiria en esos días, con un total de 60,0 mm. Durante el mes de junio en Puerto Cabello y la Orchila se produjeron fuertes precipitaciones durante los últimos diez días del mes, debidas a una vaguada en la altura y a una ligera influencia de masas de aire del norte y de la Zona de Convergencia Intertropical, que ocasionaron lluvias en casi todo el país. Igualmente para esta fecha se produjeron fuertes vientos y marejada, que obligaron a tomar precauciones en la navegación aérea y marítima. Estos vientos fuertes fueron originados por una intensificación y acercamiento de la alta presión del Atlántico hacia nuestras costas. La diferencia de presión entre esta alta y las bajas presiones ecuatoriales forman una fuerza de gradiente bárico que traslada el aire a gran velocidad produciendo fuerte oleaje.

Las condiciones meteorológicas antes mencionadas afectaron también las costas orientales (Guiria y Barcelona). Durante la primera semana del mes de julio hubo fuertes precipitaciones en casi toda la costa, producto de una vaguada en la altura combinada con influencia de la Zona de Convergencia Intertropical. Además el huracán Amy (primero de la temporada) se encontraba situado, el día 3 a las 08.00 hora legal de Venezuela, a 38°N y 60°W, o sea al norte de Venezuela. Todos estos factores determinaron la situación reinante en estos días, en las costas venezolanas, principalmente el litoral central, donde hubo que suspenderse más de 20 vuelos debido a la lluvia y fuertes vientos de hasta 80 km/h en el aeropuerto de Maiquetía. En el mes de agosto hubo fuertes precipitaciones en Puerto Cabello, debidas a una vaguada en la altura con penetración de la Zona de Convergencia Intertropical por un lado, y a ondas del este, por el otro. Los días 11 y 12 hubo torrenciales aguaceros y fuertes vientos (75 km/h) que azotaron el litoral central.

Durante los últimos meses del año encontramos un marcado incremento de las precipitaciones en septiembre y octubre, una disminución de las mismas en noviembre, para terminar con fuertes lluvias en diciembre. En el mes de septiembre ocurrieron inundaciones en Coro, causadas por precipitaciones originadas por una vaguada en la baja troposfera localizada sobre el área, también se destacan fuertes vientos en el litoral central (65 km/h) durante el día 9 ocasionados por otra vaguada. Igualmente el día 21 una nueva vaguada en la altura causó precipitaciones y fuertes vientos con mar picado y olas de más de dos metros, lo cual trajo como consecuencia la paralización de la navegación aérea y marítima. En octubre las fuertes lluvias ocurridas fueron igualmente causadas por una secuencia de vaguadas. En el mes de noviembre reinó la influencia de una alta presión que originó una disminución

Cuadro de Precipitación Total en mm

	Estación: Barcelona												
	Ener.	Feb.	Mar.	Abr.	Mayo	Jun.	Jul.	Ago.	Sept.	Oct.	Nov.	Dic.	Total
1.975	0,0	0,0	3,0	0,1	16,6	62,5	76,6	52,6	75,3	71,5	25,0	10,0	393,2
1.950-70	9,0	5,0	5,0	6,0	40,0	107,0	132,0	130,0	75,0	51,0	43,0	41,0	644,0
Dif.	-9,0	-5,0	-2,0	-5,9	-23,4	-44,5	-55,4	-77,4	0,3	20,5	-18,0	-31,0	250,8

Cuadro de precipitación total acumulada en mm

Σ1.975	0,0	0,0	3,0	3,1	19,7	82,2	158,8	211,4	286,7	358,2	383,2	393,8	
Σ 1.950-70	90,0	14,0	19,0	25,0	65,0	172,0	304,0	434,0	509,0	560,0	603,0	644,0	
Dif.	-9,0	-14,0	-16,0	-21,9	-45,3	-89,8	-145,2	-222,6	-222,3	-201.8	219,8	-250,8	

Cuadro de precipitación total en mm

	Estación: Coro												
1.975	10,7	2,1	0,0	0,6	2,2	29,3	31,0	17,6	102,3	134,8	84,0	261,6	676,2
1.950-70	35,0	17,0	8,0	21,0	26,0	22,0	36,0	31,0	42,0	66,0	65,0	58,0	427,0
Dif.	-24,3	-14,9	-8,0	-20,4	-23,8	7,3	-5,0	-13,4	60,3	68,8	19,0	203,6	-149,2

Cuadro de precipitación acumulada en mm

Σ 1.975	10,7	12,8	12,8	13,4	15,6	44,9	75,9	93,5	195,8	330,6	414,6	676,2	
Σ 1.950-70	35,0	52,0	60,0	81,0	107,0	129,0	165,0	196,0	238,0	304,0	369,0	427,0	
Dif.	-24,3	-39,2	-47,2	-67,6	-91,4	-84,1	-89,1	-102,5	-42,2	-26,6	45,6	204,2	

Cuadro de precipitación total en mm

	Estación: Escuela Naval de Venezuela												
1.975	0,0	6,0	0	6,3	14,7	27,5	35,7	17,1	66,1	82,7	23,9	151,5	431,5
1.969-74	10,3	5,5	50,0	10,0	11,0	46,5	74,1	51,5	23,0	37,8	65,8	19,0	404,5
Dif.	-10,3	0,5	-50,0	-3,7	3,7	-19,0	-38,4	-34,5	-43,1	-44,9	-41,9	32,5	27,0

Cuadro de precipitación acumulada en mm

Σ 1.975	0,0	6,0	6,0	12,3	27,0	54,5	90,2	107,3	173,4	256,1	280,0	431,5	
Σ 1.969-74	10,3	15,8	65,8	75,8	86,8	133,3	107,4	258,9	281,9	319,7	385,5	404,5	
Dif.	-10,3	9,8	-59,8	-66,8	-59,8	-78,8	-117,2	-151,6	-108.5	-63,6	-105,5	27,0	

Cuadro de Precipitación total en mm

	Estación: Guiria												
	Ener.	Feb.	Mar.	Abr.	Mayo	Jun.	Jul.	Ago.	Sept.	Oct.	Nov.	Dic.	Total
1,975	19,4	16,1	13,1	6,4	66,9	87,3	92,9	119,3	66,9	155,2	51,0	173,7	868,2
1,950-70	37,0	27,0	15,0	23,0	55,0	125,0	129,0	135,0	121,0	99,0	96,0	68,0	930,0
Dif.	-17,6	-10,9	-1,9	-16,6	11,9	-37,7	-36,1	-15,7	-54,1	56,2	-45,0	105,7	61,8

Cuadro de precipitación acumulada en mm

Σ 1,975	19,4	35,5	48,6	55,0	121,9	209,2	302,1	421,4	488,3	643,5	694,5	868,2	
Σ 1,950-70	37,0	64,0	79,0	102,0	157,0	282,0	411,0	546,0	667,0	766,0	862,0	930,0	
Dif.	-17,6	-28,5	-30,4	-47,0	-35,1	-72,8	-108,9	-132,6	-178,7	-122,5	-167,5	-61,8	

Cuadro de precipitación total en mm

	Estación: La Orchila												
1,975	39,5	15,3	8,4	16,9	1,7	23,5	82,2	14,6	30,4	56,4	15,3	162,6	466,8
1,959-70	40,0	18,0	15,0	11,0	8,0	15,0	34,0	37,0	27,0	45,0	79,0	61,0	390,0
Dif.	-0,5	2,7	-6,6	5,9	-6,3	8,5	48,2	-22,4	3,4	11,4	-63,7	101,6	76,8

Cuadro de precipitación acumulada en mm

Σ 1,975	39,5	54,8	63,2	80,1	81,8	105,3	187,5	202,1	232,1	288,9	304,2	466,8	
Σ 1,959-70	40,0	58,0	73,0	84,0	92,0	107,0	141,0	178,0	205,0	250,0	329,0	390,0	
Dif.	-0,5	-3,2	-9,8	-3,9	-10,2	-1,7	46,5	24,1	27,5	38,0	-24.8	76,8	

Cuadro de precipitación total en mm

	Estación: Maiquetía												
1,975	0	0	0	38,0	13,4	28,6	51,8	30,5	90,1	38,6	13,1	184,3	488,4
1,950-70	53,0	39,0	31,0	19,0	37,0	50,0	58,0	51,0	51,0	49,0	52,0	64,0	554,0
Dif.	-53,0	-39,0	-31,0	19,0	-23,6	-21,4	-6,2	-20,5	39,1	-10,4	-38,9	120,3	-65,6

Cuadro de precipitación total acumulada en mm

Σ 1,975	0	0	0	38,0	51,4	80,0	131,8	162,3	252,4	291,0	304,1	488,4	
Σ 1,950-70	53,0	92,0	123,0	142,0	179,0	229,0	287,0	338,0	389,0	438,0	490,0	554,0	
Dif.	-53,0	-92,0	-123,0	-104,0	-127,6	-149,0	-157,2	-175,7	-136,6	-147,0	-185,9	-65,6	

Cuadro de precipitación total en mm

	Estación: Puerto Cabello												
	Ener.	Feb.	Mar.	Abr.	Mayo	Jun.	Jul.	Ago.	Sept.	Oct.	Nov.	Dic.	Total
1,975	15,8	2,5	0,6	2,0	66,4	68,8	15,3	113,7	78,0	91,7	82,9	159,9	697,6
1,963-70	51,0	14,0	17,0	29,0	30,0	37,0	41,0	38,0	33,0	45,0	82,0	68,0	485,0
Dif.	-35,2	-11,5	-16,4	-27,0	36,4	31,8	-25,7	75,7	45,0	46,7	0,9	91,9	212,6

Cuadro de precipitación total acumulada en mm

∑ 1,975	15,8	18,3	18,9	20,9	87,3	156,1	171,4	285,1	363,1	454,8	537,7	697,6	
∑ 1,963-70	51,0	65,0	82,0	111,0	141,0	178,0	219,0	257,0	290,0	335,0	417,0	485,0	
Dif.	-35,2	-46,7	-63,1	-90,1	-53,7	-21,9	-47,6	28,1	73,1	119,8	120,7	212,6	

de la precipitación en casi todo el país, a excepción de Coro, donde el día 1 cayeron 78,0 mm debido a una vaguada en la altura de carácter local. El mes de diciembre fue muy lluvioso y estas precipitaciones fueron causadas por varias vaguadas en la altura y en la baja troposfera, al avance de masas de aire del norte, a inestabilidad atmosférica, etc., que además ocasionaron fuertes marejadas con olas de hasta tres metros tanto en el litoral central, como en oriente y occidente, desbordamiento de ríos con las consecuentes pérdidas materiales y de vidas, deslizamientos y muchos damnificados.

4. CONCLUSIONES

De los análisis anteriores se concluye que la llamada Zona de Convergencia Intertropical que se caracteriza por ser la causa principal de las lluvias en Venezuela, no tuvo la debida influencia sobre las precipitaciones en las costas de Venezuela, durante el año 1975, pasando a ser las "vaguadas", en todos los niveles, las causas más importantes de las mismas, seguidas por las "ondas del este", por las "advecciones de aire polar modificado" provenientes del norte y, en menor grado, por la Zona de Convergencia Intertropical.

Igualmente se puede concluir que si bien los primeros meses del año 1975 fueron extremadamente secos, en los meses de septiembre, octubre y especialmente diciembre se nota un verdadero incremento de las precipitaciones, especialmente en las estaciones de la costa centroccidental (Puerto Cabello y Coro), originando un excedente notable al final del año.

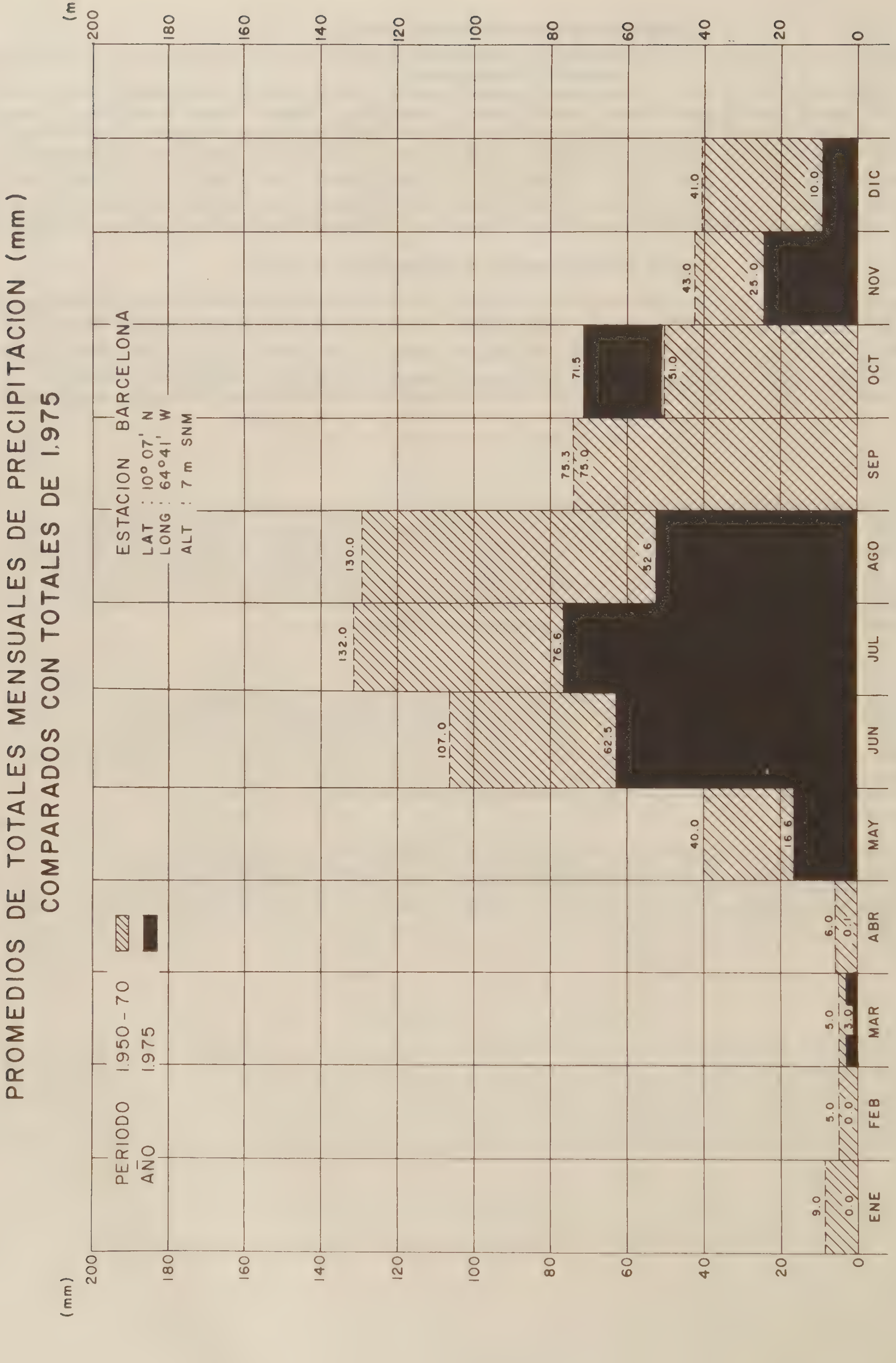

Fig. 5 Histograma de precipitación correspondiente a la estación Barcelona

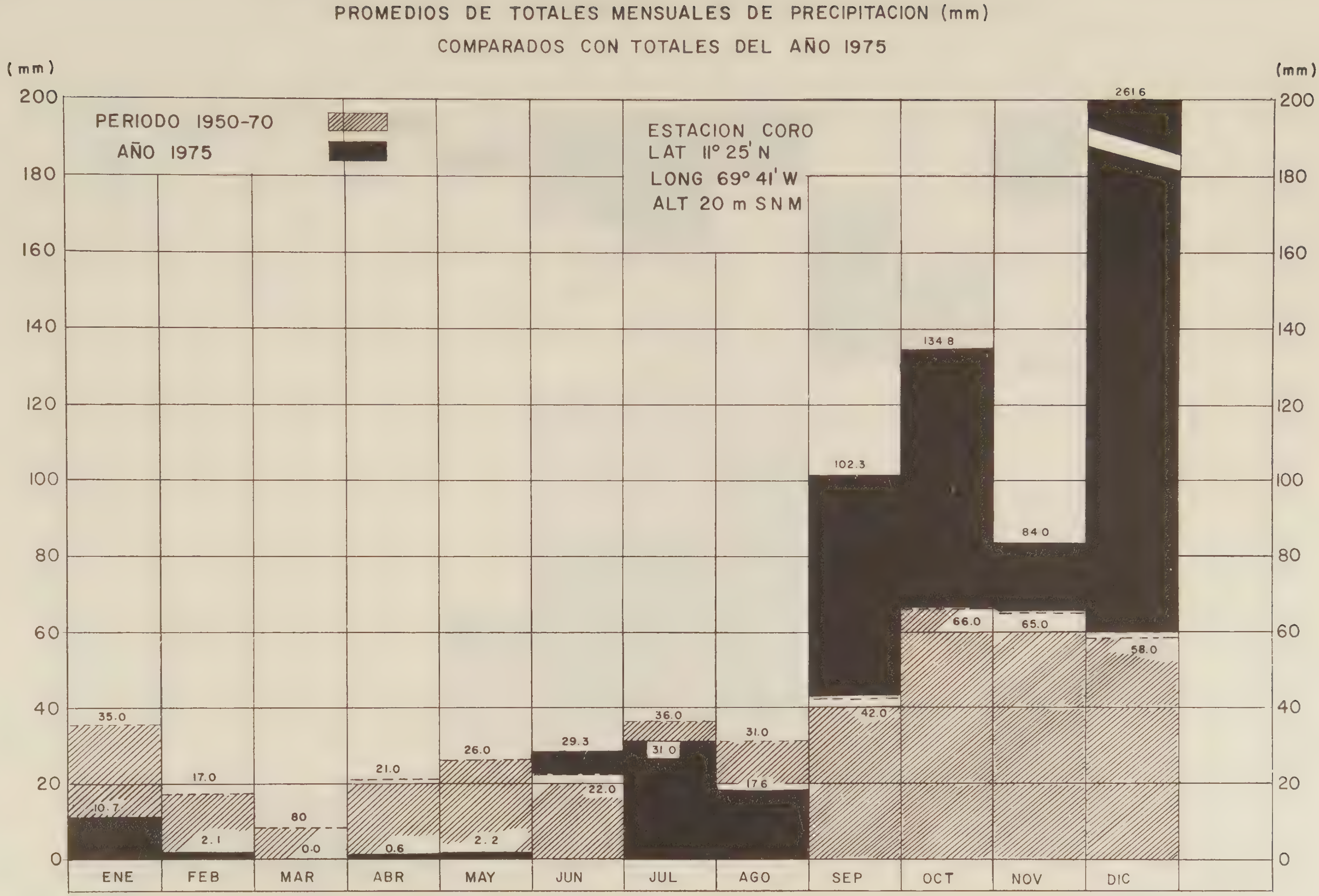

Fig. 6 Histograma de precipitación correspondiente a Coro

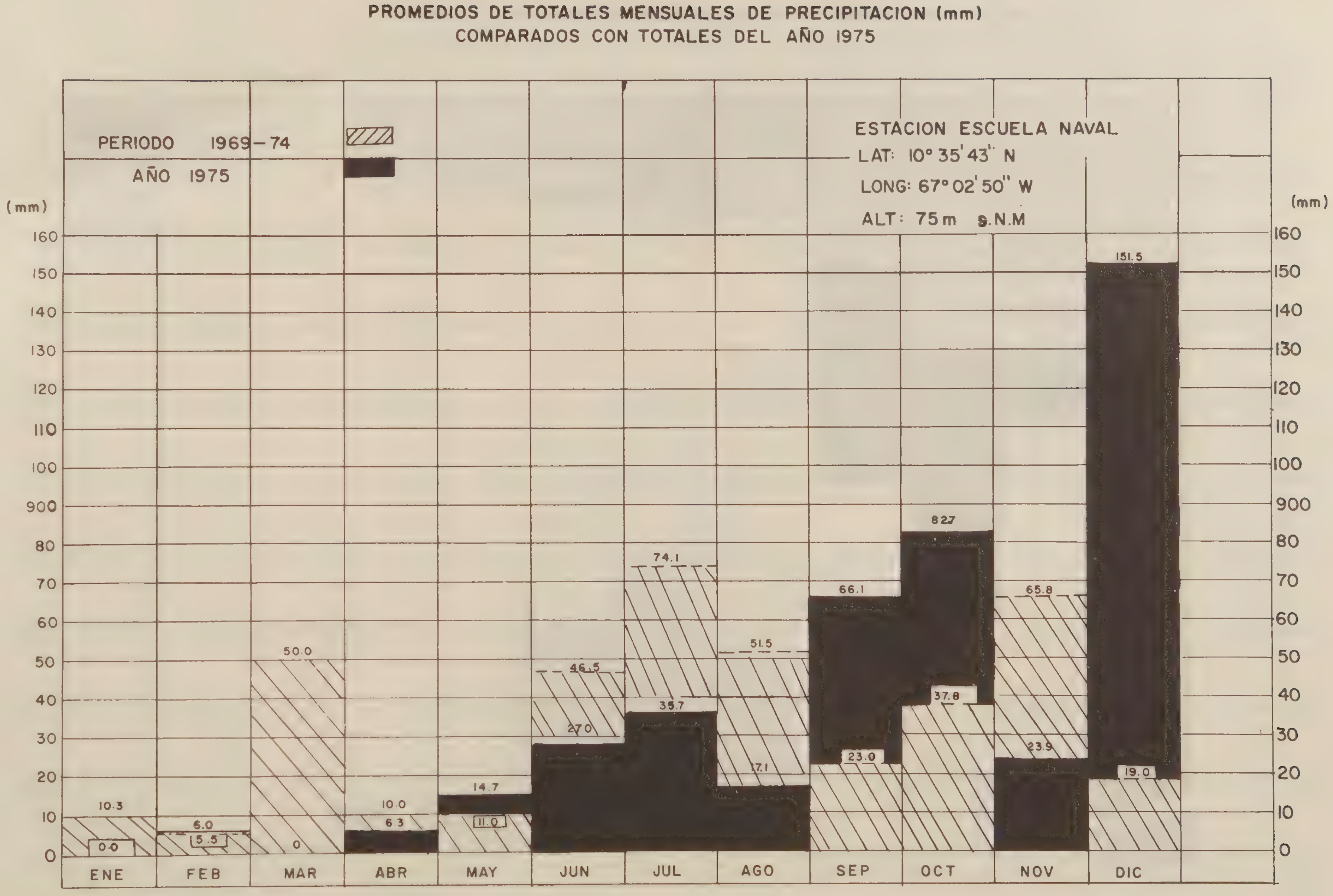

Fig. 7 Histograma de precipitación correspondiente a la Escuela Naval

PROMEDIOS DE TOTALES MENSUALES DE PRECIPITACION (mm)
COMPARADOS CON TOTALES DEL AÑO 1975

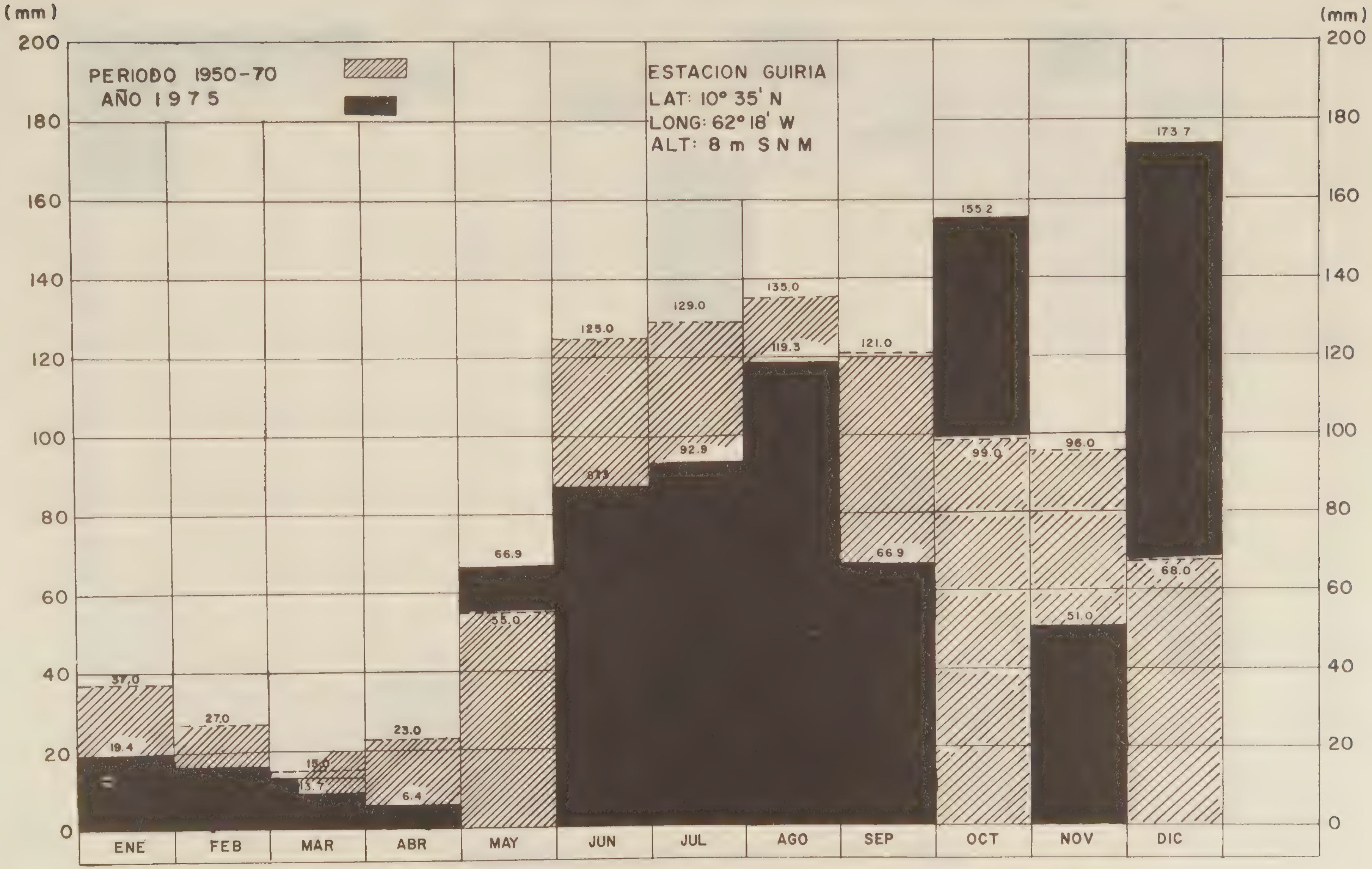

Fig. 8 Histograma de precipitación correspondiente a Guiria

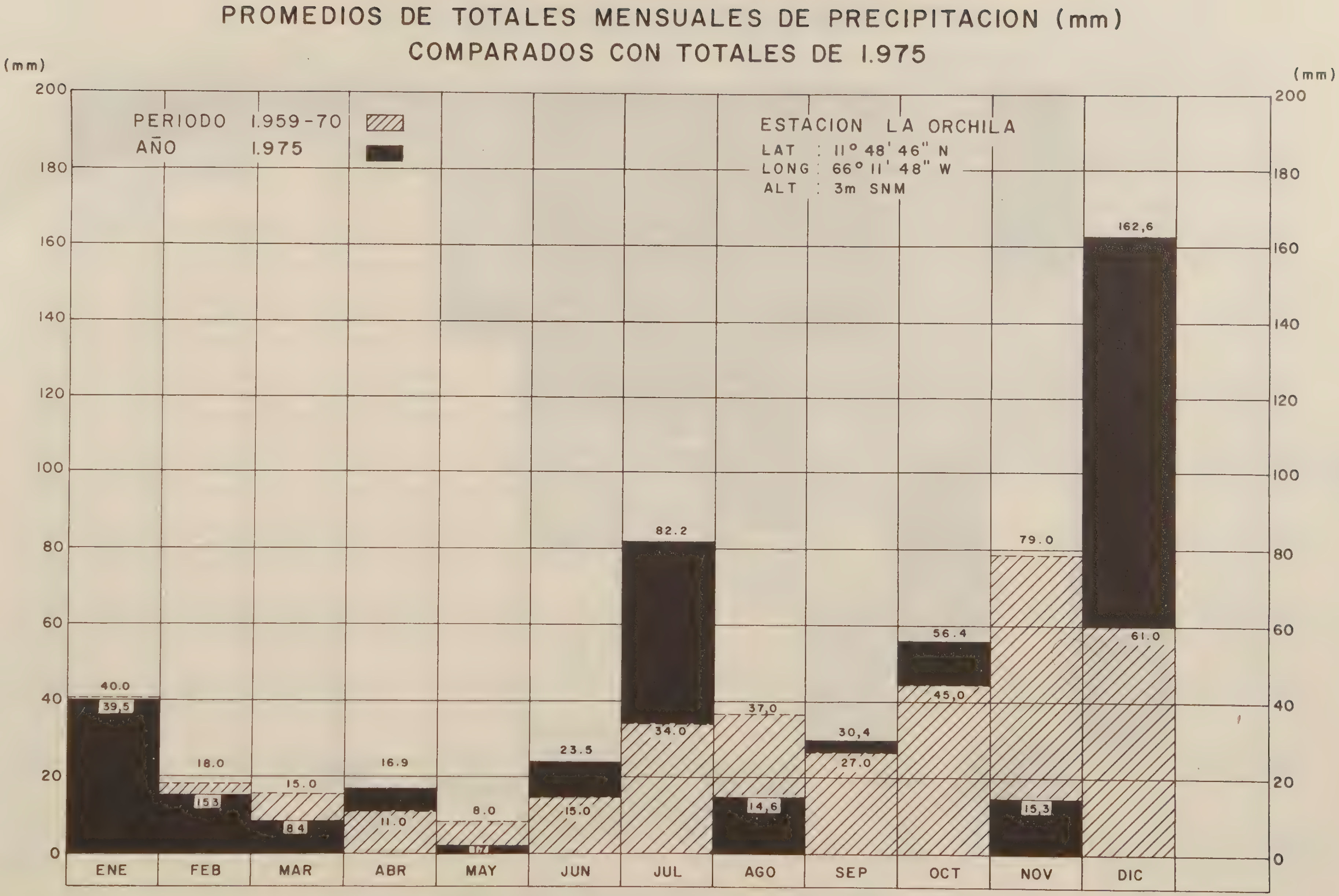

Fig. 9 Histograma de precipitación correspondiente a La Orchila

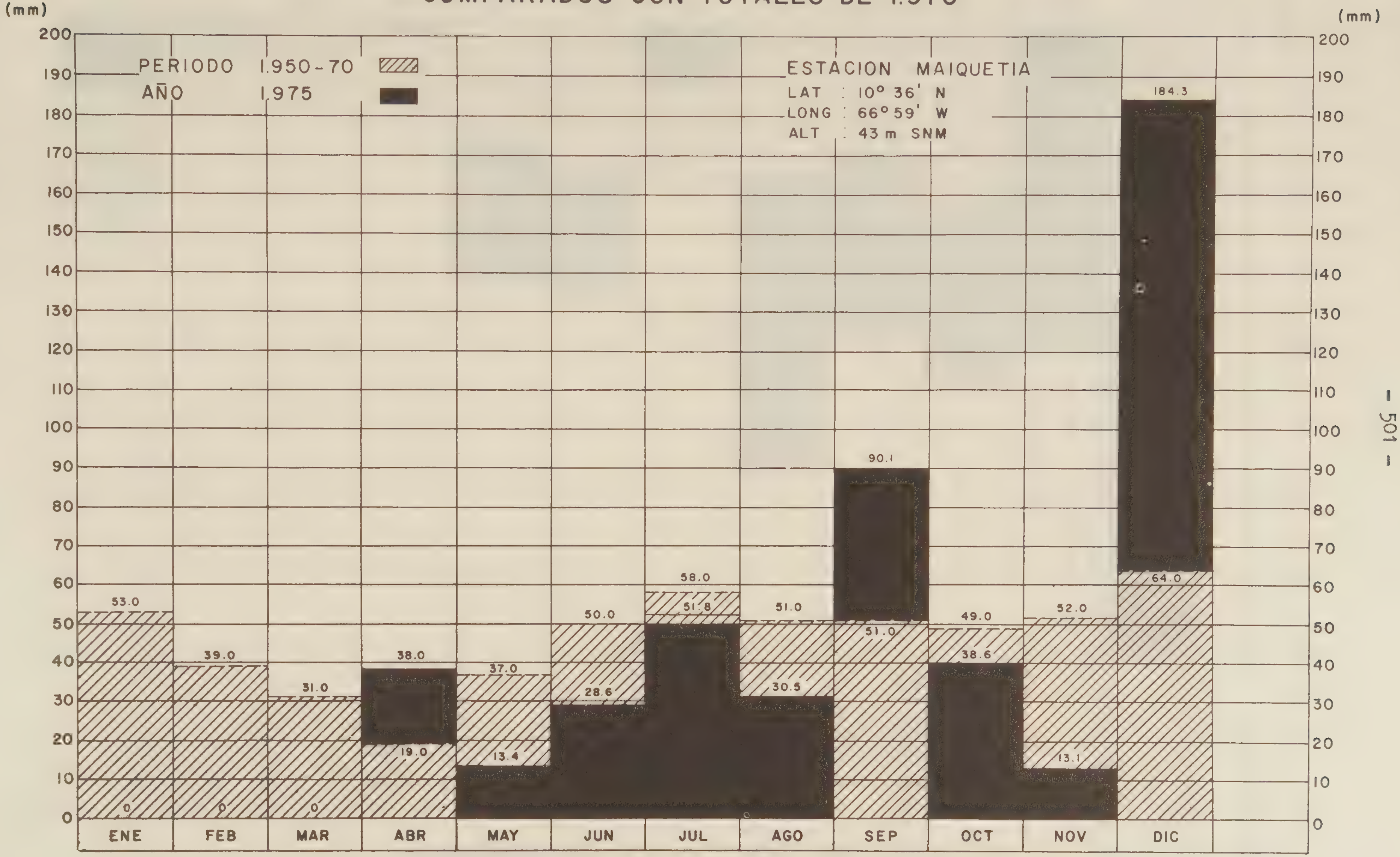

PROMEDIOS DE TOTALES MENSUALES DE PRECIPITACION (mm)
COMPARADOS CON TOTALES DE 1.975

Fig. 10 Histograma de precipitación correspondiente a Maiquetía

PROMEDIOS DE TOTALES MENSUALES DE PRECIPITACION (mm)
COMPARADOS CON TOTALES DE 1.975

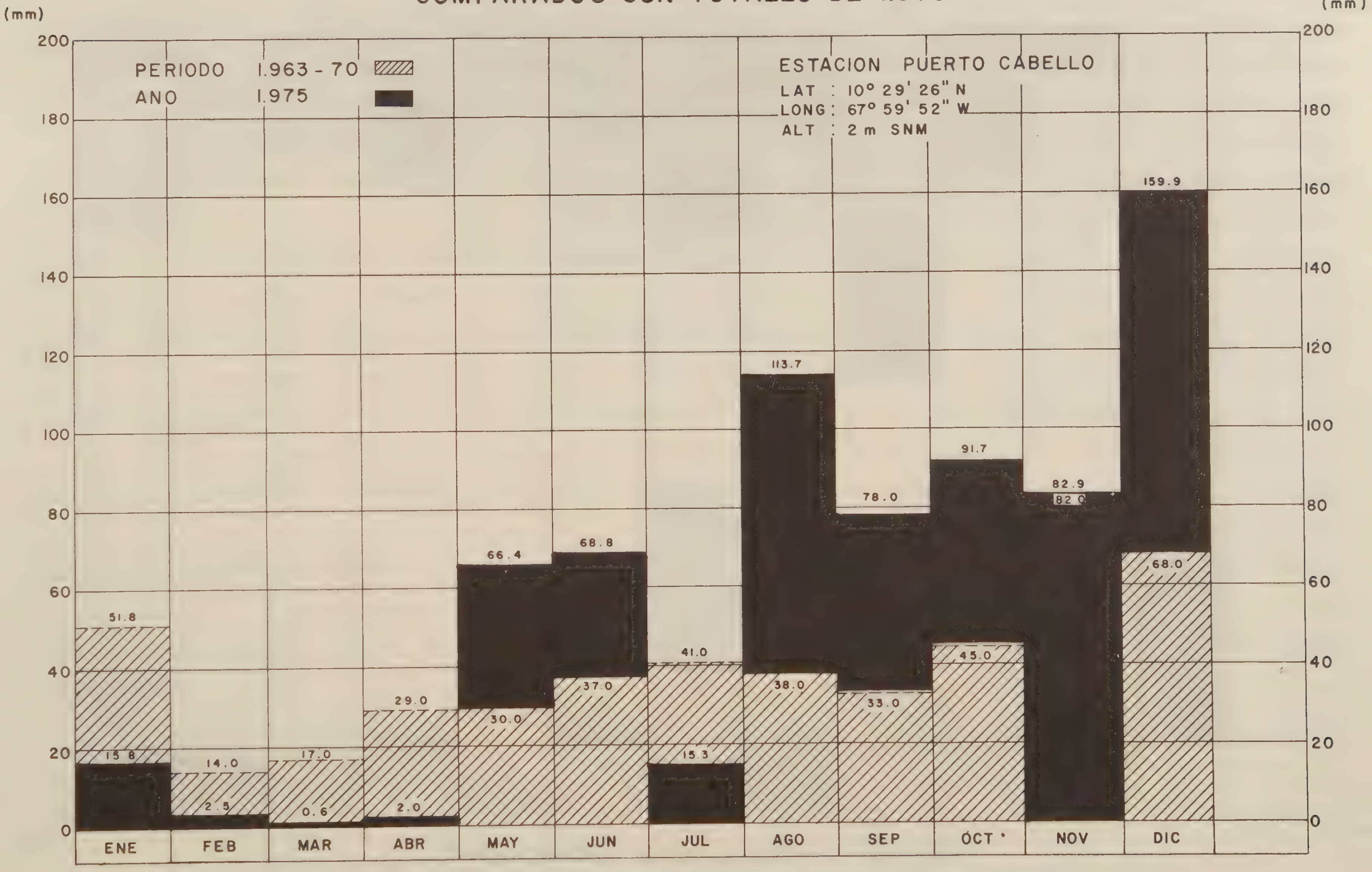

Fig. 11 Histograma de precipitación correspondiente a Puerto Cabello

5. REFERENCIAS

Gray, W., 1968 Global view of the origin of tropical disturbances and storms. Mon.Weather Rev., 96(10):669-700

Perdomo, M., 1968 Paso de un frente frío del hemisferio sur sobre el continente suramericano y Venezuela, a fines de agosto de 1966. Tesis de Grado. Caracas, Universidad Central de Venezuela

__________, 1969 Estudio del progreso de un "Frente Frío" desde Argentina hasta Venezuela. Tesis de Grado. Caracas, Universidad Central de Venezuela

Riehl, H., 1954 Tropical meteorology. New York, McGraw-Hill

Venezuela, 1975 Dirección de Hidrografía y Navegación (Observatorio Cagigal), Boletines climatológicos mensuales

Venezuela, 1975 Servicio de Meteorología y Comunicaciones, Boletines meteorológicos diarios. Caracas, Comandancia General de la Aviación de Venezuela

THE RESPONSE OF THE TROPICAL NORTH ATLANTIC TO METEOROLOGICAL FORCING FUNCTIONS

by

S. WORTHEM and F. OSTAPOFF
National Oceanic and Atmospheric Administration
Atlantic Oceanographic and Meteorological Laboratories
Sea-Air Interaction Laboratory
Miami, Florida, U.S.A.

CONTENTS

1. INTRODUCTION
2. DESCRIPTION OF FIELD EXPERIMENT
3. SYNOPTIC DATA ANALYSIS
4. CASE 1: HOMOGENEOUS REGION
5. CASE 2: LOW SALINITY PUDDLE
6. SUMMARY AND CONCLUSION
7. ACKNOWLEDGEMENTS
8. REFERENCES

Abstract

As a contribution to CICAR, an experiment to investigate the evolution of the ocean mixed layer structure in response to meteorological forcing functions, was conducted from the NOAA ship DISCOVERER between 28 September and 14 October 1971 at 21°N and 66-67°W, about 180 n mi due north of San Juan, Puerto Rico. The structure of the upper ocean was delineated using X-BT, STD, a profiling current meter system and a quartz thermometer system. Meteorological parameters were recorded from a drifting buoy allowing calculation of thermal and dynamic fluxes at the sea surface using the bulk aerodynamic formulas. This paper emphasizes the STD and X-BT measurements as they contribute to our understanding of upper ocean heat storage.

The region was selected for its lateral homogeneity and permanent thermocline depth. The permanent thermocline was sufficiently deep that the response of the mixed layer to meteorological forces could be separated from the complex internal processes occurring at the upper edge of the permanent thermocline.

The data show that the mixed layer can be divided into three zones. The surface zone is dominated by forced convection due to wave mixing. All properties are rapidly mixed uniformly in this layer, which typically extends to a depth of about 10-15 m in our measurements. The next zone is where diurnal heating processes dominate and has the character of a diffusive régime with a time scale of several hours. It extends to about 40 m in our data. The third zone is a transition region where the complex internal wave mixing processes erode the bottom of the mixed layer.

Resumen

Como contribución a las ICCRA, el buque DISCOVERER, de la NOAA, realizó un experimento, entre el 28 de septiembre y el 14 de octubre de 1971, a 21°N y 66-67°O, a 180 n. mi aproximadamente al norte de San Juan de Puerto Rico, con el fin de investigar la evolución de la estructura de la capa mixta oceánica como respuesta a las funciones de compulsión meteorológica. La estructura del océano superior pudo conocerse utilizando X-BT, STD, un sistema de medición de corrientes mediante secciones verticales, y un termómetro de cuarzo. Los parámetros meteorológicos fueron registrados por una boya flotante, que permitía calcular el flujo térmico y dinámico de la superficie del mar utilizando las fórmulas aerodinámicas globales. En este documento se ponen de relieve las mediciones STD y X-BT porque nos permiten comprender mejor el almacenamiento de calor en el océano superior.

La región fue elegida por su homogeneidad lateral y por la profundidad de la termoclina permanente. La termoclina permanente era lo suficientemente profunda para poder distinguir la capa mixta a las fuerzas meteorológicas de los complejos procesos internos que se producen en el borde superior de la termoclina permanente.

Los datos muestran que la capa mixta puede dividirse en tres zonas: en la zona de superficie domina la convección forzada, debida a la mezcla de olas. En esa capa, que en nuestras medidas llega normalmente a una profundidad de 10-15 m, aproximadamente, todas las propiedades se mezclan uniformemente, y con rapidez. En la zona inmediata dominan los procesos de calentamiento diurno, y se caracteriza por un régimen difusivo, con una escala de tiempo de varias horas: en nuestros datos, llega hasta unos 40 m. La tercera zona es una región de transición, en la que los complejos procesos internos de mezcla de olas erosionan el fondo de la capa mixta.

1. INTRODUCTION

Understanding the evolution of the upper ocean in response to meteorological forcing functions is necessary in order to predict the heat storage. The sea surface temperature is determined by dynamical processes in the upper ocean, which acts as a heat reservoir for the atmosphere. This, in turn, modifies the meteorological processes. For example, hurricanes generally intensify over a warm sea surface and are maintained over regions of relatively high sea surface temperature. They typically degenerate and modify over an area of sufficiently cool sea surface. The vapour pressure, which controls the latent heat flux, is proportional to the saturation vapour pressure which has an exponential dependence on sea surface temperature. An approximate boundary between a "warm" and "cool" sea surface for a hurricane is about 26.5°C (Ooyama, 1969).

As a contribution to the Cooperative Investigation of the Caribbean and Adjacent Regions (CICAR), a field experiment was carried out to study the response of the upper ocean to meteorological forcing functions on a time scale of hours and days. The experiment was conducted from the NOAA ship the R/V DISCOVERER from 28 September to 14 October 1971 in the region of 21°N and 66°-67°W which is about 300 km due north of San Juan, Puerto Rico. This paper describes the structure and evolution of the upper ocean in two different régimes. One régime is the characteristic low latitude upper ocean configuration of a surface layer of small gradients of temperature, salinity, and density above a sharply stratified permanent thermocline or pycnocline region (Case 1).

The other régime is that of a relatively low salinity lens of approximately 20-40 km diameter floating in the surface layer (Case 2). Low salinity puddles of similar scale have been found in the Gate B-scale area (Rooth, 1973). The origin of such puddles is thought to be the rain from atmospheric convective systems. The fresh water forms a quite stable stratified lens or puddle which has been observed to persist for a period of days or weeks floating on the surface.

Diurnal variations of the temperature and heat budgets have been studied by several investigators (e.g., Stommel and Woodcock, 1951; Shonting, 1964; Stommel et al., 1969; Howe and Tait, 1969; Bowden et al., 1970; Hasse, 1971; Fedorov, 1972; Hoeber, 1972; Denman and Miyake, 1973 and Ostapoff and Worthem,1974). Our understanding of upper ocean structure based on these results is limited to conditions which we call the Case 1 situation - the classical textbook case.

Various local models exist which can be applied to describe the evolution of the upper ocean due to meteorological forcing (e.g., Kraus and Turner, 1966; Foster, 1971; Pandolfo and Jacobs, 1972; Denman, 1973 and Mellor and Durbin, 1975). The model formulations, except for that of Pandolfo and Jacobs (1972) have generally assumed that temperature is a valid indicator of stability. The result of this assumption is that the effects of precipitation and evaporation on salinity and, thus, on the stability of the water column, is neglected. These assumptions, while generally valid in the mid-latitude regions for which the models were designed, are not necessarily applicable in the tropics, as will be demonstrated by the data which will be presented in this paper. Conceptually, it appears that including the effects of salinity variation and a surface salinity source/sink in the models should be a relatively minor modification.

2. DESCRIPTION OF FIELD EXPERIMENT

In this experiment, current profiles of the upper 300 m were taken every three hours from the drifting ship using the current profiler described by Düing and Johnson (1971). Approximately hourly X-BT profiles to 400 m were made. During periods when the ship was drifting, approximately hourly STD profiles staggered with the X-BT profiles were made to a depth of at least 100 m. From the bow of the NOAA DISCOVERER, downward- and upward-looking pyranometers as described by Hanson and Poindexter (1972) provided total sun and sky radiation data (285-2 800 n mi) at three-minute intervals. Two MAMOS buoys were used which are identical in construction to the Navy's NOMAD buoys (Naval Air Systems Command, 1967). One buoy was carrying instrumentation to record once a minute the wind speed, relative humidity and air temperature at a height of 6 m and sea surface temperature at a depth of 25 cm. The other buoy was instrumented with an array of quartz thermometers and a thermistor chain (Aanderaa) as described by Ostapoff and Worthem (1974). To minimize advective heat storage changes for the purpose of energy budget calculation, the buoys were attached to drogue chutes of about 9 m diameter which were deployed at 30 m depth.

The region was selected for its lateral homogeneity and permanent thermocline depth. The permanent thermocline was sufficiently deep that the mixed layer evolution in response to meteorological inputs could be separated from the mixing processes occurring at the upper edge of the permanent thermocline.

3. SYNOPTIC DATA ANALYSIS

The ship track is shown in Fig. 1. The track was determined using satellite navigation. The solid lines in the figure denote drifting and dashed lines steaming portions of the track. The lines crossing the track indicate hourly positions. The ship steamed and drifted to stay within a few miles of the drifting buoys. The buoy tracks are shown in Fig. 2, and their track lines were determined from hourly positions using the ship's navigational radar. Hourly positions are indicated by dots on the buoy tracks in the figure. As can be seen from the buoy tracks, the period can be divided into two régimes. The change from an essentially smooth westward drift to a complicated drift pattern with a predominantly southwestward component occurs at about 66°36'W. Measurements made east of this boundary will be referred to as the previously defined Case 1 régime, and west of this boundary will be the Case 2 régime.

Contours of surface salinity are determined from the STD profiles shown in Fig. 3. The surface salinity was approximately constant in the Case 1 region. The presence of a low salinity area is apparent in the Case 2 region. There is an extremely strong surface salinity gradient at about 66°36'W, 20°58'N. The surface salinity decreases toward the south, with a frontal region running approximately along 20°58'N. The surface salinity to the east of 66°36'W is generally in the range 36.36 °/oo-36.38 °/oo, and can be considered essentially constant. The minimum surface salinity in the frontal region was about 35.50 °/oo.

The salinity difference between 30 m depth and the surface is shown in Fig. 4. The salinity difference contours are very similar to the surface salinity contours with low surface salinity corresponding to high salinity difference. Thus, the salinity at 30 m is approximately constant over the region. The salinity east of 66°36'W is essentially constant down to about 35-40 m depth.

The low salinity region is a relatively shallow feature as can be seen in Fig. 5, in which mixed layer depths are shown. The low salinity region is generally less than 20 m deep. There appears to be no correlation between the mixed layer depths shown in Fig. 5 and the surface salinities and salinity anomalies shown in Figs. 3 and 4.

The vertical salinity gradient in the interfacial region between the low salinity puddle above and the horizontally homogeneous environment below is quite sharp. Using data from the current profiles, the gradient Richardson number Ri, was estimated in both the homogeneous and frontal regions. In the homogeneous region, $Ri \approx 0$, indicating turbulent mixing was a dominant process. In the maximum salinity anomaly region, the local gradient Richardson number at the interface was as high as 6.0, indicating high stability. Thus we believe that a turbulence cannot be maintained in the frontal region, and the low salinity lens is quite stable. In the presence of such a stable interface, a wide spectrum of internal waves is possible. We believe the mixed layer depth variability is significantly affected by the presence of internal waves. This will be discussed further in Section 5.

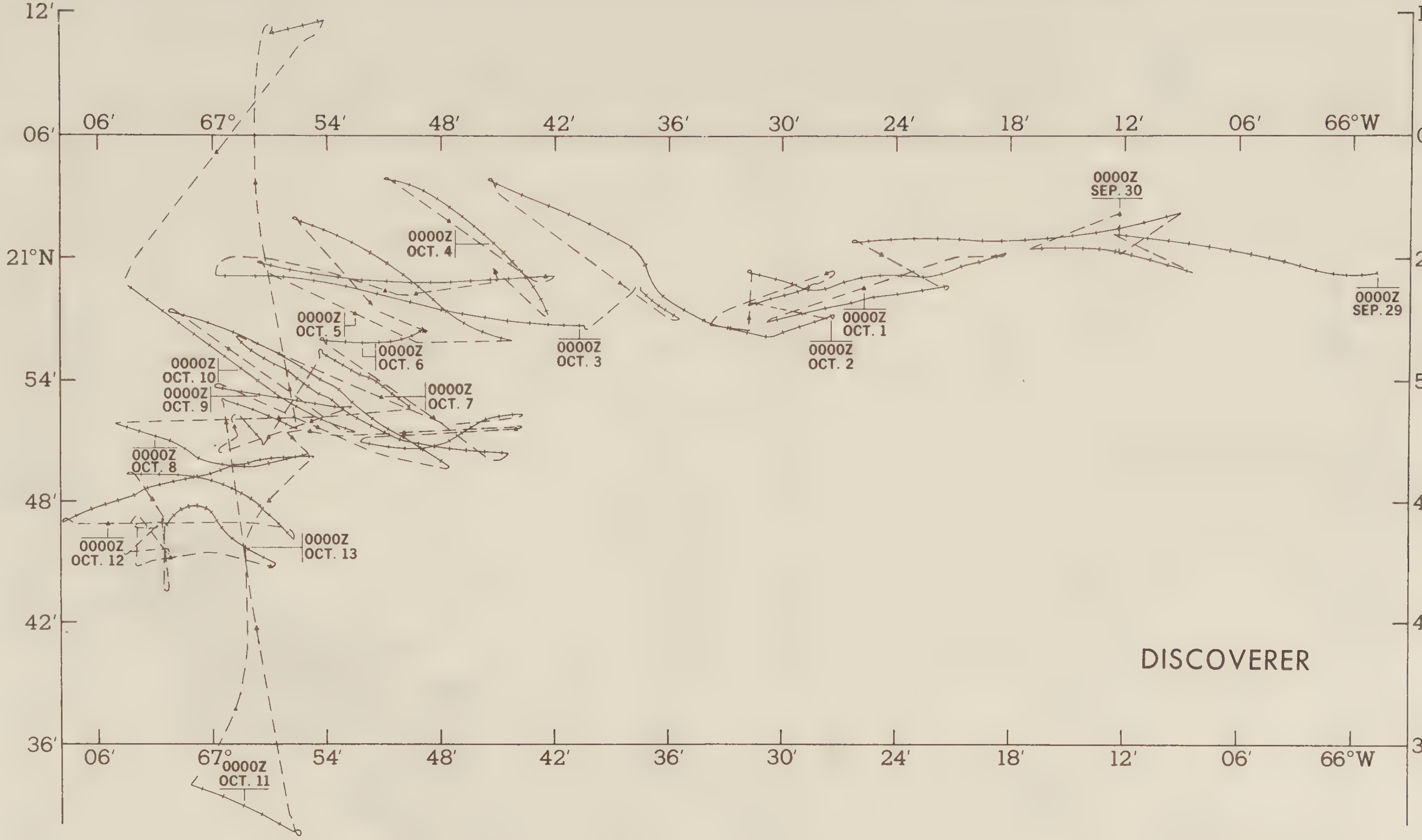
DISCOVERER
12′
06′
21°N
54′
48′
42′
36′
06′
67°
54′
48′
42′
36′
30′
24′
18′
12′
06′
66°W
0000Z SEP. 29
0000Z SEP. 30
0000Z OCT. 1
0000Z OCT. 2
0000Z OCT. 3
0000Z OCT. 4
0000Z OCT. 5
0000Z OCT. 6
0000Z OCT. 7
0000Z OCT. 8
0000Z OCT. 9
0000Z OCT. 10
0000Z OCT. 11
0000Z OCT. 12
0000Z OCT. 13

Fig. 1 Ship track with solid lines denoting drifting, dashed lines denoting steaming. Lines crossing the track indicate hourly positions

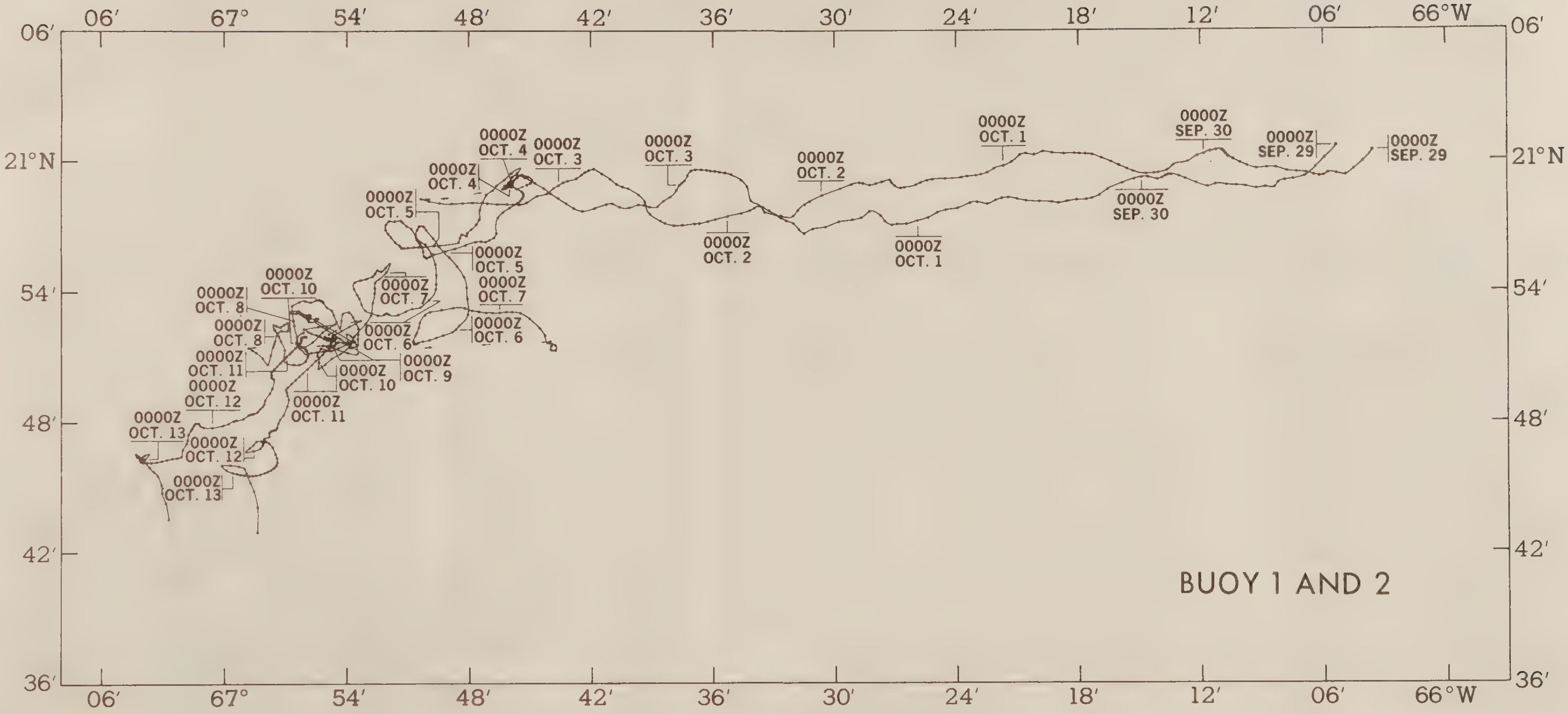
06'
67°
54'
48'
42'
36'
30'
24'
18'
12'
06'
66°W
06'
21°N
54'
48'
42'
36'
BUOY 1 AND 2
0000Z SEP. 29
0000Z SEP. 29
0000Z SEP. 30
0000Z SEP. 30
0000Z OCT. 1
0000Z OCT. 1
0000Z OCT. 2
0000Z OCT. 2
0000Z OCT. 3
0000Z OCT. 3
0000Z OCT. 4
0000Z OCT. 4
0000Z OCT. 5
0000Z OCT. 5
0000Z OCT. 6
0000Z OCT. 6
0000Z OCT. 7
0000Z OCT. 7
0000Z OCT. 8
0000Z OCT. 8
0000Z OCT. 9
0000Z OCT. 10
0000Z OCT. 10
0000Z OCT. 11
0000Z OCT. 11
0000Z OCT. 12
0000Z OCT. 12
0000Z OCT. 13
0000Z OCT. 13

Fig. 2 Buoy tracks with dots indicating hourly position

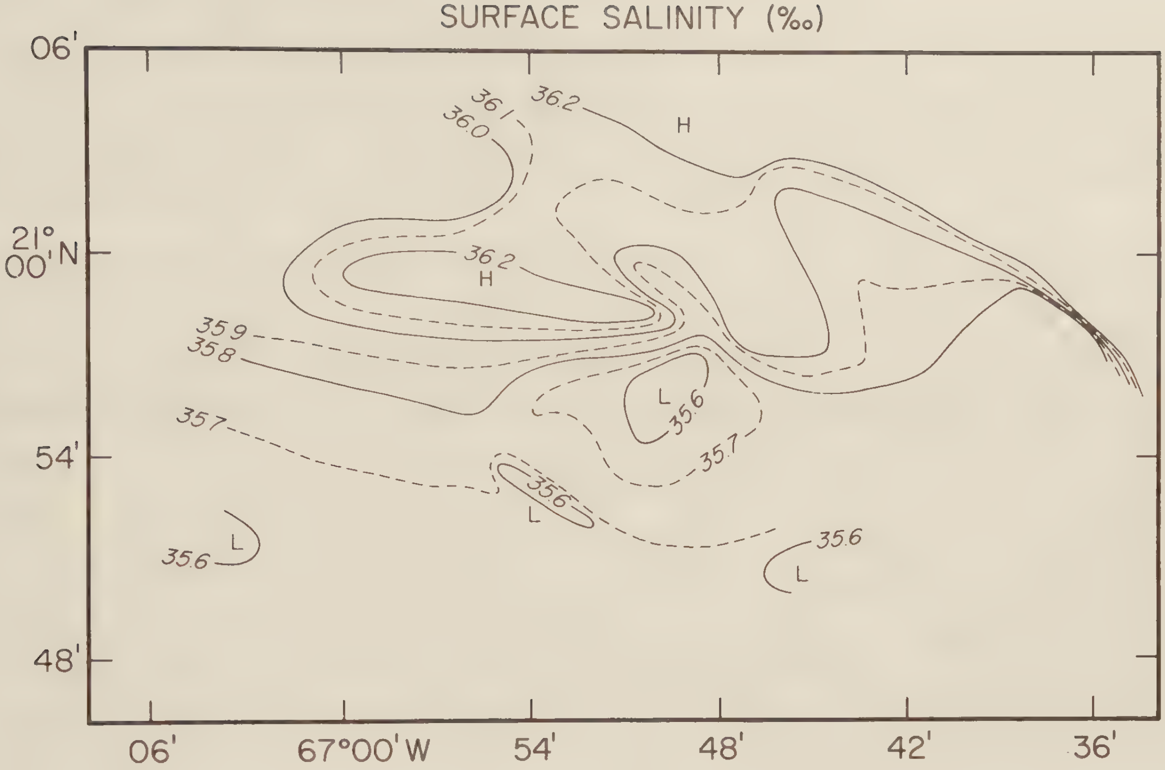
SURFACE SALINITY (‰)

06'
21°
00' N
54'
48'
06'
67°00' W
54'
48'
42'
36'
36.2
36.1
36.0
H
36.2
H
35.9
35.8
L
35.6
35.7
35.7
35.6
L
35.6
L
35.6
L

Fig. 3 Surface salinity

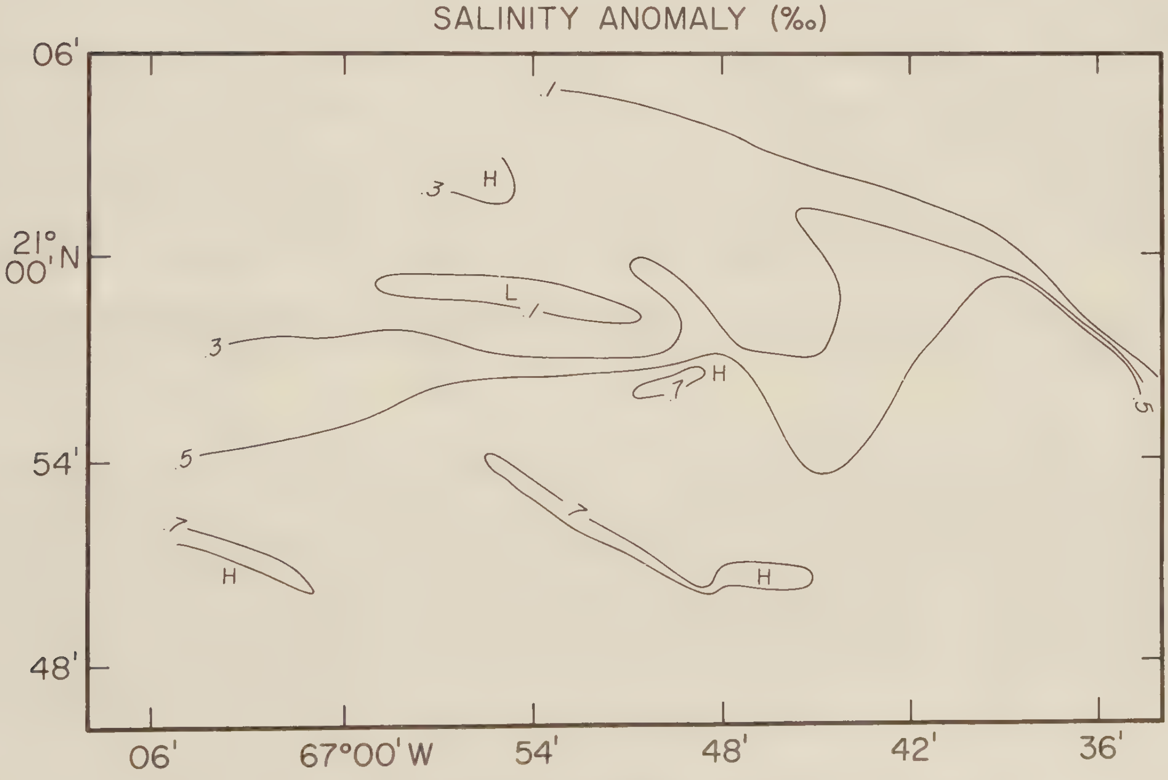
SALINITY ANOMALY (‰)

06'
21°
00' N
54'
48'
06'
67°00' W
54'
48'
42'
36'
.1
.3
H
L
.1
.3
.7
H
.5
.5
.7
H
.7
H

Fig. 4 Salinity difference between 30 m and the surface

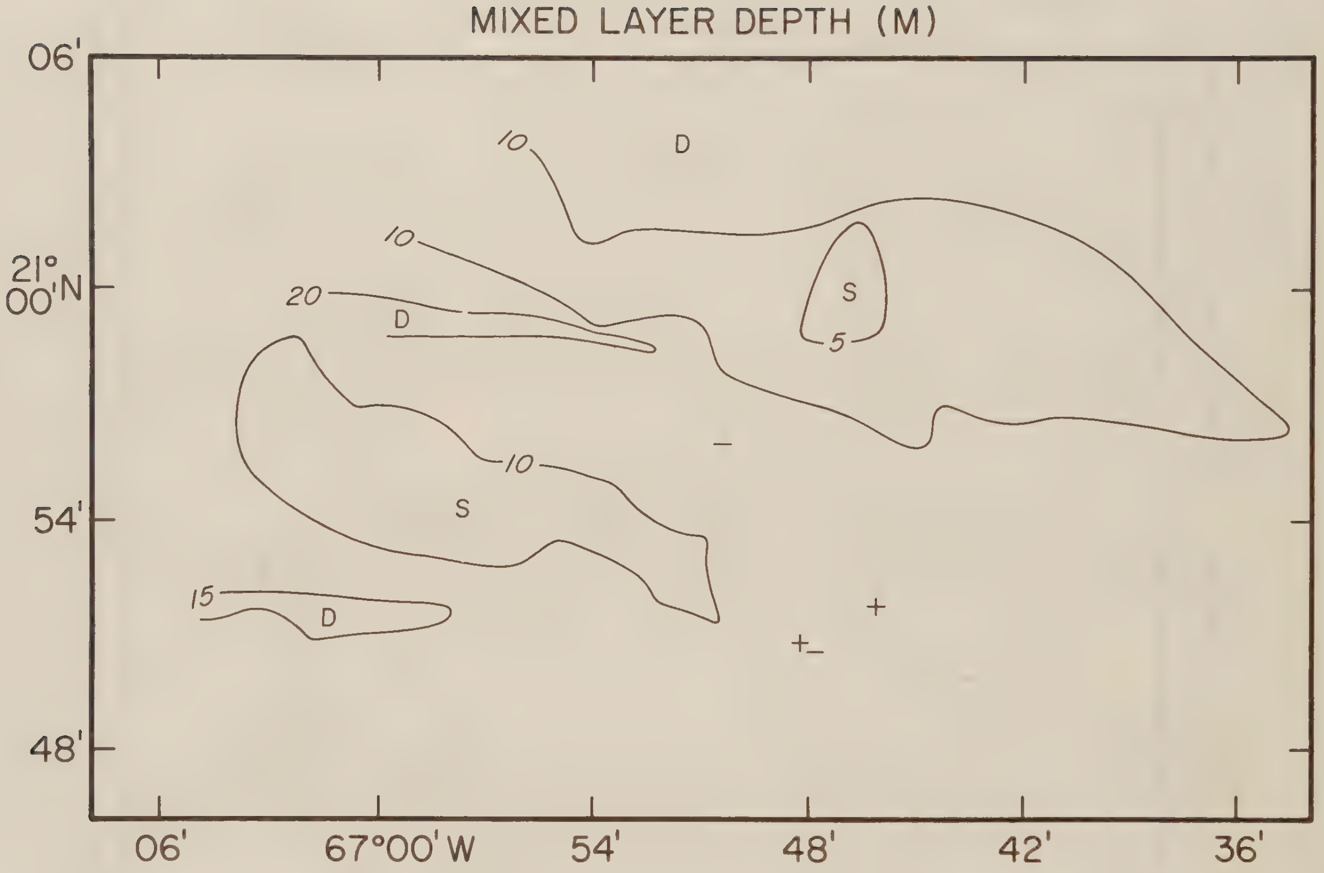
MIXED LAYER DEPTH (M)
06'
21°
00'N
54'
48'
06'
67°00'W
54'
48'
42'
36'
10
D
10
20
D
S
5
10
S
15
D
+
+

Fig. 5 Mixed layer depth

To create such a low-salinity lens, we estimate that 39.6 cm of fresh water would be necessary. This was calculated using the extreme salinity anomaly, ΔS, of 0.8 $^{o}/oo$ over a depth, h, of 18 m, using the relation $\epsilon \sim h \Delta S/S_0$. This relation was derived using the conservation of salt in the water column. The environment salinity, S_0, was taken to be 36.36 $^{o}/oo$. Before overturning of the layer or deep mixing would occur, a temperature decrease of 2.0°C could occur for a salinity anomaly of 0.8 $^{o}/oo$, as can be calculated from the linearized equation of state. Thus the surface layer could lose 3 600 cal cm^{-2} and sustain a 2.0°C bulk temperature decrease, thus reducing the Richardson number, before mixing of the water column to the permanent thermocline would occur.

Since the diurnal variability of the temperature very close to the sea surface is of the order of 1.0°C, the presence of the salinity lens obscures the diurnal heating cycle. This can be seen from the quartz thermometer record shown in Fig. 6. The time series of quartz thermometers at 10, 20, 30, 40 and 50 m depth are shown. The 50 m record shows the presence of large fluctuations due to internal waves. The dominant signal in this record is the semi-diurnal internal tide. The 50 m record was taken at the upper edge of the permanent thermocline. The upper three records show the typical diurnal heat-wave pattern until 1 400 LT (1 800 GMT) on 2 October 1971. At that time a sharp change in régimes is obvious in both the 10 and 20 m records. It is just barely apparent in the 30 m record. After that time, the diurnal cycle is completely obscured. Notice particularly the anomalously cold temperatures in the 10, 20, and 30 m records for the 14-hour period beginning at 07.00 h LT on 3 October. This time period would normally be expected to correspond to solar radiational heating and a corresponding temperature increase in the top 30 m of the water column. A prediction of the sea surface temperature during this period based on the measured solar radiation, which was normal for a meteorologically undisturbed period, and a density profile determined by temperature alone, i.e., from a prior X-BT profile, using an average salinity from the homogeneous region would be quite incorrect. Therefore, it is necessary to measure both temperature and salinity to predict sea surface temperature and heat storage.

Using the three-hourly current profile data and the ship drift velocity calculated from the ship track, the average current velocity in the upper 40 m has been calculated. It is shown in Fig. 7. The arrows represent the current speed in proportion to their length and are aligned in the current direction. Each long tail on the arrows indicates a speed of 10 cm/sec^{-1}, with the length of the smaller tails in proportion. The surface current appears to be approximately southwestward east of 66°36'W in the homogeneous region. The low salinity region is more complex. In this region the surface current becomes more southerly at southern positions. There is a region of high horizontal current shear at approximately 66°48'W and 20°57'N. This corresponds to the northward low surface salinity intrusion shown in Fig. 3. It is possible to visualize several eddy regions in Fig. 7. These roughly correspond to the high and low regions in the surface salinity shown in Fig. 3.

The current shear between 17.5 m and 37.5 m, i.e.

$$\frac{\Delta V}{\Delta Z} = \left[(U_{17.5}-U_{37.5})^2 + (V_{17.5}-V_{37.5})^2 \right]^{1/2} / 2\,000$$

was calculated from the current profile data which had previously been smoothed to obtain 20 m averages. This is shown in Fig. 8. Areas of high current shear appear to be separated by approximately 15 km. A comparison of Figs. 8 and 5 shows that the high current shear region at approximately 67°W and 20°54'N corresponds to the shallow mixed layer depth region. The relatively low shear at 66°54'W and 20°58'N corresponds to a deep mixed layer. This correlation would lead us to conclude that vertical mixing had occurred in the low shear region, perhaps enhanced by shear instability in the interfacial region. Other areas of high and low shear do not appear well correlated with mixed layer depth and could be primarily caused by internal waves.

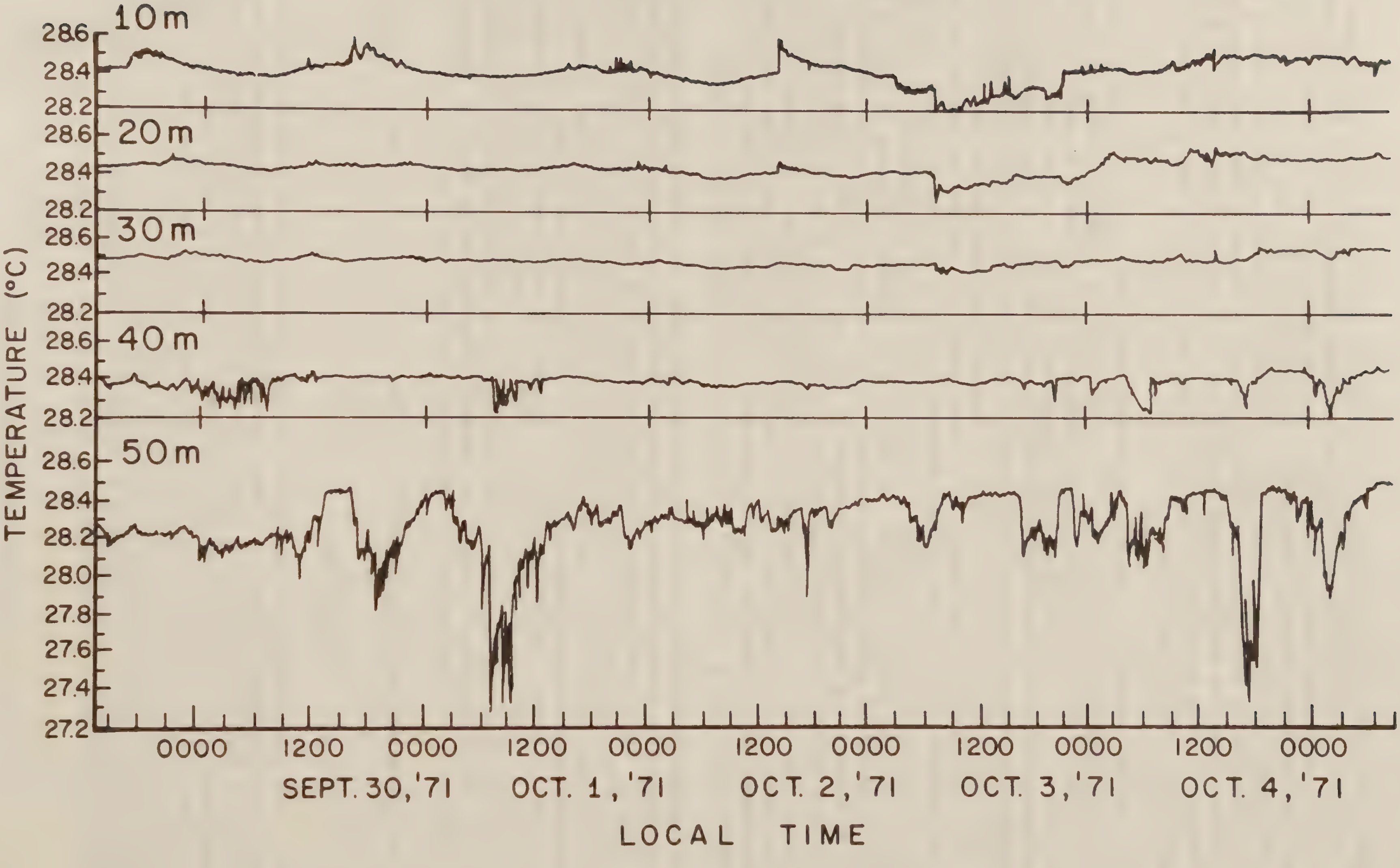

Fig. 6 Quartz thermometer time series

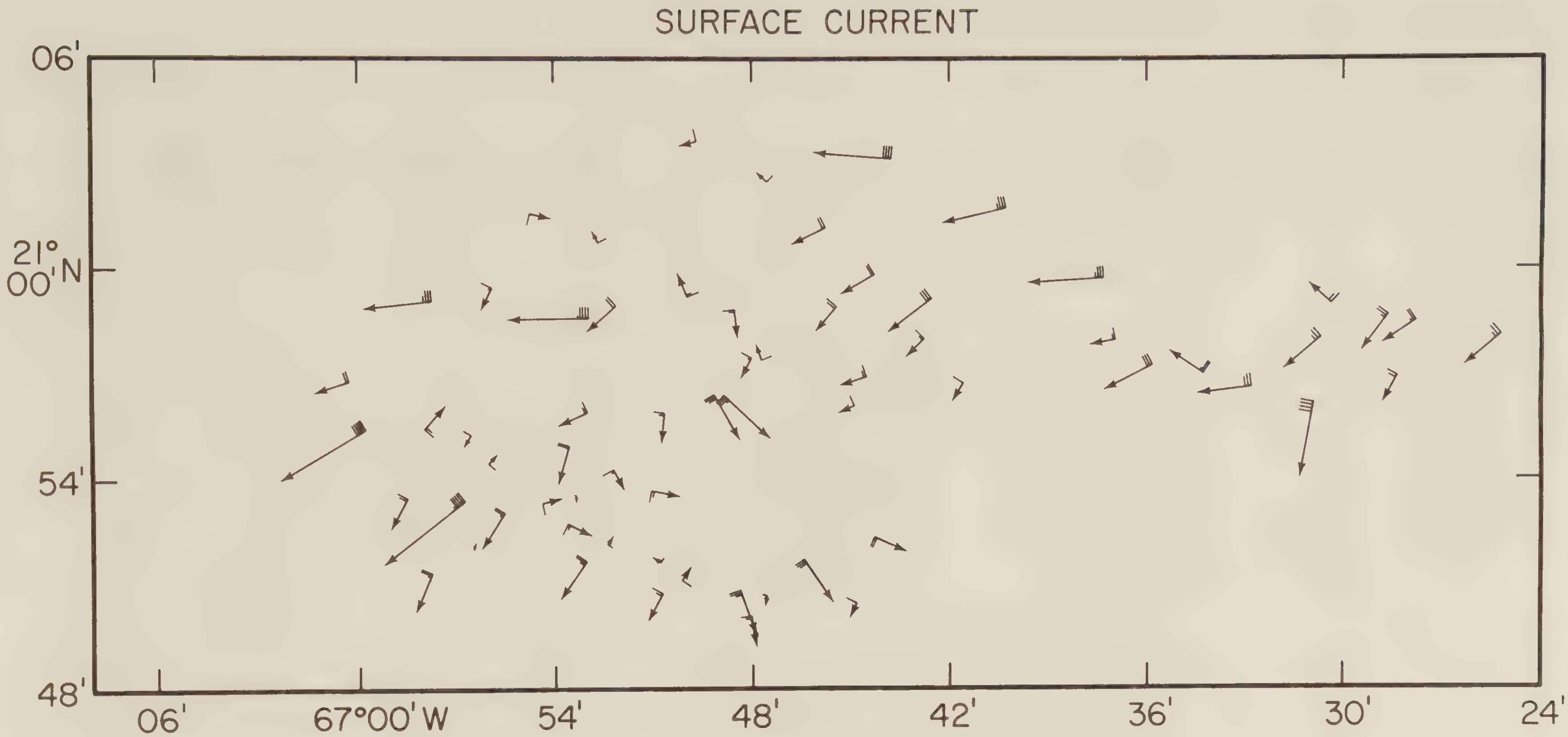
SURFACE CURRENT

06'
21° 00'N
54'
48'
06'
67°00'W
54'
48'
42'
36'
30'
24'

Fig. 7 Average current in the upper 40 m

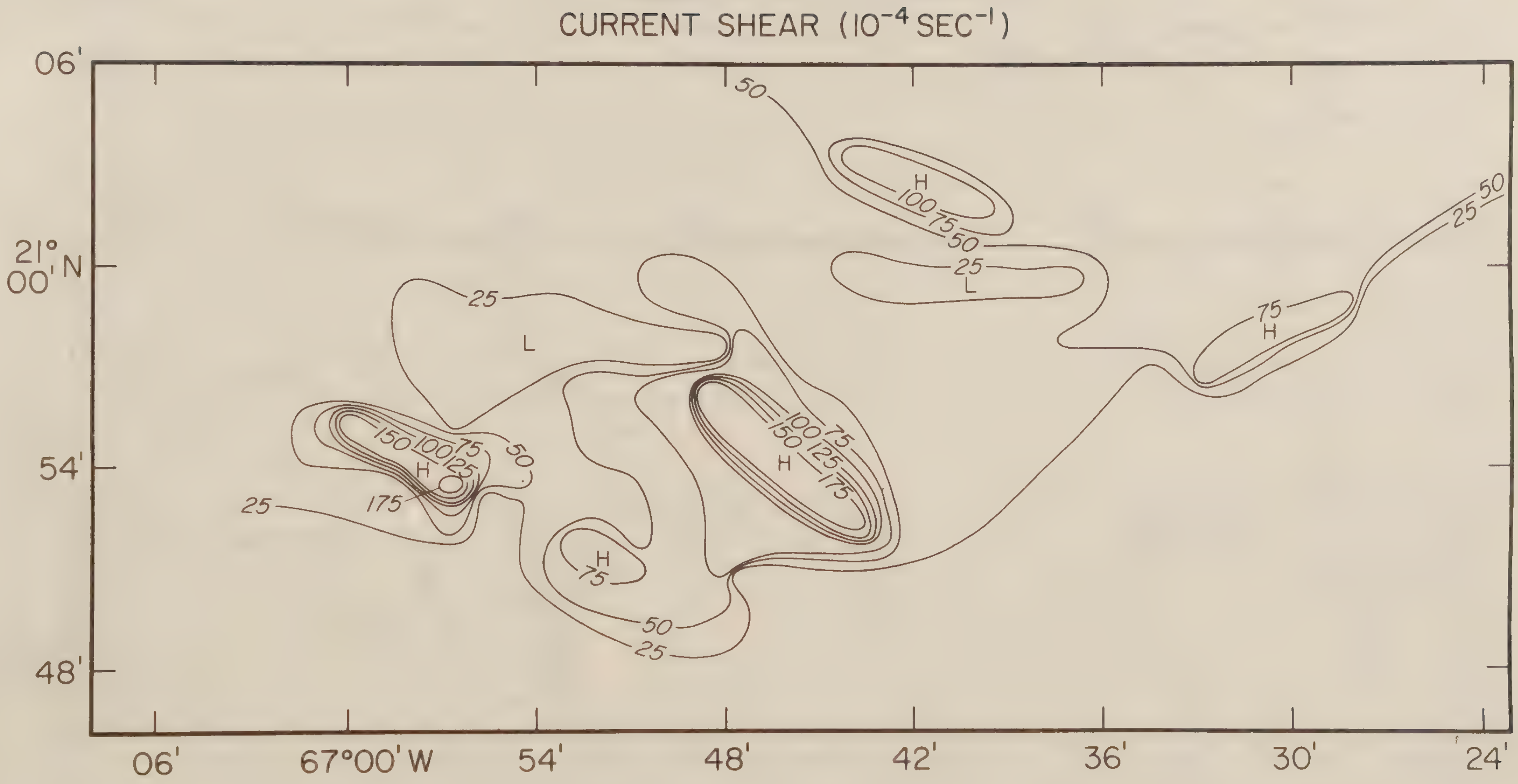

CURRENT SHEAR (10^{-4} SEC^{-1})

06'
21° 00' N
54'
48'
06'
67°00' W
54'
48'
42'
36'
30'
24'
50
H
100
75
50
25
L
25
L
75
H
50
25
150
100
75
50
H
125
175
25
100
150
75
125
H
175
H
75
50
25

Fig. 8 Current shear between 17.5 m and 37.5 m from 20 m averaged current profile data

A comparison of Figs. 8 and 3 shows that, in general, high shear corresponds to low surface salinity (large salinity anomaly) and conversely. Thus, in regions of large stratification, relatively high shear between the low salinity layer and underlying water occurs. This also supports the conclusion that low shear regions are where vertical mixing has occurred. In particular, the relatively high surface salinity area at about 66°54'W and 20°58'N corresponds to a low shear region.

Near the edge of the low salinity region, a series of low and high current shear regions appear. This could indicate an instability in the frontal region, causing internal waves to occur.

4. CASE 1: HOMOGENEOUS REGION

The physical processes which are typically observed in the upper ocean are shown schematically in Fig. 9. Atmospheric forcing functions act at and through the ocean surface. The time scale of meteorological events is of the order of several minutes to a couple of weeks. Solar radiation penetrates the upper ocean and provides a depth-dependent heat source. There is sensible heat flux caused by the air-sea temperature difference at the surface. Evaporation from the sea surface causes a latent heat flux. The sea surface temperature produces a long wave radiative flux. Evaporation (precipitation) at the sea surface produces a salinity source (sink) at the surface. The wind blowing over the sea surface produces a surface stress.

The upper ocean typically has a weakly stratified region (mixed layer) overlying a strongly stratified region (thermocline). The top of the mixed layer is dominated by "wave mixing". This is a forced convection régime in which properties are mixed on a time scale of minutes. Below this is a turbulent mixing régime which is called the "layer of the diurnal thermocline" in the figure. It is maintained by meteorological buoyancy and shear forces. This régime can be dominated by forced or free convective. It has a response time of the order of hours. The permanent or "main thermocline" is a very stably stratified region. It is maintained by longer-term processes. Internal waves in this strongly stratified region alternately squeeze and stretch the mixed layer. There is a sharp "transition layer" between the strongly stratified thermocline régime and weakly stratified mixed layer régime. Here, both internal waves and turbulent mixing processes occur.

Bulk or mean field temperature and salinity in the upper ocean typically vary more over a 100 m depth change than over a 1 000 km horizontal distance. In this case, vertical exchange processes are more important than horizontal advection and mixing, and the upper ocean can be assumed to be statistically homogeneous horizontally.

A temperature contour plot made from hourly X-BT files taken on 28 September 1971 is shown in Fig. 10. It shows a "textbook case" evolution of the mixed layer during a diurnal heating cycle during which there is no net heat gain over the period. This record was taken in the laterally homogeneous region which we refer to as the Case 1 régime. The situation is analogous to the mid-latitude seasonal heating cycle, as described, for example, by Kraus (1972).

In the tropical ocean, the air is typically a fraction of a degree cooler than the sea surface, except in deep convective systems with extensive down-draft regions (Ostapoff and Worthem, 1976) where the air-sea temperature difference may exceed 5°C. The wind is steady in the trade wind region. Thus, the sensible and latent heat fluxes transfer heat from the ocean to the atmosphere, as does the long-wave back radiation. Net evaporation also causes a slight increase in surface salinity. Thus, before the sun rises, there is typically cooling at the surface and neutral or very slightly unstable stratification (cf., Ostapoff and Worthem, 1974) in the mixed layer region. Mixing occurs down into the transition layer and is inhibited by the permanent thermocline. As soon as there is a net heat flux into the ocean, a stable shallow layer forms. As long as there is an increasing net heating rate, the layer stability increases, sea surface temperature rises and the layer remains relatively shallow.

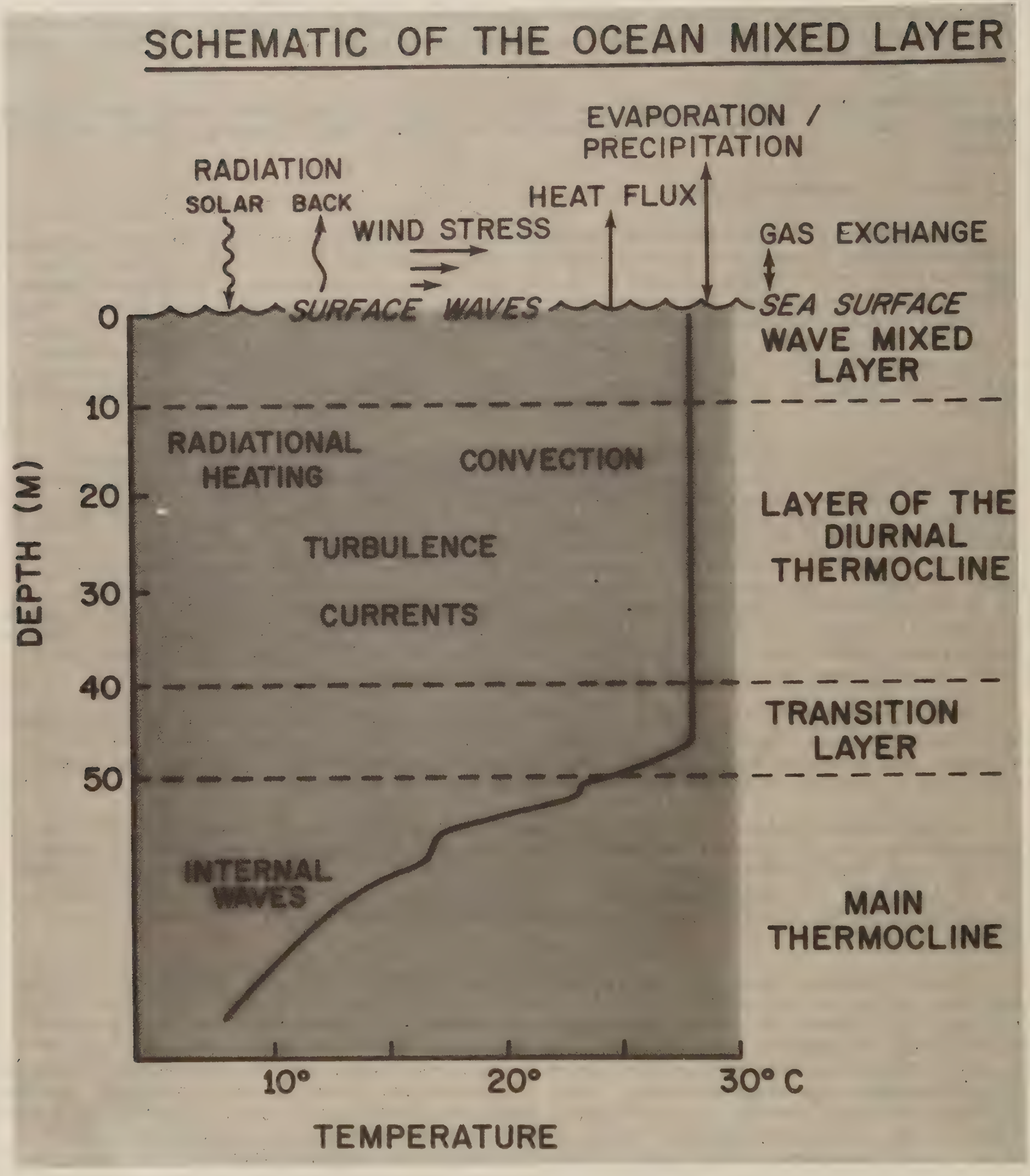
SCHEMATIC OF THE OCEAN MIXED LAYER
RADIATION
SOLAR
BACK
WIND STRESS
HEAT FLUX
EVAPORATION / PRECIPITATION
GAS EXCHANGE
SURFACE WAVES
SEA SURFACE
WAVE MIXED LAYER
RADIATIONAL HEATING
CONVECTION
TURBULENCE
CURRENTS
LAYER OF THE DIURNAL THERMOCLINE
TRANSITION LAYER
INTERNAL WAVES
MAIN THERMOCLINE
DEPTH (M)
0
10
20
30
40
50
10°
20°
30° C
TEMPERATURE

Fig. 9 Schematic diagram of ocean mixed layer

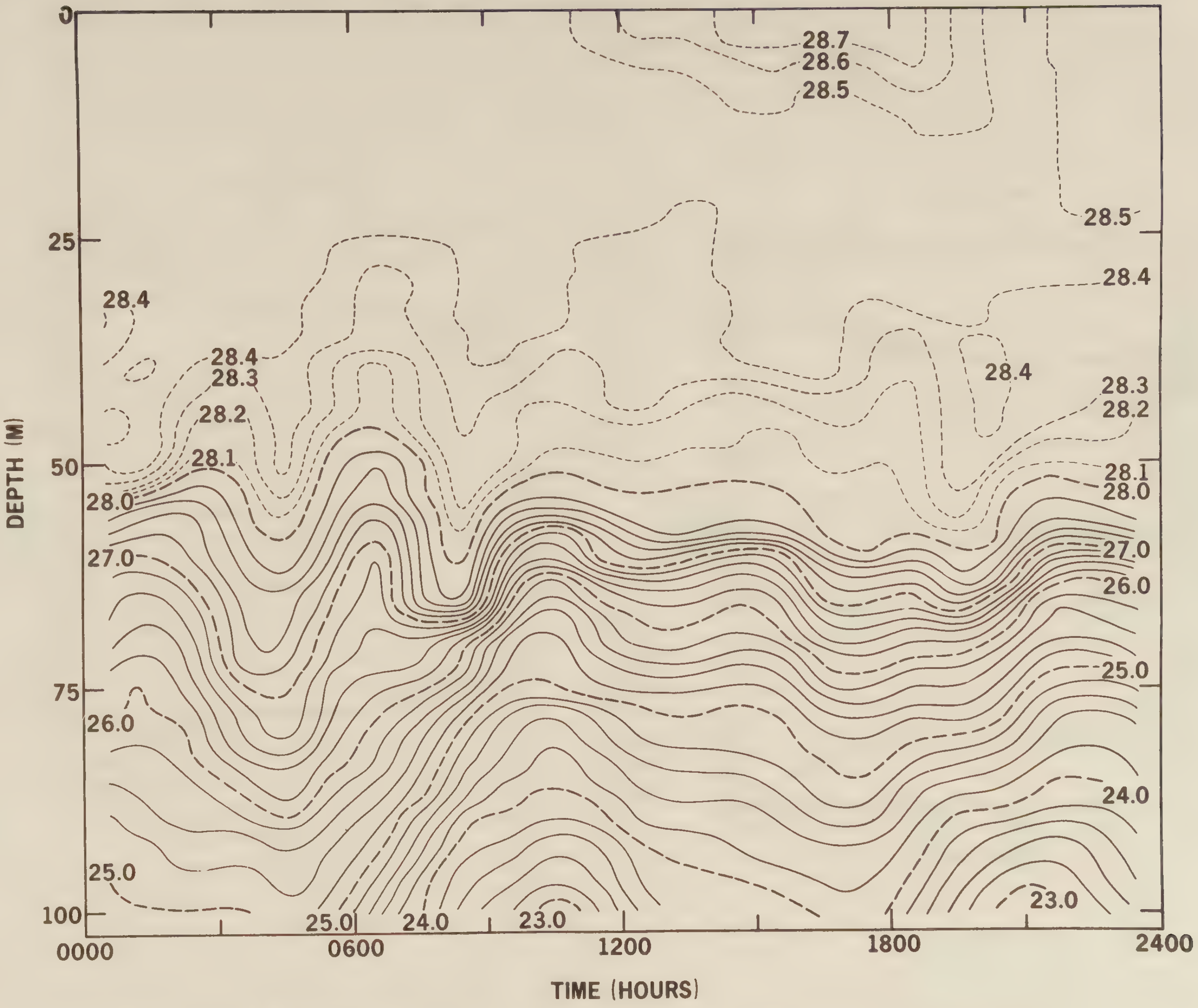

Fig. 10 28 September 1971, X-BT temperature contours. Time shown is local time

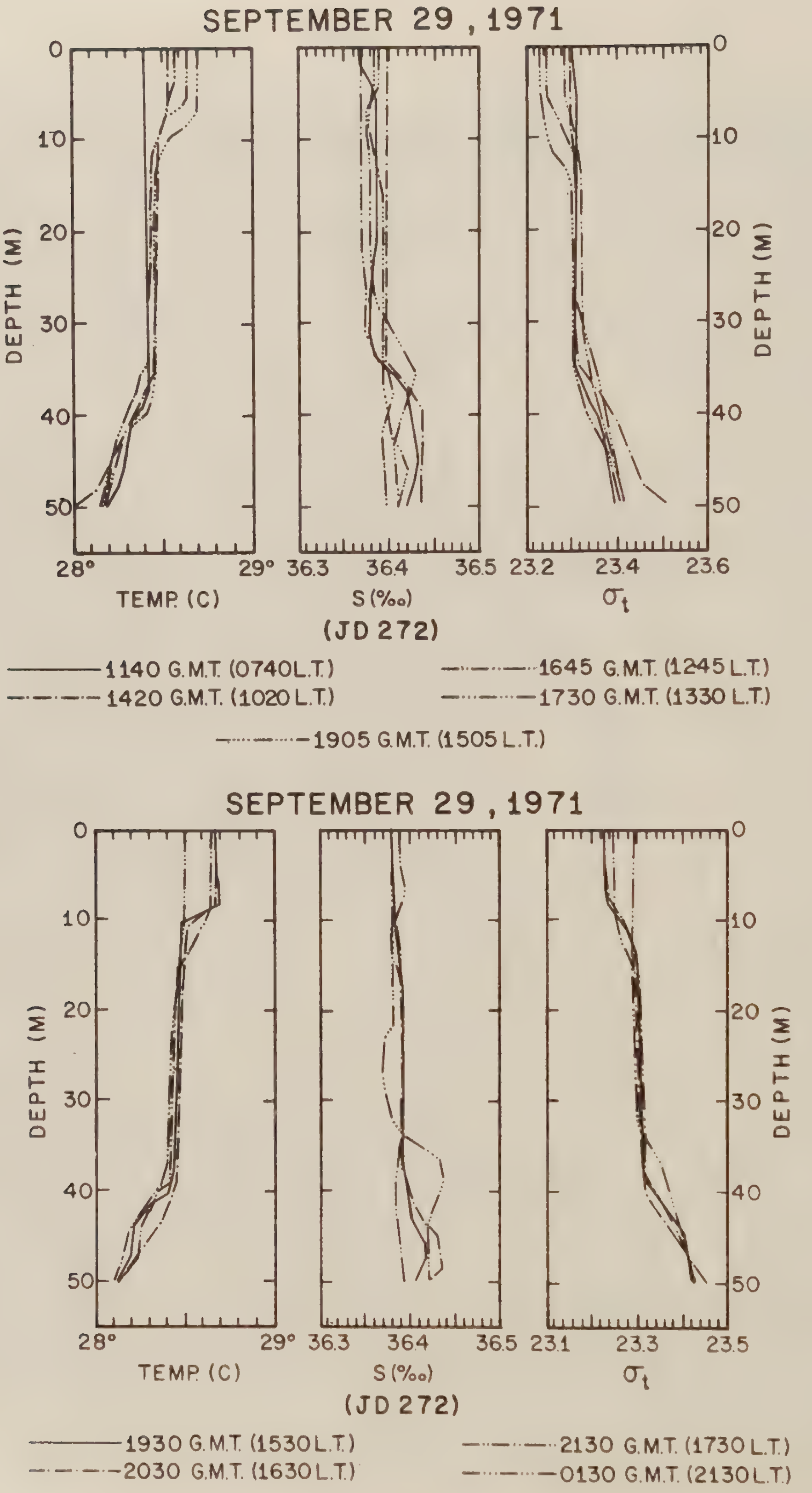

Fig. 11 29 September 1971, STD temperature, salinity, and σ_t profiles

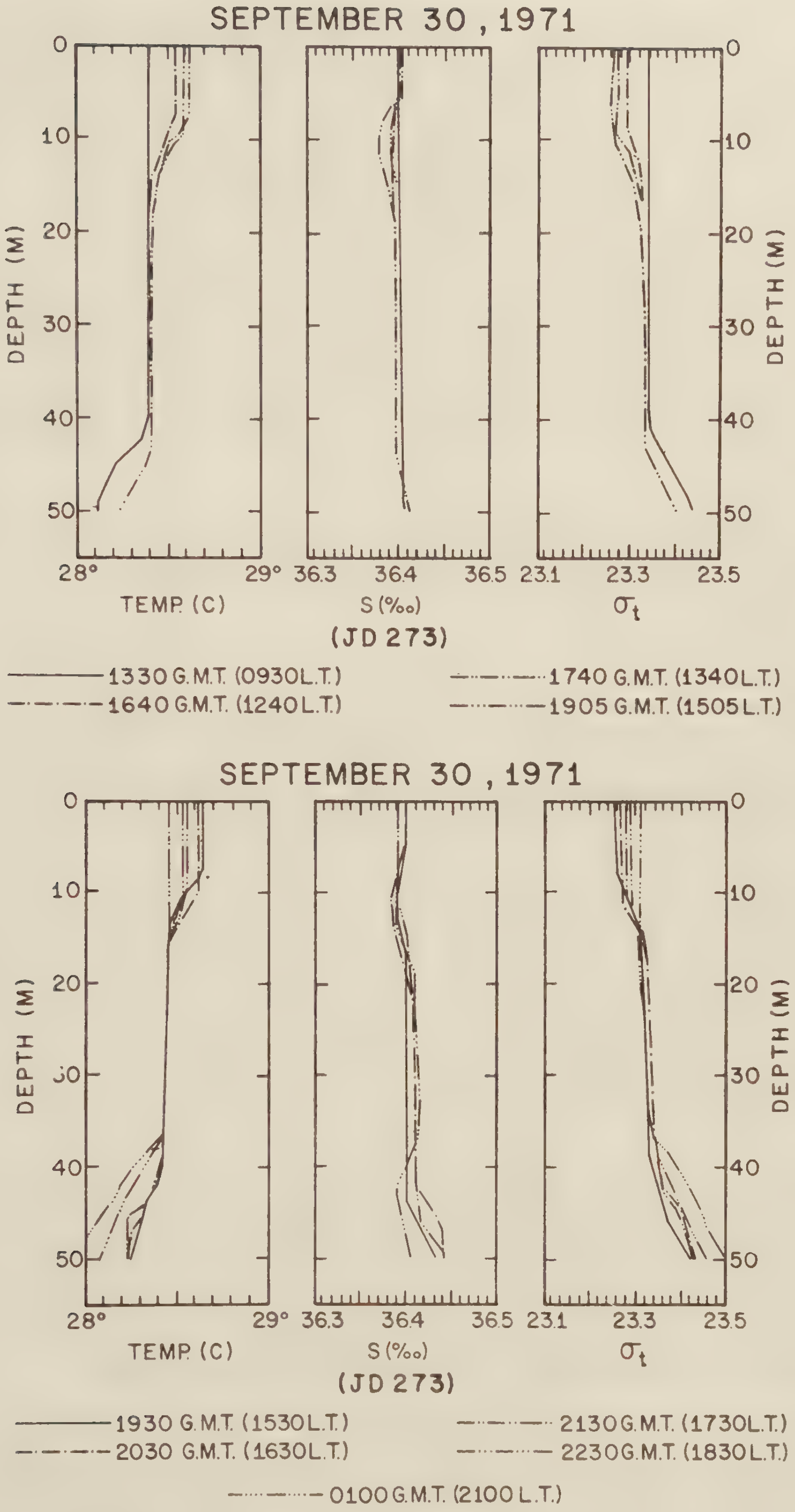

Fig. 12 30 September 1971, STD temperature, salinity, and σ_t profiles

This layer is relatively uniform. It is maintained by forced convective mixing caused by the wind stress and surface wave mixing. As the heating maximum is passed, the heating rate decreases. As long as there is net heating, the sea surface temperature generally increases. However, with a decreasing rate of buoyancy input, turbulent diffusion becomes more efficient at diffusing the heat downward, and the layer slowly deepens. As the net heating rate again becomes negative with the setting of the sun, turbulent mixing dominates and rapid deepening of the layer occurs. The layer soon disappears. Mixing occurs throughout the mixed layer, and neutral stability is re-established above the permanent thermocline.

Figs. 11 and 12 show temperature, salinity and computed σ_t profiles obtained using the STD on 29 and 30 September 1971. Figs. 11a and 12a show the portion of the diurnal cycle during which the sea surface temperature is increasing from the initial neutral stratification. Figs. 11b and 12b show the decrease of the diurnal heating layer temperature and vertical diffusion of the diurnal heat wave. These records show the typical Case 1 conditions. The salinity is uniform throughout the mixed layer and relatively constant. The density in the mixed layer is thus controlled by the temperature. Therefore, the temperature is a good indicator of density and stability. The diurnal cycle is about 0.3°C and σ_t has a range of 0.08.

During this period, the wave mixed layer is about 10 m deep, as can be seen from Figs. 11 and 12. The diurnal thermocline layer extends to approximately 35 m. The transition layer extends from about 35 m to 55 m (Ostapoff and Worthem, 1974).

5. CASE 2: LOW SALINITY PUDDLE

Various processes contribute to the observed structure in the low salinity puddle régime. Depending upon the spatial uniformity of the precipitation which produced the puddle, we expect some natural spatial variability in the surface layer salinity. Then diffusion and mixing rates may vary spatially due to the differences in stability, thus increasing the variability. The presence of mean field shear instability as well as turbulent eddies can cause erosion and mixing near the interface. Internal waves in the interfacial region can cause a temporary local increase in the mean field shear, increasing the possibility of a local instability and resultant mixing. In addition to these processes, the diurnal heating cycle including the nocturnal net cooling provide some density and temperature variation.

Figs. 13 through 18 show selected time series of STD temperature, salinity, and computed σ_t profiles during the period 2 to 6 October 1971. During this period, the ship traversed various portions of the low salinity puddle. During the 2-3 October 1971 profile series the ship drifted westward from the low surface salinity area through the neck of the low salinity northward intrusion and into the centre of the region of high surface salinity, as can be seen by comparing Figs. 1 and 3. During this time, there is a net cooling, and the surface temperature becomes cooler than the 30 m temperature. The density is essentially controlled by the salinity.

Fig. 14 shows a time series taken from approximately the time of maximum sea surface temperature in the diurnal cycle to the middle of the net heat loss period. This would normally be a time for surface layer deepening. However, the surface layer as defined by σ_t appears to become shallower through the 2235 LT profile and suddenly deepens at the 2335 LT profile. Also, the salinity profiles show a mixing and then sharpening structure in the 14 to 28 m depth range. This has the appearance of a classic case of mixing of two horizontally adjacent water masses (e.g., McLellan, 1968). Comparing Figs. 1 and 3, the ship track during this period crosses the frontal region at around 66°48'W and 20°59'N.

Fig. 15 shows a daytime profile series from about 66°42'W to 67°W at 21°N. Although the sea surface temperature range looks reasonable for the diurnal heating cycle, the profiles and absolute temperatures could not be explained without looking at the salinity profiles. The region traversed has a high salinity variability and shows what could be an oceanographer's nightmare if he were trying to measure the diurnal heating cycle and failed to record salinity. This figure also shows the mixing in the 14 to 28 m depth range discussed previously.

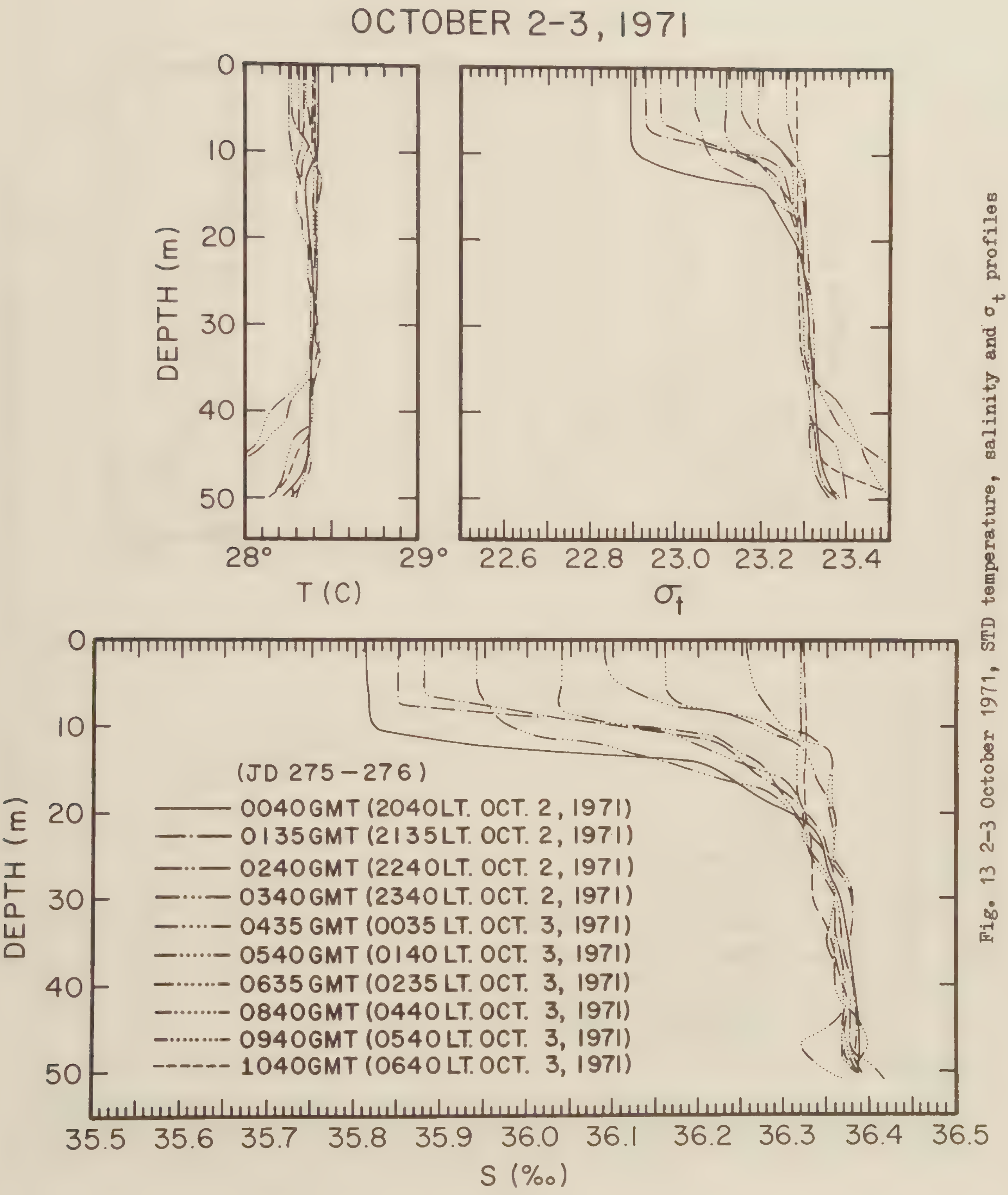

Fig. 13 2-3 October 1971, STD temperature, salinity and σ_t profiles

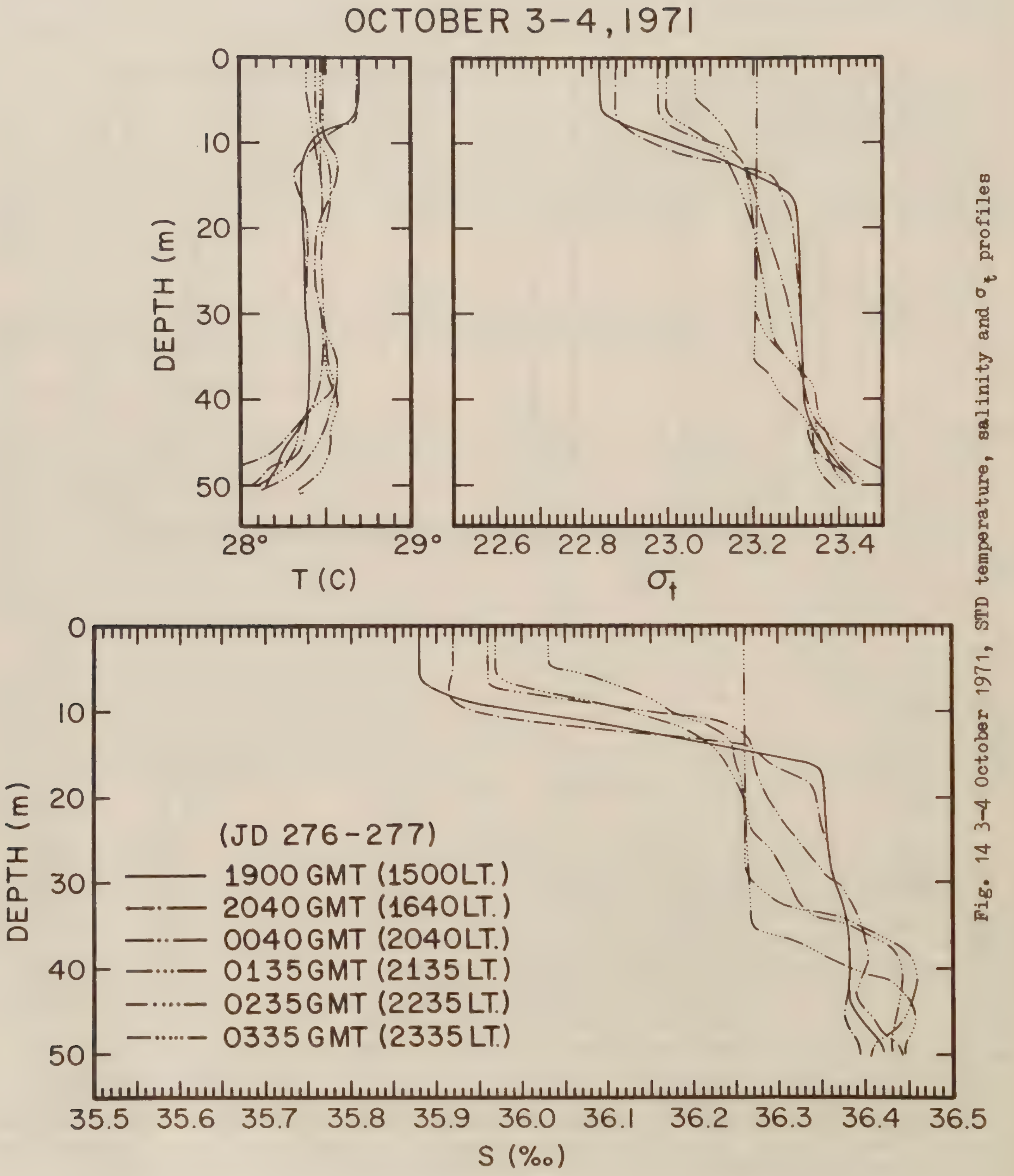

Fig. 14 3-4 October 1971, STD temperature, salinity and σ_t profiles

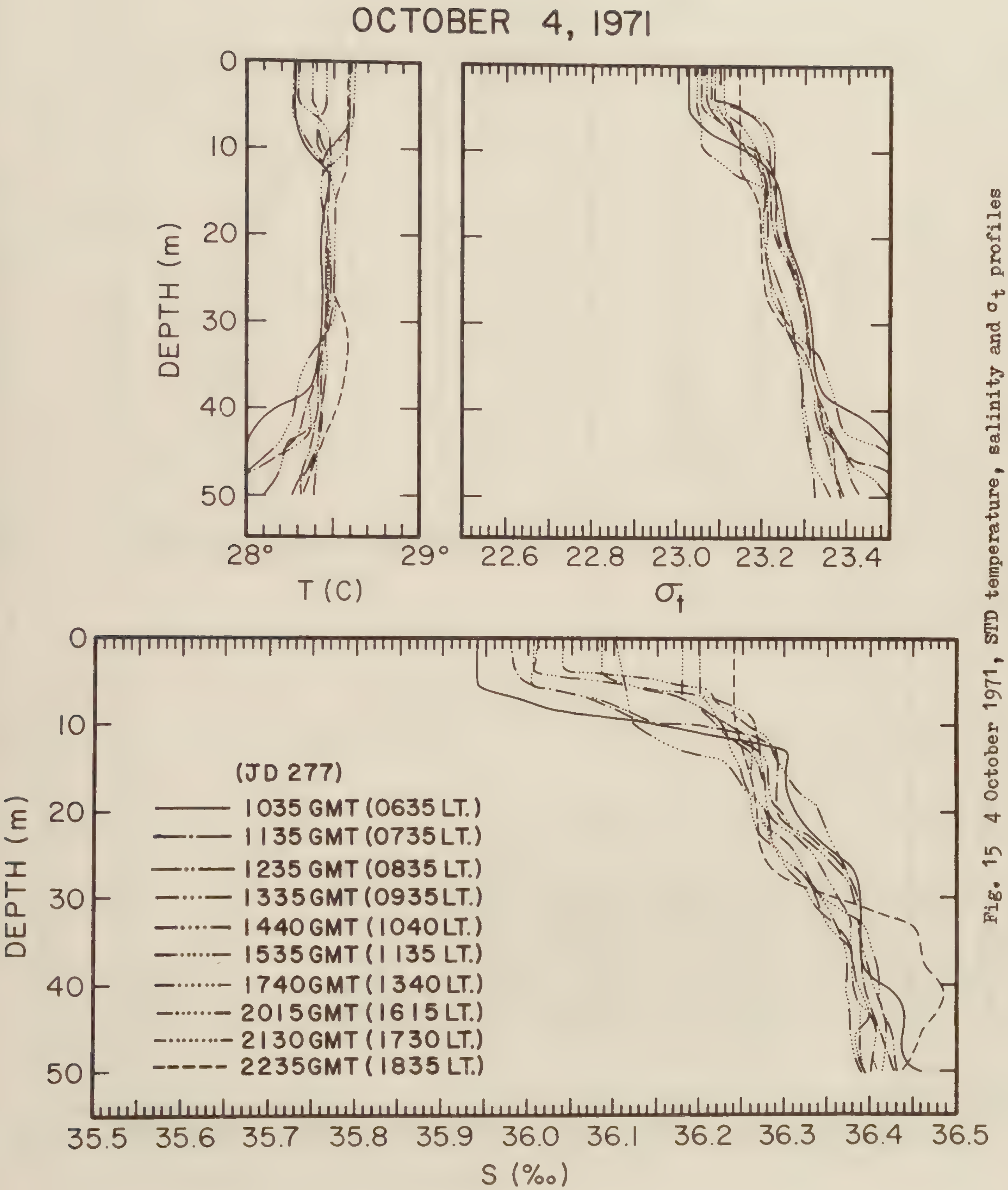

Fig. 15 4 October 1971, STD temperature, salinity and σ_t profiles

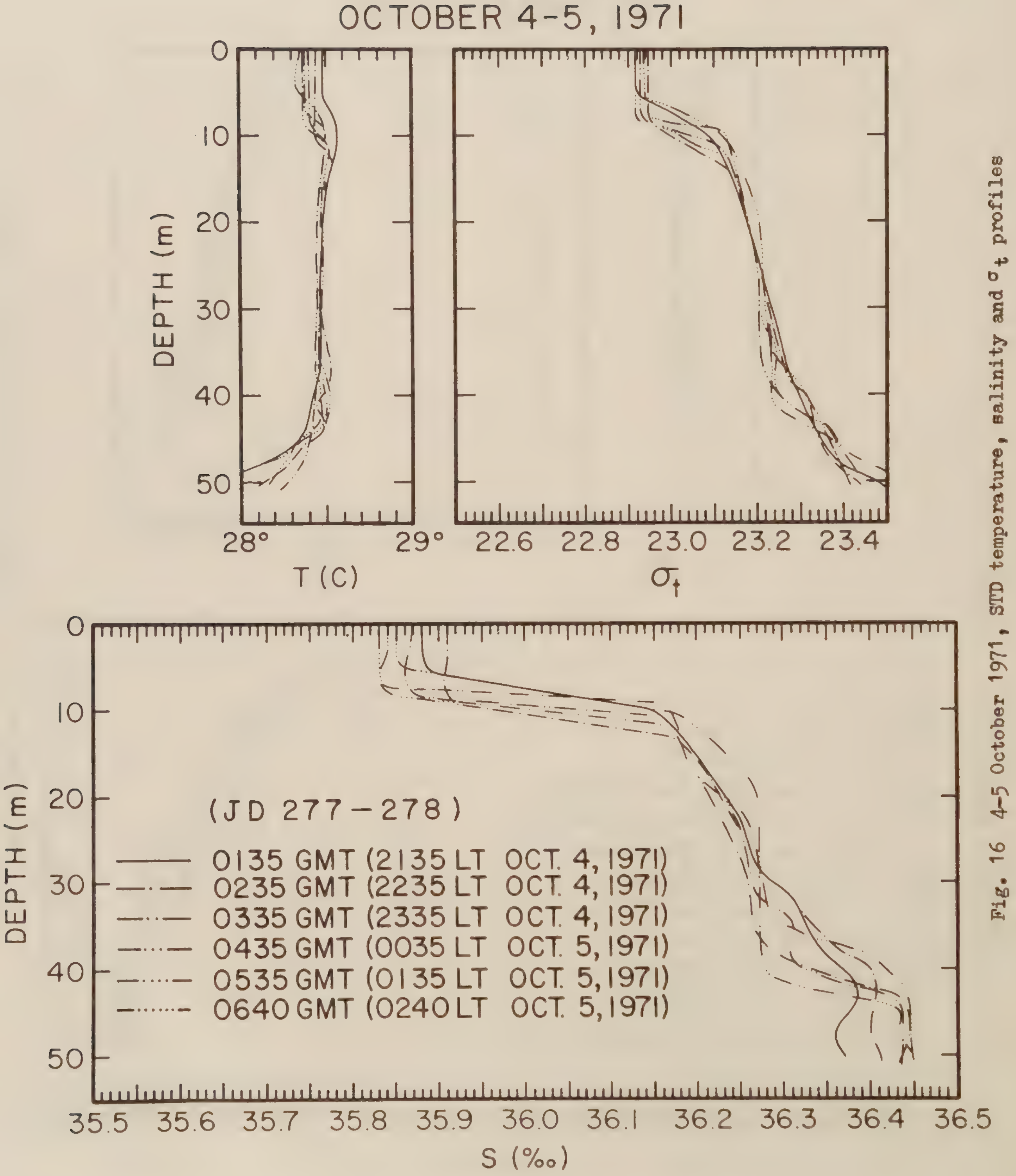

Fig. 16 4-5 October 1971, STD temperature, salinity and σ_t profiles

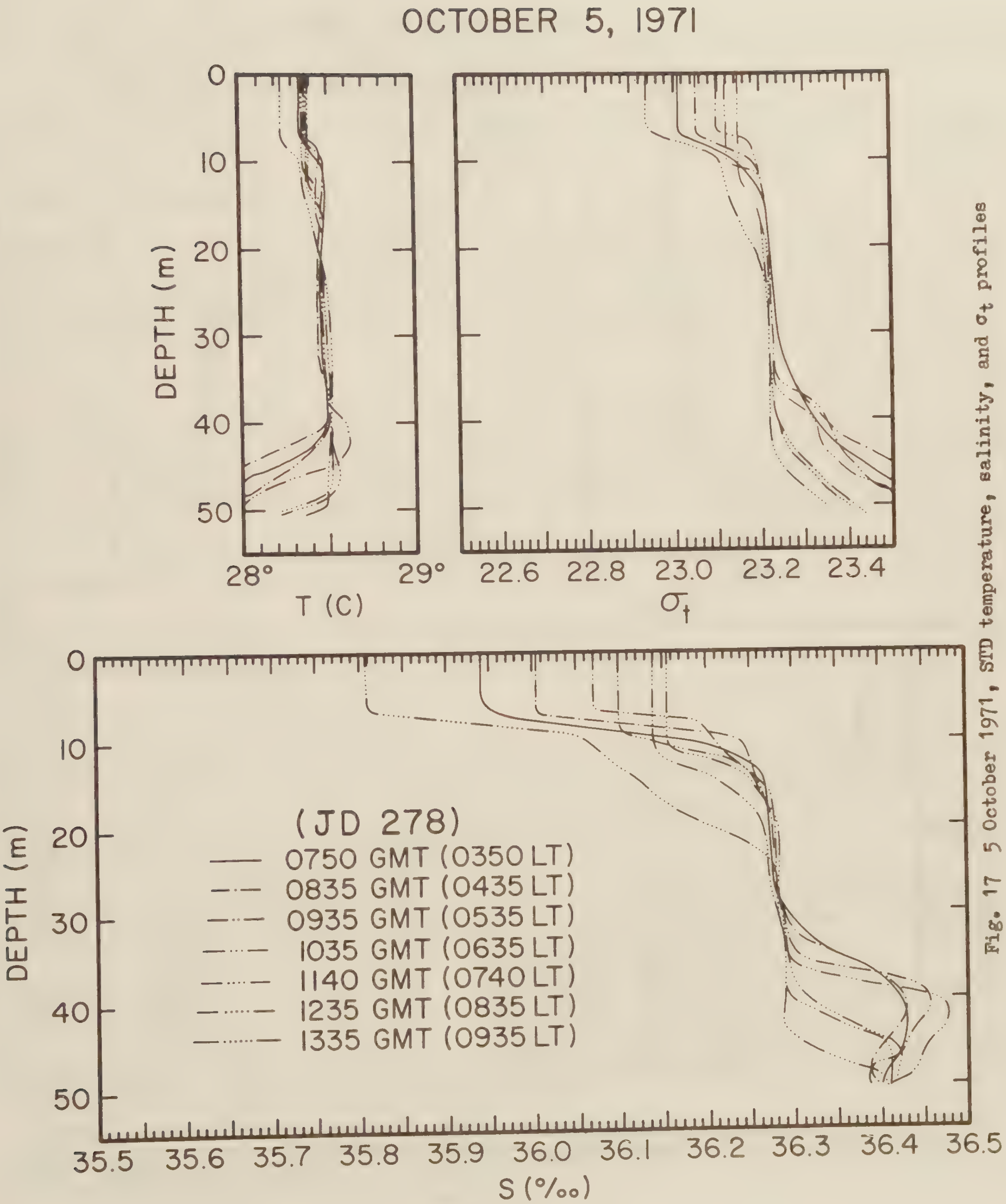

Fig. 17 5 October 1971, STD temperature, salinity, and σ_t profiles

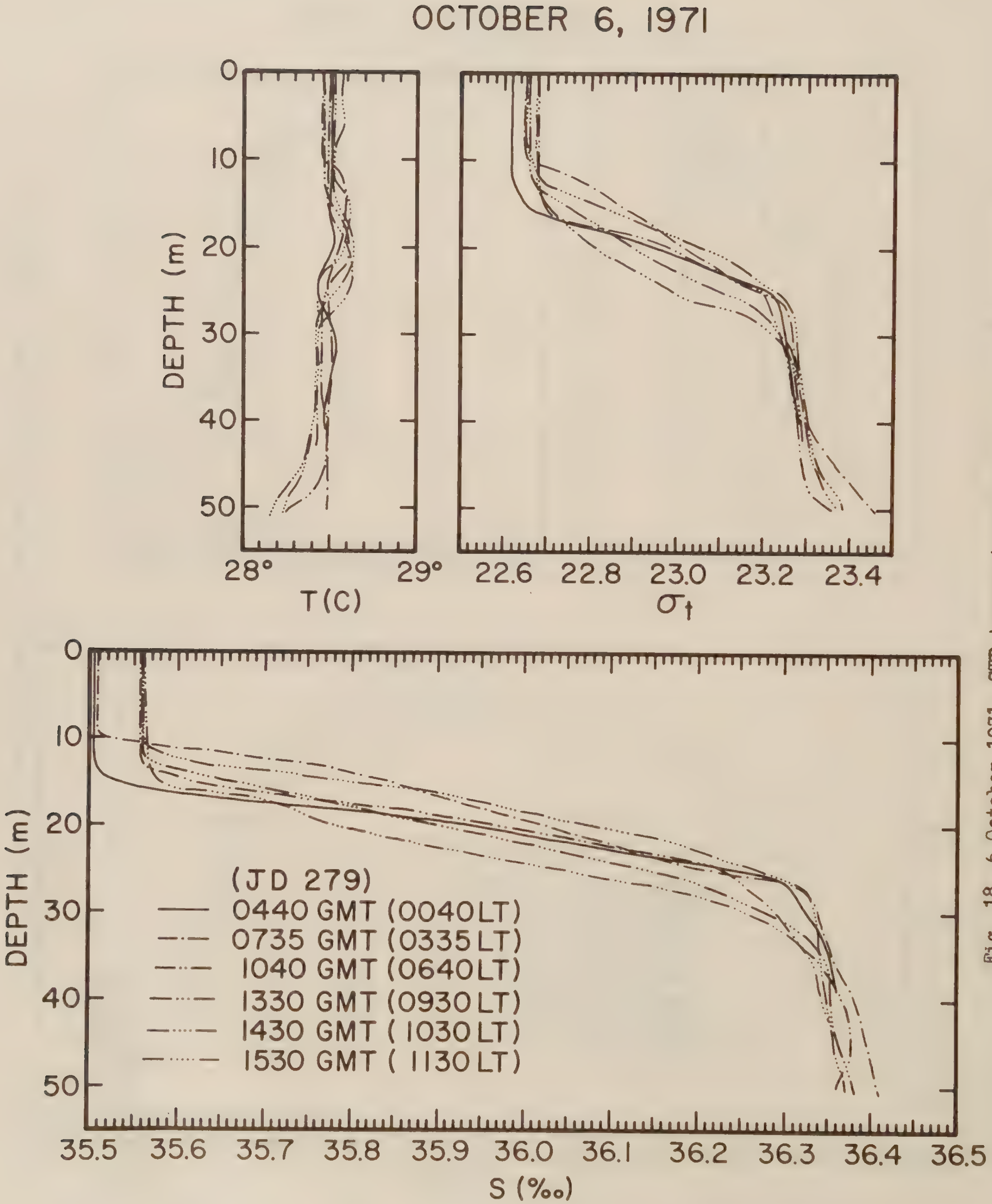

Fig. 18 6 October 1971, STD temperature, salinity, and σ_t profiles

Fig. 16 shows the structure of the salinity lens and increased nocturnal cooling of the surface layer. The variability in surface layer depth is probably due to internal waves on the interface, because the shape of the interfacial region appears relatively constant as though the isopycnals were just squeezed and stretched vertically.

The ship drifted from the centre of the low surface salinity northward intrusion northwest to the higher surface salinity region during the profiles in Fig. 17. The surface layer temperature is colder than the 30 m temperature during this period.

Fig. 18 shows a time series in the area of minimum surface salinity at about 66°54'W and 20°53'N. The variability in mixed layer depth here also appears to be determined by internal waves.

6. SUMMARY AND CONCLUSION

As can be seen from the data presented here, both salinity and temperature can be important in determining stability in the upper ocean. Strong horizontal spatial inhomogeneities may occur due to persistent low salinity puddles which originate in another area and may advect into an otherwise uniform, meteorologically ideal region. Therefore, both temperature and salinity should be measured during the duration of an experiment.

7. ACKNOWLEDGEMENTS

Portions of this work were supported by the National Science Foundation under IDOE Grant AG-282, which is gratefully acknowledged. We appreciate the fine cooperation of the Commanding Officer of the DISCOVERER, Captain R. Munson and the Operations Officer, Commander R. Allbritton, without whose skill and enthusiasm this field work could not have been accomplished. Lieutenant T. Ruszala diligently worked up the navigational data, which we gratefully acknowledge.

8. REFERENCES

Bowden, K.F., M.R. Howe and R.I. Tait, A study of the heat budget over a seven-day period at
1970 an oceanic station. Deep Sea Res., 17:401-11

Denman, K.L., A time-dependent model of the upper ocean. J.Phys.Oceanogr., 3(2):173-84
1973

Denman, K.L. and M. Miyake, Upper layer modification at ocean station "Papa". Observations
1973 and simulation. J.Phys.Oceanogr., 3(2):185-96

Düing, W. and D. Johnson, High resolution current profiling in the straits of Florida.
1971 Sci.Rep.U.Miami, (ML 71085):39 p.

Fedorov, K.N., On the summer daily heating and diurnal heat budget of the upper ocean layer.
1972 In Studi in onore de G. Aliverti. Napoli, Istituto de Meteorologia e Oceanografia, Università Navale di Napoli, pp. 27-40

Foster, T.D., A convective model for the diurnal cycle in the upper ocean. J.Geophys.Res.,
1971 76(3):666-75

Hanson, K.J. and M.F. Poindexter, Atenuance of broad-band solar irradiance in the ocean. In
1972 Preprint Volume of the Conference on Atmospheric Radiation, August 7-9 1972, Fort Collins, Colorado. AMS, Mass., pp. 165-8

Hasse, L., The sea surface temperature deviation and the heat flow at the sea-air interface.
1971 Boundary Layer Meteorol., 1:368-79

Hoeber, H., Eddy thermal conductivity in the upper 12 m of the tropical Atlantic. J.Phys.
1972 Oceanogr., 2:303-4

Howe, M.R. and R.I. Tait, Some observations of the diurnal heat wave in the ocean. Limnol.
1969 Oceanogr., 14:16-22

Kraus, E.B., Atmosphere-ocean interaction. London, Oxford University Press, 275 p.
1972

Kraus, E.B. and J.S. Turner, A one-dimensional model of the seasonal thermocline. 2. The
1966 general theory of its consequences. Tellus, 18(2):98-106

McLellan, H.J., Elements of physical oceanography. London, Pergamon Press, 151 p.
1968

Mellor, G.L. and P.A. Durbin, The structure and dynamics of the ocean surface mixed layer.
1975 J.Phys.Oceanogr., 5(4):718-28

Ooyama, K., Numerical simulation of the life cycle of tropical cyclones. J.Atmos.Sci.,
1969 26:3-40

Ostapoff, F. and S. Worthem, The intradiurnal temperature variation in the upper ocean
1974 layer. J.Phys.Oceanogr., 4(4):601-12

___________, Air-sea interactions during conditions of squalls and deep convection.
1976 FAO Fish.Rep., (200) Suppl.

Pandolfo, J.P. and C.A. Jacobs, Numerical simulations of the tropical air-sea planetary
1972 boundary layer. Boundary Layer Meteorol., 3:15-46

Rooth, C., Unpublished results
1973

Shonting, D.H., Some observations of short-term heat transfer through the surface layers of
1964 the ocean. Limnol.Oceanogr., 9:576-88

Stommel, H. and A.H. Woodcock, Diurnal heating of the surface of the Gulf of Mexico in the
1951 spring of 1942. Trans.Am.Geophys.Union, 32:565-71

Stommel, H. et al., Observations of the diurnal thermocline. Deep Sea Res., 16:269-84
1969

U.S. Naval Air Systems Command, Handbook Operation, Service and Overhaul Instructions with
1967 Illustrated Parts Breakdown Meteorological Station, Automatic, Marine (AN/SMT-1.
NAVAIR 50-30 SMTI-2):200 p.

ENERGY FROM THE SEA: OCEAN THERMAL ENERGY CONVERSION POSSIBILITIES IN THE CARIBBEAN

by

C.P. DUNCAN and D.K. ATWOOD
Departamento de Ciencias Marinas
Universidad de Puerto Rico
Mayaguez, Puerto Rico

M.C. STALCUP
Woods Hole Oceanographic Institution
Woods Hole, Mass.
U.S.A.

CONTENTS

1. INTRODUCTION
2. BACKGROUND
3. THE TROPICS
4. THE CARIBBEAN AS AN OTEC REALM
5. PLANT DESIGN AND SITE REQUIREMENTS
6. A POSSIBLE SITE NEAR PUERTO RICO
7. CONCLUSIONS
8. ACKNOWLEDGEMENTS
9. REFERENCES

Abstract

The Caribbean Sea has considerable potential as a site for Ocean Thermal Energy Conversion (OTEC) plants. Such plants could provide fuel and clean electrical energy. In principle, OTEC uses the temperature differences of the ocean to drive a motor attached to an electrical generator - with a Carnot efficiency of approximately 5 percent. In practice an OTEC plant would use warm water from the surface as a heat source and pump cold water from depths of between 600 and 1 000 m to act as a heat sink. The water motion caused by the temperature difference would turn the turbines. The plants can be situated either on land or at sea on floating platforms. They could supply electricity to factories situated on the coast, at sea, or possibly be used to produce a hydrogen fuel by electrolysis. The basic requirements for potential localities are: (1) warm surface water throughout the year, (2) cold water at a convenient depth, (3) a zone relatively free of storms, and, if the electricity produced was to be transmitted directly to the mainland, a further requirement would be, (4) cold water at a convenient distance from the coast. The southern coasts of the Greater Antilles meet these requirements well. In particular, the steep continental slope of most of the islands means that cold water is available at distances of 5 km and less, while the geostrophic tilt of the isotherms caused by the westward-flowing Caribbean Current creates a deep wedge of warm water against their coasts. A study off Yabucoa, Puerto Rico indicates that this site is oceanographically ideal for the placement of an OTEC plant. It has an excellent temperature profile, a very steep continental slope, a thick surface layer of warm water, and plentiful deep cold water. It is protected from most rough weather (except hurricanes) and is close to the Puerto Rican island-wide electrical power grid.

Resumen

El mar Caribe reúne muchas de las condiciones necesarias para la instalación de fábricas de conversión de la energía térmica marítima (OTEC), que podrían proporcionar energía eléctrica y combustibles no contaminantes. La conversión de la energía térmica oceánica consiste en principio en aprovechar las diferencias de temperatura de las aguas de los océanos para accionar un motor acoplado a un generador de electricidad, con un rendimiento de Carnot del 5 por ciento aproximadamente.

En la práctica, la instalación OTEC utilizaría como fuente de calor el agua caliente de la superficie, y bombearía el agua fría desde profundidades de 1 000 m, la cual actuaría como sumidero térmico: el movimiento del agua causado por la diferencia de temperaturas accionaría las turbinas. Las instalaciones podrían situarse en tierra firme o en el mar, sobre plataformas flotantes, y podrían suministrar electricidad a las fábricas de la costa, o flotantes, o tal vez servir para producir hidrógeno por electrólisis. Los posibles lugares de emplazamiento de estas fábricas tendrían que reunir las siguientes condiciones: (1) que el agua superficial esté caliento todo en año, (2) que haya agua fría a una profundidad conveniente, (3) que la zona esté exenta, relativamente, de tormentas, y (4) que haya agua fría a una distancia conveniente de la costa: esta última condición es necesaria cuando la electricidad que se produzca vaya a transmitirse directamente a tierra firme. Las costas meridionales de las Grandes Antillas reúnen casi todas estas condiciones. Dada la abrupta vertiente continental de casi todas las islas, se encontrará agua fría a 5 km, o menos, de distancia, y, al mismo tiempo, la inclinación geostrópica de las isotermas causada por la corriente del Caribe que fluye hacia el oeste, crea una profunda penetración de agua caliente en sus costas.

Un estudio realizado en aguas de Yabucoa (Puerto Rico) revela que es un lugar oceanográficamente ideal para el emplazamiento de una fábrica OTEC, ya que tiene un excelente perfil de temperaturas, una vertiente continental muy abrupta, una gruesa capa superficial de agua caliente y toda el agua fría, procedente de las profundidades, que se necesite. Está, además, protegido contra el mar tiempo, salvo contra los huracanes, y está cerca de la red de energía eléctrica de toda la isla de Puerto Rico.

1. INTRODUCTION

This is a brief resumé of known facts on the conversion of ocean thermal energy to electrical energy applied to the Caribbean, with the discussion of a possible site off Puerto Rico. Ocean Thermal Energy Conversion (OTEC) is an attempt to use the rapid thermal gradient between the warm mixed layers of tropical seas and the underlying cold waters of polar origins to operate a heat engine and thus extract energy from the sea. The concept recognizes the surface of the tropical seas as a vast solar collector which can also store the collected energy in a high heat capacity fluid, i.e., water. The energy stored in this way is orders of magnitude greater than that available from exploitation of waves or tides. It is also an environmentally clean source.

2. BACKGROUND

The ocean is a vast collector, distributor and reservoir of energy which man is only beginning to tap. The most obvious demonstrations of this energy are the waves and the tides. Indeed, the most successful ocean energy project so far is the hydroelectric project at Rance, so the question arises: why thermal energy?

The thermal energy resources of the ocean greatly exceed wave, tide or current power. A quick slide-rule comparison shows that even in the Gulf Stream thermal energy exceeds the kinetic energy by a factor of at least ten thousand (Düing *et al.*, 1975) because of the high heat capacity of water. Fig. 1 (from Chemical and Engineering News, 9 February 1976 reproduced by permission) gives some idea of the relative magnitudes of oceanic energy sources. Note that the figure is drawn on a logarithmic scale. Over 98 percent of the available energy is in the form of thermal gradients, and it seems reasonable to investigate first the source with the greatest potential. Thermal gradients may be compared to a low-grade ore which only needs an economically viable process to become valuable. An OTEC power plant should be competitive in cost with oil, nuclear or coal plants, although the first will probably be heavily subsidized as a feasibility study.

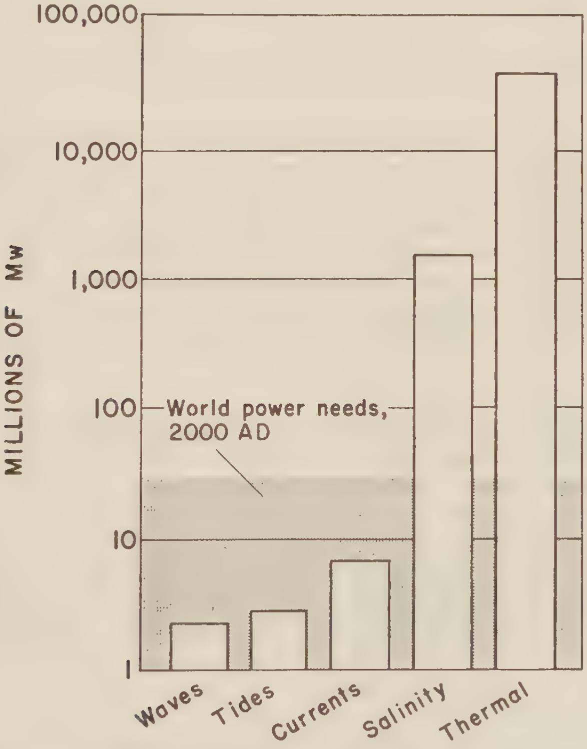

Fig. 1 Oceanic energy resources (from Chemical and Engineering News)

If the thermal gradients can be tapped economically, they are not as dependent on particular favoured localities as kinetic schemes are (e.g., Rance, Passamaquoddy for tidal power, Straits of Florida for current driven power) but are much more general. The surface waters of the tropics are generally warmer than 25°C and the cold polar water masses which underlie the oceans of the world provide virtually limitless supplies of water at 6°C or less below 1 000 m throughout the Atlantic Ocean.

An OTEC plant provides a means for using solar energy night and day, without the expense of building a large solar energy collector. A typical example of the oceanic temperature structure in the tropics is given in Fig. 2 drawn from CICAR data. The warm mixed layer from the surface to about 60 m represents a heat source of stored solar energy, and the cold deep waters are a vast ocean-wide heat sink. The potential energy in the thermal gradient between the heat source and the heat sink can be converted to electrical energy. Fig. 3 gives a schema of the process. The thermodynamic efficiency of such a Carnot cycle is calculated from the formula Efficiency = $\frac{T_1 - T_2}{T_2}$ where temperatures are in degrees Kelvin. It is about 5 percent for the temperature difference illustrated in Fig. 2. Large amounts of water are therefore needed. For a 100 MW OTEC plant about 500 m^3/sec is needed. This is a very small quantity compared to oceanic flow. The Caribbean Current, for example, transports more than 2 x $10^6 m^3$/sec (Atwood et al., 1975). An OTEC plant would be equivalent to a strip of the Caribbean Current about 10 m wide.

3. THE TROPICS

The higher the temperature difference between the heat source and the heat sink, the greater the efficiency of the plant, so that the only practicable place for a pilot plant is the tropics where the largest temperature differences are found. This conclusion was reached by George Claude when he built his pre-war OTEC plant in Cuba. Once the system is proved to be economical, then the minimum usable ΔT can be determined and the northernmost limits of OTEC plants can easily be determined.

4. THE CARIBBEAN AS AN OTEC REALM

The Caribbean is particularly favoured oceanographically as a site for an OTEC plant. A survey of historical data shows the following advantages:

(1) The thermal axis of the Atlantic Ocean lies well north of the equator and there is a plentiful supply of warm surface water the year round. As the surface waters of the Atlantic receive heat from the sun they move westward with the North Equatorial Current and are directed into the Caribbean by the shape of South America. The thermal collection, storage and advection region may be considered as a solar "catchment area" which extends to Africa, and covers about 10 million km^2. The Caribbean being downstream receives a free gift of about 15 x $10^6 m^3$/sec of water warmer than 20°C. This is sufficient to "fuel" about 30 000 OTEC plants. Figs. 4 and 5 have been drawn from U.S. and German meteorological atlases.

(2) Throughout the Caribbean the warm mixed layer is adequate for OTEC plants although it varies in thickness. Between Venezuela and Puerto Rico it is shallow in the south, deepens to a maximum at 15°N and then shoals gently to the north. Fig. 6 illustrates the average vertical temperature distribution in the surface layer, drawn from data taken along 67°W (CICAR Standard Section (j)) by the University of Puerto Rico. This displacement of the isotherms results as the density field and the westward flowing Caribbean Current approximate geostrophic equilibrium. The cooler surface water along the coast of Venezuela, which is such a noticeable feature of Figs. 4 and 5, is another expression of the same effect.

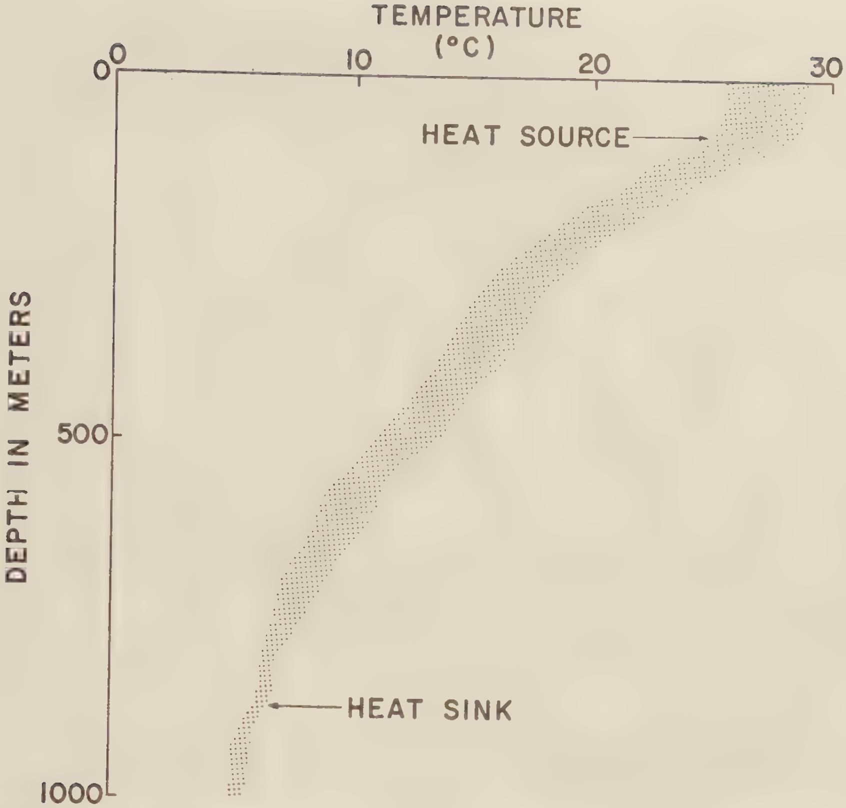

Fig. 2 Temperature/Depth envelope for all data at PESCA serial station at 17°40'N, 67°00'W, 1971-1973

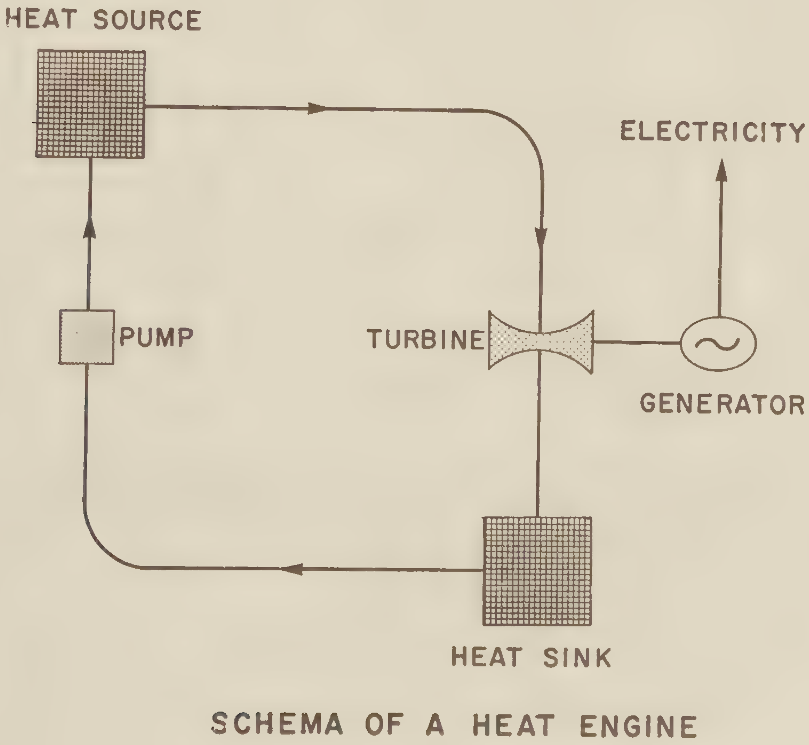
HEAT SOURCE
ELECTRICITY
PUMP
TURBINE
GENERATOR
HEAT SINK
SCHEMA OF A HEAT ENGINE

Fig. 3 Schema of a heat engine

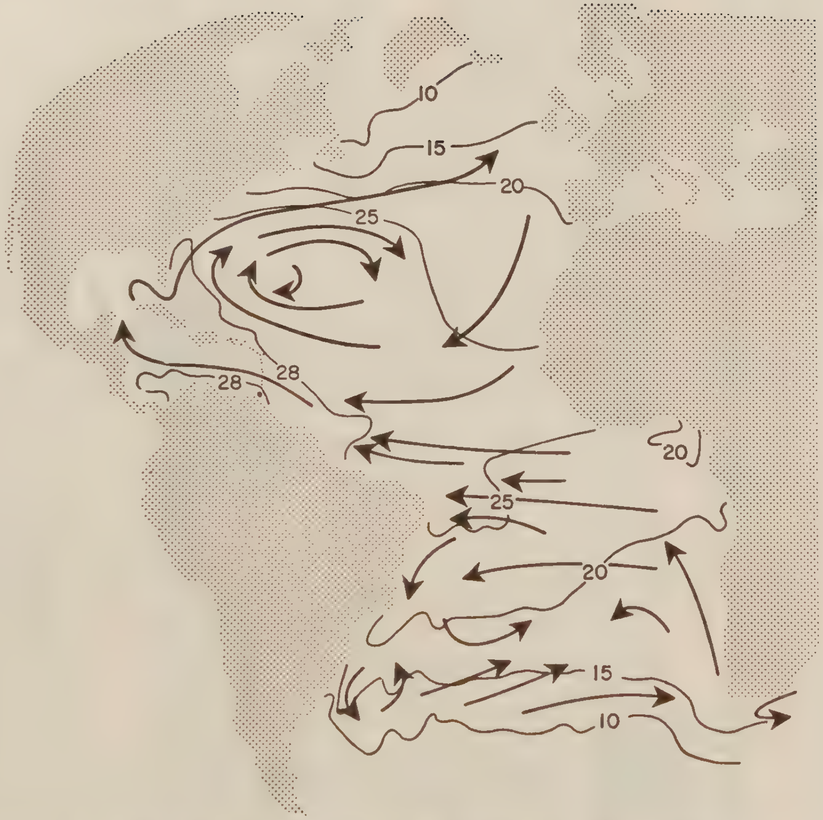
10
15
20
25
28
28
20
25
20
15
10

Fig. 4 Sea surface currents (schematic) and temperatures (°C) Atlantic Ocean in August

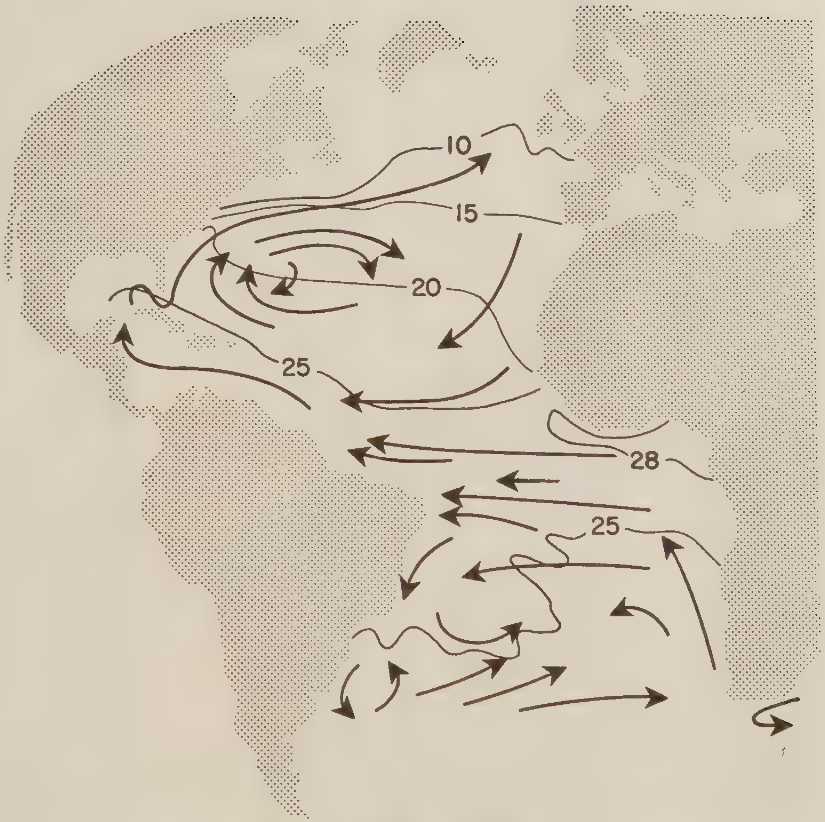
10
15
20
25
28
25

Fig. 5 Sea surface currents (schematic) and temperature (°C) Atlantic Ocean in February

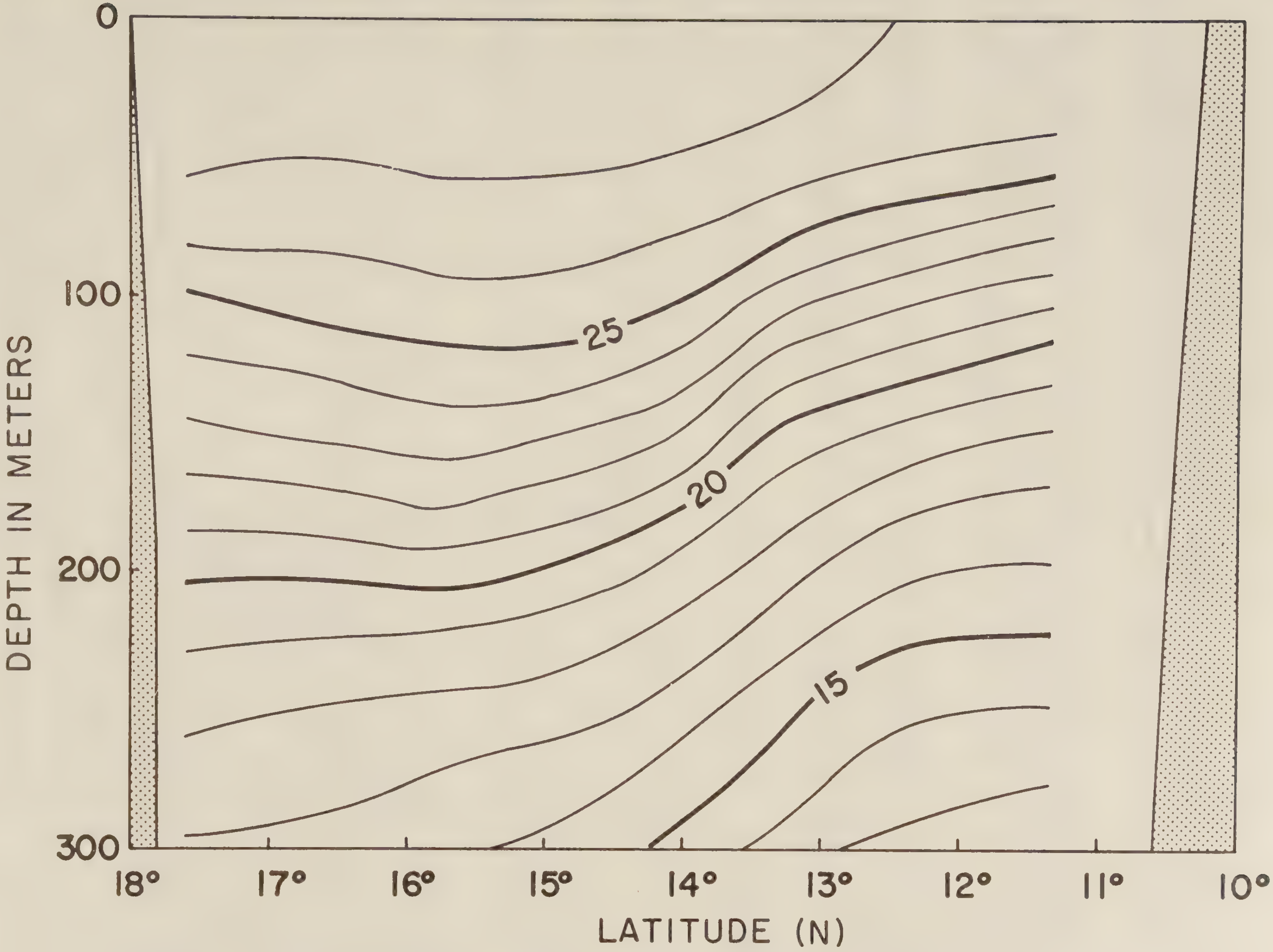

Fig. 6 Vertical section of mean temperatures (^{o}C) along 67^{o}W

(3) $15 \times 10^6 m^3$/sec of warm Atlantic water which flows past the Lesser Antilles is rapidly and efficiently distributed westward throughout the Caribbean by the Caribbean Current at surface speeds up to 0.76 m/sec as calculated geostrophically along CICAR Standard Section (j). Fig. 7 gives the geostrophic surface velocity along 67°W showing that south of 15°N the current is a dependable vehicle for this distribution on a large scale but that north of 15°N currents are likely to be variable and of more local significance.

(4) Fig. 2 illustrates the rapid thermocline break which sharply separates the heat source and sink in the northern Caribbean near Puerto Rico. For a pilot plant which must reach about 1 000 m for a dependable ΔT of 20°C the sharpness of the thermocline is not too significant but when plants are built which can use a smaller ΔT, the Caribbean will be even more attractive as an OTEC realm and the southern Caribbean will be even more attractive than the north. (Compare the temperature difference between the surface and 250 m at 17°N and 12°N in Fig. 6.)

(5) There is a plentiful supply of cold water at depth from the North Atlantic across the Anegada-Jungfern Sill between the Greater and Lesser Antilles.

(6) The Lesser Antilles have steep continental slopes which mean that cold water is found close to shore, so that the direct supply of electricity to shore is reasonably achieved.

(7) There is good weather for erection and maintenance of the plant.

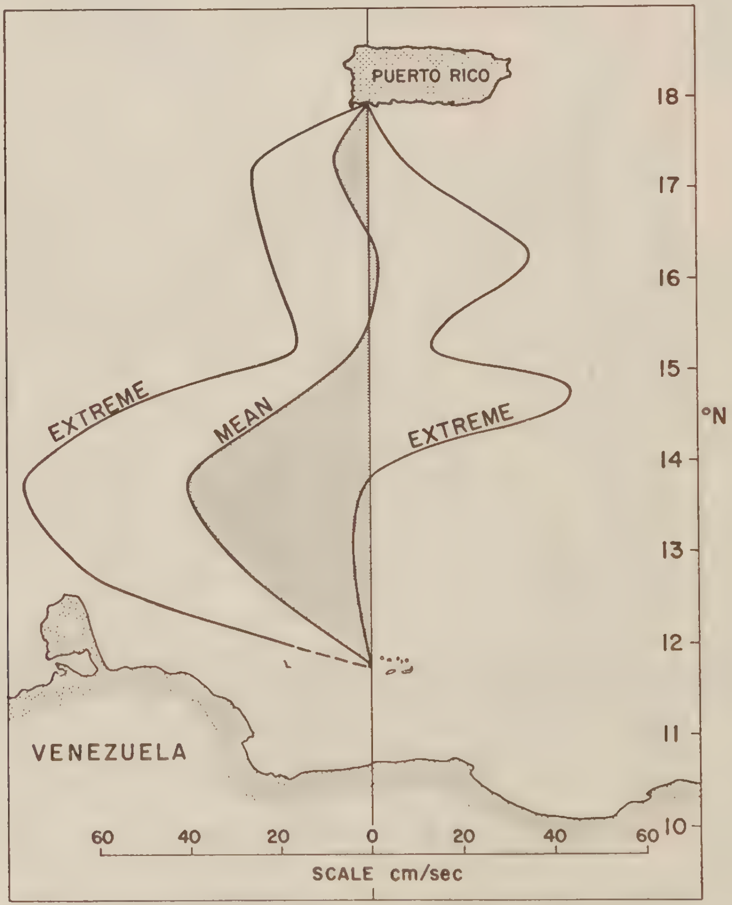

GEOSTROPHIC SURFACE CURRENTS AT 67° W
FROM PROVISIONAL CICAR DATA

Fig. 7 Geostrophic surface currents at 67°W from provisional CICAR data

5. PLANT DESIGN AND SITE REQUIREMENTS

Several plant designs are being considered at present but all are limited by the conditions imposed by the principle, the basic oceanography, and the economics. The design features which follow are abstracts from reports by Sea Solar Power, United Engineers and Lockheed Ocean Systems.

(1) All present designs have been limited to state-of-the-art-technology. They feature a long concrete pipe which reaches the cold water so that it can be pumped to a heat exchanger at the surface rather than a heat exchanger at depth. For the best temperature difference (20°C) the pipe will have to reach about 1 000 m below the surface, but a 16°C difference is available at 600 m. For adequate flow, the pipe will have to be about 20 m in diameter (Figs. 8, 9 and 10 used by permission).

(2) Most designs are for a moored floating plant, but a shore-based plant with pipes laid on the sea bed is also possible. Even free-floating plants which are moved to the best locations as the seasons change are possible. This refinement is unnecessary in the Caribbean. Power lines from a floating plant, or the pipes to a shore-based plant are expensive, and the shorter they are, the better. The ideal site must have cold water at a depth of 1 000 m close to the land mass, i.e., a narrow continental shelf and a steep continental slope. In some parts of the Caribbean depths of 1 000 m are found only 2 km offshore.

(3) The temperatures and conditions encountered do not require the exotic technology of nuclear or even conventional power plants. Heat exchangers required to function at 25°C can easily be made of plastic. Plastic has the additional advantage of being non-corrosive.

(4) With such low temperature differences very efficient heat exchangers are needed, so they will probably have to be made of non-corrosive metal - perhaps titanium - with irregular and turbulence-producing surfaces for better heat conduction.

(5) Whatever the heat exchangers are made of they will tend to bio-foul very rapidly, as they will present ideal surfaces for marine growth. With the vast amounts of water being pumped, any chemical treatment such as the addition of chlorine to the intake, is out of the question. A mechanical system which employs little balls in the circulating water to bump off the growth is standard technology and will probably be used.

(6) Some plants are designed to pump the cool effluent from the condensor out near the surface. The opinion is occasionally advanced that OTEC plants will have a vast impact on local fisheries, because of the enrichment of surface waters by water pumped up from depth. Figs. 11 and 12 illustrate the basic nutrient distribution on which this kind of reasoning is based. The surface waters are usually poor in nutrients but the deep waters contain a plentiful supply. Its composition is ideal for oceanic fertilizer for the growth of phytoplankton which feed zooplankton, small fish and higher levels of the food chain. However, at a pumping rate of 500 m^3/sec, i.e., 43 million m^3/day, the fertilizer supply is equivalent to only about 0.1 percent of the rate at which nutrients are carried into the photic zone by the Caribben Current. To be of use to phytoplankton the cold nutrient-rich water will have to be pumped into the photic zone. Unfortunately, if the cold water is discharged near the surface, it may short-circuit the OTEC plant by lowering the temperature of the surface hot water supply (Fig. 13). If the nutrient-rich water is pumped into 1 m deep land-based ponds, and held for a week to give plankton time to bloom, at 43 million m^3/day, 300 km^2 would be needed. Our conclusion is that it will be better to mix the two outflows to form water of a density sufficiently high to sink below the warm mixed layer (Fig. 14).

(7) A floating plant moored in mid-ocean, or perhaps on a seamount to save on the mooring line, could use its electrical power:

(i) to smelt aluminium or titanium or lithium or other metals needing large amounts of energy;
(ii) to produce hydrogen by electrolysis to be used ashore as a clean fuel;
(iii) to produce ammonia as fertilizer from hydrogen and nitrogen obtained by liquefaction of air, and
(iv) for any really dirty process that needs power. (This is an unwelcome possibility that will need international regulation.)

6. A POSSIBLE SITE NEAR PUERTO RICO

The Marine Science Department of the University of Puerto Rico in Mayaguez has investigated a high potential site near Puerto Rico. The study was funded by the National Science Foundation/Research Applied to National Needs (NSF/RANN), Advanced Technology Research Program and provides for a review of the historical data and a particular inspection of a proposed site off Yabucoa on the south-east coast of Puerto Rico. Four short cruises to the site were made by the R.V. CRAWFORD of the University of Puerto Rico which confirmed conclusions drawn from historical data. These cruises were made in September 1975 and January, March and May 1976. The following summarizes the major points contained in Interim Report on Ocean Thermal Energy Project (Atwood et al., 1975).

The Yabucoa site benefits from all the advantages of the northern Caribbean and the geological structure of the Greater Antilles.

(1) The bathymetry at Yabucoa is ideal for an OTEC plant. Water 1 000 m deep is found within 2 km of the shore, and this water is directly connected with the North Atlantic through the Anegada Passage so that an ample supply of cold water is assured.

(2) The general temperature structure for the region was known from the CICAR-connected PESCA serial station at 17°38'N, 67°00'W which has been occupied twelve times a year by the University of Puerto Rico for the last seven years. Fig. 2 shows the envelope for these data, which also encompasses the data for the site. The year round ΔT is greater than 20°C between the surface and 1 000 m.

(3) Nutrient salts (silicate, phosphate, nitrate, nitrite), salinity, and dissolved oxygen were also measured at the OTEC site and they, too, conformed to the expected pattern. The surface waters are depleted of nutrients which is typical for the tropics, while the deep water shows high values. Although we recommend discharging used water below the mixed layer, it is interesting to note the effects of pumping it out in the photic zone. Phosphate is probably a limiting factor for productivity in the Caribbean; hence, productivity would be determined by the amount of phosphate pumped up. Diatoms among the phytoplankton, and radiolarians and silico-flagellates among the zooplankton use silicate for their skeletons so one can expect blooms of these life-forms. Since Yabucoa is so close to land, a significant amount of the increased productivity could pass to sessile forms and a large increase in sessile biomass could occur.

(4) The site is well protected from open-ocean swell. The southern exposure of the Greater Antilles enjoys over 85 percent "calm" swell even in winter, whereas in the open ocean less than 19 percent "calm" swell is observed. Similarly, swell in the coastal area is never observed in the quadrant N to E (0° to 90°) but in the open ocean this quadrant accounts for over two thirds of all observed swell, and nearly all observations greater than 3.6 m (H.O. 21). These figures are important for installing and servicing the plant from surface vessels and will not affect its endurance, because it will have to be designed to survive hurricanes anyway.

7. CONCLUSIONS

The Caribbean Sea, particularly the northern half, is ideal for the exploitation of the concept of ocean thermal energy conversion (OTEC). The area has a year-round warm surface layer derived from the tropical Atlantic with a current régime such that geostrophy maintains this layer at a depth between 50 and 100 m in the northern half. Currents throughout the northern half are strong enough to provide a constant supply of this warm water to an OTEC plant and thus help prevent temperature short circuiting, but not so strong as to prevent mooring. Below this layer, a rapid thermocline results in water cold enough to be used for OTEC condensors at depths of from 600 to 1 000 m. The bathymetry is such that OTEC floating plants using this cold water can be placed within a few kilometres of shore, providing ready access all year round.

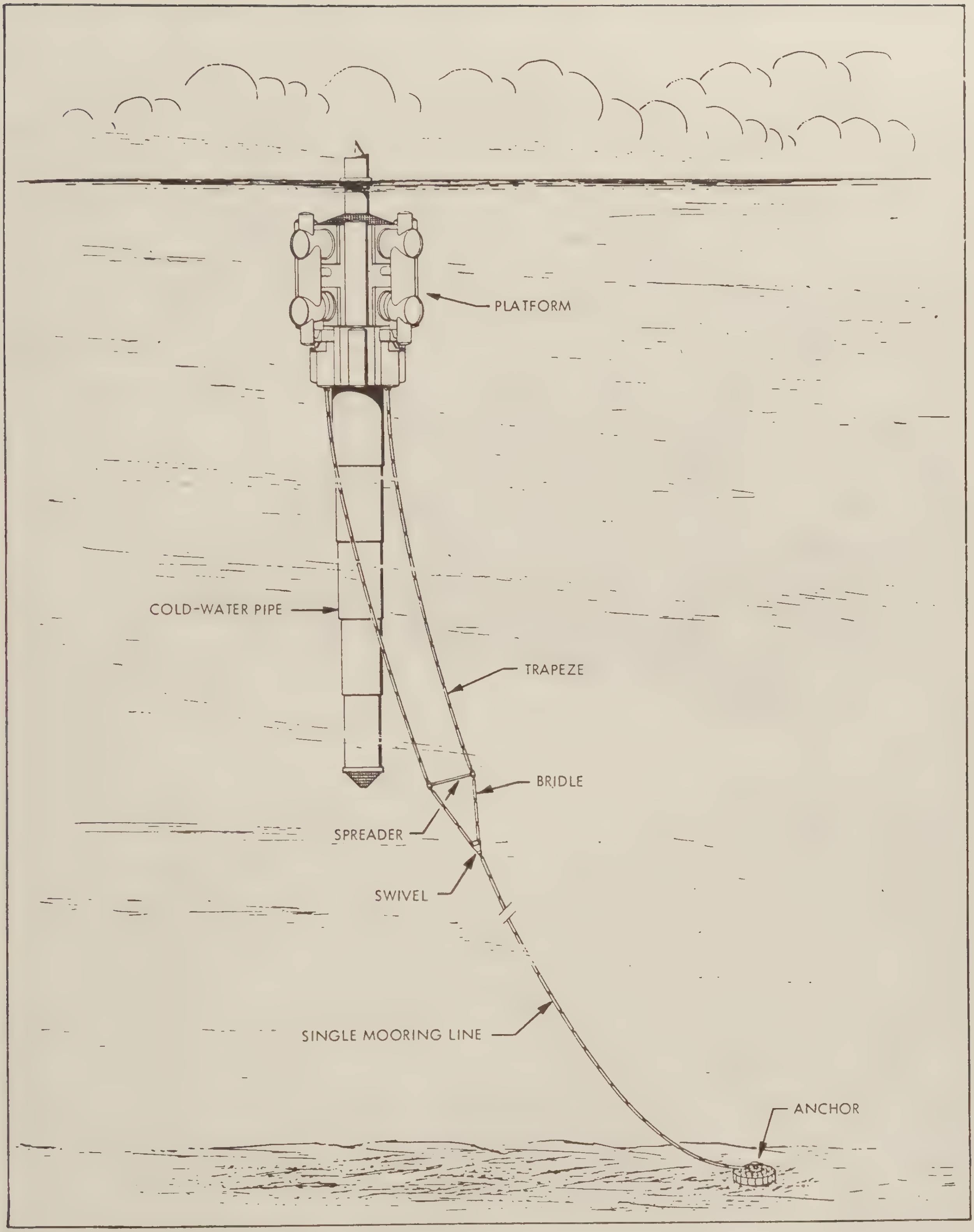
PLATFORM
COLD-WATER PIPE
TRAPEZE
BRIDLE
SPREADER
SWIVEL
SINGLE MOORING LINE
ANCHOR

Fig. 8 Design for an OTEC plant (Lockheed Ocean Systems)

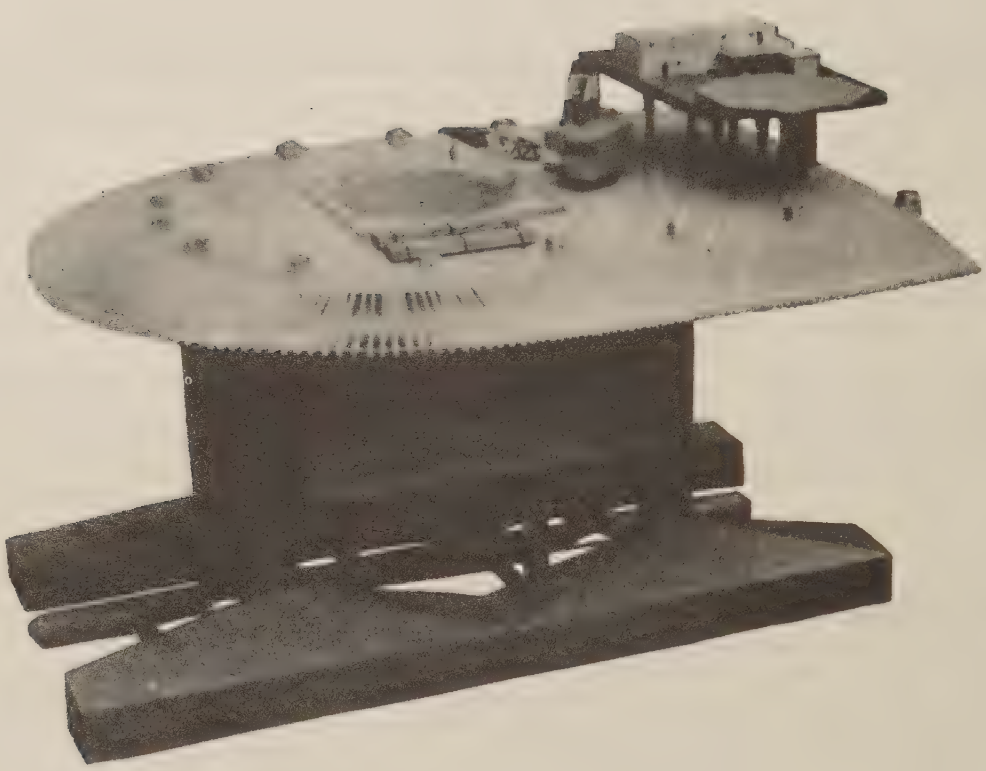

MODEL OF SEA SOLAR POWER PLANT

Fig. 9 Design for an OTEC plant (Sea Solar Power, Inc.)

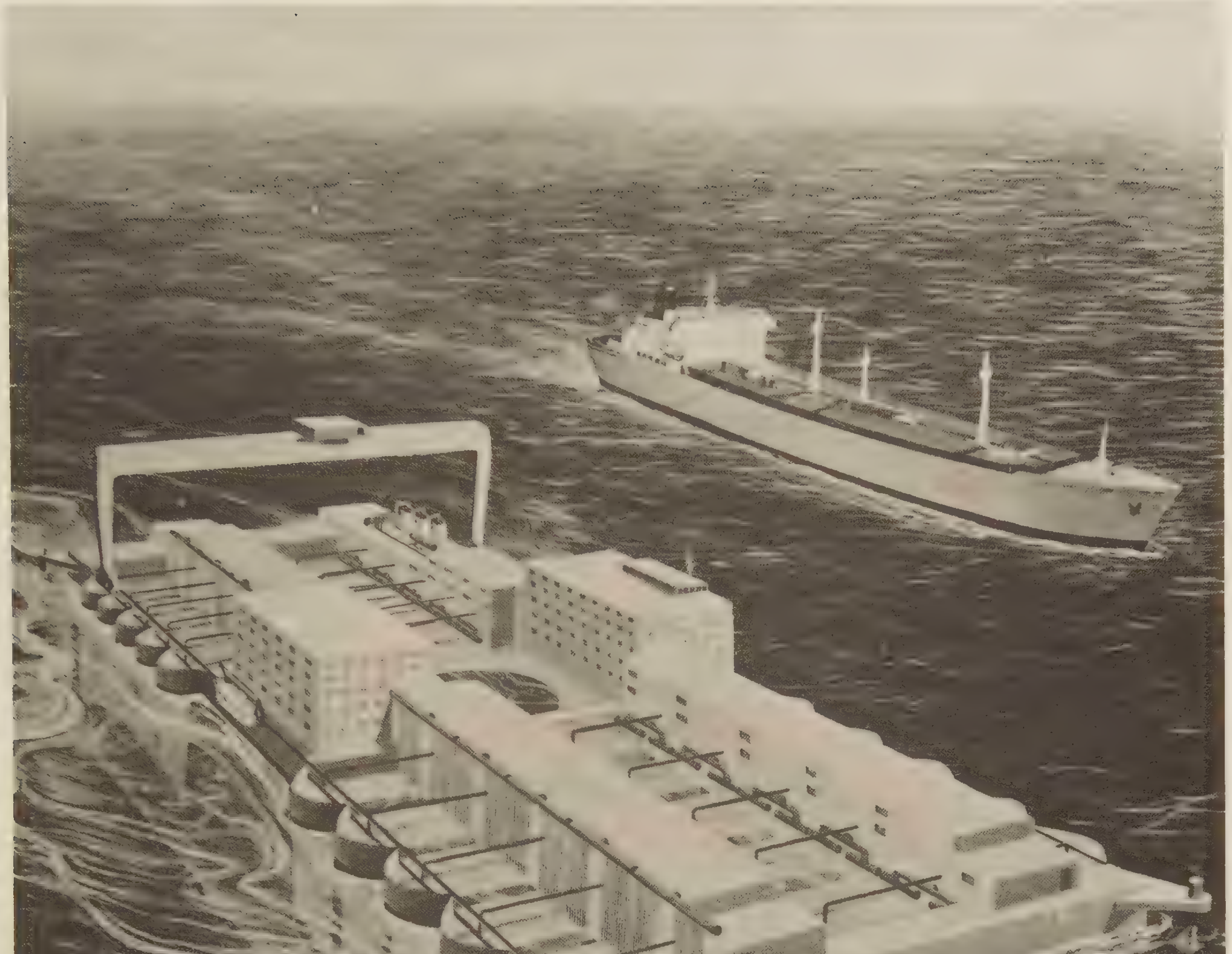

Fig. 10 Design for an OTEC plant (The Johns Hopkins University)

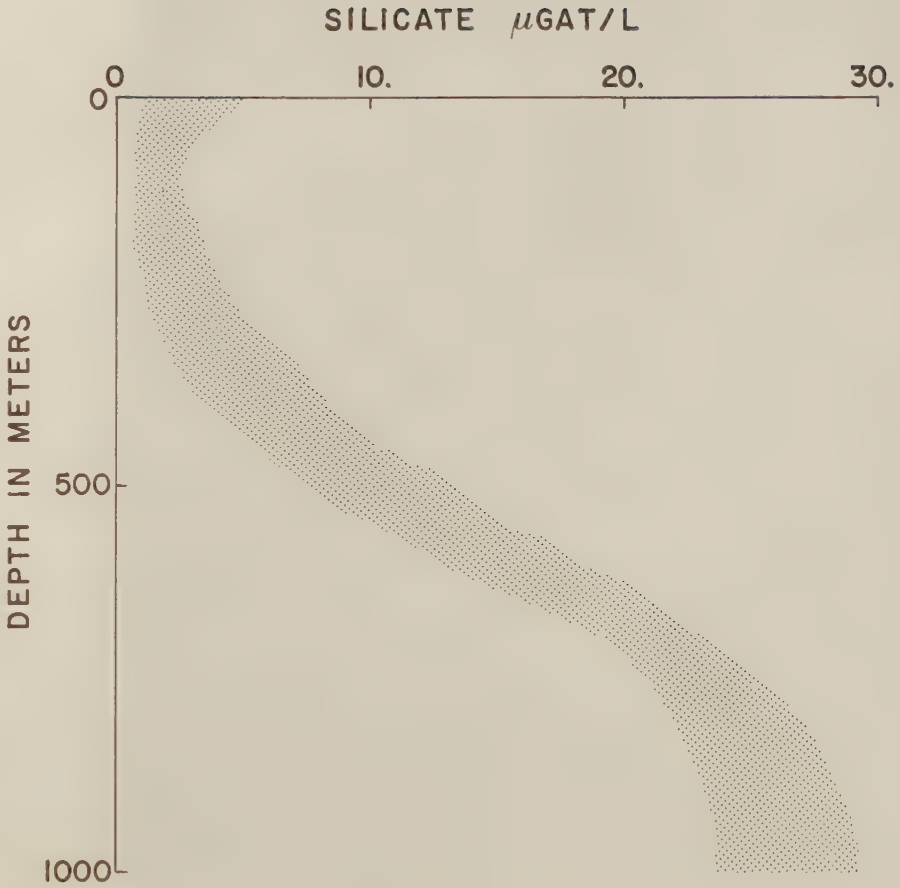

SILICATE / DEPTH AT PESCA SERIAL STATION

Fig. 11 Silicate/depth envelope at 17°38'N, 67°00' W from provisional CICAR data

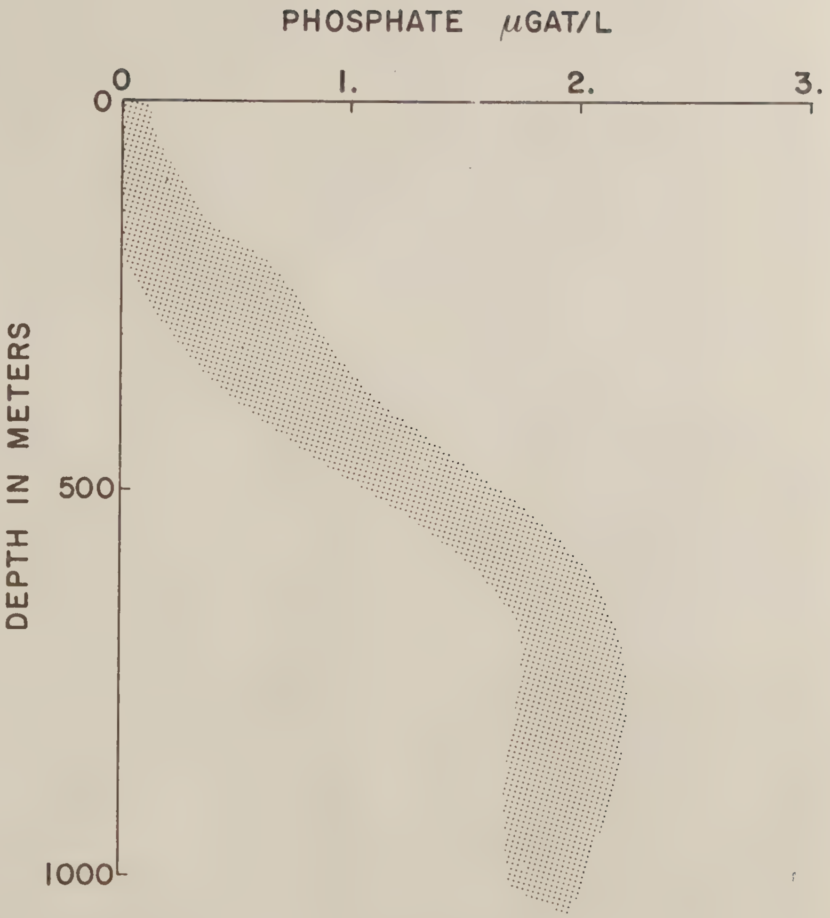

PHOSPHATE / DEPTH AT PESCA SERIAL STATION

Fig. 12 Phosphate/depth envelope at 17°38'N, 67°00'W from provisional CICAR data

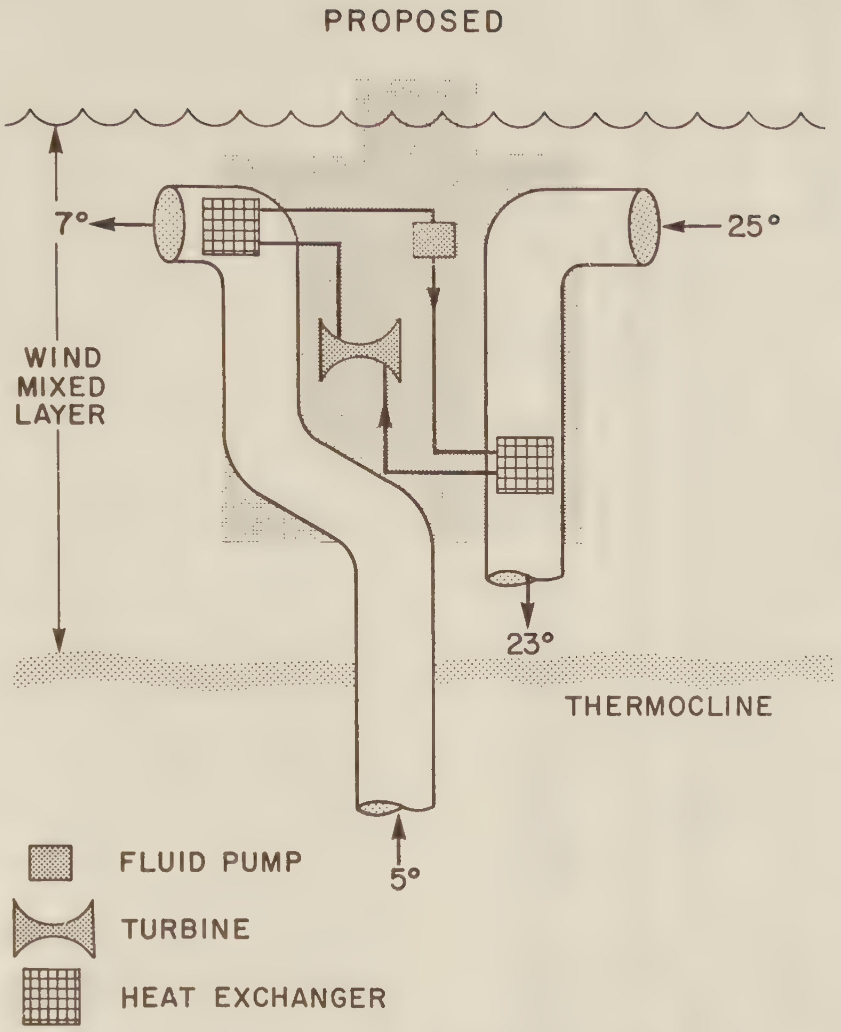
PROPOSED
WIND MIXED LAYER
7°
25°
23°
THERMOCLINE
5°
FLUID PUMP
TURBINE
HEAT EXCHANGER

Fig. 13 Proposed flow system for an OTEC plant

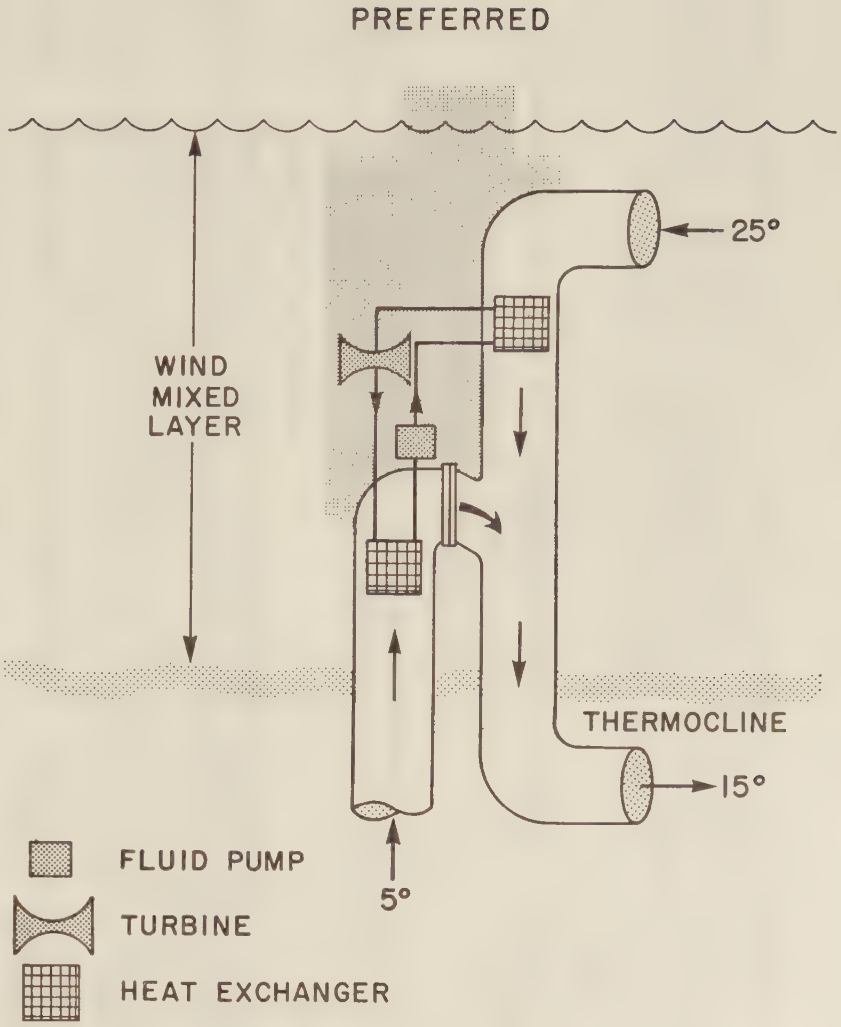
PREFERRED
WIND MIXED LAYER
25°
THERMOCLINE
15°
5°
FLUID PUMP
TURBINE
HEAT EXCHANGER

Fig. 14 Preferred flow system for an OTEC plant

A resource assessment has been made of one specific site off the south-east coast of Puerto Rico by the University of Puerto Rico and it has been shown to have excellent potential for OTEC. Advantages include all of those given above for the northern Caribbean in general plus deep water ports nearby, and power generated can be readily coupled to the existing Puerto Rico power grid.

8. ACKNOWLEDGEMENTS

We wish to thank Mrs. Evangelina Fradera Hernández for preparing the illustrations from our pencil originals.

Corrigendum

In Fig. 14 the evaporator should preferably be placed below the condensor to save energy in pumping the working fluid. (With thanks to Mr. James H. Anderson Jr., Sea Solar Power Inc.)

9. REFERENCES

Atwood, D.K., J.R. Polifka and C.P. Duncan, Temporal variation in mass transport in the
1975 eastern Caribbean Sea. Paper presented to the Eleventh Meeting of the Associated Island Marine Laboratories of the Caribbean, St. Croix, U.S.V.I.

Atwood, D.K. *et al.*, Interim report on ocean thermal energy project. Report to National
1975 Science Foundation, Grant No.AER 75-00145

Düing, W, P. Duncan and J. Meincke, Study questions in physical oceanography. Coral Gables,
1975 University of Miami

Lockheed Missiles and Space Company, Inc. (Ocean Systems), Ocean thermal energy conversion
1975 (OTEC) power plant technical and economic feasibility. Report (NSF/RANN/SE/GI-C937/FR/75/1, LMSC - DO 56566), 12 April 1975

Sea Solar Power, Inc., A conceptual feasibility and cost study for a 100 MWe sea solar power
n.d. plant. Philadelphia, United Engineers and Constructors Inc.

Seltzer, J., Efforts to tap ocean thermal energy gain. *Chem.Eng.News*, 9 Feb. issue:19-20
1976

U.S. Navy Hydrographic Office, Sailing directions. Washington D.C., U.S. Government Printing
1958 Office. (H.O. 21) as revised

PRESENT AND PLANNED SATELLITE OBSERVATIONS OF THE GULF OF MEXICO AND THE CARIBBEAN SEA

by

R. LEGECKIS
National Environmental Satellite Service, NOAA
Washington, D.C. 20233, U.S.A.

CONTENTS

1. INTRODUCTION
2. SATELLITES AND SENSORS
3. LIMITATIONS OF SATELLITE DATA IN OCEANOGRAPHIC APPLICATIONS
4. OPTIMIZATION OF SATELLITE DATA IN OCEANOGRAPHIC APPLICATIONS
5. APPLICATION OF THE SATELLITE DATA TO THE STUDY OF THE GULF STREAM AND THE LOOP CURRENT
6. FUTURE PROGRAMMES
7. CONCLUSIONS
8. REFERENCES
APPENDIX

Abstract

Data from the National Oceanic and Atmospheric Administration's (NOAA) operational satellites have greatly increased our capabilities for oceanographic research. Methods are being developed to improve the mapping and monitoring of ocean currents using the visible and thermal infra-red imagery from the polar orbiting and geostationary satellites. The limitations and capabilities of the satellite data in ocean applications are summarized. The results of two studies are presented to illustrate the use of high resolution data from the NOAA polar-orbiting satellites. The first study shows the effects of bottom topography in controlling the path of the Gulf Stream at latitude 32°N. In the second study the position of the Loop Current in the Gulf of Mexico is mapped during the winter of 1974.

Resumen

Los datos obtenidos por los satélites de la National Oceanic and Atmospheric Administration (NOAA) representan una importante contribución a las investigaciones oceanográficas. Se están estudiando métodos para mejorar la representación gráfica y la observación de las corrientes oceánicas, utilizando las fotografías visibles y de infrarrojos térmicos obtenidas desde los satélites geoestacionarios o en órbitas polares. Se resumen las posibilidades e inconvenientes de los datos obtenidos por estos satélites para las aplicaciones oceánicas. Se exponen los resultados de dos estudios, que ilustran sobre el empleo de los datos de alta resolución obtenidos desde los satélites en órbitas polares de la NOAA. El primer estudio muestra los efectos de la topografía del fondo del mar en la observación de la trayectoria de la corriente del Golfo, a 32°N de latitud. El segundo estudio es una representación gráfica de la posición de la corriente circular del Golfo de México durante el invierno de 1974.

1. INTRODUCTION

Environmental satellites have been used extensively for gathering global meteorological data since 1960. These satellites were developed jointly by the National Aeronautics and Space Administration (NASA) and the National Oceanic and Atmospheric Administration (NOAA) and were then transferred to the National Environmental Satellite Service (NESS), near Washington, D.C., for daily utilization. These satellites have provided weather forecasters with global views of weather systems and improved their prediction capability.

With the improvement of satellite technology in the past decade, new applications in hydrology and oceanography have become possible. In this presentation, an overview is given of the capabilities and the limitations of satellite data for ocean applications. Preliminary results of two satellite data studies are summarized to illustrate: (1) the topographic control of the Gulf Stream, and (2) the seasonal variation of the Loop Current.

2. SATELLITES AND SENSORS

There are two types of satellite systems presently operated by NESS. One system, called the Improved TIROS Operational satellite (ITOS), employs spacecraft that are in a near-polar, sun-synchronous orbit at an altitude of 1 500 km. They are capable of viewing the same area of the earth twice per day. The second system is the Synchronous Meteorological Satellite (SMS), in which the spacecraft remain stationary above a fixed location of the earth in the equatorial plane at an altitude of 36 000 km. The SMS monitors that part of the globe within its field of view every 30 min. There are presently two stationary satellites in orbit: SMS-1 is located at 75°W over North and South America and SMS-2 is at 135°W over the Pacific Ocean. A more complete description of these two satellite systems can be obtained from Schwalb (1972), Fortuna and Hambrick (1974), and Bristor (1975).

Among the sensors carried by these satellites, the most useful for oceanographic applications are the scanning type radiometers. They can detect sea surface temperature differences of approximately 0.5°C with their infra-red channels and identify cloud-free areas of the ocean with their visible channels. The ITOS carries a Scanning Radiometer (SR) which measures reflected solar radiation in the range 0.5-0.7 µm and emitted infra-red radiation in the atmospheric "window" region of 10.5-12.5 µm. The ground resolution of the SR is 4 km in the visible and 8 km in the infra-red and it is capable of providing day and night coverage of the entire globe.

A second type of radiometer on the ITOS is the Very High Resolution Radiometer (VHRR) which is sensitive to energy in the 0.6-0.7 µm and 10.5-12.5 µm bands and has a ground resolution of 1 km. The VHRR covers the United States and adjacent ocean areas. In addition, it has the capability to acquire data from other areas of the globe using an onboard recorder to store the data. The stored data are limited to an area of about 3 000 km on a side. The VHRR data have provided the most detailed data yet available concerning the surface temperature structure of ocean currents and eddies.

The SMS carries a Visible and infra-red Spin-Scan Radiometer (VISSR) with a spatial resolution of 1 km in the visible (0.55-0.75 µm) channels and 8 km in the infra-red (10.5-12.6 µm). Although the VISSR was designed to provide cloud images at 30-min intervals, the high frequency of observations also improves the chances of viewing cloud-free areas of the ocean.

3. LIMITATIONS OF SATELLITE DATA IN OCEANOGRAPHIC APPLICATIONS

There are several factors that limit the usefulness of the infra-red sensors in oceanographic applications. These factors are shown below:

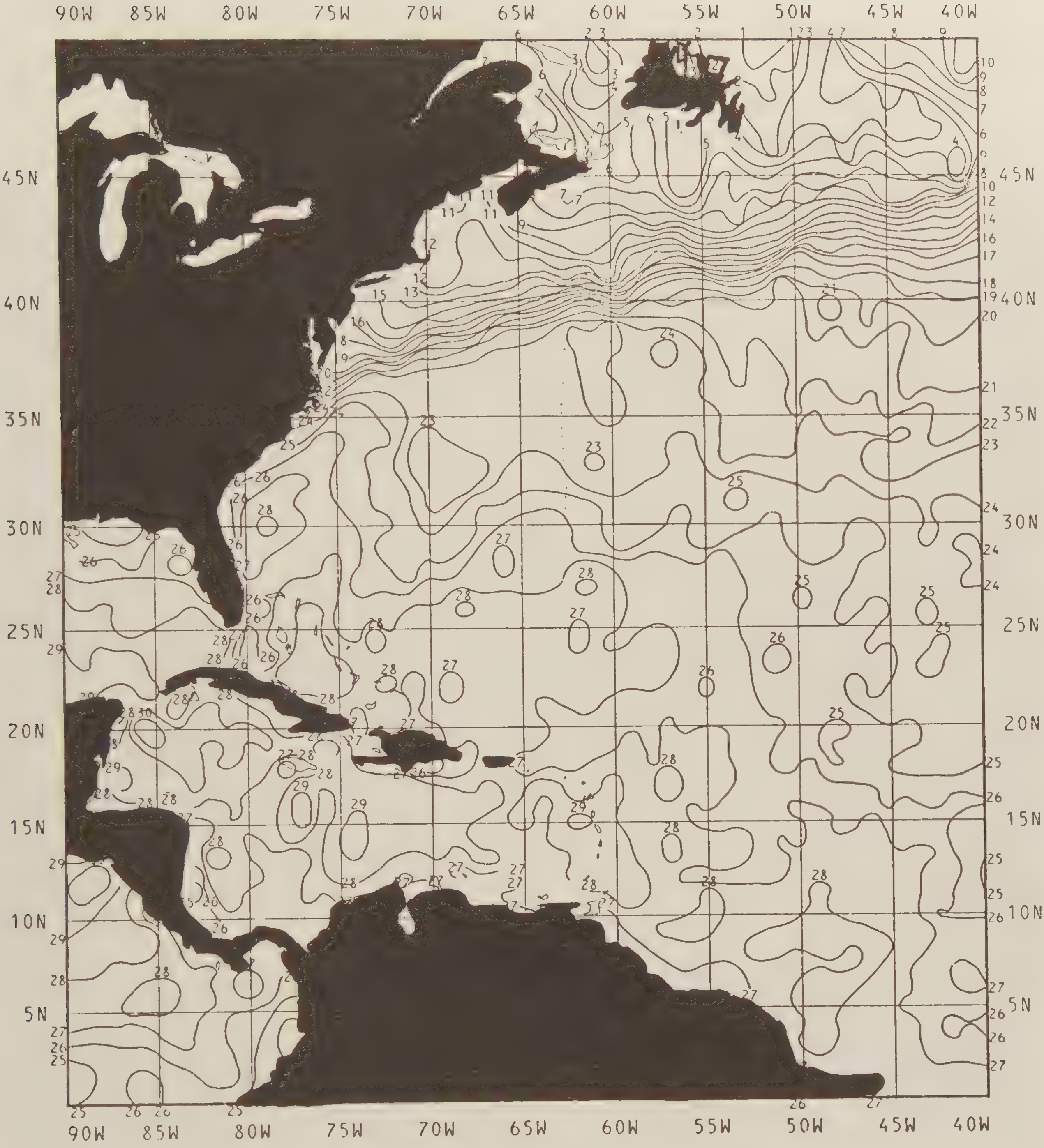
90W
85W
80W
75W
70W
65W
60W
55W
50W
45W
40W
45N
40N
35N
30N
25N
20N
15N
10N
5N

Fig. 1 Global Operational Sea Surface Temperature Composite (GOSSTCOMP) is shown for 1 June 1976. The temperature contours have been plotted at 1°C intervals. Only the western Atlantic Ocean is shown in this sample

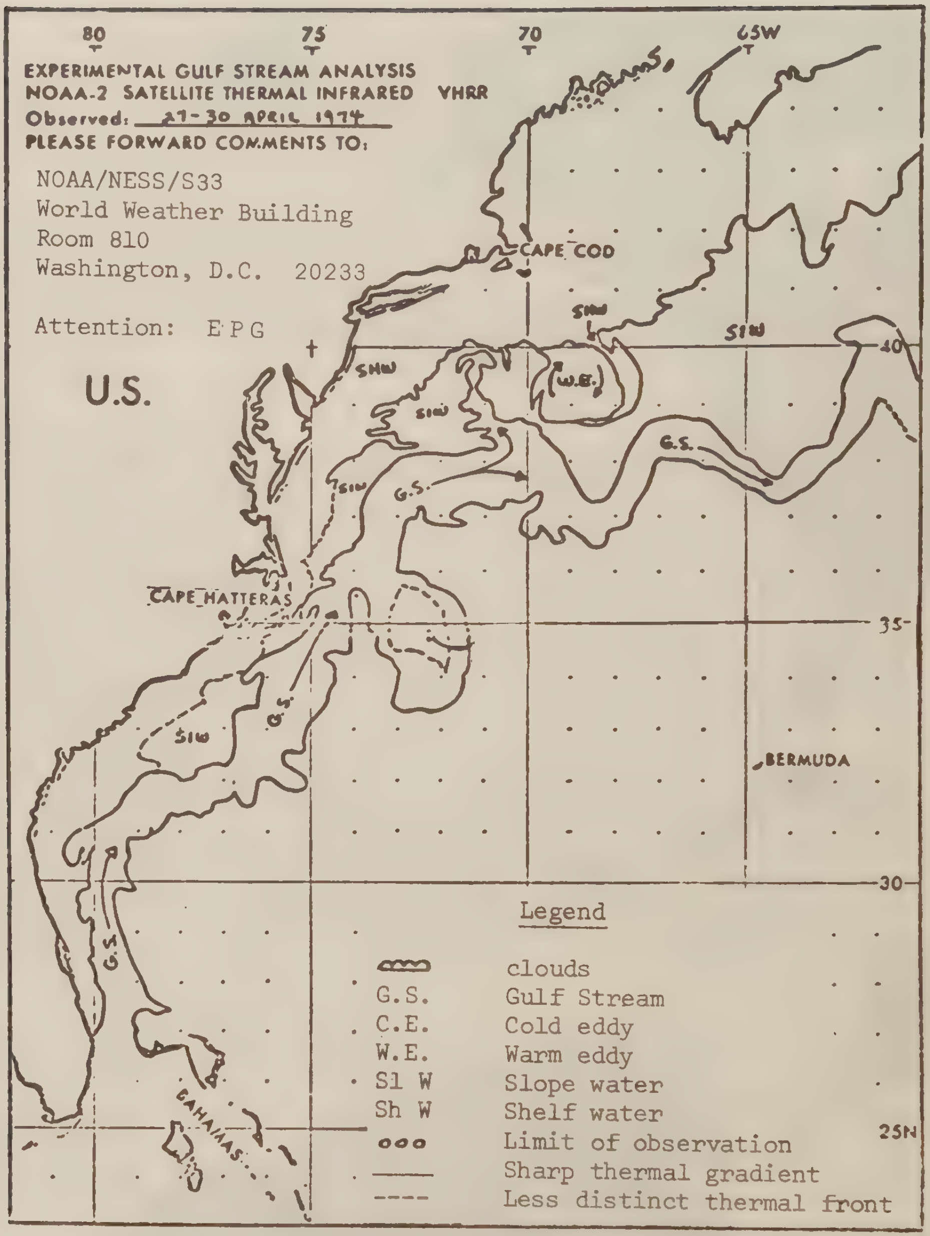
80
75
70
65W
EXPERIMENTAL GULF STREAM ANALYSIS
NOAA-2 SATELLITE THERMAL INFRARED VHRR
Observed: 27-30 APRIL 1974
PLEASE FORWARD COMMENTS TO:
NOAA/NESS/S33
World Weather Building
Room 810
Washington, D.C. 20233
Attention: EPG
U.S.
CAPE COD
ShW
SlW
SlW
ShW
(W.E.)
SlW
G.S.
SlW
G.S.
40
CAPE HATTERAS
35
G.S.
SlW
BERMUDA
30
G.S.
BAHAMAS
25N
Legend
clouds
G.S. Gulf Stream
C.E. Cold eddy
W.E. Warm eddy
Sl W Slope water
Sh W Shelf water
ooo Limit of observation
Sharp thermal gradient
Less distinct thermal front

Fig. 2 The position of the Gulf Stream is shown in the Gulf Stream Analysis product prepared by the Environmental Products Group (Appendix A). This analysis is produced each week and is based on VHRR infra-red data from the ITOS spacecraft

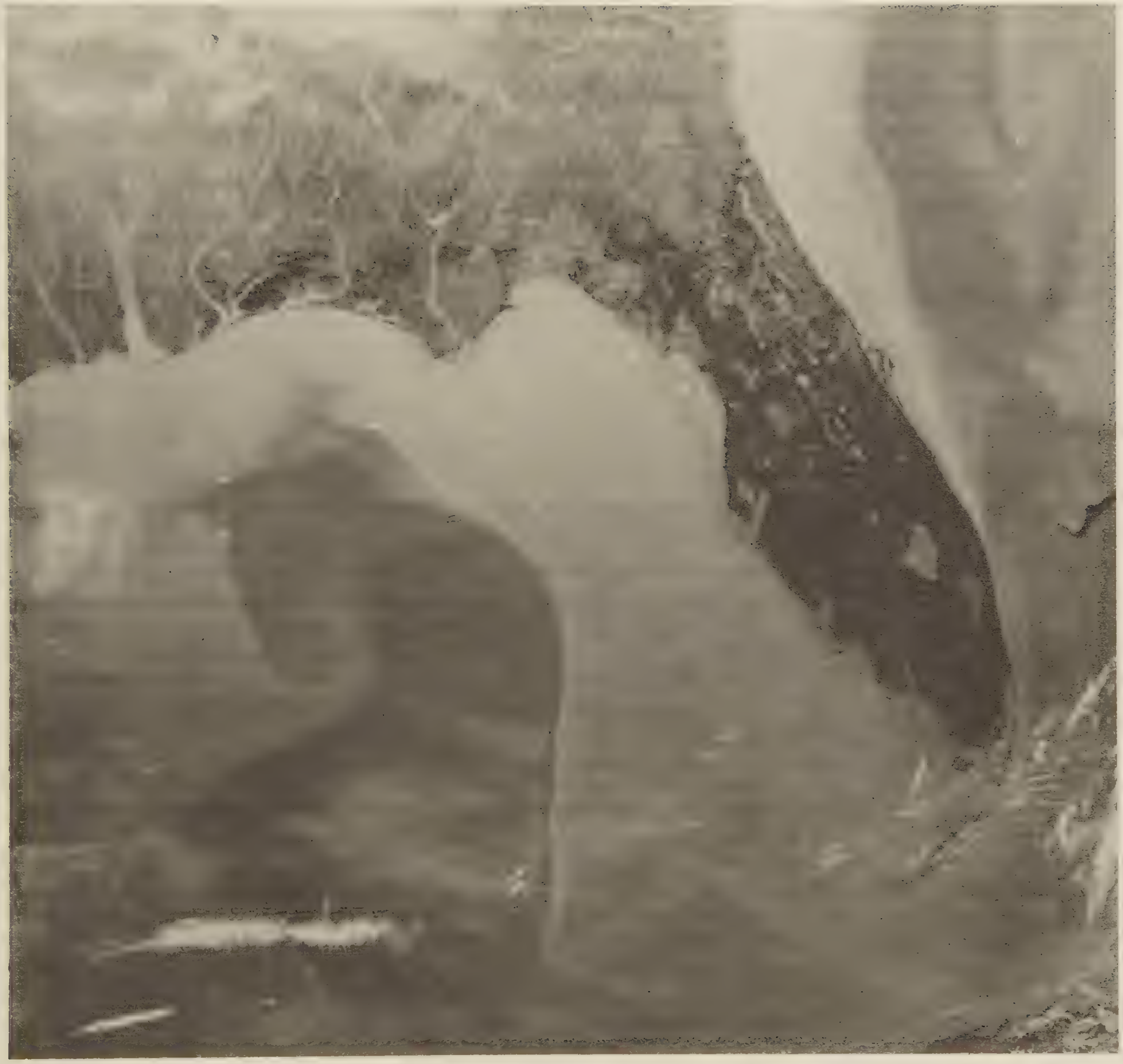

Fig. 3 An enhanced infra-red VHRR image of the Loop Current and the Gulf Stream is shown from the ITOS (NOAA-3) satellite for 31 March 1974. The darkest shade of grey represents the warmest temperature

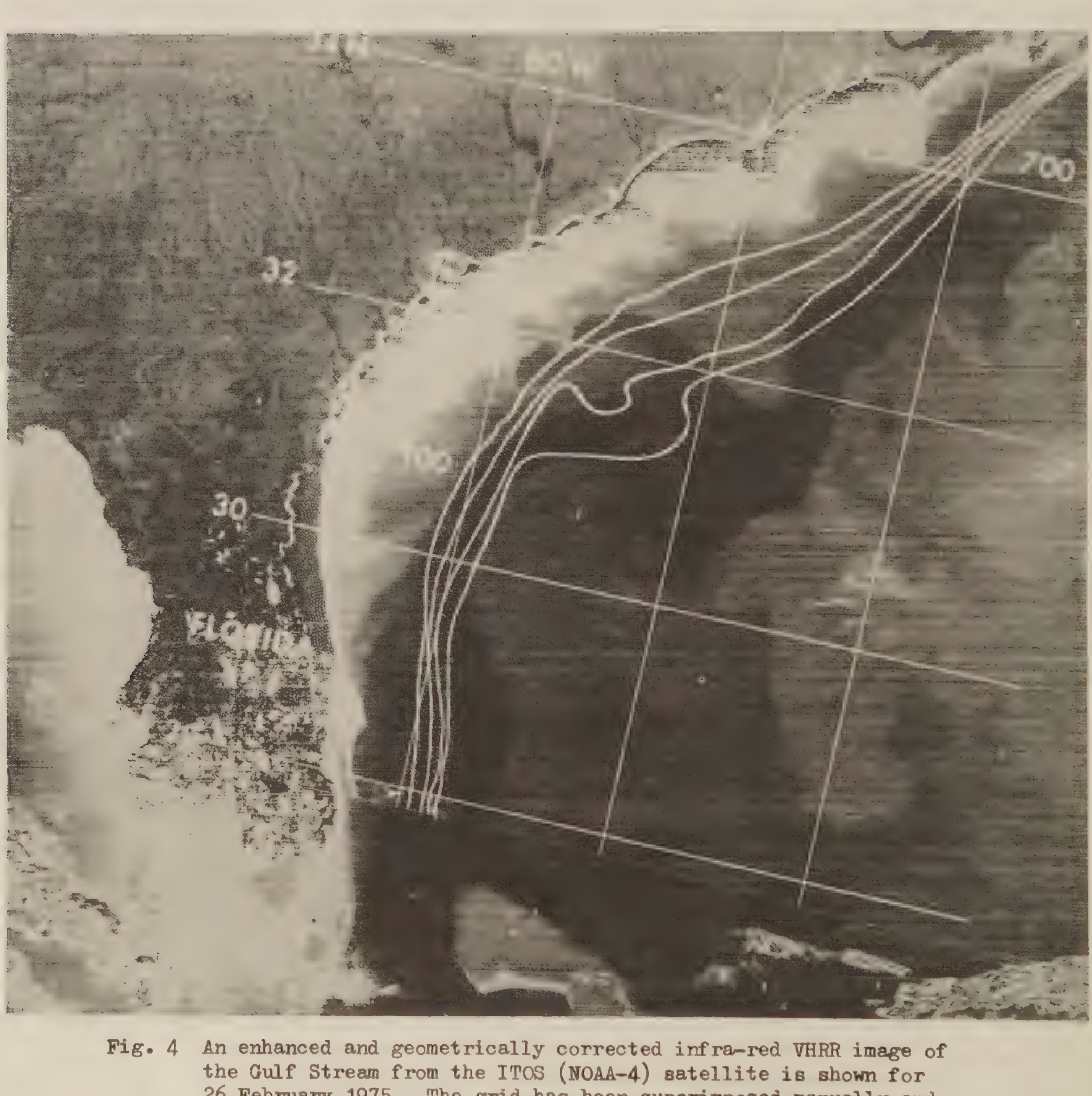

Fig. 4 An enhanced and geometrically corrected infra-red VHRR image of the Gulf Stream from the ITOS (NOAA-4) satellite is shown for 26 February 1975. The grid has been superimposed manually and the bathymetry contours are in metres. The eastward deflection of the current at 32°N is apparent in this image. A composite of the positions of the western boundary of the current during the winter of 1975 is shown in Fig. 5

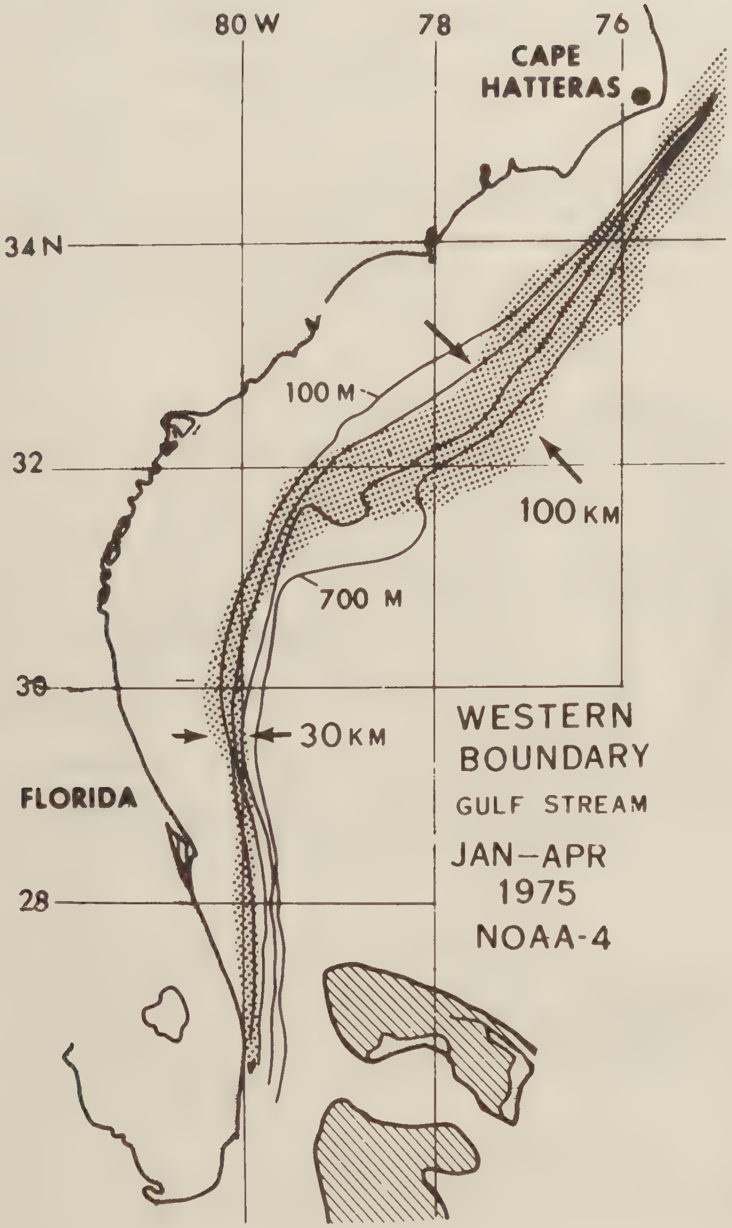
80 W
78
76
CAPE HATTERAS
34 N
32
30
28
100 M
100 KM
700 M
30 KM
FLORIDA
WESTERN BOUNDARY
GULF STREAM
JAN–APR 1975
NOAA-4

Fig. 5 The shaded area is a composite of 20 positions, of the Gulf Stream's western boundary as observed from the ITOS VHRR imagery from January to April of 1975. The displacement of the Gulf Stream position, perpendicular to the 100 m isobath, increases from 30 to 100 km downstream of latitude 32°N

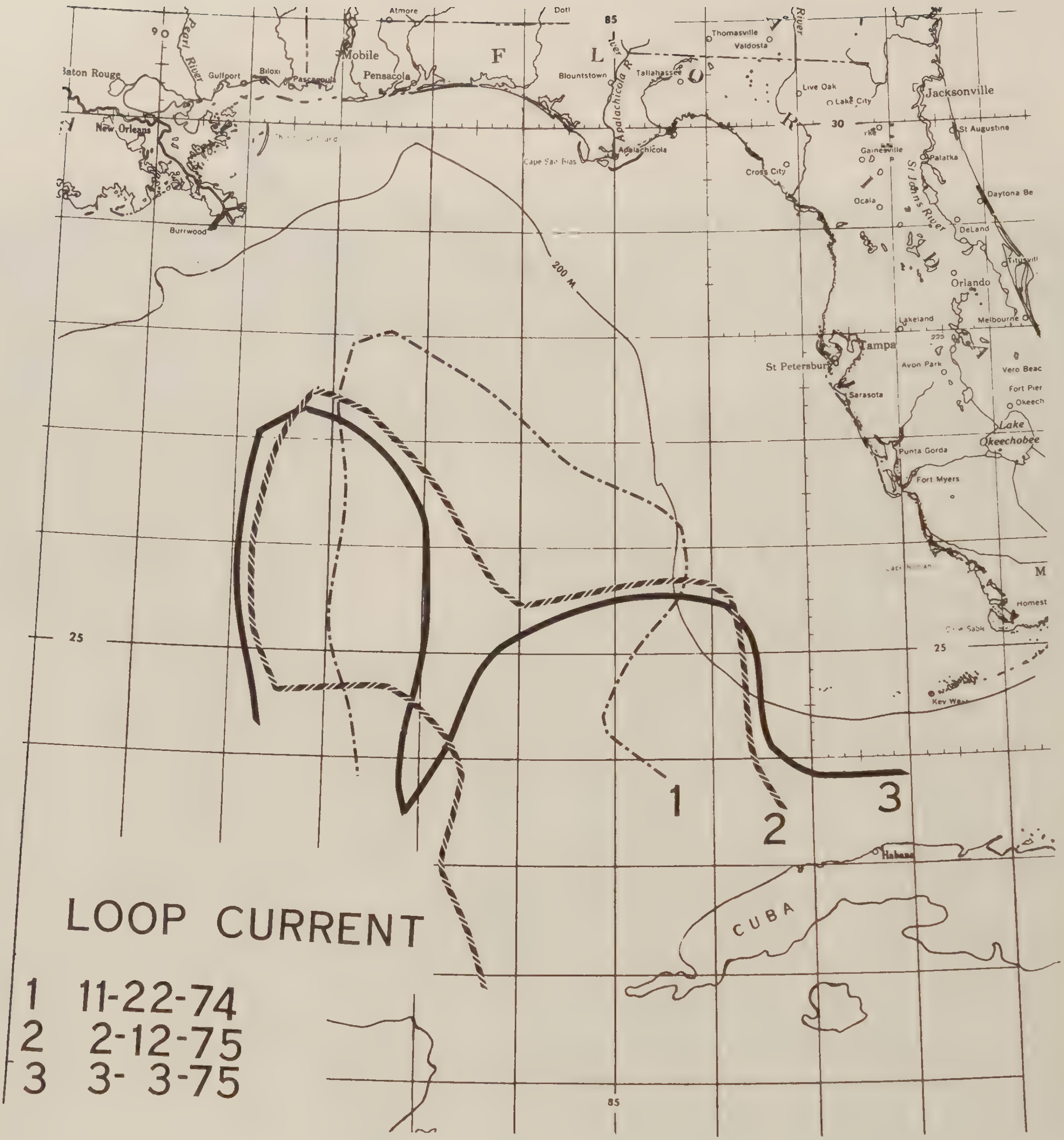
LOOP CURRENT
1 11-22-74
2 2-12-75
3 3- 3-75
1
2
3
200 M
25
85
90
30
Baton Rouge
New Orleans
Burrwood
Pearl River
Gulfport
Biloxi
Pascagoula
Mobile
Atmore
Pensacola
F L O R I D A
Blountstown
Tallahassee
Apalachicola R
Apalachicola
Cape San Blas
Thomasville
Valdosta
Live Oak
Lake City
Jacksonville
St Augustine
Gainesville
Palatka
St Johns River
Cross City
Ocala
Daytona Be
DeLand
Titusvill
Orlando
Lakeland
Melbourne
Tampa
St Petersburg
Avon Park
Vero Beac
Fort Pier
Okeech
Sarasota
Lake Okeechobee
Punta Gorda
Fort Myers
M
Homest
Key West
Habana
CUBA

Fig. 6 The positions of the Loop Current is shown for: (1) 22 November 1974, (2) 12 February 1975, and (3) 3 March 1975. These positions were obtained from ITOS VHRR infra-red imagery. The sea surface temperature gradients were used to locate the current. This is a preliminary plot and there is a +/-20 km uncertainty in the position measurements

(1) clouds,
(2) atmospheric moisture,
(3) solar insolation,
(4) satellite system noise, and,
(5) resources available for data processing.

3.1 Clouds and Atmospheric Moisture

Clouds obscure the ocean surface and prevent measurements of the sea surface temperature. In cloud-free areas of the ocean, atmospheric moisture attenuates the infra-red signal and introduces an error in the determination of the absolute values of the sea surface temperature. Methods of resolving this problem have been proposed by Smith et al. (1970), Braun (1971), Maul and Sidran (1973), and Cogan and Willand (1974).

3.2 Solar Insolation

Another limiting factor is that increased solar insolation during the warmer seasons produces a nearly isothermal sea surface. This prevents the detection of temperature gradients associated with quasi-geostrophic currents and eddies. For example, the sea surface temperature gradients due to the Gulf Stream south of Cape Hatteras and the Loop Current in the Gulf of Mexico are detectable only during the winter and spring months. The solar insolation effect has also prevented the detection of sea surface temperature gradients associated with currents in the Caribbean Sea. However, along the western coasts of Mexico and Nicaragua, areas of intense upwelling have been detected by Stumpf (1975) in spite of the strong solar insolation at that latitude.

3.3 Satellite Systems Noise

Electronic noise associated with the sensor, and introduced during data recording and transmission, limits the detection of small sea surface temperature gradients and increases the error in the absolute temperature measurements. The noise factor for ITOS can become as large as 1°C to 2°C, whereas for the SMS it is about 0.5°C.

3.4 Resource Availability

The last limitation which must be considered is the availability of resources to reprocess and optimize the satellite data for oceanographic applications. Satellite data reprocessing in ocean applications is necessary because the satellites were designed primarily to meet meteorological imaging requirements. The large volume of data involved, and the limited resources presently available have made it impossible to reprocess anything beyond selected data for ocean studies.

4. OPTIMIZATION OF SATELLITE DATA IN OCEANOGRAPHIC APPLICATIONS

Different methods have been developed to optimize the satellite data for ocean applications. These are shown below:

(1) Statistical model of global sea surface temperatures
(2) Image interpretation
(3) Digital data processing
(4) Image enhancement
(5) Geometric corrections
(6) SMS time-lapse sequences (movie loops)

4.1 Statistical Model of Global Sea Surface Temperatures

The ITOS SR infra-red data are being used to produce experimental maps of global sea surface temperatures (called GOSSTCOMP). A complex statistical method is used to filter out clouds in 100 km-square ocean areas and to select the temperature that is most representative of the sea surface temperature in each area. This temperature is corrected for atmospheric attenuation effects using moisture information from the Vertical Temperature Profiling Radiometer (VTPR) carried by ITOS. An example of a contoured temperature map made by this procedure is shown in Fig. 1. A more complete description of the statistical method can be obtained from Brower et al. (1976).

4.2 Image Interpretation

All of the scanning radiometer data are presently available in the form of grey tone photographic images of visible and infra-red scenes. Some ocean-oriented image interpretation is provided by NESS. For example, the Environmental Products Group publishes a weekly summary of the position of the Gulf Stream based on VHRR images as shown in Fig. 2. Similar position summaries of the Loop Current and the Gulf Stream, based on SMS images, are available from the Miami office of the NESS's Satellite Field Services Stations (SFSS). The sources of the satellite data are listed in Appendix A.

4.3 Digital Data Processing

It is important to note that satellite infra-red and visible data can be manipulated with greatest flexibility when they are available in digital form. Therefore, much of the optimization of satellite data for specific ocean applications cannot begin unless the data are acquired in digital form. At present, only the ITOS data are available to interested users from NESS. However, plans are being formed to extend this service to include SMS data. Digital data can be requested through the sources listed in Appendix A.

4.4. Image Enhancement

The satellite infra-red detectors have a temperature response from approximately -90°C to +60°C. The infra-red data in this temperature range are normally displayed by NESS on grey tone photographic film to produce images of clouds, land and water. The colder scenes, such as clouds, are assigned lighter shades of grey; the warmer scenes, such as land and water, appear as darker shades of grey. Because the range of sea surface temperature extends from about 0°C to 40°C, it is advantageous to assign the available shades of grey to this narrower temperature range, thus allowing the ocean features to be distinguished more clearly. This process is called image enhancement. A sample of an enhanced VHRR image of the Gulf Stream and the Loop Current is shown in Fig. 3.

It is also possible to enhance the satellite visible or infra-red data by assigning colours to specific radiance values and displaying the scene on a video monitor. At NESS, this capability is achieved on the Man-Machine Interactive Processing System (MMIPS) located at the World Weather Building near Washington, D.C. Since the operator of this system can control the relationship between each colour and temperature increment, it is possible to interpret the colours quantitatively.

4.5 Geometric Corrections

The ITOS VHRR imagery is distorted because of the Earth's curvature and rotation. Presently, a universal perspective grid is used to geographically locate ocean features in the VHRR imagery. The user can then transfer these features to a map. However, it is also possible to reprocess the VHRR digital data to remove the geometric distortions as described by Legeckis and Pritchard (1976). The geometrically corrected images can be compared directly with each other and can also be projected on an equal area map (Modified Universal Transverse Mercator Projection). This procedure allows the ocean features to be related directly to the coastlines and to the ocean's bathymetry. A sample of a geometrically corrected image of the Gulf Stream with a map overlay is shown in Fig. 4.

The SMS imagery is also geometrically distorted due to the Earth's curvature. However, since the SMS is stationary relative to the earth, the SMS images always have the same geometric distortion. Therefore, direct comparisons of images can be made without time-consuming geometric corrections. This is especially useful in making time-lapse sequences of SMS images.

4.6 SMS Time-Lapse Sequences (movie loops)

Time-lapse sequences of SMS images, called movie loops, are presently used operationally at NESS to track clouds and storms. Upper-level wind vectors are computed over the ocean on a daily basis from these movie loops. Since ocean thermal patterns change slowly in the course of a week, they appear nearly stationary relative to the rapidly moving clouds. This technique has been used to study ocean currents by Maul and Baig (1975) and Legeckis (1975). Movie loops, enhanced for sea surface temperatures, are now being made operational for the Gulf Stream and the Gulf of Mexico and are available from the Miami SFSS (Appendix A).

5. APPLICATION OF THE SATELLITE DATA TO THE STUDY OF THE GULF STREAM AND THE LOOP CURRENT

To illustrate how the data from the ITOS VHRR sensor can be used to provide useful information in ocean applications, the results of two studies are summarized. Geometrically corrected and enhanced images were used in these studies.

The Gulf Stream south of Cape Hatteras and the Loop Current in the Gulf of Mexico are detectable in the satellite infra-red imagery in the winter and spring seasons. At latitude 32°N, a persistent deflection of the Gulf Stream occurs; this was noted in satellite data as early as 1971 by Pashinski and Maul (1973). To obtain a better understanding of this deflection, the ITOS VHRR imagery has now been reviewed from 1973 to 1976. The results show that the western boundary of the current is deflected from 50 to 150 km eastward and is controlled by the rise in bottom topography at 32°N in accordance with the conservation of potential vorticity. In addition to this deflection, the western boundary of the current is time-dependent and exhibits wavelike perturbations along its length. Downstream of 32°N, these waves can reach amplitudes of 100 km whereas upstream of 32°N, the wave amplitudes do not exceed 30 km. This result is shown in Fig. 5 in which the positions of the western edge of the Gulf Stream have been composited between December 1974 and April 1975. The change in the wave amplitude at 32°N shows that bottom topography may act as an additional perturbation mechanism for the time-dependent motions of the Gulf Stream.

Preliminary results of a second study are shown in Fig. 6. Three positions of the Loop Current are plotted between November of 1974 and March of 1975. This sequence of events shows that the Loop Current pinches off between 12 February 1975 and 3 March 1975. The detachment process has been reported previously by Leipper (1970) from direct measurements of the position of the 22°C isotherm. Therefore, the ITOS VHRR data offer the opportunity to study the growth and decay process of the Loop Current during the winter and spring months.

Although both of these studies are being made using the ITOS VHRR imagery, similar results can be obtained from the SMS. Both the Gulf Stream and the Loop Current are presently plotted on a regular basis at the Miami SFSS and interested parties may contact S. Baig (Appendix A) for the availability of these products.

6. FUTURE PROGRAMMES

In 1978, the ITOS satellite system will be replaced by the next generation of NOAA polar orbiters called TIROS-N (Ludwig, 1974). This system will have the capability for global (4 km resolution) and regional (1 km resolution) observations of the oceans four times each day. Because of several improvements in the new radiometer and in the data transmission procedures, it is expected that the electronic noise will be reduced; thus the sea surface temperature measurements will be more accurate. In addition, the infra-red sensor will have two channels (3.55–3.99 µm) and 10.5–11.5 µm). The data from the two infra-red channels will be used jointly to improve the atmospheric attenuation corrections, and this will increase the accuracy of the absolute sea surface temperature measurements.

Some of the other satellite systems that are planned by NASA and that have potential applications in oceanography are briefly summarized below. Landsat-C will be launched in late 1977; it will be able to make infra-red measurements with a resolution of 250 m, but only with an 18-day cycle over any given area. A description of Landsat-C can be obtained from NASA (1976). In 1978, two other systems will be launched: SEASAT-A will be dedicated to oceanographic applications. It will be used to measure ocean tides, waves, winds, and currents primarily by means of microwave sensors. The SEASAT-A potentials and systems are described by Nagler and McCandless (1975). NIMBUS-G will carry a Coastal Zone Color Scanner which will be capable of detecting chlorophyll and sediment concentrations in the oceans. In addition, a scanning, multichannel, microwave radiometer will measure ocean surface winds. A more complete description of the NIMBUS-G sensors is given by Streaker (1975).

7. CONCLUSIONS

Perhaps the greatest advantage of satellite data is that it offers the opportunity to view the oceans on a synoptic scale. Although there are limitations in the application of satellite data to ocean studies, these limitations will decrease as satellite technology continues to improve. The challenge for oceanographers, in the coming decade, is to find the human and material resources to make satellite data a useful tool in ocean research.

8. REFERENCES

Braun, C., 1971 Limits on the accuracy of infrared radiation measurements of sea-surface temperature from a satellite. NOAA Tech.Memo., (NESS 30)

Bristor, C.L., 1975 Central processing and analysis of geostationary satellite data. NOAA Tech.Memo., (NESS 64)

Brower, R. *et al.*, 1976 Satellite derived sea-surface temperatures from NOAA spacecraft. NOAA Tech.Memo., (NESS 78), National Environmental Satellite Service, Washington, D.C. 20031

Cogan, J.L. and J.H. Willand, 1974 Mapping of sea surface temperature by the NOAA-2 Satellite. Prepared for the Environmental Prediction Research Facility, Naval Postgraduate School, Monterey, California, by Environmental Research and Technology, Inc. 72 p.

Fortuna, J.J. and L.N. Hambrick, The operation of the NOAA Polar Satellite System. NOAA Tech.Memo., (NESS 60)

Legeckis, R., 1975 Application of synchronous meteorological satellite data to the study of the time dependent sea surface temperature change along the boundary of the Gulf Stream. Geophys.Res.Lett., 2(10):435–8

Legeckis, R. and J. Pritchard, 1976 Algorithm for correcting the VHRR imagery for geometric distortions due to the earth's curvature and rotation and roll attitude errors. NOAA Tech.Memo., (NESS 77)

Leipper, D.F., A sequence of current patterns in the Gulf of Mexico. J.Geophys.Res.,
1970 73(3):637-57

Ludwig, G.H., The future polar orbiting environmental satellite system. In Proceedings
1974 of IEEE Electronics and Aerospace Systems Conference, Oct. 7-9, 1974. Washington, D.C., IEEE, pp. 498-502

Maul, G.A. and S. Baig, A new technique for observing mid-latitude ocean currents from
1975 space. In Papers from the 41st Annual Meeting, American Society of Photogrammetry, Mar. 9-14, 1975. Falls Church, Va., American Society of Photogrammetry.

Maul, G.A. and M. Sidran, Atmospheric effects on ocean surface temperature sensing from
1973 the NOAA satellite scanning radiometer. J.Geophys.Res., 78:1909-16

NASA, Office of International Affairs, Code I. Washington, D.C., U.S. Government Printing
1976 Office

Nagler, R.G. and S.W. McCandless, Jr. Operational oceanographic satellites. Report to
1975 NASA under Contract NAS-7-100, 12 p.

Pashinski, D.J. and G. Maul, Use of ocean temperature while coasting between the straits
1973 of Florida and Cape Hatteras. Mar.Weather Log, 17(1):1-3

Schwalb, A., Modified version of the improved TIROS operational satellite. NOAA Tech.
1972 Memo., (NESS 35)

Smith, W.L. et al., The determination of sea-surface temperatures from satellite high
1970 resolution infrared window radiation measurements. Mon.Weather Rev., 98:604-11

Streaker, M.D., The NIMBUS-G sensor systems: a preliminary description. Goddard Space
1975 Flight Center, (X-430-74-72):39 p.

Stumpf, H.G., Satellite detection of upwelling in the Gulf of Tehuantepec, Mexico.
1975 J.Phys.Oceanogr., 5(2):383-8

APPENDIX

Satellite data and application services are provided by NOAA's National Environmental Satellite Service (NESS), the Environmental Data Service (EDS), and the NESS's Satellite Field Services Stations (SFSS). These are listed below and readers may contact them for the latest inventory of ocean-related products.

Dr. E.P. McClain
Environmental Sciences
NOAA/NESS - S33
World Weather Building (Room 810)
Washington, D.C. 20233

Mr. R. Koffler
Environmental Products Group
NOAA/NESS - S126
World Weather Building (Room 806)
Washington, D.C. 20233

Mr. E. Hoppe
Environmental Data Services - D543
NOAA/World Weather Building (Room 606)
Washington, D.C. 20233

Mr. R. Mairs
NOAA/NESS/SFSS (S1223)
World Weather Building (Room 506)
Washington, D.C. 20233

Mr. L. Breaker
NOAA/NESS/SFSS (S1229)
660 Price Avenue
Redwood City, California 94063

Dr. S. Baig
NOAA/NESS/SFSS (S1224)
P.O. Box 8286
Coral Gables, Florida 33124

GUIDELINES FOR REGIONAL BASELINE STUDIES OF CONTAMINANTS IN COASTAL AREAS

by

E.F. MANDELLI
UNDP/Unesco
Centro de Ciencias del Mar y Limnología de la
Universidad Nacional Autónoma de México

CONTENTS

1. INTRODUCTION
2. DEVELOPMENT OF THE BASELINE EXERCISE
3. SUMMARY REMARKS
4. REFERENCES

Abstract

Baseline regional studies concerning marine contaminants should be aimed at the control of contaminant inputs, whether or not the present levels are considered dangerous to marine organisms and/or man. In the organization of such studies it is reasonable to assume that some problems will arise due to coordination procedures, shortage of manpower, and/or availability of funds and resources. International programmes are now being developed to formulate appropriate guidelines to implement baseline studies. In this paper I will discuss the necessary steps that will minimize the problems arising from the implementation of such guidelines, particularly in the Caribbean and adjacent areas.

Resumen

Los estudios básicos regionales sobre contaminantes en el medio marino deben tener como finalidad controlar las descargas de estos contaminantes, sean o no peligrosos para la salud de la población o para los organismos marinos, sus niveles actuales. Al organizar esos estudios regionales, es de suponer que surjan problemas de coordinación, de escasez de personal capacitado, o de falta de fondos. Se están preparando actualmente programas internacionales, con las normas apropiadas para la ejecución de dichos estudios. En este trabajo se discuten las medidas necesarias para minimizar los problemas que plantee la ejecución de tales normas, particularmente en el Caribe y zonas adyacentes.

1. INTRODUCTION

As man relies more and more upon the mobilization and use of natural products, as well as on an increasing number of synthetic chemicals, it is reasonable to assume that these products will become widely dispersed in the environment. This is particularly true for certain persistent compounds that are important ingredients in various products and by-products of urban, industrial and agricultural activities.

Strategies designed for the solution of contamination problems have usually been overridden by economic and social considerations. In general, efforts to solve critical problems of marine contamination by large international organizations have been both noble and futile. Therefore, regional agreements to deal with these problems seem to be the best approach.

Regional networks of cooperative laboratories for baseline studies can be established by scientists of different regions under the auspices of relevant UN Specialized Agencies, such as UNEP, FAO, ICES and IOC. A beginning in this organization can be effected either during pollution workshops or as a follow-up to such events.

In some regions, laboratories are already closely associated in their baseline research activities. For example, in the North and Baltic Seas, marine laboratories are effectively linked through ICES (1974). A recent cooperative venture is the coordinated project on pollution in the Mediterranean Sea, in which fourteen countries are conducting a baseline exercise under the auspices of FAO (GFCM) and UNEP (1975).

Thus far, the only successful baseline studies on marine contamination have been those with clearly defined and limited goals in regions with well established marine laboratories. However, in the developing world, there are few laboratories where studies in marine contamination are being undertaken. Therefore, it is particularly difficult to set up networks of cooperating laboratories to carry out baseline and other joint studies. Consequently, it is in these areas that regional association to solve common problems needs to be encouraged.

In the Caribbean and adjacent regions, several selected programmes have been drawn up to facilitate future implementation on a cooperative basis (IOCARIB Ad hoc I/13, 1976). More specifically, programme number seven of that document deals with a marine pollution monitoring exercise among the Member States of IOCARIB (CICAR).

In considering research exercises of this type for developing areas, it is recommended that a coordinator be appointed (by joint decision of the member countries and the international agencies) to convene a working group of scientists of the participating nations. For the initial stage, an outline of the proposed study should be circulated to administrators and scientists to determine their willingness to participate. In practice, it is important to establish good channels of communication among the various representatives of participating countries, the coordinator, and the sponsoring international agencies.

A diagram of one possible way to design the basic structure for a regional cooperative programme is shown in Fig. 1, considering IOC as the international component.

2. DEVELOPMENT OF THE BASELINE EXERCISE

After the appointment of the coordinator, a cooperative programme of this nature can be divided into the following stages or phases: (1) Evaluation, (2) Preparation, (3) Screening, and (4) Operation. The time involved in the development of these stages is difficult to estimate for regions composed predominantly of nations with different scientific and technological capabilities. Under present circumstances, we anticipate an on-going programme with participating nations moving through the stages at their own pace. Consequently, participation in the exercise should not be limited to research centres already able to deal with the complex tasks called for, but should also include those centres capable of only limited initial contribution. Other centres will be joining the programme at a later date as their basic scientific and technological gaps are closed.

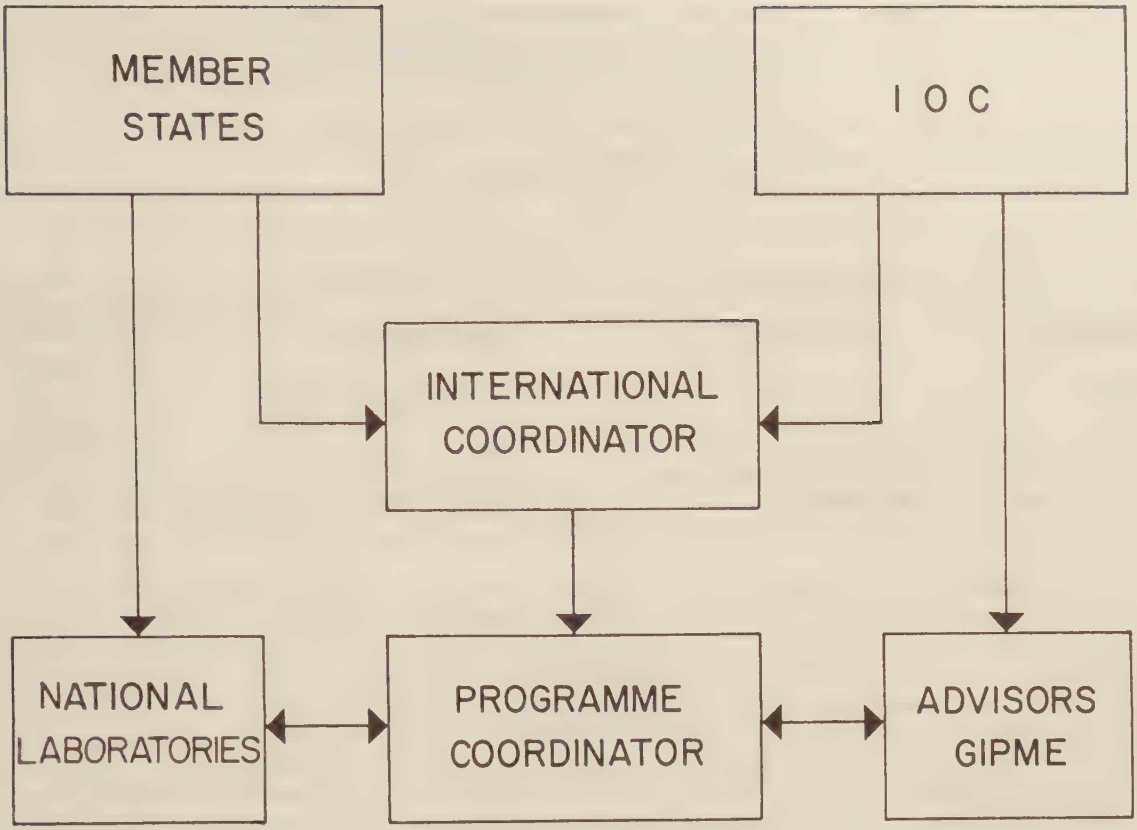

Fig. 1 Regional organization

2.1 Evaluation

The purpose of the evaluation phase is to gather and summarize information on the research capabilities of each country which has expressed a desire to participate in the baseline study.

This preliminary, but very important, phase would be conducted by the programme coordinator. It should require six to eight months to execute. During this phase, a geographical list of interested scientists would be assembled, which showed the expertise of each individual. Also, the research capabilities of each participating laboratory should be summarized according to personnel, equipment, vessels and geographical locality. A thorough evaluation of the entire personnel roster of the region should be carried out to determine whether or not gaps exist regarding professional and technical personnel, together with identification of training and educational centres in the region or adjacent areas (Fig. 2).

2.2 Preparation

Careful planning and adequate funding are the basis of success during the preparatory phase of the baseline exercise. At this point the programme coordinator should have adequate funds and staff to carry out coordinating activities. During this phase all existing knowledge concerning contaminant levels in the coastal and estuarine areas of the region should be summarized and stored in a data bank. References from other regions should also be summarized and stored, particularly if they include contaminant levels in organisms found within the region under study.

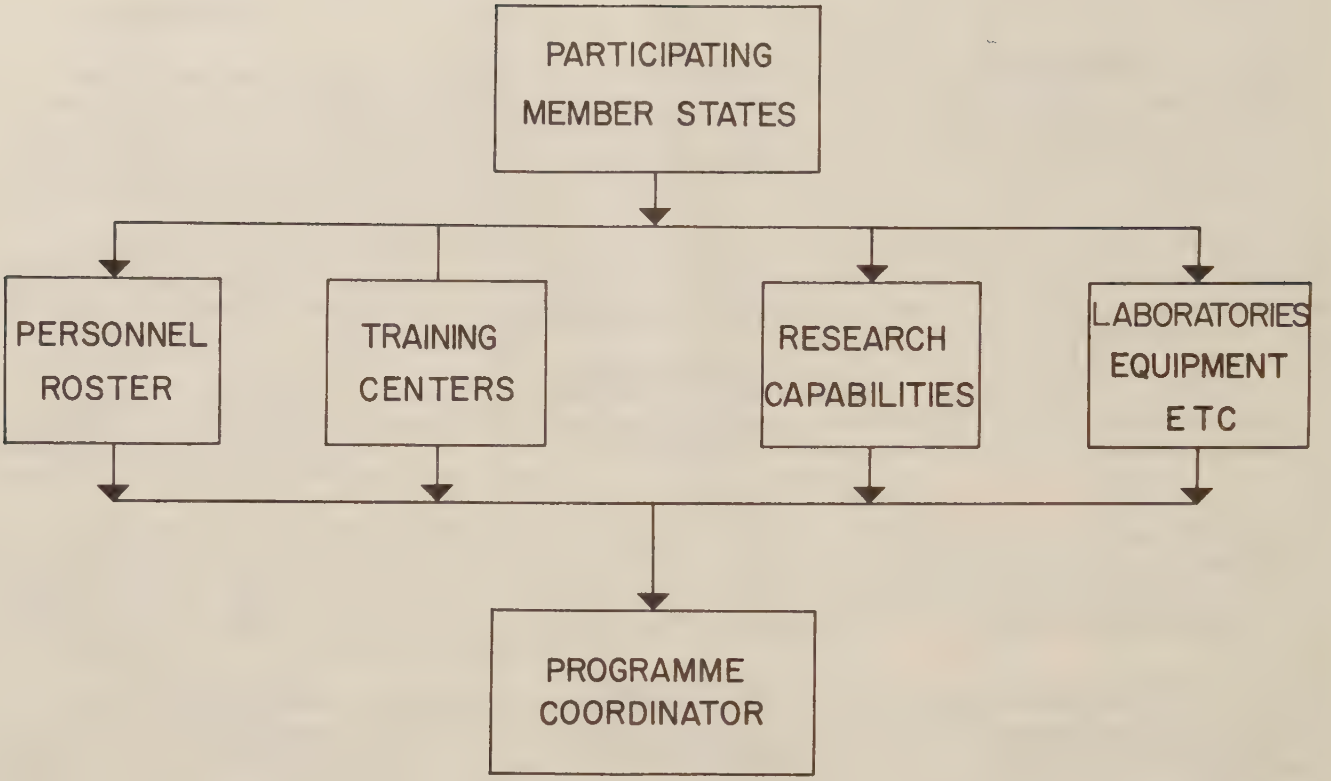

Fig. 2 Evaluation stage

The lack of adequately trained personnel to perform some of the more sophisticated analytical tasks will seriously hinder the full participation of some national marine laboratories. Therefore, fellowships for training should be available at the beginning of this phase. The trainees should be selected from national laboratories and other research centres which can assure that the trainee will continue to work on the programme upon return to his home country. This will require the identification of both existing and future training centres, preferably within the region. In this regard, TEMA can be of great assistance. Later a "critical mass" of scientific manpower will be developed within each nation and basic "in home" training can be initiated.

The contaminants that require the urgent attention of baseline studies are the following (according to ICG/GIPME IOC/INF. 276, 1976): heavy metals and other toxic trace elements (e.g., Lead, Mercury, Cadmium), chlorinated aromatic hydrocarbons (DDT, PCBs and other less studied compounds), petroleum and petroleum persistent petroleum products, micro-organisms related to sewage discharges, and artificial radioactivity (e.g., Plutonium).

The most straightforward approach would undoubtedly be directed toward public health; however, effects of contaminants on living resources and man-generated activities should also be seriously considered. Furthermore, it is necessary to point out that baseline surveys on the distribution of contaminants are very important, not only in areas already affected by this problem, but also to document undisturbed zones before specific large-scale human activities are begun.

Any list of contaminants to be monitored in a given region will depend on the evaluation of present knowledge, as well as the availability of appropriate instruments and trained personnel in the region. In the preparatory phase, the need to improve the analytical facilities of many of the participating laboratories must also be taken into consideration. Selection of recipient laboratories should be based on the actual needs of such facilities, especially the needs of national laboratories in the less developed countries.

The selection of instruments should be based on performance and easy maintenance. It is also of great importance that the recipient laboratories possess an adequate infrastructure for the installation, maintenance and operation of the instruments in accordance with the needs of the exercise.

It is imperative that the aims and direction of the baseline study programme be developed correctly at this stage (see Fig. 3). Perhaps during this preparatory phase short-term consultants, as well as active investigators, will be needed by some of the participating nations.

2.3 Screening

The main goals of the screening phase can be summarized as follows (see Fig. 4): (1) general organization and proper function of the baseline exercise; (2) training of technicians; (3) the adequate functioning of equipment, and (4) the intercalibration exercise.

The types of contaminants to be monitored should be selected after taking the regional situation into account. Document IOC/INF. 276 states that contaminants should be monitored in seawater, in marine organisms, in sediments and in the atmosphere near the sea surface. Through the experience of baseline surveys in the North and Baltic Seas, it was learned that priority should be given to insecticide residues, PCBs and certain metals in fish and shellfish. The necessary analytical and sampling techniques for such priorities are relatively well developed. Monitoring of contaminants in seawater has revealed considerable problems in achieving comparable results. Sediments have only been used in localized studies, and the transfer of contaminants from the atmosphere to the sea surface has not yet been attempted in baseline studies.

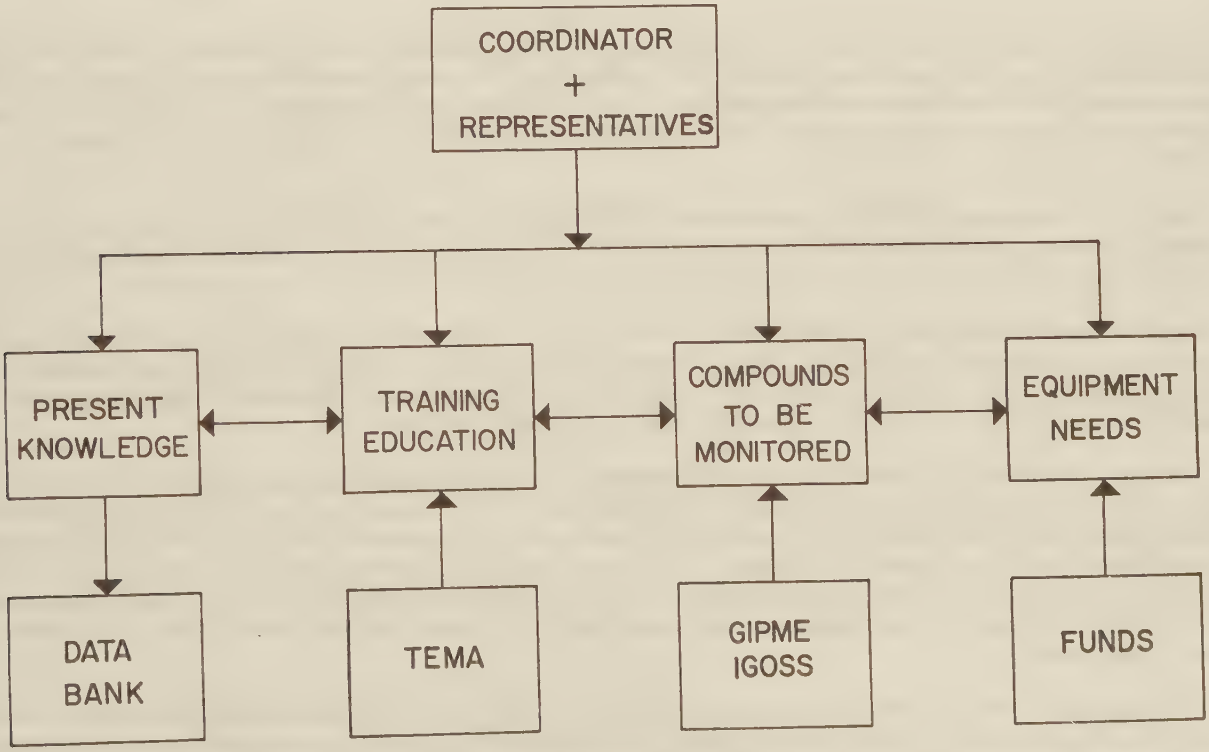

Fig. 3 Preparational stage

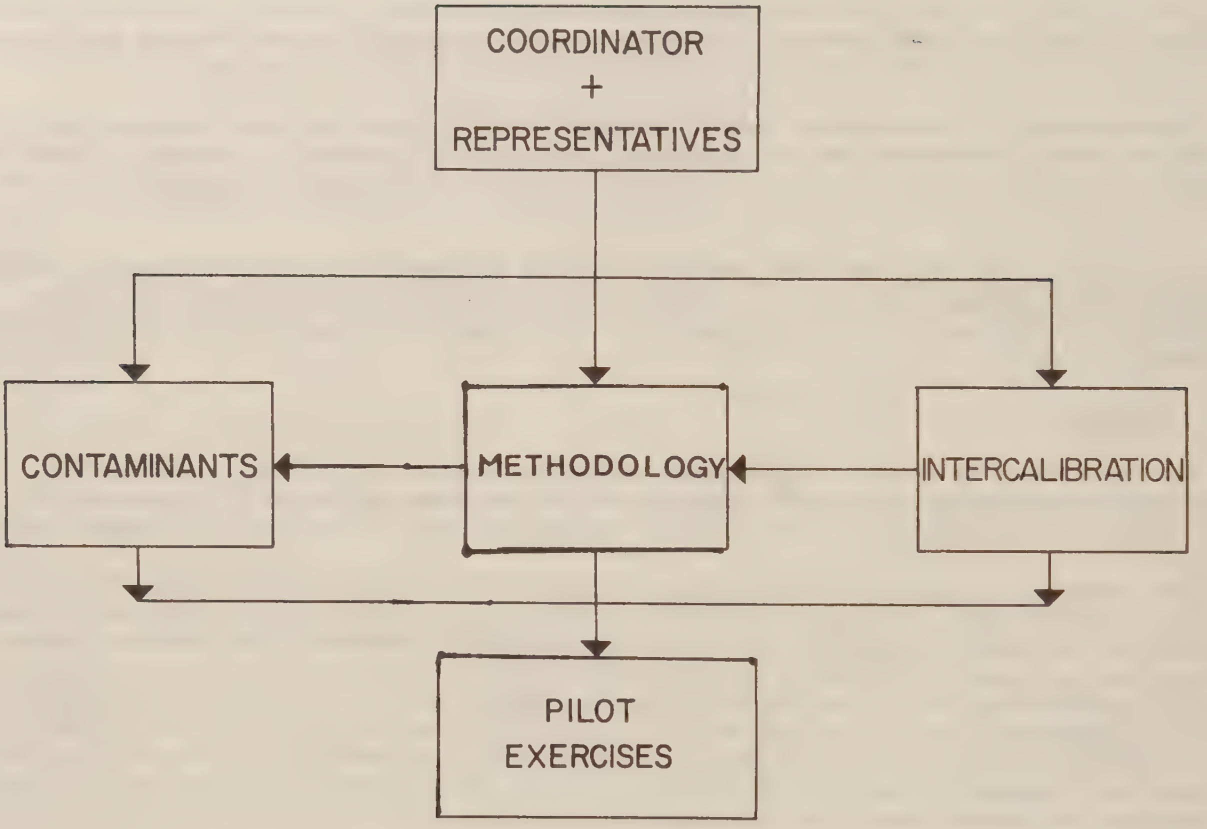

Fig. 4 Screening stage

In view of the limitations of a programme of this nature, due to technical and analytical considerations, as well as the shortage of personnel, it would be advisable to agree upon a limited number of substances and organisms. In selecting the organisms, material for comparison between different regions needs to be considered, and some common organisms should be included.

Sampling frequency for all recommended species will be seasonal (four times a year). In special areas, where particular contaminants are expected, more frequent sampling should be carried out.

Guidelines for sampling procedures, storage and treatment of samples, prior to chemical analysis, will be kept uniform as far as possible in order to ensure the highest degree of comparability for the results obtained. The "Manual of Methods in Aquatic Environmental Research" Part I (FAO, 1975) is a useful guide for this purpose.

Intercalibration of techniques will constitute an important aspect of the screening stage. For each group of contaminants it is advisable to assign to one of the laboratories responsibility for organizing the intercalibration exercise among the laboratories charged with analysing samples from the region. The organizing laboratory should arrange for each cooperating laboratory to receive samples from all the media chosen for the baseline exercise. In allocating the analytical tasks, great care must be taken to ascertain the true capacity of each laboratory.

If possible, the reference samples should be drawn up from uncontaminated areas, as well as from those areas with moderate and heavy contamination, so as to provide a useful range. The laboratory encharged with the intercalibration exercise should make both standard and reference samples available.

Small-scale pilot studies should be undertaken during the screening phase by all participating laboratories, primarily for the purpose of testing all laboratories. Meetings should be held after intercalibrating exercises to discuss any problems which arise and their possible solutions.

2.4 Operation

Once the baseline study has been designed and the various tasks have been allocated to the laboratories concerned and the intercalibration and testing exercises have been conducted or are under way, the programme should be put into operation (Fig. 5).

Attention should be given to the manner in which results are reported, as experience has shown that data have been rendered meaningless by failure to record vital information. The operational phase will be successful only if there has been adequate planning and funding and efficient coordination. Furthermore, sufficient communication of activities is imperative during the operational phase. The coordinator should keep each laboratory informed of the overall progress of the programme and be kept informed by each participating laboratory.

With so many laboratories participating in the baseline study, it is reasonable to assume that problems will arise, such as a breakdown of equipment, lack of supplies, or a change in personnel. Therefore, the coordinator should have sufficient power and resources available to make quick decisions to solve problems as they arise. The solution to any problem during the operational stage will be easier if contingency plans and emergency procedures are prepared in advance.

Each participating laboratory should be responsible for compiling and processing the data; that is, a general scheme should be agreed to and followed by the participating laboratories.

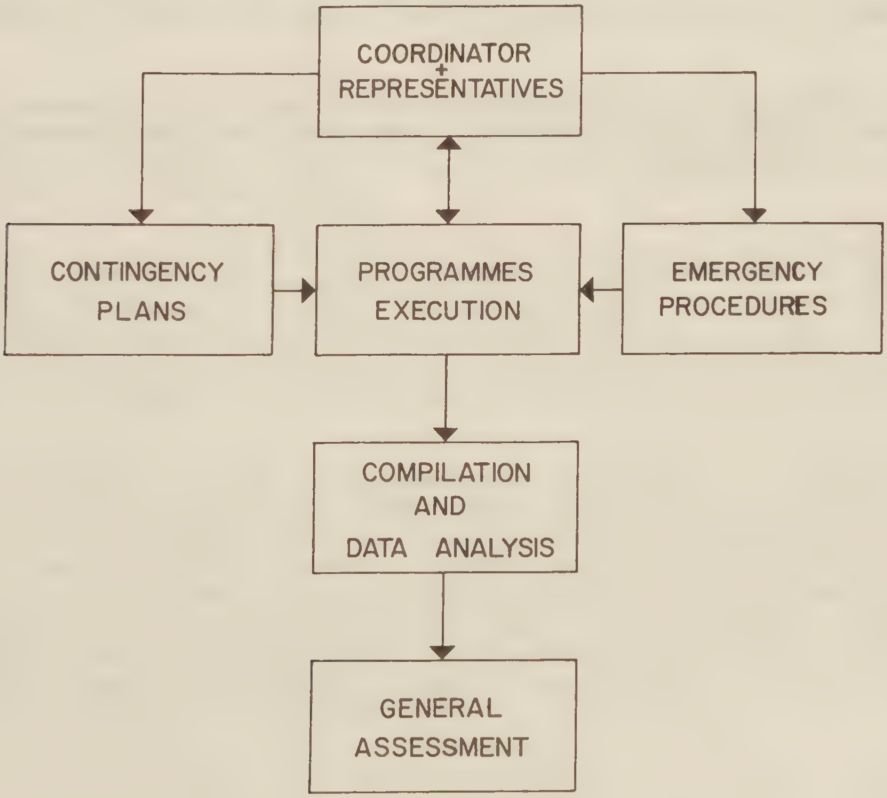

Fig. 5 Operational stage

The results of the baseline exercise should be tabulated for each contaminant, for each participating laboratory and country, for each medium, in great detail for biological samples. All such data should be published in the collective name of the supervisory panel which drew up the plans. Consequently, sufficient time and money should be made available at the end of the study to complete the analysis and interpretation of data.

3. SUMMARY REMARKS

The ultimate objective of a comprehensive baseline exercise is to provide a sound scientific basis for the assessment and regulation of marine contamination. In studies of a local or regional nature, there will be the intention to control input rates, should the levels revealed by the initial measurements be considered dangerous to either man or marine organisms. Such an intention will also require information on rates of input of contaminants, thus adding another dimension to the study. The needs are well defined and the task challenging; the starting point is the recognition of the problem by political leaders and the scientific community alike.

4. REFERENCES

FAO, Manual of methods in aquatic environment research. Part 1. Methods for detection,
1975 measurement and monitoring of water pollution. FAO Fish.Tech.Pap., (137):238 p.

FAO(GFCM)/UNEP, Pollution in the Mediterranean. Joint Coordinated Project, Report of the
1975 FAO(GFCM)/UNEP Expert Consultation on the Joint Coordinated Project on Pollution in the Mediterranean. Rome, 23 June - 4 July, 1975. Rome, FAO, 42 p.

ICES, Report of Working Group for the International Study of the Pollution of the North Sea
1974 and its effects on living resources and their exploitation. Coop.Res.Rep.ICES, (39):191 p.

IOC/INF. 276, Report of the IOC/ICES Working Group on Baseline Study Guidelines.
1976

IOCARIB, Meeting of *Ad hoc* Group of Experts on Future Programmes and Co-operation in Marine
1976 Science in the Caribbean and Adjacent Regions. Mayaguez, Puerto Rico, 1-4 March, 1976. IOCARIB *Ad hoc* I/3

DISTRIBUTION OF PHYSICAL AND CHEMICAL OCEANOGRAPHIC DATA IN THE CICAR REGION

by

T. WINTERFELD
CICAR Data Coordinator
CICAR Regional Data Center
NOAA Environmental Data Service
National Oceanographic Data Center
Washington, D.C. 20235
U.S.A.

CONTENTS

1. INTRODUCTION
2. CICAR DATA MANAGEMENT PROCEDURES AT RDC CICAR - WDC/A
3. INVENTORY REPORTS AND DATA RECEIVED
4. DISTRIBUTION OF CICAR PHYSICAL-CHEMICAL DATA STORED IN STANDARD FORMATS ON MAGNETIC TAPE
5. THE COMPUTER PLOT DISPLAYS
6. REFERENCES

Abstract

The National Oceanographic Data Center (NODC) of the U.S.A. is designated to serve as the Regional Data Center for CICAR. CICAR participants submit standard CICAR inventory reports of all types of data and samples to either the World Data Center (WDC/A-Oceanography) or the RDC CICAR shortly after their collection.

This operation has worked well during the CICAR programmes. Recently the CICAR Data Inventory (CICARDI) form has been phased out and replaced with the new IOC approved standard general purpose inventory form. At the end of the field phase of CICAR the flow of data is considered to be more important than the format of the inventory reports. The information from the CICARDI forms and other inventory forms and other inventory forms clearly related to CICAR is presently summarized by the Regional Data Centre in its publication "Guide to CICAR Data".

Data received by the data centres are indexed in detail in the "Guide" and in the annually updated WDC/A-Oceanography publication, 'Catalogue of Data". After indexing, the data are either directly archived or further processed on a priority basis onto magnetic tape in U.S. NODC standard formats. Analog materials, such as bathymetric charts or non-standard types of data are archived in the "Unprocessed Archives". All processed cruise data are merged with the NODC's worldwide applications oriented, geographically sorted data files. These magnetic tape files consist of data from all years of record and are sorted by 10° and 1° rectangles worldwide; and it is these files which can provide a user with the total processed, quality-controlled data set available in the CICAR area.

Resumen

El Centro Nacional de Datos Oceanográficos (NODC) de los EE.UU., sirve como centro regional de datos para las ICCRA. Los participantes en estas ICRRA presentan al Centro Mundial de datos (WDC/A-Oceanografía), o al Centro Regional de Datos de las ICCRA, inventarios-tipo de las ICCRA de toda clase de datos y muestras, poco tiempo después de haberlos obtenido. Durante los programas de las ICCRA, esta operación se ha realizado perfectamente.

Desde hace poco tiempo se está suprimiendo progresivamente el "Inventario de datos para las ICCRA" (CICARDI) substituyéndolo con el nuevo inventario-tipo de IOC, aprobado para fines generales. Al final de la fase operativa de las ICCRA, la serie de datos se considera más importante que el formato de los inventarios. La información procedente de los CICARDI y de otros inventarios claramente relacionados con las ICCRA, es actualmente resumida por el Centro Regional de Datos en su publicación "Guía para los datos de las ICCRA". Los datos recibidos por los centros son clasificados con arreglo a un índice en dicha "Guía", y en la publicación "Catálogo de datos", del Centro Mundial de Datos (WDC/A-Oceanografía), que es puesta al día cada año. Después de ser clasificados con arreglo a un índice, los datos son archivados directamente, o bien elaborados de nuevo, con carácter prioritario, en una banda magnética, en formatos-tipo del Centro Nacional de Datos Oceanográficos. Materiales análogos, como los mapas batimétricos o los tipos de datos no unificados, son archivados en los "archivos de datos no elaborados". Todos los datos elaborados que han sido obtenidos en los recorridos marinos, son incorporados a los archivos de datos, geográficamente clasificados, y destinados a las aplicaciones mundiales del Centro Nacional de Datos Oceanográficos (NODC). En esos archivos de bandas magnéticas están los datos que se han recogido todos los años, clasificados por rectángulos de 10° y 1°, que abarcan todo el globo terrestre, y estos archivos son los que pueden proporcionar a los usuarios la serie total de datos elaborados, y de calidad controlada, obtenidos en la zona de las ICCRA.

1. INTRODUCTION

At the second meeting of the International Coordination Group for CICAR (ICG CICAR) in 1969, the U.S. NODC was designated to serve, in collaboration with the colocated WDC/A-Oceanography as Regional Data Center (RDC) for CICAR. It was also agreed at that ICG and at subsequent meetings that CICAR participants would submit standard CICAR inventory reports of all types of data and samples to either the WDC/A-Oceanography, or the RDC CICAR shortly after their collection. Most types of data were also to be actually sent to the RDC CICAR as soon as processed, whenever possible in agreed-upon standard formats. Now, after seven years of operation it is possible to state that this early plan for the management of CICAR data has in fact worked rather well in most respects. Large numbers of many types of data have been reported on inventory forms, and, perhaps more importantly, in the case of physical and chemical data more data have actually been received by the RDC than has been reported on inventories. Not surprisingly in a period of 7 years there have been some changes in emphasis from the original plan. The standard "CICAR Data Inventory" (CICARDI) inventory form which was an important tool in monitoring the early phases of progress of CICAR, is phasing out and is being replaced by the new IOC approved standard general purpose inventory form "Report of Observations/Samples Collected by Oceanographic Programmes" (ROSCOP II). In the early years of CICAR there was also a special effort to inventory marine geological data. The CICAR inventory form used for that purpose is now being replaced in favour of the IOC International Geological/Geophysical Cruise Inventory" (IG/GCI) form. Thus, especially in the past three years, while general purpose inventory report forms are being widely used throughout the international oceanographic community, fewer of the data reported are being specifically identified as CICAR. Now, however, at the end of the field phase of CICAR, the flow of actual data should for the time being be considered rather more important than inventory reports.

2. CICAR DATA MANAGEMENT PROCEDURES AT RDC CICAR - WDC/A

The procedures followed by the RDC CICAR and WDC/A-Oceanography, in processing CICAR inventory reports and CICAR data received from CICAR participants are illustrated in a much simplified form in Fig. 1.

Ten participating countries have submitted inventory reports and data to RDC CICAR either directly or through WDC/A-Oceanography. Such submissions generally take place through the National Oceanographic Data Centres (NODCs) or Designated National Agencies (DNA) of the various countries.

The information from CICARDI forms and ROSCOP and other inventory forms clearly related to CICAR is presently summarized by the RDC in its publication "Guide to CICAR Data". The compilation of the first edition of the "Guide", which contains a ship-by-ship and cruise-by-cruise index to inventories and data received by RDC CICAR (or WDC/A-Oceanography) between 1969 and 1975, has been completed as of 1 June 1976. Distribution is planned for late 1976, but limited advance manuscript copies of the "Guide" are available at the CICAR II Symposium. In previous years RDC CICAR and/or WDC-A had prepared summary reports of data and inventories primarily for limited distribution to participants at the meetings of the ICG for CICAR.

The internal flow of CICAR data received from CICAR participants by the RDC CICAR (or by the WDC/A) is shown by the heavy arrows in Fig. 1. The extent of processing the data received, however, depends on the type of data and the form in which they are submitted. As a first step upon receipt, the data are indexed (Accessions Processing) in some detail by the RDC CICAR for internal purposes. All accessioned CICAR data are also indexed in the "Guide to CICAR Data" and most of the data, especially those from Declared National Programmes (DNP) are additionally indexed in the annually updated WDC/A-Oceanography publication Catalogue of Data.

After Accessions Processing the data are either directly archived or further processed on a priority basis onto magnetic tape and in U.S. NODC standard formats. Examples of data archived in the Unprocessed Archives (Box A in Fig. 1) include analog materials such as bathymetric charts or non-standard types of data, such as certain biological data and data that do not lend themselves to further processing. For the past three years analog mechanical BT data, which are no longer being digitized by the U.S. NODC, are mostly also included in this category as are original source materials containing data that are fully processed by NODC. CICAR Unprocessed Archive data can be made available to requestors provided it is technically possible to reproduce them.

Intensive data processing is performed by the RDC CICAR primarily on physical-chemical data, i.e., Station data (Nansen Cast or serial depth data), digital STD/CTD data, and X-BT data. These types of data, along with Mechanical BTs digitized in the past, have been the data that have been submitted by CICAR participants in by far the largest amounts, and which thus furnish the best oceanographic data coverage for the CICAR area.

Processing of Station/STD CTD data consists of conversion of originator's format to the U.S. NODC format, quality control, computer interpolation of standard depth values, computation of density and Dynamic Depth Anomaly and subsequent storage on magnetic tape. X-BT data are digitized with high resolution (ICES 1969 standards) by special semi-automated equipment, either by NODC or more commonly by arrangements with other facilities and, also, subsequently stored on magnetic tape. The NODC standard formats for these and some other types of data are described in the NODC Users Guide.

All fully processed CICAR Station/STD/CTD, X-BT and M-BT data stored on magnetic tape are maintained (actually or virtually) by cruise sequence, i.e., in order of the ship's cruise (including all data that may be taken as part of the cruise outside the CICAR area). These files are the CICAR Data Files (Box B in Fig. 1). The data in this file are indexed by NODC Reference I.D. Number in the "Guide". Copies of most of the data in the cruise ordered file which are DNP, or had been originally accessioned through WDC/system are routinely exchanged with WDC/B-Oceanography, Moscow.

All processed cruise data, with the exception of those which may have processing or quality problems of one sort or another, are also merged with the NODC's worldwide applications-oriented, geographically sorted data files (Box C in Fig. 1). These magnetic tape files consist of data from all years of record and are sorted by 10° and 1° rectangles worldwide, and it is these files which can provide users with the total processed quality controlled data set available in the CICAR area.

It should be noted that these geographically sorted files, as completed up to 1973, were used to produce a recently released CICAR related atlas, the U.S. NODC publication "Temperature, Salinity, Oxygen and Phosphate in water of Eastern Central America and Northern South America".

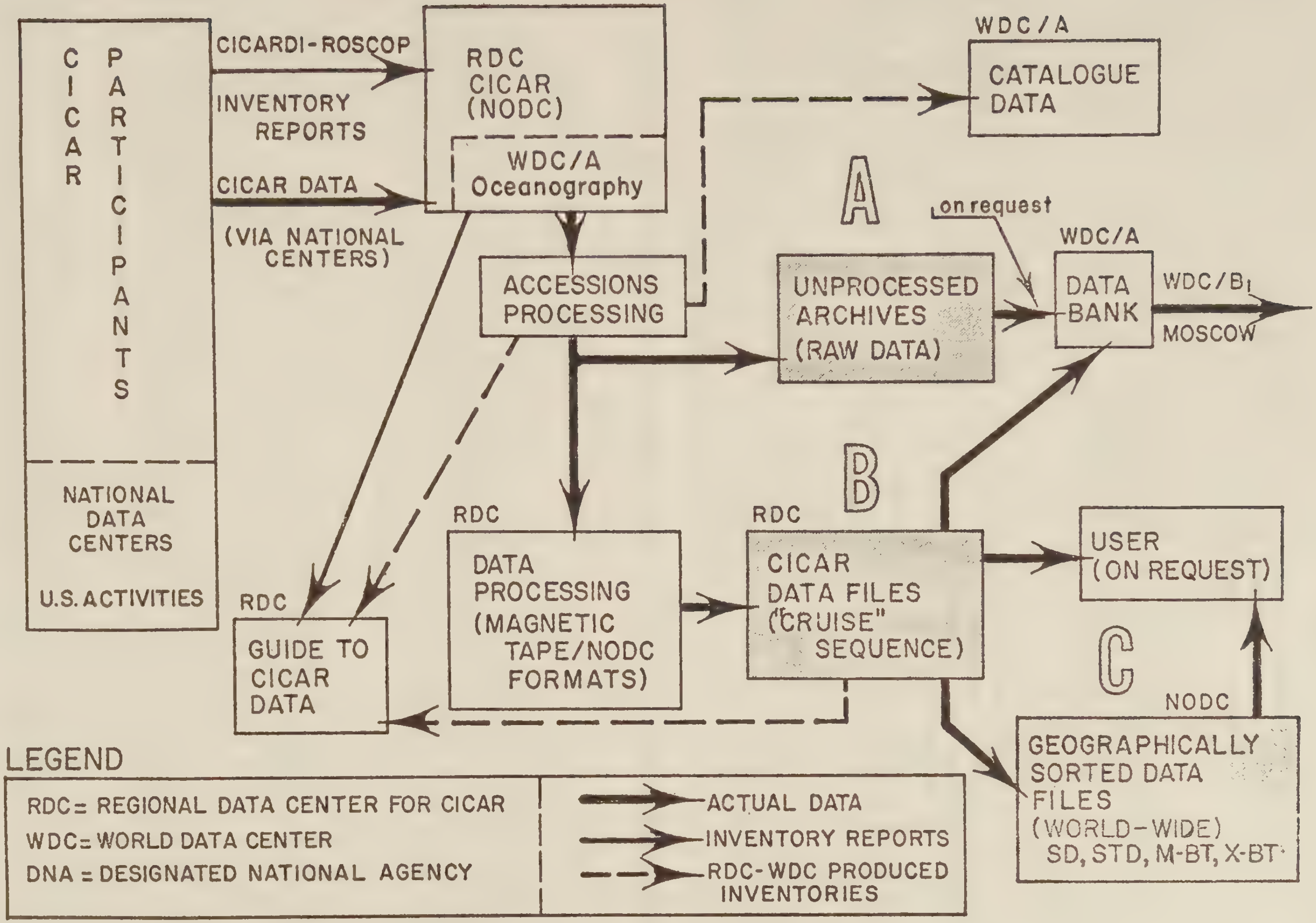
CICAR PARTICIPANTS
NATIONAL DATA CENTERS
U.S. ACTIVITIES
CICARDI-ROSCOP
INVENTORY REPORTS
CICAR DATA
(VIA NATIONAL CENTERS)
RDC CICAR (NODC)
WDC/A Oceanography
ACCESSIONS PROCESSING
WDC/A
CATALOGUE DATA
A
on request
UNPROCESSED ARCHIVES (RAW DATA)
WDC/A
DATA BANK
WDC/B1
MOSCOW
RDC
GUIDE TO CICAR DATA
RDC
DATA PROCESSING (MAGNETIC TAPE/NODC FORMATS)
B
RDC
CICAR DATA FILES ("CRUISE" SEQUENCE)
USER (ON REQUEST)
C
NODC
GEOGRAPHICALLY SORTED DATA FILES (WORLD-WIDE) SD, STD, M-BT, X-BT
LEGEND
RDC= REGIONAL DATA CENTER FOR CICAR
WDC= WORLD DATA CENTER
DNA = DESIGNATED NATIONAL AGENCY
ACTUAL DATA
INVENTORY REPORTS
RDC-WDC PRODUCED INVENTORIES

Fig. 1 CICAR Regional Data Center
"Management of inventory reports and data"

3. INVENTORY REPORTS AND DATA RECEIVED

Table I summarizes by IOC member states participating in CICAR and the type of data, the data inventoried and received and the grand total by all countries combined. It is obvious from Table I that the flow of data into the RDC CICAR archives has been quite satisfactory for those types of classical oceanographic data for which well-established international exchange procedures and formats already existed prior to CICAR. However, less commonly exchanged and less standardized data such as primary productivity and geological observations have been inventoried, but generally have not been submitted to the RDC. It should be pointed out, that to serve the purposes of requestors of such data, the identity of the activities holding data inventoried but not submitted can generally be determined from the RDC CICAR Guide to Cicar Data.

Table II shows data and inventories for three major data types, Station Data/STD/CTD, X-BT, and M-BT, accessioned by the RDC CICAR by year of collection of the data. Table II shows that the CICAR related data collection effort for Station and X-BT data seems to have peaked in 1973 and then dropped off dramatically. The collection M-BTs has been declining steadily as a result of being phased out in favour of the more accurate X-BT. Some of the apparent drop-off in 1974 and 1975 may of course be accounted for by the fact that a good part of the data probably have not yet been processed at the national level and have not yet reached the RDC. Another indication of this lag in submission is the fact that the number of data inventoried in 1974 and 1975 exceed the number of data received; e.g., a minimum of about 1 300 inventoried Station Data (mainly STDs) are still outstanding; this despite the also obvious overall decreasing trend in CICAR inventory reports which began in 1973. For example, in 1973, of 2 326 CICAR stations actually received by the RDC CICAR only 1 422 had been previously identified as CICAR on inventory forms.

4. DISTRIBUTION OF CICAR PHYSICAL-CHEMICAL DATA STORED IN STANDARD FORMATS ON MAGNETIC TAPE

Table III shows the total Station/STD/CTD, X-BT and M-BT data fully processed by the RDC CICAR and available on magnetic tape for the CICAR period (Box B in Fig. 1) and the totals for all years of data contained in the NODC geographically sorted magnetic tape files (Box C in Fig. 1). The limits of the CICAR archive-inventory area, arbitrarily defined for computer applications purposes, are shown on Page 1 of Part II of this paper. (Not reproduced here; reference in footnote on next page - Ed.) Only data falling inside this area and processed as of January 1976 are included in the totals. Additional CICAR data are in processing and will be added in periodically.

It should also be pointed out that while the data volume in the CICAR cruise files (Box B in Fig. 1) is generally increasing the volume of data in the NODC geographically sorted files (Box C in Fig. 1) may fluctuate upward or downward at three to six month intervals as individual cruises are temporarily withdrawn in order to allow reprocessing, applications of corrections of various sorts and as new cruises are added during the routine update cycle.

It is gratifying to note from Table III that over the seven years of the CICAR field period the volume of Station/STD/CTD data in the CICAR region has been increased by more than 40 percent over that collected in the period 1917-68, a percentage that will certainly increase even further when all CICAR data have been received and processed.

The X-BT data effort did not really get underway until the mid-1960s and most of the available 25 000 digital X-BT observation in the CICAR area were actually collected during the CICAR period. While only about 9 500 of these data were clearly identified as having been collected as part of CICAR programmes, the entire X-BT file is, however, available for applications purposes.

In comparison with the flood of X-BT data, the volume of digitized Mechanical BT (M-BT) data collected during the CICAR period has taken a drastic downturn since 1969, increasing existing data holding by less than 10 percent. The X-BT which yields relatively accurate temperature data to depths of 450 m (or even 750 m) has obviously proved more attractive than the M-BT which, though useful for measuring thermal gradients, has poor reliability in respect to temperature unless processed with great care, is limited to 300 m in depth and more difficult to process and digitize.

5. THE COMPUTER PLOT DISPLAYS[1]

Part II of this paper, titled Computer Plot Displays contains charts of the geographic distribution of data stored by the RDC CICAR/NODC on magnetic tape. One of the most important attributes of computer processed files stored on magnetic tape is the ease with which they lend themselves to further computer manipulations. Thus, while it would have been prohibitively expensive and time-consuming to plot the geographic distribution of CICAR data archived at the RDC manually, such plots were generated rapidly and at comparatively low cost by the computer and computer-linked plotting equipment. Obviously, however, such geographic distribution plots can only be produced from data that are stored in standard formats, and, therefore unprocessed data or non-standard CICAR data could not be included on these charts.

The geographic limits of the area of data coverage on the charts are shown on page 1. Problems related to plotting scale, reproduction, and legibility have made it necessary to divide the CICAR region into a western part (A) and an eastern part (B).

The geographic distribution of Station Data/STD/CTD, X-BT and M-BT are shown on pages 2 through 22 for both the CICAR period (titled: "Distribution of Processed Data") using the CICAR Data Files (Box B in Fig. 1) and for all years combined (including most CICAR data) using the NODC geographically sorted data files (titled: "Distribution of Geographically Sorted Data") (Box C in Fig. 1). The distribution of both types of data sets is presented in two ways:

(1) on plots showing by Xs the actual geographic location of each observation, and

(2) on plots showing the distribution of data (regardless of depth of observation) numerically by the number of observations falling within the degree rectangles of latitude and longitude.

It should be noted that large numerical data bases will unavoidably have some small residual error rates despite time-consuming and costly quality control efforts during processing and that users of such files must use some caution. Thus, a few of the M-BT observations have errors in geographic position and are plotted as falling on land (some allowance must also be made for the inexactness of the land mass plotting programme). However, the actual percentage of such errors is generally very low, i.e., less than 0.1 percent of the observations in the file.

The fully processed Station/STD/CTD data available as of January 1976 for the CICAR area (Box B and C in Fig. 1) have also been presented as the annual average distribution of temperature, salinity and (computed) density (sigma-t) by 2 degree square rectangles at selected standard depths (Part II, pages 23 through 66). These Standard Depth Level Plots were produced by one of NODC's routine general applications (GAS) programmes. The number of available observations and the maximum and minimum value in each square are also shown. Vertically interpolated values are used at those depths of a station (Nansen Cast) at which no observed values were available.

The annual average standard depth distributions were included in this paper to:

(1) serve as a long-term average "base line" distribution against which individual CICAR data sets can be compared, and

---

[1] Winterfeld, T., 1976 Distribution of physical and chemical oceanographic data in the CICAR region, United States Department of Commerce, National Oceanic and Atmospheric Administration, Washington D.C.

(2) serve as a special type of parameter-oriented inventory illustrating both the nature of the data and decrease in the sampling rate as a function of depth.

Ideally, the maxima and minima are illustrative of the range of the value of the parameter within a 2 degree rectangle. Quite obviously, by virtue of their being maxima and minima, they may also act as an indication of erroneous or anomalous data which fall well outside normal limits. Thus, inspecting, for example, the maxima of salinity and density there are a few 2 degree rectangles (e.g., in the Yucatan Straits) which are marked by implausibly high values. Though only a small amount of "bad" data may give rise to such implausible values and while the average value actually may not be affected, these data must be identified and corrected. It is one of the continuing tasks of the RDC/NODC, in collaboration with the originator of the data, to correct and reprocess any cruises containing potential errors that are to be included in the NODC geographically sorted data files (Box C in Fig. 1). (At the time of this paper, 85 cruises of the many hundreds of cruises falling in the CICAR area are scheduled for reprocessing.) Cruises that cannot be reprocessed are nevertheless permanently retained as part of the CICAR data archives either in the cruise sequenced data files (Box B in Fig. 1) or in the Unprocessed Data Files (Box A in Fig. 1).

TABLE I

Inventory reports and data received by RDC CICAR, 1969-1975 (as of May 30 1976)

Total (all countries)	Data reported on inventories	Data actually received
Stations (Nansen)	5 675	6 103
STD/CTD	3 384	2 471
X-BT	10 098	9 398
M-BT	5 786	4 346
Phytoplankton	2 027	78
Zooplankton	3 273	26
Micronekton	1 775	0
Primary productivity	756	0
Fish observations	919	0
Current	4 925	2 063
Geology	3 690	398
Pollution	197	0
Drift Bottles	15 949	716
Zoobenthos	398	0
Phytobenthos	75	0
Ichthioplankton	171	0
Neuston	248	0
Bongo	145	0
Bottom photographs	227	0
Animal sounds	276	0

Table I continued

	Data reported on inventories	Data actually received
BRAZIL		
Stations (Nansen)	152	143
STD	43	0
M-BT	270	85
Current	17	0
Zoobenthos	75	0
Phytobenthos	75	0
Geology	478	116
Pollution	66	0
CANADA		
Stations (Nansen)	139	136
M-BT	195	0
Zooplankton	673	0
Micronekton	673	0
Geology	6	0
Pollution	52	0
Fish observations	19	0
COLOMBIA		
Stations (Nansen)	168	150
M-BT	93	57
Phytoplankton	66	0
Primary Productivity	50	0
Drift Bottles	18	0
CUBA		
Stations (Nansen)	225	292
M-BT	141	0
Zoobenthos	38	0
Observations	90	0
Current	2	0
Ichthioplankton	84	0

Table I continued

	Data reported on inventories	Data actually received
MEXICO		
Stations (Nansen)	1 092	394
STD	33	0
X-BT	182	12
M-BT	378	0
Zooplankton	495	0
Phytoplankton	507	0
Primary productivity	161	0
Current	237	0
Fish observations	38	0
Drift bottles	3 300	0
Neuston	38	0
Ichthioplankton	87	0
NETHERLANDS		
Stations (Nansen)	169	140
STD	139	0
XBT	76	0
M-BT	1 536	1 330
Zooplankton	961	0
Phytoplankton	961	0
Micronekton	961	0
Drift Bottles	550	0
Zoobenthos	180	0
Geology	1 050	0
Primary productivity	460	0
Current	19	0
Fish observations	x	0
UNITED KINGDOM		
Stations (Nansen)	17	15
STD	46	0
X-BT	265	264
M-BT	55	55
Zooplankton	5	0
Current	68	51
Geology	231	171

Table I continued

	Data reported on inventories	Data actually received
U.S.S.R		
Station (Nansen)	525	1 224
M-BT	655	83
Zooplankton	28	26
Phytoplankton	78	78
Primary productivity	35	35
Geology	98	97
Current	388	0
U.S.A.		
Station (Nansen)	2 809	3 390
STD/CTD	3 123	2 471
X-BT	9 575	9 010
M-BT	2 315	2 068
Zooplankton	1 111	0
Primary productivity	50	0
Fish observations	742	0
Phytoplankton	415	0
Micronekton	141	0
Current	4 194	2 012
Drift Bottles	12 071	716
Geology	1 768	14
Pollution	79	0
Zoobenthos	105	0
Neuston	210	0
Bongo	145	0
ICITA	225	0
Bottom photographs	227	0
Animal sounds	276	0
VENEZUELA		
Stations (Nansen)	379	179
M-BT	148	668
Geology	59	0
Fish observations	30	0

TABLE II

Inventory reports and data received, number of observations (approx.) by year of observation

Year of observation		1969	1970	1971	1972	1973	1974	1975
Station Data/STD/CTD	Inventory	351	1 840	1 639	2 386	1 422	832	522
	data	483	1 343	1 541	1 732	2 326	478	378
X-BT	Inventory	589	2 021	1 981	1 920	1 398	845	1 348
	data	542	1 999	1 358	1 871	1 977	976	656
M-BT	Inventory	637	1 791	1 699	1 038	372	126	0
	data	1 515	1 647	645	62	216	150	74

TABLE III

Processed data in CICAR area archived on magnetic tape (May 1976)

Type of data	Total	CICAR period (1969- 75)
Station Data/STD/CTD	1914-1975 19 547	5 870
X-BT (digitized)	1965-1975 25 098	>15 000 (estimated)
M-BT (digitized)	1942-1975 58 450	3 836

6. REFERENCES

Halminski, S.J., Temperature, salinity, oxygen and phosphate in waters off eastern Central
1975 America and northern South America. NOAA EDS/NODC Key Oceanogr.Rec.Doc., (4):189 p.

National Oceanographic Data Center, Environmental Data Service, User's guide to NODC's data
1973 services. NOAA EDS/NODC Key Oceanogr.Rec.Doc., (1):72 p.

___________, Gas systems reference manual. Washington D.C., NOAA, 75 p.
n.d.

Unesco, Intergovernmental Oceanographic Commission, Manual on international oceanographic
1973 data exchange. Third Edition (revised). Tech.Ser.IOC, (9):63 p.

World Data Center A, Oceanography, Catalogue of data. Washington, National Academy of Sciences, World Data Center

INVESTIGATION OF MIXING PROCESSES OF NORTH SOUND LAGOON, GRAND CAYMAN

by

J. Darbyshire[1], I. Bellamy[2] and B. Jones[3]
Marine Science Laboratories
Menai Bridge
Anglesey, United Kingdom

CONTENTS

1. INTRODUCTION
2. THEORETICAL CONSIDERATIONS
3. DISTRIBUTION OF V & $h/\bar{V}^3$
4. SEASONAL DEVELOPMENT AND THE CONTROLLING EFFECT OF TOPOGRAPHY
5. TRANSIENT FRONTAL DISTURBANCE
6. LAGOON FLUSHING AND ASSOCIATED ECOLOGICAL PROBLEMS
7. REFERENCES

Abstract

During the period May 1974 to April 1975, an intensive oceanographic study of the coastal waters of Grand Cayman was mounted by the Overseas Development Administration and the Cayman Island Government. Primarily, the seasonal and short-term response of water movement to prevailing oceanic and meteorological conditions in the shallow tidal lagoon, North Sound, was investigated. Stratification was found to take place in the interior regions of the lagoon during stable meteorological conditions in contrast to fringing reef and immediate back-reef areas where strong mixing induced by the oceanic flow occurred. The subsurface horizontal density gradient along the lagoon axis (extending from the lagoon interior northward to the fringing reef) was found to be reinforced during periods when stratification was strong. Hence the stratification and the flushing time of the lagoon were found to be interdependent. This relationship is developed quantitatively and related to the main lagoon flushing mechanisms.

These mechanisms control the detrimental effects on the ecology of the lagoon caused by the dispersal of contaminants. Such dispersal has recently increased dramatically because of the commercial development of the lagoon coastline, and it is therefore necessary to supply developers with reliable estimates as to the lagoon's ability to remove pollutants.

Resumen

El Gobierno de la isla del Caimán y el Organismo de Desarrollo de los Territorios de Ultramar organizaron, entre mayo de 1974 y abril de 1975, un estudio oceanográfico intensivo de las aguas costeras del Gran Caimán. Primero se estudió la reacción, durante las estaciones

---

[1] Professor of Physical Oceanography, Marine Science Laboratories. Menai Bridge, Anglesey U59 5EK, U.K.

[2] Executive Research Assistant. Marine Science Laboratories. Menai Bridge, Anglesey U59 5EK, U.K.

[3] Oceanographer, Oceaneering International Services. Aberdeen AB2 8EF, U.K.

y en periodos más cortos, de las aguas poco profundas de la laguna costera North Sound a las condiciones meteorológicas y oceánicas. Cuando las condiciones meteorológicas eran estables, se producía estratificación en las regiones interiores de la laguna, mientras que en los arrecifes marginales y en las zonas adyacentes inmediatas se observaron fuertes mezclas, debidas al flujo oceánico. El gradiente horizontal de densidad superficial a lo largo del eje de la laguna - que va desde el interior de la laguna, en dirección norte, hasta el arrecife marginal - aumentaba durante los períodos de fuerte estratificación, de lo que se dedujo que la estratificación y el tiempo de renovación de las aguas de la laguna eran interdependientes. Esta relación es desarrollada cuantitativamente y relacionada con los principales mecanismos de renovación de las aguas de la laguna.

Estos mecanismos regulan los efectos perjudiciales que la dispersión de contaminantes ejerce sobre la ecología de la laguna. Tal dispersión ha aumentado enormemente en estos últimos tiempos a causa del desarrollo comercial del litoral de la laguna, por lo cual es necesario que los interesados conozcan la capacidad de eliminación de contaminantes de la laguna.

1. INTRODUCTION

Here we describe observations of current vector and sigmat distribution made by conventional methods and develop a simple energy model showing how density distribution can be related to prevailing forcing functions and therefore also to the lagoon flushing time.

NOTATIONS

B	buoyancy flux
$\dot{E}$	rate of supply of K.E. to mix water column
g	acceleration of gravity
h	depth of water column
k	wave number
k_s	surface drag coefficient
k_B	bottom drag coefficient
t	time
u	horizontal component of the velocity of a water particle
u_i	vector associated with mixing agent i in horizontal direction
V	mixing energy introduced from atmosphere
$\overline{V}^3$	represents a function of u_i vectors
z	verticle coordinate
ρ	water density
$\overline{\rho}$	water density, vertically meaned
ϵ	fraction of energy used to increase the energy of the water column
ζ	wave frequency
τ	shear stress

To initiate an understanding of lagoon mixing processes it is necessary to zone the lagoon into two regions by a boundary CD (Fig. 1) whose location is diurnally and seasonally dependent. The northern regime is one of a permanently mixed system but in the deeper interior waters of the lagoon (Fig. 2) a seasonal development of stratification occurs as a response to increased atmospheric heating and precipitation (Fig. 3).

2. THEORETICAL CONSIDERATIONS

We assume the mixing energy introduced to the water column due to atmospheric heating and precipitation,

$$V = \frac{1}{h}\int_{-h}^{0} (\rho - \overline{\rho})gz\,dz;\ \overline{\rho} = \frac{1}{h}\int_{-h}^{0} \rho\,dz \qquad (1)$$

as in a work of Simpson, Hughes and Morris (1976), where h is the depth, z is the vertical spatial coordinate and ρ is the density of the water with mean $\overline{\rho}$. A physical interpretation of V is seen to be the amount of mechanical energy required to bring about complete vertical mixing of the water column. To do this, a fraction ϵ of the total energy dissipated from tidal, wind and wave induced turbulence at a rate $\dot{E}$ is needed to work against gravity. The remainder is dissipated by viscosity.

At the boundary CD there is a balance and

$$\dot{V} = \dot{E} = \epsilon(\tau^{s}_{u_i} u_i + \tau^{B}_{u_i} u_i);\ \tau = k\rho u_i^2 \qquad (2)$$

assuming no interaction between τ^s (surface) and τ^B (bottom), where τ_{u_i} represents the momentum flux introduced to the water column by mixing agent i, and u_i is the appropriate representative surface or bottom vector. ϵ is the fraction of energy available for increasing the potential energy of the water column. The suffix i represents w (wind current) s (surface waves), o (oceanic current), t (tide), and s^1 (swell waves). k is the drag coefficient in the assumed quadratic friction law.

The momentum flux from the wind is $\tau u_w + \tau \bar{u}_s$, where $\bar{u}_s$ is the mean horizontal wave velocity (Phillips, 1969), and the first two terms can be written as:

$$k_s \rho (u_w + \bar{u}_s)^3$$

where u_w, the surface drift velocity, has been used instead of the more usual u (surface friction velocity = $\sqrt{\tau/\rho}$) because of the investigations of Kullenberg (1976). k_s is the surface drag coefficient ~ 0.0013.

The energy flux term to the waves is of the same order as the direct energy flux to the current since $\bar{u}_s \sim u_w$.

The remaining terms are:

$$k_B \rho (u_o + \bar{u}_t + \bar{u}_{s'})^3$$

where k_B is the bottom drag coefficient, ~ 0.002, $\bar{u}_t$ is the surface tidal mean velocity and $k_B \rho \bar{u}_t^3 = \frac{4}{3\pi} k_B \rho u_t^3$, where u_t is the velocity amplitude.

The horizontal component of the velocity of a water particle induced by wave motion is:

$$u = \frac{a\zeta \cosh k(z + h)}{\sinh kh} \cos k(x - ct)$$

where c = speed, t = time and $-h < z < 0$. This is a maximum when $x = ct$ by intuition. Also, for kh small:

$$\tanh kh = kh$$

for kh large:

$$\tanh kh = 1$$

Then the max surface wave induced horizontal component at the surface is given by:

$$u_s = a\zeta$$

and the max swell wave induced horizontal component at the bottom is given by:

$$u_{s'} = \left[\frac{a\zeta}{kh} \right].$$

Equation (2) is now:

$$\dot{E} = \epsilon\rho \left[k_B \left\{ u_o + \bar{u}_t + \bar{u}_{s'} \right\}^3 + k \left\{ u_w + \bar{u}_s \right\}^3 \right] ; \; \bar{u}_i^3 = \frac{4}{3\pi} u_i^3 \tag{3}$$

Assuming V is constant for the time and area of interest, it can quite easily be shown that (Phillips, 1969):

$$e \alpha \frac{hB}{\bar{V}^3} ; \; B = \frac{g}{\rho} \left\{ Q \frac{\alpha}{c} - S \right\}$$

where Q and S are the fluxes of heat and salt, α is the expansion coefficient, c is specific heat, B is the buoyancy flux and $\bar{V}^3$ is a vector representing the terms on the RHS of (3).

ϵ can therefore be interpreted as being a measure of the extent to which the development of externally generated turbulence is inhibited by buoyancy input and stratification will occur when ϵ exceeds a critical value.

All the necessary measurements have been obtained to evaluate the RHS of equation (2). The distribution of KE available from swell and fetch waves along Section AB (Fig. 4) was obtained from predicted wave parameters chosen to fit values obtained from periodic field observations. u_w was chosen to be 3 percent of W (Kullenberg, 1976). u_o and u_t were obtained from current meter and drogue studies.

Values of V and $h/\overline{V}^3$ are shown in Fig. 7 and can be compared to the sigmat distributions of Figs. 5 and 6. The sections in Fig. 6 are based on a 30-element array of data points where temperature and salinity values obtained from the surface to the bottom usually at 1 m intervals have been used for calculating σ_t. A similar horizontal array was used to obtain the σ_t contours of Fig. 5.

3. DISTRIBUTION OF V AND $h/\overline{V}^3$

Fig. 7 shows the distribution of V along Section AB. During July, the mid-summer period of maximum stratification yields the greatest values of $V \sim 240$ ergs/cm^3 in the lagoon interior. Values are lower ~ 35 ergs/cm^3 as the mixed oceanic region of shallower water is approached where $V = 0$. The transition is dramatically sudden, happening in a very small horizontal distance. During early summer when stratification is not strong values of V decrease as do horizontal gradients. During winter V is effectively zero throughout the lagoon. Generally, stratification is associated with a value

$$V = 35.0 \text{ ergs/cm}^3$$

Fig. 7 also shows the distribution of $h/\overline{V}^3$ along Section AB. A good agreement with V contours is evident and the value $h/\overline{V}^3 = 120$ is associated with $V = 35$ ergs/cm^3.

4. SEASONAL DEVELOPMENT AND THE CONTROLLING EFFECT OF TOPOGRAPHY

The appearance of the front is dependent upon the balance between V and E suggesting that increasing V and decreasing E should produce a front advancing oceanward as mid-summer is reached, assuming uniform depth. However, the pronounced dependence of ϵ $(\propto h/\overline{V}^3)$ on h is emphasized by the effects apparent in Fig. 6. Transient seasonal front development begins under favourable conditions as early as March, to the south of the 23.72 contour, coincident with the 2.4 m depth contour. Stratification is well established by May. As mid-summer is reached, V has increased sufficiently so that a pronounced front has developed together with the associated stratification. Only a relatively small frontal excursion oceanward has occurred however, suggesting that V is not sufficient to produce a balance with the $\overline{V}^3$ terms in the shallower water. Inspection of Fig. 7 leads to the conclusion that $h/\overline{V}^3$ increases rapidly as the front is approached from A due to decreasing values of u_o. Topographic discontinuity then produces an intensification of the horizontal $h/\overline{V}^3$ gradient until the 5.5 contour (bottom) is reached when changes in $h/\overline{V}^3$ values depend on the increase in u_w and u_s. The horizontal σ_t discontinuity peaks during July/August at 0.6. The vertical σ_t discontinuity is 0.3 at this time. During October gradients diminish until they are completely removed by high $\overline{V}^3$ values caused by the appearance of low pressure fronts in November (Fig. 6).

5. TRANSIENT FRONTAL DISTURBANCE

The front was also observed via transparency data and visual observation or turbidity from above the surface (Plate 1) and by divers. Plate 1 shows a well defined summer front during low $\overline{V}$ input conditions shortly after a strong SE wind. The colouring of lagoon water is due to the suspension of fines caused by wave-induced turbulence. High u_s and u_w values associated with summer low frontal systems for periods of typically two days produce a transient disruption of the frontal system in the main channel area. Lagoon water penetrates into oceanic areas inducing a transport of suspended material oceanward through Main Channel. To achieve mixing to a greater depth at the critical ϵ value, assuming no change in V, $\overline{V}^3$ must change appropriately according to the RHS of 3. Also assuming only u_w and u_s increase on response to the increase in wind vector W, then a minimum value of $W = 7\ m\ s^{-1}$ is required before interior lagoon water can be removed during the summer.

Thermocline re-establishment upon the resumption of usual $\overline{V}$ values occurred over a period of 17.5 hours. This temporal response can be used to show that for $V \sim 240\ ergs/cm^3$, $1/\overline{V}^3 \sim 2.9$.

$$\epsilon \sim \frac{V}{\bar{E}\ T} = \frac{1}{1\,350} = 0.00133$$

suggesting that less than 0.2 percent of all available KE is used to increase the potential energy of the column, in good agreement with typical values of elsewhere (Simpson, Hughes and Morris). Also the depth of the thermocline is given by (Phillips, p. 309):

$$D = 0.75\ \overline{V} \Big/ \left(\frac{g}{\bar{\rho}} \cdot \frac{d\rho}{dz} \right)^{\frac{1}{2}}$$

and using:

$$\overline{V} = 10\ cm\ s^{-1}\ ; \quad \frac{d\rho}{dz} = \frac{.0006}{600}$$

$$D \sim 2.4\ m$$

in good agreement with Fig. 6 (July).

6. LAGOON FLUSHING AND ASSOCIATED ECOLOGICAL PROBLEMS

Crucifix drogue tracking and the results of a numerical model (Jones, 1976) indicate residual velocity vectors of the order of 5 cm s^{-1} parallel to the front. The area to the north of CD is subject to strong oceanic and tidal influences which at all times of the year provide enough energy to forbid the development of any form of stratification and cause flushing in less than two days. The location of CD changes (Fig. 5) seasonally, but is to a large extent dependent upon the 2.3 m depth contour (Fig. 4). The seasonal thermocline also develops at about this depth during the summer when the front is established. Then, water exchange between the ocean and the lagoon is of a transitory nature, inhibited by closed circulations and occurring during storms with associated wind speeds $> 7\ m\ s^{-1}$ only (once in August and twice in October during 1974). During winter months the absence of stratification at the boundary means that the horizontal density gradient along AB supports advection caused by tidal action, wind stress, and wave transport. Calculations based on this assumption suggest a maximum flushing time of a month (Darbyshire, Bellamy and Jones, 1976).

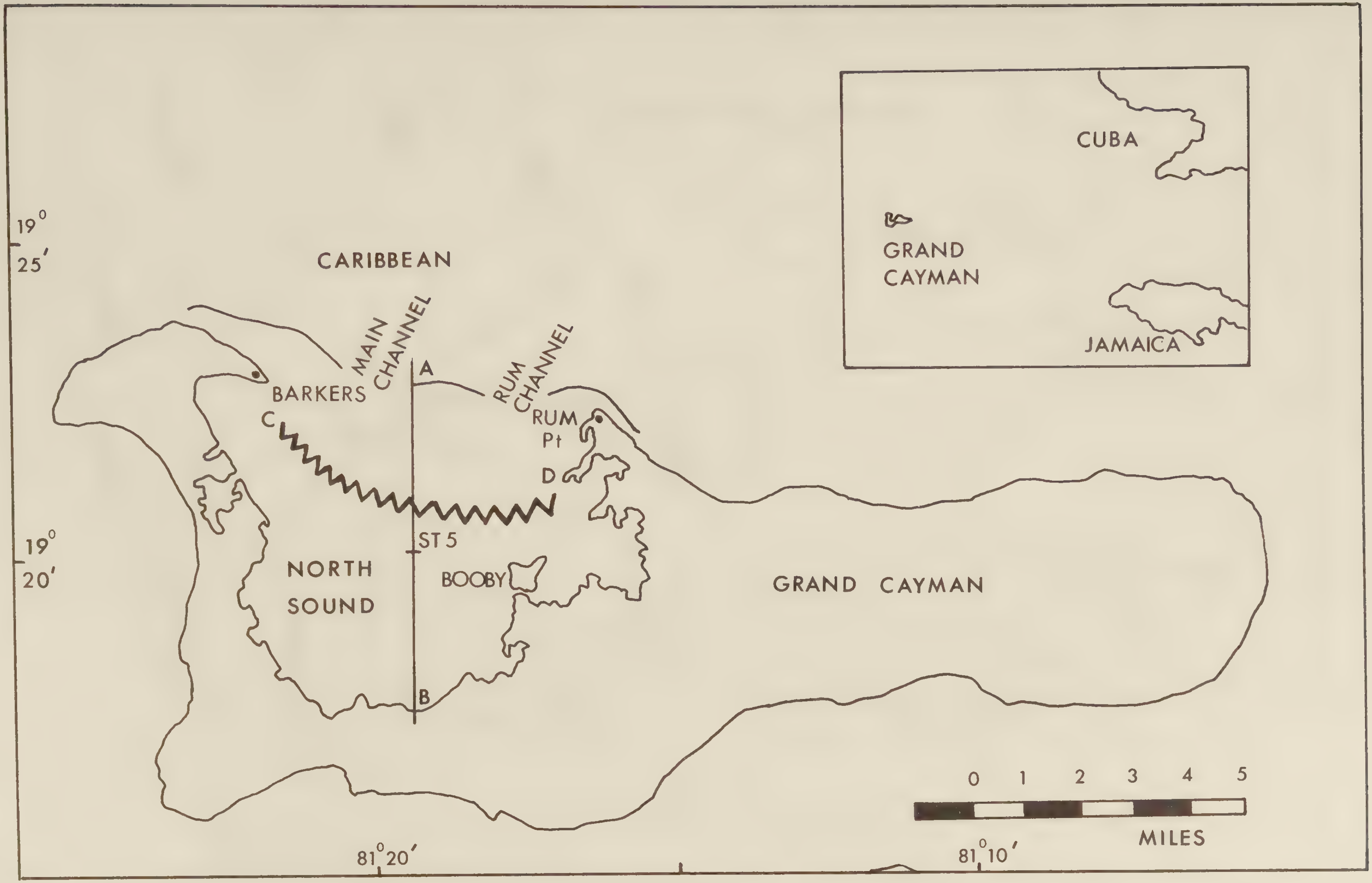
19°
25′
19°
20′
CARIBBEAN
MAIN
CHANNEL
RUM
CHANNEL
A
BARKERS
C
RUM
Pt
D
ST 5
NORTH
SOUND
BOOBY
B
GRAND CAYMAN
CUBA
GRAND
CAYMAN
JAMAICA
0 1 2 3 4 5
MILES
81°20′
81°10′

Fig. 1 Location of study area

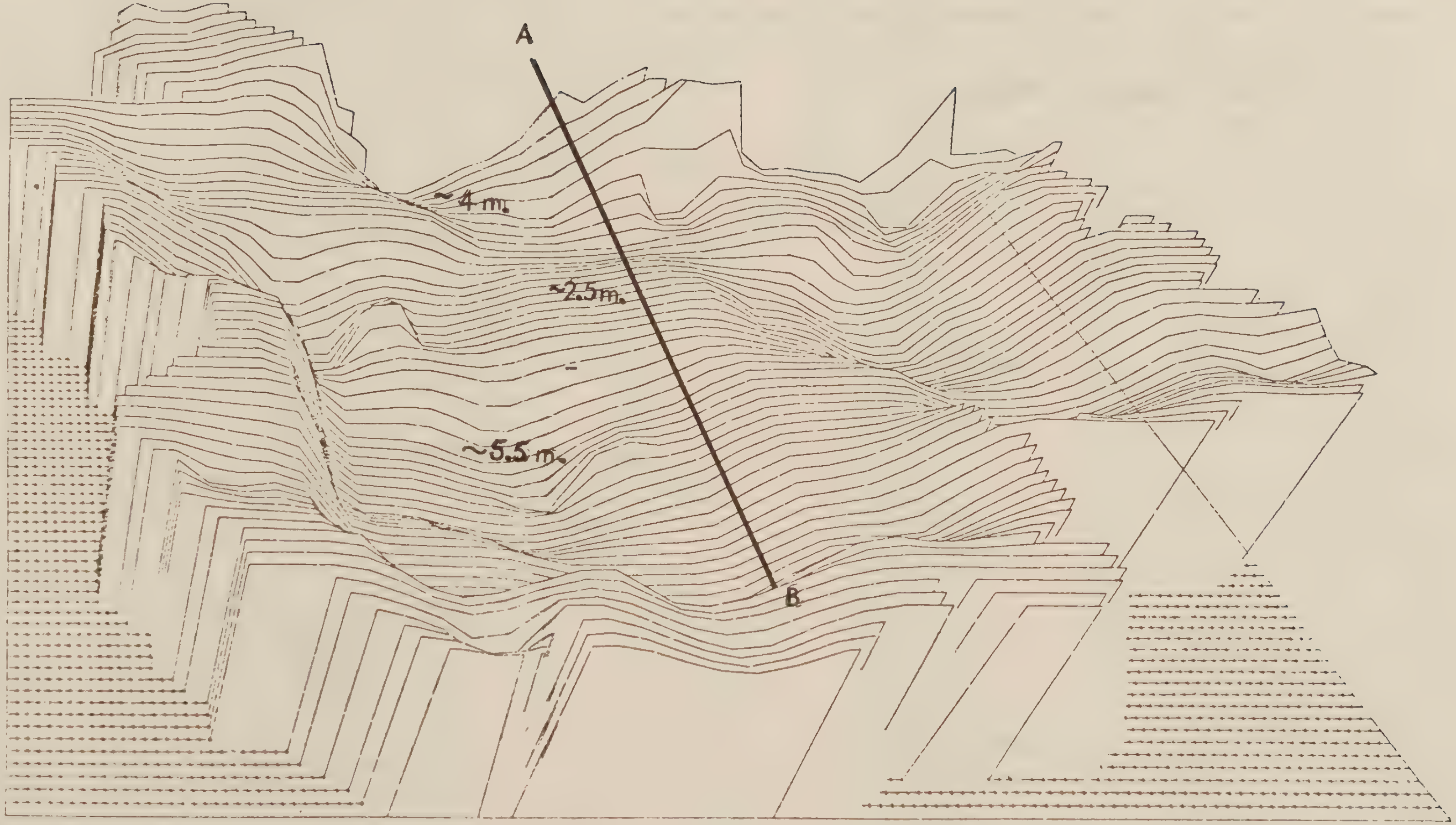

Fig. 2 North sound tri-di projection

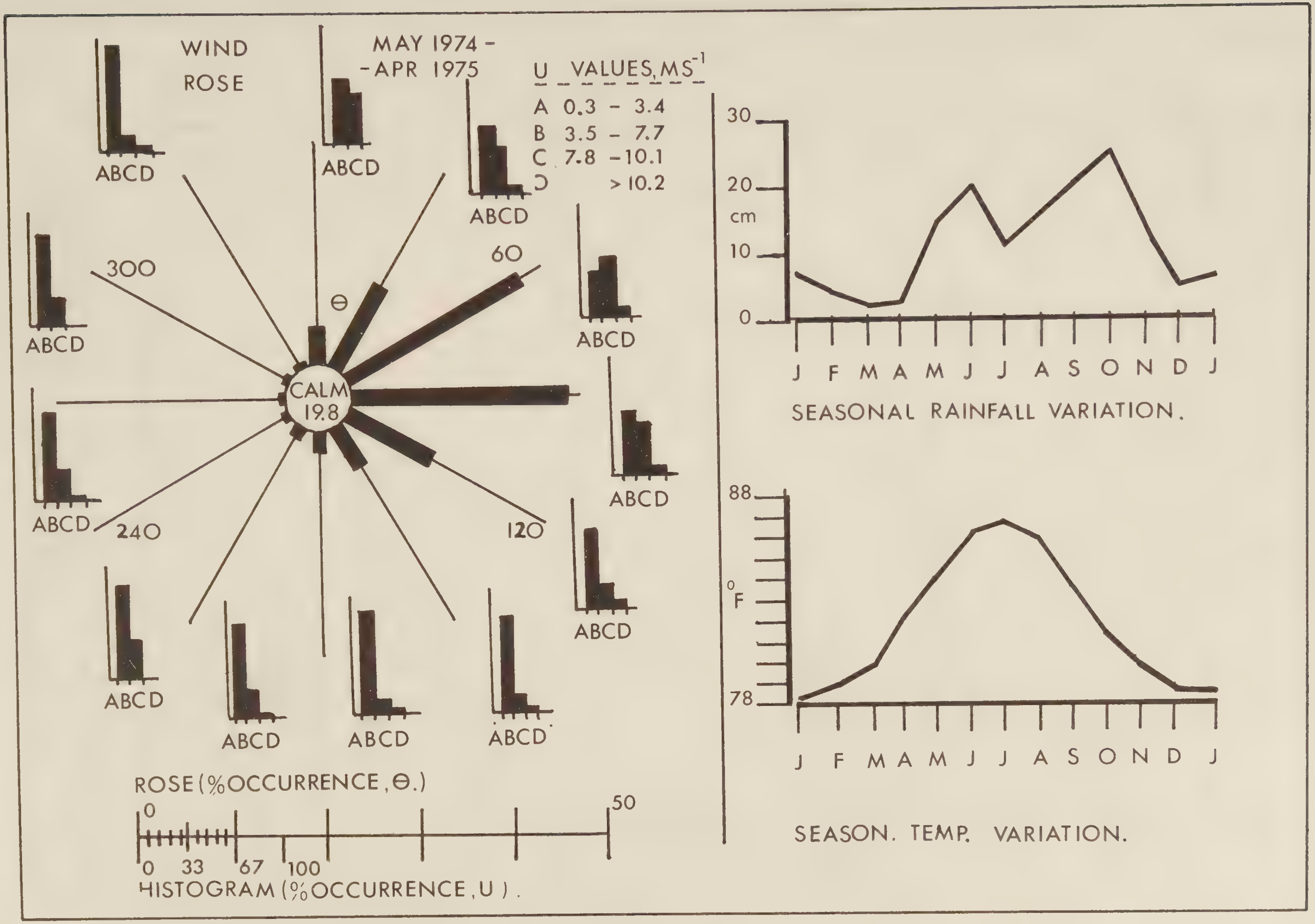
WIND ROSE
MAY 1974 - -APR 1975
U VALUES, MS^{-1}
A 0.3 - 3.4
B 3.5 - 7.7
C 7.8 -10.1
D >10.2
ABCD
CALM 19.8
Θ
60
120
240
300
ROSE (%OCCURRENCE, Θ.)
0
50
0 33 67 100
HISTOGRAM (%OCCURRENCE, U).
30
20
cm
10
0
J F M A M J J A S O N D J
SEASONAL RAINFALL VARIATION.
88
°F
78
J F M A M J J A S O N D J
SEASON. TEMP. VARIATION.

Fig. 3

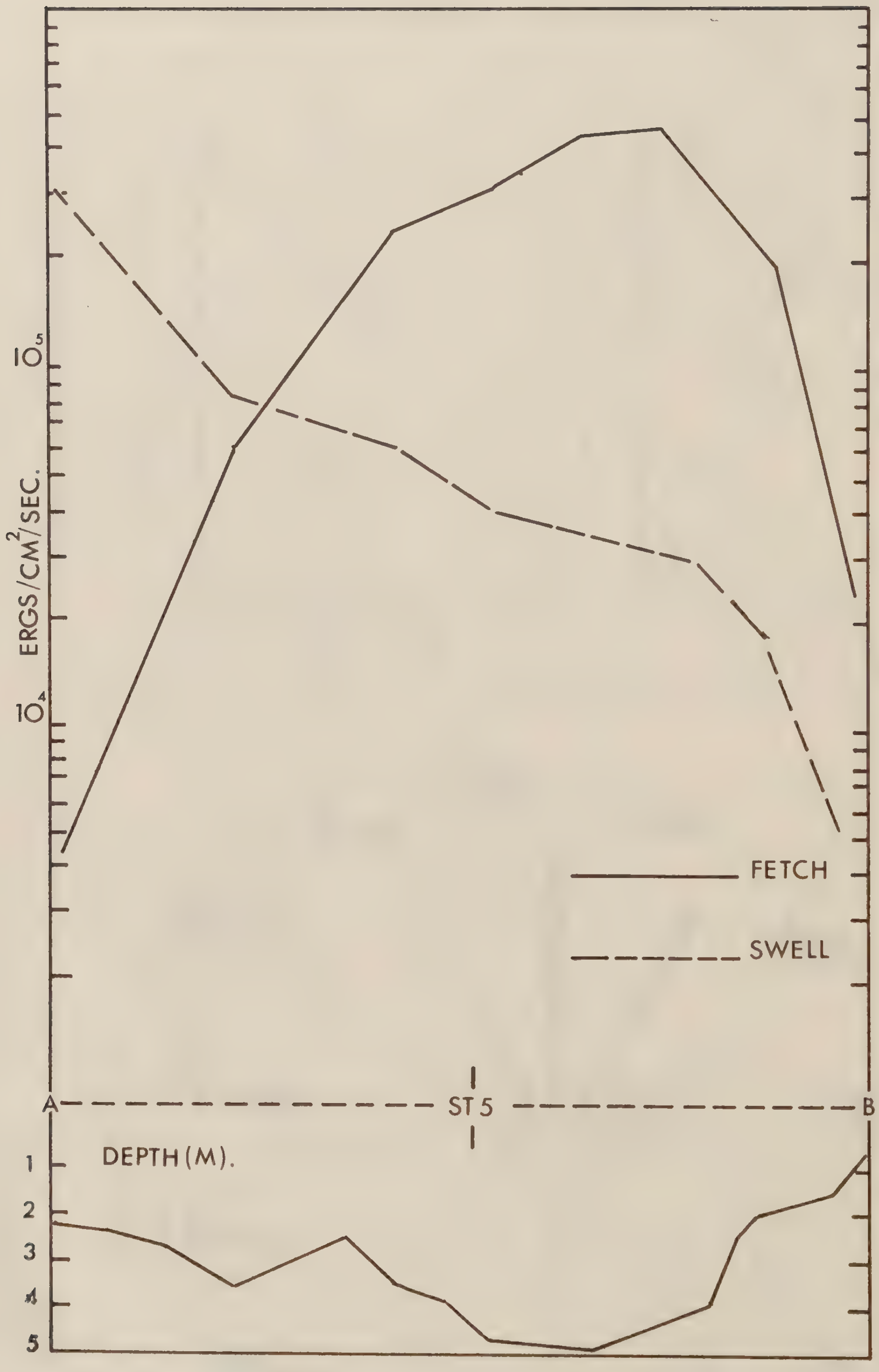

Fig. 4 Depth profile and mean wave energy distribution section AB

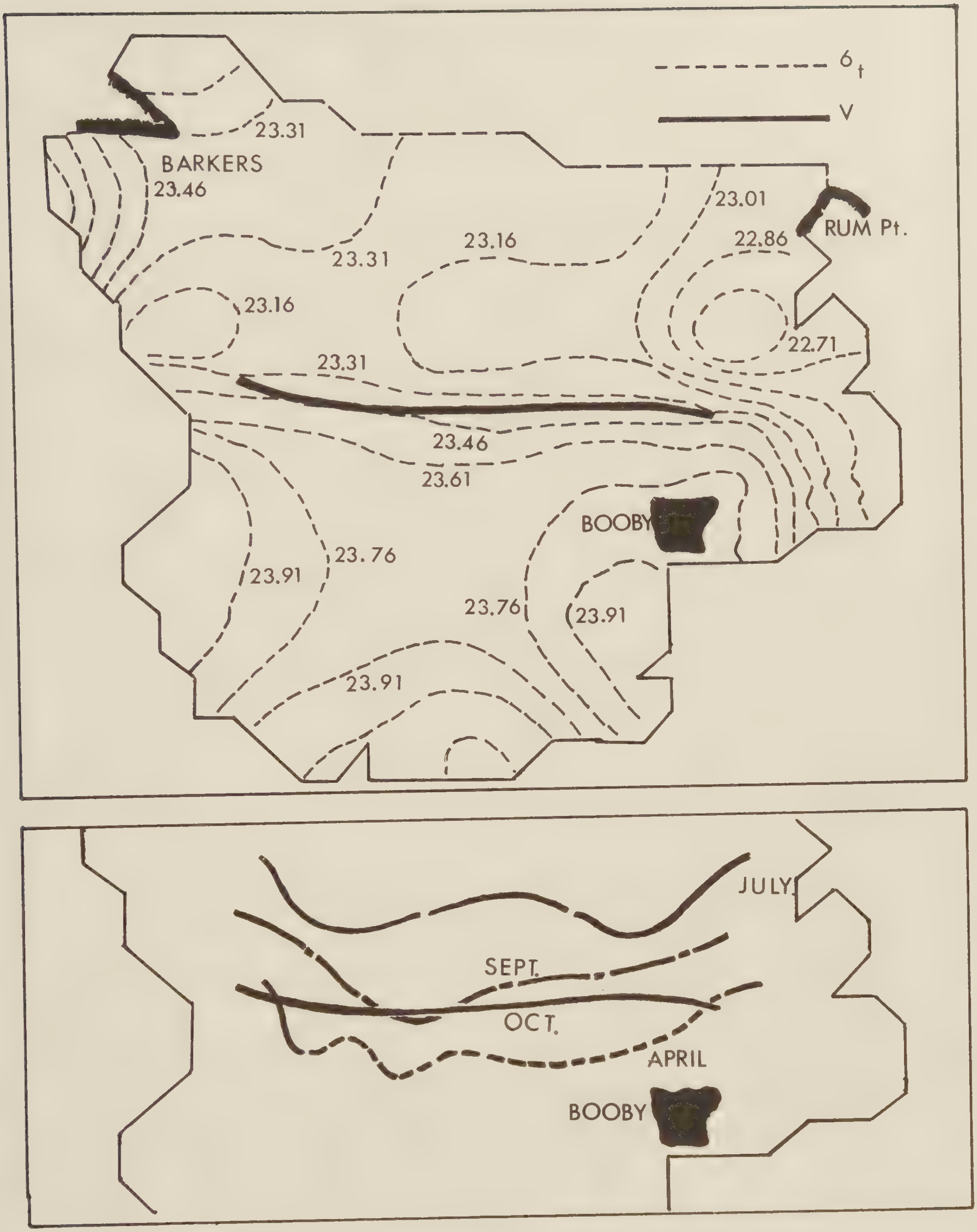
6t
V
BARKERS
23.31
23.46
23.31
23.16
23.01
RUM Pt.
22.86
23.16
22.71
23.31
23.46
23.61
BOOBY
23.76
23.91
23.76
23.91
23.91
JULY
SEPT.
OCT.
APRIL
BOOBY

Fig. 5 (1) σ_t contours at 01m depth, October 1974, and associated position of maximum horizontal σ_t gradient, (2) similarly located maximum σ_t gradients during the months indicated

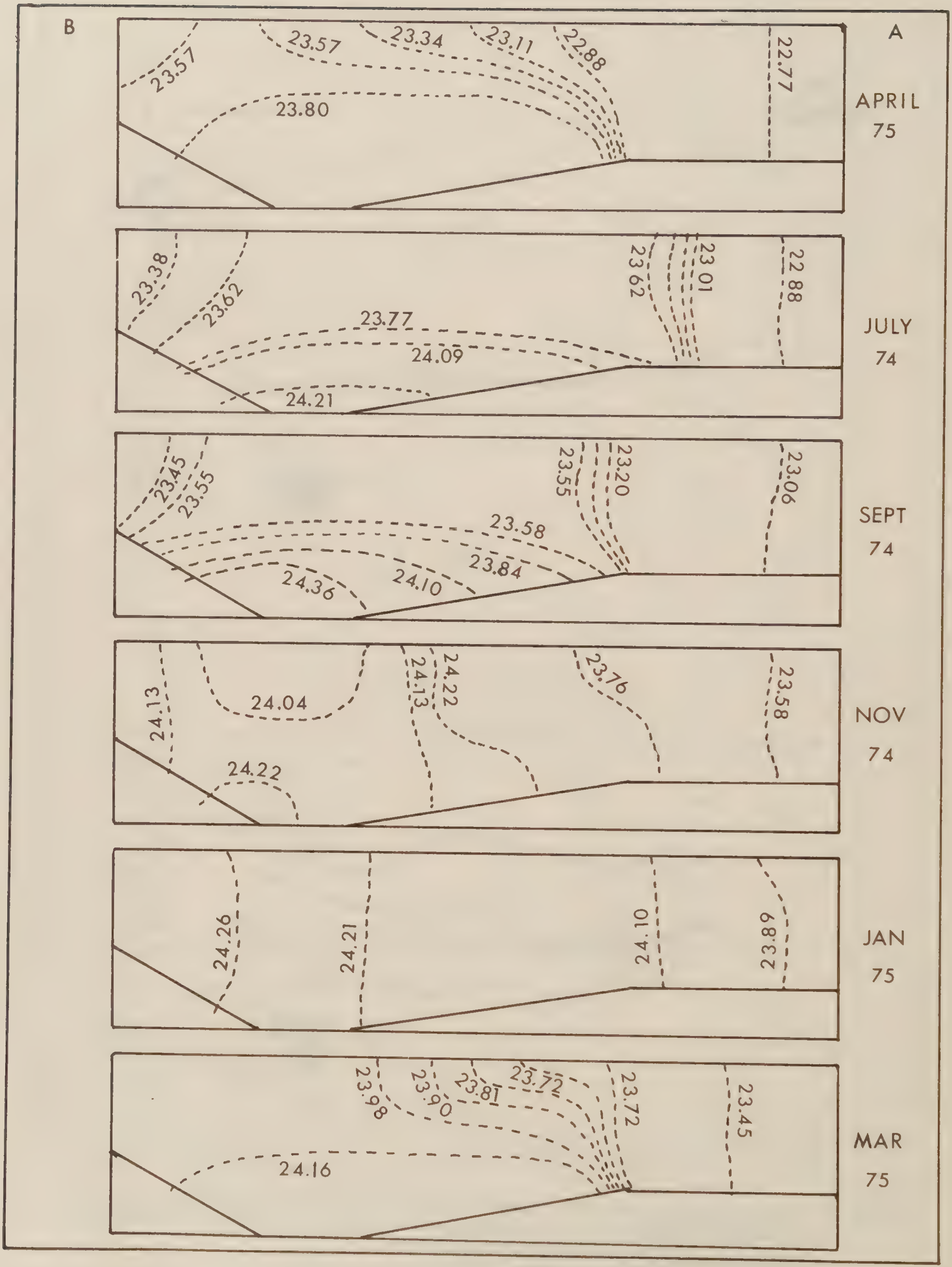

Fig. 6 σ_t Section AB

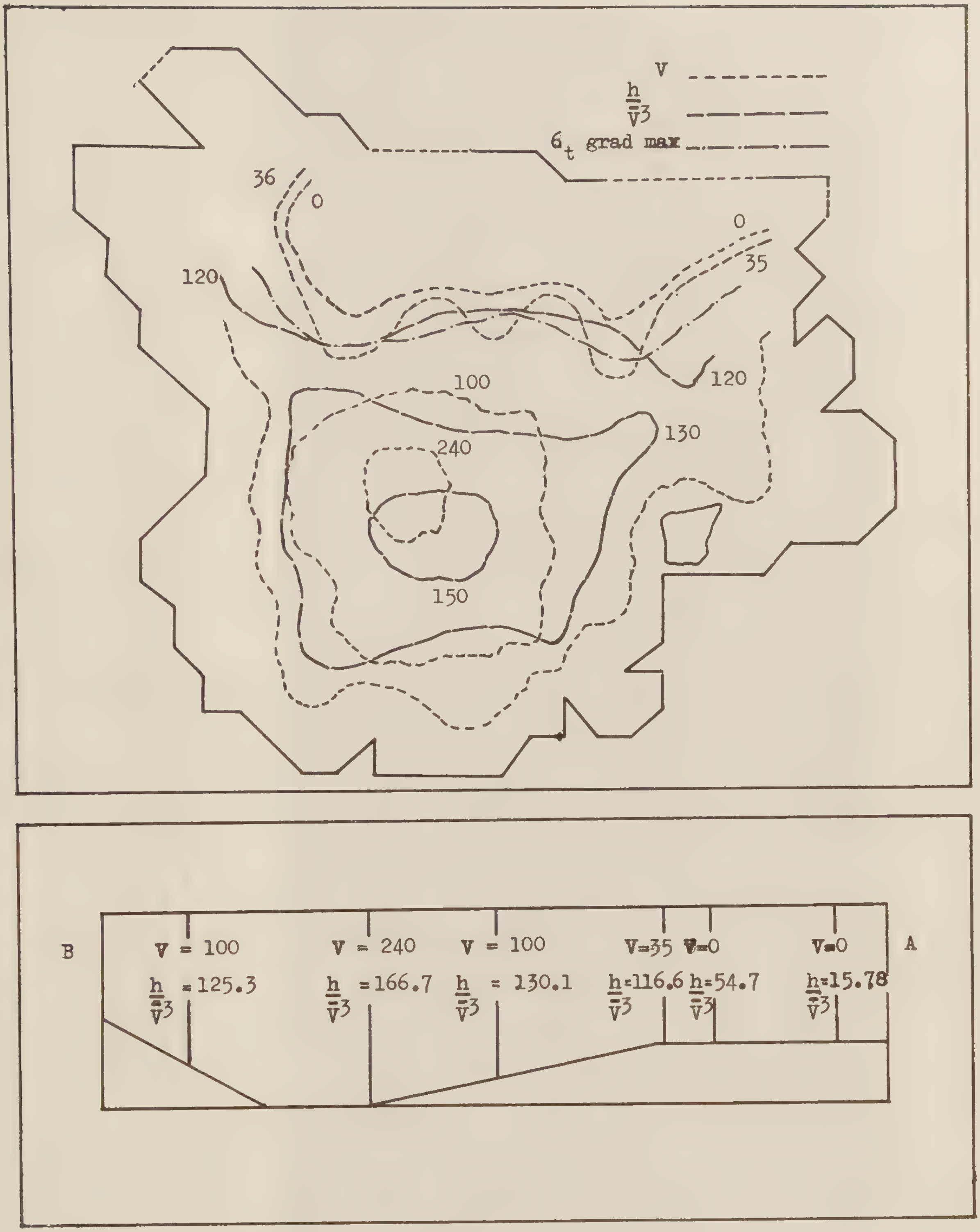
V
h/V̄3
6t grad max
36
0
120
0
35
100
120
130
240
150
B
V = 100
h/V̄3 = 125.3
V = 240
h/V̄3 = 166.7
V = 100
h/V̄3 = 130.1
V=35
h/V̄3=116.6
V=0
h/V̄3=54.7
V=0
h/V̄3=15.78
A

Fig. 7 (i) Contours of V and h/$\overline{V}^3$

(ii) Values of V and h/$\overline{V}^3$ (surface) July 1974, Section AB

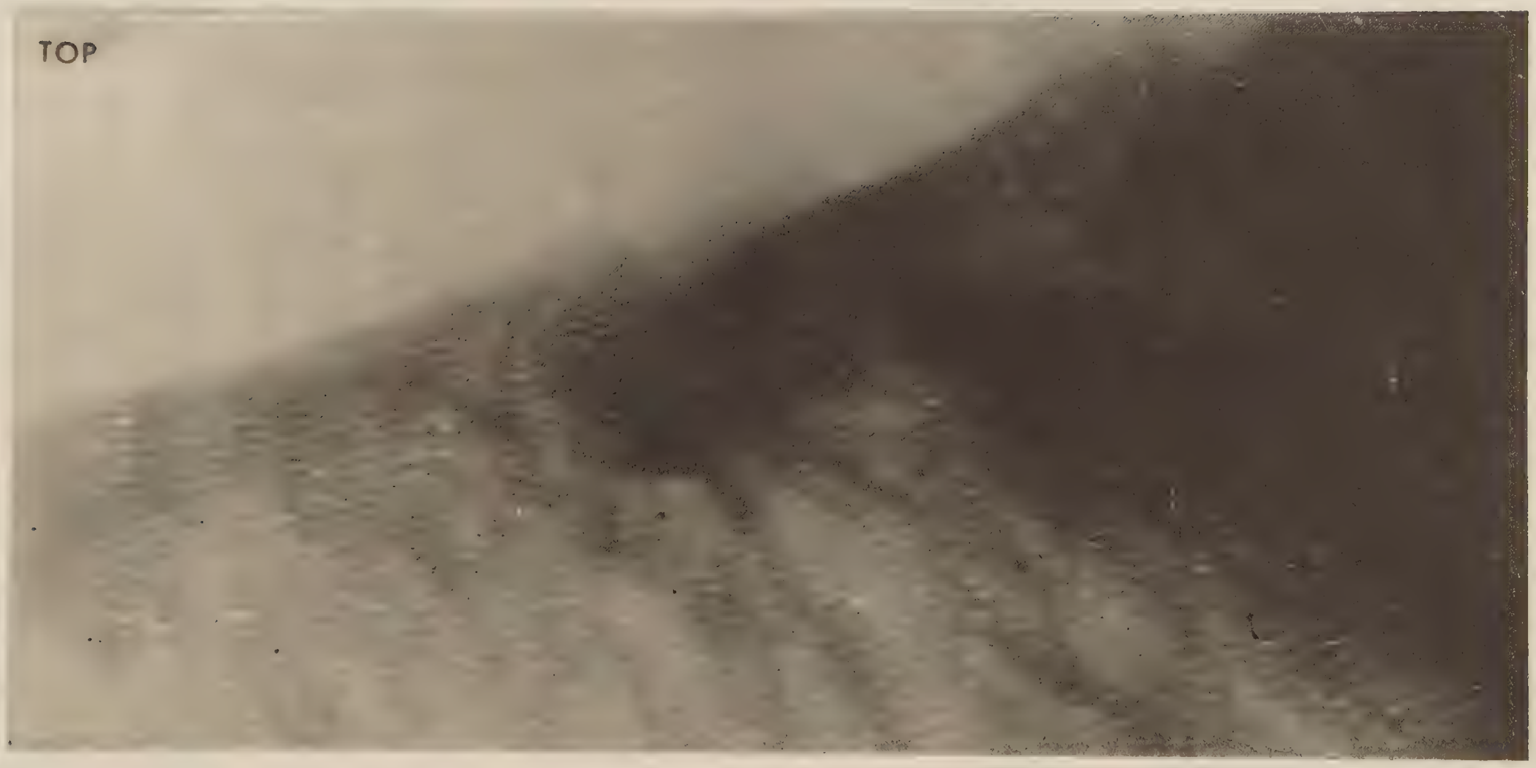

Plate 1 The summer front deliniated by clear ocean water (top) and sound water (bottom) discoloured by suspended fines and mangrove run-off. The photograph was taken after the subsidence of a storm before suspended materials settled, but during storms (winds 7 m sec^{-1}), plumes of water extend oceanward through Main Channel

A parallel biological study has indicated the occurrence of nutrient accumulation in the bottom summer layer, caused by the absence of mixing with the surface layer. At this time the underwater light climate is also more favourable because of lower u_i values. Thus the combination of long retention time and higher transparencies contributes to the efficient utilization of the nutrients available; the plant and animals acting as a "trap". Interference with the ecological balance during this period is dangerous. The introduction of fines to the surface layers, e.g., the wastage from a dredging device could effectively "blanket" the bottom layer from sunlight for a period of months until the onset of a storm, after which particulate matter could settle before the reappearance of stratification.

7. REFERENCES

Darbyshire, J., I. Bellamy and B. Jones, Ministry of Overseas Development Cayman Islands
1976 Natural Resources Study. Part III. Results of the investigations into the physical oceanography. London, Ministry of Overseas Development

Jones, B., A study of the circulation of North South Lagoon, Grand Cayman W.I. Thesis.
1976

Kullenberg, G.E.B., On vertical mixing and the energy transfer from the wind to the water
1976 Tellus, 28:159-65

Phillips, O.M., The dynamics of the upper ocean. Cambridge, Cambridge University Press,
1969 262 p.

Simpson, J.H. and J.R. Hunter, Fronts in the Irish Sea. Nature, Lond., 250(5465):404-6
1974

Simpson, J.H., D.G. Hughes and N.C.G. Morris, The relation of seasonal stratification to tidal mixing on the continental shelf (submitted for publication)

Turner, J.S., Buoyancy effects in fluids. Cambridge, Cambridge University Press, 367 p.
1973

THE 1972-1973 CYCLE OF THE GULF LOOP CURRENT
PART II: MASS AND SALT BALANCES OF THE BASIN

by

G.A. MAUL
National Oceanic and Atmospheric Administration
Atlantic Oceanographic and Meteorological Laboratories
Miami, Florida 33149

CONTENTS

1. INTRODUCTION
2. HYDROGRAPHIC DATA
3. GEOSTROPHIC TRANSPORTS
4. MASS BALANCE OF THE GULF
5. SALT BALANCE OF THE GULF
6. SUMMARY AND CONCLUSIONS
7. ACKNOWLEDGEMENTS
8. REFERENCES

Abstract

Hydrographic sections were made across the Yucatan Strait and the Straits of Florida approximately every month from May 1972 to September 1973. These data encompass a cycle of the Gulf Loop Current from eddy separation to eddy separation. The data suggest that the 5°C water near the bottom of the Yucatan Strait is forced out of the Gulf of Mexico when the Loop starts to form. About mid-way through the growth phase, resident Gulf waters advect out the Straits of Florida between the continental shelf of the United States and the Florida Current. After separation of an eddy, the 5° water flows back into the basin, continuity being maintained by continued flow along the Florida coast. In the upper 700 m, approximately 10% of the water flowing into the basin through the Yucatan Strait is exchanged with resident Gulf waters before flowing out the Straits of Florida. The eddy separation causes an injection of 10^{16} g of salt into the western Gulf, and accounts for approximately 75% of the total salt exchange between the Gulf Loop Current and resident Gulf waters. Even though the basin has an excess of evaporation over precipitation, river runoff more than accounted for the atmospheric loss of fresh water during the 1972-1973 cycle.

Resumen

Desde mayo de 1972 hasta septiembre de 1973 se hicieron secciones hidrográficas, aproximadamente cada mes, a través del estrecho de Yucatán y de los estrechos de la Florida. Los datos, que pertenecen a un ciclo de la corriente del Golfo entre dos separaciones de remolinos, indican que las aguas a 5°C situadas cerca del fondo del estrecho de Yucatán vienen forzadas desde el Golfo de México, al empezar a formarse el bucle: cuando la fase de crecimiento está en su mitad, aproximadamente, las aguas del Golfo calientan por advección los estrechos de la Florida, entre la plataforma continental de los Estados Unidos y la corriente de la Florida. Después de la separación de un remolino, el agua a 5°C, afluye de nuevo a la cuenca, y la continuidad se mantiene por el flujo constante a lo largo de la costa de la Florida. En los 700 m superiores, el 10 por ciento aproximadamente, del agua que afluye

a la cuenca a través del estrecho de Yucatán se intercambia con las aguas del Golfo, antes de afluir a los estrechos de la Florida. La separación del remolino causa una inyección de 10^{16} g de sal en el Golfo occidental, cantidad que representa el 75 por ciento, aproximadamente, de todo el intercambio de sal entre la corriente circular del Golfo y las aguas permanentes del Golfo. Aunque, en la cuenca, la evaporación es mayor que la precipitación, las pérdidas atmosféricas de agua dulce durante el ciclo 1972-1973 se debieron principalmente a la escorrentía fluvial.

1. INTRODUCTION

Between May 1972 and September 1973, 14 cruises were made into the eastern Gulf of Mexico to study the Gulf Loop Current. A multi-ship study was made in May 1972 to investigate the Yucatan Current (Molinari and Yager, 1977), the Florida Current (Brooks and Niiler, 1975) and the Gulf Loop Current (Morrison and Nowlin, 1977). Individual cruises were made in June 1972 and May 1973 by Texas A & M University, and a time-series of 12 cruises was made at 36-day intervals starting in August 1972 (Maul, 1977). The latter included STD sections across the Straits of Florida and the Yucatan Strait as well as XBT surveys to map the path of the current from Yucatan to Key West.

Data from these investigations encompass one complete cycle of the Gulf Loop Current as proposed by Leipper (1970): spring intrusion, autumn spreading, and eddy separation. Maul (1977) noted that there was a great deal of year-to-year variability of this idealized pattern and calculated that the Yucatan Current transport exceeds the Florida Current transport during the period of Loop intrusion and spreading by 4×10^6 m^3 s^{-1}. During the intrusion and spreading phase, Maul (1977) concluded that a southward flow at the bottom of the Yucatan Strait may be the mechanism that preserves mass continuity.

In this paper, the STD and XBT data across the two straits are discussed, followed by an error analysis and calculations of the year-long cycle of geostrophic transports. Since direct computation of transport imbalances between the two sections involves determination of a small difference between two large numbers, an indirect method involving water mass identification is employed. Within the error limits imposed by the available data, a synthesis of the mass balance of the Gulf of Mexico basin is then made. The quantity of salt exchanged into the Gulf from the separation of the 1972 anticyclonic eddy is calculated next, and the fresh water required to maintain the mean salinity of resident Gulf water is determined from 1972-1973 river runoff data. Finally, the evaporation-precipitation role in the basin is investigated to complete the mass and salt balance study.

2. HYDROGRAPHIC DATA

Cross-sections of the Straits of Florida (between the Florida Keys and Havana) and of the Yucatan Strait (between Cape San Antonio, Cuba and Contoy Island, Mexico) were made during every cruise except January 1973, when weather prevented observations. Station spacing was approximately 18 km. Stations were occupied to within 22 km of the Cuban coast, and approximately to the 50 m isobath off Mexico and Florida. Seven stations were in the Straits of Florida section, and nine were across the Yucatan Strait. STD data were obtained to a depth of 1 000 m or close to the bottom for each cruise except February and March 1973 when SBT data only were obtained; in September 1972, XBT data only were obtained in the Yucatan Strait.

The STD used was a Plessey model 9060, which is a battery-operated, graphic-recording instrument. Manufacturer's specifications of accuracy for this instrument are S=0.05°/oo, T=0.1°C, D=0.25% (~5 m); resolution specifications are S=0.02°/oo, T=0.05°C, and D=0.1% (~2 m). Bathythermograph observations were made using Sippican T-7 SBT probes whenever possible, which gives temperature to a maximum depth of 750 m. In a few instances, depths of less than 750 m were observed because of mechanical (STD winch) or logistical difficulties.

Calibration samples of salinity and temperature were available at the surface for each XBT or STD station. Since no calibration data were available at depth, the historical salinity minimum of 34.84°/oo in the Antarctic Intermediate Water (Molinari, 1974) was used as a deep salinity calibration point. Linear corrections were applied to the STD salinity data after digitization in 20 m depth increments, at 0.01°C and 0.01°/oo resolution. Intercomparisons between surface STD values and surface calibration values show that the standard error estimate is T = ± 0.13°C, and S = ± 0.05°/oo.

Since the interest here is to calculate transport, a salinity assignation is necessary in order to include the sections where only XBT data are available. Emery (1975) reviewed the problem and concluded that in the North Pacific Ocean, when the T-S relationship is "tight", dynamic height can be computed from XBT data alone. That is (Emery, 1975), the difference between dynamic height found by using the mean T-S relation and observed temperature and salinity was smaller than either the theoretical measurement error (0.04 dynamic metres) or observed variation in dynamic height at two ocean station sites (Victor and November), but not at a third (Papa). Nowlin and McLellan (1967) found that the T-S relation in waters cooler than 17°C was extremely consistent throughout the southeastern Gulf of Mexico, but in the waters warmer than 17°C, there are two distinctly different water masses. It is necessary to distinguish between these two water masses for two reasons: (1) transports estimated by using T-S correlations for XBT data are affected, and (2) to avoid the aforementioned difficulty of determining a small transport difference between two large values.

There are several reasons why a direct calculation of the transport difference between the Yucatan Strait and the Straits of Florida will not be attempted with these data, not the least of which is item number two in the paragraph above. In order to include the SBT sections, a geostrophic reference level must be selected at 750 m or less; the Gulf Stream System is known to have velocities of from 5 to 20 cm s^{-1} at this depth. Another significant uncertainty is due to the lack of measurements near Cuba; the importance of transport near the Cuban coast will be demonstrated by recalculating Montgomery's (1941) section from Key West to Havana. Using hydrographic data only means that the geostrophically balanced baroclinic component of the transport is known; uncertainties due to the barotropic component are probably as large as the transport difference between the Yucatan Current and the Florida Current. To solve the problem, the water mass transports in the Straits of Florida will be separated into two groups: transport of the current itself, and transport of non-Gulf Stream water. Transport estimates of this non-Gulf Stream water are less subject to the above mentioned errors because it was spatially well sampled in 1972-1973, observations were taken to near the bottom, geostrophic current speeds near the bottom are probably small, barotropic uncertainties are minimized because a small cross sectional area is involved and only low frequency (i.e., baroclinically adjusted) phenomena will be discussed. Identification and transport calculations of the water masses are presented in the next section, followed by a discussion of the inferred mass balance of the Gulf of Mexico.

3. GEOSTROPHIC TRANSPORTS

Wennekens (1959) labelledtwo distinct water masses in the Straits of Florida: Yucatan Water, which is herein named Florida Current Water (FCW), and Continental Edge Water (CEW). The 1972-1973 data set does not have salinity observations each month, therefore, the T-S properties cannot be used as the primary means of distinguishing Florida Current Water from Continental Edge Water. However, since both Leipper (1970) and Maul (1977) used the 22°C isotherm at 100 m depth to locate the cyclonic side of the current, it seems natural to pose the hypothesis that the T-S properties of waters where the 22°C isotherm is at or greater than 100 m depth (22°C $\geq$ 100 m) are different from those waters where the 22°C isotherm is at a depth less than 100 m (22°C < 100 m). To investigate how well using the depth of 22°C isotherm identifies water masses, plots were made (Fig. 1) of the T-S relation for stations in the Straits of Florida where the 22°C isotherm was at a depth of 100 m or greater (left panel) and for those stations where the 22°C isotherm was at a depth of less than 100 m (right panel). Comparison between the two panels of Fig. 1 is facilitated by reference to Fig. 2, which is a plot of the mean T-S values. In Fig. 2, water in the Straits of Florida where the 22°C isotherm was at a depth of less than 100 m is labelled Continental Edge Water, water where the 22°C isotherm was at a depth of 100 m or greater is labelled Florida Current Water. The curve labelled Yucatan Current Water (YCW) is the mean T-S correlation of all stations taken in the Yucatan Strait where the 22°C isotherm was at a depth of 100 m or deeper.

The two most striking features of the T-S plots are: (1) the remarkable similarity of the correlation in the cool waters ($\leq$ 15°C in these data; cf. Nowlin and McLellan, 1967), and (2) the distinctly different patterns in waters warmer than 15°C. T-S correlations in the right-hand panel of Fig. 1 are qualitatively similar to what Wennekens (1959) called Continental Edge Water, and what Nowlin and McLellan (1967) pointed out as being typical of resident Gulf (non Eastern Gulf Loop Current) Water. The left-hand panel of Fig. 1 is quantitatively similar to what Wennekens called Yucatan Water, Nowlin and McLellan called Eastern Gulf Loop Current Water, or what is characteristic of Caribbean Water (Wüst, 1964).

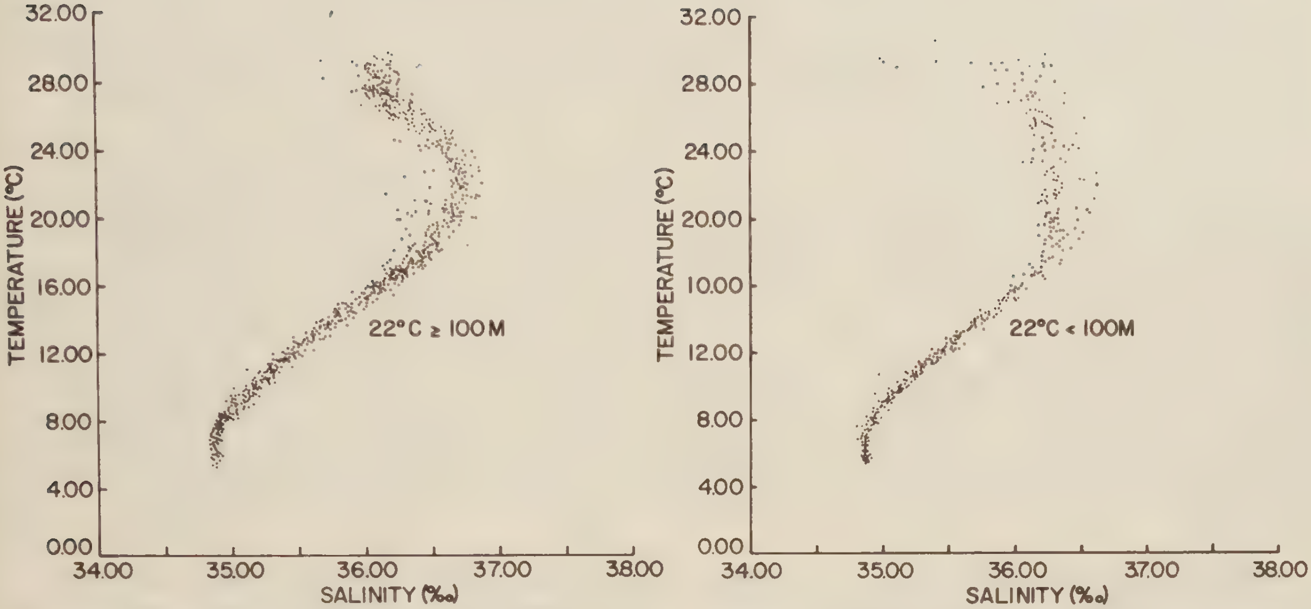

Fig. 1 Temperature-salinity correlation for the Straits of Florida. Left Panel: correlation for 35 stations that had 22°C ≥ 100 m. Right Panel: correlation for 24 stations that had 22°C < 100 m

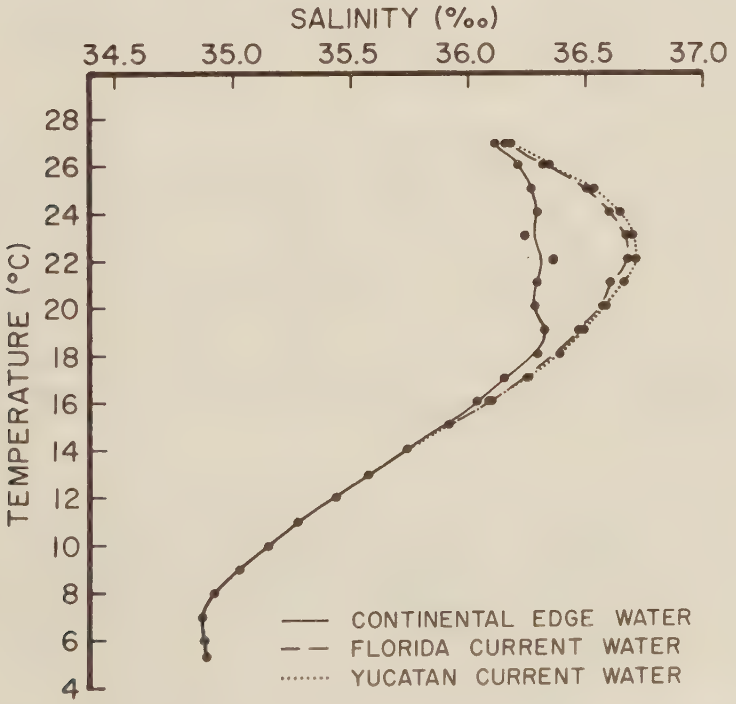

Fig. 2 Mean temperature - salinity correlations for the three water masses observed during the 1972-1973 time series

In Fig. 2, a distinction is made between Yucatan Current Water and Florida Current Water. In the Subtropical Underwater (i.e., in the temperature range $18^\circ C \leq T \leq 24^\circ C$), the salinity of the Yucatan Current Water is approximately 0.05 °/oo higher than in the Florida Current Water. It would be interesting to speculate that this 0.05 °/oo difference is due to mixing at the edge of the Loop Current, as the data frequently suggested small eddies (e.g., Maul, Norris, and Johnson, 1974; Lee, 1975; Maul, 1977) and complex thermal patterns (as observed in satellite infra-red images). However, judging from the scatter of points in the T-S correlation (cf. left-hand panel of Fig. 1) and the calibration results of the 9060 STD, a straightforward discussion of mass and salt exchange along the current path is not possible with these data. An investigation of the salt balance of the entire basin using an indirect method is possible; this will be discussed in the section entitled Salt Balance of the Gulf.

Returning to the problem of using temperatures (only) to distinguish water masses, it is clear from Fig. 1 and 2 that to first-order, the depth of the 22°C indicator isotherm distinguishes two water masses. When the data are examined in detail, stations in the transition zone between Continental Edge Water and Florida Current Water were found to have temperatures greater than 22°C at 100 m, but with T-S properties more like those of Continental Edge Water than Florida Current Water. Conversely, stations were found to have a temperature of less than 22°C at 100 m, but with T-S properties more like those of Florida Current Water than Continental Edge Water. This is seen in Fig. 1 as scatter about the main trend in the T-S correlations. A station pair in June 1973 had a geostrophic surface velocity (relative to 700 m) of 1.5 m s^{-1}, yet the T-S correlation for both stations was a mixture of Continental Edge Water and Florida Current Water. These examples highlight the difficulty of water mass identification at the edge of a current, even when the T-S data are available.

The XBT only transects were incorporated into the analysis by including all stations where the 22°C isotherm was at a depth of 100 m or greater in the Florida Current Water summation, and by including all station pairs where one station had the 22°C isotherm at a depth of 100 m or greater in the Florida Current Water summation. The reason for the second criterion is that, on the average, the 22°C isotherm at 100 m depth was 11 km to the south of the surface manifestation of the Florida Current (Maul, 1975). The mean transport of Continental Edge Water (see Table I) using temperature criteria only to identify the water mass, was compared to transports when temperature and salinity were available; uncertainty in the mean transport from using observed temperature and T-S correlations is calculated to be less than ± 7%.

The reliability of using T-S correlations in transport calculations of the main current was investigated by recalculating the August 1972 STD transect of the Yucatan Strait, using both the T-S correlation of Continental Edge Water and the historical mean T-S for Yucatan Current Water prepared from NODC data by Molinari (1974). In this transect, the RMS deviation of the dynamic height difference between the actual station data and T-S correlated data is 0.02 dynamic metres using either T-S correlation. Relative to 700 m, the transport calculated from the observed values in the August 1972 transect was $26.6 \times 10^6\ m^3\ s^{-1}$; the transport calculated from the historical T-S correlation, using observed temperatures, was $25.8 \times 10^6\ m^3\ s^{-1}$; the transport using the T-S for Continental Edge Water and observed temperatures was $27.0 \times 10^6\ m^3\ s^{-1}$. These calculations suggest, that when using the appropriate T-S correlation with XBT data, the geostrophic transport relative to 700 m can be estimated to within ± 3%.

The geostrophic transports for the 1972-1973 data set are summarized in Table I. Two dates are given in the first column: The first is that of Yucatan Strait observations, and the second is for those in the Straits of Florida. Means and standard deviations ($\pm\sigma$) for each column are given at the bottom of the table. Transport of Continental Edge Water is included in the total value for the Straits of Florida and also is separated into an individual column.

TABLE I

Summary of Geostrophic Transports
Relative to 700 m Depth

Date	Yucatan Strait		Straits of Florida		
	Total Transport	Surface Speed	Total Transport	Surface Speed	Transport CEW
1972	($10^6 m^3 s^{-1}$)	($m s^{-1}$)	($10^6 m^3 s^{-1}$)	($m s^{-1}$)	($10^6 m^3 s^{-1}$)
22,25 Aug	26.6	0.88	21.8	1.03	1.2
27,29 Sep	17.5	0.82	22.9	0.87	1.2
1, 5 Nov	19.9	0.63	29.0	1.13	0
7,11 Dec	31.1	0.95	22.2	1.00	0
1973					
16,15 Feb	30.9	0.92	12.4	0.61	1.3
24,23 Mar	32.6	1.22	17.8	0.61	2.3
29,27 Apr	23.0	0.66	12.5	0.48	2.2
4, 2 Jun	22.5	0.73	19.1	0.77	5.1
9, 7 Jul	19.7	0.88	11.4	0.64	3.9
14,12 Aug	30.3	1.16	21.4	0.63	8.3
20,18 Sep	25.3	0.73	23.2	1.05	4.1
Mean	25.4	0.87	19.5	0.80	2.7
σ	±5.3	±0.19	±5.4	±0.22	±2.5

Reference level for the values reported in Table I was chosen as 700 m in order to include all the SBT data and for comparison with other investigations (e.g., Schlitz, 1973; Morrison and Nowlin, 1977; Molinari and Yager, 1977). When water depths were less than 700 m, the method of Jacobsen and Jensen (1926) was used to estimate velocities in shallow water with respect to the deeper stations. This method affected the Yucatan Strait calculations more than the Straits of Florida calculations, because strong currents were frequently found close to the Mexican coast in shallow water, but not so off the Florida coast. One remaining problem affects the September 1972 values; namely that the Yucatan XBT section was sampled to only 460 m and the Florida STD section to only 580 m due to mechanical difficulties. Corrections of 1.2 x 10^6 m^3 s^{-1} for the 460 - 700 m layer in the Yucatan Strait and 0.5 x 10^6 m^3 s^{-1} for the 580 - 700 m layer in the Straits of Florida, were calculated from sections whose transports were similar to September 1972.

Recent investigations into the transport of the Yucatan Current have been made by Schlitz (1973), Morrison and Nowlin (1977), Molinari and Yager (1977) and by Hansen and Molinari (1978). Schlitz compared geostrophic transports relative to 1 900m and relative to 700 m, and found a difference of only 1 x 10^6 m^3 s^{-1} for April 1970. Schlitz reports 22 x 10^6 m^3 s^{-1} relative to 700 m. Contrary to Schlitz's (1973) experience with the reference level, the transport in the Yucatan Strait is 26.6 x 10^6 m^3 s^{-1} for August 1972 relative to 700 m (Table I), but is 34.0 x 10^6 m^3 s^{-1} relative to 1 000 m. Molinari and Yager (1977) used a surface float for a reference and report 19.9 x 10^6 m^3 s^{-1} and 18.2 x 10^6 m^3 s^{-1} in the upper 700 m during May 1972; the 1972-1973 data yield values of 23 x 10^6 m^3 s^{-1} in April-June (Table I) using 700 m as a reference level. Morrison and Nowlin (1977) calculated a Yucatan Strait transport for May 1972 of 30 x 10^6 m^3 s^{-1} using the deepest station pair as a reference level; Hansen and Molinari (1978) calculated geostrophic transports of 25.8 x 10^6 m^3 s^{-1} and 27.1 x 10^3 m^3 s^{-1} in October 1970 relative to the deepest common data point between adjacent stations (~2 000 m for the deepest pair). The reference level difficulty in the Yucatan Strait has also been discussed by Carder *et al.* (1978); they concluded that the choice of reference level had a much more dramatic effect on calculated currents below 1 000 m than above because the choice of the reference affected the sign of the transport in the deep layer. The average value of 25.6 ± 5.3 x 10^6 m^3 s^{-1}, reported herein, is too low by as much as 15% when compared with some geostrophic estimates which had measurements extending to the bottom, but is 22% higher than another. Nevertheless, based on the August 1973 calculations and the work cited above, the 1972-1973 transports in the Yucatan Strait must be interpreted as representing only the upper layer geostrophic variability.

Geostrophic transports in the Straits of Florida (off Miami) were investigated by Broida (1969) over a 13-month period. Broida's average transport, using the depth of the deepest station pair as a reference level, was 17.9 ± 2.1 x 10^6 m^3 s^{-1}. Niiler and Richardson's (1973) value using the dropsonde technique was 29.5 ± 4.8 x 10^6 m^3 s^{-1}. Niiler and Richardson's value includes both the baroclinic and barotropic components of transport, but they did not separate one from the other. The average geostrophic transport (Table I) in the Straits of Florida for the 1972-1973 data, 19.5 ± 5.4 x 10^6 m^3 s^{-1}, is significantly less than that for the Yucatan Strait. Brooks and Niiler (1975), using a dropsonde technique, report 20.2 x 10^6 m^3 s^{-1} during May 1972 down to the depth where σ_t = 27, in the Straits of Florida off Key West. Molinari and Yager (1977) found that the May 1972 Yucatan Strait transport down to σ_t = 27 was 20.8 x 10^6 m^3 s^{-1}. Morrison and Nowlin (1977) report a value near 23 x 10^6 m^3 s^{-1} for the waters above σ_t = 27. The agreement between Brooks and Niiler, and Molinari and Yager may be fortuitous because neither value includes measurements close to the Cuban coast.

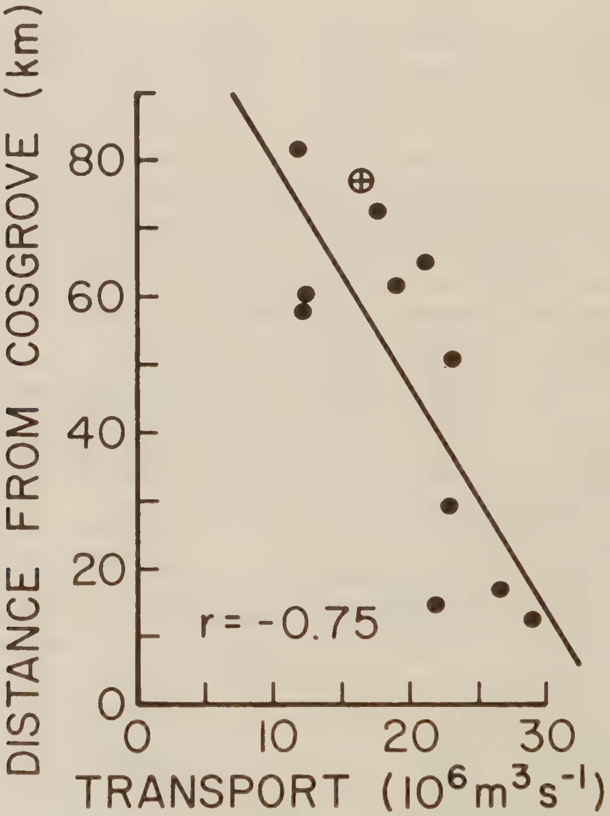

Fig. 3 Correlation between the distance south of Cosgrove Lighthouse (near Key West, Florida) to the Florida Current, and total volume transport through the Straits of Florida

The importance of measuring the transport near the Cuban coast in the Straits of Florida (Fig. 3) by plotting the distance from the 100 m isobath at Cosgrove Lighthouse (northern terminus of the sections) to the point where the 22°C isotherm was at 100 m, versus the total outflowing baroclinic transport above 700 m (summarized in Table I). The least squares line linearly relates the distance (D) from Cosgrove to the transport (T) by $D = -3.3T + 113$; the correlation coefficient, r, is -0.75. Statistically, the *t* test shows that the probability of distance and transport not being related is less than 0.01. These data suggest that the transport of the Florida Current near Havana can be large during those times of the year when the current is far to the south.

As an independent check of the relation between total transport and distance south of the Florida Platform, the section reported by Montgomery (1941), which had a station within 7 km of Havana, was recalculated using 700 m as a reference level. Montgomery's total transport relative to 1 200 m was 26×10^6 m^3 s^{-1}, relative to 700 m it is 22.8×10^6 m^3 s^{-1}. Transport in the section within 23 km of the Cuban coast relative to 700 m was 6.2×10^6 m^3 s^{-1}, or 27% of the total. The total transport in Montgomery's section relative to 700 m, less the last 23 km, is 16.6×10^6 m^3 s^{-1}. The situation in his data, taken in March 1938, is similar to that of the spring of 1973: the 22°C indicator isotherm at 100 m was well south of the Florida Platform. The circled cross in Fig. 3 is the correlation between D and T based on a recalculation of Montgomery's (1941) data.

Limitations in the 1972-1973 data prohibit a discussion of annual variability in the Florida Current Water. The Yucatan Strait transport cycle however, is markedly different from the cycle reported on by Niiler and Richardson (1973); similarly the average surface speed cycle is not in agreement with that reported by Fuglister (1951) and Cochrane (1965). Cochrane, Niiler and Richardson, and Fuglister report a maximum during the summer, whereas the 1972-1973 data have a minimum in May, June, and July. Greatest transports and speeds in the 1972-1973 data occur in December, February, and March, whereas the opposite is true in the above references. It is difficult to isolate the cause, whether it be due to using 700 m as a reference level, not having a station near Cape San Antonio, or to the inherent difficulties of geostrophic transport estimates in a narrow channel as discussed by Broida (1969). If a barotropic current of ±5 cm s^{-1} exists in a channel like the Yucatan (say 100 km wide by 1 500 m deep) the 1972-1973 values could be in error by $\pm 7.5 \times 10^6$ m^3 s^{-1}. Uncertainties of this magnitude debilitate analysis of variability in the Yucatan Current, but are not so severe a limitation when considering variability in Continental Edge Water transport as is discussed in the next section.

4. MASS BALANCE OF THE GULF

When the Loop Current grows and penetrates into the Gulf of Mexico, continuity requires that waters must be displaced. Maul (1977) suggested that the southerly flow near the sill of the Yucatan Strait (Hansen and Zetler, 1972; Schlitz, 1973) could account for this displacement. Rossov (1966) concluded that the countercurrent he observed at 100-150 m in the western Yucatan Strait arises because "the Atlantic water flowing in from the east and the Caribbean water from the south is not compensated for by the flow out through the Straits of Florida". On the eastern side of the Yucatan Strait, a southward flow is often reported (e.g., Gordon, 1967). Brooks and Niiler (1975) report a westward flow of what appears to be Continental Edge Water in the Straits of Florida off Key West. These observations suggest that a complicated flow pattern can exist at any one time. Based on the 1972-1973 data set, the low frequency (geostrophically adjusted), mass balance will be investigated, and is the subject of this section.

In order to investigate the mass balance, the contribution discussed in the previous paragraph must be assessed. The deep water flowing out of the Gulf of Mexico through the Yucatan Strait is about 5°C or less. Assuming the deep water temperatures have reached a steady state on inter-annual time scales, the ≤ 5°C water must return again to the Gulf of Mexico through the Yucatan Strait because the sill depth of the Straits of Florida (768 m) is too shallow to be a source of cold, deep renewal water. A similar conclusion was reached by Carder et al. (1978) based on silica data, and this implies that the net flow near the bottom of the Yucatan Strait is approximately zero when integrated over several years.

Rossov's (1966) observation is not seen in the 1972-1973 data; if a southward transport in the western Yucatan Strait exists, it is probably small or intermittent because the Yucatan Current almost always occupies the western side. On the eastern side, the southward flow has T-S characteristics of Yucatan Current Water, and therefore this current near Cape San Antonio is not a compensatory flow involving resident (non-Loop Current) Gulf of Mexico waters. In the mean, the Straits of Florida appears to be the only significant exit port of resident Gulf of Mexico surface waters, which, from the earlier discussion on T-S properties, is labelled Continental Edge Water.

Transports of Continental Edge Water (cf. Table I) are subject to the same range of errors discussed in the previous section on the waters in the current itself, except that the barotropic component is much smaller. The area with which to estimate barotropic effects depends upon how far south of the Florida platform the current is found. Assuming an average distance south of 25 km, a triangular area 700 m deep offshore, and again ± 5 cm s^{-1} barotropic flow, the error in transport is ± 0.4 x 10^6 m^3 s^{-1}, or about 15% of the average transport of Continental Edge Water. Summing up the errors in transport due to using T-S relations for salinity (3%), for using the 22°C isotherm to identify water masses (7%), and for the barotropic errors, the transports of Continental Edge Water are estimated to be valid to within ± 25%.

The effect of errors on the average geostrophic transport of Continental Edge Water will be assessed by an independent estimate of average transport based on the volume change of the Gulf Loop Current over the year-long cycle. With reference to 700 m, the surface area bounded by the 22°C isotherm at 100 m (Maul, 1977) defines an estimate of the volume of resident Gulf Water displaced. The minimum area covered was 66 x 10^3 km^2 in early November 1972; the maximum area covered was 209 x 10^3 km^2 in July 1973. Averaging the areal difference over the period from eddy separation to eddy separation (June 1972-August 1973), a transport of 2.5 x 10^6 m^3 s^{-1} is calculated; during the nine-month period that the Loop Current intrudes, the value is 4.2 x 10^6 m^3 s^{-1}. Average transport (T) of Continental Edge Water for the 1972-1973 data set is 2.7 x 10^6 m^3 s^{-1}; during the nine-month period when the Loop Current intrudes, the value is 3.9 x 10^6 m^3 s^{-1}. Agreement of the independent calculations of average Continental Edge Water transports is well within the geostrophic error estimate.

If there are no other sources or sinks, 2.7 x 10^6 m^3 s^{-1} is the outflow of resident Gulf water displaced by water in the upper 700 m entering through the Yucatan Strait. Assuming that for 0 - 700 m of the water column

$$\overline{\phantom{T_{YWC}}} \, T_{YWC} = \overline{\phantom{T_{FCW}}} \, T_{FCW} = \overline{\phantom{T_{CEW}}} \, T_{CEW} , \qquad (1)$$

then the mean transport of Continental Edge Water is 10% of the total. This implies that about 10% of the Yucatan Current Water was exchanged with resident Gulf Waters over the 1972-1973 cycle.

Equation (1) has to be modified if the time-dependent transport balance is to be investigated. The time-dependent equation is

$$T_{YCW} + \Delta_{YBW} = T_{FCW} + T_{CEW}, \qquad (2)$$

where T refers to the 0 - 700 m transport as before and Δ_{YBW} is hypothesized to be the transport of the deep water below the inflowing Yucatan Current Water. To solve equation (2) it will be assumed that $T_{YCW} - T_{FCW}$ is temporally related to the surface area change. In Fig. 4, the averaged geostrophic volume transport of Continental Edge Water between cruises (solid line) is shown to be temporally related to the surface area of the basin enclosed by the 22°C isotherm at 100 m (dashed line). The area covered by the Loop Current between November 1972 and January 1973 begins to increase before T_{CEW} begins to increase.

Similarly, between August and September 1973 the area is seen to decrease while T_{CEW} continues to increase. These observations suggest that $T_{YCW} - T_{FCW}$ are not balanced by T_{CEW} alone.

An interpretation of the 1972-1973 observation vis-a-vis the mass balance is as follows: In the autumn of 1972 the area covered by the Gulf Loop Current remained fairly constant and the inflow of Yucatan Current Water equalled the outflow of Florida Current Water (the mean transport of these two currents for the first four cruises is 23.8×10^6 m^3 s^{-1} and 23.4×10^6 m^3 s^{-1} respectively, while the mean value for the Continental Edge Water is 0.6×10^6 m^3 s^{-1} during the same period). In the winter and late spring, when transport of the Yucatan Current increased, an intrusion of the Loop Current forces resident Gulf waters to be displaced. However, in January, February, and March 1973, the Loop Current is close to the Florida Platform northwest of Dry Tortugas. The flow of Continental Edge Water is thus restricted, and is insufficient to account for the displacement of resident Gulf Waters required by the Loop's intrusion. Continuity is conserved by a southerly flow of deep water through the Yucatan Strait (Δ_{YBW}). In the early summer, when the transport of the Yucatan Current decreases, the Florida Current is found further to the south which permits an increased flow of Continental Edge Water. In late summer, during the time when an anticyclonic eddy is separating from the main flow, the continued flow of Continental Edge Water is balanced by a reversal in the deep flow of the Yucatan Strait.

To quantify these notions, the inferred transport difference of Yucatan Current Water and Florida Current Water (YCW - FCW) from the change in area covered by the 22°C isotherm at 100 m, is compared to the averaged Continental Edge Water (CEW) transports between cruises (Table II), 700 m is used as the reference; the time between cruises is 36 days. The column labelled YBW (Yucatan Bottom Water) is the transport difference between the Continental Edge Water and the inferred transport from areal measurements (column 2 minus column 1). The differences are chosen such that (+) implies a northward flow into the Gulf below 700 m in the Yucatan Strait, and (-) implies a southward flow. The mean

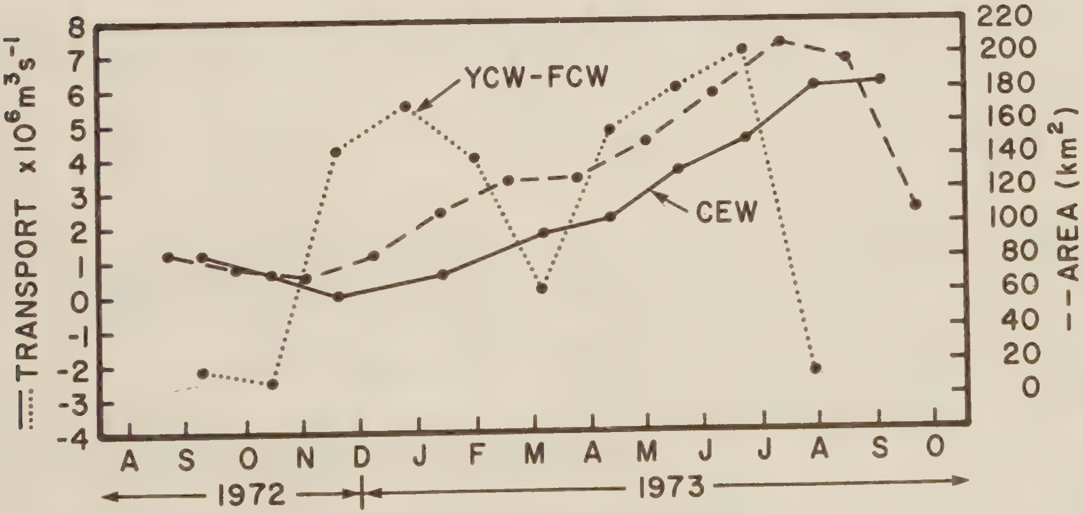

Fig. 4 Volume transport of Continental Edge Water in the Straits of Florida (solid line), inferred transport difference Yucatan Current Water - Florida Current Water (dotted line), and area enclosed by the Gulf Loop Current (dashed line) for 1972-1973

Yucatan Bottom Water transport is almost zero as is expected from the discussion on conserving 5°C water. Table II shows that there is a net southward transport below 700 m of about 2.3 x 10^6 m^3 s^{-1} in the winter; Schlitz (1973) reported 4 x 10^6 m^3 s^{-1} for April 1970.

TABLE II

Inferred Annual Cycle of Yucatan Bottom Water

	Months	Area Difference	(1) Inferred Difference (YCW-FCW)	(2) Observed Transport of CEW	YBW (2-1)
		km^2	$(10^6\ m^3\ s^{-1})$	$(10^6\ m^3\ s^{-1})$	$(10^6\ m^3\ s^{-1})$
1972	A-S	- 9,376	-2.1	1.2	+3.3
	S-ON	-11,113	-2.5	0.6	+3.1
	ON-D	19,100	4.3	0	-4.3
	(December-February)[a]			0.6	-4.2
1973	J-F	17,712	4.0		
	F-M	694	0.2	1.8	+1.6
	M-AM	21,184	4.8	2.2	-2.6
	AM-J	27,088	6.1	3.6	-2.5
	J-J	31,602	7.1	4.5	-2.6
	J-A	- 9,724	-2.2	6.1	+8.3
	A-S	Eddy		6.2	
	Mean		2.5	2.7	0.1

[a] There were no observations of CEW transport in January 1973

In view of the error bars associated with the observed transport of Continental Edge Water, and the assumptions on area and volume, the values in Table II are only intended as a scenario of possible events. The mean values are not unreasonable, however, when compared to observed transports. Another implication of this scenario is that if the transport imbalance in the upper layer water in the Gulf is balanced by a deep southward flow in the Yucatan Strait, there must be a deepening of the thermocline outside the current. The other alternative, that sea level rises, is dismissed based upon historical (Marmer, 1954) as well as concurrent tide gauge records. During the period the Loop Current spreads areally, the thermocline should deepen by about 35 m. Unfortunately, there were no observations in the western Gulf to test deepening of the thermocline and the historical records (Robinson, 1973) do not reflect it. In view of recent cruise data (unpublished) showing spinning-down eddies and the study of Sturges and Blaha (1976) into the variability in the western Gulf, it seems unlikely that the deepening thermocline signal can be detected against the background of other baroclinic processes.

The scenario of events of the 1972-1973 data should not be interpreted as a complete description of the Gulf Loop Current cycle. Variability on this description is becoming more and more evident with the synthesis of larger data sets (SUSIO, 1975; Behringer, Molinari, and Festa, 1977). For example, Hansen and Molinari (1978) report a southward transport of >2 x 10^6 m^3 s^{-1} in the lower layer of the Yucatan Strait in October of 1970; the configuration of the Gulf Loop Current at this time was once again such that the flow of Continental Edge Water in the Straits of Florida could be blocked. Winter intrusions of the Loop Current have now been documented (Molinari *et al.*, 1977), which suggest that the 1972-1973 sequence may not be a typical pattern. Further, recent satellite observations (Maul, deWitt, Yanaway, and Baig, in preparation) suggest that wave-like meanders of the Gulf Loop Current may have periods of the order of 10 days; if these meanders interact with the Florida Platform they could act as a variable blocking mechanism. A current meter array, presently moored 100 m above the sill of the Yucatan Strait, will provide even more data with which to test the hypothesis discussed herein.

5. SALT BALANCE OF THE GULF

The salt balance of the basin cannot be directly calculated from the 1972-1973 observations for the same reasons which were discussed in the section on the mass balance. An indirect approach involving an estimate of the salt exchanged into the Gulf by the May 1972 eddy will be made, followed by an estimate of the fresh water from river runoff required to keep the mean salinity of resident Gulf waters constant. First, an estimate of the salt transported (T_{salt}) by Continental Edge Water will be made from

$$T_{salt} = \int_{CEW} \int_{0}^{700} \rho\,(x,z)\; S(x,z)\; V(x,z)\; dz\; dx \qquad (3)$$

where ρ is the in situ density, S is salinity, and V is the velocity normal to th x,z plane. Evaluation of equation (3) for the 1972-1973 Continental Edge Water transports, and averaging the eleven values, gives a mean salt transport of 9.6×10^{10} g s^{-1}. Multiplication by the time interval between the May 1972 and August-September 1973 eddy separation events gives a total of 3.8×10^{18} g of salt transported out of the Gulf of Mexico in the 0 - 700 m layer by Continental Edge Water.

Dissolved solids from the United States' rivers contribute only 1.7×10^{4} g yr^{-1} to the Gulf of Mexico (Leifeste, 1974; contributions from other than United States sources are unknown). Another source of the 3.8×10^{18} g may be due to small-scale exchange processes along the perimeter of the current. But the single most important contribution is probably due to the periodic separation of an anticyclonic eddy. This latter notion will be quantified by computing the amount of salt in the May 1972 eddy and comparing this with the salt in an equal volume of resident Gulf of Mexico Water.

The eddy can be approximated by a cylinder with a surface area equal to the area enclosed by the eddy. The 22°C isotherm at 100 m plus 14 km is chosen as the outer boundary; Maul (1975) showed that this was average distance from the edge of the current to the 22°C isotherm at 100 m. Total salt in the cyclinder ($\hat{S}$) is calculated from

$$\hat{S} = 2 \int_{0}^{206} X \int_{0}^{700} \rho\,(z) S(x,z) dz \;\; dx \qquad (4)$$

where X is the radial distance from the centre of the eddy. In equation (4), S(x,z) is the distribution of salinity, ρ (z) is the in situ density; the eddy is considered to be 700 m deep and the radius of the 1972 eddy is estimated to be 206 km.

The historical temperature data on file at NODC were studied (SUSIO, 1975) to see if this is a characteristic size. Data available between 1952 and 1971 show nine eddies; their mean radius (using the same criterion) was 192 km. The September 1973 eddy was 89 000 km^2, or approximately 168 km in radius. This suggests that the 1972 eddy is of average size and that the salt balance is probably typical.

The distribution of S(x,z) in the eddy and in the juxtaposed waters was obtained from the measurements of Morrison, Merrell, and Nowlin (1973) and Molinari (1974). Five stations were used to define the eddy and three stations for the resident Gulf waters. T-S correlation for the station in the eddy centre is similar to the curve in Fig. 2 labelled Florida Current Water, and the T-S correlation for resident Gulf Waters is similar to the curve labelled Continental Edge Water. Equation (4) is numerically evaluated for both water types.

It is of interest to compare the salt transported by Continental Edge Water (3.8×10^{18} g) with the value calculated from equation (4) for the May 1972 (2.9×10^{18} g). Comparison requires that the eddy spin-down time scale be similar to the advective time scale of Continental Edge Water, because, the T-S characteristics of the eddy have to be altered by mixing to the T-S characteristics of Continental Edge Water. To date, there are no explicit measurements of anticyclonic eddy spin-down in the Gulf of Mexico. Leipper's (1970) data suggest that an eddy which was detected in November 1965 was largely mixed into the resident western Gulf waters by October 1966. An eddy detected in NOAA satellite imagery in the spring of 1977 was observed to have a maximum depth of only 140 m at its 20°C isotherm in October 1977; the 20°C isotherm was deeper than 250 m when the May 1972 anticyclonic eddy separated from the Loop Current. On the other hand, Cheney and Richardson (1976) estimate the life of cyclonic Gulf Stream Rings in the Sargasso Sea to be about two years. However, if it is assumed that anticyclonic Loop Current eddies are a quasi-annual event, and that the mean salinity of the western Gulf of Mexico is not changing, then it is reasonable to propose that the mean spin-down time scale is matched by the transport of Continental Edge Water averaged over one cycle. Based on that assumption, the May 1972 eddy accounts for approximately 75% of the exchange.

While it seems reasonable that the contribution of a detached eddy is the major consideration in the salt budget, it is not the only factor. Lee (1975) reported on spinoff eddies along the cyclonic shear zone of the Florida Current north of Miami. Somewhat larger eddy-like features were observed along the cyclonic side of the Gulf Loop Current along its northern periphery (Austin, 1971). 12-32 km sized eddies of Loop Current Water were observed on the west Florida Shelf (Maul, 1977) and on the Mississippi-Alabama shelf (Gaul, 1967). Eddies such as these are almost always seen to be present in infra-red satellite imagery (e.g., DeRyke and Rao, 1973; Legeckis, 1975). Radiance patterns in these images show a complicated thermal pattern of small eddies, plumes and entrained filaments which have been interpreted as reflecting advection (Voorhis, Schroeder, and Leetmaa, 1976; Bernstein, Breaker, and Whritner, 1977). The effect of mixing, however, is evident from infra-red patterns of isolation of warm current waters and cooler resident Gulf waters, and suggests that water from the current is continually exchanged all along its periphery.

Computing $\hat{S}$ for the May 1972 eddy and subtracting $\hat{S}$ for the juxtaposed resident Gulf waters gives an estimate of the salt added to the Gulf by the eddy after spin-down and mixing. The result of the calculation is that there is approximately 2.6×10^{16} g more salt in the eddy than in an equal volume of resident Gulf of Mexico waters outside the Loop Current. This salt must be combined with sufficient fresh water to keep the mean salinity of the upper waters of resident Gulf Water (above ~ 15°C) approximately as observed: 36.2°/oo. The quantity of fresh water required to do this is 7×10^{17} g, or 700 km^3. If the May 1972 eddy accounts for only 75% of the salt, 935 km^3 of fresh water is required to maintain the mean salinity. Since the Gulf is a net evaporation basin, the only significant source of this fresh water is river discharge.

The amount of fresh water entering the Gulf of Mexico was calculated from river gauge data supplied by the U.S. Geological Survey and from the Secretaría de Recursos Hidráulicos (Mexico). Runoff from five countries drains into the Gulf, including more than half of all runoff from the conterminous United States. Fig. 5 shows the drainage basin and the river runoff gauge sites used to calculate runoff.

As can be seen from Fig. 5, a substantial fraction of ungauged areas exist near the coast. A standard technique to estimate the contribution of these areas is to calculate the ratio of the ungauged drainage area to the area of similar gauged streams (Bue, 1970). Whenever this was done, gauged streams in the same geographic region were chosen with drainage areas of approximately the same size and with a similar discharge-volume/drainage-area ratio. The average of at least three such streams was used to estimate the contribution of ungauged areas whenever possible.

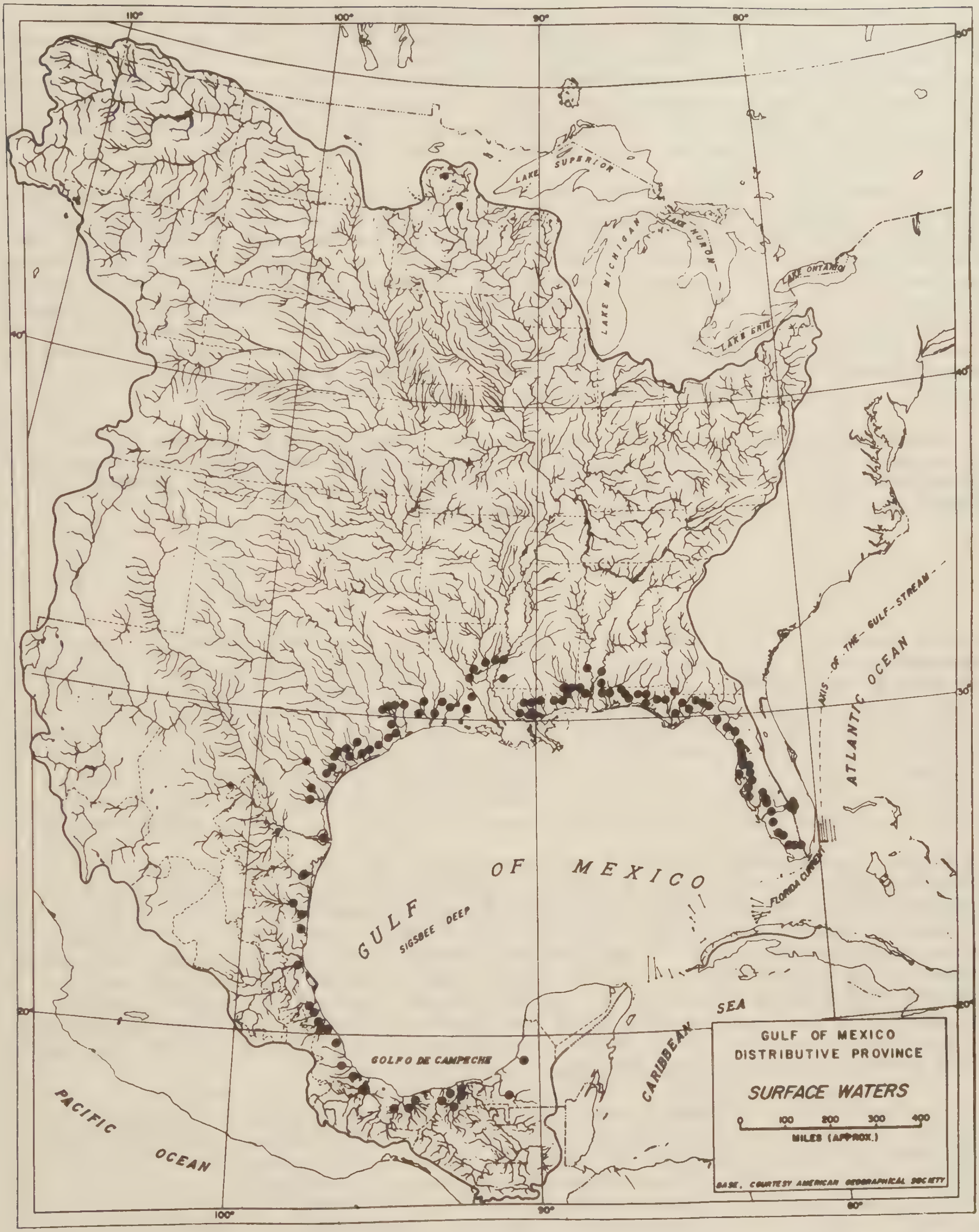
110°
100°
90°
80°
30°
40°
20°
LAKE SUPERIOR
LAKE MICHIGAN
LAKE HURON
LAKE ONTARIO
LAKE ERIE
AXIS OF THE GULF STREAM
ATLANTIC OCEAN
FLORIDA CURRENT
GULF OF MEXICO
SIGSBEE DEEP
GOLFO DE CAMPECHE
CARIBBEAN SEA
PACIFIC OCEAN
GULF OF MEXICO DISTRIBUTIVE PROVINCE
SURFACE WATERS
0 100 200 300 400
MILES (APPROX.)
BASE, COURTESY AMERICAN GEOGRAPHICAL SOCIETY

Fig. 5 Location of river runoff gauging stations in the Gulf of Mexico (after Moody, 1967), which were used to calculate the total amount of fresh water discharged into the basin

In general, the downstream-most gauging station was chosen. Care was taken not to choose a station between a major city's water source and discharge site, as Bue (1970) has shown this can contribute a substantial error. Certain areas such as the Yucatan Peninsula and southwestern Florida have no well-defined rivers or determinable drainage areas. Judging from Florida flood control records, these areas do not contribute substantial volumes to the Gulf. This, and the lack of records from Cuba, means that the estimates discussed below must be considered conservative. The results are summarized in Table III.

During the 15-month period between eddy break-off events, 1 832 km^3 of river water discharged into the Gulf. In the absence of other processes, this would raise the level of the entire basin 1.2 m. For water year 1973 (October 1972 - September 1973), 11581 km^3 was received by the Gulf. This volume is 57% larger than the values reported by other investigators based on long-term averages (see Table IV). However, the discharge of the Mississippi River alone was 77% above its 45-year average during the water year 1972-1973. This supports the notion that 1581 km^3 is a conservative estimate. In Table IV, the estimate based on Leifeste's (1974) value for the United States only (793 km^3) is made using Moody's (1967) 21% and Franceschini's (1961) 22% estimate of the contribution of the Mexican rivers. The 1973 water year data show that Mexican rivers contributed 15% of the total.

A summary of the excess of evaporation (E) over precipitation (P) for the Gulf of Mexico is given in Table V. Both Franceschini (1961) and Hall (1969) have used values of E-P, along with river runoff (R) data, to study the water balance of the Gulf. They considered the mass (M) balance in the Gulf of Mexico using

$$\frac{dM}{dt} = o = \rho(E-P) + \rho(R) + \rho(I-O) \qquad (5)$$

where M is conserved on time scales of one year or longer, i.e., they tacitly assume that the advective time of T_{SALT} (equation 3) and eddy spin-down are matched. Their conclusion is that $E-P > R$, and therefore the Yucatan Current must transport more water into (I) the Gulf than the Florida Current transports out (O). The values are small compared to total transports: Franceschini (1961) calculated $I-O = 0.015\ 10^6\ m^3\ s^{-1}$, and Hall (1969) estimated $I-O = 0.033 \times 10^6\ m^3\ s^{-1}$. Franceschini and Hall argued that if the mean salinity of the Gulf is not increasing, then $I > 0$, and the mean salinity of the outflowing ($\bar{S}_o$) waters must exceed that of the inflow ($\bar{S}_I$). Franceschini (1961) estimated that the mean increase must be 0.06 percent; Hall's (1969) estimate was that $\bar{S}_o$ was 0.13 percent higher than $\bar{S}_I$.

A proper investigation of the salt balance requires the evaluation of equation (3) across both straits. Even if such observations were available, it is unlikely that sufficiently precise calculations could be made to test Franceschini's (1961) or Hall's (1969) results. How to measure $\bar{S}_o$ or $\bar{S}_I$ is also difficult to interpret; it is not the average salinity in a section. Two observations during 1972-1973 argue against the conclusion that $\bar{S}_o > \bar{S}_I$ during this period: Continental Edge Water has lower salinity in the upper layers than Florida Current Water, and Continental Edge Water accounts for 10% of the transport; the mean surface salinity in the Straits of Florida (35.74°/oo) is less than in the Yucatan Strait (36.05°/oo). These observations not only suggest that $\bar{S}_I > \bar{S}_o$, but also that $E-P < R$ during the period investigated herein.

River runoff for the 1972-1973 period was well above the average. If the May 1972 eddy was the only source of high salinity water supplied to the basin, then only 700 km^3 of fresh water are required to keep the salinity constant. This leaves 1 131 km^3 of R to balance E-P. Adjusting this 16-month value to one year, $E-P = 55\ cm\ yr^{-1}$, which is in reasonable agreement with the values given in Table V. If the May 1972 eddy represente 75% of the total exchange, then $E-P = 41\ cm\ yr^{-1}$ which is in agreement with Jacobs (1951), but not others.

TABLE III

Summary of River Runoff Data ($m^3 s^{-1}$)

Month	Florida	Alabama	Mississippi	Louisiana	Texas	Mexico	Totals
JUN 72	1 497	740	141	12 250	660	7 902	23 189
JUL 72	1 656	785	140	14 119	442	11 221	28 364
AUG 72	1 134	568	108	12 621	271	15 232	29 952
SEP 72	1 028	523	71	10 238	329	11 954	24 173
OCT 72	803	416	81	12 454	301	9 855	23 912
NOV 72	979	813	194	26 863	691	6 778	36 318
DEC 72	2 463	2 843	874	36 135	546	6 561	49 422
JAN 73	3 359	4 729	853	37 814	1 218	4 006	51 980
FEB 73	4 546	3 584	1 019	39 564	1 705	3 478	53 896
MAR 73	4 029	5 025	1 672	41 767	2 373	2 821	57 687
APR 73	7 271	6 628	1 947	63 967	3 949	2 737	86 500
MAY 73	3 594	3 919	919	63 192	2 259	3 129	77 013
JUN 73	3 637	2 770	468	40 158	4 520	6 806	58 361
JUL 73	1 979	1 440	262	19 735	1 673	9 538	34 628
AUG 73	2 167	906	273	14 610	873	16 781	35 611
SEP 73	1 852	858	742	12 414	1 919	18 107	35 893
Average	2 625	2 284	610	28 619	1 483	8 557	50 102
%	5.9	5.2	1.4	64.8	3.4	19.4	

TABLE IV

River Runoff into the Gulf of Mexico

Volume	Period	Source
1 088 km^3	Climatological	Moody (1967)
964 km^3	Climatological	Leifeste (1974)
975 km^3	1959	Franceschini (1961)
757 km^3	1963–1965	Hall (1969)
1 581 km^3	1973	
1 073 km^3	Mean	

TABLE V

Evaporation–Precipitation for the Gulf of Mexico

E–P	Period	Source
35 cm yr^{-1}	Climatological	Jacobs (1951)
121 cm yr^{-1}	1950	Starr, Peixoto and Lividas (1958)
100 cm yr^{-1}	1959	Franceschini (1961)
57 cm yr^{-1}	1963–1965	Cummings (1968)
78 cm yr^{-1}	Mean	

Franceschini (1961) and Etter (1975), using different approaches, both show that E-P is much larger over the eastern Gulf than the western. Franceschini calculates that E-P is six times greater over the eastern basin. From the studies of Chew, Drennan, and Demoran (1962), Gaul (1967), and others, the net drift of the Mississippi River is known to be to the west, although there is a great deal of month-to-month variability. So except for times when the Loop Current penetrates as far north as the Delta and advects fresh water out of the basin (e.g., August 1973), most of the river discharge into the Gulf is into the western portion (cf. Table III where the runoff from Louisiana, Texas, and Mexico accounts for 88% of the total). Allowing only half of the water from Louisiana to flow into the western Gulf, 55% of R contributes to the hydrologic balance. As an example with the 1972-1973 data, using 0.55R and the fresh water required to dilute the May 1972 eddy (δ), E-P in the western Gulf would be 34 cm yr^{-1}; Franceschini's (1961) estimate for 1959 is E-P = 14 cm yr^{-1}. In either case, there is a net transport from the western Gulf which amounts to 0.02 x 10^6 m^3 s^{-1} during 1972-1973 to account for $0.55R \leq \delta \leq (E-P)$. This value is numerically in agreement with Franceschini (1961) and Hall's (1969) estimate of I-0 but is of the opposite sign.

It would be imprudent to surmise that the 1972-1973 data set provides a conclusive description of the salt balance of the Gulf of Mexico. Each of the terms E, P, R, δ in the hydrologic balance equation are independent variables, and conclusions for one year may not be representative of others. It is more important to recognize the hydrologic variability and to relate that variability to ocean-atmospheric interactions. For example, Shukla and Misra (1977) related the sea surface temperature and wind speed over the Arabian Sea to monsoon rainfall over India. In a similar way, winds over the Gulf of Mexico behave as monsoons providing rain to the agricultural heartland of the United States. Variability in evaporation (which is a function of temperature and salinity) may be influenced by the Gulf Loop Current and detached anticyclonic eddies. The climatic implication of this variability is an important topic for future research.

6. SUMMARY AND CONCLUSIONS

Between August 1972 and September 1973, eleven hydrographic transects were made of both the Yucatan Strait (between Cape San Antonio and Contoy Island) and the Straits of Florida (between the Florida Platform and Havana). Most of the data were from STD casts, but several sections were XBT data. In order to incorporate all available data into the transport analysis, salinities were assigned to the SBT's from historical T-S correlations and the reference level was chosen to be 700 m (which is approximately the sill depth of the Straits of Florida off Miami).

Mean and standard deviation of the geostrophic transport in the Yucatan Strait was 25.4 ± 5.3 x 10^6 m^3 s^{-1}. While the mean value appears to be about 20% too low, probably due to the shallow reference level, the range of variability is in agreement with dropsonde measurements reported by Niiler and Richardson (1973), which suggests that the variability is baroclinic in nature. Contrary to the measurements made by Niiler and Richardson, the maximum flow (~32 x 10^6 m^3 s^{-1}) occurred in December, February and March; the minimum flow (~22 x 10^6 m^3 s^{-1}) occurred in April, June and July. Average transport in the Straits of Florida is 19.5 ± 5.4 x 10^6 m^3 s^{-1}, but this value is influenced by the location of the northern edge of the Florida Current, which varies from 0 km to over 50 km from the Florida Platform. The further south the current is found, the lower the measured transport; this implies that in the 22 km unmeasured section in the offing of Havana, high velocities (and transports) are related to current meandering in the Strait.

Penetration and spreading of the Loop Current is associated with an imbalance in the upper layer transport of Yucatan Current Water and Florida Current Water. Continuity is maintained by the transport of resident Gulf of Mexico water through the Straits of Florida, where resident waters are identified by their T-S properties as Continental Edge Water. The transport imbalance, $(T_{YCS} - T_{FCW})$, inferred from an estimate of the volume of Gulf of Mexico water displaced, is approximately equal to the mean transport of Continental Edge Water, 2.7 x 10^6 m^3 s^{-1}, when averaged over the 1972-1973 cycle of eddy separation to eddy separation. When examined month by month, it is found that $(T_{YCW} - T_{FCW}) \neq T_{CEW}$. The hypothesis is made and quantified, that there is a north-south zero net transport of deep water through the Yucatan Strait to maintain the mass balance.

Continental Edge Water is volumetrically about 10% of the inflowing Yucatan Current Water. Calculations of Continental Edge Water salt transport suggest that about 75% of the salt can be accounted for by the May 1972 anticyclonic eddy. Because the eddy is a remnant of the high salinity Subtropical Underwater, it injects 2.6 x 10^{16} g of salt into the Gulf. River runoff into the basin exceeded 1 800 km^3 in the period between eddy events in 1972-1973, only 700 km^3 of which are required to mix this 2.6 x 10^{16} g of excess eddy salt to the mean salinity in the upper layer ($T \geq 15°C$) of resident Gulf of Mexico water. While it appears that the periodic separation of these (typically) 400 km diameter anticyclonic eddies dominates the mass and salt exchange, ther is evidence that the remaining exchange involves smaller (< 50 km diameter) eddies.

Results based on the 1972-1973 data set indicate that river runoff can exceed evaporation minus precipitation, contrary to prior conclusions. In addition, because of the eddy exchange, the balance equation

$$E-P \lessgtr R-\delta \qquad (6)$$

must include an extra term, δ, to account for the excess salt injected into the Gulf of Mexico. Therefore, even though $E > P$, the Gulf of Mexico is not an "American Mediterranean" because of the term $R - \delta$ which has no counterpart in the arid lands of the eastern hemisphere

7. ACKNOWLEDGEMENTS

The many persons who assisted in collecting these data were acknowledged in the first article of this series. Data processing for Part II was assisted by M. McCaslin, N. Bright, and M. Pryslak. The manuscript was critically reviewed by Drs. A. Leetmaa, F. Chew, R. Molinari, D. Behringer, W. Sturges, and D. Hansen; the author especially thanks them for their suggestions and ideas. This paper was orally presented at the CICAR II Symposium, July, 1976, in Caracas, Venezuela.

8. REFERENCES

Austin, H.R., The characteristics and relationships between the calculated geostrophic
1971 current component and selected indicator organisms in the Gulf of Mexico Loop Current system. Ph.D. Dissertation, Florida State University, Tallahassee, 369 p.

Behringer, D.W., R.L. Molinari and J.F. Festa, The variability of anticyclonic current
1977 patterns in the Gulf of Mexico. J.Geophys.Res., 82(34):5469-76

Bernstein, R.L., L. Breaker and R. Whritner, California Current eddy formation. Science,
1977 Wash., 195:353-92

Broida, S., Geostrophy and direct measurements in the Straits of Florida. J.Mar.Res.,
1969 27(3):278-92

Brooks, I.H. and P.P. Niiler, The Florida Current at Key West: Summer 1972. J.Mar.Res.,
1975 33(1):83-92

Bue, C.D., Streamflow from the United States into the Atlantic Ocean during 1931-60. U.S.
1970 Gov't Printing Office, Geological Survey Water - Supply Paper 1899-I, 36 p.

Carder, K.L. et al., Washington, D.C., Dissolved silica and the circulation in the Yucatan
1978 Strait and deep eastern Gulf of Mexico. Deep Sea Res., (in press)

Cheney, R.E. and P.L. Richardson, Observed decay of a cyclonic Gulf Stream ring. Deep Sea
1976 Res., 23(2):143-55

Chew, F., K.L. Drennan and W.J. Demoran, Some results of drift bottle studies off the
1962 Mississippi Delta. Limnol.Oceanogr., 7(1):252-7

Cochrane, J.D., The Yucatan current. In Annual report, Project 286. College Station, Texas
1965 A&M University, Ref(65-17T):10-7

Cummings, A.D., Climatological aspects of the balance of water vapor in the atmosphere
1968 overlying the Gulf of Mexico, M.S. Thesis, Texas A&M University, 50 p.

De Rycke, R.J. and P.K. Rao, Eddies along a gulf stream boundary from a very high resolution radiometer. J.Phys.Oceanogr., 3:490-2
1973

Emery, W.J., Dynamic height from temperature profiles. J.Phys.Oceanogr., 5(2):369-75
1975

Etter, P.C., A climatic heat budget study of the Gulf of Mexico. M.S. Thesis, Texas
1975 A&M University, College Station, 87 p.

Franceschini, G.A., Hydrologic balance of the Gulf of Mexico. Ph.D. Dissertation, Texas
1961 A&M University, College Station, 58 p.

Fuglister, F.C., Annual variations in current speeds in the Gulf Stream. J.Mar.Res.,
1951 10:119-27

Gaul, R.D., Circulation over the continental margin of the northeastern Gulf of Mexico.
1967 Ph.D. Dissertation, Texas A&M University, College Station, 172 p.

Gordon, A.L., Circulation of the Caribbean Sea. J.Geophys.Res., 77(24):6207-3
1967

Hall, C.S., An investigation of the Water Balance of the Basin of the Gulf of Mexico.
1969 M.S. Thesis, Texas A&M University, College Station, 39 p.

Hansen, D.V. and B.D. Zetler, Deep currents in the Yucatan Strait. EOS,Trans.Am.Geophys.
1972 Union, 53(4):392

Hansen, D.V. and R.L. Molinari, Deep currents in the Yucatan Strait. J.Geophys.Res.
1978 (submitted for publication)

Jacobs, W.C., The energy exchange between sea and atmosphere and some of its consequences.
1951 Bull.Scripps Inst.Oceanogr., 6(2):27-122

Jacobsen, J.P. and A.J.C. Jensen, Examinations of hydrographical measurements from the
1926 research vessels *Explorer* and *Dana* during the summer of 1924. Rapp.P.-V.Réun.
CIEM, 39:31-84

Lee, T.N., Florida Current spin-off-eddies. Deep-sea Res., 22:753-65
1975

Legeckis, R., Application of synchronous meteorological satellite data to the study of
1975 time dependent sea surface temperature changes along the boundary of the Gulf
Stream. Geophys.Res.Lett., 2(10):485-8

Leifeste, D.K., Dissolved-solids discharge to the oceans from the conterminous United
1974 States. Circ.U.S.Geol.Surv., (685):8 p. Geological Survey: 8 pgs.

Leipper, D.F., A sequence of current patterns in the Gulf of Mexico. J.Geophys.Res.,
1970 75(3):637-57

Marmer, H.A., Tides and sea level in the Gulf of Mexico. Fish.Bull.U.S.Fish.Wildl.Ser.,
1954 56(89):101-18

Maul, G.A., An evaluation of the use of the earth resources technology satellite for
1975 observing ocean current boundaries in the Gulf Stream system. NOAA Tech.Memo. (ERL 335-AOML 18): 125 p.

Maul, G.A., D.R. Norris and W.R. Johnson, Satellite photography of eddies in the Gulf Loop
1974 Current. Geophys.Res.Lett., 1(6):256-8

Molinari, R.L., Data from the NOAA ship Virginia Key and the SUSIO ship Bellows, collected
1974 during CICAR survey, Month II. NOAA Tech.Memo., (ERL AOML-22):153 p.

__________, An overview of the Cayman Sea - Gulf of Mexico circulation based on CICAR
1978 survey month and other data. FAO Fish.Rep., (200) Suppl.

Molinari, R.L. and R. Yager, Upper layer hydrographic conditions at the Yucatan Strait
1977 during May, 1972. J.Mar.Res., 35(1):11-20

Molinari, R.L. et al., Winter intrusions of the Loop Current. Science,Wash., 198:505-7
1977

Montgomery, R.B., Transport of the Florida Current off Havana. J.Mar.Res., 4:198-220
1941

Moody, C.L., Gulf of Mexico distributive province. AAPG Bulletin, 51(2):179-99
1967

Morrison, J.M. and W.D. Nowlin, Jr. Repeated nutrient, oxygen, and density sections through
1977 the Loop Current. J.Mar.Res., 35(1):105-28

Morrison, J.M., W.J. Merrel, Jr. and W.D. Nowlin, Jr. The waters of the eastern Gulf of
1973 Mexico as observed during May 1972. College Station, Texas A&M University, Ref. (73-10):330 p.

Niiler, P.P. and W.S. Richardson, Seasonal variability of the Florida Current. J.Mar.Res.,
1973 31(3):144-67

Nowlin, W.D. and H.J. McLeilan, A characterization of the Gulf of Mexico waters in winter.
1967 J.Mar.Res., 25(1):29-59

Robinson, M.K., Atlas of monthly sea surface and subsurface temperature and depth of the
1973 top of the thermocline, Gulf of Mexico and Caribbean Sea. Scripps Inst.Oceanogr. Ref.(73-8):105 p.

Rossov, V.V., Water circulation in the Gulf of Mexico and Caribbean Sea. Dokl.Akad.Nauk
1966 SSSR, 166:202-4 (in Russian)

Schlitz, R.J., Net total transport and net transport by water mass categories for Yucatan
1973 Channel based on data for April 1970. Ph.D. Dissertation, Texas A&M University, College Station, 107 p.

Shulka, J. and B.M. Misra, Relationships between sea surface temperature and wind speed over
1977 the central Arabian Sea, and monsoon rainfall over India. Mon.Weather Rev., 105:998-1002

Starr, V.P., J.P. Peixoto and G.C. Lividas, On the meridianal flux of water vapor in the
1958 northern hemisphere. Goefys.Para Appl., 39(1):174-85

Sturges, W. and J.P. Blaha, A western boundary current in the Gulf of Mexico. Science,Wash., 1976 192:367-9

SUSIO ((Florida) State University System Institute of Oceanography), Compilation and summation 1975 of historical and existing physical oceanographic data from the eastern Gulf of Mexico. St. Petersburg, Fla., Final Report, BLM Contract 08550-CT4-16, 97 p.

Voorhis, A.D., E.H. Schroeder and A. Leetmaa, The influence of deep mesoscale eddies on 1976 sea surface properties in the North Atlantic subtropical convergence. J.Phys. Oceanogr., 6(6):953-61

Wennekens, M.P., Water mass properties of the straits of Florida and related waters. 1959 Bull.Mar.Sci., 9(1):1-52

Wüst, G. and A. Gordon, Stratification and circulation in the Antillean-Caribbean basins. 1964 Part 1.

BASIC RESULTS OF RESEARCH CARRIED OUT BY THE MARINE HYDROPHYSICAL INSTITUTE OF THE UKRAINIAN S.S.R. ACADEMY OF SCIENCES ACCORDING TO THE INTERNATIONAL OCEANOGRAPHIC PROGRAMME "CICAR"

by

B.A. NELEPO
Marine Hydrophysical Institute
Ukrainian S.S.R. Academy of Sciences
Sevastopol, U.S.S.R.

CONTENTS

1. INTRODUCTION
2. CIRCULATION OF WATER
3. WATER MASSES
4. WATER CIRCULATION THEORY
5. HYDRO-OPTICAL PROPERTIES
6. GEOLOGICAL AND GEOPHYSICAL INVESTIGATIONS
7. SUMMARY
8. REFERENCES

Abstract

In 1970-1975, as part of the international CICAR programme, the Marine Hydrophysical Institute of the Ukrainian S.S.R. Academy of Sciences carried out a complex oceanographic research programme in the Caribbean Sea. The main operations were associated with the following research areas:

(1) the circulation, hydrological structure, and dynamics of the waters of the region;

(2) its hydrochemical condition, and

(3) the geomorphology and bottom topography of the basin.

During this period, the R/V AKADEMIK VERNADSKY of the Ukrainian S.S.R. Academy of Sciences performed three specialized cruises to the Caribbean in accordance with the national programme of research. In addition, operations on the CICAR programme were carried out in a number of complex expeditions for research on several programmes in various regions of the Tropical Atlantic.

As a result of many years of research, vertical and horizontal distributions of basic hydrological characteristics and their spatial and temporal variation have been studied and schemes of surface and deep circulation of the Caribbean waters have been constructed.

Observations performed at buoy stations made it possible to determine the characteristics of tidal phenomena in the basin and to calculate harmonic constants of tidal currents.

Data on the fine structure of the velocity and temperature fields were obtained. Theoretical research on large-scale currents of the Caribbean was conducted, and the problem of currents of the basin was solved with due regard for non-uniformity of sea water and the bottom topography of the basin.

New data were obtained on the distribution of biogenous elements, trace elements, and the isotopic characteristics of the waters of the region.

Using results of the geophysical research, gravimetric charts were compiled for the Caribbean in the "free-air" reduction and in residual topographo-isostatic anomalies.

Resumen

Como parte del programa internacional de las "ICCRA", el Instituto de Hidrofísica Marina de la Academia de Ciencias de la R.S.S. de Ucrania llevó a la prática el importante programa de investigaciones oceanográficas en el Caribe, cuyas operaciones principales fueron el estudio de las cuestiones siguientes:

(1) la circulación, estructura hidrológica y dinámica de las aguas de la región;

(2) sus condiciones hidroquímicas;

(3) la geomorfología y topografía del fondo de la cuenca.

Durante este período, el buque de investigaciones AKADEMIK VERNADSKY, de la Academia de Ciencias de la R.S.S. de Ucrania, hizo tres cruceros especiales por el Caribe, previstos en el programa nacional de investigaciones. También hicieron varias importantes expediciones previstas en el programa de las ICCRA, que incluía el estudio con arreglo a diversos programas de varias regiones del Atlántico tropical.

Como resultado de muchos años de investigaciones, se conocen actualmente las distribuciones, vertical y horizontal, de las características hidrológicas fundamentales, y de su variación en el tiempo y en el espacio, y se han podido elaborar los sistemas de circulación, en superficie y en profundidad, de las aguas del Caribe.

Las observaciones realizadas en las estaciones flotantes permitieron determinar las características de las mareas de la cuenca, y calcular las constantes armónicas de las corrientes de marea.

Se obtuvieron datos sobre la estructura delgada de los campos de velocidades y temperaturas, haciéndose estudios teóricos sobre las grandes corrientes del Caribe, y resolviéndose el problema de las corrientes de la cuenca teniendo debidamente en cuenta la falta de uniformidad de las aguas marinas y la topografía del fondo de la cuenca.

Se obtuvieron neuvos datos sobre la distribución de los elementos biógenos, de los oligoelementos, y de las características isotópicas de las aguas de la región.

Con los resultados del estudio geofísico, se hizo una compilación de mapas gravimétricos del Caribe en la reducción al "aire libre" y en anomalías topográfico-isostáticas residuales.

1. INTRODUCTION

The Marine Hydrophysical Institute of the Ukrainian S.S.R. Academy of Sciences conducts complex oceanographic research in accordance with the national programme of the U.S.S.R. within the Cooperative Investigation of the Caribbean Sea and Adjacent Regions (CICAR).

The R/V AKADEMIK VERNADSKY made three special cruises to the Caribbean Sea (1970-1971; 1972-1973; 1973) during which 53 buoy stations and 176 hydrological stations were performed (Fig. 1). Complex research was carried out in the eastern and central Caribbean Sea, in the passages of the Greater and Lesser Antillean islands, as well as in the Yucatan and Florida Straits. Hydrological, hydro-optical, hydrochemical and geologo-geophysical observations were conducted in two standard sections along the 88°30' and 60° W meridians chosen by the International Conference. In addition, operations on the CICAR project were carried out in a number of complex expeditions making provision for research on several programmes in various regions of the Tropical Atlantic (Naukova Dumka, 1966; Neuymin and Sukhovei, 1973; Akademia Nauk, 1974).

2. CIRCULATION OF WATER

The measurements taken of velocity and direction of currents made it possible to interpret in a new way a scheme of the water circulation in the Caribbean Sea and to find precise values of water exchange between the Gulf of Mexico, the Caribbean Sea and the Atlantic Ocean through the straits which connect them (Akademia Nauk, 1974; Sukhovei, 1971). Numerous passages of the Lesser Antillean islands offer free access for waters of the Southern and Northern Trade Wind Currents to the Caribbean. Waters of the Guiana Current which is a branch of the Southern Trade Wind Current, enter primarily through the channel situated between the coast of South America and Grenada. In view of the fact that the depth of the Grenada Strait does not exceed 750 m, surface tropical and subsurface subtropical waters pass through it. The Subantarctic Intermediate Waters discovered in the sea from minimum values of salinity enter through the deeper central straits of the Lesser Antillean island ridge.

A total volume of Atlantic waters entering through passages in island arcs of the Antilles toward the Yucatan Strait is equal to 155 km^3/hour.

Sections made in the straits using buoy stations allowed one to study in considerable detail the structure of both entering and leaving flows. Below the entering Atlantic waters, flows of backward direction were situated which realized the discharge of waters from the Caribbean into the ocean. Thus, in the Windward Passage the average daily velocity of the entering flow was as high as 30 cm/sec at 1 600 m from measurements during the third cruise of the R/V AKADEMIK VERNADSKY; in 1965 one observed a backward current there running at a velocity of 23 cm/sec according to measurements from the R/V MIKHAIL LOMONOSOV. High velocities of both entering and leaving flows appear to take place in the bottom portion of the trench rather often since geological investigations show exposures of bed rock and almost complete absence of mud sediments. This indicates that inflow of deep Atlantic water to the Caribbean and discharge from the Caribbean to the Atlantic Ocean at sill level is a fixed fact. In that case, Worthington's assumption concerning the complete isolation of Caribbean deep waters is not supported by observations.

Water discharge in the Yucatan Strait from the Caribbean Sea to the Gulf of Mexico occurs in the upper layer to 700-1 000 m (Fig. 2). In the lower portion of the strait, both waters flowing into the Gulf of Mexico and backward discharge to the Caribbean were observed.

The main axis of the Florida Straits is directed along the slope of Florida where velocities reach 190 cm/sec and slowly decrease with depth (Fig. 3).

Numerous observations with electromagnetic current meters ("ЭМИТ"), materials of buoy stations in the central and eastern parts of the sea, on the slope of the Campeche Bank and calculated water discharges through all the straits enable the construction of a new scheme of the circulation of water in the Caribbean region (Fig. 4).

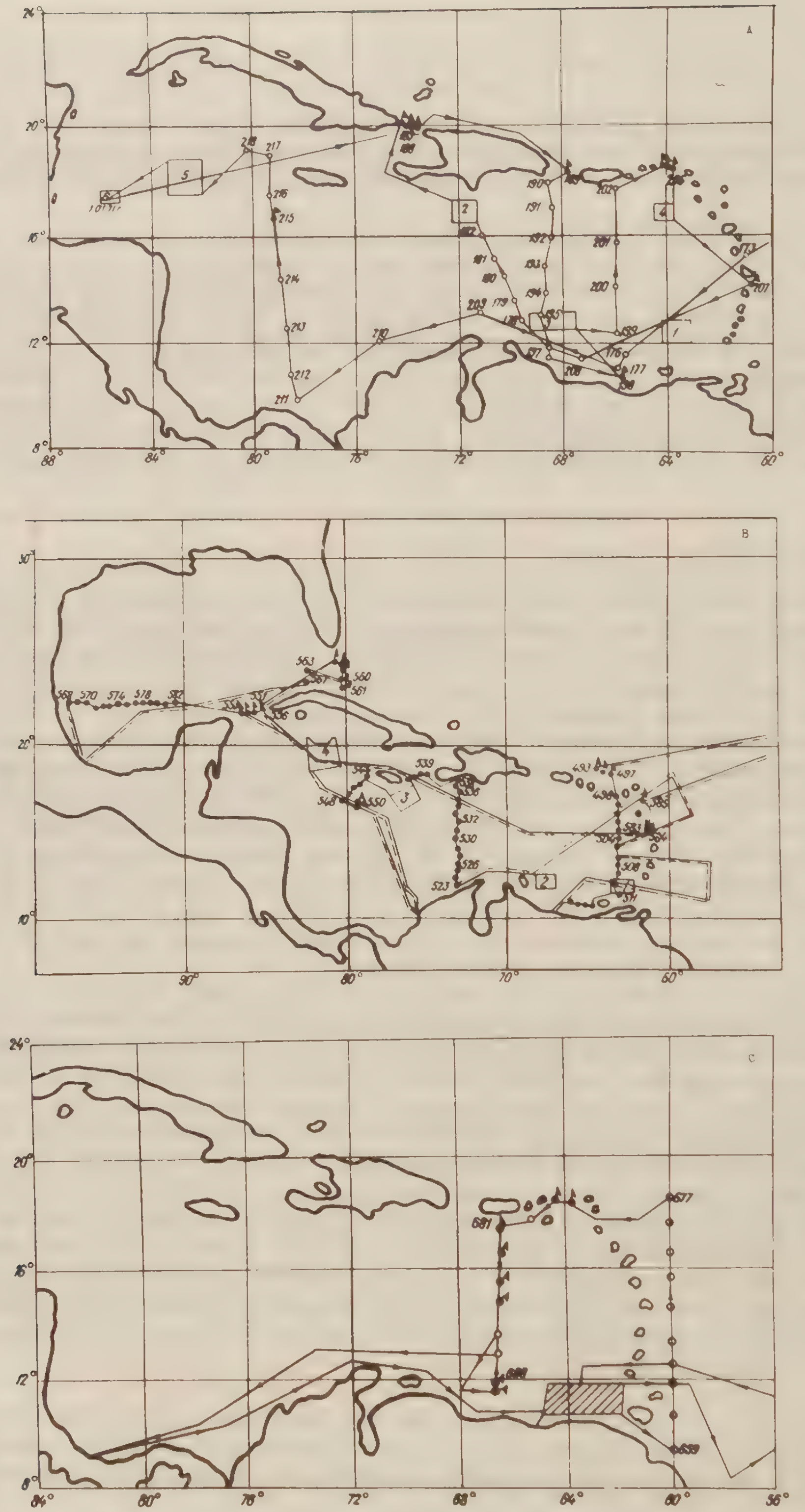
A
24°
20°
16°
12°
8°
88°
84°
80°
76°
72°
68°
64°
60°
5
2
4
1
B
30°
20°
10°
90°
80°
70°
60°
4
3
2
C
24°
20°
16°
12°
8°
84°
80°
76°
72°
68°
64°
60°
56°
677
681
659

Fig. 1 (a) a scheme of sections, buoy stations and proving grounds during the third cruise of the R/V AKADEMIK VERNADSKY
(b) a scheme of sections, buoy stations and proving grounds during the sixth cruise of the R/V AKADEMIK VERNADSKY
(c) a scheme of sections, buoy stations and proving grounds during the seventh cruise of the R/V AKADEMIK VERNADSKY

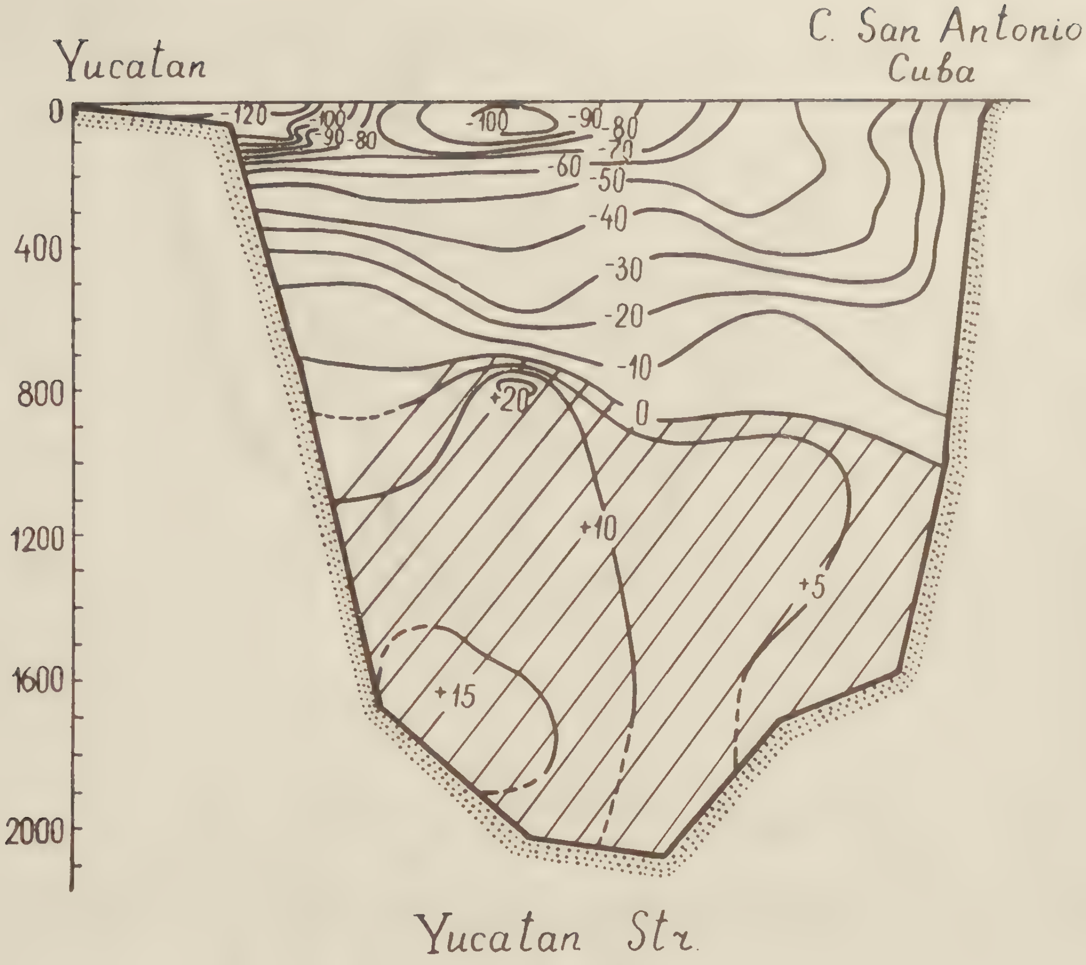

Fig. 2 Position of isotachs in the Yucatan Strait (current component normal to a section plane)

Atlantic waters entering the Caribbean Sea through all straits proceed toward the Gulf of Mexico. However, parallel with the general drift, a surface countercurrent is also present in certain regions. Thus, along the southern coast of Cuba a band of the current exists which is directed from the Yucatan Strait to the Windward Passage (Naukova Dumka, 1966). While leaving the strait this current together with a flow of the Bahama Channel forms an anticyclonic circulation in the region between the Bahama Islands and the Windward Passage. The surface countercurrent is also found along the southern coast of Haiti and Puerto Rico. Leaving the Gulf of Mexico the major flow runs toward the Florida Straits; besides the main branch of the current there are two more. In the Florida Straits these branches join the main axis of the current; one of them makes a loop in the eastern part of the Gulf, another one passes round the entire Gulf in a clockwise direction.

A narrow strip of the coastal current extends from the northern coasts of the Gulf of Mexico along the continental shelf to the Gulf of Campeche. It differs sharply in the colour and content of suspended matter, from more transparent water flowing around the Gulf in a clockwise direction.

In the Yucatan Strait a narrow strip of the current is revealed. The current enters the Caribbean Sea near the Yucatan coast. Flowing southward this current produces a cyclonic gyre in the Gulf of Honduras. The second cyclonic gyre occurs off the coasts of Panama and Costa Rica. This is due to large amounts of atmospheric precipitation and considerable coastal run-off which dilutes coastal waters.

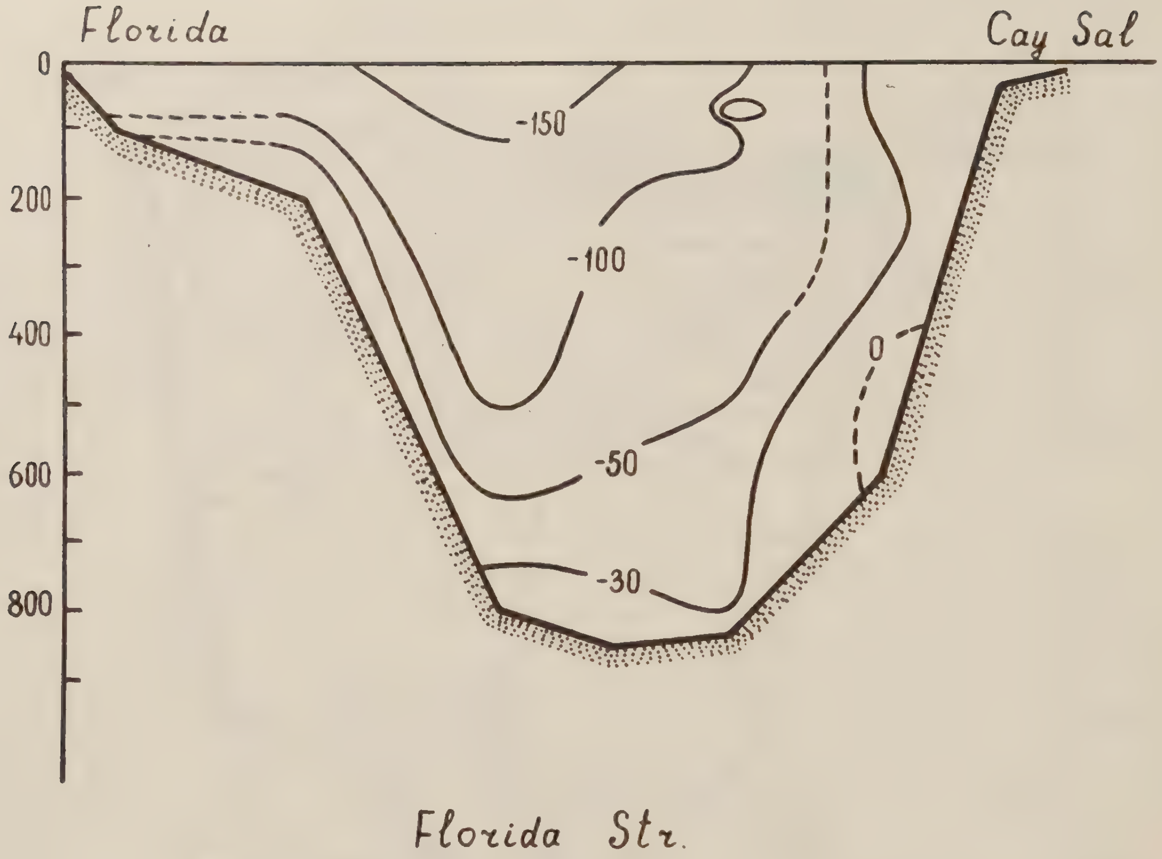

Fig. 3 Position of isotachs in the Florida Straits

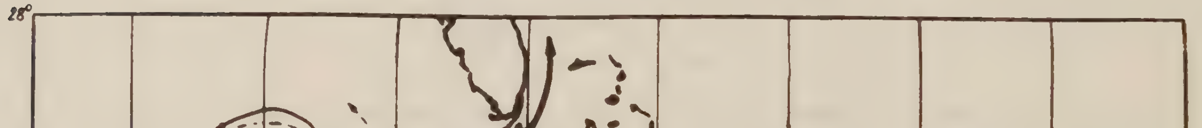
28°
24°
20°
15°
12°
8°
92°
88°
84°
80°
76°
72°
68°
64°
60°
1
2

Fig. 4 A scheme of surface and deep currents of the Caribbean Sea:
1 - surface currents; 2 - deep currents

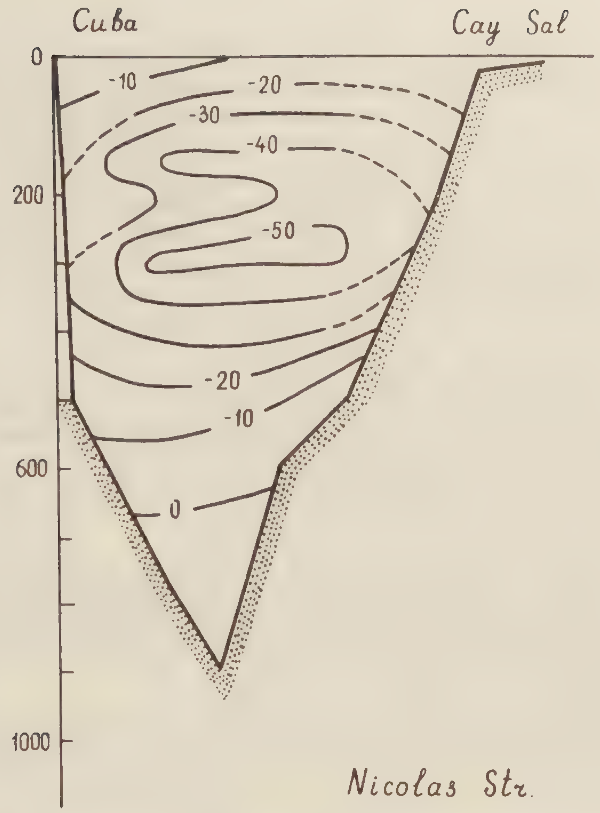
Cuba
Cay Sal
0
200
600
1000
-10
-20
-30
-40
-50
-20
-10
0
Nicolas Str.

Fig. 5 Position of isotachs in the Nicolas Strait

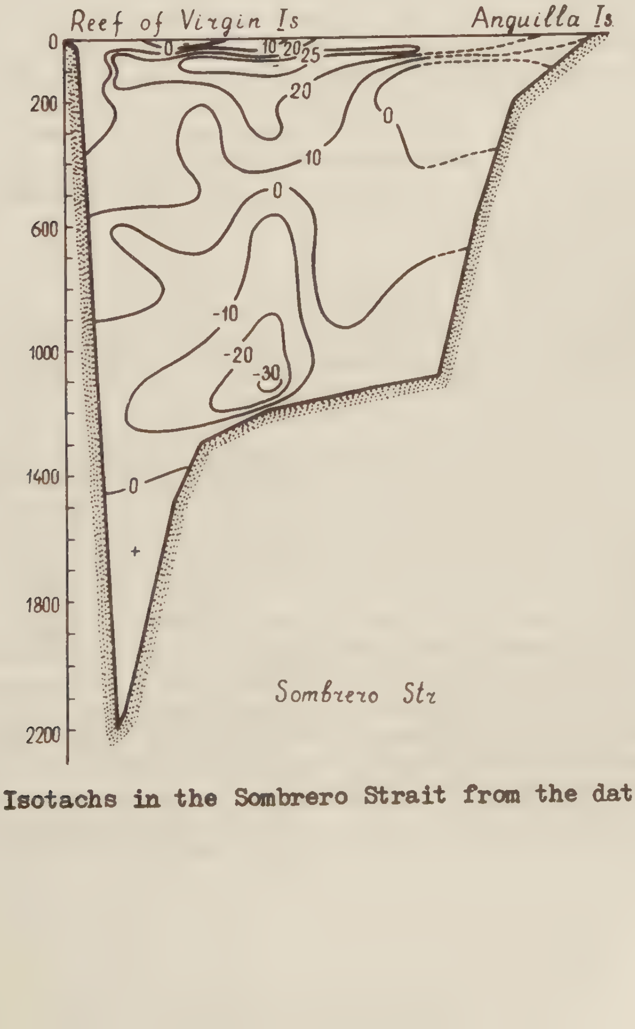
Reef of Virgin Is
Anguilla Is
0
200
600
1000
1400
1800
2200
0
10
20
25
20
0
10
0
-10
-20
-30
0
+
Sombrero Str

Fig. 6 Isotachs in the Sombrero Strait from the data of 1972

In the Nicolas Strait and along the slope of the Kai-Sal Banks in the Florida Straits weak deep backward flows are found which cannot play an important rôle in the formation of deep currents in the Gulf of Mexico and the Caribbean owing to their insignificant discharges (Fig. 5). The appearance of strong deep backward currents is caused by inflow to the Gulf of Mexico of large volumes of water from the Caribbean Sea both in the upper and lower layers. Deep waters mainly enter from the ocean through the Windward Passage (Sukhovei, 1971). The rise of the level in the Gulf of Mexico results in substantial horizontal gradients of pressure and in the development of deep currents. The discharge of deep waters through the Straits of Florida and Nicolas together with the basic flow is impossible because of high sills.

The extensive Campeche Bank accounts for the counter-clockwise direction of the deep flow. Along the slope of the Bank the current re-enters the Yucatan Strait and the Caribbean Sea. One branch of this current passes the Cayman Trench and escapes into the ocean through the eastern part of the Windward Passage. The second branch flows from the western extremity of the Cayman Ridge with its extensive banks and penetrates into the Colombian basin through a narrow trench of the Jamaico Ridge.

Deep circulation also exists in the eastern Caribbean Sea and is ascribed to inflow of deep water through the Strait of Sombrero (Fig. 6). Discharges of both the entering and leaving flows through this strait are rather high,which provides the renewal of deep water in the Grenadean and Venezuelan Troughs.

Thus, materials of investigations corroborate the existence of the intensive deep circulation in the Caribbean Sea and the Gulf of Mexico which contributes to permanent ventilation of deep waters.

3. WATER MASSES

Caribbean waters are well stratified to a depth of 800 m; between 800 and 1 700 m they are weakly stratified and, below 1 800 m they are uniform down to the bottom. This stratification characteristic is associated with sill depth in the Greater and Lesser Antilles passages. Major water masses of the Caribbean enter from the Atlantic Ocean (Akademia Nauk, 1974).

In summer, surface waters have temperature equal to 29°C and in winter 25°C; salinity varies from 34.85 to 35.85°/oo and is determined by not only waters entering from the Atlantic Ocean, but also by a fresh water balance. Oxygen saturation is 100-103% and these waters are marked by low phosphate content.

Owing to the fact that the drift in the Caribbean Sea has a general east to west direction surface waters are observed to be driven away to northern shores of the sea. In certain regions situated along the coasts of Venezuela and Colombia driving away of waters leads to coming to the surface of highly saline and colder subsurface waters.

Subsurface Subtropical Waters show maximum salinity at 75-150 m depth. In this layer salinity is as high as 37.00°/oo. Oxygen concentration varies from 3.0 to 4.0 ml/l, in the southern regions oxygen content is slightly lower than that in the northern regions. These areas also differ in phosphate concentration: in the southern regions it is 10-20 µg/l, in the northern regions under 5 µg/l. Values of pH are within 8.00-8.20.

Subtropical Intermediate Waters (700-900 m) are formed in the South Atlantic and enter the Caribbean Sea through the passages of the Lesser Antillean islands. Intermediate minimum of salinity (in the core - 34.70°/oo), the greater range of changes in oxygen concentration and high content of inorganic phosphorus is characteristic. In the layer of oxygen minimum, oxygen values decrease with depth from 4.0 to 2.6 ml/l, then they increase again to 4.4 ml/l at the lower boundary of the water mass. The entire layer of intermediate waters is marked by high concentrations of phosphates - from 40 to 60 µg/l, the highest concentrations are observed at a depth of 800 m.

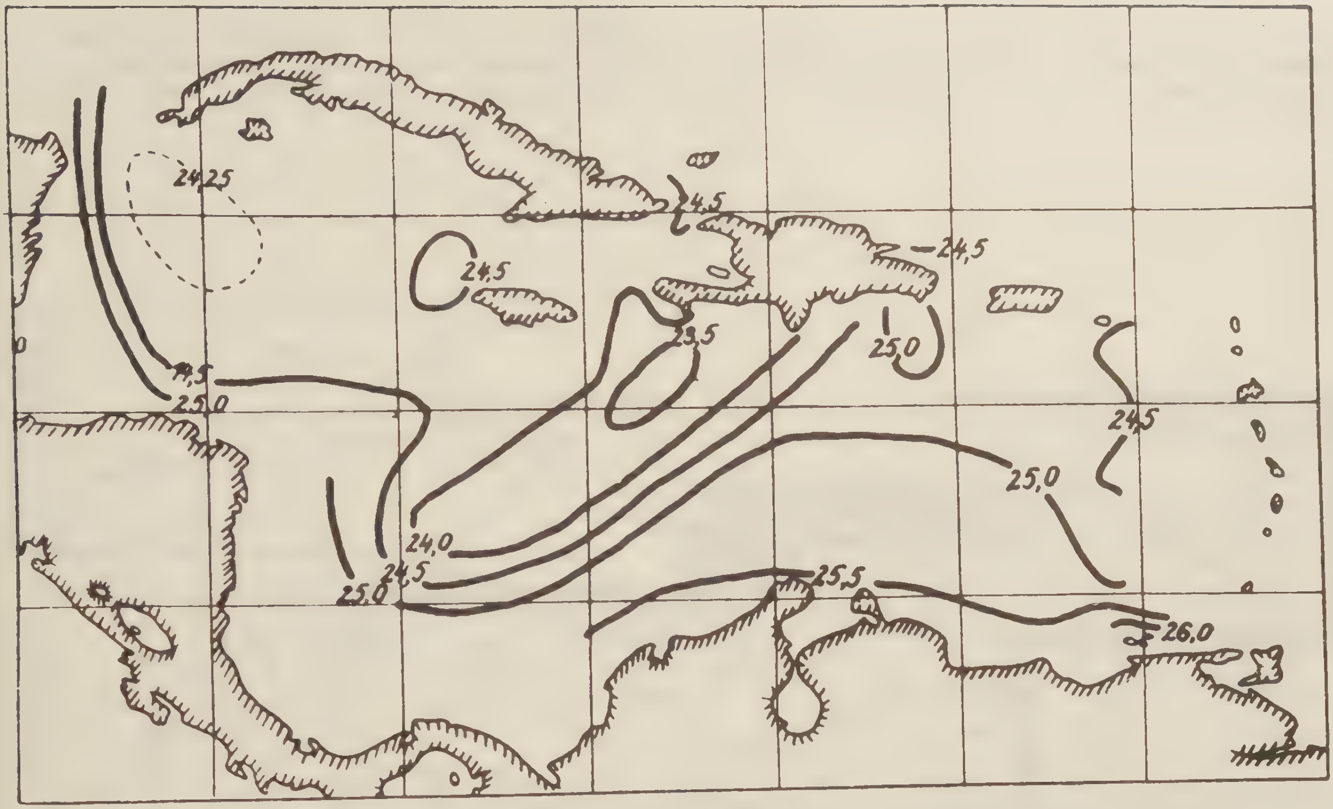

Fig. 7 Isolines of conventional density at a depth of 100 m for winter season

A deep portion of the Caribbean Sea is occupied by a relatively homogeneous water mass with a temperature of about 4°C and salinity of 35.00°/oo. Oxygen concentration increases down to the bottom from 4.5 to 5.0 ml/l. Phosphate concentration is 40-50 µg/l and slowly decreases with depth whereas the pH value increases from 8.00 to 8.15 (Akademia Nauk, 1974).

4. WATER CIRCULATION THEORY

A hydrodynamic model of the Caribbean Sea has been developed by scientists of the Marine Hydrophysical Institute of the Academy of Sciences of the Ukrainian S.S.R. The model takes into account the stratification of the sea, discharges in the straits and non-unicoherence of the area (Korotaev and Shapiro, 1975). The density field on the upper boundary of thermocline which was calculated using this model is in good agreement with that at a depth of 100 m (Fig. 7) according to observational data. The integral circulation in the Caribbean basin except for the western boundary layers where its intensification takes place, represents a zonal transport for the most part. Isolines of integral stream function indicate that the basic integral transport occurs between Jamaica and Haiti (Fig. 8) (Korotaev and Kosnyrev, 1975).

Currents in the baroclinic layer penetrating into the Caribbean Sea through its eastern boundary and northern straits extend in a south-western direction. Near the western boundary they become intensified, turn northward, round the Mosquitos Bank and, along the eastern coast of the Yucatan Peninsula, leave through the Yucatan Strait. Off the eastern coast of the Mosquitos Bank, a branch is separated from the main stream which rounds Jamaica.

Deep circulation (Fig. 9) is caused by sinking of water off the southern and western boundaries, the rise in the rest of the sea and the abyssal discharges through the Mona and Sombrero Straits. Deep countercurrents are situated off Jamaica near the northern and southern boundaries of the eastern Caribbean Sea. In addition to this, there is a deep countercurrent in the Yucatan Strait, the presence of which is responsible for the intensive water upwelling near the north-eastern extremity of the Yucatan Peninsula. The most interesting theoretical result is the initiation of a deep countercurrent in a passage between the Mosquitos Bank and Jamaica (Korotaev and Shapiro, 1975) which is evidenced by observational data.

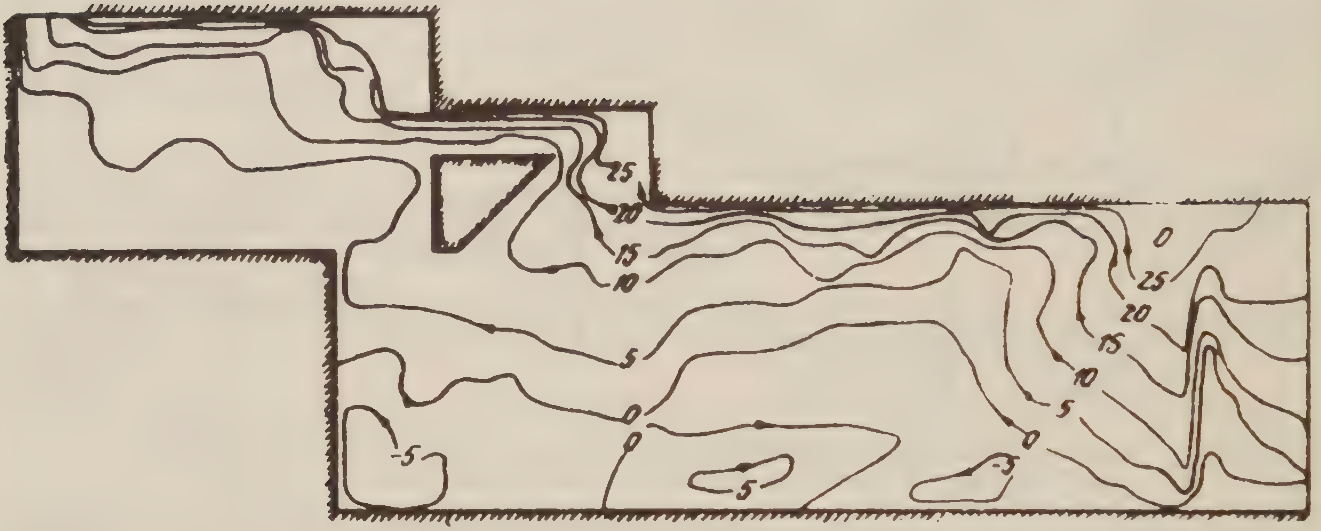

Fig. 8 Isolines of integral stream function in the Caribbean

Consequently, a theoretical picture of integral transports is close to a scheme of surface and deep currents of the Caribbean constructed as a result of processing and analysis of observations.

5. HYDRO-OPTICAL PROPERTIES

Measurements of hydro-optical characteristics of waters of the Caribbean Sea, the Gulf of Mexico and the adjacent Atlantic are conducted. The largest amount of materials is obtained on the distribution of index of directed light attenuation in various parts of a visible region of spectrum and on index of colour of surface waters (Akademia Nauk, 1974). As a whole, waters of the Caribbean and adjacent regions exhibit high transparency (25-30 m Secchi disc) and are fairly uniform over depth, with the exception of some shallow water regions (Campeche Bank, shelf of St. Vincent and Grenada as well as the spreading zones of these currents which carry waters with the high content of biogenous material).

In the most of the Caribbean Sea two water layers are found: surface (less transparent) waters and deep (more transparent) ones. Their interface is situated at depths of 50 to 100 m and usually coincides with levels of maximum gradients of density. In some regions the uppermost layer is slightly more transparent which is obviously due to features of the vertical distribution of phytoplankton. In a number of cases thin unstable layers of lower transparency - the so-called "scattering layers" - are observed during sounding. These layers are greatly affected by the presence of a measuring instrument.

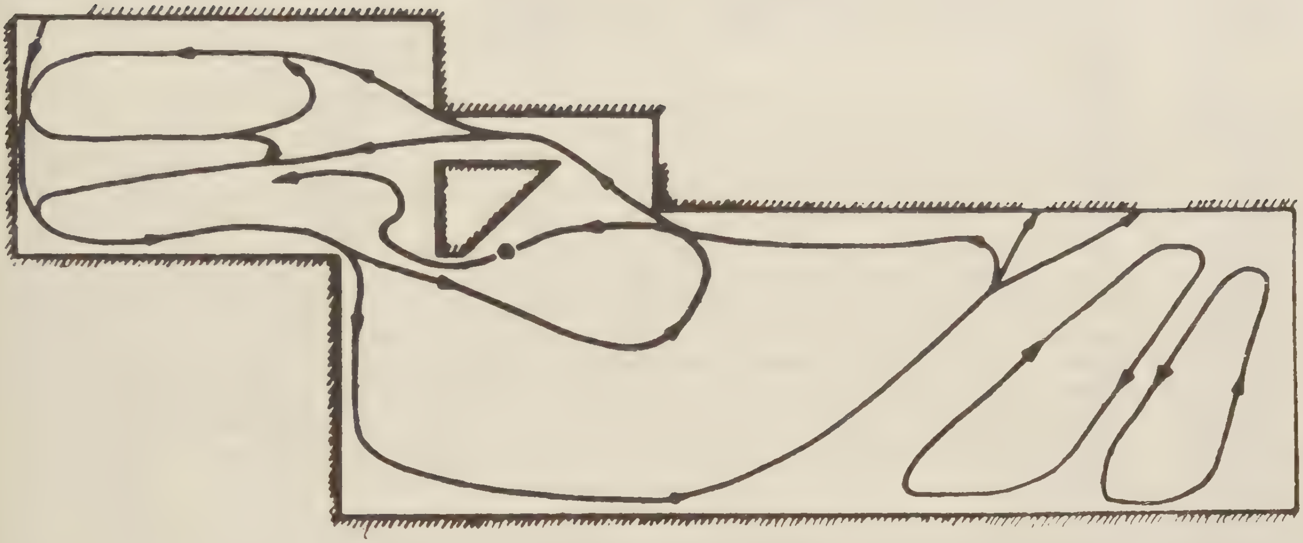

Fig. 9 A scheme of deep currents in the Caribbean

In the eastern Caribbean, optical properties are determined to a considerable extent by the inflow of Atlantic water through the passages in the ridge of the Lesser Antillean Islands. There, flows of transparent oceanic water (Fig. 10) can be easily traced, as can turbid flows of waters of the Orinoco in the straits adjacent to the South American continent. One can follow a fine structure of currents in this part of the Caribbean from spreading of turbid water.

The Cariaco Trench area is highly intensive with respect to distribution of optical properties. The optical structure of water discovered here is very close to that in the central part of the Black Sea, which can be the result of the presence of deep hydrogen sulphide zone.

In the central part of the Gulf of Mexico the area of less transparent water is encountered which can probably be attributed to a divergent character of currents in this region. In the northern part there is a well pronounced turbid layer of surface water resulting from the Mississippi runoff. This layer is carried away by the flow of the Florida Current.

Measurements of index of colour which is a sensitive indicator of biological productivity of water, indicate that low productivity is characteristic of surface waters of the Caribbean basin except for the regions with turbid water where colour index values are very high. Measurements of index of colour conducted continuously when ship is en route show that the regions of the Atlantic Ocean east and south-east of the Lesser Antilles feature a mosaic structure: dark blue transparent oceanic water and greener water occur in turns on account of the discharge of the Orinoco and the Amazon. Bioluminescence is low as a whole, which is in good agreement with low biological productivity of the region.

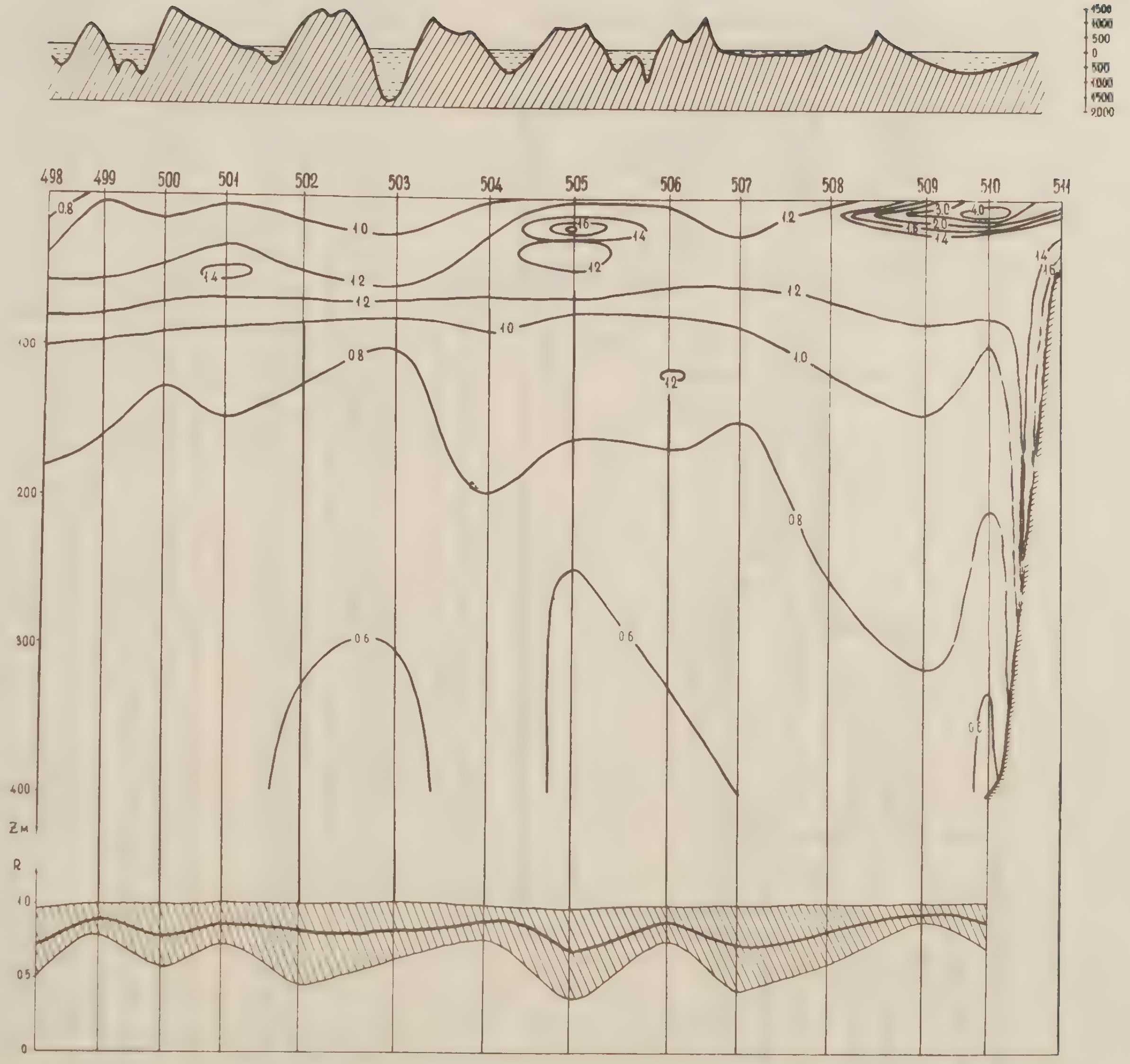

Fig. 10 (a) a schematic profile of the Lesser Antillean arc
(b) vertical distribution of index of directed light attenuation in the section along 63°W
(c) correlation coefficient value

6. GEOLOGICAL AND GEOPHYSICAL INVESTIGATIONS

On the basis of data of geological and geophysical studies carried out in 1971, the chart "Bottom Topography of the Caribbean Sea" compiled at the Marine Hydrophysical Institute of the Ukrainian S.S.R. Academy of Sciences was published (Akademia Nauk, 1970). In subsequent years a number of previously unknown sea mountains have been discovered in the Yucatan and Colombian Troughs and the submarine Nicaraguan Rise. Structural and morphological characteristics of the continental margin of Venezuela, the Curaçao Ridge, the Los-Roex Trench, the mid-oceanic rise in the Cayman Trench and the island arc of the Lesser Antilles were defined more precisely and in more detail (Akademia Nauk, 1971). Data of echo-sounding performed in 1971-1975 formed the foundation for compiling new charts.

The Cayman Trench is the northern boundary of the Caribbean lithospheric plate; in this region zones of regional linear-positive magnetic anomalies are found which are related to fractures of the earth's crust and are due to outpouring of basalts (Akademia Nauk, 1975). The calculation of bedding depth of upper edges of magnetic bodies shows that they are confined to the lower boundary of the layer of unconsolidated sediments and to the roof of basaltic layer of the earth's crust. The block structure of the Cayman Trench is conditioned by the existence of the mid-rise,dividing it into the western and eastern halves. Along the saddle of the rise a deep fracture of submeridional extension is found which is fixed by anomalies of T_a seismisity and bottom topography. Along the fracture a southward displacement of the western half of the trench relative to the eastern one by approximately 100 km is found. The location of the fracture permits one to define more precisely the north-western structure of the boundary of the Caribbean plate. With the establishment of the fracture extending in the north-eastern direction in the mid-rise area, a slips-like contact of plates occurs.

Data on the calculation of upper edges of magnetic bodies of the magnetic field of the Nicaraguan Rise (Fig. 11) are indicative of fairly wide volcanic activity in the past, which resulted in the appearance of sources of magnetic anomalies in the sediment cover (Akademia Nauk, 1975a). The block break-up of the submarine Nicaraguan Rise is determined by the fractures of sublatitudinal and submeridional strikes (Fig. 12).

Based on new data of gravimetric measurements and published works,distributions of gravity field of the Caribbean region in the free-air anomaly and Bouguer gravity anomaly have been analysed and generalized.

Calculation of isostatic anomalies of gravity defines to what extent the Caribbean lithosphere is close to equilibrium. This means that intensive horizontal gradients of gravity anomalies as well as disturbances of isostasy are timed to marginal framing of the region; the Caribbean proper is quite close to full isostasy.

On the basis of comparison between disturbances of isostasy and a character of bottom topography, seismisity and other geophysical parameters, the borders of the Caribbean plate are defined more accurately and a character of movements in the boundary zones is discussed. The compression of edges of the lithospheric plate due to a westward displacement of North and South Americas leads to differentiated motions and crushing of the lithosphere into smaller blocks.

7. SUMMARY

As a result of complex research conducted by the Marine Hydrophysical Institute of the Ukrainian S.S.R. Academy of Sciences in the Caribbean on the CICAR programme a large volume of field data has been obtained, processed and analysed. Hydrological, hydro-optical, hydrochemical and geological/geophysical investigations broadened our knowledge of properties of water of the Caribbean region and enabled a deeper understanding of the processes which occur there. The materials obtained are of prime importance in connexion with planning of the most efficient utilization of food and mineral resources of the Caribbean Sea and adjacent water areas. In parallel with this, the investigations carried out are of great importance to oceanography as a whole, since the Caribbean basin is one of the basic links in the chain of the general circulation of water of the Atlantic Ocean.

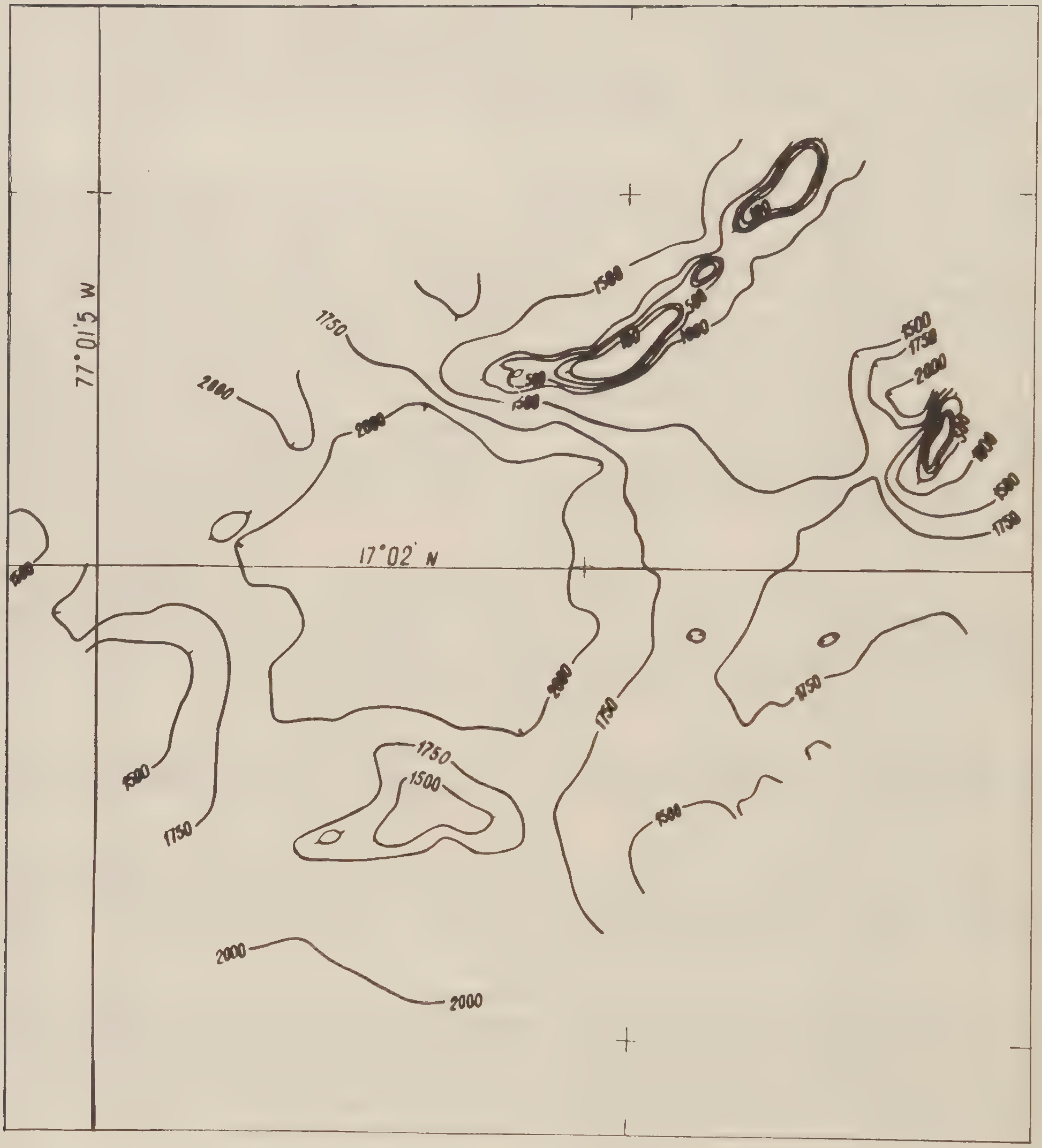
77°01'5 W
17°02' N
1750
2000
2000
1500
1500
500
1000
1500
1750
2000
1000
1500
1750
2000
1750
1750
1750
1500
1500
1750
1500
2000
2000

Fig. 11 Chart of the anomalous magnetic field of the Nicaraguan Rise

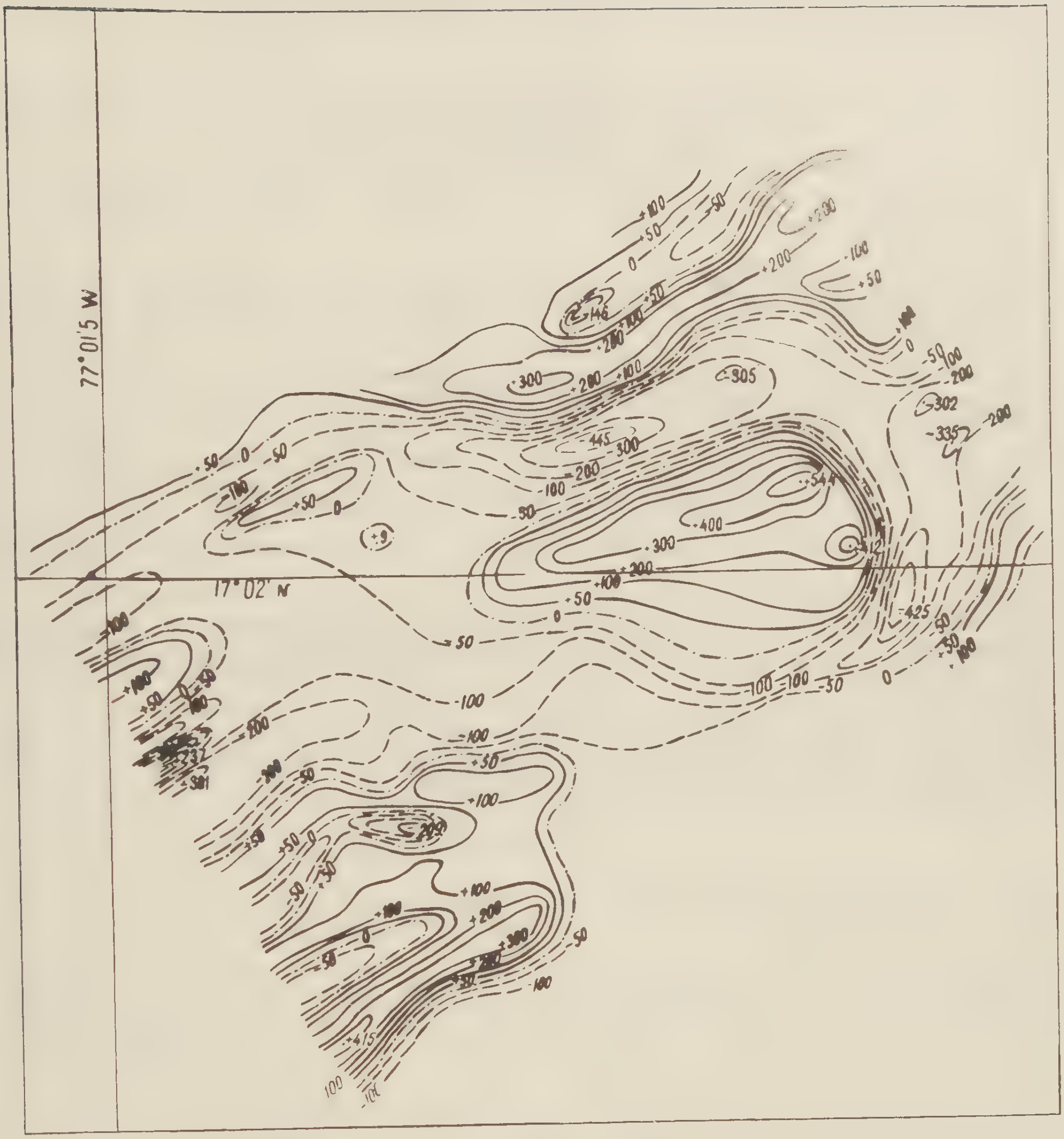
77°01'5 W
17°02' N
+100
+50
-50
0
+200
-100
+50
-146
-200
-300
-280
-305
-302
-335
-200
-445
-300
-200
-100
-544
-400
-300
+200
+100
+50
0
+9
-50
-425
-100
-100
-50
0
-100
-200
-232
-301
-100
+50
+100
-209
+100
+200
+300
-280
-301
-100
+415
100
-100

Fig. 12 Chart of bottom topography of the Nicaraguan Rise

8. REFERENCES

Akademia Nauk, Morskie Gidrofizicheskie Institut, (A new chart of bottom topography of the
1970 Caribbean Sea). Morsk.Gidrofiz.Issled., 48 (2) (in Russian)

Akademia Nauk, Morskie Gidrofizicheskie Institut, (The structure of the Caribbean Sea bottom).
1974 Sevastopol, Morskie Gidrofizicheskie Institut (in Russian)

Akademia Nauk, Morskie Gidrofizicheski Institut, (Research on the Caribbean Sea. Materials
1974 of expeditions). Sevastopol, Morskoi Gidrofizichescki Institut (in Russian)

Akademia Nauk, Morskie Gidrofizicheski Institut, (Anomalous geomagnetic field and bottom
1975 morphology of the western part of the Caribbean). Morsk.Gidrofiz.Issled., 70(3) (in Russian)

Akademia Nauk, Morskie Gidrofizicheskie Institut, (Some peculiarities of the Nicaraguan
1975 Rise from magnetic data). Sevastopol, Morskie Gidrofizicheskie Institut (in Russian)

Korotaev, G.K. and N.B. Shapiro, (On the theory of large-scale currents in the Caribbean Sea.
1975 Morsk.Gidrofiz.Issled., (68)(1) (in Russian)

Korotaev, G.K., V.K. Kosnyrev and N.B. Shapiro, (On the theory of deep currents in the
1975 Caribbean Sea). Morsk.Gidrofiz.Issled., 69(2) (in Russian)

Nauka Dumka, (Research on the Central American seas). Kiev, Naukova Dumka (in Russian)
1966

Neuymin, H.G. and V. Sukhovei, (Research during the sixth cruise of the R/V AKADEMIK
1973 VERNADSKY (September 1972-January 1973). Morsk.Gidrofiz.Issled., 61(2) (in Russian)

Sukhovei, V.F. et al., (Water exchange between the Caribbean Sea and the Atlantic Ocean
1971 through the northern straits). Morsk.Gidrobiol.Issled., 55(5) (in Russian)

ESTRUCTURA GEOLÓGICA Y PRINCIPALES FASES DE DESARROLLO DE LA PARTE ORIENTAL DE LA REGIÓN DEL CARIBE [1]

por

B.F. ZERNETSKY
Instituto de Ciencias Geológicas de Kiev
Academia de Ciencias de Ucrania
Kiev, U.R.S.S.

Resumen

Los buques soviéticos de investigación ACAD. A. KOVALEVSKY, M. LOMONOSOV (1964-67) ACAD. VERNADSKY (desde 1970) han obtenido datos geológicos y geofísicos en los mares de América Central, que han permitido conocer mejor el desarrollo geológico de la parte oriental de la región del Caribe, y que podrían servir para la verificación de varias hipótesis geotectónicas sobre el origen de toda la zona del Mediterráneo americano. Los principales elementos morfoestructurales del Caribe oriental - crestas emergentes o sumergidas (Aves, Pequeñas Antillas, Curaçao, Barbados) y hondonadas oceánicas (Venezuela, Granada, Tabago, Cariaco, Bonaire) se distinguen por sus estructuras y desarrollos geológicos, esencialmente diferentes. La distribución de los sedimentos del fondo revela su dependencia de las corrientes dominantes, así como de la topografía del fondo y de la estructura de las islas adyacentes.

El arco de las Pequeñas Antillas se considera como la estructura más joven del paleoceno-eoceno comprendida entre las del mesozoico. La cresta Aves y la hondonada oceánica Granada descansan en rocas granítico-plutónicas, mezcladas con otras básicas, y se unen al sur, con las rocas graníticas de las islas Leeward, al fondo de la hondonada Los Roques, y sobre la cresta de Curacao. A partir de la vertiente septentrional del continente sudamericano, estas estructuras están delimitadas por fracturas regionales. Por el este, el arco de las Pequeñas Antillas se une a granitos cretáceos que sirven de base a la hondonada de Tabago hasta la cresta de Barbados, que se formó antes del período triágico superior. La brusca desaparición de los sedimentos de carbonatos de la isla Mary Galan indica la existencia de la fractura, que también confirman los datos geofísicos.

La existencia de espilitas almohadilladas en la isla Deseada permite incluir esta zona en la ortogéosinclinal de las Grandes Antillas.

El análisis del desarrollo geológico de la parte oriental de la cuenca del Caribe pone de manifiesto que su estructura tectónica es más complicada de lo que suponen los que defienden la nueva tectónica global.

Abstract

The geological and geophysical data obtained in the Central American seas by the Soviet research ships ACAD. A. KOVALEVSKY, M. LOMONOSOV (1964-67) and ACAD. VERNADSKY (beginning from 1970) throw light on the geological development of the eastern part of the Caribbean region and may aid in the verification of different geotectonic hypotheses concerning the origin of the whole area of the American Mediterranian. The main morphostructural elements in the eastern Caribbean - above-water and submerged ridges (Aves, Lesser Antilles, Curaçao, Barbados) and oceanic troughs (Venezuela, Grenada, Tobago, Cariaco, Bonaire) are distinguished by their essentially different geological structure and development. The distribution of the bottom sediments shows the dependence upon the dominant currents as well as upon the bottom topography and the structure of the adjacent islands.

---

[1] Abstract only submitted

The Lesser Antilles island arc is considered to be the youngest Paleocene-Eocene structure enclosed between the mesozoic ones. The Aves Ridge and the Grenada oceanic trough are underlain by the granite pluton intruded by the more basic rocks; it adjoins in the south the granite rocks occurring on the Leeward Islands, at the bottom of the Los-Rokes Trough and on the Curaçao Ridge. From the northern slope of the South American continent these structures are delimited by regional fracture. In the east the island arc of Lesser Antilles adjoins the cretaceous granite underlying the Tobago Trough up to the Barbados Ridge, which was formed before the Late Jurassic time. The abrupt disappearance of the carbonate sediments on the Mary Galan Island suggests the existence of the fracture also confirmed by the geophysic data.

The occurrence of the Late Jurassic pillow spilites on the Désirade Island makes it possible to include this area in the ortogeosincline of the Greater Antilles.

The analysis of the geological development of the eastern part of the Caribbean Basin shows its more complicated tectonic structure as it has been supposed by the supporters of the new global tectonics.

M-40
ISBN 92-5-000707-8